SHAFT CONFIGURATION AND BEARING CAPACITY OF PILE FOUNDATION

T. W. Adejumo [1*], I. L. Boiko [2]

[1, 2] Department of Geotechnics and Environmental Engineering, Faculty of Civil Engineering, Belarusian National Technical University, Minsk.

*adejumo.taiye@futminna.edu.ng, +2349033795541.

ABSTRACT

This paper presents the results of recent research on shaft configuration and bearing capacity of pile foundation from both laboratory as well as field experimental investigations. Prototype piles of cylindrical, prismatic and conical sections were tested in the laboratory, with piles of corresponding (chosen) configurations/cross sections used as test piles on the field. Using experimental models and load tests, the study compares the values of bearing capacities of pile of various shape tested on weak soil in Minsk area of Belarus. Prismatic piles yielded lower strength at the early loading than both conical and cylindrical piles. But as the loading increases, it showed higher resistance to load than cylindrical, but still lower than conical piles. The results of test piles in a close test point proximity area, showed that conical piles have the highest bearing capacity, 1.5 – 2 times higher than prismatic piles, and 2 - 3 times higher than cylindrical piles. It further revealed that, for non-homogenous (layered) soil, mostly encountered in construction sites, pile installed by driven or boring have bearing capacity increment of 10 - 14% in bored piles, 18 - 24% hammer driven piles, and 20-30% in vibrated driven piles. For the investigated prototype modelled piles, as well as test piles, the tapering and wedging effects are responsible for increase in normalized skin friction and normalized lateral stresses of tapered conical piles. In all, tapered conical pile offers larger resistance than the cylindrical piles and prismatic piles, and is therefore recommended for use, with other factors being considered.

Keywords: Shape factor, Pile foundation, Bearing capacity, Soft/weak soil, Pile installation techniques.

1. INTRODUCTION

In foundation engineering practice, the main point of concern is the bearing capacity of soil. Pile foundation is a type of foundation in which pile is usually used as the source to transfer the load to deeper soil levels. Piles are long and slender structural members that transfer the load to stronger soil ignoring or through the soil of low bearing capacity. Piles foundations are therefore, recommended to provide a safe carrying capacity to support a structure when the bearing capacity of the soil is insufficient to do so. Modified form of the general bearing capacity equation may be used to account for the effects of footing shape, ground surface slope, base inclination, and inclined loading (Bridge Design Specification, 2003).

The compaction of the soil mass around a driven pile increase its bearing capacity. The pile end-bearing capacity in sand is not only affected by its compressibility, shear stiffness, and strength, but also by the angle of tapering of the pile. Not many researchers have noticed the effects of tapering angle in end-bearing resistance when penetrated downward in a frictional mode (Manandhar et al., 2010).

The determination of the ultimate bearing capacity, Qu, of a deep foundation based on most theories is a very complex one, since there are many factors, which are not taking into consideration in most of them. Most theories assume that the soil is homogenous and isotropic, which is normally not the case. All the theoretical equations are obtained based on plain strain conditions. Only shape factors are applied to take care of the three-dimensional nature of the problem. Compressibility characteristics of the soil even complicate the problem further (Murthy, 2007). According to De Beer, the base resistance of bored and cast-in-situ pile is about one third of that of driven pile (De Beer, 1965). Sitnikov et al., who investigated on soils in Belarus, established that the shape of the longitudinal section of the pile affects the unit bearing capacity, and concluded that, the unit bearing capacity of square piles varies significantly with their cross-sectional dimensions,

and increases with a reduction in their sectional dimensions (Sitnikov et. al., 1980).

Meyerhof concluded that, when a pile is driven into loose sand, its density is increased, and the horizontal extent of the compacted zone has a width of 6-8 times pile diameter (Meyerhof, 1959, & 1976). However, Kerisel opined that, in dense sand, pile driving decreases the relative density because of the dilatancy of the sand and loosened sand along the shaft has a width of 5 times pile diameter (Kerisel, 1964a & 1964b). Vesic opined that, only punching shear failure occurs in deep foundation irrespective of the density of the soil, provided the depth to width ratio is greater than four (Vesic, 1964). Kishida proposed from model and field tests, that the angle of internal friction decreases linearly from a maximum value $\varphi2$ at the tip of the pile to a lower value $\varphi1$ at a distance 3.5 times pile diameter; $\varphi1$ and $\varphi2$ being pre-installation and post-installation angle of internal friction respectively (Kishida, 1967). Based on theoretical relations to plastic equilibrium, a critical state frictional angle (φ'_{cv}), which is effective and a rational practical application as a strength parameter has been derived by researchers (Yasufuku*et al*, 1997,Yasufuku*et al*, 1998 andBolton, 1993). Adejumo, through experimental investigations, confirmed that, among other determinants, the bearing capacity of piles is a function of method of installation of the piles, especially in layered soil [Adejumo, 2015a, Adejumo, 2015b].

A comparative study of the observed base resistances of piles by Nurdlund(Nurdlund, 1963) and Vesic(Vesic, 1964), presented by Tomlinson (Tomlinson, 1986) , showed that, the bearing capacity factor Nq values established by (Berezantsev et al. 1961), which take into account the depth to width ratio of the pile, most nearly conform to practical criteria of pile failure. The ultimate unit skin friction of piles in a given sand or clay is practically independent of the pile diameter (Meyerhof, 1976 & 1983).

The collapsibility properties of a highly porous layered soil diminish with depth, from 2-3% to 1 - 1.5%, while the unit bearing capacity of bored piles reduces 2-3 times on the average (Belyaev et al., 1979). The lateral deformation of piles decreases with increase in distance from the pile centerline, while outward radial deformations recorded around the pile decreases downwards along the length (Adejumo, 2013). The skin friction and radial stress are highly influenced by tapered piles compared with conventional piles. The tapering and wedging effects are responsible for increase in normalized skin friction and normalized lateral stresses. Taper-shaped piles offer a larger resistance than the cylindrical piles (Manandhar et al. 2011 and 2012].

This paper therefore, presents the results of a series of modelled pile tests as well as field tests on the effects of pile shaft configuration on the bearing capacity of pile foundations in layered soil. The investigation was conducted with piles of cylindrical, prismatic and tapered conical cross sections in the research laboratory, Geotechnical and Environmental Engineering Department, Belarusian National Technical University, Minsk and construction site, also in Minsk region of Belarus. This study is useful in the understanding of the analytical techniques of pile design in relation to determination of the bearing capacity, especially in multi-layered soil.

2. MATERIALS AND METHODS

A detailed research plan was developed for the two-pronged laboratory and field investigations. Laboratory tests were conducted on soil samples taken from sites around Minsk province of Belarus, where field tests were also carried out. Consolidated in a specially constructed multipurpose test tank, Figure 1, the soil samples were properly pulverized and mixed to the desired water content and bulk densities Table I. The testing tank has a relatively rigid steel framework support, with a one sided steel panel

having open and close apertures for drained and undrained tests. The frontal panel is made with transparent Plexiglas (plasto-fiber material), which is strong enough to withstand consolidation induced pressure and strikes. The transparent strong Plexiglas allows proper monitoring of sample's state during the test as well as ensures visual observation of failures in the tested soils in terms of depression, heaving or wobbles. The weights of the soil required to obtain designed unit weight were packed into the test tank in lifts, with the interface between the lifts being made uneven, to reduce the bedding effects, and clearly marked to give room for proper monitoring during loading and unloading. After layer by layer densities were achieved, axial compressive load was applied through the upper surface layer. The testing tank was then made rigid and ready for pile installation by driving (hammering and by vibration), as well as by boring, Figures 1 - 3. Loading was introduced through the centerline of the pile which is connected to a Pile Design Analyser (PDA) for monitoring and analysis.

Seven soil condition cases were modelled with the three chosen shapes of piles for the laboratory investigations in the testing tank. They are: 1) Strong Silty clay soil exclusive; 2) Soft Silty clay layers over stiff; 3) Soft clay layers in-between stiff clay layers; 4) Soft silty clay exclusive; 5) Coarse sand exclusive 6) Medium sand layers in-between coarse sand layers; 7) Medium sand layers over coarse sand layers.

The field investigations were performed on 13 No instrumental piles of cylindrical, prismatic and tapered conical sections, (5 cylindrical, 4 prismatic and 4 conical cross sectional piles respectively) at a construction site for high-rise residential buildings in Partisankaya district of Minsk, Belarus. Static loads were applied and maintained using a hydraulic jack (of 200T capacity) and were measured with a load cell as shown in Figure 4. Reaction to the jack load is provided by a steel frame that is attached

to an array of steel H-piles located at least 1.5m away from the test piles. Pile cap settlements were measured relative to a fixed reference beam using 2 dial gauges. Displacement/settlement of soils around the piles measurements were made in reference to the pile cap using 5 dial gauges, Figure 5. The piles were subjected to axial compressive loads until the allowable pile settlement of 0.1d (10% of pile diameter) is reached or exceeded in line with the submission of (Al–Saoudi and Salim, 1998; Phanikanth et al. 2010), as well as Europe code 7 (ENV 1997-1 Eurocode 7, 1994, Bauduin, 2001). The settlement was taken with time until the time when the settlement change was insignificant.

The bearing capacity of prototyped modelled piles of different shapes were determined using the established methods of static bearing capacity equations and field load test method. The results were analysed, and inferences on the effects of shaft configuration on the bearing capacity of the pile were made thereafter.

Fig. 1: Testing Tank for Laboratory Work
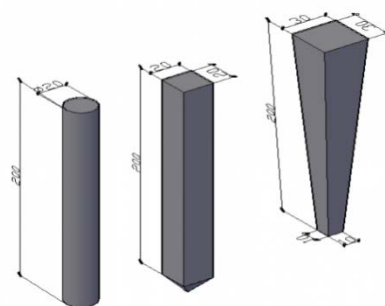
Fig. 2: Modelled Pile Shaft Configurations

Fig. 3: Modelled Test Piles Bored into the Soil

Fig. 4:2000T HJ as Loading Device

Fig. 5: Dial gauges for Settlement Reading

Fig. 6: Load Test Modelled Test Piles

3. RESULTS AND DISCUSSIONS

Table 1 shows the summary of geotechnical properties of the dominant soil in the profiles of the investigated samples. The silty-clay soil has high void ration (e) and cohesion, which indicated the compressibility of the soil. The results classified the main or dominant soils to range between, Clayed Gravel – GC (USCS), A-6 (AASHTO); Silty/clayed Gravel sand – GC (USCS), A-2-4 (AASHTO); Sandy clay – SC (USCS), A-4 (AASHTO).

Table 1: Index Properties of Samples from Test Points.

Test point/Pile No	LL (%)	PL (%)	PI (%)	GS	OMC (%)	MDD (kg/cm^3)
P1	32	20	12	2.49	13.2	1842
P2	35	22	13	2.44	18.7	1593
P3	37	20	17	2.51	17.6	1624
P5	38	23	15	2.46	15.6	1769
P6	36	24	12	2.57	16.2	1664
P7	28	21	7	2.46	20.0	1617
P8	29	22	7	2.45	19.1	1614
P10	36	22	14	2.57	16.2	1664
P12	35	21	14	2.56	16.3	1666
P13	34	23	11	2.55	16.2	1663
P20	39	24	15	2.44	18.7	1598
P22	37	20	17	2.51	17.6	1627
P23	33	20	13	2.49	13.3	1848

Using static bearing capacity equations and field load tests method, the increment in bearing capacity for a 5mm design settlement, (for a 2.5D critical state design, where D is pile diameter), for modelled single piles in the 7-modeled soil/loading (cases), were analysed and shown in Figures. 7 - 13.
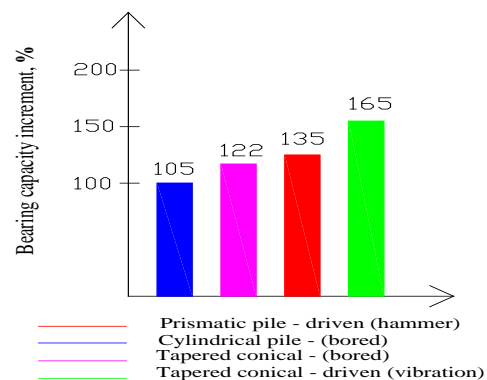

Fig. 7: Bearing Capacity of Piles - Case 1

Case 2 - Soft Silty clay layers over stiff
For settlement, S = 5mm

Prismatic square pile - (bored)
Cylindrical pile - (driven)
Tapered conical - driven (vibration)

Fig. 8: Bearing Capacity of Piles - Case 2

Case 3 - Soft clay layers in-between stiff clay layers
For settlement, S = 5mm

Prismatic pile - driven (hammer)
Cylindrical pile - (bored)
Tapered conical - driven (vibration)

Fig. 9: Bearing Capacity of Piles - Case 3

Case 4 - Soft silty clay exclusive
For settlement, S = 5mm

Prismatic pile - driven (hammer)
Cylindrical pile - (bored)
Cylindrical pile - (driven)
Tapered conical - driven (hammer)
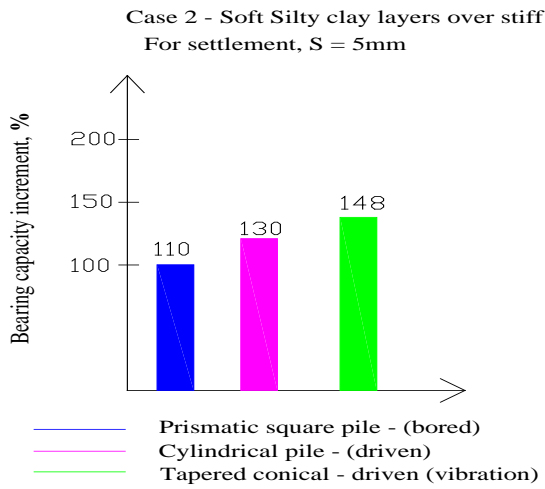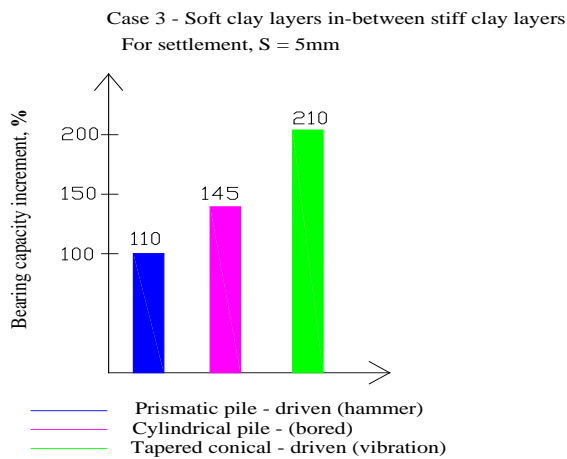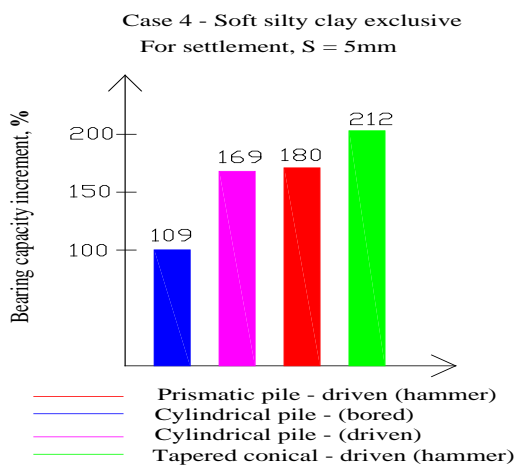
Fig. 10: Bearing Capacity of Piles - Case 4

Case 5 - Coarse sand exclusive
For settlement, S = 5mm

Prismatic pile - driven (vibration)
Cylindrical pile - (driven)
Cylindrical pile - (bored)
Tapered conical - driven (vibration)
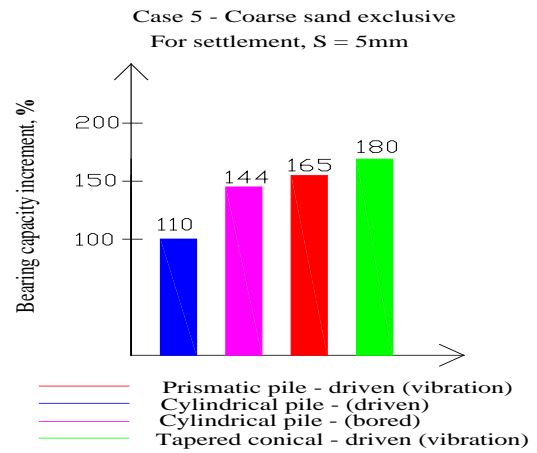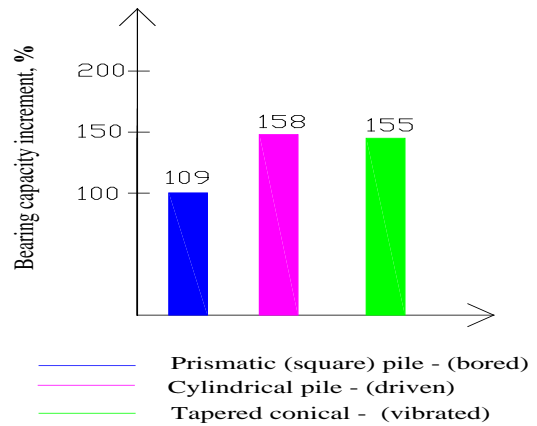
Fig 11: Bearing Capacity of Piles - Case 5

Case 6 - Medium sand layers in-between coarse sand layers
For settlement, S = 5mm

Prismatic (square) - driven (hammer)
Cylindrical pile - (bored)
Tapered conical - driven (hammer)

Fig.12: Bearing Capacity of Piles - Case 6

Case 7 - Medium sand layers over coarse sand layers
For settlement, S = 5mm

Prismatic (square) pile - (bored)
Cylindrical pile - (driven)
Tapered conical - (vibrated)

Fig. 13: Bearing Capacity of Piles - Case 7

The Load-settlement for a limiting 5mm design settlement, (for a 2.5D critical state design, where D is pile diameter), for static load test in the laboratory which corresponds to 40 mm settlement on the field, for modelled single piles in the 7-modelled soil conditions (cases), were analysed and shown in Figures 14 - 20.
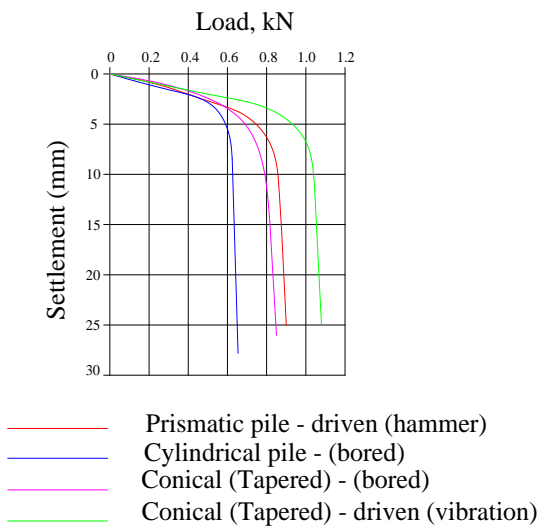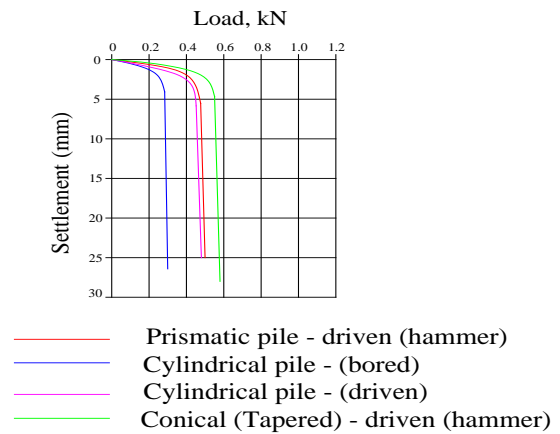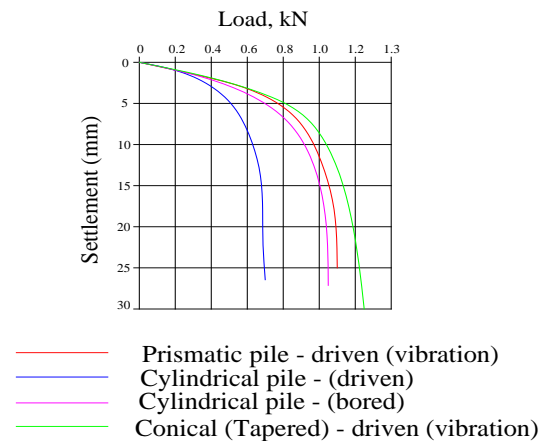

Fig. 14: Load-Settlement for Test Piles - Case 1
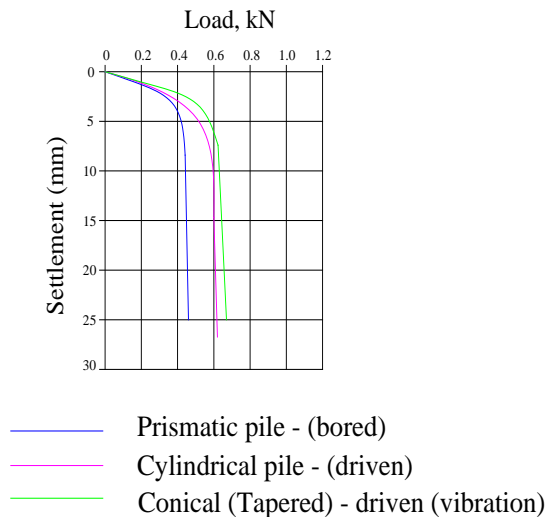
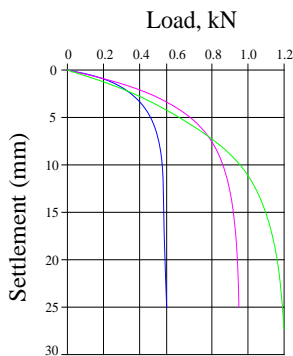**Fig. 15**: Load-Settlement for Test Piles - Case 2
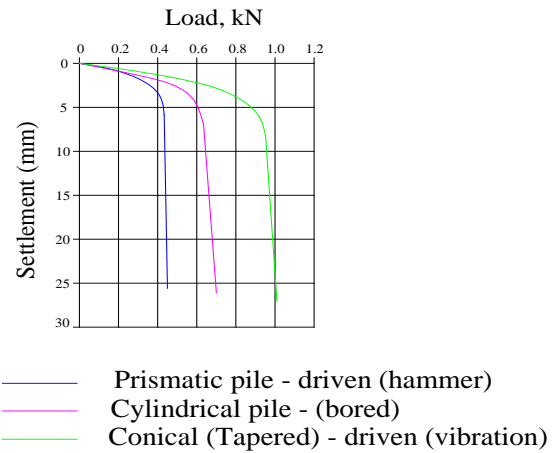
Fig. 16: Load-Settlement for Test Piles - case 3

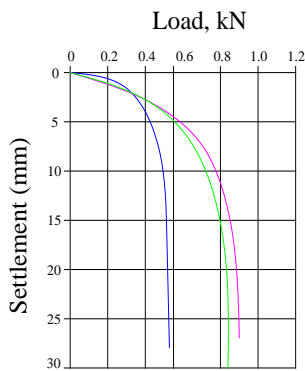**Fig. 17**: Load-Settlement for Test Piles - Case 4

Fig. 18: Load-Settlement for Test Piles - Case 5

Fig. 19: Load-Settlement for Test Piles - Case 6

Fig. 20: Load-Settlement for Test Piles - Case 7

Load-settlement curves for the 13 test piles is shown in Figure 21, while the normalized load-settlement for the ultimate load ratio is shown in Figure 22. Prismatic piles yielded lower strength at the early loading than both conical and cylindrical piles. But as the loading increases, it showed higher resistance to load than cylindrical, but still lower than conical piles.
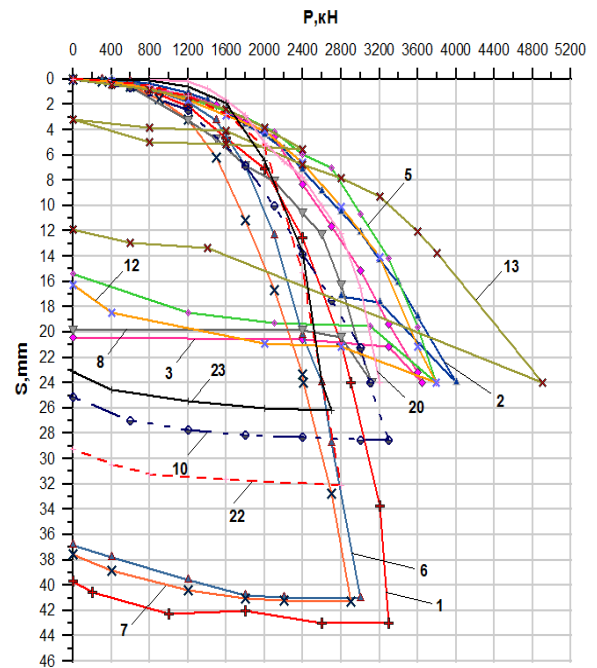
Fig. 21: Load-Settlement Curves for the 13 Test Piles
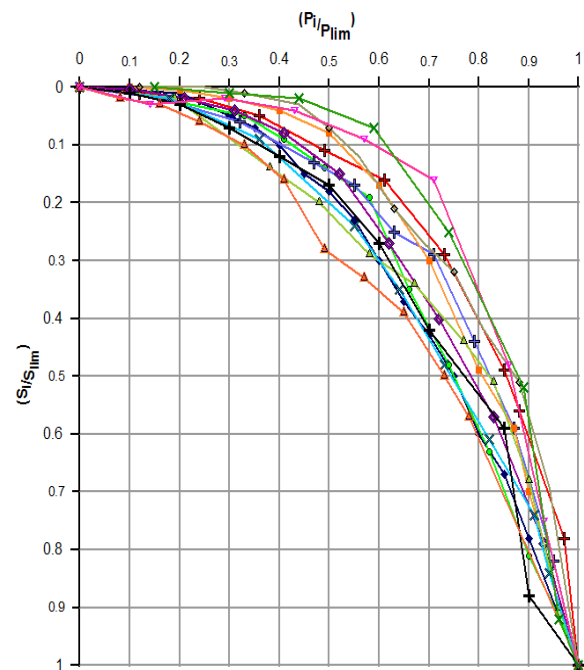
Fig. 22: Normalised Load-Settlement Curves for the 13 Test Piles

4. CONCLUSION

From laboratory and field investigations conducted on shaft configuration and bearing capacity of pile foundation, the following conclusions could be drawn:

1. In silty-clay and clayed gravel soil, tapered conical piles yielded higher bearing capacity than cylindrical and prismatic piles.

2. For a give test area, for a given test areas (close test proximity) conical piles have the highest bearing capacity, 1.5 – 2 times higher than prismatic piles, and 2 - 3 times higher than cylindrical piles

3. For non-homogenous (layered) soil, pile installed by driven or boring have bearing capacity increment of 10 - 14% in bored piles, 18 - 24% hammer driven piles, and 20-30% in vibrated driven piles.

4. Prismatic piles yielded lower strength at the early loading than both conical and cylindrical piles. But as the loading increases, it showed higher resistance to load than cylindrical, but still lower than conical piles.

5. The results of field investigations and laboratory tests for modelled piles have an 85% agreement, which is within acceptable limits of correlation.

6. Where applicable therefore, conical piles of tapered cross section is recommended for use in weak layered soil.

ACKNOWLEDGEMENTS

REFERENCES

Adejumo, T. W., (2013) "Settlement and Deformation Pattern of Modelled Wooden Piles in Clay," International Journal of Advanced Technology and Engineering Research, IJATER, Vol.3 (3), pp. 94 – 99.

Adejumo, T. W., (2015a) "Effects of Shape and Technology of Installation on the Bearing Capacity of Pile Foundations in Layered Soil," Scholars Journal of Engineering and Technology, SJET, SAS Publishers, Vol. 3, No. 2A, pp. 104 - 111.

Adejumo, T. W., (2015b) "Influence of Shaft Configuration and Method of Installation on Load Carrying Capacity of Pile Foundations," Journal of Environmental Science, Computer Science and Engineering & Technology, JECET, Section C; Vol.4. No.1, pp. 170-182.

Al–Saoudi, N. K. S. & Salim, H. M. (1998) "The Behaviour of groups of reinforced concrete model piles in expansive soil," Proceedings of the 2nd International Conference on Unsaturated Soils, Beijing, Vol.1, pp. 321-326.

Bauduin, C. (2001) "Design procedure according to Eurocode 7 and analysis of the test results. Proceedings of the symposium Screw Piles: Installation and design in stiff clay. Rotterdam, Balkema, pp. 275 – 303.

Belyaev, V. I. &Rud, Y. P, (1979) "Effect of boring method on bearing capacity of short cast-in-place piles," Soil Mechanics and Foundation Engineering, Vol. 16(4), pp. 194 – 197.

Berezantse, V. G., Khristoforov, V. V., &Golubkov, V. (1961) "Load Bearing Capacity and Deformation of Pile Foundations," Proc. 5th Int. Conf. of Soil Mech. and Found. Eng., Vol.2, pp. 1 - 9.

Bolton, M. D. (1993) "What are partial factor for, Proceedings of the International on Limit State Design in Geotechnical Engineering," Danish Geotechnical society for ISSMFE TC23, DGF Bulletin, Copenhagen, Vol. 10, pp. 565 – 583.

De Beer, E. E. (1965) "Bearing Capacity and Settlement of Shallow Foundations on Sands," Proceeding, Symposium on the Bearing Capacity and Settlement of Foundations, Duke University, Durham, NC, pp. 15 – 34.

ENV 1997-1 (1994) Eurocode 7 – Geotechnical design, part 1: General rules. CEN/TC 250/SC7. Bruxelles, ComitéEuropéen de Normalisation.

General Requirements and Materials, Bridge Design Specification (2003), Section 4 – Foundations, Caltrans: Part A, 4–1-4–8.

Kerisel, J. (1964a) "Foundation Profoundes en Milieu Sableux," Proceeding of 5th Intern. Conf. SM and Found. Eng., Vol. 2.

Kerisel, J., (1964b) "Deep Foundation – Basic experimental facts," Proceeding of North Amer. Conf. on Deep Foundations, Mexico City, Vol. 1.

Kishida, H., (1967) "Ultimate Bearing Capacity of Piles Driven into Loose Sand," Soil and Foundations, Vol. 7, No. 3.

Manandhar, S., Yasufuku, N., Omine, K. & T. Kobayashi, T., (2010) "Response of tapered piles in cohesionless soil based on model tests," Journal of Nepal Geological Society, Vol. 40, pp. 85 – 92.

Manandhar, S. &Yasufuku, N. (2011) "Evaluation of skin friction of tapered piles in sands based on Cavity Expansion Theory," Memoirs of the Faculty of Engineering, Kyushu University, Vol. 71(4), pp. 101 – 126.

Manandhar, S., Yasufuku, N. &Omine, K. (2012) "Application of cavity expansion theory for evaluation of skin friction of tapered piles in sands, International Journal of Geo-Engineering, 4(3), pp. 5–17.

Meyerhof, G. G., (1959) "Compaction of Sands and Bearing Capacity of Piles," JSFMD, ASCE, Vol. 85: SM 6.

Meyerhof, G. G., (1976) "Bearing capacity and settlement of pile foundations, 11th Terzaghi Lecture, 5th November 1975, Journal of Geotech. Eng. Div. Am. Soc. of Civ. Engr., 102, GT3:195 – 228.

Meyerhof, G. G. (1983) "Scale Effects of Ultimate pile Capacity," Journal of Geotechnical Engineering; 109 (6), pp. 797–806.

Murthy, V. N. S. (2007) "Advance Foundation Engineering, Geotechnical Engineering Series," 1st edition, CBS Publisher & Distributors, New Delhi, pp. 251 – 534.

Nordlund, R. L., (1963) "Bearing Capacity of Piles in Cohesionless Soils," JSMFD, ASCE, 1963; Vol.89: SM 3.

Phanikanth, V. S., Choudhury, D. & Reddy, G. R. (2010) "Behaviour of Fixed Head Single Pile in Cohesionless Soil under Lateral Loads," Electronic Jour. of Geotech. Eng., EJGE, Vol.15 (M): pp.1243 - 1262.

Sitnikov, M. A., Shaitarov, L. D. &Lozovik, M. A. (1980) "Introduction of rectangular pyramidal piles in Belorussia, Soil Mechanics and Foundation Engineering, Vol. 17(1), pp. 5–10.

Tomlinson, M. J., (2001) "Foundation Design and Construction," 7th Edition, Pearson Education Ltd., England: Prentice Hall, pp. 276 – 387.

Vesic, A. S. (1964) "Investigation of Bearing Capacity of Piles in Sand," Proceeding of North Amer. Conf. on Deep Foundations, Mexico City, Vol. 1, pp. 4-12.

Vesic, A. S., (1967) "A Study of Bearing Capacity of Deep Foundations," Final Report, School of Civil Engineering, Georgia Institute of Technology, Atlanta, U.S.A.

Yasufuku, N., Ochiai, H., & Maeda, Y., (1997) "Geotechnical analysis of skin friction of cast-in-place piles," Proceedings of the 14th International Conference on Soil Mechanics and Foundation Engineering (SMFE '97), Hamburg: pp. 921 – 924.

Yasufuku, N., Ochiai, H., Kwag, J. M., & Miyazaki, K. (1998) "Effectiveness of critical state friction angle of volcanic ash soils in design applications," Proceedings of the International Symposium on Problematic Soils, IS-Tohoku, Vol. 1, pp. 189 – 193.

Transesterification of waste frying oil to methyl ester using activated carbon supported Mg-Zn oxide as solid-base catalyst

. M.A. Olutoye[1], E.J.Eterigho[2], B. Suleiman[3], O.D. Adeniyi[4], I.A. Mohammed[5],U. Musa[6]

[1]Department of Chemical Engineering, Federal University of Technology, Minna Nigeria.

[*]Corresponding Author: m.olutoye@futminna.edu.ng, 08034059454

.**Abstract**

An activated carbon-supported Mg-Zn catalyst (Mg-Zn/AC) was prepared by using co-precipitation combined with incipient wetness impregnation methods. The catalyst structure was characterized by powder X-ray diffraction (XRD), N_2 adsorption–desorption, Fourier transform infrared spectroscopy (FTIR), its microstructure was studied by the use of scanning electron microscopy (SEM)and the catalytic performance toward synthesis of methyl esters from waste frying oil (WFO) was investigated. The properties studied provided insight into the catalytic performance of the catalyst whereby the large surface area and pore volume of the support facilitated the distribution of metal particles and high dispersion of metals. The optimum reaction conditions were obtained by varying parameters such as methanol to oil ratio, catalyst loading, temperature and time. Under the conditions of reaction time of 5 h, temperature, 150 ^{o}C and catalyst dosage of 2.5 wt%, the methyl ester yield of >86% was achieved using 64 g of WFO, 38 g of methanol. The results showed that Mg-Zn/AC catalyst presented efficient activity during the transesterification reaction and is a promising heterogeneous catalyst for the production biodiesel fuel from vegetable oil feedstock.

Keywords: Activated carbon; Mg-Zn oxide supported catalyst; Waste frying oil; Biodiesel; Transesterification

1. INTRODUCTION

The dwindling reserves of fossil fuel and surging prices for the petroleum-based fuels has triggered the pressing needs for renewable energy as sustainable fuel substitute (Singh and Singh, 2010). According to the statistical data reported by the International Energy Agency, a 53% increase in the global energy consumption is foreseen by 2030. The energy consumption is mainly based on fossil fuels which account for 88.1 %. At the current production rates, the global proven reserves for crude oil and natural gas are forecasted to last for the next 41.8 and 60.3 years (Ong et al., 2011).Several researches on alternative renewable energy sources, namely solar, wind, hydrothermal, geothermal and biofuels have been carried out extensively (Cheng et al., 2010; Gnansounou and Dauriat, 2010; Yin et al., 2010).

Biodiesel, produced by Transesterification of vegetable oils, fats and fatty acids is recognized as a new emerging sector in fuel industry, due to the similarity it possesses with the conventional diesel in term of its chemical structure and energy content. Several types of vegetable oils which have been used for the preparation of biodiesel includes palm (Zabeti et al., 2009), sundowner(Granados et al., 2007), rapeseed (MacLeod et al., 2008),

Canola(D'Cruz et al., 2007), and soybean (Furuta et al., 2004; Kim et al., 2004; Suppes et al.,2004).Another attraction of biodiesel as diesel fuel is that it is a clean-burning fuel, nontoxic with liquid nature-portability, has higher combustion efficiency, provides low emissions of carbon monoxide, particulate matter, unburned hydrocarbons and zero percent of sulfur content compared to petroleum-based fuel, lower sulfur and aromatic content, higher cetane number and it is biodegradable. Simultaneously, no modification in diesel engine is required as biodiesel is compatible with the existing transportation engine models (Al-Zuhair, 2007; Yung and Gon, 2010; Zhang et al., 2009).

Many researches have been conducted in quest for suitable heterogeneous catalysts that have high performance during Transesterification reaction of vegetable oils with methanol. The development of catalysts loaded on support or carrier is very promising and has shown good conversion results in this regard. Heterogeneous catalysts can be designed to give higher activity, selectivity and longer catalyst lifetime (Hillion et al., 2003). Briefly, heterogeneous catalysts such as alkali metal (Li, Na, K)-promoted alkaline earth oxides (CaO,BaO, MgO), as well as K_2CO_3 supported on (Al_2O_3), have been used for Transesterification of Canola oil with molar ratio of alcohol to oil of 11.48:1, catalyst loading of 3.16 wt%, at 60 $^{\circ}$C,, for 2 h with more than 85% conversion. Also, Transesterification of unrefined or waste oil over lanthanum-promoted zinc oxide ($ZnO-La_2O_3$) catalysts, with a 3:1 ratio of zinc to lanthanum, at 170–220 $^{\circ}$C, 126 g of oil, 180 g of methanol, and 3 g of catalyst gave over 96% in 3 h (Yan et al., 2009). Others include KNO_3/Al_2O_3 (Vyas et al., 2009), La_2O_3/ZrO_2(Sun et al., 2010), K_2CO_3 on alumina/silica support (Lukic et al.,2009) and KNO_3/KL zeolite and KNO_3/ZrO_2 (Jitputti et al., 2006).

In this study, we describe the performance of supported Mg-Zn on activated carbon (AC) for the Transesterification of WFO with methanol. To obtain maximum conversion for the process, different reaction parameters such as WFO to methanol molar ratio, reaction temperature, catalyst loading, and reaction time were studied. The activated carbon is chosen due to its high porous structure as well as low cost compared to conventional supports such as alumina and silica. Structural, functional and surface chemistry of the prepared catalyst were performed. Moreover, the catalyst reuse and stability were elucidated.

2. METHODOLOGY

2.1. Chemicals

Waste frying oil (WFO) was obtained from the University of Science, Malaysia cafeteria. The properties of theoil such as kinematic viscosity, acid value and density were determined as 3.65 x $10^{-4}m^2s^{-1}$, 2.02 mg KOH g^{-1}oil and891 kg m^{-3}, respectively. Others are the average refractive index over three determinations, 1.47, moisture content, 0.09% and shear stress, 7.98 N/m^2. Analytical grade of KOH (>85%), Mg(NO_3)$_2$. $6H_2O$(>99%), Zn (NO_3)$_2$. $6H_2O$(>98%), KNO_3 (99%), used to synthesize the catalysts were purchased from Sigma–Aldrich Pty Ltd., Malaysia. Analytical reagent grade 99.9% methanol (HPLC) purchased from Merck (Malaysia)was used for the Transesterification reactions. The reference standards which are methyl stearate (>99.5%), methyl palmitate (>99.5%), methyl myristate (>99.5%), methyl oleate (>99.5%) and methyl linoleate (>99.5%)as well as methyl heptadecanoate (99.5%) used as internal standard for gas chromatography (GC)analysis was purchased from Sigma–Aldrich (Malaysia) and n-hexane (96%) used as solvent for GC analysis was purchased from MERCK, (Malaysia). All the chemicals used were analytical reagent grade.

2.2. Preparation of catalyst

Activated carbon supported Mg-Zn oxides was prepared by co-precipitation and impregnation of the AC with an equimolar (0.5 M) aqueous solution of the nitrates of Magnesium, Mg $(NO_3)_2.6H_2O$ and zinc,Zn $(NO_3)_2. 6H_2O$ which was used as precursor for Mg-Zn oxides. The equimolar solution of Mg-Zn was precipitated with 4 M solution of ammonia water. The activated carbon used has previously been prepared and characterized and was used without any pretreatment. The solution mixture was stirred for 3 h at 60 ^{o}C to homogenize. The catalyst was obtained by loading constant amount of AC support, 100 g for each batch preparation, to the precursor under constant agitation. After impregnation, the sample was allowed to age for 12 h before it was oven dried for 24 h at 100 ^{o}C. This was followed by calcinations in a furnace at the temperature500 ^{o}C for 4 h.

2.3. Catalyst characterization, activity testing, and evaluation of methyl ester content

The synthesized catalyst samples were characterized by elemental analyzer using an energy dispersive X-ray detector(EDX) mounted on the microscope and Philips XL30S model Scanning Electron Microscope (SEM), X-ray powder diffraction analysis was conducted on a diffractometer, model Philips PW1710, with Cu Kα radiation at 40 kV and 40 mA. The surface areas and textural characteristics of the prepared catalysts were determined using the Brunauer Emmett Teller(BET) method. The data were acquired on Micromeritics ASAP2020 adsorption analyzer (Micromeritics instruments corporation, USA) at -197°C.Fourier transform infrared spectroscopy (FTIR) was used to qualitatively identify the chemical functionality of the catalysts. FTIR spectra were recorded between 4000 and 400 cm^{-1}. Scanning Electron Microscopy (SEM) analysis was carried out to study the textural morphologies of the as-synthesized catalysts. Gas chromatography GC-2010 plus (Schimadzu,Japan) supplied by Fischer Scientific (M) Sdn, Bhd with Flame ionization detectors (FID-2010 plus) and split/split less injection unit (SPL-2010 plus) equipped with a capillary column (Nukol30 m x 0.53 mm x 1 μm) was used for sample analysis. Helium was used as the carrier gas. The injection was performed in split mode with a split ratio of 100:1. The analysis of methyl ester yield for each sample was carried out by dissolving 20 μL of FAME into250 μL methyl heptadecanoatewhich was used as internal standard to give a dilution factor of 14.1 μL of the prepared solution sample was withdrawn and injected into the GC and the methyl ester yield was calculated using appropriate standards and methods for GC calibration and analysis (Munari et al., 2007).

2.4. Transesterification of waste frying oil with methanol

Prior to charging WFO into the reactor, it was filtered with a fine screen cloth to remove impurities such as food bits and sludge. The oil was pretreated by heating at 80°C for1 h to separate adhered water and volatile food particles. A 300 mL stainless steel batch reactor PARR 4842 from Autoclave Engineers equipped with a stirrer, thermocouple and a pressure device surrounded by a heating mantle controlled by a proportional integral derivative (PID) temperature controller was used for the Transesterification reaction. A measured quantity of

the pretreated oil and methanol in the desired ratio were charged into the reactor containing the catalyst. The reactor contents were kept under constant stirring at maximum speed to avoid mass transfer limitations. Similarly, the stirring commenced immediately at the start of the reaction to allow sufficient contact between the participating species and was maintained throughout the duration of the reaction. In a particular batch experiment

with the WFO, 52 g oil was measured and charged into the reactor with 17 g of methanol equivalent to a molar ratio of methanol to oil of 9:1 was used with 2.5 wt% catalyst (1.317 g) based on oil at a temperature of 120°C.

2.5 Catalyst stability

The possibility of reusing the catalyst was investigated to check its capacity to provide the same performance during Transesterification reaction. To achieve this, the supported catalyst was recovered after first run, washed with n-hexane to remove oil adhered to its surface, filtered and oven dried 70°C for 12 h. It was then used in the second experimental run and the procedure was repeated for the third and fourth runs for methyl ester synthesis by Transesterification reaction between methanol and WFO.

3. RESULTS AND DISCUSSIONS

3.1. Catalyst characterization

The textural properties of any catalyst are important features that provide insights as concerns its performance. To this effect, BET surface area, average pore size, and pore volume of the catalyst were determined as 91.44 m²/g, 8.52 nm, and 0.19 cm³/g, respectively. The external surface area of the as-synthesized catalyst was observed to favour its reactivity. In this study, AC support helped to improve the surface area of the catalyst forming a composite structure with Mg-Zn oxides. The surface of the AC used is comprised of well pronounced and orderly pores developed over the surface after activation. A typical SEM image for one of the synthesized catalyst is as shown in Fig.1. It was observed that there was agglomeration of particles on the surface over the AC support. The AC layer seems to be embedded due to the precursor which penetrates the support. It was also observed that the penetration into the support was inhomogeneous and was at least a few micrometers in depth with few porous

opening. The exhibited nature is as a result of different materials made up of AC and the precursors integrated together consisting of particles that are not all of the same degree or dimensions. It was also observed that for a fixed concentration of the precursor, a continuous flat layer was obtained. The layer, however, covered the rough AC support yielding a thin film. It was also observed that the agglomerates of particles consisting of the precursor oxides synergized together in a composite matrix. The presence of the metals is also confirmed by the XRD measurements which revealed that the metals are dispersed on the specific sites which could be responsible for the high performance of the as-synthesized catalyst.
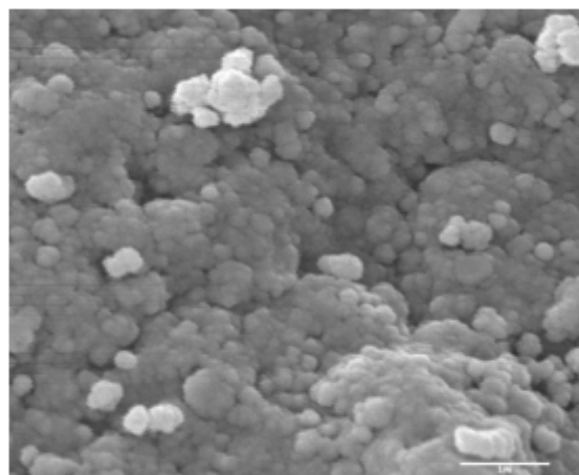
Fig.1 Scanning electron micrograph (SEM) image of Mg-Zn on AC support

The specific surface area and pore volume of the catalyst was analyzed using nitrogen adsorption at −197°C. As shown in the adsorption isotherms of Fig.2 monolayer formation was usually complete when the relative pressure reached 0.3 because the radius available for condensation was decreased by the thickness of the monolayer or by approximately two molecular diameters. Based on the results, the samples with relative pressures above 0.3 had type IV hysteresis according to the

IUPAC classifications, indicating the presence of mesoporous materials related to cylindrical pores. The relative pressure versus volume adsorbed for the catalyst with a steep increase in the isotherm of the amount of N_2 adsorbed corresponds to the filling of micro pore with N_2, this is followed by the nearly horizontal adsorption and desorption branches. The inter-crystalline textural porosity was indicated at high relative pressure (P/Po =0.99) as revealed by the observed hysteresis loop.

Fig. 2Adsorption-desorption isotherms for Mg-Zn/AC catalyst sample calcined at temperature

500 ^{o}C and time of4 h

The FTIR spectra of the used and fresh catalyst are shownin Fig. 3. The spectra show similar active surface functional groups in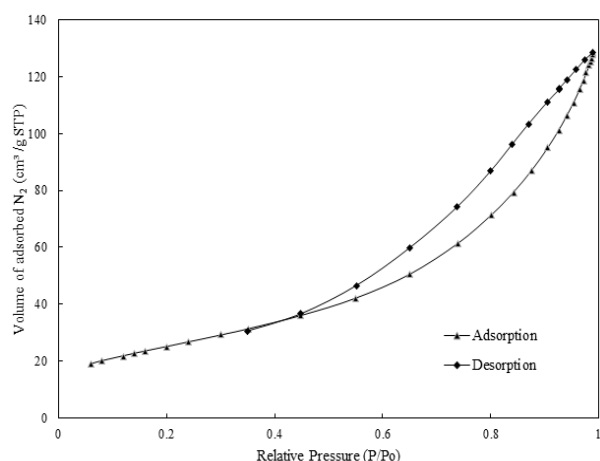 the region 3300–3550 cm^{-1} that represents the O–H stretching vibrations including hydrogen bonding in water molecules. Other peaks detected are found at bandwidths of 1620–1560 cm^{-1} that is vibration of surface hydroxyl groups attached to the metals and undissociated water molecules forming the surface hydrated layer. However, there are distinct differences between the catalysts spectra in the region

1150–420 cm^{-1}. The peaks at 2925 and 2860 are ascribed to C-H aliphatic stretching. Other important peaks at 1030cm^{-1} and 1100-1120 cm^{-1}represent C-O stretching. The peaks of symmetrical stretching of C=C are also observed at 1614-1699cm^{-1}. It was observed at 1385 cm^{-1} a peak which could be due to the presence of –CH$_3$ stretching. The intensity of peak at 2925 and 2860cm^{-1}, 1100-1120 cm^{-1}were decreased due to the intensities in the interaction between the precursor and the activated carbon. The band sat 1150–920 cm^{-1} could be ascribed to M–O–H stretching vibrations, whereas those between 580 and 500cm^{-1} are assigned to M–O bending vibrations. These observations could be due to the different interaction of the precursor's oxides on the activated carbon. The peaks for the both spectra are assigned based on existing data from literature (Miller and Wilkins, 1952). The spectra of both catalysts are found to be similar in all respect but for some new peaks established.
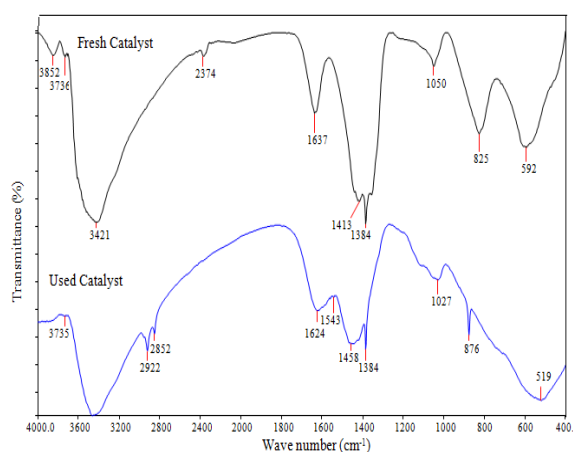

Fig.3 FTIR spectra analysis for the fresh and used Mg-Zn/AC catalyst

XRD analysis was performed in order to identify the crystalline phases present in the Mg-Zn/AC catalyst. The diffractograms for fresh and 3rdcycle reused samples is as

shown in Fig. 4. The sample calcined at 500 °Cfor4 h exhibited the XRD peaks at 2θ= 30°, 50.6° and 60.3° (strong) assigned to the tetragonal phase. It also showed weak XRD peaks at 2θ= 34°,
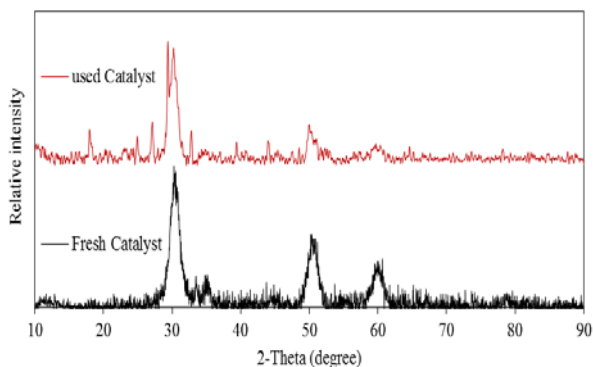
Fig. 4 XRD spectra for the fresh and used Mg-Zn/AC catalyst

35.8°, and 78°assigned to the monoclinic phase. The presence of both phases is responsible for the observed catalytic activity. Magnesium has strong intensity at2θ = 30° while other peaks are weakly dispersed. The EDX analysis was used to characterize the catalyst and the results of the analyzed samples are presented Fig.5. The spectra clearly showed the existence of Zn,Mg, and C with prominent peaks and the elemental composition further revealed the presence of carbon as the source of activated carbon used for the support with the value is as high as 15.26 wt%. The composition of the catalyst was verified by using an EDX mounted on the microscope and the elemental analysis revealed that the sample contained 10.12 wt% K, 28.03 wt% Zn, 11.28 wt% Mg and 35.31 wt% O. This was in good agreement with the XRD diffractograms
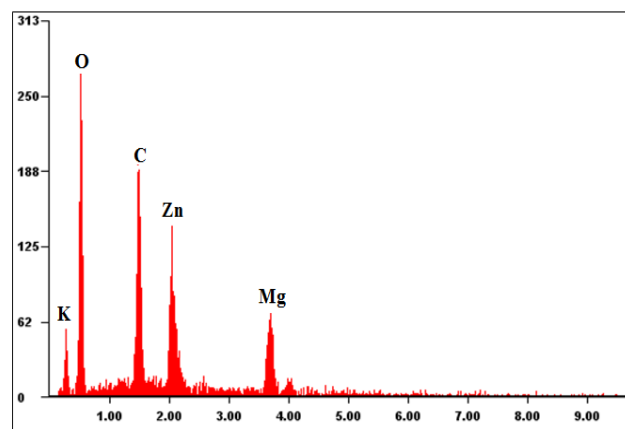
Fig.5 Energy dispersive X-ray (EDX) spectra of the Mg-Zn/AC catalyst

3.2 Thermal Gravimetric Analysis (TGA)

The thermal stability of the catalyst given in Fig.6was studied via thermal gravimetric analysis in oxygen at a heating rate 10°C/min in the range of 34-800°C.The thermal gravity curve showed that the synthesized compound had a weight loss of approximately 46.25% between 190°Cand 486°C. This corresponds to the decomposition of the organic component of the activated carbon and the metal oxide layers. When the temperature is increase over 480 °C, an increase in mass was observed, which could be attributed to the oxidation of metal precursors as the compound transforms into crystalline oxides.
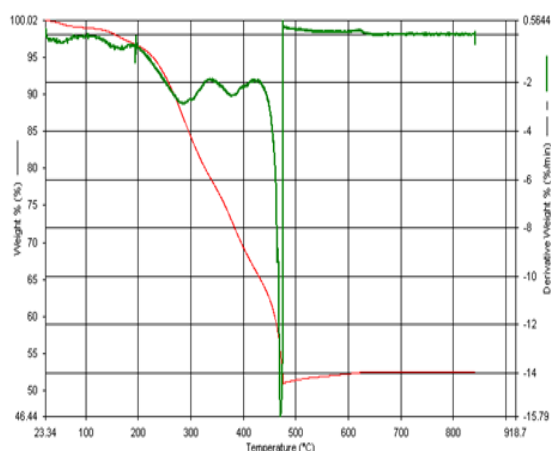
Fig.6 Thermal gravimetric analysis of the Mg-Zn/AC catalyst at a flow of 60 cm^3/min of N_2

and a heating rate of 10 ^{o}C/min from 34 ^{o}C to 800 ^{o}C

catalyst performance was observed when it was calcined above this temperature. The reason could be due to sintering at temperature > 500 ^{o}C as observed in the TGA analysis where further increase in temperature is no longer economical for Transesterification. Therefore, 500 ^{o}C was chosen as the calcinations temperature and was employed in the subsequent experimental runs.
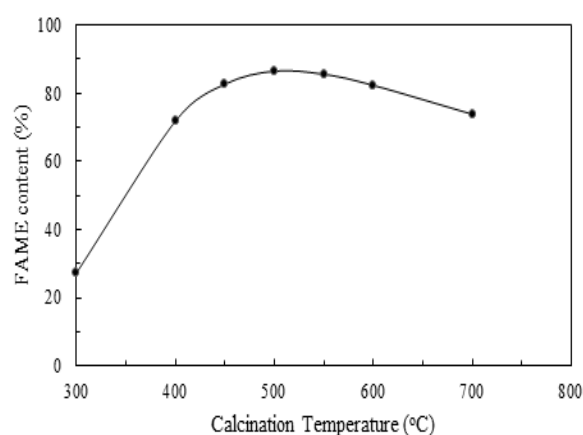
Fig.7 Yield of methyl esters at different calcined temperatures

3.3 Heat treatment effect on MgZnO/AC catalyst and test of performance

The catalyst was subjected to different calcinations temperatures in the range of 300-700°C for 4 h and the activity was examined on the Transesterification of waste frying oil with methanol. As shown in Fig. 7, the performance of the catalyst increased as the calcinations temperature is increased. This can be explained by the fact that the precursors undergo phase transition as the temperature is increased, and this is supported by the XRD and the TGA analysis where crystalline formation of MgZnO, MgO and ZnO existed in the specified range. The phase transformation could have resulted due to the basic character of the catalyst which provides a favourable condition for Transesterification of low free fatty acid oil feedstock. FAME content of above 84%was obtained with the catalyst calcined at 500 ^{o}C and a decrease in the

3.4 Effect of reaction time

Reaction time is an important factor that during Transesterification reaction. The diffusion and mass transfer limitations of heterogeneous catalyst result to slow reaction and the stirrer speed was set to maximum to overcome the mass transfer limitations. Thus, at the commencement of the reaction, the FAME content was low during 1 h of reaction. However, Fig. 8showsthat the FAME content increased gradually after 2 h of reaction time, and thereafter remained nearly constant at 84% during5 h reaction time. It was also observed that further increase in time up to 12 h produced no significant change to the FAME content rather a slight decrease was noticed as the reaction time was extended with FAME content of 78%. This observation could be as a result of a backward

16

shift in the reaction being a reversible process; the reaction complex formed at this extended period no longer favoured the yield of methyl esters.
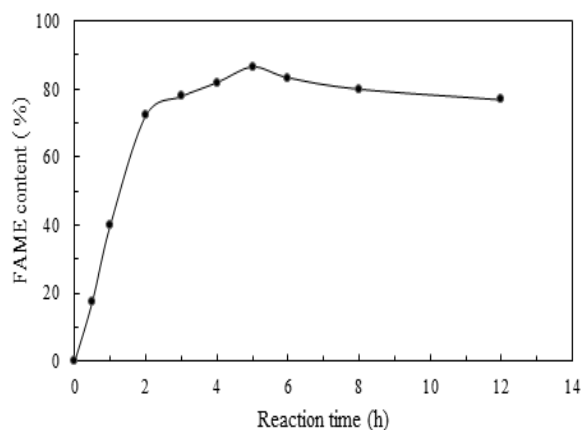
Fig.8 Yield of methyl esters at different reaction time

3.5 Effect of catalyst loading

The effect of catalyst dosage on the yield of esters was investigated with the amount of catalyst varied in the range 0.5-6.5 wt% (catalyst to oil). Fig. 9 show that FAME content increased gradually (> 84%) with the increment of catalyst to oil weight ratio from 0.5 to 2.5 wt%. After that, the FAME content started to decrease with further addition of catalyst amount. The observed trend could be due to resistant of mixing involving triglyceride molecules, product and solid catalyst in which case the viscosity increased as the catalyst loading was increased Thus, a good value of 2.5 wt% was found suitable for high FAME content in this process.
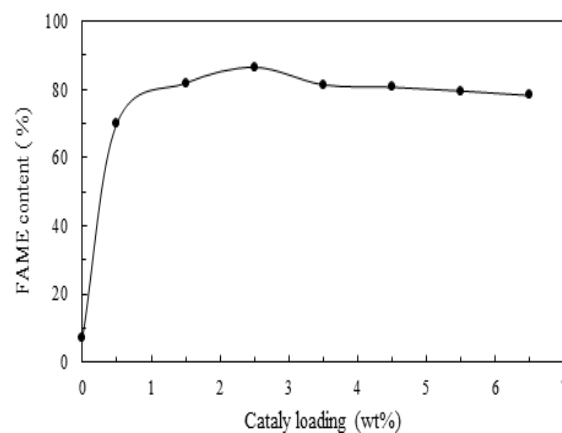
Fig.9 Yield of methyl esters at different catalyst loading

3.6 Effect of methanol to oil molar ratio

Transesterification reaction requires stoichiometrically, three moles of methanol to one mole of triglyceride. To shift the reaction forward, an excess of methanol to oil ratio is needed. It was observed from Fig. 10 that FAME content increase as expected, up to a maximum value of 86%. Beyond this point, as the ratio of alcohol to oil was further increased, there was a decline in the FAME content. The observed decrease in yield as the alcohol-oil ratio was increased could be due to dilution effect caused by the excess methanol making the separation difficult and also reduce the catalyst concentration.
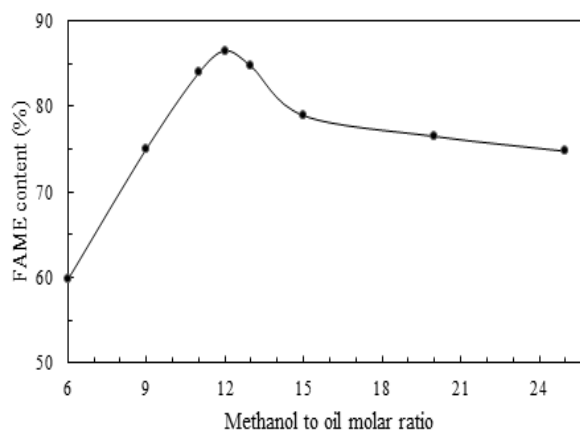
Fig. 10Yield of methyl esters at different methanol to oil molar ratio

3.7 Effect of reaction temperature

The effect of the reaction temperature was investigated in the range of 70-180 ^{o}C. During the preliminary runs reaction temperature below 70 ^{o}C produced methyl esters lower than 55% which increased to more than 76% at a higher temperature of 120 ^{o}C. The highest ester content was obtained at 150 ^{o}C as shown in Fig.11. From a kinetic performance, reaction rate is expected to increase with increase in temperature because an increase in collision among molecules lowers the activation energy barrier resulting in more product conversion. However, in this study, at higher temperature beyond 150 ^{o}C, a decrease in FAME content was obtained, an indication of temperature inhibiting effect of the catalyst which affects its activity during the Transesterification reaction. Thus, 150 ^{o}C was chosen as a suitable operating temperature in this study.
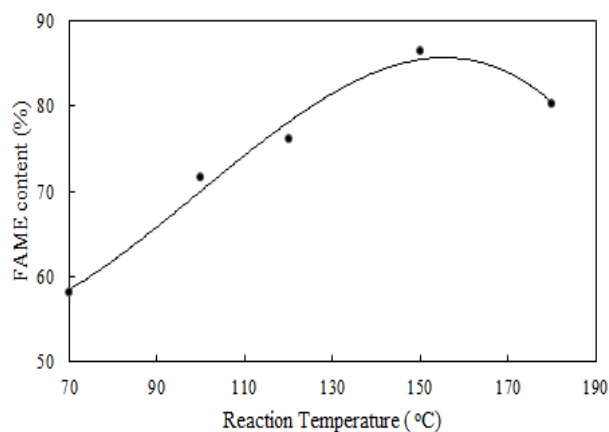
Fig. 11 Yield of methyl esters at different reaction temperature

3.8 Catalyst stability during Transesterification

The reusability was examined after the first run. After the first run, the catalyst was filtered from the product and was washed with n-hexane until all adhered oil and glycerol were removed, then it was dried at 70°C for 12 h and was placed in contact with fresh methanol and WFO for the next run. The result of the catalyst performance during reusability test is shown in Fig. 12. It can be seen from the profile that the yield of ester decreased with increase in the experimental runs. Yields of 86% ester was obtained at first run, while the second, third and fourth runs resulted in 80%,70%, and 58% of esters, respectively. The result could be due to deactivation of the active sites as a result of clogging by some triglyceride molecules. Also, the observed decrease could be due to loss of material during manipulation which resulted in fewer active sites of the catalyst for the Transesterification reaction in subsequent runs.
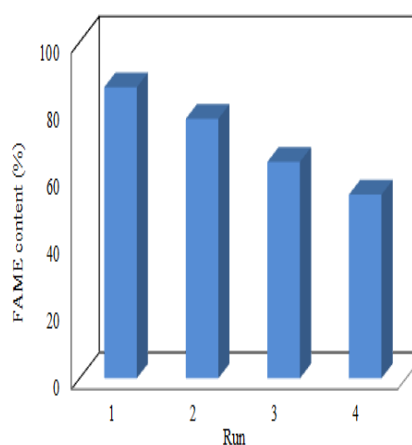
Fig. 12 Yield of methyl esters at different runs during stability studies

4. CONCLUSION

The MgZnO/AC supported catalyst was synthesized by incipient wetness impregnation method and was used in Transesterification of waste frying oil. The catalyst showed good

activity towards the synthesis of methyl esters with optimum conditions obtained at methanol to oil molar ratio of 12:1, catalyst loading 2.5 wt%, temperature 150 ^{o}C, and reaction time 5 h to give over 86% yield methyl ester when the catalyst was calcined at 500 ^{o}C for 4h. Catalyst separation from the product mixture is simple and reusable for three cycles. The current investigation showed that Mg-Zn/AC catalyst presented efficient activity during the Transesterification reaction of WFO and could be a promising heterogeneous catalyst for the production biodiesel fuel from other vegetable oil feedstock.

.REFERENCE

Al-Zuhair, S., 2007. Production of biodiesel: possibilities and challenges. Biofuels

Bioprod.Biorefin.1, 57– 66.

Cheng, H.F., Hu, Y.N., 2010. Municipal solid waste (MSW) as a renewable source of

energy: Current and future practices in China. Bioresour.Technol. 101, 3816-3824.

D'Cruz, A., Kulkarni, M.G., Meher, L.C., Dalai, A.K., 2007. Synthesis of biodiesel from

canola oil using heterogeneous base catalyst. J. Am. Oil Chem. Soc. 84, 937–943.

Furuta, S., Matsuhashi, H., Arata, K., 2004.Biodiesel fuel production with solidsuperacid catalysis in fixed bed reactor under atmospheric pressure.Catal.Commun. 5, 721–723.

Gnansounou, E., Dauriat, A., 2010. Techno-economic analysis of lignocellulosic ethanol:

A review.Bioresour.Technol. 101, 4980-4991.

Granados, M.L., Poves, M.D.Z., Alonso, D.M., Mariscal, R., Galisteo, F.C., Moreno-Tost,

R., Santamaria, J., Fierro, J.L.G., 2007. Biodiesel from sunflower oil by usingactivated calcium oxide. Appl. Catal. B: Environ. 73, 317–326.

Hillion, G., Delfort, B., Pennec, D., Bournay, L., Chodorge, J., (2003). Biodiesel production by a continuous process using a heterogeneous catalyst. American Chemical Society, Division Fuel Chemistry. 48 (2), 636-638

Jitputti, J., Kitiyanan, B., Rangsunvigit, P., Bunyakiat, K., Attanatho, L.,Jenvanitpanjakul, P., 2006. Transesterification of crude palm kernel oil andcrude coconut oil by different solid catalysts. Chem. Eng. J. 116, 61–66.

Kim, H.-J., Kang, B.-S., Kim, M.-J., Park, Y.M., Kim, D.-K., Lee, J.-S., Lee, K.-Y., 2004.

Transesterification of vegetable oil to biodiesel using heterogeneous basecatalyst.Catal. Today 93–95, 315–320.

Lukic, I., Krstic, J., Jovanovic, D., Skala, D., 2009. Alumina/silica supported K2CO3 as a

catalyst for biodiesel synthesis from sunflower oil. Bioresour.Technol. 100,4690–4696.

MacLeod, C.S., Harvey, A.P., Lee, A.F., Wilson, K., 2008. Evaluation of the activity and

stability of alkali-doped metal oxide catalysts for application to an intensifiedmethod of biodiesel production. Chem. Eng. J. 135, 63–70.

Miller, F. A. and Wilkins, C.H., (1952). Infrared Spectra and Characteristic Frequencies of Inorganic Ions. Analytical Chemistry. 24 (8), 1253-1294

Munari, F., Cavagnino, D., Cadoppi, A., 2007. Determination of Total FAME and Linolenic Acid Methyl Ester in Pure Biodiesel (B100) by GC in Compliance with EN14103. Thermo Fisher Scientific, Milan, Italy.

Ong, H.C., Mahlia,T.M.I., Masjuki, H.H., 2011. A review on energy scenario and sustainable energy in Malaysia. Renewable Sustainable Energy Rev. 15, 639-647.

Singh and Singh, (2010).Biodiesel production through the use of different sources and characterizationof oils and their esters as the substitute of diesel: A review. Renewable and Sustainable Energy Reviews. 14, 200-216

Sun, H., Ding, Y., Duan, J., Zhang, Q., Wang, Z., Lou, H., Zheng, X., 2010.Transesterification of sunflower oil to biodiesel on ZrO_2 supported La_2O_3 catalyst. Bioresour. Technol. 101, 953–958.

Suppes, G.J., Dasari, M.A., Doskocil, E.J., Mankidy, P.J., Goff, M.J., 2004.Transesterification of soybean oil with zeolite and metal catalysts.Appl. Catal.A: Gen. 257, 213–223.

Vyas, A.P., Subrahmanyam, N., Patel, P.A., 2009. Production of biodiesel throughtransesterification of Jatropha oil using KNO3/Al2O3 solid catalyst. Fuel 88, 625–628.

Yan, S., Salley, S. O. and Simon Ng, K.Y., (2009). Simultaneous transesterification and esterification of unrefined or waste oils over $ZnO-La_2O_3$ catalysts. Applied Catalysis A: General. 353 (2), 203-212

Yin, S.D., Dolan, R., Harris, M., Tan, Z.C., 2010. Subcritical hydrothermal liquefaction of cattle manure to bio-oil: Effects of conversion parameters on bio-oil yield and characterization of bio-oil. Bioresour.Technol. 101, 3657-3664.

Yung B.C., Gon S., 2010. High activity of acid-treated quail eggshell catalysts in the transesterification of palm oil with methanol.Bioresour.Technol. 101, 8515-8519.

Zabeti, M., Daud, W.M.A.W., Aroua, M.K., 2009.Optimization of the activity of CaO/Al_2O_3 catalyst for biodiesel production using response surface methodology.Appl. Catal. A: Gen. 366, 154–159.

Zhang, Z.Y., Qu, W.W., Peng, J.H., Zhang, L.B., Ma, X.Y., Zhang, Z.B., Li, W., 2009. Comparison between microwave and conventional thermal reactivations of spent activated carbon generated from vinyl acetate synthesis. Desalination. 249, 247-252.

Optimum Design of Reinforced Concrete Slabs to Eurocode 2 using Target Reliability Approach

Jibrin Mohammed Kaura[1*], Salisu Dahiru[2], Yakubu Kasimu Galadima[3], Ibrahim Aliyu[4]

[1,3,4]Department of Civil Engineering, Ahmadu Bello University, Zaria

[2]Department of Civil Engineering Technology, Nuhu Bamalli Polytechnic, Zaria

*Corresponding Author: jmkaura@abu.edu.ng, Phone Number: 2348023583817

ABSTRACT

Eurocode 2 is based on limit state design method, that ensures the attainment of low probability of failure of reinforced concrete structures through the use of partial safety factors. This approach is semi-probabilistic; uncertainties in individual design variables were not properly accounted for, and it is not clear how far the design from failure is. To address the issue of uncertainties and at the same time maintain a known and uniform level of safety a reliability-based optimum design aids, in form of design charts for simply supported one-way reinforced concrete slabs are presented in this paper. The chart was generated based on a target safety index on 3.0.

Keywords: Deterministic, Optimum, Target reliability, Safety factors, Uncertainties, Reinforced concrete labs

1. INTRODUCTION

Structural performance is directly affected by uncertainties associated with model or its physical parameters and loading (Eugen and Andrew, 1999: Melchers, 1999; Ditlevsen and Madsen, 2005). The traditional design approach has been to adopt safety factors to ensure that the risk of failure is sufficiently small. The European design code for design of reinforced concrete (Eurocode 2, 2008) is based on this approach. It adopts a limit state design philosophy. Limit state design safeguard engineering structures against failure through the use of partial safety factors. These factors are applied to both the loading and material properties with the view to achieve low probability of failure. The criticisms of the limit-state design approach include:

1. The application of partial safety factors alone to loading and material properties do not address the uncertainties associated with individual design variables.

2. Limit state design concept recognized the existence of uncertainties and already used the concept of probability in the treatment such uncertainties; it is however not clear how far the limit-state of any is given design criteria from failure (Afolayan, 1992; Enrique et al, 2003).

Today, structural engineers are not only interested in the design of safe systems but also best systems (Arora, 2004). The design of best system can be achieved using reliability based optimum design. Probabilistic approach will also be used in order to fully accommodate uncertainties. Probabilistic design permits a more rigorous quantification of the various uncertainties, and ultimately will facilitate a more efficient design process (Enrique et al, 2003). The paper, presents a reliability-based optimum design charts for one-way simply supported reinforced concrete slabs based on the Eurocode 2 design requirements. The design charts were developed through a developed FORTRAN 77-based computer program that considered a first order reliability analysis program; FORM5 developed elsewhere (Gollwitzer et al., 1988) as a subroutine. The program listing is shown in Appendix1.0.

2. METHODOLOGY

2.1 Limit State Design Philosophy

A limit state is a situation where a structure ceases to fulfil one or more of the specific functions for which it was originally designed. Some typical limit states are shown in Table 1.0.

Table 1.0: Some Typical Limit State
(Source: Melchers, R. E. 1999)

Limit state type	Description
Ultimate (Safety)	Collapsed of all or part of the structure
Damage	Damage to structure
Serviceability	Disruption of normal use

In practice, the study of structural safety is concerned with the violation of the ultimate limit state (Melchers, 1999; Detlevsen; 2005).

2.2 Limit State Code Format

In limit state design, the structural inadequacy or failure is expressed through the following equation

$$\Phi R = \gamma_D S_D + \gamma_L S_L \qquad (1)$$

Where R is the member resistance, Φ is the partial safety factor of R. S_D, and S_L are the dead and live load effects respectively. γ_D, and γ_L are the partial safety factors on S_D, and S_L respectively.

Equation (1.0) was originally developed during the 1960's for reinforced concrete codes (Melchers, 1999). It enable the live load to have greater "partial" safety factor than the dead load, in view of the former's greater uncertainty and it allowed a measure of workmanship variability and uncertainties about resistance modeling to be associated with the resistance (MacGregor, 1976).

The inconsistency of the level of safety and unexpected failure of some structures due to uncertainties on design variables, justify a code review not only to check and maintain safety level but also to achieve uniformity in safety levels and properly accommodate uncertainties in the structural design process. In this paper, the

probabilistic based optimum design is compared with the current semi-probabilistic approach of the Eurocode 2.

2.3 First Order Reliability Method (FORM)

First and Second Order Reliability Method (FORM/SORM) are other approximation methods. The Safety level of a structure is measured by a reliability index. There are different definitions of reliability index, β. The first was introduces by Cornell in the late 1960s (Cornell, 1969). Given the performance function as:

$$M = R - S = g(X_1, X_2, \ldots , X_n) \qquad (2)$$

and the safety index is defined as the ratio of the mean and standard deviation of the performance function, given by

$$\beta_C = \frac{\mu_M}{\mu_S} \qquad (3)$$

2.4 The Limit State Function

The reliability-based optimum design charts were developed based on the following limit-state function, for the bending moment capacity of one-way simply supported reinforced concrete slabs to Eurocode 2 (2008):

$$G(X) = \rho b d^2 f_y (1 - \frac{0.55 \rho f_y}{f_c}) - \frac{(\gamma_g G_k + \gamma_q Q_k)L^2}{8} \qquad (4)$$

Where ρ is the reinforcement ratio, b is unit width of the slab, d is the effective depth, f_y is the yield strength of the reinforcing steel, f_c is the compressive strength of concrete, G_k is the characteristic dead load, Q_k is the characteristic imposed load. L is the length of the slab, γ_g and γ_q are the partial safety factors for the dead load and imposed load respectively.

The structural design is said to be satisfactory if the computed safety index β_c is greater than or equal to target safety index. β_t. A uniform reliability is said to be achieved if the computed safety indices for all design situations are approximately equal to the design target safety index β_t. Target safety index β_t of 3.0 was adopted based on the recommendation of Abubakar (2005).

The procedure of First Order Reliability Method (FORM) as earlier presented was used in the computation of the reliability indices. The design procedure was coded in FORTRAN 77 module to formulate the main program

called "section". A First Order Reliability program (FORM5) developed elsewhere (Gollwitzer, et al, 1988) was linked with the main program as a subroutine. The program is given in Appendix 1.0.

Table 2: Statistical Models of the Basic Design Variables

S/No	Variable	Variable Type	Mean	Coefficient of Variation	
1	Reinforcement Ratio, ρ	Deterministic	Nominal	Nil	Nil
2	Slab with, b (mm)	Random	1000	0..020	Normal
3	Effective depth, d (mm)	Random	Nominal	0.020	Normal
4	Yield strength of steel, f_y (N/mm^2)	Random	460/250	0.107	Lognormal
5	Compressive strength of concrete, f_c (N/mm^2)	Random	25/30	0.180	Lognormal
6	Dead load safety factor, γ_g	Deterministic	1.35	Nil	Nil
7	Imposed load safety factor, γ_g	Deterministic	1.50	Nil	Nil
8	Dead load, G_g (kN/m)	Random	Nominal	0.10	Normal
9	Imposed load, Q_k (kN/m)	Random	Nominal	0.40	Gumbel
10	Slab length, L (m)	Deterministic	Nominal	Nil	Nil

2.5 Statistical Models of the Basic Design Variables

To perform reliability analysis for engineering structures, statistical models of the basic design variables are required. These include the mean values, coefficients of variation and theoretical distribution models. The statistical models of the basic design variables used in this study (Table 2.0) were obtained from previous work (Renjian et al., 1994).

2.6 Evaluation of the Limit State Function

A reliability-based optimum design problem can be formulated in the following form:

Minimise $\beta = ||\mu||^2 = \mu^T.\mu$

Subject to: $g(\mu) = 0$ (5)

Where μ is the vector of standard normal variates; $g(\mu)$ is the limit state function; β is the reliability index. The problem in Eqn.(5.0) is a constrained nonlinear optimization problem. The optimisation operation is continuous until the following stopping criteria are achieved.

$\beta_{computed} - \beta_{target} \approx 0.001$ (6)

where $\beta_{computed}$ is the computed reliability index and β_{target} is the target reliability index.

3. RESULT AND DISCUSSION

Figs 1.0 to 4.0 displayed the plots of safety indices against M/bd^2. Where M is the applied bending moment of slabs, b

is the unit with of the slab (1000mm) and d is the effective depth. In the plots, BETA is the computed safety index, and BETAT is the target safety index. In Fig. 1.0 it is clear that, the Eurocode 2, design criteria of a one-way simply supported slab will only meet the target reliability of 3.0 if and only if the value of M/bd^2 is maintained at 1.75, when the specified characteristic strength of concrete and steel are respectively equal to $25N/mm^2$ and $250N/mm^2$. When the specified characteristic strength of concrete and steel are respectively equal to $25N/mm^2$ and $460 N/mm^2$ (Fig. 2.0). The target reliability is only achieved when M/bd^2 is maintained at 2.25.
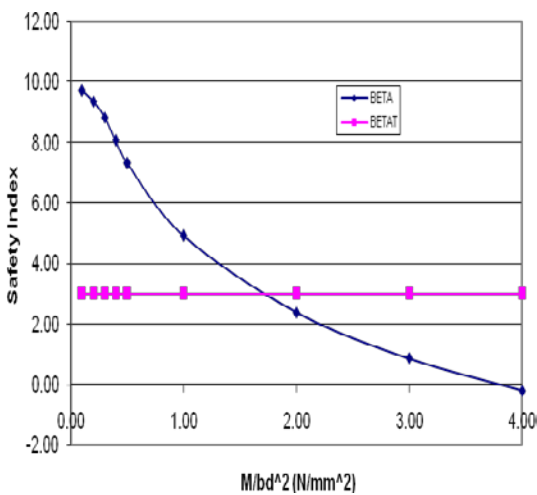
Figure 1: Safety indices against M/bd^2 for $f_{cu} = 25N/mm^2$, and $f_y = 250N/mm^2$
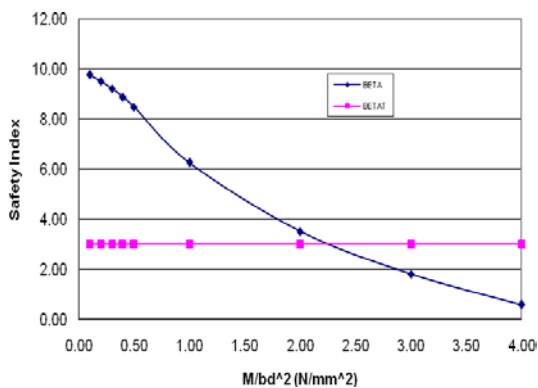
Figure 2: Safety indices against M/bd^2 for $f_{cu} = 30N/mm^2$, and $f_y = 250N/mm^2$
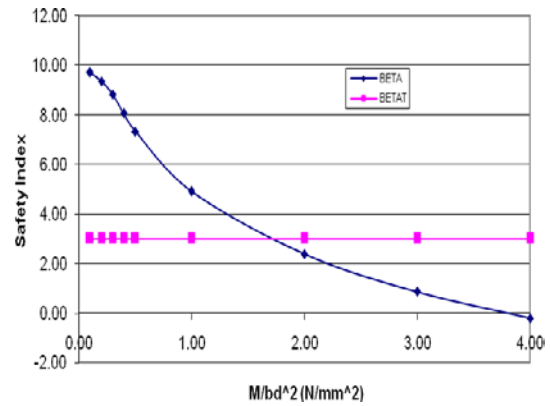
Figure 3.0 Safety index against M/bd^2 ($f_{cu} = 25 N/mm^2$, $f_y = 460 N/mm^2$)
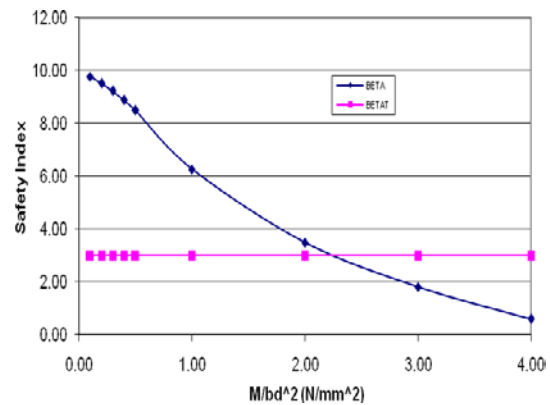
Figure 4.0 Design chart two ($f_{cu} = 30 N/mm^2$, $f_y = 460 N/mm^2$)
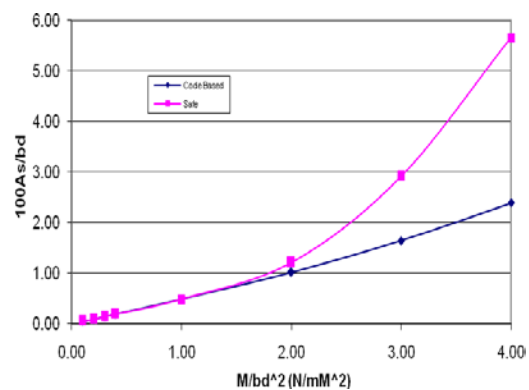
Figure 5.0 Design chart one ($f_{cu} = 25 N/mm^2$, $f_y = 250 N/mm^2$)

When the specified characteristic strength of concrete and steel are respectively equal to 30N/mm^2 and 460 N/mm^2 (Fig. 4.0). The target reliability is only achieved when M/bd^2 is maintained at 2.25.

The general observation is that the Eurocode 2 design criteria of a one-way simply supported reinforced concrete slabs do not guarantee uniform reliability for all design situation. This calls for the need for a more consistent approach to achieve uniformity in safety levels for all design situations.

In Figs 5.0 to 8.0, the design charts for the deterministic and reliability-based optimum design of one-way simply supported reinforced concrete slabs to Eurocode 2 are presented. In the optimum design, the uncertainties associated with the individual design variables were fully accommodated. The optimisation is base on target reliability approach, with target reliability (safety) index of 3.0. Uniform reliability is ensured by the optimum design chart. The design charts are functions of 100A$_s$/bd (reinforcement ratio) and M/bd^2. Once the bending moment, depth of member and effective depth are specified, the required reinforcement ratio can then be determined, from which the required area of reinforcing steel are determined. As observed in Figs 5.0 and 6.0, both the deterministic design chart (code-based) and the optimum design chart coincided at a value of M/bd^2 ranging from 0 to 1.5. This implied, with the current design criteria of the Eurocode, is optimum at this range, with reliability index of 3.0. When M/bd^2 is above 3.0, the optimum safety level will not be achieved with the deterministic approach of the Eurocode 2.

Also as observed in Figs 7.0 and 8.0, both the deterministic design chart (code-based) and the optimum design chart coincided at a value of M/bd^2 ranging from 0 to 2.0. This implied, with the current design criteria of the Eurocode, is optimum at this range, with reliability index of 3.0. When M/bd^2 is above 3.0, the optimum safety level will not be

achieved with the deterministic approach of the Eurocode 2.

It is also clear from the plot that the optimum design chart will require higher cross sectional area of steel than the deterministic design. The addition cost for optimum design will however be compensated by the level of confidence in the design due to the fact that, the uncertainties in the basic design variables are fully accommodated in the Eurocode 2 design criteria. Also, for all design situation, a uniform target reliability corresponding to reliability index of 3.0 will be achieved.
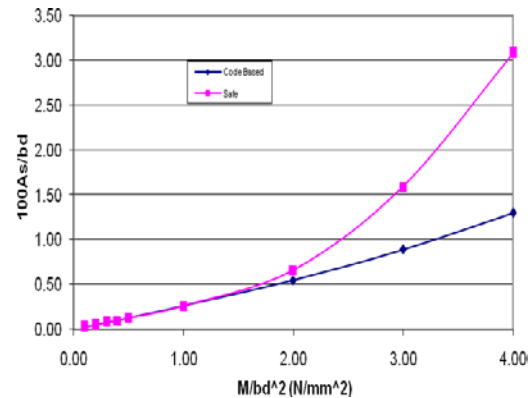
Figure 6.0 Design chart four (f$_{cu}$ = 25 N/mm^2, f$_y$ = 460 N/mm^2)
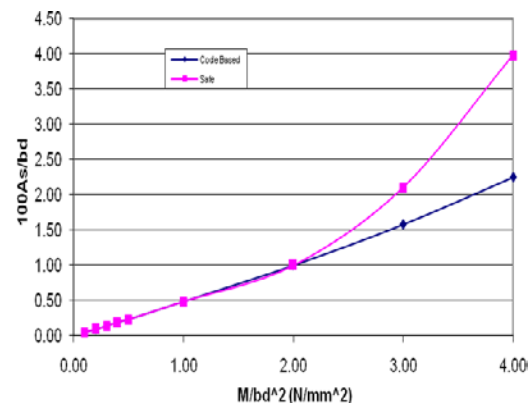
Figure 7.0 Design chart four (f$_{cu}$ = 30 N/mm^2, f$_y$ = 250 N/mm^2)
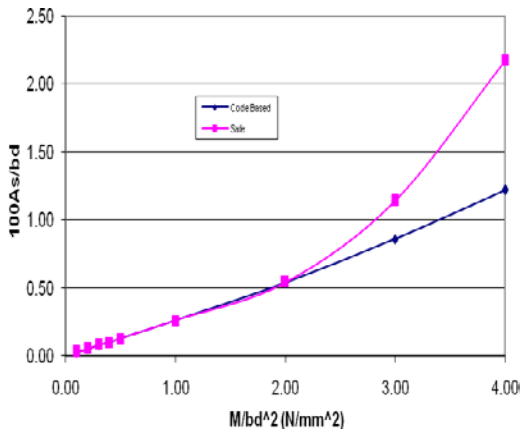
Figure 8.0 Design chart four (f_{cu} = 30 N/mm^2, f_y = 460 N/mm^2)

4. CONCLUSIONS

In this paper, reliability-based optimum design chart for singly reinforced concrete members with uniform reliability were presented. The charts were based on the requirements of Eurocode 2 (2008). The general observation on the optimum design chart is that reinforcement ratio for probabilistic design is higher than that required for deterministic reliability when the value of M/bd^2 is above 1.5 for charts in Figs. 5.0 and 6.0, and 2.0 in Figs. 7.0 and 8.0. This is however compensated by the guarantee of uniform safety that is ensured in the use of the probabilistic optimum design chart. The optimum design charts should be use in conjunction with the specification for shear and serviceability limit states as prescribed in Eurocode 2 (2008).

REFERENCES

Abubakar, I., (2006). "Reliability analysis of structural design parameters of strip footing.", Journal of Applied Science and Research, Vol. 2 No. 7, pp. 397-401.

Afolayan, J. O. (1992)."Reliability-Based Analysis and Design", Departmental Seminar, Department of Civil Engineering, Ahmadu, Bello University, Zaria. 2nd June, 1992.

Arora, J. S. (2004). "Introduction to Optimum Design". Second Edition 2004, Elsevier Inc, London

Ang, H. S. and Tang, W. H. (1975). "Probability Concepts in Engineering Planning and Design. Volume 1 – Basic principles". John Wiley and Sons, New York

Ditlevsen, O. and Madsen, H. O. (2005). Structural Reliability Methods. internet edition. Retrieved Januarey, 2015.

Andrew, S. D. (1999) "Reinforced and Prestressed Concrete Design: The Complete Process". Longman, London

Enrique, C., Antonio, J, Roberto, U. and Carmen C. (2003) An alternative approach for addressing the failure probability-safety factor method with sensitivity analysis. Reliability Engineering and System Safety. Vol. 82, pp 207-216

Eurocode 2, part 1-1 (2004). Design of Reinforced Concrete Structures – Part 1-1: General –Common Rules for Buildings. CSI, Prague, December 2004.

Gollwitzer S, Abdo T., and Rackwitz R. (1988). "First Order Reliability Method: FORM Software". User Manual.Munich

Melchers, R. E. (1999) "Structural reliability analysis and prediction". Chichester, John Wiley.

MacGregor, J.G. (1976) Safety and limit state design for reinforced concrete, Can. J., Civ,. Engg. Vol 3 No. 4, pp 484-513

Renjian, L. Yuanhui, L. Joel, P. C. (1994). "Reliability evaluation of reinforced concrete beams". Structural Safety, Vol. 14, pp 277-298

.
APPENDIX: Program Listing

```
PROGRAM RC SECTION BY J. M. KAURA

    IMPLICIT DOUBLE PRECISION (A-H,O-Z)

    COMMON FORM5, ICRT

    COMMON XX(5),FX,IER


COMMON/KHAFSAH/SPAN,ALPHA,BETA,FCUCOV,EDCOV

    COMMON EX(5)
```

```
        OPEN(10,FILE='ABA3.RES',STATUS='OLD',ERR=20
        )

              GOTO 30

        20    OPEN(10,FILE='ABA3.RES',STATUS='NEW')

        30
        OPEN(11,FILE='AB3.RES',STATUS='OLD',ERR=222
        21)

              GOTO 22222

        22221 OPEN(11,FILE='AB3.RES',STATUS='NEW')

        22222
        OPEN(50,FILE='AAGEND.RES',STATUS='OLD',ERR=
        55755)

              GOTO 55855

        55755
        OPEN(50,FILE='AAGEND.RES',STATUS='NEW')

        55855 READ(50,55655)DIA,COVER,H,SPAN,ALPHA

        55655 FORMAT(5X,5F10.5)

              WRITE(*,*)'   INPUT XTICS STRENGTH OF
        CONCRETE IN N/mm^2'

              WRITE(*,*)'    '

              READ(*,*)FCU

              FCUCOV = 6.0/FCU

              WRITE(*,*)'   INPUT XTICS STRENGTH OF
        STEEL IN N/mm^2'

              WRITE(*,*)'    '

              READ(*,*)FY

        50    WRITE(*,*)'    INPUT M/BD2 IN N/mm^2'

              WRITE(*,*)'            '
```

```
              READ(*,*)RATIO

              ED = H-(DIA/2.0)-COVER

              EDCOV = 11.9/ED

              B=1000.0

              SAM1 = (B*(ED**2))*RATIO

              SAM = SAM1 *1.0D-6

              DL = (SAM*8.0)/(SPAN**2)

              GK = DL/(1.4+(1.6*ALPHA))

              QK = ALPHA*GK

        C     ULTIMATE BENDING MOMENT

              RATI = (SAM*1.0D6)/(B*(ED**2)*FCU)

              Z1 = 0.25-((RATI)/0.9)

              Z2 = Z1**0.5

              Z3 = 0.5+Z2

              Z  = ED*Z3

              ASR = (SAM*1.0D6)/(0.87*FY*Z)

              RHO = ASR/(ED*B)

              ASR1 = ASR

              RRHO = RHO*100.0

        11113 EX(1) = FCU

              EX(2) = ASR

              EX(3) = ED

              EX(4) = GK

              EX(5) = RHO

              N5 = 5

              CALL KHAFSAH(N5,EX,TARG)
```

27

```
      BETA = TARG

      WRITE(11,22225)BETA

22225 FORMAT(5X,'BETA =',F10.5)

      BETAT = 3.0D0

      IF(BETA.LT.BETAT)THEN

      GOTO 11111

      ELSEIF(BETA.GE.BETAT)THEN

      GOTO 11112

      ENDIF

11111 ASR = ASR+10.0

      GOTO 11113

11112 ABAR = (3.142*(DIA**2))/4

      ANO = ASR/ABAR

      RRHO2 = (ASR/(ED*B))*100.0

      ASPACE = B/ANO

      WRITE(11,11114)

11114 FORMAT(5X,'RELIABILITY ASSESSMENT OF
SINGLY REINFORCED',/,

     +5X,'RECTANGULAR CONCRETE SECTION',/,

     +5X,'BY JIBRIN MOHAMMED KAURA',/,

     +5X,'(BEng(ABU;MSc(ABU);MNSE)',/,

     +5X,'DEPARTMENT OF CIVIL
ENGINEERING',/,

     +5X,'AHMADU BELLO UNIVERSITY ZARIA')


WRITE(11,70)RRHO,RRHO2,RATI,RATIO,FCU,FY

70    FORMAT(5X,/,

     +5X,'CODE BASED STEEL PERCENTAGE
(100As/BD)        =',F10.2,/,

     +5X,'SAFE STEEL PERCENTAGE (100As/BD)
=',F10.2,/,

     +5X,'MOMENT RATIO K (0.156 = MAX)
=',F10.2,/,

     +5X,'M/bd^2 (N/mm^2)
=',F10.2,/,

     +5X,'CHARACTERISTIC STRENGTH OF
CONCRETE (N/mm^2) =',F10.2,/,

     +5X,'CHARACTERISTIC STRENGTH OF STEEL
(N/mm^2)    =',F10.2)

      WRITE(11,140)BETA,BETAT

140   FORMAT(5X,/,

     +5X,'COMPUTED SAFETY INDEX
=',F10.2,/,

     +5X,'TARGET SAFETY INDEX
=',F10.2)

      WRITE(*,*)'  RESULT SEE FILE
AB3.RES'

      STOP

      END

SUBROUTINE KHAFSAH(N5,EX,TARG)

      IMPLICIT DOUBLE PRECISION (A-H,O-Z)

C    LIMIT STATE FUNCTION DECLARED
EXTERNAL

      EXTERNAL QHAFSAH

      DIMENSION EX(N5)

      DIMENSION
XX(5),SX(5),VP(10,5),COV(5,5),ZES(3),
```

```
      +              UU(5),EIVEC(5,5),IV(2,5)

       CHARACTER*10 PRT


COMMON/KHAFSAH/SPAN,ALPHA,BETA,FCUCOV,EDCOV

       DATA N/5/,NC/5/,NE/5/,IRHO/0/

C      MEAN AND STANDARD DEVIATION OF THE
VARIABLES AS WELL

C      AS THE PARAMETERS OF FORM5 ARE GIVEN
IN THIS DATA BLOCK

       SX(1) = EX(1)*FCUCOV

       SX(2) = EX(2)*4.0D-2

       SX(3) = EX(3)*EDCOV

       SX(4) = EX(4)*5.0D-2

       SX(5) = EX(5)*3.0D-2

       NAUS = 10

       ICRT = 0

       CALL YINIT(N,IV,VP,IRHO,COV,NC)

       IV(1,1) = 3

       IV(1,2) = 3

       DO 100 I = 1,N

100    XX(I) = EX(I)

       V1 = 0.5D0

       BETA = 1.0D0

C      THE STOCHATIC MODEL IS PRINTED USING
"YKOPF"

       CALL YKOPF (NAUS,N,IV,EX,SX,VP,IRHO)

C      PRINT ALSO TO SCREEN
```

```
       WRITE(ICRT,*)'  START OF FORM5'

       WRITE(ICRT,*)'  STOCHASTIC MODEL'

       CALL YKOPF (ICRT,N,IV,EX,SX,VP,IRHO)

       PRT = 'COV'

       CALL YMAUS (NAUS,NC,N,COV,PRT)

       CALL FORM5
(N,IV,EX,SX,VP,QHAFSAH,IRHO,COV,NC,

      +
EIVEC,NE,V1,NAUS,BETA,XX,UU,ZES,IER)

       PRT = 'UU'

       CALL YFAUS (NAUS,N,UU,PRT)

C      COMPUTE THE SAFETY INDEX AND THE
CORRESPONDING

C      PROBABILITY OF FAILURE

       TARG = BETA

       PRT = 'ZES'

       CALL YFAUS (NAUS,3,ZES,PRT)

       WRITE(ICRT,*)'  END OF FORM5 : IER =
',IER

       RETURN

       END

SUBROUTINE QHAFSAH(N,XX,FX,IER)

C      LIMIT STATE FUNCTION

       IMPLICIT DOUBLE PRECISION (A-H,O-Z)

       DIMENSION XX(N)


COMMON/KHAFSAH/SPAN,ALPHA,BETA,FCUCOV,EDCOV

       IF(ALPHA.GT.0.0)THEN
```

29

```
    QFX = 0.156*XX(1)*XX(2)*XX(3)/XX(5)

    FX = QFX-
(((XX(4)*(1.4+(1.6*ALPHA))*(SPAN**2))/8.0)*
1.0D6)

    IER = 0

    ELSE

    FX = 1.D+20

    IER = 1

    ENDIF

    RETURN

    END
```

APPENDIX 2.0: TYPICAL OUTPUT

```
    RELIABILITY ASSESSMENT OF SINGLY
REINFORCED

    RECTANGULAR CONCRETE SECTION

    BY JIBRIN MOHAMMED KAURA

    (BEng(ABU;MSc(ABU);MNSE)

    DEPARTMENT OF CIVIL ENGINEERING

    AHMADU BELLO UNIVERSITY ZARIA


    CODE BASED STEEL PERCENTAGE (100As/BD)
=     1.02

    SAFE STEEL PERCENTAGE (100As/BD)
=     1.21

    MOMENT RATIO K (0.156 = MAX)
=     0.08

    M/bd^2 (N/mm^2)
=     2.00
```

```
    CHARACTERISTIC STRENGTH OF CONCRETE
(N/mm^2) =     25.00

    CHARACTERISTIC STRENGTH OF STEEL
(N/mm^2)    =     250.00

    COMPUTED SAFETY INDEX
=     3.02

    TARGET SAFETY INDEX
=     3.00
```

IMPACT OF DEMOGRAPHIC FEATURES ON HEALTH AND SAFETY PRACTICES OF CONSTRUCTION CONTRACTORS IN ABUJA, NIGERIA

Abdullateef A. Shittu[1*], Ahmed D. Ibrahim[2], Yahaya M. Ibrahim[3] & Kulomri J. Adogbo[4]

[1,2,3,4]Department of Quantity Surveying, Faculty of Environmental Design, Ahmadu Bello University, Zaria – Nigeria

*aishatabdulahi2007@yahoo.com or funsho@futminna.edu.ng, 08034767554

ABSTRACT

The construction sector plays a vital role in the economic development of developed and developing nations. Surprisingly, it also contributes greatly to the occupational accidents and ill-health record. To address this problem, this study set out to evaluate the impact of demographic features on the health and safety (H&S) management practices of Nigerian construction small and medium-sized enterprises (SMEs). The study explored whether these demographic features (years of experience, number of employees and age of firm) could significantly predict/influence the major H&S practices of the SMEs. The study involved the conduct of a survey using questionnaires with both closed and open-ended questions to obtain data. The data obtained were used to determine associations between independent variables identified in the literature and 46 H&S practices of SMEs which addressed five H&S core practice areas. The questionnaire was presented to 436 SMEs which were randomly sampled from the 2219 construction contractors registered with Corporate Affairs Commission (CAC) in Abuja. Factor analysis was employed to reduce the 46 H&S practices to eight major H&S practices used for further analysis. The use of hierarchical multiple regression analysis was finally employed to establish the relationship between demographic features and H&S practices of construction SMEs. It was established that all the demographic features are good, positive and significant predictors of H&S practices of construction the SMEs. It was therefore recommended that construction SMEs should lay great emphasis on training and orientation for all level of employees to address the issue of poor safety performance and poor attitude.

Keywords: *Construction, Demographic Features, Health and Safety Practices, Impact.*

1. INTRODUCTION

The importance of the construction industry in the National Development of a Nation cannot be over emphasized. This is because at least 50% of the investments in various development plans are primarily in construction. It is the next employer of labour after agriculture in developing countries; about 10% of labour force (Okeola, 2009). In developed countries, activities in the construction industry especially building and civil works are used as indices of economic growth and buoyancy or recession. The output of the industry in Nigeria, as reported by Okeola (2009), accounts for over 70% of GDP and therefore it is a stimulator of national economy. Alongside the attractiveness of the construction industry in nation building as identified above, it has also been identified as the most risky and hazardous of all industries in terms of health and safety because its activities pose serious health and safety risks to workers,

users of construction facilities and the public. It has been acknowledged that 25% – 40% of fatalities in the world's occupational settings are contributed by construction (ILO, 2001, 2005a & 2005b; Murie, 2007).

Okpan and Agha (2013) added that the problem of health and safety in the workshop, sites, built facilities and the field in Nigeria cannot be overemphasized, hence, careless attitudes, overconfidence and failure to provide healthy and working safety measures and periodic health and safety seminar for the stake holders and general public triggers a high risk of accidents in construction industry. In the recent past in Nigeria, especially 2005 till date, death tolls, permanent disability and severe environmental threat had been on the increase through collapse of buildings and major operational accidents especially in Abuja, Lagos and Port Harcourt (Awodele and Ayoola, 2005; Olatunji and Aje; 2007). For instance, a study of 40 contractors in Nigeria conducted by Idoro (2011) revealed that the

accident and injury rates in Nigerian construction industry are high (in 2006 - the best safety ratios were 2 accidents per 100 workers and 5 injuries per 100 workers). This unfortunate scenario has been a monumental threat to productivity and the overall performance of construction projects in Nigeria.

Idubor and Oisamoje (2013) emphasized that all organizations have a duty of care to ensure that employees and other persons who may be affected by the company's undertakings remain safe at all times because maintaining a high standard of operational health and safety is for the benefit of all. Adeniran (2013) reported that it was with realization of the fact in the ILO declaration that "labour is not a commodity" but an essential economic factor which has to be well protected that Federal Government of Nigeria created, staffed and funded various departments in relevant Ministries, parastatals and agencies to formulate and administer policies, laws and regulations that protect the workers against illness, disease and injuries arising from employment of labour. It is sad that despite this effort the cases of occupational accidents and illnesses are recorded higher annually, hence the need for an enabling framework to facilitate proper implementation and enforcement of the Occupational Health and Safety (OHS) laws and regulations.

The construction industry comprises many different participants including clients, consultants and construction businesses that perform different roles from conception to commissioning of a typical construction project (contractors). Contractors occupy a significant position and are regarded as the major players in the construction industry. Researchers regard them as one of the most important participants in the industry. This claim is borne out of the fact that contractors produce majority of construction products in Nigeria. Since contractors are responsible for executing construction projects and they employ the workers that do the jobs, as reported by Idoro

(2011), they are therefore one of the parties that influence the OHS conditions of the industry. In developing countries, there are fewer large construction businesses compared with small and medium sized construction businesses (Addo-Abedi, 1999 and Kenny, 2007 cited in Kheni, 2008). Construction Small and Medium Sized Enterprises (Construction SMEs) play an important role in the economies of developing countries. The majorities of contractors in developing countries, including Nigeria, are SMEs and operate within domestic markets (Koehn *et al.,* 1995; Kheni *et al.* 2006; Idoro, 2011). These domestic construction businesses which operate within the domestic construction market are managed as family businesses, rarely employing up to 200 employees (Addo-Abedi, 1999). Due to this, most SMEs die within their first five years of existence. Another smaller percentage goes into extinction between the sixth and tenth year thus only about five to ten percent of young companies survive, thrive and grow to maturity.

As a result of the high population of the SMEs, which majority of the clients patronize in developing countries, the health and safety risks posed by their activities cannot be ignored. Kheni et al. (2007) and Kheni et al. (2008) discovered that foreign contractors operating in developing countries, especially Ghana, effectively manage health and safety whereas indigenous construction businesses have no effective arrangements in place for controlling health and safety risks because health and safety standards on sites are rarely enforced to the latter due to lack of resources for enforcement and lack of enabling environment which promotes occupational health and safety. In the light of this, Kheni (2008) recommended that the particular context of developing countries requires a holistic view of health and safety management that takes account of the contextual environments of construction SMEs in the areas of economic, legal, institutional and cultural background which are defined by organizational characteristics and the

health and safety management practices of these construction SMEs.

Nigeria being a developing nation like Ghana has its construction industry faced with similar problems as the ones identified by Kheni et al. (2007) and Kheni et al. (2008). This therefore necessitates the importance for this study to be based on the philosophy of studying the demographic features (important components of organizational characteristics) influences on health and safety performance within the contextual environment of Nigerian construction SMEs using a case study of Abuja. Abuja is the capital city of Nigeria where construction activities take place most because it experiences rapid population increase and new developmental projects daily due to rapid urbanization and rural-urban migration leading to constant increase in demand for shelter for both residential and commercial purposes.

1.1 Organizational/Demographic Characteristics of Construction SMEs

According to Chinowsky *et al.* (2007) an organization is the overall corporate entity of a company including all levels of management and staff personnel. Organizational characteristics are therefore the unique or distinguishing features which defines an organization or a corporate entity. The organizational characteristics of a construction firm are therefore the unique features which define the performance of the construction firms. Different researchers have used different parameters as organizational characteristics to define or determine the performance of construction firms.

Okafor (2007) identified four organizational characteristics in the study of the relationship between organizational characteristics and performance of Nigerian quoted companies. The four variables used by Okafor (2007) to define organizational characteristics are staff, style, skills and shared values. Dada *et al.* (2012) used five variables to define the organizational characteristics of construction

firms in carrying out a survey of selected construction industry organizations in Lagos State, Nigeria. These five organizational characteristics are years of experience of firm, type of organization (consulting, contracting or client), size of organization (in terms of annual turnover and growth rate), number of employees and number of projects handled within the last five years. Odediran et al (2012 and 2013) identified five organizational characteristics in the study of the business structure of indigenous firms in the Nigerian construction industry. These organizational characteristics identified are firm's size (which was determined using annual turnover, staff strength and equipment capacity), area of specialization (which was grouped in to building, civil and industrial/heavy engineering), type of client (which was grouped in to public, federal ministries/parastatals, state ministries/parastatals, local governments, private individual/institutions, international agencies and Non Governmental Organizations), business type (which was grouped in to build only, design & build or package deal, design, build & finance and design, build & operate), project funding arrangement (which was grouped in to bank loans, retained earnings, share capital and mobilization) and years of experience of firm.

The most commonly used organizational characteristics of firms, which are demographic, were used in this study to define the distinguishing features of the Nigerian construction SMEs. These are years of experience, age of firms and number of employees.

1.2 Review of Major H & S Practices of Construction Contractors

Past research has shown that certain practices can lead to improved health and safety performance and therefore constitute good health and safety practices. These findings as summarized by Kheni (2008) and findings from the

review of literature from this study are presented in Table 1.

Table 1: Summary of Researches on H&S Management Practices

Year and Authors	Summary of Research	Health and Safety Management Practices
Simonds and Sahrai (1977) cited in Kheni (2008)	Identified factors that distinguished firms with lower injury frequency rates from those with higher rates.	The distinguishing factors include the following: top management involvement; higher average age of workers; longer average length of employment; adequate working space and neat environment; and higher percentage of married workers.
Liska et al. (1993) cited in Kheni (2008)	Identified zero accident techniques.	Identified the following to be associated with safety success: safety training and orientations; provision of safety incentives; safety pre-task planning included in safety goals; safety person or personnel; safety policies and procedures; fire protection programme; accountability/responsibility and safety budget; alcohol-and substance-abuse programme in place; accident and near-miss investigation; and, record keeping and follow-ups.
Jaselskis et al. (1996) cited in Kheni (2008)	Strategies for achieving excellence in construction safety performance.	Companies with lower recordable incidence rates were characterized by the following: more detailed safety programmes; * expended large percentage of revenue on safety programmes; greater safety training time; more formal safety inspections per month; and, * more safety meetings.
Gallagher (1997) cited in Kheni (2008)	Identified factors associated with improved health and safety performance.	The study identified the following factors the associated with better health and safety performance: high level of top management commitment; health and safety responsibility known; supervisor involvement encouraged; active involvement of health and safety representatives who have a broad role; effective health and safety committees; planned identification of risk and hazard elimination/control emphasis; and, comprehensive approach in inspections and investigations.
Aksorn and Hadikusumo (2008) cited in Kheni (2008)	Investigated the effectiveness of safety programmes in the construction industry.	Safety performance was found to be influenced by the nature of the implemented programmes. Particular elements of safety programmes found to be positively associated with safety performance included: accident investigations; jobsite inspections; job hazard analysis; safety inductions; safety record keeping; safety committees; safety incentives; and, control of subcontractors.

Source: Kheni (2008)

Table 1 (Continued)

Year and Authors	Summary of Research	Health and Safety Management Practices
Idoro (2011)	Studied the influence of mechanization on OHS performance of the Nigerian Construction Industry.	Mechanization was discovered to have the tendency to worsen OHS performance of the construction industry when not properly managed. It was then recommended that: stakeholders should give more attention to OHS management plan; and, hazard management plan in the use of plant and equipment on site should be given more priority.
Agwu (2012(a))	Studied the implications of integrating safety and social responsibility initiatives at the organizational level in the Nigerian construction industry.	It was concluded that integrating safety and social responsibility in construction activities results in better corporate performance. The following were suggested as linking factors between safety and social responsibility: the use of ISO 26000; holding top management accountable for safety; and, communicating safety value to corporate stakeholders.
Agwu (2012(b))	Assessed the impact of employees' safety culture on organizational performance.	The organizational cultural factors identified to be improving employees safety performance at work are: visibility of management commitment to construction employees' safety culture; establishment of monthly safety incentive schemes for employees; training and retraining of employees on safe work procedure; increase in site safety audits; and, focusing on monthly safety meetings on employees' attitudinal change towards safety.
Belel and Mahmud (2012)	Studied safety culture of Nigerian construction workers in Yola.	It was discovered that: Construction workers' attitude toward s safety is influenced by their perception of risk, safety rules and procedures. Lack of training of workers was ranked the most severe factor that hinders workers' safety on site. Reduce accident cost was ranked the most important benefit of safety on site while Poor understanding of the risks associated with the work was ranked second and these could all be attributed to the poor safety culture in the Industry.
Okolie and Okoye (2012)	Assessed the impact of national culture on the safety climate of construction workers in South-East, Nigeria.	Four cultural dimensions were identified having positive correlation with safety climate and which invariably influence the safety perceptions and behaviour of construction workers. These are: * Long Vs Small power distance; * Individualism Vs Collectivism; * Strong Vs Weak uncertainty avoidance; and, Masculinity Vs Femininity.

Source: Authors' review of literature on H&S Management Practices (2014)

Table 1 (Continued)

Year and Authors	Summary of Research	Health and Safety Management Practices
Idubor and Oisamoje (2013)	Examined background of OHS practices in Nigeria by highlighting the importance of mitigating OHS challenges identified from moral, legal and financial dimensions.	Reasons for frequent violation of OHS standards and norms by the operators, against the background of extant health and safety legislation in Nigeria, were identified as: bribery and corruption in the system; the Nigerian factor; monitoring institutions; low level education of employees; and, inadequate funding; Problems of unemployment.
Okolie and Okoye (2013)	Developed a framework for incorporating cultural elements in issues relating to construction businesses.	The study identified cultural factors influencing behaviour and perceptions of construction workers towards safety in South - East Nigeria to be: collectivism; uncertainty avoidance; long term orientation; power distance; and, masculinity.
Okoye and Okolie (2014)	Assed the cost of health and safety performance of building contractors in Nigeria and the relationship between cost performance and success of building projects.	It was concluded that health and safety performance of contractors affect success of building projects in terms of delivery time, quality, cost and productivity.
Agumba and Haupt (2014)	Examined the validity and reliability of health and safety practices and respondents demographic attributes perception on these health and safety practices implementation of South African construction SMEs.	It was established that th health and safety practices were valid for construction SMEs. It was also discovered that the number of years (experience) of employers/employees in an organization and perception towards health and safety did not differ, while educational level of employer/employee in an organization and perception towards health and safety differed.

Source: Authors' review of literature on H&S Management Practices (2014)

1.3 Summary of Findings from Previous Research

On a general note from the review of literature in this study, health and safety management literature suggests a move towards stricter health and safety legislation and more proactive approaches to managing health and safety risks. Literature on health and safety tends to focus on legislation and on workplace arrangements for effectively dealing with health and safety risks. As reviewed in this study, it was discovered that the characteristics of construction SMEs make them present unique problems in health and safety management and therefore unique solutions need to be devised.

The literature discussions in this chapter conclusively give rise to two key issues - difficulties in adoption of health and safety practices by SMEs and the roles the contextual environments of construction SMEs and their organisational characteristics play in health and safety management. Three critical research questions with regards to these key issues are:

- What are the constraints limiting the capability of Nigerian construction SMEs from carrying out their operations in a healthy and safe manner?

- What are the main health and safety management practices/procedures adopted by the Nigerian construction SMEs in controlling the risks of hazards in the construction industry?

- What is the influence of organizational characteristics on the health and safety management practices of Nigerian construction SMEs?

The following propositions (P_1 and P_2, derived from the third question and literature discussions relating to it, summarize the relationships between SME demographic characteristics and health and safety practices:

P_1: construction SMEs with few employees are less likely to adopt health and safety practices. Those with a large number of employees are likely to be health and safety conscious and adopt measures to control health and safety risks.

P₂: long established SMEs are more likely to adopt health and safety measures than newer companies.

In the light of the above and seeking answers to the research questions and investigating the propositions stated above, the study aims to evaluate the impact of demographic features on the H&S management practices of Nigerian construction SMEs. In order to achieve this aim, the specific objectives of the study are stated thus:

- To identify the constraints limiting the capability of Nigerian construction SMEs from carrying out their operations in a healthy and safe manner.

- To assess the health and safety management practices/procedures adopted by the Nigerian construction SMEs in controlling the risks of hazards in the construction industry.

- To establish the influence of demographic features on the health and safety management practices of Nigerian construction SMEs.

2. METHODOLOGY

This study adopted the mixed methods approach or what Kheni (2008) referred to as multimethodology. Multimethodology, according to Kheni (2008) refers to the combining of whole or parts of qualitative and quantitative research methods either originating from the same or different paradigms in particular research situation. This is a multi-paradigmatic position argued to follow from the study's context (SMEs) and the diversity of information needed to shed light on health and safety management. The study involved the conduct of a survey using questionnaires with both closed and open-ended questions which were used to examine the significance and incidences of health and safety practices of construction SMEs within the study setting and the constraints to the management of health and safety. The data obtained was used to determine associations between independent variables identified in the literature and health safety

management practices of SMEs. A pilot study carried out revealed that 46 H&S practices were very important and considered to have major impact to improve H&S performance of SMEs. These H&S practices comprised the final questionnaire to the SMEs in the Nigerian construction industry. The 46 practices addressed five H&S core practice areas. The respondents, who are experts with reasonable years of experience in construction, were required to indicate their level of agreement with the H&S practices. The questions were ranked on a five-point Likert's scale; where 1 = least important, 2 = less important, 3 = undecided, 4 = Important and 5 = most important.

Other sections of the questionnaires were designed to get the respondents' demographic information: size and age of firms. The questionnaire was pilot tested with ten (10) top management personnel and experienced H&S officers. The final version was presented to 436 SMEs which were randomly sampled from the 2219 construction contractors contained in the list of construction contractors registered with Corporate Affairs Commission (CAC) in Abuja, Nigeria. This sample was based on Watson's (2001) formula for getting a representative sample size from a large population. Out of the 436 questionnaires distributed, 235 were returned and found useful for analysis, thereby giving a good response rate of 53.9%. The study employed the use of both descriptive and inferential methods of analysis to analyse the collected data in order to achieve the objectives of the study. In order to achieve the first objective of the study, frequency/counts/percentage was employed to determine the major constraints facing the SMEs in the proper management of H&S on site. To achieve the second objective of the study, the use of Literature Review was employed to identify the the H&S management practices adopted by the Nigerian construction SMEs in controlling the risks of hazards on construction sites. The identified H&S management

practices adopted by the Nigerian construction SMEs in controlling the risks of hazards on construction sites are thereafter ranked respectively with the use of Mean Item Score (MIS) and percentages in order to determine the level to which they are been implemented.

Factor analysis was employed, based on the work of Pallant (2013), to reduce the 46 H&S practices identified from the review of literature to eight major health and safety management practices/ which were used for further analysis to explore the relationship between demographic features (years of experience of employees, age of firm and number of full-time employees in firm) and the eight set of H&S practices (domestic health and safety practices of firms, practices given as provisions in conditions of contract, use of outside health and safety consultants, workers' consultation and participation, health and safety communication, pre-contract health and safety panning, contract health and safety planning, health and safety education and training) explored. The use of SPSS 13.0 computer software package was employed to determining whether research data set was suitable for factor analysis or not by considering the sample size, and the strength of the relationship among the variables (or items). After confirming the suitability of the research data for data analysis, factor extraction was done using the principal components analysis techniques which are Kaiser's criterion; scree test; and parallel analysis. After the factors have been extracted, the results are then interpreted based on the number of factor rotation components done by SPSS software by checking the variables that load strongly on each component.

The use of hierarchical multiple regression analysis was employed to establish the relationship between organizational characteristics and H&S practices of construction SMEs in Nigeria, based on the recommendation of Agumba and Haupt (2014). The following tests were carried out to confirm the suitability

of the data in this study for multiple regression analysis before being subjected to multiple regression analysis:

- Normality test by inspecting the Normal Probability Plot (P-P) of the Regression Standardized Residual and the Scatterplot.
- Linearity test by inspecting the Normal Probability Plot (P-P) of the Regression Standardized Residual and the Scatterplot.
- Multicollinearaity test by inspecting the Normal Probability Plot (P-P) of the Regression Standardized Residual and the Scatterplot.
- Homoscedasticity test by inspecting the Normal Probability Plot (P-P) of the Regression Standardized Residual and the Scatterplot.
- Outliers Test by inspecting the Scatter plot and Mahalanobis distances produced by the multiple regression program.

3. RESULTS AND DISCUSSIONS

3.1 Results of Descriptive Analysis

3.1.1 Results of Demographic Features

The results revealed that most of the respondents (69.36%) have had between 1 and 15 years of experience at the construction firm and majority of others (representing 23.4% of the total number of respondents and 76.4% of others) have years of experience between 16 and 20 years. In the light of this, the respondents are discovered to be suitable to provide accurate answers to the questions in the research questionnaire. It was also revealed that majority of the firms (62.13%) have been in existence for more than 10 years implying that the firms are suitable and old enough to provide accurate response to the questionnaire. It was gathered from the results that 38% of the construction SMEs has a size band of less than 30 workers while 31% of the construction SMEs have the size band of 31 – 70 workers and 31% of the construction SMEs has a size band of 71 – 200 workers. This reveals that most of

the construction firms (62%) are Small and Medium – sized Enterprises.

3.1.2   Results of Important H&S Practices

The descriptive analysis of results of the important H&S practices of SMEs which are capable of enhancing H&S performance revealed 46 important H&S practices under 5 major or core H&S practices which are *company's commitment*, *workers' consultation & participation*, *H&S communication*, *H&S planning* and *H&S education & training*. Twelve important H&S practices were identified under company's commitment with Relative Importance Index (RII) ranging between 0.92 and 0.71. The practices here range from *provision of first aid box* which is the highest ranked (0.92) to *implementation of employee drug testing* which is the least ranked (0.71). Four important H&S practices were identified under workers' consultation and participation. These are *rewarding workers who demonstrate exemplary safe behaviour on site* with RII of 0.81 and *consulting trade union representatives on health and safety matters* with RII of 0.78. H&S communication comprises of 8 H&S practices ranging from *using health and safety posters & other signs to give safety education* (RII = 0.88) to *communicating health and safety through company newsletter* (RII = 0.70). The twelve important H&S practices discovered under H&S planning range between *identifying hazards on sites before work commences* (RII = 4.50) and *obtaining a labour certificate for every contract* (0.70). The fifth core H&S practice which is H&S education & training has 6 H&S practices ranging between *organizing health and safety training and retraining for supervisors and/or senior management* (RII = 0.88) and *organizing alcohol- and substance-abuse programme* (RII = 0.74). Table 2 summarizes these results.

Table 2: Ranking of H&S practices

S/NO	COMPANY'S COMMITMENT	RII	RANK
1	Provision of first aid box	0.92	1st
2	Provision of personal protective equipment	0.88	2nd
3	Keeping of safety record keeping and follow-ups	0.88	3rd
4	Provision of procedures for investigating accidents and nearmisses	0.87	4th
5	Existence of formal health and safety policy	0.86	5th
6	Provision of adequate work space and neat environment	0.84	6th
7	Having a designated safety personnel	0.84	7th
8	Having fire protection programme	0.84	7th
9	Provision of cloak and toilet	0.82	9th
10	Provision of procedures for reporting accidents	0.79	10th
11	Using outside health and safety consultants	0.78	11th
12	Existence of minimization policy for cost of ill-health and injury	0.83	12th
13	Provision of drinking water on site	0.76	13th
14	Provision of canteen service on site	0.74	14th
15	Use of ISO 26000 to identify social responsibilities of employees	0.74	14th
16	Implementing employee drug testing	0.71	16th
S/NO	HEALTH & SAFETY COMMUNICATION	RII	RANK
17	Using health and safety posters and other signs to give safety education	0.88	1st
18	Using verbal communication with operatives during site tours.	0.88	1st
19	Communicating safety value to corporate stakeholders and use of two-way safety communication	0.84	3rd
20	Discussing health and safety during site meetings	0.83	4th
21	Communicating health and safety performance to employees	0.83	4th
22	Focusing your monthly safety meetings on employees' attitudinal change towards safety	0.83	4th
23	Networking with other companies/institutions	0.78	7th
24	Communicating health and safety through company newsletter	0.70	8th
S/NO	HEALTH AND SAFETY PLANNING	RII	RANK
25	Identifying hazards on sites before work commences	0.90	1st
26	Providing job hazard analysis	0.90	1st
27	Documenting risk assessments	0.88	3rd
28	Carrying out post-accident investigation	0.87	4th
29	Price health and safety in preliminaries	0.85	5th
30	Carrying out safety pre-task planning	0.85	5th

Table 2 (Cont.)

S/NO	HEALTH AND SAFETY PLANNING	RII	RANK

S/NO		RII	RANK
31	Documenting method statements	0.84	7th
32	Exercising disciplinary measures to correct wrong behaviours relating to health and safety	0.83	8th
33	Providing emergency response plan	0.81	9th
34	Providing insurance cover for sites and Employer-paid group insurance plan	0.77	10th
35	Ensuring adequate welfare provisions on site	0.74	11th
36	Obtaining a labour certificate for every contract	0.70	12th
S/NO	WORKERS' CONSULTATION AND PARTICIPATION	RII	RANK
37	Rewarding workers who demonstrate exemplary safe behaviour on site	0.84	1st
38	Asking workers for their ideas on health and safety matters	0.80	2nd
39	Involving workers to participate in hazard identification on sites	0.80	2nd
40	Consulting trade union representatives on health and safety matters	0.78	4th
S/NO	HEALTH & SAFETY EDUCATION AND TRAINING	RII	Rank
41	Organizing health and safety training and retraining for supervisors and/or senior management	0.88	1st
42	Organizing orientation on safety for new workers	0.88	1st
43	Organizing health and safety training of operatives - first aid, manual lifting etc	0.88	1st
44	Organizing site inductions for operatives	0.86	4th
45	Organizing toolbox talks	0.74	5th
46	Organizing alcohol- and substance-abuse programme	0.74	5th

3.2 Factor Analysis

Factor analysis was employed to reduce the 46 H&S practices identified to 8 major H&S practices. Each of the 5 core H&S practices were subjected to Principal Component Analysis (PCA) using SPSS Version 13.0. Prior to the performance of PCA, the suitability of the data for Factor Analysis was assessed. Inspection of the correlation matrix revealed the presence of many coefficients of 0.5 and above. The Kaiser-Meyer-Okin (KMO) value was 0.916, exceeding the recommended value of 0.6 (Kaiser, 1970, 1974 cited in Pallant, 2013) and

Bartlett's Test of Sphericity (Bartlett, 1954 cited in Pallant, 2013) with the value of 0.000 reached statistical significance of $p < 0.05$, supporting the factorability of the correlation matrix in all cases. The eight major H&S practices which the 46 practices were reduced to and used for further analysis (hierarchical multiple regression) are summarized below:

- Domestic Health and Safety Planning of Firms
- Practices Conforming to HSE Requirements in Conditions of Contract
- Using Outside Health and Safety Consultants
- Workers' Consultation and Participation
- H&S Communication
- Pre-contract Health and Safety Planning
- Contract Health and Safety Planning
- Education and training

3.3 Results of Hierarchical Multiple Regression Analysis

The use of hierarchical multiple regression analysis was employed to explore the relationship between the three demographic features which are years of experience of employee in firm, age of firm and number of employees in firm, and the 8 major H&S practices of firms identified from the Factor Analysis carried out. Preliminary analyses were conducted to ensure no violation of the assumptions of normality, linearity, multicollinearaity and homoscedasticity for each of the cases. The preliminary analyses revealed that there was no violation of the assumptions of normality, linearity, multicollinearaity and homoscedasticity because the tolerance value was greater than 0.10, variance inflation factor (VIF) value less than 10, Normal P-P Plot points lie in a reasonably straight diagonal line from bottom left to top right and the Scatterplot standardized residuals roughly rectangularly distributed. The presences of outliers were also checked and it was observed that the maximum Mahalanobis Distance value was greater than the critical value (24.32)

indicating absence of outliers. The maximum Cook's Distance in all the analysis was less than 1 indicating the absence of any undue influence on the results of for the whole model.

3.3.1 Relationship between Demographic Features and Domestic Health and Safety Planning of Firms

This analysis revealed that Number of Employees beta (beta = 0.484; $p < 0.001$), Years of Experience of Employees (sig (p) value of 0.024 ($p < 0.05$)) and Age of Firm (sig (p) value of 0.000 ($p < 0.05$)) were statistically significantly related with Domestic Health and Safety Planning of Firms at 95% confidence limit.

3.3.2 Relationship between Demographic Features and Company's Commitment

It was revealed from this analysis that Years of Experience (sig = 0.035; $p < 0.05$ beta = 0.137), Age of Firm (sig = 0.001; $p < 0.005$; beta = 0.229) and Number of Employees (sig =0.004; $p < 0.05$; beta = 0.228) were respectively observed to be statistically significant with Company's Commitment from HSE Requirements in Conditions of Contract at 95% confidence limit.

3.3.3 Relationship between Demographic Features & company's commitment to using outside H&S consultants

None of the demographic features was observed to be significantly related with Company's Commitment to Using outside H&S Consultants at 95% confidence limit from this analysis.

3.3.4 Relationship between Demographic Features and Workers Consultation & Participation

Number of Full-time Employees (beta = 0.321; $p < 0.001$), Years of Experience of Employees (sig (p) value of 0.021 ($p < 0.05$)) and Age of Firm (sig (p) value of 0.000 ($p < 0.05$)) were observed in this analysis to be significantly related with Workers Consultation & Participation at 95% confidence limit.

3.3.5 Relationship between Demographic Features and H&S Communication

Number of Full-time Employees (beta = 0.369; $p < 0.005$), and Age of firm ((p) value of 0.000 ($p < 0.05$)) were observed to be statistically significant with H&S Communication at 95% confidence limit in this analysis.

3.3.6 Relationship between Demographic Features and Pre-contract Health & Safety Planning

It was discovered from this analysis that there exists a statistically significant relationship between Pre-contract H&S Planning and Number of Full-time Employees (beta = 0.500; $p < 0.005$), Years of Experience of Employees (sig (p) value of 0.017 ($p < 0.05$) and beta value of 0.155) and Age of Firm (sig (p) value of 0.000 ($p < 0.05$) and beta value of 0.416).

3.3.7 Relationship between Demographic Features and Contract H&S Planning

Number of Full-time Employees (beta = 0.360; $p < 0.005$), Years of Experience of Employees (sig (p) value of 0.023 ($p < 0.05$) and beta value of 0.148) and Age of Firm (sig (p) value of 0.000 ($p < 0.05$) and beta value of 0.320) were statistically significant with Contract H&S Planning at 95% confidence limit as revealed in this analysis.

3.3.8 Relationship between Demographic Features and H&S Education & Training

It was shown from the results of this analysis that Number of Full-time Employees with a beta value of 0.477 (beta = 0.477; sig = 0.000 i.e. $p < 0.005$) and Age of Firms with sig (p) value of 0.000 ($p < 0.005$) and beta value of 0.382 were observed to be significantly related with H&S Education & Training.

The results of all the analyses discussed above led to the rejection of the hypothesis formulated based on literature

findings, third research questions and the study's proposition, except in the third analysis between Demographic Features and company's commitment to using outside H&S consultants. This hypothesis is stated thus:

H0: There is no significant relationship between demographic features and health and safety management practices of Nigerian construction SMEs.

3.4 Constraints to Construction Site H&S Management

It was discovered from the responses of the questionnaires distributed to construction SMEs that the construction firms face a lot of challenges which limit their ability to effectively perform activities on construction sites in a safe and healthy manner. About 60% of the respondents express their experience on the challenges they face in effective health and safety management on site. Some of these construction SMEs face the problem of poor attitude of their workers towards safety while some of them face the problem of being able to retain experienced workers. This implies that a large proportion of the respondents indicated that they experience difficulties in the management of health and safety. Lack of proper awareness of some health and safety regulations is the problem facing some of the construction SMEs while some face the problem of inadequate capital base. The major constraints faced by the construction SMEs, in order of severity, are discussed below based on the opinions of respondents.

3.4.1 Literacy Level

It has been discovered that most of the workers, especially the unskilled workers, are not literate. Some of them are either not well educated or they are not educated at all. It is therefore usually difficult to give them the appropriate health and safety orientation/education to make them work better in a healthy and safe manner except if there is

someone to interpret to them in their native dialect. One of the respondents had this to say:

"There is high level of illiteracy among the site operatives which, to a reasonable extent, contributes to their inability to understand safety directions on site" (Respondent Number 4).

3.4.2 Poor Attitude of Construction Workers

About 75% of the respondents indicated that problem of poor attitude towards health and safety exists in their organizations. Most of the workers fail to wear their personal protective equipments even when they are provided on sites especially when they are not being monitored. A respondent had this to say:

"Human beings generally are difficult to manage on site, especially when you remind them of safety on site; they will say "I know sir". Seeing you he will act immediately, but as soon as you leave, he removes his helmet and gloves" (Respondent Number 152).

3.4.3 Financial Constraints. Some constructions

SMEs lack the financial capability or buoyant capital base to adequately fund health and safety procedures on sites in terms of human and material resources. One of the respondents shared this on financial constraints:

"We sometimes experience financial constraint in meeting up with HSE Requirements. This makes us to cut down of the budget for health and safety" (Respondent 101).

3.4.4 Environmental Influences

This is another serious problem to health and safety management on site which many firms either do not take note of, or do not take seriously. When some workers go to sites where the natives there have uncultured teen-agers or adults, they can influence workers of their peer-groups in to bad habits like smoking and drinking of alcohol.

3.4.5 Cost of Health and Safety

Some of the respondents expressed that the cost of putting health and safety procedures on sites is very expensive because most of the good health and safety equipments are imported or foreign materials which are expensive and scarce. In the light of this, most construction firms are not able to afford them but instead go for local substitutes which are usually of a lower quality or inferior in nature to the imported ones. One of the respondents simply put it this way:

> "Cost of HSE is expensive if it is to be appropriately estimated in a bill" (Respondent Number 123).

3.4.6   Lack of Basic Facilities

It was revealed by some of the respondents that some of the rural communities lack some basic facilities like ambulance, clinics, experienced medical personnel and drugs. If there is any emergency case on site it will be difficult to get urgent attention. A respondent simply expressed it this way:

> "In rural communities, access to medicine facilities in terms of accidents is a problem" (Respondent Number 135).

3.4.7   Job Security and Continuity

Some respondents stated job security and continuity as a factor that compelled them from relying greatly on casual labour and labour only subcontractors which they thought did not promote the effective management of health and safety. An owner/manager responded as thus:

> "…… because we don't know how long it will take us to get another contract after completing one, most of our unskilled workers are casual workers and so they don't take HSE seriously as the HSE Budget does not cover their HSE issues adequately" (Respondent Number 86).

3.4.8   Lack of Awareness and Orientation from Government Regulatory Agencies

About 40% of the respondents revealed that the agencies responsible for regulating health and safety standards on sites, like the Factory Inspectorate Department, Labour Department and Federal Environmental Protection Agency, do not perform their functions effectively. This therefore results in to lack of proper awareness of some basic health and safety regulations and requirements by some construction firms.

3.4.9   Weather Condition

Poor weather condition is another challenge faced by construction SMEs. When the weather is extremely hot workers find it not conducive to properly put on their safety wears. When the weather is very cold or when there is heavy rain, work on site may have to stop and the health of workers may also be affected.

3.5 Discussion of Results

The study used three demographic features which define the H&S practices of construction SMEs. These demographic features are age of firm, experience of employees and number of employees which have also been used in many previous studies which includes that of Kheni (2008), Choudhry *et al*. (2009) and Masood and Choudhry (2012). The study also identified 46 important H&S practices which are capable of enhancing positive H&S performance of the construction SMEs. These H&S practices were reduced to 8 core H&S practices using factor analysis. These 8 H&S practices which range between domestic H&S practices and H&S education & training have also been studied by Kheni (2008) and Agumba and Haupt (2014). The relationship between the identified organizational characteristics and H&S practices was explored with the use of hierarchical multiple regression analysis as suggested by Agumba and Haupt (2014).

Number of full-time employees in firms was discovered to be a good predictor of 7 major health and safety practices

adopted by the construction SMEs namely: domestic HSE practices, HSE requirements con forming to the requirement in conditions of contract, workers' consultation and participation, H&S communication, pre-contract H&S planning, contract HSE planning and H&E education and training. The result of the study carried out by Idoro (2011) is evidence to the findings discussed above because it revealed that the protection provided to workers engaged by multi-national and national contractors is higher than the protection provided to workers engaged by regional and local contractors in order to protect workers from sustaining injuries in the event of accident. The findings of Adeogun and Okafor (2013) also corroborates with the finding of this study because it revealed that most of the indigenous establishments see HSE myopically such as cleanliness of the environment alone while the few companies that recognize occupational health and safety are the large companies or big multinationals who are running the policies as constituted in their parent countries of origin. Majority of the construction SMEs undertaking mainly civil engineering construction works are the medium-sized firms among which have a tendency of becoming large or multinational firms.

It was also discovered that years of experience of owner/managers significantly and positively correlated with five major H&S practices namely: domestic H&S practices, company's commitment to the H&S practices in the requirements in the conditions of contract, workers' consultation and participation, pre-contract H&S planning and contract H&S planning. The results of the study also indicate that age of construction SMEs is a significant predictor of 5 H&S practices which are: domestic H&S practices, company's commitment to the H&S practices in the requirements in the conditions of contract, workers' consultation and participation, H&S communication and pre-contract H&S planning. As a result of this, the second

proposition that long established SMEs are more likely to adopt health and safety measures than newer construction SMEs is supported. This is supported by the results reported in studies of Fang et al (2006), Choudhry *et al*. (2009) and Masood and Choudhry (2012) who consensually discovered that age, gender and experience among other variables have significant impact on health and safety management practices. On the contrary the study of Agumba and Haupt (2014) revealed that the number of years the respondents was involved in the construction industry (experience) and their perception towards H&S management practices were not different in the South African construction industry.

The study also identified 9 major constraints to the effective H&S management practices of the construction SMEs which are literacy level, poor attitude of construction workers, financial constraints, environmental influences, cost of health and safety, lack of basic facilities, job security and continuity, lack of awareness and orientation from government regulatory agencies and weather condition. Most of these constraints have also been identified in previous studies as major hindrances to H&S management practices of construction SMEs especially in the study of Kheni (2008).

4. CONCLUSIONS

It was established that low literacy level, poor attitude of construction workers, financial constraints, environmental influences, cost of health and safety, lack of basic facilities, job security and continuity, lack of awareness and orientation from government regulatory agencies and weather condition are the major constraints limiting the capability of Nigerian construction SMEs from carrying out their operations in a healthy and safe manner.

It was also established that domestic health and safety planning of firms, practices conforming to H&S requirements in conditions of contract, using outside health

and safety consultants, workers' consultation and participation, H&S communication, pre-contract health and safety planning, contract health and safety planning and education and training, were very important H&S practices which are capable of enhancing high H&S performance of Nigerian construction SMEs.

It was also established that all the demographic features have positive and significant relationship with the H&S practices except with the practice of using outside health and safety consultants. The demographic features are therefore good predictors of H&S practices. The propositions of the research therefore hold. Thus implying that construction SMEs with few employees are less likely to adopt H&S practices than those with a large number of employees; and long established SMEs are more likely to adopt H&S measures than newer companies.

5. RECOMMENDATIONS

In view of the conclusions from the research findings, it was therefore recommended that construction SMEs should lay great emphases on training and orientation for all level of employees in order to address the issue of poor safety performance and poor attitude. Older firms should assist younger firms with H&S orientation and training while older and more experienced employees in a firm should assist younger and less experienced employees with H&S orientation and training.

REFERENCES

Adeniran, D. (2013). The Role of Government in Occupational Safety. Lagos Open Parliament Report. Afrikold Technologies International, Lagos, Nigeria. At www.deboadeniran.com/the-role-of-government-in-occupational-safety-debo-adeniran/. Retrieved on 20th January, 2014.

Adeogun B.K. and Okafor C.C (2013). Occupational Health, Safety and Environment (HSE) Trend in Nigeria. *International Journal of Environmental Science, Management and Engineering Research.*

2(1): 24-29, Jan- Feb., 2013. Retrieved from http://www.ijesmer.com on 24/03/2014.

Agumba, J. N. and Haupt, T. C. (2014). Implementation of Health and Safety Practices: Do Demographic Attributes Matter? *Journal of Engineering Design & Technology.* Emerald Group Publishing Limited. 12(4): 531 – 550. Available on www.emeraldinsight.com/1726-0531.htm

Agwu, M. O. (2012(a)). Implications of Integrating Safety and Social Responsibility in Selected Construction Companies in Nigeria. In: *American Journal of Social and Management Sciences.* ScienceHuβ, ISSN Print: 2156-1540, ISSN Online: 2151-1559, doi:10.5251/ajsms.2012.3.1.30.38. Retrieved from http://www.scihub.org/AJSMS on 22/03/2014.

Agwu, M. O. (2012(b)). Impact of Employees Safety Culture on Organizational Performance in Shell Bonny Terminal Integrated Project (BTIP). *European Journal of Business and Social Sciences.* 1(5): 70 – 82. ISSN: 2235-7674. Retrieved from http://www.ejbss.com/recent-aspx on 23/03/2014.

Awodele, O. A. & Ayoola, A. C. (2005). An Assessment of Safety Programmes on Construction Sites. In: *Journal of Land Use & Development Studies,* Federal University of Technology, Akure, Nigeria. Volume 1(1): 1-13.

Belel, Z. A. and Mahmud, H. (2012). Safety Culture of Nigerian Construction Workers – A Cases study of Yola. *International Journal of Scientific & Engineering Research.* 3(9): 1 – 5. ISSN 2229-5518. Retrieved from http://www .ijser.org on 23/03/2014.

Choudhry, M.R., Fang, D.P., & Lingard, H. (2009). Measuring safety climate of a construction company, *Journal of construction Engineering and Management*, *135* (9), 890-899.

Chinowsky, P., Molenaar, K. and Realph, A. (2007). Learning Organizations in Construction. *Journal of Management in Engineering.* ASCE. 1(27): 27 – 34. Retrieved from http://pubs.asce.org/copyright on 15/06/2014.

Dada, M. O., Akpadiaha, B. and Ologunnagba, M. M. (2012). Disposition to Organizational Learning: A Survey of Selected Construction Industry Organizations in Lagos State, Nigeria. *Mediterranean Journal of Social Science.* 3(2): 487 – 496. ISSN: 2039 – 2117.

Fang, D.P., Chen Y., & Louisa W. (2006). Safety climate in construction industry: A case study in Hong Kong, *Journal of Construction Engineering and Management*, 132(6), 573-584.

Idoro, G. I. (2011). Comparing Occupational Health and Safety (OHS) Management Efforts and Performance of Nigerian Construction Contractors. *Journal of Construction in Developing Countries,* Preview Manuscript. 11, 1 – 21.

Idubor, E. E. & Oisamoje, M. D. (2013). An Exploration of Health and Safety Management Issues in Nigeria's Effort to Industrialize. *European Scientific Journal*; 9(12): 154-169. ISSN: 1857-7881 (Print) e-ISSN 1857-7431.

ILO. (2001). The construction industry in the twenty-first century: its image, employment prospects and skills requirements. International Labour Office, Geneva. Tripartite Meeting, Document number TMCIT/2001. Accessed on 30th November 2007 from http://www.ilo.org/public/english/dialogue/sector/techmeet/tmcit01/tmcitr.pdf

ILO. (2005a). Prevention: A global strategy. Promoting safety and health at work. The ILO Report for World Day for Safety and Health at Work International Labour Organisation, Geneva, Switzerland. Accessed on 15th September 2007 from http://www.ilo.org.pk/informationfiles/Prevention%20A%20Global%20Strategy.pdf

ILO. (2005b). Global estimates of fatal work related diseases and occupational accidents, World Bank Regions. International Labour Organisation, Geneva. Programme on Safety and Health at Work and Environment (Safe Work). Accessed on 10th May 2007 from; http://www.ilo.org/public/english/protection/safework/accidis/globest_2005/index.ht m

Kheni, N A, Dainty, A R J and Gibb, A G F (2007) Influence of Political and Socio-cultural Environments on Health and Safety Management within SMEs: A Ghana Case Study. *In:* Boyd, D (Ed) *Procs 23rd Annual ARCOM Conference,* 3-5 September 2007, Belfast, UK, Association of Researchers in Construction Management, 159-168.

Kheni, N A, Gibb, A G F and Dainty, A R J (2006). The management of construction site health and safety by small and medium-sized construction businesses in developing countries: A Ghana case study. In: Boyd, D (Ed.), *Procs 22nd Annual ARCOM Conference,*

4th-6th September, 2006, Birmingham, UK. ARCOM, Vol. 1, 273-82.

Kheni, N. A. (2008). Impact of Health and Safety Management on Safety Performance of Small and Medium-Sized Construction Businesses in Ghana. An unpublished PhD Thesis, Loughborough University, UK.

Kheni, N; Gibb, A.G. F. & Dainty, A. R. J. (2008). Health and safety management in developing countries: A Study of Construction SMEs in Ghana. In: *Construction Management & Economics.* 26(11): 1159-1169, ISSN 0144-6193 – online ISSN 1466-433X.

Koehn, E, Kothari, R K and Pan, C-S (1995). Safety in developing countries: Professional and bureaucratic problems. *Journal of Construction Engineering and Management,* **121**(3), 261-5.

Masood, R. and Choudhry, R. M. (2012). Investigation of Demographic Factors Relationship with Safety Climate. 48th ASC Annual International Conference Proceedings. Associated Schools of Construction. Pp. 1 – 9.

Murie, F. (2007). Building safety - An international perspective *International Journal of Occupational Environment and Health,* **13**, 5-11.

Odediran, S. J., Adeyinka, B. F., Opatunji, O. A. and Morakinyo, K. O. (2012). Business Structure of Indigenous Firms in the Nigerian Construction Industry. *International Journal of Business Research and Management (IJBRM).* 3(1): 255 – 264.

Odediran, S. J., Babalola, M. O. and Adebiyi, H. A. (2013). Assessment of Business Development Strategies in the Nigerian Construction Industry. *Journal of Business and Management.* Science and Education Centre of North America. 12(1): 34 – 45. ISSN: 2291 – 1995; E – ISSN: 2291 – 2002. Retrieved from www.todayscience.org/jbm on 15/06/2014.

Okafor, C. (2007). Organizational Characteristics and Performance of Nigerian Quoted Companies. *Research Journal of Business Management.* 1(1): 37 – 49. ISSN: 1818 – 1932.

Okeola, O. G. (2009). Occupational Health & Safety (OHS) Assessment in the Construction Industry. In: 1st Annual Civil Engineering Conference. University of Ilorin, Nigeria. Pp236-246.

Okolie, K. C, and Okoye, P.U. (2012). Assessment of National Culture Dimensions and Construction Health and Safety Climate in Nigeria. In: *Science Journal of Environmental Engineering Research.* Volume 2012, Article ID sjeer-167, 6 Pages, 2012. doi: 10.7237/sjeer/167. *Science Journal Publication*, International Open Access Publisher. ISSN: 2276-7495. Retrieved from http://www.sjpub.org/sjeer.html on 22/03/2014.

Okolie, K. C, and Okoye, P.U. (2013). Appraising the Influence of Cultural Determinants of Construction Workers Safety Perception and Behaviour. In: *International Journal of Engineering and Medical Science Research.* 1(1): 11-24. European Centre for Research Training and Development UK (www.ea-journals.org). Retrieved 22/03/2014.

Okolie, C. U. and Okolie, K. C. (2014). Exploratory Study of the Cost of Health and Safety Performance of Building Contractors in South- East Nigeria. *British Journal of Environmental Sciences.* European Centre for Research Training and Development, UK.. 2(1): 21-33. www.ea-journals.org.

Okpan, A. & Agha, K. A. (2013). Assessment of Health and Safety Management of Building and Infrastructure Projects in South East Geo-political Zone. In: A. D. Ibrahim, K. J. Adogbo & Y. M. Ibrahim (Eds). Proceedings of Nigerian Institute of Quantity Surveyors: 1st Annual Research Conference – AnReCon. Ahmadu Bello University Press Limited, Zaria. 190 – 198.

Olatunji, O. A. & Aje, O. I. (2007). Evaluating Health and Safety Performance of Nigerian Construction Site. CIB World Building Congress, (CIB 2007 – 051). 1176 – 1190.

Pallant, J. (2013). SPSS Survival Manual: A Step by Step Guide to Data Analysis Using SPSS (5th Edition). Allen & Uwin Publishers, Australia.

Watson, J. (2001). How to Determine Sample Size: Tip sheet #60, University Park, P.A: University Cooperative Extension, Pennsylvania State University. Retrieved from http://www.extension.psu.evaluation/pdf/TS60.pdf on 7/4/2013

BUFFERING CATION PERMEATION BY MINERAL BARRIER

Agbenyeku Emem-Obong Emmanuel[1*], Muzenda Edison[2], Msibi Mandla Innocent[3]

[1,2]Department of Chemical Engineering, University of Johannesburg, South Africa

[2]Department of Chemical, Materials and Metallurgical Engineering, Botswana International University of Science and Technology, Palapye, Botswana

[3]Research and Innovation Division, University of Johannesburg, South Africa

[*]emmaa@uj.ac.za; kobitha2003@yahoo.com, +27 11 559 6396

ABSTRACT

Laboratory test of failed membrane in a geo-composite barrier under leachate permeation through a circular defect was investigated using a bespoke apparatus. Zeolitic mineral barrier-24 mm thick, polythene plastic (PP)-2 mm thick with 5 mm centralized puncture simulated the circular failure in the membrane and a 225 mm thick mineral layer as buffering strata (BS) comprised the experimental setup. The bespoke device-160 mm diameter coupled to a hydraulic pressure frame imposed up to 150 kPa pressure to the barrier. Permeant through the barrier-BS system was evaluated for tests under varying pressures. In this study, measured permeation rates for conditions of good interface contact were found to be valid but unachievable for conditions of perfect contact. However, tests results displayed significant reduction in permeation rates with increased pressure, p, on the system. This is conceivably due to reduced system transmissivity, θ, and densification of the zeolitic barrier. After compactibility tests, cation concentrations revealed permeation through the failed membrane-mineral barrier, nevertheless, a fairly reasonable buffering ability of the zeolitic mineral to permeating cations was observed.

Keywords: *Zeolite, leachate, Membrane, Cations.*

1. INTRODUCTION

In recent decades, civilization and globalization has warranted increased human activities to meet dire needs and challenges. This has led to diverse transformations in industries and households, resulting in massive generation of solid wastes. It has therefore become imperative as observed by Rowe (2011) that these by-products of human activities are properly disposed in engineered waste containment facilities. However, in present times, recycling is the first and best option of dealing with waste before landfilling is considered in the face of handling difficulties by other methods (Goodrich, 2000). Land disposal has come a long way as a method of ridding off various generated waste and will remain the commonest form of disposal for a long time to come. Landfills are known to produce gases and leachates whose breakaway and eventual permeation into surrounding soil and ground water could have detrimental human and environmental health effects. For these reasons, Bouazza et al. (2002) argues that leachate migration be curbed to the lowest minimum if not entirely prevented. Rain, runoffs and

waste containing high moisture in landfills propel the decomposition and production of leachate contaminants by microbial actions. Hence, protecting regimes of soil and ground water resources against leachate pollution is of major interest. In the developed world, barrier systems are well employed in guarding against contaminant permeation to regions of consequential impacts. However, in developing countries, where the construction of engineered facilities may be expensive, the prevention of contaminant permeation depends on the geological formation of the disposal site (Agbenyeku et al., 2014a). In some occasions, membrane which forms part of a geo-composite barrier may fail from fabrication, installation or due to ultraviolet radiation in its service life. In some other occasions, constructing disposal facilities around vital water sources may be unavoidable as such, it must be done with integrity to ensure protection of soil and ground water regions from waste bodies (South African Department of Water Affairs and Forestry, 2005). This can be achieved by utilizing mineral clay barriers/compacted clay liners (CCL) as components of geo-composite lining systems to

prevent permeating contaminant from reaching ground regions with consequential impacts in cases of membrane failures e.g., failures of Geomembrane (GM) or Geosynthetic Clay Liner (GCL). Hence, membrane-soil barriers are recommended globally and are actively used in waste containment which forms a major component for multiple systems in engineered landfills. The utilization of geosynthetics is recognized as reported by Bouazza (2002) in designs for better services and is rapidly expanding as engineers and manufacturers develop improved materials and new analysis routines. However as observed by Agbenyeku et al. (2014b), failure of membranes in-situ is inevitable. Conversely, the daily generation and disposal of more than 41,000 tons of solid waste in South Africa has attracted attention, particularly, in the Gauteng province and Johannesburg city where cumulatively, over 25,000 tons of waste is dumped daily (EIAR, 2005). Health, environmental and aesthetic challenges are often associated with waste disposal. Pollution of soil and groundwater resources is among the many effects of landfilling which requires to be addressed. This concern gave course for the study which investigated the impact of pressure on permeation rate, cation permeation mechanism in zeolitic soil barrier as CCL and its buffering tendencies since much have not been documented. Furthermore, considering that over 75 % of Municipal Solid Waste (MSW) in South Africa ends up in landfills, the barriers are thus subjected to pressure from waste piles. Landfill surveys from this study, showed an estimated 200 kPa of waste imposing the barriers. Therefore, the study investigated pressure effects on leachate permeation through a failed PP barrier overlying a zeolitic mineral soil liner as CCL and BS. Pressure effects on permeation rate, cation permeation and the buffering behaviour of zeolitic mineral clay barrier are reported herein.

2. METHODOLOGY

For the purpose of this study zeolitic soil was collected and used as CCL and BS. As seen in Figure 1, the natural mineral soil was collected in Johannesburg, South Africa, from a landfill site slightly far from the actual dump to ensure a certain degree of purity. The zeolitic sample was then mechanically and chemically tested to determine applicable engineering and compositional properties. Figure 2 holds the grain size distribution curve while Figure 3 shows the compaction curve expressing the relationship between optimum moisture content (OMC) and maximum dry unit weight (MDUW) of the soil determined by compaction test in accordance with ASTM D-698.

Fig. 1: Sampling vicinity

The standard proctor compaction test was done with a light self-weighted rammer of about 0.0244 kN and striking effort of about 595 kN-m/m^3. The tests yielded OMC of 15.5 % and MDUW of 17.1 kN/m^3 for the zeolitic soil. Values for permeability coefficient gotten in conformance with ASTM D-2434 were measured by falling head test.
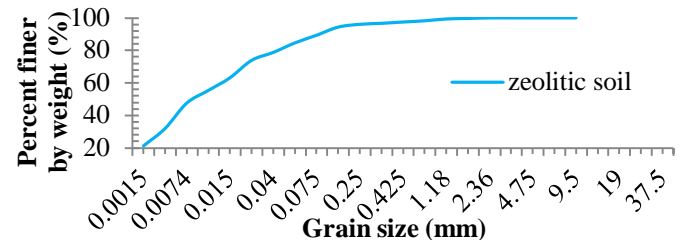
Fig. 2: Zeolitic soil grain size distribution curve

The BS was prepared with relatively low water content through the testing phases and was lightly compacted in simulation of in-situ conditions of natural soils. The

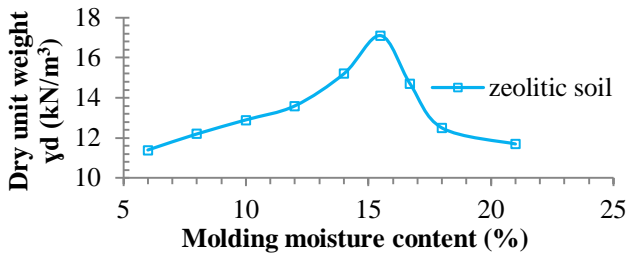relationship between the permeability and dry unit weight of the natural soil is presented in Figure 4.

Fig. 3: Zeolitic soil compaction curve

The permeant used was scooped from the leachate basin at the landfill. The basin was designed to hold generated leachate formed by decomposition of waste, infiltrated storm water and/or intercepted surface water in contact with the waste body on site as seen in Figure 5. The leachate was sampled from different points within the basin and vigorously stirred to ensure a proper leachate composition.
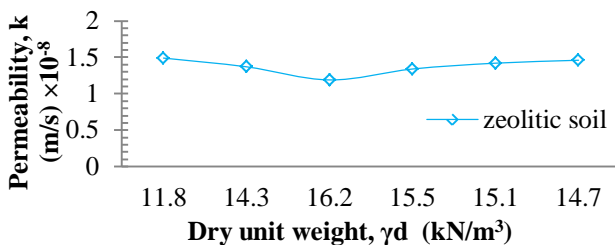

Fig. 4: Permeability variation of zeolitic soil

From the chemical analyses of the sampled leachate, Table 1 gives the initial concentrations (mg/l) of the targeted contaminant specie. The cationic contaminants were of interest to the study based on their ion exchange behaviours when permeating charged clay surfaces used as buffers. Also, establish closure for the obtained results herein and in similar works by the authors (Agbenyeku and Akinseye, 2015; Agbenyeku et al., 2014a, b; 2013a, b).

Fig. 5: Permeate sampled from leachate basin

Full spectral analysis method was used to measure the cation content on both the leachate influent and effluent which was compared to the South African standard of drinking water in consonance with Water Services Act No. 108 of 1997 and ASTM D-5673.

Table 1: Analysis of leachate for soil compactibility test

Parameter	ASTM Test	Conc. (mg/l)	Drinking water standard (mg/l)[*]
Mg	D 511	25	145
Ca	-	170	200
K	D 4192	18	-
Na	D 4191	130	250

Source: [*](Water services authorities South Africa, 1997)

Noting the complexity and nature of the contaminant species capable of being formed from the degradation of solid waste in landfills, the scarcely available spectral testing materials made it possible to detail a few compositional features and characteristics of the products. As such, cation tests for intrusion and retention of selected ions in the cores of the BS from the leachate was done. Generally, the selection of the cation species was based on: (i) the availability and concentration of the ions present in the leachate generated at the landfill and; (ii) the potential hazardous impact expected in the case of the contaminant escape to subsurface regions. As such, the parameters analyzed were the dominant intruding cations at the landfill i.e., the alkali metals (Group IA) and the alkaline earth metals (Group IIA) e.g., Na and K, Ca and Mg respectively. On the fabricated test device, the leachate reservoir was marked to hold a constant head of 250 mm throughout the testing. A pictorial and schematic view of the fabricated device is shown in Figure 6 (a) and (b).

The device comprises of three sections:

(1) the bottom part called the buffering section; which contained the natural soil strata acting as the natural earth/BS below the geo-composite system as seen in Figure 7.
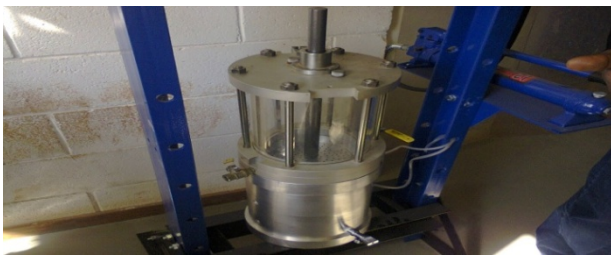
(a) Pictorial view
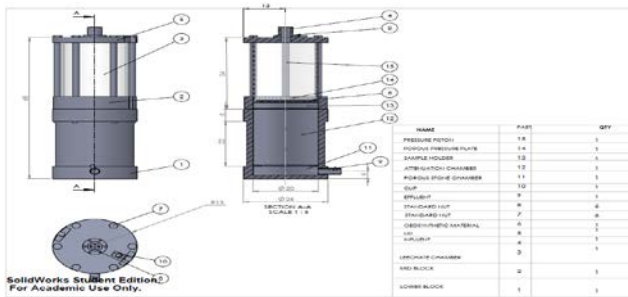
(b) Schematic view

Fig. 6: (a) and (b) Fabricated column device

(a)   (b)

**Fig. 7:** (a) Hydrated geotextile on porous stone to prevent outlet clogging (b) Lightly rammered BS to simulate loosed subsoil

(2) the mid-block called the sample carrier; which contained the designed geo-composite barrier (natural soil as CCL and failed PP membrane) overlying the buffering section as shown in Figure 8 (a) and (b), and (3) the upper part above the geo-composite barrier; which functioned as the leachate reservoir as displayed in Figure 9 (a) and (b).
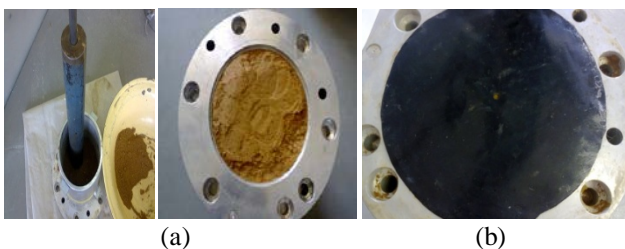
(a)   (b)

Fig. 8: (a) Compacted soil (as CCL) in sample carrier (b) Failed PP with 5 mm centred puncture overlain the CCL

Soil layers were prepared in the bottom section, the mid-block sample carrier and the failed PP membrane was placed over the soil layer. O-rings, gasket corks and silicon sealants were used to ensure an airtight and leakage free connection in the assembled device. The hydraulic frame was set up (for tests which required loading), the leachate was then added and the desired load was imposed. The vertical hydraulic conductivity, k_z value, in stratified soil (hydraulic conductivity of a barrier-BS) was calculated and used to determine the permeation rate, Q.

(a)   (b)

Fig. 9: (a) Leachate in reservoir (b) Loaded barrier

In the first test conducted no load was imposed on the system. Subsequently, samples collected from six sectioned cores of the BS were tested and measured for concentration of target source ions in the pore water using pulverized pore fluid extraction method and silver thiourea method. The analyses were done by using the 902 Double Beam Atomic Absorption Spectrophotometry as specified by Laboratory Manual EPS, 2011.

3. RESULTS AND DISCUSSIONS

3.1. Leachate Permeation Test

Outside confirmatory tests conducted in the course of the study, one major compactibility test was eventually adopted. Table 2 gives a clear summary of the test features initiated for the study. The conditions, durations, constituents and material characteristics properties under which the testing procedures were carried out are duly recorded. The observed leachate-soil interaction from

permeation behaviours through the failed barrier under loading and non-loading effects are also recorded herein.

Table 2: Test features initiated in the study

| Parameters	Properties
MDUW (kN/m^3) of barrier (CCL)	17.1
MDUW (kN/m^3) of Buffer (BS)	12.8
Geosynthetics	2mm thick PP
Puncture size, type and position	5mm failure
Pressure (kPa)	0→25→50→100→150
Test duration	≤100days

Test to ascertain the cation concentrations and permeation through the BS was done. The mechanism of cationic contaminant permeation through the barrier and the buffering behaviour of the zeolitic soil to the cations were also investigated. At the end of every test, measurements and analysis were done. The results of the permeation rates through the barrier system are graphically shown in Figure 10 (a) to (e). Hydrated geotextile over the porous stone acted as filter in preventing fines from clogging the outlet of the chamber. The effluents from results showed steady increase over the test periods. It was observed that steady or quasi steady state was reached in approximately 20 days into the tests and the permeation rates were measured up to 25 days. The permeation rate, Q, for p = 0 kPa was seen to slowly increase to a steady value as seen in Figure 10 (a).
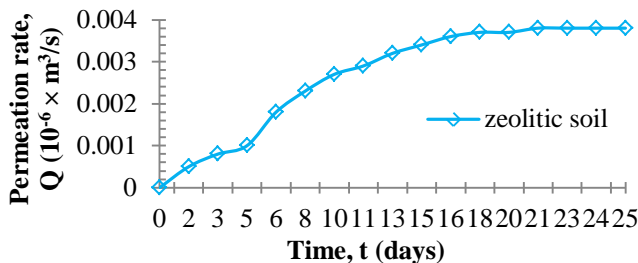
Fig. 10: (a) Permeation rate VS time for p = 0 kPa

However, with the imposition of load to the system as shown in Figure 10 (b) to (e), the permeation rates were observed to reduce. The first pressure, p, of 25 kPa was imposed on the system and steady state was reached after roughly 18-20 days as shown in Figure 10 (b) and the permeation rate was monitored and measured for a duration up to 23 days.
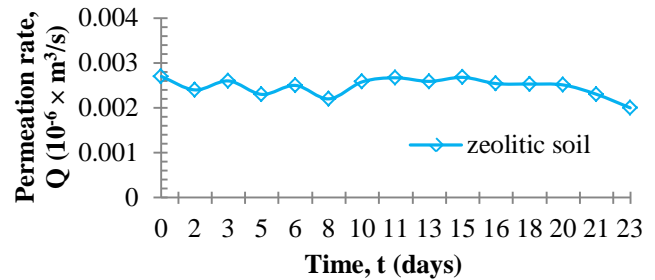
Fig. 10: (b) Permeation rate VS time for p = 25 kPa

For more investigation on the effect of pressure on the system's permeation rate, the load was increased from 25 to 50, 100 and 150 kPa respectively. This was done to closely simulate the waste load imposing the barrier of the visited landfill. The permeation rate was measured for respective loadings. The measured relationship between permeation rates, Q, versus time, t, for loads of 50-150 kPa are shown in Figure 10 (c) to (e). An increasing pressure on the membrane showed the permeation rates to gradually reduce to a steady value.
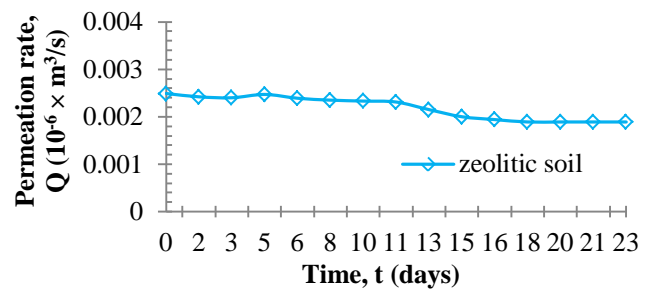
Fig. 10: (c) Permeation rate VS time for p = 50 kPa
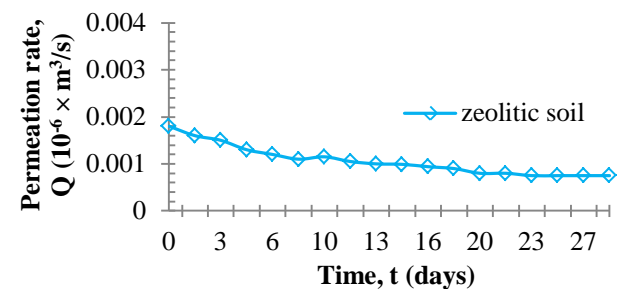
Fig. 10: (d) Permeation rate VS time for p = 100 kPa
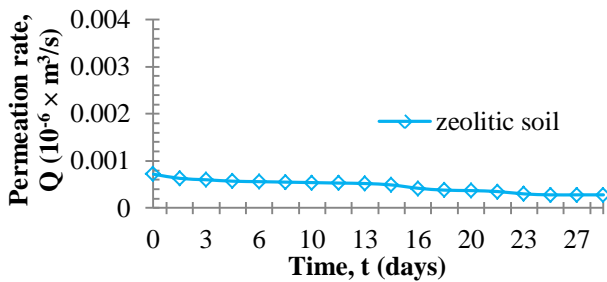
Fig. 10: (e) Permeation rate Vs time for p = 150 kPa

Figure11 therefore, reveals the relationship between the measured permeation rates, Q, versus the pressure, p.
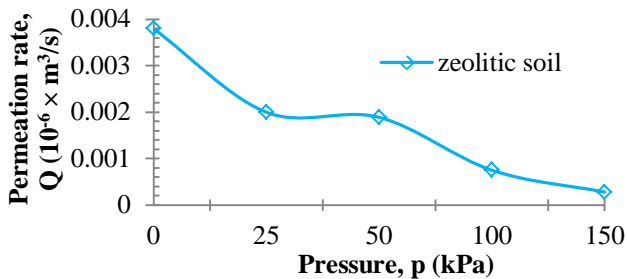
Fig. 11: Permeation rate VS pressure values

The changing loads induced a change in density which caused a decrease in the permeability of the soil barrier. Also, the applied pressure created a fair contact between the PP membrane and the soil barrier thereby reducing the interface transmissivity; reducing the interface thickness and transmissivity, θ, which plausibly explains the gradual decrease to a steady state of the permeation rates, Q.

3.2. Zeolitic Mineral Buffer of Permeating Cations

The leachate formed by decomposition of buried solid waste at sanitary landfills is often associated with appearance of substantial concentration of major cations. These cations in certain concentrations could pose threats to ground water quality. Nevertheless, analysis of the pore fluid chemistry of the studied zeolitic soil revealed the pore fluid to be rich in Na ions while other cations such as K, Ca and Mg were present only in low concentrations. The cations present in the leachate solution are believed to have originated from the decomposition of the dumped

refuse as well as the dissolution of minerals in the soil top cover at the landfill. Results from the permeation compactibility test confirmed a degree of buffer to the selected cations; which were contained in the leachate as they permeated through the BS of the zeolitic soil. This implied that the selected cations, in a mineral-water system do not permeate in any peculiar manner through the cores of the natural zeolitic BS. The major cations were plausibly buffered mainly by cation exchange replaceability caused by isomorphic substitution since clay particles usually possess negative charges. The counter ions (for negatively charged surfaces, i.e., cations or positive ions) are attracted and accumulated close to the charged surfaces. As such, there was no significant permeation of the selected cations through the soil cores as they were mostly retained at the surface of the BS. Other processes which could also be responsible for the buffering of cations are; electrostatic adsorption (physical sorption) and/or incorporation into the structure lattice (chemisorptions). The effluent relative concentration for the cations with respect to the pore volume for the permeated zeolitic soil after reaching steady state is shown in Figure 12.
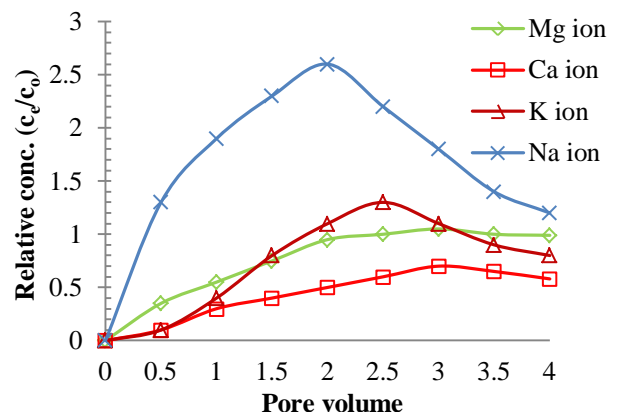

Fig. 12: Cation relative conc. (Co and Ce = initial and final conc.)

The amount of reduction observed in the concentration of a given element as it permeated the soil core was reflected

by the; (i) shift of the breakthrough curve towards higher pore volume passages and (ii) extent to which relative concentration remained below unity i.e. $(Ce/Co \neq 1)$.

In this study however, negative buffer or elution of Na^+ from the zeolitic tested soil was observed after pore volume passages of permeates. The relative concentration value greater than 1.0 is an indication that Na^+ eluted from the system at higher concentration than those of the effluent leachate. In the permeation compactibility tests, collected leachate cationic contaminants permeated the zeolitic soil cores with and without loading effects. Generally, the natural zeolitic soil exhibited fair to good buffering tendencies toward the permeating cationic pollutants through the BS. The permeation profiles depth for the natural zeolitic soil is therefore displayed in Figure 13 (a) to (d) for the respective selected cations.
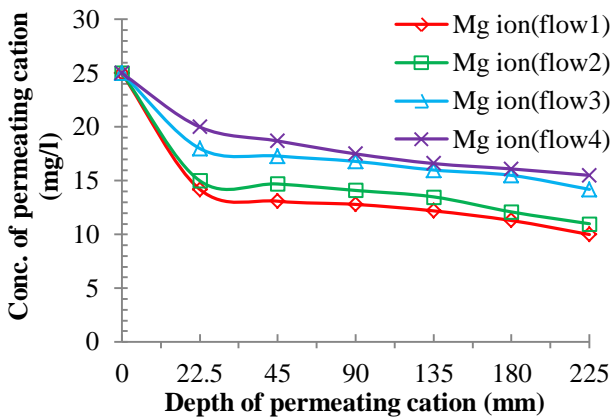
Fig. 13: (a) Permeation profiles of Mg ion through the BS

Soil ion exchange sites are capable of exchanging certain ions within soils as ions in leachates permeate the soil cores. This ability is also seen in various natural systems such as living cells, proteins, cellulose and resins. The synthetic resins are primarily used for purifying water, but also for various applications including elemental separations.
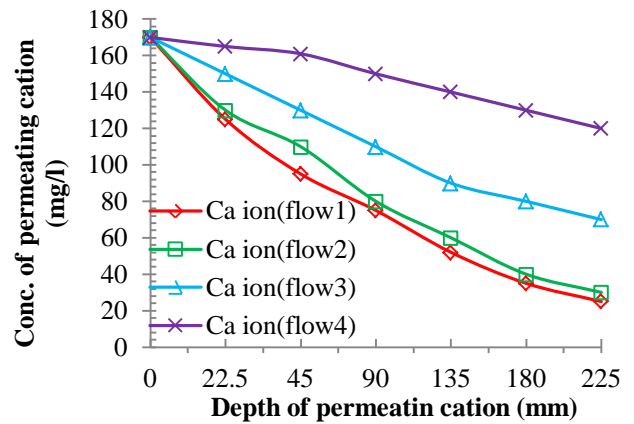
Fig. 13: (b) Permeation profiles of Ca ion through the BS

In the Na^+ elusion process, the permeating leachate is softened as it percolates the cores containing Na^+ cations but binds Ca^{2+} and Mg^{2+} more strongly than Na^+. The cores take up Ca^{2+} and Mg^{2+} and releases Na^+ thereby making for a 'softer' effluent. It was therefore noted that the reasonable buffer found for the measured selected cation species were due to factors such as; (a) properties of the soil (b) characteristics of the solution transport system and (c) reactions of the specific contaminants that determine the shape of the breakthrough curve of the permeating cation species. Ideally, only a few of these characteristics are primarily responsible for the rate of permeation that determines the final shape and the breakthrough point.
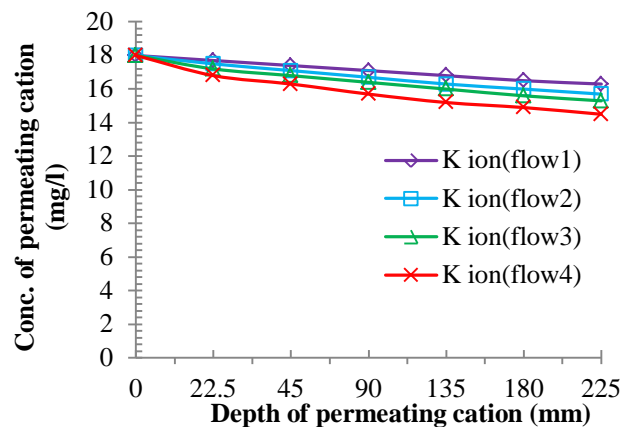
Fig. 13: (c) Permeation profiles of K ion through the BS

Therefore, the study examined the effects of soil cation exchange capacity on the cations species buffering properties. Cation exchange resulted in the storage of some cations on the exchange sites on the clay surfaces and the release of other cations to the pore fluid solution as seen in the breakthrough curves for the respective cationic contaminant species as shown in Figure 13 (a) to (d).
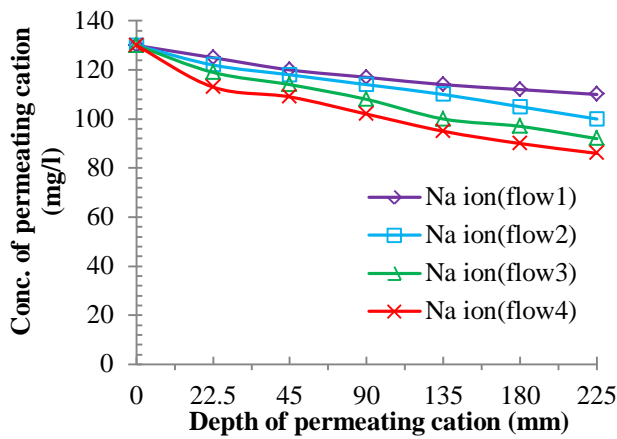
Fig. 13: (d) Permeation profiles of Na ion through the BS

The quantities of cations exchange along the flow path were estimated by determining: (i) the cation-exchange capacity of the clay soil matrix in the leaching system and (ii) the chemical equilibrium between the input cations and the exchangeable ones. The changes in the net storage of cations on exchange sites in the buffering system were also estimated using standard mass balance and mass-action relations, as well as selectivity coefficients. This was done to investigate the reasonable ability of the tested zeolitic clay mineral barrier as buffer towards permeating cationic contaminants often generated from the decomposition of waste in landfills.

4. CONCLUSION

An investigation on a geo-composite barrier under leachate permeation from a failed PP was conducted with a fabricated laboratory device. Loading effects on permeation rates, permeation and buffering of cationic pollutants (Mg, Ca, K and Na) were studied. From results and analysis, the following conclusions were reached:

o The increase in load on the barrier system caused significant reduction in permeation rates; which implied that the reduction was due to reduced membrane-soil interface transmissivity, θ, and densification of the barrier.

o The tests with failed PP revealed interface flow between the membrane and soil barrier; which indicated that a perfect membrane-soil barrier contact was not achieved.

o The results from the permeation compactibility test and analysis of pore fluid concentration of the permeated cations confirmed the flow through the membrane-soil interface.

o The concentration of cation contaminants in the sectioned cores of the BS after the permeation test showed the natural zeolitic soil to have fair to good buffering capacity towards the pollutants; showing that significant amounts of the selected cations were retained in surface of the BS of the zeolitic soil.

o The Na^+ was eluted from the system at high concentrations; which indicated the possibility that sodium was replaced with calcium and magnesium in the exchangeable sites of the zeolitic profile/charged soil surface. However, further study is recommended on the buffering of other pollutant species not addressed by the study using zeolitic mineral barriers.

In summary, the buffering of cation contaminants is mainly by cation exchange replaceability caused by isomorphic substitution of negative charges in clay particle surfaces. This study has therefore demonstrated that the zeolitic soil used in the experimental works to contain the generated landfill leachate can tolerably buffer the selected contaminant species. Consequently, the data obtained have

demonstrated that the tested soil can release potential contaminants under permeation of leachate as in the case of the eluted sodium ion. Hence, it is noted that the buffering capability of the zeolitic soil is not infinite. As such, care must be taken since high permeation of cationic pollutants to vital regions can pose consequential effects of deteriorating groundwater quality.

ACKNOWLEDGEMENTS

REFERENCES

Agbenyeku E.E. & Akinseye S.A. (2015) Leachate Percolation through Failed Geomembrane of a Geo-Composite Soil Barrier *World Journal of Environmental Engineering, 2015, Vol. 3, No. 2, 52-57.*

Agbenyeku E.E. Muzenda E. & Msibi I.M. (2014a) "Zeolitic Mineral Liner as Hydraulic and Buffering Material", International Conference on *Earth, Environment and Life sciences* (EELS-2014) Dec. 23-24, 2014 Dubai (UAE).

Agbenyeku E.E. Muzenda E. & Msibi I.M. (2014b) "Buffering of TOC-Contaminant Using Natural Clay Mineral Liner", International Conference on *Earth, Environment and Life sciences* (EELS-2014) Dec. 23-24, 2014 Dubai (UAE).

Agbenyeku E.E. Okonta F.N. & Ojuri O.O. (2013a) Leachate Flow through Composite Barrier from Defected Geomembrane. 2nd African Regional Conference on Geosynthetics, Accra, Ghana, 18-20 November (CD ROM).

Agbenyeku E.E. Okonta F.N. & Ojuri O.O. (2013b) Evaluation of Empirical Equations for Leachate Migration through Composite Barrier with Defected Geomembrane. 2nd African Regional Conference on Geosynthetics, Accra, Ghana, 18-20 November (CD ROM).

American Society for Testing and Materials (2006) Standard Test Method for Permeability of Granular Soils (Constant Head). ASTM D-2434.

American Society for Testing and Materials (2010) Standard Test Method for Elements in Water by Inductively Coupled Plasma-Mass Spectrometry. ASTM D-5673.

American Society for Testing and Materials (2012) Standard Test Methods for Laboratory Compaction Characteristics of Soil Using Standard Effort (12 400 ft-lbf/ft^3 (600 kN-m/m^3)). ASTM D-698.

Bouazza A. Zornberg J.G. and Adam D. (2002) Geosynthetics in waste containment facilities. Recent advances, Proceedings 7th International Congress on Environmental Geotechnics, Delmas, Gourc and Girard (eds), pg: 445-507.

Department of Water Affairs and Forestry (2005) Minimum Requirements for Waste Disposal by Landfill. Third Edition, Retrieved 04 July, 2013, from: http://www.dwaf.gov.za/Dir_WQM/Pol_Landfill.PDF.

Environmental Impact Assessment Regulations (2005) Waste Collection and Disposal. Retrieved 07 May, 2012, from: http://www.dwaf.gov.za/Dir_WQM/Pol_Landfill.PDF.

Goodrich M. (2000) "Beam by Beam," *Recycling Today,* December: 48-52.

Rowe R.K. (2011) Systems engineering; the design and operation of municipal solid waste landfills to minimize contamination of groundwater. Geosynthetics International, September, 18 (6), pg: 319-404.

Water Services Act No. 108 (1997) Monitoring requirements and regulations of the South African National Standard (SANS). 241 Drinking Water Specification.

Development of an Optimal Reconfiguration Model for Radial Distribution using Enhanced Particle Swarm Optimization

Abubakar A. S [#1], [*2], Sadiq. B. O, Salisu S, Okafor E and Kabir M. T

[#]Department of Electrical and Computer Engineering, Ahmadu Bello University, Zaria
Nigeria
[1] abubakaras@abu.edu.ng , 08067910975

ABSTRACT
The paper present an efficient approach to solving the problem of reconfiguration considering active power loss, total voltage deviation for a typical distribution network. The method developed is based on selective particle swarm optimization technique to determine the optimal location of tie and sectionalizing switches, with a view to yield an optimal performance for the network. The reconfiguration model was implemented and simulated using matlabV7.0. The efficiency and validity of the proposed model was tested on a standard 33 IEEE-Bus distribution network, with a reduction of 36.4 % in active power loss as compared to the initial configuration. The feasible switching state of 7, 9, 14, 28 and 31 as compared to its base case of 33, 34, 35, 36 and 37.

Keywords:_Selective particle swarm optimization, Optimal, elitism, feasible switching state, tie and sectionalizing Switches_
.

1.0 INTRODUCTION

The problem of minimizing distribution systems losses has been a major focus for researchers and utility companies due to the need of better quality of service and better utilization of available energy(Charlangsut A, 2012). Researchers working under the field of distribution system automation have adopted the use of different technique and approaches in reducing the losses in a given network. There are different techniques for reducing losses within the distribution level which include reconfiguration, capacitor placement, load balancing, introduction of higher voltage level and reconductoring (J, A, & Y, 1994; Y, Mekhamer, M, & L, 2012). These methods of reducing losses are quite numerous but the major concern is about their technical implications on the network. Introduction of new equipment at distribution level offers tremendous financial burden on the utilities that cannot be justified by the potential saving. The use of fixed compensators offers optimal reduction in losses for specific demand condition, but the control systems required are very expensive (J, A, & Y, 1994). The choice of reconductoring is not an option due to the cost associated with relaying the feeder, while

the introduction of higher voltage level requires upgrading the rating of the transformer and other equipment in the network (J, A, & Y, 1994). The problem of reconfiguration of distribution network has been explored in this work due to its flexibility, ability to use existing equipment and other pragmatic approaches to offer dynamic means of reducing losses within the distribution level. Distribution systems are designed as radial systems in which tie (NO) and sectionalizing switches(NC) play a critical role in determining the configuration of the system(V & S, 2012). Therefore reconfiguration of the distribution network is the process of altering the topology of the distribution network implemented via manoeuvring the position of normally closed and normally open (C, 2002). Due to the candidate switching combinations in the distribution system, reconfiguration is a complicated combinatorial, non-differentiable constrained optimization problem (Y. Mekhamer M et al. 2012). The reconfiguration problem is one of the multi criteria and multi objective optimization types, where the solution is chosen after the evaluation of some indices such as active power loss, reliability indices, branch load limit and voltage drop limit which represent multiple functions. These criteria can be grouped into

objective functions that can be minimized and the constraints that must be included with some bounds while some criteria are often modelled along with their objective functions(Tomoigo. B, 2013). Many techniques such as branch and bound, analytic approach, heuristic, expert system, linear programming, artificial intelligence etc have been developed by numerous researcher. The earlier reconfiguration problems were mostly represented by a single objective (J, A, & Y, 1994)(E & F, 1989; Nara. K, 1992). The major issues with works (J, A, & Y, 1994;V & S, 2012;C, 2002;Tomoigo. B, 2013;Nara. K, 1992) formulates the problem as a single objective function aimed at reducing the active power losses in the network and the results do not guarantee an effective solution. The works in (C, 2002),(Kumar. Y, 2006; Royteleman. I, 1995; Yang. J, 2012) addressed the problem using multi-objective approach. The major limitations of some of this approaches are transforming the multiple cost function into single objective function by using weighted parameter which are highly subjective, thus avoiding the complexity associated in solving a typical multi-objective problem. The advent and increasing connectivity of distributed energy sources to distribution network, has necessitated the need to consider other parameters that are critical to the network (total voltage deviation, reliability index, expected energy not served). This work addressed the problem of distribution network reconfiguration using particle swarm optimization considering active power loss and total voltage deviation as the objective functions, within a reasonable convergence time. The rest of this work is organized as follows: Section II formulate the problem of reconfiguration, section III, described the concept of the particle swarm optimization technique. Section IV detail of the developed methodology, Section V validation of the developed approach using standard 33-Bus IEEE distribution network. Section VI result, discussion and conclusion.

1.1 Formulation of the Problem

This work adopted the use of active power loss

 A. Minimization of total power losses,

 B. Maximization of voltage profile

A. Minimization of Total Power Losses

The power loss reduction is the primary aim of the reconfiguration of the distribution system. Hence it is considered as the main objective function. The power loss reduction can be expressed in terms of current variable by using:

$$P_{Loss} = \min \sum_{i=1}^{N-1} kI^2(i)R(i) \quad (1)$$

B. Minimization of Total Voltage Deviation

This bus voltage describes the security and service quality indices for the distribution system. The total voltage deviation is described by:

$$TVD = \min \sum_{i=1}^{N} (V_{rate} - V_i) \quad (2)$$

Lower value of TVD, indicate a higher quality voltage profile and better security of the considered network configuration.

Constraint

 i. Branch current limit

$$I_{\min}(i) \leq I(i) < I_{\max}(i) \quad (3)$$

 ii. Power Flow constraint

$$f(P_i, Q_i, V_i, \theta_i) = 0 \quad (4)$$

 iii. Radial structure constraint

1.2 Concept of Particle Swarm Optimization

The particle swarm optimization was formulated by Edward and Kennedy in 1995. The pso algorithm was inspired by social behavior of animals such as fish schooling and bird flocking(Haupt. L. R, 2004). The

algorithm was found to be suitable in solving non-linear optimization problem and has a distinctive feature of utilizing few parameters(Tamer. M. Khalid, 2012). There are different version of particle swarm optimization that aim to extent its area of applicability in searching for a selected space domain(Khalid. M. Tameer, 2012). For each dimension search space, the velocity and position for each particle and the best position for all particles are presented by vectors and described by the vectors in equations (5-8) respectively (Khalid. M. Tameer, 2012):

$$\mathbf{X}_i = [X_{i1,}......X_{id}] \quad (5)$$

$$V_i = [V_{i1,}......V_{id}] \quad (6)$$

$$Pb_i = [Pb_{i1}......Pb_{in}] \quad (7)$$

$$Gb_i = [gb_{i1}........gb_{in}] \quad (8)$$

At each iteration, the velocity and position of the particle in d-dimensional are updated by using equations (9-10) (Haupt, L. R. 2004;Tamer. M. Khalid, 2012):

$$\mathbf{V}_{id}^{k+1} = wV_{id}^{k} + C_1 r_1(Pb_{id}^{k} - X_{id}^{k}) + C_2\, r_2(gb_{id}^{k} - X_{id}^{k}) \quad (9)$$

$$X_{id}^{k+1} = X_{id}^{k} + V_{id}^{k+1} \quad (10)$$

Where $i = 1.....n$: n is the Set particle swarm population $pop = [\mathbf{X}_1.....X_n]$; V_i is the Velocity of particle; Pb_i is the position of particle: Gb_i is the best position of particle; w is the inertia weight; $C_1\, C_2$ are the acceleration constants or learning factor; $r_1 r_2$ are the random values ranging [0,1]. In the works of (Haupt L. R, 2004)(Kennedy. J, 1997) have adopted PSO to search the binary spaces by applying sigmoid transformation to the velocity and the positions of particle components to a range of 0-1. This work employed a similar technique adopted in the works of (Tamer. M. Khalid, 2012);Khalid. M. Tameer, 2012) to constrain the search within each d-dimension of the search space $S_d = [s_{d1}, s_{d2},...s_{dn}]$.

Where dn is a set of selected positions in dimension d. The velocity and particle position are highlighted in equations (11) and (12)(Tamer. M. Khalid, 2012);Khalid. M. Tameer, 2012):

$$sigmoid(v_{id}^{k+1}) = dn \frac{1}{1 + \exp(-v_{id}^{k+1})} \quad (11)$$

$$x_{id}^{k+1} = \begin{cases} s_{d1}, if\ sigmoid\ \exp(-v_{id}^{k+1}) < 1 \\ s_{d2}, if\ sigmoid\ \exp(-v_{id}^{k+1}) < 2 \\ s_{d3}, if\ sigmoid\ \exp(-v_{id}^{k+1}) < 3 \\ .... \\ s_{dn}, if\ sigmoid\ \exp(-v_{id}^{k+1}) < n \end{cases} \quad (12)$$

The velocity values are to restrain $\begin{bmatrix} V_{min} & V_{max} \end{bmatrix}$ using equations 13-14.

$$v_{id}^{k+1} = \begin{cases} V_{max}, if\ v_{id}^{k+1} > V_{max} \\ v_{id}^{k+1}, if\ |v_{id}^{k+1}| \le V_{max} \\ V_{min}, if\ v_{id}^{k+1} < V_{min} \end{cases} \quad (13)$$

$$v_{id}^{k+1} = \begin{cases} rand \text{ x } v_{id}^{k+1}, if\ |v_{id}^{k+1}| = |v_{id}^{k+1}| \\ v_{id}^{k+1} \qquad\qquad \text{otherwise} \end{cases} \quad (14)$$

2.0 Developed Approach

The methodology adopted for this work is based on selective particle swarm optimization technique, due to its robustness and the need for selecting few parameter (Haupt, L. R. 2004; Khalid. M. Tameer, 2012. The developed approach is similar to the works of (Yang. J, 2012;Tamer. M. Khalid, 2012) but consider all the tie switches regarding of their duplication in any loop. The status of the normally open switches are considered and tested on a standard 33-Bus IEEE distribution network as contained in Figure 1. The detail steps are outlined as follows:

i. Close all tie switches or normally open switches to form a five (5) loop or mesh network as shown in Table 1.

ii. Determination of possible branches that constitute each loop or mesh network.

iii. The number of branches in each loop constitute the search space dimension.

iv. Generation of random search space based on the numbers of element in each loop or dimension.

v. Constraint checking is perform to ensure that generated particle are void from loops and possible islanding. The constraint check comprises of checking for loops, islanding, searching the network to ensure that generated population have radial structure while ensuring load flow solution.

vi. Evaluation of the fitness functions as contained in equation (1) and (2).

vii. Update the velocities, positions for each dimension using equations (9), (11) (12) (13) and (14).

viii. Increase the number of iteration and perform steps iv-vii.

ix. If the stopping criteria are meet, terminate process.

The Flow chart of the developed approach is shown in Figure 2
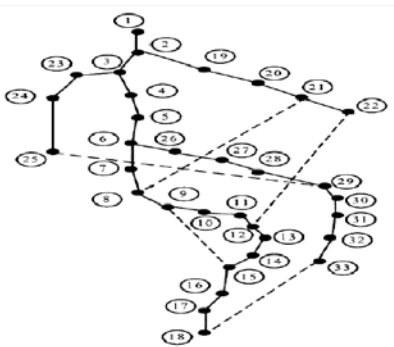
Figure 1: Standard 33-Bus Distribution Network

Figure 2: Sequential Steps of the Developed Approach Test Systems

The test system as shown in Figure 2 is a 12.66kV, 33-bus standard IEEE distribution network with 32 branches and 5-tie lines (33, 34, 35, 36, 37), and the detail of the line and load data is contained in the work (L, 2009). With the tie or normally open switch closed the number of branches that constitute the loops is contained in Table1. The simulation parameters are similar to the work of (Yang. J, 2012; Tamer. M. Khalid, 2012) with $c_1 = c_2 = 2$, $[V_{min} \quad V_{min}] = [0.9, 1]$, number of generation =30 population size= 20 and inertia weight $w = 0.9$.

Table 1 Number of Loops in standard 33-Bus Network

Loop Number	Branches
Loop1/Sd1	2, 3, 4, 5, 6, 7, 33, 20, 19, 18
Loop2/Sd2	8, 9, 10, 11, 35, 21, 20, 19, 18, 2, 3, 4, 5, 7
Loop3/Sd3	37, 28, 27, 26, 25, 5, 4, 3, 22, 23, 24
Loop4/Sd4	9, 34, 14, 13, 12, 11, 10
Loop5/Sd5	25, 26, 27, 28, 29, 30, 31, 32, 36, 17, 16, 15, 34, 8, 7, 6

RESULTS AND DISCUSSIONS

Discussion

Figure 3 shows a plot of the active power loss as a function of number of 30 iteration. The optimal location of the tie switches was found to be 7, 9, 14, 28 and 31, with reduction of 36.4% (129.2163kW)in active power loss as compare to the active power loss (202.8kW) of the initial configuration after reconfiguration. This reduction in active power loss is accompanied with an improvement in the total voltage deviation via a minimum voltage of 0.9354V as compared to the initial configuration of 0.914V.
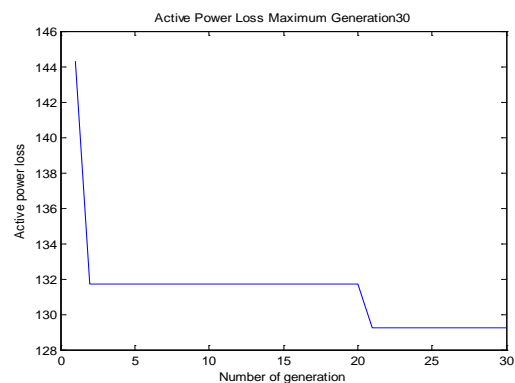
Figure 3 Active power loss Vs Number of iteration

The developed approach was compared with other standard developed model as a means of validation as contain in Table 2. The result shows that the developed model is in conformity with other works

CONCLUSION

This work has presented a reconfiguration model based on selective particle swarm algorithm considering active power loss in a distribution network to determine the optimum switching state of the network. Based on results obtain the real power losses are reduced significantly with a corresponding improvement in voltage profile as such enhancing the security of the distribution network.

| 33 Bus System	Switching state	Base Active Power Loss (kW)	Active power Loss (kW)	% Improvement in Power Loss
Initial configuration	33 34 35 36 37	202.8	202.8	
Baran and Wu, (1989)	7 9 14 32 37	202.2	139.5	31.01
Srinivasa et al.,2009	33 14 8 32 28	202.71	135.7	33.01
Moshtagh and Ghasemi, (2013)	37 32 14 9 7	203.45	140.17	31.10
Rashtchi and Pashai (2012)	32 14 9 37 7	199.3	136.5	31.51
Tameer and Alexandra, (2012)	7 9 14 37 32	203	139.5	31
Developed Approach	7 9 14 28 31	202.8	129.2163	36.4

REFERENCE

C, H. Y. (2002). Enhanced Genetic Algorithm-based Fuzzy Multi-objective Approach to Distribution Network Reconfiguration. *IEEE Proc-Gener-Distrib, 149*(2), 615-620. doi: 10.1049/ip-gtd; 20020512

Charlangsut A, R. N., Auchariyamel. S, . (2012). Heuristic Optimization Techniques for Network Reconfiguration in Distribution System. *64*, 1-4.

E, B. M., & F, W. (1989). Network Reconfiguration in Distribution Systems for Loss Reduction and Load Balancing. *IEEE Transaction on Power Delivery, 4*(2), 1402-1407.

Haupt. L. R, E. S. H. (2004). Practical Genetic Algorithms. *Second Edition John Wiley Publication*, 189-190.

J, S. R., A, M. M., & Y, C. A. (1994). Distribution System Reconfiguration for Loss Reduction: A New Algorithm Based on a Set of Quantified Heuristic Rules. *IEEE Transaction on Power Delivery, 1*.

Kennedy. J, E. R. (1997). A Discrete Binary Version of the Particle Swarm Algorithm. *Proc. IEEE int. conf on systems, man and cybernetics (SMC 97), 5*, 5.

Khalid. M. Tameer, A. V. G. (2012). Selective Particle Swarm Optimization. *International Journal of Multi Disciplinary Sciences and Engineering, 3*(4), 4.

Kumar. Y, D. B. a. S. J. (2006). Service Restoration in Distribution Using non-dominated Sorting Genetic Algorithm. *Electric Power Systems Research*, 8. doi: 10.1016/j.espr.2005.10.008

L, S. R. N. S. V. (2009). A New heuristic Approach for optimal reconfiguration in distribution system. *International Journal of Engineering and Applied Science., 5*(1), 7.

Nara. K, S. A., Kitagawa. M and Ishihara. T. (1992). Implementation of Genetic Algorithm for Distribution Systems Loss Minimum Re-configuration. *IEEE Transaction on Power Systems, 7*(3), 7.

Royteleman. I, M. V., Lee. S. S. H and Lugtu. R. L. (1995). Multi-Objective Feeder Reconfiguration By Distribution Management System. *IEEE Transaction on Power Delivery, 6*(65), 517-522.

Tamer. M. Khalid, A. V. G. (2012). Reconfiguration for Loss Reduction of Distribution Systems Using Selective Particle Swarm Optimization. *International Journal of MultiDisciplinary Sciences and Engineering, 3*(6), 17-18.

Tomoigo. B, M. C., Andreas. S, Antoni. S, and Roberto. V. R. (2013). Pareto optimal Reconfiguration of Power Distribution System Using a Genetic Algorithm Based on NSGA II. *Open Access Journal on energies, 2*(1), 1439-1440. doi: doi:10.3390/en6031439

V, R. V., & S, P. (2012). Network Reconfiguration in Distribution Power system with Distribution Generators for Power Loss Minimization. *International Conference on Advance in Computer and Electrical Engineering*, 5.

Y, A. A., Mekhamer, S. F, M, M. F., & L, B. M. A. (2012). A Modified Particle Swarm Technique for Distribution System Reconfiguration. *Open Access Journal on Electronic and Electrical Engineering, 1*(2), 7.

Yang. J, C. Z., Jian. S, Xu. J and Qi. J (2012). The NSGA-II Based Computation for the Multi-objective Reconfiguration Problem Considering the Power Supply Reliability. *China International Conference on Electricity Distribution, 3*(164), 1-5.

Physical and Mechanical Properties of Raphia (*Raphia farinifera*) Seed essential for Handling and Processing Operations

[*1]O. A. Fabunmi, [1]U. Omeiza [2]B.A. Alabadan

[1]Department of Agricultural and Bioresources Engineering, Federal University of Technology, Minna, Nigeria
[2] Department of Agricultural and Bioresources Engineering, Federal University of Oye-Ekiti, Ekiti State, Nigeria

*Corresponding Author's Email- fabunmifutminna@gmail.com; +2348036730494

ABSTRACT
The knowledge of the engineering properties of agricultural products are essential in processing operation of agricultural produces and also the result obtained can be used in the design of processing machine. In this study, the physical and mechanical properties of raphia seed were investigated using standard methods. The geometric mean diameter and sphericity are 32.85 mm and 50.74 %, respectively. The peak values of force and deformation at break were 12.925 kN and 14.050 mm, respectively. The pressure in cracking the seed in longitudinal position is greater than when placed in transverse or natural position. The results are important in the design of raphia seed oil expelling machine. The engineering properties obtained can be used in the design of processing machines.

Keyword—Physical, Mechanical, Engineering properties, Raphia seed

1. INTRODUCTION

Raphia palm (*farinifera*) is the largest palm in Africa and is restricted to the tropical rain forest, the ideal ecological condition for the Raphia palm (Ndon, 2003). It is one of the most economically useful plants in Africa, the leaves are used for shelter and the stem produces palm sap, which is drank as beverage. The fermented sap could be distilled into alcohol or local gin. Succulent, oily larvae of weevils and beetles are obtained from infected palms and serve as delicacy. The trunk could serve as firewood. The mesocarp of the ripe fruit yields edible oil (Otedoh, 1976, 1990). While the leaf petiole yield the fibrous piassava. In farm structures and design of processing machineries for agricultural bio-materials, knowledge of basic properties of these bio-materials are required. The physical and mechanical properties among others are important in the farm structure and in the design of machine equipments for various

agricultural operations. The physical and mechanical properties are important in the sizing, separating, grinding, and oil extraction machines. Likewise the true density, bulk density and porosity (the ratio of inter granular space to the total space occupied by the grain) are used in design of storage bins and silos, separation of desirable materials from impurities, cleaning and grading and quality evaluation of the products are important factors. The static coefficient of friction of the grinding against the various surfaces is also necessary in designing of conveying, transportation and storage structures. Also the knowledge of moisture content, volume and density play an important role in numerous technological processes and in evaluating product quality during drying and also in the design of silo and other storage structures (Olaniyan and Oje, 2002). Raphia (*farinfera*) is monoecious, meaning that male and

female flowers, which are reddish in colour and have a sharp, prickly tip, are borne on the same plant. The seeds of this palm are variable in size and shape, but are generally large, up to 9.5 centimeters in length, ovoid with a narrow base, and reddish-brown in colour. Each fruit is covered in symmetrical rows of large, shiny, overlapping scales, and contains a curved or spindle-shaped seed. Most raphia palms shed large numbers of seeds, often leading to dense, uniform stands of the same species, although the fruits attract a range of animals which may aid in seed dispersal. Like all palms of this group, Raphia farinifera flowers only leaves once and then dies (Otedoh, 1990).

Raphia *farinifera* occurs in freshwater swamps and on river banks in the Guinea Zone of West and Central Africa. It generally does not tolerate saline conditions; near the Guinea coast it is replaced by raphiapalma-pinus. In some places (e.g. Southern Benin and South-Eastern Nigeria) human activity (cutting of dicotyledonous, trees planting of raphia *farinfera*) has turned natural swamp vegetation into 'rafiales', in which raphia *farinfera* is the dominant species. The soils of Nigerian freshwater swamps are light textured and generally acidic (Aghimien, 1984). Managed stands of raphia *farinifera* are mostly left to rejuvenate naturally by seed. In Nigeria, selected trees are left untapped for this purpose. Occasionally, raphia (*farinifera*) is propagated from seed. The 1000-seed weight is about 25 kg. The germination period may range from 1–24 months, and the germination rate from 30–60%. Young plants are easily transplanted. In nurseries, a spacing of 30 cm ×

30 cm is recommended. It has been claimed that seeds should be sown ventral side upwards, because the embryo is located on this side, but research has shown that seed orientation does not influence germination or seedling growth (Otedoh,1981). In Nigeria, Raphia *farinifera* sometimes serves as support for yams. In Benin, tomatoes, cassava, sugar cane, red pepper and other crops are sometimes grown on earth ridges in raphia *farinifera* swamps.

Flowering in raphia *farinifera* usually occurs only after a prolonged period of vegetative growth, perhaps lasting years, at the end of which a burst of growth causes the central axis of the palm to elongate to four meters or more in height. This is followed by the development of large, complex, branched inflorescences which can reach an impressive three meters in length and which, unusually for this genus are held erect. A full survey of raphia *farinifera* populations has been recommended throughout its range, in order to better assess its conservation status. It has also been suggested that local people should be encouraged to use the more common species raphiafarinifera in building and palm wine production, in preference to raphia *regalis*. Although previous authors (Ndon, 2003) have reported works on the various uses of this exudate but there is however scanty report on the physical and mechanical properties of the raphia seed. The objective of this research is to determine the physical and mechanical properties of the Raphia seed, which will enable the evaluation of its application or its potentials.

2. Materials and Methods

2.1 Sample Preparation

The raphia seed was collected from the fresh water swamp forest of opobo village in Nkoro Local Government Area Council of Rivers State, Nigeria. The seeds was removed from the bunches and left after a week. The epicarp, mesocarp and endocarp was separated, washed and air dried. The seeds are shown in Figure 1.
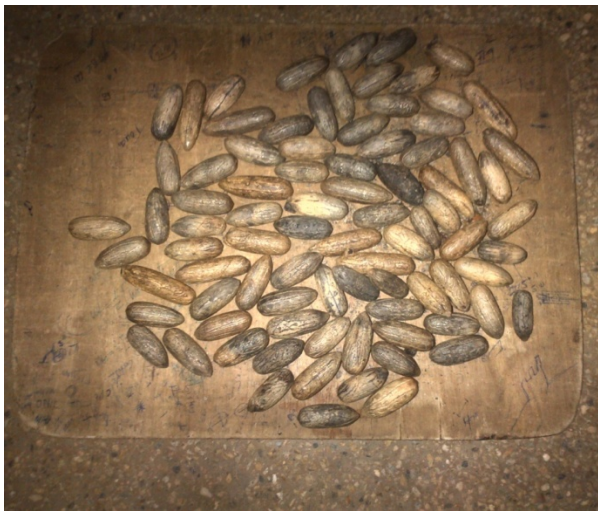

Figure 1: Raphiafarinifera Seeds

2.2 Determination of Physical Properties of Raphiafarinifera Seeds

Hundreds seed weight was measured by counting 200 raphia seed and then weighed in the digital weighing balance of 0.01 g accuracy (Hojat et al 2009). The colour of raphia seed was determined by using reflectivity and absorptivity character of the electromagnetic radiation [e-Radi (zadiac 0034612-2004 Y)] in the Physics Department Laboratory of the Federal University of Technology, Minna. The weight and volume were determined by using electronic weighing balance and toluene (C_7H_8)

displacement method. Toluene was used instead of water displacement method because the seed will not be able to absorb much toluene which can affect both the and volume of the seed engineering properties.The geometric mean diameter of the seed was determined from the major (a).minor (b) and intermediate (c) diameter using the relationship given by Moshenin (1992). The moisture content of a produce simply indicate the amount of water present in that agricultural produce and this is of great importance to both food scientist and agricultural engineers as it helps in determining certain adaptation and resistance to processing stages such as drying, storage, cooking , and consumption. It can be expressed in dry or wet basis. This is a measure of how close the material is to a sphere. The sphericity of raphia seed was determined by obtaining the values of the major, minor and intermediate diameter of the seed.The sphericity was calculated using the formular below (Moshenin, 1992). Surface area is defined as the total area over outside of the seeds. The surface area was measured by wrapping aluminum foil round the seed and cutting the foil into pieces. The pieces was passed through an area meter to find the area of the foil, which represents the surface area of the seeds. The area meter was used to measure only the apparent area of the foil which was not affected by creases in the foil. (Eissa and Gamea 2003). This was determined by weighing 20g of raphia seed which was poured into 250ml graduated cylinder. The cylinder was taped ten times against the palm and placed gently on the table and the final volume was taken. This final volume was used to calculate the bulk density as g/ml. This was done for five replicates and the average was taken (Usuf, et al., 2004). Volume of the seeds was determined by toluene (C_7H_8) displacement method. Toluene was

use as its level of absorption and surface tension was very low compared to water thereby enabling it to flow smoothly over the seed surface (Moshenin, 1992). Toluene was poured into a measuring cylinder of $1000cm^3$. The amount of toluene displaced was determined by hanging each of the seeds in the graduated measuring cylinder and the increase in the weight of the seed was calculated. The mass of each seed was obtained using an electronic balance with sensitivity.This was computed from the obtained values of the true density and bulk density of the raphia seed (Moshenin, 1992). The coefficient of static friction of raphia seed was determined on three different surfaces (plywood, glass and mild steel)for all the three samples. It was determined by filling a hollow plastic box with seeds. The box will be placed on the surface, which was gradually tilted until the box just began to slide down the surface. The angle the surface made with the horizontal was taken. Coefficient of friction (μ) was obtained by finding tangent of the angle. The specific gravity was determined as a function of moisture content by the use of a void meter manufactured by Jecons Scientific Limited, Bedfordshire, England. Raphia seed was placed in the sample jar and water was added to determine the percentage void content by reading value from the scale on the tube. After this, the material was weighed and the mass was recorded. The percentage void content of the sample was computed on the basis of the mass of the sample in the sample jar which was subtracted from the mass of the sample in the jar. The value obtained was used to divide the weight of the sample to obtain the specific gravity.

2.3 Determination of the Mechanical Properties of Raphia Seed

The mechanical properties of the raphia seed was carried out at Federal Institute of Industrial Research Oshodi, (FIIRO) Lagos. The compressive test was conducted using Testometric Machine (ZDM50-2313/56/18, Germany). The Testometric Machine is shown in Figure 2.

Figure 2: M 500- 25KN TESTOMETRIC AX MACHINE.

3   Results and Discussion

3.1   Physical properties of Raphia Seed

The results of the physical properties of raphia seed is shown in Table 1.

The shape of the seed was obtained by tracing the projected boundary outlines of the raphia seed was compared with shape on the charted standard, which gave an oblong shape. The length, width and thickness obtained for the 200 samples of the raphia

seeds were in the range of 52.6-89.5, 20.3-28.3, 12.7-26.1mm with mean values 65.24, 24.57, 22.31 mm respectively. The calculated values of the geometric mean diameter and sphericity ranged from 23.93-37.78 mm and 39.43-60.42 % with mean values as 32.85 mm and 50.74 % respectively. The values were higher than the corresponding values reported for oil bean seed (Oje and Ugbor, 1991), as well as that reported for bread fruit seed (Omobuwajo et al, 1999). The low sphericity and geometric mean diameter of the seed indicated that the Raphia seed is likely to slide rather than rolling. The average thousand seed weight obtained for the seed was 23.39 kg. This result shows the seed has a considerable high weight which can be used as aggregate in farm structures. The average bulk density obtained for the seed was 0.70 g/cm^3 while the true density varied from 0.76- 0.80 g/cm^3 with mean value and standard deviation as 0.80 g/cm and 0.05 respectively. It was observed that the mean value of the bulk density is higher than the true density. The estimated value for the porosity varied from 38.06-39.02 %. The result obtained indicated that there is relatively low level of

void solace in the material which indicated that the seed can be used as aggregate in structural constructions. The porosity of the seed is important because it shows the resistance of the seed to airflow during drying process. The results of the surface area varied from 1495–3844mm with a mean value of 1373.33mm and standard deviation as 987.01. The result indicated that there is high variation in the surface area of the seeds. The of the coefficient of friction obtained on glass surface, sheet metal and wood surface varied from 0.36-0.39, 0.42-0.53 and 0.51-0.53, with mean values as 0.38, 0.49 and 0.52 and standard deviation as 0.01, 0.05 and 0.01 respectively. It was observed that the seed had the highest coefficient of friction on wood surface and the least coefficient of friction on glass surface. This occurred because the least frictional resistance on the glass surface and higher frictional resistance on the wood surface. This property is of paramount importance in determining the steepness of storage container, hopper and any other loading and unloading device.

Table 1: Physical Properties of Raphia Seeds at 20.43% (d.b) Moisture Content

PARAMETERS	Mean values	Maximum values	Minimum values	Standard Deviation
Length(mm)	65.24	89.5	52.6	0.74
Width(mm)	24.57	28.5	20.3	0.13
Thickness(mm)	22.31	26.1	12.7	0.16
Geometric Mean Diameter(mm)	32.85	37.78	23.93	0.17
Surface Area (mm^2)	1373.33	3844.00	1495.00	987.01
Sphericity(%)	50.74	60.41	39.43	3.92
Hundreds Seed Mass (kg)	24.39	24.39	24.39	0.01
Bulk Density (g/cm ^{3})	0.70	0.70	0.70	0.00
True Density (g/cm ^{3})	0.80	0.87	0.76	0.05
Porosity (%)	36.92	39.02	33.86	2.21

Coefficient of Friction				
Glass Surface	0.38	0.39	0.36	0.01
Sheet Metal Surface	0.49	0.53	0.42	0.05
Wood Surface	0.52	0.53	0.51	0.01
Specific Gravity	1.54	1.55	1.53	0.01

3.2 Mechanical behaviour of Raphia Seed

The Table showing the results of some of the mechanical properties raphia seed test carried out are presented in the appendix pages (Tables 2 and 3). This tables present the graphically behavior of the raphia seed under load or force both longitudinally and transversely. With anvil height set on Tensometric Machine for the 200 pieces of raphia seed samples when the seed is placed longitudinally the compressive force at break were 3.08, 4.033, 6.052, 8.000, 10.085, 6.920 and 7.000 kN, while the deformations at break were 9.200, 9.221,9.301,9.302,11.230, 12.225, 13.099, 14.055 and 15.000 mm. Sample B, when the seed is placed transversely, the compressive force at break were 8.023 kN, 9.580, 9.801, 10.022, 12.925, 9.999, 13.501, 13.011 and 12.925kN, respectively. For sample C, when the seed is in its natural position, the compressive force at break were 8.501, 8.520, 10.20, 9.80, 9.60, 9.50, 12.99, 13.80, and 14.41 kN and the deformation at break were 4.80, 5.40,5.70, 5.90, 6.00, 6.20, 6.75, 9.00 and 9.40 mm, while for sample D, when the seed is placed longitudinally were 7.902, 12.510, 12.58, 13.30, 13.400, and 14.100 kN respectively and the deformation at break were 6.580, 8.20, 4.700, 6.750 and 7.510 mm, respectively. Also, for sample E, when the sample is placed transversely the compressive force at break were 6.501, 6.200, 6.000, 6.500, 8.500, and 3.890 kN while the deformation at break were 11.540, 11.580, 12.000, 12.540, 13.530, and 14.050 mm, respectively.

Table 2: Longitudinal Results of Mechanical Properties of Raphia Seed

Test	Force @break (N)	Deformation @Break (mm)	Force @Break (N)	Deformation @Break (mm)
Min	3818.0	11.689	4743.0	11.951
Mean	6258.7	12.682	6792.0	13.077
Median	6482.0	12.664	6862.0	13.375
Max	8530.0	14.259	8124.0	14.035
S.D	1505.4	1.047	1148.8	0.782

The mechanical results of the seeds when it was placed longitudinally i.e. the force @break and deformation @break on the testometric machine.

Table 3: Transverse Results of Mechanical Properties of Raphia Seed

Test	Force @break (N)	Def @Break (mm)	Force @Break (N)	Def @Break (mm)	Force @Break (N)	Def @Break (mm)
Min	3737	9.187	7474	4.8520	8171	5.4850
Mean	6306	11.518	10328	6.5768	11063	6.9028
Median	6484	11.315	9627	6.0560	10065	6.4200
Max	10549	15.002	14281	9.3530	13561	8.9300
S.D	2525	2.355	2451	1.5724	1999	1.3199

The mechanical results of the seeds when it was placed transversely i.e. the force @break and deformation @break on the testometric machine.

Figures 3 to 7 shows that more pressure is expected on the seed samples as it begins to extend towards it axis, thereby causing a break or crack which increase as more load is placed on it thereby giving the rise and fall slope on the graph due to variation of strength within the see product. From the values obtained, it shows that the pressure in cracking the seed in longitudinal position is greater than when placed in transverse or natural position, this can be concluded that increase of storage and bagging, the seed should be placed at longitudinal position because it takes more force to break or crack at longitudinal position compared to the transverse and natural positions. This knowledge is essential for the farm product designers which can be applied in the design process of handling, harvesting machines and storage devices for raphia seed.
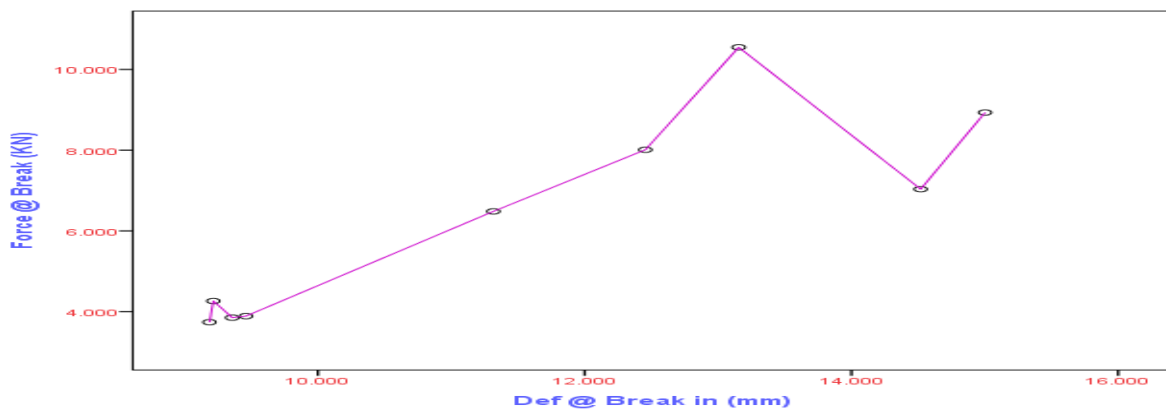
Figure 3: Compressive Force @Break against Deformation
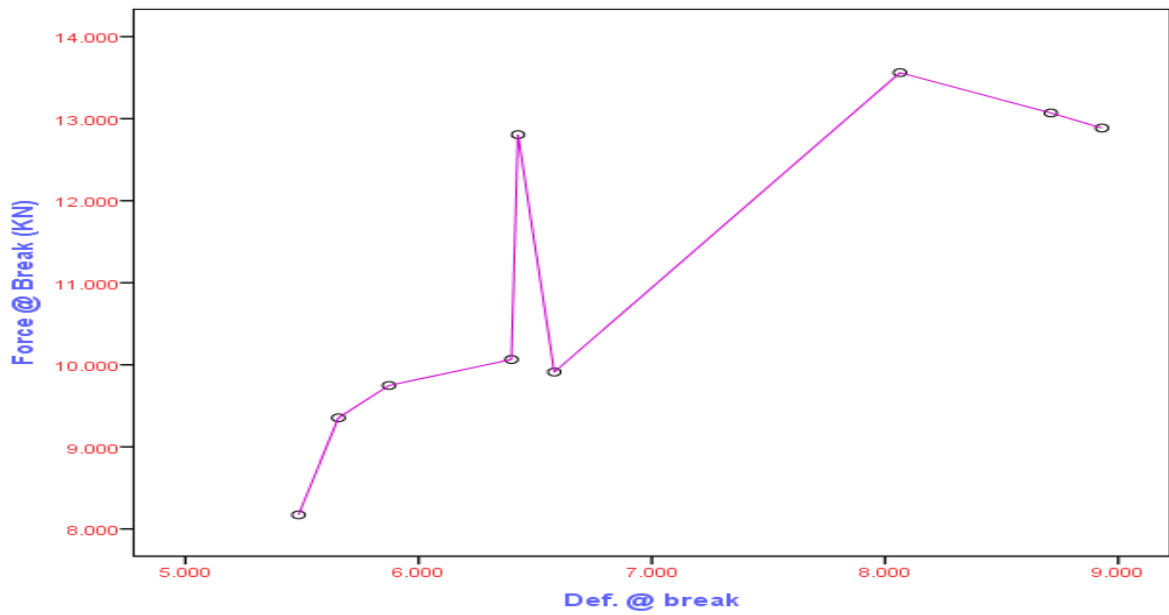
Figure 4: Compressive Force @Break against Deformation
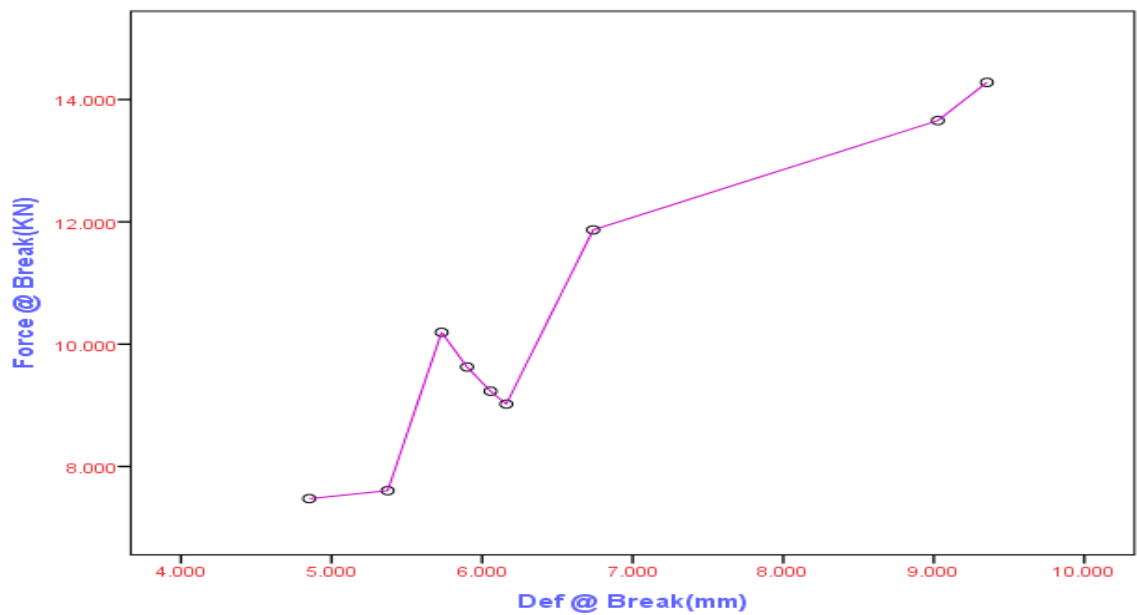
Figure 5: Compressive Force @Break against Deformation
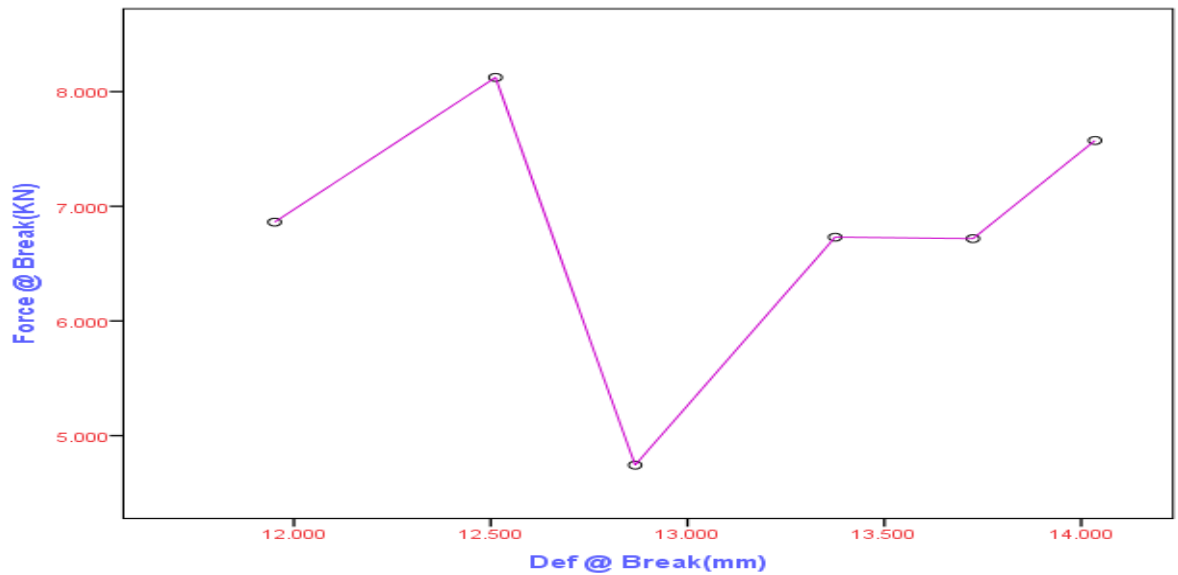
Figure 6: Compressive Force @Break against Deformation
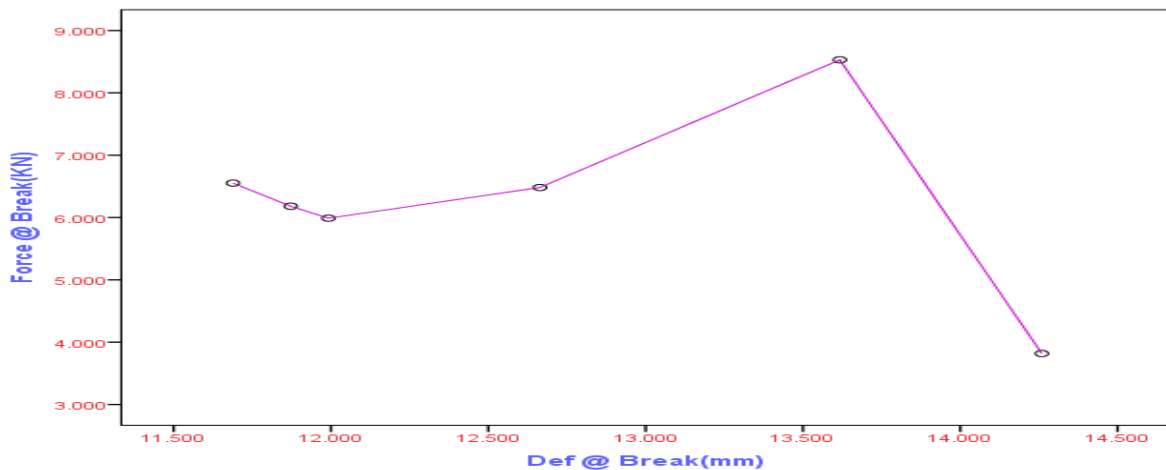
Figure 7: Compressive Force @Break against Deformation

4.0 Conclusions

The study into the physical and mechanical properties of raphia seed revealed that seed had an ovate shape and the particle density of raphia seed had a lesser value than their aspect ratio. Densities have been of interest in breakage susceptibility and hardness studies. The sample A (when the seed was placed longitudinally) has the highest compressive load while, sample B (when seed was placed transversely) has the lowest compressive load. Knowledge of compressive strength is vital to engineers handling agricultural products. From the data obtained for the selected physical and mechanical properties of raphia (*farinifera*), it was established that, they are useful in design of post harvesting, handling and processing operations. The physical and mechanical properties of raphia seeds was investigated to enable the

knowledge of compressive strength which is vital to engineering handling agricultural products. The determined physical properties of raphia had an oblong shape and the particle density of raphia seed has a lesser value than their aspect ratio. The mechanical properties of raphia seeds when the seed was placed longitudinally have the highest compressi ve load. These parameters are important in designing equipment for handling and processing operations of the product.

Reference

Aghimien, A.E. (1984): Distribution and Transformation of Phosphorus in Hydromorphic Soils,Supporting Raphia Palm Species in South-Eastern Nigeria. *A paper presented at the 24th Annual Conference of the Science Association of Nigeria.* 2003, pp. 1-20.

Eissa, A.H, and Gamea, G.R. (2003): Physical and Mechanical properties of Bulb Onions. *Journal of Agricultural Engineering*, 20 (3): 661-676.

Ezeike, G.O. (1986): Quasi – Static hardness and elastic properties of some tropical seed, grains and tomato fruit. Agrophysics, 2 (1): pp. 15 – 29.
.
Hojat, A., Jalal K., Seyed, S. and Ali, R. (2009); Some Physical and Mechanical Properties of Fennel Seed. *Journal of Agricultural Science,* 1(1).

Moshenin, N.N. (1992): Thermal properties of food and agricultural materials, Gordon and Breach Science publishers, New York, N.Y.

Ndon,(2003): Some morphological and chemical characteristics of developing fruits of Raphiafarinifera Journal of Experimental Botany 36 (172): 1817–1830.

Ndon, B.A. (2003): The Raphia palm (Economic Palm Series). Concept Publication Limited, Lagos, Nigeria. pp.155.

Ndon, B.A. (2003): The raphia palm: 1st ED. p. 16. Concept Publication Ltd, Lagos, Nigeria.

Omobuwajo, T.O., Akande, E.A. and Sanni, L.A. (1999): Selected physical, mechanical and aerodynamic properties of African breadfruit seeds. *Journal of Food Engineering*, 40: 241-244.

Olaniyan, A.M. and Oje, K. (2002): Some aspect of the mechanical properties of shear nut. Bio-systems Engineering, 81: 413- 420.

Otedoh, M.O. (1990): Ph.D. Thesis. The Systemic Studies of *Raphia*Palms.University of Reading, London.pp. 157.Sweet *Raphia*Palm Wine.The Nigerian Field. 55: 59-64

Otedoh, M.O. (1976): *Raphia* palm: Their Utilization in Jeremi Clan of Mid-Western Nigeria.Nigeria Agricultural journals. 9(2): 174-182.

Otedoh, M.O. (1991): Raphia palms; their utilization in jeremi clan of Mid- Western Nigeria. Nigeria Agricultural journal 9(2): 174-182.

Usuf, A.B., Pual, C.B. Fatima, A., Ester, I.B., Grace, K., Onyelwu, S.C. and Aliu, A. (2004): Laboratory manual on food Technology, Nutrition and Dietetics for School and industries. *National Science and Technology Forum Kaduna Polytechnic, Kaduna. Nigeria.* Pp. 60-82.

A FACTORIAL EXPERIMENTAL DESIGN APPROACH FOR THE SYNTHESIS OF TEMPLATED ZEOLITE Y

Muhammad A. T,[1*], A. S Kovo[2], Makarfi Y. I[3]

[1]Scientific Equipment Development Institute, PMB 37 Tunga goro, Minna. Niger State, Nigeria.
[2] Department of chemical Engineering, Federal University of Technology, Minna. Niger State, Nigeria. [3]Cape Peninsula University of Technology (CPUT), Cape Town, Western Cape, South Africa.
[*]abubakartakuma@gmail.com, 08036541959.

ABSTRACT. The factorial experimental design approach for the synthesis and characterization of templated zeoliteY was carried out by the hydrothermal process procedure using high temperature, low cost chemicals and simple apparatus. Using a batch composition $23.4Na_2O$: Al_2O_3: $83.4SiO_2$: $4.2(C_6H_{12}N_4)$: $3750H_2O$ and structural directing agent (SDA) Hexamethylene tetramine ($C_6H_{12}N_4$). A 2^3 fractional factorial design of experiments was applied in the design of the synthesis conditions used to conduct the experiment. The samples obtained were characterized by the use of powdered X-ray diffraction (XRD) and the scanning electron microscopy (SEM) methods. The results of the characterization showed that, the XRD patterns of the as-synthesized zeolite matched with those of the commercial Zeolite Y show sharp and narrow XRD peaks predominantly crystalline, while the images were of spherical crystals and represent a typical morphology for zeolite Y. It also showed a uniform size crystal distribution across the SEM images with an average size of 71 μm, while the highest percentage crystallinity was 48.52 %. A Mathematical model for the templated zeolite Y was derived from the experimental data and validated by the predicted and actual values of the conditions of synthesis. The optimal conditions for the synthesis of templated zeolite Y are: crystallization time of 43.00 h, crystallization temperature of 177.5 °C and ageing time of 60 h. The conditions ranges crystallization time 38-48 h, crystallization termperature 165-190 °C, while the ageing time ranges 48-72 h. Given the results the model can be use as tool for interpretation of the obtained relationship and the conditions was validated with an R^2 of 0.9308 which indicates 93.08 % similarity between experimental and predicted values.

Keywords: *Zeolite Y, Experimental design, Synthesis, purity.*

1. INTRODUCTION

Faujasite aluminiosilicate FAU, zeolite Y is a very important zeolite in respect to its volume in research activity and large scale in commercial use (Karami & Rohani, 2009). The synthetic zeolite Y has found applications principally in the field of catalytic cracking (FCC) of vacuum gasoil and in adsorption of volatile organic from wet off-gas streams (Jolanta, 2010). The faujasite materials are characterized by high surface area, uniform pore size distributions with pore sizes in the range 0.9-1.2nm and high thermal stability (Karami & Rohani, 2009).

Zeolite are generally a high class of crystalline aluminosilicate materials and the major approach to preparation of zeolite is by the hydrothermal synthesis, which is similar to the naturally occurring process that produces several classes of inorganic minerals such as crystalline silica and zeolites (Siti, 2007). Many variables mostly influence the synthesis of fuajasite materials. These variables include the inorganic cations, Si/Al ratio, crystallization time and temperature, ageing time, concentration, pH, batch composition, water content (Cejka, 2007). Therefore, a multi-variable experimental design is necessary in order to investigate the factors influencing the resulting output (Dongsheng *et al, 2009*). To effectively synthesis Zeolite Y, mostly a single factorial method was applied to optimize the synthesis conditions, which involves varying one variable at a time and keeping the rest constant (Xiaming & Erdong, 2007)). In this method, many experiments were required, and it becomes very difficult to study the interactions between the variables as they may influence the synthesis of the zeolite. Therefore, multi-variable experiment will give a better

output. It involves statistical design of experiment and it is an efficient way to obtain the maximum amount of information with fewer possible numbers of experiments, which helps in the investigation of factors influencing the resulting output (Katovic *et al*, 2001)

A factorial experiment can be analyzed using analysis of variant (ANOVA) or regression analysis. It is relatively easy to estimate the main effect for a factor. To compute the main effect of a factor "A", subtract the average response of all experimental runs for which A was at its low (or first) level from the average response of all experimental runs for which A was at its high (or second) level (Box & Draper, 1987).

2. METHODOLOGY

2.1 Materials

The materials used for this work are basically the reagents, which are mostly manufactured by Chadwell Heath Essay, England. The chemicals include the Aluminium Nitrate $Al(NO_3)_3.9H_2O$, Sodium Silicate (water glass, $Na_2SiO_3.9H_2O$) and a structural directing agent Hexamethylenetetramine ($C_6H_{12}N_4$). All the equipment were obtained in Minna and used in the Chemical Engineering Departmental laboratory, Federal University of Technology, Minna, Nigeria.

2.2 Design of Experiments

In this study, a 2^3 factorial experimental design was used to determine the optimum synthesis conditions. The parameters used were the ageing time, crystallization temperature and crystallization time and were study at both low and high levels with the response been percentage purity. The high level of the ageing time was 72 h and the low level 48 h. The high level for crystallization temperature was 190 ^{o}C and the low level was 165 ^{o}C. The high level for

crystallization time was 48 h, while the low level was 38 h.

Table 2.1: Variables for 2^3 factorial designs

Factors	parameters values	
	Lower level (-1)	High level(+1)
X_1: Ageing time (h)	48	72
X_2: crystallization temp (^{o}C)	165	190
X_3: crystallization time (h)	38	48

The design matrix is as shown (Table 2.1)

2.3 Characterization

The phase identification was performed by X-ray diffraction (XRD) using a PANalytical X'Pert computerized diffractometer with Cu-Ke radiation (40 kV, 40 mA). The 2Θ value was scanned in a range of 5-80°. The morphology of the individual crystal was observed by scanning electron microscopy (SEM) with a PHILIPS XL-30 ESEM microscope (Dongsheng *et al*, 2009).. The response measured, P, was the relative crystallinity of zeolite Y samples. The value of P was calculated using the following equation (Eq. (1)) from the peak area of angle 2Θ in the XRD spectra, using a highly crystalline sample

$$\%XRDcrystallinity(P) = \frac{\Sigma sample}{\Sigma Ireference} \times 100 \qquad (1)$$

Where P is the relative crystallinity, $\Sigma Isample$ sum of the peak area of product, $\Sigma Irefernce$ the peak area of reference sample. While the average crystal sizes was calculated by the scanning electron micrograph (SEM) technique.

2.4 Zeolite Y synthesis procedure

A series of templated zeolites Y were synthesized hydrothermally, using salt solution of analytical Aluminum Nitrate Al $(NO_3)_3.9H_2O$, Sodium Silicate (water glass,

$Na_2SiO_3.9H_2O$) and a structural directing agent Hexamethylenetetramine ($C_6H_{12}N_4$). Using a batch composition $23.4Na_2O$: Al_2O_3: $83.4SiO_2$: $4.2(C_6H_{12}N_4)$: $3750H_2O$. The distilled water was divided into two equal parts of 111.7 ml. The template solution was prepared by dissolving 1.95 g of Hexamethylenetetramine ($C_6H_{12}N_4$) in 111.7 ml of distilled water and stirred vigorously. The second half of the distilled water 111.7 ml was used to dissolved 2.45 g of Aluminium Nitrate Al $(NO_3)_3.9H_2O$ and 88.4 g of $Na_2SiO_3.9H_2O$ (water glass) sodium silicate was then added to dissolve and stirred (Tshabalala,2009).

The template solution of 111.7 ml and the second solution were then poured into a blender to stir it more intensively until a smooth jellylike form was consistently obtained. The final mixture was then transferred into 100 ml plastic beaker and allowed to age for 72 h, after which the solution was then transferred to an autoclave equipped with a 50 ml Teflon vessel. The autoclave was then put in the oven and the contents were allowed to crystallize at a temperature of 190 ^{o}C for 48 h. After the hydrothermal treatment, the autoclave contents were filtered and washed with distilled water until the filtrate had a pH of 9. The resulting product was then dried at 120 ^{o}C for 6 h and later calcined at 650 ^{o}C for a period of 4 h to get rid of the organic impurities/template. The resulting product suspected to be templated zeolite Y. Using the same procedure, the entire procedure was repeated for seven (7) different more runs for different Ageing time, crystallization temperature and crystallization time.

3.0 RESULTS AND DISCUSSION

The characterization of the zeolite Y produced by XRD showed that the as-synthesized zeolite Y has the characteristic peaks of zeolite Y.
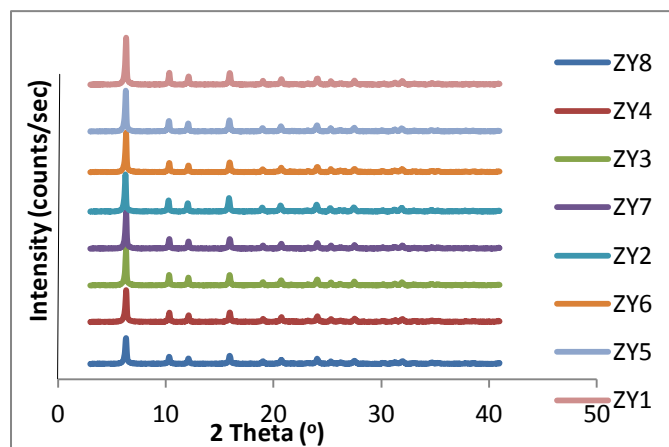
Fig. 3.1: XRD patterns of the Synthesized Templated zeolite Y.

The XRD patterns of the as-synthesized zeolite Y matched with known zeolite Y pattern which shows the required sharp and narrow XRD peaks (Dong, Bin, Guang, Qiang, Gaomeng, Lian and Jishuan, 2005) and are predominantly crystalline as shown in Figure 3.1. Also from Figure 3.1, the produced zeolite Y showed the characteristic peak of zeoliteY at 2Θ values of 6.15^o, 10.2^o, 11.0^o, and 16.0^o and there is a clear broadening of the reflection from the sample and the decrease in peak intensity from 20.2^o, 30.0^o. This can be attributed to the presence of small crystals and some impurities, noise and amorphous phase from 2Θ values of 35° to 45°.

The XRD pattern also compared well with some other work on zeolite Y as reported in literature such as in the work of (Karami & Rohani, 2009). The percentage crystallinity which serve as the purity was calculated, is depicted in Table 3.1

Table 3.1: Percentage crystallinity

Run	Factor 1 A:Ageing time(hrs)	Factor 2 B:Cry Tempt (^{o}C)	Factor 3 C:Cry Time (h)	Response Cry (%)
1	72.00	190.00	48.00	48.52
2	72.00	190.00	38.00	45.37
3	48.00	165.00	48.00	41.11
4	48.00	190.00	38.00	43.33
5	72.00	165.00	48.00	35.37
6	48.00	165.00	38.00	30.74
7	48.00	190.00	48.00	40.56
8	72.00	165.00	38.00	41.85

Table 3.1 shows the various percentage crystallinity at the runs conducted, the percentage is higher for the first run at 48.52 % while the lowest is at run 6 at 30.74 %. The percentage crystallinity is used as the response in the work and shows the purity of the synthesized zeolites (Karami et al, 2009). The Table also shows that the highest percentage crystallinity was obtained at the highest conditions of synthesis with ageing time 72 h, crystallization time 48 h and crystallization temperature 190 ^{o}C. While the lowest percentage crystallinity is at the lowest conditions with ageing time 48 h, crystallization time 38 h and crystallization temperature 165 ^{o}C respectively. This is an indication of the importance of ageing time and the crystallization time, since at highest level it gives the best results of crystallinity and at lowest the lowest respectively. But considering the factors of time and cost of running the experiment, the experimental runs 4, gives a more realistic result. The ageing and crystallization time were lower 48 h and 38 h respectively, with a corresponding temperature of 190 ^{o}C given a percentage crystallinity of 43.33 % which is within the range of the experiments best. From experiment run 4, this showed that more time can be saved thereby achieving the aim at a minimum time.

The crystallite size is one of the important parameters that influence physical properties of nano-materials. Fabrication of materials with specified properties requires close control of crystallite size (Uvarov & Popov, 2006). In order to establish the crystal size of the zeolite samples, the scanning electron micrograph (SEM) technique was used. Representative micrographs of synthesized zeolites Y are shown in Figure 3.2 to 3.6 respectively.
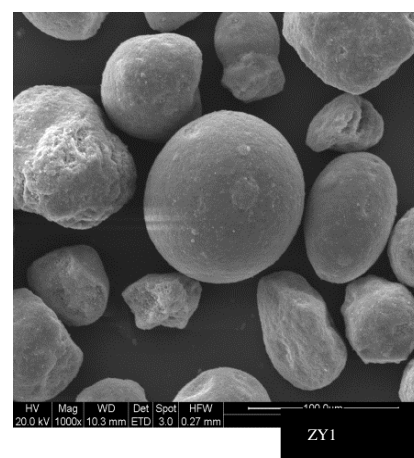
Fig. 3.2: SEM image of sample at Ageing time 72 h, Crystallization time 48 h and Crystallization temperature 190 ^{o}C
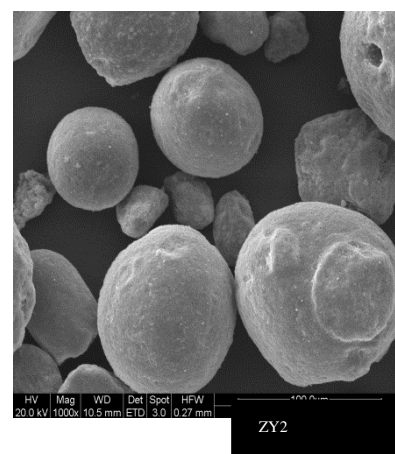
Fig. 3.3: SEM image of sample at Ageing time 72 h, Crystallization time 38 h and Crystallization temperature 190 ^{o}C
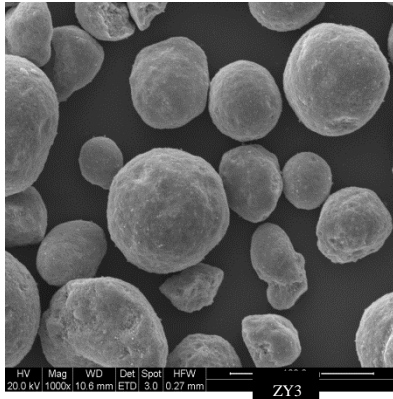
Fig. 3.4: SEM image of sample at Ageing time 48 h, crystallization time 48 h and crystallization temperature 165 ^{o}C
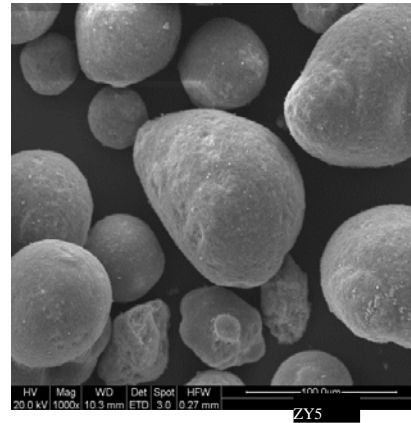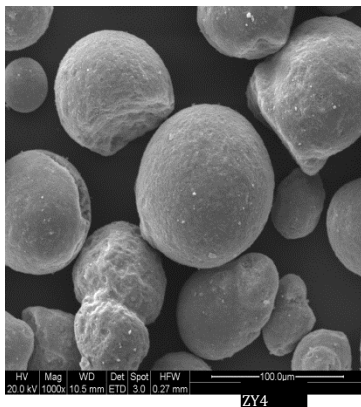
Fig. 3.5: SEM image of sample at Ageing time 48 h, Crystallization time 38 h and Crystallization temperature 190 ^{o}C

From Fig. 3.2 to 3.6 an average crystal size of around 90.49 µm for microcrystalline zeolite Y image was observed and it also showed that the crystal size distribution appears to be uniform. This is expected since the precursors are protected from aggregation during the crystallization. Based on the observation from the SEM images (Fig. 3.2 to 3.6) all had similar morphology. This typical morphology for zeolite Y was shown by other researchers as well (Uvarov et al 2006).

Fig. 3.6: SEM image of sample at Ageing time 72 h, Crystallization time 48 h and Crystallization temperature 165 ^{o}C

SEM images revealed that the sample had Spherical crystals with blunt edges, and has a defined morphology of zeolite Y (Uvarov *et al* 2006). The crystal sizes were calculated using the SEM micro-graphs of the synthesized samples.. It shows an increase in the ratios as the synthesized parameters varied.

A full factorial requires at multi level many experiments (Dongsheng *et al*, 2009). Interactions between different variables could be important in the study. Therefore one of fractional factorial design methods was used for the data analysis and was performed with the design Expert software version 7(stat-Ease Inc. Minneapolis, USA), (Karami *et al*, 2009). The analysis of a 2^3 factorial design resulted in an overlap between the main variables and their interaction terms. In this work, all interaction effects greater than 0.1000 were ignored. While the values lower than 0.1000 were statistically significant in the model.

Table 3.3: Analysis of variable (ANOVA for selected Factorial Model)

source	Sum of square	d	Mean square	F-value	P-value	Remarks
Model	211.53	4	52.88	24.53	0.0125	Significant
A-Ageing	29.38	1	29.38	13.63	0.0345	Significant
B-Cry temp	102.75	1	102.75	47.66	0.0062	Significant
AC	14.82	1	14.82	6.88	0.0789	Significant
ABC	64.58	1	64.58	29.96	0.0120	Significant
Residual	6.47	3	2.16			
Cor. Total	218.00	7				

The Model F-value of 24.53 confirmed the model to be significant. There is only a 1.25% chance that a "Model F-Value" this magnitude could occur due to noise. Values of "Prob > F" less than 0.1000 indicated model terms are significant.   In this work A, B, AC and ABC are significant model terms. Values greater than 0.1000 indicated the model terms are not significant.

Table 3.4: Calculation of the coded factors

Factor	Coefficient Estimate	df	Standard Error	90% CI Low	90% CI High	VIF
Intecept	40.86	1	0.52	39.64	42.08	
A-Ageing	1.92	1	0.52	0.69	3.14	1.00
B-Cry Temp	3.58	1	0.52	2.36	4.81	1.00
AC	-1.36	1	0.52	-2.58	-0.14	1.00
ABC	2.84	1	0.52	1.62	4.06	1.00

Table 3.4, showed the significant values of the coded factors, factor C is eliminated because the value of C was outside the given value of 0.1000.

Final Equation in terms of coded factors

$$Cry \% = +40.86+1.92*A+3.58*-1.36*A*C+2.84*A*B*C. \quad (3.0)$$

Where A is the Ageing time, B is the Crystallization temperature and C the Crystallization time, respectively.

The final equation was arrived at considering the coded factors which are very significant in this work. Table 3.5, showed the diagnostic statistics of response, while Fig 3.7 is the plot of the predicted values against the actual values in the model (Eq. (3.0)).
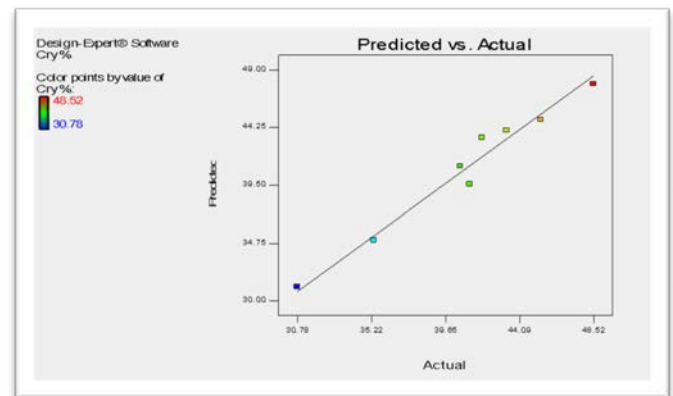
Figure 3.7: Predicted vs Actual value

As can be seen in Figure 3.7, predicted values matched experimental (actual) values reasonably well as they converged on the linear path and the "Pred R-Squared" of 0.7890 was found to be in reasonable agreement with the "Adj R-Squared" of 0.9308 for response. Therefore this model is a sufficient basis for interpretation of the obtained relationships. The response (percentage crystallization) at any regime in the interval of our experimental design can be calculated from Eq. (3.0).

The significant nature of most of the results of experiment and interaction been significant, it can magnify or diminish the effect of a factor (Dongsheng et al, 2009). The surface plot can be visualised as a three dimensional (3D) plot that showed the predicted responses as a function of the two factors keeping others constant (Dongsheng et al, 2009).
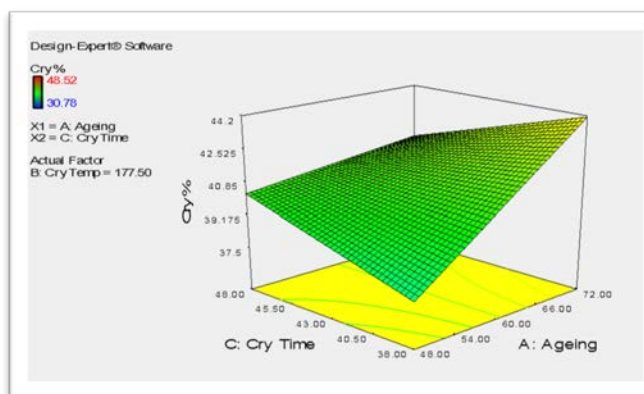
Figure 3.8: 3D view of Interaction crystallization time against Ageing time.
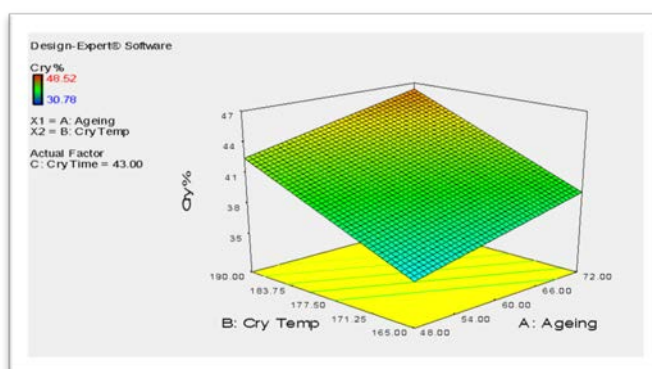
Figure 3.9: 3D view of Interaction between Crystallization Temp and Ageing time

The 3D plots in Figure 3.8, showed that as the ageing time and crystallization time increases, there is an increase in the percentage crystallization, until a time when a fall is observed in percentage crystallization. While Figure 3.9, showed that the crystallization temperature and ageing time are the most important variables. This can be seen as an increase in both resulted in an increase in the percentage of crystallization.

Considering all plots of the analysis and results, the optimal condition for the synthesis of templated zeolite Y

should be at a crystallization time of 43.00 h, crystallization temperature of 177.5 ^{o}C and ageing time of 60 h. The condition was validated with an R^2 of 0.9308 which indicates 93.08 % similarity between experimental and predicted values.

3. CONCLUSION

Synthesis of crystalline zeolite Y has been successful using hydrothermal sol gel procedure from synthesis mixtures. Zeolite Y was successfully synthesized with a single method which involved high temperatures and simple apparatus. The 2^3 factorial design and response surface analysis are found to be efficient tools for the optimization of zeolite Y synthesis. The predicted and actual values were found to be in conformity and validated the model equation and the results showed that the model was a sufficient tool for interpretation of the obtained relationship

Cry % = +40.86+1.92*A+3.58*-1.36*A*C+2.84*A*B*C. The optimal condition for the synthesis of templated zeolite Y should be at a crystallization time of 43.00 h, crystallization temperature of 177.5 ^{o}C and ageing time of 60 h. The condition was validated with an R^2 of 0.9308 which indicates 93.08 % similarity between experimental and predicted values.

REFERENCE

Box, G. E. P., & Draper, N. R. (1987). Response Surfaces, Mixtures, and Ridge Analyses, *Second Edition of Empirical Model-Building and Response Surfaces*, 54.622-654.

Camblor, M. A., Corma, A., Maetinez, A., Mocholi, F. A., & Perez, P. J. (1989). Catalytic cracking of gasoil: Benefit in activity and selectivity of small Y zeolite crystallites stabilized by a higher Silicon-to-aluminuim ratio by synthesis. Journal

of Applied Catalysis, 55. 65-74, Doi: 10:1016/S0166-9834(00)82317-9.

Cejka, J., & Heyrousky, J. (2005). Zeolites and ordered Mesopouros Materials; Progress and Prospects, Studies in Surface Science and Catalysis vol.157, Elsevier, Amsterdam.

Dong, J., Bin, W., Guang, Q., Qiang, G., Gaomeng, L., Lian, Y., & Jishuan, S. (2005). A highly efficient catalytic C4 alkane cracking over Zeolite ZSM-23. *Journal of catalysis communication*, 6, 297-300.

Dongsheng, Z., Rijie, W., Xiaoxia, Y. (2009). Application of fractional factorial design to zsm-5 synthesis using ethanol as template, *Journal of Microporous and Mesoporous Materials*, 126 (Doi: 10; 1016/j) micromeso.2009.03.015.

Jolanta, D. (2010). The influence of Alumunosilicate Gel Ageing on the synthesis of Nax Zeolite. *Scientific Journal of Riga Technical University*, 22, 308-321.

Karami, D., & Rohani, S. (2009) Synthesis of pure zeoliteY using soluble silicate, a two- level factorial experimental design, *Journal of Chemical Engineering and processing,* 13(6), 1269-1275.

Katovic, A., Cosco, M., Cozzcoli, P., & Giodano, G. (2001). The Factorial Fxperimental Design Applied to Zeolite Synthesis, Studies in Surface Science and Catalysis, 140, 323-330.

Siti, A. B. I. (2007). Synthesis and characterization of Zeolites from sodium Aluminosilicate solution, M.SC Thesis, *Department of Chemical Engineering USM, Malaysia.*

.
Tshabalala, T. E, (2009) Aromatization of n-Hexane over Metal Modified H-ZSM-5 Zeolites catalysts: A Dissertation for Master of Science, Faculty of Science, *University of Witwatersrand, Johannesburg.*

Uvarov, V. & Popov, I. (2006), Metrological Characterization of X-ray Diffraction Methods for Determination of Crystallite Size in nano-scale Materials Characterization of nanocrystalline zeolite, *Journal of Microporous and Mesoporous Materials* 58(10), 883-891.

Ursula, L., Barbara, P., & Sera, P., (1989). Y zeolite acidity dependence on the silicon/ aluminium ratio, *Journal of Physical Chemistry*, Doi: 10.1021/J1003469061

www.ijichemistry. International Journal of Industrial Chemistry, (2011) 2 (3), 140-143 ISSN (online): 2228-5547

Xiaming, D., & Erdong, Wu. (2007) Porosity of Microporous Zeolite A, X and ZSM-5 Studied by small angle X-ray Scattering and Nitrogen Adsorption. *Journal of Physics and Chemistry of Solids*, 68.1692-1699.

BEHAVIOUR OF PERCOLATION RATES IN LANDFILL MINERAL BARRIER FROM UNSATURATED ZONE EFFECT

Agbenyeku Emem-Obong Emmanuel[1*], Muzenda Edison[2], Msibi Mandla Innocent[3]

[1,2]Department of Chemical Engineering, University of Johannesburg, South Africa

[2]Department of Chemical, Materials and Metallurgical Engineering, Botswana International University of Science and Technology, Palapye, Botswana

[3]Research and Innovation Division, University of Johannesburg, South Africa

[*]emmaa@uj.ac.za; kobitha2003@yahoo.com, +27 11 559 6396

ABSTRACT

Laboratory model tests on percolation rates were evaluated for a landfill mineral barrier system as compacted clay liner (CCL) overlying unsaturated and saturated zone of known thickness respectively. The laboratory percolation model tests were done to simulate the moisture flow regime and steady/quasi steady-state percolation rates for scenarios of a landfill. The outcome of the tests showed the hydraulic conductivity of the fine textured unsaturated zone to be 1-2 magnitude order lesser than saturated zone hydraulic conductivity. However, the hydraulic conductivity of the mineral barrier and the percolation rate to underlying groundwater rely on the nature of the zone as the last line of defense to contamination migration in an event of leachate leakage. Thickness values of up to 225 mm for the fine textured zones were reached and they appeared to be effective parts of the tested landfill mineral barrier. Nevertheless, the unsaturated soil zone was found to behave better than the saturated zone in the permeability of the overall barrier system thus, outcomes of the tests showed permeability coefficient of the CCL (24 mm natural clay mineral barrier) to be the key controller of the steady/quasi steady-state percolation rates through the overall lining system.

Keywords: *Leachate, Percolation, Liner, Vadose zone.*

1. INTRODUCTION

The breakaway and subsequent percolation of landfill leachate through barrier lining systems as recorded by Rowe (2011) is one of the major contributors to soil, surface and groundwater deterioration. In South Africa as in many parts of the world, composite lining systems consisting of either a geomembrane (GM) or geosynthetic clay liner (GCL) and compacted clay liner (CCL) are used in waste containment facilities. As reported by Touze-Foltz (2006) substantial research has been done and more are ongoing on factors and impacts of leachate percolation through landfill lining barriers. In similar studies, Rowe (2004) showed how single low permeability clay liners have been effective in containing advective leachate percolation to regions of consequential impacts. It has been demonstrated that in the absence of a GM but with a leachate collection system (LCS) of typical design heads up to 0.3 m, CCL relying on the natural geology/aquitards can contain leachate percolation through landfill barrier systems as such, preventing the migration of contaminant species into vital groundwater resources (Rowe, 2005). The design and construction of landfill barrier systems therefore, requires appropriate laboratory modelling with relevant parameters such that, the potential impact of a proposed barrier system can be ascertained. Generally, software and laboratory landfill models use Darcy's law to estimate percolation from the barrier system to groundwater levels. At this point, selecting suitable permeability coefficients for CCL and the underlain soil zone is crucial in curbing migrating contaminants in the case of leachate breakaway due to membrane failures (Bouazza et al., 2002). With respect to the unsaturated zone, Freudlund and Raharjdo (1993) stated that the permeability coefficient of soils is a function of pore-water pressure; irrespective of the drastic changes that could occur in the unsaturated zone triggered by minute alteration in the soils moisture content. It has been observed that most laboratory tests and modelling software estimate percolation rates by single uniform permeability coefficient value for the CCL, disregarding the reliance of

permeability on moisture content (MC) in the unsaturated zone. This simply implies that escaped leachate percolation rates beneath the containment barriers are often underestimated leading to grave contamination in an event of a contaminant breakaway in landfills. As such, it is noted that the percolation through the entire barrier system depends on the type and sequence of the layers. It is for such reasons that this laboratory study assessed the percolation rates in landfill leachate migration using a bespoke percolation model. The study evaluated steady/quasi steady-state percolation rates into groundwater reserves/aquifer through CCL as landfill barrier system overlying unsaturated and saturated zones of known thicknesses. The zones were tested as fine textured soils collected from the landfill site. The impacts on percolation rates of uniform saturated and unsaturated permeability values, soil texture and the permeability of CCL were estimated. In this study, only the case of a single low conductivity CCL overlying a soil zone was investigated as it represents most of the cases around visited landfills in Johannesburg, South Africa. Also, the study offers a more conservative scenario reliant on the geology of a typical dump site as compared to cases of engineered landfills with composite barrier systems i.e., incorporating a LCS, GM or GCL, to a CCL overlying a soil zone. Hence, the results herein are noted to be conservative of composite landfill barrier cases.

2. METHODOLOGY

The fine textured soil in the study was sampled as clayey material used as the CCL, saturated and unsaturated zones. The clayey soil was collected in Johannesburg, South Africa, around a landfill site slightly distant from the dump as shown in Figure 1. The soil sample was mechanically tested to determine its characteristic properties with its grain size distribution curve shown in Figure 2 while its compaction curve showing the relationship between

optimum moisture content (OMC) and maximum dry unit weight (MDUW) determined by compaction test in consonance with American Society for Testing and Materials (2012) is seen in Figure 3.

Fig. 1: Sampling site

The standard proctor compaction was achieved with a light self-weighted rammer of about 0.0244 kN and striking effort of about 595 kN-m/m^3. The tests yielded OMC of 16.2 % and MDUW of 15.6 kN/m^3 for the barrier liner while the saturated and unsaturated zones had MDUW and OMC of 11.7 kN/m^3 and 22 % and 11.4 kN/m^3 and 6 % respectively. Values for permeability coefficient gotten in accordance with American Society for Testing and Materials (2006) were measured by falling head test.
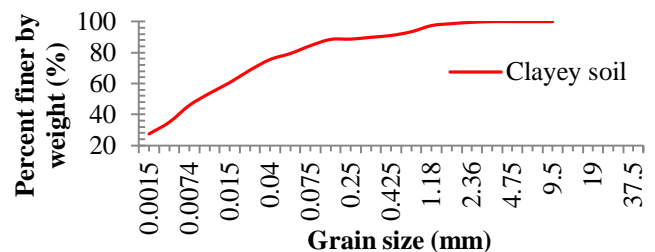
Fig. 2: Clayey soil grain size distribution curve

The unsaturated zone was prepared with relatively low water content while the saturated zone had high water content. The soil zones were lightly compacted to best simulate in-situ conditions of the natural soil respectively.
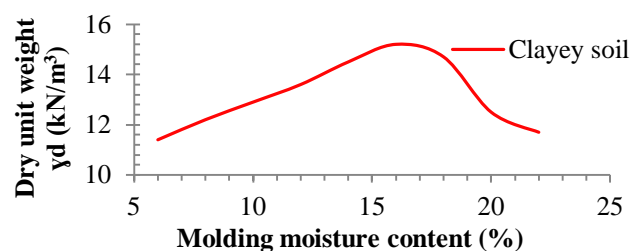
Fig. 3: Clayey soil compaction curve

The relationship between the permeability and dry unit weight of the soil used as barrier liner is shown in Figure 4. The leachate used in the study was collected from a pond at the site. The pond held generated leachate formed by decomposed waste, infiltrated storm water and/or intercepted surface water in contact with the waste pile in-situ as seen in Figure 5.
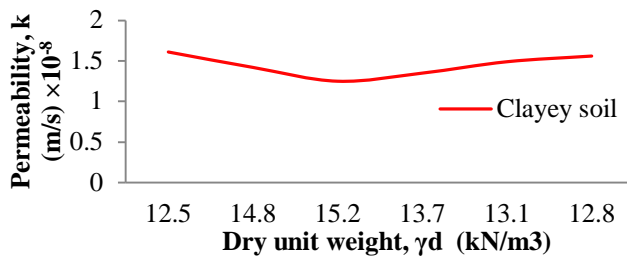
Fig. 4: Permeability variation of barrier clayey soil

The actual landfill leachate was of interest to the study such that at best, real life percolation conditions of the leachate-soil interaction can be visibly simulated and monitored in the laboratory. Also validate results of similar studies carried out by the authors with respect to landfill leachate migration through defected lining barriers (Agbenyeku and Akinseye, 2015; Agbenyeku et al., 2014a, b; 2013a, b).
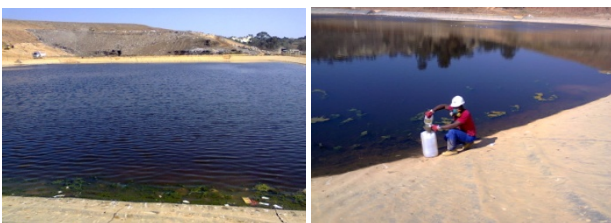
Fig. 5: Permeate collected from leachate pond

On the model device the leachate reservoir was marked to hold a constant head of 250 mm but since the mechanism to keep constant head was not designed for in the device, it was maintained by manually topping up the leachate level as it dropped throughout the test procedure. A pictorial and schematic view of the bespoke model device is shown in Figure 6 (a) and (b). For this test, the model comprised of three sections:

(1) the bottom part called the bucket section; which contained the unsaturated and saturated soil of 225 mm thickness respectively simulating the zones below the barrier liner as seen in Figure 7.
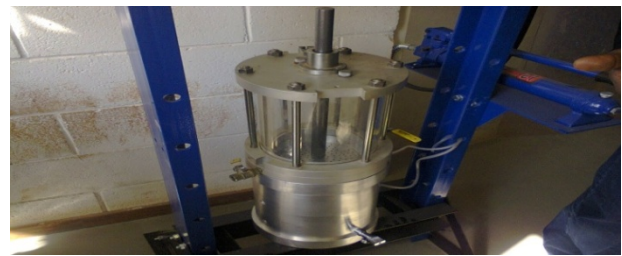
(a)   Pictorial view
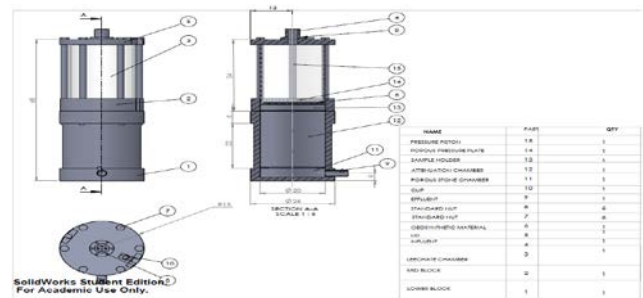
(b)   Schematic view

Fig. 6: (a) and (b) bespoke model device

(a)   (b)

Fig. 7: (a) Moist geotextile on porous stone to prevent outlet clogging (b) Lightly compacted simulated saturated and unsaturated zone

(2) the mid-block called the barrier holder; which contained the compacted soil barrier (natural clayey soil as CCL) overlying the respective zones as seen in Figure 8 (a) and (b), and (3) the upper part above the soil barrier liner; which functioned as the leachate pond as shown in Figure 9 (a) and (b) was filled with de-ionized water to saturate the system before the actual leachate was introduced. Soil layers were prepared in the bottom section and the mid-block sample holder and leakage free

connection was ensured by using O-rings, gasket corks and sealants to secure an airtight assembled device.
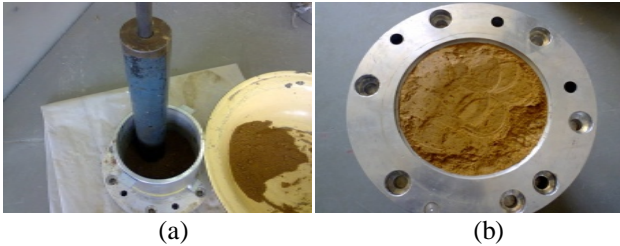
Fig. 8: (a) Standard proctor compaction of soil (as CCL) in barrier holder (b) Designed barrier liner

The leachate was then added and the vertical hydraulic conductivity, k_z value, in stratified soil (overall hydraulic conductivity of barrier-vadose system) was calculated and used to determine the percolation rate, Q, through the entire system on the assumption that since the barrier liner and the soil zones are not in direct contact, leachate that percolated the barrier went straight into the zones. This was further benched on the fact that the hydraulic conductivities of the soil zones were higher than the CCL since the zones were only lightly tampered to simulate a porous substrate and was not prepared at OMC.
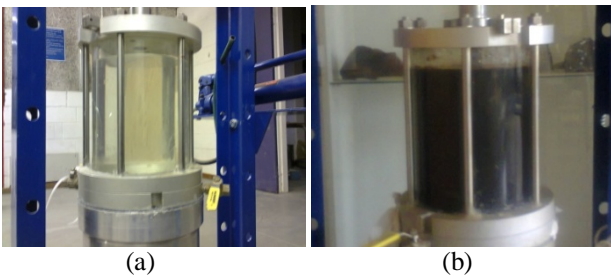
Fig. 9: (a) De-ionized water in reservoir (b) Actual leachate in reservoir

This part of the experimental work studied the changes in the hydraulic conductivity through the soil-leachate interaction. Four main test series were structured and done in this study outside other confirmatory tests. However, the conditions of two series of main concern to the study are reported herein. "Equations (1) to (3)" were used to determine:

The hydraulic conductivity (k) expressed as;

$$k = QL/Ath \qquad (1)$$

Where; k is the hydraulic conductivity, Q, is the volume of water collected, L, is the length of the sample, A, is the cross-sectional area of the sample, t, is the duration of effluent collection and h, is the total head. While the hydraulic conductivity of a barrier liner-soil zone (stratified soil layer) system was calculated and used to determine the percolation rate through the entire system. The vertical hydraulic conductivity in a stratified soil (k_z) is given as;

$$k_z = \sum H_i / \sum H_i/k_i$$

Therefore, $\quad k_z = H_1 + H_2/(H_1/k_1) + (H_2/k_2)$

$$(2)$$

Where; k_z is the vertical hydraulic conductivity in a stratified soil, H_1, is the thickness of the barrier liner, k_1, is the hydraulic conductivity of the barrier liner, H_2, is the thickness of the soil zone, k_2, is the hydraulic conductivity of the soil zone. The percolation rate through the entire system for the test by Darcy's Equation is expressed as;

$$Q = k \, \Delta h A/L \qquad (3)$$

Where; k = hydraulic conductivity of the entire system, Δh = leachate head drop, A = cross-sectional area of the system and L = thickness of the barrier liner-soil zone system. The clayey soil was moulded with de-ionized water and compacted in the mid-block to simulate water-wet clay barrier. The samples in the bucket section were gently compacted to simulate a loose substrate layer as the soil zone thereby increasing its porosity and hydraulic conductivity.

3. RESULTS AND DISCUSSIONS

3.1. Test for Leachate Percolation Rate

Outside validatory tests done in the study, two main test series were adopted. Table 1 summarizes the test conditions used for the study. The observed leachate-barrier soil interaction from percolation behaviours through the barrier system are recorded herein.

Table 1: Test series and conditions for the study

Test No.	Barrier as CCL		*Eft	Soil as vadose zone		**Eft
	MDUW (kN/m^3)	OMC (%)		MDUW (kN/m^3)	MC (%)	
1	15.2	16	25b/l	11.4[+]	6[+]	Gentle
2	15.2	16	25b/l	11.7[++]	22[++]	Gentle

*Standard Proctor Compaction Test (ASTM D-698)
**Gently compacted to simulate a loosed substrate
[+]Unsaturated zone [++]Saturated zone

Through each test, measurements were taken after the actual test leachate solution was introduced into the leachate chamber. This was done after the hydraulic conductivity value using de-ionized water as initial permeant stabilized to values in the order of 10^{-7} to 10^{-8} m/sec. The results of the percolation rates in the overall lining system for the unsaturated and saturated zones are graphically shown in Figure 10 (a) and (b) respectively. Moist geotextile over the porous stone served as filter to moving fines thus, prevented clogs at the chamber outlet. Due to temperature variations and atmospheric conditions, it was difficult to arrive at an absolute steady state in the laboratory. Nevertheless, for the purpose of this work the steady state adopted, implied a relatively steady/quasi steady state. Considering test with the unsaturated zone, it was observed that by day 16 steady/quasi steady state was reached however, to carter for factorial changes the test was monitored up to 20 days. The percolation rate, Q, for the overall lining system with unsaturated zone was seen to gradually increase to a steady value of 0.0043×10^{-6} m^3/s after breakthrough as shown in Figure 10 (a).
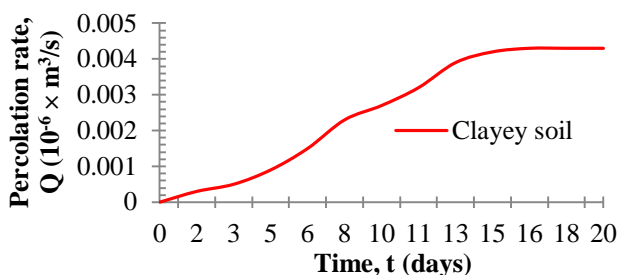
Fig. 10: (a) Percolation rate VS time with unsaturated zone

In the case of the saturated zone, it was observed that by day 13, steady/quasi steady state had been reached however, to also carter for factorial changes measurements were taken 16 days. Hence, the percolation rate, Q, for the overall lining system with saturated zone as shown in Figure 10 (b) was seen to gradually increase to a steady value of 0.0061×10^{-5} m^3/s after breakthrough was reached.
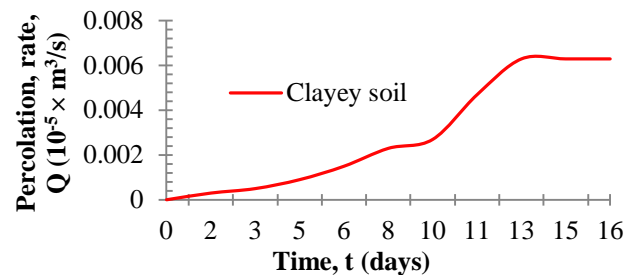
Fig. 10: (b) Percolation rate VS time with saturated zone

Pressure effects on the barrier liner in this study were neglected i.e., p = 0 kPa. Since it is considered that the constant low leachate head of 250 mm simulated in the study would have negligible impact on the percolation rate (Rowe, 2011). Moreover, previous studies by the authors have investigated the effect of waste load on leachate migration through barrier liners (Agbenyeku and Akinseye, 2015; Agbenyeku et al., 2014a, b; 2013a, b). Conversely, a 1-2 order of magnitude difference was recorded between the unsaturated and saturated zone tests. The plausible reason could be the difference in pore-water pressure; as the hydraulic conductivity of soil is a function of MC as such, increases with increased moisture intake. Also, the loose cohesive force between the soil particles of the saturated zone and the light compaction contributed by allowing easier flow thus, accounting for the higher percolation rate than in the unsaturated zone observed in the study as was also recorded by Rowe et al., (2004).

3.2. Mineral Barrier System of CCL Overlying Clayey Unsaturated and Saturated Zones

From the percolation rates of the barrier system with fine textured soil zones, it is clear that there is considerable difference between the barrier system of unsaturated and saturated zones. It has therefore been established through laboratory soil mechanical and percolation tests that water content, pore-water pressure and soil density can affect the hydraulic conductivity of barrier lining systems with respect to the soil zone. The percolation rate measured for a structure of unsaturated zone was 1-2 orders of magnitude less than the saturated zone structure. Thus for laboratory simulated 225 mm thickness of unsaturated and saturated zones under similar conditions (same MDUW, OMC and thickness for the designed clayey soil barrier liner), no significant threat will be posed by the hydraulic conductivity and percolation rate to vital ground regimes in a case of contaminant escape from landfills. This is based on consideration of the 24 mm designed barrier liner (CCL) tested in the laboratory in relation to the standard 150 mm CCL initiated in landfills. More retention capacity due to density and waste load effects will be expected thereby reducing the percolation rates significantly in real life scenarios.

3.3. Impact of Mineral Soil as CCL on Percolation Rate of a Barrier System

The behaviour of natural mineral soil to hydraulic conductivity as CCL and its impact on the overall performance of a barrier system was estimated from the permeability test carried out under various MDUW. The hydraulic conductivity value of 1.41×10^{-8} m/s for the CCL overlying both unsaturated and saturated zones decreased to steady/quasi-steady state. The percolation rates into groundwater as measured in the study for the overall barrier lining system is reflected in Figure 10 (a) and (b) respectively. Hence, the effect of hydraulic conductivity of

the mineral soil as CCL was observed to be highly influential over the tested zones. As such, should be crucially considered in the design of a functional mineral barrier system. Furthermore, it has been considerably proven in this study by laboratory simulation of percolation tests that the soil barrier liner constitutes a major controlling factor for leachate permeation into ground regions of consequential impacts.

3.4. Impact of Unsaturated Zone in Containment of Contaminant Influx

Rowe (2007) reported that increase in soil thickness sandwiched by barrier liner and underlying groundwater significantly reduces advective and diffusive contaminant migration to vital regions. Nevertheless, the efficiency of the unsaturated zone as containment to percolating contaminants relies on the water content, pore pressure and the nature of the leachate contaminant. On one hand, non-volatile contaminants will easily diffuse through water but not air. As such, unsaturated soil as observed from the study forms better barrier against percolating leachate contaminants than saturated soil. In the event of a diffusive percolation, Rowe et al., (2004) reported that the contaminants can only diffuse through the water phase hence; a saturated soil offers such medium for diffusive contaminant percolation. For this reason, Rowe et al., (2004) proposed equations for estimating coefficient of diffusion for unsaturated soils. On the other hand, volatile contaminants in forms of dichloromethane, 1,2 dichloroethane, trichloroethene (trichloroethylene), benzene, toluene, ethylbenzene, m&p-xylene and o-xylene will diffuse in higher magnitude faster in a dry medium than they will through a saturated medium. In the case of an unsaturated medium, the contaminants will diffuse in both the gaseous and dissolved phases. However, diffusion will mainly occur through the gas-filled pores if the water

content is low enough to have considerable number of continuous gas filled pores.

4. CONCLUSION

An investigation on mineral soil barrier system to estimate the impact of unsaturated zone on leachate percolation behaviour was studied. A laboratory bespoke percolation model was used in the testing procedure together with materials sampled from an actual landfill site. The overall percolation rate for the barrier lining system was estimated under certain conditions outlined in the study. It was therefore noted that failure to consider the presence of an unsaturated zone underlain a CCL can result in significant underestimation of the percolation through the clay barrier. This consideration is based on the effect of the unsaturated zone on the percolation through the CCL. It was also stated that hydraulic conductivity of soil is a function of water content among other factors. From results and analysis, the following conclusions were drawn:

- o In the fine textured soils, the unsaturated zone had a 1-2 difference in order of magnitude lesser than the saturated zone; plausibly due to difference in MC, pore-water pressure and density of zones.

- o The percolation rate for the overall mineral barrier system for the unsaturated and saturated zones were estimated as 0.0043×10^{-6} m^3/s and 0.0061×10^{-5} m^3/s after breakthrough was reached respectively.

- o The unsaturated soil zone was found to behave better than the saturated zone in the permeability of the overall barrier system.

- o The unsaturated zone can function both as an effective advective barrier as was the case in the study, as well as an effective diffusive barrier in an event of inorganic contaminant breakaway.

- o The tests showed permeability coefficient of the CCL to be the key factor of steady/quasi steady-state percolation rates through the overall lining system.

In a nutshell, the effect of hydraulic conductivity of the mineral soil as CCL was observed to be highly influential over the tested zones. Therefore, it is imperative that crucial considerations be given in the design of a functional mineral barrier system. Ultimately, the study has considerably established by laboratory simulation of percolation tests that the soil barrier liner constitutes a major controlling feature for leachate permeation into ground regions of consequential impacts.

ACKNOWLEDGEMENTS

REFERENCES

Agbenyeku E.E. & Akinseye S.A. (2015) Leachate Percolation through Failed Geomembrane of a Geo-Composite Soil Barrier *World Journal of Environmental Engineering, 2015, Vol. 3, No. 2, 52-57.*

Agbenyeku E.E. Muzenda E. & Msibi I.M. (2014a) "Zeolitic Mineral Liner as Hydraulic and Buffering Material", International Conference on *Earth, Environment and Life sciences* (EELS-2014) Dec. 23-24, 2014 Dubai (UAE).

Agbenyeku E.E. Muzenda E. & Msibi I.M. (2014b) "Buffering of TOC-Contaminant Using Natural Clay Mineral Liner", International Conference on *Earth, Environment and Life sciences* (EELS-2014) Dec. 23-24, 2014 Dubai (UAE).

Agbenyeku E.E. Okonta F.N. & Ojuri O.O. (2013a) Leachate Flow through Composite Barrier from Defected Geomembrane. 2nd African Regional Conference on Geosynthetics, Accra, Ghana, 18-20 November (CD ROM).

Agbenyeku E.E. Okonta F.N. & Ojuri O.O. (2013b) Evaluation of Empirical Equations for Leachate Migration through Composite Barrier with Defected Geomembrane. 2nd African Regional Conference on Geosynthetics, Accra, Ghana, 18-20 November (CD ROM).

American Society for Testing and Materials (2006) Standard Test Method for Permeability of Granular Soils (Constant Head). ASTM D-2434.

American Society for Testing and Materials (2012) Standard Test Methods for Laboratory Compaction Characteristics of Soil

Using Standard Effort (12 400 ft-lbf/ft^3 (600 kN-m/m^3)). ASTM D-698.

Bouazza A. Zornberg J.G. & Adam D. (2002) Geosynthetics in waste containment facilities: recent advances. *Proceedings 7th International Congress on Environmental Geotechnics,* Delmas, Gourc & Girard (eds): 445-507.

Freudlund D.G. & Raharjdo H. (1993) Soil Mechanics for Unsaturated Soils. John Wiley and Sons Inc., USA. pp. 136–140.

Rowe R.K. (2005) Long-term performance of contaminant barrier systems 45th rankine lecture. Geotechnique 55 (9), 631-678.

Rowe R.K. (2007) Advances and remaining challenges for geosynthetics in geoenvironmental engineering applications, 23rd manual Rocha lecture. Soils and Rocks 30 (1), 3–30.

Rowe R.K. (2011) Systems engineering; the design and operation of municipal solid waste landfills to minimize contamination of groundwater. Geosynthetics International, September, 18 (6), pg: 319-404.

Rowe R.K. Quigley R.M. Brachman R.W.I. & Booker J.R. (2004) Barrier Systems for Waste Disposal Facilities. Taylor & Francis Books Ltd. (E&FN Spon), London. p. 587.

Touze-Foltz N. Duquennoi C. & Gaget E. (2006) Hydraulic and mechanical behavior of GCLs in contact with leachate as part of a composite liner. Geotextiles and Geomembranes 24 (3), 188-197.

CAPILLARY ACTION THROUGH GEOSYNTHETIC CLAY LINER FROM SUBSOIL: A CLOSED SYSTEM EXAMINATION

Agbenyeku Emem-Obong Emmanuel[1*], Muzenda Edison[2], Msibi Mandla Innocent[3]

[1,2]Department of Chemical Engineering, University of Johannesburg, South Africa

[2]Department of Chemical, Materials and Metallurgical Engineering, Botswana International University of Science and Technology, Palapye, Botswana

[3]Research and Innovation Division, University of Johannesburg, South Africa

[*]emmaa@uj.ac.za; kobitha2003@yahoo.com, +27 11 559 6396

ABSTRACT

A constant mass of soil moisture considered as closed system in this study was prepared in the soil chamber of a bespoke device. The capillary action through three geosynthetic clay liners (GCLs) from subsoil pore water was examined. Pyrophyllite bentonite GCL often used in most landfills in Johannesburg, South Africa was selected for the hydration test however; the three GCLs had different descriptive properties under the same test conditions. A 5 kPa pressure plate was imposed on the setup to give close contact between the GCL and soil surface thereby, simulating waste load effect on the GCL barrier in-situ. The GCL overlying the closed system setup was periodically sampled and tested to examine a range of variables and ultimately, the hydration behaviour of the GCL through capillary action. The laboratory test required occasional removal of the barrier from the soil chamber. Simple parameters were measured to monitor the hydration changes over time. Laser measurement techniques have been used in similar studies to monitor changes in GCL thickness during hydration however, in this study, measurements were manually done using vernier dials and the results obtained showed GCL type and GCL-soil interaction to constitute a major role in its hydration by capillary action from subsoil.

Keywords: *Capillary action, Subsoil, GCL, Landfills.*

1. INTRODUCTION

In the area of waste containment, one major concern remains the prevention of leachate contaminants from migrating to vital regions below the ground surface. Issues on soil, surface and groundwater pollution are often results of contaminant migration in the event of leachate breakaway from waste containment facilities as explained by Rowe (2011). Primarily, needs have stemmed to adequately address the importance to the assessment of contaminant generation, subsurface contamination and development of relevant control systems drawn from a variety of engineering and applied science fields. The protection of groundwater is now a major consideration in the design of waste containment facilities in many countries including South Africa as reported by Environmental Impact Assessment Regulations (2005). As stated by Bouazza et al., (2002) geosynthetics play an important role in the protective task because of their versatility both mechanically and hydraulically. Changing environmental conditions however, have diminished the ability of land to contain the vastly generated contaminant

species with no apparent consequence. Hence, Agbenyeku et al., (2014a, b) emphasized the need for composite materials i.e., geosynthetic clay liner (GCL), compacted clay liner (CCL) and Geomembranes (GM) in waste containment facilities to be used together with the natural geology to prevent leachate escape from landfills to vital ground levels. GCLs which are vastly used in landfills, comprises of a layer of low permeability clay (bentonite) sandwiched by two layers of geotextile (a nonwoven cover geotextile and either a woven or nonwoven carrier geotextile) with the components bound together by needle-punching. GCLs are often used as part of composite liners with a geomembrane liner placed over the GCL. These composite liners have gained widespread recognition for use in waste lining systems and other containment applications. A study by Rowe (2005) on GCLs revealed effective prevention of groundwater contamination provided: (i) the GCL is adequately hydrated and (ii) there is an overlap between the panels. In-situ, GCL absorbs moisture by capillary action from underlying soil and once hydrated it has been reported by Rowe (2007) to function better as barrier to contaminant migration. In the design of

a landfill barrier system, and for decisions to be taken with respect to potential GCL performance, data is needed to assess the hydration of GCL through capillary action. Therefore, it is noted that the operation of GCL as barrier will rely partly on the hydration of the GCL among other factors. Hydration of GCLs has gained attention in recent years however; the behaviour and hydrating rate of dry GCLs overlying subsoil have not been sufficiently documented. Data on GCL underlain by sand have been fairly reported whereby, at 3 % moisture content (MC) of sand, an air dry GCL reached 88 % MC after 40-45 days (Daniel et al., 1993). While in another case reported by Eberle and von Maubeuge (1997) air dry GCL reached MC of 100 % in less than 24 hrs and 140 % after 60 days for sand with MC of 8-10 %. Nevertheless, there is dire need to look into other soil types i.e., silty and clayey soils underlain a GCL as not much have been examined. The rate of GCL hydration is vital as recorded by Rowe (2005) in terms of assessing how fast the composite barrier system must be covered with soil/waste if defects are to be minimized by virtue of desiccative cyclic impacts. Hence, this study found the impetus to investigate the behaviour and hydration of GCL through capillary action overlying clayey strata. The laboratory barrier setup investigated herein is based on real life scenarios in most landfills around Johannesburg, South Africa. Thus, effect of GCL type and the potential GCL-soil interactions were studied.

2. METHODOLOGY

The fine textured soil used in the study was sampled as clayey material used as the subsoil underlying the tested GCLs throughout the test procedure. The clayey soil was collected in Johannesburg, South Africa, around a landfill site relatively far from the dump area as seen in Figure 1. The sampled soil was mechanically tested to determine its characteristic properties. Its properties indicated it is a clayey soil with over 70 % passing the 0.075 mm sieve and its fines were found to be plastic with plastic limit of 25.

Fig. 1: Sampling area

Figure 2 shows the grain size distribution curve of the clayey soil while the compaction curve showing the relationship between optimum moisture content (OMC) and maximum dry unit weight (MDUW) determined by compaction test in conformance with American Society for Testing and Materials (2012) is shown in Figure 3.
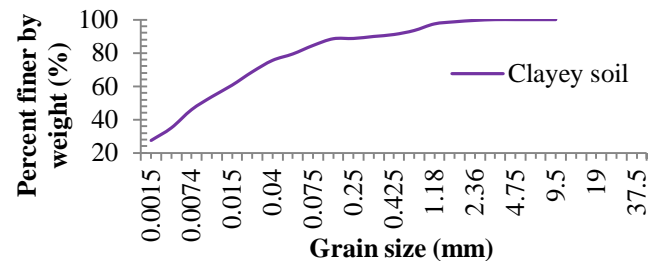
Fig. 2: Clayey soil grain size distribution curve

The standard proctor compaction was achieved with a light self-weighted rammer of about 0.0244 kN and striking effort of about 595 kN-m/m^3. The tests yielded OMC of 16.2 % and MDUW of 15.6 kN/m^3. The compaction was done lightly in the soil bucket of the bespoke model to best simulate in-situ conditions.
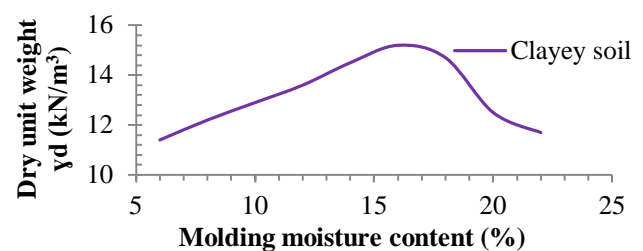
Fig. 3: Clayey soil compaction curve

A pictorial and schematic view of the bespoke model device is shown in Figure 4 (a) and (b).

(a) Pictorial view
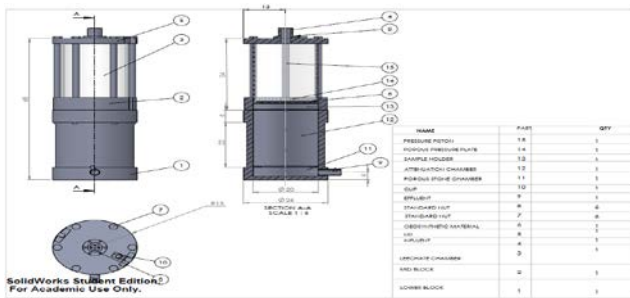
(b) Schematic view
Fig. 4: (a) and (b) bespoke model device

For this test, the model comprised of two sections:

(1) the bottom part called the bucket section; which contained the lightly compacted 225 mm thick layer to simulate in-situ subsoil as shown in Figure 5 (a) and (b).

(a)   (b)
Fig. 5: (a) Standard proctor compaction of soil (as subsoil)
(b) Lightly compacted subsoil in bucket section

(2) the upper chamber coupled to the bucket section; which functioned to keep the system airtight and in position under applied pressure using O-rings, gasket corks and sealants to ensure a well coupled device as seen in Figure 6. Three GCLs collected from the landfill operation store room with different descriptive properties under the same test conditions were used for the study. Table 1 summarizes the GCL properties.

Fig. 6: Bucket section coupled to upper chamber

Smaller portions of the GCL were sliced open as shown in Figure 7 and the bentonite material was scraped out and tested for hydroscopic MC whose respective values are also presented in Table 1.

Fig. 7: GCL sliced open to remove bentonite material

Table 1: Description of GCLs test properties for the study

Desig.	MC*(%)	Upper GT	Lower GT	Bond Type	Mass/area (kg/m²)
GCL-A	9	NW	NW	NP	4.05
GCL-B	10	NW	W	NPHT	4.17
GCL-C	11	NW	RSNW	NP	4.21

*Hydroscopic moisture content, GT=Geotextile, NW=Nonwoven, W=Woven, RS=Reinforced scrim, NP=Needle punched, HT=Heat treated

The selected GCLs were composed of granular pyrophyllitic bentonite and were hand cut as shown in Figure 8 (a) and (b) from a larger portion to fit the test conditions. The GCLs had mass per unit area of 4.05-4.21 kg/m² cut to 160 mm diameter and 24 mm thickness.
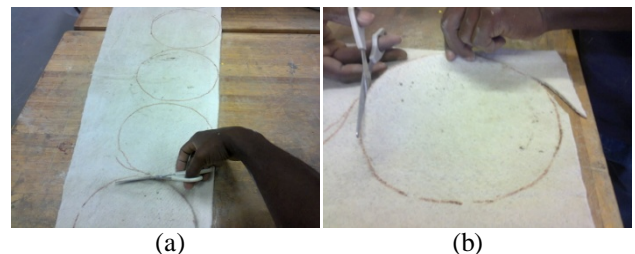
(a)   (b)
Fig. 8: (a) GCL marked 160 mm diameter on parent portion (b) 24 mm thick GCLs cut from larger portion

The upper chamber of the bespoke device is made of a rigid cylindrical cell constructed of transparent, high

strength and corrosion resistant polymethyl (methacrylate) acrylic glass that allows for visual observation during testing. While the bucket section 225 mm high with diameter of 160 mm is made of polished anodized aluminium (to prevent corrosive attacks and resist scratches during dismantling). This part of the experimental work used the bespoke device in the closed system hydration of the respective GCLs by capillary action from the simulated 225 mm high clayey subgrade. The well equilibrated clayey soil of known void ratio and MC was lightly compacted in three layers in the bucket section. The cut GCL was immediately placed over the soil with enough swelling headspace as seen in Figure 9. The GCLs for the respective tests were periodically removed and measured to monitor the hydration behaviour in relation to time.

Fig. 9: (a) 24mm thick GCL placed over 160 mm diameter subgrade with headspace to accommodate swelling

The measurements for the GCL thickness were manually done in this study using vernier dials. However from similar studies, Figure 10 shows a laser measurement technique used to monitor GCL swelling evolution.

Fig. 10: Laser measurement of GCL (Rayhani et al., 2008)

Also to ensure a closed system, a thin 2 mm thick polyethylene plastic membrane (PPM) was placed over the GCL as in Figure 11 to simulate field conditions as well as

reduce potential evaporation into the headspace. To foster a GCL-soil interaction, a 5 kPa pressure was imposed on the system simulating the waste load effects in field conditions by a pressure plate as shown in Figure 12.
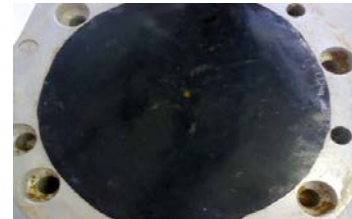
Fig. 11: 2mm thick PPM overlying the GCL

This was done for the three series of test on the respective GCLs. However, a fourth test was done without applied stress as seen in Figure 13 simulating a situation where there is a gap between the PPM and the GCL such that its impact on GCL hydration could be assessed.

Fig. 12: 5 kPa pressure on the system by pressure plate

It was ensured that throughout the different series tested, the MDUW and MC were kept constant, and the GCL types and GCL-soil interaction were examined.
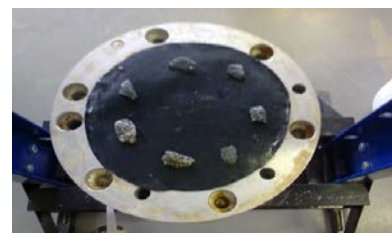
Fig. 13: 0 kPa pressure on the system

For the purpose of the study two sets of data were gathered from the test series. A manual vernier dial measurement was used to measure the thickness changes of the GCL at intervals during hydration by capillary movement. For the first set of data; the GCL thickness was periodically monitored and measured by manually taking readings off the vernier dial before and after the GCL was removed for

weight measurement on a weekly basis. For the second data set; the mass of the GCL was measured to determine MC changes over time. Table 2 therefore shows the working details of the tested GCL and subgrade for the study while graphical relationships between changes in GCL thickness and MC with respect to time for the respective series were generated.

Table 2: Experimental details initiated in the study

Desig.	MDUW (kN/m^3)	Soil MC (%)	Pressure (kPa)	GCL Thickness (mm)
GCL-A	15.6	16.2	0	24
GCL-B	15.6	16.2	0	24
GCL-C	15.6	16.2	0	24
GCL-C	15.6	16.2	5	24

3. RESULTS AND DISCUSSIONS

3.1. Effect of Capillary Action on GCL Hydration

From the hydration tests due to capillary action on the tested GCLs, it was observed that over the test period of 4 weeks (28 days) GCL-A with initial MC of 9 % gravimetrically increased to about 84 %. The GCL-B with initial MC of 10 % increased to about 86 % while the GCL-C with 11 % initial MC increased to about 93 % and 107 % for the 0 kPa and 5 kPa pressure respectively. The higher uptake of moisture in GCL-C to about 107 % can be accounted for by the pressure effect on hydration from capillary action. The Table 3 therefore shows the initial MC and the final MC after capillary action for all the tested GCLs. To further investigate the hydration behaviours of the respective GCLs, they were exposed to free saturation by submergence in water. Their respective moisture uptake values as well as approximate degree of saturations are also presented in Table 3. However, GCL-A was observed to take in more moisture to a value of about 167 % while GCL-B and GCL-C had values of 112 % and 135 % respectively.

Table 3: Values of moisture uptake for the tested GCLs

Desig.	Initial MC (%)	*Final MC (%)	Submerged MC (%)	Approx. Deg. of Sat.
GCL-A	9	84	167	75
GCL-B	10	86	112	70
GCL-C	11	93	135	60
+GCL-C	11	107	135	60

*4 weeks (28 days) of hydration, +5 kPa imposed pressure

This difference in free saturation moisture uptake can plausibly be due to the respective geotextile bonding types as well as the needle punches provided by the manufacturers.

3.2. Effect of Hydration on GCL Thickness

For the purpose of this test, the initial GCL thickness for the series of tests was kept constant at 24 mm over the 28 days hydration from capillary movement. The thickness of GCL-A was observed to increase up to 25.1 mm and 24.8 mm in GCL-B while GCL-C for the 0 kPa and 5 kPa surcharge increased to 24.5 mm and 25.6 mm respectively. The Table 4 shows the difference in the respective GCL thickness due to hydration over the 28 days test duration.

Table 4: Difference in GCLs thickness due to hydration

Desig.	Initial Thickness (mm)	Final Thickness (mm)	Change in Thickness (mm)
GCL-A	24	25.0	1.0
GCL-B	24	24.8	0.8
GCL-C	24	24.9	0.9
GCL-C	24	25.6	1.6

The higher thickness change in GCL-C under 5 kPa stress effect can be accounted for by the increased GCL-soil interaction. This allowed for a more contact surface between the surfaces of the GCL-C and the subgrade thus, leading to increased uptake of moisture which must have triggered the swelling of the GCL. Conversely, the thickness change recorded for the other series can also be reasonably attributed to the uptake of moisture through the GCL-soil surface interaction over the test period which led to swelling.

3.3. Effect of GCL Type on Hydration

Further tests were conducted on the three pyrophyllitic bentonite GCLs under the same test conditions. This test was opted for to examine the effect of GCL manufacturing, bentonite type, bonding and geotextile configuration on hydration of the GCLs by capillary action from the prepared subgrade. The tested GCLs were placed over the prepared subgrade as previously done. However, the respective tested GCLs in this case were subjected to similar pressures of 5 kPa as previously described. From the outcome of this extra test series, it was observed that GCL type plays a key role in the hydration of the GCL from subgrade. The Figure 14 show the relationship between MC and duration of hydration with respect to the effect of GCL type on GCL hydration.
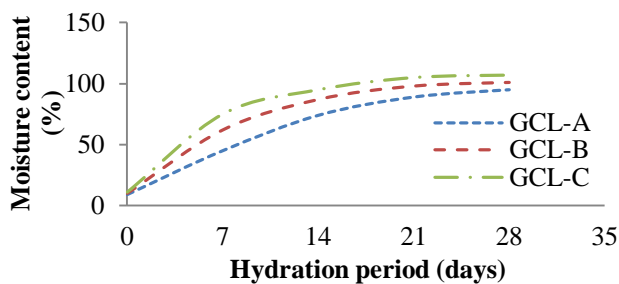
Fig. 14: Effect of GCL type on hydration of GCL

From Figure 14, it can be seen that all the tested GCLs behaved relatively alike. With respect to GCL type and bonding, the pyrophyllitic bentonite and the nature of the manufactured geotextile bonding may have resulted in the similar behaviours observed. However, GCLs are seen to have similar patterns in their moisture uptake due to capillarity. This may have resulted from the nonwoven and needle punched properties of the respective GCLs. Nevertheless, GCL-C clearly showed a considerably higher hydration as compared to GCL-B and GCL-A under a constant testing conditions. Under a constant pressure of 5 kPa and test duration of 28 days for the tested GCLs, the hydration of GCL-C was about 107 %, while that of GCL-B and GCL-A were 101 % and 95 % respectively. Nonetheless, it is noted that the higher MC of GCL does not essentially imply a better performance.
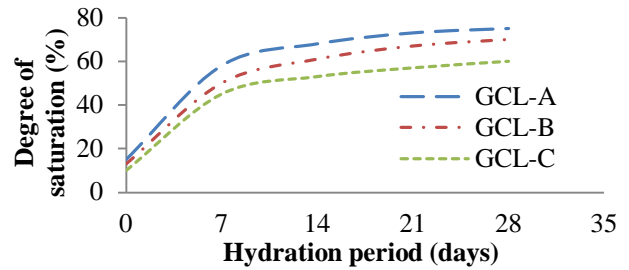
Fig. 15: Sat. degree-hydration time relationship for GCLs

Hence, as recorded by Rayhani et al., (2008) the GCL needs to be near saturated to show low hydraulic conductivity. As shown in Table 3 and Figure 15, the GCL-A was found to have a higher degree of saturation as compared to GCL-B and GCL-C.

3.4. Effect of Potential Gap/Imperfect Interface of PPM on Hydration of GCL

Form the test conducted herein, simulation of the waste load effect in field conditions on potential gap during the hydration of GCL from capillary movement was done. This was achieved using the GCL-C where a pressure of 0 kPa and 5 kPa was imposed on the GCL. Figure 16 shows the pressure effects on the hydration behaviour of the GCLs by moisture uptake.
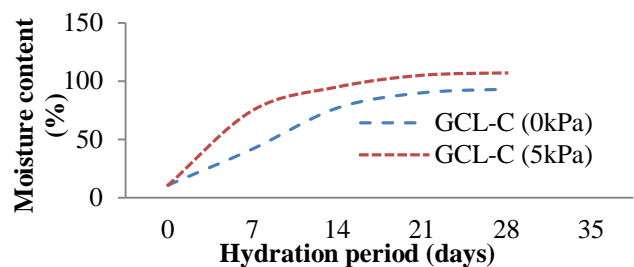
Fig. 16: Pressure effect on hydration by GCL-soil contact

It was observed that for GCL-C with 5 kPa imposed pressure from a pressure plate, there was increased interaction between the GCL and subgrade as compared to GCL-C with no imposed load. It was clear that the imposition of load on the GCL revealed considerable effect on the rate of capillary action in a closed system subgrade. Hence, the GCL-C with 5 kPa imposed pressure indicated higher MC as compared to the GCL-C with 0 kPa pressure under the same controlled testing conditions.

As such, a moisture uptake variation of about 10-15 % was recorded.

4. CONCLUSION

A laboratory closed system examination of GCL hydration behaviours from capillary action was conducted in the study. Three fixed pyrophyllitic bentonite type with varying initial MCs and geotextile bonding types were used. The GCL samples were respectively placed over a laboratory closed system prepared subgrade as in standard conditions reported in the study. A fourth test under similar testing conditions but with an imposition of 5 kPa pressure to the GCL was also conducted. This was done to simulate the effect of waste load in field conditions on GCL hydration for a potential case of imperfect contact/gap in the PPM. Furthermore, a test to examine the effect of pressure on all tested GCLs for their respective hydration behaviours by moisture uptake was also conducted. All the tests herein were done in a laboratory bespoke model in simulation of field conditions typical of most landfills around Johannesburg, South Africa. Hence, from the analysis of results, the following conclusions were drawn:

- o The GCL in all tested series were hydrated by capillary action form the pore-water of the subgrade.
- o The respective MC and thickness of the tested GCLs were found to increase with respect to hydration periods due to moisture uptake by the GCLs from capillary movement.
- o The manufacturers GCL type; geotextile bonding, weave and needle punching were also found to affect the GCL-soil interaction based on moisture uptake by capillarity as well as when exposed to full saturation by submergence in water.
- o The rate of hydration in GCL-C was found to be higher as compared to GCL-B and GCL-A respectively. Although it was observed that the

degree of saturation for GCL-A and GCL-B were respectively higher than GCL-C. Hence, as noted by Rayhani et al., (2008) a higher MC does not necessarily imply a better GCL barrier performance since a higher degree of saturation could lead to low permeability of the GCL as barrier material.

In summary, constant mass of soil in a closed system was studied using a laboratory bespoke device. Capillary action through three GCLs from subsoil pore water was examined. An imposed 5 kPa pressure on the setup gave close GCL-soil surface contact simulating field condition waste load effects on the GCL barrier. The GCLs were underlain by the constant mass of soil periodically tested to examine a range of variables. Ultimately, the outcomes of the study showed GCL type and GCL-soil interaction to constitute a significant role in the hydration of GCL by capillary action from subgrade. It is therefore recommended that further tests be conducted on the permeability of the respective hydrated GCLs at respective hydration periods. This will aid the determination of their performance as barriers in landfill waste containment.

REFERENCES

Agbenyeku E.E. Muzenda E. & Msibi I.M. (2014a) "Zeolitic Mineral Liner as Hydraulic and Buffering Material", International Conference on *Earth, Environment and Life sciences* (EELS-2014) Dec. 23-24, 2014 Dubai (UAE).

Agbenyeku E.E. Muzenda E. & Msibi I.M. (2014b) "Buffering of TOC-Contaminant Using Natural Clay Mineral Liner", International Conference on *Earth, Environment and Life sciences* (EELS-2014) Dec. 23-24, 2014 Dubai (UAE).

American Society for Testing and Materials (2012) Standard Test Methods for Laboratory Compaction Characteristics of Soil Using Standard Effort (12 400 ft-lbf/ft^3 (600 kN-m/m^3)). ASTM D-698.

Bouazza A. Zornberg J.G. & Adam D. (2002) Geosynthetics in waste containment facilities: recent advances. *Proceedings 7th International Congress on Environmental Geotechnics,* Delmas, Gourc & Girard (eds): 445-507.

Daniel D.E. Shan H.Y. & Anderson J.D. (1993) Effects of Partial Wetting on the Performance of the Bentonite Component of a Geosynthetic Clay Liner, *Proceedings of Geosynthetics* '93, Vancouver, B.C., IFAI, March 30-April 1, pp. 1483-1496.

Eberle M.A. & von Maubeuge K. (1997) Measuring the in-situ moisture content of geosynthetic clay liners (GCLs) using time domain reflectometry (TDR), *6th Int. Conf. on Geosynthetics*, Atlanta, 1: 205-210.

Environmental Impact Assessment Regulations (2005) Waste Collection and Disposal. Retrieved 07 May, 2012, from:
http://www.dwaf.gov.za/Dir_WQM/Pol_Landfill.PDF.

Rayhani M.H.T. Rowe R.K. Brachman R.W.I. Siemens G. & Take A. (2008) Closed-system investigation of GCL hydration from subsoil, GeoEdmonton, *GeoEngineering Centre at Queen's-RMC, Queen's University, Kingston, Canada.*

Rowe R.K. (2005) Long-term performance of contaminant barrier systems 45th rankine lecture. Geotechnique 55 (9), 631-678.

Rowe R.K. (2007) Advances and remaining challenges for geosynthetics in geoenvironmental engineering applications, 23rd manual Rocha lecture. Soils and Rocks 30 (1), 3–30.

Rowe R.K. (2011) Systems engineering; the design and operation of municipal solid waste landfills to minimize contamination of groundwater. Geosynthetics   International, September, 18 (6), pg: 319-404.

A BOND GRAPH MODELLING APPROACH FOR MULTI PROCESS SYSTEMS

Ikpo C. Valentine, Mu'azu .B. Muhammed, Tajudeen. H. Sikiru, Okafor Emmanuel.

Department of Electrical and Computer Engineering, Ahmadu Bello University, Zaria – Nigeria.

ezeval7@yahoo.com, 07031310628.

ABSTRACT

This paper presents a graphical based mathematical modelling of a nonlinear multi input multi output (MIMO) quadruple tank system using Bond Graph (BG) technique. The procedure adopted in actualizing this modelling includes; identification of the input/output (I/O) relationship, contribution of various elements to the entire system, and validation of the causal nonlinear mathematical model derived using 20-sim software application. The nonlinear model of the quadruple tank system was validated using 20-sim, which established the accuracy of bond graph model technique. Linearization was achieved using Taylor series and system response of the input and output relationship was also presented.

Keywords:*BG, I/O, Nonlinear, MIMO, Validation, 20-sim.*

1. INTRODUCTION

The dynamic behaviour of a physical system is the outward manifestation of the energy transaction within the system. Hence, benchmark setups such as those composed of tanks are physical systems used to study and design reliable, controllable and high performing industrial processes. Benchmark tank configurations popularly found in open literature include those modelled using techniques like variation methods, network methods and use of first principle derivations (Bhat and Osting, 2011).

The single conical tank that describes a nonlinear model for level control and real time was design and simulated in SIMULINK(Aravind et al., 2013). The work of (Deepa and Arulselvi, 2014, Chu et al., 2014) showed the modelling of two tank systems and its simulation, three tanks systems modelling and control by (Bregon et al.,

2012, Triki et al., 2014). Most of these works were based on first principles. The work of (Vijula and Devarajan, 2013) also describes the modelling of a quadruple tank based on first principles. Moreover, the techniques were characterised by potential challenges arising from approximation errors, over assumptions and ill-posed boundary conditions. This paper proposes the modelling of a quadruple tank system using bond graph technique which is based on a unifying concept (energy and power) that captures most physical variables and dynamics of a nonlinear system and provides a symbolic platform for visualization.

The remaining part of this paper is divided into sections; section two describes methodology adopted, by describing the modelling of the quadruple tank system using bond graph method. The analysis of significant result obtained

are presented in section three. While section four concludes the work and provides areas for further work.

2. METHODOLOGY

The physical system of the quadruple tank in this work is based on the experimental setup in the work of(Rajanikanth Vadigepalli, 2001). The various combinations of input and output configurations that can be implemented include; Single Input Single Output (SISO) systems, Single Input Multi Output (SIMO) systems, Multi Input Single Output (MISO) systems, and Multi Input Multi Output (MIMO) systems (Rosinova and KozǍ˘kovǍ˘, 2012). The quadruple tank used in this work is a MIMO. A typical illustration of the quadruple tank system is shown in Figure 1
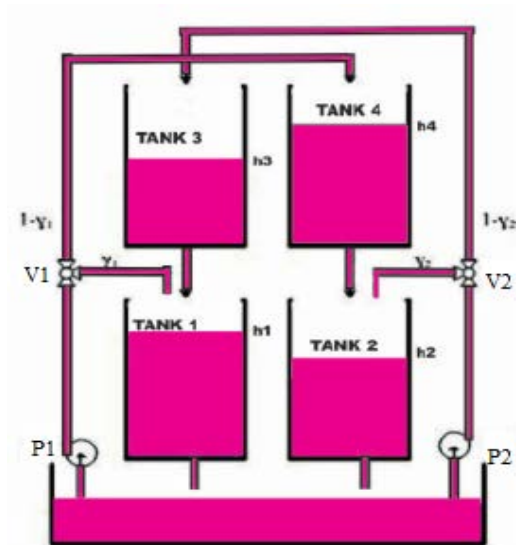
Figure 1: The Quadruple Tank System

The quadruple tank system consists of three basic units;

(i) Input Unit: This unit is made up of two inputs that consist of pump 1 (P1) and pump 2(P2).

(ii) Control Unit: This is responsible for regulating the flow rates in valve V1 and V2 which are three-way configured.

(iii) Output Unit: This accounts for the output response obtained from the quadruple tank system. This is determined based on the difference in height of the output variables which consist of h1 of tank 1 and h2 of tank 2.The target is to control the level of the two lower tanks; Tank 1 and Tank 2 and their in-let flow rates. The output of each pump is split into two by using a three- way valve. Thus, each pump output goes to two tanks, one lower (Tank 1) and the other upper (Tank 4) diagonally opposite and the ratio of the split is controlled by the position of the valve. With the change in position of the two valves, the system can be appropriately placed either in the minimum phase or in the non-minimum phase (Garg and Tangirala, 2014).

2.1. BOND GRAPH MODELLING OF QUADRUPLE TANK

The nature of the constitutive equations lay demands on the causality of the connected bonds (Wolfang, 2013). Bond graph elements are drawn as letter combinations (mnemonic codes) indicating the type of element. The bond graph consists of the following elements:

(i) C - Storage element for a q-type variable,e.g. capacitor (stores charge), spring (stores displacement).

(ii) I - storage element for a p-type variable,e.g. inductor (stores flux linkage), mass (stores momentum).

(iii) R - Resistor dissipating free energy, e.g.electric resistor, mechanical friction.

(iv) Se Sf sources, e.g. electric mains (voltagesource), gravity (force source),pump (flow source).

(v) TF - transformer, e.g. an electric transformer, toothed wheels, lever.

(vi) GY - gyrator, e.g. electro-motor, centrifugal pump.

(vii) 0 and 1 {junctions, for ideal connection of two or more sub-models.

While considering the elements of the bondgraph as lump parameters, the electrical and hydraulic components share the same characteristics (Das, 2009). This means that their modelling patterns and considerations are almost similar (The capacitance/capacity exhibited by Tank/Capacitors, the resistance by the Resistor/Pipe, the transformation by Transformer/Valve. The supply by pump and voltage source (Li et al., 2014).

2.2 MODEL DERIVATION

In deriving the equations of the quadruple tank system, certain factors need to be considered.

1. What is the contribution of each element to the entire system?

2. Consideration of what the system gives back to each storage element?

Furthermore, the procedures for the derivation of equations from a causal bond graph include the following steps:

(i). Write the constitutive equations for all independent sources. Their outputs are given functions of time.

(ii). Identification of input and out relationship.

(iii). Identification of elements and their individual contributions using characteristic behaviour of each element (storage, dissipater, transformer.

(iv). Identification of the various 1 and 0nodes.

(v). Causality application from which the resultant algebraic equations will result depending on either integral or derivativecausality outcomes and validation(Benmoussa et al., 2014)

(vi). Integrating the various variables, elementsand junctions, a quadruple tank is obtained using symbolic bond graph as shown in Figure 2.

A. Quadruple Tank System Variables

The vector H denotes the power port of the quadruple tank system which is derived from the product of individualeffortsand flows at designated port, and can be deduced from bond graph model of Figure 2.

$$H=[e_{14}f_{14}; e_{13}f_{13}; e_1f_1; e_2f_2; e_{10}f_{10}; e_8f_8; e_{17}f_{17}; e_{19}f_{19}] \qquad (1)$$

Where: $e_1, e_2 \ldots e_{19}$ are referred to as the efforts

$f_1, f_2 \ldots f_{19}$ are referred to as the flows

This implies that the power port comprises of 8 power variables. In same vein, it is possible to determine the modulated source flow (MSF) vector (K) of the quadruple tank by computing four possible modulated source flows for the designated ports.

$K = [MSF_1; MSF_2; MSF_3; MSF_4].$
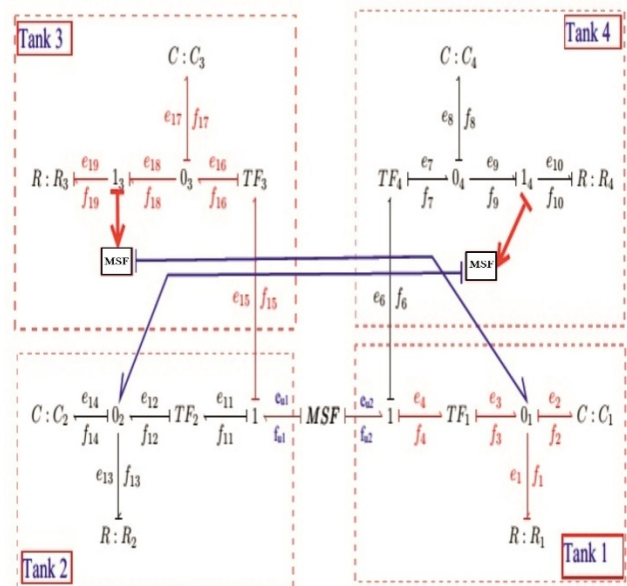
Figure 2: The Quadruple Tank Crossed Looped Information Scheme.

The quadruple tank system model is shown in Figure 2, which shows the interconnectionof the various subsystems of each of the tanks and their corresponding source flows. With the aid of Bond Graph.

B. Mathematical Model of Quadruple Tank System

The mathematical model of the various subsystems of the quadruple tank system can be described based on the principle of Bond Graph. This model is presented in equation (2).

$$F13 : R : R_1 \to f_1 = |a| * \sqrt{|e_1|},$$
$$F14 : R : R_2 \to f_{13} = |a| * \sqrt{|e_{13}|}$$
$$F15 : R : R_3 \to f_{19} = |a| * \sqrt{|e_{19}|}$$
$$F16 : R : R_4 \to f_{10} = |a| * \sqrt{|e_{10}|}$$
$$F17 : C : C_1 \to e_2 = 1/C_1 \int f_2 dt \quad \text{(2)}$$
$$F18 : C : C_2 \to e_{14} = 1/C_2 \int f_{14} dt$$
$$F19 : C : C_3 \to e_{17} = 1/C_3 \int f_{17} dt$$
$$F20 : C : C_4 \to e_8 = 1/C_4 \int f_8 dt$$

Where

F13, F14…. F20: refers to the flow effects

|a|: is the absolutevalue of the cross sectional area of each of thetank pipe.

$\to$: Means such that

: Marks the end of a bond graph code

\ Means points of energy

In order to obtain the contributions of each the tank; tank1, tank2, tank3, and tank4 as subsystems of the quadruple tank, there is a need to consider each of the various subsystem configurations used. This subsystem is presented in Figures 3, Figure 4, Figure 5 and Figure 6 respectively.
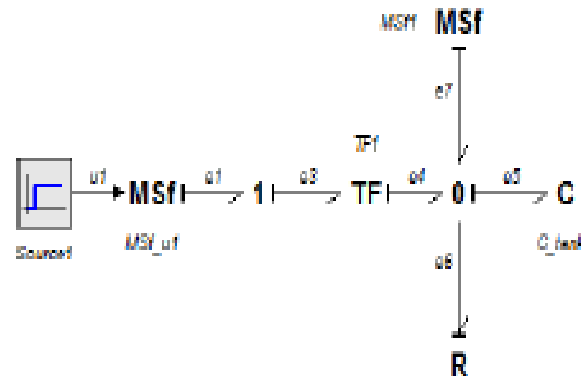
Figure 3: Bond Information of Tank 1
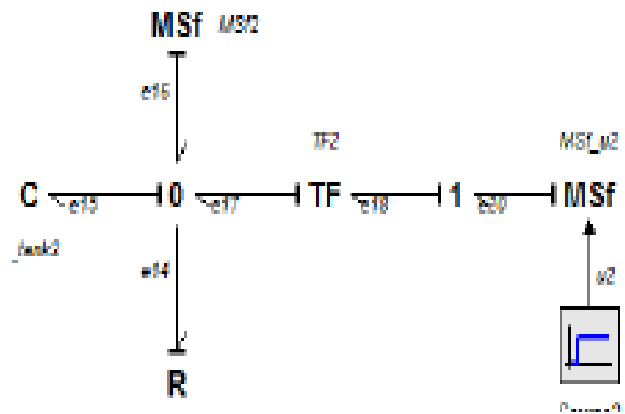
Figure 4: Bond Information of Tank 2
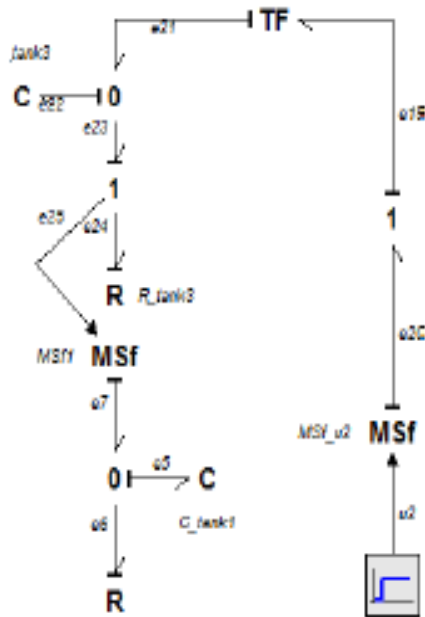
Figure 5: Bond Information of Tank 3
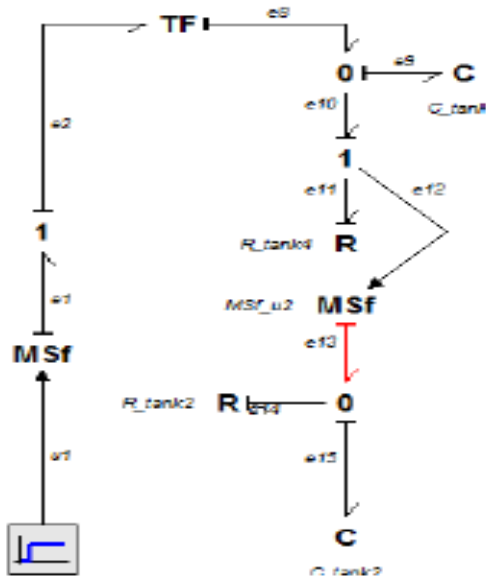
Figure 6: Bond Information of Tank 4

$$R_{tk1} \backslash p.f = C_{tk1} \backslash p.e / R_{tk1} \backslash r;$$
$$R_{tk2} \backslash p.f = C_{tk2} \backslash p.e / R_{tk2} \backslash r;$$
$$R_{tk3} \backslash p.f = C_{tk3} \backslash p.e / R_{tk3} \backslash r;$$
$$R_{tk4} \backslash p.f = C_{tk4} \backslash p.e / R_{tk4} \backslash r;$$
$$C_{tk1} \backslash p.f = (TF_1 \backslash p2.f + R_{tk3} \backslash p.f) - R_{tk1} \backslash p.f;$$
$$C_{tk2} \backslash p.f = (TF_2 \backslash p2.f + R_{tk4} \backslash p.f) - R_{tk1} \backslash p.f;$$
$$C_{tk3} \backslash p.f = TF_3 \backslash p2.f - R_{tk3} \backslash p.f;$$
$$C_{tk4} \backslash p.f = TF_4 \backslash p2.f - R_{tk4} \backslash p.f;$$

$$(3)$$

Where

R_{tki} and C_{tki} (I = 1, 2, 3, 4) are the resistance and capacitance components of the tank1 to tank4;

$\backslash p.f$ is the flow direction.

$\backslash p.e$ is the effort direction.

r is the resistive point offered by pipe.

$TF_1...TF_4$ is the energy transformer for designated valves.

The physical tanks when represented by tick dark lines geometry, when superimposed upon by the bonds are visually illustrated as shown in Figure 7. This configuration was implemented in 20-sim software application.

The dynamic equations of the system are derived based on the information present in Figures 3 to 6.

C. **Quadruple Tank System Dynamic Equations**

The dynamics of the quadruple tank system with respect to flows and efforts are derived as follows:
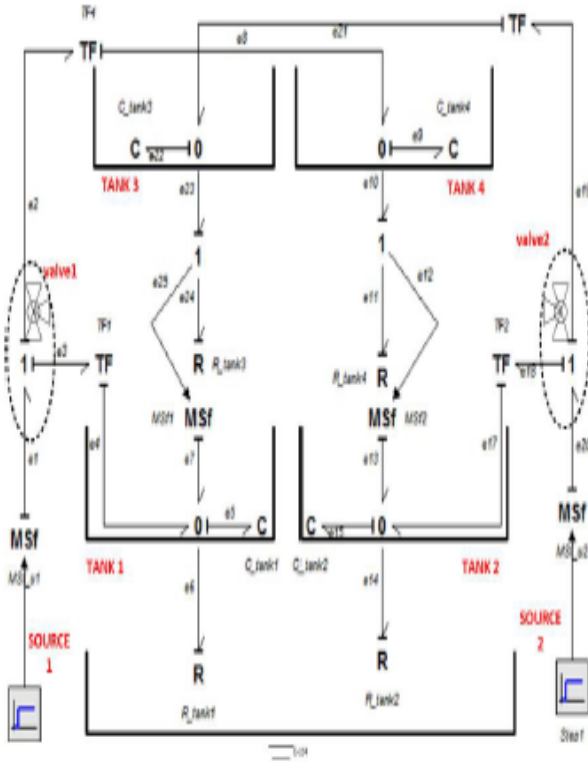
Figure7: Bond Graph Model of a Quadruple Tank Showing the Complete Mechanism and Information Block

D. System Nonlinear Model

The system nonlinear model equations are obtained as follows:

$$C_{tk1} \setminus state = \int (C_{tk1} \setminus p.f, C_{tk1} \setminus state\_initial); \tag{4}$$

$$C_{tk4} \setminus state = \int (C_{tk4} \setminus p.f, C_{tk4} \setminus state\_initial); \tag{5}$$

$$C_{tk3} \setminus state = \int (C_{tk3} \setminus p.f, C_{tk3} \setminus state\_initial); \tag{6}$$

$$C_{tk2} \setminus state = \int (C_{tk2} \setminus p.f, C_{tk2} \setminus state\_initial); \tag{7}$$

Where

h1, h2, h3 and h4 represents the liquid levels of tank1, tank2, tank3 and tank4 respectively;

A1, A2, A3, and A4 are the cross-sectional areas of the tanks' (A = h*h), respectively related to tanks hydraulic capacities by the mathematical relation

$$C_{tki} = \frac{A_{tki}}{\rho g}$$ (i = 1, 2, 3, 4); ρ is the constant densities of

the liquid, g is the gravitational acceleration while a1, a2, a3 and a4 are the cross-sectional area of the pipes (assumed equal).

The sources are given by $k_1 u_1$ and $k_2 u_2$ for the two inputs. [\state, \p.f, \p.e, \p_i.f, \p_i.e, \r: symbolises system-mode and port of exchange with regards to flow and effort].

Therefore, the differentiation of the equations (4 to 7) yields equations (8 to 11) which is similar to the derivation as presented in open literature by (Vijula and Devarajan, 2013):

$$\frac{dh_1}{dt} = -\frac{a_1}{A_1}\sqrt{2gh_1} + \frac{a_3}{A_1}\sqrt{2gh_3} + \frac{\gamma_1 \kappa_1}{A_1} u_1 \tag{8}$$

$$\frac{dh_2}{dt} = -\frac{a_2}{A_2}\sqrt{2gh_2} + \frac{a_4}{A_2}\sqrt{2gh_4} + \frac{\gamma_2 \kappa_2}{A_2} u_2 \tag{9}$$

$$\frac{dh_3}{dt} = -\frac{a_3}{A_3}\sqrt{2gh_3} + \frac{\gamma_2 \kappa_2}{A_3} u_2 \tag{10}$$

$$\frac{dh_4}{dt} = -\frac{a_4}{A_4}\sqrt{2gh_4} + \frac{\gamma_1 \kappa_1}{A_4} u_1 \tag{11}$$

E. Linearization

The linearization of the nonlinear model of the quadruple tank as obtained in the equations (8), (9), (10), and (11) were achieved using Taylor series method that is present in Simulink toolbox of Matlab 2013b. Hence, the compact representation of the non-linear model of the quadruple tank system is presented as follows:

$$\dot{h} = f(h,u)$$
$$y = g(x,u)$$
(12)

The linearized state equation is presented in equation (13):

$$\dot{h} = f(\bar{x}, \bar{u})$$
(13)

The linearized state space modelparameters of the quadruple tank system is then gotten by:

$$A = \left[\frac{\partial f}{\partial x}\right]; B = \left[\frac{\partial f}{\partial u}\right]; C = \left[\frac{\partial g}{\partial x}\right]; D = \left[\frac{\partial f}{\partial u}\right]$$
(14)

The approximated states space modeltherefore becomes:

$$\dot{x} = Ax + Bu$$
$$y = Cx + Du$$
(15)

This state space model is better represented as:

$$\dot{x} = \begin{bmatrix} -\frac{1}{T_1} & 0 & \frac{1}{T_3} & 0 \\ 0 & -\frac{1}{T_2} & 0 & \frac{1}{T_4} \\ 0 & 0 & -\frac{1}{T_3} & 0 \\ 0 & 0 & 0 & -\frac{1}{T_4} \end{bmatrix} x + \begin{bmatrix} \frac{\gamma_1 \kappa_1}{A_1} & 0 \\ 0 & \frac{\gamma_2 \kappa_2}{A_2} \\ 0 & \frac{\gamma_2 \kappa_2}{A_3} \\ \frac{(1-\gamma_1)\kappa_1}{A_4} & 0 \end{bmatrix} u$$
(16)

$$y = \begin{bmatrix} k_c & 0 & 0 & 0 \\ 0 & k_c & 0 & 0 \end{bmatrix} x$$
(17)

Where

x = [h1, h2, h3, h4]^T, and u = [v1, v2]^T, y = [h1, h2]^T.

The time constant was obtained using the formula:

$$T_i = \frac{A_i}{a_i}\sqrt{\frac{2h_i^0}{g}}$$ such that i = 1,2,3,4. The open–loop response of the multi process; Multi Input Multi

Outputsystem is obtained by simulation of the system at one of its equilibrium points [h$_1$ = h$_2$ = h$_3$ = h$_4$ = 0cm] as shown in Figure 9 in the results and discussions section.

3.0 RESULTS AND DISCUSSIONS

Results shows that by differentiating the integral model obtained using 20-SIM, resulted in a system similar to the nonlinear algebraic model obtained via bond graph symbolic procedures. This model obtained is also in agreement with the models obtained as shown in literature(Vijula and Devarajan, 2013)though via first principles method. The responses of the linear quadruple tank system at one of its equilibrium points which shows first order system characteristics of each tank's dynamics are illustrated in Figure 9.
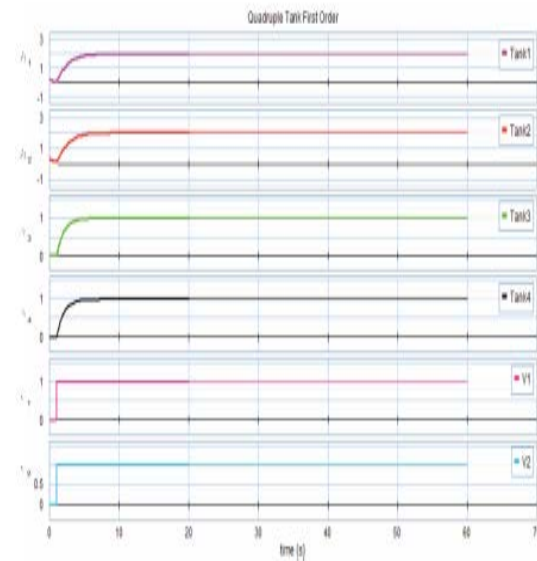
Figure 9: 20-SIM Step Response of Open-loop System from Initial Equilibrium Condition.

The response shown in Figure 10 resulted from the open-loop quadruple tank system modelled. With some perturbation, the system showed stability after been excited.
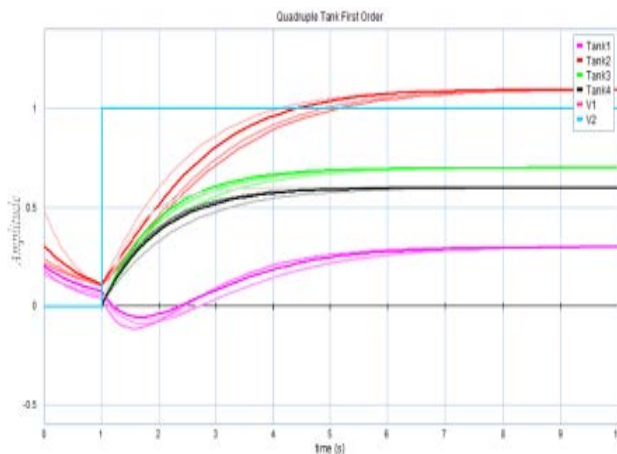
Figure 10: Step Response under Multiple Excitations

4.0 CONCLUSION

The quadruple tank is a MIMO benchmark system which can be modelled and simulated to appreciate the dynamics of most industrial complex systems. The concept of energy in modelling captures a systems' dynamics accurately and demonstrates a robust efficient methodology towards reproducing perfect models. The bond graph technique achieves this using dynamic graph with causality. The equations modelling the quadruple tank and its dynamics were validated using 20-sim(Li et al., 2014). The linearized model of the quadruple tank system showed stable response under multiple excitations.

This work recommends modelling and control of systems with increased number of tanks (Tanks > four) with bond graph.

REFERENCE

ARAVIND, P., VALLUVAN, M. & RANGANATHAN, S. 2013. Modelling and Simulation of Non Linear Tank. *International Journal of Advanced Research in Electrical, Electronics and Instrumentation Engineering,* 2**,** 842-849.

BENMOUSSA, S., BOUAMAMA, B. O. & MERZOUKI, R. 2014. Bond Graph Approach for Plant Fault Detection and Isolation: Application to Intelligent Autonomous Vehicle. *Automation Science and Engineering, IEEE Transactions on,* 11**,** 585-593.

BHAT, H. S. & OSTING, B. 2011. Kirchhoff's laws as a finite volume method for the planar Maxwell equations. *Antennas and Propagation, IEEE Transactions on,* 59**,** 3772-3779.

BREGON, A., BISWAS, G. & PULIDO, B. 2012. A decomposition method for nonlinear parameter estimation in TRANSCEND. *Systems, Man and Cybernetics, Part A: Systems and Humans, IEEE Transactions on,* 42**,** 751-763.

CHU, Y., ÆSØY, V., ZHANG, H. & BUNES, Ø. Modeling and simulation of an offshore hydraulic crane. 28th European Conference on Modelling and Simulation, 2014.

DAS, S. 2009. *Mechatronic Modeling and Simulation Using Bond Graphs*, CRC Press.

DEEPA, N. & ARULSELVI, S. 2014. Design and Implementation of Neuro Controllers for a Two-Tank Interacting Level Process. *International Journal of ChemTech Research,* 6.

GARG, A. & TANGIRALA, A. K. Interaction Assessment in Multivariable Control Systems through Causality Analysis. Advances in Control and Optimization of Dynamical Systems, 2014. 585-592.

LI, Y., ZHU, Z. & CHEN, G. 2014. Bond Graph Modeling and Validation of an Energy Regenerative System for Emulsion Pump Tests. *The Scientific World Journal,* 2014.

RAJANIKANTH VADIGEPALLI, E. P. G., AND FRANCIS J. DOYLE III 2001. Robust Control of a Multivariable Experimental Four-Tank System. *Ind. Eng. Chem. Res,* 40.

ROSINOVA, D. & KOZÁ̌KOVÁ̌, A. Decentralized Robust Control of MIMO Systems: Quadruple Tank Case Study. Advances in Control Education, 2012. 72-77.

TRIKI, S., MEKKI, T. & KAMOUN, A. 2014. Modeling Switched Behavior with Hybrid Bond Graph: Application to a Tank System. *arXiv preprint arXiv:1402.2925.*

VIJULA, D. A. & DEVARAJAN, N. 2013. Design of Decentralised PI Controller using Model Reference Adaptive Control for Quadruple Tank Process. *International Journal of Engineering and Technology*.

WOLFANG, B. 2013. Bond Graph Modelling and Simulation of Mechatronic Systems An Introduction into the Methodology. *European Control Conference (ECC).*

Design of (7, 4) Hamming Encoder and Decoder Using VHDL

Usman Sammani Sani[1*], Ibrahim Haruna Shanono[2]
[1,2]Department of Electrical Engineering,
Bayero University, Kano, P.M.B. 3011, Nigeria
Corresponding Author's Email: usmanssani@live.com, Phone Number: 08025791503

ABSTRACT

Hamming code is one of the commonest codes used in the protection of information from error. It takes a block of k input bits and produce n bits of codeword. This work presents a way of designing (7, 4) Hamming encoder and decoder using Very High Speed Integrated Circuit Hardware Description Language (VHDL). The encoder takes 4 bits input data and produces a 7 bit codeword. The encoder was designed through the usual generator matrix multiplication while in the decoder design the computation of the syndrome vector was ignored. Meanwhile, the different states that can represent a particular input were calculated and the decoder was designed to identify each codeword representing a particular input. Results have shown that the method is also reliable.

Keywords: Hamming, VHDL, Encoder, Decoder, Syndrome vector.

1. INTRODUCTION

Hamming codes are used in error detection and correction in digital communication circuitries. Hamming codes belong to the class of block codes which are codes that work on a block of bits rather than individual bits of data. A block code designated by (n, k) means k bits of input data is used in producing a codeword, C with n bits of data (Edward and David, 1994), (Richard, 2003). The n – k bits added are called parity check bits. Thus a (7, 4) Hamming encoder produces 7 bits from 4 bits and the codeword has 4 parity check bits. Hamming codes are usually generated by multiplying the input block, x by a generator matrix, G (John, 2007). Digital communications involves 0s' and 1s'. Both the generator matrix and the input matrix are in form of 0s' and 1s'. The addition involved during the multiplication of the two matrices is modulo – two addition (Edward and David, 1994). For example a (7, 4) Hamming code has the generator matrix

$$\mathbf{G} = \begin{bmatrix} 1 & 0 & 0 & 0 & 1 & 1 & 0 \\ 0 & 1 & 0 & 0 & 1 & 0 & 1 \\ 0 & 0 & 1 & 0 & 0 & 1 & 1 \\ 0 & 0 & 0 & 1 & 1 & 1 & 1 \end{bmatrix} \quad (1)$$

For an input x,

$$C = Gx \quad (2)$$

Hamming codes are decoded by multiplying the codeword received, r by a parity check matrix, H to see whether there is an error or not. The resulting matrix is called a syndrome vector, Z. If Z is zero, it means there is no error while if Z is not zero, then the position of the bit that is in error is indicated by Z. Hamming codes can only correct a single bit error (Peter, 2002) and are mostly used in Random Access Memory for error correction purpose (Mistri et al, 2014).

$$\mathbf{H} = \begin{bmatrix} 1 & 1 & 0 & 1 & 1 & 0 & 0 \\ 1 & 0 & 1 & 1 & 0 & 1 & 0 \\ 0 & 1 & 1 & 1 & 0 & 0 & 1 \end{bmatrix}$$
$$(3)$$

For a codeword C,

$$Z = Hr \quad (4)$$

In this work, a (7, 4) Hamming encoder and decoder is designed using Very High Speed Integrated Circuit Hardware Description Language (VHDL). VHDL is a programming language that became popular in the 1990s'. It is similar to other high level programming languages such as C but in its own case it doesn't have a compiler but has a synthesizer. The synthesizer translates the written source code into an equivalent hardware described by the source code. The process of this translation is called synthesis (Enoch, 2006).

2. METHODOLOGY

The G and H matrices above were used in the process. The encoder and decoder design will be discussed separately.

2.1 Encoder Design

The encoder has a generator matrix in which it produces the codewords. The codeword is a vector with seven bits. Each bit is obtained by multiplying the input matrix by a column in G as shown below:

C(1) = x(1)
C(2) = x(2)
C(3) = x(3)
C(4) = x(4)
C(5) = x(1) XOR x(2) XOR x(4)

C(6) = x(1) XOR x(3) XOR x(4)
C(7) = x(2) XOR x(3) XOR x(4)

C(n) stands for the nth bit in the codeword and x(n) stands for the nth bit of the input bits. The VHDL code was then developed and synthesized using XILINX ISE 10.1 software.

2.2 Decoder Design

For restoring the original message, the codewords corresponding to the 16 possible combinations of input were calculated using some Matlab codes. The results of the 16 combinations of 4 bit input data resulted in the table below:

Table 1. Codewords for 4 input data.

S/N	X	C
1	0000	0000000
2	0001	0001111
3	0010	0010011
4	0011	0011100
5	0100	0100101
6	0101	0101010
7	0110	0110110
8	0111	0111001
9	1000	1000110
10	1001	1001001

S/N	x	C
1.	0000	0000000
		1000000
		0100000
		0010000
		0001000
		0000100
		0000010
		0000001
2.	0001	0001111
		1001111
		0101111
		0011111
		0000111
		0001011
		0001101
		0001110
3.	0010	0010011
		1010011
		0110011
		0000011
		0011011
		0010111
		0010001
		0010010
4.	0011	0011100

11	1010	1010101
12	1011	1011010
13	1100	1100011
14	1101	1101100
15	1110	1110000
16	1111	1111111

Hamming codes can correct a single error. So in this work, bits of a codeword representing a particular input were altered one by one and each new codeword represents that same input. Therefore in this case the need of computing the syndrome vector and later on correcting the bit in error has been abandoned, unlike in (Saleh, 2015), where the syndrome vector was computed. This method also differs from that of (Hosamani and Karne, 2014), in which the parity bits were inserted directly without the use of a defined generator matrix at the encoder and then the received parity bits were also computed at the decoder. Thus in our own case, each of the 16 input combinations has 8 different codewords representing it. The whole seven bits possible combinations of codewords has thus been assigned the correct input representing it (i.e. $2^7 = (16 \times 8) = 128$). The table below shows the different combinations of codewords and there corresponding inputs.

Table 2. Codewords extension of 4 bits input.

S/N	x	C
		1011100
		0111100
		0001100
		0010100
		0011000
		0011110
		0011101
5.	0100	0100101
		1100101
		0000101
		0110101
		0101101
		0100001
		0100111
		0100100
6.	0101	0101010
		1101010
		0001010
		0111010
		0100010
		0101110
		0101000
		0101011
7.	0110	0110110
		1110110
		0010110

No.	x	C
		0100110
		0111110
		0110010
		0110100
		0110111
8.	0111	0111001
		1111001
		0011001
		0101001
		0110001
		0111101
		0111011
		0111000
9.	1000	1000110
		0000110
		1100110
		1010110
		1001110
		1000010
		1000100
		1000111
10.	1001	1001001
		0001001
		1101001
		1011001
		1000001
		1001101
		1001011
		1001000
11.	1010	1010101
		0010101
		1110101
		1000101
		1011101
		1010001
		1010111
		1010100
12.	1011	1011010

No.	x	C
		0011010
		1111010
		1001010
		1010010
		1011110
		1011000
		1011011
13.	1100	1100011
		0100011
		1000011
		1110011
		1101011
		1100111
		1100001
		1100010
14.	1101	1101100
		0101100
		1001100
		1111100
		1100100
		1101000
		1101110
		1101101
15.	1110	1110000
		0110000
		1010000
		1100000
		1111000
		1110100
		1110010
		1110001
16.	1111	1111111
		0111111
		1011111
		1101111
		1110111
		1111011
		1111101
		1111110

Codes were also written in VHDL to describe the decoder.

3.   RESULTS

Figure 1. Register transfer level of the encoder.
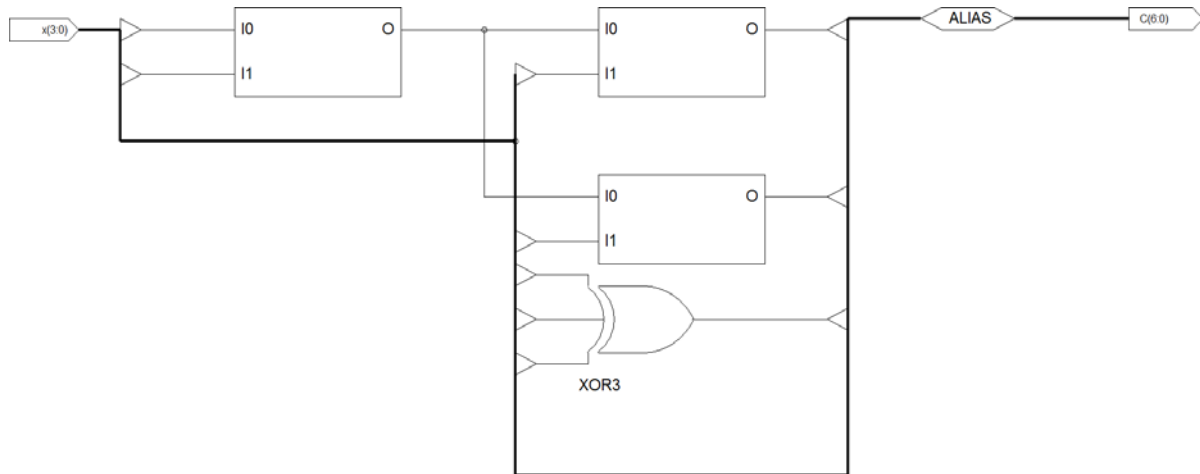
Figure 2. Component view of the encoder
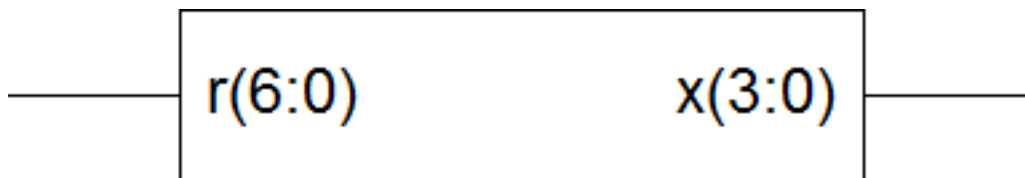
Figure 3. Register transfer level of the decoder
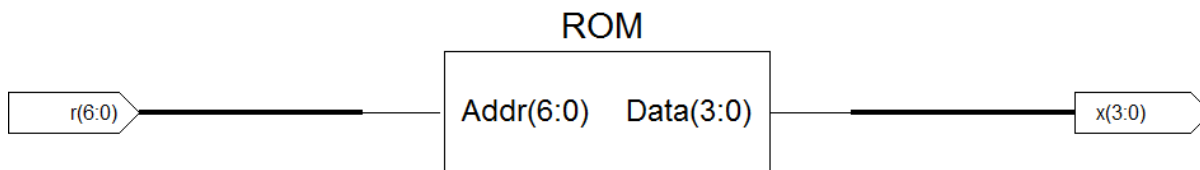
Figure 4. Component view of the Decoder

5. CONCLUSION

The paper has presented a way of designing (7, 4) Hamming encoder and decoder using VHDL. The encoder was designed the normal way while some modifications were made in the decoder design that avoided the computation of a syndrome vector. Results have shown how VHDL simplifies the design of digital hardware and how the design procedure is effective. The same process can be used in the design of any Hamming encoder and decoder. The designed circuits can be used in places they would be applicable or even be left as trainers for students to understand the concept of Hamming encoding and decoding. Thus several digital logic circuits meant for experiment could be designed so that they can be used on a single target device such as a Field Programmable Gate Array. This reduces the cost of setting up a laboratory.

REFERENCES

Edward A. L., David G.M., Digital Communication, Kluwer Academic Publishers, 1994, pp613-617.

Enoch O. H., Digital Logic and Microprocessor Design with VHDL, La Sierra University, 2006, pp 23-26.

Hosamani R., Karne A.S., design and Implementation of Hamming Code on FPGA Using Verilog, International journal of Engineering and Advanced technology, Vol.4, Issue 2, 2014, pp 181-184.

John P., Masoud S., Digital Communications, McGraw-Hill, 2007, pp 413-418.
Peter S., Error Control Coding; from theory to practice, John Wiley and Son's ltd, 2002, pp 67–69.

Mistri R. K. et al, Reduced Area and Improved Delay Module Design of 16 bit Hamming Codec Using HSPICE 22nm Technology Based on GDI Technique, international Journal of Scientific and Research publications, vol. 4, Issue 7, 2014, pp 1-6.

Richard E. B., Algebraic Codes for Data Transmission, Cambridge University Press, 2003, pp54.

Saleh A.H., Design of Hamming Encoder and Decoder Circuits for (64,7) Code and (128,8) Code Using VHDL, Journal of Scientific and Engineering Research, Vol. 4, Issue 1, 2015, pp 1-4.

DEVELOPMENT OF A REAL TIME DISTRIBUTED WIRELESS SENSOR NETWORK USING LABVIEW

Suleiman U. Hussein[1*], Paul McKenna[2], Emmanuel Okafor[3], Abdullahi I. Audu[4]

[1,2]School of Engineering and Built Technology, Glasgow Caledonian University, Scotland, United Kingdom

[3,4]Department of Electrical and Computer Engineering, Ahmadu Bello University, Zaria, Nigera

*elsuligh@gmail.com, +2348037847476.

ABSTRACT

This paper entails the development of a real time distributed wireless sensor network system using Laboratory Virtual Instrument Engineering Workbench (LabVIEW) and instruments form NI (National Instruments) with ZigBee wireless technology. The system was accomplished by configuring the wireless sensor network on a host controller, extraction of measurement data with the aid of LabVIEW and Implementation of several subsystems such as; radio link failure and time recorder, file storage, logging table, Audio-visual alarm system, system initializer and initial system time delay. Hence, the subsystems are then integrated to form the wireless sensor network. This system is intended to acquire the temperature of a system remotely ranging from temperature of $-200^0 C$ to $1250^0 C$ base on type-K thermocouple material used. Also, the audio visual alarm system addressed the effect of safety in a Wireless Sensor Network using ZigBee technology. Result showed that the real time system was working satisfactorily, displaying temperature reading of $27.37^o C$ for duration 2740 to 2767s.

Keywords: *Wireless Sensor Network, Thermocouple,ZigBee, LabVIEW.*

1. INTRODUCTION

Wireless sensor networks (WSNs) have gained world-wide attention in recent years, particularly with the proliferation in Micro-Electro-Mechanical Systems (MEMS) technology which has facilitated the development of smart sensors. These sensors are small, with limited processing and computing resources, and they are inexpensive compared to traditional sensors. These sensor nodes can sense, measure, and gather information from the environment and, based on some local decision process, they can transmit the sensed data to the user (Abuzneid et al., 2015; Yick et al., 2008) . In addition to its area of application, WSN can be used in ZigBee based multilevel parking vacancy, monitoring system, design of intelligent warehouse, measurement and control system (Somani

&Patel, 2012). Also, ZigBee based wireless sensor networks finds relevance in the area of environmental monitoring (Kaushal et al., 2014).

Wireless Sensor Network (WSN) is made up of tiny wireless devices capable of taking various environmental measurements, such as temperature, humidity, vibrations, and luminance (Nakayama et al., 2007). Therefore, it can be defined as a network of devices, denoted as nodes, which can sense the environment and communicate the information gathered from the monitored field (e.g., an area or volume) through wireless links (Buratti et al., 2009; Ye et al., 2011)

A typical WSN comprises of host controller, gateway and nodes. The sensor nodes sense, measure, and gather information from an environment and, they can also

transmit the sensed data to the user based on locally designed decision process (Yick et al., 2008).

WSN is inexpensive and has reduced cost of implementation (Chi & Xinchun, 2012). In support of this, Lueders and Accutech (2005) states that 'when no wires are required for power or signal transmission, monitoring devices becomes less costly to own and operate, and can easily be installed more quickly'. Toteda(2008),considered the environmental safety using wireless sensor in order to ensure safe monitoring of critical process parameters and equipment condition. In addition to its merits, wireless sensor network finds application in both biological and ecological activities which provided new avenues for inquiry at greater spatial and temporal resolution, and collection of diverse types of data such as: temperature, imagery and sound (Porter et al., 2005).

However, WSN is faced with problem of poor energy management ability of the node if not properly designed from inception could be expensive than a wired network. In order to mitigate this challenge, Lewis (2004) suggested that an increase in the lifetime of sensor nodes through power generation, power conservation, and power management scheme would in turn improve sensor network. Also, Royo et al. (2009) designed a power-aware link protocol to reduce energy wastage due to idle listening time of nodes and the work had the ability to lower the radio duty cycle by turning the radio on and off.

Moreover, Toteda (2008) focused on time-synchronized communication which was critical in conservation of battery life by allowing sensors to operate on the equivalent of two AA-batteries for seven to ten years or more. Also, the work considered the optimal reliability performance of the wireless sensor network

However, limited works have been carried out using LabVIEW application in analysing remote temperature sensing and safety design for abnormal temperaturein open literatures.

In this paper, the design and implementation of a real time wireless sensor network using LabVIEW with the view of determining the temperature of an environment remotely was actualized. Also, the audio and visual alarm implementation for abnormal temperature which factored in safety was achieved. Furthermore, data logging was implemented for saving abnormal temperature for reference purpose. The remaining parts of this paper are divided into Sections: the methodology adopted in the implementation of distributed wireless sensor network which determines the temperature of an environment is presented in Section 2. Section 3 discusses the results and provides a real time performance of the system at normal working condition. Section 4 concludes the work and recommends areas for further work.

2. METHODOLOGY

The graphical programming platform used by LabVIEW in the implementation of a real time distributed wireless sensor networks is described using the flowchart presented in Fig1.
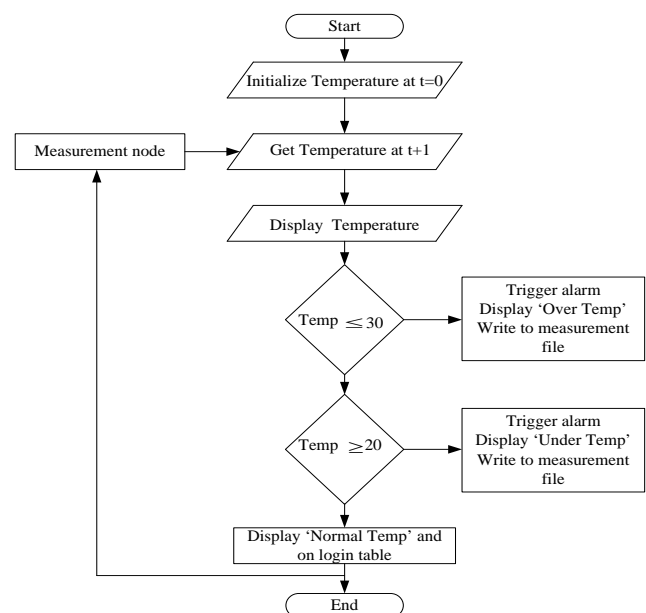
Fig 1: Flowchart Showing the Programmatic Implementation of a Real Time Distributed Wireless Sensor Network using LabVIEW

It is pertinent to note that LabVIEW is a graphical programming application which uses symbolic blocks in developing program codes. This application can be used to perform task such as simulation, visualization and computation. In this work LabVIEW was used to design a real time distributed wireless sensor networks.

The steps adopted in actualizing this development are discussed as follows:

2.1 Configuration of the Wireless Sensor Network on the Host Controller

To configure Wireless Sensor Network on our Host controller, NI Measurement and Automation Explorer was launch and configured the WSN. The following steps explain how this can be achieved:

i. Launch Measurement & Automation (MAX) and expand Remote Systemsto be sure that MAX has auto-detected the WSN-9791.

ii. If plugged into the Ethernet port on the local subnet or directly into the PC host, the gateway appears in Remote Systems.

iii. If the gateway is plugged into a port that is not on the subnet, it can manually be configured using the WSN gateway.

iv. To change the default setting, enter the default host name of the device,"NI-WSN9791''followed by the serial number: NI-WSN9791-014A41F2.

v. Select the Network Setting tab and obtain an IP address automatically. Alternatively, if we know the gateway IP address, such as 192.168.0.2, then we can enter it and click finish.

vi. Add the measurement nodes to the Wireless Sensor Network by selecting WSN nodes tab and clicking the Add WSN Node button.

vii. Enter the type, serial number, and ID number for the measurement nodes and click Apply to save change.

viii. To establish a connection with the gateway, press the Signal Strength button on the node for at least five seconds.

ix. When connected, refresh the WSN Nodes tab to view the last communication time, battery state, link quality, and mode of the measurement nodes.

2.2 Extracting Measurement Data with LabVIEW

LabVIEW and NI-WSN was used in extraction of measurement data which was achieved using the following steps;

i. Start up theLabVIEW application, click through the activation screen in order to initialize the start menu window.

ii. Select empty project to bring up a new project explorer window.

iii. Add NI WSN-9791 Ethernet gateway to the LabVIEWProject.The measurements nodes configure with the network automatically.

iv. Create a host VI by right-clicking on My Computer and selecting New.

v. To monitor thermocouple temperature, drag the corresponding Input/Output variables to the LabVIEW block diagram.

vi. We also monitored node attribute like battery voltage and link quality by dragging the corresponding input/output variables to the block diagram.

vii. We added measurement functions and indicators to the front panel of our LabVIEW to view the system response.

viii. After, completing the design phase, we clicked Run to start acquiring data from the NI WirelessSensor with the aid of ZigBee wireless technology

2.3 Implementation of the Various Sub-System

i.   Implementation of Radio link failure and Time recorder in LabVIEW

Implementation of radio link failure and time recorder was carried out with LabVIEW to show when there is failure in the radio link. The LabVIEW code for the implementation is shown in Fig 2.
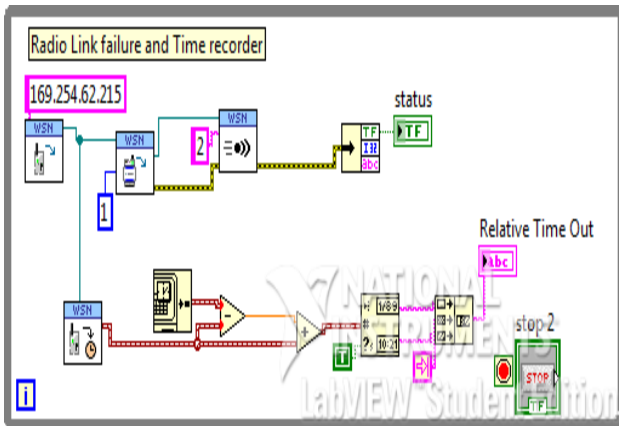
Fig 2: LabVIEW Code for Radio Link and Time Record

ii.   Implementation of a File Storage

This was done to write temperature outside a set limit of between 20-30°C with the aid of LabVIEW code. The "file name out" and "saving data" blocks were designed and then written into the "write to measurement file", for easy access to temperature. The "write to measurement file block" writes data to text-based measurement file (.lvm) or binary measurement files (.tdm or .tdms). While, the "file name out block" displays the full path to the file to which data is written to.

iii.   Implementation of Build (Logging) Table

It is implemented to keep all the measured temperature within the limit of 20-30°C for reference.

iv.   Implementation of Audiovisual Alarm system

Several Boolean and mathematical operators have been used to implement the alarm system, and a speaker was used to get an audio sound that would sound a continuous warning to the operator in the event of abnormal temperature. The LabVIEW program code which account for safety in the WSN is shown in Fig 3.
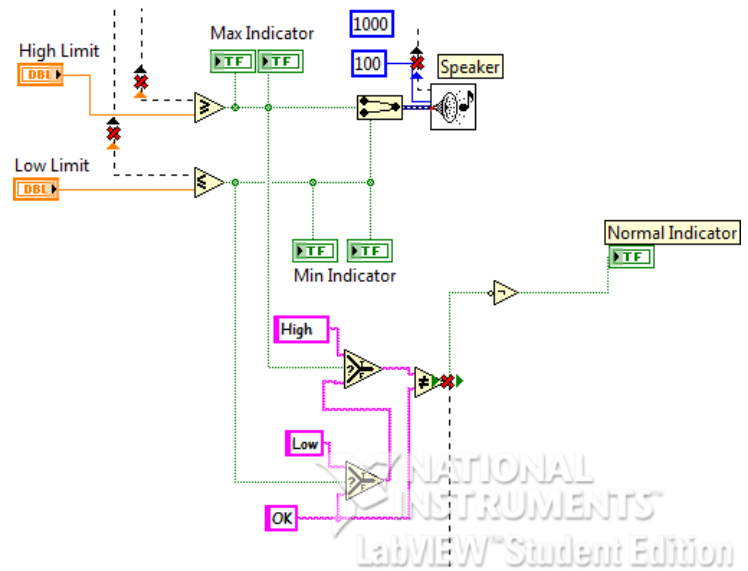
Fig 3: LabVIEW Code for Alarm System

v.   Implementation of System Initializer

This reset the radio link quality, battery, and temperature indicator to the value of zero at the start of the wireless sensor network for temperature measurement.

vi.   LabVIEW implementation of Initial System Time delay

The system is design to wait for 20ms at start up, in order to give proper measurement of the environmental temperature. This repeats the sub-diagram inside it until the conditional terminal, an input terminal, receives a particular Boolean value (gives TRUE or FALSE information). The Boolean value depends on the continuation behaviour of the while loop. The while loop keeps the system running until the stop button is pressed.

vii.   Integration of the Subsystem of the Wireless Sensor Network

The integration of all the implemented sub system to form a complete wireless sensor network system is shown in Fig 4.

110
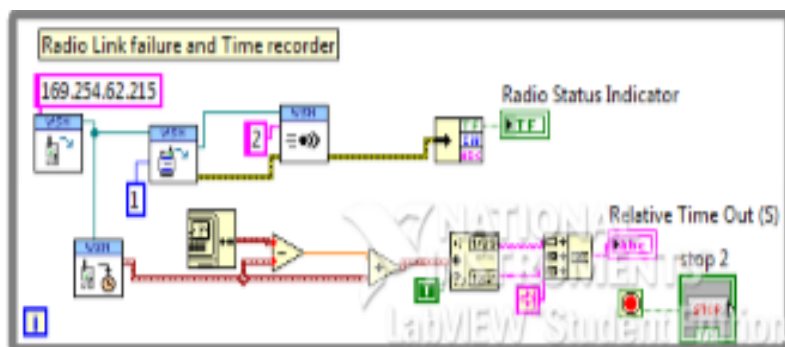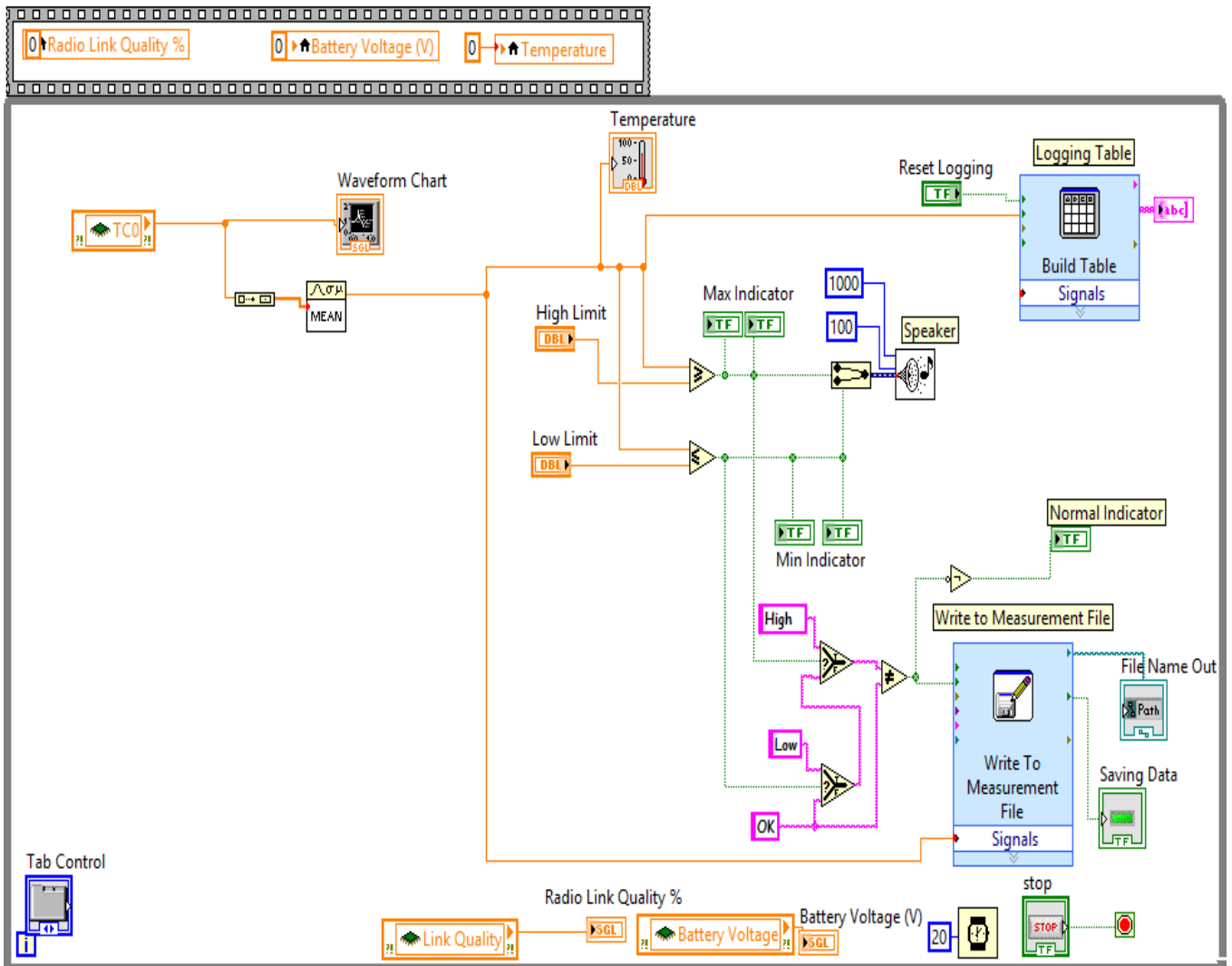
Fig 4: Complete Block Diagram of the Wireless Sensor Network

While, the control panel for the system which shows the graphical user interface that enable users perform environmental monitoring task is shown in Fig 5.
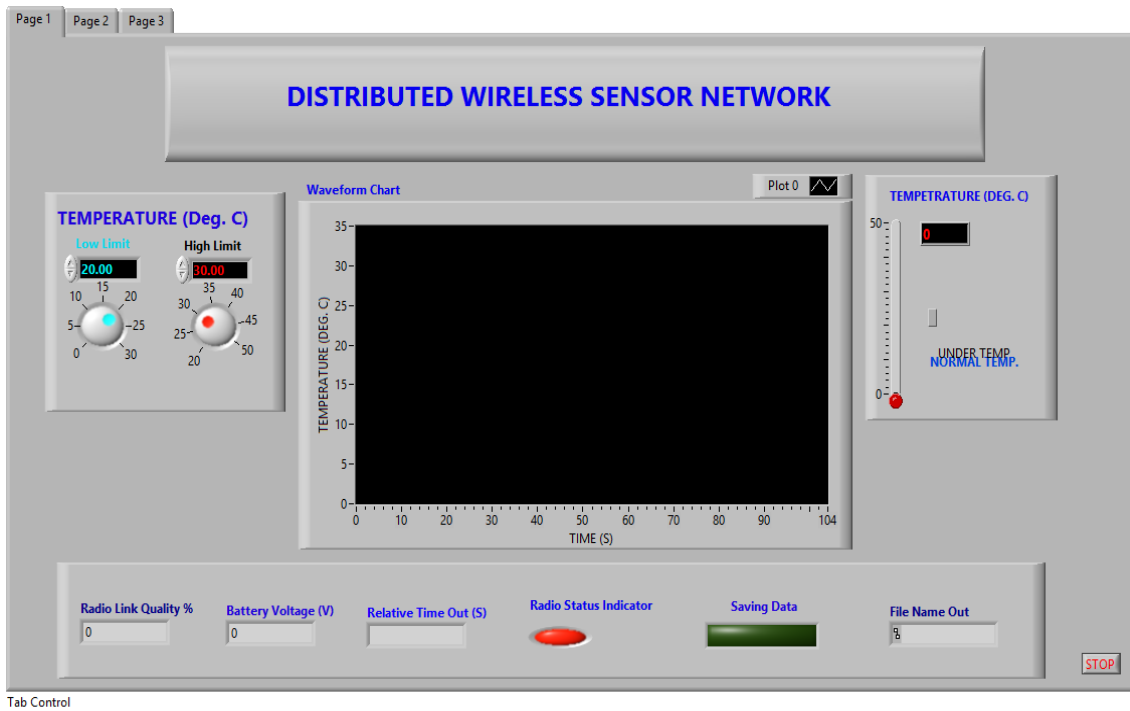
Fig 5: The Control Panel of the Distributed WSN

3. RESULTS AND DISCUSSIONS

Once the run button on the front panel of the LabVIEW is pressed, the type K thermocouple senses the temperature of the heat source or environment, while the NI WSN-3212 performs the signal conditioning of the sensed signal by the thermocouple, and transmit it wirelessly with the help of the attached radio linkusing ZigBee technology to the NI WSN-9791 Ethernet gateway. The gateway sends the aggregated data from the node to the host controller (laptop in this case) through the RJ45 Ethernet cable. The measured temperature (in degree Celsius) is displayed on the front panel of the LabVIEW program as shown in Fig 6. The system is design to measure temperature within a set limit by the operator (in this case 20-30°C) and as long as the measured temperature remain within the desired limit, there is an indicator that shows that the temperature is within the limit by blinking the inscription 'Normal temperature' in green colour for the operator to see. The desired measured temperature is logged into a table on the front panel for the operator to make reference to.
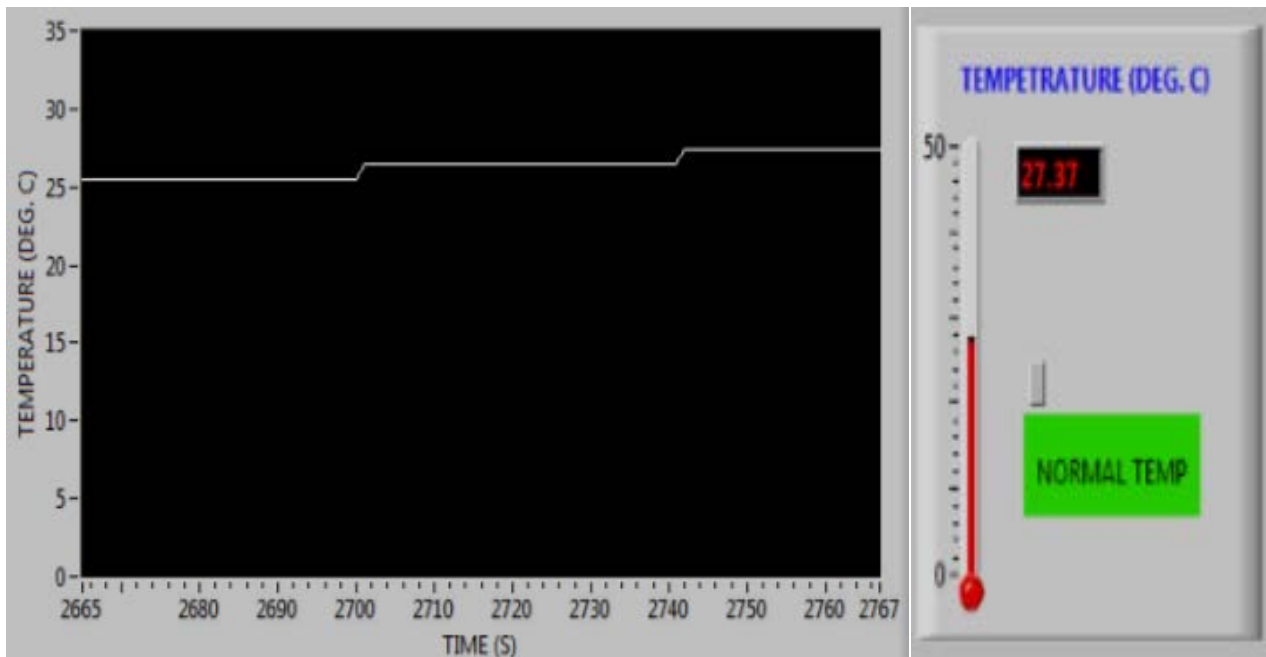
Fig 6: Temperature Reading from Distributed Wireless Sensor

4. CONCLUSION

The development of a real time distributed wireless sensor network system using LabVIEW (National Instrument (NI)) with the aid of ZigBee wireless technology was achieved. The system was designed and implemented by adopting the following methods: configuring the wireless sensor network on a host controller, extraction of measurement data with the aid of LabVIEW and Implementation of several subsystems such as; radio link failure and time recorder, file storage, logging table, Audio-visual alarm system, system initializer and initial system time delay. Hence, the subsystem are then integrated to form the wireless sensor network. Result showed that the real time system was working satisfactorily displaying temperature reading of $27.37^o C$ for a duration 2740 to 2767s. Further works should examine the incorporation of controller to maintain a specified range of temperature in a scenario where there is either excessive temperature or under temperature in an area.

REFERENCE

Abuzneid, A.-s., Sobh, T., & Faezipour, M. (2015). *An enhanced communication protocol for anonymity and location privacy in WSN*. Paper presented at the Proceedings of the IEEE Wireless Communications and Networking Conference, New Orleans, LA, USA, country.

Ahamed, S. R. (2009). The role of zigbee technology in future data communication system. *Journal of theoretical and applied information technology, 5*(2), 129.

Buratti, C., Conti, A., Dardari, D., & Verdone, R. (2009). An overview on wireless sensor networks technology and evolution. *Sensors, 9*(9), 6869-6896.

Chi, X., & Xinchun, L. (2012). Temperature and Humidity Monitoring System Based on ZigBee-WSN [J]. *Microcontrollers & Embedded Systems, 6*, 013.

Gary, F. F. (2011). Measuring Temperature by Direct Contact. *Chemical Engineering Progress, 107*(9), 26-30.

Kaushal, K., Kaur, T., & Kaur, J. (2014). ZigBee based Wireless Sensor Networks. *International Journal of Computer Science and Information Technologies, 5*(6), 7752-7755.

Lewis, F. L. (2004). Wireless sensor networks. *Smart environments: technologies, protocols, and applications*, 11-46.

Lueders, W., & Accutech, A. (2005). Wireless sensors for environmental compliance. *Chemical engineering, 112*(8), 40-43.

Nakayama, H., Ansari, N., Jamalipour, A., & Kato, N. (2007). Fault-resilient sensing in wireless sensor networks. *Computer Communications, 30*(11), 2375-2384.

Porter, J., Arzberger, P., Braun, H.-W., Bryant, P., Gage, S., Hansen, T., . . . Kratz, T. (2005). Wireless sensor networks for ecology. *BioScience, 55*(7), 561-572.

Royo, F., Olivares, T., & Orozco-Barbosa, L. (2009). A synchronous engine for wireless sensor networks. *Telecommunication Systems, 40*(3-4), 151-159.

Somani, N. A., & Patel, Y. (2012). Zigbee: A Low Power Wireless Technology For Industrial Applications. *International Journal of Control Theory and Computer Modelling (IJCTCM) Vol, 2*.

Toteda, S. (2008). Wireless sensor. *InTech, 55*(10), 60-63.

Ye, M., Chen, T., & Yu, C. (2011). ZigBee-based positioning and navigation system for robot. *Journal of Convergence Information Technology, 6*(1), 135-146.

Yick, J., Mukherjee, B., & Ghosal, D. (2008). Wireless sensor network survey. *Computer networks, 52*(12), 2292-2330.

APPLICATION OF BOX-BEHNKEN DESIGN FOR OPTIMIZATION OF CATION EXCHANGE CAPACITY OF ZEOLITES LINDE-TYPE A AND Y

Oyinade Adewolu[1*], A. S Kovo[1], Alechine E. Ameh[2], Patrick Hill[3]

[1]Federal University of Technology Minna, Nigeria.
[2]University of Western Cape, Cape Town, South Africa.
[3]University of Manchester, United Kingdom.
[*]oyinade.adewolu@st.futminna.edu.ng, +234-8055272827.

ABSTRACT

Zeolites Linde – Type A and Y were synthesized from sodium metasilicate, alumina, sodium hydroxide and water using hydrothermal method. Response Surface method called Box – Behnken was used to design the number of experiments considering three factors affecting the synthesis [(i) hydrothermal treatment time (A), (ii) hydrothermal treatment temperature (B) and (iii) ageing time (C)]. The synthesized zeolite products were characterized using XRD and SEM, and their cation exchange capacity (CEC) was calculated. The ammonium ion CEC for LTA ranges from 4.94 – 8.37meq/g while that of zeolite Y ranges 3.40 – 6.51meq/g. Also, the calcium ion CEC for LTA ranges from 5.99 – 8.04meq/g while that of zeolite Y is from 4.17 – 8.55meq/g. This may be attributed to low Si/Al as a result of high aluminium content in these products. The X–ray diffraction XRD pattern peak of samples LTA (A4) and zeolites Y were quite consistent with the reference sample as reported by Traecy and Higgins. The XRD pattern of sample (A4) and (Y6) showed the highest percentage crystallinity of 32.84% and 75.03% respectively. The SEM showed a cubic face centred structure for Zeolite A and hexagonal crystal shape for zeolite Y.

Keywords: Zeolite, *Linde – Type A, Faujasite Y, CEC, RSM , Box – Behnken.*

1. INTRODUCTION

Zeolites are three-dimensional crystalline solids with micro-pores and well-defined structures that contain aluminium, silicon, and oxygen with a regular framework (Breck, 1974). The silicon and aluminium atoms are tetrahedrally coordinated with each other through shared oxygen atoms. Since silicon typically exists in a +4 oxidation state, the silicon-oxygen tetrahedral are electrically neutral, while aluminium-oxygen tetrahedral forms centres that are electrically deficient of one electron because aluminium typically exists in the +3 oxidation state. The presence of aluminium in the framework results in a negative framework charge, which is balanced by positively charged ions such as Na^+, NH_4^+, Ca^{2+} (Szostak, 1989).

Cation exchange capacity (CEC) is a measure of absorbed cations that can be displaced by exchange with other cations in milliequivalents per 100 grams of material (Reganold and Harsh, 1985). The greater the aluminium content the more the extra framework cations needed to balance the charge, hence, the higher the cation exchange capacity of the zeolites. Zeolites have high cation exchange capacities and unparalleled ability to selectively latch on to specific cations from mixtures with other cations (Dyer, 2007).

According to Ruen-ngam and co-workers, (2009), CEC values can be calculated on a mass balance concept after which the sodium ion in the exchange solution has been determined by spectrophotometry as follows;

$$CEC = \frac{(c_0 - c_b)}{MW * m} * V \qquad (1)$$

Where C_0 is the sodium ion concentration (mg/L).

C_b is the sodium ion concentration in the blank (mg/L).

V is the volume of the aqueous phase (mL).

m is the mass of zeolite (g).

MW is the molecular weight of sodium or absorbed cation (g/mol) (Ruen-ngam *et al.,* 2009).

Box Behnken design is a type of response surface design that does not contain an embedded factorial or fractional factorial design and it requires a fewer number of runs. This response surface design does not have axial point (i.e. it is rotatable), it ensures that all design points fall within a safe operating zone and that all factors are not set at their high levels at the same time (Box and Draper, 1987).

Past work has been done using factorial and response surface methods. Karami and Rohani used four methods (gelling of soluble silicate to silica – alumina gel, precipitation of soluble silicate to precipitated silica alumina gel, gelling of soluble silicate by sulphuric acid plus alumina impregnation and precipitation of soluble silicate by sulphuric acid plus alumina impregnation) for the synthesis of zeolite Y. They used a 2 by 4 factorial design to study the influence of four different variables; mixing rate, alkalinity, ageing time and synthesis time on the purity of zeolite Y. Using the first method, they found that ageing time was the most significant variable and the other three factors were statistically significant. The best synthesis condition of the first method was applied for the other three method and only the fourth method yielded pure zeolite Y. They concluded that in synthesizing pure zeolite Y, the effect of silica – alumina precursor preparation is very important (Karami and Rohani, 2009).

Matlob and co-workers, (2011) used response surface method (Box Behnken design) to determine the optimum conditions for the synthesis of zeolite A from coal fly ash. Using three factor; SiO_2/Al_2O_3 ratio (0.5 – 1.5),

incubation temperature (70 – 120°C) and incubation time (2 – 4days), they observed the highest yield of zeolite A was at SiO_2/Al_2O_3 of 1, temperature of 70°C and 4days. They concluded that duration of incubation has no significant effect on yield percent while SiO_2/Al_2O_3 ratio and incubation temperature decreases with an increase in the yield percent (Matlob, Kamarudin, Jubri and Ramli, 2011).

Musyoka and colleagues synthesized zeolites from coal fly ash using 2 by 4 factorial experimental design using CEC as the model response. The synthesis variables studied were sodium hydroxide concentration, ageing temperature, hydrothermal treatment time and temperature. They found from the analysis of linear and nonlinear interaction, that the main factors which showed interaction among each other were ageing temperature, hydrothermal treatment time and temperature (Musyoka, Petrik, Balfour, Ndungu, Gitari and Hums, 2012).

1.1 Aim and Objectives

The aim of this paper is to study the effect of ageing time, the crystallization temperature and crystallization time on crystallinity and to study the effect of Cation Exchange Capacity (CEC) on the synthesized Zeolites Linde-type A and Y using a Response Surface Methodology (RSM) – Box Behnken design. To accomplish this, a study was completed with the accompanying targets:

1. To synthesize Zeolite A (Linde – type A) and Zeolite (Faujasite) Y from commercial precursors.
2. To characterize the morphology of synthesized zeolites using Scanning Electron Microscopy (SEM), the percentage crystallinity and crystal sizes using X-Ray Diffractometer (XRD).

2. METHODOLOGY

Chemicals used in this study were Sodium metasilicate (Fischer Scientific, 99%), Aluminium Oxide (Loba, 99%), Sodium hydroxide (BDH, 96%), Ammonium acetate (Lab Tech, 99%), Calcium acetate (Merck, 99%), Distilled water (Laboratory made).

2.1. Design of Experiment

The data analysis was carried out with Design Expert® software version 7, applying response surface methodology with Box-Behnken design. The effect of three (3) variables [hydrothermal treatment time (A), hydrothermal treatment temperature (B) and ageing time (C)] on the products were studied. According to the Box-Behnken design, the total number of experiments is $N = 2k * (k - 1) + c_p$, where k is the number of factors and c_p is the number of central points (Matlob *et al.,* 2011). In this work, there were no central points, hence, twelve (12) experiments were carried out for each zeolites synthesized.

Table 1.0 Levels of Independent Variable for Zeolite Linde – Type A

Levels	Low	Medium	High
Coding	-1	0	+1
Hydrothermal Treatment Time (A) h	2	3	4
Hydrothermal Treatment Temp. (B) ^{o}C	85	90	95
Ageing Time (C) h	16	18	20

Table 2.0 Levels of Independent Variable for Zeolite Y

Levels	Low	Medium	High
Coding	-1	0	+1
Hydrothermal Treatment Time (A) h	5	6	7
Hydrothermal Treatment Temp. (B) ^{o}C	90	95	100
Ageing Time (C) h	24	30	36

All factors were adjusted at three levels (-1, 0, +1) with equally spaced intervals between the levels and the range of the variables as shown in Table 1.0 and 2.0. The twelve (12) samples of Linde – type A and Faujasite Y were analysed by CEC and these results were the basis for the response variable.

2.2. Preparation of Zeolite Linde – Type A

The aluminosilicate gel used for the synthesis of zeolite A was prepared from reaction mixture with molar composition $3.29Na_2O:1Al_2O_3:1.697SiO_2:107.8H_2O$.

4.167g of sodium hydroxide pellet was weighed and transferred to the beaker, dissolved in 60mL of deionised water and was continuously stirred until a clear solution was obtained. The solution was divided into two equal volumes. To the first portion, 3.473g of alumina was added. To the second portion, 12.261g of sodium metasilicate was added in the beaker.

The alumina and silicate solutions were mixed in a beaker and stirred to achieve homogenization. The mixture was transferred into a Teflon bottle and left to age at room temperature and varying time between 2 and 4 hours .

The aged mixtures were transferred into the capped 100mL Teflon autoclave for hydrothermal treatment in an oven at autogenous pressure, maintained at distinguishable crystallization temperature and time using the Box-Behnken design matrix. At the end of the hydrothermal treatment, the mixture was cooled at room temperature and the resulting solid products were separated by filtration, washed with deionised water until filtrate pH was about 9. The solid products in various cases were transferred to the watch glass and dried in an oven at 60°C overnight. The samples obtained were weighed and placed in plastic bottles.

2.3. Preparation of Zeolite Y

Zeolite Y was synthesized from aluminosilicate gel mixture with molar composition $7.99Na_2O:1Al_2O_3:20.2SiO_2:323.41H_2O$.

1.198g of alumina was added to 30mL of deionised water and stirred for a while. 19.915g of sodium metasilicate was added to another 30mL deionised water to form a homogenous solution in a beaker. The alumina and silicate mixtures were mixed together and stirred for about 20 minutes until the gel appeared somewhat smooth in the beaker.

The overall gel was transferred into a 100mL autoclavable Teflon bottle (sealed) and was aged for varying time at room temperature. The aged mixture was transferred into an autoclave for hydrothermal treatment in an oven under autogenous pressure, maintained at distinguishable crystallization temperature and time using the Box-Behnken design matrix, until gel separated into solid and supernatant liquid showing a complete crystallization, and then cooled to room temperature.

The resulting solid product was separated by filtration, washed with deionised water until the filtrate pH was about 9. The solid products in various cases were transferred to the watch glass and dried in an oven at 100°C overnight. The zeolite Y was weighed and placed in a plastic bottle.

2.4. Characterization and Analysis

X-ray diffraction patterns were measured by AXS Bruker advance-8 Diffractometer using CuKα (λ = 0.1541nm) radiation at 40kV and 40mA. The diffraction patterns of the synthesized zeolites were obtained at a scan speed of 0.04° 2θ/88sec. The areas, peak positions and widths were estimated using ORIGIN®8. The percentage crystallinity of synthesized zeolites were estimated by comparing seven (7) characteristic peak areas appearing at 2θ from 12 to 55° to that of the reference sample according to the following equation:

$$\% \, crystallinity = \frac{\sum P}{\sum P_s} \times 100 \quad \text{(Rios, William and Fullen, 2008)} \tag{2}$$

Where P is the total areas of seven (7) characteristics peaks patterns of pure sample.

P_s is the total areas of seven (7) characteristics peaks of standard.

The crystal sizes were estimated from the XRD pattern using Scherrer's formula given as;

$$CS = \frac{K * \lambda}{\beta * \cos \theta} \tag{3}$$

Where K = 0.94 is the shape factor for spherical crystal with cubic symmetry,

λ = 0.1541nm is the wavelength of the diffraction,

β is the full width at half maximum (FWHM) in radians,

θ is value of 2θ/2 in radians.

The morphology of zeolites A and Y were done by Scanning Electron Microscopy (SEM) at 20kV and magnification of 500x and 2000x using the FEI Quanta 200 instrument. The Elemental Dispersive Analyser X-ray (EDAX) showed the composition in weight percent, the matrix correction parameters describing the atomic number effect (Z), the absorption effect (A), and the fluorescence effect (F).

Sodium ion analysis for cation exchange capacity were carried out by flame photometer. Calcium ion anlaysis were done by Bulk Scientific atomic absorption spectrophotometer (Accusys 211) and ammonium ion were measured with ultraviolet spectrophotometer using Nessler's reagent.

3.0. RESULTS AND DISCUSSION

3.1. XRD pattern
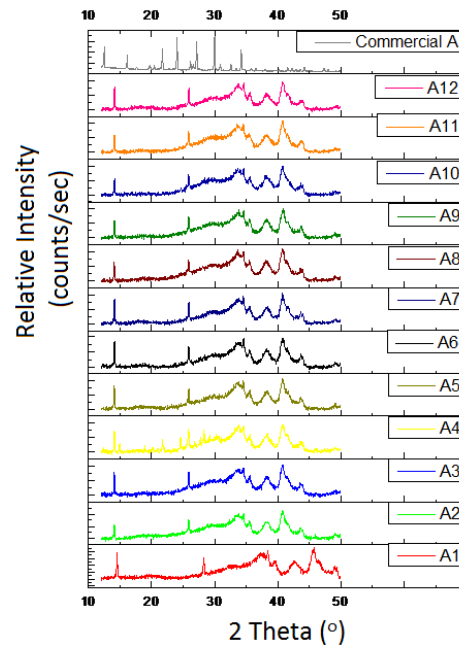
Figure 1.0 X- ray diffraction pattern for the synthesized and commercial LTA

The 7 characteristics XRD peak of LTA (A4) at 2θ: 12.4°, 23.6°, 25.8°, 34.5°, 43.6°, 47.3°, 49.1° which are quite consistent with the reference sample as shown in figure 1.0. Sodalite was however present at 14.1° and amorphous aluminium oxide was observed between 35.5° and 40.8° for (A1) to (A12) with the exception of (A4).

From the XRD pattern obtained, sample (A4) showed better crystalline peaks at crystallization time of 4h, crystallization temperature of 95°C and ageing time of 18h. Linde type A and sodalite phase contribute to the main crystallinity with some amount of aluminium oxide. The XRD background attributed to the presence of amorphous glass increased between 2θ: 30° to 42°. The amorphous aluminosilicate glass and aluminium oxide can be effectively converted to zeolites. Sample (A4) was observed to have the highest percentage crystallinity of 32.84%. Sample (A1) clearly showed XRD characteristic for aluminium oxide.

According to Kovo, (2010), there was no zeolite formation observed by the first two hour of crystallization of zeolite A. This could be attributed to the fact that at the initial period of crystallization after mixing of the aluminosilicate solution, some time is taken before dissolution is completed. The ageing process was expected to promote some degree of dissolution and possibly influence quick formation of zeolite A during crystallization. Kovo, (2010) observed that the gel formed remained amorphous during the first two (2) hour of crystallization. However, increase in the synthesis time of up to 6h show further crystal growth taking place with XRD analysis indicating crystallinity better than that of the commercial sample (Kovo, 2010).
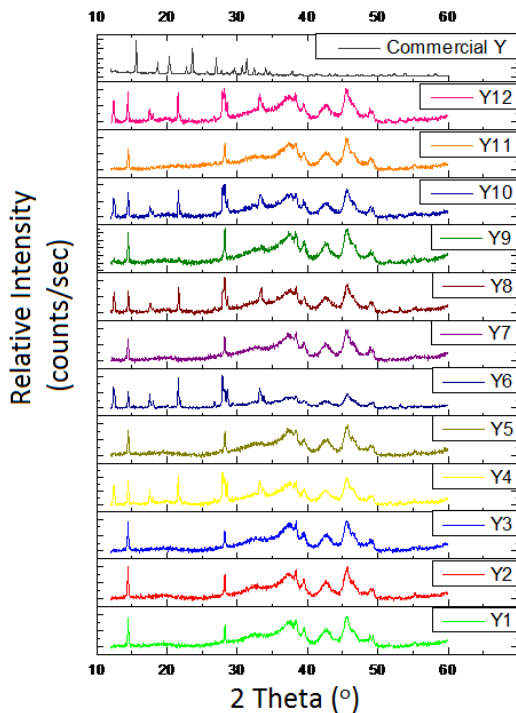
Figure 2.0 X-ray diffraction pattern for the synthesized and commercial Faujasite Y.

The 7 characteristics XRD peak of Faujasite Y at 2θ: 14.5^o, 21.7^o, 28.2^o, 33.2^o, 38.4^o, 49.3^o, 55.3^o which are quite consistent with the reference sample as shown in figure 2.0. Zeolite P appeared at 2 theta: 12.5^o and 17.6^o.

Zeolite Y and P contribute to the main crystalline phase with small amount of unreacted aluminium oxide. Y6 showed the highest percentage crystallinity of 75.03% and has the least amorphous background.

3.2. Scanning Electron Microscopy
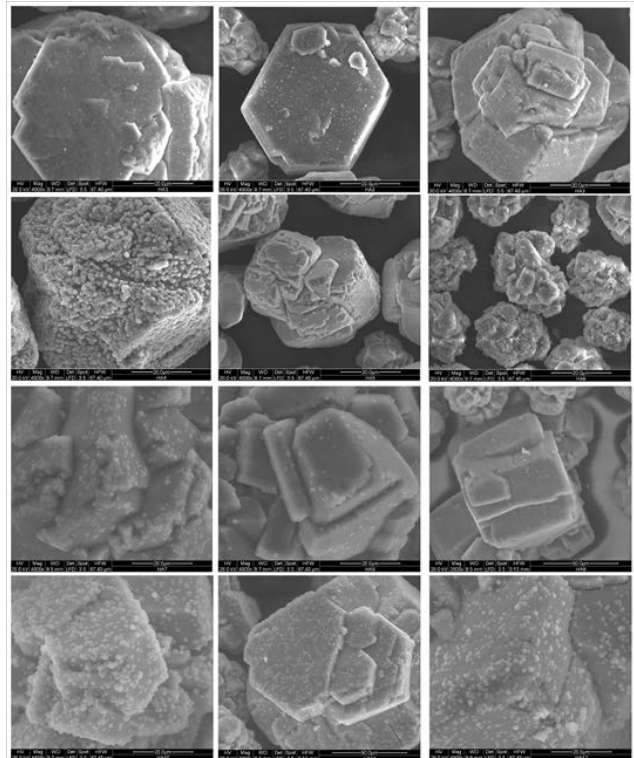
Figure 3.0 Scanning Electron Microscope of LTA

The cubic face centred structure of sample (A4) in figure 3.0 shows a typical morphology of zeolite A. The appearance of small particles in the other samples is due to the incomplete conversion of zeolite LTA and the presence of amorphous unconverted precursors in the reaction medium. The crystals are a mixture of cubic particles with imperfect edges and amorphous aluminosilicate in different symmetry and magnitude and their totality.
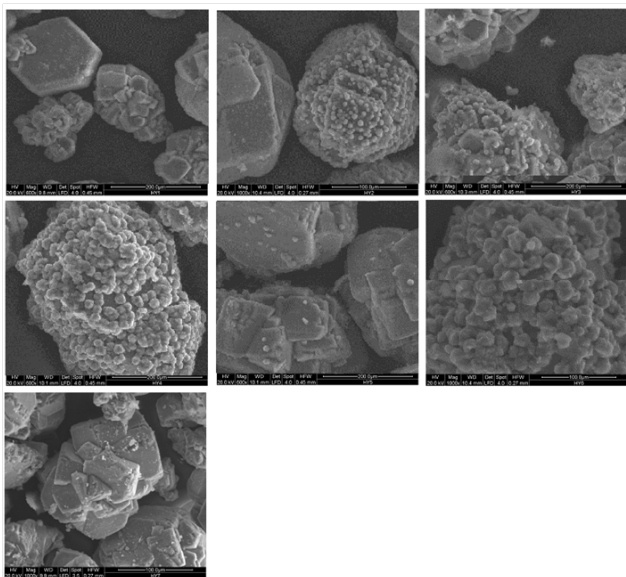
Figure 4.0 Scanning Electron Microscope of zeolite Y

The hexagonal crystal shape of samples products in Figure 4.0 shows the morphology of zeolite Y. Analogous growth and intergrowth of poly crystals was observed explaining the clustering of nuclei.

3.3 Effect of Crystallization Time, Temperature, Ageing Time and Cation Exchange Capacity on Zeolites Synthesis Results and Discussion

3.3.1 Effect of Crystallization Time on Zeolite A Synthesis

Synthesized samples at low time of 2h had lower average crystal size and percentage crystallinity, but as crystallization time increases, percentage crystallinity also increases to about 30% as shown in figure 5.0. The crystal sizes however, are low with one exception at higher crystallization time as percentage crystallinity reaches maximum at 4h. Samples synthesized at low crystallization time had low CEC values compared to those synthesized at high crystallization time when other factors were fixed.

Figure 5.0 A 3D plot showing relationship between crystallization time, crystal size and percentage crystallinity for Zeolite A

3.3.2 Effect of Crystallization Temperature on Zeolite A Synthesis

Temperature tends to have a better crystallization effect on synthesis of zeolite as it helps in the crystal formation from the nuclei. At 85^oC, an average crystal size of 20nm and lower percentage crystallinity were obtained. At 90^oC crystal sizes decreased while better percentage crystallinity were obtained. At 95^oC however, crystal size were lower with one exception and the highest percentage crystallinity was obtained at this temperature as shown in figure 6.0.

Samples synthesized at low temperature gave low CEC, which increased with increase in temperature. The very high CEC value of sample (A1) is due to its high aluminium content (Mumpton, 1999), as the XRD shows that zeolite conversion was minimal at this condition.
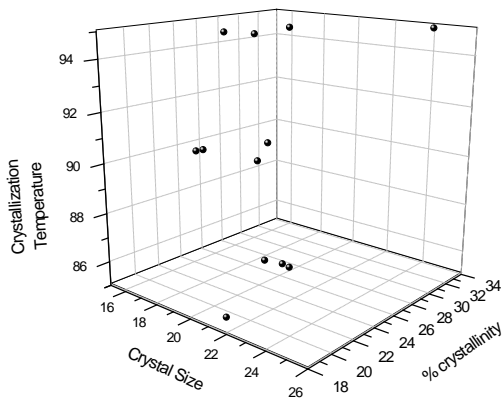
Figure 6.0 A 3D plot showing relationship between crystallization temperature, crystal size and percentage crystallinity for Zeolite A

Figure 7.0 A 3D plot showing relationship between Ageing time, crystal size and percentage crystallinity for Zeolite A

3.3.3 Effect of Ageing Time on Zeolite A Synthesis

Ageing which helps with nuclei formation shows that low percentage crystallinity and crystal sizes which ranges from 16 to 20nm as shown in figure 7.0. Maximum percentage crystallinity and crystal size were obtained at 18h of ageing time. Although percentage crystallinity increased at higher ageing time, crystal sizes were very low.

Ageing time which showed a positive effect on zeolite nucleation showed that CEC values increased with increase in ageing time. From the XRD and SEM results, however, 18h showed the optimum ageing time.

3.3.4 CEC Results and Discussion for Zeolite LTA

Table 3.0 Cation Exchange Capacity for Zeolite LTA

Samples	NH_4^+ CEC (meq/g)	Ca^{2+} CEC (meq/g)
A1	6.646252454	7.809733081
A2	6.860922724	6.187813982
A3	6.416832237	6.5552079
A4	8.372493259	7.423840387
A5	5.347826198	6.479071226
A6	8.270583772	5.991924154
A7	6.576541773	6.176291051
A8	7.687235387	7.50572098
A9	4.935636458	6.762654603
A10	7.546515381	7.326158277
A11	5.457548226	6.982896225
A12	7.17088543	8.039431113

Zeolite LTA exchange with ammonium ion cation exchange capacity varies from 4.94 meq/g to 8.37 meq/g while the zeolite LTA exchange with calcium ion cation exchange capacity varies from 5.99 meq/g to 8.04 meq/g as compared to 5.48meq/g (Shoumkova, 2012). The high CEC value is as a result of high aluminium concentration.

3.3.5 Effect of Crystallization Time on Zeolite Y Synthesis

Low crystallization time had predominantly low percentage crystallinity and crystal sizes. At 6h, however, percentage crystallinity increased but the crystal sizes were still low as seen in figure 8.0 below. At 7h, percentage crystallinity and crystal size increased till it reached a maximum value. Increase in crystallization time resulted in a significant increase in CEC values of synthesized zeolite Y.

the case of calcium ion exchange, a decrease was observed with increase in temperature when other conditions were kept constant as seen in table 4.0. High aluminium content in the products and the type of cation been used for exchange in samples (Y1, Y9 and Y11) could be used to explain why these samples have high CEC values when compared to their counterparts (Y3, Y10 and Y12) at same time and ageing condition. Thus, crystallization temperature had a positive effect on crystallization of the samples to lower its aluminium content, hence, its cation exchange capacity.

Figure 8.0 A 3D plot showing relationship between crystallization time, crystal size and percentage crystallinity for Zeolite Y
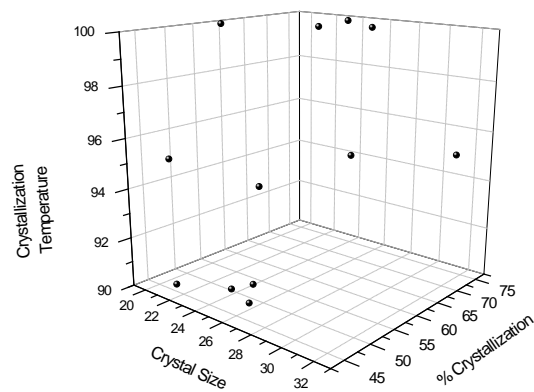
Figure 9.0 A 3D plot showing relationship between crystallization temperature, crystal size and percentage crystallinity for Zeolite Y

3.3.6 Effect of Crystallization Temperature on Zeolite Y Synthesis

Low temperature resulted in low crystal sizes and percentage crystallinity as shown in figure 9.0. At a temperature of $95^{o}C$, crystal sizes and percentage crystallinity increased until maximum values were obtained. At $100^{o}C$, crystal sizes were lower compared to those obtained at $95^{o}C$, however, percentage crystallinity were high.

Increase in crystallization temperature resulted in increase in CEC values when other factors were fixed. However, in

3.3.7 Effect of Ageing Time on Zeolite Y Synthesis

Low ageing time gave better crystal sizes and gradual increase in percentage crystallinity. As ageing time increases, crystal sizes were relatively low but the percentage crystallization increased as shown in figure 10.0. Optimum ageing time of 24h gave the highest percentage crystallinity and crystal size.

Increase in ageing time showed better nucleation of the samples as shown in the SEM results in figure 4.0 above while other factors were kept constant. CEC values decreases with increase in ageing time with the exception of samples (Y9) and (Y11) whose CEC value increases

with increase in ageing time. Samples obtained at higher ageing time showed better nucleation.
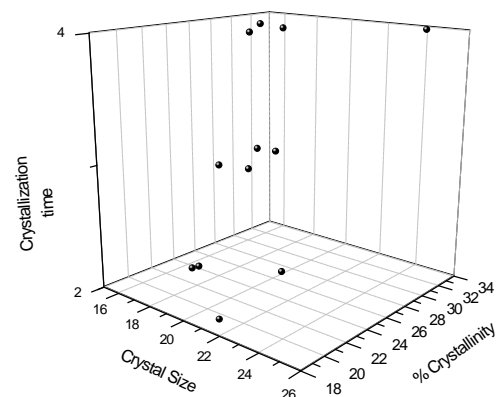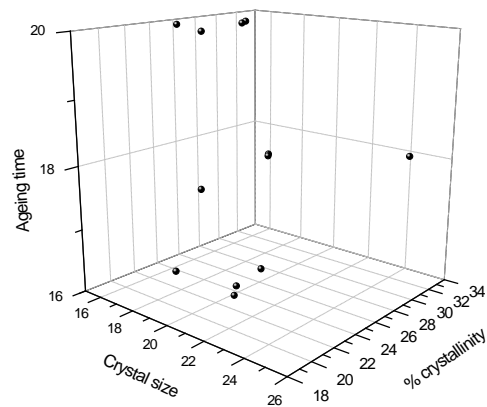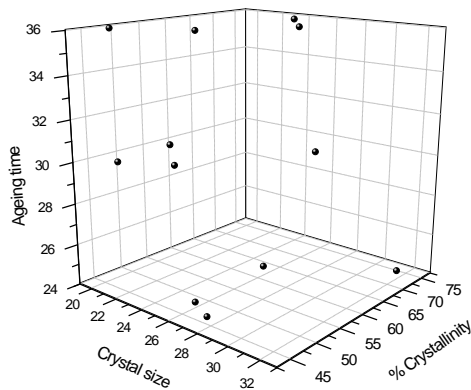

Figure 10.0 A 3D plot showing relationship between ageing time, crystal size and percentage crystallinity for Zeolite Y

3.3.8 CEC Results and Discussion for Zeolite Y

Table 4.0 Cation Exchange Capacity for Zeolite Y

Samples	NH_4^+ CEC (meq/g)	Ca^{2+} CEC (meq/g)
Y1	3.973058144	8.552444627
Y2	4.38925596	4.172875399
Y3	4.523902736	6.078533807
Y4	6.269816339	6.828341563
Y5	4.162036762	6.557161001
Y6	3.807950916	7.332497074
Y7	3.403332144	5.226326779
Y8	6.51419818	6.936727937
Y9	3.818647407	6.675599049
Y10	6.020470889	5.617428894
Y11	6.061805155	7.927399654
Y12	5.541809659	5.885380109

Zeolite Y exchange with ammonium ion cation exchange capacity varies from 3.4 meq/g to 6.51 meq/g while the exchange with calcium ion cation exchange capacity varies 4.17 meq/g to 8.55 meq/g as compared to 3.26 meq/g (Shoumkova, 2012). In the exchange process, more sodium ion was displaced with calcium ions compared to ammonium ions due to the ionic charge of the incoming ion.

3.4 Response Surface Method; Box – Behnken Design

The results are discussed based on cation exchange capacity (CEC) which is the response factor. Statistical testing of the model was performed with F – test to obtain the mathematical relationship between the response and process variables.

The quantity R – squared measured the proportion of total variability in the data as explained by ANOVA. Adequate Precision measures the signal to noise ratio and acts as a good indicator of whether the response surface method are applicable. The Predicted Error Sum of Squares (PRESS) is a measure of how precise the model will predict responses in a new experiment.

The response surface method was used to determine the region in space at which a combination of different variables gives a product withe high Cation Exchange Capacity. The cube plots are predicted values and shows how the three (3) factors; hydrothermal time, temperature and ageing time interact to affect the cation exchange capacity.

3.4.1. Cation Exchange Capacity for Ammonium Ion Exchanged Zeolite A

The relationship between independent variables and response was described by a second – order polynomial equation. The result for the analysis of variance (ANOVA) for the reduced model containing a quadratic model is shown in Table 5.1:

Table 5.1 Results of ANOVA for the Zeolite A Exchange with Ammonium ion CEC at Lambda = 3

Source	Sum of Squares	DF	Mean Square	F value	p-value Prob>F	
Model	2.253E+05	4	56324.81	11.54	0.0033	Significant
A – Hydrothermal time	1.092E+05	1	1.092E+05	22.38	0.0021	
B – Hydrothermal Temp.	70368.99	1	70368.99	14.42	0.0067	
AB	21507.13	1	21507.13	4.41	0.0739	
A^2	24221.47	1	24221.47	4.96	0.0611	
Residual	34153.55	7	4879.08			
Correlation total	2.595E+05	11				

The Model F-value of 11.54 implies the model is significant. For the assumed model, there is only a 0.33% chance that a "Model F-Value" this large could occur due to noise. Values greater than 0.1000 indicate the model terms are not significant and were not included in the model. In this case A, B, AB, A^2 are significant model terms.

Table 5.2 Statistical Parameters for NH_4^+ Zeolite A Data Analysis from Model

Standard deviation	69.85	R-squared	0.8684
Mean	333.86	Adjusted R^2	0.7931
Coefficient of Variation (C.V.) %	20.92	Predicted R^2	0.5728
Predicted Error Sum of Squares (PRESS)	1.108E+05	Adequate Precision	10.491

The value 0.8684 explains that about 86.84% of variability is obtained in zeolite A cation exchange capacity with ammonium ion. The Predicted R-Squared of 0.5728 is not as close to the Adjusted R-Squared of 0.7931 as one might normally expect. The Predicted R – squared value explains about 57% of the variability in the new data. The Adequate Precision (signal to noise ratio) of 10.491 indicates an adequate signal.

Final Equation in Terms of the Significance of the Experimental Factors:
(CEC A $NH_4^+)^3$ = 3049.02393 – 1774.87416* Hydrothermal Time – 25.2384* Hydrothermal Temperature + 14.66531*Hydrothermal Time * Hydrothermal Temperature + 95.30505*Hydrothermal Time^2.

The equation showed that Hydrothermal Time has the largest coefficient hence, has the greatest impact. The CEC for zeolite A exchanged with ammonium ion increases with decrease in hydrothermal time and temperature.
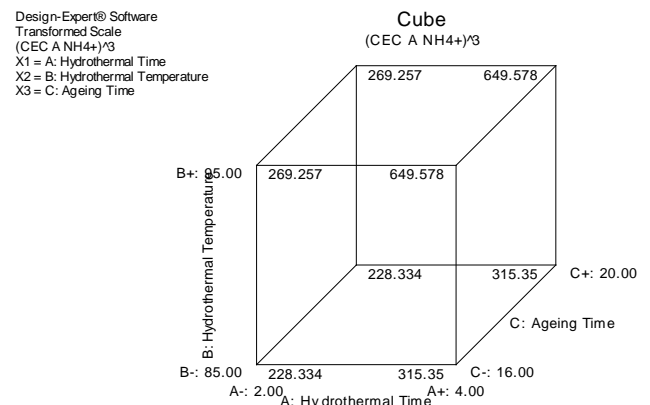
Figure 11.0 A Cube plot representation of the CEC for Zeolite A exchanged with ammonium ion.

The cube plot in figure 11.0 shows that cation exchange capacity increases with increase in Hydrothermal Time and Temperature but constant with increase or decrease in Ageing time. It was shown that maximium CEC was obtained at hydrothermal time of 4h, hydrothermal temperature of 95°C and at constant ageing time.

125

3.4.2 Cation Exchange Capacity for Calcium Ion Exchanged Zeolite A

The result for the analysis of variance (ANOVA) for the reduce model containing a cubic model is shown in Table 5.3:

Table 5.3 Results of ANOVA for the CEC for Calcium ion Exchanged Zeolite A at Lambda = -1.42

Source	Sum of Squares	DF	Mean Square	F value	p-value Prob>F	
Model	8.786E-04	9	9.763E-05	20.00	0.0485	Significant
A – Hydrothermal time	2.479E-05	1	2.479E-05	5.08	0.1530	
B – Hydrothermal Temp.	8.647E-05	1	8.647E-05	17.71	0.0521	
C – Ageing Time	9.007E-05	1	9.007E-05	18.45	0.0502	
AB	2.620E-04	1	2.620E-04	53.67	0.0181	
AC	1.754E-04	1	1.754E-04	35.93	0.0267	
A^2	3.172E-05	1	3.172E-05	6.50	0.1256	
B^2	7.895E-05	1	7.895E-05	16.17	0.0566	
A^2B	3.493E-05	1	3.493E-05	7.15	0.1160	
AB^2	4.950E-05	1	4.950E-05	10.14	0.0861	
Residual	9.764E-06	2	4.882E-06			
Correlation total	8.884E-04	11				

The Model F-value of 20.00 implies the model is significant. For the assumed model, there is only a 4.85% chance that a Model F-Value this large could occur due to noise. Values greater than 0.1000 indicate the model terms are not significant. In this case B, C, AB, AC, B^2, AB^2 are significant model terms.

Table 5.4 Statistical Parameters for Ca^{2+} Zeolite A Data Analysis from Model

Standard deviation	2.210E-03	R-squared	0.9890
Mean	0.065	Adjusted R^2	0.9396
Coefficient of Variation (C.V.) %	3.41	Predicted R^2	N/A
Predicted Error Sum of Squares (PRESS)	N/A	Adequate Precision	12.771

The R – squared value of 0.9890 explains that about 98.90% of variability is obtained in Zeolite A cation exchange capacity with calcium ion. For case(s) with leverage of 1.00, the Predicted R-Squared and Predicted Error Sum of Squares (PRESS) statistic are not defined. Adequate Precision (signal to noise ratio) of 12.771 indicates an adequate signal. This model can be used to navigate the design space.

Final Equation in Terms of the Significance of the Experimental Factors:

$(CEC\ A\ Ca^{2+})^{-1.42} = -7.94033 + 0.16414 *$ Hydrothermal Temperature $+ 8.25593E-03 *$ Ageing Time $- 0.042452 *$ Hydrothermal Time * Hydrothermal Temperature $- 3.31122E-03 *$ Hydrothermal Time * Ageing Time $- 8.4828E-04 *$ Hydrothermal Temperature^2 $+ 1.98989E-04 *$ Hydrothermal Time * Hydrothermal Temperature^2

The coefficient for hydrothermal temperature reveals that it is the most significant factor. The CEC for zeolite A exchanged with calcium ion increases with increase in hydrothermal temperature and ageing time.

Design-Expert® Software
Transformed Scale
(CEC A Ca2+)^1.42
X1 = A: Hydrothermal Time
X2 = B: Hydrothermal Temperature
X3 = C: Ageing Time
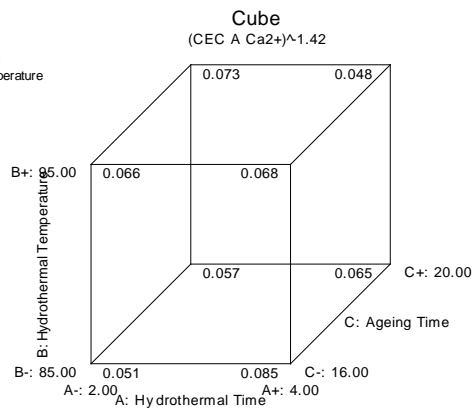
Figure 12.0 A cube plot representation of the CEC for zeolite A exchanged with Calcium ion.

The cube plot in figure 12.0 of the CEC for zeolite A exchanged with calcium ion showed that CEC increased with increase in hydrothermal time, hydrothermal temperature and ageing time at the low level of hydrothermal time. CEC however, decreases with increase in hydrothermal time, hydrothermal temperature and ageing time at high level of hdrothermal time. Maximum CEC was obtained at the lowest temperature (85°C), the highest hydrothermal time (4 h) and lowest ageing time (16 h).

3.4.3 Cation Exchange Capacity for Ammonium Ion Exchanged with Zeolite Y

The result for the analysis of variance (ANOVA) for the reduced model containing a 2 Factor Interaction (2FI) model as shown in table 5.5:

Table 5.5 Results of ANOVA of the CEC for Ammonium ion Exchanged with Zeolite Y at Lambda = 1.42

Source	Sum of Squares	DF	Mean Square	F value	p-value Prob>F	
Model	95.09	6	15.85	6.13	0.0327	Significant
A – Hydrothermal time	23.89	1	23.89	9.24	0.0288	
B – Hydrothermal Temp.	16.16	1	16.16	6.25	0.546	
C – Ageing Time	13.91	1	13.91	5.38	0.682	
AB	3.90	1	3.90	1.51	0.2741	
AC	22.65	1	22.65	8.75	0.0316	
BC	14.58	1	14.58	5.64	0.0636	
Residual	12.93	5	2.59			
Correlation total	108.02	11				

The Model F-value of 6.13 implies the model is significant. For the assumed model, there is only a 3.27% chance that a Model F-Value this large could occur due to noise. Values greater than 0.1000 indicate the model terms are not significant. In this case A, B, C, AC, BC are significant model terms.

Table 5.6 Statistical Parameters for NH_4^+ Zeolite Y Data Analysis from Model

Standard deviation	1.61	R-squared	0.8803
Mean	9.62	Adjusted R^2	0.7366
Coefficient of Variation (C.V.) %	16.73	Predicted R^2	0.3103
Predicted Error Sum of Squares (PRESS)	74.50	Adequate Precision	8.202

The R – squared 0.8803 explains that 88.03% of variability is obtained in zeolite Y CEC values for ammonium ion. The Predicted R-Squared of 0.3103 is not as close to the Adjusted R-Squared of 0.7366 as one might normally

expect. The predicted R – squared indicated that the model would be expected to explain 31% variability in the new data. Adequate Precision (signal to noise ratio) of 8.202 indicates an adequate signal.

Final Equation in Terms of the Significance of the Experimental Factors:

$(CEC\ Y\ NH_4^+)^{1.42}$ = – 31.78673 – 28.92997* Hydrothermal Time + 1.00865* Hydrothermal Temperature + 3.88671* Ageing Time + 0.39656* Hydrothermal Time * Ageing Time – 0.063645 Hydrothermal Temperature * Ageing Time.

The order of coefficients by experimental values shows the relative importance of each factor to the response (CEC). The equation shows Hydrothermal Time is the most significant followed by ageing time. The equation shows that the CEC for zeolite Y exchanged with ammonium ion increases with decrease in hydrothermal time, increase in hydrothermal temperature and increase in ageing time.
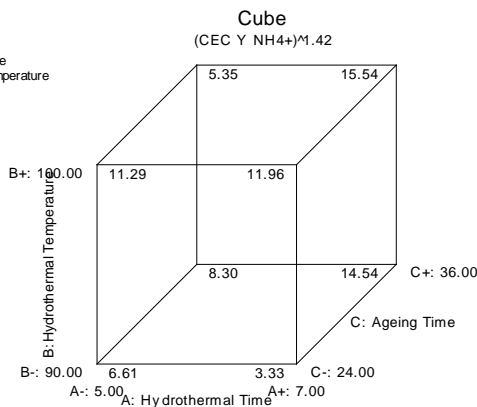
Figure 13.0 A cube plot representation for Faujasite Y CEC with Ammonium ion.

The cube plot in figure 13.0, showed how the three (3) factors interact affects the CEC for zeolite Y exchanged with ammonium ion. The CEC values increases with hydrothermal temperature and ageing time. However, at low hydrothermal time, low hydrothermal temperature and high ageing time, the CEC which was 8.30meq/g decreased to 5.35meq/g as the temperature increased. The interactions at temperature of 100^oC and time of 7h and ageing time of 36 h resulted in maximum CEC values.

3.4.4. Cation Exchange Capacity for Calcium Ion Exchanged Zeolite Y

The result for the analysis of variance (ANOVA) for the reduced model containing a cubic model as shown in table 5.7:

Table 5.7 Results of ANOVA of the CEC for Calcium ion Exchanged with Zeolite Y at Lambda = 1.81

Source	Sum of Squares	DF	Mean Square	F value	p-value Prob>F	
Model	611.48	5	122.30	4.74	0.0423	Significant
A – Hydrothermal time	100.97	1	100.97	3.91	0.0952	
B – Hydrothermal Temp.	215.78	1	215.78	8.36	0.0276	
AB	214.83	1	214.83	8.33	0.0278	
B^2	7.43	1	7.43	0.29	0.6107	
AB^2	172.25	1	172.25	6.68	0.0415	
Residual	154.79	6	25.80			
Correlation total	766.27	11				

The Model F-value of 4.74 implies the model is significant. For the assumed model, there is only a 4.23% chance that a "Model F-Value" this large could occur due to noise. Values greater than 0.1000 indicate the model terms are not significant. In this case A, B, AB, AB^2 are significant model terms.

Table 5.8 Statistical Parameters for Ca^{2+} Zeolite Y Data Analysis from Model

Standard deviation	5.08	R-squared	0.7980
Mean	31.15	Adjusted R^2	0.6297
Coefficient of Variation (C.V.) %	16.30	Predicted R^2	0.1861
Predicted Error Sum of Squares (PRESS)	623.64	Adequate Precision	6.973

Figure 14.0 A cube plot representation for Faujasite Y CEC with Calcium ion.

The R – squared value of 0.7980 explains that about 79.80% of variability is obtained in zeolite Y CEC with Calcium ion. The Predicted R-Squared of 0.1861 is not as close to the "Adj R-Squared" of 0.6297 as one might normally expect. The predicted R – squared indicated that the model would be expected to explain about 18% of variability in the new data. Adequate Precision (signal to noise ratio) of 6.973 indicates an adequate signal.

Final Equation in Terms of the Significance of the Experimental Factors:

(CEC Y Ca^{2+})$^{1.81}$ = 21637.99339 – 3484.42973* Hydrothermal Time + 445.70599* Hydrothermal Temperature + 71.99648* Hydrothermal Time * Hydrothermal Temperature – 0.37121* Hydrothermal Time * Hydrothermal Temperature^2.

The equation shows hydrothermal time is the most significant factor followed by hyydrothermal temperature. The equation confirms that the CEC for zeolite Y exchanged with calcium ion increases with decrease in hydrothermal time and increase in hydrothermal temperature.

The cube plot in figure 14.0 showed how the three (3) factors interacted to affect the CEC for zeolite Y exchanged with calcium ion. The CEC decreased with increase in hydrothermal time and temperature but remained constant with increase in ageing time. Maximum CEC was obtained at interactions of temperature of 90°C, time of 5h and ageing time 36h. Although, CEC values remained constant with increase in ageing time, hence, ageing time had little or no effect on zeolite Y CEC values with calcium ion.

4.0. CONCLUSION

The morphology of synthesized zeolite LTA had a face centred cubic shape while zeolite Y had a hexagonal crystal structure. Although not all the synthesized zeolites gave high crystallinity, zeolite samples A4 and Y6 gave a value of 32.84 and 75.03% for percentage crystallinity respectively.

Zeolite LTA A4 had 8.37meq/g ammonium ion CEC and 7.42meq/g calcium ion CEC while zeolite Y6 had 3.80meq/g ammonium ion CEC and 7.33meq/g for calcium ion CEC.

The effect of ageing time, crystallization temperature and crystallization time were studied and it was observed that the ageing time in the zeolite A with ammonium ion CEC and zeolite Y with calcium ion CEC had little or no effect on the response – cation exchange capacity. However, crystallization temperature and ageing time had significant effect on zeolite A ammonium ion CEC and zeolite Y calcium ion CEC, but at low and high crystallization time respectively.

ACKNOWLEDGEMENTS

REFERENCES

Box, G. E. and Draper, N. R. (1987). Empirical Model: Building and Response Surfaces. John Wiley and Sons, New York pp 477.

Breck, D.W. (1974). Zeolite Molecular Sieves. John Wiley and Sons Ltd, New York.

Dyer, A. (2007). Ion Exchange Properties of Zeolites and Related Materials In: Cejka, J., van Bekkum, H., Corma, A. and Schuth, F. Editions, *Introduction to Zeolite Science* and Practice 3rd Revised Edition, Elsevier.

Karami D. And Rohani S. (2000). Synthesis of Pure Zeolite Y using Soluble Silicate, A Two level Factorial Experimental Design. Chemical Engineering and Processing 48:1288 1292.

Kovo, A. S. (2010). Development of Zeolites and Zeolite Membrane from Ahoko Nigerian Kaolin. PhD Thesis, University of Manchester.

Matlob, A. S., Kamarudin, R. A., Jubri, Z. and Ramli, Z. (2011). Optimized Conditions for the Synthesis of Na – A Zeolite from Coal Fly Ash by Applying the Response Surface Methodology. Solid State Science and Technology 19(1):88-100.

Musyoka, N. M., Petrik, L. F., Balfour, G., Ndungu, P., Gitari, W. M. and Hums, E. (2012). Synthesis of Zeolites from Coal Fly Ash: Application of a Statistical Experimental Design. Research on the Chemical Intermediates 38:471-486. Doi0.1007/s11164011-0364-1.

Reganold, J. P. and Harsh, J. B. (1985). Expressing Cation Exchange Capacity. *Journal of Agronomic Education* 14: 84-90.

Rios, C. A., William C. D. & Fullen M. A. (2008). Nucleation of Growth History of Zeolite LTA Synthesis from Kaolinite by 2 different Method. *Applied Clay Science* doi:10.1016/j.clay.200805.006

Ruen-ngam, D., Rungsuk, D., Apiratikul, R. and Pavasant, P. (2009). Zeolite Formation from Coal Fly Ash and its Adsorption Potential. *Journal of the Air and Waste Management Association* 59:1140-1147. Doi0.3155/1047-3289.59.10.1140.

Shoumkova, A. (2012). Zeolites for Water and Waste-Water Treatment: An overview. *Australian Institute of High Energetic Materials* (ABN: 68 126 426 917) p1-61.

Szostak, R. (1989) Molecular Sieves. In: Weitkamp J. J. Edition Science and Technology Springer, Berlin.

DEVELOPMENT OF AN INTERACTIVE PLATFORM FOR LTE MOBILE ACCESS NETWORKS ENERGY SAVING ANALYSIS BASED ON DYNAMIC SCHEDULING

E. Obi[1*], O.E. Ochia[2], B.O. Sadiq[3] M.T. Kabir[4]

[1]Department of Electrical and Computer Engineering

Ahmadu Bello University, Zaria.

[*]eobi@abu.edu.ng, emmirald@gmail.com, sadiqbashirolaniyi@gmail.com, mtkabir@abu.edu.ng

ABSTRACT

This paper presents the development of a graphical user interface (GUI) for the energy saving analysis in Long Term Evolution (LTE) mobile access networks. The GUI runs a dynamic energy saving algorithm which utilizes off mode, sleep mode and multi-cell cooperation at the eNodeBs. The dynamic energy saving algorithm is an integration of two algorithms, namely: energy estimation algorithm and load/traffic sharing algorithm. The energy estimation algorithm estimated the energy consumption of the eNodeBs when they are all powered on, irrespective of their traffic loading.The load/traffic sharing algorithm transfers traffic between eNodeBs which enabled the off mode, sleep mode and multi-cell cooperation of the eNodeBs. The dynamic energy saving algorithm and the GUI for the energy saving analysis were implemented in MATLAB 2013b environment. The energy saving analysis for the LTE mobile access network was done for various energy-load proportionality constant at a particular call blocking probability using the developed GUI for LTE mobile access network energy saving analysis based on dynamic scheduling.

Keywords: *LTE Network, Load Utilization Factor, Bandwidth Efficiency, Data rate and Signal-to-interference-noise-ratio.*

1. INTRODUCTION

The LTE standard was developed by the 3rd Generation Partnership Project (3GPP) to cope with the rapid increase of mobile data usage (Sesiaet al., 2009). The energy consumption as well as CO_2 footprint of mobile cellular networks is increasing at an alarming rate due to the exponential growth in mobile data traffic (Wu et al., 2015). This is because current cellular networks are typically designed and operated to meet a given coverage and capacity level by considering the peak traffic demand, while energy efficiency takes a minor (or no role at all) at the design and operation stages (Oh et al., 2013). Consequently, minimization of energy consumption at base stations will considerably enhance the energy efficiency of LTE cellular networks (Zhang and Wang, 2013). Remarkably, contemporary base stations have a high-degree of non-load-energy proportional consumption characteristic and consume asignificant amount of energy even at no-load condition (Xiang et al., 2014). On the other hand, cellular mobile network traffic exhibits a high-degree of temporal-spatial diversity, which means that traffic demand varies both in time and space (Peng et al., 2011). This variation is directly related to the random call making behavior and mobility pattern of the mobile stations (Paul et al., 2011). However, under the current network operation approach, all base stations are kept powered on irrespective of traffic load (Wu and Niu, 2012).This traditional network operation and the aforementioned non-load-energy proportional utilization at base stations are the major causes behind the substantial amount of energy wastage in existing cellular networks (Chiaraviglio et al., 2012). Thus, it is imperative to exploit the non-load-energy proportional utilization of eNodeBs to devise techniques to manage the energy consumption of LTE mobile access networks more efficiently (Hasan et al., 2011). Switching-off eNodeBs during low traffic situations has been proposed for future LTE systems; however the standard so far does not specify implementation schemes (Hossain et al., 2011). This is the primary focus of green cellular communication which finds radio networking solutions that can greatly improve

energy saving and resource efficiency without compromising the quality of service of mobile stations (Han et al., 2014). Given the nature of energy wastage, natural traffic diversity and the exponential traffic growth trend, it is crucial to develop an interactive platform for energy saving analysis in LTE mobile access networks based on dynamic scheduling.

2. METHODOLOGY

The step by step approach of the proposed methodology is itemized as:

i. Development of mathematical model of the LTE cellular environment.

ii. Development of mathematical model for the energy saving and quality of service constraint (QoS) at the LTE eNodeBs.

iii. Development of the energy saving algorithm

iv. Development of a MATLAB GUI for the simulation and analysis of the LTE access network energy saving.

2.1. Modeling the LTE Cellular Environment

The LTE environment comprises of the eNodeBs, the Cell structure, adjacent cells, and the mobile stations. Mobile stations are initially generated uniformly across the entire network. A set of randomly active mobile stations for a particular distribution factor D is selected from the group of uniformly distributed mobile stations N_u given as (Obi et al., 2015):

$$N_u = 6D^2 + 8D + 3$$
(1)

2.2. Modeling the Energy Saving and QoS Constraints

The eNodeB power consumption model is used for evaluating the energy consumption of an LTE cellular network. The mathematical representation of the instantaneous power consumed by the jtheNodeB is given as (Hossain et al., 2013):

$$P_j(t) = \begin{cases} (1-q)\rho_j(t)P_j^a + qP_j^a ; & active\ mode \\ P_j^s ; & sleep\ mode \\ 0 ; & off\ mode \end{cases}$$
(2)

Where: $P_j(t)$ is the operational power of the jth eNodeB at time t; P_j^a is the maximum operational power of the jth eNodeB; $\rho_j(t)$ is the load utilization factor of the jth eNodeB at time t and $q \in [0,1]$ is called the energy-load proportionality constant of the eNodeBs which determines the level of dependency of the operational power of an eNodeB on it load utilization factor.

The operational power, P_j^a of the jth eNodeB is given as (Shahab et al., 2015):

$$P_J^a = aP_{TX,j} + b$$
(3)

The sleep mode power, P_j^s consumed by the jth eNodeB is given by as (Hossain et al., 2013):

$$P_j^s = qb$$
(4)

Where: $P_{TX,j}$ is the transmit power of the jth eNodeB; the parameters 'a' and 'b' are termed as the power profile parameters.

The load utilization factor at the jth eNodeB, $\rho_j(t)$ at time t is given as (Hossain et al., 2013):

$$\rho_j(t) = \frac{N_{used.rb.j}(t)}{N_{rb.j}}$$
(5)

Where: $N_{used.rb.j}(t)$ is the number of used physical resource block at the jth eNodeB at time t; $N_{rb.j}(t)$ is the number of available resource block at the jth eNodeB.

Also, the number of used physical resource blocks at the jth eNodeB at time t is given as (Hossain et al., 2013):

$$N_{used.rb.j}(t) = \sum_{i=1}^{N_u} z_{i,j}(t)w_{i,t}(t)$$
(6)

Where: $z_{i,j}(t)$ is an assignment indicator variable which is equal to 1 when ith mobile station is served by jth eNodeB at time t and zero otherwise; $w_{i,t}(t)$ is the

approximate number of physical resource block allocated by the jth eNodeB to the ith mobile station at time t.

The approximate number of physical resource block allocated by the jth eNodeB to the ith mobile station at time t is given as (Hossain et al., 2013):

$$w_{i,t}(t) = \frac{R_{i,j}(t)}{W_{RB} e_{i,j}(t)} \qquad (7)$$

Where: W_{RB} is the bandwidth per physical resource block and it is $180\ kHz$; $R_{i,j}(t)$ is the bit rate requirement of the ith mobile station from the jth eNodeB at time t; $e_{i,j}(t)$ is the average bandwidth efficiency of the ith mobile station from the jth eNodeB at time t.

The average bandwidth efficiency of the ith mobile station from the jth eNodeB at time t is usually expressed using equation (6) when considering adaptive modulation and coding (Hossain et al., 2013):

$$e_{i,j} = \begin{cases} 0 & if\ \gamma_{i,j} < \gamma_{min} \\ \xi \log_2(1 + \gamma_{i,j}) & if\ \gamma_{min} \le \gamma_{i,j} < \gamma_{max} \\ e_{max} & if\ \gamma_{i,j} \ge \gamma_{max} \end{cases}$$

(8)

Where: $0 \le \xi \le 1$ is the attenuation factor accounting the implementation loss; γ_{min} is the minimum signal-to-interference-noise-ratio; γ_{max} is the maximum signal-to-interference-noise-ratio; e_{max} is the maximum bandwidth efficiency and $\gamma_{i,j}(t)$ is the instantaneous received signal-to-interference-and-Noise ratio of the ith mobile station from the jth eNodeB.

The simulated traffic arrival pattern of an eNodeB follows a poisson distribution model given as (Obi et al., 2015):

$$A(t) = \frac{p(t,\mu)}{\max[p(t,\mu)]}$$

(9)

$$p(t,\mu) = \frac{\mu^t}{t!} e^{-\mu} \qquad (10)$$

Where: $A(t)$ is normalized traffic at time t, p is the poisson distribution function, t is the specific time in a day and μ is mean value where peak number of traffic occurred.

The load factor of each eNodeB in the LTE access network is normalized using the instantaneous traffic normalization

factor $A(t)$. This is to make the traffic behaviour at each eNodeB of the propose model exhibits the temporal diversity of a typical cellular network. The load factor of jth eNodeB after normalization is given as (Obi et al., 2015):

$$\rho_{j,new}(t) = A(t)\rho_j(t)$$

(11)

Where: $\rho_{j,new}(t)$ is the normalized instantaneous load factor of the jth eNodeB at time t; $A(t)$ is the instantaneous traffic normalization factor and $\rho_j(t)$ is the calculated load factor of the jth eNodeB at time t.

Thus, the instantaneous power consumed by the LTE access network of N eNodeBs at time t is given as (Obi et al., 2015):

$$P_N(t) = \sum_{j=1}^{N}[(1-q)\rho_{j,new}(t)P_j^a + qP_j^a]$$

(12)

The total energy consumed by the N eNodeBs over a period of 24 hours can be computed using equation (12) and is termed as the original/base-case energy E_N^{orig} which is given as (Obi et al., 2015):

$$E_N^{orig} = \sum_{t=0}^{24} P_N(t) \qquad (13)$$

Energy saving is achieved when active eNodeBs dynamically transfer their loads/traffic to their adjacent cells in other to switch to sleep or off mode depending on the status of the adjacent eNodeBs. This load/traffic sharing results in an instantaneous increase in power consumed by the adjacent eNodeBs due to the increase of its transmission power to extend it coverage area to the off or sleep eNodeB. This increase in the instantaneous power of the $j\ th$ eNodeB to cover the coverage area of an off or sleep mode adjacent eNodeBs can be computed using (Hossain et al., 2011):

$$P_{INC.j} = \frac{m(t)P_{TX,j}}{6} \qquad (14)$$

Where: $m(t)$ is the number of off or sleep mode, adjacent eNodeB whose load is been transfer to the jth eNodeB at time t.

The total energy consumed by N eNodeBs over a period of 24 hours with the energy saving algorithm is termed as the energy-with-scheduling E_N^{wshc} and is expressed using (Hossain et al., 2013):

$$E_N^{wshc} = \sum_{t=0}^{24} \left[\sum_{j=1}^{N} [S_j(t)\left((1-q)\rho_{j,new}^+ P_j^{a+} + qP_j^{a+}\right) + \left(\left(1 - S_j(t)\right)P_j^s\right)] \right] \qquad (15)$$

Where: $S_j(t)$ is the operating mode indicator of the $j\,th$ eNodeB at time t and it is given as (Hossain et al., 2013):

$$S_j(t) = \begin{cases} 1 & active\ mode \\ 0 & sleep\ mode \end{cases} \qquad (16)$$

$\rho_{j,new}^+$ is the new normalized load factor of the jth eNodeB after implementing dynamic scheduling at time t.

P_j^{a+} is the new operating power of the jth eNodeB after coverage extension and it is expressed using(Hossain et al., 2012):

$$P_j^{a+} = a\left(P_{TX,j} + P_{INC,j}\right) + b \qquad (17)$$

Thus, the proposed net energy savingsE_S, in the network is expressed using (Chiaraviglio et al., 2012):

$$E_S = \left(\frac{E_N^{orig} - E_N^{wshc}}{E_N^{orig}} \right) \times 100\% \qquad (18)$$

The blocking probability of a new call/mobile station at the jth eNodeB at time t is expressed using (Hossain et al., 2012):

$$Pr_{b,j}(t) = \frac{\frac{\left(N_{rb}\rho_{j,max}(t)\right)^{N_{rb}}}{N_{rb}!}}{\sum_{k=1}^{N_{rb}} \frac{\left(N_{rb}\rho_{j,max}(t)\right)^{K}}{K!}} \qquad (19)$$

Where:$\rho_{j,max}(t)$is the maximum allowable load utilization factor of the jth eNodeB at time t.

The quality of service constrain is imposed at each eNodeB while performing scheduling/load transfer. The quality of service constrain is represented using:

$$Pr_{b,j}(t) \leq Pr_{b,max} \qquad (20)$$

Where: $Pr_{b,max}$ is the maximum allowable blocking probability at the jth eNodeB.

2.3.*Energy Saving Algorithm*

The energy estimation algorithm (Obi et al., 2015) and the load/traffic sharing algorithm are integrated to form the energy saving algorithm. The following set of instructions form the proposed load/traffic sharing algorithm.

i. Generate the neighbour matrix
ii. Replace each neighbour by its traffic and sort the neighbours in descending order of their traffic size/load factor.
iii. Determining the available space in each neighbour while imposing the safety margin constrain/blocking probability.
iv. For each of the eNodeB, attempt traffic sharing from the eNodeB with highest traffic to the eNodeB with the lowest traffic.
v. If traffic sharing is not possible for a particular eNodeB, go to the next eNodeB with the lower traffic and continue until the entire eNodeB are exhaust.
vi. For each successful sharing, increment the sharing counter.
vii. Determine the new load factor of each of the eNodeB after sharing process is completed
viii. Determine the number of sleeping and off eNodeBs
ix. Subtract the number of sleeping and off eNodeB to obtain the number of active eNodeBs.

The flow chart of the energy saving algorithm is given in Figure 1.
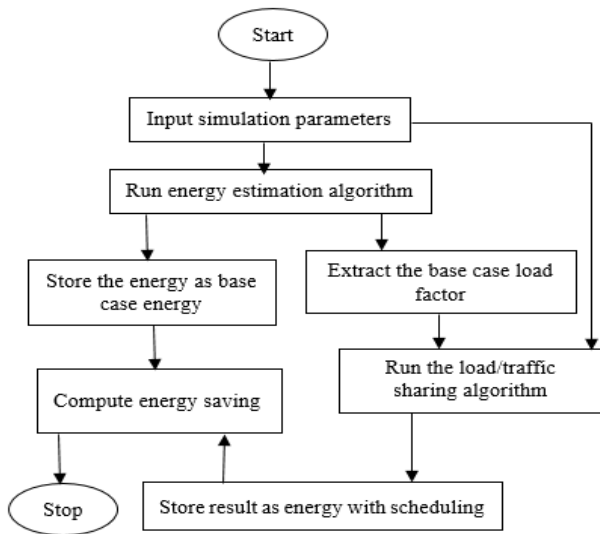
Figure 1: Flow Chart of the Energy Saving Algorithm

The performance of the proposed dynamic energy saving algorithm was evaluated by simulation. The simulated LTE access network consists of 50 macro cells with a distribution factor of 4 and 100 active mobile stations per eNodeB. The choice of 50 eNodeBs is based on the number of eNodeBs which was used in the energy saving algorithms for LTE access networks proposed by(Hossain et al., 2013).The standard parameters used for the simulation are shown in Table 1 which are consisted with the simulation scenario recommended by 3GPP (3GPP TR. 36.942, 2012):

2.4.Graphical User Interface

Figure 2 shows the developed MATLAB GUI. The GUI takes in inputs through the text boxes provided on the user interface. When the correct inputs are entered and the desired bottom is pressed, the GUI feeds the inputs to the set of MATLAB function that performs the required task. If the Energy Saving bottom is selected the program run the energy saving algorithm and various results are displayed on the user interface.

Table 1: Standard Simulation Parameters

PARAMETER	VALUE
Transmit power of eNodeBs	46 dBm
System bandwidth	20 MHz
Carrier frequency	2 GHz
Bandwidth per Resource	180 kHz
Resource block per eNodeB	100
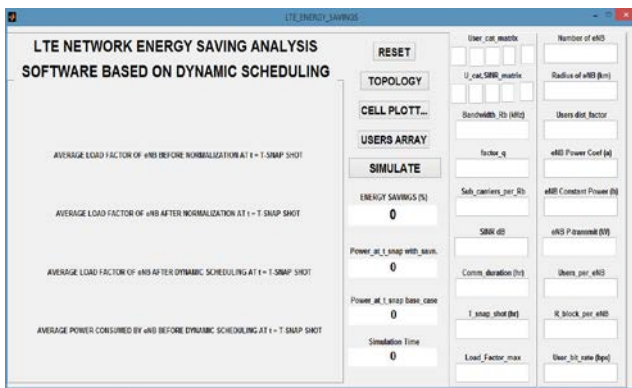
Figure 2: MATLAB GUI for Energy Saving Analysis

2.5.Simulation Setup

The radius of the macro cell is chosen as 1.5 km. Adaptive modulation and coding (AMC) set parameters are given as $\xi = 0.75, \gamma_{min} = -6.5\ dB, \gamma_{max} = 19\ dB$ and $e_{max} = 4.8\ bps/Hz$(Hossain et al., 2013). Five classes of real time constant data rate having data rates equal to 64 kbps, 128 kbps, 256 kbps, 384 kbps and 512 kbps are randomly selected by mobile stations. It is assumed that only one resource block can be allocated to a mobile station from any class. Thus, the required signal-to-interference-noise-

ratio of the five classes, calculated using equation $(7) - (8)$, are found equal to $-4.1\ dB$, $-0.3\ dB$, $4.3\ dB$, $7.9\ dB$, and $11.1\ dB$ respectively. The eNodeBs power profile parameters are: $a = 21.45$ and $b = 354.44$ for macro cells. These parameters provide the maximum operating power of the eNodeBs. The energy load proportionality constant q ranges from 0 to 1. A snap shot of the simulated network is as shown in Figure 3.
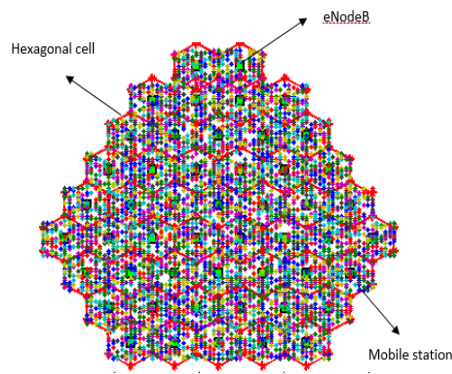
Figure 3: Simulated Network of 50 eNodeBs

3. RESULTS AND DISCUSSIONS

The daily energy saving resulted from using the developed GUI of the LTE access network was plotted against the energy load proportionality constants which ranges from 0 to 1 at an interval of 0.1 for the call blocking probability of $0.001\%, 0.01\%, 0.1\%, 1\%$ and 10%. The dependency of the energy saving on the energy-load proportionality constant for the various call blocking probability is as shown in Figure 4.
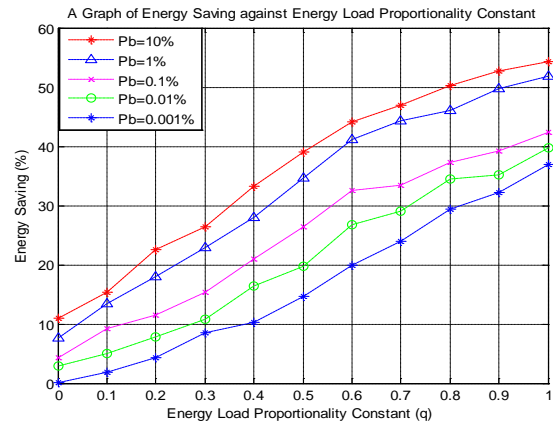
Figure 4: Energy Saving against Energy Load Proportionality Constant

The energy saving from Figure 4 is highest for the energy load proportionality constant of 1, which corresponds to constant energy-load proportionality constant. This is because for the constant energy load proportionality constant, the eNodeBs consume constant power irrespective of their traffic level which result to the highest amount of energy consumption of the LTE access network and consequently the highest amount of energy saving which correspond to $36.87\%, 39.67\%, 42.32\%, 51.84\%$ and 54.24% for the call blocking probability of $0.001\%, 0.01\%, 0.1\%, 1\%$ and 10% respectively. However, as the energy-load proportionality constant tends toward zero, the dependency of the energy consumption of the eNodeBs increases with its load utilization level, hence the energy consumption and energy saving decreases. Subsequently, for the energy load proportionality of zero, the energy consumption of the eNodeBs fully depends on its load utilization, and hence the energy saving is lowest and corresponds to $0.12\%, 2.95\%, 4.23\%, 7.56\%$ and 10.91% for the call blocking probability of $0.001\%, 0.01\%, 0.1\%, 1\%$ and 10% respectively. This is because the network incurs extra power (additional transmit power) in transferring the mobile stations from the off/sleep mode eNodeBs to the neighbouring active eNodeBs.

4. CONCLUSION

The GUI for the energy saving analysis in LTE mobile networks that utilized the energy saving algorithm has being developed. The LTE network environment and the eNodeBs power consumption models were developed with a view to implementing the dynamic energy saving algorithm which comprises of the energy estimation algorithm and the load/traffic sharing algorithm. The dynamic energy saving algorithm was implemented on MATLAB 2013b environment. The analysis of the energy saving resulted from the energy saving algorithm was done using the developed MATLAB GUI called the LTE network energy saving analysis software based on dynamic scheduling for the energy load proportionality constant ranging from 0 to 1. The results show that the energy saving in the network increases as the energy-load proportionality constant and call blocking probability increases.

REFERENCES

3GPP TR.36.942, (2012). 3GPP, "Technical Specification Group Radio Access Network; Evolved Universal Terrestrial Radio Access (E-UTRA); Radio Frequency (RF) system scenarios," *Technical Report*.

Chiaraviglio, Luca, Ciullo, Delia, Koutitas, George, Meo, Michela, and Tassiulas, Leandros. (2012). Energy-efficient planning and management of cellular networks. *Wireless On-demand Network Systems and Services (WONS), 2012 9th Annual Conference on*, 159-166.

Han, Shengqian, Yang, Chenyang, & Molisch, Andreas F. (2014). Spectrum and energy efficient cooperative base station doze. *Selected Areas in Communications, IEEE Journal on, 32*(2), 285-296.

Hasan, Ziaul, Boostanimehr, Hamidreza, & Bhargava, Vijay K. (2011). Green cellular networks: A survey, some research issues and challenges. *Communications Surveys & Tutorials, IEEE, 13*(4), 524-540.

Hossain, Md Farhad, Munasinghe, Kumudu S, & Jamalipour, Abbas. (2011). *An eco-inspired energy efficient access network architecture for next generation cellular systems.* Paper presented at the Wireless Communications and Networking Conference (WCNC), 2011 IEEE.

Hossain, Md, Munasinghe, Kumudu S, & Jamalipour, Abbas. (2013). Distributed inter-BS cooperation aided energy efficient load balancing for cellular networks. *Wireless Communications, IEEE Transactions on, 12*(11), 5929-5939.

Obi, E., Garba, S., & Sani, S.M. (2015). Development of an Energy Estimation Algorithm for LTE Mobile Access Networks. *International Journal of Engineering Research & Technology (IJERT), 4*(07), 313 - 317.

Oh, Eunsung, Son, Kyuho, & Krishnamachari, Bhaskar. (2013). Dynamic base station switching-on/off strategies for green cellular networks. *Wireless Communications, IEEE Transactions on, 12*(5), 2126-2136.

Paul, Utpal, Subramanian, Anand Prabhu, Buddhikot, Milind M, & Das, Samir R. (2011). *Understanding traffic dynamics in cellular data networks.* Paper presented at the INFOCOM, 2011 Proceedings IEEE.

Peng, Chunyi, Lee, Suk-Bok, Lu, Songwu, Luo, Haiyun, & Li, Hewu. (2011). *Traffic-driven power saving in operational 3G cellular networks.* Paper presented at the Proceedings of the 17th annual international conference on Mobile computing and networking.

Sesia, Stefania, Toufik, Issam, & Baker, Matthew. (2009). *LTE: the UMTS long term evolution*: Wiley Online Library.

Shahab, Suhail Najm, Abdulkafi, Ayad Atiyah, & Zainun, Ayib Rosdi. (2015). Assessment of Area Energy Efficiency of LTE Macro Base Stations in Different Environments. *Journal of Telecommunications and Information Technology*(1), 59.

Wu, Junyong, Zhang, Ye, Zukerman, Moshe, & Yung, Edward. (2015). Energy-Efficient Base Stations Sleep Mode Techniques in Green Cellular Networks: A Survey. *IEEE Communications*(99), 1-25.

Wu, Yiqun, & Niu, Zhisheng. (2012). *Energy efficient base station deployment in green cellular networks with traffic variations.* Paper presented at the Communications in China (ICCC), 2012 1st IEEE International Conference on.

Xiang, Lin, Ge, Xiaohu, Wang, Cheng-Xiang, Li, Frank Y, & Reichert, Frank. (2014). Energy efficiency evaluation of cellular networks based on spatial distributions of traffic load and power consumption. *arXiv preprint arXiv:1412.5356*.

Peng, Chunyi, Lee, Suk-Bok, Lu, Songwu, Luo, Haiyun, & Li, Hewu. (2011). *Traffic-driven power saving in operational 3G*

Zhang, Xi, & Wang, Ping. (2013). Optimal trade-off between power saving and QoS provisioning for multicell cooperation networks. *Wireless Communications, IEEE, 20*(1), 90-96.

APPLICATION OF ANALYTICAL-FIREFLY ALGORITHM FOR OPTIMAL LOCATION AND SIZING OF DISTRIBUTED GENERATOR IN STANDARD IEEE 30-BUS DISTRIBUTION NETWORK

Abdulrahman Olaniyan[1], Jimoh Boyi[2], Yusuf Jibril[3]

[1,2,3] Ahmadu Bello University, Zaria

*olaniyanabdulrahman@gmail.com, +2348027331685.

ABSTRACT

This paper presents a combined method which integrates the analytical approach into a firefly algorithm for optimal location and sizing of Distributed Generators (DG) in power system distribution networks. Optimal location and sizing of DGs are key to achieving an improvement in the system's reliability, stability and reduction of power losses. The combined method was then tested on the standard IEEE 30-bus radial distribution system and results obtained showed high precision for location and accuracy in sizing.

Keywords: *Distributed Generation, Analytical Approach, Firefly Algorithm, Loss Minimization*

1. INTRODUCTION

Due to continuous economic development which has brought about an increase in load demands in distribution networks, developing nations like Nigeria, have their power systems operating very close to the voltage instability boundaries. The decline in voltage stability margin is one of the important factors which restricts increment in load served by distribution companies (Jain et al., 2014). This rapidly increasing need to improve the stability and reliability of power systems, the need to provide more electrical power and difficulties in providing the required capacity using traditional solutions, such as transmission network expansions and substation upgrades, provide a motivation to select a Distributed Generation (DG) option. A DG is understood to be a type of generation system which is embedded, integrated and controlled on the distribution voltage side of the power system network. DG can be integrated into distribution systems to improve voltage profiles, power quality and the system generally. (Muttaqi et al., 2014).

These DG units when integrated into distribution networks provide ancillary services such as spinning reserve, reactive power support, loss compensation, and frequency control. On the other hand, poorly planned and improperly operated DG units can lead to reverse power flows, excessive power losses and subsequent feeder overloads (Atwa *et al.*, 2010).

Several methods, objectives and constraints for finding the optimal location and size of DGs in distribution networks have been introduced by different researchers. Methods used include the classical or numerical method by Atwa et al., (2010), Ochoa & Harrison, (2011) and Rau & Wan, (1994); the analytical approach by Wang & Nehrir, (2004), Acharya et al., (2006), Gözel & Hocaoglu, (2009) and Hung et al., (2010), Hung et al., (2013), Hung et al., (2014). Another method used is the heuristic approach by Abou El-Ela et al., (2010), Akorede et al., (2011), López-Lezama et al., (2012), Soroudi & Ehsan, (2011) and Vinothkumar & Selvan, (2011, 2012). Combined and hybrid solution approaches were also proposed in Afzalan & Taghikhani, (2012) and Moradi & Abedini, (2012). These methods have also presented different kinds of objective functions varying from single to multiple objectives and different types of constraints have also been addressed. The analytical method for optimal DG allocation was developed based on the 2/3 rule for capacitor placement. It is simple to understand and non-iterative but it can only get an approximate solution.

Furthermore, the analytical method is computationally exhaustive and time consuming thus it becomes more complex as the complexity of the distribution network increases. On the other hand, the firefly algorithm is robust and easy to use for optimal DG allocation but it hardly produces an optimal result. This is because the sizing is treated as an iterative process which may give a size which is theoretically optimal but practically not applicable. This iterative procedure for sizing also makes convergence take a longer period.

However, the analytical method proposed in Hung et al., (2010) has shown precision and accuracy in the aspect of DG sizing as each optimal DG that is suitable for each bus can be calculated before location of the best DG is done. This is more precise, specific and accurate for DG sizing only and the placement can then be treated as an iterative problem. Similarly, the firefly algorithm as applied in Nadhir et al., (2013) has shown very good performance in iterative problems and can be used for optimal location of DGs when it is treated as an iterative problem.

This paper presents a new approach which combines the analytical method and firefly algorithm for optimal DG allocation. The incorporation is done by using the analytical approach for sizing of the candidate DGs required for each bus while the firefly algorithm is used to randomly search for the optimal location of these DGs. The algorithm is implemented on MATLAB R2015a platform and it is tested on a standard IEEE 30-bus radial distribution test system.

The remainder of this paper is outlined as follows:

Section 2 presents the methodology which explains the problem formulation, necessary background and the proposed method. Section 3 presents the results obtained and discussions while Section 4 is the conclusion.

2. METHODOLOGY

This section is divided into four subsections which are problem formulation, analytical method, the firefly algorithm and the proposed method. The first three subsections discuss necessary backgrounds required to understand the proposed method.

2.1. Problem Formulation

The aim is to minimise the total loss in the system and improve the voltage profile by incorporating DG into a typical distribution network. The size and location of this DG must be optimal. The variables of the DG to be located are defined as (Sulaiman et al., 2012):

$$x = [x_{1L}, x_{1S}, \dots x_{nL}, x_{nS}] \tag{1}$$

Where x is the parameter of the DG which indicates candidate size and location, L is the location, S is the size of the DG at each location as obtained using the analytical method, and n is the maximum number of buses.

The objective function which was formulated based on the constraints in equation (1) by minimizing the total power loss in a distribution network is defined as:

$$f(x) = \min\left(\sum_{j=1}^{n} P_{Loss}\right) \tag{2}$$

Where $f(x)$ is the optimal result obtained after the minimisation of total loss, P_{Loss} based on the parameters of the DG in (1).

2.2. Analytical Method

The analytical method originated from the 2/3 rule and is implemented based on the exact loss formula. The exact loss formula used for calculating the total active loss in a distribution system having N-number of buses is given as a function of the respective real and reactive powers as (Hung et al., 2013):

$$P_{loss} = \sum_{i=1}^{N} \sum_{j=1}^{N} [\alpha_{ij}(P_i P_j + Q_i Q_j) - \beta_{ij}(Q_i P_j - P_i Q_j)] \tag{3}$$

Where;
$$\alpha_{ij} = \frac{r_{ij}}{V_i V_j} \cos(\delta_i - \delta_j) \tag{4}$$

$$\beta_{ij} = \frac{r_{ij}}{V_i V_j} \sin(\delta_i - \delta_j) \tag{5}$$

$$r_{ij} + jx_{ij} = Z_{ij} \tag{6}$$

V_i and δ_i are the complex voltage magnitude and angle at any bus i and (6) represents the i,j element of the impedance matrix. Pi and Pj are active power injections at buses i and j respectively while Qi and Qj are the reactive power injections at buses i and j respectively.

The total power to be delivered by the DG and its corresponding power factor at any bus i can be found using (Hung et al., 2014):

$$P_{DG_i} = P_{D_i} - \frac{X_i}{\alpha_{ii}} \qquad (7)$$

$$pf_{DG_i} = \cos(\tan^{-1}(\frac{\alpha_{ii}Q_{D_i} - Y_i}{\alpha_{ii}P_{D_i} - X_i})) \qquad (8)$$

$$\text{Where; } X_i = \sum_{\substack{j=1 \\ j \neq i}}^{N} (\alpha_{ij}P_j - \beta_{ij}Q_j) \qquad (9)$$

$$Y_i = \sum_{\substack{j=1 \\ j \neq i}}^{N} (\alpha_{ij}Q_j - \beta_{ij}P_j) \qquad (10)$$

P_{DG_i} is the DG size at any bus i, pf_{DG_i} is the power factor of the DG, while P_{D_i} and Q_{D_i} are the corresponding real and reactive powers of the bus having the DG.

2.3. Firefly Algorithm

The firefly algorithm is a nature-inspired meta-heuristic algorithm which mimics the social flashing behaviour of fireflies. The algorithm was proposed by Xin-She Yang (Yang, 2009) for solving complex optimization problems. The flashing light in fireflies serves as a means of communication to attract mating partners and potential preys. Three ideal rules are proposed in order to simplify the modelling of the algorithm. These are (Yang, 2010):

1. All fireflies are unisex such that one firefly will be attracted to any other firefly irrespective of their sex.

2. Attractiveness is proportional to brightness for any two fireflies. Thus, the less bright firefly will move towards the brighter one.

3. The brightness of any firefly is determined or affected by the landscape of the objective function.

For any optimization problem, the brightness can simply be proportional to the value of the objective or fitness function. The pseudo code for implementing the firefly algorithm is depicted in Figure 1 (Yang, 2009).

Objective function $f(x)$, $x = (x_1,..., x_d)^T$
Generate initial population of fireflies $\mathbf{x}_i$ $(i = 1,2,...,n)$
Light intensity I_i at x_i is determined by $f(\mathbf{x}_i)$
Define light absorption coefficient, γ
while $(t < \text{MaxGeneration})$
for $i = 1$:n all n fireflies
 for $j = 1$:i all n fireflies
  if $(I_j > I_i)$, Move firefly i towards j in d-dimension; **end if**
 end for j
end for i
Rank the fireflies and find the current best
end while
Post process results and visualization

Figure 1: Pseudo code of Firefly Algorithm

The describing equation which shows the movement of a firefly i to a more attractive (i.e. brighter) firefly j is described using (Yang, 2009):

$$x_i^* = x_i + \beta_o e^{-\gamma r_{ij}^2}(x_j - x_i) + \alpha \in_i \qquad (11)$$

Where x_i^* is the new position of firefly i, x_i is the initial position of firefly i, x_j is the position of firefly j, β_o is the initial attractiveness of the firefly, γ define the characteristic length, α is the randomization parameter, $\in_i$ is a vector of random numbers drawn from Gaussian or uniform distribution and r_{ij} is an Euclidean distance defined in equation (12).

$$r_{ij} = \|x_i - x_j\| \qquad (12)$$

This represents the Cartesian distance between any two fireflies defined as:

$$\|x_i - x_j\| = \sqrt{(x_i - x_j)^2 + (y_i - y_j)^2} \qquad (13)$$

The describing equation (11) is an ordinary random walk which is biased towards the brighter firefly. If $\beta_o = 0$,

equation (11) becomes an ordinary random movement.

2.4. *The Proposed Method*

The proposed method presents a heuristic procedure guided by the analytical method described in subsection 2.2.The flow chart for the proposed method is shown in Figure 2.
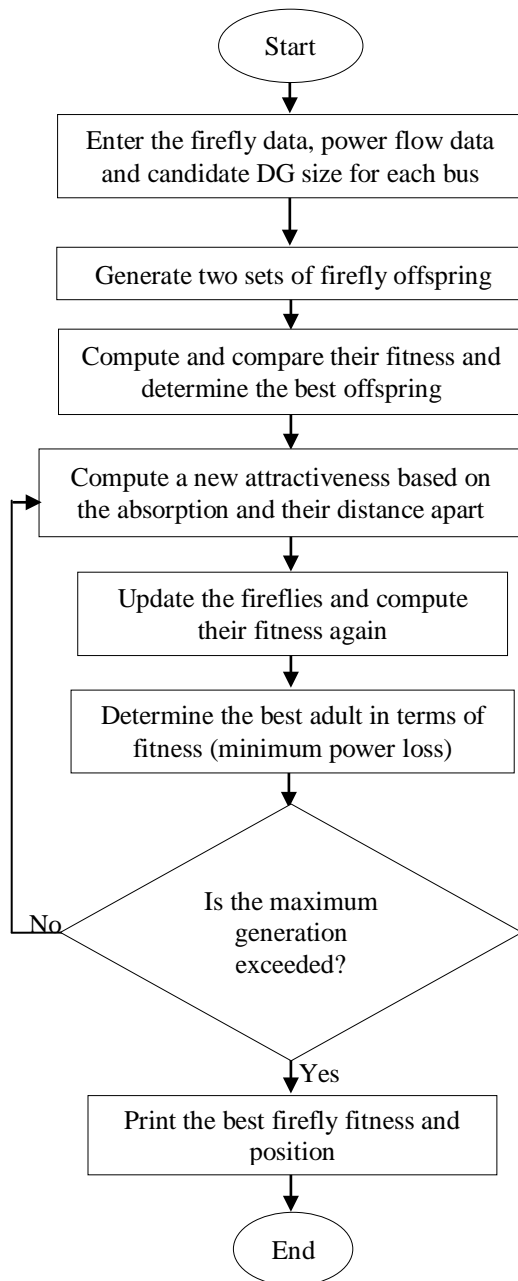
Figure 2: Flow Chart of the Proposed Method

The analytical method was used to calculate the size of DG

to be placed at each bus while the firefly algorithm was used for location of the DG. The location was done based on a fast random search in order to reduce computational time.

The step by step procedure for implementing the proposed method (shown in Figure 2) are as follows:

1. Input bus and line data
2. Input firefly parameters (i.e. number of fireflies, maximum generation, stopping criteria, scaling parameters, minimum value of attractiveness and absorption coefficient)
3. Run base case load flow
4. Compute candidate DGs for each bus using equations (7) and (8)
5. Determine the best location as a fitness offspring using firefly algorithm;
6. Display best location and its candidate size.
7. Print result
8. Stop.

3. RESULT AND DISCUSSIONS

The proposed method was tested on the IEEE 30-bus radial distribution system. The single line diagram of the system is shown in Figure 3 and the line and bus data of the system were obtained from Mojtaba *et al.*,(2014).
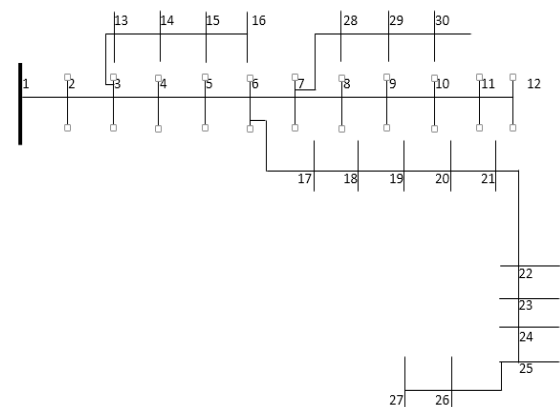
Figure 3: IEEE 30-bus Radial System

The parameters of the firefly algorithm used for simulation were set as shown in Table 1to ensure an optimum

performance of the algorithm.

Table 1: Parameters of Firefly Algorithm

S/N	Parameters	Values
1	No. of Fireflies	30
2	Maximum Generation	30
3	Scaling Parameter α	0.25
4	Attractiveness β_o	0.2
5	Absorption Coefficient γ	1

To show the impact of the DG installation, a base case load flow analysis was first run on the system before DG allocation was done, then the voltage profile of the base case scenario was plotted against that of the optimized case after DG allocation.

The voltage profile comparison is shown in Figure 4 while Figure 5 shows the plot minimization process of the objective function as against the number of iterations. This is to indicate the quick convergence of the proposed method.

The results obtained are presented in Table 2.
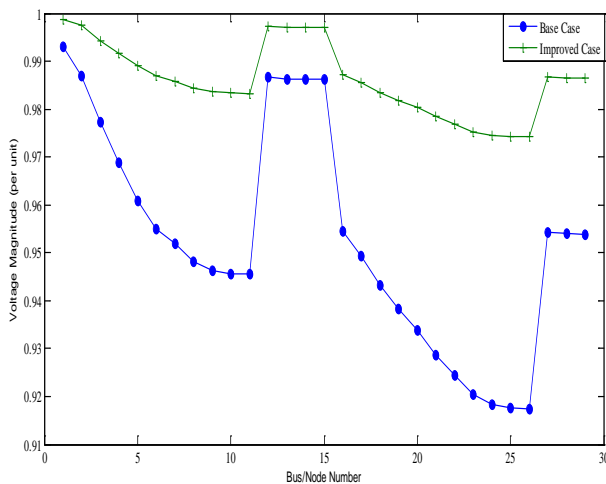
Figure 4: Voltage Profile of 30-bus system

It can be observed from Figure 4, that the DG installation has improved the voltage profile of the system. The blue line indicates the base case voltage profile while the green line represents the improved voltage profile after DG installation. The bus with the minimum voltage as shown in Table 2 (i.e. bus 27) recorded an improvement from 0.9236 p.u to 0.9534 p.u.
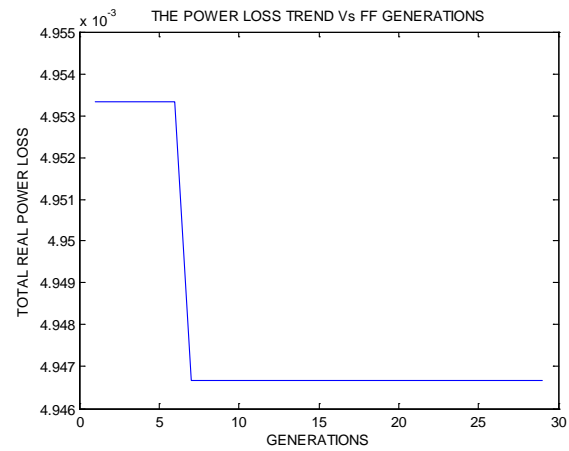
Figure. 5: Objective function against iteration

The overall voltage profile also recorded a 21.07% improvement while the total real power loss was also reduced from 542 kW to 495 kW. Figure 5 shows the trend of the power loss as against the number of iterations. It can be seen that the minimum loss was achieved after the seventh iteration which indicates the fast convergence speed of this method as compared to the conventional analytical method proposed by Hung *et al.*, (2010).

Table 2: Summary of Results Obtained

Particulars	Base Case	Optimized Case
Real Power Loss	542 kW	495kW
Bus with Minimum Voltage	Bus 27 with 0.9236 p.u	Bus 27 with 0.9534 p.u
DG Location	-	Bus 2
DG Size	-	183kW

As seen in Table 2, the simulation results showed that the optimal DG location and size were found to be bus 2 and 183 kW respectively.

4. CONCLUSION

This paper presented a combined method for optimal DG allocation in radial distribution networks. The method was tested on a standard IEEE 30-bus radial distribution system. The results obtained showed that the problem of inaccuracy associated with the firefly algorithm solution and the time consumption associated with the analytical method has been successfully addressed by this method.

REFERENCES

Abou El-Ela, A., Allam, S., & Shatla, M. (2010). Maximal optimal benefits of distributed generation using genetic algorithms. Electric Power Systems Research, 80(7), pp869-877.

Acharya, N., Mahat, P., & Mithulananthan, N. (2006). An analytical approach for DG allocation in primary distribution network. International Journal of Electrical Power & Energy Systems, 28(10), pp669-678.

Afzalan, M., & Taghikhani, M. (2012). DG Placement and Sizing in Radial Distribution Network Using PSO&HBMO Algorithms. Energy and Power, 2(4), pp61-66.

Akorede, M. F., Hizam, H., Aris, I., & Ab Kadir, M. (2011). Effective method for optimal allocation of distributed generation units in meshed electric power systems. Generation, Transmission & Distribution, IET, 5(2), pp276-287.

Atwa, Y., El-Saadany, E., Salama, M., & Seethapathy, R. (2010). Optimal renewable resources mix for distribution system energy loss minimization. Power Systems, IEEE Transactions on, 25(1), pp360-370.

Gözel, T., & Hocaoglu, M. H. (2009). An analytical method for the sizing and siting of distributed generators in radial systems. Electric Power Systems Research, 79(6), pp912-918.

Hung, D. Q., Mithulananthan, N., & Bansal, R. (2010). Analytical expressions for DG allocation in primary distribution networks. Energy Conversion, IEEE Transactions on, 25(3), pp814-820.

Hung, D. Q., Mithulananthan, N., & Bansal, R. (2013). Analytical strategies for renewable distributed generation integration considering energy loss minimization. Applied Energy, 105, pp75-85.

Hung, D. Q., Mithulananthan, N., & Lee, K. Y. (2014). Optimal placement of dispatchable and nondispatchable renewable DG units in distribution networks for minimizing energy loss. International Journal of Electrical Power & Energy Systems, 55, pp179-186.

Jain, S., Agnihotri, G., Kalambe, S., & Kamdar, R. (2014). Siting and Sizing of DG in Medium Primary Radial Distribution System with Enhanced Voltage Stability. Chinese Journal of Engineering, 2014.

López-Lezama, J. M., Contreras, J., & Padilha-Feltrin, A. (2012). Location and contract pricing of distributed generation using a genetic algorithm. International Journal of Electrical Power & Energy Systems, 36(1), pp117-126.

Moradi, M., & Abedini, M. (2012). A combination of genetic algorithm and particle swarm optimization for optimal DG location and sizing in distribution systems. International Journal of Electrical Power & Energy Systems, 34(1), pp66-74.

Muttaqi, K., Le, A. D., Negnevitsky, M., & Ledwich, G. (2014). An algebraic approach for determination of DG parameters to support voltage profiles in radial distribution networks.

Nadhir, K., Chabane, D., & Tarek, B. (2013). Distributed Generation Location and Size Determination to Reduce Power Losses of a Distribution Feeder by Firefly Algorithm. International Journal of Advanced Science & Technology, 56.

Ochoa, L. F., & Harrison, G. P. (2011). Minimizing energy losses: Optimal accommodation and smart operation of renewable distributed generation. Power Systems, IEEE Transactions on, 26(1), pp198-205.

Rau, N. S., & Wan, Y.-h. (1994). Optimum location of resources in distributed planning. Power Systems, IEEE Transactions on, 9(4), pp2014-2020.

Soroudi, A., & Ehsan, M. (2011). Efficient immune-GA method for DNOs in sizing and placement of distributed generation units. European Transactions on Electrical Power, 21(3), pp1361-1375.

Sulaiman, M., Mustafa, M., Azmi, A., Aliman, O., & Abdul Rahim, S. (2012). Optimal allocation and sizing of distributed generation in distribution system via firefly algorithm. Paper presented at the Power Engineering and Optimization Conference (PEDCO) Melaka, Malaysia, 2012 Ieee International.

Vinothkumar, K., & Selvan, M. (2011). Fuzzy embedded genetic algorithm method for distributed generation planning. Electric Power Components and Systems, 39(4), pp346-366.

Vinothkumar, K., & Selvan, M. (2012). Distributed generation planning: A new approach based on goal programming. Electric Power Components and Systems, 40(5), pp497-512.

Wang, C., & Nehrir, M. H. (2004). Analytical approaches for optimal placement of distributed generation sources in power systems. Power Systems, IEEE Transactions on, 19(4), pp2068-2076.

Yang, X.-S. (2009). Firefly algorithms for multimodal optimization Stochastic algorithms: foundations and applications (pp. 169-178): Springer.

Yang, X.-S. (2010). Firefly algorithm, stochastic test functions and design optimisation. International Journal of Bio-Inspired Computation, 2(2), pp78-84.

ECONOMIC BENEFITS OF ALUMINIUM ORES DEPOSITS IN NIGERIA AS ALTERNATIVE SOURCE OF FOREIGN EARNING

Omeye Levi Ugwuanyi, Orji-Daniels Kennedy, O. and Abdulrahman, A. S.

Department of Mechanical Engineering, School of Engineering and Engineering Technology, Federal University of Technology Minna, Nigeria.

Email: delevino@gmail.com Tel: 07036114787
Email: kennyjubris@gmail.com Tel: 08037782268
Email: asipita.salawu@futminna.edu.ng Tel: 08036812724.

ABSTRACT

The economic benefits of Aluminium deposits in Nigeria as alternative source of foreign earnings cannot be overemphasized. Nigeria's economy has since the discovery of crude oil been monolithic, paying more attention to petroleum than other non-oil sectors including the solid mineral sector. The adverse effects of these on the nation's economy ranging from Naira devaluation to lack of employment opportunities for Nigerian graduates have necessitated this research work. The research looked into the chemistry of aluminium as an element and the deposits of the ore in the country. The research equally explored the existing government policies as it affects the solid mineral sector. The processes involved in mining aluminium ore (bauxite), processing of the ore and the refining were also considered. The research also looked into the states of the existing aluminium production plants such as the Aluminium Smelter Company of Nigeria (ALSCON) and other downstream production companies. The cost implication of aluminium production, the consumption level of the products and the expected revenue generation for the country were also analyzed. It was ascertained that aluminium ore deposits are found in Delta, Ekiti and Kebbi state areas of the country and that government (though needs to be more target driven) have been making favorable policies on the solid mineral sector but the policies have not translated to the intentions for which they were formulated and this has kept ALSCON and the entire sector in the condition they are presently. Research results also showed that aluminium production is capital intensive and electricity takes about 35% of the total production cost. The country's aluminium per capita consumption was found to be about 0.3kg as against world's average of 5kg which means that about 45,000 tons of aluminium is required for a country of about 150 million people. Research showed that for the month of May 2015, the US exported aluminium of 99.5% purity level at the rate of USD 1,804.04 per metric ton and this x-rays the lucrative nature of harnessing the aluminium deposits, if Nigeria is to put attention to the sector.

Keywords: *Solid minerals, Bauxite, Aluminium production, National economy, foreign exchange.*

1. INTRODUCTION

Nigeria is a crude oil rich nation with Gross Domestic Product (GDP) of USD 522 billion (norminal; 2015 est). But the country's growth rate is 6.2% (First Quarter, 2014) driven by non–oil production activities such as Agriculture: 22%, Services: 52%, Manufacturing: 6.8%; and oil and gas contributes only 14.4% (2014 est). Mining contributes only 1% to Nigeria's GDP and 33.1% (2013 est) of the country's population still live below poverty level (Nigeria National Bureau of Statistics, 2015). According to Channels Television News of May 15, 2015, 6.4% of the workforce are still suffering unemployment. The US Dollar continues to appreciate over the Naira (above

₦200 as at First Quarter, 2015). Petroleum constitutes 95% export of the country (2012 est). Though the petroleum sector is important, it remains in fact a small part of the country's overall vibrant and diversified economy and until this ideology of monolithic economy is corrected, the nation's economic growth rate will continue to remain low. The crude oil is refined outside the shores of the country and this helps neighboring and other beneficiary countries grow economically at a very rapid rate at the expense of the Nigerian citizens. Nigeria has indigenous refineries but continues to import refined petroleum products at very high cost. With this, there is no way the country can move forward

if the local refineries are not put to full operation and modern ones built.

To improve the economic situation of the country there is urgent need to diversify the economy. One important area of such diversification is the exploration of the solid mineral sector. According to Auwal, 2010, Nigeria is richly blessed with solid mineral deposits with over 34 different minerals in 500 known mineral deposits across the 36 states and Federal Capital. The commercial value of Nigeria's solid mineral has been estimated to run into hundreds of trillions of Dollars with 70 percent of these minerals buried in the bowel of Northern Nigeria and it is just unfortunate that Nigeria since her independence in 1960 has failed to put in place structures that will make the countless benefits therein available to the citizens (*Vanguard News,* June 13, 2014). According to the audit report by the Nigeria Extractive Industries Transparency Initiative (NEITI), Nigeria is losing billions of Naira that should accrue to the federation account from the mining sector because Nigeria mining regulators are not efficient enough. For the period covered by the maiden report (2007 - 2010), over 70 percent of mining title holders in Nigeria's solid mineral sector are inactive, causing the government huge revenue losses (Ata, 2012). All these if put in proper shape will not only add to the GDP but at the same time serve a source of employment to the unemployed graduates whose number increases geometrically as a result of yearly graduating students who only come out to join a system that creates no avenue to absorb the existing ones.

Aluminium is one among many of such minerals to include Iron, Tin, Limestone, Dolomite to mention but a few. Aluminium is a silvery–white metal that occurs chiefly as bauxite. Bauxite consists of minerals mostly gibbesite $Al(OH)_3$, boehmite γ–AlO(OH) and diaspora α–AlO(OH) mixed with the two iron oxides goethite and haematite, the clay mineral coalinite and small amount of anastase TiO_2. Aluminium was discovered by a Danish chemist Hans Christian Oersted in 1825 (Siteseen, 2015). It is the third most abundant element in the earth's crust after oxygen and silicon and the most widely used metal after iron. Aluminium is paramagnetic and the third in electrical conductivity after silver and copper. It is a light metal (specific gravity 7.874 at 20^0C) with good thermal conductivity (Anne, 2015). A combination of these critical properties earn aluminium various applications, some in pure forms (such as electricity cables) and mostly in alloyed form such as cooking pots and pans, cutleries, automobile parts and soda cans. Other applications are: in production of boats and ships, airplanes and plant tubes (Siteseen, 2015). Aluminium forms a protective impervious oxide layer on early corrosion and so it is used in form of foils in packaging food. Aluminium is also used extensively in the building industries.

2. METHODOLOGY

Theoretical approach was adopted in this study. The method relates to collection of relevant information from textbooks, government gazettes relating to the subject matter and on–line information. On the whole, the bulk of the data used were obtained from the official records of government establishments.

2.1. THE CHEMISTRY OF ALUMINIUM

Aluminium does not exist as a pure element in nature. It exhibits relatively high chemical reactivity and hence tends to bond with other elements to form compounds. More than 270 minerals in Earth's rocks and soil contain aluminium compounds (William, 2015). Aluminium is a group 3 and period 3 element of the periodic table with atomic number 13 and atomic weight 26.981539. Aluminium belongs to the *p*–block elements with electronic configuration of $1s^2\,2s^2\,2p^6\,3s^2\,3p^1$.

Aluminium derives its name from alum - from the latin name *alumen* which means bitter salt. Aluminium is a soft, light, silvery white metallic solid at 300K with the following physical and chemical data.

Physical Data

Density at 300K: 2.6989 g/cm^3

Density at melting point: 2.375 g/cm^3

Specific gravity: 7.874

Melting point; 933.47 K, 660.32^{0}C

Boiling point: 2792 K, 2519^{0}C

Critical point: 8550 K

Heat of fusion: 10.67 kJ/mol

Heat of Vaporization: 293.72 kJ/mol

Molar heat Capacity: 25.1 J/mol.K

Specific Heat: 24.200 J/g.k (at 20^{0}C)

Chemical Data

Oxidation states: +3 (most common) +2, +1

Electronegativity: 1.610

Electron affinity: 41.747 kJ/mol

Atomic Radius: 1.43Å

Atomic Volume: 10.0 cm^3/mol

Ionic Radius: 51 (+3e)

Covalent Radius: 1.24Å

First Ionization Energy: 577.539 kJ/mol

Second Ionization Energy: 1816.667 kJ/mol

Third Ionization Energy: 2744.779 kJ/mol

Source: Aluminium Facts, Chemical and Physical Properties (Anne, 2015)

Aluminium has face–centered cubic structure. Though aluminium has 23 known isotopes ranging from ^{21}Al to ^{43}Al, it has two naturally occurring isotopes namely, ^{27}Al occurring for nearly 100% of all natural aluminium and ^{28}Al found in traces with nearby stable half-life of 7.2 x 10^5 years.

2.2. ALUMINIUM ORE DEPOSITS AND SOLID MINERAL POLICIES IN NIGERIA

The top three countries that mine aluminium ore are Guinea, Australia and Vietnarn but Australia, China and Brazil lead the world's aluminium production (Anne, 2015). Bauxite is aboundant in commercial exploitable reserves in Nigeria. The deposits are found in Delta, Ekiti and Kebbi states of the country (Akinrele, 2014). Figure 1 below shows a typical aluminium ore. The red colour seen is as a result of the presence of iron oxides.

Figure 1: Aluminium Ore (Bauxite)

The vast potential of Nigeria mineral wealth has not always been so ignored. Before the oil boom of the 1970's the nation's economy was largely sustained by agriculture and exploitation of solid minerals. Coal and Tin were among the minerals mined on large scale with the former being used to generate electricity, power the railway network and meet the demands of regional and international markets. Lead and Zinc were a significant source of export revenue and Nigeria was the world's largest exporter of columbite. The Federal government has acknowledged the potentials in solid minerals as an alternative to the petroleum industry for foreign exchange earnings and has set some policies in favour of revitalizing the sector. This is because mineral resources are the foundation upon which an

industrialized economy is built and this idea in recent times has been rejuvenated following the global economic recession of the late 1980s and early 1990s that made the badly hit developing countries especially African and Latin American to turn towards liberalizing their trade to improve balance of payment and increase economic growth. This left Nigerian's economy which is monolithic in nature vulnerable to fluctuations in oil prices with the attendant shock on the economy. This informed the Federal government's decision to diversify the nation's economy base from oil to non–oil sectors including the development of solid mineral resources. The Federal Government after internal analysis and in reaction to the global economic recession embarked on key policy review which was completed and endorsed at the middle of the 1990s for implementation. This led to a number of important actions including the creation of the Ministry of Solid Minerals Development in 1995. Substantial efforts and polices were made towards developing the sector some of which are:

- The new National Policy on Solid Mineral Development, 1998.
- The enactment of the Mineral and Mining Act, 1999 known as Sustainable Management by Mineral Resources Project.
- Development of the Seven-Year Strategic Action Plan for Solid Minerals Development in Nigeria (2002 - 2009).
- Establishment of Nigeria Geological Survey Agency, 2002 to act as a repository of mineral information and ensure that this is available to private sector.
- Establishment of Sustainable Management of Mineral Resources Project – a World Bank assisted Programme, 2004 where World Bank announced to spend the sum of USD 120 million to fund the sector. (Akinrele, 2014)

- Establishment of the Mining Cadastre Office to grant mining permits and licenses.
- Establishment of the Mines Environment Compliance Department to outline best International Practice.
- Establishment of the Artisanal and Small Scale Mining Department as a focused department for small entrepreneur and local content.
- Enactment of the Mineral and Mining Act 2007.

Although previous policy decisions and instruments well meaning, they have not produced the desired results and the outcomes for which they were formulated. Consequently, for the sector to develop beyond its low level, it became apparent that a reform of the policy is inevitable. The development of decisions and instrument in recent times has led to a meaningful change in perception and interest in the sector. However it is now necessary that the interest be deepened and the sector carried to the next level by developing further enabling environment in the national mining industry and to situate this within the context of Millennium Development Goals (MDG) and Nigeria's development agenda especially to National Economic Empowerment and Development Strategy NEEDS 1, (2004) and NEEDS 2, (2007) (Ministry of Mines and Steel Development).

2.3. ALUMINIUM ORE MINING AND PROCESSING

Aluminium does not occur naturally in its pure state. It is estimated that aluminium constitutes 8% of earth's crust and usually found in oxide form known as bauxite. Australia, Guinea and Jamaica accounted for 60% by world's bauxite output in 1994 while Australia, the USA and China together accounted for around 50% of alumina total output. As mentioned earlier, there are

bauxite deposits in Delta, Ekiti and Kebbi states of Nigeria but remain commercially untapped as a result of challenges in the sector.

Bauxite mining involves the removal of an entire layer of the lateritic soil profile after clearing the trees. Then the top soil is stock piled and mining proceeds. After mining, the ironstone or clay underneath is deeply ripped and the soil is replaced. Bauxite mining processes are in five steps namely: preparation of the mining area, bauxite mining, crushing and grinding, ore transportation and rehabilitation. Figure 2 below shows a typical mining and crushing site.

Figuire 2: Bauxite mining and crushing site

During crushing, coarse bauxite stones are crushed using primary crusher followed by cone crusher or impact crusher which are used as fine crushers. Finally ball mill plays important role in grinding the bauxite.

The bauxite is then converted to aluminium Oxide (Al_2O_3) called Alumina through Bayer process as shown in Figure 3 below.
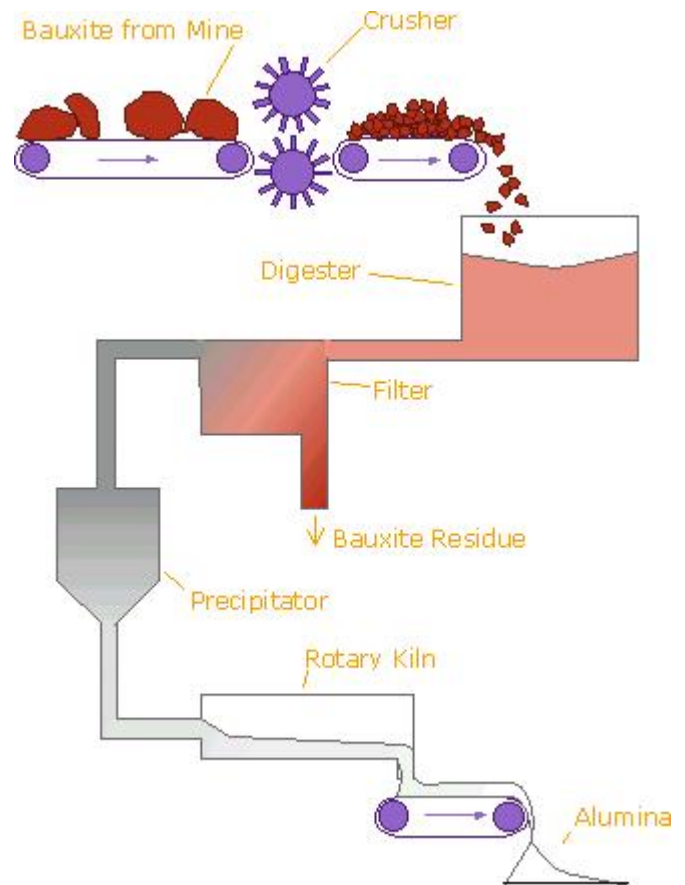
Figure 3: Bayer process of bauxite processing
Source: Bayer Process on Industrial Scale by Sam Davyson

2.4 ALUMINIUM PRODUCTION IN NIGERIA

The Federal government of Nigeria intended to use locally produced bauxite and subsequently import some of the bauxite from neighboring West African countries for her 180,000 metric ton per year capacity plant, the Aluminium Smelter Company of Nigeria (ALSCON) in Ikot Abasi Akwa-Ibom State, Southern Nigeria (David, 2005). When fully operational, ALSCON will have the confidence to mine bauxite and establish an alumina refinery rather than import all its 375,000 tons per year requirement from Guinea (Mbendi, 2015).

Unfortunately, ALSCON has remained a very unprofitable smelter since the divestment of the Federal

Government's equity holding from the privatized plant. ALSCON, a subsidiary of United Company UC RUSAL a Russian Company is yet to fully stamp its foot on ground as a business enterprise (*Daily Trust Nigeria,* October 17, 2013). The Russian firm holds 85% stake in the smelter. However, in February 2008, ALSCON was re-launched after the modernization completed by UC RUSAL. As at 2013 the company was running at a great loss, utilizing only 11% of its production capacity as a result of unfavorable business climate.

Should ALSCON reach its full capacity, it will create 1,900 local jobs and 90% of the employees will be Nigerian citizens. Additionally, 20,000 jobs could be created in the downstream aluminium manufacturing sector and through the development of infrastructure around the smelter, resulting in a positive improvement in the standard of living for Akwa-Ibom state residents and the country at large.

However, there seems to be no definite date for the completion of the project by the Federal government and the cost of the project when completed would be far higher than is needed for ALSCON to remain profitable. The availability of a back–up gas pipeline promised by the Federal Government which remains the necessary precondition for ALSCON's survival is not feasible at the moment. Unless urgent steps are taken to put the gas pipeline issue in place, Nigeria's desire of an aluminium revolution may remain a pipe dream (*Business and Finance News,* December 15, 2010).

Other downstream aluminium manufacturers such as the First Aluminium Nigeria, the Tower Aluminium Nigeria and many others convert aluminium ingots to various shapes and sections to satisfy the various areas of aluminium applications. The first Aluminium Rolling Mill was established in 1959 by then Eastern region

government in Trans–Amadi in Port Harcourt. The mill which represents the second stage in the processing of aluminium into one of its many end products was intended to produce aluminium coils and aluminium circles. The coils being the primary input in the fabrication of aluminium roofing sheets and circles being the primary input in the production of aluminium pots, pans and hollow ware.

Since then, the aluminium industry has experienced tremendous growth with good number of rolling mills and aluminium extrusion plants in the country. The extrusion plants produce the aluminium profiles used in the fabrication of windows, doors, curtain walling systems, partitions etc. (commonly referred to as the Windows and Doors subsector of the Aluminium building products industry). Imported aluminum coils and extrusions today are resorted to in order to augment the outputs of these mills and plants. Indeed, it is thought that the tonnage of imported profiles now exceed by far that of the local mills by 2:1. Imported aluminium coils also account for close to 50% of the total tonnage in the market (Ebubec, 2014). Most of these imported finished aluminium products are substandard (*Business Day,* September 15, 2014).

Secondary aluminium production also utilizes aluminium scraps in the production of beverage cans, tripod pots and frying pans, and aluminium automotive parts such as engine blocks (US Energy Information Administration – Today in Energy, August 16, 2012).

2.5. ALUMINIUM REFINING AND RECYCLING

Aluminium is too high in the electrochemical series to be extracted from its ore by carbon reduction. The temperatures needed are too high to be economical. Instead, it is extracted by electrolysis (Jim, 2005). The relevant chemical equations are:

$$Al_2O_3 + 2NaOH \rightarrow 2NaAlO_2 + H_2O$$
$$2H_2O + NaAlO_2 \rightarrow Al(OH)_3 + NaOH$$
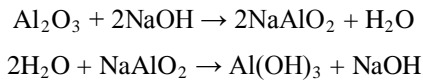
The intermediate sodium aluminate ($NaAlO_2$) dissolves in strongly alkaline water while other components are insoluble. Depending on the quantity of the bauxite ore, twice as much waste called red mud is generated compared to the amount of alumina. The conversion of alumina to aluminium metal is achieved by the Hall–Heroult electrolytic process as shown in Figure 4 below.
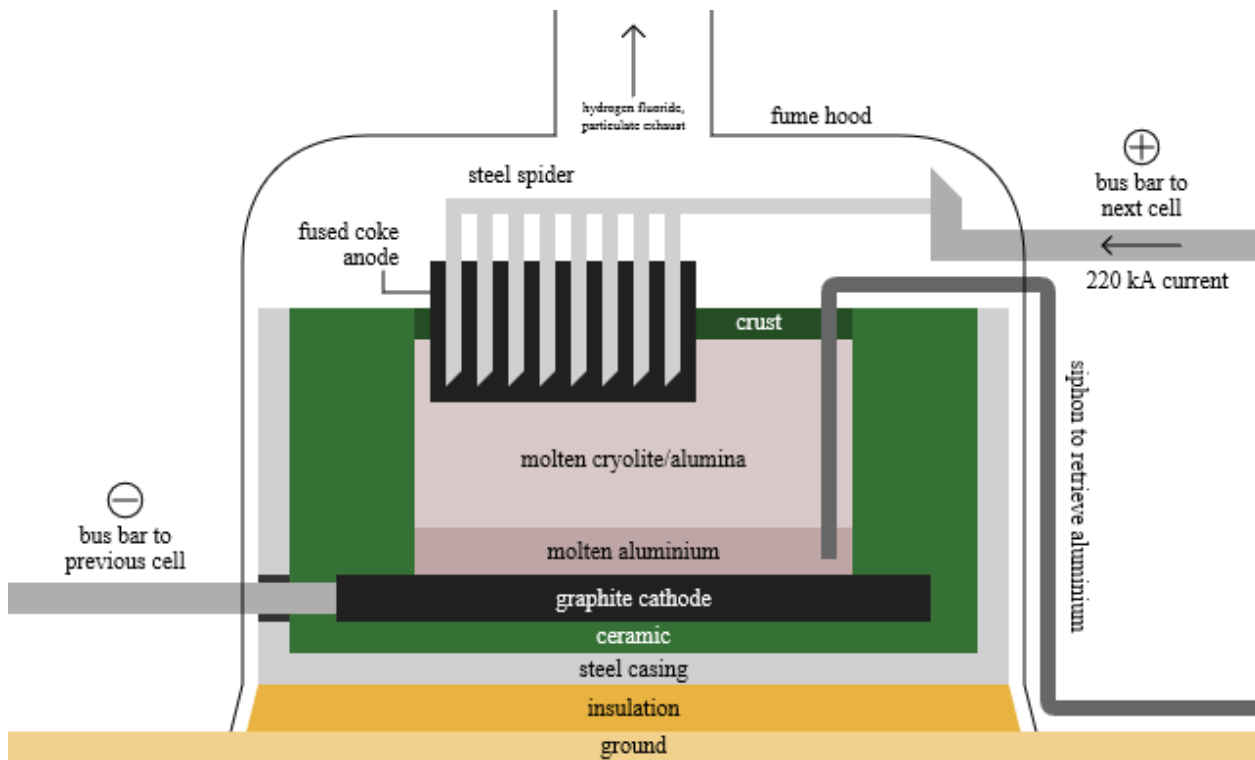
Figure 4: Hall-Heroult Electrolytic cell

In this energy intensive process, a solution of alumina in a molten (950 and 980^0C) mixture of cryolite (Na_3AlF_6) with calcium fluoride is electrolyzed to release the metal.

$$Al^{3+} + 3e^- \rightarrow Al$$
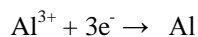
Oxygen gas is formed at the anode

$$2O^{2-} \rightarrow O_2 + 4e^-$$
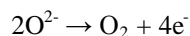
The aluminium metal formed (above 99% purity) sinks to the bottom of the solution and is tapped off. This is called primary aluminium and could be cast into large blocks called aluminium billets for further processing. Further purification can yield 99.99% purity level using Hoopes process – a process that involves the electrolysis of molten aluminium with a sodium, barium and aluminium fluoride electrolyte.

Aluminium is theoretically 100% recyclable without any loss of its natural qualities. Recovery of the metal through recycling has been an important advantage of the aluminium industry. Recycling involves melting the scrap, a process that requires only 5% of the energy used to produce aluminium from ore, though a significant part (up to 15% of the input material) is lost as dross. An aluminium stack melter produces significantly less dross with values reported below 1%. The dross can undergo a further process to extract

151

aluminium. Recycled aluminium is known as secondary aluminium.

2.6. ALUMINIUM PRODUCTION COST ANALYSIS

Principal cost elements in aluminium production are: Alumina, Electrical energy, Carbon anodes, Management and Labour, Gas for heating, Chemicals (principally cryolite) and Mill overheads (Stuart, 2009).

During the electrolytic extraction, the carbon anode is consumed by subsequent reaction with oxygen to form carbon dioxide and so, anodes in the reduction cell must be replaced regularly since they are consumed in the process. The cathode do erode mainly due to electrochemical processes and metal involvement. After five to ten years, depending on the current used in the electrolysis, a cell must be rebuilt because of cathode wear.

In terms of power, the worldwide average specific energy consumption is apparently 15 ± 0.5 kilowatt–hour per kilogram of aluminium produced (52 to 56 MJ/kg). The most modern smelters achieve approximately 12.8 kWh/kg (46.1 MJ/kg). (Compare this with the heat of reaction 13 MJ/kg and Gibbs free energy of reaction 29 MJ/kg). Reduction line currents for older technologies are typically 100 to 200 kA; state–of–the–art smelters operate at about 350kA. Electric power represents about 20 to 40% of the cost of producing aluiminium depending on the location of the smelter and electricity tariff.

Trying to cut down cost in aluminium refining regardless of the production methodology proposed, all alternative processes have some common elements. The primary inputs will be alumina, electrical energy, some carbon and possibly some recyclable chemicals; outputs are aluminium and varying amounts of carbon oxides. Heat will always be released because all alternatives involve high temperatures. Based on these, the best process would be one that occurs at as low a temperature as possible, but with the highest productivity per unit volume reactor while possessing the fewest number of processing stages in the overall conversion process. Some of the alternative processes are shown with their features in Table 1 below.

Table 1: Alternative processes investigated for aluminium production

Production Process	Features
Drained-Cell Technology[*]	Cathode sloping and coated with aluminium-wettable TiB_2. By eliminating metal pad, anode-cathode gap could be halved to ~25 mm, enabling substantial voltage lowering. Other basics would remain the same as present technology ($E° \sim 1.2$ volts, $\Delta_{min, electrolysis} = 6.34$ kWh/kg).
Inert Anode Cells[*] (Oxygen Evolution)	Eliminate consumable carbon anode by having an electrode material that evolves oxygen. Although the electrochemical potential would increase by 1 V ($E° \sim 2.2$ volts), the voltage increase would be (hopefully) less because of lower anode polarization ($\Delta_{min,electrolysis}=9.26$ kWh/kg). The superstructure of the existing cell could be refined, reducing capital costs. If drained-cell materials development were successful, further design options are possible.
Chloride Process[†]	Aluminous material converted to (anhydrous) $AlCl_3$ of adequate purity. $AlCl_3$ electrochemically decomposed in a multi-electrode cell at ~700°C ($E° \sim 1.8$ volts, $\Delta_{min, electrolysis} = 6.34$ kWh/kg). Electrochemically generated chlorine is recycled.
Sulphide Process[†]	Aluminous material converted to (anhydrous) Al_2S_3 of adequate

Production Process	Features
	purity. Aluminium sulphide electrochemically decomposed to recyclable S_2 and aluminium ($E° \sim 1.0$ V) in a multipolar ($\Delta_{min,electrolysis}$ = 5.24 kWh/kg) cell.
Carbothermal Reduction[†]	Convert aluminous material to an intermediate Al_4C_3 (or oxycarbide) chemically at T > 1,700°C. React carbide with further oxide to evolve CO and produce aluminium (or alloy) at T > 2,000°C. Refine the metal quality to a usable grade ($\Delta_{minimum}$ = 9.0 kWh/kg).
* Substantial retrofits using cryolite-alumina electrolytes.	
† Processing using intermediates derived from alumina.	

Source: Aluminium Smelting Overview by Barry, J. Welch (1999)

Figure 5a below shows sectorial representation of the cost of the elements required in aluminium production while Figure 5b shows possible trade–offs with alternative technology.
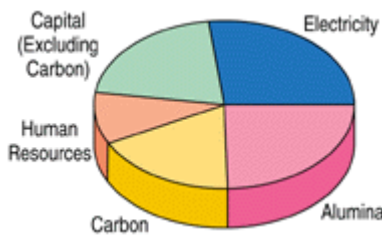
Figure 5 (a) Contributions to the cost of aluminium production
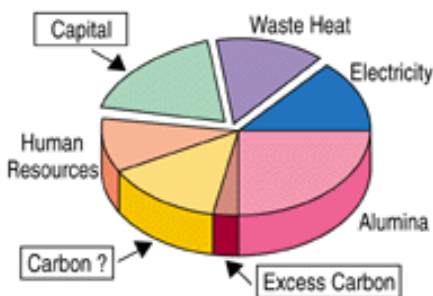
Figure 5 (b) Potential areas for cost reduction with alternative technology

2.7. ALUMINIUM CONSUMPTION IN NIGERIA AND EXPECTED REVENUE GENERATION

Due to its inherent properties chief among which are good electrical and thermal conductivity, high strength to weight ratio especially in alloyed form, ability to form protective oxide coating, non–poisonous nature, recyclability among others, aluminium finds vast areas of application in building and constructions, transportation and machinery, electrical and electronics, food industries for packaging, cooking utensils and cutleries and many more. Although there is small number of bauxite deposits in the country, the ore is cheaply available in neighboring West African countries and its recyclability nature is a huge asset being tapped on. This is what some of the downstream aluminium producers exploit in trying to meet the ever increasing demand of aluminium products in the country.

The consumption of aluminium and other metal products is regarded as a major index of industrialization of a nation. By that yardstick, when compared with even some developing nations, Nigeria is lagging far behind in industrial development. By current estimate, the annual per capita consumption of aluminium in Nigeria is 0.3kg while the corresponding world average is 5kg. This is an indication that Nigeria with an estimated population of over 150 million has large room and huge potential domestic market that can sustain rapid growth in aluminium and other related metal product sector.

While export orientation of Aluminium Smelter Company of Nigeria is very relevant, it is recognized that the long–term viability would largely depend on accelerated and orderly growth of domestic consumption of products. In fact from value addition

point of view, it is the downstream industries that should be encouraged to export, after satisfying domestic market, so as to enhance the foreign exchange earning of the country (Farri consulting, February 3, 2011)

For the month of May 2015, the US exported aluminium (99.5% purity) at the rate of USD 1,804.04 per metric ton (Yinka, 2015). Nigeria with per capita aluminium consumption of 0.3kg across the population of about 150 million people needs about 45 million kg (45 thousand tons) aluminium to satisfy the product need of the citizens before considering exportation and the resultant foreign exchange earnings. This represents a lucrative area of investment which the country would never regret venturing into.

2.8. THE CHALLENGES

The benefits of exploiting aluminium deposits in Nigeria cannot be over emphasized, ranging from the consequent economic growth to creation of employment to the teeming Nigerian youths among others.

Notwithstanding, the attendant challenges ranging from its capital intensive nature to sustainability cannot just be pushed aside. The following are some of the big challenges that must be considered and confronted in order to achieve the feasibility of aluminium production.

- Lack of interest on the part of government: The people saddled with the responsibility of to move the sector forward do not pay attention to the deserved areas of attention and only pay lip services and the sector remains the same or even worse off.
- Inadequate power supply: Aluminium production is capital intensive and about 35% of the total cost is attributed to electric power. With the poor state of power in the country, sustainability of the venture will seriously be challenged.

- Political instability and ethnicity: The problem of dwindling political situation in the country and the question of who comes from where hampers the focus on aluminium and solid mineral exploration in the country.
- Poor policy implementation: Nigerians are good at making sound policies but lack the culture to implement them. Several good policies in solid minerals development but are just on paper.
- Obsolete technology: The technologies of companies established long ago but never reached 10% of installed capacity are phasing out. Good examples are the Aluminium Smelter Company of Nigeria and the famous Ajaokuta Steel Company Limited. New technologies emerge everyday with lower running costs.
- International Politics: Some foreign interests because of mutual coexistence and inter dependency sign some agreements which are detrimental to the development of some sectors in the country.
- Environmental Implications: The control of environmental pollution and other hazards have significant cost implications in aluminium production.

3. CONCLUSION AND RECOMMENDATIONS

At the end of the research, I have appreciated the fact that Nigeria is a country blessed with abundant solid mineral deposits. Lucky enough, the nation is also blessed with abundant human resources capable of tapping the resources in order to enhance growth and

development while at the same time reducing the over dependency on the importation of these items.

Aluminium deposits though not in many areas of the country, can be exploited to satisfy the ever increasing needs and everyday application of the metal in various areas of our lives. Thank God for huge deposits in neighbouring West African countries of Guinea and Ghana, but secondary aluminiium production and recycling still remain supportive to the actualization and sustainability of the giant Aluminium Smelter, Company of Nigeria (ALSCON) project which has been in a pitiable shape for years now.

The country with a huge population of more than 150 million people is a good market when the trend of aluminium usage is considered. The country can also at some point embark on exportation of aluminium products, it only takes policy creation, implementation and tackling of some salient issues that are spelt out in the following recommendations.

i. Nigeria's attention should favour solid mineral sector rather than only on crude oil.

ii. The power issue cannot just but fixed in order to liberalize industrial development. Aluminium production is capital intensive and up to 35% of the cost is only on electricity.

iii. The Federal government should ensure the revitalization and completion of the Aluminium Smelter Company of Nigeria in order to tap the benefits for which the project is meant which has been wasting since its establishment.

REFERENCES

Akinrele, F.O. (2014), "Overview of The Nigerian Mining Sector" A Newsletter publication, September, 2014, pp 1 – 5.

Anne, M.H. (2015), Aluminium Facts, Chemical and Physical Properties.

Ata, U. (2012), "How Nigeria Loses Billions in Solid Mineral Sector" An Audit Report by the Nigeria Extractive Industries Transparency Initiative, NEITI (2007 – 2010).

Auwal, M.I. (2010), "Policy Brief on Solid Mineral Sector for the National Assembly" A Publication of Civil Society Legislative Advocacy Centre, pp 3.

Barry, J.W. (1999), "Aluminium Smelting: Overview of Aluminium Production Paths in the New Millennium" The Member Journal of The Minerals, Metals and Materials Society, pp 24 - 28.

Business and Finance News, (2010) "Why Nigeria's Aluminium Production Falters" December, 15. www.thenigerianvoice.com/nvnews/41034/1/whynigerians-aluminium

Business Day, (2014), "Nigerian Aluminium Industry Choked By Imports, High Energy/Labour Costs" September, 15. www.businessdayonline.com

Channels Television News, (2015) "National Bureau of Statistics Rates Nigeria's New Unemployment Statistics at 6.4%" May 15, 2015.

Daily Trust, (2013), "ALSCON – A Tale of Vainly Privatized Smelter" October, 17.

David, I. (2005), "The Mineral Industry of Nigeria" pp 598.

Ebubec, (2014), "Aluminium Industry Survey Nigeria, Chapter Six" Geoscience Boot Camp, August, 11.

Farriconsulting, (2011), "Aluminium and Steel Consumption; Critical to Nigeria's Economic Development" Investment Opportunity in Nigeria, Thursday, February 3.

Jim, C. (2005), "Extracting Aluminium from Bauxite" www.chemguide.co.uk/inorganic/extraction/aluminium.html

Mbendi, (2015), "Bauxite Mining in Nigeria – Overview" Mbendi and its Associate Information Providers, June, 26. www.mbendi.com/indy/ming/baux/af/ng/p005.htm

Ministry of Mines and Steel Development, "National Policy on Minerals and Metals in Nigeria"

Nigeria National Bureau of Statistics, 2015.

Sam, D. "Aluminium Extraction" Bayer Process on Industrial Scale. sam.davyson.com/as/physics/aluminiunm/site/extraction.html

Siteseen Ltd (March, 2015), "The Element Aluminium" www.elementalmatter.info/element-aluminium.htm

Stuart, B. (2009), "Cost Build up Model for Primary Aluminium Ingot Production" February, 27.

The Punch Newspaper, (2015), "Only 4.67 million Nigerians are Unemployed - National Bureau of Statiatics" May 15, 2015.

US Energy Information Administration; "Energy Needed to Produce Aluminium" An Article Published in "Today in Energy" August 16, 2012.

Vanguard News, (2014), "Nigeria and Solid Mineral Gains" June, 13.

William, H. (2015), "How Aluminium Works"

Yinka, F. (2015), "Aluminium Monthly Prices – US Dollars per Metric Ton" Index Mundi Real Price Survey.

Chemical and Geotechnical Analyses of Soil Samples from Test Pits at Active Open Dump sites in Minna, Nigeria

Agapitus Amadi

Department of Civil Engineering, Federal University of Technology, Minna, Nigeria

agapitus.amadi@futminna.edu.ng, agapitusahamefule4@yahoo.com, 08034516603.

ABSTRACT

The objective of this study is to evaluate the contribution of open waste dumping in contamination of host soil and the effect of such contamination on geotechnical properties of soils. The open dump sites in Bosso and Maikunkele, Minna were selected for this study. Soil samples (n = 6 + 6) were taken from three test pits each in areas covered by wastes and adjacent locations established to represent control sites in the two dump sites. Tests were conducted to measure some chemical properties (pH, Organic matter, carbonate, chloride, sulphate) and geotechnical properties (natural moisture content, particle size distribution, consistency limits, compaction parameters, permeability as well as the shear strength) of soil samples. Test results show that the measured chemical parameters were higher at the dump sites areas than in the control locations for the two sites. In addition, the liquid limit (LL), plasticity index (PI), permeability (k) and shear strength of samples were found to be higher for soil samples taken from test pits in waste disposal areas when compared with that of control locations.

Keywords: *Leachate, Municipal solid wastes, Open dump sites, Soil contamination*

1. INTRODUCTION

Due to population growth, a progressive living standard and industrial progress in the recent past, cities all over the world have witnessed high volume of wastes far beyond their handling capacities and the need to dispose of these wastes in an environmentally responsible way is now top priority in society commitments. As a result, cities are now grappling with the methodologies and technologies of disposal, the costs involved and the negative impact on the local environment (Ekenta, 2001; Tchobanoglous et al., 1977). These problems have however provided a window of opportunity for cities to find solutions involving innovative technologies and disposal methods. While cities in developed countries moved away from old disposal practices of open dumping to engineered landfills, most of their counterparts in developing countries like Nigeria continued with the unscientific waste disposal techniques of open dumping.

The system of solid and liquid wastes disposal by open dumping have resulted in contamination of soil and groundwater systems (Amadi, 2007; Ali et al., 2014). Large areas of land are currently being used for this purpose. At any of the dumping sites scattered in all parts of the country such as the ones shown in plates 1 and 2, tons of wastes which includes municipal solid wastes, chemical and industrial wastes are being dumped without shredding and segregation (Ekenta, 2001). Moreover, the status of the dump sites indicate that leachate generated from such landfill sites infiltrate into the geoenvironment without any hindrance (Robison and Gronow, 1992; Amadi, 2007). As a result of high precipitation, substantial releases of leachate from dump sites have occurred during the past few years. These releases may have also covered extensive areas adjacent to the dumping area resulting in ground contamination.

Leachate is a contaminated liquid from decomposed waste in a landfill or waste dump. Much like the source material, leachate composition varies from state to state, city to city, site to site as well as from season to season. It is produced when water or another liquid comes into contact with waste (Gibbon etal., 1992; Barlaz and Ham, 1993). Source water includes rainfall, snow, surface or groundwater intrusion, water in the waste itself. The composition of leacahtes ranges from inorganic and organic chemicals to

microbiological components (Gibbon etal., 1992; Barlaz and Ham, 1993; Robinson and Gronow, 1992). Its flux in the soil is characterized by a slow, unsteady and non - uniform type of flow (Fang, 1997).

Plate 1: Section of Bosso waste dumpsite

Plate 2: Section of Maikunkele waste dumpsite

Generally, all types of contamination have direct or indirect effects on geotechnical properties of affected soil and invariably, on already existing structures such as foundation embankments, clay liners, footings, caissons, piles and sheet piles. Previous studies (Fang, 1997; Amadi, 2007; Ali etal., 2014) have confirmed that some types of contaminants change the index and engineering properties of their host soils and this behavior has been shown to be dependent on the concentration of the

contaminant solution. Though the effects of contaminants on soils are complex, changes in engineering properties of contaminated soils are primarily due to accumulation of particles and increase in void space resulting from ion exchange and flocculation of soil particles.

In connection with any possible applications of such material for embankment or roadway sub-base etc which is a common practice in construction, knowledge of the chemical and geotechnical properties of the contaminated soil is required and hence the present investigation was carried out.

2. MATERIALS AND METHODS

2.1 Soil samples

Two dump sites located in Bosso and Maikunkele Minna were selected for the study. The wastes in the two dump sites are generated mainly from residential, commercial and industrial sources and are deposited on open land without shredding and segregation. Soil samples for analysis/tests (n = 6 + 6) were taken at 1m depth. First, soil samples (6 in number) were taken from three (3) test pits in areas covered by wastes and then another set of soil samples (6 in number) to represent control samples were obtained from three (3) test pits in adjacent locations away from the disposal areas for comparative assessment. The samples were then prepared for tests/analysis by air drying and sieving.

2.2 Chemical Tests

Each soil sample was estimated for pH in a soil to water ratio of 1:5, Organic matter (OM), carbonate, chloride, sulphate contents based on the standard methods described in BS 1377 (1990) as well as Head, (1994a).

2.3 Geotechnical Properties Test

Laboratory tests were conducted following standard procedures outlined in British standards (BS 1377, 1990) and Head (1994a,b) to determine the particle size distribution, index (consistency limits and compaction

parameters) and engineering properties (permeability, shear strength) of soil samples from the dump sites and the control sites.

3.0 RESULTS AND DISCUSSION

3.1 Comparison of parameters at control and waste dump sites

3.1.1 Chemical properties

The pH measurements of soil samples from the two dump sites indicate higher pH values for samples from areas covered by wastes. The mean values of pH at dump site areas in Bosso and Maikunkele are 9.46 and 9.39 respectively while that of pH at control locations are 6.70 and 6.30 for the dump sites in Bosso and Maikunkele respectively (Table 1).

Similarly, the mean OM content for soil samples from Bosso disposal area is 0.43% while that of the control sites is 0.17% as reported in Table 1. For samples from the Maikunkele dump site, the mean OM was 0.48% for areas covered by wastes and 0.14% for the control sites.

The average values of the chemical contents of soil samples from disposal area in Bosso dump site are 4.0, 3.7 and 10.26 mg/l for carbonate, chloride and sulphate respectively while 1.1, 0.7 and 0.2 mg/l were recorded for carbonate, chloride and sulphate for the control sites. Similarly, at Maikunkele disposal site, the average values of these chemical parameters were found to be higher at waste disposal locations as compared to control sites as highlighted in Table 1.

3.1.2 Geotechnical Properties

The particle size analysis indicates a slight variation in the soil textural composition at the sampling sites. Soil samples from the disposal area at both Bosso and Maikunkele sites contain higher percentage of sand and slightly lower fine fraction (percent passing No. 200 sieve) than the control samples. The mean values

for sand and fines contents for samples from the disposal area at Bosso dump site are 24% and 66% respectively while the sand and fines fractions recorded 20% and 72% in that order for control locations (Table 1). The data in Table 1 also shows mean values of 14% and 70% for sand and fines fractions and corresponding values of 12%, 78% for control locations at Maikunkele site.

Table 1: Mean Soil properties of control sites and waste dump sites.

	Bosso		Maikunkelele	
	TP(W)	TP(C)	TP(W)	TP(C)
Soil Parameters				
pH	9.46	6.70	9.39	6.30
NMC	29.78	8.88	26.53	9.56
OM (%)	0.43	0.17	0.48	0.14
Carbonate (mg/l)	4.00	1.10	4.60	0.80
Chloride (mg/l)	3.70	0.70	3.40	0.60
Sulphate (mg/l)	10.26	0.20	10.87	3.10
Sand (%)	24.00	20.00	14.00	12.00
Fines (% passing No. 200 sieve)	66.0	72.0	70.0	78.00
LL (%)	48.46	57.0	50.0	60.00
PI (%)	20.0	26.0	24.0	33.00
British Standard Light Compaction				
MDD (g/cm^3)	1.73	1.71	1.66	1.60
OMC (%)	15.2	14.75	14.85	14.5
k x 10^{-5}(cm/s)	5.67	0.0444	8.75	0.125
UCS (kN/m^2)	200.0	180.45	176.9	168.24

TP(W) – Test pit waste area; TP(C) - Test pit Control area

Table 1 also highlights the average LL and PI of soil samples from the disposal areas and control locations in both Bosso and Maikunkele sites. The LL and PI of soils from the disposal areas at both sites were found to be higher than at the control locations. The average LL values of soils from disposal areas and control locations are 48.46%, 50% and 57%, 60% correspondingly. Likewise, average PI values of 20%, 24% and 26%, 33% were recorded for disposal areas and control locations in that order at Bosso and Maikunkele sites. The relatively high regime in LL and PI of soil samples from the contaminated

areas is attributable to changes in pore fluid characteristics of soil beneath the wastes.

For the compaction parameters namely the maximum dry density (MDD) and optimum moisture content (OMC), their mean values at control and areas covered by wastes are not much different (Table 1). While mean values of MDD for the two dump sites at the contaminated areas are $1.73 g/cm^3$ and $1.66 g/cm^3$, it is $1.71 g/cm^3$ and $1.60 g/cm^3$ at the control locations for Bosso and Maikunkele sites respectively. Similarly, the average OMC of soil samples from contaminated areas are 15.2% for Bosso site and 14.85% for Maikunkele site. On the other hand, the average OMC for control samples are 14.75% and 14.5% for Bosso and Maikunkele sites respectively.

In terms of soil permeability, samples from the disposal areas of both dump sites yielded higher permeability values when compared with the values for samples from the control locations. It is shown in Table 1 that for Bosso site, the mean value of permeability for waste disposal areas is 5.67×10^{-5} cm/s while 4.44×10^{-7} cm/s was established for the control locations. For Maikunkele dump site, mean values of 8.75×10^{-5} cm/s and 1.25×10^{-6} cm/s were achieved for contaminated areas and control locations respectively. The increase in permeability is due to the flocculant structures in the soil matrix created by leachate that resulted in the decrease in adsorbed double diffuse layer thickness and thus an increase in permeability of the soil.

The results obtained for shear strength of soils at both control and waste disposal sites are presented in Table 1. The average values of the unconfined compressive strength (UCS) for soils from contaminated areas are slightly higher than the average values for control samples at the two dump sites. The average UCS values are 200 kN/m^2, 176.88 kN/m^2 and 180.45 kN/m^2, 168.24 kN/m^2 for contaminated soil samples and control samples respectively. The higher average UCS values for soil samples from the contaminated areas is perhaps as a result of textural changes in soils resulting from soil – leachate interaction.

4 CONCLUSION

An extensive laboratory testing program was carried out to assess the impact of wastes on the chemical and geotechnical properties of soils collected from test trenches in both areas covered by wastes and control locations at active dump sites in Bosso and Maikunkele, Minna. The chemical (pH, Organic matter, carbonate, chloride, sulphate) and geotechnical (natural moisture content, particle size distribution, consistency limits, compaction parameters, permeability as well as the shear strength) properties of soil samples encountered in these test trenches were evaluated based on methods published in standard codes. Test data indicate that soils at the disposal sites showed higher regime in chemical properties when compared with soil samples encountered in locations designated as control sites at the two dump sites.

Similarly, the geotechnical properties were found to be higher in soil samples taken from test pits in waste disposal areas than in soil samples from control locations. The variation in the geotechnical properties are due to textural changes in the soil beneath the waste resulting from leachate intrusion.

REFERENCES

Ali, S. M., Pervaiz, A., Afzal, B., Hamid, N. and Yasmin, A. (2014). Open dumping of municipal solid waste and its hazardous impacts on soil and vegetation diversity at waste dumping sites of Islamabad city. Journal of King Saud University - Science, Vol. 26, Issue 1, 59–65. doi:10.1016/j.jksus.2013.08.003

Amadi, A. (2007). Unsafe waste disposal practices in Nigerian cities: Geoenvironmental perspectives. Nigerian Society of Engineers (NSE) Technical Transactions, Vol. 42, No. 2, 31– 44.

Barlaz, M. A. and Ham, R. K. (1993). Leachate and Gas Generation. Geotechnical Practice for Waste Disposal. Ed.: D. E. Daniel, 113 – 136.

BS 1377 (1990). Methods of testing soil for Civil Engineering Purposes. British standards institute London.

Ekenta, O. E. (2001). Solid Waste Management in Awka Municipality: An Environmental Pollution Control Study. Proc. National Eng. Conf. and Annual General Meeting of the Nig. Soc. of Engrs. held in Portharcourt, 86 – 92.

Fang, H. Y. (1997). Introduction to Environmental Geotechnology, CRC Press, U.K

Gibbon, R. D., Dolan, D., Keough, H. O'Leary, K. and O'Hara, R. (1992). A Comparison of Chemical Constituents in Leachate from Industrial Hazardous Waste and Municipal Soild Waste Landfills. Proc. of the Annual Madison Waste Conf., Madison, 251 – 276.

Head, K.H. (1994a) 'Manual for soil laboratory testing', Vol. I, Soil Classifi cation and Compaction Tests, Halsted Press, New York.

Head, K.H. (1994b) 'Manual of soil laboratory testing', Permeability, Shear Strength and Compressibility Tests, 2nd ed., Vol. 2, Pentech Press, London.

Robinson, H. and Gronow, J. (1992). Groundwater Protection in UK: Assessment of Landfill Leachate Source Term. J. of Inst. of Water & Environ. Mgt, No. 6, Vol. 2, 225 – 235.

Tchobanoglous, G., Theisen, H. and Eliassen, R. (1977). Solid Wastes, McGraw-Hills, Inc., New York.

CHARACTERIZATION OF UNDERGROUND WATER RESOURCES OF MINNA, NIGERIA FOR DOMESTIC USES

[1]Nuhu A. Ademoh; [2]Sadiq S. Lawal

[1,2]Department of Mechanical Engineering, Federal University of Tecvhnology, Minna, Nigeria.

Corresponding author's e-mail: nuhuadam@yahoo.com; Phone Number:-+2348038441442

ABSTRACT

The general water shortage afflicting Minna, the capital of Niger State of Nigeria has made people resort to access underground and subsurface water through sinking of shallow, intermediate and deep wells to alleviate their problems particularly during dry seasons of the year when temperatures are quite high (above 40^0C) and most surface water is dried up coupled with minimal supplies from state public water board. This study adopted 11 sample wells in the categories affordable by most citizens located at different parts of the town for physic-chemical and biological characterization to ascertain compliance of their water samples with the World Health Organization's guidelines for safe drinking water. They were measured with tape rule and found to belong to the shallow well category as their depths ranged from 1.2 to 15.0m and widths 1.0 to 5m. Standard test methods as described by Degrémont (2010) schedule of water analyses were adopted for the physic-chemical examinations that included turbidity, PH, temperature, alkalinity, hardness, colour and chloride ions. Bacterial micro-organisms present were determined with Eosin methylene blue agar (EMB) system. The result showed that all samples were unsuitable biologically as each well water contained bacterial presence in excess of Nill/100ml and none satisfied the physic-chemical qualities specified by WHO standard. Appropriate mechanical, biological or chemical treatment would be needed to purify water from each well to make it suitable for human consumption so as to solve un-investigated problems that ignorant consumptions of the raw well water might have been causing to citizens.

KEYWORDS: Minna, well water, physic-chemical, WHO guideline, e-coli, enterobacter/aerogen.

1.0   INTRODUCTION

Water is one of the critical natural resources desperately needed for survival of all living things. Water is needed by man for drinking, food preparation, cleaning/hygiene, growing his crop, tendering animals and other essential use in commerce and industry. Accessibility to safe water is universally considered as a basic right of every country citizen. Unfortunately this necessity remains unrealized for a large majority of people living in rural and urban settlements in most developing countries of the world that includes Nigeria. Although the world is made up of over 70% of surface and underground water, most of this water contains certain mineral, gases, bacteria/virus, solid/liquid contaminants, undesired taste and odour [1]. Presence of these organic and inorganic matters in water causes many life threatening diseases like dysentery, gastroenteritis, cholera, typhoid e. t. c. It is in respect of this danger posed by consumption of unsafe water to human health that United Nations declared provision of portable water for citizens as one of Millennium Development Goal (MDG). However by 2015, the targeted year for the realization of these goals, many Nigerian communities just like most developing countries are yet to have access to safe water.

This shortage has forced citizens to individual effort of sourcing water from any available and affordable means for daily sustenance. Common sources of water include rain water (seasonal), public water supply (available to only a few), underground water through shallow/deep wells and surface water from rivers and streams. In Minna, Niger State of north central Nigeria, general water shortage afflicting the country has made people resort to access underground and subsurface water through sinking of shallow and intermediate/deep wells to alleviate the problem particularly during dry seasons of the year when temperatures are very high (above 40^0C) and most surface

water is dried up coupled with minimal supplies from state public water board. Due to poor economic situations of most people using this type of water they cannot afford the high cost of the technology for sinking wells up to the depths that produce clean water nor that for treating such water. They use the water as obtained from the wells. The state department responsible for sampling, testing such water for suitability or otherwise for human and advice users accordingly are not forthcoming with vital service. These expose people that consume such water to high risks of water borne diseases.

Well water contains organic compounds originating from decaying organic matters from agricultural runoffs. It also contains synthetic inorganic materials resulting from use of some processed products like detergents, pesticides, herbicides, solvents, domestic and industrial wastes. Presence of the contaminants influences quality and usefulness of natural water resource. Those who are aware of dangers of untreated water and resort to packaged water popularly referred to as sachet water or pure water in Nigeria for drinking are still not completely protected from water related diseases contacted through other uses of water. Moreover most packaged water producers in town source their raw water from these same wells and lack the required treatment technology to make the water absolutely safe for human despite regulations by the National Agency for Food and Drug Administration and Control (NAFDAC) in Nigeria [2]. Hence the need for its treatment before use by man to forestall health hazards [3]. Treatment will bring the main chemical constituents common with well water within acceptable limits for human consumption and other domestic/industrial uses.

As a part contribution towards finding solution to this problem this research paper is aimed at identifying some strategic shallow/intermediate and deep wells in Minna town from which most citizens draw their water for characterization to ascertain their suitability or otherwise for human consumption. The main objectives of this are to obtain World Health Organisation's (WHO) standard for water quality for human consumption, characterize sampled water from wells at different parts of Minna for chemical and biological analyses and to compare result obtained with WHO standard to ascertain the level of contamination, usability and otherwise for domestic uses. The significance of the work when completed lie in the fact that citizens of Minna would become better informed about the qualities of sub-surface and underground water resources available to them and guide them on use and treatment of water. This will reduce incidences of water borne disease and improve living standard.

2.0 MATERIALS AND PROCEDURES

2.1   Materials:-The major materials used for the experimental aspect of this work included raw water samples collected from eleven (11) wells located at different parts of Minna town, wooden tape rule, assorted chemical reagents obtained from licensed industrial and laboratory chemical dealers in Minna, spectrophotometer, digital PH meter, burettes, glass beakers, pipettes, glass test tubes, hand gloves, plastic containers of varied sizes and WHO standard for safe drinking water (table 1) [4].

Table 1 WHO Guidelines for safe drinking water

Parameters	WHO Permissible Limits
Temperature	30^0C
Odour	Unobjectionable/odorless
PH	6.5-8.5
Hardness	500mg/l
Total Dissolved Solids	1500mg/l
Turbidity	5NUT
Conductivity	$120YS/cm^3$
Chloride Ion	250mg/l
Alkalinity	100mg/l
Colour	15TCU
Appearance	Clear
Bacteriological	
Coliform	Nil/100ml

E.Coli	Nil/100ml

2.2 Experimental Procedures

A wooden tape rule calibrated to take linear measurement was used to determine vertical depth of each of the wells investigated. Water sample was collected from each well through the mounted pumping facilities (for motorized well) and manually collected for non-motorized wells. Samples were stored in clean/labelled plastic containers to protect it from any environmental contamination awaiting tests and analyses. The experimental works were broken into two parts and conducted as follows:

2.2.1 Physico-Chemical Analysis of raw water samples obtained from wells:-Standard analysis was done to determine the physical parameters sample to evaluate water portability. Digital PH meter was used to measure the PH of water and turbidity meter was used to measure turbidity of water samples. A spectrophotometer was used to measure light transmission ability of water samples in accordance with Degrémont, A.8 [5]. For total alkalinity, methyl orange was used in titration. Alkalimetric reagent was made up of two acids, HCl and H_2SO_4 and was also used in the titration in accordance with Degrémont, A.21, A.24 [5]. Test for hardness was done with 20 drops of KIO buffer that helped to bring specimen to uniformity with 5 drops of erichrome black or net measured and added as the indicator. Procedures stated in Degrémont, A.29 was adopted by which disodium ethylene chiamine tetraocetate was used in the titration process. For chlorine and ion tests, 4 drops of phenolphthalein was added to raw well water specimens with 5 drops of potassium dichromate indicator before sample was titrated with silver nitrate as recommended by Degrémont, A.5 [5].

2.2.2 Bacteriological analysis:-This was carried out on raw water samples to determine extent and types of bacterial presence. This will enable adequate information on the biological treatment that should be recommended

for a water sample to adequately domesticate as safe for human use. The multiple tube fermentation method of preliminary processing of raw water for analyses was used prior to carrying out bacteriological analysis on cultured test sample [6]. Analyses were conducted in sequences of presumptive and confirmative tests.

(a) Presumptive test:- In this stage, lactose broth (liquid) was used for the analysis. Exactly 10ml of each raw well water sample was inoculated in 10ml lactose broth. Each sample was then inoculated between at temperature of 37^oC to 38^oC for 24 hours. On observation, presence of gas, acid and cloudy appearance accordingly showed test sample was contaminated. This was adopted as in the WHO annex 5 guideline for drinking water quality [4].

(b) Confirmatory test: Raw well water samples were streak on an EMB plate (Eosin methylene blue agar). Specimens were then inoculated for a period of 24hours and when exposed to presence of green metallic shine showed presence e-coli (Escherichia coli); as an indication of any faecal contaminants. After exposure, a pinkish growth with dark spots showed presence of enterobacter aerogen while a pure pinkish growth indicated presence of other coliforms. The tests and their interpretations were all done in compliance with WHO Guidelines for drinking-water quality [7]; [8]. Pysico-chemical and bacteriological analyses were carried out in the departments of Chemistry and Chemical Engineering of the Federal University of Technology Minna and the facilities at the water quality laboratory of Niger state Water Board, Minna, Nigeria.

3.0 RESULTS AND DISCUSSION

The vertical depths of the wells as obtained with wooden meter rule used for dimensioning them. The diameters of the wells measured 100cm to 500cm as presented in table 2. Wells selected for study were all mounted with either concrete or metal top protective covers to secure its water.

From the table it is observed that the wells fall within the shallow hand dug category which can yield relatively large quantities of water from the shallow sources and are

most extensively employed for individual water supplies in areas containing unconsolidated glacial and alluvial deposit (Watt S. B., 1985). However due to the hard rocky nature of Minna most citizens who depend on this type of water sources do not have financial strength to dig deep wells that go beyond depth of surface solid contaminants.

Table 2:- Vertical depths of the sampled wells

S/N0	Well Sample/Location	Depth (m)
1	Well A (Central Minna)	4.3m
2	Well B (Central Minna)	5.2m
3	Well C (Central Minna)	4.6m
4	Well D (Central Minna)	5.5m
5	Dutsen Kura well	5.2m
6	Fadipe well	1.2m
7	Sauk Kahuta well	1.8m
8	Maikunkele well	9.7m
9	FQS well	15.0m
10	Chanchanga well	5.6m
11	Tunga Maje well	4.4m

Solid content of natural water extremely vary as a result of geomorphologic and hydraulic characteristics of the environment in which water collects and of the manner in which it is withdrawn. These factors were not readily controllable with these types of well that are mostly for low income public uses. Therefore, the well water when properly analysed may contain colloids, organic matter, humic compounds like tannin, lignin, phenol, amino acids and hydrocarbon products of decomposition of vegetable matter that will require appropriate treatment processes to make the water safe for human consumption [9]; [10].

Mineral constituents dissolved in natural water constitute dissolved solids. More than 500 mg/l is undesirable for drinking and many industrial uses. Less than 300 mg/l is desirable for dyeing of textile and manufacture of plastics, pulp paper, and rayon. Dissolved solids cause foaming in steam boiler. The maximum permissible content decreases with increase in operating pressure [3]; [10]. Natural minerals commonly contain less than 5,000 mg/l; some brines contain as much as 300,000 mg/l. The rocky sub-terrain nature of Minna could have highly enriched minerals that could generate lots of dissolvable solids into shallow wells that may require treatment for the water.

Table 3 presents the phsico-chemical analyses of the water characteristics which include the PH, turbidity, temperature, total alkalinity, hardness, colouration and chloride ion content in the raw untreated state of the water samples for each of the 11 wells studied.

Table 3:-Result of physico-chemical tests on the raw well water samples

S/N	Water Sample	Turbidity (NUT)	PH	Temp. (^{O}C)	Total Alkalinity	Total Hardness (mg/l)	Colour (TCU)	Chloride ion (mg/l)
1	Well A (Central Minna)	10.5	6.6	31.6	230.0	196.0	151	63.9
2	Well B (Central Minna)	15.7	6.3	31.5	160.0	176.0	169	45.4
3	Well C (Central Minna)	15.8	6.3	31.3	200.0	280.0	119	44.0
4	Well D (Central Minna)	23.7	7.5	31.6	100.0	252.0	0ver range	56.8
5	Dutse kura well	3.7	7.7	32.0	210	356	32	120.7
6	Fadipe well	10.5	7.8	31.8	204	166	3	18.5
7	Sauka-kahuta well	4.8	7.1	31.8	228	132	53	42.6
8	Maikunkele well	10.9	7.6	31.8	120	300	68	12.8
9	FQS well	1.4	7.1	31.7	200	234	1	49.7
10	Chanchanga well	26.6	7.0	31.5	142	210	174	17.2
11	Tunga-maje well	4.9	6.9	31.8	200.0	384.0	33	213.0

The results presented in table 3 were compared with the WHO standard presented in table 1 to ascertain level of suitability of each of the well water sample for humans. Out of the total of 11 wells, only water samples taken from Dutse kura (well with 3.7NUT), Sauka-kahuta (well with 4.8NUT), FQS (well with 1.4 NUT) and Tunga-maje (well with 4.9NUT) satisfied the WHO maximum recommended turbidity of 5NUT for drinkable water. All the samples fell within the upper limits of acceptable WHO PH of 6.5-8.5 for portable water. Based on the ambient sample temperatures, well water samples were slightly above WHO value of 30^0C. This is acceptable because, daily meteorological data always maps Minna as one of the hottest towns of Nigeria. The water from Well D located in central part of Minna with a total alkalinity of 100mg/l was the only sample that satisfied the WHO standard of 100mg/l. Except water from Maikunkele well which was marginally above the requirement all the other wells had water alkalinity quite above WHO standard [3].

The maximum water hardness of 500mg/l that is recommended by WHO was reasonably satisfied by all the well water samples; in fact no sample had a hardness of up to 50% of the standard. By colouration, WHO specifies a value of 15TCU as the maximum that is acceptable for drinking water whereas only the water from Fadipe and FQS wells satisfied this condition. All the other well samples were extremely higher than WHO

standard because of heavy presence of series of organic and inorganic compounds that co-exist as micro-pollutants, that even in small quantities are dangerous to a man's health. Concentrations of these substances are such that their removal would require some treatment [11]. The nature of well shallow and absence of concrete ring sealant against pervious earth layer surrounding well. Fadipe well (with a depth 1.2m) is located in that rocky environment which sealed it from contamination by decomposed organic/inorganic matter seepage. The depth of water collection in FQS well (15.0m) was far below the top soil that causes contamination. Each of the samples had chloride ions below 250mg/l recommended by the WHO and are therefore certified suitable for human use. Tunga-maje had 230mg/l and Dutse kura well had about 121mg/l chloride content. These also indicated the dissolved solid in water sample. Chief source of chloride is sedimentary rock that evaporates while the minor sources are igneous rocks that are very prevalent in Minna as shown by the two samples [3]. Chloride in the excess of 100mg/l imparts salty taste that may cause physiological damage [12]. Food process industries require below 250mg/l, implying that water from Tunga-maje and Dutse-kura wells require chloride reduction treatment [13]; [14].

Table 4 shows result of bacteriological analyses on 11 raw well water samples studied. Bacterial organism discovered were enterobacter, aerogen and escherichia-coli as displayed per well in the

table. WHO standard (table 1) shows Nill/100ml concentration of the escherichia-coli and other bacterial microorganism present in safe drinking water. However all the well water samples had substantial presence of enterobacter, aerogen and echerichia-coli and therefore do not satisfy WHO requirement for safe drinking except it is treated appropriately [14], [15].

Table 4:-Result bacteriological analysis for raw well water samples.

S/N	Well Sample	Bacteria Present
1	Well A (Central Minna)	Enterobacter/Aerogen
2	Well B (Central Minna)	Enterobacter/Aerogen
3	Well C (Central Minna)	Enterobacter/Aerogen
4	Well D (Central Minna)	E.Coli/Enterobacter/ Aerogen
5	Dutsen Kura	Enterobacter/Aerogen
6	Fadipe	Enterobacter /Aerogen
7	Sauka Kahuta	Enterobacter /Aerogen
8	Maikunkele	E.Coli/Enterobacter/ Aerogen
9	FQS	E.Coli/Enterobacter/ Aerogen
10	Chanchanga	Enterobacter /Aerogen
11	Tunga Maje	Enterobacter /Aerogen

Presence of the harmful bacteria/virus, solid and liquid contaminant, doesn't only give water the undesired taste and odour but also causes many life threatening diseases like cholera, dysentery, gastroenteritis, typhoid e. t. c. Thus, appropriate conditioning treatment of well water from these locations inevitable in order to make such water safe for human consumption for healthier living and longevity [16]; [17].

4.0 CONCLUSION

The research work showed that the depth of the wells analysed fell within the shallow categories of wells due to the economic status of users of the wells and the rocky hard nature of the land where they are located. Their low depths were responsible for presence of decomposed organic matter and other contaminants that affected the physio-chemical and the micro-organic quality of samples. None of the raw well water sample was exactly suitable for human consumption without prior chemical or biological treatment as each contained micro-organisms that including enterobacter, aerogen and escherichia-coli; the presence of which WHO guidelines totally reject in safe human water.

REFERENCES

Brock T.D. (1991)-"Biology of micro organisms, zoological description". Biology of microorganisms. 6th Edition. Prentice Hall, New Jersey.

WHO (2011)-"Guidelines for drinking-water quality". 3rd edition; volume 3. World Health Organization, Geneva.

Arbelot A. (1994)-"Public Health Engineering in Emergency Situation". Water testing in emergencies. Médecins Sans Frontières, Paris, France.

WHO (2011)-"Guidelines for drinking-water quality". 3rd edition; volume 3. World Health Organization, Geneva.
Degrémont ; Manual for Water Treatment Handbook 10th Edition.

Barnes (1983)-"Water filtration using rice hull ash". Waterlines, vol. 2, pp.21-3.

WHO (2004)-"Guidelines for drinking water quality". 2nd edition volume 3.

WHO (2004)-"Community water supplies; a critical situation". WHO Chronicles 23, NO.8

Reed A. (1979)-"Summary of water quality testing parameters''

Frankel R.J. (1979). Alternative Filter Media'. Operation of coconut fibre/burnt rice husks filter for supplying drinking water to rural communities in Southeast Asia. AJPH vol.69 (1), pp.75-6.

Feacham R.G. (1975). "Water supplies in low-income communities of developing countries".

Shaw R. (1999)-"Technical Briefs, Including Overview of Treatment Processes". Running Water: more technical briefs on health, water and sanitation. Intermediate Technology, London, UK, p.103.

Journal of environmental engineering division proceedings ASCE 101, EES.

I R.C. (1981)-"Overview of sand filtration among other processes". Small community water supplies: Technology of small water supply systems in developing dountries. Hofkes, E.H. (Ed.) Technical Paper Series 18. IRC, Rijswijk, the Netherlands.

C. W. C (1995). "Alternative filter media". Evaluation of crushed recycled glass as a filtration medium in slow rate sand filtration. CWC, Seattle, USA.

Schulz C.R. and Okun D.A. (1984)-"General overview of rapid sand filtration". Surface water treatment for communities in developing countries. IT, London.

Stapleton C.K. (2000)-"Tube wells and their construction". Water aid's health and safety policy, wells and their construction IT Publications.

ANALYSIS OF HEAT EXCHANGER NETWORKS FOR MINIMUM TOTAL ANNUAL COST (TAC) USING PINCH ANALYSIS

Y. Lukman[1]*, B. Suleiman[1] and O.S.Azeez[1]

[1]Department of Chemical Engineering, Federal University of Technology Minna,
Niger State

*Correspondent Author: yusuflukman55@yahoo.com, 08035873224.

ABSTRACT

This study presents pinch analysis of some heat exchanger networks (HENs) problems using Hint integration software to analyzer heat exchanger networks (HENs) problems. Three problem examples reported to have been solved using different approaches by various researchers to obtain the least possible total annual cost (TAC) was solved using HINT software and the result obtained is presented. It shows that this approach was the best in solving problem example 2 and 3 type and second best for problem example 1.However,it was observed in this study that reduction in piping cost in the absence of split does not necessarily translate into the lowest TAC. The overall assessments of the various approach to solve these problems shows that HINT has proven to be the best in handling different kind of heat exchanger network problem aimed at minimizing total annual cost.

Keywords:HENS, TAC, HINT, networks, integration.

1. INTRODUCTION

Energy integration offers a novel approach that reduce energy consumption and total annual cost where the existing system required modification to improve performance (Akande, 2007). Energy is needed to drive the heat exchangers system in the process line, where a set of hot process streams to be cooled and a set of cold streams to be heated. This call for the energy integration in the form of heat exchanger networks (HENS) design. In process integration, the external heating and cooling utilities are reduced to save energy and total annual cost (TAC) (Smith, 1995). The optimization of chemical processes in industries is being given serious attention because of the need to reduce energy consumption in the face of increasing energy cost. This will ultimately lead to reduction in production costs, improved product quality, meeting safety requirements, reduction in energy consumption, and compliance with environmental regulations. The main objective is often economics and is stated in various terms such as return, profitability or payback period of an investment (Smith, 2005).

Pinch analysis begins and has now advanced to solve problems in engineering where heating and cooling of process materials required effluent quality, improvement in product yield, debottlenecking, and safety of the process. The concept of pinch analysis evolved over the years as a result of various research efforts made by a substantial number of researchers. The general progress that has been made over the years to accomplish energy minimization in HENs and also to develop an optimal heat exchanger network design using pinch analysis have been presented in literature (Hohmann, 1971; Linnhoff and Flower, 1978; Linnhoff *et al*., 1982). Specific researchers that have adopted mathematical techniques include Yee and Grossman (1990), Isafiade and Fraser (2008), Azeez, *et al.* (2012) and Azeez, *et al.* (2013). Lawler and wood (1966) optimized energy exchange to obtain a network design of minimum cost without putting stream split into consideration. The use of modified pinch analyzer (Hint software) is hereby investigated to optimize TAC for problems that have been solved by other researchers as presented in the three examples in this paper.

2.0 METHODOLOGY

2.1.1 Materials

Data extraction: The materials used include previous research journals for data extraction.

Soft wares: The software used is HINT

Computer System: HP 620, 64 bit operating system, 2G RAM, 2.3 GHz processor, Window 7 operating system.

2.1.2 Methodology

The methodology of this research work consist of data extraction from literature, data input and simulation in HINT; Design of Grid Diagram in simulation environment; Optimization of ΔTmin in HINT and finally comparison of the results obtained using the packages as summarized in Figure 1.
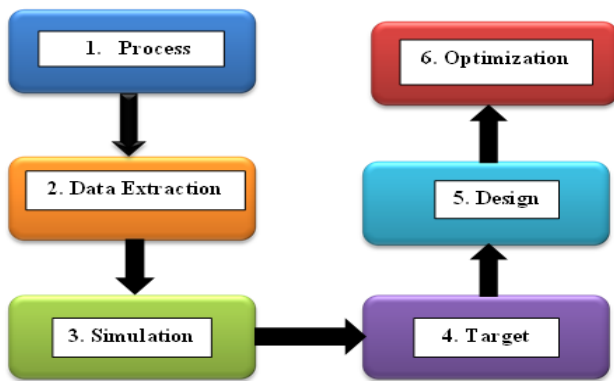
Figure 1 Phases involved in Pinch analysis

Data input and simulation in HINT

The data obtained from the work of previous researchers were used as input to the simulation environment of HINT (indicated as add stream dialogue box) from which composite and grand composite curves are generated as well as the grid diagram with the assumption of ΔTmin in the menu bar.

Design of Grid Diagram in HINT

The matching and splitting of the streams was carried out on the grid through the following procedures: the matching was carried out using MCp rule that said above the pinch the number of hot streams ≤ Number of cold streams and MCp of hot streams ≤ MCp of cold streams. The second rule emphasized that below the pinch the number of hot streams ≥ Number of cold streams while MCp of hot

streams ≥ MCp of cold streams. Stream split was carried out where the MCp rule is violated. The utility heater and cooler were placed after all possible matching was achieved at points where heating and cooling are required respectively. The matching which has various options above and below the pinch was verified using remaining problem analysis (RPA) to obtain the best possible total heat flow area close to the area target after all exchangers above and below the pinch is installed. Though RPA analysis can be based on energy and capital cost other than target area selected in this work. After the RPA based on target area, the energy target, minimum number of units and cost target was evaluated and displayed for the optimal minimal area selected.

Optimization of ΔTmin in HINT

The result of the total minimum cost was optimized using optimal ΔTmin. The ΔTmin for energy targets was selected for optimization in the diagram menu ΔTmin analysis. The optimal ΔTmin can be identified on the cost target versus ΔTmin graphs plotted in HINT.

3. RESULTS AND DISCUSSIONS

Examples

In all the three examples presented, RPA based HINT package approach was used in the modelling of heat exchanger networks with objective function of minimum total annual cost optimization.

Example1: Linnhoff *et al.* (1982)

This example was previously reported in the work of Linnhoff *et al.* (1982). It consists of two hot streams, two cold streams, along with steam and cooling water as utilities. The Stream and cost data are as shown in Table 1. The Linnhoff *et al.* (1982) solution to this problem using pinch analysis was followed by other approaches including mathematical approaches (Yee and Grossmann, 1990; Grossmann, 1985; Azeez*et al.,* 2012). Table 2 shows the

result obtained for this example using HINT-RPA package to solve this problem and comparison of the result with those of previous researchers has been made with the grid diagram presented in Figure 2. The optimal minimum TAC of $ 83,107/year obtained in this work was the least after Stage wise superstructure (SWS) of Yee and Grossmann (1990) with percentage difference of 3.53 % from the least TAC. This significant improvement obtained can be linked to the use of the remaining problem analysis (RPA) for best stream matches that were not considered in the work of Linnhoff *et al.* (1982) pinch analysis. The number of heat exchanger unit obtained is five (5) which was the least obtained in the previous research works. This shows that the pinch technique is able to simultaneously minimize the competing costs in HEN. The absence of split in the solution obtained using HINT-RPA is another added advantage of making piping easier. It should be noted that Yee and Grossmann (1990) approach that resulted into best TAC used DICOPT++ in GAMS which is non-linear optimization step.

Table 1: Stream and Cost Data for Example 1 Linnhoff *et al.* (1982)

Stream	Ts (K)	Tt (K)	F (kW K^{-1})	Cost ($ kW^{-1} year^{-1})
H1	443	333	30	-
H2	423	303	15	-
C1	293	408	20	-
C2	353	413	40	-
S1	450	450	-	80
W1	293	313	-	20

U = 0.8 kW m^{-2} K^{-1} for all matches without steam. U = 1.2 kW m^{-2} K^{-1} for matches with steam. Heat exchanger annual cost = $1000 (A) $^{0.6}$ (A in m^2).
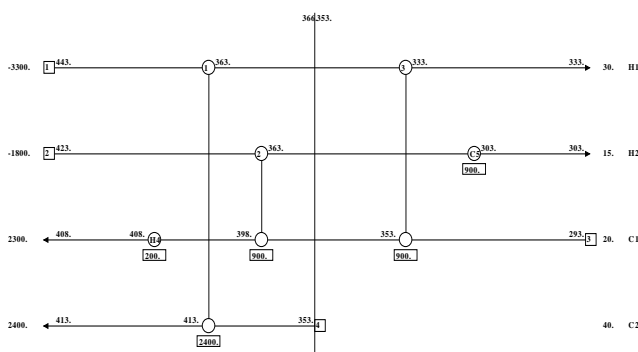
Fig.2: Grid Diagram for Example 1

Table 2: Comparison of Results for Example 1

Method	Stream splits	No. of units	TAC ($/year)	Difference (%)
Supply & target based superstructure (S&TBS) (Type 1) Azeez et al. 2012	1	5	93,391	16.34
Supply & target based superstructure S&TBS (Type 2) Azeez et al. 2012	1	5	90,672	12.95
Supply based superstructure (SBS) of Azeez*et al.* 2013	2	7	90,521	12.77
Magnets Solution of Grossman (1985)	-	6	89,832	11.91
Pinch technique of Linnhoff *et al.* (1982)	-	7	89,832	11.91
Target & Supply based superstructure (T&SBS)	2	6	87,611	9.14
Pinch technique (HINT), present study	0	5	83,107	3.53
Stage wise superstructure (SWS) of Yee and Grossmann (1990)	2	5	80,274	0.00

Example 2 Yee and Grossmann (1990)

This problem was previously reported in Magnet user Manual and Yee and Grossmann (1990) adopted it for analysis using SWS method capable of handling cases requiring stream splits. The problem consists of five hot streams, one large cold stream, one hot utility (steam) and cold utility (cooling water). The stream and cost data are shown in Table 3 and Figure 3 shows the grid diagram obtained in this work. The problem was analysed by many researchers with high expectation of having as much number of splits as possible as demonstrated by the results obtained as contained in Table 4. Previous attempt to minimize the total annual cost with least number of split in this problem was carried out by many researchers (Yee and Grossman, 1990; Isafiade and fraser, 2008a; Azeez*et al*., submitted for publication; Azeez*et al*., 20012) with the expectation of many splits. The application of RPA based HINT technique to evaluate this problem resulted into two stream splits as reported to have been obtained in previous work (GA of Lewin, 1998). The number of units obtained is 8 slightly lower than that of GA of Lewin (1998). This number of splits is the highest maximum obtained in all

previous work with unit number close to the average obtainable as shown in Table 4. The approach used in this work resulted into the least total annual cost (TAC) of $ 562,331/year when compared with the least obtained by Azeez *et al.* (2013) with 1.19 % difference. Comparison has shown that the objective function of minimum total annual was achieved in this work and the potentials of remaining problem analysis as a rebust optimization tool in this type of pinch has been revealed. The use of pinch without RPA by Linnhoff *et al.* (1982) resulted into 11.91 % higher total annual costs. This variation and improvement in RPA base HINT can be linked to its ability to select the best match among all the available possibilities that can give the least optimal minimum area compute by the area target.

Table 3: Streams and Cost Data for Example2.

Stream	Ts (K)	Tt (K)	F (kW K^{-1})	Cost ($ kW^{-1} year^{-1})
H1	500	320	6	-
H2	480	380	4	-
H3	460	360	6	-
H4	380	360	20	-
H5	380	320	12	-
C1	290	660	18	-
S1	700	700	-	140
W1	300	320	-	10

U (kW m^{-2} K^{-1}) = 1 for all matches, heat exchanger annual cost =$1200(A)$^{0.6}$ for all exchangers (A in m^2).
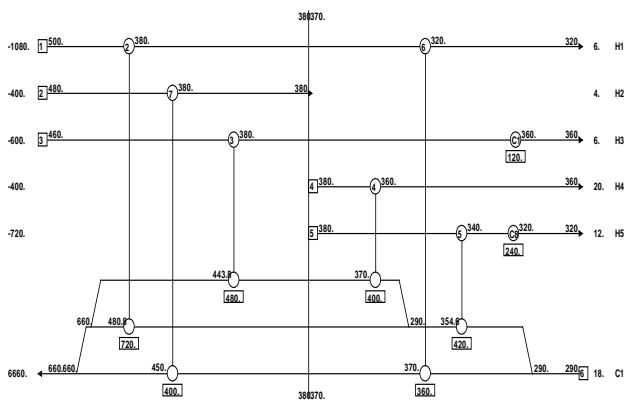
Fig.3: Grid Diagram for Example 2

Table 4: Comparison of Results for Example2 (Magnets Problem)

Method	No. of intervals	Stream splits	No. of units	TAC ($/year)	Difference (%)
Cold stream based Interval based mixed integer non-linear programming MINLP superstructure (IBMS)Isafiade and Fraser (2008)	3	1	7	595,064	5.821
Target & Supply based superstructure (T&SBS) of Azeez (2011)	6	1	7	581,954	3.490
Hot stream based Interval based mixed integer non-linear programming MINLP superstructure(IBMS) of Isafiade and Fraser (2008b)	7	1	7	581,942	3.487
Supply & target based superstructure S&TBS (Type 1) (2012)	7	1	7	581,942	3.487
Supply based superstructure (SBS) of Azeez et al. (2013)	6	1	8	580,023	3.146
Supply & target based superstructure S&TBS (Type 2) (2012)	7	1	10	577,602	2.716
Stage wise superstructure (SWS) of Yee and Grossmann (1990)	5	1	7	576,640	2.545
Genetic algorithm (GA) of Lewin (1998)	-	2	9	573,205	1.934
Pinch technique (HINT), present study	-	2	8	562,331	0.00

Example 3 Krishna and Murty (2007)

This example is an aromatic plant problem reported in previous works (Linnhoff and Ahmed, 1990; Lewin, 1998; Krishna and Murty, 2007) that attempted to determine cost optimal network of heat exchangers. The problem consist of four hot streams and five cold streams having significantly different heat transfer coefficients as shown in Table 5 with its grid diagram in Figure 4. The result obtained using HINT software shows that two (2) stream splits and eleven (12) number of units was obtained. Total annual cost of $2.881 million/year was obtained and is the best when compared to the least minimum annual cost reported literature as shown in Table 6. The least number of splits obtained in previous works for this problem is 2 which correspond to the number obtained in this work. The minimal number of splits signifies reduction in the cost of

piping. Sequential match reduction approach of Pettersson (2005) gives the best minimum cost of $M2.905/year. The highest cost is that obtained by the DEM of Krishna and Murty (2007) with a cost of M$3.146/year and percentage difference of 8.30 % higher. The results obtained shows that the HINT is a robust tool capable of identifying optimal network of heat exchangers proved by the annual cost, splits and number of units obtained which can be linked to the optimal placement of heat exchangers through best matches selection and ΔTmin optimization.

Table 5: Stream and Cost Data for Example3 (Krishna and Murty, 2007)

Stream	Ts (K)	Tt (K)	F (kW K^{-1})	h (kW m^{-2} K^{-1})
H1	600.15	313.15	100	0.50
H2	493.15	433.15	160	0.40
H3	493.15	333.15	60	0.14
H4	433.15	318.15	400	0.30
C1	373.15	573.15	100	0.35
C2	308.15	437.15	70	0.70
C3	358.15	411.15	350	0.50
C4	333.15	443.15	60	0.14
C5	413.15	573.15	200	0.60
Hot oil	603.15	523.15	-	0.50
CW	288.15	303.15	-	0.50

Plant lifetime = 5 years; rate of interest = 0%; exchanger cost = $10,000+350(A) (A in m^2); cost of hot oil = 60 ($/year)/kW; cost of cooling water (CW) = 6 ($/year)/kW.
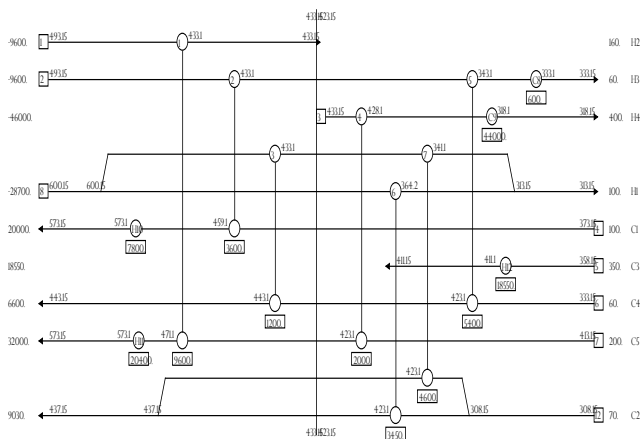
Fig. 4: Grid Diagram for Example 3

Table 6: Comparison of Results for Example 3 (Krishna and Murty, 2007)

Method	Stream splits	No. of units	Cost (M$/year)	Difference (%)
Differential evolution method (DEM) of Krishna and Murty (2007)	2	-	3.146	
Block decomposition technique of Zhu et al. (1995)	0	10	2.980	9.19
Supply & target based superstructure (S&TBS) (Type 1) of Azeez et al. 2011	3	13	2.979	3.43
Supply based superstructure(SBS) of Azeez et al. (2013)	6	14	2.976	3.40
Linnhoff and Ahmad (1990)	0	13	2.960	3.29
Genetic algorithm (GA) of Lewin (1998)	0	11	2.946	2.74
Differential evolution method (DEM) of Krishna and Murty (2007)	0	15	2.942	2.25
T&SBS of Azeez et al. (2011)	7	17	2.922	2.11
Sequential match reduction approach of Pettersson (2005)	7	17	2.905	1.42
Pinch technique (HINT), present study	2	12	2.881	0.83
				0.00

1. CONCLUSION

The search for optimal cost of heat exchanger network by previous researchers for three (3) different reported problems has been examined using HINT software to examine its potentials. The HINT software has been proven to be suitable for the solution of such problems and the potentials of remaining problem analysis (RPA) is revealed. The extent of HINT performance varies with the type of problem but is excellently adequate in all heat exchanger network problems solution. The result shows that using HINT, there was a successful reduction in the minimum number of units, additional piping cost and the overall total annual cost.

REFERENCE

Akande, H. F. (2007), Energy Integration of Thermal Hydro-dealkylation Plant, M. Eng. Thesis, FUT Minna, Minna, Nigeria. Pp.2

Azeez, O.S., Isafiade, A.J and Fraser, D.M. (2011), Supply and target based superstructure synthesis of heat and mass exchanger network, Chem. Eng. Res.Des (in Press).

Azeez, *el al.,* (2012), Supply and target based superstructure synthesis of heat and mass exchanger network, Chem. Eng. Res. Des (in Press).

Ahmad, S. Linnhoff, B. & Smith, R. (1990). Cost optimum heat exchanger networks-2. Targets and design for detailed capital cost models. Comp and Chem. Eng., 14(7): 751 -767.

Floudas, C. A. (1995). Nonlinear and Mixed Integer Optimization: Fundamental sand Application, Oxford University Press, New York.

Heat Integration (2008). Department of Chemical Engineering andEnvironmentTechnologyUniversityofValladolid Spain.Retrieved from http//www.iq.uva.es/integ/hint.zip/

Hohmann, E. C. (1971). Optimum networks for heat exchanger. Ph. D. Thesis of

Isafiade, A.J. (2008).Interval Based MINLP Superstructure Syntheses Heat and Mass Exchange Networks, PhD Thesis, University of Cape Town.

Krishna, M. Y. & Murty, C.V.S. (2007). Synthesis of cost-optimal heat exchanger networks using differential evolution. Comp. & Chem. Eng. 32: 1861-1876.

Lewin, D. R., (1998). A generalized method for HEN synthesis using stochastic optimization- II. The synthesis of cost-optimal networks. Comp. & Chem. Eng. 22(10):1387-1405.

Linnhoff, B. & Ahmad, S. (1990). Cost optimum heat exchanger networks (Part I). Comp. & Chem. Eng., 14(7): 729-750.

Linnhoff, B & Flower, J. R. (1978). Synthesis of heat exchanger networks, I. Systematic generation of energy optimal networks, AICHE J., 24(4): 633- 642.

Linnhoff, B., Townsend, D. W., Boland, D., Hewitt, G. F., Thomas, B. E. A.,Guy, A. R. &Marsland, R. H. (1982). A User Guide on ProcessIntegration for the Efficient Use of Energy. The Institute of Chemical Engineering, U.K.

Pettersson, F. (2005). Synthesis of large-scale heat exchanger networks using a sequential match reduction approach. Comp. & Chem. Eng. 29(5): 993-1007.

Smith, R. (2005), Chemical Process Design and Integration John Wiley & Sons, Ltd. England.

Yee, T.F. & Grossmann, I.E. (1990). Simultaneous optimization models for heat integration- II Heat exchanger network synthesis, Comp. & Chem. Eng., 14(10): 1165 - 1184.

ENHANCED APPROACH FOR CYBER SECURITY WEB APPLICATIONS IN NIGERIA

Suleiman Mustafa[*], Mohammed Dauda[2], AbdullahiAliyu Danlami[3], Muhammad AshafaShehu[4]

[1]National Agency for Science and Engineering Infrastructure

[1]PMB 391, Garki, Abuja, Nigeria

[*]mustafa.suleiman@naseni.org,+234 (0) 70626 41324.

ABSTRACT

Cyber security is rapidly becoming an important aspect of ICT around the globe. In Nigeria there have been increase in the rate of cyber crime and various organizations have become targets of cyber criminals. Cyber crime can pose a high risk to the economy and security of a nation. The most common types of cyber crime committed in Nigeria include hacking, cyber-theft, viruses and worms, spamming, financial fraud, identity theft, cyber and website cloning. The techniques for carrying out these activities include tricks and scams such as beneficiary of will, money laundering, lottery and winning ticket, next of kin, bogus cashier check and online charity. This paper examines the vulnerabilities of websites owned by various organizations in Nigeria from across different sectors that handle sensitive data. Finally the work revealed certain types of cyber crime and vulnerabilities that are common in Nigeria. Several recommendations for tackling such problems were offered for website developers.

Keywords: Cyber security, Cyber crime,
Nigerian organizations, Website vulnerabilities.

1. INTRODUCTION

The increases and widened access to computer and mobile technology has resulted in development of the Internet for work and business activities, as well as those engage in illegal activities. The rise of technology and communication has not only produced a dramatic increase in the incidence of criminal activities, has also resulted in the emergence of what appears to be a new variety of criminal activities (1). Both the increase in the incidence of criminal activities and the possible emergence of new variety pose challenges for secure systems, as well as for law enforcement (2).

Cyberspaces and its underlying infrastructure are vulnerable to a wide range of risk stemming from both physical and cyber threats and hazards. Cyberspace is particularly difficult to secure due to a number of factors: the ability of malicious actors to operate from anywhere in the world, the linkages between cyberspaces and physical systems, and the difficulty of reducing vulnerabilities and consequences in complex cyber networks. An information technology becomes increasingly integrated with physical infrastructure operations, there is increased risk for wide scale or high-consequences events that could cause harm or disrupt services upon which our economy and the daily lives of millions of Nigerians depend (2).

It has been established that Nigeria is an impressionable country. The advent of the Internet to her was both welcome and full of disadvantages. The exceptional outbreak of cyber-crime in Nigeria in recent times was quite alarming, and the negative impact on the socio-economy of the country is highly disturbing (3). Nigeria is operating on a weakened technology platform and digitally illiterate environment that is in urgent need of expert solution, laws on cybercrime, and indeed effective and efficient cyber security policies (4).

This paper hopes to look at the forms of cyber attack in Nigeria, the vulnerability of its organizations to cyber attack and suggest techniques for software developers to prevent such risks.

2. CYBER ATTACKS PERCULIAR TO NIGERIA

While some types of cyber crimes are specific to Nigeria such as phishing, electronic spam, fake copycat websites etc., others such as identity theft and false statements are also common across other countries (6). The most common cybercrime activities in Nigeria include Next of Kin Scam, Online Charity, Internet Service Time Theft, and Beneficiary of Will Scam etc. However, these are carried out using tricks and scams and are mainly targeted at individuals. More sophisticated cyber attacks aimed at organizations can be more damaging. These are targeted information systems, infrastructures, networks and personal devices by various means of malicious acts that either steals, alters, or destroys a specified target by hacking into a susceptible system (7). The aim of these attackers for either to obtain information that could valuable or cause denial of service. As a result online website and web applications with valuable information and data are obvious targets for such attacks in Nigeria.

Web application vulnerabilities may result in stealing of useful data, breaking of data integrity. Thus one of the most useful tasks now in ICT in the security of web application, according to Acunetic survey 60% of found vulnerabilities were web applications (2).

The most common way of securing web application is searching and eliminating vulnerabilities therein. Example of another way of securing web application includes safe development, implementing intrusion detection and protections system and web application firewalls. But data-stealing attacks, many of which get the attention of media, are also a big threat (8). Now, we need a greater emphasis on protecting web servers and web applications. Web servers are especially the best platform for these cyber criminals

to steal the data. Hence one must always use a safer browser especially during important transactions in order not to fall as a prey for these crimes (6).

Common targets for hackers are government websites. According to recent statistics, the number of cases involved with the defacement of government websites in Nigeria has continued to rise from 10% back in 2010 to 60% as at 2012, reports Centrex Ethical Lab, a cyber-security and intelligence firm based in Abuja. In January 2015, The Nigeria Defence Headquarters website was defaced 'ISIS style' by unknown hackers and a day after elections in March, hackers using the name, Nigerian Cyber Army, hacked into the website of the Independent National Electoral Commission (INEC) (9).

3. METHODOLOGY

The objective of this paper is to examine the vulnerabilities of websites in Nigeria to cyber attacks. A risk analysis was carried out by testing for sets of alerts that will identify weaknesses in website coding. A sample of twenty-five websites was selected. The websites examined cut across various sectors such as banking and financial, government, education, healthcare, aviation and security agencies.

Using OWASP ZAP (open-source web application security scanner Zed Attack Proxy), a thorough analysis of all the web pages linked to the 20 selected sites was conducted. There are various applications for testing the vulnerability of websites such as Grabber, WebScarab, Wapiti,W3af etc. The advantage of ZAP is that it can be used to find a wide range of vulnerabilities in web applications and is simple and easy to use for penetration testing of web applications. It allows manipulation of traffic that passes through it including from https.

The websites were selected because they deal with high amount of sensitive user data and information. For instance, websites that accept or store credit card numbers and bank account information are prominent hacking targets, because of the potential for immediate financial gain from transferring money, making purchases, or selling the information. Military installations have also been the target of hacks; vital government infrastructure such as police and intelligence agency communications are also potential targets. Data breaches at large corporations have become common, largely for financial gain through identity theft. (10)

The alerts tested using the software to detect penetrations are:

A. Cross Site Scripting (Reflected): Cross-site Scripting (XSS) is an attack technique that involves echoing attacker-supplied code into a user's browser instance. A browser instance can be a standard web browser client, or a browser object embedded in a software product such as the browser within WinAmp, an RSS reader, or an email client. The code itself is usually written in HTML/JavaScript, but may also extend to VBScript, ActiveX, Java, Flash, or any other browser-supported technology (11).

B. Remote OS Command Injection: Attack technique used for unauthorized execution of operating system commands. This attack is possible when an application accepts not trusted input to build operating system commands in an insecure manner involving improper data sanitization, and/or improper calling of external programs (3).

C. Application Error Disclosure: This page contains an error/warning message that may disclose sensitive information like the location of the file that produced the unhandled exception. This information can be used to launch further attacks against the web application. The alert could be a false positive if the error message is found inside a documentation page.

D. X-Frame-Options Header Not Set: X-Frame-Options header is not included in the HTTP response to protect against 'Click-Jacking' attacks by which users are tricked into clicking on things triggering important actions. Usually they are authenticated at the website containing the elements they are tricked to click on (12).

E. Directory Browsing: It is possible to view the directory listing. Directory listing may reveal hidden scripts, include files, backup source files etc which be accessed to read sensitive information (13).

F. Cookie set without Http Only flag: When an attacker gets a user's browser to execute his/her code, the code will run within the security context (or zone) of the hosting web site. With this level of privilege, the code has the ability to read, modify and transmit any sensitive data accessible by the browser. A Cross-site Scripted user could have his/her account hijacked (cookie theft), their browser redirected to another location, or possibly shown fraudulent content delivered by the web site they are visiting (14).

G. Cross-Domain JavaScript Source File Inclusion: A cookie has been set without the secure flag, which means that the cookie can be accessed via unencrypted connections.

H. Cross-Domain JavaScript Source File Inclusion: The page at the following URL includes one or more script files from a third-party domain.

I. Private IP Disclosure: A private IP address has been found in the HTTP response body. This information might be helpful for further attacks targeting internal systems.

J. Web Browser XSS Protection Not Enabled: Web Browser XSS Protection is not enabled, or is

disabled by the configuration of the 'X-XSS-Protection' HTTP response header on the web server (12).

K. X-Content-Type-Options Header Missing: The Anti-MIME-Sniffing header X-Content-Type-Options was not set to 'no-sniff'. This allows older versions of Web browsers such as Internet Explorer and Chrome to perform MIME-sniffing on the response body, potentially causing the response body to be interpreted and displayed as a content type other than the declared content type (15).

L. Incomplete or No Cache-control and HTTP Header Set: The cache-control and HTTP header have not been set properly or are missing allowing the browser and proxies to cache content.

M. Password Auto complete in browser: AUTOCOMPLETE attribute is not disabled in HTML FORM/INPUT element containing password type input. Passwords may be stored in browsers and retrieved.

N. Secure Page Includes Mixed Content: The page includes mixed content, i.e. content accessed via http instead of https.

4. RESULTS AND DISCUSSIONS

From the sample of 25 websites, 3 could not be tested using the software. These 3 were military/paramilitary sites with mil.ng domain extensions therefore due to added security the penetration tests failed. The alerts were classified into low, medium and high risk. Majority of the websites tested failed 3 of the alerts but two of them where low risk and one medium risk. Of he two high-risk alerts only two websites failed the risk assessment. The other low and medium alerts ranged from a few, half and third of the websites found to be vulnerable. Below is a graph showing the

risk against the number of websites. Examples of figures and tables are given in Figure1 and Table1.

Table 1: Vulnerability attack test results.

ALERT	RISK	NO. OF VULNERABLE WEBSITES
CROSS SITE SCRIPTING	High	1
REMOTE OS COMMAND INJECTION	High	1
SECURE PAGE INCLUDES MIXED CONTENT	Medium	4
APPLICATION ERROR DISCLOSURE	Medium	8
X-FRAME-OPTIONS HEADER NOT SET	Medium	22
DIRECTORY BROWSING	Medium	1
COOKIE SET WITHOUT HTTP ONLY FLAG	Low	13
COOKIE SET WITHOUT SECURE FLAG	Low	6
CROSS-DOMAIN JAVASCRIPT SOURCE FILE INCLUSION	Low	15
PRIVATE IP DISCLOSURE	Low	4
WEB BROWSER XSS PROTECTION NOT ENABLED	Low	21
X-CONTENT-TYPE-OPTIONS HEADER MISSING	Low	21
INCOMPLETE OR NO CACHE-CONTROL AND PRAGMA HTTP HEADER SET	Low	8
PASSWORD AUTOCOMPLETE IN BROWSER	Low	8

Source: Fieldwork: 2015
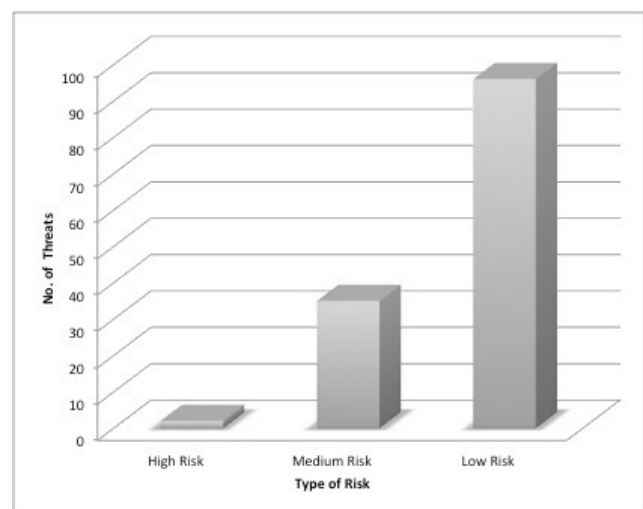
Fig.1: Risk Level against Number of Threats

5.   CONCLUSION AND RECOMMENDATIONS

This study reviews 25 websites for risk of penetration and categorized the risk in to three levels. From our investigations on cyber attacks to Nigerian websites we conclude that cyber crime poses a great treat to the peace, security and economy of the country due to the number of low and medium alerts. Although it is encouraging that the high risk are very few. Web application developers and coders in Nigeria therefore still have room for improvement in security when it comes to design and development of such applications. We therefore make the following suggestions to be employed by developers to address security challenges:

1.To prevent against Application Error Disclosure, review the source code of the page. Implement custom error pages. Consider implementing a mechanism to provide a unique error reference/identifier to the client (browser) while logging the details on the server side and not exposing them to the user

2.As most modern Web browsers support the X-Frame-Options HTTP header. Ensure it's set on all web pages returned by your site if you expect the page to be framed only by pages on your server.

3.Use a vetted library or framework that does not allow web cookies to be set without HttpOnly flag weakness easier to avoid or provides constructs that make it such.

4.Whenever a web cookie contains sensitive information or is a session token, then it should always be passed using an encrypted tunnel. Ensure that the secure flag is set for cookies containing such sensitive information.

5.Ensure JavaScript source files are loaded from only trusted sources, and end users of the application cannot control the sources.

6.Ensure that the web browser's XSS filter is enabled, by setting the X-XSS-Protection HTTP response header to '1'.

7.Ensure that the application/web server sets the Content-Type header appropriately, and that it sets the X-Content-Type-Options header to 'nosniff' for all web pages.

8.Whenever possible ensure the cache-control HTTP header is set with no-cache, no-store, must-revalidate, private; and that the pragma HTTP header is set with no-cache.

9.A page that is available over TLS must be comprised completely of content, which is transmitted over TLS. The page must not contain any content that is transmitted over unencrypted HTTP. This includes content from unrelated third party sites.

REFERENCE

(1) OlayemiO. J, (2014), "A socio-technological analysis of cybercrime and cyber security in Nigeria", International Journal of Sociology and Anthropology, Vol. 6(3), pp. 116-125.

(2) Gabi D. et al, (2014) "Towards the use of New Forensic Approach as a Panacea in Investigation of Cybercrime", International Journal of Science and Engineering Research, Volume 5, Issue 7, 2014.

(3) Frank I. and Odunayo E., "Approach to cyber security issues in Nigeria", International Journal of Cognitive Research in Science, Engineering and Education (IJCRSEE),2013.

(4) K. S. Adewole et al, (2011)"An Inquiry Into The Awareness Level of Cyber Security Policy and Measures In Nigeria", International Journal of Science and Advanced Technology (ISSN 2221-8386) Volume 1 No 7, 2011.

(5) Reddy G. N. and ReddyG. J. U., (2014)"A Study of Cyber Security Challenges and Its Emerging Trends on Latest Technologies", International Journal of Engineering and Technology Vol. 4 No. 1.

(6) Wada F. and OdulajaG.O., (2012)"Assessing Cyber Crime and its Impact on E-Banking in Nigeria Using Social Theories". African Journal of Computing & ICTs. Vol 5. No. 1.

(7) Karnouskos S. (2011)"Stuxnet Worm Impact on Industrial Cyber-Physical System Security". 37th Annual Conference of the IEEE Industrial Electronics Society (IECON 2011), Melbourne, Australia, 7-11 November 2011.

(8) ZemberC. and McGibbon T., (2014)"New and Enhanced Cyber Security and Information Systems Information Analysis", DoD Information Analysis Centers, Center CSIAC, Journal of Cyber Security and Information Systems. Vol. 1 No. 1.

(9) Cyber Attacks At Nigerian Government Websites Increased By 60% In 2012 Report Available Online at http://techloy.com/2013/01/17/nigerian-government-websites-cyber-attack-report/

(10) Grossman J. et al. (2008) "XSS Attacks: Cross-Site Scripting Exploits and Defense". Elsevier Science & Technology via Google Book Search. pp. 70, 156. ISBN 1-59749-154-3.

(11) Cross-site Scripting (XSS) Available Online at https://www.owasp.org/index.php/cross_site_scripting

(12) Braun F. and Heiderich M., "X-Frame-Options: All about Clickjacking? How else do X-Frame-Options protect my website" Available Online athttps://frederik-braun.com/xfo-clickjacking.pdf Retrieved June 11, 2015.

(13) An Overview of vulnerability scanners. The government of the Hon Kong special administration region, 2008. Available Online at http://www.infosec.gov.hk/english/technical/files/vulnerability.pdfRetrieved June 14, 2015

(14) HttpOnly Available Online at https://www.owasp.org/index.php/HttpOnly

(15) List of useful HTTP header Available Online at https://www.owasp.org/index.php/List_of_useful_HTTP_headers

(16) Tope O., (2012)"Patterns Of Internet Security In Nigeria: An Analysis of Data Mining, Fraud Detection and Mobile Telecommunications in Unsupervised Neural Networks"Available Online at, https://egoboosterbooks.files.wordpress.com/2011/12/patterns-of-internet-security-in-nigeria-front.pdf. Retrieved June 14, 2015

(17) Podhorec M., (2012)"Cyber Security Within The Globalization Process", Journal of Defense Resources Management, Vol. 3, Issue 1(4).

(18) BasamhS. S., (2014) et al. "An Overview on Cyber Security Awareness in Muslim Countries", International Journal of Information and Communication Technology Research (ISSN 2223-4965), Volume 4 No. 1, January 2014.

(19) Cleary F. and Felici M., (2014) "Cyber Security and Privacy: Communications in Computer and Information Science", 3rd Cyber Security and privacy EU Forum, CSP Forum, May 2014.

(20) Kizza J. M., (2014) "Computer Network Security and Cyber Ethics 4th Edition" pp 60-81. ISBN 978-0-7864-9392-0.

180

Geoscience Investigation of selected sites in Minna for siting a Sanitary Landfill

Amadi[1*], A. N., Ameh[1], I. M., Okunlola[2], I. A., Dan-Hassan[3], M. A. and Tukur[4] Aminu

[1]Department of Geology, Federal University of Technology, Minna, Nigeria
[2]Department of Chemical and Geological Sciences, Al-Hikmah University, Ilorin, Nigeria
[3]Rural Water Supply and Sanitation Department, FCT Water Board, Garki, Abuja
[4]Katsina State Rural Water Supply and Sanitation Agency, Nigeria

[*]Corresponding Author's Email Address: geoama76@gmail.com or an.amadi@futminna.edu.ng,
Phone Number: 08037729977

ABSTRACT

An integrated geoscience investigation was carried out on 3 selected sites in Minna, North-Central Nigeria in order to determine their suitability for use as sanitary landfill. Geological and hydrogeological mapping of the area was executed to determine the rock type and aquifer properties of the area. Subsurface geophysical investigations of the area employing the 1-D and 2-D subsurface resistivity imaging techniques were undertaken. Four lithological layers: lateritic top soil, mottled zone, clayey soil and the weathered to fresh basement rock were delineated from the geo-electric sections. The clay layer thickness varies between 2.8m to 8.0m with resistivity range of 18 Ωm to 86 Ωm and the depth of about 3.8m to 9.3m. The 2-D resistivity images using Wenner-Schlumberger and Wenner-Alpha arrays revealed the presence of an overwhelmingly dominant clay interval in the subsurface. The grain size distribution curve showed that the soil is dominated by fines (clay and silt. The soils liquid limit, plastic limit and plasticity index values ranged between 20 % to 90 %, 13.2 % to 26.8 % and 11.3 % to 24.7 % respectively. This implies that the soil is of low hydraulic conductivity. Permeability coefficient of the soils ranged from 3.4×10^{-6} cm/s to 5.68×10^{-8} cm/s, which is within the 10^{-8} to 10^{-6} range required for attenuation of leachate by natural geological materials with no potential of lateral migration of leachate. The analysis of results from geological, hydrogeological, geophysical, geotechnical and structural investigations revealed that two out of the three sites are suitable for siting a sanitary landfill.

Keywords: *Geoscience Investigation, Sanitary Landfill, Minna, and Groundwater Pollution*

1. INTRODUCTION

The management of waste in Nigeria is yet to take a definite shape and this can be attributed to non-enforcement of existing environmental laws. Most developed nations of the world have properly managed their wastes within their domain as a result of proper planning and effective waste management policies (Oyediran and Adeyemi, 2011; Amadi *et al*., 2012a).

Properly sited municipal solid waste sanitary landfill has been recognized as one of the environmentally friendly ways of waste disposal (Ranke, 2001; Ige, 2013). The concept of a well-engineered municipal sanitary landfill technology is aimed at minimizing soil and groundwater contamination and other associated environmental hazards. The sanitary landfill system is designed and constructed to include lined leachate containment with minimal risk of vertical and horizontal leakage into surface and groundwater systems. The merit of the sanitary landfill over other types of waste disposal methods is that handling and management of waste is kept to a minimum level (Ige, 2013; Amadi *et al*., 2012b). The local geology, hydrogeology and geotechnical characteristics of a site are key determinants of the suitability of a site for use as sanitary landfill, hence the need for this study.

Daniel (1993), Kabir and Taha (2006), Rowe *et al,* (1995), Edelman (1999), Ige and Ogunsawo (2009), Oyediran and Adeyemi (2011) in their various investigations have proposed certain recommendations that must be attain for a soil to be considered for use as barrier soil for sanitary landfill. Four major open dump-sites apart from some minor ones scattered all over the metropolis are currently in use in Minna. They constitutes public nuisance by the smell and smoke generated in the course of their decomposition and burning respectively.

Groundwater is an essential natural resource that needs to be protected at all cost, because once it is contaminated it is difficult and expensive to clean up (Amadi *et al*., 2014). A study targeted at assessing the suitability of a site for use as a landfill in order to ensure protection to the soil and water system and avoid the occurrence of water-borne diseases should be encouraged by all. The choice of site for sanitary landfill construction is critical as the consequences of a wrong choice leads to soil and groundwater pollution, environmental degradation and various health impact (Rowe, 2011). No effort should be spared in making accurate decisions that would lead to the

choice of suitable sites for locating a solid waste sanitary landfill system.

1.1. Study Area

The investigated sites (A, B and C) are located within Minna metropolis and lie between longitudes $6^O24'E$ to $7^O00'E$ of the Greenwich Meridian and latitudes $9^O30'N$ to $10^O00'N$ of the Equator and are accessible through major roads (Figure 1). The River Chanchaga catchment basin forms the drainage system for th area and the tributaries are ephemeral. The area has two seasons: the rainy and dry seasons. The average annual rainfall of about 1100mm while the temperature is about 29ºC. The vegetation of the study area belongs to the savannah type. The major rock type in the area is granite, granite-gneiss and schist with relics of quartz-veins and pegmatites as minor intrusions.

2. MATERIALS AND METHODOLOGY

Geological mapping was carried out in the area to know the rock types in the area. Fresh rock samples were collected and subjected to both micro-photographic and mineralogical analyses to understand the mineralogical composition and mode of occurrence. The petrographic thin section analysis was carried out at the Geological Laboratory, Federal University of Technology, Minna while the mineralogical analysis was carried out the Nigerian Geological Survey Agency, Kaduna. Geophysical investigation employing the 1-D and 2-D resistivity subsurface imaging were undertaking in the study area to obtain lateral and vertical subsurface information. Hydrogeological mapping was undertaking to establish the aquifer types and groundwater flow direction. Static water level values were collected from 45 hand-dug wells within the vicinity of the investigated sites. Soil samples were collected from trial pits across the sites. A total of five trial pits were excavated at each site. The samples were transported to the Civil Engineering Laboratory at Federal University of Technology, Minna, and Federal Polytechnic, Bida in polythene bags, for relevant geotechnical analysis. The analyses were carried out in accordance with BS 1377 standard.

3. RESULTS AND DISCUSSIONS

3.1. Geological Mapping

Information obtained from the geological mapping shows that the area is underlain by three rock types namely granites, granite-gneiss and schist. The schist is dipping toward the east, with dip ranging from 12º to 64º east. The predominantly joint direction is NE-SW. The petrographic thin section identified biotite, microcline, quartz and plagioclase as the major constituents of the rock from the study area (Plates 1a and 1b).
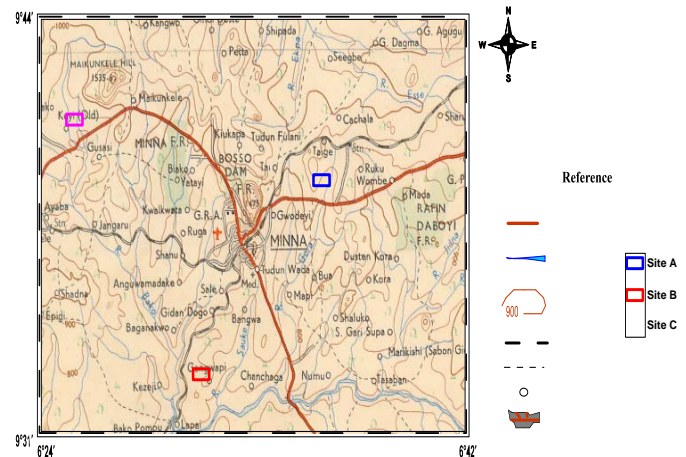
Figure 1: Topo map of Minna, showing the three sites
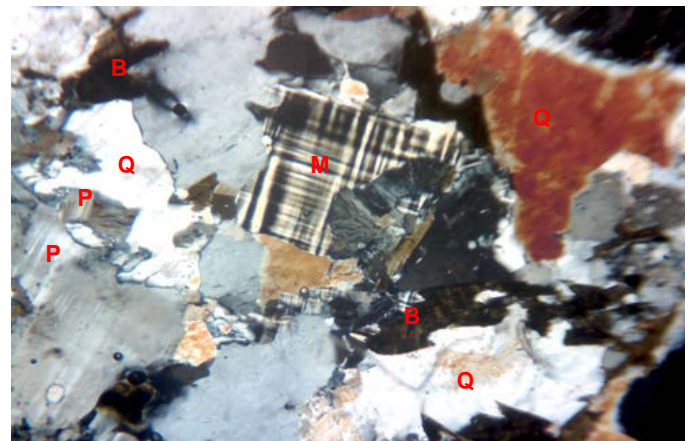
Q= Quartz   M= Microcline   B= Biotite   P= Plagioclase

Plate 1a: Photomicrograph of granite-gneiss

Q= Quartz   B= Biotite   P= Plagioclase

Plate 1b: Under cross polarize light (Magnification X40)

3.2. Geophysical Investigation

The 1-D model sounding curves show three layers indicating four lithological units in the subsurface formations across the study area. Lateritic soil, mottled zone, clayey soil and weathered/fresh basement rocks were the different layers delineated from the VES curves and geoelectric sections. The mottled zone is a transitional layer that exists between the lateritic soil and clay soil. The dominant curve type in the area is HA (Figure 2).

Table 1: Geoelectric parameters indicating Curve Types for profile B

	RESISTIVITY ((Ωm) / Thickness h (m)								
	Profile 1B			Profile 2B			Profile 3B		
LAYER	VES 1B	VES 2B	VES 3B	VES 4B	VES 5B	VES 6B	VES 7B	VES 8B	VES 9B
Layer1 ℓ1/h1	141/0.9	93/1.4	380/0.7	64/0.8	130/1.0	100/1.1	89/1.5	118/1.3	99/1.3
Layer 2 ℓ2/h2	71/7.2	113/7.4	112/6.0	22/4.4	68/5.7	60/7.3	86/5.2	83/6.3	72/8.0
Layer 3 ℓ3/h3	300/∞	290/∞	863/∞	231/∞	245/∞	274/∞	504/∞	303/∞	265/∞
CURVE TYPE →	HA	A	HA	HA	HA	HA	A	HA	HA

Fig. 3a. Geoelectric Section 2B for site B
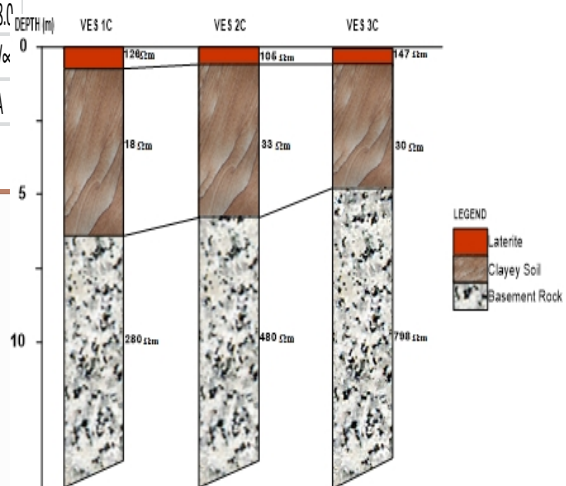
Fig. 3b. Geoelectric Section 1C for site C

Figure 2: Sounding Curve Type for HA

The geoelectric section as constructed from the geoelectric parameters obtained from VES contained in Table 1 indicates different layers. The resistivity of the mottled zone ranged between 74 Ωm to 96 Ωm to the depth of about 1.0m to 1.4m while that of laterite ranged between 100 Ωm to 174 Ωm to the depth of about 0.9m to 1.3m. The top layer is underlain by clayey soil characterized with low resistance which ranged between 18 Ωm to 86 Ωm with a thickness range of 2.8m to 8.0m to the depth of 3.8m to 9.3m. The last layer is the crystalline basement rock unit with varying degree of weathering which has resistivity values range between 231 Ωm to 366 Ωm to a fairly infinite depth. From the geoelectric sections (Figures 3a and 3b) the clay soil, show low resistivity values due to their charged surfaces and associated boundary layers of attracted ions.

The 2-D subsurface images identified different lithologic layers which are distinguishable based on the response to electrical current. The resistivity increases away from the blue colour to the red and pink colours as indicated on the inverses model resistivity sections (Figures 4a and 4b). The inverse model shows a highly conductive clay layer as the top layer with resistivity values less than 100 Ωm and depth extend of about 12m. Underlying the clay layer is the weathered basement rock unit with resistivity value range of 110 Ωm to 500 Ωm. The last layer is the highly resistive bed rock with resistivity values range of 558 Ωm to greater than 1433 Ωm extending to a fairly infinite depth.

3.3. Hydrogeological Mapping
The study area is made up of two aquifer units which are; the regolith aquifer and the fractured aquifer.
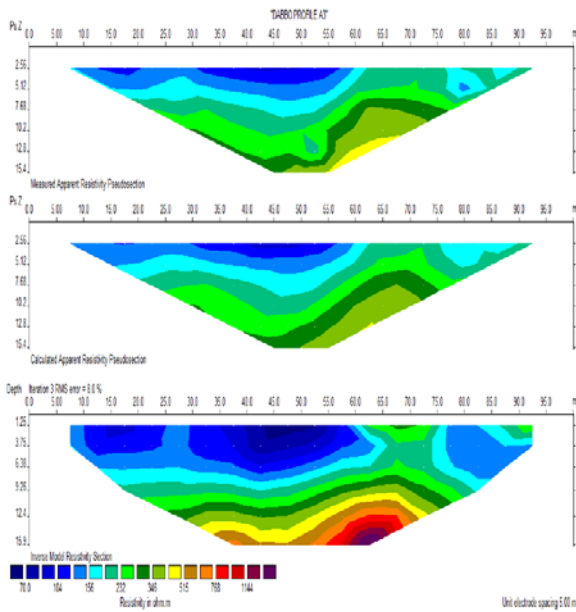
Fig.4a. Inverse Model resistivity section for profile B3
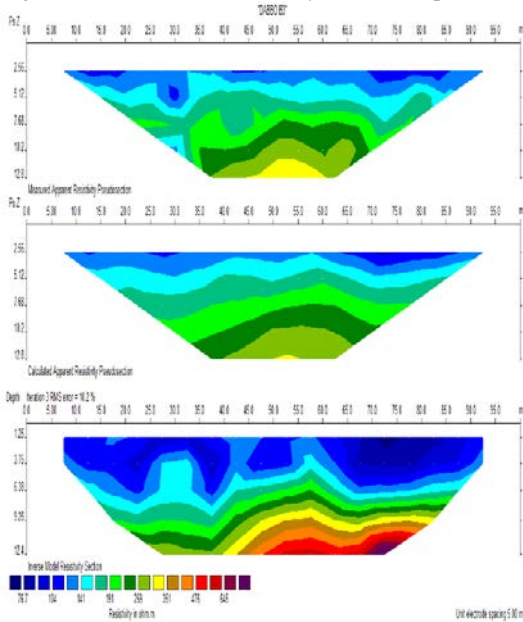
Fig.4b: Inverse Model resistivity section for profile C3

Table 2: Representative Hydrogeological Well Data.

S/N	Co-ordinates		Altitude (m)	SWL (m)	Depth of well (m)	Hydraulic Head
	N (°)	E (°)				
1	9.63275	6.57119	286	6.9	7.2	279.1
2	9.63328	6.57150	278	4.6	6.3	273.4
3	9.63103	6.57386	299	7.6	8.3	291.4
4	9.63008	6.57583	288	3.5	5.2	284.5
5	9.62992	6.57553	273	6.0	6.2	267.0
6	9.62950	6.57583	276	5.0	5.4	271.0
7	9.62936	6.57578	269	3.7	3.8	265.3
8	9.62900	6.57611	295	3.6	3.9	291.4
9	9.62925	6.57606	289	3.7	5.0	285.3
10	9.62919	6.57542	296	3.5	4.6	292.5
11	9.62853	6.57619	284	4.8	5.0	279.2
12	9.62869	6.57603	284	3.4	4.3	280.6
13	9.62817	6.57619	298	3.9	4.0	294.1
14	9.62761	6.57772	280	3.6	4.6	276.4
15	9.62761	6.57789	234	0.9	4.6	233.1
16	9.62742	6.57811	203	1.2	5.3	201.8
17	9.62794	6.57825	284	1.0	3.8	283.0
18	9.62828	6.57861	285	2.0	4.0	283.0
19	9.62842	6.57958	293	3.0	5.4	290.0
20	9.62844	6.58017	294	6.7	7.1	287.3
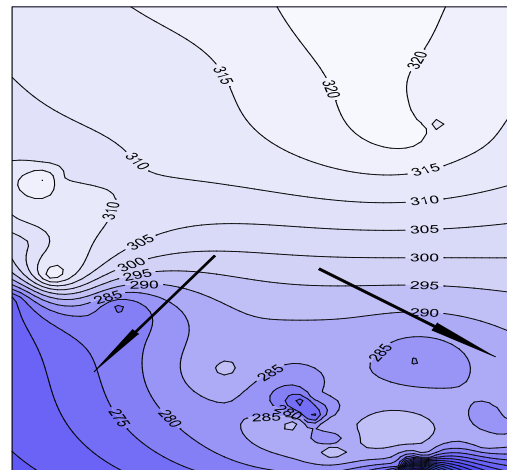
Figure 5: Groundwater flow direction of the study area

3.4 Grain size distributions
The result of the grain size distribution and a representative grading curve are presented in Table 3. Particle size distribution is one of the key factors that influence the hydraulic characteristic of soil. Daniel, (1993), Rowe et al, (1995), Ige, (20013), Oyediran and Adeyemi, (2011) suggested the minimum of 30% fines and less than 30% gravel size particles for soil to be used as mineral seals in sanitary landfill. Declan and Paul, (2003)

From the data (Table 2), the average depth to static water level in the study area is about 4m. The depth of the wells ranged from 2.6m to 10m depending on the thickness of the overburden material. The groundwater flow direction map generated from the water level data (Figure 5) indicates a NE-SW flow direction is mainly toward the southern portion of the mapped area. This finding is in line with the result of the principle joint direction. This implies that the groundwater in the area is structurally controlled.

suggested 10% clay content as requirement for soil to qualify for use in sanitary landfill as mineral seal.

From the grain size analysis the soil retained on the BS sieve No.4 ranged from 0.0% to 10%. The sand size fraction ranges from 8.2% to 42.1% while the amount of fine particles passing the BS sieve No.200 ranged from 50% to 91.8%. The results of the grain size distribution are within the limits suggested by previous authors. The high percentage of the fine particles predominantly clay fractions will influence the low permeability of the soils. Ogunsawo, (1996) observed that soils containing adequate amount of sand particle could prevent the soil from volumetric shrinkage when used as mineral seal.

Table 3: Summary of particle size distribution of soils in percentage

Site	Samples	Gravel %	Sand%	Fines%
A	A	0.9	36.5	62.6
	B	1.8	42.1	56.1
	C	0.2	28.2	69.6
	D	1.5	28.9	69.6
B	E	0.0	25.5	74.5
	F	1.1	24.4	74.5
	G	1.0	21.9	77.1
	H	0.2	25.8	74.0
C	I	0.0	8.2	91.8
	J	0.2	25.8	74.0
	K	10.0	40.0	50.0
	L	0.1	24.0	75.9
Minimum		0.0	8.2	50.0
Maximum		10	42.1	91.8
Mean		1.4	30.0	71.6

3.5. Atterberg Consistency Limits

The result of the Atterberg consistency limits are presented on Table 4. The consistency limit tests indicate that the liquid limit of the soils ranged from 24.5% to 51.5% while the plastic limit varied from 13.2% to 26.8%. The plasticity index ranged from 11.3% to 24.7% (Table 4). The plasticity index indicates the fines portion soil and their ability to change shape without a change in volume. Declan and Paul (2003) and Benson et al. (1994) suggested a minimum liquid limit of 90% and 20% respectively for soil to be used as mineral seal in sanitary landfill. This implies that the soils have the potential to exhibit low hydraulic conductivity.

Daniel (1993), Rowe et al. (1995) and Ige, (2007), suggested that plasticity index for soil to be used as mineral seal must be greater than 7%. The analysed soils possess liquid limits greater than 20% but less than 90% and plasticity index greater than 7%. This indicates that the soils have the potential to exhibit low hydraulic

conductivity, display minimal expansion rate when in contact with fluid and have low potential for developing secondary leachate pathways (Benson *et al* 1994). This finding is in agreement with the recommendation of Benson *et al* (1994) for soil to be used as mineral seal in sanitary landfill.

Table 4: Summary of Atterberg limits results in percentage

Sites	Label	Liquid Limit (%)	Plastic Limit (%)	Plasticity Index
A	A	33.5	17.1	16.4
	B	39.9	21.5	18.4
	C	34.9	18.5	16.4
	D	35.0	18.5	16.4
B	E	42.0	24.1	17.9
	F	40.0	20.0	20.0
	G	36.0	18.1	17.9
	H	34.0	19.1	14.9
C	I	51.5	26.8	24.7
	J	47.5	23.6	23.6
	K	44.0	22.2	21.8
	L	24.5	13.2	11.3
Minimum		24.5	13.2	11.3
Maximum		51.5	26.80	24.70
Mean		38.6	20.23	18.21

4.6. Compaction Test

This test method was used to determine the relationship between Maximum Dry Density (MDD) and the Optimum Moisture Content (OMC) of the soil samples. The amount of mechanical energy applied to soil mass is known as the compaction energy. The standard and modified Proctor compaction energies were employed in this work. The results of the MDD and the OMC and a representative plot of dry density versus moisture content are contained in Table 5. The peak of the curves indicates the MDD and the corresponding OMC (Fig. 9). The result of the MDD and OMC of the standard Proctor energy ranged from 1.58 KN/m3 to 1.82KN/m3 and 16.5% to 25.9% respectively while for the modified proctor energy, the soils MDD and OMC ranged from 1.74KN/m3 to 2.10KN/m3 and 11.0% to 18.9% respectively. Kabir and Taha (2004) stated that for a soil to use as mineral seal it should possess MDD not less than $1.45g/cm^3$ for standard Proctor and $1.64g/cm^3$ for modified Proctor. The analyzed soils have values that compete favourably with the recommendations of Kabir and Taha (2004). Ige and Ogunsawo (2009) stated that MDD increases and OMC decreases with an increase in compactive efforts. This may be due to the fact that more parallel orientation of the phyllosilicate mineral particles occurs at higher compaction energy. A higher unit weight of compaction occurs as the clay particles become closer on higher compactive effort. Hence, the modified compaction effort is preferable as it does significantly reduce the hydraulic conductivity of the soil.

Table 5: Summary of the MDD and OMC of the two Compaction Energies

Sample Label	Standard Proctor		Modified Proctor	
	MDD (KN/m^3)	OMC %	MDD (KN/m^3)	OMC %
A	1.70	19.0	1.94	14.0
B	1.76	17.6	2.00	12.0
C	1.71	20.1	1.89	14.0
D	1.74	18.1		
E	1.59	24.0	1.88	13.5
F	1.64	18.5		
G	1.49	19.1	1.74	18.9
H	1.58	25.9	1.80	16.5
I	1.68	19.9		
J	1.70	19.7		
K	1.82	17.9	2.10	11.0
L	1.68	16.5	1.87	15.5
Minimum	1.49	17.9	1.74	11.0
Maximum	1.82	25.9	2.10	18.9
Mean	1.67	19.96	1.88	15.08

3.7. Coefficient of Permeability

The results of the permeability coefficient are presented in Table 6. Coefficient of permeability is one of the critical factors in the choice of soil or site for sanitary landfill. It is the function of the structure and grain size of the soil. The coefficient of permeability of all the analysed soils ranged from 3.4 x 10^{-6} cm/s to 5.68 x 10^{-8} cm/s. USEPA (1978) suggest a permeability of 1x10^{-4}cm/s as the boundary between permeable and impermeable linears. Allen (2000) suggested that natural geological materials considered for attenuation of leachate in landfill should possess an optimum coefficient permeability range of 10^{-6}cm/s to 10^{-8}cm/s. For a soil to be used as mineral seal for the attenuation of leachate it should have a maximum permeability coefficient of 1x10^{-7}cm/s (Rowe *et al*, 1995, Ige and Ogunsawo, 2011, Oyediran and Iroegbuchu, 2013). All the analysed soil samples are in line with the findings of Allen (200); Rowe et al (1995) and Ige and Ogunsawo (2011). The soils have the potential to exhibit low to practically impermeable permeability characteristics which will enhance grater attenuation of leachate contaminant in sanitary landfill system.

Table 6: Coefficient of Permeability of the Soil Samples

Soil	A	B	C
k (cm/s)	5.53 x 10^{-6}	4.58 x 10^{-6}	4.73 x 10^{-6}
Soil	D	E	F
k (cm/s)	3.56 x 10^{-6}	4.81 x 10^{-7}	3.85 x 10^{-7}
Soil	G	H	I
k (cm/s)	1.88 x 10^{-7}	4.73 x 10^{-6}	4.65 x 10^{-8}
Soil	J	K	L
k (cm/s)	5.68 x 10^{-8}	3.40 x 10^{-6}	6.42 x 10^{-7}

3.8. Clay Mineralogy

Chemical weathering of rock results in the formation of clay at or near the earth's surface. The formation of clay as a result of weathering activities is dependent on four major factors which include; mineralogical and textural composition of the parent rock, porosity and permeability of the parent rock, composition of the aqueous solution and the morphology (position of the weathered parent rock) (Thair and Olli, 2008).

Table 7: Facial mineralogical composition of some clay samples

Clay Soil		Mineralogy (decreasing order)				
		Quartz	Kaolinite	Muscovite	Goethite	Hematite
	Compound name	Silicon Oxide	Aluminum Silicate Hydroxide	Potassium Aluminum Silicate Hydroxide	Iron Oxide Hydroxide	Iron Oxide
	Chemical formula	SiO$_2$	Al$_2$Si$_2$O$_5$(OH)$_5$	KAl$_2$(Si, Al)$_4$O$_{10}$(OH)$_2$	Fe$_3$O(OH)	Fe$_2$O$_3$
	Crystal system	Hexagonal	Anorthic	Monoclinic	Orthorhombic	Orthorhombic
Sample B		✓	✓	✓		
Sample F		✓	✓			
Sample I		✓	✓		✓	
Sample J		✓	✓	✓		✓

From the mineralogical composition of the representative clay soil, kaolinite is the most dominant clay mineral in all the soil analysed (Table 7). From the oxide composition of the rock and clay samples as determined by XRF (Table 8), the major oxides found are SiO$_2$, Al$_2$O$_3$ and K$_2$O. These oxides form the composition of potassium feldspar and kaolin, and it is the transformation of potassium feldspar into kaolin that forms clay as justified from the equation: 2 KAlSi$_3$O$_8$ + 3 H$_2$O Al$_2$Si$_2$O$_5$ (OH)$_4$ + 4 SiO$_2$ + 2 K (OH) (Thair and Olli, 2008). This therefore implies that the clays are non-expendable with low cations exchange capacity (CEC). The clays will exhibit less effective surface area of about 10-30m^2/g (Thair and Olli, 2008). With the effective surface area been small, the clays will exhibit low to moderate expansion on wetting and low to moderate expansion on drying. The high occurrence of quartz as indicated in the diffractograms (Figure 6) may be responsible for the significant percentage of sand size particles in the grain size distribution.

3.9. Soil Classification

Soils for engineering purposes are classified in accordance to the Unified Soil Classification (USCS) and American

Association of State Highway Transport Officials (AASHTO) Classification systems.

Figure 6: X-Ray Diffractogram for a sample

Table 8: Major Oxide Composition of Rock and Soil Samples

Oxide	Rock Samples			Clay soil Samples			
	MK1	MA1	DB1	B	F	I	J
SiO_2	74.3	75.10	66.80	56.2	50.80	44.10	46.20
TiO_2	0.30	0.21	0.81	0.94	1.20	1.21	1.94
Al_2O_3	14.70	14.90	16.50	23.30	27.20	27.50	26.80
Fe_2O_3	4.16	3.75	6.23	4.58	4.44	8.84	5.70
MnO	0.10	0.11	0.29	0.03	0.04	0.05	0.04
MgO	0.36	0.81	1.03	1.96	0.96	2.50	2.43
CaO	2.43	2.07	3.26	0.45	0.48	0.29	0.60
Na_2O	1.62	1.17	2.04	2.01	2.24	2.41	2.09
K_2O	1.03	0.78	1.78	0.82	0.84	0.88	1.17
P_2O_5	0.15	0.13	0.19	0.01	0.006	0.02	0.008
BaO	0.11	0.05	0.24	0.006	0.11	0.04	0.001
LOI	0.74	0.92	0.83	9.64	11.68	12.16	12.42
Total	100	100	100	99.946	99.996	100	99.399

In accordance to the USCS all the soil samples indicate PI greater than 7 and LL less than 50% except for sample I which have LL greater than 50%. Based on the soil classification, all the soil are classified as inorganic clay materials of low to medium plasticity with the exception of sample I which is classified as inorganic clay with high plasticity. According to the AASHTO classification system, the soil samples analysed have more than 35% soil particles passing the No.200 sieve, the PI of the soils is greater than 10% and the LL less than 40%. Hence, the soil samples are clayey soil with the symbol A-7-6.

On the plasticity chart (Figure 7), samples A, B, C, D, E, F, G and H fall within the A-7-6 section which indicate that they are inorganic clay (CL) of low to intermediate

plasticity. Soil sample I is classified as inorganic clay of high plasticity (CH) because it has liquid limit greater than 50% and occur above the A line. Soil samples J, K and L fall within the A-6 section of the plasticity chart, which indicate that they are inorganic clays (CL) of low plasticity. Soil which fall under groups A-7-6 and A-6 contain appreciable amounts of fine which makes the soils suitable for use as sanitary landfill liners.

Figure 7: Plasticity chart of the clay soils

4. CONCLUSION

An integrated geoscience approach was used to investigate three sites in Minna, for the purpose of generating a data that will aid the siting (design and construction) of a sanitary landfill. The area was underlain by granite, granite-gneiss and schist. The soil profile of the study areas are in the order of: top humus soil, laterite/mottle zone, clay soil and weathered to fresh basement rock. Inverse model resistivity sections shows a thin to thick highly conductive clayey layer underlain by weathered basement rock which overlays the fresh basement rock. The safe depth of excavation is between 7m to 9m, due to the inhomogeneous nature of the sites. The study area is made up of the regoliths and fractured aquifer units. The groundwater flow direction is NE-SW in accordance with the principle joint direction in the area. Hence care should be taking to protect the groundwater vulnerable area by minimizing leachate infiltration into groundwater system, since the direction of groundwater flow can also serve as conduit for leachate movement.

The soils are generally well graded possessing the required amount of fines, clay minerals and sand size fraction required for a soil to be used as mineral seal. The clays possess low, intermediate to high plasticity with low shrinkage abilities. The coefficients of permeability of the soils indicate very low permeability with the soils falling within the favourable range ($1x10^{-6}$ cm/s to $1x10^{-8}$ cm/s) of optimum hydraulic conductivity for attenuation. Although the sites indicated favourable geotechnical properties, site A is geological and hydrogeological unsuitable for a

sanitary landfill as a result of the high weathering and fracture of the underlying rocks. The fractures can serve as conduits for possible migration of leachates. Site B and C have competent rocks that have not experience significant weathering and fracturing and hence suitable for siting sanitary landfill system. The integrated approach employed in evaluating the sites for sanitary landfill are more rewarding to using any single method to investigate the sites.

References

Ajibade, A. C. (1982).The origin of the Older Granites of Nigeria: some evidence from the Zungeru region. *Nigerian Journal of Mining and Geology*, 19, 223-230.

Allen, A. R. (2000). Attenuation landfills the future in landfilling. Retrieved from www.tu.koszalin.pl/towarzystwo/2000/17allen.

Amadi, A. N., Nwankwoala, H. O., Eze, C. J., Alkali, Y. B. & Waziri, S. H., (2012a). A review of waste management techniques in parts of Niger Delta, Nigeria. *Centre for Human Settlement and Urban Development Journal,* 3(1), 98 – 108.

Amadi, A. N., Ameh, M. I. & Jisa, J., (2012b). The impact of dumpsites on groundwater quality in Markurdi Metropolis, Benue State. *Natural and Applied Sciences Journal,* 11(1), 90 – 102.

Amadi, A. N., Ameh, I. M., Ezeagu, G. G., Angwa, E. M. & Omanayin, Y. A. (2014). Bacteriological and physico-chemical analysis of well Water from villages in Edati, Niger State, North-central Nigeria. *International Journal of Engineering Research and Development* e-ISSN: 2278-067X, p-ISSN: 2278-800X, www.ijerd.com 10(3), 10-16.

Benson, C. H., Zhai, H., & Wang, X. (1994). Estimating Hydraulic Conductivity of Clay Liners. *Journal of Geotechnical Engineering*, 120, 366-387.

British Standard Institution (1990). Methods of Test for Soils for Civil Engineering Properties (BS 1377). British Standard Institution. London, UK. 143.

Daniel, D. E. (1993). Clay liners. In Geotechnical practice for waste disposal, (Ed. David E. Daniel) Chapman & Hall, London, UK, pp 137-163.

Declan, O. & Paul, Q. (2003). Geotechnical engineering & environmental aspects of clay liners for landfill projects. Retrieved 12 January 2015 from http://scholar.oauife.edu.ng/ijs/files/oyediran_and_i roegbuchu.

Edelmann, L., Hertweck, M., & Amann, P. (1999). Mechanical Behaviour of Landfill Barrier Systems. *Journal of Geotechnical Engineering*, 137, 215-224.

Ige, O. O. & Ogunsanwo, O. (2009). Assessment of Granite-derived Residual Soil as Mineral Seal in Sanitary Landfills. Researcher. 1(6), 80-86. Retrieved from http://www.sciencepub.net/researcher.

Ige, O. O. (2010). Assessment of geotechnical properties of migmatite-gneiss derived residual soil from Ilorin, Southwestern Nigeria, as barrier in sanitary landfills. *Continental Journal of Earth Sciences*, 5 (1), 32 – 41.

Ige, O. O. (2013). Geological and Geotechnical Evaluation of an Open Landfill for Sanitary Landfill Construction in Ilorin, Southwestern Nigeria. *Journal of Environment and Earth Science*, 3(3), 9-17.

Kabir, M. H. & Taha, M. R. (2004). Assessment of Physical Properties of a Granite Residual Soil as an Isolation Barrier, *Electronic Journal of Geotechnical Engineering,* 92, 13-18.

Ogunsanwo, O. (1996). Geotechnical Investigation of Some Soil from Southwestern Nigeria for Use as Mineral Seals in Solid Waste Disposal Landfill. *Bulletin of the International Association of Engineering Geology*. 54, 120-123.

Oyawoye, M. O. (1972). The basement complex of Nigeria. In: Dessauvagie TFJ and Whiteman, A. J. (eds) African geology. Ibadan University Press. 66–102.

Oyediran, I. A. & Adeyemi, G. O. (2011). Geotechnical Investigations of a Site in Ajibode, Southwestern Nigeria for Landfill. *Ozean Journal of Applied Sciences*. 4(3), 265-279.

Oyediran, I. A. & Iroegbuchu, C. D. (2013). Geotechnical Characteristic of Some Southwestern Nigerian Clays as Barrier Soils. *Ife Journal of Science*, 15(1), 17-30.

Rahaman, M. A. (1976). Review of the basement geology of South-Western Nigeria. In: Kogbe, CA (ed) Geology of Nigeria, (2nd ed.). Lagos, Elizabethan Publishers, 41–58.

Ranke, H. G. (2001). Appropriate Design and Operation of Sanitary Landfill in Sustainable Economic Development and Sound Resource Management in Central Asia, Proceedings of an International Conference, Nottingham, United Kingdom.

Rowe, R. K. & Fraser M. J (1995). Waste Disposal Facility Site Selection and Design Considerations. Retrieved from www.geoeng.ca/.../waste%20disposal%20facility.

Rowe, R. K. (2011). Systems engineering: the design and operation of municipal solid waste landfills to minimize contamination of groundwater. Geosynthetics International, 18, (6), 391–404. http://dx.doi.org/10.1680/gein.2011.18.6.391.

Thair A., & Olli S. (2008). Clay and Clay Mineralogy. Geologian Tutkuskeskus. Geological Survey of Finland.

USEPA, (1978). Process Design Manual: municipal sludge landfills, Document No. EPA-625/1-78-010; SW-705, Cincinnati, Ohio, *Environmental Research Information Centre.* 12-17.

IMPACT OF SOIL COMPACTION ON AMARANTHUS (*Amaranthus Caudatus L.*) YIELD AND SOIL BULK DENSITY

Olayaki-Luqman, M.[1*], Dauda, K. A.[2]

[1]Agricultural and Bio-environmental Engineering, Institute of Technology, Kwara State Polytechnic, Ilorin, Kwara State, Nigeria.
[2.]Agricultural and Bio-environmental Engineering, Institute of Technology, Kwara State Polytechnic, Ilorin, Kwara State, Nigeria.

[*]daudaabdulkadir@yahoo.com, 08035796934

ABSTRACT

A field experiment was conducted on Amaranthus at the Department of Agricultural and Bio-Environmental Engineering Technology, Institute of Technology, kwara State Polytechnic, Ilorin, Kwara State, Nigeria under a rain fed farming between the months of May to August, 2014 to examine the impact of soil compaction on Amaranthus growth and soil bulk density in which the experimental plot of $8 \times 11m^2$ was prepared and divided into three (3) plots; disturbed, undisturbed and fallowed plot. Soil auger was used to collect three soil samples from each plot at a depth of 10cm and 20cm. The results of average bulk density at depth of 0-10 cm for cultivated, uncultivated and compacted soil before planting are; $1.83g/cm^3$, 1.72g/cm3 and $1.64g/cm^3$, respectively. Result of average bulk density after harvest at the depth of 0-20cm for cultivated, uncultivated and compacted soil is; 1.74g/cm3, 1.65g/cm3 and 1.58g/cm3, respectively. The total yield from the first harvest for the cultivated, uncultivated and compacted soil is; 49.2kg, 38.3kg and 31kg, respectively. Therefore, the compacted plot had the least yield because; some moisture and air needed for growth had been expelled out of the soil during compaction process which has led to reduction in the soil pores.

Keywords: Soil, compaction, Vegetable, Growth, Crop

1. INTRODUCTION

Compaction of agricultural soils has been of great concern for many years due to heavy field traffic which may reduce plant growth. Plants depend on loose and crumby soil to spread their roots deep into the ground, well established root provides the plant with strength against environmental stresses, like drought. If the soil is compacted, it is too difficult for the roots to break through as a result; the plant maintains a shallow root system with little nutrient and moisture absorption opportunities (USDA, 2012).

In practice, conservation tillage can be achieved by minimizing tillage operations temporally and spatially for example reducing the number of times over a field or in the width or depth tilled and managing surface residues (Magdoff and Van, 2000). The lack of tillage coupled with residue on the soil surface maintains cooler soil temperatures for longer periods in the spring (Teasdale and Mohler, 1993).

Alterations in the soil structure due to compaction influence many aspects of the soil such as air, water and heat, which in turns affect root growth and crop production. Quantification of soil compaction effects is essential to develop management strategies that minimize the harmful compactive effects (Lipiec and Hatano, 2003).

It is in the light of the above this study is aimed at assessing the impact of soil compaction on Amaranthus

growth and soil bulk density, comparing the growth yield of Amaranthus on compacted, uncultivated and cultivated beds, and determines the bulk density on cultivated plot to compacted and uncultivated plot.

2. METHODOLOGY

The experiment was conducted at the Institute of Technology, Kwara State Polytechnic, Ilorin, Kwara State, Nigeria. The study area is located at latitude $8^0 26'$ N and longitude $4^0 30'$ E of the Greenwich meridian. It lies on the altitude of approximately 345m. It is a transitional zone between the climate of southern Nigeria and semi-Sudan savanna of the northern part of Nigeria.

2.1 Field Preparation

A land of 8 x 11m^2 was divided into three (3) plots laid along the general slopes of the field area. The first plot labeled (A) was disturbed and raised. The second plot labeled (B) was undisturbed but cleared and the third plot labeled (C) was fallowed.

2.2 Planting Operation

The planting operation was done by hand broadcast on the 16th of May, 2014, the second day after rainfall event in the study area. A mass of 0.46kg of Amaranthus seeds was evenly broadcasted on each plot. After two weeks of planting, weeding operation by hand picking was done. The description and length of growth stages are presented in table 1.

Table 1: Description and length of growth stages of Amaranthus vegetables

S/N	Developmental stages	Day after planting
1	Seed	1-6 days
2	Seedling	6-21 days
3	Vegetative	21-35 days
4	Flowering	35-49 days
Total		49 days

Source: FAO, 1991

Amaranthus plants were harvested after 50 days (Maturity period of the variety planted ranged between 50-60days), plot by plot and the yield per plot was weighed and recorded.

2.3 Determination of Bulk Density

This was determined at the harvest period of the experiment. The soil samples collected from the auger were poured into polythene bags and labeled sample A_1, A_2, A_3; B_1, B_2, B_3; and C_1, C_2, C_3, respectively. The samples were taken to the laboratory for analysis using core method. The core sampler was pushed into the soil and inner cylinder was filled up. It was pressed softly in order not to compact the soil. The core was dug out carefully to preserve the soil in it. Then, the outer cylinder was separated while the inner one was retained with undisturbed soil. The soil was trimmed carefully at the two open ends of the cylinder using a Knife. The two ends were covered with metal disk and put in plastic bag which was folded to keep the soil in place and the opening of the bag was taped. The samples were then taken to the laboratory for analysis. The cylinder and wet soil were weighed and the value was recorded. The soil was dried in an oven at a temperature of 105^0C for 24 hours to a constant weight and the bulk density was calculated using equation 1.

$$Soil\ bulk\ density = \frac{X3 - X1}{V}$$

(1)

Where,

X_1 = weight of empty cylinder (g)

X_3 = weight of oven dried soil + cylinder (g)

V = volume of soil (cm3)

Source: Taylor and Fujioka, 1992.

3. RESULTS AND DISCUSSIONS

3.1 Bulk Density

The results of soil bulk densities at depths 10cm and 20cm are presented in Table 2.

Table 2: Results of soil bulk density

S/N	Plot Number	Bulk density at 0-10cm (g/cm3)	Bulk density at 0-20cm (g/cm3)
1	A1	1.87	1.79
2	A2	1.79	1.73
3	A3	1.79	1.72
4	B1	1.68	1.60
5	B2	1.72	1.65
6	B3	1.74	1.70
7	C1	1.67	1.63
8	C2	1.56	1.52
9	C3	1.69	1.59

The results showed that the bulk densities at depth 10cm for all treatments (cultivated, uncultivated and compacted) were higher than the bulk densities at 20cm. The results also showed that bulk density for the compacted plot was the lowest, while bulk density at the cultivated plot has the highest. The result revealed that the compacted soil has less water for the survival of Amaranthus growth due to the effect of compaction. Excessive soil compaction impedes root growth and therefore limits the amount of soil explored by roots. This, in turn, can decrease the plant's ability to take up nutrients and water. From the standpoint of crop production, the adverse effect of soil compaction on water flow and storage may be more serious than the direct effect of soil compaction on root growth (J. DeJong-Hughes et al, 2001).

3.2 Amaranthus Vegetable Yield

The yields of Amaranthus vegetable for all the treatments for the two (2) harvests are presented in Table 3. The results revealed that cultivated plot has more yield of Amaranthus than the uncultivated and compacted plots because soil tillage usually create a more favourable condition for plant growth and improves soil aeration. Also, cultivated plot had enough water for the growth of Amaranthus plants than other plots. The compacted plot had the least yield because some moisture and air needed for growth had been expelled out of the soil during compaction which led to reduction in the soil pores.

Table 3: Amaranthus yield

S/N	Treatment	Yield per harvest (kg/8.75m2)		Total (kg/8.75 m2)	Average (kg/8.75 m2)
		1	2		
1	A1	7.9	8.0	15.9	8.0
2	A2	8.3	8.5	16.8	8.4
3	A3	8.1	8.5	16.5	8.3
				49.2	
4	B1	6.0	6.2	12.1	6.1
5	B2	6.4	6.2	12.6	6.3
6	B3	6.7	6.9	13.6	6.8
				38.3	
7	C1	5.2	5.0	10.2	5.1
8	C2	5.3	5.1	10.4	5.2
8	C3	5.0	5.4	10.4	5.2
				31.0	

3.3 Physical and Chemical Properties of the Soil

The physical and chemical properties of the soil at various depths (0-10cm and 10-20cm) at the experimental plot are also presented in table 4 and 5, respectively.

Table 4: Physical properties of experimental soil (Amaranthus)

Depth (cm)	FC (%)	Bulk density(g/cm3)	Clay %	Silt %	Sand %	Texture class
0-10	30	1.91	6	20	74	Loamy-sand
10-20	26	1.71	10	18	72	Loamy-sand

Table 5: Chemical properties of experimental soil (Amaranthus)

Parameters	0-10cm	0-20cm
pH in water	6.10	6.30
pH in KCL	5.0	4.60
% Organic carbon	0.20	0.36
% Organic matter	0.40	0.52
% Total nitrogen	0.26	0.20
Available phosphorous (ppm)	20.05	16.85
Exchangeable Bases (Cmol/kg)		
Ca^{++}	1.15	1.20
Mg^{++}	0.68	0.80
K^+	0.19	0.17
N^+	0.60	0.12
Exchangeable Acidity	0.31	0.40
	6.80	8.20

4. CONCLUSION

Based on the results obtained, it is concluded that Amaranthus on the cultivated land performed best. Tillage system by tractor on farmland enhanced soil nutrients status and good soil structure that resulted to better grain yield. Therefore, any farmer embarking on vegetable production should choose a cultivated land over non cultivated land as this supports high productivity and yield.

REFERENCE

.

FAO (1991): Crop Evapotranspiration-Guidelines for computing reference evapotranspiration. Food and Agriculture Organisation of United Nations, Rome, Italy.

J. DeJong-Hughes, J. F. Moncrief, W. B. Voorhees, and J. B. Swan (2001): Soil compaction: causes, effects and control. Extension Service, University of Minnesota.

Lipiec, J. and Hatano, R. (2003): Quantification of the Compaction effects on Soil Physical Properties and Crop Yield. Faculty of Agriculture, Hokkaido University, Sapporo 060, Japan.

Magdoff. F. and Vanes, H. (2000): Crop rotation in Building soils for better crops (2nd edition) Handbook...63 249.122.224. Date Accessed: 04.06.2014

Teasdale, B. and Mohler, F. (1993): Response of Weed Emergency to rate of vicia villosa. Http://www.extension.org. Date Accessed: 20.06.2014.

USDA (2012): United States Department of Agriculture. Production guide for central United States. Http://www.seleckcentrals.com . Date Accessed: 20.06.2014.

Coherency based dynamic reduction of Nigerian power system in PSS/E

Shereefdeen O. Sanni[1*], Josiah O. Haruna[2], Boyi Jimoh[3] Usman O. Aliyu[4]

[1,2,3]Department of Electrical and Computer Engineering, Ahmadu Bello University Zaria, Nigeria

[4]Department of Electrical and Electronics Engineering, Abubakar Tafawa Balewa University Bauchi, Nigeria

[*]daposanni@gmail.com, 08057217550.

ABSTRACT

This paper implements a technique for network reduction of the Nigerian 330kV power system in PSS/E. The technique involved identification of coherent generators, aggregation of the generators and elimination of load buses by topology reduction. Coherent generator was identified by inspection of the swing curves of the generators in the external system following a disturbance. Disturbances were simulated on the equivalent and original system. Results from the simulation showed that the dynamic characteristics of the equivalent system closely follow the original system. The developed equivalent network can be used for the assessment of the transient stability of the network.

Keywords: *coherency, aggregation, reduction, PSS/E*

1. INTRODUCTION

The increase in the size of power systems around the world which stems from rising level of interconnection has increased their complexities. In such systems, studies such as off-line stability analysis and on-line security assessment become practically difficult to conduct due to factors which include amongst others, increased computation time. Increased computational time is of concern due to low computer memory. Moreover, some disturbances have little effect on the dynamics of the whole system and modelling them with great accuracy will be unnecessary (Machowski, et al., 2008). It is on this ground that network reduction becomes necessary. In network reduction, the part of the system which is of interest is called the internal subsystem and is modelled in detail, while the rest of the system is called the external subsystem and is represented by simplified models referred to as an equivalent.

Network reduction of large power system using varying form of the coherency-based technique has been reported by (Haque & Rahim, 1990) and (Mahdi & Ahmed, 2011). Transient stability analysis is crucial for system operators in the planning, operation and control of power systems. With the integration of renewable into existing power system, (Naik, et al., 2011) has reported coherency based techniques for identifying coherent generators for systems with a considerable penetration of renewable energy sources.

In identifying coherent group of generators on the Nigerian power system, the use of a combination of power variation, inertia and damping indices was presented by (Izuegbunam, et al., 2011), (Okhueleigbe & Okhueleigbe, 2014) and (Ubah & Azubuike, 2014).

Progression in the use of digital computers for the design and implementation of engineering systems has paved the way for its application in the analysis of large power system. In simulating power systems, the idea is to reproduce a close to ideal scenario for research and academic purposes.

Various power system simulation and analytical tools are available and could be categorised as either commercial or academic/research based software. While academic tools are flexible with the ability to easily prototype, commercial tools are typically computationally efficient and "closed", i.e. do not allow for the modification of source code or algorithm.

PSS/E as a commercial software is able a reliable tool for most system operators around the world. The availability of limited feature version also ensures that research/academic studies could be carried out whilst exposing the individual to a potential real life application.

This paper presents a simple and accurate means of creating dynamic equivalents using PSS/E software. This procedure is based on the report of (Yang, et al., 2005) which will be implemented on the Nigerian power system. Although PSS/E has a network reduction module within it, it has a limitation of being applicable to static condition only (Milano & Srivastava, 2009) and does not provide a reliable equivalent for use in dynamic conditions.

2. METHODOLOGY

The procedure to create dynamic equivalent of the test case used for this study as presented by (Yang, et al., 2005) are: identification of coherent generators, aggregation of coherent generators and network reduction. The first two steps are preparatory to the third which is a static equivalent procedure available in PSS/E. A brief description of the technique involved in each of the three steps follows

2.1. Identification of coherent generators

A coherent group of generators is defined as a group of generating unit oscillating with the same angular speed and terminal voltage in a constant complex ratio for a set of disturbance (Padiyar, 2008). Mathematically, this is expressed as:

$$\left.\begin{array}{l}\dfrac{\dot{V}_i(t)}{\dot{V}_j(t)} = \dfrac{V_i(t)}{V_j(t)}\, e^{j[\delta_i(t)-\delta_j(t)]} \\[4mm] = \dfrac{V_i(0)}{V_j(0)}\, e^{j[\delta_i(0)-\delta_j(0)]} = \text{constant}\end{array}\right\} \quad (1)$$

If the voltage magnitude of the coherent buses is assumed to be constant, the coherency condition of (1), simplifies to

$$\delta_i(t) - \delta_j(t) = \delta_{ij}(t) = \delta_{ij}(0) = \text{constant} \quad (2)$$

Where $\delta_i(0)$ and $\delta_{ij}(0) = \delta_i(0) - \delta_j(0)$ are the initial values of the variables calculated for the reduced model. This study identifies coherent generators when a fault is applied in the study system and the swing curves in the external systems are observed and those generators with the most identical swing curves are classified as coherent.

2.2. Dynamic Aggregation of generators

Coherent group of generating units are aggregated into an equivalent generator that exhibits the same speed, voltage and total mechanical and electrical power as the group during any disturbance where the units in the group remain constant. The aggregation of coherent generator buses is based on the Zhukov's method (Machowski, et al., 2008) in which each terminal bus is connected through an ideal transformer with complex turns ratio to the equivalent bus. The voltage of the equivalent bus is defined as the average voltage of the coherent generator buses, which can be mathematically expressed as

$$V_t = \frac{\sum\limits_{k=1}^{n} V_k}{n} \quad (3)$$

$$\Theta_t = \frac{\sum\limits_{k=1}^{n} \Theta_k}{n} \quad (4)$$

Where V_t is the voltage of the equivalent bus, V_k is the voltages at coherent buses k and θ_t is the phase angle of the equivalent bus voltage.

The turns ratio of the ideal transformer is given by

$$\dot{a}_k = \frac{\dot{V}_k}{\dot{V}_t} \quad (5)$$

The mechanical (P_m^*) and electrical (P_e^*) power of the equivalent generator is the sum of the mechanical and electrical power of all the generators in the same coherent group:

$$P_m^* = \sum_{i=1}^{n} P_{mi} \quad (6)$$

$$P_e^* = \sum_{i=1}^{n} P_{ei} \quad (7)$$

The equivalent generator is represented by the classical model with constant equivalent transient emf and the swing equation of the rotor given by

$$\left(\sum_{i=1}^{n} M_i\right)\frac{d\omega}{dt} = \sum_{i=1}^{n} P_{mi} - \sum_{i=1}^{n} P_{ei} - \left(\sum_{i=1}^{n} D_i\right)\omega \quad i = 1,2\ldots\ldots\ldots.n \quad (8)$$

Where ω is the angular frequency of the coherent generator and is assumed to be identical.

Hence the inertia (M^*) and damping (D^*) constant of the equivalent generator is given by

$$M^* = \sum_{i=1}^{n} M_i \qquad (9)$$

$$D^* = \sum_{i=1}^{n} D_i \qquad (10)$$

The transient reactance (X_d') of the equivalent generator is obtained by paralleling the transient reactance of all the coherent generators:

$$X_d' = \frac{1}{\sum_{i=1}^{n} \dfrac{1}{X_{di}'}} \qquad (11)$$

2.3. Network topology reduction

The network reduction procedure in PSS/E is the topological reduction method. This process involves deleting some load buses in order to reduce the size and complexity of the network. The selected load buses are eliminated by performing Gauss elimination operation on the admittance matrix of the external system.

The admittance matrix equation of the external system can be written in the partitioned form as

$$\begin{bmatrix} I_R \\ I_D \end{bmatrix} = \begin{bmatrix} Y_{RR} & Y_{RD} \\ Y_{DR} & Y_{DD} \end{bmatrix} \begin{bmatrix} V_R \\ V_D \end{bmatrix} \qquad (12)$$

Where subscript R and D refer to the nodes to be retained and deleted respectively.

The equivalent is obtained by rearranging the second row of (12), as

$$V_D = Y_{DD}^{-1}(I_D - Y_{DR}V_R) \qquad (13)$$

Substituting (13) into the first row of (12) to give

$$I_R = Y_R V_R + K_l I_E \qquad (14)$$

Where

$$Y_R = Y_{RR} - Y_{RD}Y_{DD}^{-1}Y_{DR} \qquad (15)$$

$$K_l = Y_{RD}Y_{DD}^{-1} \qquad (16)$$

The admittance matrix Y_R corresponds to a reduced equivalent network that consists of the retained buses and the equivalent branches linking them. The matrix K_l is often referred to as the distribution matrix which passes the node currents from the eliminated buses to the retained buses. The first term of (14) specifies a set of equivalent branches and static shunt elements connecting the retained nodes, while the second term specifies a set of equivalent currents which must be impressed on the retained nodes to reproduce the effect of load currents at the deleted nodes. These equivalent currents may be translated into equivalent constant real and reactive power loads and added to the original loads at the retained buses. It is pertinent to note that the efficiency of the equivalent network thus created by this process within PSS/E is improved with when external system is divided into subsystem (Power Technology International (PTI), 2010).

3. RESULTS AND DISCUSSIONS

The test network has 31 bus, 7 generators and 33 transmission lines interconnecting them. The network is essentially a radial system with 3 hydro-powered plants located in the north and 4 thermal power plants located in the south. The generators, transmission lines and load parameters are available from reference (Nwohu, 2011). Figure 1 shows the single line network diagram illustrating the area of interest. The area of interest has only one generator i.e. Egbin generator and the south west buses; this is identified as the study system.
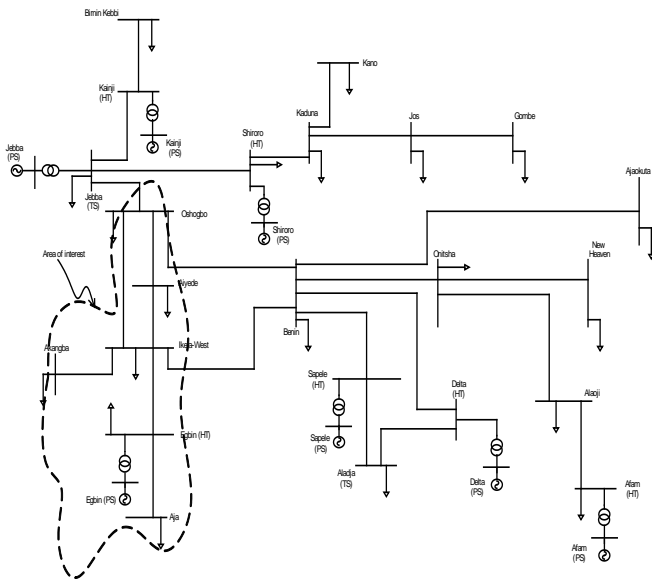
Fig. 1: The Nigerian 330kV transmission network showing the area of interest

Fig. 2: Rotor angle response of generators in the external systems

Two other subsystems known as the external systems were created based on the type of generation i.e. hydro or thermal and geographical location. Time domain simulation is performed on the network with a three phase fault applied in the study system in order to identify the coherent generators. Figure 2 show the response (swing) of the generators to a three phase fault on Ikeja-west bus at 0.1 second which was cleared by the tripping of the Ikeja west- Oshogbo line at 0.2 second. The results show that the swing curves of the generators in close proximity to each other are more coherent even though there are more generators within the same area. Two groups of coherent generators were identified as shown by the swing curves. The groups are: {Jebba, Kainji} and {Delta, Sapele}, generators at Shiroro and Afam did not fall into any of the groups.

The coherent generators in each group are lumped into an equivalent generator and the network reduced by deleting the load buses except the boundary buses of the two external systems at Jebba and Benin.

The equivalent network thus obtained is reduced to 5 generators, 17 loads, 13 buses and 14 branches. Figure 3 is the reduce network model in PSS/E.
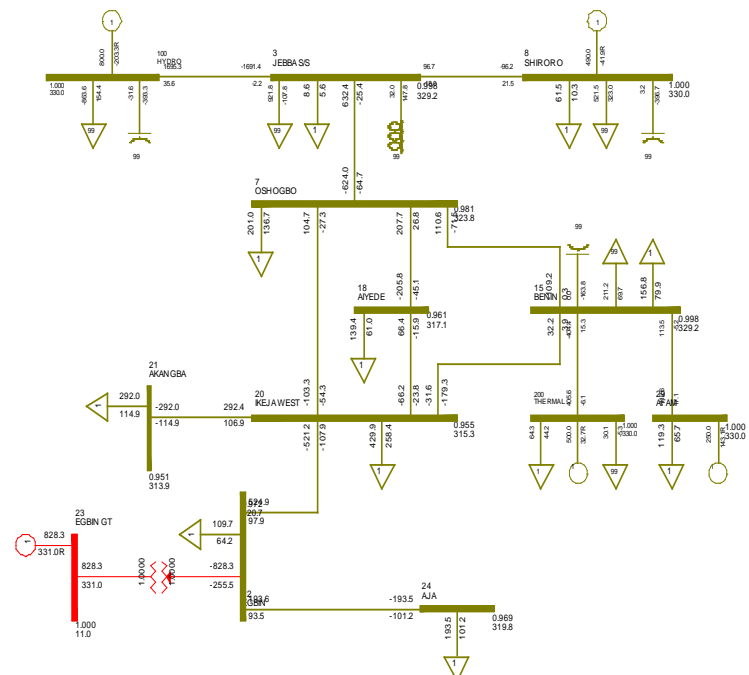
Fig. 3: The Reduced Nigerian 330kV transmission network

Table 1 gives a comparison between the original and reduced system.

Table 1: Comparison between the original and equivalent system

	Generators/Loads	Buses/Branches
Original	7/21	31/33
Reduced	5/17	13/14

The reduced system is tested with a disturbance which is the sudden loss of the largest load in the network. Figures 4 to 6 shows the performance of the reduced system under this condition as compared with the original system.
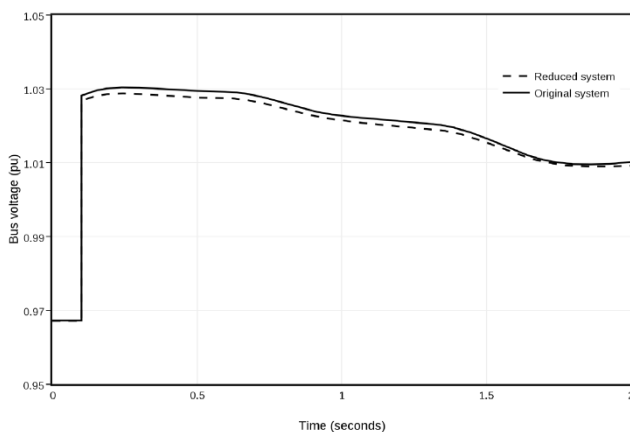
Fig. 4: Bus voltage profile of the faulted bus at Ikeja-west
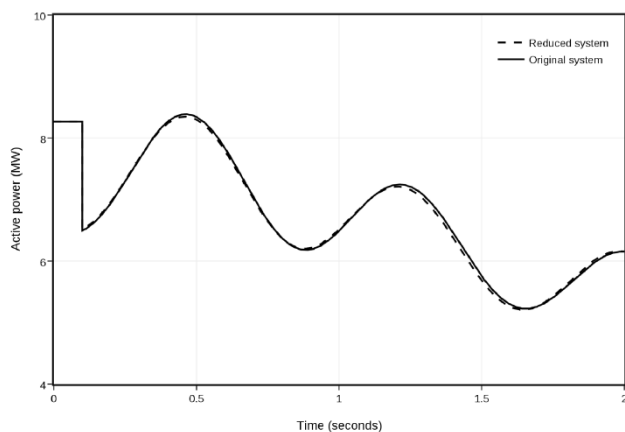
Fig. 5: Active power response of the machine at Ebgin
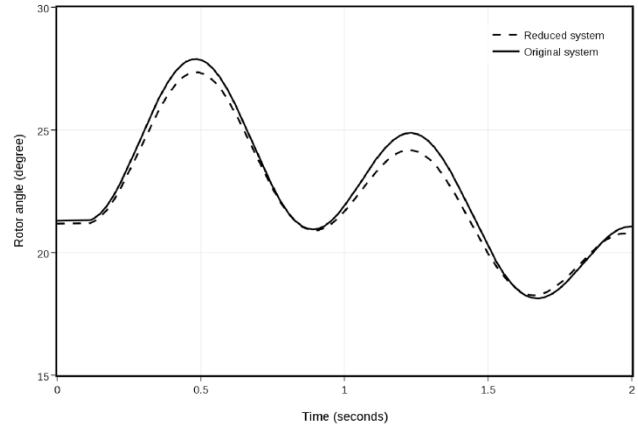
Fig. 6: Rotor angle response of generator at Egbin

With the sudden loss of load the voltage at the Ikeja-west bus increases and slowly returns to its original value as illustrated in figure 4. Voltage magnitudes of the reduced system reliably reproduce the behaviour of the voltage of the original system. The generator electrical power response of the generator at Egbin is shown in figure 5. The response of the network is reproduced when the network is reduced and when it is full. Rotor angle oscillates after the load loss but has reduced amplitude with time as illustrated in figure 6.

The response from the figures shows that the reduced system follows closely the original system and can be used for transient stability analysis of the network.

4. CONCLUSION

This paper implemented a coherency based technique for reducing power systems in PSS/E. In the procedure, the coherent generators were aggregated after their identification and the static network reduction procedure within PSS/E implemented. The Nigerian 330kV network was used as the test case with a disturbance simulated on the original and reduced network. Results obtained reveals that the reduced system adequately captures the response

of the original system and can be used for transient stability analysis.

REFERENCE

Haque, M. H. & Rahim, A. M., 1990. Identification of Coherent Generators Using Energy Function. IEEE Proceedings, July, 137(4), pp. 255-260.

Izuegbunam, F. I., Okafor, E. C. & Ogbogu, S. O. E., 2011. Coherent generator based Transient Stability Analysis of the 16 machines, 330KV Nigeria Power System. Journal of Emerging Trends in Engineering and Applied Sciences , 2(3), pp. 456-461.

Machowski, J., Bialek, J. W. & Bumby, J. R., 2008. Power System Dynamics Stability and Control. s.l.:John Wiley & Sons, Ltd.

Mahdi, M. M. E.-A. & Ahmed, F., 2011. Identification of Coherent Generators for Large-Scale Power Systems Using Fuzzy Algorithm. WSEAS TRANSACTIONS on SYSTEMS and CONTROL, June, 6(6), pp. Issue 6, Volume 6, June.

Milano, F. & Srivastava, K., 2009. Dynamic REI equivalents for short circuit and transient stability analyses. Electric Power Systems Research, p. pp.878–887.

Naik, P. K., A.i, Q. W. & K., N. N., 2011. Identification of Coherent Generator Groups in Power System Networks with Windfarms. Brisbane, QLD, IEEE, pp. 1-5.

Nwohu, M. N., 2011. Low-frequency power oscillation damping enhancement and voltage improvement using unified power flow controller (UPFC) in multi-machine power system. Journal of Electrical and Electronics Engineering Research, July, 3(5), pp. pp. 87-100.

Okhueleigbe, E. I. & Okhueleigbe, A. O., 2014. Identification of Multi-Machine Power System Coherent Group in Nigeria. JOURNAL OF ADVANCEMENT IN ENGINEERING AND TECHNOLOGY, 1(3), pp. 1-3.

Padiyar, K. R., 2008. Power System Dynamics Stability and Control. Hydrabad: BS Publications.

Power Technology International (PTI), 2010. PSS/E 30.0.5 Program Application Guide. Vol. I and II. s.l.:Siemens Energy.

Power Technology International (PTI), 2010. PSS/E 30.0.5 Program Operation Manual.. s.l.:Siemens Energy.

Ubah, B. C. & Azubuike, K., 2014. Computer Simulation of Power Deviation, Admittance Distance, Coherency Indices, and Dynamic Equivalents for Electric Power Systems. International Journal of Computer Applications, September, 101(7), pp. 6-17.

Yang, J. P., Cheng, G. H. & Xu, Z., 2005. Dynamic Reduction of Large Power System in PSS/E. Dalian, China, IEEE, pp. PP.1-4.

Influence of catalyst concentration and temperature on Reactive Extraction of *Moringa oleifera* oil seed for biodiesel Production

Mohammed I. A., Musa Umaru., B. Suleiman., M. Auta., K.R.Onifade and Baaki Monica A

Department of Chemical Engineering, Federal University of Technology, P.M.B 65, Main Campus, Gidan Kwano-Minna, Niger State, Nigeria

*umar.musa@futminna.edu.ng,   08032318723.

ABSTRACT

This paper presents the study of reactive extraction (in situ tranesterification) of moringa oleifera oil seed. In this study the effect of catalyst concentration (0.1–1.8 wt %) and reaction temperature (30–60 ∘C) on the synthesis of moringa methyl ester yield (MOME) via reactive extraction at a constant particle size, molar ratio of methanol to oil, reaction time and agitation speed of < 5 mm, 1:350, 60 minutes and 350 rpm, 60 respectively. Experimental results show that lower catalyst concentration promotes the methyl ester yield positively until an optimum of 1 wt % NaOH after which a decline in yield was observed. The reaction temperature exhibit small but noticeable effect on the reaction as the yield increases slightly with temperature increase. The optimum biodiesel yield of 80 % with a corresponding purity of 98.4 % against the European Union set limit of 96.5 wt % was obtained at a catalyst concentration of 1 wt % and a temperature of 60°C. The result of the characterization of the MOME biodiesel shows that it compares favorably with ASTM standard for biodiesel.

Keywords: Moringa *oleifera*, Reactive extraction, Biodiesel, *in situ* transesterification, catalyst, temperature characterization

1. INTRODUCTION

Biodiesel is a mono alkyl ester of fatty acid produced from the transesterification of vegetable oil/animal fat with an alcohol in the presence of a catalyst (Gerpen *et al.,* 2004). Biodiesel is presently enjoying wide popularity as a possible alternative to petroleum diesel due to ever increasing demand for energy resulting from population explosion, industrialization and the menace of environmental degradation largely attributed to the over dependency and usage of fossil derived diesel fuel (Madankar *et al*., 2013). The fuel can be used in conventional diesel engines as a substitute for petro diesel (Musa and Aberuagba, 2012). It is known to be an attractive biofuel because it is essentially renewable, non toxic, biodegradable, emit less carbon, sulphur free, have high flash point, good lubricity, non flammable and miscible with petroleum diesel in all ratio (Musa *et al*., 2014). The most prominent feedstock for biodiesel production are soya bean oil Silva *et al.,* 2011, palm oil , sunflower oil, canola (Musa *et al*., 2014a) corn oil (Lu *et al.,* 2009), palm kernel oil (Alamu *et al.,* 2007) Jatropha curcas oil, castor oil, cotton seed oil, olive oil, , tallow, waste grease, peanut oil, madhuca indica, pongamia pinnala, fish oil, and linseed oil (Musa *et al.,* 2014b).

Transesterification is the most common technology employed for the production of biodiesel from vegetable oils (Abdulkareem *et al.,* 2011). Biodiesel production using these techniques involves a number of stages; such as extraction of oil from precursor, purification of the oil before esterification/transesterification. These multiple steps are reported to account for over 70 % of the total biodiesel production cost (Shuit *et al.,* 2010). In order to reduce the cost of biodiesel production a number of ways have been identified. According to Reefaat *et al*., 2008, there is the need to minimize the cost of biodiesel

production by improving on the process technology through optimization of the process variables that affects the biodiesel yield and purity.

The development of *in situ* transesterification (reactive extraction) as a process of biodiesel production has the potential to drastically reduce the cost of biodiesel. This new technology differs from conventional transesterification process as it permits the synthesis of biodiesel from oil bearing seed directly through a single step process that involves in situ extraction and transesterification (Zakari and Harvey, 2011; Ponsak *et al.,* 2013). The technique essentially allows both extraction of oil from its seed and subsequent conversion to biodiesel to take place in one single step with the alcohol acting as a solvent for extraction and a reagent for transesterification (Shuit *et al.,* 2011). This makes both extraction and transesterification to take place simultaneously thereby eliminating the step of extraction, refining and further processing before tranesterification (Haas *et al.,* 2004, Georgogianni *et al.,* 2008). A number of study has been reported on the in situ transesterification of oil bearing seeds for biodiesel synthesis; some of seeds include rapeseed (Zakaria and Harvey, 2011), rice bran oil seed and rubber oil seed (Abdulkadir *et al*., 2014) castor seed (Madankar *et al.,* 2011), Jatropha curcas seed (Shuit *et al.,* 2010) and cotton seed (Kazim and Harvey, 2011), Palm fruit (Ponsak *et al.,* 2013). Besides process optimization the present increase in human population and the current renewed interest in oleo-chemicals products and lipids derived fuels such as biodiesel has necessitate the need to search for new underutilized vegetable oils bearing seeds. Quite a number of this plants seed have been identified, however the dearth of information on their chemical composition has limited their applications as potential oilseed crop (Anwar and Rashid, 2007).

Moringa oleifera is a multi- purpose plant. The leaves, fruits, flowers and immature pods of this tree are edible and are part of traditional diets in many countries of the tropics and sub-tropic (Anwar and Rashid, 2007). Moringa *oleifera* is commonly known as Never Die tree, West Indian, Ben tree, Horseradish tree Drumstick tree and Radish tree In English. Moringa *oleifera* Lam belongs to an *onogeneric* family of shrubs and tree. Moringa seed kernels contain about 30 – 50 % oil (Zaku *et al.,*2012). The oil is commercially known as "Ben oil" or "Behen oil". Moringa seed oil content and its properties show a wide variation depending mainly on the species and environmental conditions (Anwar and Rashid, 2007). Moringa seed oil contains about 74 % oleic acid making it an ideal feedstock for biodiesel synthesis in term of improved oxidative stability (Anwar, 2005). One of the major threats against the use of vegetable oils for industrial purposes is the shortage of food supply. Abdulkareem *et al.,* (2011) reported that Moringa oleifera seed oil is not a popular edible oil in Nigeria and many other parts of the world; hence its usage for biodiesel production will not pose any food challenge. The author also establishes the potential of these oilseeds for biodiesel production

The objective of this work is to investigate the influence of in situ transesterification catalyst concentration and reaction temperature on the yield of moringa oleifera methyl ester (MOME) by reactive extraction for biodiesel production.

2.0 MATERIALS AND METHODS

2.1 Moringa *oleifera* seed

The oil seed was collected from Minna, Nigeria. These seeds were stored in very dark air tight container.

2.1.1 Preparation of Moringa *oleifera* seed

The seed including its shell were ground using a pestle and mortar in a fine particle of less than 5 mm and dried in an

oven (Dakai, Korea) for an hour at a temperature of 105 ^{0}C.

2.1.2 Determination of oil content

2g of the ground and dried moringa seed was weighed into thimbles. The thimbles were inserted in the soxhlet apparatus and the boiling flask was filled with 300 ml of n-hexane. The soxhlet apparatus was set up, powered and allowed to reflux for 6 hours. The thimbles were occasionally removed and weighed until a constant weight was observed. The thimbles were finally removed and the n-hexane was drained from the top of the apparatus. There liquid in the boiling flask was removed and oven dried at 105 ^{o}C to get rid of any trace of n-hexane. The sample was then cooled and weighed (Ibitoye, 2005).

$$\% \, Oil = \frac{weight \, of \, oil}{weight \, of \, sample} \qquad (1)$$

2.2 Chemical and reagent

Methanol with a purity of 99.8%, NaOH, acetic acid, hexane were obtained from the Fisher scientific Co, U.S.A.

2.3 Reactive Extraction for Biodiesel Production

The reactive extraction experiments were conducted in a sealed conical flask. About 0.792g of sodium hydroxide (1% wt of oil) was first dissolved in 125.2 ml of methanol (i.e. alcohol to oil molar ratio of 1:350). This was then poured into the 500 ml conical flask and heated to a desired temperature of 60 ^{o}C. 20g of ground and dried moringa seed powder was poured into the alkaline alcohol and agitated for 60 minutes in a water bath agitator set to 60 ^{o}C. After 60 minutes, the agitation was stopped and a known amount of glacial acetic acid was poured into the mixture to stop further reactions. A funnel equipped with a filter paper was used to separate the liquid from the meal. Excess methanol was used to wash the residue to recover

every methyl ester trapped in the meal. The excess methanol was recovered using a rotary evaporator equipped with a vacuum pump. The remaining mixture of glycerol and biodiesel was separated using a separating funnel. The mixture in the separating funnel formed two distinct layers; the biodiesel rich upper layer and the lower layer of glycerol which was further removed. An equal volume of warm acidified water was used to wash the biodiesel to increase its purity. The washed biodiesel was the oven dried (Kasim, *et al.,* 2012).

2.4 Biodiesel Analysis

2.4.1 Biodiesel yield

The biodiesel yield was calculated by dividing the mass of biodiesel obtained by the mass of oil in the moringa oilseed.

$$Biodiesel \, yield \, (\%) = \frac{weight \, of \, ester}{weight \, of \, raw \, oil} \times 100 \quad (2)$$

2.4.2 Characterization of Biodiesel

The flash point was determined in a Pensky–Martens closed-cup tester (ISL, Model FP93 5G2) using ASTM D 93. Cloud point and pour point determinations were determined using ASTM D 2500 and ASTM D 97. The kinematic viscosities were determined at 25 °C, using a Viscometer (Model VT-03) following the ASTMD 7042 procedure. The cetane index was calculated from the iodine value and saponification value as given by Krisnangkura below.

$$CI = 46.3 + \frac{5458}{SV} - \frac{0.225}{IV} \qquad (3)$$

SV = Saponification value of ethyl ester; IV = Iodine value of ethyl ester.

The cetane number was therefore calculated from the cetane index as given by Patel in the equation below.

$$CN = CI - 1.5 \qquad (4)$$

3.0 RESULT AND DICUSSIONS

3.2.1 Effect of Catalyst Concentration

The presence of catalyst is play a key role in reactive extraction of oilseed to biodiesel.
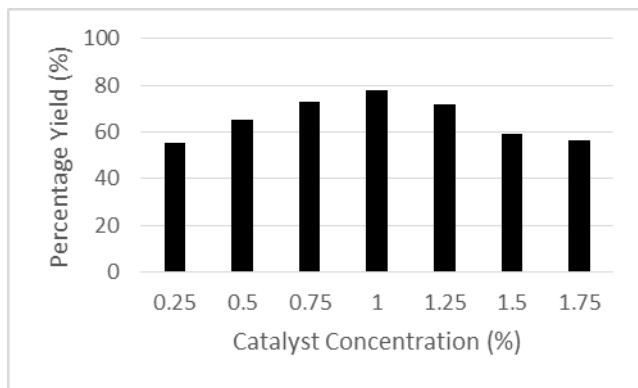
Figure 1: Effect of catalyst concentration on MOME yield

Different catalyst (NaOH) concentration (0.25, 0.50, 0.75, 1.0, 1.25, 1.50 and 1.75 %wt) other parameter such as temperature, molar ratio of methanol to oil, reaction time and agitation speed were kept constant at 50 ^{0}C, 1:350, 60 minutes and 300 rpm respectively. The result gave an average yield of 55.3, 65.3, 72.9, 77.9 71.6, 59.0 and 56.5 % with a corresponding methyl ester content (purity) of 83, 86.5, 93.1, 94, 90.5, 82.5 and 83.3 % respectively The clearly revealed that the methyl ester yield increased linearly with increase in catalyst concentration until an optimum of 77.9 % was obtained at 1 % wt catalyst concentration. The yield of methyl ester does not necessarily depend on high catalyst concentration but on a sufficient catalyst concentration required to penetrate the oilseeds and aid the oil extraction as well as methyl ester synthesis. Catalyst concentration below the optimal point (i.e. 1%) even under the same operating conditions of alcohol, temperature and time resulted into lower biodiesel yield. The result compares favourably with the work of Chandu *et al.,* 2012. The decrease in biodiesel yield at catalyst concentrations above 1 % can be attributed to increase in hydroxide ions which lead to side reactions such as soap formation.

3.2.2 Effect of Temperature

Generally temperature affects the diffusion of solvent into oil seed core and subsequent synthesis of the biodiesel (Zakaria and Harvey, 2012). The result of Figure 2 shows that the increase in temperature from 30 - 60 ^{0}C leads to an increase in biodiesel yield and purity
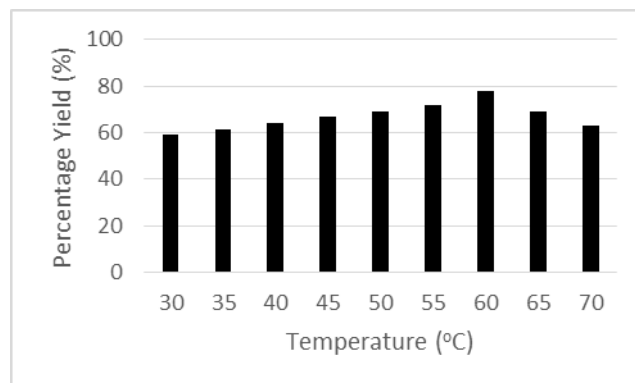
Figure 2: Effect of temperature on MOME yield

The highest yield of 80 % was obtained at a temperature of 60 ^{o}C beyond this point the yield began to drop. This result is in agreement with the report by Zakaria and Harvey, 2011, who reported that the solubility of the oil in the solvent into seed is usually increased at elevated temperature due to substantial decrease in parent oil viscosity which results higher diffusitivity of the solvent in to oilseed core. The findings from this work differ from the report of Chandu *et al.,* 2012 who reported the same yield at a temperature of 65 ^{o}C during the reactive extraction of castor methyl ester. Other researchers such as Kasim and Harvey (2011) have also reported insignificant effect of temperature beyond 30°C. According to Kasim *et al.,* 2010 the pronounced contradictions on the effect of temperature variation might probably be dependent upon the feedstock used, as different raw materials are characterized by different internal structures and effective diffusitivity.

3.3 3.1 Characterization of Moringa Oleifera seed oil Biodiesel

Table 3.4: Fuel properties of biodiesel

Fuel property	Experimental Values	Rashid *et al.*, 2008	European Norm (EN)	ASTM standard
Kinematic viscosity at 40°C (mm^2/s)	4.4667	4.83	3.5- 5.0	1.9 – 6.0
Specific gravity g/ml at 15 ^{o}C	0.88	-		0.88-0.93
Flash point (^{o}C)	192	-	> 101	> 130
Cloud point (^{o}C)	5	18		
Pour point (^{o}C)	3	17		-15 – 10
Cetane number	66.8	67.07	> 51	> 47

The kinematic viscosity of any fuel is of utmost importance as it affects the atomization and distribution of the fuel (Gerpen *et al.,* 2004). According to ASTM D6751 the kinematic viscosity of biodiesel must be within the range of 1.9 - 6.0 mm^2/s. The kinematic viscosity of the biodiesel produced in this work is 4.4667mm^2/s at 40°C which is within the EN and ASTM D6751 standard and also shows close proximity to the report of Rashid *et al*., 2008 as shown on Table 1. Excessive high kinematic viscosity will result in higher drag, higher pressures and higher injection volumes into the injection pumps particularly for engines under low temperature conditions (Sarada, 2011).

The flash point is the least temperature at which vapours of a fuel will be ignited by an applied ignition source. Flash point measures the tendency of a fuel to form flammable mixture with air (Gerpen *et al.,* 2004). The flash point of the moringa biodiesel was found to be 192 ^{0}C which is reasonably within the acceptable EN and ASTM D6751 standard. Biodiesels with higher flash points are safer to

use. This makes moringa biodiesel a better option when compared to others like castor biodiesel with a flash point of 189.3 (Chandu *et al.,* 2012).

The cloud and pour point are important fuel properties which determine the use of that fuel for low temperature applications. The cloud and pour point of moringa biodiesel was determined to be is 5 ^{o}C and 3 ^{o}C respectively which were quite impressive when compared to 18 ^{o}C for cloud point and 17 ^{o}C for pour point reported by Rashid *et al*, (2008). The cloud point and pour point values of moringa biodiesel obtained present it as a very good fuel for low temperature applications.

The cetane number was found to be 66.9 which is just a little bit above the ASTM D6751 standard of 47-65 and slightly below the value of 67.07 reported by Rashid *et al.,* 2008 and this implies short delay in ignition and better ignition properties. This result confirms the report by Rashid et al, 2008 that moringa biodiesel has one of the highest Cetane numbers ever reported. When compared

with castor and jatropha, both with a cetane number of 52 (Mohammed, 2012; Salihu 2012).

The specific gravity was found to be 0.88 which is within the acceptable range of 0.88-0.93 by ASIM D6751 standard for biodiesel. This implies that moringa biodiesel is not only less viscous but also light. Comparing the specific gravity of moringa biodiesel with that of castor (0.89) and jatropha (0.91), moringa biodiesel have a lower specific gravity both castor and jatropha biodiesel.

The density of the diesel was also found to be $0.8837 g/cm^3$ as against the density of $0.9032 g/cm^3$ of the parent oil. The sharp change in this value is an indication of a decrease in the trigylceride content of the oil. The result of the characterization of moringa biodiesel obtained, the properties of the moringa biodiesel produced fall within EN and ASTM D6751 standard.

4.0 CONCLUSION

The study have attempted the reactive extraction (*in situ* tranesterification) of moringa oleifera oil seed studying the effect of catalyst concentration (0.1–1.8 wt %) and reaction temperature (30–60 ∘C) on the synthesis of moringa methyl ester yield (MOME) at a constant particle size, molar ratio of methanol to oil, reaction time and agitation speed of < 5 mm, 350 rpm, and 60 minutes respectively. The findings revealed an optimum yield of 80 % at 1.0 wt % catalyst concentration and a temperature of 60 ^{0}C. The characterization of the resultant biodiesel presents moringa oleifera oilseed as a good feedstock for biodiesel production as its properties conforms to the acceptable EN and ASTM standard. The innovation in this manuscript is that it is one of the very first attempt to document the reactive extraction of biodiesel from moringa oleifera oilseed.

REFERENCES

Abdulkadir Bashir Abubakar, Wilson Danbature, Fai Y. Yirankinyuki, Buhari Magaji and Muhammad M. Muzakkir (2014) In Situ Transesterification of Rubber Seeds (Hevea brasiliensis), Greener Journal of Physical, Vol. 4 (3), pp. 038-044

.

Abdulkareem, A.S., H. Uthman, A.S. Afolabi and O.L. Awenebe (2011). Extraction and Optimization of Oil from Moringa Oleifera Seed as an Alternative Feedstock for the Production of Biodiesel, Sustainable Growth and Applications in Renewable Energy Sources, Dr. Majid Nayeripour (Ed.), ISBN: 978-953-307-408-5.

Alamu, O.J, Waheed, M.A; Jekayinfa, S.O (2007) Alkali-Catalysed Labouratory Production & Testing of Biodiesel Fuel from Nigerian Palm Kernel oil Agricultural *Engineering International. The CIGRI Journal of Scientific Research S^l*

American society for Testing Materials, *Standard Specification for biodiesel fuel* (B100) *Blend stock for distillate fuels, Designation D6751-02, ASTM* international, West Conshohocken, PA. (2002).

Anwar F., Ashraf M., Bhanger MI. 2005. Interprovenance variation in the composition of *Moringa oleifera* oilseeds from Pakistan. *J.Am.Oil.Chem.Soc.* 82 (1), 45-51.

Anwar F., Zafar N.S., Rashid U., (2006). Characterization of *Moringa oleifera* seed oil from drought and irrigated regions of Punjab, Pakistan. Pp 160-168, 2006, ISSN: 0017-3495.

Anwar F and Rashid U (2007) Physico-chemical characteristics of moringa oleifera seeds and seed oil from a wild provenance of pakistan , Pak. J. Bot., 39(5): 1443-1453, 2007.

Chandu, M. S., Pradhan, S., Naik, S.N., (2012). Parametric study of reactive extraction of castor seed (*Ricinus communis* L.) for methyl ester production and its potential use as bio lubricant. Industrial crops and products, 43 (2013) 283-290.

Georgogianni K.G., Kontominas M.G, Pomonis PJ, Avlonitis D, Gergis V., (2008). Alkaline conventional and *in situ* transesterification of cottonseed oil for the production of biodiesel. *Energy Fuel*. 22(3), 2110–2115.

Georgogianni K.G., Kontominas MG, Pomonis P.J., Avlonitis D., Gergis V., (2008).Conventional and *in situ* transesterification of sunflower seed oil for the production of biodiesel. *Fuel Process. Technol*. 89(5), 503–509 .

Gerhard, K. Gerpen, J.V. and Jurgen K. (2005). *The biodiesel handbook, AOCS press,* Champaign, Illinois, pp 14-19.

Haas, M.J., (2004) In situ alkaline transesterification: an effective method for the production of fatty acid esters from vegetable oils, J. Am. Oil Chem. Soc. 81 (1) (2004) 83–89.

Ibitoye A.A. (2005). Basic Methods of Plant Analysis, pp 63-85.

Kasim F.H; and Harvey P.A., (2011). Influence of various parameters on reactive extraction of Jatropha curcas L. for biodiesel production. Chemical Engineering Journal 171 (2011) 1373– 1378.

Kasim F.H., Harvey P.A., & Zakaria R., (2010). Biodiesel production by *in situ* transesterification, School of Chemical Engineering and Advanced Material, Merz Court, Newcastle University, NE1 7RU, UK, future science group. pp 1-11

Ma, F. & Hanna, M. A., (1999). Biodiesel production: a review. *Bioresource Technology*, Vol. 70, pp. 1–15, ISSN 0960-8524.

Madankar, C.S., Pradhan, S., Naik, S.N., (2012). Parametric study of reactive extraction of castor seed (*Ricinus communis* L.) for methyl ester production and its potential use as bio lubricant. Industrial crops and products 43 (2013) 283-290.

Musa Umaru and F. Aberuagba (2012) Characteristics of a Typical Nigerian *Jatropha curcas* oil for Biodiesel Production. *Research Journal of Chemical Science*, Vol.2 (10),7-12.

Musa Umaru, Aboje A.A., Mohammed Ibrahim.A, Member, Aliyu M. A., Sadiq M. M. and Olaibi Aminat. O (2014a)The Effect of Process Variables on the Transesterification of Refined Cottonseed Oil, Proceedings of the World Congress on Engineering 2014 Vol I, WCE 2014, July 2 - 4, 2014, London, U.K, 622-624.

Musa Umaru , Mohammed, Ibrahim A., M. M. Sadiq, A. M. Aliyu, B. Suleiman, and Talabi Segun (2014b). Production and Characterization of Biodiesel from Nigerian Mango Seed Oil, Proceedings of the World Congress on Engineering 2014 Vol I, WCE 2014, July 2 - 4, 2014, London, U.K, 645-649

Ponsak Jairurob , Chantaraporn Phalakornkule , Anamai Na-udom , Anurak Petiraksakul (2013) Reactive extraction of after-strippig sterilized palm fruit to biodiesel, Fuel, 107, 282–289. http://dx.doi.org/10.1016/j.fuel.2013.01.051

Rashid U.; Anwar F.; Moser B. R.; Knothe G., (2008). Moringa oleifera oil: A possible source of biodiesel. Bioresource Technology, 99, 8175–8179.

Shuit, Siew Hoong, Keat Teong Lee , Azlina Harun Kamaruddin, Suzana Yusup (2010) Reactive extraction and in situ esterification of Jatropha curcas L. seeds for the production of biodiesel, *Fuel* 89 (2010) 527–530

Zakaria R. & Harvey P.A., (2012). Direct production of biodiesel from rapeseed by reactive extraction/in situ transesterification. Fuel Processing Technology 102 (2012) 53–60.

Zaku, S.G, Emmanual, S.A, Isa A.H, & Kabir A. (2012) Comparative Studies on the Functional Properties of Neem, Jatropha, Castor, and Moringa Seeds Oil as Potential Feed Stocks for Biodiesel Production in Global Journal of Science Frontier Research Chemistry Volume 12 Issue 7 Version 1.0 Year 2012

PERFORMANCE ANALYSIS OF TRANSMISSION SCHEMES OVER A MIMO SYSTEM IN RICEAN FADING CHANNELS

O.E. Ochia [1*], E. Obi[2], B.O. Sadiq[3] Abubakar A.S.[4]

Department of Electrical and Computer Engineering,

Ahmadu Bello University, Zaria.

[*]emmirald@gmail.com, eobi@abu.edu.ng, bosadiq@abu.edu.ng

.

ABSTRACT

This paper presents a comparative performance analysis of different transmission schemes over a multiple input-multiple-output (MIMO) communication system. The physical layer of a wireless MIMO system is modelled using a simulator in Matlab. It is assumed that the communication channel exhibits Ricean fading i.e. there exist a line-of-sight signal path between transmitterand receiver antenna pairs. Three techniques for transmitting data into the channel are investigated for the Ricean channel model namely spatial multiplexing with zero forcing, spatial multiplexing with V-BLAST and space-time coding using Alamouti scheme. The Symbol Error Rate (SER) is computed for different values of Signal-to-Noise-Ratio (SNR) for the different transmission schemes and the results plotted with the SNR axis on a decibel (dB) scale. It is observed that the spatial multiplexing schemes perform better than the Alamouti scheme in situations where the system power requirements are not high i.e. low SNR and their complexities are lower than the Alamouti scheme for the same transmission rate. Also, the Alamouti scheme can always be used regardless of the channel characteristics i.e. Rayleigh fading, Ricean fading and line-of-sight conditions and because of its higher diversity order; itcan be used for highly sensitive systems where the bit error rate must be low.

Keywords: *Multiple-Input-Multiple-Output(MIMO), Ricean Fading, Spatial Multiplexing, Zero Forcing, V-BLAST, Alamouti*

1. INTRODUCTION

MIMO systems have received large attention over the last few decades. A lot of research has been carried out and solutions have been proposed for improving spectral efficiency and conserving bandwidth and transmit power while maintaining the data rate requirements for present and future communication applications(Goldsmith, 2005). Digital modulation techniques especially the M-ary modulation schemes deliver high data-rates in multipath fading channels as they achieve better bandwidth utilization and give higher data rates compared to other digital transmission systems. When combined with MIMO systems a gain in spectral efficiency is attained. However in mobile communications, the radio channel puts a limit on the performance of communication systems as a consequence of the Shannon theorem and due to various natural phenomena such as multipath propagation, time dispersion and fading. This introduces errors like intersymbol interference and other distortions into the signals transmitted over the wireless channel. To combat errors, various methods of mapping data and symbols to the multiple antennas at the transmitter end have been proposed and researched on.The first attempt to develop Space Time Codes (STC) was presented in (Seshadri and Winters, 1994) and was inspired by the delay diversity scheme of Wittneben (Wittneben, 1993). However, the key development of the STC concept was originally revealed in (Tarokh et al, 1998) in the form of trellis codes, which

required a multidimensional (vector) Viterbi algorithm at the receiver for decoding. These codes were shown to provide a diversity benefit equal to the number of TX antennas in addition to a coding gain that depends on the complexity of the code (i.e. number of states in the trellis) without any loss in bandwidth efficiency. In (D.Gesbert, 2003) a combined Space-Time Block (ST-BC) with MIMO Equalizer (MIMO-EQ) was proposed. In this system, MIMO-EQ equalized the channel into a temporal Inter-symbol Interference (ISI) - free channel and then simple linear processing was used to perform maximum likelihood (ML) decoding for ST-BC. The simulation results showed that the proposed system can achieve the full spatial diversity gain. This was due to the fact that the simple ML decoding of ST-BC required the orthogonality between signals at the receiver. This paper attempts to synthesize the above reviewed works by comparing the performance of the different transmission schemes in the presence of a Ricean fading environment.

2. METHODOLOGY

The MIMO system is modelled with N transmitter antennas and M receiver antennas as shown in Figure 1. In the presence of a rich line-of-sight (LOS), the channel closely follows a Ricean distribution with a factor, K which is the ratio of the signal power in the line-of-sight between the transmitter and receiver pairs and the signal power in other multi-paths (Gesbert, 2014). Let the *1 x N* transmitted signal vector be represented as **s**, and the *M x 1* received signal vector be represented as **y**. Let the *M x N* channel matrix be represented as **H**.
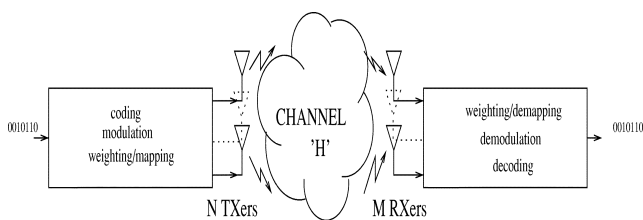
Fig 1.Diagram of a MIMO wireless transmission system

Figure 1 shows a MIMO wireless transmission system. The transmitter and receiver are equipped with multiple antenna elements. Coding, modulation, and mapping of the signals onto the antennas may be realized jointly or separately (Alamouti, 1998). The noise introduced by the system is random and is modeled as an *M x 1* vector, **n** of additive noise terms, assumedi.i.d. complex Gaussian with each element having a variance equal toσ^2. For convenience, we normalize the noise power so that σ^2 is unity(Alamouti, 1998). In the presence of a rich line of sight, the linear system describing the transmission and reception of arbitrary signals is given as (Gesbert, 2014).

$$y = \frac{1}{N}Hs^T + n \qquad (1)$$

Where;

$$H = \sqrt{\frac{1}{K+1}}H_{NLOS} + \sqrt{\frac{K}{K+1}}H_{LOS} \quad (2)$$

Equation (1) describes a single MIMO user communicating over a Ricean fading channel with additive white Gaussian noise (AWGN). It is also worth noting that there is no channel state information at the transmitter (no CSIT) hence the need to transmit at equal powers on all antennas. In (2), the first term corresponds to the non-line-of-sight component of the channel while the second term corresponds to the line-of-sight component which is given by an all-ones *M x N* matrix.*K* is the Ricean factor which depends on the strength of the line-of-sight signal and *T*is the transpose operator. The normalization by *N* isto ensure a fixed total transmit power. Three algorithms for transmitting the data into the channel are systematically applied, namely: spatial multiplexing with zero-forcing (ZF), spatial multiplexing with V-BLAST and Alamouti schemes. In both ZF and V-BLAST schemes 4-QAM modulation is used and in the case of Alamouti schemes 16-QAM modulation is used. This is to maintain the same data rate in each transmission scheme and ensure a fair

comparison of the performance of the algorithms (Alamouti, 1998).

2.1. Alamouti Space-Time Block codes (STBC)

Alamouti (Alamouti, 1998) discovered a remarkable space–time block coding scheme for transmission with two antennas. This scheme supports maximum-likelihood (ML) detection based only on linear processing at the receiver. This scheme was later generalized in (Tarokh et al, 1999) to an arbitrary number of antennas. Here, the basics of Alamouti STBCs will be reviewed as it has been extensively discussed in literature. Figure 2 shows the baseband representation for Alamouti STBC with two antennas at the transmitter.
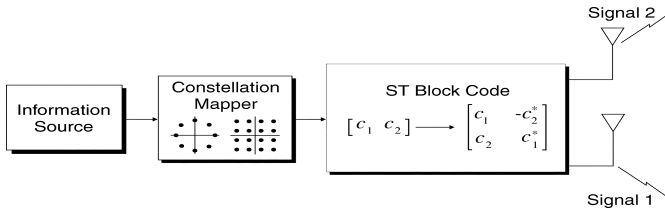
Fig.2. Transmit Diversity with Alamouti Space Time Block Code

The input symbols to the space–time block encoder are divided into groups of two symbols each. At a given symbol period, the two symbols in each group, $\{c_1, c_2\}$ are transmitted simultaneously from the two antennas. The signal transmitted from antenna 1 is c_1 and the signal transmitted from antenna 2 is c_2. In the next symbol period, the signal $-c_2^*$ is transmitted from antenna 1 and the signal c_1^* is transmitted from antenna 2. Let h_1 and h_2 be the channels from the first and second TX antennas to the RX antenna, respectively. The major assumption here is that h_1 and h_2 are scalar and constant over two consecutive symbol periods. It is assumed that the receiver has a single RX antenna. The received signals over two consecutive symbol periods are denoted as r_1 and r_2. The signals can be expressed as (Gesbert et al, 2003):

$$r_1 = h_1 c_1 + h_2 c_2 + n_1 \quad (3)$$

$$r_2 = -h_1 c_2^* + h_2 c_1^* + n_2 \quad (4)$$

Where n_1 and n_2 represent the AWGN and are modelled as i.i.d. complex Gaussian random variables with zero mean and power spectral density $N_0/2$ per dimension. The received signal vector r is defined as $[r_1 r_2]^T$, the code symbol vector c as $[c_1 c_2]^T$ and the noise vector n as $[n_1 n_2]^T$. Equations (3) and (4) can be rewritten in a matrix form as:

$$r = Hc + n \quad (5)$$

Where the channel matrix H is given as

$$H = \begin{bmatrix} h_1 & h_2 \\ h_2^* & -h_1^* \end{bmatrix} \quad (6)$$

H is now only a virtual MIMO matrix with space (columns) and time (rows) dimensions, not to be confused with the purely spatial MIMO channel matrix defined in the previous section. The vector $\mathbf{n}$ is a complex Gaussian random vector with zero mean and covariance $N_0 I_2$. The matrix $\mathbf{C}$ is defined as the set of all possible symbol pairs $\mathbf{c}$ given as $\{c_1, c_2\}$. Assuming that all symbol pairs are equiprobable, and since the noise vector $\mathbf{n}$ is assumed to be a multivariate AWGN, it can easily be deduced that the optimum ML decoder is

$$\hat{c} = arg\,\min_{\hat{c}\,\varepsilon\,c} ||r - H.\hat{c}||^2 \quad (7)$$

It is also straightforward to verify that the SNR for c_1 and c_2 will be

$$SNR = \frac{\alpha.E_S}{N_0} \quad (8)$$

Where;

$$\alpha = |h_1|^2 + |h_2|^2 \quad (9)$$

Hence, a two branch diversity performance (i.e., a diversity gain of order two) is obtained at the receiver. By extension, the Alamouti STBC can be applied to a MIMO system. When the receiver uses M RX antennas, the received signal vector r_m at RX antenna m is (Gesbert et al, 2003).

$$r_m = H_m \cdot c + n_m \quad (10)$$

Where n_m is the noise vector at the two time instants and H_m is the channel matrix from the two TX antennas to the receive antenna. In this case, the optimum ML decoding rule is (Gesbert et al, 2003)

$$\hat{c} = arg \min_{\hat{c} \, \varepsilon \, C} \sum_{m=1}^{M} ||r_m - H_m \hat{c}||^2 \quad (11)$$

The diversity order provided by this scheme is *2M*.

2.2. Spatial Multiplexing with Zero Forcing

In spatial multiplexing, multiple signals are sent into the channel; the receiver learns the channel matrix and inverts it to separate the data (Gesbert, 2014).

Assuming a block of independent data, **C** of size *N x L* is transmitted over the *M x N* MIMO system, the receiver will obtain **Y = H C + N** where **Y** is of size *M x L.*

In order to perform symbol detection, the receiver must unmix the channel, in one of several various possible ways.

Zero-forcing (ZF) techniques use a straight matrix inversion with the resulting decoded symbol matrix $\hat{C}$ given as(Gesbert, 2014):

$$\hat{C} = \sqrt{M} W \, Y \quad (12)$$

Where

$$W = H^{-1} \quad (13)$$

2.4. Spatial Multiplexing using V-BLAST

The V-BLAST method also called 'Onion peeling' method or 'Successive Interference Canceling' in literature is an iterative procedure used to decode each of the transmitted symbols starting with decoding the first received symbol, cancelling it out and decoding successive symbols till only the last symbol is left. It is given by the following procedure:

$$\hat{s}_1 = w_1^H y \quad (14)$$
$$\dot{s}_1 = Slicer(\hat{s}_1) \quad (15)$$
$$y_1 = y - h_1 \dot{s}_1 \quad (16)$$
$$\dot{s}_2 = w_2^H y_1 \quad (17)$$

3   RESULTS AND DISCUSSIONS

In this section, the MIMO system is simulated using MATLAB scripts and function files.The SER-SNR curves are plotted for the different schemes. The plot is madefor two values of Ricean Factor; K = 0dB (No line-of-sight) and K = 20dB (strong line-of-sight). The diversity orders of the 3 schemes correspond to the slopes in the plots, so from figure 4, itcan be deduced that the diversity orders for the 3 schemes are:

ZF: diversity order of 1

V-BLAST: diversity order of a little bit more than 1

Alamouti: diversity order of 4. (For 2 x 2 MIMO)
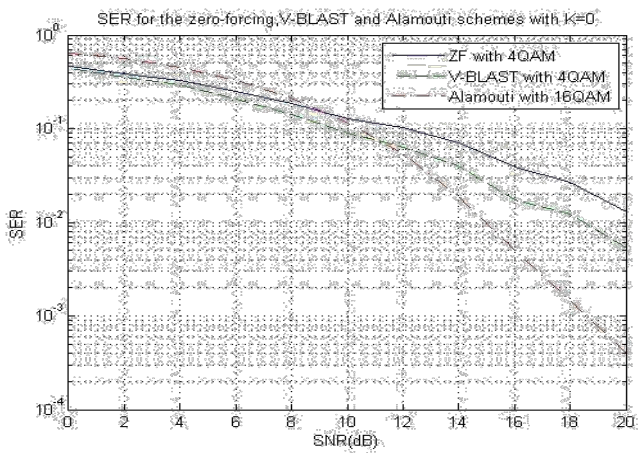
Fig 3. SER-SNR curves for Zero-Forcing, V-BLAST and Alamouti schemes with K= 0.
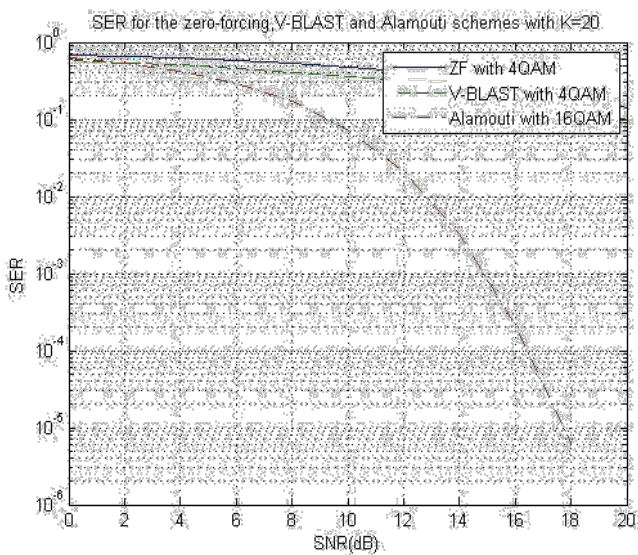
Fig.4. SER-SNR curves for Zero-Forcing, V-BLAST and Alamouti Schemes with K = 20

3.1. SER performance comparison with K=0.

In Figure 3, itis evident that the V-BLAST scheme has a lower SER than the ZF scheme for all values of SNR. This is because the V-BLAST scheme makes use of successive interference cancelling, and consequently the inter-symbol interference in the SINR expression becomes lower during eachiteration of V-BLAST. This leads to a better SER performance. The performance of the Alamouti scheme is the worst at low values of SNR but at high SNR values the Alamouti scheme gives the best performance. This is because the symbols in the 16-QAM constellation are closest to each other compared to 4-QAM and so it is easier to make errors in detecting them and this makes the Alamouti the worst of the 3 when the SNR is not too high, and since the Alamouti scheme has a higher diversity order (in our case Alamouti has a diversity order of 4), the curve of its SER will have a higher slope than the other 2 schemes. At high SNR, the performance of Alamouti is much better.

3.2. SER Performance comparison with K = 20

In Fig. 4, It can be seen that the performance of the ZF scheme and V-BLAST schemes of K is 20 are much worse than that for the case of K is 0. This is because the line of sight component is stronger in the channel and the channel matrix H is "ill conditioned". So in the ZF and V-BLAST scheme the interference and noise will be much amplified and the performances become much worse than the case of K=0.We also notice that the SER performance of Alamouti with K=20 is better than that for the case of K=0. This is due to the fact that first of all, the Alamouti scheme is not by the channel characteristics (it does not matter if the channel is Rayleigh fading or Rician fading or without fading). Secondly since the formula of SER of Alamouti scheme with 16QAM is of the form, $A*\mathrm{erfc}\sqrt{(B.\,SNR)}$ and the erfc() function is concave; it can be shown mathematically that the randomness in channel coefficients and consequently the randomness in SNR will always increase the average SER. This means with a higher value of K, we have less randomness in the channel coefficients and the resulting average SER will decrease. This explains why the Alamouti scheme has a better performance when K is 20.

4   CONCLUSION

In this paper, three mechanisms for transmitting signals into a MIMO system in the presence of Ricean channel fading, have been implemented via simulations in MATLAB. The analyses show thatfor low SNR values, theAlamouti scheme performs worsecompared to the other two schemes. This is because the modulation scheme adopted is 16-QAM and hence there is a higher SER due tocloseness of the symbols in the QAM constellation. On the other hand, the Alamouti scheme outperforms the other two schemes at high SNR values because it fully exploits the diversity in the number of antennas present in the system.The Spatial Multiplexing schemes perform worse in the presence of a strong line-of-sight because the channel gains becomehighly correlated thereby resulting in a higher SER. On the other hand, the Alamouti scheme is insensitive to the nature of the channel conditions and its performance is relativelyunaffected. It can be deduced that the choice of transmission schemes depends on the application. For sensitive, low power applications with minimal retransmission bandwidth, the spatial multiplexing schemes will be the better choice while for high power systems with more retransmission bandwidth, the Alamouti scheme will be the better choice. This paper addresses the single user MIMO communication model. More research needs to be carried out in multi-user MIMO scenarios to establish the performance of these schemes in order to determine the optimal scheme in different channel conditions and SNR ranges.

REFERENCES

A. Goldsmith, (2005) "Wireless Communications"Cambridge University Press.

N. Seshadri and J. H. Winters (1994) "Two schemes for improving the performance of frequency-division duplex (FDD) transmission systems using transmitter antenna diversity," *Int. J. Wireless Information Networks*, vol. 1, pp. 49–60.

A. Wittneben, (1993) "A new bandwidth efficient transmit antenna modulation diversity scheme for linear digital modulation," in *Proc. IEEE ICC'93*, vol. 3, Geneva, Switzerland, pp. 1630–1634

V. Tarokh, N. Seshadri, and A. R. Calderbank, (1998) "Space–time codes for high data rate wireless communication: Performance criterion and code construction," *IEEE Trans. Inform. Theory*, vol. 44, pp. 744–765.

D.Gesbert, M. Shafi et al, (2003)"From theory to practice: An overview Of MIMO space-time coded wireless systems" IEEE *Journal on Selected Areas in Communications*, vol. 21, No. 3, pp. 281-302.

S. Alamouti, (1998) "Space block coding: A simple transmitter diversity technique for wireless communications," *IEEE Journal on Selected Areas in Communications*, vol. 16, pp. 1451–1458.

V. Tarokh, H. Jafarkhani, and A. R. Calderbank, (1999) "Space–time block   codes from orthogonal designs," *IEEE Transactions. Information. Theory*, vol. 45, pp. 1456–1467.

D.Gesbert, (2014) "Advanced Topics in Wireless Communications" "Course notes given at Institut Eurecom, Sophia Antipolis, France".

EFFECT OF DRYING TECHNIQUES ON THE NUTRIENTS OF MORINGA LEAVES

Y. B. Umar*, A. H. Isyaku, I. A. Mohammed-Dabo, S. Bilal, A. H. Mashi and M. S. Adamu

Department of Chemical Engineering, Ahmadu Bello University, Zaria, Kaduna State, Nigeria

* Corresponding Author; E-Mail: yumzebally@yahoo.com, Phone Number:+234(0)8034512713

ABSTRACT

This study investigates the effects of different drying techniques on the nutrients of *Moringa oleifera* leaves. Fresh samples of *Moringa oleifera* leaves were collected, sorted and dried using four different methods viz; freeze-drying, oven-drying, sun-drying and shade-drying. Proximate analysis was carried out on fresh and dried samples for moisture, protein, fibre, fat and carbohydrate content. Elemental analysis was also carried out to determine the presence of iron, magnesium, potassium, calcium and phosphorus. For all the various drying processes, moisture content was observed to reduce from 72.5 % in the fresh sample to 5.88 %, 5.37 %, 6.43 % and 7.23 % for freeze-dried, oven-dried, sun-dried and shade-dried leaves respectively. The proximate composition of the fresh moringa leave and the dried leaves using the 4 different drying methods varied from 7.48 to 8.96 %, 6.34 to 27.56 %, 7.30 to 14.76 %, 1.23 to 9.33 % and 5.15 to 37.20 for fat, crude protein, crude fibre, ash and carbohydrate content respectively. Similarly elemental composition varied from 1.28 to 2.85 %, 2.50 to 5.40 mg/g, 5.17 to 6.27 mg/L, 5.04 to 5.39 mg/L and 2.30 to 4.65 % for Potassium, Phosphorous, Iron, Calcium and Magnesium respectively. The overall assessment of the performance of the four drying methods base on nutrients retention and moisture removal revealed that freeze-drying is most efficient whereas sun drying is the least efficient technique.

Keywords: *Moringa, Freeze-drying, Shade-drying, Sun-drying, Oven-drying, Proximate, Elements*

1. INTRODUCTION

Moringa (*Moringa spp.*) belongs to a monogenetic family, the Moringacae. *Moringa oleifera* is also known as "Miracle Tree" (Kumari, 2006). It is the best known of the thirteen species of the genus Moringacae. *Moringa oleifera* has a host of other country specific vernacular names (Kumari, 2006) such as *Babati* in Ewe, Ghana; *Zogalla* in Hausa, Nigeria, *Shingo* in Swahili, Kenya; *Alim* in Arabic, Sudan and Chad and many more. Moringa tree is known for its significance around the world. It is a small fast-growing ornamental tree. The trees is reported to originate from Agra and Oudh in North Western region of India to South of the Himalayan Mountains (Ramachandran, 1980). Presently it is widely cultivated in many countries of Africa, Asia and South America regions and the Middle East, Central and South America, Sri Lanka, India, Mexico, Malaysia and the Philippines (Gupta, 2007). Various varieties of *Moringa oleifera* have been developed to meet the tastes of local populations (Anwar, 2003). Moringa leaves are edible and are of high nutritive value.

Until recently, *moringa oleifera* has been one of many underutilized vegetables found in Nigeria. Almost every part of the moringa plant has nutritional value. The pods, the seeds and the roots are eaten and used for seasoning, in some cases it is used as nutritional supplement. The seeds are used as a flocculant in water purification and as a source of highly stable non-drying oil, called Ben oil (Broin and Armelle, 2010). The oil has been reportedly used for lubricating watches and other delicate machinery. Moringa may also be used in fish and poultry feeds. The bark yields a blue dye which has the potential to be used for tanning of clothes. The wood can be used for paper production. Significant part of the plant is the leaves, which are highly nutritious; as it is a significant source of beta-carotene, vitamin C, protein, iron and potassium. *Moringa oleifera* leaves is reported to contain more of vitamin A than carrot, more vitamin C than oranges, more potassium than bananas and the protein quality compares very well with that of milk and eggs (Gardener and Ellen, 2002). Apart from food and seasoning, Moringa leaves are also used for animal fodder, cosmetics and medicine (Rebecca, 2006).

Drying is one of the methods of food preservation employed to reduce losses in quantity and quality (Habou *et al*., 2003). The drying of green leafy vegetables such as *Moringa oleifera* is very important so as to preserve its numerous nutrients, easy storage and transportation. Processing plant vegetable makes it safe for consumption because the effects of pathogens is greatly minimized. The processing of vegetable food matter like moringa leaves are affected by a number of factors such as sensitivity of the nutrient to light, heat and oxygen (Morris *et al*., 2004). Vegetables have been dried using numerous techniques (Mishra *et al*., 2012; Gyamfi *et al*., 2011). These techniques include air-drying, freeze-drying, sun drying or solar-drying and oven drying. Each of these techniques have varying significance on the quality and availability of minerals, vitamins and other essential nutrients. Several researches have documented losses of nutrients from vegetables during drying (Yadav and Sehgal, 1997) and cooking (Kachik *et al*., 1992; Kidmose *et al*., 2006). The micronutrient in dried moringa leaves was also reported (Mahmood *et al*., 2010; Price, 2007).

This study was aimed at determining the effect of four different drying techniques (which includes shade drying, freeze drying, oven drying and sun drying) on the proximate and elemental nutrient composition of *moringa oleifera* leaves sourced from Zaria in Northern Nigeria.

2. METHODOLOGY

2.1. Collection and Identification of Plant Sample

Fresh, mature and healthy leaves of *moringa oleifera* were used for this study. The leave samples were collected from '*Panhauya'* village in Zaria Kaduna state in Northern Nigeria in the morning when the average temperature was 22°C. The samples were collected at the same time to avoid the effect of environmental factors. The samples were collected at the same place and from the same tree to avoid the effect of soil variation on the micronutrient content of the leaves. The samples collected were taken to the laboratory for further analysis.

2.2. Preparation of Leaves for Drying

Fresh, green, un-wilted, and non-insect infested leaves were selected while the bruised, discoloured, decayed and wilted leaves were discarded before washing. The stalks of the leaves were cut from the main branches and the leaves washed thoroughly with plenty of water to remove all the adhering dust and dirt particles. Thin branches of the moringa leaves were carefully handled during washing for easy handling of the leaves. The excess water was drained out from leaves. After removing the excess moisture, all the stems and branches of the leaves were removed and only the leaves of *moringa oleifera* were dried.

2.3. Drying

The fresh washed leaves were weighed, divided into five portions and the four drying methods; freeze drying, shade drying, sun drying and oven drying were employed to dry the samples. The last portion was immediately taken for analysis as the control sample. The sample for sun drying was placed on tray and covered with a net to keep off dust and insects while exposing it to direct sunlight between 9.00 am to 5.00 pm daily for 7 days. Sample for shade drying was spread on a tray under a net and dried for 14 days in a well ventilated room where natural current of air and an average room temperature of 25 °C were prevalent. The samples for oven drying were similarly spread and then subjected to a steady temperature of 60 °C for 4 hrs in the oven (PETERSON SCIENTIFIC Digital Vacuum Oven). Freeze drying the fourth sample was performed by pre-freezing the sample for an hour and then drying for about 6 hrs at sample temperature of 15 °C and condition temperature of -60 °C.

2.4. Determination of nutritional composition

The fresh and the dried leaves were analysed for proximate composition (moisture, protein, fat, fibre, carbohydrate and ash), using the methods described by Association of Official Agricultural Chemists (AOAC, 2000). Similarly, elemental nutrients (calcium, phosphorus, potassium, iron, and magnesium) of the samples were determined according to methods recommended by the same body.

Atomic Absorption Spectrophotometer (AA500 by PG Instruments) was used to determine Iron (Fe), calcium (Ca) and magnesium (Mg). Phosphorus (P) was determined using a Sherwood Calorimeter 257 while Potassium (K) was determined with a JENWAY flame photometer.

3. RESULTS AND DISCUSSIONS

Table 1 shows the proximate composition of moringa leave samples while Table 2 shows the elemental composition of the moringa under the four different techniques.

3.1. Proximate analysis

The proximate analysis consists of experimental determination of moisture, fat, crude protein, crude fibre, ash and carbohydrate.

Table 1: Proximate composition of moringa leave samples from different drying techniques

Sample	Moisture content (%)	Fat (%)	Crude protein (%)	Crude fibre (%)	Ash (%)	Carbohydrate (%)
Fresh leave	72.50	7.48	6.34	7.30	1.23	5.15
Freezedried	5.88	8.15	27.02	13.39	8.36	37.20
Ovendried	5.37	8.86	24.94	14.76	9.33	36.74
Sundried	6.43	8.96	26.06	12.65	8.92	36.98
Shade dried	7.23	8.62	27.56	12.49	8.41	35.69

Moisture is a basic requirement for the growth and development of vegetable pests and bacteria. Since leafy vegetables are seasonal and highly perishable, special processing (e.g. drying) is required to minimize their vulnerability to bacteria and pests attack, which could bring about decaying or losing of nutritional values. A reduction in the moisture content of the fresh leaves from 72.50 % to a minimum amount of 5.37 % was achieved by oven drying. Freeze drying, sun drying and shade drying of moringa leaves also reduced the moisture content of the leaves to 5.88, 6.43, and 7.23 % respectively.

The crude protein composition ranged from 6.34 to 27.56 % with shade dried samples having the highest value of 27.56 % and the fresh leaves samples having the least at 6.34 %. The freeze dried, oven dried and sun dried samples had their protein content as 27.02, 24.94, and 26.06 % respectively as shown in Table 1. Apparently, drying of

moringa oleifera leaves increases the protein content. This is because the loss in moisture content in the processed leavesincreases the nutrient density of the leaves. The oven dried had the least value of protein content among the dried samples and this might be as a result of the high temperature in the oven. Air dried and freeze dried sample have relatively higher percentage of protein content perhaps, because of the lower temperature involved in the drying processes. Moringa oleifera is a good source of protein having a protein content twice that found in yoghurt (Fuglie, 1999).

Fat was also retained in the dried samples of moringa leaves. The fresh leaves have a fat content of 7.48 %. Whereas the freeze dried, oven dried and shade dried moringa leaves contain 8.15, 8.86, and 8.62 % respectively. Sun dried leaves however, demonstrated highest percentage of 8.96 % fat. The fat content of moringa leaves is relatively low compared to the protein content. This suggests that the leave can be consumed as a better dietary for individuals that require low fat diet. Similarly, the analysis for crude fibre shows that it was preserved in the dried leaves. Fresh leaves sample had the least fibre content of about 7.30 % while the oven dried moringa leaves had the highest content of 14.76 %. The result implies that the fibre concentration almost doubled by drying the leaves. The freeze dried, sun dried and shade dried moringa leave had their crude fibre content as 13.39, 12.65 and 12.49 % respectively. Fibre has been reported to cleanse digestive tract by removing potential carcinogens from the body and hence prevents the absorption of excess cholesterol. In addition, fibre adds bulk to food and reduces the intake of excess starchy food, which is a characteristic dietary for low income earners (Sodamade et al., 2013). Hence supplementing dietary with moringa leaves will guard against metabolic conditions such as hypertension and diabetes mellitus.

The ash content ranges from 1.23 - 9.33 %. The fresh leave sample had ash content of about 1.23 %. Oven dried

moringa leaves again has the highest ash content of about 9.33 % followed by sun dried (8.92 %) then shade dried (8.41 %,) and lastly freeze dried samples (8.36 %). The carbohydrate content of the five samples of moringa leaves analysed in this study ranged between 5.15-37.20 %. The fresh leaves had 5.15 % carbohydrate. Freeze dried leaves (37.20 %) has the highest carbohydrate content followed by sun dried (36.98 %) then oven dried (36.74 %) and shade dried leaves has the least (35.69 %). Carbohydrate content increased as a result of drying by at least 6 times the initial concentration. Green vegetables and leaves are important sources of carbohydrates. Mustapha and Babura (2009) reported that the carbohydrate level in *Moringa* is comparatively higher (10.1 %) when compared to other vegetables such as carrot (8.7 %) and sorrel (7.1 %).

3.2. Elemental analysis

The elemental analysis consists of the determination of the elements present in a sample e.g. iron, potassium, calcium, magnesium, nitrogen, sulphur, manganese, zinc, phosphorus, sodium etc. In this study, only five elements were considered which includes iron, potassium, phosphorus, magnesium and calcium. Table 2 shows the result of the elemental analysis of the fresh leave and the four different drying methods employed.

Table 2: Elemental composition of moringa leave samples from different drying techniques

Sample	Potassium (%)	Phosphorus (Mg/g)	Iron (Mg/L)	Magnesium (Mg/L)	Calcium (%)
Fresh leaves	1.28	2.50	5.17	5.04	2.30
Freeze drying	2.40	5.40	6.27	5.19	4.65
Oven drying	1.60	3.56	5.27	5.35	3.20
Sun drying	2.35	0.45	5.33	5.28	3.95
Shade drying	2.85	4.83	6.17	5.39	4.23

The potassium content of the fresh moringa leaves and the dried leaves using the four drying methods varied from 1.28 % to 2.85 %. The fresh leaves had the lowest value of 1.28 % while the shade dried leaves had the highest value of 2.85 %. The freeze dried, oven dried, and sun dried moringa leaves had potassium content of 2.40 %, 1.60 %, and 2.85 % respectively. From the result it can be seen that

reducing the moisture content of moringa leave had effect on the potassium concentration. The dried leaves had more potassium content than the fresh/unprocessed leave. Among the dried leaves, the oven dried sample had the lowest value of potassium content; this was due to the high heat applied for the drying of the leaves. The potassium content of moringa leave obtained in this study is reasonably close to the 3.65 % reported by Moyo *et al.*, (2011). Potassium is a mineral that is needed by the body system to work properly. It is a type of electrolyte. The human body needs potassium to build proteins, break down and use carbohydrates, build muscle, maintain normal body growth, control the electrical activity of the heart, control the acid-base balance etc. The potassium content of moringa leave is said to be three times that contained in banana and as such can serve as a good food supplement to the body (MedlinePlus, 2015).

The phosphorus concentration in the dried moringa leaves increased by more than twice that available in the fresh moringa leaves by the removal of moisture. The fresh leaves have a low concentration of 2.50 mg/g. Freeze dried leaves had the highest value of 5.40 mg/g and the sun drying has the least with a quantity of 3.56 mg/g. The dried moringa leaves have a higher value of phosphorus content than the fresh leaves. This is attributed to the removal of the moisture to avoid degradation of the leaves. The sun dried had the lowest value of phosphorus for the dried samples because of the heat applied. Phosphorus is a mineral that makes up 1 % of a humans' total body weight. It is present in every cell of the body. It is needed for the body to make protein for maintenance, growth, and repair of cells and tissues (MedlinePlus, 2015).

The iron content of the fresh moringa leave and the dried leaves using the 4 different drying methods varied from 5.174 mg/L to 6.267 mg/L. The fresh leaves had the lowest value of 5.174 mg/L while the freeze dried leaves had the highest value of 6.267 mg/L. The oven dried, sun dried, and shade dried moringa leaves had iron content value of

5.274 mg/L, 5.333 mg/L, and 6.167 mg/L respectively. The same trend that was observed for the phosphorus content was also observed for the iron content of the moringa leave. It was observed that when the temperature used for dehydration is reduced, the iron content of the leave increases. The human body needs iron to make the oxygen-carrying proteins haemoglobin and myoglobin. Haemoglobin is found in red blood cells and myoglobin is found in muscles (MedlinePlus, 2015). Magnesium content of the fresh moringa leaves and the dried leaves ranged from 5.035 mg/L to 5.385 mg/L. The fresh leave had the lowest value of 5.035 mg/L while the shade dried leaves had the highest value of 5.385 mg/L. The freeze dried, oven dried, and sun dried moringa leaves had magnesium content of 5.185 mg/L, 5.345 mg/L, and 5.275 mg/L respectively. Magnesium is needed for more than 300 biochemical reactions in the body. It helps to maintain normal nerve and muscle function, supports a healthy immune system, keeps the heartbeat steady, and helps bones remain strong. It also helps regulate blood glucose levels and aid in the production of energy and protein (MedlinePlus, 2015). Calcium content of the fresh and dried moringa leaves varied from 2.30 % to 4.65 % (Table 2). The fresh leaves had the lowest value of 2.30 % while the freeze dried leaves had the highest value of 4.65 % followed by shade dried samples with 4.23 %. The sun dried and oven dried samples had the least content, 3.95 % and 3.20 % respectively. The same trend that was observed in the phosphorus and iron content was also observed in the calcium content of the moringa leave i.e. freeze dried > shade dried > sun dried > oven dried. The calcium content of *moringa oleifera* obtained in this study is within significant range with that reported by Moyo *et al.* (2011) of 3.65 %. Calcium is one of the most important minerals required by the human body. Calcium helps form and maintains healthy teeth and bones. Proper levels of calcium over a lifetime can help prevent osteoporosis. Moringa leaves are said to contain four times the calcium

of milk (MedlinePlus, 2015). This is an indication of the numerous nutrients available in the leaves.

3.3. Overall performance of the four drying techniques

The overall performance of individual drying methods was statistically analysed using Microsoft excel ranking and are presented in figure 1.
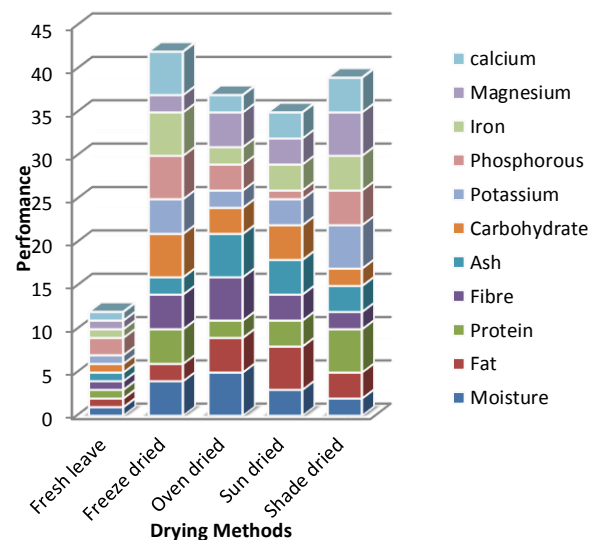
Fig.1: Performance of drying techniques base on moisture removal and nutrient concentration

The major drying techniques analysed in this study were freeze drying, oven drying, sun drying and shade drying. A common trend from Figure 1 shows the cumulative performance of the four drying methods in the order; freeze drying > shade drying > oven drying > sun drying. The cumulative performance was determined as a function of nutrient retention ability and moisture reduction capability. Sun drying and oven drying reduces the concentration due to heat. Thus freeze drying retained best the nutrients due to absence of heat and photo reaction.

4. CONCLUSION

Moringa oleifera leaves were dried using the methods of freeze-drying, oven-drying, sun-drying and shade-drying. Proximate and elemental analyses of the dried samples and that of fresh samples were carried out to investigate the effects of the four drying techniques on the nutrients of

moringa oleifera leaves. The major nutrients considered for the investigation were crude protein, crude fibre, fat, carbohydrate, iron, magnesium, potassium, calcium and phosphorus. Fresh *moringa oleifera* leaves have been found to be rich in all these nutrients and even richer when properly dried. In the various drying processes, moisture content reduction from 72.5 % in the fresh sample to 5.88 %, 5.37 %, 6.43 % and 7.23 % for freeze-dried, oven-dried, sun-dried and shade-dried leaves respectively were achieved. Of the four drying methods analysed, freeze dried samples recorded highest cumulative nutrient retention in the order: freeze dried > shade dried > oven dried > sun dried.

REFERENCE

Anwar, F. and Bhanger, M. I., (2003). "Analytical characterization of moringa oleifera seed oil grown in temperate regions of Pakistan". Journal of Agricultural and Food Chemistry. 51 6558–6563.

AOAC, (2000). "Official method of analysis". 16th edition. Washington D.C: Association of Official Analytical Chemists.

Broin, M. and Armelle, S. S. (2010). "Growing and processing moringa". Moringa Association of Ghana (MAG), Accra Ghana.

Fuglie, L. J., (1999). "The miracle tree: *moringa oleifera*: natural nutrition for the tropics". Church World Service, Dakar. 68 pp.; revised in 2001 and published as The Miracle Tree: The Multiple Attributes of Moringa, 172 pp.

Gardener and Ellen, (2002). "Moringa tree has many uses, from food to firewood". Yumasun Portal market, Moringa Tree Powder.

Gupta. R., Dubey,D. K. Kannan,G. M. and Flora,S. J. S., (2007). "Concomitant administration of Moringa oleifera seed powder in the remediation of arsenic-induced oxidative stress in mouse". Cell. Biol. Int. 31 44–56.

Gyamfi, E. T., Kwarteng, I. K., Ansah, M. O., Anim, A. K., Ackah, M., Kpattah, L. and Bentil N. O. (2011). "Effects of processing on Moringa oleifera". Proceedings of the International Academy of Ecology and Environmental Sciences, June 2011: 179-185.

Habou, D. A., Asere A. and Alhassan A. M., (2003). "Comparative study of the drying rate of tomatoes and pepper using forced and natural convection solar dryers". Nigeria Journal of Renewable Energy, 14: 36-40.

Kachik, F., Goli, M., Beecher, G. R., Holden, J. Lusby, W. R., Tenorio, M. D. and Barrera, M. R., (1992). "Effects of food preparation on qualitative and quantitative distribution of major carotenoids constituents of tomatoes and several green vegetables". Journal of Agricultural and Food Chemistry, 40: 390-398.

Kidmose, U., Yang, R. Y., Thilsted, S. H., Christensen, L. P. and Brandt, K. (2006). "Content of carotenoids in commonly consumed Asian vegetables and stability and extractability during frying". Journal of Food Composition and Analysis, 19: 562-571.

Kumari, P., Sharma, P., Srivastava, S. and Srivastava, M. M. (2006). "Biosorption studies on shelled Moringa oleifera Lamarck seed powder: Removal and recovery of arsenic from aqueous system". Int. J. Miner. Process. 78 131–139.

Mahmood, K. T., Mugal, H., and Haq, I., (2010). "Moringa oleifera: a natural gift-A review". Journal of Pharm. Sci. & Res. Vol.2.

MedlinePlus. (2015). Medical Encyclopedia. Available Online at http://www.nlm.nih.gov/medlineplus/encyclopedia.htm. Retrieved on May 20, 2015.

Morris, A., Barnett, A. and Burrows, O. J., (2004). "Effect of processing on nutrient content of foods".Caj articles, 37 (3): 160-164.

Moyo, B., Masika, P. J., Hugo, A. and Muchenje, V. (2011). "Nutritional characterization of Moringa (Moringa oleifera Lam.) leaves, South Africa". African Journal of Biotechnology Vol. 10(60), pp. 12925-12933.

Mustapha, Y. and Babura, S.R. (2009). Determination of carbohydrate and β-carotene content of some vegetables consumed in Kano metropolis, Nigeria. Bayero Journal of Pure and Applied Sciences, 2(1): 119 - 121

Price, M. L., (2007). "The Moringa Tree". Moringa-An Echo Technical Note.

Ramachandran, C., Peter, K. V.,Gopalakrishnan, P. K., (1980). "Drumstick (Moringa oleifera) a multipurpose Indian vegetable". Econ. Bot. 34, 3, 276–283.

Rebecca, H. S. U., Sharon, M., Arbainsyah, A. and Lucienne, D., (2006). "Moringa oleifera: medicinal and socio-economic uses". International Course on Economic Botany, September 2006. National Herbarium Leiden, Netherlands. pp: 2-6.

Sodamade, A., Bolaji, O. S. and Adeboye, O. O. (2013). "Proximate Analysis, Mineral Contents and Functional Properties of MoringaOleifera Leaf Protein Concentrate". Journal of Applied Chemistry.Vol. 4, Issue 6 PP 47-51.

Yadav, S. K. and Seghgal, A., (1997). "Effect of home processing on ascorbic acid, beta carotene content of bathua (Chenopodiumalbum) and fenugreek (Trigonellafoenungraecum) leaves". Plant Foods for Human Nutrition, 50: 239-247.

Evaluation of Mechanical Properties of Aluminium Casting using Sand Deposits in Niger State

Katsina Christopher BALA[1]* Jabiru SHUAIBU[2], Matthew S. ABOLARIN[3]

[1,2,3]Department of Mechanical Engineering, Federal University of Technology, P.M.B. 65 Minna, Nigeria
*Corresponding Author's Email Address: katsina.bala@futminna.edu.ng, Phone Number: +2348035980302

ABSTRACT
Mechanical properties of aluminium casting using sands from GidanMangoro, Tagwai Dam,TunganMallam,Wuya and Zungeru in Niger State of Nigeria was evaluated according to the American Foundry Society (AFS) standard. Tensile, Hardness and Metallographic tests were carried out on the aluminium cast specimens produced from the five different sand samples. The results obtained for the aluminium alloy cast compared favourably with standard values. Hence the sand deposits can be used for casting of aluminium products.

Keywords:S*and Casting;Tensile strength;Aluminium;*

1. INTRODUCTION

Sand casting, otherwise known as sand moulded casting, is a metal casting process whereby sand is used as the mould material. It is relatively cheap and sufficiently refractory for steel foundry use. Khan (2005) identifies sand casting as the most widely used casting process in the casting industry, worldwide. Abolarin*et al* (2010) share the view in stating that sand is the major moulding material used in casting all over the world and it is used for the production of all types of metals casts both ferrous and nonferrous metals. In explaining the reason for the high utilization of sand casting, Aweda and Jimoh (2009) noted the particle size of sand which is packed finely and tightly together provides an excellent surface for the mould. A large variety of moulding materials is used in foundries for manufacturing of moulds and cores. They include moulding sand, system sand or backing sand, facing sand, parting sand, and core sand. The choice of moulding materials is based on their processing properties. The properties that are generally required in moulding materials are; Refractoriness, Permeability, Green Strength, Dry Strength, Hot Strength, Collapsibility, Bala and Khan (2013).

The much desired development of Nigeria can only be achieved through industrialization and the back bone of any industrialized country is very much dependent on its production capacity from the availability of raw materials to the technology utilized in transforming the raw materials to finished products. Nigerian economy over the years has continue to depend on oil as the major source of revenue neglecting other sectors that would boost its industrial and economic development, Abolarin*etal* (2004). The abundance of mineral deposits all over Nigeria is greatly underutilized, sand being one of them. Asuquo*etal* (2013) in investigating the nature and quality of Zircon sand from Jos Plateau State and sand samples from Idah, Kogi State for foundry application, noted that Nigeria is blessed with large quantity of natural resources that have numerous applications which can be used in producing expensive High Performance Engineering equipment, which are not being utilized to the optimum.

Nigeria is aiming to be among the twenty most developed nations by the year 2020, this can only be achieved through rapid industrialization and this cannot be achieved without sufficient production that would serve the country and even provide for export to other nations. Sheidi (2012) noted that the production of castings is necessary for the development of every nation, as almost all human aspect is reliant upon casting of equipment in construction, transportation, petroleum, mining, farming, and in water supply. Nuhu (2008) noted the significance of Ajaokuta steel rolling company situated in Kogi state operating at

full capacity will draw a large number of ancillary and small to heavy industries to the region that require large foundry plants for the spare and completely knocked down parts.

Niger state with a land mass of 99,000 km^2 situated in central Nigeria and also the largest state in terms of land mass in Nigeria has tremendous potential in the casting industry if only it would be harnessed properly. The growing desire for increase in local content in the production industries and the quest for rapid industrialization in Nigeria necessitates that more and more local materials be soughtto replace imported materials. Shuaibu (2014) investigated the properties of sand collected from GidanMangoro,Tagwai Dam, TunganMallam, Wuya and Zungeru ofNiger state and found that the sand deposit could be used for casting purposes and other foundry applications. This paper presents mechanical properties of aluminium casting using the moulding sands of GidanMangoro, Tagwai Dam, TunganMallam, Wuya and Zungeru.

2. METHODOLOGY

Sand samples were collected from each of the location and used to produce moulds in its natural state i.ewithout the addition of bentonite and other additives because the sand samples were observed to have high clay content to act as binder. Wooden patterns of rectangular shape (length = 150mm, breadth = 30mm height = 6mm) and cylindrical

shape of diameter 30mm and height 150mm were made.The rectangular pattern was used to produce cast for hardness test and microstructure analysis, while the cylindrical pattern was used to produce cast for tensile test. The aluminium alloyAA6063(Al-Si-Mg) used for the experiment was obtained from the Nigerian Aluminium Extrusion Company, Lagos. The chemical composition of the aluminium alloy is presented in Table 1.

2.1. Melting and Casting Processes

The alloy of aluminium was melted using a fuel-fired crucible furnace. The molten alloy was thoroughly stirred and slag removed at a pouring temperature of 680°C. Melting of the aluminium alloy took an hour and fifteen minutes. A ladle was used to scoop the molten metal and poured into the sand mould and allowed to solidify and cool. The solidified cast was then removed from the mould.

2.2. Tensile Test Procedure

Tensile test was carried out using the Universal Testing Machine at the Strength and Materials Laboratory, Ahmadu Bello University, Zaria, Nigeria. The aluminium cast was machined to ASTM E-8 standard size in dimension for tensile strength testing of gauge length of 30mm, Ayoola*etal* (2012). The test piece was inserted into the jaws of the universal testing machine and gripped firmly.

Table 1:Chemical Composition AA6063

Alloying Element	Al	Si	P	Ca	Ti	V	Cr	Mg	Mn	Fe	Ni	Cu	Zn	Pb	As	Sn
Percentage Composition	87.45	10.87	0.2	0.05	0.019	0.12	0.068	0.20	0.29	0.27	0.007	0.034	0.015	0.007	0.06	0.34

Tensile force was then applied gradually using 5kN load, the loading was applied continually at steady rate until the aluminium cast fractured and failed as shown in Plate I. The maximum load before fracture was read and recorded. The fractured test piece was removed from the universal

testing machine. The fractured parts were put together to enable thedetermination of the increase in length as well as the necking diameter for the calculation of elongation and

reduction in area.

Plate I: Alumiunm Cast Samples after Tensile Tests

Plate II: Aluminium Cast Samples showing Indention of Hardness Tests

2.3. Hardness Test Procedure

Hardness test is carried out to ascertain the level or degree of resistance of material to wear, cutting, crushing when the material is under loading. Hardness test was carried out at the foundry laboratory in Federal Institute Industrial Research Oshodi, Nigeria using a Brinnel Hardness testing machine. The aluminium specimen was placed in position under the testing machine. The test was carried out using a 10mm diameter steel ball. The test piece was then brought into contact with the steel ball with the gradual application of force. The loading was done until a clear indention was made. After the indention had been made, the load was removed and the steel ball removed from the top of the aluminium cast test piece leaving an indention on the cast as shown in Plate II. The diameter of the indention was measured using a Venier calliper and the force applied was recorded.

2.4. Metallographic Test Procedure

The microstructure or metallographic test was carried out at the Metallurgical and Materials Engineering Laboratory of University of Lagos, Nigeria. The cast aluminium test piece was cut and polished to a good smooth surface using aBelt Grinder(B.G-20) with fine grades of abrasive papers to ensure better surface finish. The aluminium test specimen was then washed in warm water, rinsed thoroughly and allowed to dry. Etching was done using a chemical reagent of 0.5 % hydrofluoric acid after which it was allowed to dry before placing the specimen under the microscope to view and record the microstructure of the surface at a magnification of x400μm.

3. RESULTS AND DISCUSSIONS

3.1. Mechanical Test Results

The mechanical tests results for the aluminium casts from the five different sands samples tested include,tensile strength, hardness, elongation and reduction in cross sectional area are presented in Tables 2 to 6.

Table 2: Mechanical Tests Results of Aluminium Cast Sample Using GidanMangoro Sand

S/No	Original Length (mm)	Final Length (mm)	Elongation (%)	Original Diameter (mm)	Final Diameter (mm)	Reduction Area (%)	Ultimate Tensile Stress (N/mm^2)	Average Elongation (%)	Average Reduction Area (%)	Average Ultimate Tensile Stress (N/mm^2)	Hardness (HB)
1	30	31.25	4.17	6.00	5.85	4.94	132.45	4.54	5.59	128.44	44.14
2	30	31.25	4.17	6.00	5.82	5.91	116.32				
3	30	31.58	5.27	6.00	5.82	5.91	136.55				

Table 2 presents the mechanical test results of GidanMongoro aluminium cast sample. The average

ultimate tensile stress of 128.44 N/mm^2, average percentage elongation of 4.54 %, also an average reduction

area of 5.59 % and Brinell hardness number of 44.14.

Table 3: Mechanical Tests Results of Aluminium Cast Sample Using Tagwai Sand

S/No	Original Length (mm)	Final Length (mm)	Elongation (%)	Original Diameter (mm)	Final Diameter (mm)	Reduction Area (%)	Ultimate Tensile Stress (N/mm^2)	Average Elongation (%)	Average Reduction Area (%)	Average Ultimate Tensile Stress (N/mm^2)	Hardness (HB)
1	30	31.25	4.17	6.00	5.85	4.94	120.23	4.54	5.26	118.81	39.34
2	30	31.25	4.17	6.00	5.85	4.94	124.32				
3	30	31.58	5.27	6.00	5.82	5.91	111.89				

Table 3 presents the mechanical test results of Tagwai Dam aluminium cast sample. The average tensile stress of 118.81 N/mm^2, average percentage elongation of 4.54 %, also an average reduction area of 5.26 % and Brinell hardness number of 39.34.

Table 4 presents the mechanical test results of TunganMallam aluminium cast sample. The average tensile stress of 129.26 N/mm^2, average percentage elongation of 4.90 %, also an average reduction area of 4.94 % and Brinell hardness number of 42.26.

Table 4: Mechanical Tests Results of Aluminium Cast Sample Using TunganMallam Sand

S/No	Original Length (mm)	Final Length (mm)	Elongation (%)	Original Diameter (mm)	Final Diameter (mm)	Reduction Area (%)	Ultimate Tensile Stress (N/mm^2)	Average Elongation (%)	Average Reduction Area (%)	Average Ultimate Tensile Stress (N/mm^2)	Hardness (HB)
1	30	31.58	5.27	6.00	5.85	4.94	136.76	4.90	4.94	129.26	42.26
2	30	31.25	4.17	6.00	5.85	4.94	121.95				
3	30	31.58	5.27	6.00	5.85	4.94	131.07				

Table 5: Mechanical Tests Results of Aluminium Cast Sample Using Wuya Sand

S/No	Original Length (mm)	Final Length (mm)	Elongation (%)	Original Diameter (mm)	Final Diameter (mm)	Reduction Area (%)	Ultimate Tensile Stress (N/mm^2)	Average Elongation (%)	Average Reduction Area (%)	Average Ultimate Tensile Stress (N/mm^2)	Hardness (HB)
1	30	31.58	5.27	6.00	5.85	4.94	123.17	4.90	5.26	114.17	39.25
2	30	31.25	4.17	6.00	5.82	5.91	102.64				
3	30	31.58	5.27	6.00	5.85	4.94	116.70				

Table 5 presents the mechanical test results of Wuya aluminium cast sample. The average tensile stress of 114.17 N/mm^2, average percentage elongation of 4.90 %, also an average reduction area of 5.26 % and Brinell hardness number of 39.25.

Table 6 presents the mechanical test results of Zungeru aluminium cast sample. The average tensile stress of 114.99 N/mm^2, average percentage elongation of 4.71 %, also an average reduction area of 5.59 % and Brinell hardness number of 39.66.

Table 6: Mechanical Tests Results of Aluminium Cast Sample Using Zungeru Sand

S/No	Original Length (mm)	Final Length (mm)	Elongation (%)	Original Diameter (mm)	Final Diameter (mm)	Reduction Area (%)	Ultimate Tensile Stress (N/mm^2)	Average Elongation (%)	Average Reduction Area (%)	Average Ultimate Tensile Stress (N/mm^2)	Hardness (HB)
1	30	31.58	5.27	6.00	5.82	5.91	102.57	4.71	5.59	114.99	39.66
2	30	31.25	4.17	6.00	5.85	4.94	127.43				
3	30	31.41	4.70	6.00	5.82	5.91	114.99				

3.2. Metallographic Test Result and Analysis

The metallographic results show the microstructures of the casts from the five different sand samples as shown in plates 1 to 5. The microstructures generally consists of fine crystals of aluminium (Al), magnesium silicide (Mg$_2$Si), and Al-Mg$_2$Si phases. These structures basically consists of primary alpha solid solution of magnesium silicate in rich solid aluminium (α)) in a matrix of eutectic magnesium silicate (Mg$_2$Si). The aluminium rich portion of the Al-Mg$_2$Si is a precipitation of the magnesium silicide (Mg$_2$Si). The primary solid solution of silicon in aluminium is revealed in white patches while the eutectic magnesium silicide (Mg$_2$Si) is seen as dark patches in the micrographs in Plates 1-5. There is also a very thin gray structure indicating the presence of Fe$_3$SiAl$_2$. TunganMallam sand shows white patches of primary alpha solid solution of silicon in aluminium in matrix form (α) is visible but it is not as pronounced as that of GidanMangoro in Plate1. Similar observation shows that Tagwai dam area (Plate 3) sand has more white patches in Plate 3 than in Plate1. Plate 4 and 5 shows the microstructure of aluminium cast produced from Wuya sand. It shows similar characteristics in terms of primary alpha solid solution of silicon in aluminium (α) in matrix form and magnesium silicide (Mg$_2$Si) in the eutectic state with the microstructure of Plate 3.
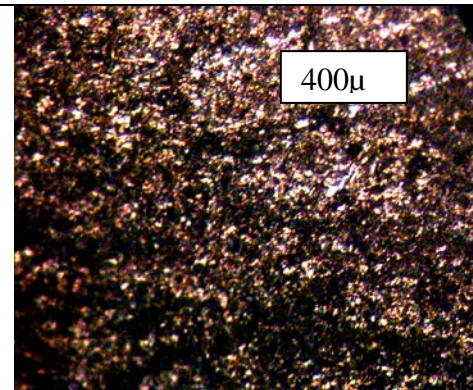

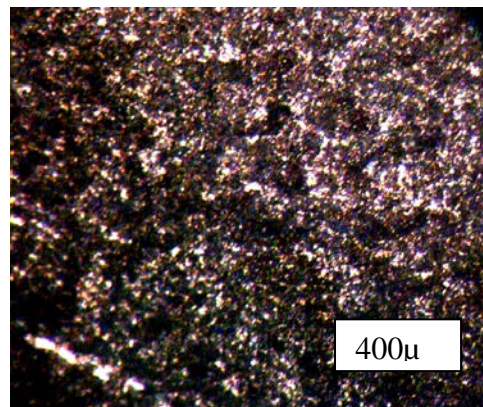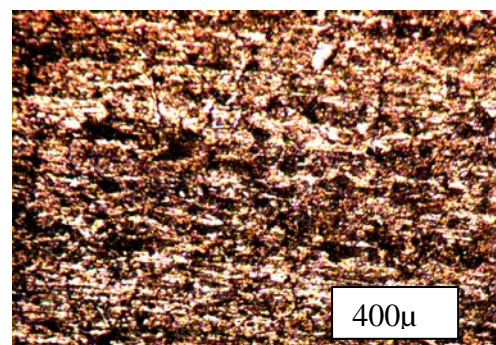Plate 1. Micrograph of etched Aluminium test sample using GidanMangoro sand

Plate 2. Micrograph of etched Aluminium test sample using TunganMallam sand

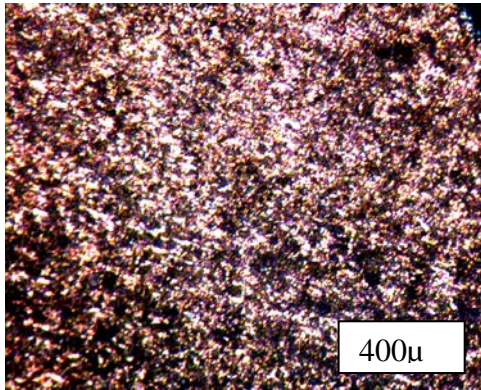Plate 3. Micrograph of etched Aluminum test sample using Tagwai Dam sand

Plate 4. Micrograph of etched Aluminium test sample using Wuya sand
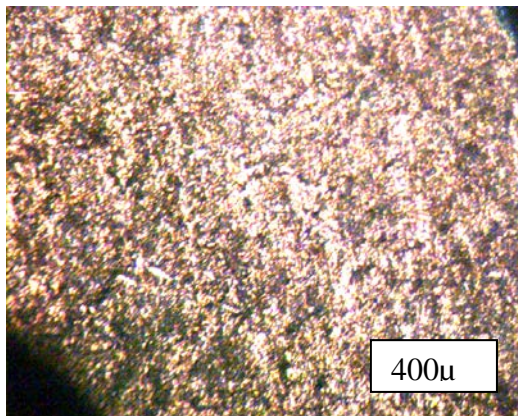

Plate 5. Micrograph of etched Aluminium test sample using Zungeru sand

The aluminium alloy casts produced from all the five sand samples indicates that the sand with low permeability (Shuaibu, 2014)had microstructures in which the white patches of primary alpha solid solution of silicon in aluminium (α) to be more pronounced i.eZungeru, Tagwai and Wuya sands, these sands exhibited very similar permeability number while the sands with higher permeability showed less white patches of primary alpha solid solution of silicon in aluminium (α) with TunganMallam sand microstructure showing the least primary alpha solid solution of silicon in aluminium (α). The relationship between the microstructure and permeability can be explained by the fact that permeability is a measure of gas passage through the sand. The ability of air to pass through sand affects the temperature of casting and the rate of cooling which consequently affects the solidification process and time also affects the types of phase and grains formed. Similarly, the average tensile strength and the hardness values of the three sands from Zungeru, Tagwai and Wuya were very close as compared to the other values which implies that the microstructure of the sand produced are in agreement with the mechanical tests carried out.

4.0 CONCLUSION

The investigation has shown that all the sand collected from the five locations were suitable forcasting aluminium alloy. The Mechanical tests carried out included tensile strength, hardness, elongation and reduction in cross sectional area. Results from the mechanical tests of the aluminium casts from all the five different sand were also compared with standard ranges of mechanical tests for aluminium alloy cast using sand moulds.

REFERENCES

Abolarin, M. S., Lawal, S. A.,&Salawu, A. A., (2010)"Effect of Moisture Content on the Moulding Properties of River Niger Sand Using Tudun-Wada Clay as a Binder",Assumpta University Journal of Technology, Vol. 13 No.3, pp.170-174.

Abolarin, M. S., Olugboji, O. A., &Ugwoke, I. C., (2004)"Experimental Investigation on Local Refractory Materials for Furnace Construction",5th AnnualEngineeringConference Proceedings, Federal University of Technology, Minna, Nigeria,pp.82-85.

Asuquo, L. O., Bassey, E. N., &Ihom, A. P.,(2013) "Characteristics of Zircon Sand andthe Effect on Foundry Casting",Journal of Mechanics & Industry Research, Vol.1 No.1, pp. 27-32.

Aweda, J. O.&Jimoh Y. A., (2009) "Assessment of Properties of Natural Moulding in Ilorin and Ilesha, Nigeria",Journal of Research Information in Civil Engineering, Vol. 6 No. 2, pp. 68-77.

Ayoola, W. A., Adeosun, S. O., Sanni, O. S. &Oyetunji, A.., (2012) "Effect of CastingMouldson Mechanical Properties of

6063 Aluminium Alloy",Journal of Engineering Science and Technology, Vol. 6 No.1, pp. 89-96.

Bala, K..C.&Khan, R..H., (2013) "Characterization of Beach/River Sand for Foundry Application",Leonardo Journal of Sciences, Vol.12 Issue 23, pp.77-83.

Khan, R. H., (2005) "Metal Casting Technology In Nigeria-Present Status and FutureProspects", Inuagural Lecture Series, Federal Univerity of Technology, Minna: p34.

Nuhu, A. A.,(2008) "Evaluation of the Foundry Properties of River Niger Sand Behind Ajaokuta Steel Company, Nigeria",American-Eurasian Journal of ScientificResearch, Vol.3 No.1, pp.75-83.

Sheidi, H. M.,(2012) "Investigation on Properties of Local Zircon Sand for Sound Casting: Azara-Lafia Deposit, Nigeria",Research Journal in Engineering andApplied Sciences,Vol.1 No.6, pp. 404-407.

Shuaibu, J., (2014), Evaluation of Moulding Properties of Sand in Niger State for Aluminium Casting and other Foundry Applications, M.Eng. Thesis, Mechanical Engineering Department, Federal Univerity of Technology, Minna

Investigation of impressed current protection of underground steel pipeline

A.S. Abdulrahman[1*], K.C. Ajani[2], J.J Augustine[3]

[1,2,3]Department of Mechanical Engineering, School of Engineering and Engineering Technology, Federal University of Technology, P.M.B 65, Minna, Nigeria

[*]salawu.asipita@futminna.edu.ng, +2348036812724.

ABSTRACT

Buried Pipelines are exposed to aggressive soil, varying climatic conditions, microorganism and stray currents that engenders corrosion, hence, the need for a viable means of tackling this menace. This paper presents the mitigating effect of Cathodic Protection system using impressed current technique on the corrosion of a buried steel pipeline. The theoretical work was validated by conducting the actual soil test and the soil pH was 6.97 with soil resistivity of 7850 ohm-cm. The specimens were buried in the soil at a depth of 1.0 m, for a total underground exposure of 60 days. The soil samples analyzed was found to be mildly corrosive and non-aggressive toward the mild steel pipelines. After the exposure period, the specimens were cleaned prior to final analysis. Surface morphological examination shows that both uniform and galvanic corrosion occurred on the buried steel sample. Corrosion rates were calculated for both protected and unprotected steel samples using weight loss method for all the specimens. The average corrosion rate result for unprotected mild steel is 4.649 mpy compare to Corrosion rate for the cathodically protected mild steel sample which is 0.379 mpy and the efficiency obtained was 92%, thus making Cathodic protection a viable corrosion control measure.

Key words: *Pipelines, Corrosion Inhibition efficiency, cathodic protection, Impressed Current, Weight loss*

1. INTRODUCTION

Corrosion is the destructive attack of a material as a result of reaction with its environment (Roberge, 2000). Corrosion in the modern society is one of the most challenging problems facing the industry. Buried pipelines are exposed to aggressive soil, varying climatic conditions, microorganism and stray currents that initiate corrosion processes (Onyechi et al., 2014). Pipelines are constructed and designed to maintain their integrity but undesirable phenomena like corrosion make it difficult to avoid the occurrence of leakage in a pipeline system during its lifetime (Banerjee, 2000). Recently, industrial catastrophes and pipeline insecurity show that many industries have lost several billions of dollars as a result of corrosion. (Kevin, 2010).

Corrosion in an industrial plant has been causing a lot of concern to petroleum, mechanical, chemical engineers and even chemists(Oyelami and Asere 2011).

Corrosion returns the metal to its thermodynamically stable state in chemical compounds that are identical to the minerals from which the metal was extracted. The amount of metal that will be removed is directly proportional to the amount of current flow. Corrosion can be changed by cathodic protection using impressed current to the underground steel pipe, the general result is that the original anode (steel pipe) become as cathode and other metal for example cast Iron will become anode. In order to protect the pipeline from corrosion effectively, a good knowledge of corrosion is required. By applying the concept of corrosion mechanism, it is then easier to understand various conditions which cause active corrosion cells in buried pipeline (Mohd, 2009).

Corrosion in a buried pipeline occurs as a result of electrochemical processes in which a currentleaves a structure at the anode site, passes through an electrolyte, and re-enters the structure at the cathode site (Mohd, 2009). The generated corrosion currents leaves the pipe to enter the soil at certain selective locations. Corrosion occurs at these selective locations of the pipe structure. Since corrosion can be controlled at these selective locations there is no need to replace a complete piece of pipe.

In order to mitigate these undesirable phenomena, cathodic protection does not only eliminate corrosion, it also

removes corrosion from the structure being protected and concentrates the corrosion at another known location. This method required installation of anodes made from electrically dissimilar metals, buried in the ground near the pipeline, which acts as the anode, and the corrosive action of ground water is thereby arrested (Banerjee and Mishra 2000).

Therefore cathodic protection in essence is a method of mitigatingcorrosion by utilizing the difference in potential between anode and cathode, this is achieved by applying a current to the system to be protected (such as pipeline) from outside source. When sufficient current is applied, the whole structure will be at the same potential, thus, anode and cathode sites will no longer exist.The direct current forced to flow from the external source to the pipeline when properly adjusted onto all surfaces of the pipeline will overpower corrosion current discharging from all anodic sites on the pipeline and there will be a net current flow onto the pipe surface at these points. The entire structure will now become cathode and the protection is assured(Banerjee and Mishra 2000).

 By using impressed current technique the steel pipe will be made the cathode and hence, will be protected from corrosion but the other metal (anode) will corrode. In designing this method,parameters such as factor affecting corrosion, the amount of anodes and rate of corrosion must be considered.

Pipelines play an important role throughout the world as a means of transporting petroleum products such as gases and other liquids over a very long distance from their source to the end users. Pipelines are exposed to varying climatic conditions, aggressive soil, microorganism and stray currents that initiate corrosion processes (Onyechi et al., 2014)

 A buried pipeline in the earth represents a big challenge, since they are made of steel which are thermodynamically unstable due to significant amount of energy is involved in the extraction process which places it in a high-energy state and will tend to seek a lower energy state, which is an oxide or some other compound.The process by which metals reverse back to the lower-energy oxides can be called corrosion. It is the duties of the corrosion engineer to study the properties of this material to ensure that the pipelines are well protected from deteriorating. In order to solve this problem, cathodic protection provides a valuable extra precaution against corrosion attack.Therefore, the aim of this study is to evaluate impressed current cathodic protection system of buried steel pipeline.

2.   METHODOLOGY

2.1.   Collection and pre-treatment of samples

The soil samples was obtained from the Nigeria National Petroleum Corporation (NNPC) pipeline product and marketing company (PPMC) located at Paiko along Suleja road, Minna Niger state. The three soil samples were taken from a depth of about 1 meter from the ground level and about 100 meters apart.

2.2.   Preparation of coupon

Locally produced mild steel known as RST37-2, widely used in petroleum, oil pipelines and chemical industries was cut mechanically into coupons. A hole was drilled on the sample using drill bit of 4mm. It was then weighed using a digital weighing balance and recorded, the coupon have the following dimensions (4.8×3.5 × 0.5cm).

2.3.   Soil pH measurement

10g of soil sample A was measured into 50 ml beaker, 25 ml of distilled water was added and stirred for 5 minutesand the resulting suspension was left for 1hour undisturbed. A calibrated pH meter was inserted and the pH of the solution was obtained. The above procedure was repeated for samples B and C.

2.4.   Soil resistivity measurement

In order to measure the soil resistivity, the potential pins in the soil box was removed first, the box was then carefully filled and compacted to the top with the soil sample. The

potential pins were then inserted and the soil re-compacted to ensure solid contact between the soil and the pins and for proper contact with the plates. The soil sample in the box was levelled and flushed with the top of the box so that the cross sectional area of the soil sample is the same with that of the box. The equipment (figure 1) was turned on to pass current through the soil sample and the voltage drop was recorded. The soil resistivity was calculated using equation 1 (Pierre, 2000).

$$\rho = \frac{R \times W \times H}{C} \qquad (1)$$

where, ρ= soil resistivity in ohm-cm

R= resistance in ohm,W= width of the soil box in cm, 4.47cm, H= height of the soil box in cm, 4.47cm

C= electrode spacing in the soil box, 2cm.

$$\rho = \frac{R \times 4.47 \times 4.47}{2} = 9.99R$$

2.5. Determination of Corrosion rate by Weight loss method

Corrosion test was conducted to determine corrosion rate using weight loss method in which coupons with known initial weights were buried in the soil for a specified period of time.in order to measure the weight losses, six samples were cut from locally made mild steel and surface prepared mechanically. The initial weights of each samples were measured with the aid of digital weighing balance and recorded.

Weight loss of the steel sample W=W_1–W_2 (2)

where W_1 = initial weight and W_2 = final weight

The test was carried out for a total period of 60 days with six weight measurements taken at an interval of 10 days. The corrosion rates of the samples measured in mils per year (mpy), was determined using equation (Abdulrahman et al., 2013)

Corrosion Rate= $\dfrac{W \times k}{\rho \times A \times T}$ (3)

W is the weight loss (g), ρ is the metal density in g/cm^3, A is the exposed area of the test coupon in cm^2, T is the exposure time in hours.

2.6. Design Simulation

Cathodic protection design for a steel pipeline was determine using (4) - (8) (Naseer et al., 2013). Calculation for voltage required by the system Current required by the system

$$I = (A) \times (i) \times (1.0\text{-CE}) \qquad (4)$$

where,

    I = Total protective current, mA.

    A_1 = Total exposure structure surface area, m^2.

    i = required current density, mA/m^2.

    CE = Coating efficiency, decimal value.

(It should be noted that A = surface area of the steel sample - circular surface drilled off + internal curved surface area of the hole)

The number of anodes needed to satisfy manufacturer's current density limitations, N is giving by

$$N = \frac{I}{A_a \times I_1} \qquad (5)$$

where,

I = Total protection current, milliamperes.

A_a = Anode surface area, m

I_1= Recommended maximum current density output, milliamperes.

$$N = 0.41/ (0.0015 \times 10734)$$

$$N = 0.0255$$

Number of anodes needed to meet design life requirement

$$N = \frac{n \times I}{1,000 \times W} \qquad (6)$$

where,

N = Number of anodes.

I = Total protection current, mA.

n = Life in years, 25

W = Weight of one anode, kg

N=25×0.41/ (1000×0.0166)

N=0.617

In order to determine the minimum Voltage (V_{min}) required by the System

V=IR   (Ohm's Law)

Therefore, $V_{min} = I \times R_T$ (7)

$R_T= (R_W + R_C + R_P)$ (8)

where,

R_W = wire resistance (0.12 ohm)

R_C = coating resistance (0.38 ohm), R_P= pipeline resistance (2.0 ohm)

V_{min} = 0.41×2.5=1.025V

Total minimum voltage required for the four samples = 1.025×4 = 4.1Volts

2.7. Cathodic Protection simulation using Impressed Current method

Plastic rubber was filled with soil sample connection cables were connected to the steel sample (cathode) Another cable wire was connected to the cast iron (anode) The steel and cast iron were buried separately inside soil in the plastic rubber. The other edge of the wire on the steel was connected to the negative terminal of the battery Likewise, the other edge of the wire on cast iron was connected to the negative terminal of the battery. In the procedures listed above, the steel serve as the cathode, the cast iron served as the anode, the soil serve as the electrolyte and the cable wires served as a returning metal path.

2.8. Determination of Cathodic Protection Efficiency

The efficiency of cathodic protection was calculated using equation 9 (Ajani *et al* 2014).

$$\eta = \frac{C_{wt} - C_w}{C_{wt}} \times 100 \ (9)$$

Where, η= protection efficiency, C_{wt} = corrosion rate without cathodic protection, C_w= corrosion rate with cathodic protection.

Fig.1: Impressed current cathodic protection setup.

3. RESULTS AND DISCUSSION

The outcome of the various experiment carried out to evaluate the impressed current cathodic protection system and the corrosion rate of locally made RST37-2 steel are presented in Tables 1 and 2 and Figures 2-6. Laboratory tests such as soil pH and soil resistivity have been conducted and the results are discussed appropriately as shown in Table 1.

The first step in analyzing the soil parameters was to carry out two basic tests namely; the soil pH and soil resistivity test. The soil resistivity is subsequently a function of the soil moisture content and the concentration of the current carrying soluble ions and the major controlling factors in corrosion control for buried steel pipelines.

Table 1 Result of soil pH and soil resistivity test

Samples	A	B	C
pH	6.96	6.59	6.80
Soil resistivity (ohm-cm)	7850	7900	7830

Table 2: Result of the weight loss, corrosion rate and Efficiency

S/N	time (days)	loss.g (unprot.)	loss g (prot.)	CR (unprot.)	CR (prot.)	I%(η)
1	10	0.113	0.009	4.932	0.395	91.99
2	20	0.231	0.017	5.041	0.373	92.60
3	30	0.332	0.027	4.830	0.395	91.82
4	40	0.387	0.032	4.332	0.351	91.87
5	50	0.496	0.038	4.330	0.347	91.98
6	60	0.609	0.045	4.430	0.355	91.99
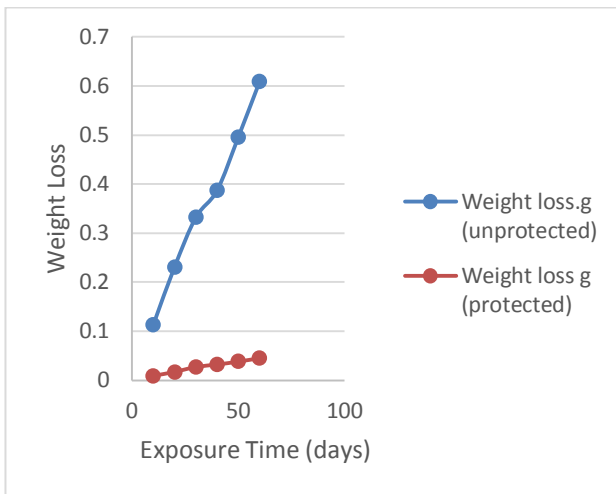
Fig. 2: Variation of Weight loss Vs. Exposure Time for unprotected and protectedmild steel samples
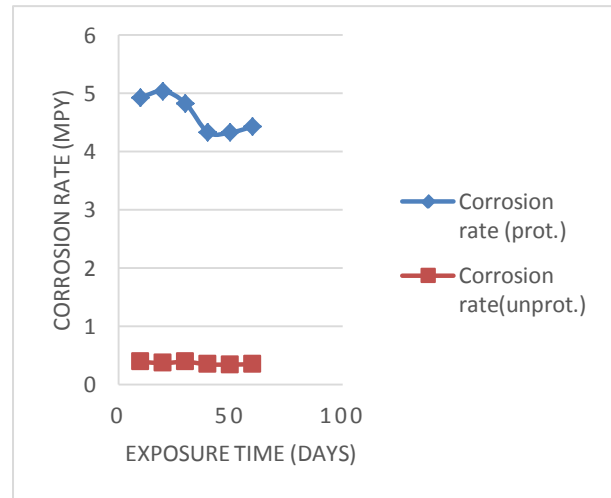
Fig. 3: Variation of corrosion Rate Vs. Exposure Time for unprotected samples.
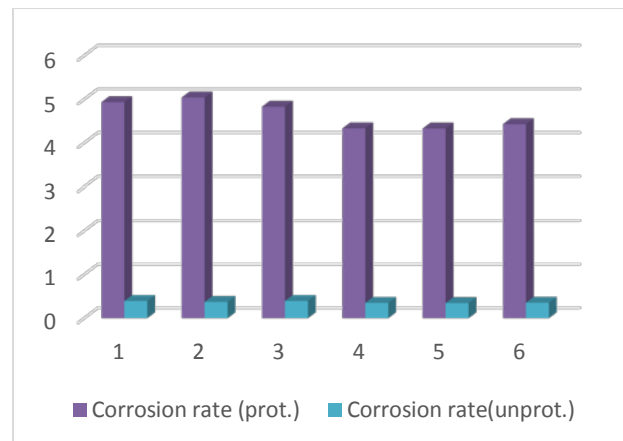
Fig. 4: Effect of impressed current cathodic protection

oncorrosion rate

Fig. 5: Unprotected coupon buried for 60 day.
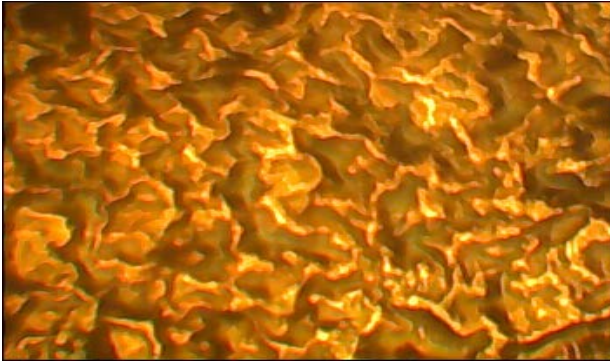
Fig. 6: Microstructure specimen×400.

3.1. Soil pH

All the three soil samples collected from the study area were neutral in nature, as such the soil is non-aggressive. But as suggested by Oguzie et al. (2004) that buried metallic structures are susceptible to corrosion at any pH value, therefore, the soil samples analyzed in this study were assumed to be mildly corrosive towards the mild steel pipelines.

3.2. Soil resistivity

The soil resistivity values for all the three samples collected from the study areas revealed that all the samples are mildly corrosive in nature toward the buried structures based on ASTM and NACE standards. All soil samples were tested at room temperature of 25^{0}C.

3.3. Variation of weight loss with exposure time

As shown in Figure 2, the weight loss by the steel sample increases as the exposure time increases for both the protected and unprotected. The weight loss however in the protected coupons are lesser than those of the unprotected samples. This implies that the steel releases energy to become thermodynamically stable by gradually returning into its original oxide called hematite (Fe_2O_3) (Abdulrahman et al, 2011)

3.4. Variation of corrosion rate and impressed current with time of exposure

From the Figure 4, the corrosion rate of a steel sample varies between 4.330 mpy to 5.041 mpy. The corrosion rate increases first with time of exposure and later decreases slightly as number of days increases. The effect of the impressed current is also as shown in Figure 5.There is reduction in corrosion rate with time. This is as a result electrons introduced into the system to replenish the electron loss by the corroding system.

3.5. Protection efficiency

Cathodic protection evaluation was carried out by calculating the efficiency of the corrosion control to ascertain the level of impressed current cathodic protection. It can be seen from Table 2, the cathodic protection efficiency result shows that there is a drastical reduction in corrosion rate between the two systems, the highest efficiency obtained is roughly 92%. With this result, corrosion rate has been reduced from 4.932 to 0.376 mpy.

3.6. Surface morphological examination of buried specimen

The surface morphological examination of the mild steel sample was carried out after prolonged underground exposure for a total period of 60 days in the studied soil using microscope at X200 and X400. Figure 5reveals the buried sample for 60 days while the microstructural view at X400 magnification is as shown in figure 6.Interestingly, small pits with distinct shapes were observed on the surface of the specimen, hence, indicating pitting corrosion. The surface was filled with corrosion products as viewed using microscope as shown in Figure 6. The corrosion products were found to cover almost all the exposure area uniformly.

4. CONCLUSION

The impressed current cathodic protection experiment of a small pipeline segment protected with cast iron in a soil was carried out. Cathodic protection is found to be an outstanding and reliable corrosion control method especially for buried and submerge pipelines and structures. The cathodic protection simulation enables the engineer to test and predict system prior to installation to reduce cost. From the experiment carried out, the highest efficiency obtained was 92% which validates the effectiveness of the impressed current cathodic protection.

REFERENCES

Abdulrahman, A.S., M. Ismail and M.S. Hussain, (2011). Corrosion inhibitors for steel reinforcement in concrete: A review, Scientific Research and Essays, 6(20): 4152-4162.

Abdulrahman, A.S. and Mohammad Ismail, (2014). Electrochemical assessment of concrete inhibitor used in retarding corrosion steel reinforcement. ARPN Journal of Engineering and Applied Sciences, 9(5): 750-756.

Ajani K.C., Abdulrahman A.S. and Mudiare E., Inhibitory (2014). Action of Aqueous Citrus aurantifolia Seed extract on the Corrosion of Mild Steel in H_2SO_4 Solution, World Applied Sciences Journal (WASJ), 31 (12): 2141-2147.

Banerjee T. and Mishra G. (2000). Cathodic protection — a proven corrosion control means in immersed or buried pipelines in oil, natural gas and petrochemical industries. Journal of Metallurgy and Materials Science. Vol. 42, pp. 167-176.

Kean and Davies, (2003) Kean, R. L. and Davies, K. G. (2003).www.npl.co.uk/ncs/docs/cathodic-protection.pdf.

Kevin G Davies (2010). Dealing with Corrosion: Helical Piling

Mohd Saiful Nizam Bin Mohamad (2009) Cathodic Protection of underground Steel pipelines by using Sacrificial anodes.

Naseer A. Al Habobi and Shahad F. Abed (2013) Simulation of Cathodic Protection System Using Matlab Iraqi Journal of Chemical and Petroleum Engineering.Vol.14 No. 25- 37

Oguzie EE, Agochukwu IB, Onuchukwu AI. (2004). Monitoring the corrosion susceptibility of mild steel in varied soil textures by corrosion product count technique. Materials chemistry and physics. Vol. 84, (1), pp. 1-6.

Onyechi, Pius C, Obuka, Nnaemeka S.P, Agbo, Cornelius O and Igwegbe, Chinenye A (2014). Monitoring and evaluation of Cathodic Protection performance for oil and Gas Pipelines: a Nigeria situation. International journal of advanced scientific and technical research vol. 1

Oyelami BO, Asere AA (2011). Mathematical Modeling: An application to corrosion in a petroleum industry. NMC Proceedings Workshop on Environment. National Mathematical Centre, Abuja, Nigeria.

Pierre R. Roberge (2000), Handbook of Corrosion Engineering.

Roberge PR (2000) Handbook of corrosion engineering. McGraw-Hill, New York.

LANDFILLS: WHAT WAS AS TO WHAT IS

Agbenyeku Emem-Obong Emmanuel[1*], Muzenda Edison[2], Msibi Mandla Innocent[3]

[1,2]Department of Chemical Engineering, University of Johannesburg, South Africa

[2]Department of Chemical, Materials and Metallurgical Engineering, Botswana International University of Science and Technology, Palapye, Botswana

[3]Research and Innovation Division, University of Johannesburg, South Africa

[*]emmaa@uj.ac.za; kobitha2003@yahoo.com, +27 11 559 6396

ABSTRACT

Landfills are well known components of landscapes in many countries as they are incorporated into cities master plans and in some countries are extensively designed and engineered. Landfills are also severely censured by the public as it threatens the health and safety of humans and the environment. As in the past, landfills will continue to play a significant role in municipal solid waste (MSW) management and remain the commonest means of waste disposal for a long time. On one hand, landfills in some parts of the world particularly in developing countries constitute various human, environmental and social menaces. On the other hand however, most developed countries have ascended levels where; gone are the past challenges associated with landfills i.e., by-products from waste decomposition causing soil, groundwater and air contamination. In developed countries, modern landfills, in contrast to those mostly found in developing countries, are highly engineered containment facilities that are designed and operated to diminish the impacts of MSW on human and environmental health. Hence, need for proper containment and monitoring systems to minimize contamination is crucial, especially in developing countries. Thus, improvements in waste containment around the world, gave this paper the impetus to propagate the need for paradigm shift in developing Africa. The paper highlighted the evolution of landfills from yesteryears to present day such that; the general public, contractors and government parastatals can consider the beneficial sides of a modern landfill towards energy sustainability, environmental conservation and social benefits.

Keywords: *Contamination, Landfill, Waste, Contaminant.*

1. INTRODUCTION

It is now clear that growth in one sector of an industrialized system consequently impacts another. Such that in striving to meet globalized demands and through population growth, energy resource use, infrastructure development and civilization, enormous waste are been generated. Despite every recycling measure presently harnessed, waste is continually generated at work places, homes and surrounding vicinity (EIAR, 2005). In the United States, 254.7 million tons of municipal solid waste (MSW) was generated in 2005 alone with over 138.3 million tons disposed in landfills (EPA, 2006). In South Africa however, where industrialized activities are gigantic as compared to other countries on the continent, approximately 15 million tons of MSW was generated in 2005 with over 10.5 million tons of these wastes destined for landfills (EIAR, 2005). These enormous amounts of waste constantly generated and disposed in landfills require proper containments to keep harmful substances in

check. Therefore, to make sure that our waste inflicts no harm to human and environmental health, modern day-state-of-the-art landfills are technically built with highly sophisticated and regulated up to date features. For instance, the use composite lining features ensure the protection of important ground regimes from impacts of leachate contaminants. Also a geomembrane feature; forming part of a composite liner may fail due to defects from fabrication, installation or aging. In other cases, siting landfills near important water sources may be inevitable as such, requires reliable barrier features in separating waste bodies from ground water to prevent contaminant percolation (Agbenyeku and Akinseye, 2015). Generally, "landfills" are mostly referred to as "municipal solid waste landfills" to differentiate them from "open dumps" of the past which are still practiced in many developing countries. However, as described by Bouazza et al., (2002) modern landfills in contrast to old dumps are comprised of specially engineered protective liners, leachate collection

systems (LCS), groundwater monitors/monitoring systems (GMS), gas collection equipments/systems and environmental reporting tools. This paper on a general note highlights the evolution of landfills from "what it was to what it is". It pinpoints the beneficial transformation of landfills and offers information on the design, operation and regulation of modern landfills towards human and environmental protection, natural resource and energy conservation, as well as social benefits.

2. MODERN LANDFILLS

2.1. Transitory Phases of Waste Disposal System

From time immemorial, human activities have always generated waste. Waste disposal however, was never a problem in ancient time as people were more of wanderers than settlers as such, left their trash behind. By 10,000 BC, people gradually settled in groups and communities, and with that came the dumping of generated waste on the ground around settlements. At that time, settlements had no need for optional methods of waste disposal until waste heaps became platforms for waging attacks thereby, wrecking smaller communities. By 500 BC, Athens, Greece, became the first in the western world to establish municipal waste dumps by ridding of waste some 1-2 miles away from the city's fence such that, attackers would not cross into their premises using elevated waste piles. Nevertheless, waste dumping within cities as shown in Figure 1 was the main disposal method in Europe and the United States till the late 1800s when there was an outbreak of disease resulting from poor environmental conditions. By the end of the 19th Century, many cities knew of the health and political implications of street waste dumping. In bid for solution, the advent of an organized city waste collection and disposal system using horse-drawn wagons as seen in Figure 2 to pick up waste and dispose of it in water bodies, incinerators or open dumps was born. By the 1920s, there was enormous idle

waste ash as a result of waste incineration used mainly together with other waste types in reclaiming nearby wetlands.

Fig. 1: Late 1800s city street side dumps (NSWMA, 2008)

Fig. 2: Horse carts for waste collection (NSWMA, 2008)

The beginning of the then "modern landfilling system" started in California in 1935, where collected waste was thrown into dug pits and occasionally covered by trash. From thereon, landfilling system took a different toll as domestic disposal regulations were gradually formed and enforced. In 1959, the American Society of Civil Engineers published the first guidelines for a "sanitary landfill" that recommended daily compaction of waste and covering it with a layer of soil to minimize odoriferous discharges and control burrowing animals. The first federal legislation of solid waste management was the Solid Waste Disposal Act of 1965 (SWDA) that formed a national office of solid waste. By the mid-1970s, all states had solid waste management regulations. However, the contents of these regulations were different across states. In some states, sanitary landfilling was done as laws prohibited open waste burning at dumps. While in some other states, disposal facilities needed to have permits and met minimal design and operational standards to operate. The U.S.

House of Representatives in 1976 as recorded by NSWMA (2008) passed the Resource Conservation and Recovery Act (RCRA) that expanded the federal government's role in managing waste disposal. Wastes were divided into hazardous and non-hazardous categories and RCRA mandated the EPA to develop design and operational standards for sanitary landfills as well as upgrade or close existing open dumps that did not meet the set sanitary landfill standards. EPA developed criteria for sanitary landfills in 1979 that addressed: siting restrictions in floodplains; protection of surface and groundwater; open burning prohibitions; fire prevention through the use of cover materials; explosive gas (methane) control; endangered species protection; disease and vector (rodents, birds, insects) control and prevention of bird hazards to aircraft (NSWMA, 2008). The RCRA was then amended in 1984 that required EPA to assess and, if appropriate, revise the sanitary landfill requirements. In 1991, EPA initiated new federal standards for MSW landfills that upgraded location and operation standards; inclusive of design standards, groundwater monitoring requirements, corrective action requirements for known environmental emergencies, closure and post-closure care requirements and financial assurance requirements to show the ability to pay for long-term care of the landfill (NSWMA, 2008).

2.2. Landfill Operations at Safer Locations

From what was, little or no concern was neither given to landfill location nor its operation. From what is however, modern landfills are sited and constructed in locations that safeguard human and environmental health, and also ensure the structural reliability of the landfill. For instance, modern landfills are prohibited from being built in:

i.   Fault areas, seismic impact zones and unstable areas: - only if the landfill is designed and constructed to withstand shocks and maintain structural integrity in an event of a geological disaster.

ii.   Floodplains: - except proper engineering measures to prevent a flood from either infiltrating or washing MSW out of the landfill into local streams or rivers are set in place; and

iii.   Wetlands: - except there are engineering measures put in place to properly separate the waste body from the wetland as such, let no considerable degradation or loss of the wetland be encountered.

Furthermore, modern landfills have established various protective operational measure; they have plans and structures in place to ensure hazardous waste is not accepted and disposed of at the facility, open waste burning is disallowed, unauthorized access is controlled, bulk and non-containerized fluids are rejected etc. In addition, owners and operators of modern landfills track, record and routinely report to regulatory bodies on groundwater, surface water and air monitoring activities (NSWMA, 2006).

2.3. Improvements in Landfill Designs

According to EPA, (2006) landfills in the globalized world have transformed drastically from what is was- dug pits in the ground to what it is- highly engineered, high-tech containment systems requiring large capital expenditures and generating just as much. From what it was, older landfills were designed and constructed by excavating a trench, filling the excavation with garbage and covering it with soil/dirt. In most cases, wastes were placed directly on the underlying soils without a lining barrier to prevent leachate contaminants from reaching groundwater, as containment relied on the natural geology of the site (Agbenyeku et al., 2014a). In other cases, wastes were burnt in open air as shown in Figure 3 to create space for future dumping, thereby, causing air pollution and related health hazards. At a set height, a layer of soil was used to cover the waste and sometimes was revegetated. Often, revegetation failed due to emission of methane gas (a

natural by-product of waste decomposition) escaping through the soil cover. In grave instances, the landfill gas could flow off-site into nearby buildings and homes posing risks of explosion.

Fig. 3: Waste burning in landfills

On the contrary, modern landfills are specially designed and constructed to protect human and environmental health by containing leachate and gas discharges. Combination of barrier liner and LCS function together to contain landfill leachate as such prevents contamination of groundwater reserves (Rowe, 2011). The Figure 4 shows the cross section of a typical modern landfill. Also, as noted by Bouazza et al., (2002) liners prevent leachate and gas from escaping landfill while directing liquids to the LCS.
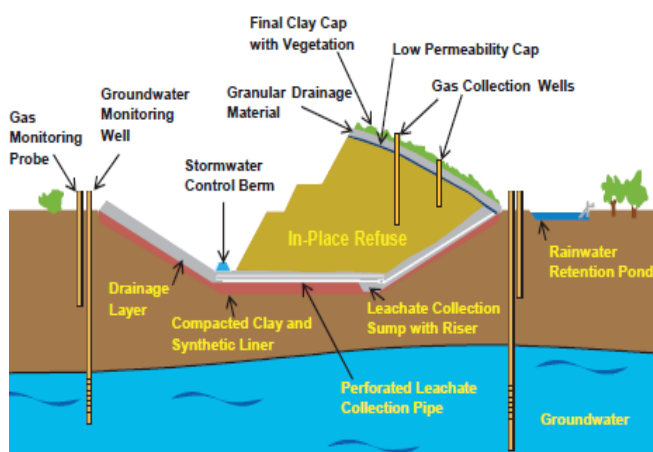
Fig. 4: Cross view of a modern landfill (NSWMA, 2008)

Barrier lining systems are basically constructed with layers of low permeability, natural materials (compacted clay soil) and/or synthetic materials (high/low-density polyethylene) while the LCS functions to remove liquid restrained by the liner. From bottom to top, a typical LCS consists of a perforated leachate collection pipe placed in a gravelly drainage layer, a filter blanket and a leachate collection layer. Waste is placed directly above the LCS in layers, as also deposited waste on working face is maintained to control odours and vectors. Heavy compactor machines move the waste into the working face to reduce wastes volume and increase densification as shown in Figure 5.

Fig. 5: Waste compaction in landfill

Additionally, at the end of each day, delivered waste is covered with six inches of soil or an optional cover e.g., tarps waste ash, foams or compost to control vectors, odors, fires and blowing litter (EPA, 2005). Once the landfill has been filled to acceptable requirements, it is closed, engineered and constantly monitored to guard against infiltration of runoffs by installing low permeability cover similar to the barrier system. The final cover may constitute a compacted clay and/or synthetic material. As described by NSWMA (2008) granular drainage layer is placed on top of the low-permeability barrier layer to channel water away from the top of the landfill. A protective cover is placed on top of the filter blanket and topsoil is spread on the final layer in case of revegetation. Essentially, the engineered systems in a modern landfill is basically to offer proper containment of waste contaminants thereby, ensuring that landfill leachate is kept in check as well as prevent the interaction of water with the general waste body. Consequently, this containment system is designed to confidently ensure the protection of human and environmental health while in some cases, carefully collects landfill gas beneficially used as alternative source of energy.

236

3. MODERN LANDFILLS AS ECO-FRIENDLY

3.1. Improved Human-Environmental Protection

From what was, open dumps were linked to various human and environmental challenges i.e., soil, surface and groundwater contamination, air pollution and related hazards. However, from what is, modern landfill designs and operations have been beneficially transformed to eradicate or at worst prevent any impacts on the health of humans and the environment. On the disposal of MSW in landfills, biological decomposition of waste occurs due to activities of naturally occurring microorganisms. Waste decomposition rates are often influenced by the temperature and amount of water present in the waste body. From the series of microbial actions, methane (as main constituent of natural gas) and carbon dioxide in almost equal proportions are formed from the degraded organic waste portion. Through the processes involved minute amounts of organic compounds are also generated. Furthermore, as explained by NSWMA (2008) some organic compounds contained in decomposed household waste i.e., from cleaning agents, may be released into the gas. These non-methane organic compounds (NMOC) that may be present in the natural gas amount to < 1 % of the total produced gas. Additionally, as noted by EPA (2006) landfill generated gas when not trapped as an energy source or destroyed if not needed can pose severe danger to human and environment health if allowed to migrate off site. A gas collection well used in modern landfills to safeguard public health and the environment by preventing methane from escaping the landfill is shown in Figure 6. The Federal Clean Air Act Standard in the United State requires larger modern landfills with estimated uncontrolled emissions of $\geq$ 55 tons/year of NMOC to install gas collection (GCS) and destruction systems (EPA, 2006). Nevertheless, smaller landfills also willingly install gas collection and destruction systems for reasons of; gaining emission reduction credits by minimizing greenhouse gas (GHG) emissions towards human and environmental benefits.

Fig. 6: Modern landfill gas well

GCS conveys gas to a central location where it can be processed and treated depending on its final use. At this point, gas can either be destroyed in a loose flare or alternatively, be used as energy source to power vehicles, produce electricity or used as substitute natural gas.

3.2. Improved Quality and Destruction of Gas

Report from studies by EPA (2006) showed that what is- a modern landfill, forms considerably lesser concentrations of NMOCs as compared to what was- an old dump site. In modern landfills, out of 48 NMOCs regulated by Federal Clean Air Act rules, 58% of them are 1-3 orders of magnitude lower in concentration than in older landfills. More to this, their reports showed that at modern landfills, 5 out of 28 NMOC compounds were below detection. While in older landfills, they were found to be present in high concentrations. Figure 7 shows GCS at a modern landfill. Also, as stated by NSWMA (2008) considering that comparable data are from test programs conducted in the late 1980s, older landfills are likely to have higher concentrations of NMOCs than modern landfills.

Fig. 7: Modern landfill GCS (NSWMA, 2008)

Consequently, the environmental benefits of lower concentrations of NMOCs in gas from modern landfills compared to older ones cannot be over emphasized. The potential risks of gases from what is- modern landfills, on human and environmental health is considerably lower than what was- older landfills. This significant huge difference can be plausibly accounted for by the devices (as seen in Figure 8) currently used to combust gas; having destruction efficiencies $\geq 99\%$ for methane and $\geq 98\%$ for all other NMOCs (NSWMA, 2008).

Fig. 8: Modern landfill combustion system

3.3. Modern Landfills for Alternative-Green Energy

As earlier mentioned, landfill generated gas can be collected and used to produce electricity or heat for powering industrial facilities, as fuel to drive vehicles or provide lighting and heating systems for homes and public buildings. According to data from EPA (2006) as recorded by NSWMA (2008) there are more than 455 operational gas-to-energy projects ongoing in some states. These projects collect up to 7245 Million Metric Square Cubic Feet Per Day pending on landfill gas to produce up to 1,383 MW of electricity yearly. Currently, environmental merits of landfill gas-to-energy projects are considered an equivalent of:

(a) Limiting the use of ≥ 177 million barrels of oil;

(b) Removing $CO_2 \geq 14.5$ million car emissions;

(c) Planting ≥ 20.5 million acres of forest yearly; and

(d) Offsetting the use of 370,000 railcars of coal (EPA, 2006). However, since methane is a potent GHG (having nearly 21 times more global warming potential than carbon dioxide), a plus to the merit of modern landfill gas collection and destruction systems is the total prevention or at worst drastic minimization of methane released to the atmosphere where it adds to global warming. More beneficial outcomes from modern operating landfills are appreciated in the GHG net emissions. In 2006 126.2 Tg of CO_2 equivalents ($TgCO_2E$) was recorded as against 149.6 $TgCO_2E$ recorded in 1990 (EPA, 2006). It is clear that modern landfill practices used in 2006 prevented the discharge of 23.9 $TgCO_2E$ as against the quantity that would have been emitted if the practices from 1990 were still in use. Although, in most African countries, a lot of transformation is yet to occur as the entire continent requires a speedy paradigm shift. Since modern landfills are considered a sink for carbon, sequestering of about 10.5 $TgCO_2E$, proper and sustainable safe waste management practices towards human and environmental benefits is crucial.

3.4. Leachate Control in Modern Landfills

In the past very few landfills had liners and leachate collection systems, as much of them relied on the geology of the site to contain leachate from escaping the landfill. This practice is still undertaken in most developing countries and for such reasons, Agbenyeku et al., (2015; 2014a, b; 2013a, b) investigated the impact of mineral barriers in containing leachate contaminants. Modern landfills however, are built with liners and LCSs as reported by Bouazza et al., (2002) that functions to keep leachate from escaping the facility and contaminating water reserves. Recent EPA studies have shown liners and LCS constructed to standard specification to have 99-100% efficiency. Further outcomes have shown that most trace chemicals from modern landfills leachate are either below detection or detected in minute concentrations as compared to older ones with high concentrations of chemical contaminants. In most instances, contaminant concentrations in leachate from modern landfills are 1-2 orders of magnitude less as against older landfills.

Furthermore, research expects that the quality of leachate will continually improve as further changes registered in modern landfills increases. Figure 9 shows a modern landfill leachate treatment facility with high efficiency of contaminant constituent removal. This implies that the release of trace constituent contained in modern landfill leachate will virtually be eliminated as improvements are made in the collection, removal and treatment processes.

Fig. 9: Modern landfill leachate treatment facility (NSWMA, 2008)

In modern landfills, generated leachate is either treated in-situ or pumped off-site for treatment. In most landfills in South Africa however, generated leachate is often left open in leachate ponds (as shown in Figure 10) to evaporate since not much effort has been invested in leachate treatment.

Fig. 10: Leachate basin in a landfill

In the United States, Federal requirements mandate that treatment of landfill leachate must meet drinking water quality standards. This is done primarily to safeguard public health and protect sensitive environmental resources e.g., quality streams, trout streams, groundwater reserves etc (EPA, 2006). Research has shown that leachate treatment facilities at modern landfills are capable of removing 100% trace organics and over 85% of heavy metals. Groundwater monitoring wells are usually installed in modern landfills to ensure the liner and LCS are functioning properly. Groundwater monitors around the landfills are regularly tested for indications of the slightest releases from the landfill which could degrade water quality. As such, groundwater quality reports are supplied to the relevant authorities routinely. On event of landfill contaminant influx; detected by groundwater monitors at levels posing threat to both humans and the environment, the landfills are charged with the responsibility of correcting the problems and restoring to original quality the affected features i.e., soil, surface and groundwater.

4. LANDFILL RECLAMATION AND REUSE

4.1. Functional-Merits of Reclaimed Landfill

As earlier heighted, what was- older dump sites were typically covered with a thin layer of dirt and in rare cases were sparingly revegetated. In present times, the availability of virgin land for developmental projects is scares and the cost of land insistently on the rise. Running out of open space and considering the heightened environmental awareness, many communities push to reclaim and make functional use of older landfill sites. This is often difficult, as it is considered very expensive and unstable to be developed; since no initial designs were made for future upgrades. However, from what is- modern landfills are designed and constructed from the start to secure the environment and public health. Modern landfills are also initially designed to ensure that on closure in the future, safe and productive use of the site can go on. Some functional merits of modern landfills after closure can be categorized into the following three:

I.   Open space, agricultural, and passive recreation;

II.   Active   recreation,   parking,   or industrial/commercial activities; and

III. Intensive uses such as residences, industry, and commercial development.

As recorded by NSWMA (2008) category I functional merits are the least recognizable and most numerous because they often appear to be just open fields. For instance, in many parts of the United States, category I uses are seen in agricultural land, cemetery, clear zone around runways as seen in Figure 11, as well as hiking paths.

Fig. 11: Clear zone around runways built on reclaimed category I landfill (NSWMA, 2008)

Additionally, in some other developed countries category I reclaimed landfills are beneficially used as solar energy farms towards greener energy conservation as seen in Figure 12.

Fig. 12: Solar energy farm on category I reclaimed landfill

In the case of Category II, uses are more frequent and are typically characterized by lightweight structures. The site may contain certain basic utilities, lighting systems or paving. For instance, golf courses and minor league baseball fields, parks, softball fields, soccer fields and children's play areas as seen in Figure 13 (a) and (b) can be category II functional merits of reclaimed modern landfills.

(a)   (b)

Fig. 13: (a) and (b) Children's park and soccer field built on reclaimed landfill for category II functional use

While in the case of category III, functional merits are the most intensive and are typically characterized by major structures. The site may hold steel and concrete works used in the construction of basic and social amenities. For instance, football stadium (as shown in Figure 14), shopping centers and malls, post offices, libraries and clinics etc.

Fig. 14: Football stadium built on reclaimed category III landfill (NSWMA, 2008)

5. LANDFILLS AND THE WAY FORWARD

5.1. Future Growth of Landfills

The waste industry continually investigates on the way forward in terms of innovative designs and operations modern landfills. This is such that further protection of human and environmental health can be guaranteed while boosting social and economic benefits. An ongoing innovative design and operation in modern landfills is the promising bioreactor. As reported by EPA (2006) a bioreactor landfill adds liquids and/or air to the waste body, thereby accelerating the rate of waste bio-decomposition and stabilization as shown in Figure 15.

Fig. 15: Innovative bioreactor liquid sprayed on waste

Outcomes of research have shown the environmental benefits of a bioreactor landfill to include the following:

o Shorter time periods (7-10 years) over which air and water emissions are generated compared to 30 or more years in a conventional landfill;

o Shorter post-closure care periods (10-15 years) as against ≥ 30 years for conventional landfill;

o Increased efficiency of the GCS; and

o Faster return of property to functional end-use.

Also, the innovative design and use of biocovers to further reduce air emissions at landfills is fast gaining grounds. Biocovers as seen in Figure 16 are composted yard waste used as a final cover in modern landfills (NSWMA, 2008).

Fig. 16: Innovative biocovers spread as final landfill cover

The merits of biocovers are that air emissions of methane and other organic compounds are oxidized and destroyed in the biologically active compost. Thus far, research has shown biocovers to effectively control air emissions when used:

▪ On faces to carry more waste in the future that lacks/have a nonfunctioning GCS; or

▪ To control air emissions when the GCS is temporarily out of use due to repairs/maintenance (NSWMA, 2008).

6. CONCLUSION

Landfills are well known in many countries as they take up huge land spaces in many communities and constitute a host of public nuisance. Landfills in some countries are extensively designed and engineered while in others, they exist simply as dump sites. Generally, landfills poses various threats to health and safety of humans and the environment as such are often kicked against by the general public. Nevertheless, landfills will continue to play a significant role in MSW management hence, should be better improved or upgraded to standard requirements of modern landfills. As such, the paper highlighted the evolution of landfills from early days to present day. Since landfills will remain the commonest means of waste disposal for a long time to come, the following conclusions were drawn:

➤ That as it was- with older landfills, modern landfills as it is- will remain a significant part of MSW management system.

➤ That unlike human and environmental problems associated with older landfills, modern landfills are highly engineered containment systems designed and operated to minimize impacts on human and environmental health.

➤ That with modern landfills, safer and efficient operations can be undertaken and monitored as against older landfills that relied solely on site geology.

➤ The there is continuous innovative explorations on landfill designs and operations to better safeguard human and environment health towards improved economic and social benefits.

In summary, as to what is- modern landfills are driven towards greener and more sustainable human, environmental, social and economic benefits as compared to what was- older landfills with severe consequential impacts and no benefits. In many parts of the world,

particularly developing Africa, need for proper containment and monitoring systems to minimize contamination is dire. Thus, as the paper highlighted through the evolutionary changes in landfills, it is expected that the general public, contractors and government parastatals will shift towards embracing the beneficial impacts of adopting modern landfills i.e., in energy sustainability, environmental conservation, social and economic benefits as against sticking to the older and more consequential waste dumping system.

ACKNOWLEDGEMENTS

REFERENCES

Agbenyeku E.E. & Akinseye S.A. (2015) Leachate Percolation through Failed Geomembrane of a Geo-Composite Soil Barrier *World Journal of Environmental Engineering, 2015, Vol. 3, No. 2, 52-57.*

Agbenyeku E.E. Muzenda E. & Msibi I.M. (2014a) "Zeolitic Mineral Liner as Hydraulic and Buffering Material", International Conference on *Earth, Environment and Life sciences* (EELS-2014) Dec. 23-24, 2014 Dubai (UAE).

Agbenyeku E.E. Muzenda E. & Msibi I.M. (2014b) "Buffering of TOC-Contaminant Using Natural Clay Mineral Liner", International Conference on *Earth, Environment and Life sciences* (EELS-2014) Dec. 23-24, 2014 Dubai (UAE).

Agbenyeku E.E. Okonta F.N. & Ojuri O.O. (2013a) Leachate Flow through Composite Barrier from Defected Geomembrane. 2nd African Regional Conference on Geosynthetics, Accra, Ghana, 18-20 November (CD ROM).

Agbenyeku E.E. Okonta F.N. & Ojuri O.O. (2013b) Evaluation of Empirical Equations for Leachate Migration through Composite Barrier with Defected Geomembrane. 2nd African Regional Conference on Geosynthetics, Accra, Ghana, 18-20 November (CD ROM).

Bouazza A. Zornberg J.G. & Adam D. (2002) Geosynthetics in waste containment facilities: recent advances. *Proceedings 7th International Congress on Environmental Geotechnics,* Delmas, Gourc & Girard (eds): 445-507.

Environmental Impact Assessment Regulations (2005) Waste Collection and Disposal. Retrieved 07 May, 2012, from: http://www.dwaf.gov.za/Dir_WQM/Pol_Landfill.PDF.

Environmental Protection Agency (2005) Municipal Solid Waste LandfillRegulationshttp://www.epa.gov/epaoswer/nonhw/muncpl/landfill/msw_regs.htm.

Environmental Protection Agency (2006) Municipal Solid Waste in the United States 2005 Facts and Figures. EPA 30-2-06-011.

National Solid Wastes Management Association (2008) Landfill Institute, Environmental Programs, North America.

Rowe R.K. (2011) Systems engineering; the design and operation of municipal solid waste landfills to minimize contamination of groundwater. Geosynthetics International, September, 18 (6), pg: 319-404.

RELATIONSHIP BETWEEN COST OF FIRE INCIDENCE AND CAPITAL EXPENDITURE IN KWARA STATE

A. A. Shittu[1*], J. E. Idiake[2], W. P. Akanmu[3]

[1, 2](Department of Quantity Surveying, Federal University of Technology, Minna, Nigeria)

[3](Department of Building, Federal University of Technology, Minna, Nigeria)

[*]aishatabdulahi2007@yahoo.com or funsho@futminna.edu.ng, 08034767554.

ABSTRACT

The incidence of fire outbreak has been identified as a threat to both citizens and the Government which makes it a threat to national development. This study addressed the problem of incidence of fire outbreak, resulting to losses amounting to a sizeable proportion of capital expenditure in Kwara State. To solve this problem, this study set out to determine the relationship between cost resulting from fire incidences and annual capital expenditure in Kwara State. The study's background revealed that the incidence of fire outbreak increases annually, resulting to loss of lives and property worth huge amount of money. Data were collected from secondary source, which is from records of Kwara State Fire Service and National Bureau of Statistics. Bar and line graph was employed to carry out trend comparison of the variables studied, while regression and correlation analyses were used to determine the relationship between the variables studied. Major findings from the study showed that fire occurs due to electrical faults than gas faults; the amount of financial loss (=N=6,533,988,401.50) was about 4% of the capital expenditure (=N=178,347,461.00); and number of fire cases recorded correlated significantly with the amount of capital expenditure. It was concluded that there is no improvement in the trend of fire incidents in Kwara State over the study period.

Keywords: *Capital Expenditure, Electrical/Gas fault, Financial Loss/Salvage, Fire, Public/ Residential building.*

1. INTRODUCTION

In Nigeria, there has been a serious disaster confronting the homes, lives and property of people. The most common ones are flood, building collapse and fire. A lot has been written on flood and building collapse, but the incidence of fire is still lax in literature. Fire is the result of flammable materials being combusted and the essential ingredient for the propagation of fire is air, which is sufficient to start ignition or means of ignition and oxidation (Oyeyode, 2003; University of Gulph; 2003).

For longer than recorded history, fire has been a source of comfort and catastrophe for the human race. Fire is rapid, self-sustaining oxidation process accompanied by the evolution of heat and light in varying intensities. Fire is believed to be based on three elements being present: fuel, heat and oxidizer. Fire disasters can occur above the ground (in tall buildings and on planes), on the ground, and below the ground (in mines). Sometimes they occur in circumstances that are unexpected or unpredictable. All fire incidents can be divided in many ways depending on the cause of fire outbreak, but broadly there are two types of fires: one is natural and the other is man-made. Fires can be either due to natural or man-made reasons. All residential and non-residential structural fires are largely man-made. Similarly, all industrial and chemical fires are due to explosions or fires made by humans or due to machine failures.

Firestorms can also be natural or human generated. Fires which are considered as natural are basically earthquake, volcanic eruption and lightning - generated fires. Fire caused by human/machine errors are considered as man-made fires, e.g. industrial or chemical fire disasters, fires at social gatherings due to Electrical short circuit fires, incendiary bombing, accidental fire and kitchen-fires. Rural and urban residential and non-residential structural fires are also largely man-made fires.

The slightest contact of highly inflammable liquid contents, such as gasoline (petrol), paraffin (kerosene), or gas with fire brings explosive services of destruction, inferno and loss of lives and property (Adeleke, 1993). It was in these light that the Aqua group (1984) reported that there must be presence of three basic elements or

ingredients of fire, which is referred to as fire`s own eternal triangle before fire can break out (see Appendix 1). According to Oludare (2000), there has been emphasis on the provision of fire fighting equipment for the fire service offices in the country. Millions of Naira are been spent to train fire-men in fire-men combat, but little has been done to look at fire safety practices in the buildings where there is likely to be occurrence of fire. In most times, fire-fighters are been blamed for fire incidents in public building, and all their possible loopholes seriously explored. But little has been said or explored about the activity of the other stakeholders in the construction and uses of public buildings, which are mostly responsible for the causes of fire outbreak (Makanjuola et al, 2009).

Some instances of fire outbreak in Nigeria included the one that occurred where two students loss their lives in University of Ilorin, Kwara State in 2009 as a result of electrical fault. Another serious and memorable incidence of fire outbreak in Nigeria was the fire which struck the six – storey building of the Nigerian Port Authority (NPA) in Marina on Thursday the 19th day of June, 2008 (Odueme and Ebimomi, 2008). The Nigerian Telecommunications Limited (NITEL) headquarters in the same Marina was gutted by mysterious fire in the early 80s during the Second Republic. Also not too long Ibadan branch of the Central Bank of Nigeria (CBN) was up in flame leading to loss of several vital documents. In the same vein, it was reported in www.leadership.ng (2011) that fire outbreaks in Nigeria records 1,000 deaths and 7,000 fire accidents annually. One of such cases is shown in the Appendix.

The findings by many researchers, among which are Mogbo (1998), Anyawata (2000), Shittu (2001); Shittu (2007), Shittu (2009) and Shittu et al (2013a & b), confirmed the fact that fire incidences affect buildings of individuals, corporate organizations, government and government parastatals. The major causes of fire outbreak are electrical and gas faults, resulting in to financial and non financial losses. The incidences of fire outbreak and losses resulting from them increase annually as reported by these authors. In view of this background, the incidence of fire outbreak in Nigeria has become a threat not only to the citizens but also to the Government and this makes it a threat to national development.

In the light of the above, Shittu (2001) studied the incidence of fire outbreak in residential and public building of Kwara State and discovered that the amount of financial loss due to fire on the average was about 4% of the capital expenditure (i.e. ₦14,548,694.00). In the same vein, Shittu et al (2013b) discovered that the incidence of fire outbreak increases annually and a greater frequency of fire incidents occur in domestic rather than public buildings and that fire outbreak occurs more as a result of electrical faults rather than other causes of fire. These studies however did not look at the effect of incidence of fire outbreak on the capital expenditure budget which is of a major concern to the construction sector as a whole.

It is a known fact that incidence of fire leads to damage to lives and property and eventually financial loss. In an attempt to offer assistance to victims, Government gives compensation to victims of domestic building fire incidences and carry out rehabilitation/reconstruction during public building fire incidences. The money used for these compensation and reconstruction comes directly or indirectly from the capital expenditure budget. In the light of this, capital expenditure depends on frequency of fire incidence. It is against this background that this study set out to study the relationship between cost resulting from the incidences of fire outbreak and the amount of capital expenditure in Kwara State in order to minimize or halt the trend and save the government cost that can be diverted to capital projects, to enhance growth and development in the construction sector. To achieve this aim, the study set out to: i. present a trend analysis of the amount of financial loss due to the incidence of fire outbreak in comparison

with the amount of financial salvage from fire outbreak incidence; ii. compare trends of fire incidences between residential and public buildings/causes of fire; iii. establish the relationship between amount of financial loss and annual capital expenditure of Kwara State from 1990-2013.

The result of this study will assist the Government to understand how consequential the increase in the number of fire incidence can be to the national economy aside its effects on lives and property. Individuals will also be awakened to the need for putting a proactive fire prevention/precaution in place to prevent or discover incidence of fire in good time.

This research covered the total number of recorded fire cases; fire outbreak due to electrical and gas faults; amount of financial loss/salvage due to fire incidence; and the annual capital expenditure in Kwara State from 1990-2013. The limitation of the study was that cost resulting from fire incidence (financial loss) in public buildings was not separated from the amount of financial loss and as a result the study could not relate capital expenditure to financial loss from public building fires but only to total amount of financial loss.

2. METHODOLOGY

The data collected for the study was from the secondary source. Data on recorded fire cases and causes of fire were obtained from the archive of Kwara State Fire Service, while data on annual capital expenditure were gathered from the record of National Bureau of Statistics.

The use of tables and bar charts were employed to present the collected data to make data more comprehensive and useable. The use of bar and line graph was employed to carry out trend comparison of the variables of the study. The study also employed the use of regression and correlation analyses, with the aid of SPSS 15.0 software, to determine the relationship between the amount of financial

loss/salvage due to fire outbreak and the annual capital expenditure of Kwara State from 1990-2013. The use of regression analysis has also been adopted in the studies of Anyawata (2000), Shittu (2001); Shittu (2007), Shittu (2009) and Shittu et al (2013a & b). These studies used regression analysis to establish the relationship between frequency of fire incidence and financial and non – financial losses resulting from fire incidence. This study therefore adopts this technique in order to achieve the objectives stated in the introductory section of this paper. The Correlation and Regression analyses carried out for the study were based on the following decision rules:

i. *Coefficient of Correlation (R)*

If R ≥ 50% (50-100%); there is strong correlation.

If R < 50%; there is weak correlation.

ii. *Coefficient of Determination (R^2)*

If R^2 is from 50-100%; there is strong relationship.

If R^2 is less than 50%; there is weak relationship.

iii. *Level of Significance*

(a) *Probability (P) Test of Significance:*

If P value < 0.05; relationship is significant.

If P value > 0.05; relationship is not significant.

(b) *F-Test of Significance:*

If F calculated > F tabulated; relationship is significant.

If F calculated < F tabulated; relationship is not significant.

It is important to note that F calculated is the F value obtained from analysis while F tabulated is the F value obtained from statistics table by checking Degree of Freedom 1 under Degree of Freedom 2 (DF1 and DF2). The regression analysis was carried out to test the following hypotheses.

i. There is no significant relationship between the number of fire cases and the amount of financial loss/salvage.

ii. There is no significant relationship between the number of fire cases and the amount of capital expenditure of Kwara State.

iii. There is no significant relationship between the amount of financial loss and the amount of capital expenditure of Kwara State.

3. RESULTS AND DISCUSSIONS

3.1 Data Presentation

The data collected on the recorded cases of fire incidence, causes of fire, types of fire, the amount of financial loss/salvage due to incidence of fire outbreak and the capital expenditure of Kwara State from 1990 to 2013 are presented in Tables 1 and 2.

Table 1: Data on Recorded Fire Cases

Year	No. of fire incidence	Electrical Faults Fire	Gas Faults Fire	Residential Buildings Fire	Public Buildings Fire
1990	107	10	2	34	11
1991	142	43	4	53	7
1992	160	73	4	70	11
1993	128	24	1	38	1
1994	77	17	1	25	4
1995	45	8	1	9	1
1996	67	21	1	33	7
1997	84	21	3	32	5
1998	78	23	1	30	15
1999	73	26	1	44	8
2000	70	18	1	9	1
2001	71	14	3	12	8
2002	60	12	1	13	2
2003	61	15	2	10	1
2004	50	20	1	9	4
2005	54	10	1	15	3
2006	52	24	3	10	10
2007	53	21	1	9	1
2008	41	8	1	9	6
2009	32	11	1	11	4
2010	40	13	1	5	2
2011	29	8	2	7	5
2012	21	10	1	5	6
2013	27	12	2	6	4

Source: Kwara State Fire Service (2014)

Table 2: Data on Losses, Salvages and Capital Expenditure

Year	Amount of Financial Loss (=N=million)	Amount of Financial Salvage (=N=million)	Capital Expenditures (=N=million)
1990	1,720,000.00	9,120,000.00	321,102,120.31
1991	2,830,000.00	8,760,000.00	432,108,231.22
1992	18,100,000.00	126,550,000.00	612,177,280.29
1993	6,070,000.00	108,070,000.00	523,278,291.29
1994	25,490,000.00	56,230,000.00	327,723,241.47
1995	9,600,000.00	10,790,000.00	223,418,210.23
1996	11,270,000.00	33,290,000.00	101,620,203.25
1997	14,240,000.00	770,030,000.00	963,339,308.36
1998	35,810,000.00	33,870,000.00	423,426,247.19
1999	5,900,000.00	4,440,000.00	2,038,288,368.20
2000	6,284,500.00	15,937,500.00	3,047,365,382.14
2001	8,478,540.00	64,763,540.00	4,021,403,369.14
2002	3,842,350.00	38,420,575.00	5,025,416,402.12
2003	68,808,700.00	612,632,989.00	6,022,424,405.32
2004	24,759,600.00	70,812,300.00	7,033,445,506.22
2005	78,450,145.00	240,353,876.00	8,044,356,607.11
2006	46,910,000.00	25,981,000.00	9,055,467,608.11
2007	4,260,000.00	18,605,000.00	12,799,736,679.72
2008	1,326,000.00	6,800,000.00	19,890,139,850.81
2009	600,000.00	900,000.00	29,597,761,556.54
2010	1,040,921,000.00	1,807,042,000.00	25,939,122,967.51
2011	241,115,747.50	4,490,786,960.00	21,158,136,926.51
2012	2,123,088,330.00	229,283,800.00	24,066,722,11.94
2013	2,754,113,489.00	245,117,885.00	20,746,608,697.94
TOTAL	**6,533,988,401.50**	**9,028,587,425.00**	**178,347,867,461.00**

Source: i. Kwara State Fire Service (2014)
ii. National Bureau of Statistics (2014)

3.2 Data Analysis and Discussion of Results

The subsections below give a detailed presentation and discussion of results of the analyses.

3.2.1 Discussion of Results of Descriptive Analysis of Data

The results of the bar and line graphs are presented and discussed in this section. Figure 1 shows the comparison of trend between the amount of financial

loss and amount of financial salvage due to fire incidence in Kwara State from 1990 – 2013.
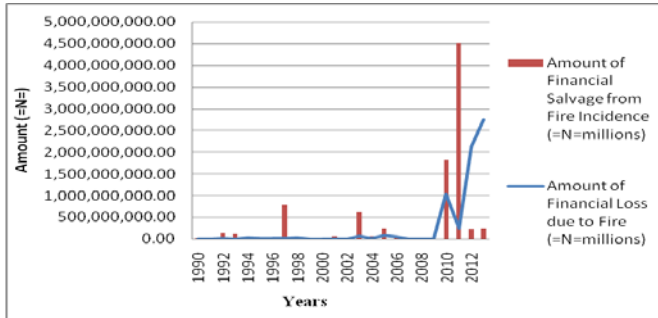
Fig. 1: Trend Comparison between Amount of Financial Loss & Financial Salvage due to Fire Incidence in Kwara State from 1990 – 2013

It was revealed from Figure 1 that over the period being reviewed the amount of financial salvage is usually greater than the amount of financial loss except in very few occasions which include the last two years. The two variables were also shown to have followed similar trend pattern on the average. It was also observed that the total amount of financial loss of =N=6,533,988,401.50 over the period under review is about 4 % of the total capital expenditure of =N=178,347,867,461.00 (see Table 1). This corresponds to the findings of Shittu (2001) cited in Shittu et al (2013a) indicating that there has not been improvement in the trend of fire outbreak till date.

Figure 2 shows the comparison of trend between the number of recorded fire cases in residential and public buildings of Kwara State from 1990 – 2013.
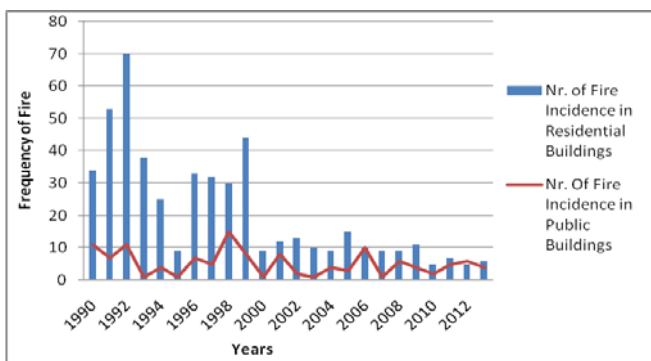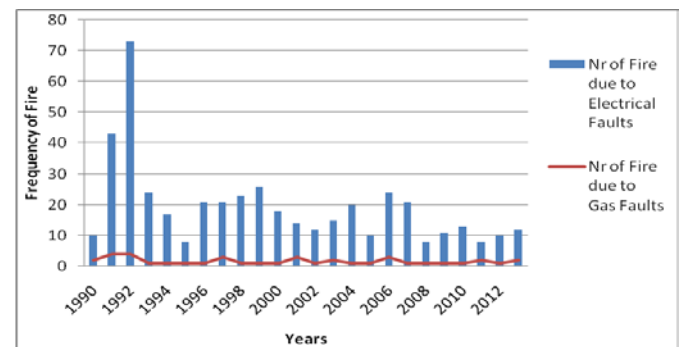

Fig. 2: Trend Comparison between Number of Fire Incidences in Domestic & Public Buildings in Kwara State from 1990 - 2013

It was noticed from Figure 2 that the number of recorded fire cases in residential buildings and the number of fire cases in public buildings of Kwara State from 1990 – 2013 did not follow similar trend pattern. Number of fire cases recorded in residential buildings was higher than the recorded cases of fire outbreak in public buildings throughout the period of study as also revealed in Figure 2. This also corresponds to the findings of Shittu (2001) and Shittu et al (2013a) indicating that there has not been improvement in the trend of fire outbreak till date in Kwara State.

Figure 3 shows the comparison of trend between the number of recorded fire cases due to electrical faults and the number of fire cases as a result of gas faults in Kwara State from 1990 – 2013.

Fig. 3: Trend Comparison between Number of Fire Incidences due to Electrical & Gas Faults in Kwara State from 1990 - 2013

It was observed from Figure 3 that the number of recorded fire cases due to electrical faults and the number of fire cases as a result of gas faults also did not follow similar trend pattern. The number of fire cases due to electrical faults was higher than the recorded cases of fire outbreak as a result of gas faults in Kwara State throughout the period of study as also revealed in Figure 3. This is also in line with the findings of Shittu (2001), Shittu (2007) and Shittu et al (2013a) showing that there has not been improvement in the trend of fire outbreak till date.

3.2.2 *Discussion of Results of Regression/Correlation Analysis*

The use of correlation and regression analyses were employed to determine the degree of association and the relationship between the variables tested in this study. The first analysis was carried out to determine the relationship between the number of fire cases and the amount of financial loss due to fire in Kwara State. It was observed that there exists a weak, negative and significant relationship between the variables. The coefficient of determination (R^2) value observed was 18% implying weak relationship and the correlation coefficient (R) observed was 43% indicating fairly strong degree of association between the variables. The negative correlation observed between the variables indicates a tendency that an increase in the number of fire cases will be followed by a decrease in the amount of financial loss due to fire in Kwara State and vice versa. The value of F calculated of 4.732 observed was greater than the value of F tabulated of 4.30 while the probability (P) value of 0.037 observed was less than 0.05. This led to the rejection of the null hypothesis which states that there is no significant relationship between the variables. This slightly differs from the findings of Shittu (2001) and Shittu et al (2013a) where it was revealed that a non-significant relationship existed between the number of fire cases and the amount of financial loss due to fire in Kwara State.

The second analysis showed a negative, weak and non-significant relationship between the number of fire cases and the amount of financial salvage from the incidence of fire outbreak in Kwara State. The R^2 value observed was 8% implying weak relationship and the R value observed was 28% indicating weak degree of association between the variables. The negative correlation observed between the variables indicates a tendency that an increase in the number of fire cases will be followed by a decrease in the amount of financial salvage due to fire in Kwara State and

vice versa. The value of F calculated of 1.863 observed was less than the value of F tabulated of 4.30 while the P value of 0.186 observed was greater than 0.05. This led to the acceptance of the null hypothesis which states that there is no significant relationship between the variables. This corresponds to the findings of Shittu (2001) cited in Shittu et al (2013a) indicating that there has not been improvement in the trend of fire outbreak till date.

The third analysis also showed a negative, weak and significant relationship between the number of fire cases and the amount of capital expenditure in Kwara State. The R^2 value observed was 36% implying slightly weak relationship and the R value observed was 60% indicating a strong degree of association between the variables. The negative correlation observed between the variables indicates a tendency that an increase in the number of fire cases will be followed by a decrease in the amount of capital expenditure in Kwara State and vice versa. The value of F calculated of 12.504 observed was greater than the value of F tabulated of 4.30 while the P value of 0.002 observed was less than 0.05. This led to the rejection of the null hypothesis which states that there is no significant relationship between the variables.

On the other hand a positive, slightly weak and non-significant relationship was discovered between the amount of financial loss due to fire cases and the amount of capital expenditure in Kwara State in the fourth analysis. The R^2 value observed was 10% implying weak relationship and the R value observed was 32% indicating weak degree of association between the variables. The positive correlation observed between the variables indicates a tendency that an increase in the amount of financial loss due to fire cases will be followed by a corresponding increase in the amount of capital expenditure in Kwara State and vice versa. The value of F calculated of 2.455 observed was less than the value of F tabulated of 4.30 while P value of 0.131 observed was

greater than 0.05. This led to the acceptance of the null hypothesis which states that there is no significant relationship between the variables.

The above discussed results of the analyses are summarized in Table 3.

Table 3: Results Summary for Inferential Analysis

Analysis No.	Variables		Inferences					
	X	Y	R/R^2 (%)	F_{cal}	F_{tab}	P_{value}	Strength of Relationship	Remark
1	Nr. Of Fire Cases	Financial Loss to Fire	43/18	4.73	4.3	0.037	Weak	SS
2	Nr. Of Fire Cases	Financial Salvage from Fire	28/8	1.86	4.3	0.186	Weak	NS
3	Nr. Of Fire Cases	Capital Expenditure	60/36	12.50	4.3	0.002	Slightly Weak	SS
4	Financial Loss to Fire	Capital Expenditure	32/10	2.45	4.3	0131	Weak	NS

KEY: SS = Statistically Significant
NS = Not Significant

4. CONCLUSION

The research findings revealed that the total amount of financial loss of =N=6,533,988,401.50 over the period under review was about 4 % of the total capital expenditure of =N=178,347,867,461.00. The amount of financial salvage from fire incidences was always higher than the amount of financial loss over the period under review. Fire incidences occur more in residential buildings than in public buildings over the period under review. Fire outbreaks were observed to be caused more as a result of electrical faults than gas faults. Significant relationship exists between number of fire cases and the amount of financial loss due to fire. Significant relationship also

exists between the number of fire cases and the amount of capital expenditure in Kwara State.

Finally, the research findings show that a positive correlation exists between the amount of financial loss due to fire cases and the amount of capital expenditure in Kwara State indicating a tendency that an increase in the amount of financial loss due to fire cases will be followed by a corresponding increase in the amount of capital expenditure in Kwara State and vice versa. This implies that more funds are being diverted for repairs and compensation by the Government yearly due to the incidence of fire outbreak. On this note, it can be concluded that there has not been improvement in the trend of fire out break recorded over the study period.

In view of the conclusions made from this study, it was recommended that the Kwara State Fire Service should strengthen their officers more in the area of rescue operations and fire fighting so that more lives and property can be saved because it was discovered that amount of financial salvage was more than the amount of financial loss and positive correlation exists between the amount of financial loss and the capital expenditure. Kwara State Government should focus more on enlightenment programme for the people on how to fight fire before the arrival of fire fighters.

In view of the limitation of the study, it was suggested that Kwara State Fire Service should improve their record keeping by separating amount of losses /salvages from fire incidence into the different building types (i.e. whether residential or public).

REFERENCES

Adeleke, S. (1993). Fire: An Ambivalent Substance. *The Herald.* 25th October. Pp 12.

Anyawata, C.H.(2000). *Analysis of fire outbreak in Niger-Delta, Nigeria.* Unpublished B. Tech Thesis, Department of Quantity Surveying, Federal University of Technology, Minna.

Aqua Group (1984). *Fire and Building.* Granada Publishing, Great Britain.

Leadeship Newspaper (2011). Nigeria Records 1,000 Deaths, 7,000 Fire Accidents Annually. *Leadership Newspaper Groups*. Y S Media Coy., Abuja. Retrieved from www.leadership.ng/articles on 6/1/2013.

Makanjuola, S.A, Aiyetan, A. O and Oke A.E. (2009), Assessment of Fire Safety Practice in Public Buildings in Western Nigeria. *RICS COBRA Research Conference*, University of Cape Town, September 2009.Pp1-21.

Mogbo, T.C (1998), Fire Outbreak and the Urban Environment in Nigeria: Implication on Public Policy and Politics. In A. A. Ndanusa (Ed.); *The Quantity Surveyor*. A Journal of the Nigerian Institute of Quantity Surveyors, Lagos. January – March. Pp31-32, 36-38.

Oludare, L (2000). Season of Fire, Shelter Watch, May/June 29-30.

Oyeyode, M. (2003). *The Construction and Design of Fire Fighting Equipment in the Building in the Building Industry*. A Term Paper of Quantity Surveying Department, Federal Polytechnic, Ede. May. 2, 4, 7 & 8.

Shittu, A.A (2001). *An Analysis of Losses due to Fire Incidence in Residential and Public Buildings of Kwara State (1990-1999)*. Unpublished B.Tech. Thesis Quantity Surveying Department, Federal University of Technology Minna, Nigeria.

Shittu, A.A (2007), Fire Outbreak in Domestic and Public Buildings of Niger State: A Comparative. Analysis of Military and Civilian Era (1993-1998 and 1999-2004). *Nigerian Journal of Environmental Science*. School of Environmental Technology, Federal University of Technology, Minna. Vol.2 November (2007) Pp139-146.

Shittu, A.A (2009), An Analysis of Losses due to Fire Incidence in Domestic and Public Buildings of Some Selected State in North-Central Nigeria. *Journal of Environmental Science*. Feculty of Environmental Sciences, University of Jos, Jos, Nigeria. Vol. 13(1) June (2009) Pp54-61.

Shittu, A. A., Oke, A. A., Adamu, A. D. & Shehu, M. A. (2013a). A Comparative Analysis of Fire Incidences in Domestic and Public Buildings during the Military and Civilian Era in Kwara State, Nigeria (1990 – 1999; 2000 – 2009). In A. S. Abdulkareem, S. A. Abdularahaman, A. A. Amadi & M. Abdullahi (Eds.). *3rd Biennial Engineering Conference: Conference Book of Proceedings.* Schoolof Engineering and Engineering Technology, Federal University of Technology, Minna, Nigeria. Tuesday, 14th – Thursday, 16th May, 2013. Pp 255 – 267.

Shittu, A. A., Adamu, A. D., Oke, A. A., Aliyu, S. & Shehu, M. A. (2013b). Appraisal of Fire Safety Provisions in Tertiary Institutions Buildings in Minna. In M. Zubairu (Ed.). *Centre for Human Settlement and Urban Development (CHSUD) Journal*. Federal University of Technology, Minna, Nigeria. December, 2013, Volume 4(1): 64 - 72.

University of Gulph (2003). http://en.wikipedia.org/wiki/Fire Classes.

APPENDIX

Appendix 1: Fire Triangle

Appendix 2: Picture Showing Firemen Trying to Put Out Fire during an outbreak of Fire in Ilorin, Kwara State.

Appendix 3: Picture Showing Firemen Trying to put out Fire during an outbreak of Fire in Kwara State, Nigeria.

Mineralogical Characterization of Agbaja (Nigeria) Iron Ore

R. A. Muriana[1,2]

[1] Department of Mechanical Engineering, Federal University of Technology, Minna, Nigeria
[2] Chemical Engineering Department, University of Johannesburg, Doornfontein, Johannesburg, South Africa
*mraremu@yahoo.com , +2347037849369.

ABSTRACT

The mineralogy of Agbaja iron ore is established in this study. Phase characterization, using X-ray Diffraction (XRD), revealed that goethite was the major iron phase in the ore while microstructures analysis at $\times 250$ contact magnification affirmed the fineness of the iron mineral grains in the ore. X-ray Fluorescence (XRF) showed 89.64% iron oxide content, which qualified the ore as metallurgical iron ore grade. The sulphur content of the ore is below 0.06% while 2.5046% of phosphorus oxide content is found to be a challenge in metallurgical applications of the ore.

Keywords: *Goethite, X-Ray Diffraction and Peaks.*

1. INTRODUCTION

The Kogi State government of Nigeria is currently considering full exploration of Agbaja iron ore. This work is aimed at providing detailed mineralogical properties of the ore to assist in an economic and gainful exploration. Agbaja iron ore deposit (Figure 1) with proven reserve of one billion metric tones can be adjudged as the largest iron deposit in Nigeria yet unharnessed (Tom and Revy, 2012). Proper exploration techniques require detailed and qualitative beneficiation techniques. Hence, there is need for mineralogical characterization of the ore to obtain clear information on its compositions, texture, morphology and concentrations of respective constituents and to recommend better beneficiation techniques. The techniques are meant to reduce the level of unwanted associate elements in the iron ore to the barest minimum. Associate elements such as sulphur and phosphorous are considered 'poisonous' to iron beyond 0.6% and 0.04% respectively. High sulphur content in iron decreases its ductility and notch impact toughness, especially in transverse direction. Weldability of steel decreases with increase in sulphure. Phosphorous weakens steel as it combines with iron to form FeTiP and Fe_3P (Xinli et al, 2010 , Brooks and Lambert 1978). The lower the sulphure content in iron the lower the hysteresis loss and the higher the magnetic flux density (Yoshihiko et al, 2002). In 2012,

Obot and Anyakwo studied the potential of micrococcus bacterial species to refine Agbaja iron ore through submerged culture technique. The efficiency of the technique was however hampered by rapid decline in microbial population as the experiment proceeded. Alafara et al (2005) also carried out direct extraction of iron mineral from Itakpe (Nigeria) iron ore samples using hot (55^oC) hydrochloric acid as the leaching reagent. Viable and economic exploration of the ore can only be achieved after proper characterization using the necessary equipment (Habashi, 1998, Baba et al 2003, Hanno, 2001). Olympus BX41 Optical Microscope, equipped with Bertrand Lens, Ultima IV Rigaku X-Ray Diffraction with monochromatic copper K-α radiation operated at 40 Kv and 30 mA over 2Theta range of 3^0 - 90^0 and Primus II Rigaku XRF operated at Rh 4.0 Kw, 24 Kv 2m A in the University of Johannesburg, Republic of South Africa were all utilized in the characterization process.

2. METHODOLOGY

Samples of iron ore used for this study were obtained from Agbaja mines located in Kogi State, Nigeria. Some 250 g of the ore were comminuted using Jocker Rock crusher and pot milled for 50 sec; the samples were test screened through 355 µm, 300 µm, 212 µm, 150 µm and 106 µm aperture sizes. Section of the ore was viewed through transmitted light microscope. Ore elemental and

mineralogical composition analyses were performed using XRF and XRD respectively. Polished section was viewed under metallurgical reflected light microscope at 250 contact magnification.

3. RESULTS AND DISCUSSION

The hand specimens were identified as sedimentary, hard and opaque ore mineral. The particle size distribution after comminuting is presented in Table 1. Fair sieve fraction distribution portrayed a hard material with highest fraction of 41.65% by weight of particles less than 106 µm. The resolution of ore minerals as infra red ray passed was captured according to Plate 1. Iron dominated field with alumina-silica patches (deep brown); invisible grain boundaries reflect the absence of coarse grains. Table 2 presents the XRF elemental compositions of the ore. The elements are in their oxide form. Iron accounted for 89.64% of the total ore with metallurgical unacceptable phosphorus level of 2.5046% which can cause cold shortness (brittleness) of iron, possible beneficiation techniques must reduce the level to less than 0.05% for ferrite stabilization, (Higgins, 1983 Zhongzhu et al 2005) . Alumino-silica accounted for less than 8% of the total ore which suggests a high grade iron ore. The ore morphology, as revealed at 250 contact magnification, will constitute a major problem for valuable mineral liberation during comminuting circuits. Plates 2 and 3 present the ore microstructure under reflected light microscope. Grain boundaries were invisible which clearly suggests fine-grained texture and extreme fineness of the ore minerals.

Table 1: Screen Test Results.

S/N	Normal Aperture size (µm)	Sieve size Range (µm)	Sieve Fractions Wt* (g)	% wt**	Cumulative % undersize	Cumulative % oversize
1	355	+355	33.95	15.19	84.81	15.19
2	300	-355+300	14.70	06.58	78.23	21.77
3	212	-300+212	28.80	12.88	65.35	34.65
4	150	-212+150	29.95	13.39	51.96	48.04
5	106	-150+106	23.04	10.31	41.65	58.35
		-106	93.13	41.65		
			Σwt =223.57			

Phases identification according to XRD analysis is shown in Figure 2. Peaks of Goethite and aluminian synthetic (($Fe_{0.83} Al_{0.17}$) O (O H)) phases accounted for 84.39%, while cristobalite-beta high (Si O_2) accounted for 15.6% of the total ore. This is in agreement with other generated results in this work. Primary lines (peaks) are majorly confined to the major constituent, which is iron mineral.
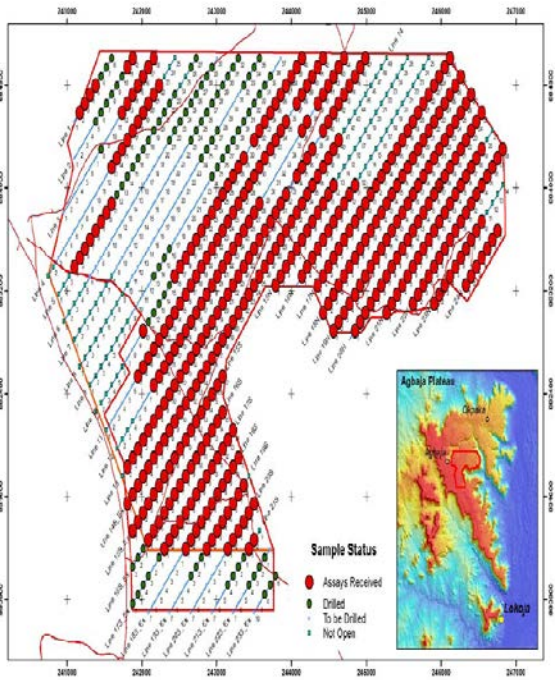
Table 2: XRF Analysis Results

S/N	Component	% Composition
1	MgO	0.0232
2	Al_2O_3	4.9733
3	SiO_2	2.3234
4	P_2O_5	2.5046
5	SO_3	0.0534
6	Cl	0.0085
7	K_2O	0.0089
8	CaO	0.1041
9	TiO_2	0.1379
10	V_2O_5	0.0598
11	Cr_2O_3	0.0193
12	MnO	0.0418
13	Fe_2O_3	89.6366
14	ZnO	0.0428
15	SrO	0.0202
16	Y_2O_3	0.0099
17	ZrO_2	0.0108
18	PbO	0.0216

Figure 1: Iron Deposit on Agbaja Plateau (Tom and Revy, 2012).

4. CONCLUSION

The mineralogy of Agbaja iron ore is goethitic with fine grains. The ore is qualified as metallurgical iron ore grade. The sulphure content of the ore is below 0.06% while 2.5046% of phosphorus oxide content is a challenge in metallurgical application of the ore.
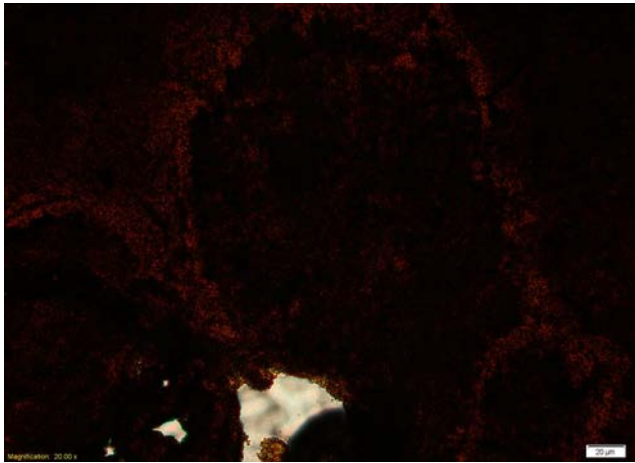
Plate 1: Petrograph showing Iron oxide Mineral in its characteristic reddish reflection as infra red light passes (×20)
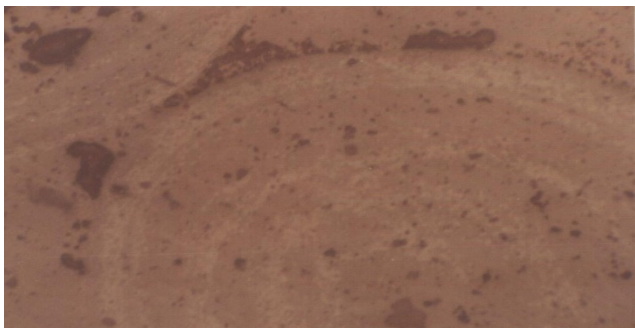
Plate 2: Extremely fine grains of Iron mineral with silica inclusions (×250).
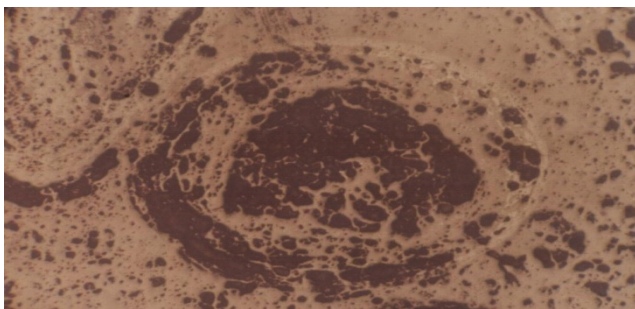
Plate 3: Patches of Silica (deep brown) dispersed in the formation (×250).
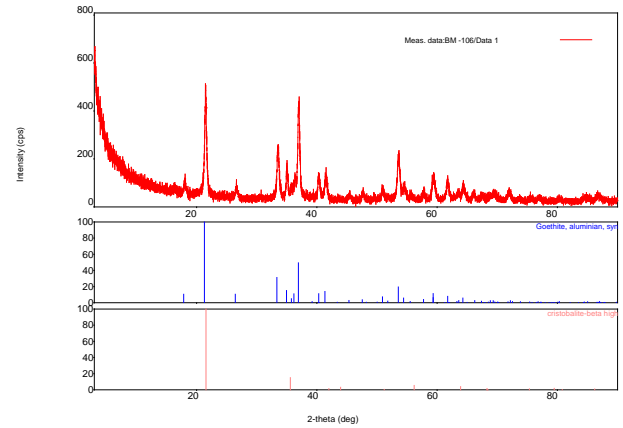
Figure 2: Goethite, aluminian, syn ((Fe0.83 Al0.17) O (O H)) : 84.39%, cristobalite-beta high (Si O_2): 15.6%

REFERENCE

Alafara A. Baba; Adekola F.A; Folashde A.O, (2005) *Quantitative leaching of a Nigeria iron ore in Hydrocholoric acid*, page 15-20.

Baba A A., Adekola F.A, Mesubi M.A and Bale, R.B, (2003).Journal of Chemistry Society of Nigeria, Vol 28, part 1, page 40-44.

Brooks J.A. and Lambert Jr. (1978). The Effects of Phosphorous, Sulfur and ferrite Content on weld Cracking of Type 309 Stainless Steel. Pp 1-6.

Habashi, F., (1998); *"Principles of Extractive Metallurgy Amalgam and Electormetallurgy"*, vol . 4, Metallurgie Extractive Quebec/ Laval University Bookstore zone, Quebec city, pp. 15-16.

Hanno Z. (2001). X-Ray Diffraction: How it Works. University of South Caroline, Bicentennial Lecture.

Higgins R.A. (1983), Applied physical metallurgy, page 220– 496

Tom and Revy, (2012). Kogi State Agbaja Plateau Iron Ore Project Report.

Xinli S., Zexi Y., Juan J., Di W., Pinghe L., and Zhaojin D. (2010). "*Effect of Phosphorous Grain Boundaries Segregation and Precipitations on Mechanical Properties of Ti-IF Steel after Recrystallization annealing*" Journal of Material Science Technology. 26 (9). Pp 793-797.

Yoshihiko O., Yasushi T., Nobuo Y., Atsushi C. and Katsumi Y. (2002). "*Ultra- Low Sulfur Non-Oriented Electrical Steel Sheets for High Efficient Motors: NKB-Core* ". NKK Technical Review, No 87. Pp 12-18.

Zhongzhu L., Yoshinano K and Kotobu N. (2005); "*Effect of Phosphorous on Sulphide Precipitation in Strip Casting Low Carbon Steel*", Materials Transactions, Vol 46,No 1. Pp 26-33. The Japan Institute of Metals.

Improvement of Multicast Algorithm for Bandwidth Utilization over Wireless Networks

Joseph Stephen Soja, Suleiman Mohammed Sani, Suleiman Garba and A.M.S Tekanyi
Department of Electrical and Computer Engineering, Ahmadu Bello University, Zaria. Kaduna state
sojsteve@gmail.com, smsani@abu.edu.ng, sgarba@abu.edu.ng and amtekanyi@abu.edu.ng

ABSTRACT

Multicasting has been given attention because of its numerous applications in many areas such as audio conferencing, video conferencing, and video-on-demand services. The service ability of these applications depends largely on how the cost of bandwidth used is minimizedduring multicast. Performance metrics such as packet delay, packet loss, throughput, congestion and packet rejection lead to large bandwidth requirement and they hinders smooth transmission of messages to destination nodes. Hence, this paper proposes an Improved Network Coding Algorithm (INCA) based on linear programming framework formulated as a mixed integer programmingproblem to address the cost of bandwidth. The proposed INCA considers packet loss and packet delay collectivelyin order to significantly minimize the cost of bandwidth during multicast. The simulation results showed that the INCA largely achieved a reduction in the cost of bandwidth when compared to the NCA used as a benchmark

Key words:Network coding, Multicast Network Model, Coded Packets, Wireless Network and Optimization

.

1. INTRODUCTION

The process of routing messages from a source to a set of destination nodes is known as multicast (Wen and Liao 2010). According to (Zhansong 2005), multicast video streaming and video conferencing has become an important application for many key requirements of computer networks supporting numerous multimedia applications (Lertpratchya et al. 2014).Multicasting requires many issues to be addressed such as bandwidth, topology, loss of packets, delay, routing, reliability, security and quality of service, before it can be fully deployed (Qadir et al. 2014).

Often there is a great challenge of bandwidth cost allocation with broadcasting, most especially, when the users are linked to a common source at a minimum cost (Bhattad et al. 2005). The problem of finding node transmission cost such that the total cost is minimized as a solution to an optimization problem is referred to as minimum cost multicast (Wen and Liao 2010). Different optimizations goals have been formulated and applied in multicast algorithms to minimize bandwidth and energy consumption. One of such goal is providing minimum delay along the tree, which is an important factor for many multimedia applications.Minimizing the total bandwidth utilization of the link and energy consumption is the goal for most optimization problems for multicast routing algorithms (Zhu et al. 1995).

Two models are usually associated with multicast: the node-based model and link based model. The node based

model is mostly used during multicasting because single transmission can be heard by several nodes rather than using a link based model where a node transmits separately to each of its neighbours resulting in increased cost of operation (Xiong and Li 2010).

The reminder of this paper is presented in sections: section I is about the introduction, section II is about network coding techniques, section III deals with the review of related works, performance metrics that affects multicast and the multicast network models. In section IV, the INCA and its implementation are described and section V discusses the experimental results, while section VI concludes the paper.

II. Network Coding Techniques

Network coding offers many benefits along with diverse dimensions of communication networks, such as throughput, wireless resources, security, complexity, and resilience to link failures(Chou and Wu 2007). Network coding requires the transmission, encoding and re-encoding of messages arriving at nodes inside the network, such that the transmitted messages can be decoded at their final destinations (Archer et al. 2004). It also improves network security because adversary node can combine packets using secure coefficient to enhance privacy and increase data integrity (Hamza et al. 2013).Packet networks involves the transmission of packets in form of 0s and 1s.
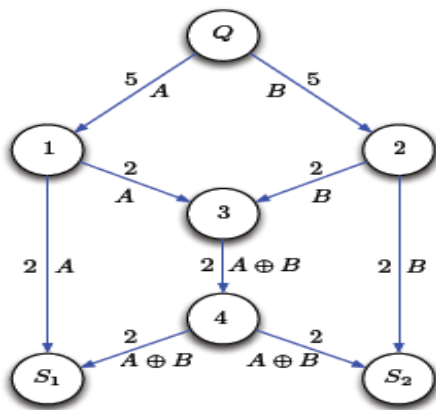

Figure 1: Network Coding Techniques (Ajibesin et al. 2012)

From Figure 1 node Q is the source node that sends packets A and B to node 1and 2, respectively. Node 3 combines the incoming packets A and B to the new packet $A \otimes B$ and sends it via 4 to both sinks $S_1$and S_2. When sink S_1 receives packet A and sink S_2 receives packet B, they can each derive the other packet by using XOR on $A \otimes B$ and A, as well as B. This process continues until packets are concurrently transmitted from a source to a set of receivers.

a). Random Linear Network Coding

Random Linear Network Coding (RLNC)concern how fast eachnode receivescomplete information, that is, the rate of information arrival at eachnode (Li et al. 2003). This is implemented by combining packet with independent, random and non-zero coefficient and it finds application in real time multicasting(park et al. 2006; Katti et al. 2006).

b). Opportunistic Network Coding

In opportunistic network coding (ONC), packets are coded at different session and each node uses the idea of what its neighbouring nodeshasand each encoded packet can be decoded immediately at the next stage (Cui et al. 2008). In these case, packets combinations are selected according to the received and lost packet states of each link, where nodes often reads packets that are not designated to them (Chen et al. 2007).

III. Related Works

(Lun et al. 2006)Provided an overview of minimizing the total cost of energy consumption for multicast packets in wired and wireless networks. They achieved reduction in the problem of multicast programming. However, some of their limitations were the stability of their decentralized algorithm under changing conditions and exploring a

specific approximation method for use in the formulation of dynamic multicast.

(Ajibesin et al. 2012)studied the performance of multicast algorithms over coded packet wireless network by using Network Coding Algorithm (NCA) and Multicast Incremental Power Algorithm (MIPA). However, the issue with this work is that the network coding based-algorithm was developed to bring improvement in packet delay only.

(Rajkumar 2014) Proposed an efficient resource allocation in multicasting over mobile ad hoc networks by choosing the closest distance from the source to any node as zone leader to communicate with its group members. However, some large numbers of packets were missing in the process of delivery and hence complete packets cannot get to the destination nodes.

(Mani 2014) Examined secured multicasting for wireless sensor networks. He used public key cryptography for authentication using signature remuneration that overcomes the vulnerability of symmetric based schemes .However, the scheme designed was only compared with only two public key cryptography scheme and can be more vulnerable to hackers.

c). Performance Metrics That Affects Multicast

i.   **Packet delay**: This is the time taken for a packet to reach its destination node. (Choi et al. 2007). It can be summarized into four components namely, the propagation delay, transmission delay, nodal processing delay and lastly queuing delay.

ii. **Packet loss:** During multicast, packets loss at various nodes directly affects the performance of the networks and this lossesvaries. Most often, lost video packet may lead to significant degradation in decoded video quality, due to the use of spatial temporal prediction and sophisticated entropy coding.

iii. **Packet congestion:** This occurs when the incoming packets at the node approaches or

exceeds that of the outgoing packets (Karthikeyan and Shankar 2014). The longer the path a packet has to travel, the higher its possibility of becoming lost due to congestion, especially under high traffic (Nguyen and Xu 2007).

iv. **Throughput**: Throughput is defined as measure of the amount of time for a packet to reach it destination node in a unit period of time.

d). Multicast Network Model

A network model isa vivid description of how a set of network layers interact. A network shown in Figure 1 is usually represented as a weighted graph G (*V, E*), where *V* is a set of nodes and *E* is a set of directed links, $\mathrm{V}(G)$ and $\mathrm{E}(G)$ denote the number of nodes and links in the network.
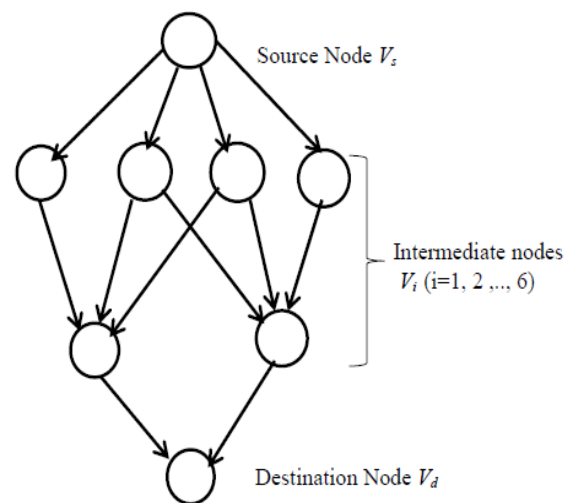
Figure 2: A Multicast Network Model (Zhansong 2005)

In figure 2,each link is associated with parameters such as link delay, link cost, link congestion, etc., which describe the current status of the link (Dutta and Mishra 2012).$M \subset V$ is a set of nodes involved in a group communication and M is called multicast group with each node $v \in M$ as a group member. Each node member v is assigned a cost $\gamma(v)$ and a delay $\delta(v)$ which are assumed to be nonnegative integers.

For a node i of the network, the cost of bandwidth required to reach another node j is given by (Duffield and Lo Presti 2000):

$$y_{ij} = c_{ij} \qquad (1)$$

where C_{ij} is the cost of bandwidth used and y_{ij} is the distance from the source node to destination nodes.

IV. IMPROVED NETWORK CODING ALGORITHM

The Improved Network Coding Algorithm (INCA) is an extension of the work carried out by [18], which can be applied to two performance metrics collectively. Considering packet delay and packet loss leads to the improvement of what the NCA did.

In developing the INCA, the value of packet delay was set to be 400ms to enhance efficient packet delivery. This also takes care of other delays such as nodal processing delay, delay on the process of transmission which is a function of link capacity, delay along the route, and queuing delay which lead to bandwidth consumption during multicast. Packet loss is set to be less than or equal to four in such a way that the cost of lost packets within this range is tolerated.

a). Mixed Integer Linear Programming Formulation

The multicast problem is formulated as a mixed integer programming because the INCA was applied to two performances metric collectively. The optimization objectives are usually defined in terms of minimizing the cost of bandwidth of the multicast tree. The objective function of this multicast problem is stated as (Das et al. 2003) :

$$\text{Min (q)} \sum_{(i,j)\in V}^{n} c_{ij} y_{ij} \qquad \forall (i.j) \in V, i \neq j \,(2)$$

Provided that equation (3) is satisfied.

$$C_{ij} \leq C_{ia_j^i} \ \forall (i,j) \in A, a_j^i \neq i \qquad (3)$$

$$\delta(p) \leq 400 \qquad \forall (i.j) \in V, i \neq j \ (4)$$

$$\rho(l) \leq 4; \ i \neq j \ \forall (i,j) \in V \ (5)$$

$$\sum_{y=1}^{n} y_{ij} > 0; \ i \neq j \ \forall i \in v/\{s\} \quad (6)$$

where:

C_{ij} = cost of the bandwidth used during multicast

y_{ij} = distance from one node to the other.

(i, a_j^i) = arc originating in node I with the lowest cost.

And also,

q = the objective function to be minimize

p = packet delay

l = packet loss

i = source node

j= destination node.

b). Installation and Configuration of the software

Visual Studio 2010 was installed along with compilers and relevant libraries for C languages and the Java Netbeans Integrated Environment (IDE) 6.7.1. In addition, the GNU linear programming kit (GLPK) was also installed, in order to launch the algorithm via revised simplex method, mixed integer linear programming via algorithms (Trapp 2009).

c). Simulation

The Java program was run first and the test file from the java program was saved in a folder and both NCA and the INCA take as input the number of randomly generated nodes from the test file and output the cost of bandwidth used during the multicast session. This process was repeated for 50, 70 and 90 randomly generated nodes multicasting to 2, 3, 4, 5, 6, 7, 8, 9, and 10 receivers in order to agree with the NCA used as a benchmark.

Figure 3: Cost of Multicast for 50 Randomly Generated Nodes to Various sets of Receivers.

V. Experimental Results and Discussion

This section shows the performance of the INCA implemented on Visual Studio 2010. The costs of bandwidth for randomly generated nodes (50, 70and 90) multicasting to various receivers (2, 3, 4, 5, 6, 7, 8, 9, and 10) were obtained.

a). Performance Evaluation of the two Algorithms

Thesummary of the results obtained for the two algorithms NCA and t INCA are shown in tables.

Table 1: Cost of bandwidth for 50 Randomly Generated Nodes Multicasting to groups of Receivers

No. of Receivers	Cost of Multicast	
	Network coding algorithm	Improved network coding algorithm
2	0.9663	0.7506
3	2.5024	1.6129
4	3.4126	2.0116
5	4.9163	2.8540
6	5.6603	4.3289
7	6.5861	5.9323
8	7.7031	6.4192
9	8.4885	6.9220
10	8.7075	7.8556

Table 2: Cost for 70 Randomly Generated Nodes Multicasting to Various Receivers

Number No. of receivers	Cost	
	Network coding algorithm	Improved network coding algorithm
2	2.1989	1.3733
3	2.4378	1.6463
4	3.9606	2.6533
5	6.5154	4.4382
6	5.8008	3.5805
7	7.5415	5.9904
8	7.3358	5.4878
9	7.5523	7.0702
10	8.6629	7.3621
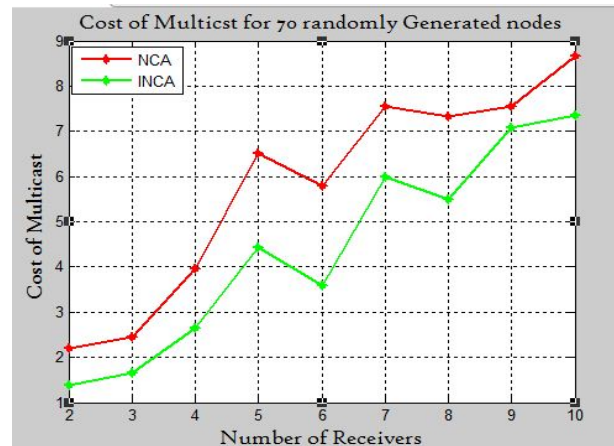
Figure 5: Cost of Multicast for 70 Randomly Generated Nodes to Various sets of Receivers.

the NCA in terms of saving or minimizing the average cost of bandwidth used during multicast by 27.9%, 23.85% and 20.9% respectively for 50, 70and 90 randomly generated nodes within the wireless network.

VI. CONCLUSION

From thetwo algorithms, it was discovered that the INCA has better performance than the existing NCA. Traffic transmission in network is now becoming coded packet instead of the present WAN, LAN and MAN which are non-traffic. This gives the coded traffic high security compare to the uncoded packets.

Table 3: Cost of 90 Randomly Generated Nodes Multicasting to Various Receivers

Number of receivers	Cost of Multicast	
	Network coding algorithm	Improved network coding algorithm
2	1.5485	1.0738
3	2.4472	2.1387
4	3.0309	2.8710
5	4.6266	4.4886
6	5.9491	2.6338
7	4.9986	4.7146
8	6.5523	5.1668
9	7.3691	5.7783
10	7.7464	6.1223

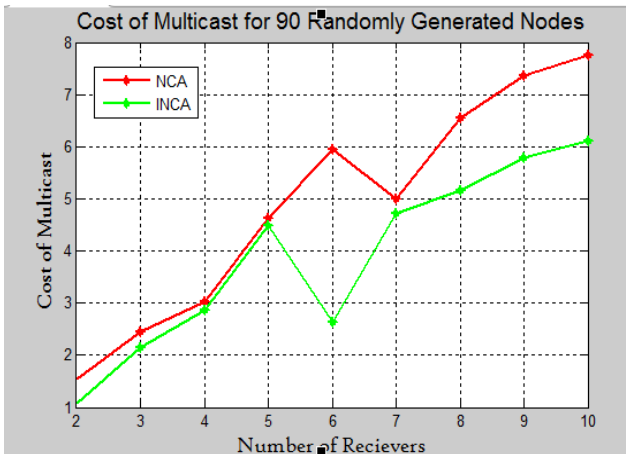

Figure 5: Cost of Multicast for 90 Randomly Generated Nodes to Various sets of Receivers.

b). Discussion

The INCA uses a node based model and the simulation results showed that the INCA algorithm with two performance metrics considered collectively outperformed the NCA. The results showed that the INCA outperformed

REFERENCES

Ajibesin, A. A., N. Ventura, H. A. Chan, A. Murgu, and O. K. Egunsola. 2012. Performance of Multicast Algorithms Over Coded Packet Wireless Networks. Paper read at Computer Modelling and Simulation (UKSim), 2012 UKSim 14th International Conference on.

Archer, A., J. Feigenbaum, A. Krishnamurthy, R. Sami, and S. Shenker. 2004. Approximation and collusion in multicast cost sharing. *Games and Economic Behavior* 47 (1):36-71.

Bhattad, K., N. Ratnakar, R. Koetter, and K. R. Narayanan. 2005. Minimal network coding for multicast. Paper read at Information Theory, 2005. ISIT 2005. Proceedings. International Symposium on.

Chen, W., K. B. Letaief, and Z. Cao. 2007. Opportunistic network coding for wireless networks. Paper read at Communications, 2007. ICC'07. IEEE International Conference on.

Choi, B.-Y., S. Moon, Z.-L. Zhang, K. Papagiannaki, and C. Diot. 2007. Analysis of point-to-point packet delay in an operational network. *Computer Networks* 51 (13):3812-3827.

Chou, P. A., and Y. Wu. 2007. Network coding for the internet and wireless networks. *IEEE Signal Processing Magazine* 24 (5):77.

Cui, T., L. Chen, and T. Ho. 2008. Energy efficient opportunistic network coding for wireless networks. Paper read at INFOCOM 2008. The 27th Conference on Computer Communications. IEEE.

Das, A. K., R. J. Marks, M. El-Sharkawi, P. Arabshahi, and A. Gray. 2003. Minimum power broadcast trees for wireless networks: integer programming formulations. Paper read at INFOCOM 2003. Twenty-Second Annual Joint Conference of the IEEE Computer and Communications. IEEE Societies.

Duffield, N. G., and F. Lo Presti. 2000. Multicast inference of packet delay variance at interior network links. Paper read at INFOCOM 2000. Nineteenth Annual Joint Conference of the IEEE Computer and Communications Societies. Proceedings. IEEE.

Dutta, B., and D. Mishra. 2012. Minimum cost arborescences. *Games and Economic Behavior* 74 (1):120-143.

Hamza, F. A., L. Romdhani, and A. Mohamed. 2013. Novel Network Coding-based Techniques for Multi-layer Video Delivery over Multi-hop Wireless testbed. *arXiv preprint arXiv:1304.7578*.

Karthikeyan, E., and R. Shankar. 2014. VoIP Packet Delay Techniques: A Survey. *Global Journal of Computer Science and Technology* 14 (3).

Katti, S., H. Rahul, W. Hu, D. Katabi, M. Medard, and J. Crowcroft. 2006. "Xors in the air: Practical wireless network coding,". *Proc. of ACM Computer Communication Review, (SIGCOMM' 2006), Pisa, Italy ,October 2006,* 36:243–254.

Lertpratchya, D., D. M. Blough, and G. F. Riley. 2014. Interference-aware multicast for wireless multihop networks. Paper read at Wireless Communications and Networking Conference (WCNC), 2014 IEEE.

Li, S. Y., R. W. Yeung, and N. Cai. 2003. Linear network coding. *Information Theory, IEEE Transactions on* 49 (2):371-381.

Lun, D. S., N. Ratnakar, M. Mêdard, R. Koetter, D. R. Karger, T. Ho, E. Ahmed, and F. Zhao. 2006. Minimum-cost multicast over coded packet networks. *Information Theory, IEEE Transactions on* 52 (6):2608-2623.

Mani, D. M. 2014. Secure Multicasting for Wireless Sensor Networks. *IJCSNS* 14 (11):70.

Nguyen, U. T., and J. Xu. 2007. Multicast routing in wireless mesh networks: Minimum cost trees or shortest path trees? *Communications Magazine, IEEE* 45 (11):72-77.

park, J.-S., ., M. Gerla, D. Lun, Y. Yi, and M. Medard. 2006. "Codecast: A network-coding-based ad hoc multicast protocol,". *IEEE Tranaction on Wireless Communications,* 13 (5):76-81.

Qadir, J., A. Baig, A. Ali, and Q. Shafi. 2014. Multicasting in cognitive radio networks: Algorithms, techniques and protocols. *Journal of Network and Computer Applications* 45:44-61.

Rajkumar, K. 2014. Efficient Resource Allocation in Multicasting over Mobile Adhoc Networks. *Indian Journal of Science and Technology* 7 (S5):71-75.

Trapp, A., ed. 2009. *Introduction to GLPK*. edited by P. I. s. chapter.

Wen, Y.-F., and W. Liao. 2010. Minimum power multicast algorithms for wireless networks with a Lagrangian relaxation approach. *Wireless Networks* 17 (6):1401-1421.

Xiong, C., and X. Li. 2010. Minimum cost optimization of multicast wireless networks with network coding. Paper read at Information Sciences and Systems

(CISS), 2010 44th Annual Conference on.

Zhansong, M. 2005. Multicast Source Routing Algorithms. *Computer science and artificail intelligent laboratory* 3:331-339.

Zhu, Q., M. Parsa, and J. J. Garcia-Luna-Aceves. 1995. A source-based algorithm for delay-constrained minimum-cost multicasting. Paper read at INFOCOM'95. Fourteenth Annual Joint Conference of the IEEE Computer and Communications Societies. Bringing Information to People. Proceedings. IEEE.

NON-INTRUSIVE NOISE REDUCTION IN GSM VOICE SIGNAL USING NON-PARAMETRIC MODELING TECHNIQUE

S.A Gbadamosi[1*], A. M. Aibinu[2], O.C.Ugweje[3], A. J Onumanyi [4], E. N Onwuka[5], & M. Aderinola[6]

[1,2,4,5]Federal University of Technology Minna, Niger State, Nigeria.

[3]Digital Bridge Institute, Abuja, Nigeria

[*]g_safiu.its@futminna.edu.ng, 08060511079.

ABSTRACT

Noise degrades the quality and intelligibility of speech. It impedes speech clarity, coding, recognition and speaker identification. To mitigate noise effect and improve speech quality, we propose Non-parametric modeling technique along with a Non-intrusive signal denoising system based on short time Fourier transforms. This paper aims to establish only the idea behind our proposed algorithm, however, we present argument to justify that our results will reduce an end to end acoustic background noise; improve quality of speech for both the speaker and the listener and eventually increase throughput. Ultimately, users' will be able to call and receive calls in a noisy environment while enjoying clarity of voice.

Keywords: *Non-parametric, Non-intrusive signal denoising system, Short time fourier transform, Speech quality.*

1. INTRODUCTION

Communication systems continue to be plagued by the limiting effects of noise. These varying noise levels degrade speech quality, especially in Global System for Mobile (GSM) communication networks, thereby creating difficulty in audio reception. An initial step towards addressing this noise challenge is being able to quantify its effect on voice signals. One performance metric for achieving this evaluation requirement is the use of speech quality[Barile et. al.2006]. Speech quality signifies the lucidity of any speaker's words as identified by the audience [Mahdi 2007].

Two main approaches used to evaluate speech quality are either the use of subjective and objective speech quality measures [Aicha 2012]. Each approach has its limitation especially in the area of reducing distortions such as noise reduction, echo cancellations, listening level, and loudness and so on [RIX, and HOLLIER 2000].

To reduce these effects, we propose noise reduction in GSM voice signals using non-parametric modelling techniques approach for evaluation of speech quality. This technique adopts the use of Non-Intrusive Signal

Denoising algorithms which employs the use of noise suppression algorithms such as Short Time Fourier Transform (STFT) algorithms. This technique will extract noise time consumption. It is user-directed and hence offers precise understanding of quality features that lead to better service acceptance from the end users. It is designed to judge speech quality alongside signal distortion, noise distortion as well as overall quality. A correlation among this specific pair of distortions and the observed quality of speech will be developed.

The paper is organised as follows. Section II introduces the related work to our research alongside with the proposed method and noise reduction techniques adopted. In section III, we elucidated the processes adopted to achieve our speech quality. In section IV, we stated the results expected to be obtained. Finally, we concluded in section V.

2. RELATED WORK

Review of related work from [Mahdi & Picovici 2009, Quackenbush et. al.1988, Rix 2006, Hansen and Pellom 1998, Noll et. al. 1976, Noll 1974, Tribolet et. al. 1978] of early simple objective measures of quality, based on metrics of overall SNR and their extension were proposed.

The limitation of the above metrics is that they lack predictive power. This lead to the discovery of linear prediction coefficients, Itakura-Saito (IS) distortion measure, loglikelihood ratio (LLR) measure, cepstral distance measure which uses cepstral coefficient and Bark spectral distortion (BSD) which measures mean squared Euclidean distance within spectral vectors of the coded utterances and the original [Rix 2006, Noll et. al 1974, Klatt et. al.1982]. The performances of the above measures predict speech quality moderately. The mathematical representation of all the above metrics can be denoted as follows [Kondo 2012];

$$SNR = 10\log_{10}\frac{\sum_n x^2(n)}{\sum_n (x(n)-d(n))^2} \tag{1}$$

$$SNRseg = \frac{10}{M}\sum_{m=0}^{M-1}\log_{10}\left(\frac{\sum_{n=Nm}^{Nm+N-1} x^2(n)}{\sum_{n=Nm}^{Nm+N-1}[(d(n)-x(n))]^2}\right) \tag{2}$$

$$fwSNRseg = \frac{10}{M}\times\sum_{m=0}^{M-1}\frac{\sum_{j=1}^{K} W(j,m)\log_{10}\frac{|x(j,m)|^2}{(|x(j,m)|-|X(j,m)|)^2}}{\sum_{j=1}^{K} W(j,m)} \tag{3}$$

$$Where \qquad W(j,m) = |X(j,m)|^\gamma \tag{4}$$

$$d_{WSS} = \frac{1}{M}\sum_{m=0}^{M-1}\frac{\sum_{j=1}^{K} W(j,m)(S_C(j,m)-S_p(j,m))^2}{\sum_{j=1}^{K} W(j,m)} \tag{5}$$

For loglikelihood ratio (LLR) measure:

$$d_{LLR}(\vec{a}_p,\vec{a}_c) = \log\left(\frac{\vec{a}_p R_c \vec{a}_p^{\,T}}{\vec{a}_c R_c \vec{a}_c^{\,T}}\right) \tag{6}$$

For Itakura-Saito (IS) distortion measure[Kondo 2012]:

$$d_{IS}(\vec{a}_p,\vec{a}_c) = \frac{\sigma_c^2}{\sigma_p^2}\log\left(\frac{\vec{a}_p R_c \vec{a}_p^{\,T}}{\vec{a}_c R_c \vec{a}_c^{\,T}}\right) + \log\left(\frac{\sigma_c^2}{\sigma_p^2}\right) - 1 \tag{7}$$

For cepstral coefficient calculation:

$$d_{CEP}(\vec{c}_c,\vec{c}_p) = \frac{10}{\log 10}\sqrt{2\sum_{k=1}^{p}[C_c(k)-C_p(k)]^2} \tag{8}$$

Where $\vec{a}_p, \vec{a}_c$ are the Linear Predictive Code (LPC) vector from the reference (original) voice signal frame and Linear Predictive Code vector from the enhanced voice frame,

respectively. While R_c is the autocorrelation matrix of the reference (original) voice signal. $\sigma_c\ and\ \sigma_p$ are the LPC (increase) gains from the reference (clean) and improve (enhanced) signals, respectively. Also $\vec{C}_c$ and $\vec{C}_p$ are the cepstrum coefficient vector from the reference (clean) and improved (enhanced) signals, respectively.

For Bark Spectral Distortion (BSD):

$$BSD = \frac{\frac{1}{M}\sum_{m=1}^{M}\sum_{i=1}^{o}[L_x^{(m)}(i)-L_d^{(m)}(i)]^2}{\frac{1}{M}\sum_{m=1}^{M}\sum_{i=1}^{o}[L_x^{(m)}(i)]^2} \tag{9}$$

Where M will be the amount of frames (speech segments) processed, O is amount of critical bands, $L_x^{(m)}(i)$ is the bark spectrum from the mth critical frame of reference (original) speech, and $L_d^{(m)}(i)$ is the mth critical frame of coded speech of bark spectrum.

In order to get better performance, many objective measures modelled approach-driven were developed, given rise to models such as Perceptual Audio Quality Measure (PAQM), Perceptual Speech Quality Measure (PSQM) [Côté 2011], Measuring Normalizing Block [BEERENDS and STEMERDINK 1994], Perceptual Evaluation of Audio Quality Measure (PEAQ) [Hekstra 2001], Perceptual Analysis Measurement system (PAMS) to Perceptual Evaluation of Speech Quality (PESQ) [Pocta 2010a]. PSQM and PESQ were adopted as ITU-T recommendation P.861and P.862 respectively [Pocta 2010b]. In spite of the high success recorded on PESQ. The search for more better, intuitive and predictive measure continues as all the above models required both the degraded signal and its corresponding clean version. The limitation of the above models is in the obtainment of the reference (clean) signal. This brings us to the counterpart method called Non-intrusive measures. The measure uses only the degraded speech signal to predict quality as against the intrusive measures. These models

range from Auditory Non-Intrusive QUality Estimation (ANIQUE) [Cote 2011], single ended assessment measure (SEAM) and so on. The basic principle adopted by Non-intrusive measure was that it depends on the relationship of three ideas released by the ITU-T as the ITU–T Rec. P.563 (2004) [Cote 2011]: (i) any derivation in the degraded signal, of various parameters relevant to the speech production system, (ii) following reconstruction of a referral signal from a degraded signal, both signals are evaluated by an intrusive model, and (iii) discovery of specific distortions in the degraded signal. Subsequently, the extracted parameters are linearly merged to anticipate voice transmission quality. Above the aggregation stage, the perceptual influence of every parameter is quantified via a distortion-dependent weighting operation [Cote 2011]. The problem of quality of speech above is that, it measures the impact of radio frequency (RF)–related impairments on hearing or Listening quality, which are not able to capture and calculate how other important voice quality impairments present in live calls e.g. background noise, acoustic echo and mismatched speech levels affect users experience. In trying to adopt this basic principle, we proposed Non-Intrusive Signal Denoising System (NISDS) using Short Time Fourier Transform (STFT) to achieve real-time execution of the algorithms as well as to obtain a trade-off in between high quality reduction in noise along with minimal computational heap. The NISDS was used to derive our reference signal before using linear predictive code (LPC) and correlation of the subjective MOS value between the Noisy speech and denoised speech (clean) to predict our quality of speech.

3.   NON-PARAMETRIC MODELLING TECHNIQUE

In contrast, non-parametric models discover the parameters for a statistical model describing a signal, system, or process. These techniques use known information about the system to determine the model. Applications for non-parametric modelling include speech and music synthesis,

data compression, high-resolution spectral estimation, communications, manufacturing, and simulation [Mathwork 1988-2015]. It usually have no sound signal to process (and thus help to make restricted utilization of perceptual techniques), but rather estimate MOS from measured properties of the underlying transport and/or terminal, for instance, echo, delay, speech levels and noise [Aicha 2012], VoIP network characteristics [Rix et. al 2000], [Mahdi and Picovici 2009], or cellular radio reception measures [Quackenbush et. al 1988]. Parametric models are traditionally used for network planning, to construct MOS estimates based on tabulated values such as the codec type, bit-rate, delay, packet loss statistics, etc. [Rix 2006]. This process demand total characterization of the system under test and consequently could be considered as Glass box approach in which no expertise in the system underneath test is required. A Non-intrusive parametric assessment such as these, would be use to address two critical issues. Firstly, estimate the occurring distortions (noise) which is a challenge since the original signal is unknown. Secondly, predict the subjective impacts of the estimated distortions. The non-intrusive parametric approach determines first, the well characterized distortions such as impulsive noise and deduced a mathematical relation among the limited set and the subjective opinions [Mahdi 2009].

4.   NOISE REDUCTION PROCESSES

In speech communication, the speech signal is always accompanied by some noise. In most cases, background noise of the environment, where the source of speech lies. The obvious effect of this noise addition is to make the listening task difficult for a direct listener. The purpose of P.835 listening tests is to assess the trade off between background Noise attenuation and foreground speech degradation that arises in noise reduction processing.

It should be noted that the improvement of overall

listening quality is not the only purpose of noise reduction processing; the removal of noise during speech pauses also helps reduce the amount of data needed for transmission. Hence, it is another form of data compression but this time eliminates distortion caused by noise. The noise reduction algorithm used in this proposal is Short time Fourier Transform (STFT). The goal of noise reduction in speech is to improve the quality of degraded speech. Two general classes of problems have been assumed depending on the point where the corrupting noise is included to the voice signal. The assumed scenarios are;

- CORRUPTING NOISE INCLUDED AT THE TALKER ENVIRONMENT: It is presumed that the person speaking is in a noisy environment while the listener is in quiet.

- CORRUPTING NOISE INCLUDED AT THE LISTENER ENVIRONMENT: It is presumed that the listener is in a noisy environment while the speaker is in quiet. i.e. a supervisor delivering guidelines to employers on a noisy factory floor [Wuhan University 2004].

5. PROPOSED ALGORITHM

This research work adopts the approach of Non-Parametric Modeling method of estimating the quality of speech using Non-Intrusive Signaling Denoising System to extract Noise parameters from Speech. A speech signal was recorded using MATLAB command and a quantified amount of synthesized Gaussian noise is mixed with it using MATLAB code to get a Noisy Speech signal. The technical conditions were in accordance with the guidelines given in ITU-T recommendation P.800. The Noisy speech has been obtained using Synthetic approach. The Noisy signal was passed into channelization chamber where it convolved with hamming window in order to obtain a windowed segmented signal. The output of the

windowed segmented signal was passed into the STFT process where the signal is analyzed, manipulated and the noise parameter in the signal is removed and any abnormal variation in the speech signal was considered as degradations. Secondly, a reference signal (denoised signal) is reconstructed from the Noisy signal with the aid of Non-Intrusive Signal Denoising system as depicted in Fig 1. In a signal comparison approach, the overall quality is finally determined from the degradation measures weighted, according to the dominant distortion identified in the speech signal and a correlation between the subjective MOS value of the degraded speech signal and the denoised (clean) speech signal.
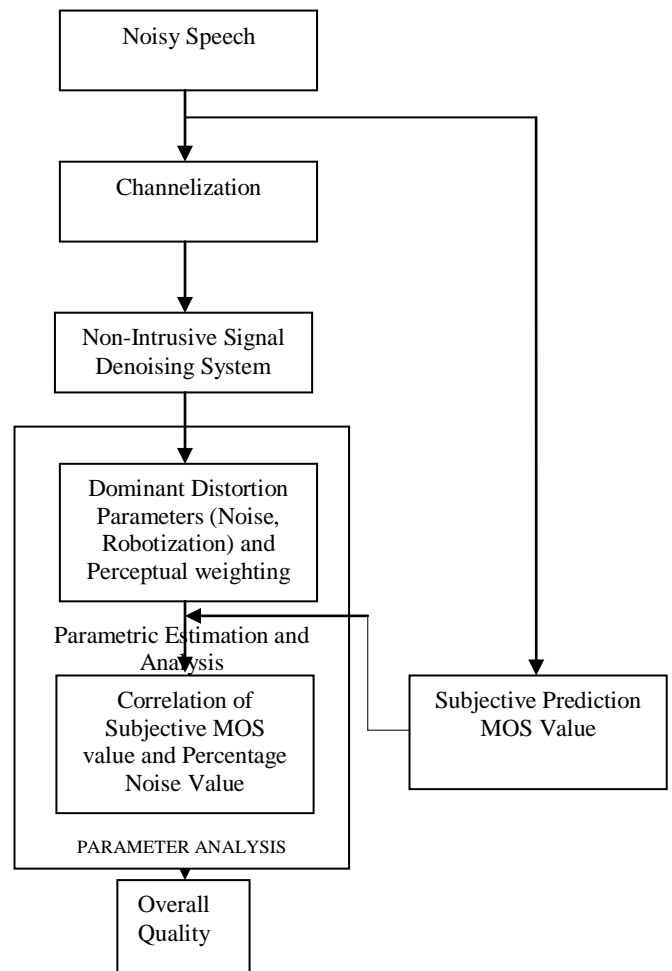

Fig 1: Block Diagram of Non-Parametric Modelling Technique

6. EXPECTED RESULT

The expected outcome of this research work will achieve an efficient model for noise reduction in GSM voice signal which will improve speech quality. Secondly, the removal of noise parameter from speech is a form of compression which increases throughput and help reduce the amount of data needed for transmission.

7. CONCLUSION

We have described how to reduce background acoustic noise in GSM voice signal using Non-Parametric modeling technique which adopts the use of Non-intrusive signal denoising system (NISDS) to reduce noise. The NISDS was based on the method of Short time Fourier transform to manipulate and analyze the noisy signal. This model when fully developed will be useful in speech analysis, recognition and of course noise reduction, which will improve speech clarity and intelligent.

ACKNOWLEDGEMENTS

REFERENCE

Ascom,*Technical White Paper Series RxQual and voice quality,* Ascom Infrasys AG

Aicha, A.B.. "Perceptual speech quality measures separating speech distortion and additive noise degradations", Speech Communication, 201205.

A.M. Noll, Cepstrum pitch determination, J. Acoust. Soc. Am. 41 (1974) 293–309.

Barile, M., Camarda, P., Dell'Aquila, R., & Vitti, N. (2006, September). Parametric Models for Speech Quality Estimation in GSM Networks. In *Software in Telecommunications and Computer Networks, 2006. SoftCOM 2006. International Conference on* (pp. 204-208). IEEE

Beerends, J., Hekstra, A., Rix, A., & Hollier, M. (1998). *Perceptual Evaluation of Speech Quality (PESQ), the new ITU standard for end-to-end speech quality assessment. Part II− Psychoacoustic model.* Technical report, ITU-T.

BEERENDS, J. G., STEMERDINK, J. A. A perceptual speech quality measure based on a psychoacoustic sound representation. J. Audio Eng. Soc., 1994, vol. 42, p. 115-123, ISSN 1549-4950

Hansen, J. H. and Pellom, B. L., \An effective quality evaluation protocol for speech enhancement algorithms," in Proc. Int. Conf. Spoken Lang. Process., 1998.

Hekstra, A.P. "Perceptual evaluation of speech quality (PESQ)- a new method for speech quality assessment of telephone networks and codecs", 2001 IEEE International Conference on Acoustics Speech and Signal Processing Proceedings (Cat No 01CH37221) ICASSP-01, 2001.

Klatt. et. al, \Prediction of perceived phonetic distance from critical-band spectra: A _rst step," in Acoustics, Speech, and Signal Processing, IEEE International Conference on ICASSP '82, 1982.

Kazuhiro Kondo. "Speech Quality", Signals and Communication Technology, 2012,

Mathworks,'Signal Processing Toolbox™ User's Guide, The MathWorks, Inc. 3 Apple Hill Drive Natick, MA 01760-2098, © COPYRIGHT 1988–2015 by The MathWorks, Inc.

Mahdi, A. E. "Voice Quality Measurement in Modern Telecommunication Networks", 2007 14th International Workshop on Systems Signals and Image Processing and 6th EURASIP Conference focused on Speech and Image Processing Multimedia Communications and Services, 06/2007.

Mahdi, A. E., & Picovici, D. (2009). Advances in voice quality measurement in modern telecommunications. *Digital Signal Processing*, *19*(1), 79-103.

Noll, P. Et. al, \Adaptive quantization in speech coding systems," in lnt. Zurich Seminar on Digital Communication (IEEE), 1976.

Nicolas Côté. "Speech Quality Measurement Methods", Integral and Diagnostic Intrusive Prediction of Speech Quality, 2011.

Peter Pocta. "Impact of fragmentation threshold tuning on performance of voice service and background traffic in IEEE 802.11b WLANs", 20th International Conference Radioelektronika 2010, 04/2010

Peter Pocta "Predictions in Case of Independent and Dependent Losses (in Presence of Receiver-Side Comfort-Noise)", Radioengineering/12102512, 20100401.

Quackenbush, S. R., Barnwell III, T. P., and Clements, M. A., Objective Measures of Speech Quality. Prentice Hall, 1988.

Rakesh Kumar, Sandeep Saini " Measuring Parameters for speech quality in cellular networks" Computer Science and Application Department, Kurukshetra University, Kurukshetra, IndiaEmail:sandeepsaini083@gmail.com, Globalize the Research.,International Journal of Advances in Computer Networks and its Security.

RIX, A. W., HOLLIER, M. P. The perceptual analysis measurement system for robust end-to-end speech quality assessment. In Proceedings of IEEE ICASSP 2000. Istanbul (Turkey), 2000, vol. 3, p. 1515-1518.

Rix, A.W. "Objective Assessment of Speech and Audio Quality—Technology and Applications", IEEE Transactions on Audio Speech and Language Processing, 11/2006

Speech Signal Processing, School of Electronic Information, Wuhan University, Chapter 5 Speech Enhancement.

Tribolet et. al, \A study of complexity and quality of speech waveform coders," in Acoustics, Speech, and Signal Processing, IEEE International Conference on ICASSP '78, 1978.

Optimal Mix of Coir Reinforced Laterite Blocks for Maximum Compressive Strength

Aguwa J. I. [1] and Gimba A. E. [2]

[1,2,] Department of Civil Engineering Federal University of Technology, Minna, Nigeria

[*] james.aguwa@futminna.edu.ng, 08033163634

.

ABSTRACT

Building construction materials like laterite and coconut fibre (coir) are available in Nigeria. But the potentials in making them into building is not explored enough. This project is centred on an experimental investigation to determine the optimum quantity of coconut fibre that can produce maximum compressive strength of coir reinforced laterite blocks. Laboratory tests such as moisture content, Atterberg limit, sieve analysis, water absorption, specific gravity, density and compaction were carried out for investigations and classifications. Two hundred cubes of size 150mm x 150mm x 150mm were moulded using coir content of 0%, 0.2%, 0.4%, 0.6%, 0.8%, 1.0%, 1.2%, 1.4%, 1.6% and 1.8% by weight of laterite, with twenty pieces of blocks per mix. These blocks were air dried in the laboratory under atmospheric condition. The compressive strength test was carried out on the blocks at 7days, 14days, 21days and 28days respectively. The compressive strengths of coir reinforced laterite blocks at 28days were measured to be 2.022, 2.089, 2.667, 2.778, 1.778, 1.378, 0.956, 0.667, 0.644 and 0.622N/mm^2 for 0.0%, 0.2%, 0.4%, 0.6%, 0.8%, 1.0%, 1.2%, 1.4%, 1.6% and 1.8% coir content respectively. The optimal mix determined from this study is at 0.6% coir content. According to NIS 87: (2004) the block with 0.6% coir content can be used successfully in load bearing wall in building construction.

Keywords: *Buildings, Coir, Compressive strength, Laterite blocks, Optimal mix*

.

1. INTRODUCTION

The need for shelter is universally acknowledged as basic for both physical and psychological comfort of mankind. After food and good health, shelter is the next most important need of man, in fact a necessity in the lives of every human being whether rich or poor. Housing shortage is a worldwide phenomenon among developing and developed countries (Arayela, 2000). Shortage of housing has been recorded in both rural and urban communities in Nigeria (Arayela, 2000). It was in recognition of the magnitude of housing needs in developing countries that made the United Nations estimate annual construction rate of between 8 and 10 dwelling units per a thousand populations as against the low level of annual production of buildings in Nigeria, estimated at between 2 and 3 dwelling units (Arayela, 2000).

The high demand and dependence on the use of Sandcrete blocks for buildings have kept the cost of the blocks as walling units in buildings financially high. This problem, has continued to deter the underdeveloped and poor nations of the world from providing houses to their rural dwellers who constitute the higher percentage of their populations. Also the choice of walling material is a function of cost, availability of material, durability, and aesthetics. In developing nations the people that are mostly hit are predominantly farmers. The high cost of Sandcrete blocks coupled with the low strength properties of commercially available Sandcrete blocks necessitates the need for alternative low cost walling materials (Aguwa, 2010).

Laterite is the term used to describe all the reddish residual and non-residual tropically weathered soils formed from decomposed rocks through clays (Arayela, 2000). Laterite are the products of intensive and long lasting tropical rock weathering which is intensified by high rainfall and elevated temperatures. For a proper understanding of laterite formation we must focus on the chemical reactions between the rocks exposed at the surface and the infiltrated rain water. These reactions are above all controlled by the mineral composition of the rocks and their physical properties (for example cleavage and porosity), which favour the access of water. The second relevant factor for the formation of laterite are the properties of the reacting water (that is, dissolved constituents, temperature, acidity pH, redox potential), which are themselves controlled by the climate, vegetation and the morphology of the landscape (Arayela, 2000).

Various research works have been carried out in the production of laterite blocks. Significant among them is the work by Aguwa, (2013), who worked on "Study of coir reinforced laterite blocks for buildings" and observed that coir has the potential to increase the compressive strength of laterite blocks by ten percent at 28days curing duration and reduction in mass by two percent. He also reported that the use of coir in reinforcing laterite blocks will minimize the environmental problem of waste disposal in addition to the reduction in the cost of building blocks. He also worked on "Performance of laterite-OPC blocks as walling units in relation to Sandcrete blocks", and observed that, laterite-OPC blocks have better engineering properties and more economical with

a saving of 30% per square metre of wall when compared with the use of Sandcrete blocks (Aguwa, 2010).

Akeem *et al.* (2012) worked on comparative analysis of Sandcrete hollow blocks and laterite interlocking blocks as walling elements. They reported that, walling materials cover about 22% of the total cost of a building. They also observed that; the compressive strength of 225mm and 150mm Sandcrete hollow blocks varies from 1.59 N/mm^2 to 4.25 N/mm^2 and 1.48N/mm^2 to 3.35N/mm^2 respectively, as the curing age increases from 7 to 28 days. For laterite interlocking blocks, the strength varies from 1.70N/mm^2 at 7days to 5.03N/mm^2 at 28days.

Akeem *et al.* (2012) also reported that cement stabilized interlocking blocks were more effective structurally and cheaper than those stabilized with lime. Aguwa (2009) worked on "The compressive strength of laterite-OPC mixes as building materials", and reported that the compressive strength of laterite-OPC blocks increased steadily with increases in the percentage of cement content up to 20% but decreased at cement contents above 20%. Aguwa (1999) on Sandcrete block mixes observed that, the 'producers of these weak Sandcrete blocks and their users lack adequate engineering knowledge on the strength quality requirements of Sandcrete blocks. Materials with high compressive strength values have relatively low tensile strength, such as bricks and aerospace composites. These are not generally tested in tension as their application do not normally require them to withstand tensile load (Monsanto, 2012).

Fibre reinforcement of mud blocks with plastic, polystyrene and barley straw in certain geometric fashion exhibited 17 to 21% compressive strength improvement (Hanifi *et el.,* 2008). Sisal and coir vegetable fibres as well as those obtained from disintegrated newsprint is found to be the most suitable fibre for building purposes.

Alutu and Oghenejobo (2006) worked on production of laterite blocks stabilized with cement at varying cement content of 3% to 15% at 2% increment. The result showed that for 7% cement content and 13.76N/mm^2 compactive pressure, blocks of strength of at least 2.0N/mm^2 at 28 days, could be produced. The laterite-cement stabilized blocks showed no fractures of wear after exposure to rain with weight losses within permissible limits.

Laterite bricks were made by the Nigerian Building and Road Research Institute (NBRRI) and used for the construction of a bungalow. From the study, NBRRI proposed the following specifications as requirement s for the laterite bricks; bulk density of 1810kg/m3, water absorption of 12.5%, compressive strength of 1.65N/mm2, durability of 6.9% with maximum cement content fixed at 5% (Agbede and Manasseh , 2008)

The aim of this work is to determine the effectiveness of coir as reinforcement in the laterite blocks and optimum quantity of coir that can produce maximum compressive strength in coir reinforced laterite blocks. In order to achieve the above aim, the following objectives are paramount; to determine the index properties of laterite and coir, to produce coir reinforced laterite blocks at various coir content which are air dried, to determine the compressive strength of coir reinforced laterite blocks at curing ages 7, 14, 21 and 28days, and to establish the maximum quantity of coir required to produce optimum compressive strength for the coir reinforced laterite blocks.

2. METHODOLOGY

2.1 Laterite

The soil sample used for this work was collected from Maikunkele borrow pit along Minna-Zungeru road between the depth of 2.5m to 3.0m using the method of disturbed sampling. The laterite was used directly as collected from the borrow pit, preliminary laboratory tests were carried out to ascertain the suitability of the laterite.

2.2 Coir

The coconut fibre used for this work was collected from Garatu farm along Minna-Bida road Niger state Nigeria. The coir were removed gently from coconut husk, washed to remove impurity and air-dried before use.

2.3 Water

Potable drinking water for construction as specified in BS 3148 (1980) and EN 1008 (2002) was used in the Civil Engineering Laboratory, Federal University of Technology Minna, Nigeria

2.4 Index Properties of the Soil

The design mix process which involves estimation of the proportions of the constituent of coir reinforced laterite block was carried out. The test procedures of natural moisture content of the laterite, Atterberg limit tests, sieve analysis, specific gravity tests, water absorption tests and compaction tests were carried out on the sample

specimens in accordance with BS 1377 (1990). Laterite blocks were moulded in accordance with Nigerian Industrial Standard (NIS 87, 2004).

2,5   Preparation of Test Specimen

In this work, three constituent materials of coir reinforced laterite blocks which include; water, laterite, and coconut fibre were used. The fibre was removed from husk and shaped to a uniform length of 5cm. The constituents were then mixed thoroughly and homogeneously using the corresponding optimum moisture content (OMC) from the compaction test as percentage of water. Ten different mixes/batches of coir reinforced laterite blocks using coir content of 0.0%, 0.2%, 0.4%, 0.6%, 0.8%, 1.0%, 1.2%, 1.4%, 1.6% and 1.8%, were prepared. Twenty blocks were moulded per mix making a total of two hundred blocks. The blocks were moulded according to NIS 87 (2004) Five blocks from each mix were air dried, weighed and subjected to compressive strength test for 7days, 14days, 21days and 28days as indicated in Plates I, II and III.

Care was properly taken to ensure that the cubes were not disturbed during curing and that extrusion was cautiously done to ensure that there was no breakage. Extra care was taken to ensure that the critical dimensions of the cubes were not disfigured, to maintain constant surface area of the cubes in contact with the crushing machine. During crushing, proper care was taken to ensure that the cubes were perfectly positioned and aligned with the axis of the thrust of the compression machine to guarantee uniform loading of the cubes (Aguwa, 2009).

Plate I: Cured Coir Reinforced Laterite blocks

Plate II: Weighing of Coir-Laterite blocks

Plate III: Coir-Laterite block under compressive strength test.

3.   RESULTS AND DISCUSSIONS

3.1   Index properties of the soil.

Table 1 shows the index properties of the laterite used for this work. The soil is classified as silty or clayey gravel and sand (Granular materials belonging to group A-2-7 (0)) using AASHTO soil classification system. Granular material have

more compressibility characteristic than the clay (Gopal and Rao, 2007). The Specific Gravity obtained for the laterite soil is 2.60 which is within the range specified by Smith (1994)

Table 1: Index properties of the laterite.

Characteristic	Laterite
Liquid limit (%)	48.50
Plastic limit (%)	31.37
Plasticity index (%)	17.13
Percentage passing sieve No 200 (%)	4.68
Group index	0.00
AASHTO Classification	A-2-7(0)
Natural moisture content (%)	15.17
Specific gravity	2.60

3.2 Compressive Strength of the Coir Reinforced Laterite Blocks

Compressive strength of material is the ratio of load applied (Compressive force) on a material to the cross sectional area of the same material. Figures 1, 2 and 3 show the result of compressive strength test on coir reinforced laterite blocks. It was observed from Figure 2 that the mass of coir reinforced laterite blocks decreases with increase in coir content, while the compressive strength increases with age of air drying as shown in Figure 3. The result also exhibited 37% improvement in compressive strength of coir reinforced laterite blocks at 0.6% coir content compared to the control blocks. The compressive strength thereafter was found decreasing with further increase in coir content as shown in Figure 1. Also the improved fibre flexibility makes them behave as a structural mesh which holds the soil together. The compressive strength of coir reinforced laterite blocks depends on the formation and bonding of coir-laterite mixture. The bonding can be affected by dimension, surface conditions and quantity of fibre present in the given volume of material. Therefore, the increase in coconut fibre content in the mixture resulted in a decrease

in bond strength of the specimen, which subsequently led to lower strength. According to the Nigerian Industrial Standard (NIS 87, 2004), the lowest crushing strength of individual load bearing blocks shall not be less than 2.5N/mm^2 for machine compaction and 2.0N/mm^2 for hand compaction blocks. Coir increases the cohesiveness among soil particles and interaction of the coir among themselves. Therefore, coir reinforced laterite blocks (percentage of coir not exceeding 0.6) may have more energy or strength compared to non-coir reinforced laterite blocks; thus making the blocks more suitable as structural materials.
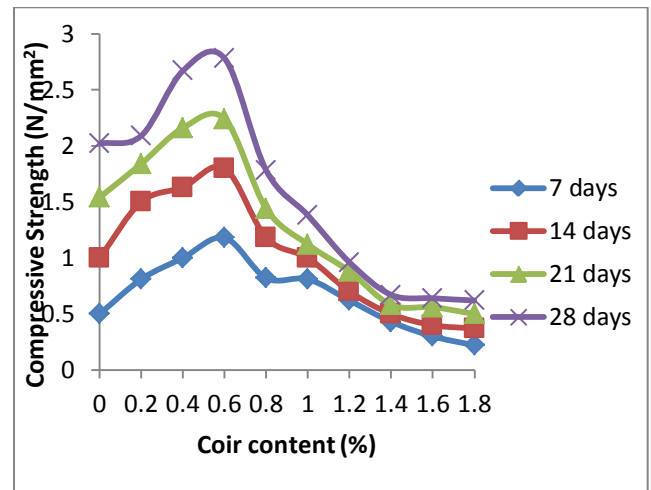

Figure 1: Compressive Strength-Coir Content Relation for Coir Reinforced Laterite blocks
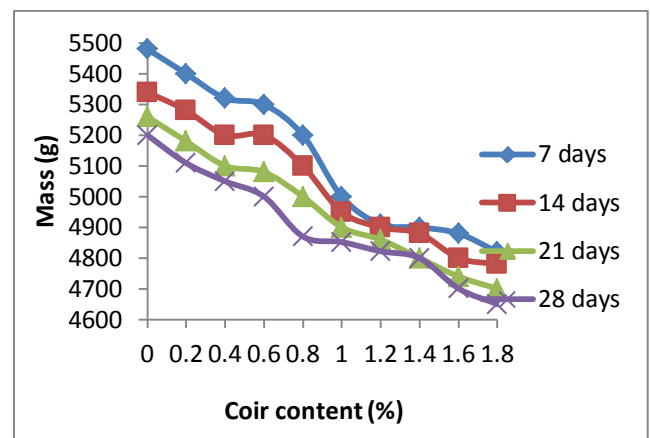

Figure 2: Mass of block-coir Content Relation for Coir Reinforced Laterite blocks.
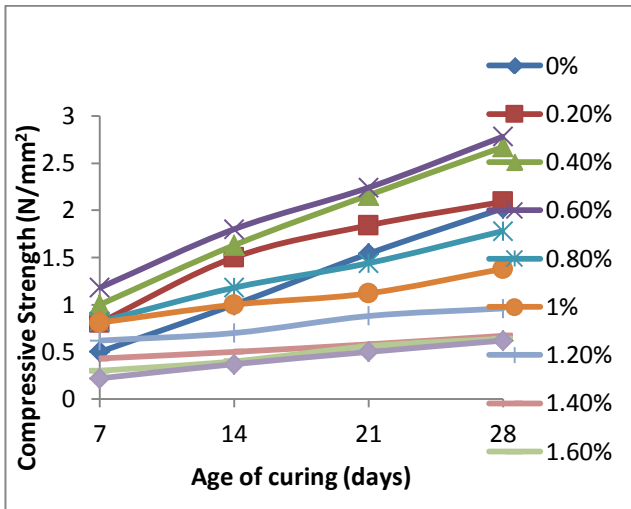
Figure 3: Compressive Strength-Age of Curing Relation for Coir Reinforced Laterite blocks

4. CONCLUSION

In conclusion, the maximum compressive strength as well as adequate cohesion of coir reinforced laterite blocks was achieved at optimal mix of 0.6% coir content. The compressive strength of the coir reinforced laterite blocks increased by 37.62% at 0.6% coir content when compared with the non- laterite reinforced blocks. This work has shown that a maximum compressive strength of 2.78N/mm2 can be gained by coir reinforced laterite blocks at an optimum coir content of 0.6%. These blocks can be used as load bearing walls. Also, the use of coconut fibre in reinforcing laterite blocks will reduce the environmental problem of waste deposal and subsequent cost reduction in building construction. This will in turn create more employment opportunities for the teaming unemployed people of the areas where coconuts are grown. Considerable improvement in the compressive strength and reduction in mass were

exhibited by coir reinforced laterite blocks compared with non-coir.

5. REFERENCE

AASHTO (1986) Standard Specifications for Transportation Materials and Method of Testing and Sampling, American Association of State Highway and Transportation Officials, Washington D. C., USA.

Agbede, I. O. and Manasseh, J. (2008). use of Cement-Sand Admixture in Laterite Bricks Production for Low Cost Housing, Leonardo Electronic Journal of practices and Technologies, ISSN 1583-1078, Issue 12, pp 163-174.

Aguwa J. I. (2009) Study of Compressive Strength of Laterite-Cement Mixes as Building Material, Assumption University Journal of Technology, Vol. 13, No 2, pp 114-120.

Aguwa J.I. (2010) Comparative study of compressive strengths of Laterite-Cement and Sandcrete Blocks as Building materials. NSE Technical Transactions – A Technical Publication of the Nigerian Society of Engineers, 45(4) 23-34.

Aguwa J.I. (2010) Performance of Laterite-Cement Blocks as Walling Units in Relation to Sandcrete Blocks. *Leonardo Electronic Journal of Practices and Technologies* ISSN 1583-1078 Issue 16, January-June 2010 p. 189-200

Aguwa J.I (2013). Study of Coir reinforced laterite blocks for buildings," *Journal of Civil Engineering and Construction Technical*, 111-115.

Akeem, A. R., Ayodeji, K. M., and Aliu, A. S.(2012) Comparative analysis of sandcrete hollow blocks and laterite interlocking blocks as walling elements, International Journal of Sustainable Construction engineering and Technology, Issue 1, pp 2180-3242

Alutu O. E. and Oghenejobo A. E. (2006). Strength durability and cost effectiveness of cement-stabilized laterite hollow blocks, Quarterly Journal of Engineering Geology and Hyrology, Vol. 39, Issue 1, pp 65-72.

Arayela O. (2000). Development of Stabilized Laterite Bricks for Building Cost Reduction in South Western Nigeria. Architecture, School of

Environmental Technology.Federal University of Technology, Akure.

BS 3148: (1980). Methods of test for water for making concrete: *British Standards Institution,* Her Majesty Stationary office, London.

BS 1377: (1990). Method of tests for soils for Civil Engineering purposes. *British Standards Institution.* pp, 13-108.

BS EN1008: (2002) Mixing water for concrete-Specification for sampling, testing and assessing the suitability of water, including water recovered from processes in the concrete industry, as mixing water for concrete.

Gopal R. and Rao A.S.R (2007) Basic and Applied Soil Mechanics. New Age International (p) Limited, Publishers. pp103-222.

Hanifa, B., Organ, A., and Tahir, S. (2008) Investigation on Fibre Reinforced Mud Brick as Building Material, Construction and Building Materials, Vol. 19, pp 313-318.

Nigerian Industrial Standard (NIS 87 : 2004). Standard of Sandcrete Blocks. Standards Organisation of Nigeria 9-10

Smith M.J. (1994) Soil Mechanics. Longman Scientific and Technical, Longman Group UK Ltd, Longman House, Burnt Mill, Harlow, Essex CM20 2JE England pp 3-4

Lateritic Soil Stabilized with Fly Ash as a Sustainable Structural Material for Flexible Pavement Construction

Agapitus Amadi[1*] and Olayemi James[2]

[1,2]Department of Civil Engineering, Federal University of Technology, Minna, Nigeria

[*]agapitus.amadi@futminna.edu.ng, agapitusahamefule4@yahoo.com, 08034516603.

ABSTRACT

This paper describes a laboratory study conducted to evaluate the improvement in engineering properties relevant to highway design and construction that can be obtained when fine grained lateritic soil is stabilized with fly ash obtained from coal fired electric power plants. The experimental program included sieve analysis of soil sample; Atterberg limits tests, compaction, Unconfined Compressive Strength (UCS) and California Bearing Ratio (CBR) tests on soil mixtures prepared with fine-grained lateritic soils at 0, 5, 10, 15 and 20% fly ash content. Specimens for UCS and CBR tests were prepared at optimum moisture content and cured for 28 days. The Nigerian General specification for Roads and Bridges and U.S Army Corps of Engineers unconfined compressive strength criteria were used for judging the performance of the soil mixtures. Test data showed that the addition of fly ash led to substantial enhancement of the soil, satisfying the Atterberg limits criteria used by regulatory agencies to assess performance of stabilized pavement materials. While all the lateritic soil - fly ash mixtures met the CBR and UCS criteria for subgrade construction, only mixture containing 10% fly ash satisfied the requirement for sub base layer. The CBR and UCS requirement for use as base course was not met in any soil mixture.

Keywords: *Fly ash, Lateritic soil, Pavement layers*

1. INTRODUCTION

As a consequence of economic growth, road traffic is increasing in vehicle numbers and in axle loads in all parts of the world. This requires extension of the road network which invariably demands large amounts of materials with good structural performance and a long service life below the asphalt or concrete. Each year, tons of these materials which require mining, quarrying, and transportation are consumed in this country for construction.

Quite often, most of the areas where these projects are executed are covered with fine grained lateritic soils that exhibits insufficient engineering properties needed to provide structural support for the imposed loads during usage and loads from construction equipments (Amadi, 2011).

Lateritic soils, a highly weathered soil type rich in iron and aluminum are distributed in many parts of the world. Some low grade lateritic soils with high percentage of fines content present many problems in road construction and maintenance (Gidigasu, 1976). Nevertheless, the use of the soil in pavement construction offer numerous benefits such

as reducing the need for quarrying and transportation of natural aggregate, which saves construction costs and energy consumption.

The properties of these soils can be improved by addition of a stabilizing agent. Among the various stabilizing agents available, lime, fly ash and cement are most widely and commonly used to accomplish this need. Many of these treatments can significantly improve the strength, stiffness, durability, permeability and stability of host materials to allow them to support the load from the structure above them (Amadi, 2013). To reduce the cost of soil improvement and for sustainable development, the replacement of cement by fly ash is one of the best alternative ways (Nicholson and Kashyap, 1993; Arora and Aydilek, 2005; Amadi, 2013).

Fly ash is the by-product produced by coal-burning electricity generating power plants. It contains siliceous and aluminous materials (pozzolans) and also certain amount of lime. Depending on the source and composition of the coal being burned, the components of the resulting fly ash vary considerably, but all fly ash contains substantial amounts of silica (SiO_2) and free lime (CaO).

When mixed with soils, it reacts chemically and forms cementitious compounds. As pozzolans, fly ash can provide an array of divalent and trivalent cations (Ca^{2+}, Al^{3+}, Fe^{3+} etc) under ionized conditions that can promote flocculation of dispersed clay particles. Several chemical reactions that occur when fly ash is mixed with clay namely cation exchange, flocculation/agglomeration of the soil particles and pozzolanic reaction are responsible for stabilization.

A number of researchers have investigated the use of fly ash in stabilizing weak soils. While Cokca (2001) studied the effect of fly ash on expansive soils, concluded that fly ash can be recommended as an effective stabilizing agent for the improvement of expansive soils, Ferguson (1993) has shown that the addition of 16% self-cementing fly ash increases the soaked CBR values of heavy clay soils into the mid 30s, which is comparable to gravelly sands (Rollings and Rollings 1996). Also Zia and Fox (2000) found that the CBR of loess increased five times with the addition of 10% fly ash, but an ash addition rate of 15% showed lower CBR than the 10% mixtures. On the other hand, unconfined compressive strengths of soils stabilized with self-cementing fly ash according to Ferguson (1993) as well as Ferguson and Leverson (1999) are typically on the order of 100 psi, but can be as high as 500 psi at seven days, depending on ash content and ash properties.

2. MATERIALS AND METHODS

2.1 Lateritic Soil Characterization

Fine grained lateritic soil sample obtained from a borrow pit in Shika – Zaria, (Latitude $11^o15'$ N and Longitude $7^o45'$ E) Nigeria at about 1.2m depth was used for this study. The soil is a reddish brown sandy clayey silt. The properties of the soil sample obtained in accordance with standard procedures outlined in BS 1377 (1990) and its oxide composition determined by Atomic Absorption Spectrometer (AAS) are presented in Tables 1 and 2,

respectively. Analysis by X – ray diffraction (XRD) method indicate that the clay fraction is dominated by koalinite clay mineral. The particle size distribution curve of the studied soil, presented in Fig. 1 indicate that the soil contains 57% fines (i.e., percentage passing BS No. 200 sieve) as determined by mechanical sieve analysis.

Table 1: Properties of the studied lateritic soil

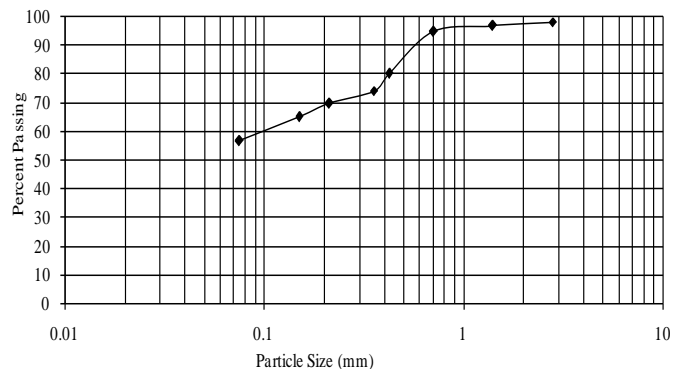| Property	Value
Natural moisture content (%)	5.80
Liquid Limit (%)	42.22
Plasticity Index (%)	22.22
Linear shrinkage (%)	9.5
USCS Classification	CL
Specific gravity	2.76
pH	6.67
Color	Reddish brown
Dominant Clay Mineral	Kaolinite

Fig. 1 Particle size distribution of lateritic soil used in the study

Typically, specifications for pavement construction limit maximum fines content (No. 200 sieve) to 35% (Nigeria General Specifications, 1997). The studied soil therefore, had fines fraction greater than the maximum suggested for pavement layers.

2.2 Properties of Fly Ash used in the study

The fly ash used in this study is a Class F fly ash following ASTM C 618, from Oji River thermal station in Enugu state, Nigeria. The fly ash has low calcium oxide (CaO) content (9.8%), and high silicon dioxide (SiO_2) content (46.02%). The specific gravity of this ash is 2.06 and as in most fly ashes is a non-plastic material. The Oxide composition of soil sample analyzed by Atomic Adsorption spectrometer (AAS) is summarized in Table 2. Only fraction passing BS sieve No. 200 was used throughout the test without additional treatment at 0, 5, 10, 15 and 20%.

Table 2: Oxide composition of study soil and Fly Ash

Oxide	(%)	
	Lateritic soil	Fly Ash
CaO	0.28	1.78
SiO_2	35.60	46.02
Al_2O_3	27.40	24.16
Fe_2O_3	2.40	13.68
MgO	0.22	1.91
SO_3	0.85	ND
Mn_2O_3	2.00	0.56
K_2O	ND	5.58
TiO_2	ND	1.86
Na_2O	ND	5.31
Loss on ignition	14.60	1.3

ND – Not determined

2.3 Atterberg limits and Compaction tests

The plasticity characteristics namely, liquid limit (LL), plastic limit (PL) and plasticity index (PI) and linear shrinkage (LS) as well as specific gravity of the various soil – fly ash mixtures were determined in accordance with procedures outlined in BS 1377 (1990) and 1924 (1990). For the compaction test, specimens with the relevant quantities of dry soil and fly ash (0, 5, 10, 15 and 20%) prepared at optimum were compacted with British Standard Heavy, (BSH) compactive effort in accordance with the relevant sections of BS 1377 (1990) as well as 1924 (1990).

2.4 CBR test

Specimens of the soils and soil–fly ash mixtures prepared at optimum moisture content were subjected to CBR testing in soaked condition following the methods described in the relevant sections of BS 1377 (1990) and BS 1924 (1990). Prior to CBR testing, soil–fly ash specimens were left in the mould after compaction, sealed using plastic wrap, and cured at about 25°C and 100% relative humidity for 28 days. A 28-day curing period was adopted to allow sufficient pozzolanic reaction. The CBR tests on soil mixtures were conducted after the 28-day curing period and 96 hours soaking.

2.5 Shear strength test

The unconfined compression test was carried out in accordance with the procedures outlined in BS 1377 (1990) and 1924 (1990). The test was conducted on specimens prepared at optimum moisture content using BSH compactive effort. The compacted specimens were stored in cellophane bags and kept in a humid environment for 28 days before testing. The test was performed on cylindrical specimens with diameters of 38 mm and lengths of 76 mm, which were trimmed from the larger compacted cylinders. The samples were tested in triaxial compression test machine without applying cell pressure.

3.0 RESULTS AND DISCUSSION

3.1 General Effects of Fly Ash Treatment

3.1.1 Plasticity Characteristics

One common and simple way of measuring the improvement of a granular material containing clay is by the reduction in its plasticity characteristics as measured

by the plasticity index (PI). This index is a significant indicator of soil behaviour; the higher the PI, the more plastic the soil will be and the more unsuitable it will be for use in road construction. Treatment with fly ash makes such soils more granular in nature and suitable for use in engineering applications.

Test data indicate that the liquid limit (LL) of the untreated soil was 42.2% (Table 1) which increased to 29.53% for specimen containing 20% fly ash content. On the other hand, the PI decreased gradually with higher fly ash content from 22.22 for 0% fly ash content to 15.87, 12.06, 7.78 and 3.54% in the same sequence of fly ash treatment (Fig. 2). Soil mixtures containing 0-15% fly ash were classified as CL and mixture treated with 20% fly ash as ML according to USCS classification system.

To be considered effective for pavement construction, the soil mixtures must exhibit LL not greater than 35%; PI not greater than 12% (Nigerian General Specification, 1997) which indicate that only mixtures containing 10, 15 and 20% fly ash satisfied the Atterberg limits criteria.

3.1.2 Compaction Parameters - Maximum Dry Unit Weight and Optimum Moisture Content (OMC)

The effect of fly ash addition on the maximum dry unit weight and optimum water content is presented in Fig. 3. The maximum dry unit weight of soil mixtures decreased slightly with corresponding increase in optimum water content as the amount of fly ash in the mixtures increased from 0 to 20%. The decrease in dry unit weight with increasing fly ash content is primarily due to the lower specific gravity of fly as which resulted in mixtures with lower specific gravity. On the other hand, the increase in OMC with higher fly ash content could be as a result of the additional water requirement for the hydration of cementitious products of soil - fly ash reaction. The optimum moisture content (OMC) ranged from 11.88% to 13% yielding dry unit weight mostly in the range 17.26 kN/m^3 to 18.78 kN/m^3.
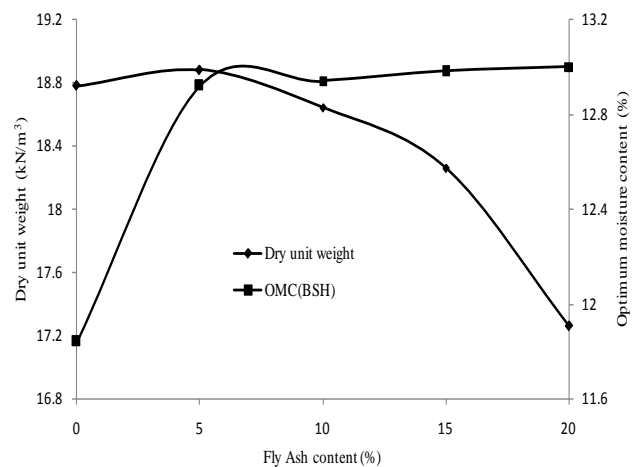
Fig. 3: Variation of maximum dry unit weight and OMC with fly ash content

Fig. 2: Changes in Atterberg limits of studied soil with fly ash content

3.1.3 California Bearing Ratio (CBR)

The CBR of the soil increased gradually with the addition of fly ash up to 10% beyond which further increase in fly ash resulted in decreasing trend in the CBR values. The value of the soaked CBR varied from 8% for unstabilized soil to 30% for stabilized soil. Improvement of the soil was

provided by the matrix formed with fly ash acting as a filler and as a cementing agent.
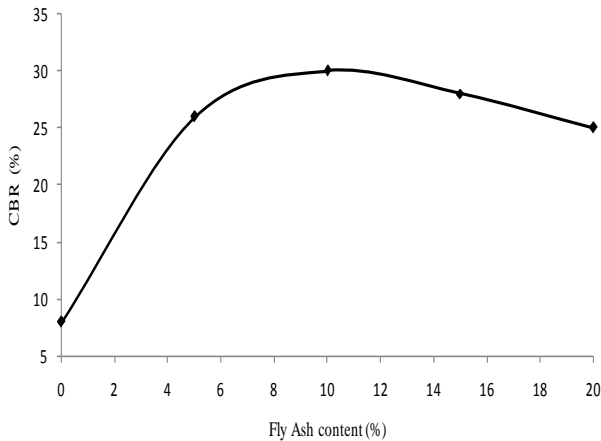

Fig. 4: Variation of CBR with fly ash content

In pavement design and construction, CBR values of 10%, 30% and 80% (standard Proctor compaction) have been adopted as criteria to be met for subgrade, sub-base and base courses, respectively (Nigeria General Specifications, 1997). The CBR requirement for subgrade was met in all the soil mixtures while the requirement for sub-base layers was only met at 10% fly ash content. All soil mixtures had CBR lower than the minimum suggested for pavement base layers.

3.1.4 Unconfined Compressive Strength (UCS)

The effect of addition of fly ash to the unconfined compressive strength of lateritic soil samples is shown in Fig. 5.

UCS of fly ash treated lateritic soil attained a compressive strength 2 – 3 times greater than that of the natural soil. The highest strength value of 1921.62 kn/m^2 was recorded on application of 10% fly ash.
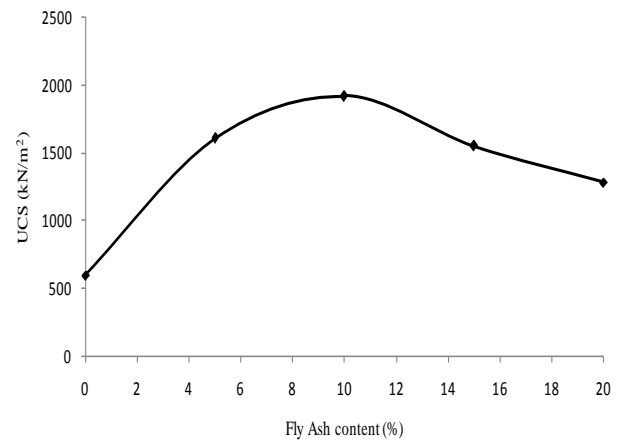
Fig. 5: Variation of UCS with fly ash content

Subsequent increase in ash content did not yield higher strength values, rather, reductions in strength values were observed. Excessive fly ash content (> 10%) behaved as low strength filler, effectively weakening the soil - fly ash mixture that led to reduction in UCS. This finding is in conformity with the results reported by zia and fox (2000). It is also important to note that strength gain was however comparatively low, probably due to the low cementing potential of the ash utilized and therefore does not possess adequate pozzolanic reactivity to fully mobilize the compressive strength of the mixtures.

Explanation for the increase in strength values with fly ash application is probably due to the coupled effects of flocculation and agglomeration of fly ash together with the neo-formations such as calcium silicate hydrates (CSH) and calcium aluminate hydrates (CAH) that coats and binds the soil particles to produce strong matrices (Edil etal., 2006).

In terms of regulatory specifications, the typical minimum UCS requirement varies from around 345 kN/m^2 for subgrades, 1340 kN/m^2 for sub base layers and 5175 kN/m^2 for base layers (United Facilities Criteria, 2004). All soil mixtures exceeded the specification requirement for subgrade course while only specimen with 10% fly ash achieved the

requisite UCS for sub base layers. The requirement of 5175 kN/m^2 for use as base course was not met in any soil mixtures.

4 CONCLUSION

A laboratory study was undertaken to determine the properties of fly ash stabilized lateritic soil for the design and construction of durable roadway pavements. Compacted specimens of lateritic soil stabilized with (0, 5, 10, 15 and 20%) fly ash were cured for 28 days and tested for unconfined compressive strength (UCS) and CBR.

In terms of plasticity, all mixtures containing fly ash were effectively improved satisfying the specification limits i.e., LL $\leq$ 50%, PI $\leq$ 35%. Moderate increases in the CBR and UCS of soil mixtures were recorded up to 10% fly ash content. The UCS requirement for a sub-base layer was met only at 10% fly ash content. However, all the lateritic soil - fly ash mixtures fall below the minimum suggested CBR and UCS for chemically stabilized base layers.

REFERENCES

Amadi, A. A. (2011). Evaluating the potential use of lateritic soil mechanically stabilized with quarry fines for construction of road bases. Nig. J. Eng., 17(2), 1 - 12.

Amadi, A. A. (2012). Utilization of Fly Ash to Improve the Engineering Properties of Lateritic Soil. Int. J. Mat. Eng. Innovation, Inderscience Publishers, 3(1), 78 –88.

Arora, S. and Aydilek, .H. (2005), "Class F Fly-Ash-Amended Soils as Highway Base Materials," *Journal of Materials in Civil Engineering*, ASCE, 17(6), pp. 640-649.

BS 1377 (1990). Methods of Tests for soils for Civil Engineering Purposes, British Standards Institute, London.

BS 1924 (1990). Methods of tests for stabilized soils, British Standard Institute, London.

Cokca, E. (2001), "Use of Class C Fly Ashes for the Stabilization of an Expansive Soil." *Journal of*

Geotechnical and Geoenvironmental Engineering, 127(7), pp 568-573.

Edil, T.B., Acosta, H.A. and Benson. C.H. (2006), "Stabilizing Soft Fine-Grained Soils with Fly Ash," *Journal of Materials in Civil Engineering,* March/April, pp 283-94.

Ferguson, G. (1993). Use of self-cementing fly ashes as a soil stabilization agent. Fly ash for soil improvement, Geotechnical Special Publication No. 36, ASCE, New York, 1–14.

Ferguson, G., and Leverson, S.M. (1999). *Soil and Pavement Base Stabilization with Self-Cementing Coal Fly Ash*, American Coal Ash Association, Alexandria, VA.

Gidigasu, M. D. (1976). Laterite Soil Engineering, Elsevier Scientific Publishing Co. New York.

Nicholson, P. G., and Kashyap, V. (1993). Flyash stabilization of tropical Hawaiian soils. Fly Ash for Soil Improvement, Geotechnical Special Publication No. 36, ASCE, New York, 15–29.

Nigerian General Specification, (1997). Roads and Bridges, Federal Ministry of Works and Housing, Abuja, Nigeria.

Rollings, M. P. and Rollings Jr., R. S. (1996). Geotechnical Materials in Construction, McGraw-Hill, New York.

United Facilities Criteria (3-250-11) (2004). "Soil Stabilization for Pavements, TM 5-822-14/AFJMAN 32/1019."Access at http://www.wbdg.org/ccb/DOD/UFC/ufc_3_250_11 on Jul. 16, 2006.

Zia, N., and Fox, P.J. (2000). "Engineering properties of loess-fly ash mixtures for road bases." *Transportation Research Record 1717*, Transportation Research Board, 49-56.

Performance analyses of dense wavelength Division multiplexing in Ring Metropolitan Area networks with and without Erbium Doped Fibre Amplifier.

A.M.S Tekanyi[1], Joseph Stephen soja[2], Hussaini James[3], Khadijat Alhassan[4]

[1,2,4] Department of Electrical and Computer Engineering, Ahmadu Bello University Zaria.

[3] Federal Polytechnic Mubi, Adamawa State

amtekanyi@abu.edu.ng, sojasteve@abu.edu.ng, hussainijames15@gmail.com

ABSTRACT

This Paper investigates the performance of dense wavelength division multiplexing ring networks implemented in the metropolitan areas for the purpose of deploying higher bit rates. The investigations were carried out in the C- band operating region by deploying four channels over a single standard mode fibre with channel spacing of 100GHz at 10Gbps. Transmissions of 108km and 7km with and without Erbium Doped Fibre Amplifier (EDFA) were achieved with a 10^{-9} fixed value of Bit Error Rate (BER). The performance was measured through a bit rate analyser using an eye diagram.

Key words: DWDM, EDFA, OADM, MAN and BER

.

1. Introduction

Wavelength Division Multiplexing (WDM) is either coarse or dense (Cisco, 2011). Dense Wavelength Division Multiplexing (DWDM) is an optical system that allows for simultaneous transmission of light at different wavelengths on a single stranded fibre**.** It is often used in public optical telecommunication networks such as Local Area Network (LAN), Metropolitan Area Network (MAN) and Wide Area Network (WAN) to link heavy groups of users over different geographic regions (Grundlehuer 2002)**.**

The ITU-T recommendation G.92 defines the window used for DWDM application with 45 channels spaced 100 GHz apart (0.8nm), spanning across the C-band from 1528.77 to 1563nm.According to Keiser (2006), DWDM channels of 50 GHz, 100 GHz and 200 GHz are governed by ITU-T recommendation G.692, where 100 GHz is the first standard and 50 GHz and 200GHz are alternatives suggestions of the recommendation. The recommendation was aligned on frequency grid 193.0THz corresponding to 1552.524nm and the channel spacing 200 GHz, 100 GHz and 50 GHz correspond to a spectral width of 1.6 nm, 0.8 nm and 0.4nm, respectively (Cisco, 2011).

The MAN ring networks deployed with numerous channels over a single fibre support several internet services (personal, business, health, and educational, etc) are described as DWDM networks DWDM is used to route protocols to users with the support of optical components such as Optical Add and Drop Multiplexer (OADM), transmitter (laser and led), receiver, Standard Single Mode Fibre (SSMF), Multiplexer, Demultiplexer and Erbium Doped Fibre Amplifiers (EDFAs) (Singh and Kaler, 2014).

This Technology has been developed to meet growing demands for bandwidth by multiplying the capacity of a single fibre. Optical add/drop filter is required for adding and dropping required WDM

channel at each subscriber's node in the WDM based optical access network. This optical DWDM ring is composed of a multiple of four channel wavelengths each driven by a distinct transmitter on a common fibre. There are three operating windows in optical telecommunication, they include 850nm, 1300nm and 1550nm. Amongst these operating windows, 1550nm window is the one with the lowest loss of about 0.2dB/km and it is frequently used for metro area networks (Cisco, 2011).

The aim of this paper is to transmit 4-channels over a ring MAN with a channel spacing of 100GHz with and without EDFA. This can be achieved by exploring the metro DWDM ring network using 1550nm window and a bit rate of 10 Gb/.

The paper is presented in different sections: Section I covers introduction, section II is about the literature review, section III presents MAN, description of EDFA, OADM, BER and OSNR. Section IV presents design of power analysis of four channel DWDM ring metropolitan network with and without EDFA. Section V presents the experimental results while section VI concludes the paper.

II. Related works

Considerable amount of work has been carried on DWDM using different approaches and some of these researches are as follows:

Jaspreet and Kochler (2015) came out with a novel approach on DWDM based metropolitan ring network. They deployed the possibilities of exploring DWMD in Metropolitan ring networks with a wavelength modulated at 2.5, 10 and 40Gbps covering both C and L band with a channel spacing of 100GHz or 50GHz. However, there were no any simulation results to achieve the realization of the specifications given. Srivastava (2014) studied the performance of OADM based on DWDM Technology. Some transmission challenges such as attenuation, dispersion and nonlinear effects which hinder the performance of OADM in DWDM were discussed. However, the study was not narrowed to a particular type of OADM. Aliosio et al., (2012) examined the performance analysis of a DWDM optical transmission system by designing a board for the experiment that hosted a DWDM link for data transmission. They introduced optical filter to increase the system performance due to the reduced amount of optical noise fed to the receiver. However, it is very expensive to implement in real time situation.

III. Metropolitan Area Networks (MAN)

In the design of metropolitan DWDM networks, considerations are made for the following: fibre capacity, amplification or regeneration of signals, channel capacity, channel count and the type of topology (Grundleher, 2002).

The fibre capacity support of transmission in MAN is within the range of ITU-T G.652 specification for low density DWDM transmission with inter-channel spacing of 100 GHz and the ITU-T G.655 recommendation for high density DWDM with 50 GHz channel spacing.

The amplification of signals through revitalization is not required in a MAN, except in situations where high speed is required and the network is approaching distances occupied by long-haul. Similarly, the channel count deals with the number

of DWDM. A single fibre can perfectly convey several channels at one occasion. According to Zhao and Yin (2012), more channels can be deployed with 100 GHz channel running at 10 Gb/s on a single fibre.

On the contrary, channel capacity in metro DWDM higher speeds have proven to be an issue as dispersion and other non-linear effects set in at higher data rates. Furthermore, the MAN ring topology is incorporated with devices such as SSMF, OADM, multiplexers, demultiplexers, transmitters and receivers among other components like couplers or connectors and they can reach very big circumferences using these components and fibres.

(a) Erbium Doped Fibre Amplifier

Erbium Doped Fibre Amplifiers (EDFA) are classified into many categories such as Praseodymium (Pr) doped fibre amplifier, Neodymium (Nd) doped fibre amplifiers, Erbium doped planar devices, Raman effect amplifiers, Plastic fibre amplifiers and Semiconductor optical/laser amplifiers (Becker and Olsson, 1999). They are optical amplifiers widely used for different purposes. EDFA consists of fibre having a silica glass host core. Since most EDFAs are designed to operate in the 1550nm region, the component uses the 980nm or 1480nm pump laser to pump energy into the doped fibre section (Srivastava, 2014).

(b) Optical Add and Drop Multiplexers

The Optical Add and Drop Multiplexers (OADMs) are mostly utilized in wide-area and metropolitan area networks and have the competency of dropping one or more signal, while maintaining the

quality and integrity of the other signals traversing through them (Rashed, 2011).
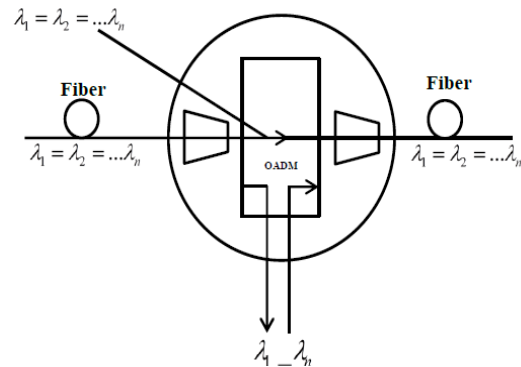
Figure 2: OADM configuration (Mahad et al., 2009).

As shown in Figure 2, when the OADM system receives arriving WDM channels on the input fibre, it drops or adds one or more selected channel(s) simultaneously without affecting traveling signals. This leads to less delay associated with OADM. In this paper, four (4) OADMs were used to drop the signal at four different locations. Most often, dynamic OADMs are always in usage and have an edge over static OADMs because they are cheaper, more flexible and can supply any wavelength on demand without altering their physical attributes (Tzanakaki, 2003).

(c) Bit Error Rate and Optical Signal to Noise Ratio

The Optical Signal to Noise Ratio (OSNR) represents the ratio of the net total power of the original signal to the net total power of noise. It is independent of factors like the formation of data, shape of the pulse and bandwidth of the optical filters (Pete, 2010). The ratio also suggests a degree of impairments when the optical signal is carried by an optical transmission system. OSNR is measured in decibels and is given as (Pete, 2010):

(1)

$$OSNR = 10\log_{10}\log(P_1/P_2)$$

where P_1 is the input signal power and P_2 is the output signal power .

The quality of a signal is specified by Bit Error Rate(BER) and it is primarily determined by OSNR. BER is the number of bits in error divided by the entire number of bits transferred through the DWDM link over a given period (Stoll et al., 2001).

IV. Power Analysis

Power analysis is carried out in order to obtain the respective power budget, power loss and power margin of a four-channel DWDM network.

(a) Four-Channel DWDM Design without EDFA

The comparison in this work is based on four-channel usage on DWDM network. The investigation is carried out in a C-band with a circumference of 7km and four OADMs without an EDFA. At the transmitter (optical source), a Pseudo Random Bit Sequence (PRBS) generator is connected to a Non- Return to Zero (NRZ) generator, which is used to derive Mach Zehnder (MZ) modulator through a low pass gaussian filter. At the other side an electrical signal of 0dBm from a continuous wave laser is coupled (fed) into the MZ frequency input for the process of modulation. All receivers used in the network, including those for signal dropped at each OADM have equal sensitivity. Bit error rates and eye diagrams for every signal are then analysed on the eye diagram analyser. Standard values of relevant parameters required in the analysis are provided in tables as shown in Table 1 and 4.

Table 1:Standard Values of Parameters for DWDM Design without EDFA (Keiser, 2006).

Components/ParametersValue	
Multiplexer Insertion Loss	4dB
Demultiplexer Insertion Loss	4dB
OADM Insertion Loss	4dB
Fibre Attenuation	0.2dB/km
Receiver Sensitivity	-30dB
Transmitted Launch Power	0dB
Loss due MZ Modulator	3dB
Operating Window	1550nm
Channel Spacing	100GHz
Polarization	0.2ps/√km
Spectral Efficiency of Modulated Channel	0.4Gb/s/Hz

The power analysis for DWDM without EDFA is carried out for all the channels in the entire network.

(i) Channel 1: Signal Drop at Multiplexer

Optical power budget (P_b) is given by (Tzanakaki, 2003):

$$P_b = P_t - P_r \qquad (2)$$

whereP_t = Transmitter power

P_r = Receiver sensitivity

From equation (2):

P_b = 0dBm – (-30dBm)

= 30dB

From Table 1, loss due to attenuation in channel 1 at 1km is 0.2dB (0.2dB/km × 1km).

Total signal power loss (P_{loss}) is given by (Aliosio, 2012):

$$P_{loss} = M_l + L_a + L_{mz} + T_{lp}$$

$$(3)$$

where M_l = Multiplexer insertion loss

   L_a = Loss due to attenuation

   L_{mz} = Loss due to MZ modulator

   T_{lp} = Transmitted launch power

From equation (3)

P_{loss} = 4+4+3+0.2

   = 11.2dB

The power margin is expressed as [8]:

P_{Margin} = P_{in} - P_{loss} + Gain - P_{rec} (4)

where P_{in} = Input power

   P_{loss} = Power due to loss

   P_{rec} = Receiver sensitivity

From equation (4):

P_{Margin} = 0 - 11.2 + 0 – (-30)

   = 18.8dB

Similarly, the computations of power margins for channels 2, 3 and 4 for signal drop at the multiplexer are carried out as shown in the analysis of that of channel 1 and results are tabulated in Tables 2.

Table 2: Signal Drop at the Multiplexer

Channel parameters

Channel	Distance	Power Margin
1	1km	18.80dB
2	2km	14.6dB
3	3km	10.4dB
4	4km	6.20dB

(ii) Channel 1: Signal Drop at Demultiplexer with OADM

From Table 1 and using equation (2), the optical power budget is 30dB.

Loss due to attenuation in channel 1 at 6km is 1.2dB (0.2dB/km × 6km).

From table 1 given the following total power loss and power margin can also be calculated at demultiplexer.

Loss due MZ modulator   = 3dB

Loss due to demultiplexer   = 4dB

Loss due to four OADM   = 4×4dB = 16dB

Transmitted Power (P_{in})   =0dB

Receiver sensitivity   =-30dB

From equation (3):

Total loss (T_{loss})   = 16+3+4+1.2

        = 24.2dB

From equation (4):

P_{Margin} = 0-24.2 + 0 – (-30)

        = 5.8dB

Similarly, the computations of power margins for channels 2, 3 and 4 at a distance of 5km, 4km and 3km for signal drop at the multiplexer are carried out in the same way as shown in the analysis of that of channel 1 and results are tabulated in Tables 2.

Table 3: Signal Drop at the Demultiplexer

Channel parameters

Channel	OADM	Power Margin
1	1st OADM (6km)	5.80dB
2	2nd OADM (5km)	10.0dB
3	3rd OADM (4km)	18.2dB
4	4th OADM (3km)	14.2dB

(b) Four - Channel DWDM Design with EDFA

Similar investigation of 10Gb/s four-channel MAN with four OADM are also implemented but this time with one EDFA amplifier, which is connected several kilometers apart. The network covers a metro area circumference of 108km. The same power analyses are also carried out as the cases were in item (i) and (ii) without EDFA to obtain values in Tables 5 and 6.

Table 4: Properties of Components/Parameters for DWDM Design with EDFA (Keiser, 2006).

Components/Parameter	Value
Multiplexer Insertion Loss	4db
Demultiplexer Insertion Loss	4db
OADM Insertion Loss	4db
Fibre Attenuation	0.2db/km
Receiver Sensitivity	-30dbm
Transmitted launch Power	0dbm
Circumference Distance	108km
Operating Window	1550nm
Channel Spacing	100GHz
Polarization	0.2ps/km
Spectral Efficiency of Modulated Channels	0.4Gb/Hz
Optical Signal To Noise Ratio	42dB
EDFA Noise Figure	3dB
EDFA Gain	28dB
Bit rate	10Gb/s

Table 5: Signal Drop at the Multiplexer

Channel parameters

Channel	Distance	Power Margin
1	40km	15.0dB
2	20km	7.0dB
3	4km	18.0dB
4	3km	26.8dB

Table 6: Signal Drop at the Demultiplexer

Channel Parameters

Channel	OADM	Power Margin
1	Ist OADM (88km)	17.4dB
2	2nd OADM (68km)	13.4dB
3	3rd OADM (47km)	5.60dB
4	4th OADM (25km)	14.0dB

V. Results and Discussion

In this paper, the improvement of signal transmission distance when Erbium Doped Fibre Amplifier was analysed using an eye diagram analyser. It was discovered that signal impairment increases with an increase in the transmission distance of the signal form the source. Impairment is reduced by employment of EDFA, thus increasing the signal transmission distance.

(a) Result without EDFA

When the required minimum BER of 10^{-9} is satisfied, the effect of distance on the signal is investigated using Eye diagram analayzer
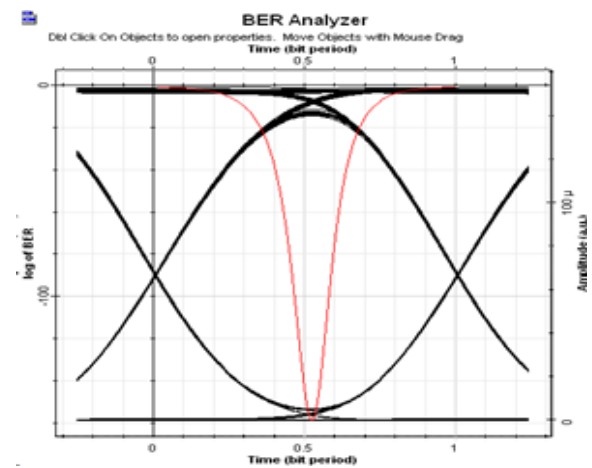
Figure 1: Signals Drop at 1km from Multiplexer.

The eye diagram of Figure 1 is very strong and has a good eye opening. The system presents a good height and eye width which shows that data can be easily sensed and recovered because there is no effect of degradation on the signal at that distance.
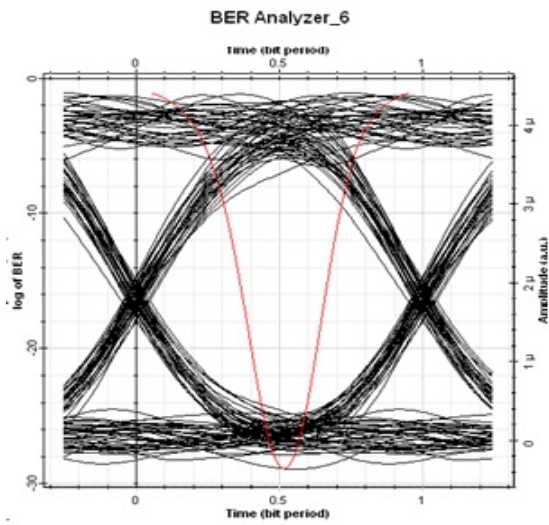
Figure 2: Signal Drop at 4km from Demultiplexer

Figure 2 represents one of the worst channels with significant effect of degradation as a result of transmission impairments as the distance increases
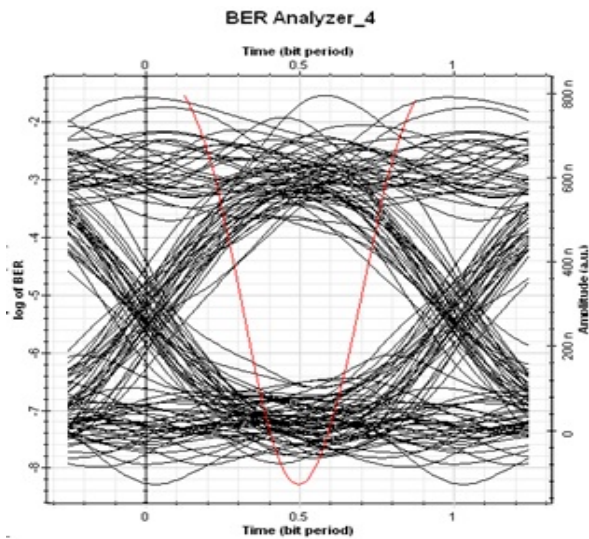
Figure 3: Signals Drop at 6km from Demultiplexer

The eye diagram in Figure 3 has a very good height and bad openning. The effect of degradation becomes very much and the signal cannot be recovered.
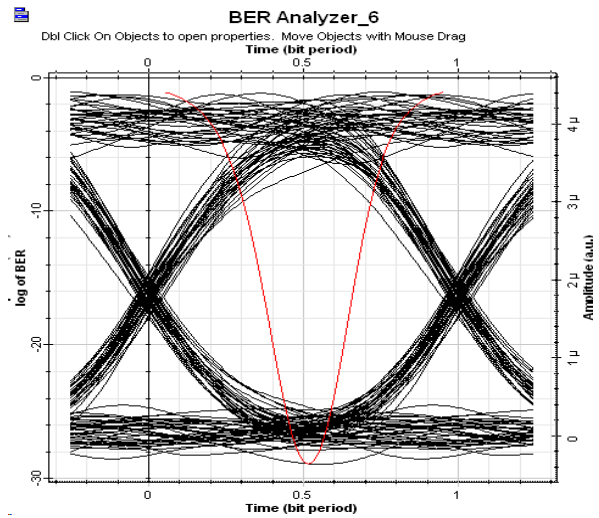
Figure 4: Signals Drop at 3km from Demultiplexer

The eye diagram is very good and can be easily recovered and there is no significant effect of degradation on the signal at that distance.

(b) Results with EDFA

When the requirement of the minimum BER of 10^{-9} is satisfied, the effect of distance on signal is investigated using Eye diagram analayzer
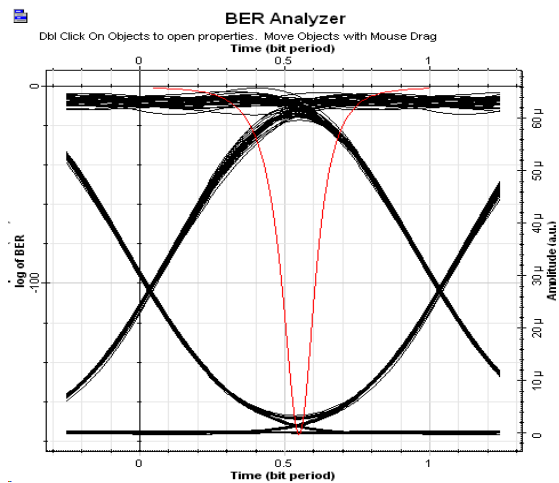
Figure 5: Signals Drop at 20km from Multiplexer.

When Erbium Doped Fibre Amplifier (EDFA) is used, the signal transmission distance is increased. With EDFA, the eye diagram in Figure 5 is still very clear and has a good opening even at 20 km from the multiplexer. There is no

effect of degradation at this distance because of the presence of EDFA used for the transmission and amplification of the signals.
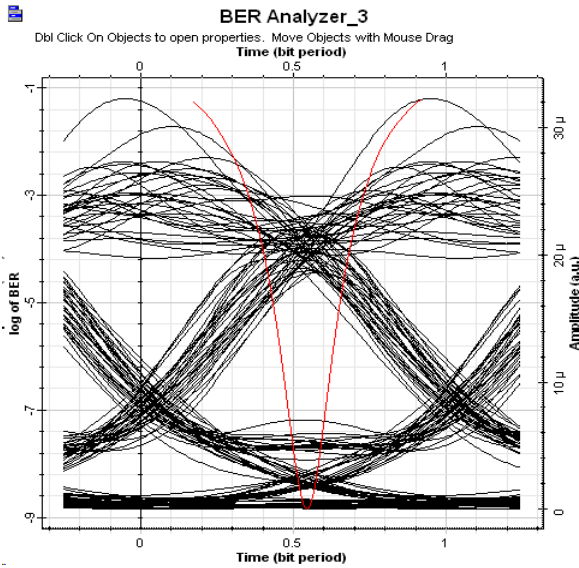
Figure 6: Signals Drop at 40km from Multiplexer

Figure 6 presents a very bad eye diagram at a distance of 40 km, the effect of degradation is more as a result of the transmission impairment and data could not easily be sensed and recovered.
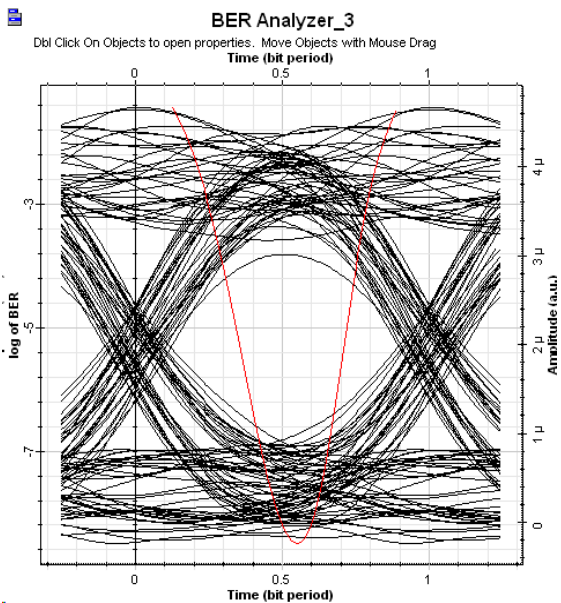
Figure 7: Signals Drop at 88km from Demultiplexer

Figure 7 eye diagram has a very poor opening. It can be observed that the transmission impairments increase as the distance increases. Data can hardly be recovered and sensed because of the effect of degradation and transmission impairments.
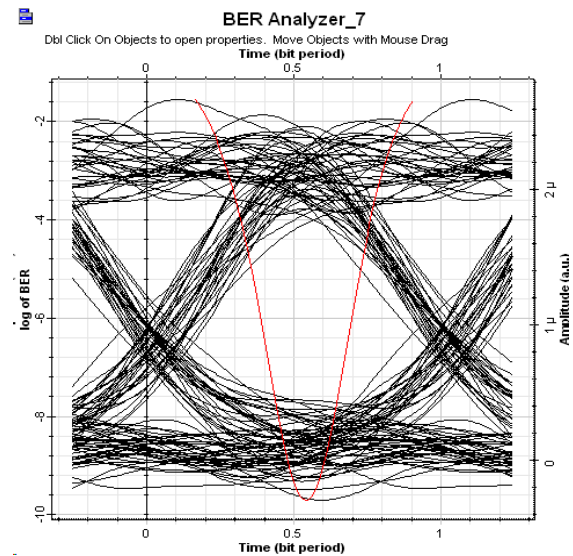
Figure 8: Signals Drop at 68km from Demultiplexer

The eye diagram of Figure 8 has a very bad opening and is not clear. This is because as the distance increases, transmission impairments also increases as a result of the degradation encountered with distance.

VI. Conclusion

The worst channels of the DWDM for a system without EDFA connotes that expansion in these channels is limited unless amplifiers are incorporated into the system to provide gain that compensates for the losses. An example of such channels included at the multiplexer, signal dropped at the 4th kilometre (channel 4) with power margin of 6.2dB and the one added at 1st OADM (channel 1 at a distance of 6km) with a power margin of 5.8dB dropped at the demultiplexer.

Due to impairments, only a transmission distance of 7km was achieved by DWDM system without EDFA deployment. It is after a distance of 7km that this resulted

to chromatic dispersion, losses due to attenuation and insertion losses associated with the devices. Hence, signals which did not propagate through longer distances experienced less loss, for example, comparing Figures 1 and 2 at the multiplexer and Figures 3 and 4 at the demultiplexer. Less losss indicated strong evidence of data recovery because of the strong opening of the eye diagram.

Similarly, other channels propagated through the amplifier (EDFA) provided reasonable power margin, which indicated the expansion could be accommondated these are represented by Figures 5 and 6 at the multiplexer and Figures 7 and 8 at the demultiplexer. A distance of 108km reached by the network when deployed with EDFA could be regarded as a reasonable improvement for a MAN incorporated EDFA system. The utilization of a four-channel Dense Wavelength Division Multiplexing ring network in metropolitan area achieved a distance of 7km without EDFA and 108km with one EDFA when operated at a bit rate of 10Gb/s with 0dBm power for each channel. Chromatic dispersion degradation factor is the major limiting effect on bit rate and distance, fibre attenuation and components insertion losses. All these factors played a major role in limiting the distance and bit rates.

REFERENCES

Cisco systems. Introduction to DWDM for metropolitan Networks. 2011

V. B. Grundlehner, "Dense Wavelength Division Multiplexing," 2002

Q. Zhao, and H. Yin, "performance analysis of dense wavelength division multiplexing secure communications with multiple chaotic optical channels" optics communications, vol. 285, no.5, pp. 693-698, 2012.

A. N. Z. Rashed, "Optical add drop multiplexer (OADM) based on dense wavelength division multiplexing technology in next generation optical networks," *Electrical and Electronic Engineering,* vol. 1, no. 1, pp. 24-32, 2011

S. Singh and R. S. Kaler, "Novel optical flat-gain hybrid amplifier for dense wavelength division multiplexed system," *Photonics Technology Letters, IEEE,* vol. 26, pp. 173-176, 2014

M. Jaspreet, and R. Kochher, "A Novel Approach on DWDM based metropolitant Ring Networks. ," *International Journals for science and Emerging,* vol. 20, no. 1, pp. 1-5, 2015

SaumyaSrivastava, "Optical Add Drop multiplexer (OADM) based on Dense Wavelength Division Multiplexing Technology: A performance Review," *Proceedings of STEER 2014:: ICIEEC 2014*, pp. 65- 67, 2014

A. Aliosio., A.Ameli., F. D'amico. *et al.*, "Performance analysis of a DWDM optical transmission system," *IEEE Transaction on Nuclear Science,* vol. 59, no. 2, pp. 251-255, 2012.

D. Stoll, P. Leisching, H. Bock *et al.*, "Metropolitan DWDM: A dynamically configurable ring for the KomNet field trial in Berlin," *Communications Magazine, IEEE,* vol. 39, no. 2, pp. 106-113, 2001

P. M. Becker, A. A. Olsson, and J. R. Simpson, *Erbium-doped fiber amplifiers: fundamentals and technology*: Academic press, 1999

F. D. Mahad, M. Supaarmet, and A. Sahmah, "EDFA gain optimization for WDM system," *Elektrika,* vol. 11, pp. 34-37, 2009.

D. Knipp, Optical Signal to Noise Ratio (OSNR). International University Bremen. Course: Photonics and Optical Communication 2005.

A. Pete, Ciena, "Optical power budgets," 2010.

S. Tibuleac and M. Filer, "Transmission impairments in DWDM networks with reconfigurable optical add-drop multiplexers," *Lightwave Technology, Journal of,* vol. 28, pp. 557-598, 2010.

A. Tzanakaki, I. Zacharopoulos, and I. Tomkos, "Optical add/drop multiplexers and optical cross-connects for wavelength routed networks," in *Transparent Optical Networks, 2003. Proceedings of 2003 5th International Conference on*, 2003, pp. 41-46.

Keiser, G. 2006. *FTTx Concept and Applications* PhotononicsCom Solution Inc, John Wiley and Sons Inc, Hoboken,New Jersey Published simultaneously in Canada.

SIMULINK BASED COMPARATIVE ANALYSIS OF VIDEO SEQUENCE USING EDGE DETECTION TECHNIQUES

B.O Sadiq[1*], Z.M Abubakar[2], A.I Abdu[3] and S. Salisu[4]

Department of Electrical and Computer Engineering,

Ahmadu Bello University Zaria

[*]bosadiq@abu.edu.ng,xeenabu@yahoo.com, s.salisu@live.com+2348156422063.

ABSTRACT

This paper presents a Simulink model for edge detection algorithm in video image processing using the proven edge detection algorithms such as the Sobel, Prewitt, Canny and the Roberts algorithms. The developed Simulink model compares the performance of the proven edge detection algorithms on real-time object tracking in video sequence. The result showed that the canny and the Sobel edge detection algorithms performed better in presence of noise as compared to the Roberts and Prewitt edge detection algorithms.

Keywords:_Simulink, Object tracking, video sequence and edge detection techniques_

1. INTRODUCTION

A number of practical video processing applications such as those requiring object detection and tracking process the visual signals in a series of stages. An advance object detection task in video processing requires breakage of task into smaller specialized stages which allows one to easily replace a component with a more advanced algorithm. The most fundamental stage in video processing is the edge detection stage. Edge detection is a low level feature in image processing [1]. Edge detection is a process of detecting sharp discontinuous in images. This is also a process of detecting high frequency component in images [2]. Edge detectors are of two types which are the gradient based edge detectors and the zero crossing order edge detectors. The presence of noise in the images makes edge detection in video sequence a highly difficult task. The developed Simulink model application will help researchers obtain a comparative analysis between the proven edge detection algorithms without having to resort to coding the algorithms when needed. The Simulink model is intended to help researchers have a better understanding of implementing edge detection in digital video hardware implementation.

2. EDGE DETECTORS

The proven edge detection algorithms are presented as follows:

i Sobel Edge Detectors

The traditional Sobel edge detection algorithm uses a 3x3 convolution kernels designed to operate in two directions, which are the vertical and horizontal directions [2]. The convolution kernel in Figure 1.0 showed the Sobel mask used in both directions. One kernel is simply the other rotated by 90^0[3]. The mask used by Sobel edge detection algorithm is shown in Figure 1.0

-1	0	+1
-2	0	+2
-1	0	+1

G_p

+1	+2	+1
0	0	0
-1	-2	-1

G_q

Figure 1.0: A 3x3 kernel of Sobel Edge Detection Algorithm

ii Prewitt Edge Detectors

The Prewitt edge detection algorithm uses the same principle as the Sobel edge detection algorithm, but

has a different convolution kernel. The Prewitt edge detection algorithm operates based on a 3x3 convolution kernel designed to operate in both horizontal and vertical directions denoted as G_p and G_q respectively. It performs better than the Sobel edge detection algorithm without the presence of noise in the image [4]. The mask used by Prewitt edge detection algorithm is shown in Figure 2. [5]

-1	0	+1
-1	0	+1
-1	0	+1

G_p

+1	+1	+1
0	0	0
-1	-1	-1

G_q
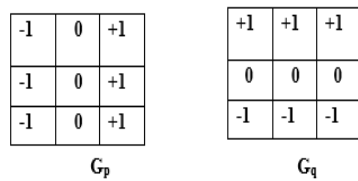
Figure 2: 3x3 kernel of Prewitt Edge Detection Algorithm

iii Roberts Edge Detectors

The Robert Edge detection algorithm used a 2x2 convolution kernel to compute the gradient magnitude and direction. Its computes the difference between the sum of squares of the diagonally adjacent pixel using discrete differentiation. Thus finding the approximate gradient in the image. The 2x2 kernel are shown in Figure 3 [6]. The Robert edge detection algorithm is highly sensitive to noise due to the smaller mask size [7].

1	0
0	-1

G_p

0	-1
-1	0

G_q

Figure 3: A 2x2 kernel of Robert Edge Detection Algorithm

iv. Canny Edge Detectors

The canny edge detectors are the most widely used edge detectors in recent times. The main advantage of the canny edge detection algorithm is its ability to eliminate multiple responses to a single edge. It possesses good localization property, the detected edges are much closer to the real edges. The response of this detector is also good, as the original edge does not result in more than one detected edge. The gradient magnitude and direction is calculated by using first order finite differences. However the algorithm is susceptible to weak edges in images and cannot perform effectively in noisy environment [8].

The flow chart for the implementation of the canny edge detection algorithm is shown in figure 4.0
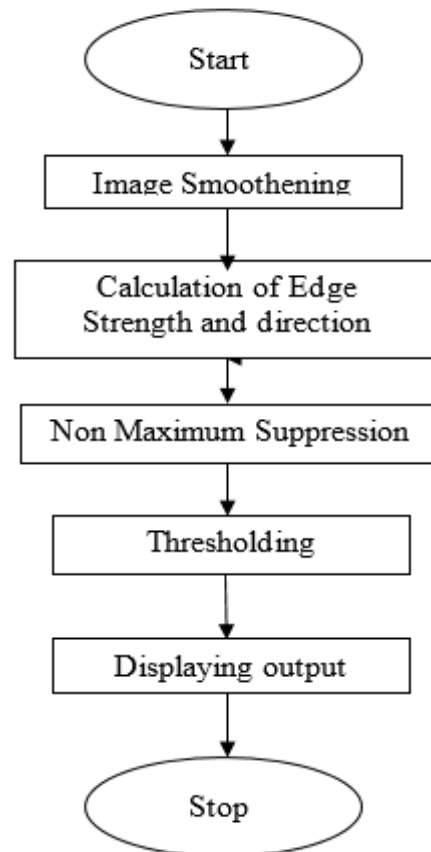
Figure 4.0: Canny Edge Detector Flow Chart

3. METHODOLOGY

The methodology adopted in realising this work follows the under listed procedures:

i. Start your Simulink Model for digital image edge detection and add the HD webcam from video device block.

ii. Add the color space conversion block, linking it to the video device block.

iii. Add noise to the image using a Gaussian noise generator with a view to testing the model in noisy environment.

iv. Attack a median filter to reduce the effect on noise present in the image.

v. Use the edge detection block set to detect edges in the video sequence.

vi. Go to the Simulation → Configuration Parameters, change the solver options type to "variable steps.

vii. Run the model to view the results

viii. Repeat the test with the Prewitt, Canny and Roberts edge detection methods.

Figure 5.0 shows the Simulink model for the edge detection algorithm.
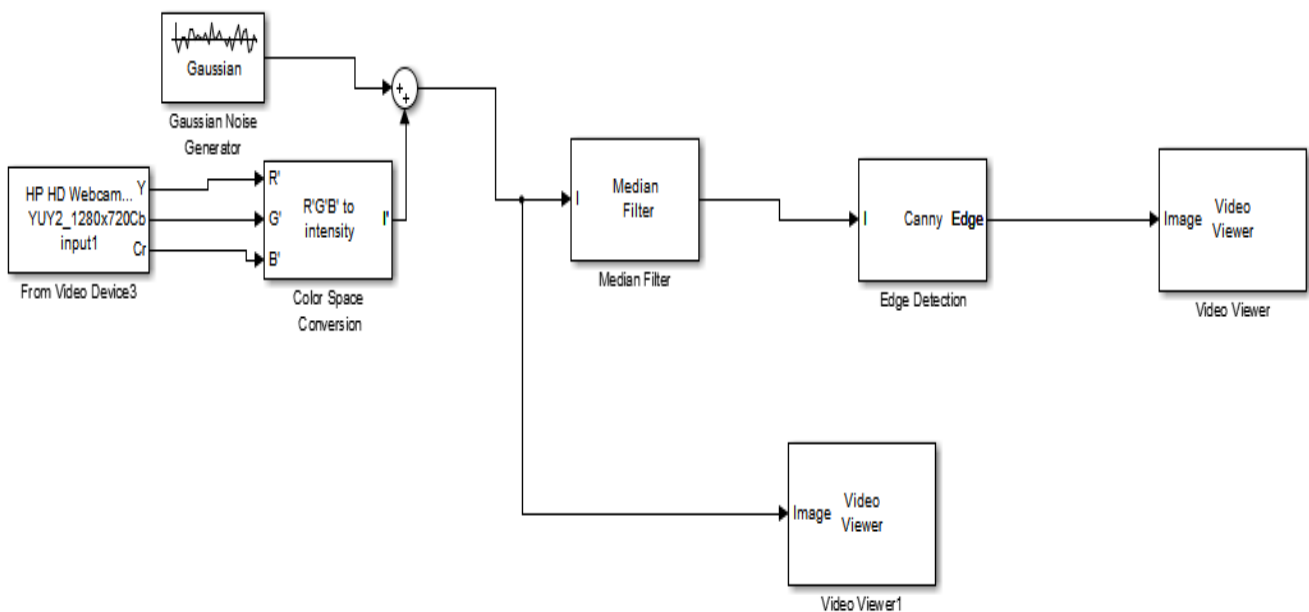
Figure 5.0: Simulink model for detection of edges in video sequence

4. SIMULATION RESULT

The output result of the Simulink model is shown in figure 6.0 (a-d). The Figure 6.0 (a) is the result of applying the Sobel Edge Detector to the video sequence, the Figure 6.0 (b) is the result of applying the Prewitt Edge Detector to the video sequence, Figure 6.0 (c) is the result of applying the Roberts Edge Detector to the video sequence and

Figure 6.0 (d) is the result of applying the Canny Edge Detector to the video sequence.

(a)

(b)

(c)

(d)

Figure 6.0: Output result of Proven Edge Detection Algorithm

From the output result shown in Figure 6.0, the Sobel, Prewitt, Robert algorithm showed missing edges in the generated output edge map. The Canny edge detection algorithm showed more detected edges, but this algorithm is highly sensitive to weak edges unlike the Sobel Edge detection algorithm.

5. CONCLUSION

This paper presents a Simulink model with a view to comparing the performance of the proven edge detection algorithms which are the Sobel, Prewitt, Roberts and the Canny. The Simulink model was developed to perform in noisy environment, and a median filter was used to reconstruct the image from noisy environment to clean environment. These reduces the effect of false and broken edges that exists with the edge detection algorithms. It can

be concluded that the canny edge detector perform better but highly susceptible to weak edges and thus false edges exists. This work can be extended to hardware based implementation with a view to detecting edges in real time video sequence.

REFERENCES

[1] Ayaz Akram and Asad Ismail (2013) "Comparison of Edge Detectors," *International Journal of Computer Science and Information Technology Research (IJCSITR),* vol. 1, pp. pp.16-24.

[2] S.M Sani B.O Sadiq , Garba.S (2015) "Edge Detection: A Collection of Pixel based Approach for Colored Images," *International Journal of Computer Applications,* vol. 113, pp. 29-32.

[3] Anila and Devarajan (2010) "Simple and Fast Face Detection System Based on Edges," *International Journal of Universal Computer Sciences,* vol. 1, pp. pp.54-58.

[4] Rashmi, Mukesh Kumar, and Rohini Saxena (2013) "Algorithm and Technique on Various Edge Detection: A survey," *Signal & Image processing : An International Journal (SIPIJ),* vol. 4, pp. pp.65-75.

[5] Raman Maini and Himanshu Aggarwal (2011) "Study And Comparism of Various Image Edge Detection Technique," *internation Journal of Image Processing (IJIP),* vol. 3, pp. pp.1-12.

[6] Syed Jahanzeb and Ayesha Siddiqui (2013) "Analysis of Edge Detection Algorithms for Feature Extraction in Satellite Images " *IEEE International Conference on Space Science and Communication (IconSpace),* vol. 3, pp. pp.238-242.

[7] Katiyar and Arun (2014) "Comparative analysis of common edge detection techniques in context of object extraction," *IEEE Transactions of Geoscience and Remote Sensing,* vol. 50, pp. pp.68-79.

[8] Vineet Saini and Rajnish Garg (2012) "A Comparative Analysis on Edge Detection Techniques Used in Image Processing " *IOSR Journal of Electronics and Communication Engineering,* vol. 1, pp. pp.56-59

STUDIES ON THE SUITABILITY OF ALUMINA AS BIMETALLIC CATALYST SUPPORT FOR MWCNTs GROWTH IN A CVD REACTOR

Kariim Ishaq[1*], Abdulkareem Ambali Saka[1,2], Abubakre Oladiran Kamardeen[1,3], Mohammed Ishaq Alhassan[2], Bankole Mercy Temitope [1,4] and Jimoh Oladejo Tijani[4]

[1] Nanotechnology Research Group, Centre for Genetic Engineering and Biotechnology (CGEB), Federal University of Technology, P.M.B 65, Bosso, Minna, Niger State, Nigeria

[2] Department of Chemical Engineering, Federal University of Technology, P.M.B 65, Gidan Kwano, Minna, Niger State, Nigeria

[3] Department of Mechanical Engineering, Federal University of Technology, P.M.B 65, Gidan Kwano, Minna, Niger State, Nigeria

[4] Chemistry Department, School of Pure Sciences, Federal University of Technology, P.M.B 65, Bosso, Minna, Niger State, Nigeria

[*]k.ishaq@futminna.edu.ng, +2348179612145.

ABSTRACT

The role of alumina (Al_2O_3) as catalyst support for improving the selectivity and uniformity in carbon nanotube growth via Chemical Vapour Deposition (CVD) technique has been widely explored. In this study, the suitability of bimetallic (Fe-Ni)/Al_2O_3 catalyst prepared via wet impregnation technique for the synthesis of multi-walled carbon nanotubes (MWCNTs) has been investigated. The surface morphology, thermal properties and the crystallinity of the bimetallic catalyst supported on aluminaand Multi-Walled Carbon Nanotubes (MWCNTs) were characterized using various analytical techniques such as HRSEM, HRTEM, EDS, SAED, TGA-DTA, and BET surface area. The results revealed that the synthesized catalyst wascrystalline with surface area of 286 m^2/g as determined by BET equipment. The bimetallic (Fe-Ni) supported alumina catalyst grown in a horizontal CVD reactor was found to produce high quality MWCNTs with 79.5 % purity. A Dynamic Light Scattering(DLS) based correlation chart revealed interdependence of length, diameter and aspect ratio of the purified and un-purified MWCNTs. This study has demonstrated that a thermally stable and high quality MWCNTs can be obtained from Fe-Ni/Al_2O_3 catalyst via wet impregnation followed by CVD technique.

Keywords: Iron–nickel catalyst*; Alumina support;MWCNTs;Characterization; DLS-Correlation*

1. INTRODUCTION

The synthesis and application of carbon nanotubes (CNTs) have attracted considerable interest among experts in the field of nanoscience and nanotechnology due to their excellent electrical, mechanical and thermal properties (Hoenlin*et al.,* 2003; Kong*et al.,* 2000; Liu *et al.,* 2011). These remarkable characteristics make CNTs a suitable materials for various applications in hydrogen storage, nanoelectric devices, reinforced materials, energy storage, chemical sensors and field emission to mention but a few. Different methods of synthesising CNTs such as laser ablation, spray pyrolysis, arc discharge and catalytic chemical vapour deposition (CVD) have been reported in literatures (Ahmad*et al.,* 2013; Lee *et al.,* 2002).

However, of all the methods, CVD is considered rather simple, easy to scale up anda cost-effective technique in terms of production of carbon nanotubes of high quality yield and purity, better structural growth, and mass production compared to the other methods (Terrado*et al.,* 2006). Ease of optimization ofthe process parameters, feasibility of exploring numerous carbon sources, and its ability to run multiple samples per experimental run, also make a suitable process technique.

Over the years, there have been considerable increases in the utilization CVD techniques for CNT synthesis based on the aforementioned advantages. Additionally, several approaches of producing CNTs including growing of metallic catalyst on support material have been

reported(Pelech*et al.,* 2009; Quian*et al.,*2003; Yeoh*et al.,*2009). The choice of metallic catalyst with or without support materials influences the yield and morphology of synthesized carbon nanotubes. Not only that the mechanism of CNT growth is complex and not fully understood (Kumar, 2012).It is also noteworthy to mention that, catalyst design, catalyst type, support material as well as their properties are integral components in the synthesis of controlled-growth of carbonnanotubes (CNTs) for various applications (Mhlanga *et al.,* 2009). The role of catalyst support in supported-catalyst lies in its ability to determine accessibility of active sites, and to influence certain properties such as the pore volume and pore-size distribution which are essential parameters in catalyst design (Storch*et al.,*1998). Thus, the efficiency of the CVD method for CNT growth is a function of catalysts preparation and metals loading (Terredo et al., 2006).

Furthermore, Iron, Cobalt and Nickel are mostly employed as an efficient catalyst for CNT growth in the CVD method. The choice of these metals as active component of catalyst is ascribed to their ability to form carbides which are metastable compounds that decompose to form a graphene-like sheet by the process called graphitization. Thus, the nature of metallic catalysts as well as the support material or template both affects the yield and purity ofthe final CNT material (Kathyayini*et al.,*2008). In the synthesis of CNTs by CVD, the catalyst aids in the decomposition of the carbonaceous materials during thermal process in the quartz chamber of CVD. However, the purity of the CNT material is still a subject of debate, due to the fact that the as-synthesized CNT is usually accompaniedbyimpurities such as fullerenes, amorphous carbons, crystallized graphite, support material and the metal (Kruusenberg*et al.,* 2011).The level of impurities is known to depend on the choice of metal, support material and other growth parameters.

Different support materials such as Al_2O_3, zeolite, MgO, SiO_2, and $CaCO_3$ have been applied as a carrier in supported-catalysts for CNT (Kathyayini *et al., 2008;* Willems*et al.,* 2000; *Mao-Lin et al.,* 2012 and Couteau*et al.,* 2003)Several researchers have reported high purity multi-walled carbon nanotubes obtained from Co-Mo supported MgO catalyst via CVDPelech*et al.,* 2009; Quian*et al.,*2003; Yeoh*et al.,*2009). Awadallah*et al. (*2012)demonstrated the synthesis of CNTs prepared via CVD methods from Ni-Mo and Co-Mo supported on Al_2O_3 catalyst.. Studies have shown that alumina supported catalysts for CNTs synthesis appeared more promising due creation of a high surface areas and mesoporous materials which promote catalysis (Kathyayini*et al., 2008*). In addition, Al_2O_3 has good thermal stability and can be easily removed after the synthesis via acid purification.

In this present study, bi-metallic Fe-Ni catalyst supported on aluminium oxide were developed and utilised to prepare CNT through CVD method. The choice of Fe-Ni as an active part of the catalyst is due to their availability and cheapness (Uddin *et al., 2008*).

2. METHODOLOGY
2.1 Material

All the chemicals used in this study are of analytical grade with percentage purity in the ranges of 98- 99.99 %. These chemicals include Nickel nitrate hexahydrate $[Ni(NO_3)_2.6H_2O]$, iron nitrate nonahydrate $[Fe(NO_3)_3.9H_2O]$, alumina $[Al_2O_3]$, distilled water and concentrated hydrochloric acid $[H_2SO_4]$ were supplied by Aldrich . The carbon source (acetylene) and carrier gas (argon) are also of analytical grade with 99.99% purity supplier by BOC Nigeria.

2.1.1 Synthesis of Supported Bimetallic Catalyst

Wet impregnation method was employed for bimetallic catalyst preparation. Bimetallic catalyst (Fe-Ni/Al$_2$O$_3$) was produced using equal weight percentage of Fe and Ni supported on Aluminium oxide. This was prepared by dissolving 4.04 g of Fe (NO$_3$)$_3$.9H$_2$O and 2.91 g of Ni (NO$_3$)$_2$.6H$_2$O in 50 ml of distilled water. The solution obtained was then added to 8 g of Aluminium oxide and the mixture was allowed to age for 45 min under constant stirring. The resulting homogeneous slurry was dried at a temperature of 115 ^{O}C for 7 hrs. The product obtained was grinded and calcined in a static air furnace at 400 ^{0}C for 2 hrs. The calcined sample was allowed to cool and was later sieved through 150 μm sieve.

2.1.2. Synthesis of CNTs

In this study, a cylindrical tube reactor of length 1010 mm with internal and external diameter of 52 mm and 60 mm respectively and thickness of 4 mm was used. 1.0 g of the supported bimetallic catalyst (Fe-Ni/Al$_2$O$_3$) was weighed and spread evenly on a quartz boat placed at the central part of the horizontal tube. The heating rate, temperature, gas flow rates were maintained at the desired rate. The entrapped gases in the quartz tube were expelled using argon as the carrier gas at a flow rate of 30 ml/min. At a temperature of 750 ^{0}C, the flow of acetylene was released into the quartz tube of catalytic reactor at 100 ml/min for 45 min with immediate increment in the flow rate of the carrier gas (argon) to 200 ml/min. As the residence time (45 minutes) of the reaction was attained, the flow of acetylene was stopped and the argon gas was left flowing at 30 ml/min until the reactor cooled to room temperature. The sample was removed, weighed and analysed. The yield of the deposited carbon was therefore determined using Equation (1)(Yeoh*et al.,* 2009; Taleshi, 2012).

$$Yield\ (\%) = \left(\frac{W_2 - W_1}{W_1}\right) \times 100 \quad (1)$$

Where W$_1$ is the initial weight of the catalyst before reaction and W$_2$ is the weight of catalyst and carbon deposited after synthesis.

2.1.3. Purification of As-synthesised Carbon Nanotubes

The as-produced CNT was treated with 30 % wt concentrated sulphuric acid, heated and stirred at a temperature of 60 ^{O}C for 30 minutes using a magnetic stirrer to remove residual fractions of Al$_2$O$_3$ or Fe-Ni in the form of sulphates. The sample was washed with distilled water until the pH was approximately 7.0 and later dried at 110 ^{O}C for 5 hours. The acid purified sample was characterized with SEM, TEM, EDS, SAED and TGA.

2.2 Characterization of the Synthesised Materials

2.2.1 Thermo-Gravimetric Analysis (TGA) and Differential Thermal Analysis (DTA)

The thermal stability, compositional and percentage purity of materials were determined using TGA 4000 (PerkinElmer). Samples were analysed in nitrogen environment at a flow rate of 20 ml/min, pressure of 2.5 bars and heating rate of 10 ^{0}C/min. To a zeroed thermal balance, sample was loaded and recorded into the equipment using pyris manager software. The analysis was then initiated after constant weight was noted using the created heating profile (temperature scan). The test results were then analysed using pyris manager for proximate and compositional analysis.

2.2.2 High Resolution Scanning Electron Microscope (HRSEM)

The surface morphology and microstructure of the synthesised materials were characterized using Zeiss Auriga HRSEM. The HRSEM equipped with EDS was further used to determine the elemental composition of the synthesised catalysts. A small quantity of the synthesised

materials was sprinkled on a sample holder and sputter coated with Au-Pd using Quorum T15OT for 5 minutes prior to analysis. The sputter coated samples was firmly attached to the carbon adhesive tape and analysed using ZeissAuriga HRSEM equipped with In-lens standard detector at 30 kV. The microscope was operated with electron high tension (EHT) of 5 kV for imaging.

2.2.3X-Ray Diffraction Patterns (XRD)

The crystal phase identification of the powdered materials were performed using Bruker AXS D8 X-ray diffractometer system coupled with Cu-Kα radiation of 40 kV and a current of 40 mA. The λ for Kα was 0.1541 nm, scanning rate was 1.5 °/min, while a step width of 0.05° was used over the 2θ range value of 20 – 80 °.

2.2.4High Resolution Transmission Electron Microscope (HRTEM)

The diameters and the crystalline nature ofas-produced and purified CNTs were determined by Zeiss Auriga HRTEM operated at 3950 V. Small quantity of the materials were suspended in 10 ml methanol and ultrasonicated until the particles completely dissolved. Few drops of the slurry was placed onto the holey carbon grid, dried via exposure to photo light and analysed.

2.2.5 Particle Size Analysis (DLS Technique)

The particle size and the hydrodynamic diameter were determined using Zetasizer Nano S at scattering angle of 173 ^{O} operating at 25°C with equilibrating time of 120 secs. 1mg of the samples were dispersed in 10 ml of ethanol then transferred into a polystyrene cuvette using a syringe with 0.22 µm filter coupled to it. This was then placed in the analysis stage of the equipment for analysis.

2.2.6 BET Surface Area

The surface area of the developed and the alumina were determined using a BET method in Nova e-series equipment. Samples were degassed at 250 ^{O}C for 4 hrs for moisture and removal. The degassed samples were then analysed for physisorption of the adsorbate (nitrogen) by

theadsorbent in liquid nitrogen environment on the on the surface.

3. RESULTS AND DISCUSSIONS

Figure 1 depicts the thermal stability of the aluminasupport and the bimetallic supported catalyst. The TGA examines the behaviours of materials as a function of percentage weight and derivative weight against temperature (Okpalugoet al.,2006). At 800 ^{O}C, the percentage weight difference retain in the catalyst increase by 1.621 % compared to the alumina support. This is resulted from the presence of active catalyst (Fe and Ni) in the composition which raised the thermal behaviour of the alumina for thermal stability for CNTs growth. The results indicated improvement of the thermal stability of the prepared bimetallic catalyst compared to the raw alumina. The BET surface area of the developed bimetallic catalyst was determined to be 285.62m^2/g under nitrogen condition, with micropore volume of 0.1023 cc/g and micropore half pore width of 32.43 Â. This surface area is little less than those reported by Abassi *et al.,* 2014. This may be due to the presence of weak bond that exixt between Fe-Al$_2$O$_3$ (Zhang et al., 2006).
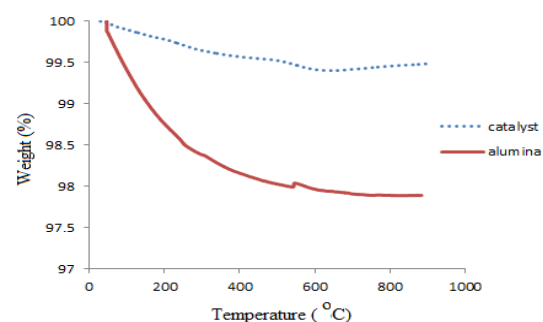
Figure 1: Thermal behaviour of the developed bi-catalyst (Fe-Ni/Al$_2$O$_3$) and raw alumina

The XRD pattern of the synthesized catalyst is presented in Figure 2 which demonstrates the presence of sharp diffraction peaks. This suggests that the prepared catalyst is highly crystalline, an indication of orderlydistribution of the metallic ions on the pore of the alumina support. The characteristics peak at 2θ value of 35. 23° suggest the
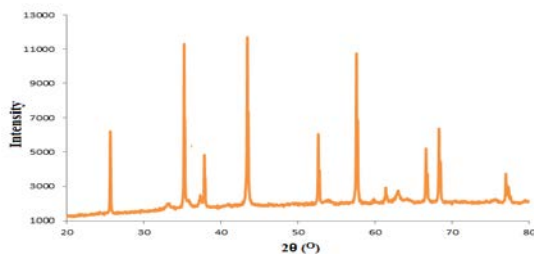
presence of alpha alumina (α-Al_2O_3) (Kathyayini*et al.,*2008).The crystalline size of the catalyst was calculated from the XRD data using the Scherer Equation shown in Equation (2) (Chen *et al.,*2006).

$$D = \frac{K\lambda}{\beta COS\theta} (2)$$

Where D is the particle size diameter, β is the full width at half maximum, λ is the wave length of X-ray (0.1541 nm), θ is the diffraction angle and K is the Scherrer constant (0.94).

Fig.2: XRD spectra of Fe-Ni/Al_2O_3 catalyst

The particle size distribution of the synthesised supported catalyst based on the respective identified peaks in the XRD pattern is presented in Figure 3. The estimated crystallite size revealed that the bimetallic catalyst is dominatedwith particle sizes of 60.94 nm and relatively the smallest particle size population of 8.86 nm. Thus, the result indicates the possibility of producing CNTs of nano size when utilizing bimetallic supported catalyst.

The results presented in Table 1showedthat 45 minutes is the optimum reaction time for CNTs synthesis using bimetallic catalyst (Fe-Ni/Al_2O_3) at a desired temperature (750 ^{O}C), argon flow rate of 200 ml/min and acetylene flow rate of 100 ml/min. Below this reaction time, acetylene possesses low decomposition rate and little of the bi-metallic catalyst's active pores are susceptible to carbon nanotube yield (Hengameh, 2006). Further increment in the residence time from 45 - 60 minutes resulted into a slight decrease in CNTs yield from 49 % to 48 %. At 60 minutes reaction time, side-way reaction

occurs which resulted in catalyst deactivation and CNTs yield decrease with increase reaction time. The initial increment in the carbon yield may be attributed to continuous deposition of carbon from acetylene into the pore volume of the catalyst until the entire pores are completely saturated (45 minute). At 60 minutes, the catalyst becomes poisoning due to saturation of the catalyst pores by carbon deposit and further leads to reduction in yield.

Table I: Effect of Residence Time on Carbon Nanotube Yield

Time (mins)	Yield (%)	Production rate (g/mins)
15	25	0.0167
30	42	0.0140
45	49	0.0109
60	48	0.008

It has been reported that porous materials such as alumina are excellent catalyst support, but they have the tendency of producing amorphous carbon during CNTs production. However, wet impregnation of the bimetallic catalyst on the alumina will reduce the porosity of thesupport. This wasconfirmed by the SEM micrograph of the synthesized catalyst as presented in Figure 4. TheHRSEM micrograph clearly showed that the synthesized catalyst is of low porosity with noticeable particles of metal ions covering the surface of the support material (Figure 4b). The influence of time on the quantity of carbon nanotubes yield was investigated and the results obtained are presented in Table 1.

Due to the possibility of presence of impurities as a result of undissolve catalyst particles, the synthesised carbon nanotubes were purified with 30% sulphuric acid to remove the undissolved metallic catalyst, support and amorphous carbon presence in the as-produced CNTs.

The carbon nano-material treated using this process becomes active and led to oxygenous functional groups generation such as carboxyl (Dalton et al., 2000).
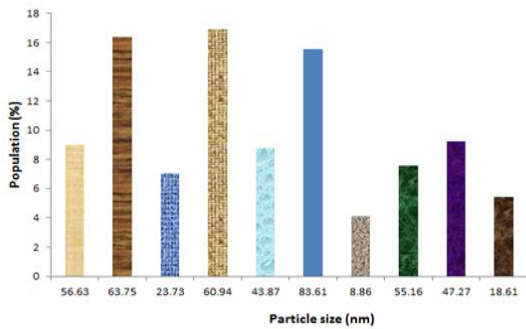
Fig.3: Percentage Population of Particle Sizes from XRD Data
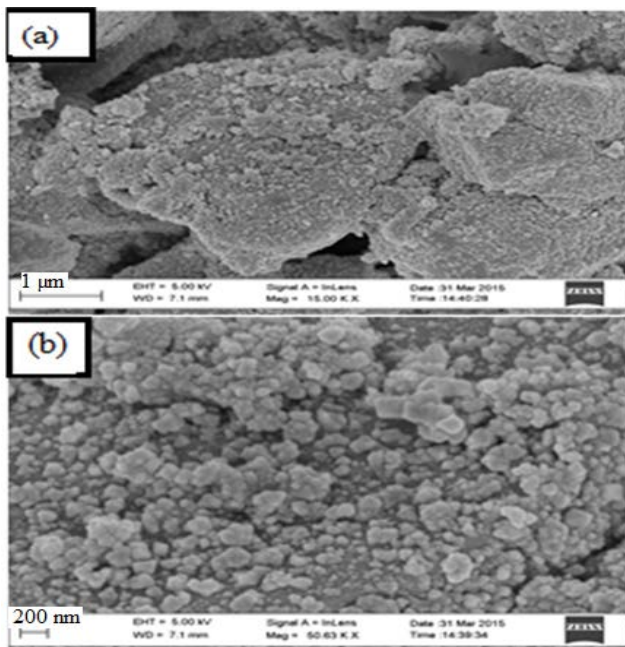
Fig.4: HRSEM Micrograph of (a) Low Magnification and (b) High Magnification of CalcinedFe-Ni/Al$_2$O$_3$Catalyst

The HRSEM micrograph, Figure 5 shows a densely populated strand of CNTs with high degree of homogeneity covering the impurity present; which is in line with the property reported by (Ratkovic et al., 2011).
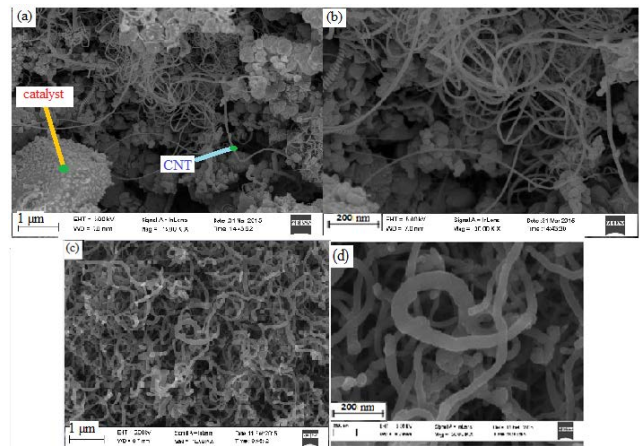
Fig.5: HRSEM Micrograph of As-Produced (a-b) and Purified (c-d) Carbon Nanotubes with Production Time of 45 Minutes

HRSEM micrograph of as-produced CNTs presented in Figures 5a and b indicate that the CNTs are several micrometres long with encapsulated catalystimpurities during CNTs nucleation process.
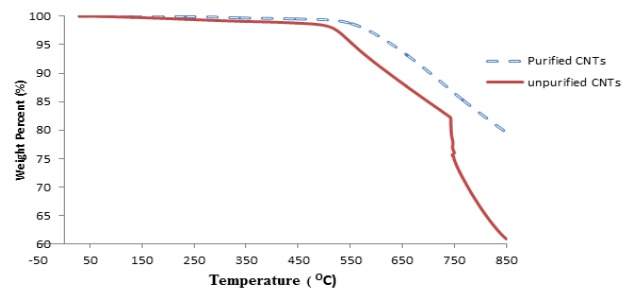
Fig.6: Thermal Behaviour of As-synthesized and Purified MWCNTs

Figures 6 and 7 represent the TGA and DTA profile of both the as-produced and purified CNTsrespectively.
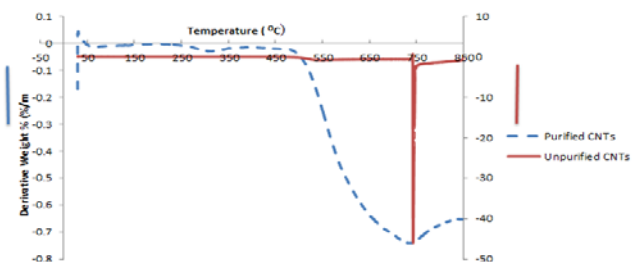
Fig.7: DTA of As-synthesized and Purified MWCNTs

Additionally, Table 2 contains information about the sample extracted from Figures 6 and 7. The results indicate that the as-produced CNTs hadlower moisture content than purified CNTs. The increment in percentage moisture content may be due to the purification process which involves distilled water and sulphuric acid solution, thus there is a possibility of water being entrapped within the pore of the CNTs. The TGA results also revealed that the percentage purity of the synthesized MWCNTs was 79.547 % with lesser volatile organic constituents compare to as-produced MWCNTs. The observable high T_P(optimum temperature of degradation) in unpurified CNTs is linked to the presence of impurities which accompany the synthesis CNTs (Ebbensen*et al.,* 1998; Eftehari*et al.,* 2005). After the purification process, the impurities in the form of amorphous carbon and metals oxides were reduced and further lower the peak temperature of the purified carbon nanotubes. Temperature at which 50 % of the material degraded, T_{50} were also determined to be greater than 850 ^{O}C which is an indication of high thermal stability of the CNTs. Hence the CNTs produced with bimetallic catalyst, Fe-Ni on alumina support is thermally stable.

Table II: Proximate Analysis of the As-Synthesized and Purified MWCNTS 750 ^{O}C

Material	Moisture Content (%)	CNTs Content (%)	Volatile Content (%)	Degradation Temp Range (^{O}C)	T_{50} (^{O}C)	T_p (^{O}C)	Onset Temp ^{O}C
As-produced MWCNTs	0.013	62.48	37.50	450.65-726.54	>850	743.64	516.71
Purified MWCNTs	0.098	79.55	19.87	519.80-806.91	>850	738.61	578.12
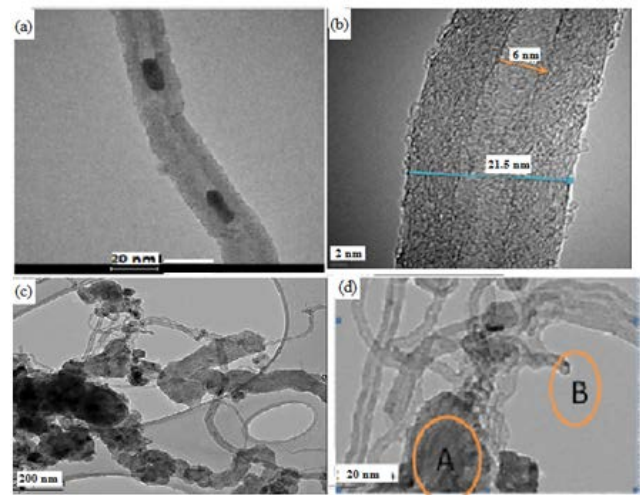
Fig.8: HRTEM Image of MWCNT (a) As-produced (b) Purified MWCNTs showing the Inner and Outer Diameter (c) As-synthesized and (d) Purified CNTs
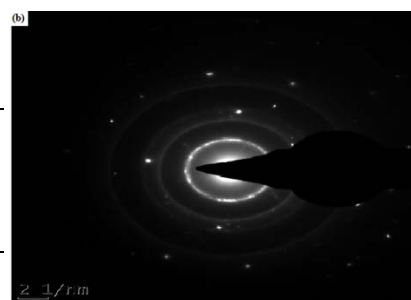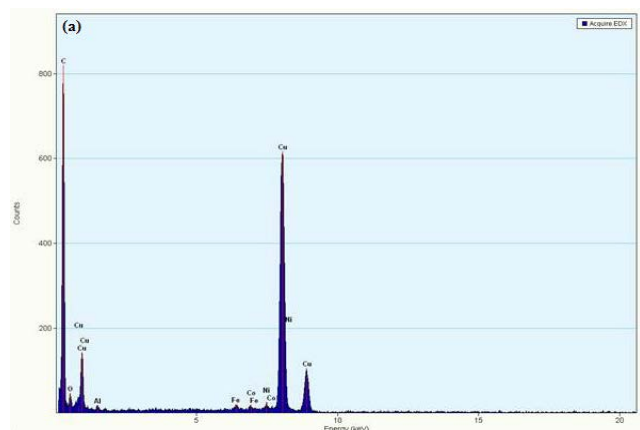
Fig.9: (a) EDS and (b) SAED of Purified Carbon Nanotubes

The morphologies and the microstructure of the unpurified and purified CNTs was examined using HRTEM and the results presented in Figure 8 a and b. According to figure 8a and b, the synthesised carbon nanotubes are multiwall

302

carbon nanotubes (MWCNTs) having a straight length structure or rope-like structure with absence of coiled-tube. In the purified HRTEM image (Figure 8b), there wasa reduction in the level of impurity present which was attributed to by the purification process by 30 % sulphuric acid. The acid aids in the precipitation of the metallic impurities in the form of amorphous carbon and metal carbide which might have not dissociate during the thermal catalysis process. The diameters and length of the microscopic images shown in Figure 7(a-d) are well represented in terms of their interrelationship in Figure 8. It can be deduced from the results presented in Figure 8c that there is no uniformity in the size distribution of the purified synthesized carbon nanotubes. However, point A shows some denser and thicker tubes which anchor some catalyst as a result of continuous overlapping and encapsulation therein with impurities of larger particles (Son *et al.,* 2008). The point marked B in Figure 8dindicates a cracked tube with thin tube end where catalysts particles were removed during the oxidative purification process. The EDS result presented in Figure 9 A also indicates that the metals impurities are not completely removed, hence, there is need to improve on the purification process. The presence of Cu in the EDS results emanated from the Cu grid used in the HRTEM analysis. The crystalline nature of the prepared MWCNTs was further evaluated via the Selected Area Electron Diffraction (SAED) pattern (Figure 9b). The SAED pattern revealed the presence of two broad crystal plane which correspond to (002) and (100) respectively. This result is in accordance with the previous studies (Cong*et al.,* 2011). The effect of acid treatment on the aspect ratio (L/D) of the purified carbon nanotubes was investigated by establishing a DLS-correlation chart. The diameter of as-produced and purified carbon nanotubes from HRTEM image was related to the D_h (hydrodynamic diameter) using modified Navier-Stokes equation (Nair *et al.,* 2008)and Stokes-

Einstein equation. The chart is aimed at determining MWCNTs aspect ratio and length at a specific diameter.

$$D_h = \frac{L}{\ln(L/d)+0.32} \quad (3)$$

Where D_h, l and d are hydrodynamic diameter, length and diameter of MWCNTs respectively. From the DLS-Nanosizer, the hydrodynamic diameter of both the as-synthesized and purified carbon nanotubes were determined to be 4847 nm and 3471 nm respectively.

From the correlation graph, Figure 10, the length and the diameter of as-synthesized MWCNTs purified with 30 % sulphuric acid shows a reduction in the diameter and the length.
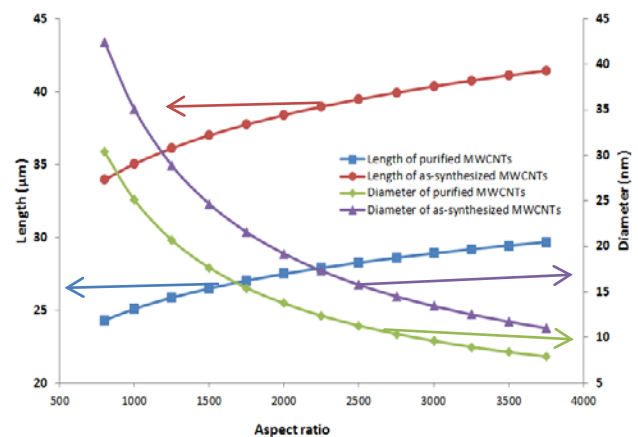
Fig.10:Aspect Ratio Correlation of Length and Diameter of Purified and As-Synthesized Long-Tube MWCNTs

This reduction in diameters and lengths confirms the removal of crystalline impurities in the as-synthesized MWCNTs. The aspect ratio (L/D) is proportional to the length and inversely proportional to the diameter of both the as-synthesized and purified MWCNTs. The correlation results also indicate a long-tube growth of purified and as-synthesized MWCNTs of 25.86 μm and 36.11 μm length respectively with 1250 aspect ratio. Based on the results of the analysis obtained, it can be concluded that bimetallic catalyst on alumina support is suitable for CNTs production.

4.0 CONCLUSION

In this study, multi-walled carbon nanotubes were developed from bimetallic supported alumina catalyst via wet impregnation followed by CVD technique. High purity and thermally stable CNTs was successfully synthesised at optimum conditions of reaction time of 45 minutes, temperature of 750 ^{o}C, argon flow rate of 200 ml/min and acetylene flow rate 100 ml/min. The average diameter of the as-produced multiwalled carbon nanotubes obtained from bimetallic Fe-Ni/Al_2O_3 catalyst was 28.89 nm whereas; the bimetallic catalyst had average particle size of 46.24 nm. The correlation chart showed that the MWCNTs produced was a long-tube multiwall carbon nanotubes with aspect ratio of 1250. Acid treatment method with tetraoxosulphate (VI) acid of 30 % was found to remove reasonable amount of impurities with little tip-tube damage. Thus, the bimetallic catalyst on alumina support developed via incipient wet impregnation method is suitable for CNTs production by CVD method.

ACKNOWLEDGEMENTS

REFERENCE

Abbasi, A., Ghasemi, M., Sadighi, S, (2014) "Effect of Lanthanum as a Promoter on Fe-Co/SiO2 Catalyst for Fischer-Tropsch Synthesis", Bulletin of Chemical Reaction Engineering & Cataly-sis, Vol. 9, No.1, pp. 23-27.

Ahmad, S. N., Hakeem, S., Alvi, R. A., Farooq, K., Farooq, N., Yasmin, F., and Saeed, S, (2013) "Synthesis of Multi-Walled Carbon Nanotubes and Their Application in Resin Based Nanocomposites" Journal of Physics: Conference Series, vol. 439, pp. 1-8.

Awadallah, A. E., Abdel-Hamid, S. M., El-Desouki, D. S., Aboul-Enein, A. A., and Aboul-Gheit, A.K., (2012)"Synthesis of Carbon Nanotubes by CCVD of Natural Gas Using Hydrotreating Catalysts",Egyptian Journal of Petroleum,Vol. 21, pp.101-107.

Chen, Y., Zhang, Y. Q., Zhang, T. H., Gan, C. H., Zheng, C. Y., and Yu, G.,(2006) "Carbon Nanotube Reinforced Hydroxyapatite Composite Coatings Produced Through Laser Surface Alloying" Carbon, Vol. 44, pp.37-45.

Cong, Y., Li, X., Qin, Y., Dong, Z., Yuan, G., Cui, Z., and Lai, X .,(2011) "Carbon-doped TiO_2 Coating on MultiwalledCarbon Nanotubes with Higher Visible Light Photocatalytic Activity", Applied Catalysis B: Environmental, Vol. 107, pp. 128–134.

Couteau, E., Hernadi, K., Seo, J.W., Thiên-Nga, L., Mikó, C. S., Gaál, R., and Forró, L., (2003) "CVD Synthesis of High-purity Multiwalled Carbon Nanotubes Using CaCO3 Catalyst Support for Large-scale Production", Chemical Physics Letters, Vol. 378, No. 1-2, pp. 9-17.

Dalton, A. B., Stephan, C., Coleman, J. N., McCarthy, B., Ajayan, P. M., Lefrant, S., Bernier. P., Blau, W. J., and Byrne, H. J.,(2000) "Selective Interaction of aSemiconjugated Organic Polymer with Single-Wall Nanotubes", Journal ofPhysical Chemistry of Solids B, Vol. 104 No. 43, pp. 10012-10016.

Ebbensen, T., Ajayan, A., and Tanigaki, K., (1994) "Purification of Nanotubes", Nature,Vol. 367, pp. 519.

Eftehari, A., Jafarkhani, P., and Moztarzadeh, F.,(2005) "High-Yield Synthesis of Carbon Nanotubes Using aWater-Soluble Catalyst Support in Catalytic Chemical Vapour Deposition", Letters to the Editor/Carbon, Vol. 44, pp. 1298-1352.

Hengameh, H., (2013) "The Interaction Effects of Synthesis Reaction Temperature and Deposition Time on Carbon Nanotubes (CNTs) Yield", International Journal of Material Science Innovations (IJMSI), Vol. 1, pp. 54-61.

Hoenlein, W., Kreupl, F., Duesberg, G. S., Graham, A. P., Liebau, M., and SeidR.,(2003) "Carbon Nanotubes for Microelectronics: Status and Future Prospects", Material Science and Engineering, Vol. 23, pp. 663.

Kathyayini, H., Vijayakumar, K. R., Nagy, J. B., andNagaraju, N., (2008)"Synthesis of Carbon Nanotubes over Transition Metal Ions Supported on $Al(OH)_3$", Indian Journal of Chemistry, Vol. 47A, pp. 663-668.

Kong, J., Franklin, N. R., Zhou, C., Chapline, M. G., Peng, S., Cho, K., and Dai, H., (2000)"Nanotube Molecular Wires as Chemical Sensors", Science, Vol. 287, pp. 622-625.

Kruusenberg, I., Alexeyeva, N., Tammeveski, K., Kozlova, J., Matisen, L., Sammelselg, V., Solla-Gullón, J.,

and Feliu, J. M., (2011)"Effect of Purification of Carbon Nanotubes on their Electrocatalytic Properties for Oxygen Reduction in Acid Solution", Carbon,Vol. 49 No 12, pp. 4031-4039.

Kumar, M.,(2012) "Carbon Nanotube Synthesis and Growth Mechanism", Department of Materials Science & Engineering Meijo University, Nagoya 468-8502 Japan.http://www.intechopen.com, Book chapter 8.

Lee, C. J., Park, J., and Yu, J. A., (2002)"Catalyst Effect on Carbon Nanotubes Synthesized by Thermal Chemical Vapor Deposition", Chemistry of Physics Letters, Vol. 360, pp. 250-255.

Liu, H., Zhang, Y., Li, R., Sun, X, andAbou-Rachid, H., (2011)"Effects of Bimetallic Catalysts on Synthesis of Nitrogen-Doped Carbon Nanotubes as Nanoscale Energetic Materials",Particuology, Vol. 9, pp. 465–470.

Mao-Lin, W.,Yong, J., Fang, F., Shuang-Sheng, Z., Pei-Yun, W., and Dai-Yin, P., (2012)"Synthesis of Single- and Double-Walled Carbon Nanotubes using the Calcined MgO Supported Commercial Metal Oxide as Catalysts", Thin Solid Films, Vol. 52, pp. 35-39.

Mhlanga, S. D., Mondal, K. C., Carter, R., Witcomb, M. J., andCoville, N. J., (2009)"The Effect of Synthesis Parameters on the Catalytic Synthesis of Multiwalled Carbon Nanotubes using Fe-Co/CaCO$_3$ Catalysts", South Africa Journal of Chemistry, Vol. 62, pp. 67–76.

Nair, N., Kim, W. J., Braatz, R. D., and Strano, RD., (2008)"Dynamics of Suspended Single-Walled Carbon Nanotubes in a Centrifugal Field, Langmuir, Vol. 24, pp. 1790-1795.

Okpalugo, T. I. T., Papakonstantinou, P., Murphy, H., Mclaughlin, J., and Brown, N. M. D., (2005)"Oxidation of Functionalization of Carbon Nanotubes in Atmospheric Pressure Filamentary Dielectric Barrier Discharge", Carbon, Vol. 4,pp. 2951-2959.

Pelech, I., Narkiewicz, U.,Kaczmarek, A., andJędrzejewska, A., (2009)"Preparation and Characterization of Multi-Walled Carbon Nanotubes Grown on Transition Metal Catalysts", Polish Journal of Chemical Technology, vol. 16, No. 1, pp. 117–122.

Quian, W., Liu, T., Wang, Z., Yu, H., Li, Z., Wei, F., and Luo, G., (2003)"Effect of Adding Nickel to Iron–alumina Catalysts on the Morphology of As-grown Carbon Nanotubes",Carbon, Vol. 41, pp. 2487–2493.

Ratkovic, S., Vujicic, D., Kiss, E., Boskovic, G., and Geszti, O., (2011) "Different Degrees of Weak Metal-

Support Interaction in Fe–(Ni)/Al$_2$O$_3$ Catalyst Governing Activity and Selectivity in Carbon Nanotubes Production using Ethylene", Mater ChemPhys, Vol. 129 No.1, pp. 398-405.

Son, S. Y., Lee, Y., Won, S., and Lee, D. H., (2008) "High-Quality Multiwalled Carbon Nanotubes from Catalytic Decomposition of Carboneous Materials in Gas−Solid Fluidized Bed" Industrial and Engineering Chemistry Research, Vol. 47 No.7, pp. 2166–2175.

Storck, S., Bretinger, H., and Maier, W. F.,(1998) "Characterization of Micro- and Mesoporous Solids by Physisorption Methods and Pore-size Analysis", Applied Catalysis A, Vol. 174 No. 1-2, pp. 137-146.

Taleshi, F., (2012)"Evaluation of New Processes to Achieve a High Yield of Carbon Nanotubes by CVD Method", International Nano Letters, pp. 2-23.

Terrado, E., Redrado, M., Munoz, E., Maser, W. K., Benito, A. M., and Martinez, M. T., (2006) "Carbon Nanotube Growth on Cobalt-Sprayed Substrates by Thermal CVD", Material Science and Engineering, Vol. C26,No (5-7), pp.1185–1188.

Uddin, M. A., Tsuda, H., and Sasaoka, E. (2008). "Catalytic Decomposition of Biomass Tars with Iron oxides Catalyst", Fuel, Vol. 87, No (4), pp. 451-459.

Willems, I., Konya, Z., Colomer, J.F., (2000)"Control of Outer Diameter of Thin Carbon Nanotubes Synthesized by Catalytic Decomposition of Hydrocarbons", Chem Phys Lett, Vol. 317, pp. 71-76.

Yeoh, W. M., Lee, K. Y., Chai, S. P., Lee, K. T., and Mohamed, A., (2009)"Synthesis of High Purity Multi-Walled Carbon Nanotubes over Co-Mo/MgO Catalyst by the Catalytic Chemical Vapour Deposition of Methane",New carbon materials,Vol. 24, pp. 60041-60044.

Zhang, C.H., Yang, Y., Teng, B.T., Li, T.Z., Zheng, H.Y., Xiang H.W., and Li, Y.W.,(2006) Study of an iron-manganese fischer Tropsch Synthesis Catalyst Promoted with Copper", Journal of Catalysis,Vol. 237,pp. 405-415.

Nanotechnology Applications in National Defence: A review

I. A. Mohammed[1,2*], M. T. Bankole[1,3], A. S. Abdulkareem[1,2], A. S. Afolabi[4], I. Kariim[1] and O. K. Abubakre[5]

[1] Nanotechnology Research Group, Centre for Genetic Engineering and Biotechnology (CGEB), Federal University of Technology P.M.B 65, Minna, Nigeria

[2] Chemical Engineering Department, Federal University of Technology, Minna, Nigeria

[3] Chemistry Department, School of Pure Sciences, Federal University of Technology, Minna, Nigeria

[4] Department of Chemical, Metallurgical and Materials Engineering, Botswana International University of Science and Technology (BIUST), Plot 10071, Buseja ward, Palapye, Botswana

[5] Mechanical Engineering Department, Federal University of Technology, Minna, Nigeria

*ichemsoft@gmail.com, +2348060134955.

ABSTRACT

Nanotechnology is believed to be the next revolutionary force after the computer revolution age, having something in common to the earlier industrial revolution era of textiles, railroad and automobile. All these are enabling technologies. Fundamental advancements in science and technology between 1771 till date have shown that such revolutionary forces come about twice a century and take an average of thirty years to introduce before their widespread adoption. Nanotechnology, described as the control and manipulation of molecular-scale matter of about 1-100 nm in size, has been extensively researched for over twenty years now and many products of its application are currently in the market. Being an enabling technology and due to its multidisciplinary nature, science and technology of nanomaterials have found application in numerous areas. In recent times, the world is witnessing multidimensional security challenges which await solution strategies to secure lives, properties and home land. Typical example is the amazing security threats posed by global climate changes. Experts have also projected that the growing nanotechnology in itself has the potential to generate political, economic and social disorders through creation of novel classes of weapons that could threaten international security. In this article, advancements in nanotechnology applications of military importance have been reviewed. Recent discoveries made in nanoscale science and technologies useful in achieving the goals of national security are explored and possible progress in *nanodefence* through improved manufacturing, water-proof and armour materials, nanomedicine and nanosensors/nano-spies were identified.

Keywords: *Nanotechnology; National defence.*

1. INTRODUCTION

Nanotechnology can be defined as the application and commercialization of nanoscience. It is the study of systems in the sub 100 nm size regime (Hamlett, 2008). A Merill Lynch economist, Norman Poire (2002) have considered nanotechnology as the next phase of the second industrial revolution following the information and communication technology era that may have reached its rapid growth phase by 2025 (Dutta, 2007). Figure 1 shows Norman Poire's prediction of nanotechnology potentials as compared to other major technological evolutions (Hamlett, 2008). The emerging industrial revolutionary force is still a baby technology but has received much attention of researchers especially within the last twenty years. Its application in medicine, electronics, catalysis, sensors, energy, mechanics, and many other fields have also become popular (Bhattacharjee *et al.*, 2011).
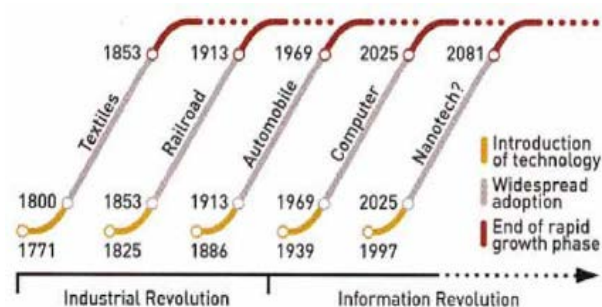
Fig.1: Trend of revolutionary forces from 1771 till date. **Source:** Dutta, 2007; Hamlett, 2008.

Presently, there is gradual acceptance of nanotechnology in addressing a number of the human needs. Majority of developed countries of the world like Europe, Japan and U.S.A. are spending heavily to fund nanotechnology

research for possible applications in various areas (Figure 2) (Almuhanna *et al.*, 2009). For instance, South Africa is expected to contribute about 3% of a projected $9 billion in carbon nanotubes global market by 2020 (Mohammed, 2015), but Nigeria's position is still uncertain. However, with the rising world population of about 6.8 billion people in 2010 to a projected 9.1 billion population by 2050 (FAO, 2009), experts have identified crime, war and terrorism as part of humanity's top ten challenges that may linger for the next fifty years (Wang, 2012). All other global problems identified are somewhat potential security threats.
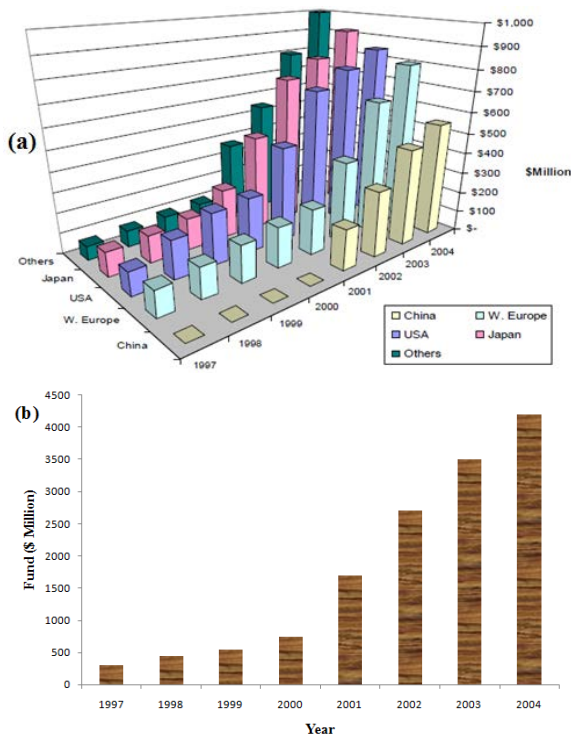
Fig. 2: Global government-funded nanotechnology (1997 – 2004) (a) by countries, and (b) total. **Source:** Almuhanna *et al.* (2009).

What are the root causes? It is certain that man cannot survive without food and water. Amidst malnutrition and hunger, the global environment is witnessing critical climate changes that affect agricultural activities, resulting in poverty and diseases (Shetty *et al.*, 2015). These and the lack of adequate education accessible to the growing world

populace have resulted in increased crime, war and terrorism (Shetty *et al.*, 2015; Abeygunawardena *et al.*, 2003). It also has the potential to increase conflicts among countries over the scarce resources because the world population is on the continuous increase. Though, it is believed that the solution to these problems is many-fold, Nanoscience and technology can be supportive in securing the future of current international security problems. While the advanced stage of molecular nanotechnology is perceived as the platform for the next technological revolution which will be possibly more beneficial than earlier ones, it could also be the most dangerous (Vandermolen, 2006). There are possibilities to cheaply mass-produce the nanomaterials in large quantity with high precision at atomic level, and hence the matured form of nanotechnology can be a threat to international security (Vandermolen, 2006). This potential hazard can be addressed by active participation of all countries at ensuring that international regulations are enforced to direct the growing nanotechnology research towards economic development rather than destructions. Notably, there are milestones that have been made which are promising discoveries and significant developments in national defence and the military, and that is presented in this review. It gives insight into various ways by which recent advancements in nanotechnology could be seen to have potential applications to achieving the goals of national security.

2. SECURITY-EXACERBATING ENTITIES

In 2003, Richard Smalley projected that humanity is bedevilled with at least ten problems which would continue till the next fifty years (Figure 3) (Wang, 2012).

Fig. 3: Humanity's top problems for the next half century.

Central to these problems is security which has strong link to all other items in the list. In the listed factors, two major security-exacerbating issues have posed significant long-term threats to national security. These are global climate change (environment) and world population growth. The duo has the tendency to worsen the risk of security threats.

2.1. Global climate change and security

Climate change is possibly the most significant long-term security threat (Morisetti, 2014). While factors such as terrorism are known to pose immediate threat, climate change has been associated with long-term security threats. The problems of demands on resources, climate change (such as drought) and increased population on the scarce mineral resources, food and water supplies are likely to lead to tension, which could result in conflict (Morisetti, 2014). In view of the growing awareness to reverse the catastrophic consequences of greenhouse gas emissions for the planet, the role of the growing nanotechnology in addressing climate changes need to be evaluated. Again, the solution to combating climate change and reducing emissions of the greenhouse gases is multidimensional. The achievement of this goal would involve the development of energy forms that are less-carbon dependent, improvement in efficiencies of the systems and reduction in the demand for fossils (Vandermolen, 2006). Within the context of nanotechnology, reducing demand may be out of its sphere of influence but as an enabling technology, if integrated with many other technologies, improved efficiencies and novel sources of energy could be made available to the market. Nanoscientists and technologists have identified specific roles that nanotechnology could play to make impact. Primarily, in the energy sector which has a link to the lingering climate change, nanotechnology applications can produce improved fuel additives that will help increase the efficiency of fuel cells and hydrogen economy; diesel engines. Other areas include manufacture of more efficient solar cells from improved photovoltaic technology;

improved energy storage from efficient batteries and super capacitors and improved insulation for houses and offices (Changseok *et al.*, 2013). Currently, nanotechnology application in fuel additives such as the use of nanoparticles to increase the fuel efficiencies of vehicles has been actualized (Nature, 2007). It was reported in the UK that about 2 to 3 million tonnes of CO_2 per annum could be saved by this technology. Nanocrystals of molybdenum disulphide (MoS_2) have also been used as catalysts in the oil industry to remove potentially harmful sulphur compounds from crude oil (Lauritsen & Besenbacher, 2006).

2.2. World population growth and security

Developed countries of the world have put in place strategies to control its population as shown in Figure 4, but it has been observed that the escalating population in developing countries is posing security challenges in a number of ways (Sherbinin, 2011).
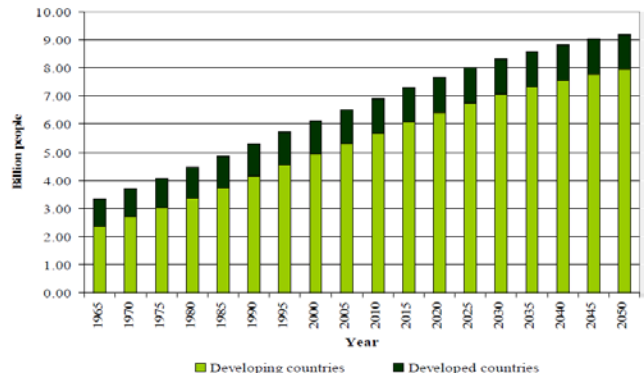
Fig.4: World Population, 1965 – 2050**. Source:** Peter (2013); FAO (2009).

Though, the rise in world population could be described as a natural phenomenon, there are concerns by the developed nations about the impact of population growth on their national security (Sherbinin, 2011). Around 1950s, the U.S response to world population growth was nonexistent despite early urgings by some prominent activists and demographers to combine fertility reduction efforts with the broader public health measures already taking place in the developing world. Later, following recommendations by

Draper Committee (set up by President Eisenhower in 1958) that the U.S. government should engage itself in population programs in any country that might request its assistance, discussion of family planning had become somewhat more politically acceptable, as a growing number of public health and religious groups endorsed birth control by the early 1960s. In the continued effort towards population control by the US, the Clinton Administration created the office of Undersecretary of State for Global Affairs to oversee population-related issues, among others. The United States did much to promote new thinking on international population issues that recognizes the crucial role of women' empowerment and education in helping to reduce fertility. According to Sherbinin (2011), population growth can affect national security of the developed world in many ways. The growing population can induce resource scarcity that could result in regional conflicts and population displacements. It is also believed that a rapid growth in the younger age groups together with growth discrepancy among various ethnic or religious groups in a country can cause political and economic instability (Sherbinin, 2011). On the part of the developing countries, feeding the overwhelming human population is a major challenge that could cause hunger, conflicts and general threats to national security (FAO, 2009). Again, the whole fear of population growth can be reduced through advancements in nanotechnology applications in creating efficient and advance technologies towards feeding the world, securing the global environment and participating in stabilizing climate conditions. The overall result would be ability to abate security threats that are related to shortage in food supply, domestic earnings and national conflicts over resources.

3. NANOTECHNOLOGY ADVANCEMENTS TOWARDS NATIONAL DEFENCE

Materials at nanoscale, single atoms or molecules exhibit important properties different from the properties of bulk materials (Musso, 2011; Das *et al.*, 2015). Nanoscience and technology make use of these nanomaterials that have unique physical, chemical, and biological properties towards innovative developments. As an enabling technology that cut across all fields, the applications offered by nanomaterials and *nanosystems* is actualized by combining nanotechnology with other appropriate technologies. In this context, advancements in nanotechnology have potentials to help solve threats to homeland security through developments of improved manufacturing, fabrics and materials, robotics, security, weaponry, vehicles, and nanomedicine for improving the health of military personnel.

3.1. Smart Fabrics and materials

Nanoscientists and technologists have been able to produce nano Teflon by Chemical Vapour Deposition (CVD) process for making water-proof and bullet-proof army tactical vests. This development is credited to Prof. Karen Gleason of the Institute for Soldier Nanotechnologies. The CVD was used to manufacture waterproof surfaces that are ultra hydrophobic shown in Figure 5 (Downing, 2003).

Fig.5: An image of the water-proof and bullet-proof Army outer tactical vest. **Source:** Downing, (2003).

Using CVD, nanolayers of Teflon was deposited on Kevlar panels which is the material used to make bullet-proof vests (Downing, 2003). Teflon is the same material that is used on kitchen frying pans.

3.2. Nano Air Vehicle (Sensor/Nano spy) - Nano Hummingbird

One of the popular successful applications of nanotechnology in different fields is in robotics (Cerofolini *et al.*, 2010; Yarin, 2010). An example is the ongoing reservoir robots (resbots) project used in crude oil wells to collect reservoir data. In a related development to

intelligence and surveillance, a nano spy which is a robot that mimics a flying hummingbird has been successfully created. Hummingbird is the smallest natural bird known that swings its wings more than fifty times per second. Figure 6 shows the nano Hummingbird while hovering (AeroVironment, 2013).

Fig. 6: Nano air vehicle (A nano spy)

The nano air vehicle was the research breakthrough of AeroVironment, based out of Monrovia, Central America. The researchers developed their Nano Hummingbird under a DARPA research contract (AeroVironment, 2013). The nano spy can fly indoors and outdoors. By this development, the next generation of fighter jets is nano-sized jets, the size of a seed that can go anywhere. The scientists are still working on this revolutionary achievement that will facilitate the collection of military intelligence. The development will enhance the operational effectiveness of soldiers and first responders.

3.3. Chemical and biological sensors

Nuclear substances such as phosgene, sarin, mustard gas, chlorine; and biological warfare such as anthrax, Ebola virus, *Brucella*, and anthrax spores have been used on battlefields and in some acts of terrorism. Some others that are both biological and chemical; toxins like botulinum neurotoxin and ricin which are produced by living organisms have also been threats to global security. It becomes important to device ways of detecting and sensing the presence of these substances. According to a study commissioned by Defense Advanced Research Projects Agency (DARPA), key sensor metrics are (Carrano, 2005):

- ❖ Sensitivity
- ❖ Probability of correct detection
- ❖ False positive rate
- ❖ Response time

Recently, it has been discovered that the development of improved detection techniques is possible through nanotechnology. Electronic nose and bio-inspired nanosensors are some of the existing nanotechnology-improved sensors. According to Shelley (2008), the application of nanotechnology can help in advancing detection of biological and chemical substances in a number of ways. Because of their small size, light weight and large reactive surface area, engineered nanostructures can improve, by orders of magnitude, the sensitivity, selectivity and response time of sensor technology. Nanosensors have certain advantages over conventional detection techniques. Some nanosensors can detect a target chemical from multiple chemical species (Shelley, 2008). Projects towards the development of more nanosensors are ongoing. For instance, iPhone chemical sensor is being developed by NASA which can help notify security agents in case of any suspected threat. With the involvement of citizens in the use of such sensors, first responders would find it easier to distinguish between false positives and true threats (Jones *et al.*, 2013). A nanosensor called electronic nose has also been created that can be used to differentiate 19 different toxic industrial chemicals (Lim *et al.*, 2009).

3.4. Electrochromic camouflage

'Going invisible' by manipulating light so that soldiers seem to disappear or invisible from their enemy is another way by which nanoscientists have attempted to advance security (Fountain, 2010). Military uniforms would have to be made from fabric which changes colours instantly to blend in with the surroundings. Objects can be made invisible through the use of optical negative-index metamaterials (NIM). The refraction of light through a conventional material is different from its refraction

through a negative-index metamaterial. Optical NIMs have also being applied in antennae, microscopes and circuits (Cai, 2007; Shalaev, 2007; and Xiao, 2010).

3.5. Nano-Armor

Lessons from nature as observed in sea snails and abalone have helped nanotechnologists in developing armour that are exceptionally strong to satisfactorily protect the contemporary combatant (Halber, 2008). With the use of a scanning electron microscope (SEM), Prof. Ortiz and her students investigated the nanostructure of the scales of the dinosaur eel, a species that is believed to have been able to survive enemy attacks for more than 96 million years (Bruet, 2008). Their studies revealed that the four layers of the scales dissipate the energy of a strike, protect the soft tissue beneath the scales, and also prevent the spread of fractures within the scale. The research findings are now being applied towards human body armour (Bruet, 2008)

3.6. Nano-medicine in military

One of the main branches of nanotechnology research is nanomedicine, which is continually breaking grounds in advancing the medical field worldwide. Sometimes, wounded soldiers could lose their lives on battlefield because of delayed medical attention. Professor Joseph Wang at the University of California at San Diego has developed method for screen printing sensors on the waistband of underwear (Yang *et al.*, 2010). On the waistband, the sensor is in close contact to the skin where it can monitor biomarkers in the sweat of the person wearing the underwear (Yang *et al.*, 2010). The anti-toxin uses nanotechnology on packaging films to detect micro-organisms like pathogens that may cause illness or disease. An adhesive chest patch worn by the soldiers is fitted with sensors and a tiny radio. They would be provided vital signs and location to medics via radio, thanks to the sensors. Also, artificial muscles are being developed to enable soldiers to leap tall walls or buildings.

3.7. All-electric warship

One of the challenges with the conventional war ships is that it requires the involvement of thousands troops to run the battleships. An all-electric warship that could be run by a crew of about 100 people is being manufactured by the US Navy researchers. But, the greatest hurdle encountered in this course lies in distributing power to the entire ship. The team of electronic experts has resorted to nanotechnology as a way out of the challenge (Fallon, 2011).
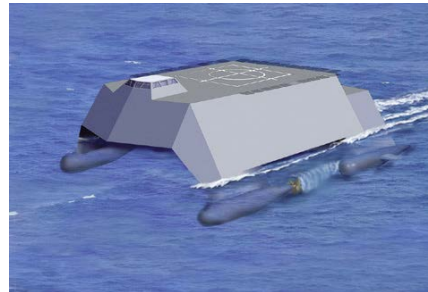
Fig.7: Artistic rendering of the All-electric warship

The overall advantages of the electric warship are in survivability, cost savings and improved effectiveness. In addition, spaces required for energy production on warships are significantly reduced, thereby freeing onboard space that can be used for other functions.

3.8. Advanced manufacturing materials

Another consequence of nanomaterials is the development of advanced manufacturing materials such as improved aircraft bodies and armour parts. Carbon nanotubes (CNTs) are examples of nanomaterials which exhibit very light weight but possess excellent mechanical, thermal and electrical properties. The CNTs are lighter but stronger than steel (Musso, 2011). Nanotubes also exhibit exceptional electrical conductivity and thermal conductivity better than the conventional copper (Musso, 2011). Hence, the nanomaterials have the potential towards development of better manufacturing materials. Many other security-related nanotechnology developments have been found. For instance, in the area of combating crime the research on nano-'fingerprints' that can aid identity

verification is ongoing. The nano-'fingerprints' can be used to verify ID cards, passports and related documents with just a scan. This nanotechnology concept can also be applied in the packaging of products and its measured accuracy has been reported to be greater than DNA tests with a reliability of about a million trillion. In addition, nanotechnologists especially researchers in the US military have recorded several breakthroughs in the direction of nondefense.

4. CONCLUSION

Nanotechnology is perceived as the next phase of industrial revolution and possibly more beneficial than earlier revolutions. Humanity is faced with a number of lingering challenges among which security is most fundamental. Thus, national security issues which are multidimensional have become extremely important aspect of global society. It involves the greater task of protecting citizens and state from organized crime, responding to natural and man-made disasters and preventing terrorist acts. Different applications areas of nanotechnology in national defence have been identified with reference to the recent advancements in nanoscience and technology. In order to promote vibrant researches in nanotechnology towards security objectives, security R&D activities are essential. This way, potential benefits exist in protecting against terrorism and crime; improving security of infrastructures and utilities; attaining efficient intelligence surveillance and border security; restoring security and safety in case of crisis.

REFERENCE

Abeygunawardena, P., Vyas, Y., Knill, P., Foy, T., Harrold, M., Steele, P.... Sperling, F. (2003), Poverty and climate change: Reducing the vulnerability of the poor through adaptation.

AeroVironment (2011), "aerovironment develops world's first fully operational life-size hummingbird". February 17, 2011 press release

Almuhanna, A. A., Aldakkan, K. A., Alsalman, H. A., Alaskar, Y. A., & Alatawi, A. A. (2009), Strategic priorities for nanotechnology programme, King Abdulaziz City for Science and Technology, Saudi Arabia.

Bhattacharjee, C. R., Nath, A., Purkayastha, D. D., Mukherjee, B., Sharon, M., & Sharon M. (2011), Synthesis and Characterization of Carbon Nanotubes Using a Natural Precursor: Turpentine Oil. *Science Journal Ubon Ratchathani University, 2 (1), 36-42.*

Bruet, B.J.F. (2008), "Materials Design Principles of Ancient Fish Armour". *Nature Materials,* 7(9), 748-756.

Cai, W. S. (2007), "Optical Cloaking with Metamaterials". *Nature Photonics* 1(4), 224-27

Carrano, J. (2005), Chemical and Biological Sensor Standards Study.

Cerofolini, G., Amato, P., Asserini, M., & Mauri, G. (2010), "A surveillance system for early-stage diagnosis of endogenous diseases by swarms of nanobots". *Advanced Science Letters,* 3(4), pp 345-352. Doi 10.1166/asl.2010.1138

Changseok, H., Andersen, J., Pillai, S. C., Fagan, R., Falaras, P., Byrne, J. A., Dunlop, P. S. M., Choi, H. & Jiang, W. (2013), Green Nanotechnology: Development of Nanomaterials for Environmental and Energy Applications, *ACS Symposium Series,* 2013. Book Chapter

Das, R., Abd Hamid, S. B., Ali, M. E., Ramakrishna, S. & Yongzhi, W. (2015), "Carbon Nanotubes Characterization by X-ray Powder Diffraction - A Review". *Current Nanoscience, 2015, Vol. 11, No. 1.*

Downing, E., (2003), "Team creates new process for waterproofing", MIT News

Dutta, J., (2007) "Nanotechnology: Overview and applications", power point presentation. Asian Institute of Technology, Thailand.

Fallon, S. (2011), "Navy Developing All-electric Warship", *Gizmodo.*

FAO (2009), "How to Feed the World in 2050", FAO Headquarters, Rome, 12 - 13 October, 2009.

Fountain, H. (2010), "Strides in Materials, but No Invisibility Cloak," *New York Times*, Nov. 8, 2010.

Halber, D. (2008), "Natural Armor: Nature's impenetrable defense systems," MIT Spectrum. http://spectrum.mit.edu/articles/normal/natural-armor/

Hamlett, C.A.E., (2008) "Utilization of nanostructured surfaces for sensing applications and the use of nanoentities for the fabrication of new materials", PhD Thesis, The University of Birmingham.

Jones, A., Nye, J., & Greenberg, A. (2013), "Nanotechnology in the military". Power point presentation

Kamat, P. V., (2005) "Energy challenge and Nanotechnology", University of Notre Dame, Notre Dame, Indiana.

Lauritsen, J. V. and Besenbacher, F., (2006) *Adv. Catalysis* **50,** 97–147 (2006).

Lim, S.H., Feng, L., Kemling, J.W., Musto, C.J., Suslick, K.S. (2009), "An Optoelectronic Nose for Detection of Toxic Gases". *Nature Chemistry*, 1, 562-567.

Mohammed, I. A. (2015), Response surface approach to formulation of bimetallic (Fe/Co) catalyst on $CaCO_3$ support for Carbon nanotube growth. MEng Thesis

Morisetti, (2014) "Climate change and security", Energy and climate intelligence unit (ECIU) Briefing, November, 2014. Available Online at www.eciu.net. Retrieved April 20, 2015.

Musso, S. (2011), "From fullerenes to Graphene passing through Carbon nanotubes: Synthesis, properties and applications of quasi-new allotropes of carbon". Presentation, Massachusetts Institute of Technology

Nature nanotechnology (editorial), 2(6), 325 (2007) "Combating climate change", *nature nanotechnology, vol. 2, (6), pp 325.* Available Online at www.nature.com/naturenanotechnology. Retrieved May 17, 2015

Norman Poire (2002), *Red Herring*, May 2002, Merrill Lynch.

Peter B. R. H. (2013), "Options for African agriculture in an era of high food and energy prices". *Agricultural Economics,* 44, pp 19-27.

Shalaev, V. M. (2007), "Optical Negative-Index Metamaterials". *Nature Photonics* 1.1 (2007): 41-48.

Shelley, S. (2008), "Nanosensors: Evolution, not Revolution… Yet", *Chemical Engineering Progress*, 104, pp. 8-12.

Sherbinin, A. D., (2011), "World Population Growth and U.S. National Security", *Features, 24 – 39.*

Shetty, S., Abdul-Raheem, T., Pimple, M., and Ponti, M. (2015), Climate change and the Millennium Development Goals. The United Nation Millennium Campaign, Accessed online at www.endpoverty2015.org

Vandermolen, T. D. (2006), "Molecular nanotechnology and national security". *Air & Space Power Journal*, Fall 2006 Issue

Wang, G.G.X. (2012), Development of clean energy and environmental technologies to address humanity's top problems. *Front. Chem. Sci. Eng.*, 6(1), pp 1–2. DOI 10.1007/s11705-011-1145-5

Xiao, S. M., *et al.* (2010), "Loss-Free and Active Optical Negative-Index Metamaterials". *Nature*, 466.7307 (2010): 735-U6.

Yang, Y. L., Chuang, M. C., Lou, S. L. and Wang, J. (2010), "Thick-film textile-based amperometric sensors and biosensors". *Analyst*, 135 (6), 1230-1234.

Yarin, A. L. (2010), "Nanofibers, nanofluidics, nanoparticles and nanobots for drug and protein delivery systems". *Scientia Pharmaceuatica,* Central European Symposium on Pharmaceutical Technology, 78(3), pp 542. Doi 10.3797/scipharm.cespt.8.L02

Synthesis and characterization of highly crystalline MWCNTs using Fe-Co/CaCO$_3$ catalyst by CVD

I. A. Mohammed[1, 2*], M. T. Bankole [1, 3], A. S. Abdulkareem [1, 2], S. S. Ochigbo[3], A. S. Afolabi [4] and O. K. Abubakre [5]

[1] Nanotechnology Group, Centre for Genetic Engineering and Biotechnology (CGEB), Federal University of Technology P.M.B 65, Minna, Nigeria

[2] Chemical Engineering Department, Federal University of Technology, Minna, Nigeria

[3] Chemistry Department, School of Pure Sciences, Federal University of Technology, Minna, Nigeria

[4] Department of Chemical, Metallurgical and Materials Engineering, Botswana International University of Science and Technology (BIUST), Plot 10071, Buseja ward, Palapye, Botswana

[5] Mechanical Engineering Department, Federal University of Technology, Minna, Nigeria

*ichemsoft@gmail.com, +2348060134955.

ABSTRACT

There is continuous research on synthesis of carbon nanotubes to meet the different specification requirements for many applications. In this study, controlled thermal decomposition of acetylene using supported bimetallic catalyst was explored via Chemical Vapour Deposition (CVD). Acetylene undergoes polymerization or dissolution around 780 ^{o}C during thermal decomposition. Therefore, selective ability of the Fe-Co/CaCO$_3$ towards the growth of multiwalled carbon nanotubes (MWCNTs) at lower acetylene decomposition temperature was explored. Fe-Co of 1 g (1:1 mass % metal ratio) on CaCO$_3$ support, developed by wet impregnation, was used for the growth of 2 g MWCNTs at 700 ^{o}C in 45 min under argon environment. Catalyst efficiency based on weight of H$_2$SO$_4$-purified MWCNT sample was found to be 110 %. The as-synthesized and purified MWCNTs were characterized by transmission electron microscopy (TEM), selected area electron diffraction (SAED/SAD), scanning electron microscopy (SEM) and Energy-dispersive X-ray spectroscopy (EDX), showing the high density of nanotubes distribution and effectiveness of the purification process respectively. TEM image showed concentric nanotube tips and SEM micrographs showed outer diameter reaching up to 40 nm which confirmed the materials as MWCNTs. The crystallographic study through TEM-SAED of the MWCNT further confirmed the known graphitic hexagonal crystal lattice structure of nanotubes. The SAED patterns of the purified MWCNT are evidence of highly polynanocrystalline material.

Keywords: *Fe-Co/CaCO$_3$, CVD, MWCNTs, TEM, SEM.*

1. INTRODUCTION

Carbon nanotubes (CNTs) have been extensively studied over the last two decades because of their promising applications in catalysis, sensors, drugs delivery, high performance materials, purification systems and many other versatile fields (Prasek *et al.*, 2011). The diverse applications are dependent on CNTs structures which are determined by number of walls, diameter, length and chiral angle (Mohamed *et al.*, 2006). For instance, smaller diameter, higher surface area and crystallinity are prerequisite for mechanical reinforcement applications in polymer composites (Kurita *et al.*, 2011; Mohamed *et al.*, 2006). Crystalline iron oxide nanotube layers have also proved to demonstrate better electrochemical properties than the amorphous types (Pervez *et al.*, 2014). Multiwalled carbon nanotubes (MWCNTs) are allotropes of carbon structurally made up of concentric graphene sheets that determine the number of walls. They are forms of carbon atoms organized in a rolled up hexagonal tube network (Das *et al.*, 2015). Among the different synthesis methods, the chemical vapour deposition (CVD) method is easily scalable for mass production. It is also the best method in obtaining high-yield, high-purity MWCNTs and it is preferred in terms of structure control and CNTs architecture (Kumar and Ando, 2010). MWCNT growth by CVD method utilizes carbon source (or precursor), carrier gas, hydrogen and/or catalyst (Das *et al.*, 2015). Acetylene gas has been successfully used by many researchers for nanotubes growth in CVD. While inert gases such as argon are used as carrier gas, the use of hydrogen gas in the process is believed to be responsible for catalyst reduction during the CNT growth (Chiwaye, 2012). Hence, hydrogen

is not necessary if acetylene is used as carbon source because the dissolution of C_2H_2 releases hydrogen which does the reduction. This explains the success behind the MWCNT growth in solely argon environment without hydrogen gas. Supported bimetallic catalysts are more efficient than monometallic types due to formation of ternary (multiple metals) oxides in final bimetallic catalyst systems (Haffer, 2013). Successful synthesis of good crystalline MWCNTs was reported by Mahajan *et al.* (2010), Mohamed *et al.* (2006) and Han *et al.* (2004) via the CVD method in different ways. However, Kumar and Ando (2010) claimed that CVD-grown nanotubes contained lots of amorphous materials and have inferior crystallinity. The present study is a report of good crystalline MWCNT growth in horizontal CVD reactor using acetylene as carbon source, argon as carrier gas, and bimetallic Fe-Co/CaCO$_3$ catalyst. SAED was used to identify the phases present in the MWCNTs.

2. METHODOLOGY

2.1. Materials

All chemicals used were of analytical grade. Fe $(NO_3)_3.9H_2O$, Co $(NO_3)_2.6H_2O$ and CaCO$_3$ were purchased from chemical stores. Distilled water was obtained from Chemistry department of Federal University of Technology, Minna. The gases, acetylene, argon and nitrogen have 99.99 % purity while sulphuric acid was 98.0 % pure.

2.2. Catalyst preparation

The bimetallic catalyst Fe-Co on CaCO$_3$ support was prepared as described by Afolabi *et al.* (2011) using wet impregnation method, which was targeted mainly at dispersing the Fe and Co metals on the CaCO$_3$ support so as to be available to reactant (i.e. acetylene). 3.62 g of Fe $(NO_3)_3.9H_2O$ and 2.47 g of Co $(NO_3)_2.6H_2O$ were weighed and dissolved in 50 cm^3 of distilled water. This was followed by the introduction of 10 g of CaCO$_3$ under continuous stirring for 60 min. The ratios of Fe

$(NO_3)_3.9H_2O$, Co $(NO_3)_2.6H_2O$, and CaCO$_3$ corresponds to final composition of Fe: Co/CaCO$_3$ = 2.5: 2.5: 95 wt %. After impregnation, the sample was dried for 12 hrs at 120 °C to remove excess liquid and to fix the catalyst species so that high-temperature calcinations will not cause significant movement or agglomeration of the well dispersed catalytic species. After this, the catalyst was calcined for 16 hrs at 400 ^{o}C to remove the nitrate, followed by grinding in a mortar and sieving using a 150 μm sieve.

2.3. MWCNTs growth

The Fe-Co/CaCO$_3$ catalyst developed was applied in producing MWCNTs in a CVD reactor. Precisely 1 g of catalyst was spread in a ceramic boat, which was inserted in the quartz tube of the CVD furnace. Heating was done at 10 ^{o}C/ min. The heating commenced in argon flow rate of 30 ml/min until reaction temperature of 700 ^{o}C was attained when acetylene was introduced at 150 ml/min and argon flow was raised to 230 ml/min. The reaction time was 45 min, after which acetylene flow was stopped and the sample was allowed to cool in argon flow of 30 ml/min. In order to remove the impurities, amorphous forms of carbon and the residual catalyst support materials that were introduced into the sample during MWCNT growth; the as-synthesized CNT was purified by acid treatment. 1 g of as-synthesized CNT sample was washed in 100 ml of 30 % H_2SO_4 by continuous stirring for 1 hr. The mixture was then washed with distilled water until a pH of 7 was achieved. Water was filtered out to obtain the wet CNT residue which was dried at 120 ^{o}C for 12 hrs.

2.4. Characterization

The catalyst was characterized for its crystallinity (XRD), thermal behaviour (TGA), morphology (SEM/EDX) and surface area (BET). Purified and as-synthesized nanotubes were characterized by transmission electron microscopy (TEM/SAED), scanning electron microscopy (SEM) and Energy-dispersive X-ray spectroscopy (EDX). The TEM

and SEM were used to study the morphology, diameter and distribution of CNTs while the EDX was used to investigate the qualitative elemental composition of as-synthesized and purified nanotubes. Both techniques were used to investigate the effectiveness of the purification process. SAED pattern was used to identify phases present in the CNTs.

3. RESULTS AND DISCUSSIONS

The results of catalyst preparation are fully reported elsewhere (Mohammed, 2015). Properties of the catalyst and its suitability for CNT growth were investigated using different characterization techniques. Thus, XRD, TGA, SEM/EDX and BET were used to study the catalyst's texture (crystallinity), thermal behaviour, morphology and surface area respectively. The XRD pattern showed that the solid catalyst is polycrystalline with different crystal sizes resulting in a number of peaks as presented in Figure 1.
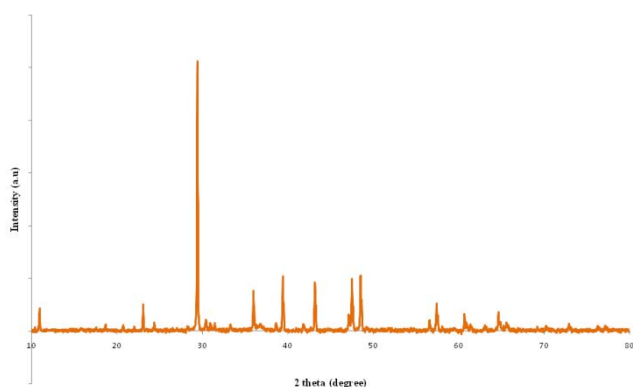
Fig.1: XRD of Fe-Co/$CaCO_3$ catalyst

The thermal decomposition of the catalyst conducted in nitrogen environment is presented as Percentage weight loss against temperature in Figure 2.
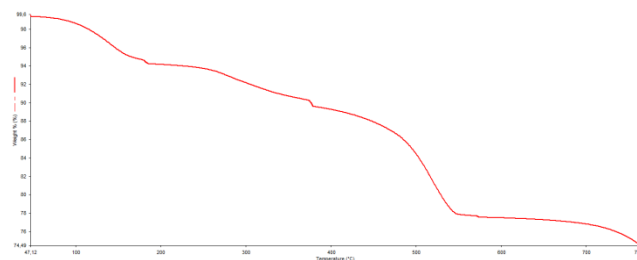
Fig.2: TGA curve of the catalyst

The catalyst thermal decomposition showed four weight loss regimes. The first slope is attributed to loss of unbound water, the next two weight losses are due to conversion of Fe and Co nitrates to form a combined oxide, most likely, $CoFe_2O_4$. The final weight loss represents the decomposition of $CaCO_3$ to evolve CO_2 and form CaO. The SEM micrograph of the catalyst and its corresponding EDX showed the morphology and qualitative elemental compositions of the sample (Figure 3).
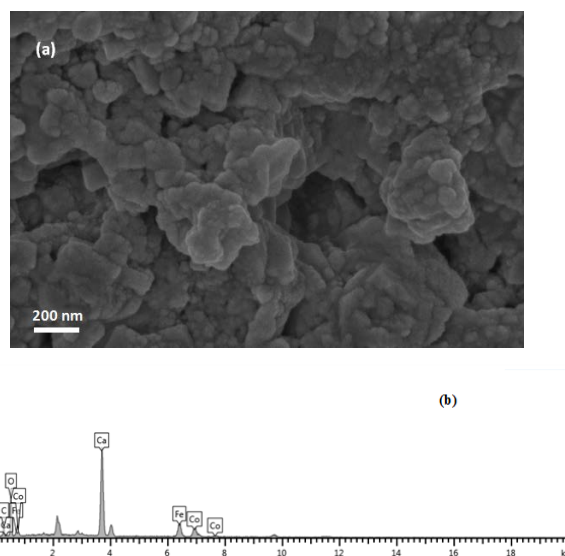
Fig.3: Fe-Co/$CaCO_3$ catalyst' (a) SEM image and (b) EDX

The SEM/EDX is evidence of Fe and Co nanoparticles dispersed in $CaCO_3$ matrix, possibly present as a ternary oxide, $CoFe_2O_4$. The BET method was used to analyse the specific surface area of the catalyst sample and a value of 3.9 m^2/g was obtained. It was observed that the catalyst

has surface area similar to that of the CaCO$_3$ powder used as support.

Figures 4 (a) and (b) show the SEM images of as-synthesized and purified MWCNTs respectively. The images are evidence of filamentous nature of CNTs. As-synthesized CNTs (Figure 4a) contained significant amount of impurities, residual catalyst and amorphous forms of carbon. The nanotubes have varying outer diameter reaching up to 40 nm, due to different sizes of catalyst metal nanoparticles or insufficient growth time to complete a uniform growth of walls throughout the sample.
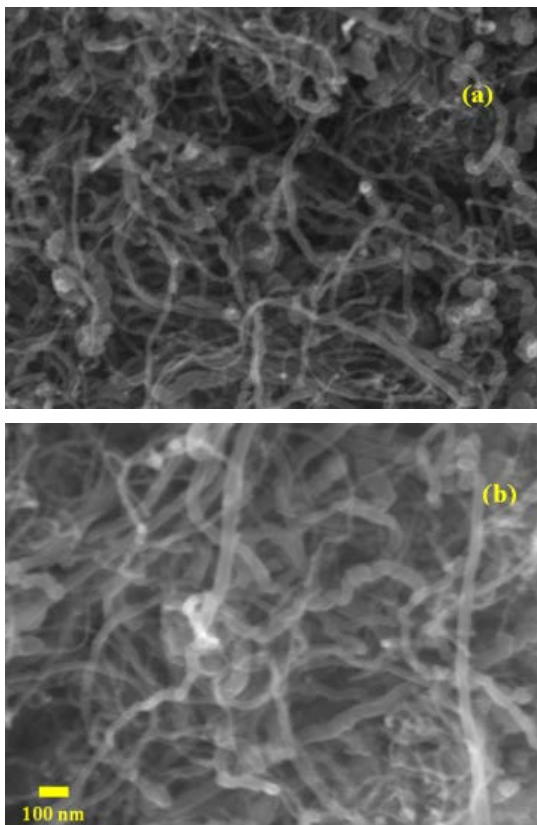
Fig.4: SEM image of (a) as-synthesized and (b) purified MWCNTs

Non-uniform or wide distribution of diameter throughout CNTs bundles is one of the property deviations of practical nanotubes compared to the theoretical 'ideal' ones, making optimization studies to be an important tool for attaining

optimum CNTs growth conditions. Another observation from the SEM micrographs is the globular nodules seen at different points along the nanotubes. These are encapsulated metal catalyst nanoparticles in the inside diameter of the CNTs. Carbon nanotubes grow by either tip or root mechanism thereby encapsulating catalyst metal nanoparticles within the tubes (Prasek *et al.*, 2011). This suggests how the nano sizes of the metal particles could affect the diameter of the final nanotubes. Mohamed *et al.* (2006) observed that Fe catalyst produced MWCNTs with larger diameter (31-38 nm) than Co-grown nanotubes (23-26 nm). Hence, the different sizes of metals in the catalyst alloy are responsible for wide diameter distributions of nanotubes. However, TEM images of the MWCNT sample shown in Figure 5(a) and (b) presents nanotubes with smaller outer diameter of about 20 nm. Clustered image of the MWCNT is shown in Figure 5(a) while Figure 5(b) shows an individual nanotube.
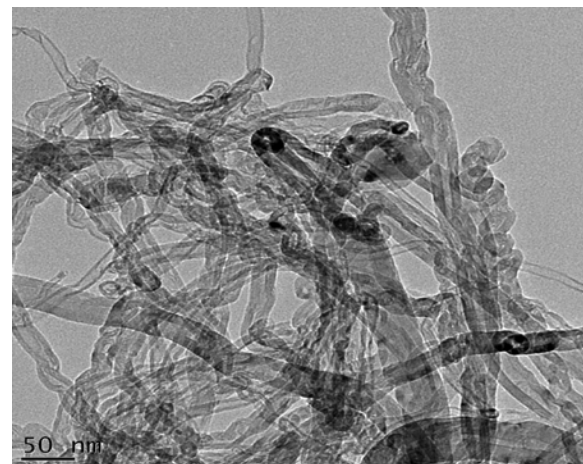
Fig.5 (a): TEM image of the MWCNT cluster
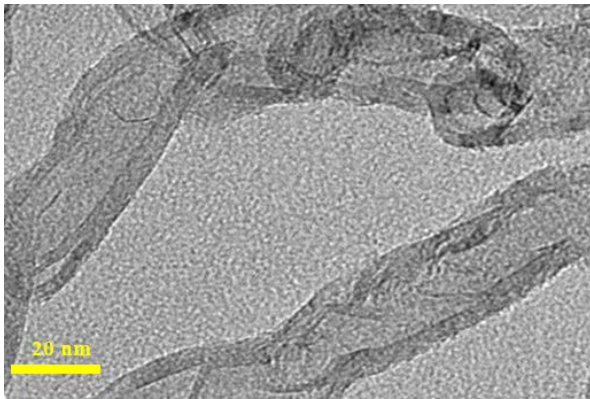
Fig.5 (b): TEM image of the MWCNT (20 nm diameter)

In order to confirm the effectiveness of the purification step, an elemental microanalysis was carried out on the MWCNT by EDX as shown in Figure 6.
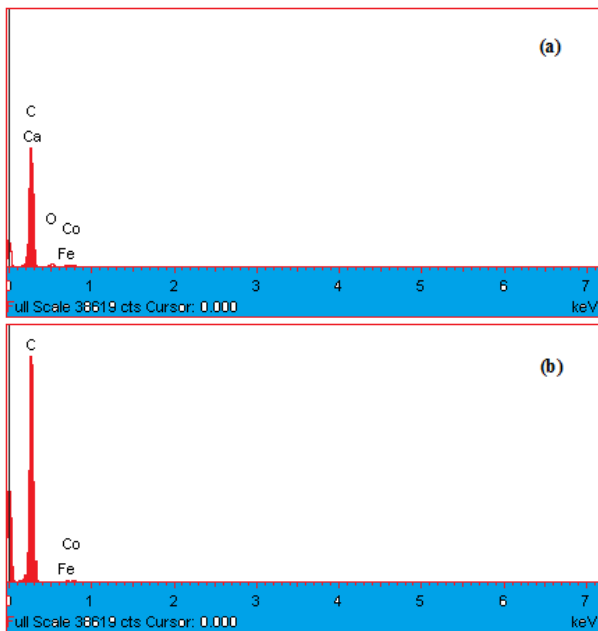
Fig.6: EDX spectrum of (a) as-synthesized and (b) purified MWCNT

As shown in Figures 6 (a) and (b), the acid purification removed residual catalyst oxides except the metal nanoparticles. The appearance of Fe and Co at lower line energy (< 1 keV) instead of their usual line energy of 6.4 and 6.9 keV respectively (Haungs, 1986) indicates that these metals were in combined state in the as-synthesized sample, most likely as oxides. The purification process by H_2SO_4 acid treatment aided the removal of residual

catalyst comprising $CaCO_3$ and CaO from as-grown CNTs according to Reaction Schemes (1), (2), (3) and (4):

$$H_2SO_4(aq) + CaCO_3(s) \rightarrow CO_2(g) + \underbrace{CaSO_4(s)}_{Precipitates\ out} +$$

$$H_2O(l) \tag{1}$$

$$H_2SO_4(aq) + CaCO_3(s) \rightarrow CO_2(g) + CaSO_4(aq) +$$

$$H_2O(l) \tag{2}$$

$$H_2SO_4(aq) + CaCO_3(s) \rightarrow \underbrace{CaSO_4(s)}_{Precipitates} + H_2CO_3(aq) \tag{3}$$

$$H_2SO_4(aq) + CaO(s) \rightarrow \underbrace{CaSO_4(s)}_{Precipitates} + H_2O(aq) \tag{4}$$
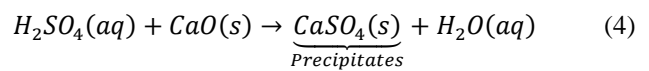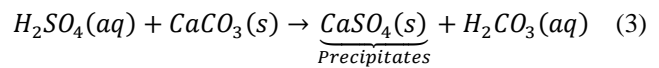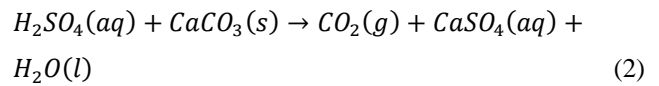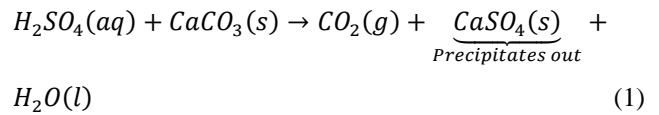
The insoluble $CaSO_4(s)$ precipitated out of solution and was easily decanted away from top layer along with some light carbonaceous substances.

The catalyst efficiency was calculated using (Magrez *et al.*, 2010);

$$Catalyst\ efficiency =$$

$$\frac{Mass\ of\ purified\ MWCNTs\ produced}{Mass\ of\ supported\ catalyst\ introduced} \tag{5}$$

In order to investigate both the crystalline phase and multiple walls of the MWCNT produced, selected area electron diffraction (SAED) pattern was collected from a high resolution transmission electron microscopy (HRTEM) of the sample. The diffraction pattern in SAED comes from the area of the sample corresponding to the image. Figure 7 shows the TEM image that reveals the multiple walls of the MWCNT from the tip. The captured tube from the sample bundle has outer diameter of about 20 nm.
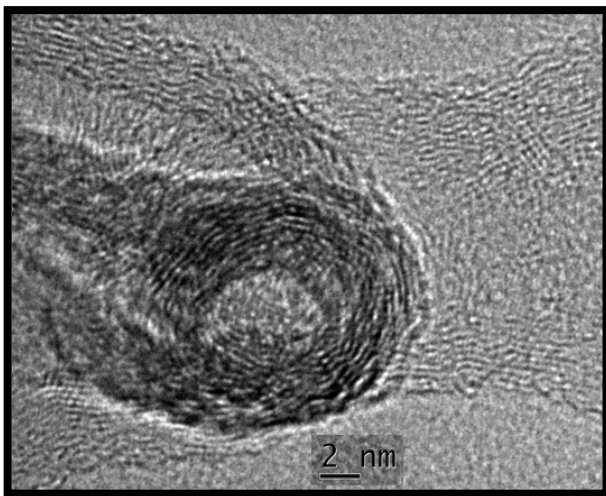
Fig.7: TEM image of the MWCNT (Evidence of multiple walls from tip)

Multiwalled carbon nanotubes have been described as graphene sheets rolled up to form concentric cylinders hence the nanotubes have hexagonal crystal lattice structure similar to that of graphite. Typical MWCNTs diffract at reciprocal lattice spacings ($1/d$) of 2.99, 4.92, 6.00 and 8.64 nm^{-1} corresponding to 002, 101, 004 and 112 planes respectively (Corrias *et al.*, 2007). A corresponding SAED pattern collected from the TEM image was used to study the crystallinity and phase of the MWCNT as shown in Figure 8.
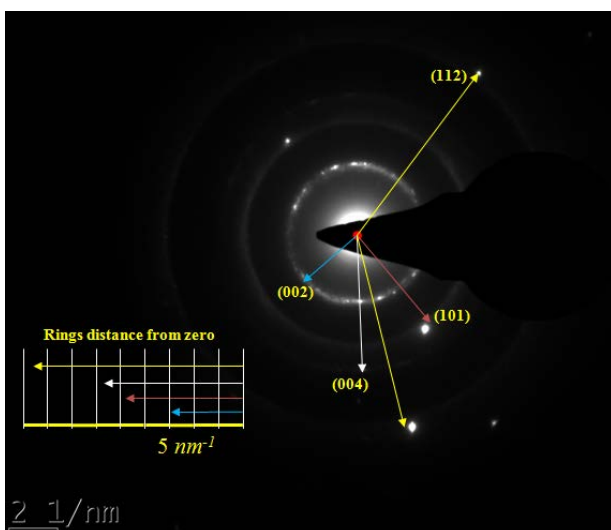
Fig.8: SAED pattern of the MWCNT

The sharp rings are evidence of polynanocrystalline material representing diffraction from few crystals. A diffuse pattern would be obtained from amorphous substances. The single bright spots are reflections from certain individual crystals. The (002) is usually the strongest graphitic plane found in MWCNTs (Das e*t al.*, 2015). The occurrence of the sharp rings at reciprocal lattice spacing ($1/d$) of 2.9, 4.8, 5.7 and 8.5 nm^{-1} are in good agreement with those reported for graphite. Corrias *et al.* (2007) also collected SAED pattern of MWCNTs and observed sharp rings attributable to the MWCNT at reciprocal lattice spacing of 3.1, 5.0, 6.0 and 8.5 nm^{-1}.

4. CONCLUSION

Good crystalline multiwalled carbon nanotubes with relatively narrow diameter were successfully produced from acetylene using Fe-Co/$CaCO_3$ catalyst via the CVD technique in solely argon environment. Varying diameter MWCNTs (20-40 nm) were produced. Sulphuric acid treatment of the as-synthesized MWCNTs proved effective as evident from EDX analysis, but its use in $CaCO_3$-supported catalyst required the simple decantation of $CaSO_4$ precipitates that are formed in the reaction of residual $CaCO_3$ and CaO with H_2SO_4. A relatively fair catalyst efficiency of 110 % was obtained with the use of $CaCO_3$-supported catalyst. But, contrary to the claim that CVD-grown MWCNTs do have relatively inferior crystallinity (Kumar and Ando, 2010), the SAED pattern collected for the MWCNTs produced in this study showed a highly polynanocrystalline material. The lattice parameters are consistent with that reported for graphite in literature, thereby affirming the hexagonal crystal structure of nanotubes. The SAED results gave accurate and precise crystallographic study. The observed good quality properties of the final nanotubes suggest that the $CaCO_3$ powder is suitable for use as catalyst support in CNT

growth. As to whether the observed crystallinity was due to H_2SO_4 acid treatment could not be established.

REFERENCE

Afolabi, A. S., Abdulkareem, A. S., Mhlanga, S. D. and Iyuke, S. E. (2011) "Synthesis and purification of bimetallic catalysed carbon nanotubes in a horizontal CVD reactor", *Journal of Experimental Nanoscience, vol. 6(3), 248-262*.

Chiwaye, N., (2012) "In Situ X-Ray Diffraction Analysis of Fischer Tropsch Synthesis", PhD Thesis. University of the Witwatersrand, Johannesburg.

Corrias, A., Mountjoy, G., Gozzi, G., and Latini, A., (2007) "Multi-walled carbon nanotubes decorated with titanium nanoparticles: synthesis and characterization", *Nanotechnology, 18, 485610 (7pp);* doi:10.1088/0957-4484/18/48/485610.

Das, R., Abd Hamid, S. B., Ali, M. E., Ramakrishna, S., and Yongzhi, W., (2015) "Carbon Nanotubes Characterization by X-ray Powder Diffraction - A Review", *Current Nanoscience, 2015, Vol. 11, No. 1*.

Haffer, S., (2013) "Mesoporous Spinel-type Cobalt oxide, Cobalt Ferrite and Alumina by Nanocasting". PhD Thesis, Paderborn University, Paderborn.

Han, I. T., Kim, H. J., Park, Y. J., Jin, Y. W., Jung, J. E., Kim, J. M., Kim, B. K., Lee, N., and Kim, S. K., (2004) "Synthesis of Highly Crystalline Multiwalled Carbon Nanotubes by Thermal Chemical Vapor Deposition Using Buffer Gases", *Japanese Journal of Applied Physics,* 43, 3631; doi:10.1143/JJAP.43.3631.

Haungs, M., (1986) "A brief table of X-ray line energies and widths".

Kumar, M. and Ando, Y., (2010) "Chemical Vapor Deposition of Carbon Nanotubes: A Review on Growth Mechanism and Mass Production", *Journal of Nanoscience and Nanotechnology Vol. 10, 3739–3758*.

Kurita, H., Kwon, H., Estili, M., and Kawasaki, A., (2011) "Multi-Walled Carbon Nanotube-Aluminum Matrix Composites Prepared by Combination of Hetero-Agglomeration Method, Spark Plasma Sintering and Hot Extrusion", *Materials Transactions, Vol. 52, No. 10 (2011) pp. 1960 - 1965*.

Magrez, A., Seo, J. W., Smajda, R., Mionić, M., and Forró, L., (2010) "Catalytic CVD Synthesis of Carbon Nanotubes: Towards High Yield and Low Temperature Growth (Review)", *Materials*, *3*, 4871-4891; doi:10.3390/ma3114871.

Mahajan, S. S., Bambole, M. D., Gokhale, S. P., and Gaikwad, A. B., (2010) "Monitoring structural defects and crystallinity of carbon nanotubes in thin films", *Pramana- Journal of Physics,* Vol. 74, No. 3, pp. 447 – 455.

Mohamed, N. M., Tan, Y. C., and Kadir, A. K., (2006) "Synthesis of Narrow Diameter Multiwalled Carbon Nanotubes (MWNTs) By Catalytic Chemical Vapor Deposition For Mechanical Reinforcement Applications", NSTI-Nanotech 2006, www.nsti.org, ISBN 0-9767985-6-5 Vol. 1, 2006.

Mohammed, I. A. (2015), Response Surface Approach to formulation of Bimetallic (Fe/Co) Catalyst on $CaCO_3$ Support for Carbon nanotube Growth. MEng Thesis, Federal University of Technology, Minna, Nigeria

Pervez, A., Doh, C. H., Kim, D., Farooq, U., Yaqub, A., and Choi, J. H., (2014) "Comparative Electrochemical Analysis of Crystalline and Amorphous Anodized Iron Oxide Nanotube Layers as Negative Electrode for LIB", *ACS Applied Materials & Interfaces, 6 (14)*; DOI: 10.1021/am501370f

Prasek, J., Drbohlavova, J., Chomoucka, J., Hubalek, J., Jasek, O., Adam, V. and Kizek, R., (2011) "Methods for carbon nanotubes synthesis—review", *Journal of Materials Chemistry, 21, 15872;* DOI: 10.1039/c1jm12254a.

PERFORMANCE ASSESSMENT OF HYDROPOWER GENERATING PLANTS

J. Y Yisa [1*], A. Nasir [2], H. T. Abdulkarim [5], H. U Ogboo [3], S. Abdulmumini [4]

[1]Department of Mechanical Engineering, Federal University of Technology, Minna, Nigeria

[2,3,4]Department of Mechanical Engineering, Federal University of Technology, Minna, Nigeria

[5]Department of Electrical/Electronic Technology, College of Education, Minna, Nigeria

[*]jojileg@yahoo.com, +2347034612371

ABSTRACT

This paper studies the performance of ahydropower scheme in Nigeria which contributes to an acute electricity supplyand has effects on the country's development. This does not only restrict the socioeconomic activities to basic human needs, but also adversely affecting the quality of life too.The expected full load installed capacity for the hydropower scheme is 522.74MW but the generated capacity for the period under review is 305.147MW. Only about 40% of the installed capacity was available.Average Capacity factor for this hydropower scheme is 47%, min. of 25% in 2014 and max. of 83% in 2013 as against the industrial best practice of 50 – 80%.Total generation reduction due to downtime of the hydropower scheme is 28165773MWh amounting to 53% of the total installed capacity. Based on Power generation reduction of 53% the loss of revenue in naira was about 186 Billion naira.To improve the annual power generation, a complete overhauling of all the generators and adequate water management practice must be in place so that the available water can sustain generation throughout the year.

Keywords:*Downtime,Running hour,Reduction, Capacity*

1. INTRODUCTION

The unreliability of public electricity supply in Nigeria is responsible to a large extent for the relatively low industrial development in the country. The Power Holding Company of Nigeria, (PHCN) the body that has the monopoly of power generation and distribution has been unable to affectively meet the electricity needs of the country according to Hart, (1992).

NEPA (as formerly called) as at June, 1992 had an installed capacity of about 600 megawatts from its eight major power stations. The maximum actual generating capacity of NEPA has however been about 3392.5 megawatts and this occurred around 15 March, 1992. This includes about 60 megawatts that is generated at Ajaokuta and other smaller stations. If this quantity is subtracted from the 3392.5 megawatts stated above, it means that only about 56% of the installed capacity is available for power generation from the major stations, (Hart, 1992). The problem of NEPA has been a long standing worry for everyone in the country but the situation seems to have defied all solutions. Before now, most of the reasons proffered for the continuing problem had not been looked at from the technical point of view according to Hart.

The prime mover of economic growth and development is energy. It is a major requirement in every home, offices and factories, therefore the issue of power generation is of utmost importance and the prosperity of any country is dependent upon the efficient and rational use of energy according to Akinbode, (2004). The world is currently experiencing a period of energy crisis of which Nigeria is not an exception. Nigeria as a country has been generating her own power for over one hundred years even right from the colonial era as noted by Akinbode, (2004). There has been a steady rising demand for energy needs in the country as a result of growth in population and infrastructural facilities. Coping with the rising demand of energy needs has been a great challenge to the agency that is responsible for generation of power in Nigeria, the Power Holding Company of Nigeria PHCN.

1.1 Principle of Hydropower

The controlling rule behind hydropower is the fundamental law of energy in which energy is neither created nor

destroyed but can be changed from one form to another. The component includes the change from potential energy to kinetic energy of water. Whereas Potential energy is the energy contained in a body by virtue of height or position, the Kinetic energy of a body is the energy contained in the body by virtue of motion.

Water from the region, is either used directly as in ROR types or gathered in big reservoirs and made to keep running from higher height to lower rise through a penstock. The water turns a water turbine or wheel, and by means of a shaft connected to an electrical generator, produces power (Figure 2.1). The combination of the turbine and generator operations converts mechanical energy into electrical energy.

At a hydropower plant, Energy is created by the power of falling water unlike thermal plant; this power is created without the generation of gas emissions. The water used to deliver power is not consumed and can be accessed for different purposes downstream. Some Energy plants are situated on waterways, streams and trenches. As a rule, a dam is obliged to store water so it is dependably accessible when expected to create power and for different purposes. The reservoir can be likened to a battery which stores energy (water) to be used later.

At the point when the control doors are opened, the reservoir water goes into a pipe called the penstock. Water moving through the penstock can be controlled and specifically coordinated to one or more turbines to generate power. Hydropower producing units have four primary parts: a stator, a rotor, a turbine, and a shaft joining the turbine to the rotor. They are shown in Figure 1. Water falls through the penstock into the turbine. The wicket doors as seen in this figure permit the measure of water guided into the turbine to be varied. The magnitude of the falling water against the razor sharp edges of the turbine pivots a shaft connecting the rotor and turbine. The pivoting shaft turns the rotor or moving bit of the generator. The outside edge of the rotor is comprised of exceptionally solid electromagnets. These electromagnets are shaped by wrapping copper wires around a steel core (pole). These magnets are positioned in order to give north and south poles around the edge of the rotor.

The stator is the doughnut shaped structure encompassing the rotor. The key part of a stator is the stator conductors or winding. In a bigger generator, stator windings are comprised of coils made of numerous turns of copper wire which is a superb conductor of electrical energy. The development of the electromagnets in the rotor causes power to flow in the copper wires (conductors).

The turbine shaft is specifically connected to the rotor. As the turbine is turned by the power of the falling water, the rotor turns. The electromagnets on the edge of the rotor sweep over the stator thereby inducing electric current. By changing the quality and strength of the electromagnets in the rotor and varying the flow rate of water in the penstock, the voltage and power generation of the generator can be controlled.
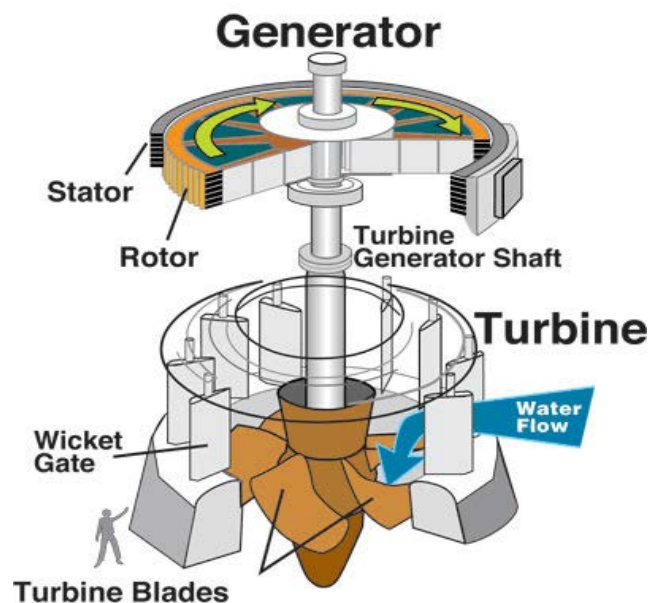
Figure 1: Schematic diagram of a Generator and Turbine
Source: U.S. Army Corps of Engineers

1.2 Hydropower in the World

The most important source of renewable energy for electrical power production in the world is Hydropower. The technically feasible hydro potential of the world is estimated as 14,371 Tera-Watt hour per year (TWh/year), which is equal to the global electricity demand today. Whereas the economically feasible proportion of this is 8,080 TWh/year. The exploited hydropower potential in the world in 1999 was 2,650 TWh which is about 19% of the world's electricity according to Paish (2002).

In 2001, Canada was the world's biggest producer of hydropower generating 350 TWh/year which is 13% of the global output. United States, Brazil, China and Russia are behind Canada in hydropower production.
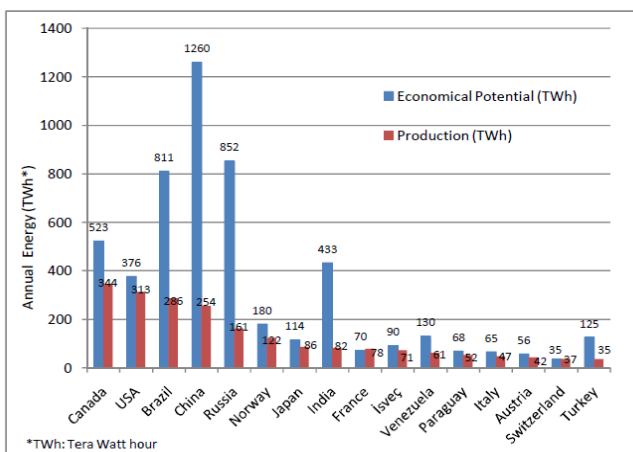
Figure 2: Hydropower Productions and Economic Potential of some Countries

Source: Paish (2002)

As we move forward in the 21st century, global energy consumption is rising to record levels never anticipated in the past. Economic development in emerging countries and the worldwide increased dependency on electric devices drives this energy consumption further to an ever-increasing scale. Yet, the majority of our energy is derived from fossil fuels, that is, oil, gas and coal that are finite (i.e. non-renewable) resources on our planet. Thus, there is a great emphasis in today's energy and technology

research to increase and improve sustainable energy options. Many people think of renewable energy as solely solar or wind energy, however above 90% of all renewable energy worldwide actually Comes from hydropower production (International Hydropower Association [IHA], International Commission on Large Dams [ICOLD], International Energy Agency [IEA] & Canadian Hydropower Association [CHA], (2000). Hydropower is considered a renewable energy because it is based on the energy provided by the Sun that drives the hydrological cycle.

Many countries produce large shares of their total electricity generation with the energy derived from water. For example, Norway, Brazil and Venezuela produce 95.7 per cent, 83.8 per cent and 72.8 per cent, respectively, of their domestic electricity with hydropower (IEA, 2011). So too does Switzerland, with approximately 54 per cent of its electricity production coming from more than 550 large hydropower installations (Bundesamt fur Energie [BFE], 2012a). The remaining share is largely produced by nuclear power with approximately 41 per cent and other electricity sources with 5 per cent. However, due to the dramatic events of the nuclear disaster in Fukushima, Japan in March 2011, the Swiss energy policy has radically changed its course. After the event, the Swiss Federal Council decided that nuclear power production will no longer be part of the Swiss electricity supply mix and shall be phased out until 2034. Naturally, this means a great change for the Swiss electricity industry and it raises the issue of how to replace the base electricity supply, which is currently provided by nuclear power plants.

1.3 Hydro-Electricity Potential in Nigeria

World Bank Study (2001) of hydro-electricity potential in Nigeria revealed that hydro power could be tapped to supplement the coal fired plants as a source of electricity. Consequent upon this, the Kainji hydro-electric power

station was built. However, it was discovered that the Kainji dam encountered a season of fluctuating water levels following draught in the Sahel region and damming of the waterways in neighboring countries. To address this problem, Government built two more hydro-electricity power stations at Jebba and Shiroro. This helped a great deal in raising the hydroelectric potential of the country but the problem of water level in River Niger affects electricity production from these hydro-electric plants.

2. METHODOLOGY

Data were collected from plant records. Information on the following parameters were used in the course of this study.

i. Gross Energy Generated (MW h).

ii. Running hours (h).

iii. Energy utilized by the plant (MW h).

iv. Energy delivered (MW h).

v. Installed capacity (MW) of the plant and the individual units.

2.1 The Plant performance indices

For the purpose of this study only the following Power Plant performance indices will be employed;

    i.   Plant capacity (P_{IC})

    ii.   Plant factors (Load factor LF, Capacity factor CF, Utilization factor UF)

    iii.   Efficiency of the plant

Other key performance indices employed in evaluating a plant's performance are: Generation unit cost, water volume utilization efficiency, breakdown maintenance, staff productivity etc.

The Economic factor considered in this work is outage cost for the plant.

The plant performance indices used in this work are as follows;

Plant Capacity (PC):

$$EPC = PPC\ (MW) \times Running\ Hours\ (h) \tag{1}$$

EPC = energy plant capacity,

PPC = power plant capacity.

Capacity Factor (CF):

$$CF = \frac{E_p}{C_{in} \times T_h} \tag{2}$$

E_p = total energy generated (MW h) in a given period,

C_{in} = the installed capacity of the plant, and

T_h = the total hours of the year.

Plant Use Factor (PUF):

$$PUF = \frac{E_p}{C_{in} \times T_{Oh}} \tag{3}$$

T_{Oh} = total number of operating hours in the given period (one year).

Load Factor (LF):

$$LF = \frac{L_{av}}{L_{md}} \tag{4}$$

Where L_{av} is the average (demand) load generated and

L_{md} is the maximum (demand) load generated in a given period (one year).

Also, Load factor is given by;

$$\frac{Total\ Energy\ Generated}{Available\ Capacity \times Hours\ witin\ the\ period} \times 100 \tag{5}$$

Utilization Factor (UF):

$$UF = \frac{L_{md}}{C_{in}} \tag{6}$$

Generation unit cost:

$$\frac{Total\ Expenditure}{Total\ Energy\ delivered} \tag{7}$$

Measured in naira per kilowatt hour

Generation unit index:

$$\frac{Actual\ Generation}{Available\ Capacity} \times 100 \qquad (8)$$

Capacity Utilization index:

$$\frac{Available\ Capacity}{Installed\ Capacity} \times 100 \qquad (9)$$

Water Volume utilization index:

$$\frac{Actual\ Generation}{Available\ Capacity} \qquad (10)$$

Measured in m^3/MWh

Energy utilised by the generating station:

$$\frac{Total\ Energy\ generated - Energy\ delivered}{Total\ Energy\ generated} \times 100 \qquad \textbf{(11)}$$

Staff cost index:

$$\frac{Total\ staff\ cost}{No.of\ employees} \qquad (12)$$

Measured in Naira per Head

Staff productivity index:

$$\frac{Energy\ delivered}{No.of\ employees} \qquad (13)$$

2.2 Power Outage Cost

Hydropower outage cost can be determined using the following equations;

$$P_T = \sum_{i=1}^{n} P_{Ai}$$

$$(14)$$

Where P_T is the total power outage cost due to system downtime for n number of years and P_A is the annual power outage cost for m number of units.

But,

$$P_A = P_R \times P_F \times C_U \qquad (15)$$

$$P_R = \sum_{j=1}^{m} P_r$$

$$(16)$$

$$P_A = P_{IC} - P_{GC} \qquad (17)$$

$$P_F = \frac{\sum G_C}{\sum I_C} \qquad (18)$$

Oyedepo*et al* (2014)

Where P_R is the annual power generation reduction for m number of unit,

P_r is the annual power generation reduction for individual unit,

P_{IC} is the annual installed energy capacity in MWh for individual units.

P_{GC} is the annual generated energy capacity in MWh for individual units,

P_F is the annual power factor for m number of units,

G_C = generated power capacity in MW for individual units,

3. RESULTS AND DISCUSSIONS

Table 2: Total Energy generation from 2004-2014

Year	Actual Energy Generation (MWh)	Average Running Hours	Capacity Factor
2004	2878774	7808.248	0.52
2005	2586929	7808.248	0.45
2006	2366716	7304.106	0.43
2007	2816749	7377.249	0.51
2008	2695223	6632.087	0.49
2009	2505663	6961.706	0.52
2010	2300991	6478.8	0.48
2011	1769060	5682.557	0.37
2012	1392353	6420.172	0.34
2013	935868	7456.653	0.83
2014	735062	5389.286	0.25
Ave	2089399	6847.192	0.47

Source: Fieldwork: 2015

Table 2: Cost of power outage for the Hydropower plant scheme

Year	Energy Plant Capacity (MWh)	Energy Generation Reduction (MWh)	Cost Of Power Outage (Naira)	% Power Reduction	
2004	5529600	2650826	20262913940	49	
2005	5529600	2942670.65	19465766350	53	
2006	5529600	3162883.45	19992586290	57	
2007	5529600	2712850.6	20338240950	49	
2008	5529600	2834577	20417458130	51	
2009	4838400	2332737	17831441630	48	
2010	4838400	2537409	17903957923	52	
2011	4838400	3069340	16694140260	63	
2012	4147200	2754847	13768725310	66	
2013	1123200	187332	11775111894	17	
2014	2937600	2202539	8094330825	75	
Total	50371200	28165773.7	186544673500	Avg = 53	

Source: Fieldwork: 2015

Fig. 4: Power available vs. power reduction

Fig. 5: Energy Generation from 2004-2014

Fig. 3: Variation of capacity factor with year
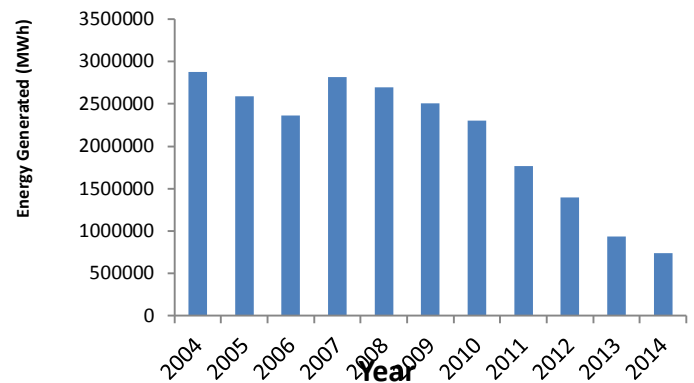
3.1 Research Findings

I. The expected full load installed capacity for the hydropower scheme is 522.74MW but the generated capacity for the period under review is 305.147MW. Only about 40% of the installed capacity was available. This is as a result of ageing generating facilities as seen in figure 5 showing that energy generation depletes over time.

II. The average Energy generated within the period under review is 2089399MWh at average running hours of 6847.19 hours. This is far from the installed capacity

III. Average Capacity factor for this hydropower scheme is 47%, min. of 25% in 2014 and max. of 83% in 2013 as against the industrial best practice of 50 – 80%. The low capacity factor of the plant in 2014 signifies that

the average energy generation is low. Generally, low CF indicates frequent failure of the plant or inadequate water supply to boost the operating head of the station, which implies that the plant's capacity for major parts of the year remains unutilized. If scheduled maintenance of the plant is significantly improved, the rate of failure will be minimized, the quantity of water in the reservoir will be judiciously utilized as against spilling of such water as a result of overflowing dams caused by unutilized amount of water in the dams. Thus, a higher capacity factor will be attained.

IV. Load factor for the scheme varies from 25% to 83% with an average of 47%. This is low when compared with the international best practice of 80% (Abam et al, 2011). The load factor is an indication of the utilization of the power plant capacity.

V. Total generation reduction due to downtime of the hydropower scheme is 28165773MWh amounting to 53% of the total installed capacity.

VI. Based on Power generation reduction of 53% the loss of revenue in naira was about 186 Billion naira.

4. CONCLUSION

This study has shown that the performance of this hydropower scheme is slightly below the international best practice standards, but offers an avenue for improvement.

The revenue loss as a result of power generation reduction from this study can be considerably reduced via improvement in the Plants operational practices and the general housekeeping of the plants, which includes overhauling of the plant at least at 25yrs intervals. Good water management practices should be implemented.

REFERENCES

Abam, F.I., Ugot, I.U., Igbong, D.I. (2011): Thermodynamic assessment of grid-based gas turbine power plants in Nigeria. Journal of Emerging Trends in Eng. and Applied Sci. (JETEAS) 2011; 2(6):1026–33.

Akinbode, F.O. (2004): Sustainable Energy Technology for twenty-first century. Inaugural Lectures series No.2. Federal University of Technology, Minna

Bundesamt fur Energie (BFE) (2012). *SchweizerischeElektrizitätsstatistik 2011*. Retrieved June 06, 2012, from http://www.bfe.admin.ch/themen/00526/00541/00542/00630/index.html?lang=dDehradun, October 2006.

Hart, H.I. (1992): Viability of Large scale power generating systems in Nigeria. NSE Technical Transactions. Vol. 28,No.3Pp 26-37http://www.swv.ch/Fachinformationen/Wasserkraft---Schweiz.

International Energy Agency (IEA) (2011). *Key World Energy Statistics 2011*. Retrieved May 15, 2012, fromhttp://www.iea.org/publications/freepublications/publication/name,26707,en.htm

International Hydropower Association (IHA), International Commission on Large Dams (ICOLD), International Energy Agency (IEA) & Canadian Hydropower Association (CHA) (2000).*Hydropower and the World's Energy Future.The role of hydropower in binging clean, renewable, energy to the world.*Retrieved April 19, 2012, fromhttp://www.ieahydro.org/Hydropower_Development13.html

Oyedepo, S.O., Fagbenle R.O., Adefila S.S., Adavbiele, S.A., (2014) Performance evaluation and economic analysis of a gas turbine power plant in Nigeria. Energy Conversion and management. 79(2014) 431-440.

Paish, O. (2002), Small Hydro Power: Technology and Current Status. Paper published in Renewable and Sustainable Energy Reviews,2002.

PERFORMANCE EVALUATION OF DOWNDRAFT GASIFIER FOR SYNGAS PRODUCTION USING RICE HUSK

J. Salisu[1*], M.B. Muhammad[2], M. Bello[3], N. Yusuf[4], A. Atta[5], I. M. Bugaje[6]

[1]Department of Chemical Engineering, Modibbo Adama University of Technology, Yola

[2, 3]Department of Chemical Engineering, Ahmadu Bello University, Zaria

[4, 5, 6] National Research Institute for Chemical Technology, Basawa, Zaria

[*]ejamilsalih@yahoo.com, +2348037179080.

ABSTRACT

Gasification is considered to be a promising clean energy option for reduction of greenhouse gas emissionsand increasing access to energy. It is a way of utilizing agricultural waste like rice husk which could otherwise create environmental risks and a way of reducing energy dependency on fossil fuels. In this paper, rice husk was characterized using ASTM standards; except for hydrogen, carbon and oxygen where correlations were used. The rice husk was used as a biomass for gasification with a downdraft gasifier installed at National Research Institute for Chemical Technology, Zaria. Air was used as a gasifying agent and the effect of 0.64, 0.3 and 0.07 L/min as flow rate were studied. It was found that higher air flow rate favouredgasification temperature and syngas quality, 0.64 L/min gives the best syngas composition of 12.07% CO, 12.69% CO_2, 2.54% CH_4 and 1.01 H_2 with gasification temperature of 733°C.

Keywords: *Rice Husk, Gasification, Downdraft Gasifier, Syngas, Biomass.*

1. INTRODUCTION

About 90% of the world primary energy consumption is from fossil (petroleum, gas and coal), (Melgara *etal*, 2009). However depleting of these fossil energy sources, the rate at which carbon dioxide (CO_2) is released into the atmosphere when they are burned and increasing demand of the world energy due to population coupled with technological advancement are challenges. These challengeshas served as motivation globally to develop alternative and renewable energylike biomass and solar that can help the present generation to meet their energy demand without jeopardizing the ability of the future generation to meet their energy demand.

By 2050 energy from biomasscould contribute 15%–50% of the world's primary energy (Beohara *etal*, 2014). Presently about 25% of biomass is used by developed countries, while 75% is used by developing country to produce heat (Sahito, 2013).Nigerian biomass energy resource is estimated to be 144 million tonnes/year (Diyoke *etal*, 2014).Sambo (2009) estimated Nigerian agricultural waste resources in million tonnes per annum as 11.2, with energy content of 147.7GJ.About 120 million tonnes of rice husks are generated annually in the world

(Omatola and Onojah, 2012). In Nigeria about 2.0 million tonnes of rice is produced annually and 400 thousand tonnes of rice husk is generated out of it (Abalaka, 2012).These large quantities of biomass resources in Nigeria offer much potential for renewable energy and can play a significant role in meeting the country's energy demand if properly harness in modern and sustainable way.

Direct combustion has been the major way of utilization of biomass in Nigeria especially inrural areas. Fuel wood is used by over 60% of Nigerians living in the rural areas. Nigeria consumes over 50 million metric tonnes of fuel wood annually with alarming rate of deforestation The rate of deforestation is about 350,000 hectares per year, which is equivalent to 3.6% of the present area of forests and woodlands, whereas reforestation is only at about 10% of the deforestation rate (Sambo, 2009).

The benefit of utilization of rice husk in a sustainable way in Nigeria includes:clean energy option for reduction of greenhouse gas emissions; reducing energy dependency on the conventional fossil source, could serve as major source of energy to rural areas;and creation of more value to growing of rice in Nigeria which will translate to overall food security and new jobs will be created.

The conversion of biomass to useful forms of energy in a sustainable way can be achieved using a number of biomass conversion technologies broadly grouped into thermochemical processes and biochemical/biological processes as in fermentation and aerobic digestion (Caputo *etal*, 2004). The thermochemical conversions of biomass are combustion, pyrolysis and gasification. They constitute one of the promising routes among the renewable energy options of future energy because virtually all types of biomass can be used as feedstock even waste.Their counterpart fermentation and aerobic digestion are very specific in their biomass feedstock requirement. Gasification is a thermochemical process which breaks down biomass completely into a combustible gas, volatiles, chars, and ash in an enclosed reactor or gasifier. The process occurs when a controlled amount of oxidant (pure oxygen, air, steam) is reacted at high temperatures with available carbon in the fuel within a gasifier. This combustible gas is known as producer gas or syngas and consists of mainly hydrogen (H_2) and carbon monoxide (CO) with methane (CH_4), carbon dioxide (CO_2), water vapour (H_2O), nitrogen (N_2), higher hydrocarbons and undesired products: particulate matter, dust, soot, inorganic pollutants and organic pollutants (tars) as well as ash (Reynolds *et al*, 2013*)*. The composition for any syngas strictly depends on the gasification principles (reactor geometry, used gasification agents, operating conditions), biomass properties.

Biomass gasification has attracted the highest interest as it offers higher efficiencies compared to combustion and pyrolysis (Sheth and Babu, 2009). Gasification is also favoured among the others thermochemical conversion processes because it provides a syngas that can be used not only to produce heat and power but also utilized in synthesis of liquid fuels and chemicals.

Gasification is a two-step, endothermic process. In the first reaction, pyrolysis, the volatile components of the fuel is vaporized at temperatures below 600°C by set of complex reactions. Included in the volatile vapours are hydrocarbon gases, hydrogen, carbon monoxide, carbon dioxide, tar, and water vapour. As biomass fuels tend to have more volatile components (70-86% on a dry basis) than coal (30%), pyrolysis plays a larger role in biomassgasification than in coal gasification. Char (fixed carbon) and ash are the pyrolysis by-products, which are not vaporized. In the second step, the char is gasified through reactions with oxygen, steam, carbon monoxide and hydrogen. The heat needed for the endothermic gasification reactions is generated by combustion of part of the fuel, char, or gases, depending on the reactor technology (Boerrigter and Rauch, 2006).

Properties of biomass are useful in order to evaluate their suitability as chemical feedstock in different processes. In evaluating gasification feedstock, the following properties are generally useful: proximate (thermo-chemical behaviour) and ultimate (elemental composition) analysis and heating value (Stahl, *et* al, 2004).Composition of every biomass has carbon (C), hydrogen (H), oxygen(O) and sulphur (S) as major chemicalelements. These element fractions can be quantified by ultimate analysis.

Proximate analysis gives the composition of the biomass in terms of gross components such as moisture content (M), volatile matter (VM), ash, and fixed carbon (FC) (Bhavanam and Sastry, 2011).

The heating value of biomass is relatively low, especially on a volume basis, because its density is very low. The heating value may be reported on two bases. The higher heating value (HHV, cross heating value)) represents the heat of combustion relative to liquid water as the product. The lower heating value (LHV) is based on gaseous water (Stahl *et al,* 2004).

Gasifiers are mainly classified according to their design as fixed bed, fluidised bed and entrainedflow bed. However gasifiers can also be classified (Arnavat, 2011): according

to gasification agent, according to heat for gasification (autothermal or allothermal), and according to pressure in the gasifier (atmospheric or pressurised).

Fixed bed gasifiers are sometimes called moving bed because the gasifying agent passes through a bed of solid fuel, when the gasifying agent is feed from the top of the reactor with the biomass it is term downdraft gasifier while if the gasifying agent is feed from the bottom moving counter currently with the biomass the gasifier is called updraft (Arnavat, 2011). In cross draft gasifiers gasifying agent flows at high velocity through a nozzle located on a side of the gasifier opposite to where the syngas leaves the reactor (Rivas, 2008).

Fixed bed gasifiers are generally easy to construct, operate and suitable for small scale applications. There are widely available in developing countries but have limited scale-up properties.

The right choices of the parameters values (type and amount of oxidant) and types of biomass play a vital role in harnessing properly the energy in biomass using gasification technology. Rajvanshi (2014) reported that 16.1% CO, 9.6% H_2, 0.95% CH_4, with energy content of 3.25 MJ/m^3 is achievable by gasifying rice husk in downdraft gasifier with air as oxidant, while Jaina and Goss (2000) reported a lower heating value of syngas of about 4 MJ. Rahardjo (2013) uses mixture of air and steam for rice husk gasification and found syngas quality of 16.62% H_2, 9.75% CO, 5.74% CH_4 and 12.84% Co_2.

This paper focuses on the effect of amount of air as oxidant on the quality of syngas andgasification temperatureusing downdraft gasifier installed at National Research Institute for Chemical Technology, Zaria

2. METHODOLOGY

2.1. Rice Husk Characterization

The proximate analysis, sulphur and nitrogen content of the rice husk were determined according to ASTM standards as shown in Table1.While for hydrogen, oxygen and carbon as part of the ultimate analysis were determined from correlation developed by Shen,*etal* (2010) as given in equations (1) to (3).

Table l: Rice Husk Characterisation Parameters.

Parameter		ASTM Method
Proximate Analysis	Moisture content	E 871
	Ash	D 1102.
	Volatile Matter	E 872.
	Fixed Carbon	Subtracted percentage summation of moisture, ash, and volatile matter from 100
Ultimate Analysis	Sulphur	E 775
	Nitrogen	E 778

$$C = 0.635FC + 0.460VM + 0.095ASH(wt.\%) \qquad (1)$$

$$H = 0.059FC + 0.060VM + 0.010ASH(wt.\%) \qquad (2)$$

$$O = 0.340FC + 0.469VM + 0.023ASH(wt.\%) \qquad (3)$$

2.2 Experimental Procedure

The gasifier is throated downdraft with an internal diameter of 30cm and a height of 82cm. Syngas passes through a cyclone and a filter for gas cleaning. The operation was started by loading the gasifier with rice husk with minimum load as the grate capacity of height10cm and diameter 36cm.After charging of the biomass the gasifier was sealed properly to avoid leakages and then ignition of the rice husk through the ignition point with the help of air blower which lasted for 10 minutes before the ignition point was closed and air blower was reserved to supply air through the air tuyere controlled by flow controller.
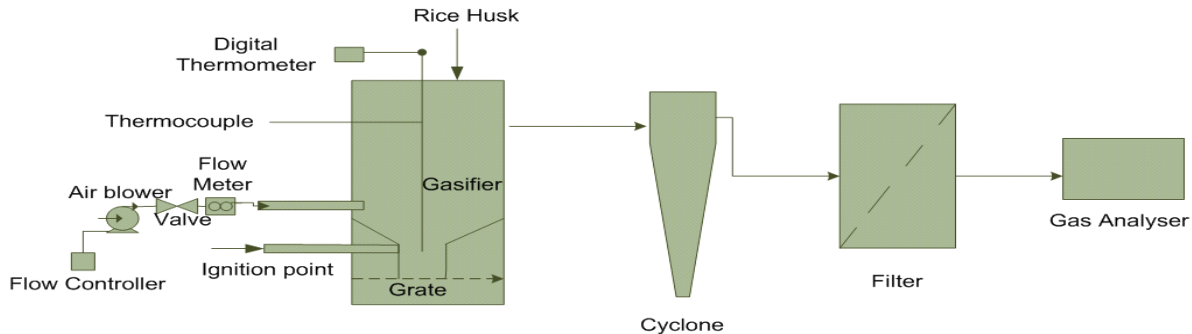
Figure 1: Schematic Diagram of the Experimental Set-up of the Gasification System.

The sampling valve was then opened which allowed syngas out of the system to a portable infrared syngas analyser (Gasboard 3100P series) where the percentage composition and energy content of the gas were analysed and recorded. K-type (chromel-alumel) thermocouple was placed down the reduction zone as a sensor to digital thermometer which helps in monitoring and recording the gasification temperature. The schematic diagram of the gasifier system is shown in Figure 1

3. RESULTS AND DISCUSSIONS

Figures2 and 3 revealed the chemical composition of the rice husk in terms of proximate and ultimate analysis.Chemical compositionof any has impact on the gasification behaviour of the biomass and the syngas composition. Moisture content was found to be 9.88 % (Dry basis) and it is desired to be low because the higher the moisture content of the rice husk, the more carbon monoxide (CO) is consumed by the water-gas shift reaction to produce CO_2 and H_2as in (7).However H_2 is produced and the reaction is exothermic. The hydrogen insignificant compare with the amount of CO loss with increase in moisture content. In addition, the small amount of heat gained due to the exothermic behaviour of the water-gas shift forward reaction is less than that will

berequired to evaporate the moisture; the overall effect is decrease in temperature which favours the exothermic reaction (Gautam, 2010). Equations (4) to (8) describes the main reactions occurring in a gasification system namely respectively as water-gas, boudouard, methanation, water – gas shift and steam reforming

$$C + H_2O \rightarrow CO + H_2 \qquad (4)$$
$$C + CO_2 \rightarrow 2CO \qquad (5)$$
$$C + 2H_2 \rightarrow CH_4 \qquad (6)$$
$$CO + H_2O \rightarrow CO_2 + H_2 \qquad (7)$$
$$CH_4 + H_2O \rightarrow CO + 3H_2 \qquad (8)$$

Biomass with moisture content above 30% makes ignition difficult due to the need to evaporate the additional moisture before combustion/gasification can occur (Arnavat, 2011).Ash was also found to be 19.7 % (Dry basis) from Figure2. When the ash content is above 5%, slagging occurs due to formation of clinkers which results into gasifier operational challenges, however successful gasification with ash-content up to 25% is possible with effective ash discharging mechanism (Gautam, 2010).Volatile matter was found to be 66.12% (Dry basis) and the higher its percentage, the more tar will be generated.
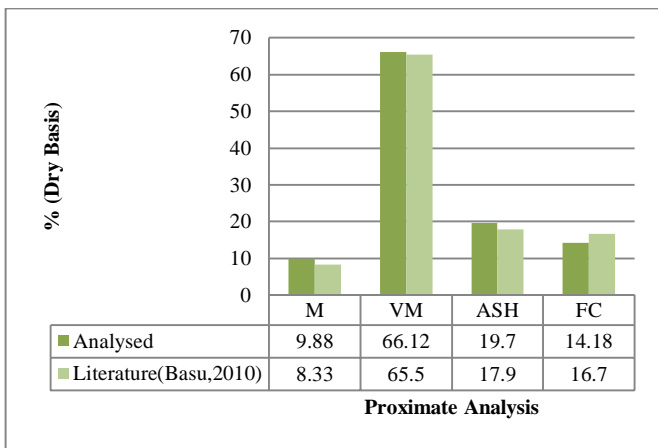
Figure 2: Proximate Analysis of Rice Husk

Fixed carbon was also found to be 14.18% (Dry basis) from Figure2 and any gasification reaction desired this value to be high because it is the carbon left for gasification reactions after devolatilization has occurred.
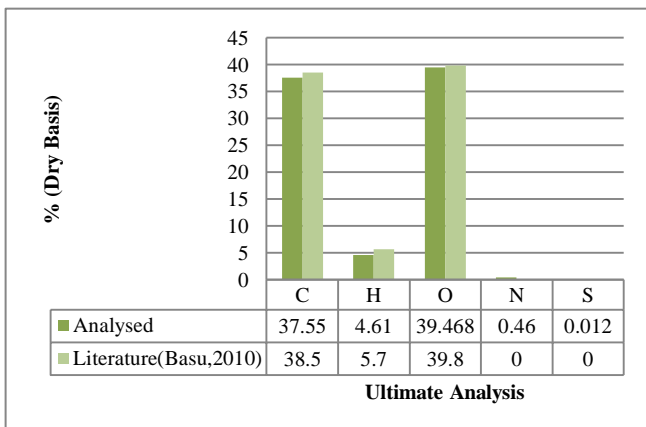
Figure 3: Ultimate Analysis of Rice Husk

Figure3 revealed the elemental composition which has effect on syngas produced of rice husk and it was found to be in weight percent dry basis as 37.54, 4.61, 37.67, 0.46 and 0.012 for carbon, hydrogen, oxygen, nitrogen and sulphur respectively.The release of pyrolysis gas is highly dependent on hydrogen/carbon ratio as well as oxygen/carbon ratio.A higher elemental carbon will increase the amount of carbon that will beavailable for gasification reaction. Higher oxygen content will require less oxygen as oxidant however its presence in higher amount will limit the percentage of carbon and oxygenin

the biomass.The amount of sulphur and nitrogen oxides that will be generated when the syngas is burned depends on appreciable percentage of sulphur and nitrogen content in the biomass. The ultimate analysis of the rice husk shows a negligible amount of sulphur and nitrogen.
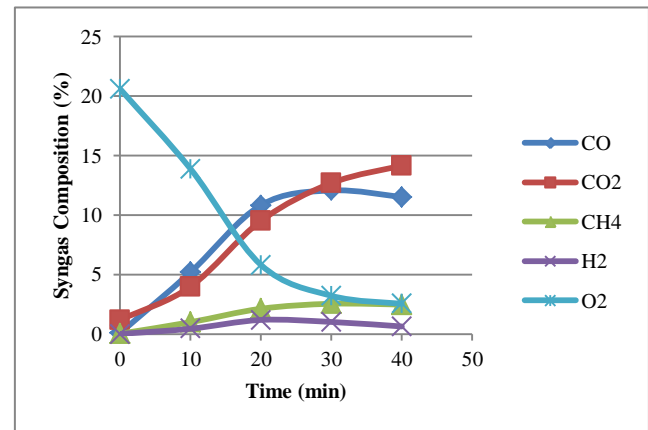
Figure 4: Variation of Syngas Composition with Time at 0.64 L/ min Air Flow Rate

Figures4, 5 and 6 showed the effect of syngas composition with respect to air flow rate of 0.64 L/min, 0.3 L/min and 0.07 L/min. It was found that the highest flow recorded the best quality of syngas composition of 12.07% CO, 12.69% CO_2, 2.54% CH_4 and 1.01 H_2, while the lowest flow rate of 0.07 L/min recorded the least quality of syngas of 6.68% CO, 10.54% CO_2, 0.95% CH_4 and 0% H_2.
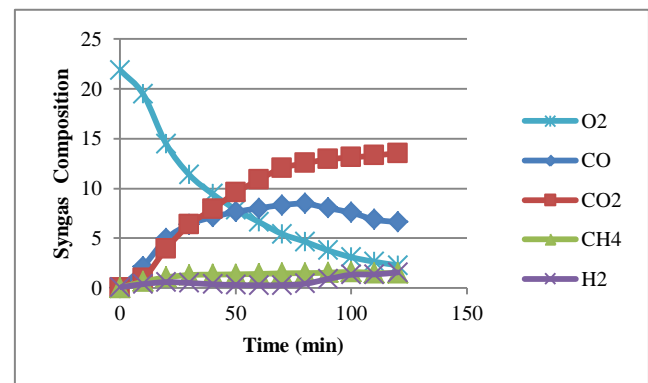
Figure 5:Variation of Syngas Composition with Time at 0.30 L/ min Air Flow Rate

In any gasification, the desire is to supply the system with deficient of oxygen, for this reason the oxygencomposition

in the syngas should be kept as low as possible, the trend from 2, 3 and 4 revealed that oxygen composition reduces with time, with reduction from maximum to minimum value of 20.61% to 2.54%, 21.89% to 2.28%, 20.85% to 5.07% for flow rate of 0.64 L/min, 0.3 L/min and 0.07 L/min respectively.
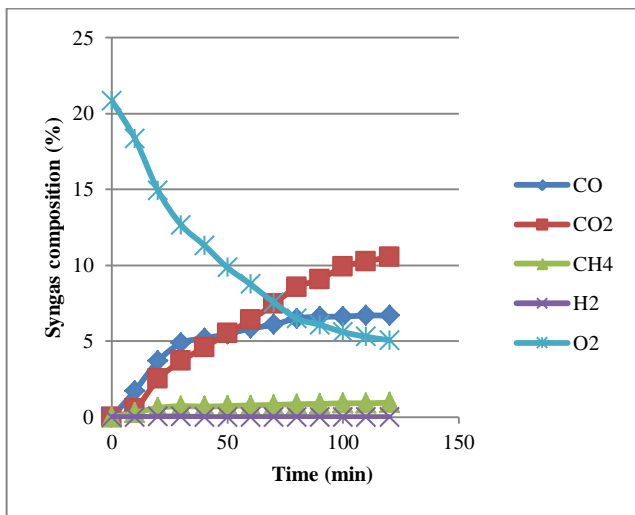
Figure 6: Variation of Syngas Composition with Time at 0.07 L/ min Air Flow Rate

Figure7 examined the effect of gasification time on temperature; it is observed that temperature rises to a peak before beginning to fall; this could be due to transition time between burnt biomass at the oxidation zone and the fresh biomass. The highest temperatures recorded were 733°C, 299°C, and 211°C for flow rate of 0.64 L/min, 0.3 L/min and 0.07 L/min respectively. It can be deduced that temperature increases with flow rate, this is justified because in an auto-thermal gasification, heat required for the system is supply by the exothermic heat released at the oxidation zone and higher supply of oxygen will generate more heat for the system. Gasification is favoured at higher temperature because both boudouard and water-gas reactions that produces carbonmonoxide are endothermic however reactions that produces methane from methanation and steam reforming are favoured at lower temperature because of their exothermic nature.
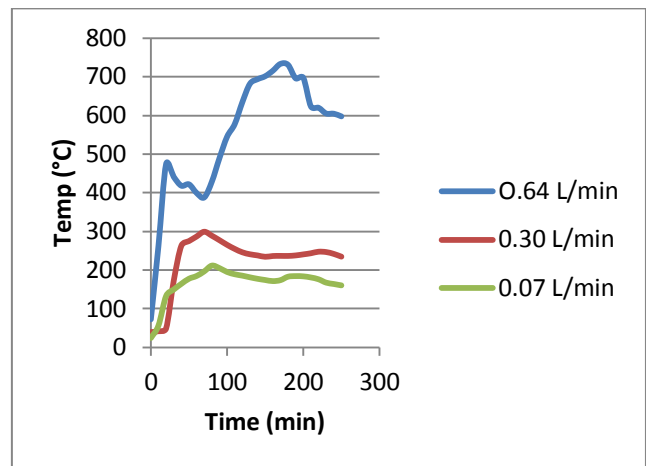
Figure 7:Variation of Temperature with Time at**Different Air Flow Rates**

Figure8 examined the syngas energy content within 250 minutes gasification, it was found that highest flow rate (0.64 L/min) recorded the highest syngas energy content of 2.75 MJ/Nm^3 while the lowest flow rate (0.07 L/min) recorded the lowest syngas energy content 0.32 MJ/m^3, this is so because syngas energy is a function of the
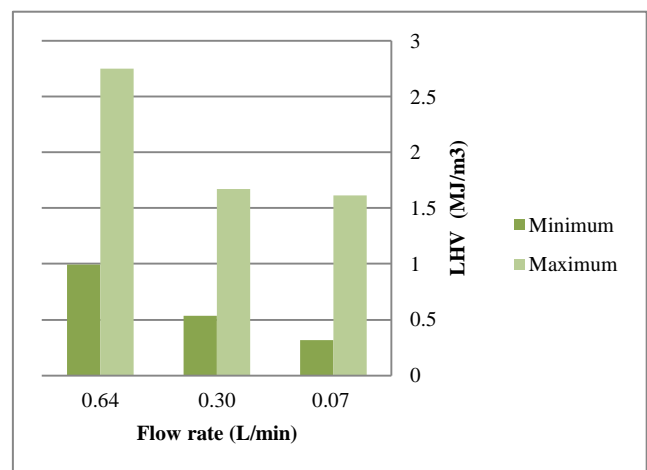
Figure8: Syngas Energy Content of Different Air Flow Rates

composition of the syngas as shown in Figure9 and best syngas composition was achieved with higher flow.Individual component of syngas has LHV in MJ/Nm^3 of 37.1, 13.1, 11.2 for methane, carbonmonoxide and hydrogen respectively (Tasma *etal*, 2009), so the higher

the percentage combination of these three components the higher the calorific value of the syngas. On the other hand carbondioxide and oxygen has no calorific values, their presence in syngas in higher percentage lessen the calorific value of the syngas.The quality of syngas produced also depends on the gasifying agent , calorific values in MJ/Nm^3 of 4-6 and 12-18, are reported for gasification with air and oxygen respectively (Vaezi,2008), though 3.25 MJ/Nm^3 was reported for rice husk specifically (Rajvanshi, 2014). Lower calorific value of gasification with air is due to inherent dilution with nitrogen present in the air.
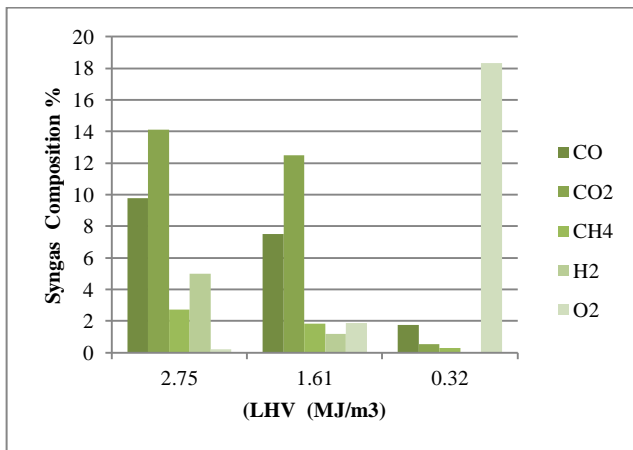
Figure 9: Effects of Syngas Composition on Energy Content.

4. CONCLUSION

Increase in air flow rate between the range of 0.64 - 0.07 L/min favours syngas composition, gasification temperature and syngas energy content. The best syngas composition recorded using air as gasifying agent with the downdraft gasifier installed at National Research Institute for Chemical Technology, Zaria was 12.07% CO, 12.69% CO_2, 2.54% CH_4 and 1.01 H_2.The highest gasification temperature and syngas energy content was 733°C and 2.75 MJ/Nm^3. The energy content shows that the syngas from the gasifier can only be applied for direct thermal applications,however higher syngas quality which could be used for liquid fuels and chemicals is possible by using pure oxygen or enriched air as the gasifying agent.

REFERENCE

Abalaka, A.E. (2012). Effects of Method of Incineration on Rice Husk Ash Blended Concrete. *ATBU Journal of Environmental Technology*. 5 (1) 34-47

American Society for Testing and Material, http://www.astm.org

Arnavat, P. M. (2011). *Performance Modelling and Validation of Biomass Gasifiers for Trigeneration Plants.* (Unpublished Doctoral dissertation),Universitat Rovira,Virgili.

Basu, P. (2010). *Biomass Gasification and Pyrolysis Practical Design and Theory.*Elsevier : Oxford

Beohara, H. Guptaa, B., Sethib, V. K., Pandeyb M., (2012). Parametric Study of Fixed Bed Biomass Gasifier: A review. *International Journal of Thermal Technologies.* 1 (2) 134-140.

Bhavanam, A and Sastry, R. C. (2011).Biomass Gasification Processes in Downdraft Fixed Bed Reactors: A Review. *International Journal of Chemical Engineering and Applications, (2) 6*,425-433.

Boerrigter, H. and Rauch, R. (2006). *Review of Applications of Gases from Biomass Gasification.*ECN biomass, coal and environment.p1-33

Caputo,C.A.,Palumbo,M.,Pelagagge,M.,Scacchia,F.(2004) .Economics of biomass energy utilization in combustion and gasification plants: effects of logistic variables. *Biomass and Bioenergy.*28(2005) 35-51

Diyoke, C., Idogwu , S., Ngwaka, U.C. (2014). An Economic Assessment of Biomass Gasification for Rural Electrification in Nigeria .*International Journal of Renewable Energy Technology Research.*1 (3) 1-17

Gautam, G. (2010). *Parametric Study of a Commercial-Scale Biomass Downdraft Gasifier: Experiments and Equilibrium Modelling.*(Unpublished master's thesis), Auburn University.

Jaina, K. A., Goss, R. J. (2000). Determination of Reactor Scaling Factors for Throatless Rice Husk Gasifier. *Pergamon Journal Biomass and Bioenergy.* (18) 249-256

Melgara, A., Pérezb, J. and Horrilloc, A. (2009). Biomass gasification process in a downdraft fixed bed gasifier: a real time diagnosis model based on gas composition analysis. *Rev. Fac. Ing. Univ. Antioquia.* pp. 9-18.

Omatola, K .M and Onojah, A.D (2012). Rice Husk as a Potential Source of High Technological Raw Materials: A Review. *Journal of Physical Sciences and Innovation.* Volume 4, 30-35

Rahardjo, B. S. (2013). Effect of Gasifiyng Agent (Air+Steam) Injection Towards Syngas Quality from Rice Husk Gasification..*International Journal of Engineering and Applied Science*(2) 74-96.

Reynolds, A., Doherty, W. and Kennedy, D. (2013). *Aspen Plus Simulation of Biomass Gasification in a Steam Blown Dual Fluidised Bed* (Unpublished master's thesis), Dublin Institute of Technology

Rivas, M. C. J. A. (2012). *The Effect of Biomass, Operating Conditions, and Gasifier Design on the Performance of an Updraft Biomass Gasifier.* (Unpublished master's thesis) Kansas State University, Manhattan, Kansas.

Sahito, A. R., Mahar, R. B., Syed, F. S., and Brohi, K. M. (2013). A Correlation for Estimating Elemental Composition of Lignocellulosic Biomass from Its Volatile and Fixed Solids Content.*Sindh University Research Journal (Science Series).* 45(4) 665-672.

Sambo, S. A. (2009). Strategic Developments in Renewable Energy In Nigeria. *International Association for Energy Economics.* Third Quarter ,15-19

Shen, J., Zhu, S., Liu, X., Zhang, H., Tan, J. (2010). The Prediction of Elemental Composition of Biomass Based on Proximate Analysis. *Elsevier Journal of Energy Conversion and Management.* (51) 983–987.

Sheth, P. N., Babu, B.V. (2009). Experimental Studies on Producer Gas Generation from Wood Waste in a Downdraft Biomass Gasifier. Bioresource Technology 100 (2009) 3127–3133.

Stahl, R., Henrich, E., Gehrmann, H. J., Vodegel, S. and Koch, M. (2004). *Renew- Renewable Fuels for Advanced Powertrains - Integrated Project Sustainable Energy Systems -Definition of a Standard Biomass.* (Report prepared under the framework of project): Germany.

Tasma, D., Uzuneanu,K., Panait, T.,(2009). The effect of excess air ratio on syngas produced by gasification of agricultural residues briquettes. *Journal of Advances in Fluid Mechanics and Heat & Mass Transfer*p203-207.

Vaezi, M., Passandideh-Fard, M., Moghiman, M. and Charmchi, M. (2008). Modelling Biomass Gasification: A New Approach to Utilize Renewable Sources of Energy. *Proceedings of IMECE2008 2008 ASME International Mechanical Engineering Congress and Exposition October.* 1-8.

RIVER GRAVEL AS ALTERNATIVE AGGREGATE IN HOT MIX ASPHALT PRODUCTION

Kolo S.S[1], Jimoh Y. A[2]., Sadiku S[1]., Jimoh O. D[1], Adeleke O. O[2]., and Enejoh D. A
[1] Department of Civil Engineering, Federal University of Technology, Minna, Nigeria.
[2] Department of Civil Engineering, University of Ilorin, Ilorin, Nigeria.
E-mails: bukysayo123@yahoo.com, +2348036879855

ABSTRACT

The world population continue to grow so the demand for more and reliable infrastructure, therefore researches into new and innovative materials are continually advancing. This research title river gravel as alternative aggregates in hot mix asphalt production was aimed determining the durability of river gravels (aggregates) as compared to crushed stone (aggregates) in hot mix asphalt production and uses. Samples of the aforementioned materials were obtained and process according to BS 812 for asphalt production and process. Various laboratories test were conducted on the river gravel, the bitumen and the resulting asphalt obtained using standard laboratory equipment in MSSR Julius Berger Nigeria Plc located in Abuja Nigeria. The aggregates were sieved and graded proportionately to obtain the required aggregate gradation in accordance to Nigerian General Specification for Road and Bridges (1999). Hot Mix Asphalt was produced with each at temperature ranging from 150°C to 165 °C, and the optimum bitumen content values for river gravel hot mix asphalt was at 6.0% and has a stability of 1,550(KN) which shows agreement with the standard for hot mix asphalt production.

Keywords: *Asphalt, Bitumen, Economy, Availability and River gravel.*

1. INTRODUCTION

Roads are established path over land for the passage of animals and vehicles (Mathew and Rao, 2006). These pathways helped in providing links, movement of people and goods from one place to another. The first footpath originated from animal paths and served as path for early hunters to reach the forest. Paths eventually grew around primitive settlements and as trade grew, longer routes were developed to transport food and other materials. The roads built by the ancient Romans were carefully planned and structurally constructed (Mathew and Rao, 2006). The increasing demand in the provision of better road, decreasing budgetary funds, and the need to provide a safe, efficient and cost effective road system has led to increase in the need to rehabilitate our existing pavement system.

Pavements are made up of several layers of different materials which functions as a structural element configured to support the wheel loads applied to the road and distribute them to the subgrade. There are two major types of road pavements namely flexible and rigid pavement. The following pavements: earth, stabilized soil and bituminous surfaces falls under the flexible pavements type (UNESCO-Nigeria Technical and Vocational project, 2008), but the rigid pavement roads are constructed to perform as a slab. It might be reinforced or mass concrete pavement with high modulus of elasticity and adequate rigidity.

While in the design of flexible pavement, the layers comprises of series of granite layer which is usually topped by a relatively high quality bituminous surface. This layers of granular materials helps to distribute and maintain load to the subgrade, the quality of these granite solely depends on the particle friction, interlocking property and strength. In the construction industry, series of granular materials can be used depending on their availability, cost and durability. River gravel is one out of such materials which is alternate materials used in road and asphalt production over the crushed stone due to its low cost effectiveness compared to crushed stone. River gravel can be used as sub-base, base and wearing surface of flexible pavement.

Asphalt is mostly used if heavy traffic is expected at the base layer. The sub grade strength has the greatest effect in

determining pavement thickness (UNESCO-Nigeria Technical and Vocational project, 2008). Generally, weaker sub grades require thicker asphalt layers to adequately bear different loads associated with different uses. The wearing surface receives the traffic and transfers its loads to the base, while at the same time serve as the base's protection material.

In achieving a comprehensive flexible pavement design procedure based on structural analysis, a complication in terms of difficulties in getting a performance model that relate the variety of pavement materials (river gravel) in relation to distress modes due to casual factors and in characterizing the component layers of the pavement structure to reflect stability.

Aggregates are of numerous types, depending on their source and properties, crushed gravel (granite) and river gravel, are the aggregates of major consideration in this study. Crushed aggregates whitish black aggregate obtained from rock blasting (which could be igneous, sedimentary or metamorphic rocks), texture and structural property places some rocks at a higher advantage over others in serving as aggregate materials. It is sourced naturally but becomes artificial after going through some changes in physical and mechanical properties. The relationship between specifications of crushed and river aggregates and their performance are often not well defined due to the fact that most specifications are based on experience with local materials. Density, durability and strength are parameter that plays important role in specification of these materials, because of the structural behaviour of the layers, being sub-base and base layer application in pavement structure. Worldwide, fundamental measures such as shear parameters from axial testing are used to satisfy this granular material.

Tensile strength, durability, economy, texture and availability of these materials play an important role in

their use, which include significant savings, resulting from the use of river gravel instead of crushed aggregates or beauty and readily availability of the crushed aggregates. Environmental issues around the use of non-renewable resources such as weathered gravels are becoming more important in developing economies and have been important for a long time in the developed world (RSDT, 2013). Even the very best calcretes and laterites perform almost as well as graded crushed stone and can be used for heavy traffic roads. However, River aggregates are always more variable than crushed aggregates (RSDT, 2013). On a general perspective more time and resources are observed to be saved in the application of river aggregates. Hence, this study tends to measure some characteristics, stimulating factors influencing the strength of the two separate aggregates

2. METHODOLOGY

The materials used for this study were river gravel/aggregates, bitumen, and produced asphalts, obtained from Kuta in Niger State. Standard method outlined in BS 812 was used to sample the river aggregates from a river in Kuta, Niger State. River aggregates is a common alternative material to crushed aggregates. On the other hand the bitumen used was grade 60/70, collected from Kaduna refinery and subjected to bitumen tests in accordance with Euro Code at the asphalt plant of Mssr Julius Berger Nig. Plc located at Mpape branch in Abuja, Nigeria. After sampling of the materials, laboratory tests such as specific gravity, water absorption, aggregate crushing value, grading of aggregates and sieve analysis of the aggregates used for mix-design using Job- Mix Formula method were carried out.

The following were the methods adopted in achieving the desired aim and objectives of this study; check on material adequacy, mix design, asphalt production and Marshall Stability test.

2.1. Physical Properties Adequacy of Materials

To ensure the effectiveness of the materials, tests were conducted in accordance to BS 812 on the sampled materials before and after mix. These tests include: aggregate specific gravity test, aggregate water absorption test, aggregate crushing value, sieve analysis and bitumen tests. Results for the above test are in Table 4 and Table 5 while grading envelope of the aggregates was also displayed in Figure 1.

2.2. Mix Design

Job mix formula was used to determine the required percentages for each graded aggregates sample as obtained in the sieve analysis which requires different percentages of aggregates and filler. The percentages and weights of the aggregates and filler used in the asphalt production are shown in Table 1. Also provided in Table 2 is the bitumen adding ranges as specified by Nigerian General Specification for Road and Bridge Works (1999) for wearing course in relation to sample weight.

Table 1: Percentage and weight of aggregates using job mix formula.

S/No	Aggregate sizes (mm)	Percentage of River Gravel/ Aggregates (%)	Weight of Aggregates (g)
1	9.5-19	15	180
2	4.75-9.5	20	240
3	0-5	50	600
4	Filler	15	180
Total			1200

Table 2: Percentage and Weight of Bitumen using Job Mix Formula.

S/No	Percentage of bitumen (%)	Weight of Bitumen (g)	Weight of Bitumen for Total Mix for Extraction, Specific gravity and Marshall Test (g)
1	5.0	60	360
2	5.5	66	396
3	6.0	72	432
4	6.5	78	468
5	7.0	84	504

2.3. Asphalt Production

The samples were prepared using Marshall Design Procedures for asphalt concrete mixes according to Nigerian General Specifications for Roads and Bridge Works (1999). The procedures involved preparation of series of test specimens for a range of bitumen contents such that test data curves showed well defined optimum values. The tests were conducted on the bases of 0.5 percent increments of bitumen content. In order to provide adequate data, three replicate test samples were prepared for each set of bitumen content used. During the preparation of the asphalt concrete samples, the aggregates were first heated for about 5 minutes to attain a temperature of 80°C bitumen was added to the heated aggregates and allowing proper absorption into the aggregates and properly mix with mixer and attaining a temperature not less than 150°C. Measured samples from the mix were taken for specific gravity and extraction after which the remaining 1200g was poured into mould and compacted on both faces with 75 blows using an automated 4.5kg-rammer falling freely from a height of 450mm. This process was repeated until last sample was done. The Compacted specimen was subjected to unit weight – Total Mix, Stability, Flow, Percent Voids – Total Mix and Percent of Total Voids filled with Binder tests. The results obtained are shown in Table 6 and used to determine the optimum bitumen content of the asphalt concrete.

2.4. Marshall Stability Test

This test was carried out to determine the durability of the produced Hot Mix Asphalts (HMA) of the river aggregates. Its a test that helps to determine the rate of deformation of asphalt to axle load. It can also be used to determine the optimum bitumen content that can provide stability, unit weight (density), flow, voids and voids filled with bitumen of the produced Hot Mix Asphalt. The standard requirement of asphaltic material is given in Table 3.

Table 3: Specified properties of compacted Asphalt Concrete according to the BS code:

S/No	Properties	Wearing Course
1	Optimum Bitumen Content	5-8%
2	Stability	≤3.5kN, ≤350kN
3	Flow	20 - 40mm
4	Voids in Total Mix	3-5%
5	Voids Filled with Bitumen	72-82%

3. RESULTS AND DISCUSSIONS

3.1. Physical Properties Adequacy

The test conducted on the aggregates material as shown in Table 4. This indicates that the major requirement of hardness and durability of a specified standard was also met by the river aggregates with crushing values of 26.3. Also looking at the specific gravity of the materials it was discovered that the materials also meet the specified standard relative to weight in quantity and volume. The water absorption rate of the river aggregates though high but still within the recommended range for asphaltic materials. The grading envelopes of the materials are presented in Figure 1.

Table 4: Specified Properties of Aggregate Test and Obtained Result from Kuta river gravel.

S/No	Properties	Specified Standard	Results obtained (River Agg)
1	Specific Gravity	2.4 – 2.9	2.65
2	Water absorption	0.2 – 1.5	0.947
3	Aggregate Crushing Value	≤ 30	26.3
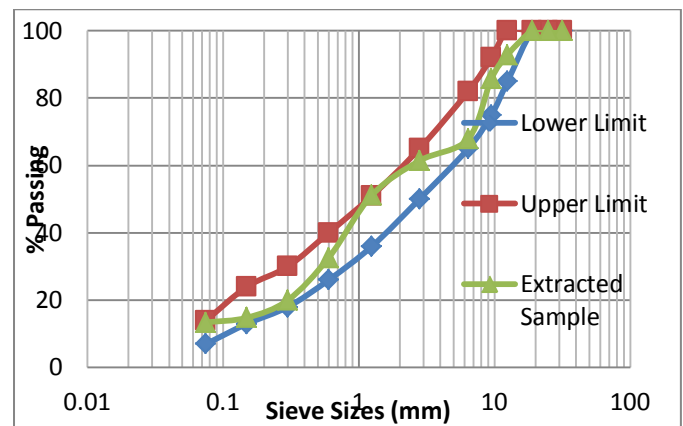
Figure 1: Gradation of river gravel

3.2. Bitumen Properties

The bitumen tests conducted was to check if the binder used was adequate and up to standard specified for Roads. It was further confirm that the bitumen used was adequate and up to standard and that the bitumen is grade 60/70 penetration. The results of the conducted test are presented in Table 5 to Table 8.

Table 5: Penetration Test Result

Trials	Penetration 1/10mm at 25°C
1	65
2	64
3	66
Average	65
Standard	60 – 70

Table 6: Specific Gravity Test Result

Trials	Softening Point R+B (°C)
1	305
2	295
3	300
Average	300
Standard	Not less than 230

Table 7: Flash Point Test Result

Trials	Specific Gravity(at 25°C)
1	1.037
2	1.044
3	1.042
Average	1.041
Standard	1.02 - 1.06

Table 8: Softening Point Test Result

Trials	Softening Point R+B (°C)
1	48.8
2	48.2
3	48.5
Average	48.5
Standard	46 – 54

3.3. Marshall Test Results

The total result obtained is shown in Table 9. From the table 6 the graphs the following parameters can be obtained; maximum unit weight (density), maximum stability, void in mix, void filled with bitumen, and optimum bitumen content.

Table 9: Marshall Test Result

Percent Binder content	5.0	5.5	6.0	6.5	7.0

Unit weight – Total Mix	2.335	2.340	2.360	2.366	2.350
Stability	1350	1380	1550	1540	1500
Flow	26.0	34.0	36.0	40.0	46.0
Percent Voids – Total Mix	4.1	4.5	3.3	2.6	2.1
Percent of Total Voids filled with Binder	73.4	73.5	80.6	85.1	88.4

3.4. Apparent Density (Unit Weight)

This is the weight of the sample after a certain amount of bitumen and compaction has been given to that sample. It shows how closely packed the aggregates are in a particular sample with the presence of the binder. Presented in Figure 2 is the graph showing the relation between the unit weight and percentage binder content of the samples. The graph shows an increase in weight with increase bitumen content until it reaches the optimum unit weight, then decreases and the maximum densities occurs at 2.360 for river gravel. The figure further shows that at binder content of 6.2% for the river gravel has a weight of 2.360 showing that the materials is suitable.
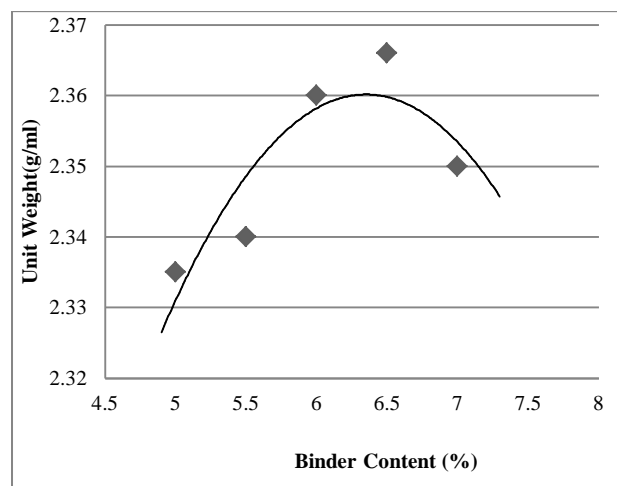
Figure 2: Graphs of Unit Weight against Binder Content

3.5. Marshall Stability:

Result of this shows the relationship between the corrected stability and the bitumen content of the sample. This graph shows an increase in strength as the bitumen content

increases, its reaches its peak and then decreases. The figure also shows that, at binder content of 6.25%, the river gravel has a stability of 1530N. The bearing capacity and the binder content conform to the specified standard (see Table 3) which confirms the reasonnableness of the determined optimum binder content.
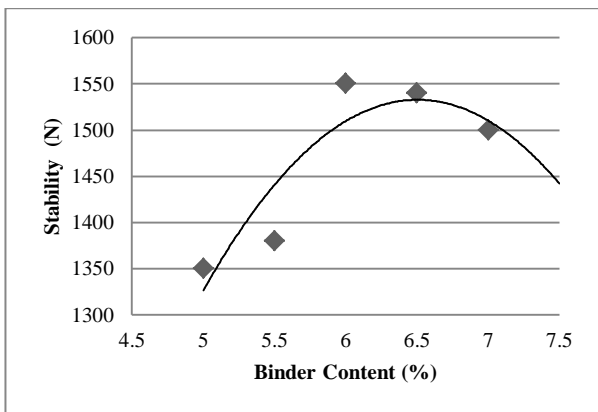
Figure 4: Graph of Stability against Binder Content

3.6. Flow:

This is the measure of the deformation of the sample or the total movement of strain in mm occurring in the sample of no load occurring at stability. The graph shows the relation between the deformation of the sample and the bitumen composition. It determines the bitumen content that correspond with the required air void. The figure also shows that at binder content of 6.0%, the river gravel has a flow of 36mm.
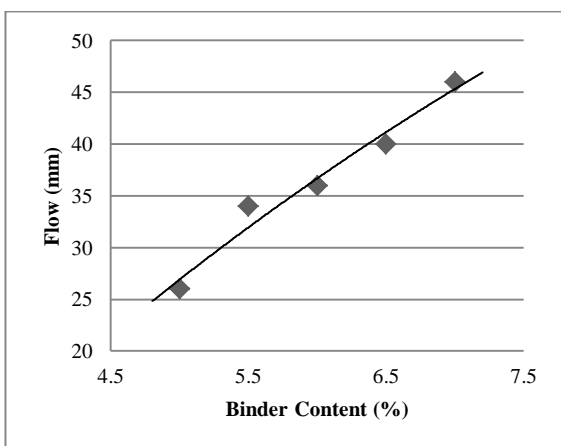
Figure 6: Graph of Flow against Binder Content

3.7. Percent Voids - Total Mix:

This is a graph showing the relationship between the percent voids in total mix and the binder content. This graph shows an increasing percentage air void with decreasing bitumen content till the maximum obtainable void value is reached then shows a decrease. The figure also shows that at binder content of 5.5%, the river gravel has a void of 4.5%.
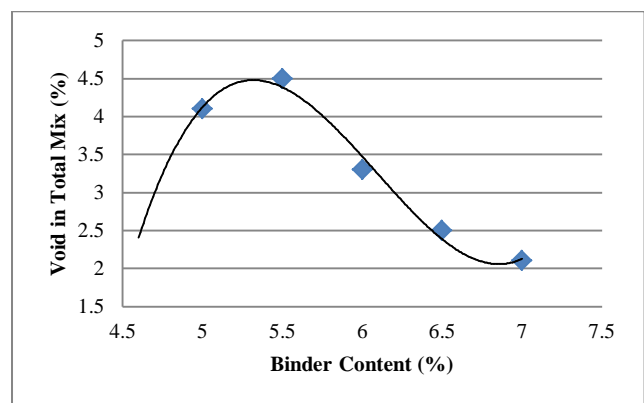
Figure 8: Graph of Percent Voids – Total Mix against Binder Content

3.8. Void Filled with Bitumen:

This graph shows the relation between the percentages of the total mixture filled with bitumen at relative bitumen content. The graph shows a curve of steady increase as the bitumen content increases. The more you increase the bitumen, the higher the void filled with bitumen. The figure also shows that at binder content of 6.7%, the river gravel has a void filled with bitumen of 87.6% which allows a permissible continuous compaction of about 13.4%.
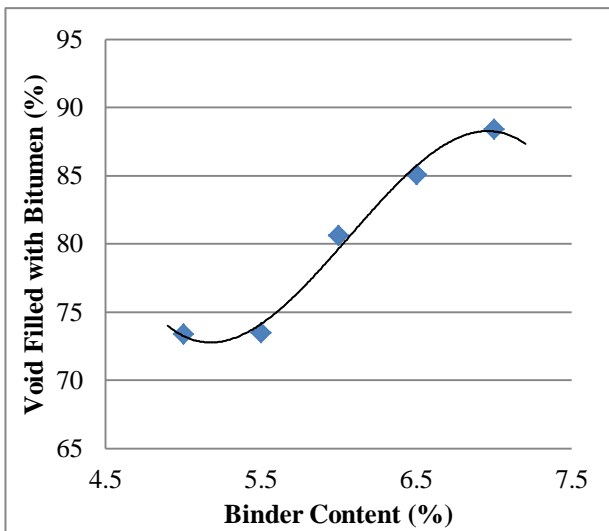
Figure 10: Graph of Percent of Total Voids filled with Binder against Binder Content

It is strongly believed that river gravel will be good for asphalt production, can be an innovative material in asphalt production thereby saving the environment from activities of blasting and other social problem associated with dynamite.

It is therefore recommended from the test results and conclusion that, river gravel asphalt can be recommended for use in road construction and maintenance work in Nigeria. This is because of the advantages it possesses over the crushed stone such as durability, less expensive, availability from natural source (rivers) and its minimal environmental hazards such as dust emission during blasting as is the case with crushed stone.

4. CONCLUSION

This research work on the Strength properties of river gravel in asphalt production compared asphalt standard as an alternative material for hot mix asphalt in Civil Engineering (highway Engineering) was focused on verifying the performance of river gravel in asphalt production and meant to check its potentials and possibilities for use in highway engineering. From the result obtained, it can be concluded that, the properties of the produced asphalt such as unit weight, stability, flow, percent voids in total mix and percent of total voids filled with bitumen met the standard specification for hot mix asphalt. Also from the graph, at optimum binder content of 6.2% the stability value of 1530N was obtained, this is in consonant with established standard for road design. If granite material is to be used for asphalt production the analyses has to be conducted on about four (4) samples and a blend of them all was needed for the requirement for asphalt production to be meet required blend, resulting to waste of time and resources while only single sieves analysis was required in the case of river aggregates.

REFERENCE

Use the Author and year style or IEEE style of referencing. Citations in the mainbody of text, appendices, tables and figures are to be made using the last name of the author (both authors when only two; first author plus et al. when more than two).For two or more papers published in the same year by the same author(s), add a, b, c, etc. to the year such as (1980a) or (1980b) and cite jointly as Jones et al. (1980a, b).

Do not use numbers in square bracket to cite reference in the body text rather insert citation within bracket as in (Sadiq and Nwohu, 2013). List of all references cited(including citations in tables, figures and appendices)in the body of text is provided in**alphabetically order** at the end of the paperaccording to the last name of the first author. The titles of papers, patents and books or monograph chapters, journal Volume,

issue/number and the initial and final page numbers are to be included.

REFERENCE STYLE

Asphalt Paving Association of Iowa, Asphalt Paving and Design Guide: 3408 woodland avenue suite 209 West Des Moines, IA 50266-6506: p 11-86.

Abraham, H. (1938) Asphalts and Allied Substances, (4th edition.). New York: D. Van Nostrand Co: p 11-16

American Society for Testing and Materials (ASTM), (2004). Test Method for Theoretical Maximum Specific Gravity and Density of Bituminous Paving Mixtures ASTM Designation D2041

Asphalt Institute, (2003). "Asphalt Hand Book," Manual series No. 04, Six Edition, Kentucky,USA.

Asphalt Institute, (2003). "Mix Design Method for Asphalt Concrete and other Hot-Mix Types," Manual series No. 02, Six Edition, Kentucky, USA.

Blades Christopher, Kearney Edward (2004), Asphalt Paving Principles, 416 Riley–Robb Hall Ithaca, New York 14853–5701: p 33-46

Colorado Asphalt Pavement Association (2006) 'Guideline for the Design and use of Asphalt Pavement for Colorado Roadways' 2nd Edition, 6880 South Yosemite Court, Suite 110 Centennial, Colorado.

Civil Engineering Napa, Adobe associate, Inc. (www.adobeinc.com).

Summers C.J. (2000/14), The Idiots Guide to Highway Maintenance.

David, M., Leonard W. (2007), 'Aggregate for Concrete' American concrete institute 38800 country club drive Farmington Hills, mi 48331 U.S.A: p 15-18.

Delmar, R. (2006), Asphalt Emulsion Technology, Transportation Research Board 500 Fifth Street, New Washington, dc 20001: p 2-5.

FERMA, (2010) 'Current and Management Conditions of Nigeria Road Network' Federal Road Maintenance Agency Abuja, Nigeria.

Smith, H.R., Jones, C.R. (1998) Bituminous Surfacings for Heavily Trafficked Roads in   Tropical Climates.

Paper 11513, p 28-33
.

FHWA (2013). "Functional Classification Guidelines" Federal Capital Territory, Abuja.

FMWH (1994), Manual of Pavement Design – 1994 Edition (FHWA), Part 4, Federal Ministry of Works and Housing, Abuja.

Krutz N. C. and P. E. Sebaaly (1993). The Effects of Aggregate Gradation on Permanent Deformation of Asphalt Concrete. In Proceedings, Vol. 62, Association of Asphalt Paving Technologists.

Momoh L. R and Fred E. A (2010) 'An Assessment of the Environmental Impact of Asphalt Production in Nigeria' Department of Geography and Regional Planning, Ambrose Alli University, Ekpoma, Edo State, Nigeria, p277-280.

Road Sector Development Team (RSDT), (2013) 'Road Sector Development Highway manual' Part1: Design, Volume 3; Pavements and material Design, Federal Ministry of Works, Abuja.

Road Note 19, (2002). 'A guide to Dense Bituminous Surfacing for developing countries' R6897, Department of International Development, 1 palace street London, UK, p 2-7.

Tom V. M and Krishna K V (2007). Introduction to Transportation Engineering.

(Unesco, 2008). 'Introduction to Highway Engineering' (Technical and Vocational Education, Version 1). P 5-40.

Urbanik, T. (2008) Road Redmond, WA: Microsoft corporation.

O'Flaherty C.A (1983)''Highway and Traffic'' Edward Arnold (publishers) Ltd. Second Edition.

Performance Metrics for Image Segmentation Techniques: A Review

Faiza Babakano Jada[1*], A. M Aibinu[2], A. J. Onumanyi[3]
[1]Department of Computer Science,
[2,3]Department of Telecommunications Engineering
Federal University of Technology Minna, Nigeria
[*]faiza.bkano @futminna.edu.ng , 08056307052

ABSTRACT

Image Segmentation has become a lot popular in recent years because of its application in computer vision and related field. This has led to an upsurge in different segmentation techniques from the research community. Different image segmentation techniques have their strengths and weaknesses and some are more geared to some specific application. The need to evaluate the performance of these techniques became necessary because of the autonomous system that do quite a lot of these segmentation. This paper reviews different types of metrics used for evaluating the performance of different image segmentation techniques. It was found out that some metrics are used by some specific image segmentation techniques and their strength and weaknesses are outlined.

Keywords: *Image, segmentation, performance, metrics*

1. INTRODUCTION

Image segmentation is an important step in the processes of Digital Image Processing (DIP). It is usually sandwiched between image pre-processing and image recognition stage. There are different techniques of image segmentation, these techniques include but not limited to clustering methods [1], thresholding methods [1], edge detection [1], region based methods [1], partial differential equations (PDE) [2] and artificial neural network (ANN) [2]. These methods can be largely divided into pixel-based methods (where pixels with similar features like color and texture are clustered) region-based methods (where pixels are clustered according to their similarities and spatial connectedness) and boundary-based methods (use pixels around the boundary of an object to define it).

Various Image Segmentation techniques have their advantages and disadvantages and some are more suitable for some applications than others. There is no comprehensive and standardized report for image segmentation evaluation metrics that can be used by evaluators. Since most of these performance measures are application dependent, naive evaluators can use the wrong metrics for the wrong application thereby giving inaccurate result. There is need to identify these metrics for measuring the performance of the different image segmentation techniques. This can be achieved if these metrics from the literatures can be thoroughly discussed, organized and summarized. Moreover, the strengths, weaknesses, adequacy and correctness of each of these metrics will be brought to light for image segmentation evaluators to make informed decisions while making use of them.

The outline of this paper is as follows: Section 2.1 gives an overview of Image Segmentation techniques. Section 2.2 discusses some of the Image Segmentation Evaluation Techniques while section 2.3 describes the performance metrics used for by the evaluation methods. Finally, conclusions are drawn in section 4. .

2. METHODOLOGY

2.1 Image Segmentation Techniques

The two main objectives of Image Segmentation are to decompose image into parts for further analysis and to perform a change of representation, which involves organizing the pixels of the image into higher-level units that are either more meaningful or more efficient for further analysis [3].

This makes image segmentation a central part in digital image processing for computer visions, robotic navigation,

content-based image retrieval and etc. There exist lots of image segmentation algorithms and the list can barely be exhausted. From the more traditional threshold method [1], clustering method [1], gradient based methods [2], region-based methods [1], gray histogram methods [2], graph partitioning methods to more recent algorithms like the Mean Shift Segmentation[4], Modified Recursive Shortest Spanning Tree (MRSST) [4], Normalized-cut method (NC) [5], Efficient graph-based method (EG) [5], Ratio-cut method (RC) [5].

With the numerous number of image segmentation techniques in existence, there have been several efforts to categorize them into different groups. Based on the criteria used for the groupings, the groups are not mutually exclusive hence some segmentation algorithms can be found under more than one category. Table 1 shows some of the grouping of image segmentation techniques found in the literature.

Table 1: Different Categorizations of Image Segmentation Techniques

Segmentation Techniques Categorization	
Category A from [6] phylosophical	a)Edge based b) Point/Pixel based c) Region based and d) Hybrid approach
Category B from [7]	a) Color based b) Texture based algorithms.
Category C From [8]	a) Classical and targeted segmentations b) Segmentation based on minimizing a piecewise-smooth Mumford-Shah functional on a graph c) Segmentation based on active contours without edges d) Random walks algorithm based segmentation e) Segmentation of non-homogenous regions of an image based on an energy fitting minimization f) Segmentation of non-homogenous regions of an image based on the level sets method
Category D from [4]	a) Mean Shift Segmentation (MS) b) Region Based Automatic Segmentation (RBAS) c) Modified Recursive Shortest Spanning Tree (MRSST) d) Spatio Temporal Video Segmentation (SEG2DT)
Category E from [1]	a) Clustering. b) Edge Detection, c) Multiple Thresholding and d) Region-Based
Category F from [9]	a) Seeded Region Growing b) Interactive Segmentation Using Binary Partition Trees

The first category consists of well-known classification for image segmentation techniques. These techniques include finding out the edges or boundary of an object. Chain-code is an example of a method that can be used for determining the edge or boundary of an object. Region growing method involves initial selection of seed points where neighbouring pixels are examined to determine if they belong to that region. Region based method is sometimes referred to point based image segmentation because an initial selection seed point is needed Hybrid method uses the combination of two or more types of the segmentation methods. A combination of region-based and edge-detection methods is an example of hybrid method. Another major classification of Image segmentation is color-based and texture based segmentations. These methods are categorized under second category. While the former groups pixels based on their color, the latter groups the pixels based on their textures.

The categories C and D are some examples of hybrid methods of image segmentation discussed previously. Most of them are developed for some specific applications. Category E as described by [1] involves segmentation methods like clustering, edge-detection, thresholding and region-based. Clustering is an unsupervised method of data analysis and is broadly divided into partitioning and hierarchical methods. Example of clustering algorithms include the K-means algorithm, Fuzzy C-means algorithm (FCM), the Expectation Maximization algorithm, Minimum Spanning Tree (MST) algorithm and etc

2.2 Image Segmentation Evaluation Techniques

Recently, there have been lots of interests in evaluating image segmentation techniques. Motivation for this is due to optimizing the existing techniques. Thus evaluation techniques are developed to aid embedded/autonomous system make the choice of the best segmentation method to apply for a particular image. Though no single approach can be said to be the best, some methods perform better for some images than others.

Zhang et al. in [10] broadly divided the segmentation evaluation techniques into Subjective evaluation and Objective evaluation depending on whether human being has evaluated the image visually or not. Subjective evaluation is the most common form of evaluation method where a human compares the segmentation results from different segmentation algorithms. On the other hand, Objective evaluation can further be divided into supervised and unsupervised methods. Supervised method requires access to ground truth segment (manually segmented reference image) while the unsupervised method does not require access to the ground truth.

The most traditional and common metrics used in performance analysis of different image segmentation techniques is the subjective methods. This means that a segmented image is compared with the original image by human inspection. However, this method is so cumbersome that it cannot be used for large number of images; more so different humans can rate the performance differently because human interpretation can be highly subjective. With the advent of more independent metrics like mean square error, entropy, color difference between regions and etc [10], the need to review these metrics became necessary.

Another categorization of image segmentation evaluations according to [4] are the theoretical and experimental. The experimental can be further divided into feature based and task based. Feature based is then divided into one with ground truth and one without ground truth.

3. RESULTS AND DISCUSSIONS

3.1 Performance Metric for Image Segmentation Algorithms

There are presently lots of unsupervised evaluation methods of image segmentation these include F', D_{WR}, E_{CW}, Busy, SE, SM and etc [10]. These evaluation methods are based on metrics like color error, metrics based on squared color error, metrics based on texture, metrics based on entropy, metrics based on average color between regions, root mean square error, metrics based on difference of color along local boundaries, metrics based on barycentre layout and metrics based on layout entropy [10].

Different researchers have been creating different metrics to objectively evaluate image segmentation algorithms, among which are Normalized Probabilistic Rand (NPR) by [12], metric based on the distance between segmentation partitions proposed by [13] and etc. Many of the performance metrics applied to large set of images shows that some of the metrics suffer from under-segmentation bias while others suffer from over segmentation bias.

Some other unsupervised evaluation criteria of segmentation results had been compared in the work of [11] namely: Zeboudj, Inter, Intra, Intra-inter, Borsotti and Rosenberger. Intra-region uniformity metrics measures the intra–region uniformity to get the performance of segmentation. Examples of Inter-region metrics are Color error, Texture, Squared color error and Entropy. The Inter-region disparity metrics on other hand includes metrics based on region color difference, local color difference, metrics based on Bary Center distance and metrics based on layout entropy.

Metrics based on color error compares the difference between a pixels original color with the average color of its region based on some pre-specified threshold value in E_{CW} evaluation method. If the value is higher than the threshold, then it is termed misclassified pixels. Z_{eb} and D_{WR} classification methods also use metrics based on square error. The squared color error metric is the square of the color and is used by evaluation methods like F, F', Q, FRC. Metrics based on texture measures the uniformity of texture of a region and is used by evaluation methods like FRC and Busy. Metric based on entropy is used by evaluation methods like E and H_r.

Mean weighted distance was a metric used by Sapna et al. [1] for evaluating different segmentation techniques including clustering, thresholding, region-based and edge-detection. Normalized Probalistic Random index is the metric used by Unniskrishnan et.al in [12] to measure the performance of image segmentation techniques. Sughandi et al. in [14] suggested quantitative measures like discrete entropy, root mean square error and visible color difference for color image segmentation algorithms.

Table 2.2: Examples of Performance Metrics for Image Segmentation Techniques

Paper	Evaluation Metrics used
[10]	Color error Texture Squared color error Region color difference Local color difference Entropy
[1]	Mean weighted distance
[15]	PETs Metrics (Young DP) including *Overall regions (OR)* *Merged regions (MR), Accuracy ACC [4]* *Negative rate metric (NRM).*
[10]	Fuzzy metric B. McGuiness Evaluation Measure, A. Unnikrishnan Probabilistic Rand Index

Finally, Jaime et al. [15] proposed a metric that can be used for all applications that will give correct result provided that reference segmentation is available. The method can estimate the quality of segmentation the same a human observer can do. Though it is a step forward, the required reference segmentation makes dependent on human intervention. An ideal one would have been one without requiring a ground truth.

Table 2: Examples of Performance Metrics for Image Segmentation Techniques

S/N	Metrics	Type	Metric Strength	Metrics Weakness
1	Color error	Intra-region uniformity measure	Ideal for D_{WR}, E_{CW} and Zeb evaluation methods	Too sensitive to noise.
2	Squared color error	Intra-region uniformity measure	Ideal for F_{RC}, η, PV, NU, F, F`, Q evaluation methods	Not ideal for noisy/textured images
3	Texture	Intra-region uniformity measure	Ideal for Busy, PV, V_{CP}, F_{RC} evaluation	Causes under segmentation
4	Region color difference	Inter-region disparity measure	Ideal for Ŋ, PV, F_{RC}, evaluation methods	Assume a single underlying distribution(eg Gaussian distribution)
5	Local color difference	Inter-region disparity measure	Ideal for V_{CP}, Zeb, V_{EST} evaluation methods	Do not complement the inter-region uniformity measures.
6	Layout Entropy	Inter-region disparity measure	Ideal for SE, E evaluation methods	Rely on low- level feature extraction and not semantic meaning of segments
7	Barycenter distance	Inter-region disparity measure	Ideal for F_{RC} evaluation methods	Assume a single underlying distribution(eg Gaussian distribution)
8	Shape	Shape measure	Ideal for SM, V_{CP} evaluation methods	Highly dependent on application and type of images

4. CONCLUSION

Reviews of different technique of image segmentation from literatures have been presented in this work. Additionally image segmentation evaluation techniques and the underlying metrics used by these metrics are discussed. The metrics are listed; the evaluation methods that used them are also listed. The type, strength and weaknesses of each metric are outlined. It is concluded that the evaluation methods are highly dependent on the underlying performance metrics and consequently affects the evaluation results given by such techniques. Problems like noise, under segmentation, use of low-level features for evaluation and assumption of single underlying distribution and all concerned with the underlying metric used by that evaluation technique .Future work include trying to solve the shortcomings of these metrics and consequently the short coming of the evaluation methods that uses them.

REFERENCE

[1] S. V. Sapna, R. Navin, and P. Ravindar, (2009). Comparative Study of Image Segmentation Techniques and Object Matching using Segmentation.

International Conference on Methods and Models in Computer Science (ICM2CS),

[2] R., Dass, Priyanka and S. Devi. (2012). Image Segmentation Techniques. International Journal of Electronics and Communication Technology (IJECT). Vol 3 Issue 1, 2012

[3] R. C Gonzalez, Richard E. Woods, Steven L Eddins "Digital image Processing using Matlab" Prentice Hall publication.

[4] L.Goldmann1, T. Adamek, P. Vajda, M. Karaman, R. M¨orzinger, E. Galmar, T. Sikora, N. E. O'Connor, T. Ha-Minh, T. Ebrahimi, P. Schallauer, and B. Huet. (2008). Towards Fully Automatic Image Segmentation Evaluation. Advanced Concepts for Intelligent Vision Systems Lecture Notes in Computer Science. Volume 5259, pp566-577

[5] F. Ge, S. Wang and T. Liu. (2007). New benchmark for image segmentation evaluation. *Journal of Electronic Imaging 16(3), 033011 (Jul–Sep 2007)*

[6] V. Deya , Y. Zhang , M. Zhong.(2010). A Review on image segmentation techniques with remote sensing perspective, IAPRS, Vol XXXVIII, Part 7A, July 5-7

[7] D. Guo, V. Atluri and N. Adam. (2005). Texture-based remote sensing image segmentation In: Proceedings of IEEE International Conference on Multimedia and Expo, pp 1472-1475

[8] M. Weingart and O.Vascan.(2013)Image Segmentation Processing- Some Techniques and Experimental Results. 4th international symposium on Electrical and Electronics Engineering (ISEEE 2013). Pp 1-8

[9] E. Askari, A. M. E. Moghadam. (2011). A Fuzzy Measure for Objective Evaluation of Interactive Image Segmentation Algorithms. IEEE International Conference on Signal and Image Processing Applications (ICSIPA2011)

[10] H. Zhang, J. E. Fritts, S. A. Goldman. (2008). Image segmentation evaluation: A survey of unsupervised methods. Computer Vision and Image Understanding 110(2008) pp 260-280

[11] R. Unnikrishnan, C. Pantofaru, M. Hebert. (2005). A Measure for Objective Evaluation of Image Segmentation Algorithms. IEEE Computer Society Conference on Computer Vision and Pattern Recognition(CVPR2005). pp34

[12] S. Chabrier, H. Laurent and B. Emile. *(2005).* Performance Evaluation of Image Segmentation. Application to Parameter Fitting.. *IEEE International Conference on Pattern Recognition*, 3:576–579, (EUSIPCO 2005).

[13] Sugandhi V. Dr. S. Sharma and C. Marwaha. (2013). Performance Evaluation of Color Image Segmentation Using K Means Clustering and Watershed Technique. 4th ICCCNT 2013 July 4-6, 2013, pp 1-4

[14] S. C. Jaime, and C.Luis (2005). Towards a Generic Evaluation of Image Segmentation. IEEE Transaction on Image Processing. Vol 14, No11

[15] S. Chabrier, B. Emile, H. Laurent, C. Rosenberger, and P. March´e. (2004)Unsupervised evaluation of image segmentation: Application to multi-spectral images. *IEEE International Conference on Pattern Recognition*, 3:576–579

Performance Evaluation of Enhanced Least Significant Bit Audio Steganographic Model for Secure Electronic Voting

Olaniyi Olayemi Mikail[1], Folorunso Taliha Abiodun[2], Abdullahi Ibrahim Mohammed[1], Nuhu Bello Kontagora[1], Abdulsalam Kayode Abdusalam[1]

[1](Computer Engineering Department, Federal University of Technology, Minna, Niger State, Nigeria)
[2](Mechatronics Engineering Department, Federal University of Technology, Minna, Niger State, Nigeria)
*mikail.olaniyi@futminna.eu.ng,.

ABSTRACT
This paper presents performance evaluation of an enhanced Least Significant Bit (LSB) audio steganographic model for secure electronic voting. The enhancement on the traditional LSB audio steganographic technique on the electronic vote was achieved through the hidden of secret information from fourth bit to sixth bit position. The sampled votes were digitally signed to ensure the integrity of the casted votes. The model was evaluated objectively using three quantitative metrics: Embedding capacity of the stego audio file, Mean Square Error (MSE) and Peak Signal to Noise Ratio (PSNR) of the cover and stego audio. The results of the quantitative evaluation of the model showed that the model was robust and imperceptible for the delivery of transparent and credible secure e-voting of high electoral integrity and confidentiality in developing countries of significant digital divide.

1. INTRODUCTION

Democratic decision making in modern society have been transformed by the introduction of Information and Communication Technology (ICT). This introduction termed, electronic democracy(e-democracy), have added improved accessibility, accuracy, reduced cost and fast casting, counting and timely dissemination of electoral results to wider populace. The most important element of democracy is the voting procedure of the electorate. The introduction of ICT in this critical element of democracy is called electronic voting (e-voting)[22]. E-voting as a distributed social information system is a security-critical application of democracy with the usage of computerized infrastructures in ballot casting as reasonable alternative to traditional procedure of opinion expressing procedures [22, 26]. Electronic voting is seen as a tool for making the electoral process extra efficient and for increasing trust in its administration. Properly executed e-voting solutions can increase the security of the ballot, speed up the processing of results and make voting a stress-free exercise.

Every electronic voting system design must fulfill certain fundamental requirements which provide a platform for delivery of a reliable, impartial and confidential election. These requirements are: Non-repudiation, accessibility, transparency, auditability, confidentiality, integrity, authentication, and non-coercibility [15].In view to produce excellent and effective democratic processes, the aforementioned criteria must be taken into consideration. Other basic criteria are [13, 14,11]:

i. **Accuracy:**All valid votes must be recorded accurately and the result must be correct.

ii. **Democracy:** Democratic principles must be enshrined through single citizen single vote mechanism and those votes must count.

iii. **Ease of access:**The developed system must be easily and readily accessible to the electorate with minimal complexity.

iv. **Transparency:** This is the quality of the developed system to be free from ambiguity.

v. **Security:** This is the protection of castedvotes from spoofing and falsification for all phases of electioneering process.

vi.   Verifiability: the casted votes must be check-balanced to ensure they meet up the basic requirements of the system.

Security in e-voting is the critical requirement amongst the aforementioned criteria whose purpose is to safeguard valued electronic data during casting, transmission, collation and audition [26]. Insecurity in voting can cause electorates to lose confidence in electoral activities. The root of credibility in democratic decision making in developing countries lies in proper provision of security requirements as well as other issues such as legislation, usability, convenience and universal accommodation of able and disable electorate in political decision making processes. The generic security issues of electronic voting systems include: authentication of near and remote voters, integrity, confidentiality and availability of electronic ballot in transit as well as verification of casted and counted votes. It is invariably impossible to develop a system that is perfect or fault free but if salient security requirements like authentication, integrity, confidentiality and verification of electorates of casted votes can be handled other features of availability and universal verifiability could be handled for the delivery of credible electronic voting exercise [13].

In this work, we present the performance evaluation of an Enhanced Least Significant Model ofSecure electronic voting as anticipated in [25]. Steganography is the science of keeping the existence of secret message in innocent media for covert communication in an unsecured channel. Since electronic voting involves secret and confidential decision making of an anonymous electorate [12]. Careful application of steganographic techniques in electronic voting could assists to deliver credible secure e-voting. In this contribution, we investigate performance of the model proposed in [25] objectively in view to guarantee a secure electronic voting. An enhanced LSB audio steganographic technique was used to develop a secure system that can

significantly cater for security issues pervading different phases of electronic voting system in our contemporary world. Steganography is an information hiding technique for communication between source and destination from third party. This communication through invisibility of voter's choice by hiding it in unobjectionable carrier file is proposed in audio medium in this work.

The paper is organized into five sections: Section two provides the review of related works,, model designed consideration was presented in section three, performance evaluation of model was accomplished in section four. Section five concludes and provides opens issues for future research.

2.   RELATED WORKS

There are several related works in literature that exploited the science of steganography for computer security especially in the field of electronic voting system design for credible and confidential electioneering process.

The design and development of a secure electronic voting system using a multifactor authentication and cryptographic hashing function were presented in [13]. In this work, significant attempt was made to improve the authentication of electorates before casting their votes as well as the integrity of the vote after being casted. After a unique id was generated, a unique short message service (SMS) code was automatically generated for instant authentication of voter. Only two of the security issues mentioned in [12] were tackled in [13] which are authentication and integrity. Hence the efficiency of the system cannot be guaranteed with only two security challenges addressed in [13]. Biometrics was added to the advantage of steganography in online voting system security in [20]. Complementary security systems are good

enough to guarantee secure voting process especially where password is added. The fingerprints of the voters were used as cover object for embedding voters' secret information. Personal Authentication Numbers (PAN) was used to authenticate voters for who they are. PSNR of the images range between 30-50db for scheme imperceptibility, but spatial domain steganography without any enhancement proposed is not secure enough to guarantee and effective secure e-votiing.

Authors in [4] designed a secure e-voting system based on homomorphic property and blind signature scheme. The proposed system in this work was implemented as embedded system on voting machine. This system employs RFID smart card to store all conditions that comply with the rule of the government to verify voters' eligibility. Central Tabulation Facility (CTF) was adopted to collect all secret ballots from local committee severs distributed across pole stations. The proposed system utilises homomorphic cryptosystem implemented using Paillier cryptosystem and blind signature based on RSA. The information stored in the RFID tags were used to track the activities of the voter and hence he/she cannot vote more than once. Security analysis was carried out using eligibility, secrecy, uniqueness, privacy and accuracy. The designed system was not in any way evaluated based on the specified issues it was built upon.

Since the major bone of contention in online voting system is information security, authors in [6] developed an online voting system powered by biometric security using steganography. The combination of science of cryptography with steganography in [6] added higher security. Fingerprint image was used as cover object for steganography while key generated was used to achieve cryptography. Cryptography helped to reduce to a great extent the risk of the system being hacked as hackers must find the secret key as well as the image. The merging of the secret key with image resulted into stego image which

is similar to the cover image with no significant difference for detection by human eyes. The strength of the system lies in the cascading of different security platforms to make the system as a whole. However, the system is limited to large information overhead that must be processed and limited consideration for integrity of hidden vote on transit.

In [22] and [23] several steganographic techniques were analysed implanting them in various categories of steganography such as text, image, audio and file system. Also, [9] demonstrated the advantages of the techniques in [22] emphasising the fact that transform domain can ensure high embedding capacity with perceptual transparency than temporal domain. A survey was carried out on general principle of hiding in information security for audio carriers in [23]. In [1], a review was carried out on binary image steganography and watermarking analysing different techniques in each domain. Different factors in watermarking and steganography were considered such as visual quality, embedding capacity, security, robustness and computational complexity in [1] for image based processing in spatial and transform domains. The limitation of image steganography is such that it can only hide limited amount of information, therefore, making it attributed to low embedding capacity and perceptual transparency.

A steganographic system for data hiding in video/audio was proposed in [5]. The system successfully hides information in different data format but the limitation is such that only small information of few bytes can be hidden in the cover files. Lempe-Ziv-Welch (LZW) universal lossless data compression technique was used for hiding information coupled with AES encryption and decryption algorithms. Hiding encrypted data in audio wave file was done by [17] building on a secret key steganographic system. The proposed system was

developed for message encryption using Data Encryption Standard (DES) and was evaluated using Signal to Noise Ratio (SNR). Authors in [16] developed apeak-shaped-based steganographic technique for mp3 audio using LSB steganography based on the MDCT by applying PSB algorithm. The Peak Shaped Model algorithm that is used for JPEG images was modified to be suited for MP3audio file in other to implement a good steganographic technique. Proposed work was actualized based on statistical properties of MP3 samples, which were compressed by Modified Discrete Cosine Transform. These coefficients were chosen with regards to the statistical relevance of individual coefficients within the distribution. The embedding capacity after performance evaluation was 12.5% and PSNR is 58.21db.The shortfall of [16] was in the low resistance to statistical attack through steganalysis.

Audio in Image Steganography based on Wavelet Transform was proposed in [7]. The work proposed an audio-image steganography, hiding an audio file inside a cover image using LSB technique and wavelet transform. The audio file was first compressed, embedded in the cover image, extracted and then reconstructed. Wavelet was achieved by carrying out some compaction ratio. Compaction was carried out in two level Haar, Daubechies and Coif wavelets. Increase in the audio file causes a corresponding decrease in the PSNR. The speech has high MSE property which cannot ensure enough safety and the size of embedded speech can significantly destroy the image if too large.

Secure Scheme in Audio Steganography (SSAS) was proposed in [10]. The authors designed a system to increase the security by addressing secret message before embedding using mathematical model and map for subsequent extraction of the secret message. The work

proposed a new technique for audio steganography using a two phase approach. The stego math selection phase embedding and extracting phase. Stego embed for embedding and P_Map for extraction. A secure stego object was obtained as the output by subjugating or abridging the probability of attach on the secret message or exchanging it. The integrity of the secret message was not put into consideration. The fourth position LSB algorithm was used for embedding with is not safe enough but rather can be improved upon to guarantee a secure information protection

In [2] authors worked towards improving robustness of security through the use of concept of Discrete Wavelet Transform (DWT) and Least Significant Bit (LSB) on audio steganographic method. Image was embedded inside a cover audio and the stego audio obtained was compared with simple Least Significant Bit insertion method for data hiding in audio. The cover audio was first converted to streams of bits; the image is also converted to bit streams and then embedded inside the cover audio. DWT was applied on the audio file for taking the higher frequency and generate a random key. 8×8 blocks for each 16bits data was taken and the last 3bits data was used to store image in the cover audio. Inverse of the algorithm was also designed for extraction of the image from the stego audio. Generation was described in detail for embedding and extracting of the image which gave a reasonably good result PSNR of more than 30decibel.

This work made a significant improvement over [2], [4], [7], [10] and [16] through the proposed enhanced LSB audio steganographic technique. Taking advantage of the advantage of Human Auditory System (HAS), we developed a technique to improve information secrecy without noticeable difference to human hearing. Our developed model provided solution for voter's

authentication as well as protection of casted votes from eavesdroppers, hackers and imposters while transmitting electronic ballot over insecure networks. This work improves on similar models in literature with the insertion into sixth bit of the LSB of the cover audio, thereby making the designed model a vehicle for the delivery of credible future e-election in societies where digital democratic dispensation is practiced.

3. MODEL ARCHITECTURAL DESIGN

The designed model shown in Fig. 1 embodies two exceptional security requirements of voting system which are: integrity and confidentiality of vote using object oriented design (OOD) metaphor in Unified Markup Language Activity diagram. Two security layers are implemented in aspects of digital signature for the vote integrity and enhanced LSB audio steganographic technique for the confidentiality of the casted votes. The

proposed e-voting model was structured around pre-electoral, electoral, and post electoral phases of e-democratic decision making in Fig. 2. The architectural design in Fig. 2 was adapted to tackle three security issues where RFID cards were used for voter's authentication and verification, digital signature were appended to the votes for integrity control and enhanced LSB audio steganography caters for the system confidentiality. The whole electioneering processes were layered into three phases of electoral processes; pre-election phase, election phase and the post-election phase of the voting exercise.. Voter's registration was carried out at the front end which is the pre-election phase. The candidates, parties and electorates information are documented for use in the subsequent phases. This information includes: name, phone no, sex, marital status, age, occupation and so on. This information helps to verify the eligibility of participants in the exercise and hence for system audit.
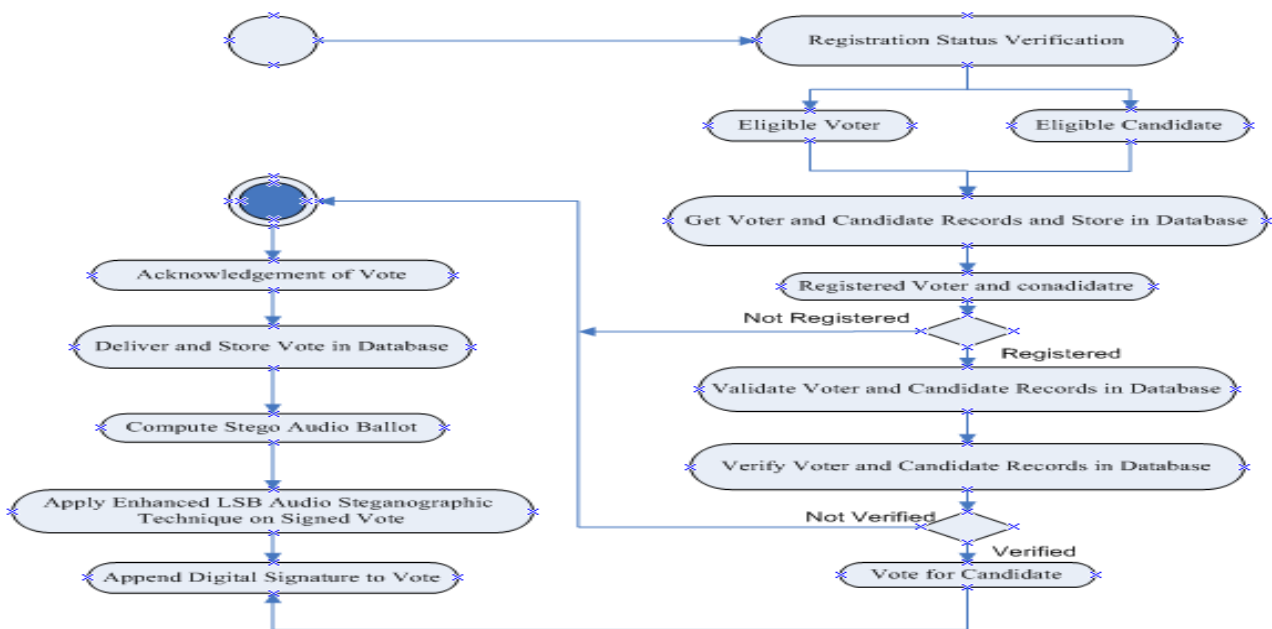
Fig. 1: Enhanced LSB Audio Steganographic Model of Secure E-voting System
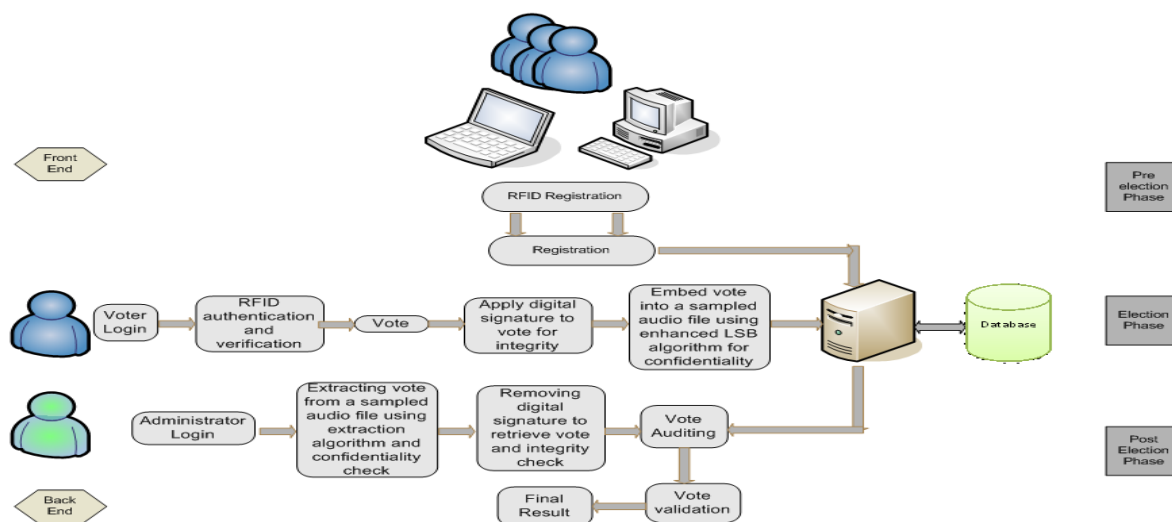
Fig. 2: Secured Electronic Voting System Architectural diagram (adapted from [26])

From Fig. 2, the model was designed around a kiosk type voting system where voters are made to move to a particular voting site for the first two phases of the electioneering process. In the registration phase, each voter is assigned a unique RFID tag which stored the voter's details in the database for further validation and verification in the election phase. This RFID tag was designed for voter's identification during voting, which is further check-balanced with the ID digit stored in the database. The casted vote (V) is sampled and digital signature is appended on it using vote MD5 hashing technique. The resultant digital object is then embedded with embedding algorithm (Em) in a digitized cover audio file using enhanced LSB audio steganographic technique of information security. Stego audio file is the end object which possesses no suspicious difference from the cover audio and the vote can be extracted by the administrator using the reverse mechanism.

In the post-election phase in Figure 2, the administrator retrieves the casted vote (V) from the stego audio (A) file using the extraction algorithm (Ex). This technique helps to protect the confidentiality of the votes from any suspicious knowledge of any adversary, imposter or hacker. This system ensures high perceptual transparency, payload capacity and reasonably robust against attack.

Our proposition is an improvement over [6], [8] and [10] from with respect to the use of RFID for voter's authentication and convenience. The electorate is only required to move his/her RFID card to the tag reader for automatic verification of ID. This has created an authentication and verification mechanism for electorates without any inconvenience. After casting vote, it is then hashed automatically application of MD5 hashing algorithm for integrity control over the casted votes. The digitally signed vote is then hidden in the sixth bit position of the sampled audio for an enhanced LSB audio technique to improved technique over the existing methods adopted by most systems designers as shown in both schemes for embedding and extraction illustrates as follows:

The following algorithm describes the embedding and extracting processes of information security on the electronic ballot:

Embedding algorithm

Input: A wave (.wav file) source audio and a payload file (vote in text form)

Output: A stego wave audio

Begin

1. Read the header information from the source audio file and generate compresses output audio file.
2. Generate 128-bit message digest(MD5 hash fuction)
3. Generate 32 digit hexadecimal text value of the vote(payload)
4. Repeat the following steps until 32-bit payload size(in bytes) are embedded:
   a. Read a sample amplitude value from the source audio file
   b. Apply the enhanced LSB algorithm on the sixth bit position to the LSB for payload embedding
   c. Write the sample value as the output audio, the stego wave audio.
   d. stop

End

Extraction algorithm

Input: A stego wave audio

Output: The extracted payload and the message digest

Begin

1. Read sample amplitude of the stego wave audio file as input.
2. Apply the inverse of the enhanced LSB algorithm on the sixth bit position to the LSB for payload extraction
3. Extract the payload
4. Extract the message digest of the payload
5. Generate 128-bit message digest (MD5-hash function) of the extracted payload.
6. Compare the two message digests to verify the authenticity of the extracted payload.
7. Save vote
8. Increment vote count by 1

End

4 MODEL PERFORMANCE EVALUATION

This entails the assessment of the developed model to determine whether it meets up with the set goal and performance as expected of an electronic voting system [15]. This can be carried out in two broad categories of subjective and objective evaluations. Subjective evaluation describes the process of subjecting the stego audio to

steganalytic test and listening hears of electoral officials, voters and observers were allowed to test the system in view to detect the slightest change in the audio files both stego and cover audio. Steganalysis tried to detect any hidden content in a digital file suspected to be carrying hidden information. This technique also exploits the disadvantages of Human Auditory System (HAS) thereby taking advantage of the disadvantage of human hears. At certain frequency, sound are not audible to human hears and this is therefore being capitalized upon. Subjective evaluation model have been carried out in [25]. In this paper, the developed model was evaluated objectively through embedding capacity, Mean Square Error (MSE) and Peak Signal to Noise Ratio (PSNR). This evaluation was carried out with regards to the three basic properties of information security: robustness, imperceptibility and payload capacity.

4.1 Objective Evaluation

This is the process of evaluating the perceptual transparency of the stego audio and embedding capacity. This describes the techniques used for detection of the level of efficiency and effectiveness of the algorithms used to develop the system.

4.1.1 Embedding Capacity

This refers to the maximum amount of information that can possibly be hidden inside a cover audio without consequently damaging or scathing the quality of the audio file. It is calculated by evaluating the ratio of the amount of secret message to that of the cover audio object.

$$EC = \frac{Size\ of\ secret\ message}{Size\ of\ cover\ object} \qquad (1)$$

4.1.2 Mean Square Error (MSE)

This is an error metrics used to represent the cumulative square error between the original audio signal and the

compressed audio (stego audio). The lower the value of the calculated MSE, the lower the error rate between the samples which shows little distortion was introduced. It is calculated by the following formula.

$$MSE = \frac{\sum_{M,N}[I_1(m,n) - I_2(m,n)]^2}{M*N} \qquad (2)$$

Where M and N are the rows and columns of the audio samples respectively. I_1 is the stego audio while I_2 is the cover audio.

4.1.3 Peak Signal to Noise Ratio (PSNR)

This is used to estimate the amount of similarities that exist between the cover audio and the stego audio. It is a function of Mean Square Error (MSE). It is a ratio of quality measurement between the two files calculated in decibels. The higher the PSNR of the comparison, the better the analysis demonstrating low distortion of the stego audio generated from cover audio

$$PSNR = 10 \log_{10} \frac{R^2}{MSE} \qquad (3)$$

Where R is the minimum fluctuation in the stego audio which is usually 255 in integer data type

4.2 Results of Objective Performance Evaluation

The outcomes of the tested developed system are described in Tables 1 and 2. Table 1 shows the audio samples evaluation with the various sizes, bit rates and embedding capacity. Table 2 on the order hand shows the results obtained from stego audio analysis after evaluating their Mean Square Error (MSE) and Peak Signal to Noise Ratio (PSNR). These analyses on MATLAB software tool obtained are tabulated as follows:

Table 1: Embedding Capacity of Audio Files

Audio File	Audio Size(KB)	Bit Rate(kbps)	Embedding Capacity (%)
Bom	768	88	0.23
Corn	415	176	0.43
One	78.1	128	2.27
Samp	434	705	0.41
Pledge	348	176	0.51

Table 2: MSE and PSNR of the Sampled Audio Files

Audio File	Audio Size (KB)	Bit Rate (kbps)	Vote Size (kb)	MSE (db)	PSNR (db)
Bom	768	88	1.77	0.2	104.6268
Corn	415	176	1.77	0.5	121.0942
One	78.1	128	1.77	0.9	139.8472
Samp	434	705	1.77	0.7	115.6010
Pledge	348	176	1.77	0.1	101.3640

After comparison of stego audio samples, the average embedding capacity obtained was 0.77%. This is the maximum amount of data size that can be hidden in a cover audio without raising any suspicion. Figure 3 also demonstrated various values obtained from MATLAB

analysis of both the stego audio and the cover audio for both bom and Corn audio media. An average value of PSNR value of 116.5066decibel was obtained after analysis of proposed model with Bom, Corn, One, Samp and Pledge audio covers. The proposed was model for secure e-voting

was 50% better than [16] and 42.9% better than [10] using

expression in (4).
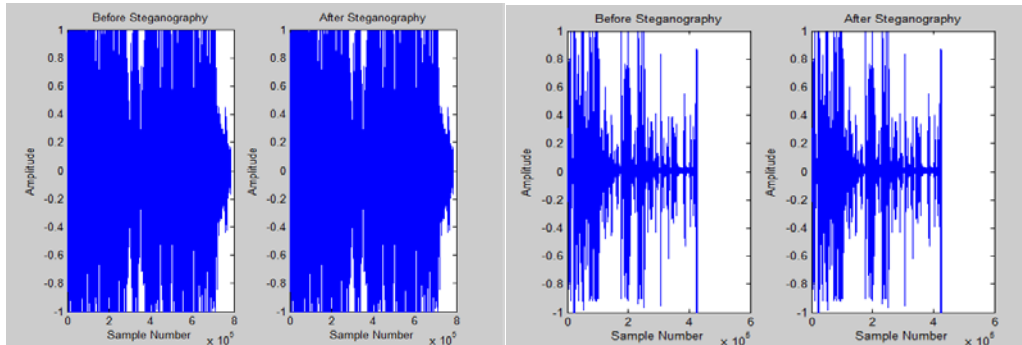
Figure 3: The Wave Plot of both Bom and Corn Audio before and after Steganography

$$\% \ Comparison = \frac{PSNR \ of \ new \ model - PSNR \ of \ existing \ model}{PSNR \ of \ new \ model} \tag{4}$$

Table 4.3: Comparative Analysis of PSNR Value of Existing Models

S/N	Compared Works	PSNR Values (db)	% improvement
1	**The proposed Model**	**116.5066**	
2	Peak-Shaped-Based Steganographic Technique for MP3 Audio (Raffaele, *et.al.*, 2013)	58.2100	50.0372
3	Audio in Image Steganography based on Wavelet Transform (Kaul, *et.al.*, 2013).	59.6548	48.7971
4	New Secure Scheme in Audio Steganography (SSAS) (Mohammed, *et.al.*, 2013).	66.4275	42.9839
5	Hiding Image in Audio using DWT and LSB (Gupta *et.al.,* 2013)	37.0733	68.1792
6	Message Guided Adaptive Random Audio Steganography using LSB Modification (Taruna *et.al.,* 2014)	86.0462	26.1448

5. CONCLUSION AND RECOMMENDATIONS FOR FUTURE WORK

This work has successfully presented the architectural design and performance evaluation of an enhanced LSB audio Steganographic model for a secure electronic voting.The model provided countermeasures over ballot integritybreach and spoofing of the ballot confidentially on transits, verification and validation of voters at kiosk site using RFID card uniquely assigned to voters. The model was quantitatively evaluated using embedding capacity, Mean Square Error (MSE) and Peak Signal to Noise Ratio (PSNR) quality metrics. The proposed model for secure e-voting was 50% better than [16] and 42.9% better than [10] similar models in literature. The proposed secure e-voting model if applied in conducting future electoral process in developing countries could assists in delivery of credible e-

election in societies where digital divide is significant. We hereby recommend the wide scale test-running and subsequent adoption of the developed model for the electoral authority in developing countries like Independent National Electoral Commission (INEC) in Nigeria for future comprehensive secure electronic voting. The following open issues can be addressed in future research endeavour:

a) **Voting Service Availability:** Future design could address voting service availability issue towards Denial of Service(DoS) and Distributed Denial of Service (DDoS) attacks.

b) **Frequency domain for higher security measures:** Improvement can be made on the

security technique through the use of enhanced frequency domain for higher imperceptibility, robustness and payload capacity of hidden information.

c) Audio linguistic steganography can also be combined with other security technologies to increase both generic and non-generic of secure e-voting.

d) Integration of speech processing for visually impaired is also recommended.

REFERENCES

[1] Chhajed G. J., Deshmukh K. V. and Kulkarni T. S. (2011). Review on Binary Image Steganography and Watermarking. International Journal on Computer Science and Engineering. 3(11). 3645-3651.

[2] Gupta N. and Sharma N. (2013). Hiding Image in Audio using DWT and LSB. International Journal of Computer Applications (0975 – 8887). 81(2).

[3] Hernandez-castro J. C., Tapiador J. E., Palomar E. and Romero-gonzalez A. (2010). Blind Steganalysis of Mp3stego. Journal of Information Science and Engineering 26, 1787-1799.

[4] Hussien H. and Hussien A. (2013). Design of a Secured E-voting System. Electronic and Communication Department. AAST Cairo, Egypt. 5.

[5] Jyotheeswari J. and Reddy V. L. (2013). A Novel Steganographic System for Data Hiding in Video/Audio. International Journal of Computer Applications. 82(11). 31-36.

[6] Katiyar S., Meka K. R. (2011). Online Voting System Powered By Biometric Security Using Steganography. Second International Conference on Emerging Applications of Information Technology, IEEE.

[7] Kaul N. and Bajaj N. (2013). Audio in Image Steganography based on Wavelet Transform. International Journal of Computer Applications (0975 – 8887) 79(3).

[8] Kohno T. Stubblefield A. (2004). Analysis of an Electronic Voting System. IEEE Symposium on Security and Privacy. IEEE Computer Society Press.

[9] Kulkarni S. A., Patil S. B. Patil B. S. (2013). A Optimized and Secure Audio Steganography for Hiding Secret Information - Review. Journal of Electronics and Communication Engineering. 12-16.

[10] Mohammed S. A., Ibrahim S., Ghazali S. and Ahmad A. (2013). New Secure Scheme in Audio Steganography (SSAS). Australian Journal of Basic and Applied Sciences. 7(6): 250-256.

[11] Okediran O. O., Omidiora E. O., Olabiyi S. O., Ganiyu R. A. and Sijuade A. A. (2011b). Towards Remote Electronic Voting Systems. Computer Engineering and Intelligent Systems. 2(4). 2011. 72-82.

[12] Olaniyi O. M., Arulogun O. T. and Omidiora E. A. (2012a). Towards an Improved Stegano-Cryptographic Model for Secured Electronic Voting. African Journal for Computer and Information Communication Technology. 5(6). 10-16.

[13] Olaniyi O. M., Arulogun O. T. and Omidiora E. A. (2013b). Design of Secure Electronic Voting System Using Multifactor Authentication and Cryptographic Hash Functions. International Journal of Computer and Information Technology. 2(6). 1122-1130.

[14] Olaniyi O. M., Arulogun O. T., Omidiora E. A. and Okediran O. O. (2014a). Performance Assessment Of An Imperceptible And Robust Secured E-Voting Model. International Journal of Scientific & Technology Research. 3(6). 127-132.

[15] Olaniyi O. M., Arulogun O. T., Omidiora E. O. and Okediran O. O. (2014c). Performance Evaluation of modified Stegano-Cryptographic model for Secured E-voting. International Journal of Multidisciplinary in

Cryptology and Information Security. http://warse.org/pdfs/2014/ijmcis01312014.pdf. 3(1). 1-8.

[16] Raffaele P, Fabio G. and Roberto C. (2013). Peak-Shaped-Based Steganographic Technique for MP3 Audio. Journal of Information Security, 4, 12-18.

[17] Sabir F. A. (2014). Hiding Encrypted Data in Audio Wave File. International Journal of Computer Applications. 91(4). 6-9.

[18] Sakthisudhan K., Prabhu P. and Thangaraj P. (2012). Secure Audio Steganography for Hiding Secret information. International Conference on Recent Trends in Computational Methods, Communication and Controls.

[19] Saurabh A. and Ambhaikar A. (2012). Audio Steganography using RPrime RSA and GA Based LSB Algorithm to Enhance Security. International Journal of Science and Research. 1(2).

[20] Tambe S. A., Joshi N. P. and Topannavar P. S. (2014). Steganography & Biometric Security Based Online Voting System. International Journal of Engineering Research and General Science. Volume 2, Issue 3. 8.

[21] Taruna and Jain R. (2014). Message Guided Adaptive Random Audio Steganography using LSB Modification. International Journal of Computer Applications. 86(7). 4-9.

[22] Gallegos-Garcia,G., Gomez-Cardenas,R and Dunchen-Sanchez, G(2010).Electronic Voting Using Visual Cryptography. Proceedings of fourth IEEE International Conference on Digital Society,IEEE Computer Society,31-36.

[23] Tatar U. and Mataracioğlu U. (2007). Analysis and Implementation of Distinct Steganographic Methods. Tübitak Uekae, Department of Information Systems Security 06700, Kavaklıdere, Ankara, Turkey.

[24] Verma S. S., Gupta R. M. and Shrivastava G. (2013). A Survey on Recent Steganography Technique Using Audio Carrier. International Journal of Advanced Research in Computer Science and Software Engineering. 3(11).

[25] Olaniyi, O.M,Folorunso, T. A.,Abdullahi I. M., and AbdulSalam, K..A(2015), "Design and Development of Secure Electronic Voting System Using Radio Frequency Identification and Enhanced Least Significant Bit Audio Steganographic Technique .IOSR Journal of Computer Engineering, *In press.*

[26] Olaniyi, O.M, O.T Arulogun, E.O. Omidiora, & Okediran O.O (2015)," Enhanced Stegano-Cryptographic Model for Secure Electronic Voting", Journal Of Information Engineering and Applications ,5(4):1-15

PHYTOREMEDIATION OF AGRICULTURAL SOILS POLLUTED WITH NICKEL AND CHROMIUM USING FLUTED PUMPKIN PLANT (*Telfairia occidentalis*)

Animashaun I. M.[1*], Otache M. Y. [1], Yusuf S. T.[2], Busari M. B.[3], Aliyu M. [1], Yahaya M. J.[1]

1. Department of Agricultural & Bioresources Engineering, Federal University of Technology, Minna, Nigeria
2. Department of Crop Production, Federal University of Technology, Minna, Nigeria
3. Centre for Genetic Engineering and Biotechnology, Global Institute for Bioexploration Unit, Federal University of Technology, Minna, Nigeria

[*]Corresponding Author's email and number: ai.iyanda@futminna.edu.ng, 08057714197.

ABSTRACT

Phytoremediation is a new remediating technology which gives a great prospect for cleanup of many harmful wastes, including heavy metals on agricultural land. This research work aimed at evaluating the potential of fluted pumpkin plant (*Telfairia occidentalis*) for phytoremediation of nickel and chromium from soil. Soil sample collected at a depth of 20 cm were used for the experiment. The pH, organic carbon, nitrogen, phosphorus and potassium content of the soil were determined. The experimental design for this study consist of 5 treatments, each of these treatment were divided into 3 replicates, each containing 4 kg of soil including soil without concentration of Ni and Cr to serve as control. Three (3) polythene bags, each contaminated with 1 g/dm^3 and 3 g/dm^3 concentration of Ni and Cr. Three (3) fresh fluted pumpkin seeds were planted on each of the soil sample at a depth of 5cm and the setup was monitored properly in crop production department nursery garden. Samples were taken for analysis at every 2 weeks interval for a period of 8 weeks. Results obtained at every 2 weeks interval showed reduction in the concentration of Ni and Cr in the soil. The analytical results of the plant assessment upon harvest confirmed an uptake and accumulation in the aerial parts and root of the plant. It can thus be concluded that fluted pumpkin plant is a good phytoplant having undistorted growth in the presence of Ni and Cr, and be used for remediating soils polluted Ni, Cr and their compounds. The implication is that fluted pumpkin meant for consumption should not be planted on soil rich in heavy metal to avoid uptake of heavy metals by man.

Keywords: *fluted pumpkin plant, heavy metals, agricultural soils, phytoplant, crop quality*
.

1. INTRODUCTION

Environmental build up of waste products which are rich in heavy metals are of great concern in recent time. Contamination of soil, air and water by these metals has been on drastic increase since the early 20th century due to rapid growth in the world population coupled with increase in exploitation, production and consumption of the earth's raw material such as fossil fuel and minerals (Appel and Ma, 2002). Soils on the other hand are the major recipients and accumulators of these metals due to its high capacity for metal retention.

Nickel (Ni) and Chromium (Cr) are among the most prominent heavy metals disturbing soil quality and human health because of their diverse roles in industrial and agricultural sectors (Appel and Ma, 2002). These metals do not only affect the quality of crop but also the quantity as they pose threat to microorganism causing abiotic stress which is often detrimental.

Phytoremediation is gaining popularity recently as an alternative to mechanical and chemical methods of removing contaminant from soil. The preference given to this method is due to the fact that it is an inexpensive technology which generates fewer secondary wastes making it environmental friendly (Cullaj et al. 2004; Usman and Shuaibu, 2011).

The search for the available indigenous plant that has the potential to survive and reproduce under heavy metal

stress field condition is pivotal to the applicability of this technology (Yoon et al., 2006). Literature has shown that some plants (vegetables inclusive) have high tolerance for heavy metal and thus accumulate them in various parts of their system (Cheng, 2003; Yusuf et al., 2002).

If an agricultural soil is rich in heavy metals, the toxic substance consistency of the cultivated vegetable on those soils will also be high. Hence, ensuring good status of soil to be used for cultivating edible crop is very paramount to both subsistence and commercial system of farming (Agbogidi and Enujeke, 2011).

To this end, this study focused on evaluating the potential of fluted pumpkin plant (*Telfairia Occidentalis*) for phytoremediation of agricultural soil contaminated with nickel and chromium.

METHODOLOGY

Study Area

The study was conducted in Crop Production Departmental Garden, in School of Agricultural and Agricultural Technology, Federal University of Technology Minna, Nigeria, Gidan Kwanu campus. The collected soil sample is well drained and has high water infiltration rate.

Materials

Fluted pumpkin seeds used for the experiment were obtained at kasua Ngwari, (Gwari market) Minna. Nickel (II) nitrate hexahydrate [Ni $(NO_3)_2.6H_2O$] and chromic nitrate [Cr $(NO_3)_2.9H2O$] were used as artificial sources of Ni and Cr in soil

Soil Sampling

Soil samples were collected within the study area at a depth of 20cm. Three fresh fluted pumpkin seeds were planted in polythene bags containing 4 kg of the soil at a depth of 5cm. The experimental design used was 5 by 3 which consist of 5 treatments (including the control) and 3 replicates. Three polythene bags without nickel and chromium to serve as control, three polythene bags contaminated with 1 g/dm^3 concentration of nickel, three

polythene bags contaminated with 3 g/dm^3 concentration of nickel, three polythene bags contaminated with 1 g/dm^3 concentration of Chromium and three polythene bags contaminated with 3 g/dm^3 concentration of Chromium (Plate 1). The control and contaminated soil samples were taken for initial analysis before planting of the seeds. After seed planting, samples were also collected and analyzed for heavy metal content at two weeks interval for a period of eight weeks. At the end of the 8th week, after the collection of soil samples, the plants were uprooted and the leaves, stem and root were also analyzed for the heavy metal content.

Plate 1: Experimental set up

Sample preparation and analysis

The soil samples in each of the polyethylene bags were dried and ground. The ground samples were then passed through 0.25 mm sieve mesh to obtain a fine particle. The samples were digested using nitric acid-perchloric acid digestion (Otaru et al, 2013). Some 0.5 g of the finely ground soil samples were weighed using a digital weighing balance and placed in a 50 ml beaker. Some 20 ml of a mixture of nitric acid and perchloric acid in 1:1 molar ratio was poured into the soil in the beaker and the content was placed on a hot plate and heated gently at low temperature until dense white fumes of $HClO_3$ appears. The digested soil sample was allowed to cool before it was filtered into a 50 ml standard volumetric flask which was made up to

mark with deionised water and the samples were placed in storage containers and taken for analysis.

At the end of 8th week, Plant samples (leaves, stem and root) were digested using method illustrated by Hornwitz (1980). The samples were oven dried and grounded to powdery form. Some 0.5 g of the sample was weighed into a 50 ml beaker. 5.0 ml of concentrated nitric acid was added and the beaker heated on a hot plate in a fume cupboard to a small volume. Same amount of concentrated Perchloric acid was also added and then boiled again for few minutes after which 15.0 ml of deionised water was added and allowed to cool to room temperature. The whole mixture was then transferred to a 100 ml volumetric flask and made up to the mark with deionised water. These solutions were placed in storage container and used for the analysis

The samples (both plant and soil) were analysed for Cr and Ni content using atomic absorption spectrometer (AAS).

Before the treatment of the soil sample, some physicochemical properties of the samples were determined. The soil textural class, soil pH and organic carbon were determined using Bouyoucos Hydrometer method, pH meter and Walkey-Black method respectively. While phosphorus was determined with flame photometer, potassium and nitrogen were determined using oxidation kjedal method respectively.

2. RESULTS AND DISCUSSIONS

The results of the physicochemical properties of the soil before contaminated with Cr and Ni are presented in Table 1. The mean value for particle distribution (74% of sand, 9% of silt and 17% of clay) of the soil showed that the soil can be classified as sandy loam based on textural classification.

pH is an important parameter, as it regulates most of the biological and chemical reaction in soil (Ahaneku and Sadiq, 2014). While high soil pH can stabilize soil toxic

Table 1: Physicochemical parameters of soil in the study area

Parameters	Mean Value
Sand (%)	74
Silt (%)	9
Clay (%)	17
pH	6.9
Organic Carbon (g/kg)	14
Available Phosphorus (mg/kg)	21
Potassium (Cmol/Kg)	0.40
Total Nitrogen (%)	1.42

elements, pH value of less than 5.5 poses a threat to most microbial activities (Li et al., 2005; Solomon, 2008). The soil used for the experiment has a mean pH value of 6.9 showing its tendency for considerable stabilization of the soil and a probable consequent of low absorbability of the metal elements from the soil solution by the plant, as opined by Ogbemudia and Mbong (2013).

The presence of organic carbon (14 g/Kg) in the soil can also favour increase in leaching of some heavy metals from the soil (Carmona et al, 2008).

The presence of phosphorus (21 mg/kg), potassium (0.40 Cmol/kg) and nitrogen (1.42%) also indicated good quality of the soil for agricultural purposes.

The potential of fluted pumpkin plant in removing chromium and nickel from contaminated soil was evaluated. The average concentration of Cr and Ni in soil sample at week zero (initial stage) was 0.11 mg/kg and 0.028 mg/kg for the control, 0.94 mg/kg and 0.83 mg/kg for soil contaminated with $1g/dm^3$ and 2.96 mg/kg and 2.29 mg/kg for $3g/dm^3$ contaminated soil sample respectively (Figure 1). The values observed in the control showed the presence of the two heavy metals in the uncontaminated soil, though at small amount. The low value observed for Ni and Cr content in the control sample was not unexpected as soil with neutral pH value are

usually low in heavy metal contents particularly Ni content as opined by Cempel and Nikel (2006).

This result agrees with the findings of Ahaneku and Sadeeq (2014) which claimed that some heavy metals are present in agricultural soils of Gidan kwano.

The observed mean concentration at the end of week 2 showed a reduction in the Cr and Ni concentration in each of the three samples (Figure 2). The control sample has a value of 0.09mg/kg for Cr and 0.02mg/kg for Ni. The values of the metals in soil contaminated with $1g/dm^3$ reduced to 0.51 mg/kg and 0.49 mg/kg, while the values in soil contaminated with $3 g/dm^3$ reduced to 2.1 mg/kg and 1.37 mg/kg for Cr and Ni respectively. This showed a probable transport of the metal into the plant via the root. While the amount lost in each of the samples varies, the highest reduction was recorded in soil samples with highest concentration ($3g/dm^3$) for both metals. This suggests that the higher the concentration of the contaminant in the soil, the more the pollutant transported to the plant

Figure 1: Sample at week 0

Figure 2: Sample at week 2

The result of the soil analysis at the end of 4th week of the experiment showed a further reduction in Cr and Ni content of the soil samples. The mean concentrations of Cr and Ni in the control sample were 0.07 mg/kg and 0.013mg/kg respectively (Figure 3). At $1g/dm^3$ contamination the respective mean concentrations of Cr and Ni were 0.27 mg/kg and 0.22 mg/kg while at $3g/dm^3$ contamination 1.46 mg/kg and 1.09 mg/kg were recorded for Cr and Ni respectively.

At the end of 6th week of experiment, the average concentrations of Cr and Ni in the control sample were 0.06mg/kg and 0.009mg/kg respectively (Figure 4). The average mean of Cr and Ni at $1g/dm^3$ contamination was 0.12 mg/kg and 0.11 mg/kg respectively, while at $3g/dm^3$ contamination; 1.08 mg/kg was recorded for Cr and 0.64 mg/kg for Ni. Likewise, the average mean level of Ni at 1g contamination was 0.11mg/kg while at 3g contamination was 0.64 mg/kg. These results showed a continuous reduction in the amount of Cr and Ni in both the controlled and the contaminated soil, indicating more quantities of both metals have probably been absorbed by the fluted pumpkin plant.

Figure 3: Sample at week 4
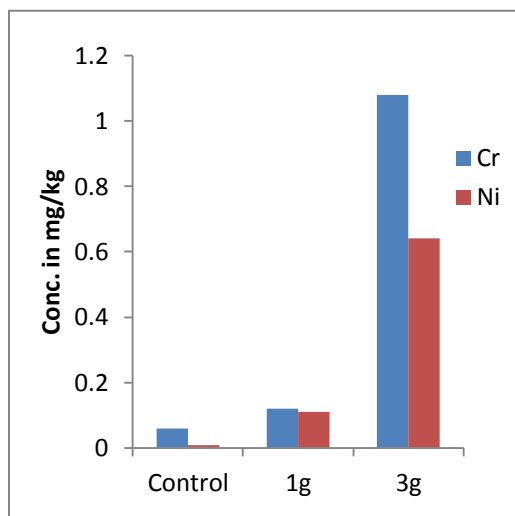
Figure 4: Sample at week 6

At end of 8th week of experiment, the mean concentrations of Cr and Ni in the control sample of the soil were 0.04mg/kg and 0.007 mg/kg respectively (Figure 5). The mean concentration of both Cr and Ni at 1g/dm³ contamination was 0.0 6mg/kg (both having the same value). At 3 g/dm³ contamination, Cr was 0.69 mg/kg while Ni was 0.31 mg/kg. The results obtained at the end of every two weeks up to week 8 showed consistence
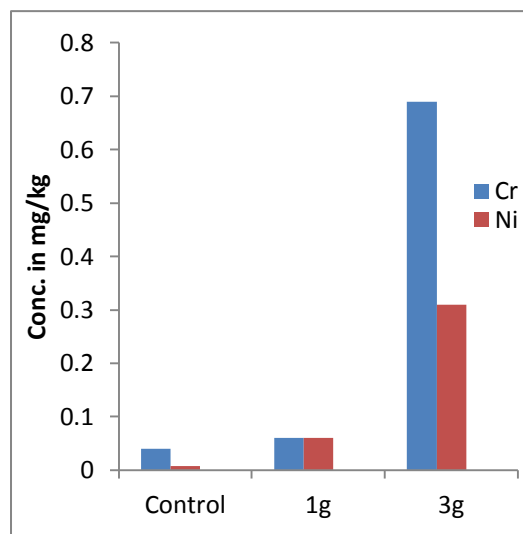
Figure 5: Sample at week 8

reduction in the amount of the heavy metal in the soil samples.

Though, the growth of fluted pumpkin plant was not distorted, the amount of heavy metals lost in the soil has probably been absorbed by the plant.

The parts of the harvested plant (leaf, stem and root) were analysed for heavy metal presence at the end of the week 8. The average mean value of Ni in the leaf, stem and root of the control sample was 0.01 mg kg-1 (all assuming the same mean value). At 1g contamination, the leaf, stem and root have mean values of 0.28 mg kg-1, 0.22 mg kg-1 and 0.20 mg kg-1 respectively for Ni content, while at 3g contamination, the leaf, stem and root have mean values of 1.06 mg kg-1, 0.59 mg kg-1 and 0.33 mg kg-1 respectively (Figure 6).

The Cr content in the leaf, stem and root of the control sample was 0.03 mg kg-1, 0.02 mg kg-1 and 0.01 mg kg-1 respectively. At 1g contamination, the leaf, stem and root have mean values of 0.32 mg kg-1, 0.24 mg kg-1 and 0.19 mg kg-1 respectively for Cr content and at 3g/dm³ contamination, the leaf, stem and root has mean values of 1.28 mg kg-1, 0.70 mg kg-1 and 0.2 mg kg-11 respectively for Cr content (Figure 7).
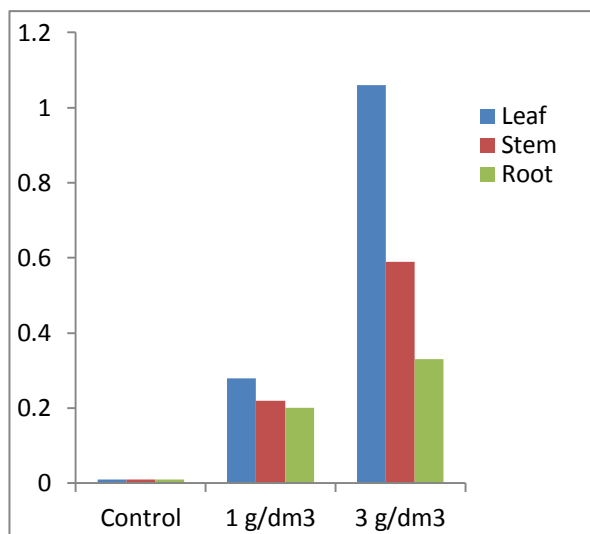
Figure 6: Concentration Nickel of in Plant Part
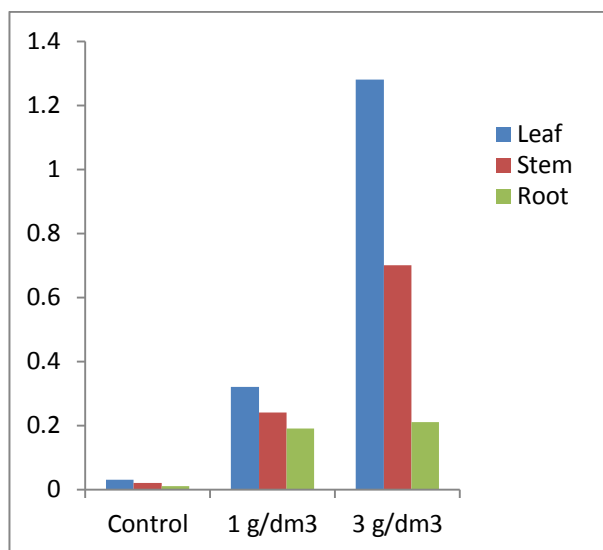
Figure 7: Concentration of Chromium in Plant Part

The results showed that though, the heavy metals are present in the aerial parts and root of the plant, the distribution varies. The leave accumulated higher contents of both metals followed by stem and root in a respective order. The results agree with the finding of Cullaj et al. (2004) and Bada and Olarinre (2012).

3. CONCLUSION

This work demonstrated the use of fluted pumpkin plant for phytoremediation of nickel and chromium. It was noted that the higher concentration of the metals (Ni and Cr) are stored in the leaves. The results of the finding also showed that the higher the concentration of the available metals, the more the uptake by the plant. It thus implies that fluted pumpkin plant meant for consumption by man or even animal should not be cultivated on highly polluted soils to avoid excess intake of the metals either directly or through food chain. More so, the study showed that the pH of the soils for cultivating fluted pumpkin plant should not be acidic to control or reduce uptake of the metals by the plant. Though, the plant uptake the two metals, it showed a relatively tolerance for nickel.

REFERENCE

Ahaneku I. E. and Sadiq B. O. (2014). Assessment of Heavy metals in Nigerian Agricultural Soils. Pol. Journal Environ. Studies. Vol. 23 No 4 pp. 1091-1100

Agbogidi, O. M. and Enujeke, E.C. (2011) Heavy metals content of three common vegetables sold in markets of Asaba metropolis, Nigeria, Proceedings of the 45th Annual Conference of the Agricultural Society of Nigeria held at Faculty of Agriculture Usmanu Danfodiyo University, Sokoto, Nigeria between 24th and 28th of October, Pp 96-99.

Appel, C., and Ma L., (2002). Heavy metals in the Environment "Concentration, pH and surface charge effects on Cd and Pb sorption in three tropical soils "Journal of Environmental Quality (JEQ) Vol. 21, pp.589-595.

Bada B. S. and Olarinre T. A. (2012) Characteristics of Soils and Heavy Metal Content of Vegetation in Oil Spill Impacted Land in Nigeria Proceedings of the Annual International Conference on Soils, Sediments, Water and Energy Vol. 17 Article 2

Carmona, D. M., Cano A. F., & Arocena J. M., (2008). Dissolved Organic Carbon and Metals, Release in Amended Mine Soil, Macla: pp. 115-117

Cempel, M., Nikel G. (2006) Nickel: A Review of Its Sources and Environmental Toxicology Polish J. of Environ. Stud. Vol.15 No. 3, pp. 375-382

Cheng, S. (2003). Effects of heavy metals on plants and resistance mechanisms. Environmental Science and Pollution Resources Vol. 10 No. 4 pp.256-264

Cullaj, A. Hasko, A. McBow, I. Kongoli, F. (2004).Investigation of the potential of several plants for phytoremediation of nickel contaminated soils and for nickel phytoextraction The European Journal of Mineral Processing and Environmental Protection Vol.4, No.2, pp. 144-151

Hornwitz Z. W. Official Methods of Analysis. Association of Analytical Chemists, Washington D.C. International Potash Institute, Bern. 1980; (13th Ed.): pp. 871-78.

Li, X. D, Wong, C. S. C., & Thornton, I. (2005). Urban environmental geochemistry of trace metals. Environ. Pollut. 129, pp.113-124.

Ogbemudia F. O. and Mbong E. O. (2013) Soil reaction (pH) and heavy metal index of dumpsites within Uyo municipality Merit Research Journal of Environmental Science and Toxicology Vol. 1, No. 4 pp. 82-85.

Otaru, A. J., Ameh, C.U., Okafor, J.O., Odigure, J. O., Abdulkareem, A.S & Ibrahim, S. (2013) Study on the Effectiveness of Phytoremediation in the Removal of Heavy Metals from Soil Using Corn. International Journal of Computational Engineering Research, Vol. 03, Issue, 4 pp. 87-93

Solomon D (2008) Presentation on the relationship in mineral soil between pH on one hand and the activity of microorganism and availability of plant nutrient on the other hand. Bahir Dar University, Bahir Dar Ethiopia

Usman O.A. Shuaibu and Abdus-Salam Nasiru (2011) Phytoremediation of Trace Metals in Shadawanka Stream of Bauchi Metropolis, Nigeria, Universal Journal of Environmental Research and Technology, Vol. 1, Issue 2: pp. 176-181

Yoon, J., Cao, X., Zhou, Q., & Ma, L. Q., (2006). Accumulation of Pb, Cu, and Zn in native plants growing on a contaminated Florida site. Science of the Total Environment, Vol. 368, 456-464.

Yusuf, A. A., Arowolo, T. O. A., & Bamgbose, O. (2002). Cd, Cu and Ni levels in vegetables from industrial and residential areas of Lagos City, Nigeria; Global Journal of Environmental Science Vol. 1, pp.1-6.

REFINING AND CHARACTERIZATION OF PALM KERNEL OIL USING TREATED CHARCOAL AND CLAY

Azeez, O. S.[1*], Olatunde, O. N.[1], Adewolu, O.[1], Olutoye, M. A.,[1]

[1]Chemical Engineering Department, Federal University of Technology, Minna

*tosin.azeez@futminna.edu.ng, +234-8068360923.

ABSTRACT

This study was aimed at refining palm kernel oil using activated charcoal and activated clay. The effects of activating both the charcoal and clay subjected to the same (chemical) activation process were studied on the refining of palm kernel oil in an adsorption column. From the results obtained, it was shown that there were increase in transmittance of palm kernel oil from 0.12 to 0.47 with activated charcoal and 0.12 to 0.52 with activated clay as a result of the removal of impurities and pigmentation of the oil. A notable change was observed in the free fatty acid (FFA) content of the oil from 6.57 mg(KOH)/g to 1.57 mg(KOH)/g with activated charcoal and 6.57 mg(KOH)/g to 1.51 mg(KOH)/g with activated clay. Hence, activated clay was a better adsorbent than activated clay.

Keywords: *clay, charcoal, adsorption column, activation, palm kernel oil, characterization.*

1. INTRODUCTION

Palm kernel oil is one conceivable item that can be centred on in light of its various employments. In Nigeria, emphasis has been on the agro-lied industries for economy enhancement. Some other types of oil that are been produced in Nigeria include vegetable oil, groundnut oil and palm oil. Palm kernel oil is consumed due to some of its nutritional benefits such as vitamins K for bone formation and it is cholesterol free nature.

The Palm kernel oil is derived from palm kernel seed of the palm tree which are grown as major crops in the southern part of Nigeria. The oil palm tree is available in the tropical rain forest region of West African countries like Ivory Coast, Cameroon, Nigeria, Ghana, Liberia (Olatunde, 2014).

The palm oil is normally obtained from the fleshy part of the palm fruit while the palm kernel oil is obtained from the kernel (seed) inside the palm fruits (Ibeawuchi, 2012). Palm kernel oil is of much economic importance both in commercial and domestic applications. It can be used in

food industries such as bakery, the production of cakes, biscuits, margarines and chocolates. Palm kernel oil can also be used in the production of cosmetics like hair and body creams, detergents and soap. They have also been tried as fuels in native lamp for lighting rural communities and as biodiesel for diesel engines.

The purification of the crude palm kernel oil in terms of decolourization of the brownish colour and deodorization of the very sharp smell of the oil was carried out in this research. High adsorbent materials such as activated clay and activated carbon can be used to remove colour and other impurities via adsorption process will be considered in this study. Activated carbon is a form of carbon that has been treated in order to make it extremely porous and have a very large surface area which favours the adsorption process.

Palm kernel oil is stable at moderately high temperature. Palm kernel oil and coconut oil comprises less than 5% of the total natural fats and oils, but they are important feedstock of the oleo chemical industry (Ibeawuchi,

2012). This importance and applications of palm kernel oil has made the study of purification of palm kernel oil necessary. Fatty acid composition of palm kernel oil as presented by John (2009) is shown in Table 1.

Table 1: Fatty acid composition of palm kernel oil (John, 2009).

Type of fatty acid	Percentage
Lauric (C12:0)	48.2
Myristic (C14:0)	16.2
Palmitic (C16:0)	8.4
Capric (C10:0)	3.4
Caprylic (C8:0)	3.3
Stearic (C18:0)	2.5
Oleic (C18:1)	15.3
Linoleic (C18:2)	2.3
Others (unknown)	0.4

The aim of this research is to study the effect of activated clay and activated carbon on colour and odour removal by comparing the results obtained in the refining of palm kernel oil with that of the crude sample. The activated carbon can be obtained from carbon containing materials like coconut shells, palm kernel shells, wood chips, animal bones, corn cobs, rice husk (Abubakar *et al.*, 2012).

2. METHODOLOGY

2.1 Materials and Equipment Used

Measuring cylinder, Heating Mantle, Weighing balance, Beakers , Conical flasks, Burette, Pipette, Separating funnel, Viscometer, Spectrophotometer, Retort stand, Filter cloth, Charcoal, clay, Oven, Furnace, Thermometer, filter cloth, filter paper, distilled water.

2.2 Chemical Activation of the adsorbents (charcoal and clay)

2.2.1 Pre-treatment stage: The raw clay from FUT staff quarters, Bosso and charcoal from Kpakungun were washed with water to remove debris, stones, unwanted particles and other impurities. The two adsorbents were dried, crushed and sieved to particle sizes of between 500 µm and 750 µm.

2.2.2 Activation stage: The pre-treated adsorbents (charcoal and clay) were activated using chemical activation method. The process is mainly divided into two stages namely; the carbonization and activation stage. The pre-treated clay was reacted with 85% phosphoric acid to inhibit the formation of tar and other unwanted particles during carbonization (Hernandez-Montoya *et al.*, 2012). The mixture which was exothermic was continuously stirred for two minutes for proper contact of the acid with the pre-treated clay and then mixed with distilled water to dissolve the un-reacted acid. The resulting solution was filtered and the residue was allowed to dry in an oven as suggested by (Osoka, 2012). The dried residue was then carbonized in a furnace at $600^{o}C$ for 30 minutes after which it was allowed to cool. The same procedure was repeated for the chemical activation of charcoal.

2.3 Characterization of the activated charcoal and activated clay

2.3.1 Ash Content Determination

2 g of dry activated sample was placed in a crucible; weight of the sample was noted to be w_2. The sample was then placed in a furnace at $450^{o}C$ for 6 hrs, after which it was removed, cooled and its content reweighed and recorded as w_3. The process was repeated twice for each

activated carbon sample to get average ash content value (Abubakar *et al.*, 2012). It was calculated as;

$$\frac{w_2 - w_3}{w_2} \times 100\%$$

2.3.2   Moisture Content Determination

5 g of sample was weighed and recorded as w_2. The sample was kept in an oven at 100^oC for 24 hrs, after which it was removed, placed in desiccators and allowed to cool. The sample was reweighed and recorded as w_3. It was repeated twice for each sample to obtain average moisture content value (Abubakar *et al.*, 2012). It was calculated as;

$$\frac{w_2 - w_3}{w_2} \times 100\%$$

2.3.3   Pore Volume Determination

2 g of each sample was weighed into a beaker and recorded as w_1. 50 mL of distilled water was poured into the beaker containing the dry sample and the mixture was boiled for 15 minutes. After the air in the pores had been displaced, the sample was drained, dried superficially and weighed as done by Abubakar *et al.*, (2012). The weight was recorded as w_F and procedure was repeated twice. It was calculated as;

$$\frac{w_F - w_1}{w_1} \times \text{density of water}$$

2.4   Refining of Palm Kernel Oil

The palm kernel oil was refined mainly in three stages namely: the degumming stage, neutralization stage, odour and colour removal stage.

2.4.1   The Degumming Stage

The approach adopted was that of Ibeawuchi, (2012) where 500 mL of crude palm kernel oil put in a separating funnel and 500 mL of distilled water at 100^oC was added. The resulting solution was mixed vigorously for about 10 minutes and allowed to settle. Two layers were obtained, the oil layer and the water layer containing the gumming materials. Using density differences, the oil of lesser density settled at the upper part and the gumming materials with water was decanted off.

2.4.2   The Neutralization Stage

0.5 M sodium hydroxide was mixed with the degummed oil as done by Ibeawuchi, (2012). The resulting mixture was well shaken after which it was filtered to obtain the neutralized palm kernel oil.

2.4.3   Odour and Colour Removal Stage

The bleaching process was done using a hollow measuring cylinder of 46 mm × 610 mm as the adsorption column. The cylinder was packed with filter cloth at the bottom to ensure that the adsorbent did not move together with the oil. The activated charcoal was put above the filter cloth to a fixed height of 10 cm and another filter cloth were placed just on top of the adsorbent to prevent impurities from entering with the oil. The measuring cylinder was supported with the retort stand and a beaker was placed at the bottom for the collection of the refined or purified oil. Distilled water was passed through the purifying bed before passing the oil through to ensure that the ashes and dust in the activated carbon was well removed before passing the oil through the bed. The collected water from the bed was compared with pure distilled water until it was clear. The set-up was allowed to dry for about 30 minutes and the oil was passed through it. A fixed volume 200 mL

of oil was passed through the adsorption column for each run. The oil that was collected at the base of the bed was then characterized. The transmittance was measured with the aid of spectrophotometer. The above procedure was repeated for the unactivated charcoal, activated clay, and unactivated clay.

2.5 Characterization of Palm Kernel Oil

2.5.1 Specific Gravity

100 g of crude palm kernel oil was heated to a temperature of 50°C and weighed. The weighed oil was put into a specific gravity bottle of known weight and the total weight was recorded. The specific gravity bottle with the oil was emptied, washed thoroughly with detergent and rinsed with distilled water to avoid contamination. It was then refilled to the same level with water at 50°C and the weight was recorded.

$$\text{specific gravity} = \frac{\text{weight of oil at 50}^{o}\text{C}}{\text{weight of water at 50℃}}$$

2.5.2 Free Fatty Acid (FFA) Content

2.8 mL of crude palm kernel oil with unknown FFA content was put into a conical flask and 25 mL of ethanol was added. Two drops of phenolphthalein indicator was added to the mixture. 0.1 M potassium hydroxide was titrated against the resulting solution until a pink colour was observed.

$$\text{FFA} = \frac{V \times M \times N}{W}$$

Where V is volume of KOH,

M is the molecular weight of oil sample used,

W is the weight of the sample,

N is concentration of KOH.

2.5.3 Iodine Value

0.5 g of oil was weighed and poured into a conical flask. 25 mL of both Carbon tetrachloride (CCl$_4$) and Wij's solution was measured accurately and mixed well. The solution was then added to the oil in the conical flask. The mixture in the flask was shaken well to ensure complete mixing. Standardized sodium thiosulphate solution is taken in a burette and titrated against the contents of the iodine flask as starch was used as the indicator (Ibeawuchi, 2012).

$$Iodine\ Value = \frac{((B-S) \times N \times 0.1269 \times 100)}{W}$$

Where B is the volume of the standard thiosulphate solution blank,

S is the volume of standard thiosulphate solution,

N is normality of standard thiosulphate solution,

W is weight of oil sample in grams.

2.5.4 Moisture Content

A beaker and a stirring rod were weighed while empty. It was reweighed after 10 g of the crude palm kernel oil sample was added into the beaker containing the stirring rod. The oil was heated using the heating mantle at a constant temperature until there was no bubbles again which indicate the absence of water. The beaker and its content were allowed to cool after which it was reweighed. The difference in weight indicated the weight of water that has evaporated during heating. Hence the moisture content can be calculated by

$$Moisture\ content\ (\%) =$$

$$\frac{weight\ of\ moisture}{weight\ of\ crude\ palm\ kernel\ oil} \times 100$$

2.5.5 Saponification Value

1 mL of crude palm kernel oil sample was measured into a conical flask; 25 mL of alcoholic potassium hydroxide was added to the oil. It was heated with the aid of heating mantle for 30 minutes and 1 mL of phenolphthalein solution was added as an indicator. 0.5 M of hydrochloric acid was titrated against the solution and the volume of the acid used was noted at end point.

2.5.6 Flash Point

It is the lowest temperature of a flammable liquid at which it can form ignitable mixture in the air, however if the ignition source is removed the liquid stops to burn. 5 g of palm kernel oil was put in an open cup and continuously heated until the smoke evolved quenched the fire from the matches stick.

3. RESULTS AND DISCUSSIONS

Table 2: Results of properties of activated clay and activated charcoal

Characteristics	Activated Clay	Activated Charcoal
Moisture content (%)	2.2	1.9
Yield (%)	92	89
Pore volume (g)	0.34	0.43
Particle size (µm)	500 – 725	500 – 725
Ash content (%)	Nil	7.50
Color change	Brown to reddish brown	Nil

Table 3: Comparison of results obtained for the characterization of oil after refining using unactivated charcoal and unactivated clay, then activated charcoal and activated clay.

Characteristics	Crude Palm Kernel Oil	Crude Oil refined with Unactivated Charcoal	Crude Oil refined with Activated Charcoal	Crude Oil refined with Unactivated Clay	Crude Oil refined with Activated Clay
FFA(mgKOH/g)	6.57	3.81	1.57	3.60	1.51
Saponification value(mgKOH/g)	417.95	308.50	221.60	283.31	202
Iodine value(g/100g)	47.2	43.20	32.60	42.70	32.20
Acid Value(mgKOH/g)	12.34	7.62	3.14	7.2	3.02
Flash point(^{o}C)	205	215	242	221	247
Moisture content (%)	8.7	6.53	3.9	6.32	3.75
pH	5.24	6.27	6.71	6.35	6.76
Specific gravity	0.93	0.94	0.94	0.94	0.94
Melting point(^{o}C)	31	30.10	29	30.10	29
Transmittance	0.12	0.14	0.47	0.14	0.52
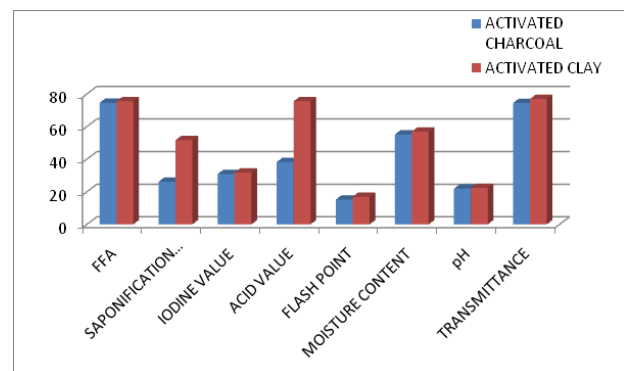
Figure 1: Efficiencies comparison of activated clay and activated charcoal

From the experimental results obtained in table 3, it was shown that the free fatty acid was reduced from (6.57 – 1.51) by the activated clay and from (6.57 – 1.57) by the activated charcoal which is in agreement with (7.2997 – 0.486) as reported by (Viele *et al., 2013)*, the flash point was increased from 205°C to 247°C by the activated clay and from 205°C to 242°C by the activated charcoal. It was also shown that the effect of activation was negligible on the specific gravity of the palm kernel oil. The acid value of crude palm kernel oil of 12.34 mgKOH/g is comparable with 11.60 mgKOH/g as reported by Atasie and Akinhanmi, (2009). The transmittance increased from

0.12 to 0.47 for activated charcoal and from 0.12 to 0.52 using activated clay indicating a reduction in the colour of the palm kernel oil. The iodine value of crude palm kernel oil of 47.2 g/100g is comparable with 41.42 g/100g as reported by Atasie and Akinhanmi, (2009). The decrease in the iodine value of the refined palm kernel oil is an indication of low level of unsaturation in the oil (atasie and Akinhanmi, 2009)

4. CONCLUSIONS

Decolourization and deodorization of crude palm kernel oil was done and results obtained from activated (clay and charcoal) and unactivated (clay and charcoal) was compared.

From the results obtained, it can be concluded that clay is a better adsorbent than charcoal both in its activated and unactivated forms. Also, transmittance was increased due to the removal of impurities and pigments from the oil. The removal of impurities also increased the flash point.

REFERENCES

Abubakar, M., Aboje, A. A., Auta, M. and Mohammed, J. (2012). A Comparative Analysis and Characterization of Animal Bones as Adsorbent. *Advances in Applied Science Research* 3 (5):3089-3096

Atasie, V. N. and Akinhanmi, T. F. (2009). Extraction, Compositional Studies of Physcio-Chemical Characteristics of Palm Kernel Oil. *Pakistan Journal of Nutrition,* 8: 800-803. Doi:10.3923/pjn.2009.800.803

Hernandez-Montoya, V., Garcia-Servin, J. and Bueno-Lopez, J. I. (2012).Thermal treatments and activation procedures in the preparation of activated carbon. ISBN 978-953-51 0197-0, DOI:10.5772/3936.

Ibeawuchi, B. E. C., (2012). Refining of Palm Kernel Oil. Master Thesis, Caritas University, Amorji-Nike, Enugu.

John, J. M. (2009). Evaluation of the Lubricating Properties of Palm Kernel Oil, page (1)107 – 114

Olatunde, O. N. (2014). Refining of Palm Kernel Oil using Activated Charcoal and Clay. Undergraduate Thesis, Federal University of Technology Minna.

Osoka, E. C. and Kamalu, C. I. O. (2012). Optimum Parameters for Bleaching of Crude Palm Kernel Oil using Activated Snail Shell. *Journal in Engineering and Applied Sciences* 1(5):323-326

Viele, E. L., Chukwuma, F. O. and Uyigue, L. (2013). Esterification ofHigh Free Fatty Acid Crude Palm Kernel Oil as Feedstock for Based-Catalyzed Transesterification Reaction. *International Journal of Application or Innovation in Engineering and Management* 2(12): 361-365

AN IMPROVED GENETIC ALGORITHM TECHNIQUE FOR ROUTE OPTIMIZATION IN A VOIP BASED CAMPUS COMMUNICATION SYSTEM.

R. Okoro, A. M. Aibinu, A. J. Onumanyi
Department of Communication Engineering
Federal University of Technology, Minna, Niger State.
remigiusokoro@gmail.com (RemigiusOkoro), 08037908072;

ABSTRACT

Wireless access technology has become a pervasive means of serving the daily telecommunications needs of society and making various services available to users. The problem associated with this technology is that its performance becomes degraded over time by the combined effect of increasing demand for connectivity, bandwidth and by most deployed multimedia services. In this paper, we are proposing an approach based on route optimization to solve the performance and Quality of Service issues experienced in a VOIP based campus communication system running on a Wireless Local Network. A Genetic Algorithm based approach will be adopted and applied on an optimal Mesh Networking routing metric to choose traffic paths that best guarantees low delay, high throughput and low packet losses suitable for real time voice communication.A reduction in end-to-end delay, increased throughput and low packet loss will be achieved from the improved routing algorithm.

Keywords: Genetic Algorithm, WMN, ILA, VOIP.

1. INTRODUCTION

This work is focused on routing optimization in Wireless Local Area Networks (WLAN) for real-time voice services. This has become important because demand for broadband services and quicker deployment of universal wireless access has necessitated the installation of WLANs or Wi-Fi systems in corporate offices, public and private enterprises, public places and university campuses. (Wang et al, 2007) stated that in the design, planning and implementation of Wi-Fi systems for mixed voice and data, priority access must be given to voice and also considerations for coverage, capacity and Quality of Service (QoS). Improvement in QoS for real time voice can be obtained by careful planning and optimization of route selection in the network.

Digitized voice signals are carried over the TCP/IP protocol as Voice over Internet Protocol (VOIP) which is the mode of voice communications in most private networks.From the work done by (Siddique&Kamruzzaman, 2008), route selection is very vital for improving performance in a VOIP based network

because of the random nature of the wireless channel. The infrastructure of the Wireless local network for a mesh configuration is made up of the Basic Service Set (BSS) consisting of the Mobile Station and the Access Points (APs), the Extended Service Set (ESS) consisting of the Mesh backbone Routers and the Core Service Set (CSS) which are the core backbone infrastructure as shown in figure 1. The AP is basically a wireless access router with a connection to a Backbone router on the network which in turn connects to the main core network router.

This study is aimed at developing an improved algorithm that will achieve route optimization in a campus VOIP network resulting in better Quality of Service (QoS) objectives such as reduced end-to-end delay, increased throughput and reduced packet losses.
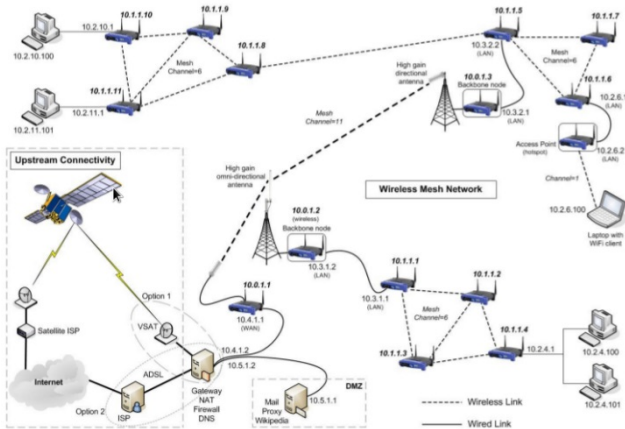
Fig.1: Wireless Mesh Network*(Courtesy Wikipedia)*

According to (Camelo and C. Omana, 2010) application of routing protocols with carefully chosen metrics will improve performance in the VOIP network and the optimization algorithm should be designed to find the best communication route for voice calls from the source to destination. This will also take into consideration the cumulative cost of any chosen route in terms of load, bandwidth, interference and length along the route.

2. METHODOLOGY

A six stage process is required to accomplish the objectives of this study from system simulation to performance evaluation.

2.1. System Simulation

A Wireless Mesh Network (WMN)system will be simulated using OMNET++ network simulator to describe a typical campus wireless architecture. The network topology implemented in this study emulates a mesh topology depicting a university campus. Candidate routes are selected from the simulated test bed in block 1 of figure 2, from which a random source and destination will be chosen depending on the number of nodes in the network. Figure 2 shows the process methodology. A set of all the likely routes that a packet will traverse from the chosen source to

its destination are identified and recorded.
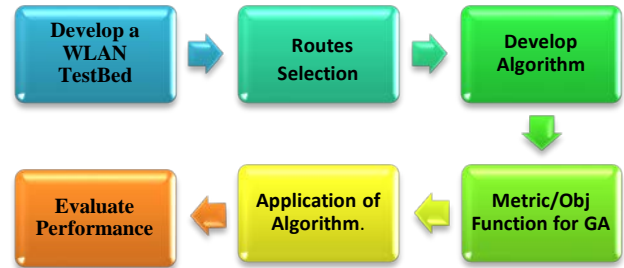
Fig.2: Process Methodology

We take note of the fact that each link in every given route will have a cost determined by parameters such as delay, interference and load (Siraj, 2014).

2.2. Algorithm Development

All the candidate routes selected from the first stage will make up the initial solution set (random population)for the GA in the selection stage (Mehboob et al, 2014) as shown in figure 3. The GA process is described as follows:
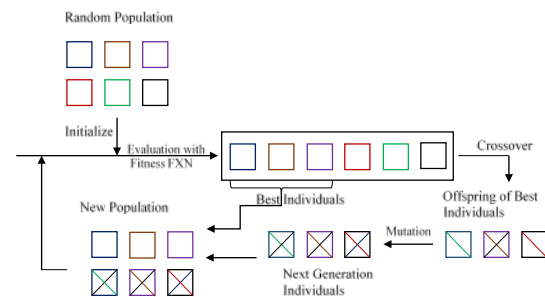
Fig.3: GA Process *(Pries et al, 2010)*

Random Population: The random population consists of all likely routes from the source to destination which shall consequently be encoded as chromosomes.

Fitness Function: A fitness function is necessary to compute the fitness value of each individual in the population randomly. This puts a weighted value on each of the routes generated in the random population.

Encoding: The encoding process generates chromosomes (binary or real numbers) that uniquely identifies each route

and shall form the basis for the GA manipulation process to generate offspring.

Selection: Selection process involves choosing individual routes from the initial population with high probability of survival as parents that will produce a new generation of fit and desirable offspring.

Crossover: This is the process of generating a new population from two parents through a recombination process. A crossover point is chosen along the string of binary or real numbers of the chromosomes of both parents, and a swap is done at this point to produce two new offspring.

Mutation: Mutation is a GA process used to avoid the problem of the solutions being stuck at a local minimum in the algorithm process. In this process, a bit position in the chromosome is flipped, thereby producing a new offspring and creating diversity (Mehboob et al, 2014).

2.3. Routing Metric/Objective Function

The most important element of the GA process is the Objective or Fitness Function which determines the success of the optimization process. The novelty in this research is that unlike other works that adopted a generalized objective function for fitness evaluation, an efficient routing metric is chosen to reflect the parameters of wireless media networks. Some routing metrics used in WMN are Expected Transmission Count (ETX), Expected Transmission Time (ETT), Weighted Cumulative Expected Transmission Time (WCETT), Metric of Interference and Channel Switching (MIC) and Interference and Load Aware (ILA) (Siraj, 2014). Of all these metrics, only ILA, a hybrid metric, takes into consideration most routing parameters of wireless routes such as interference (intraflow and interflow), throughput, load, channel switching cost and packet loss. Though it is difficult to assign weights to each of the components of ILA, it guarantees optimal paths in the network and improves on

the weaknesses of the aforementioned metrics. ILA metric is expressed as follows:

$$ILA_p = \alpha * \sum_{link\, l \in p} MTI_l + \sum_{node\, i \in p} CSC_i \qquad (1)$$

Where p is the path, MTI = Metric of Traffic Interference, and CSC=Channel Switching Cost. The parameter, MTI shows the amount of traffic generated by interfering nodes on the route expressed as follows:

$$MTI_j(Q) = ETT_{jk}(Q) * AIL_{jk}(Q), N_l(Q) \neq 0 \qquad (2)$$

$$MTI_j(Q) = ETT_{ij}(Q), N_l(Q) \neq 0 \qquad (3)$$

In equation (2) and (3), the parameter ETT differentiates between transmission rates and packet loss ratios, whereas the parameter AIL (Average Interfering Load) for nodes*(i)*and*(j)*that use channel Q for transmission is expressed as follows:

$$AIL_{jk} = \sum_{N_L} \frac{IL_{jk}(Q)}{N_L}, \qquad (4)$$

Where,

$$N_L(Q) = N_j(Q) \cup N_k(Q)$$

IL_{jk}= Neighbour Interfering Load

$N_L(Q)$ = Interfering Nodes set of neighbours *j* and *k*. A scaling factor α is applied to MTI metric for balancing the difference in magnitude of the two components (MTI and CSC). The termα can be evaluated as follows:

$$\frac{1}{\alpha} = min(ETT) * min(AIL) ; N_L(Q) \neq 0 \qquad (5)$$

$$\frac{1}{\alpha} = min(ETT) , N_L(Q) \neq 0 \qquad (6)$$

Where,

Min (AIL) = Load Average, and

Min (ETT) = Least ETT.

The CSC component is expressed as follows below:

$$CSC_j = w1\ if\ Ch_{j-1} = Ch_j \qquad (7)$$

$$CSC_j = w2\ if\ Ch_{j-1} \neq Ch_j, 0 \leq w1 < w2 \qquad (8)$$

Where,Ch_jrepresents the channel assigned for node *j*

transmission and *j-1* represents the previous hop of the node *j* along path *p*.

According to (Siraj, 2014), estimation of interfering nodes' load is the complex part of this metric, however, ILA makes up for all the weaknesses observed in other metrics such as WCETT, ETX, ETT and Hop Count. From the work done by (Shila and Anjali, 2008) the ILA metric successfully discovers least congested and low interference routes with high throughput, low loss and least delay. Interflow interference is well estimated using ILA. The drawback of this metric is that when there are two successive links, the second component CSC can capture intra-flow interference.

In this study, the objective function of the GA is modeled around this routing metric so that at the instance of route request for packet transmission, any chosen route must meet the requirements of the ILA routing metric.

2.4. Application of Proposed Algorithm

The GA routing problem could be modeled as a directed graph defined as $G = (V, A)$ where V is the vertex set of nodes and A is the arc set of links between nodes (Pries et al, 2010).

1. Initialization of Population of Routes:
    i. Randomly generate all the likely routes from a source say A to a destination node B.
    ii. Encode the weight of all the candidate routes in binary or real digits.
    iii. Compute the Fitness value of each member of the initial population using the objective function (ILA metric).

2. Selection:
    i. Select the population of all the individuals that passed the fitness test as parent routes.
    ii. The selected population is sorted in descending order of magnitude.

3. Crossover:
    i. Perform an X-point crossover on any pair of parent chromosomes.
    ii. Swap the binary weights of parent pair at the crossover points and generate a new offspring.

4. Mutation:
    i. Flip at random, a bit position of an offspring to improve the solution, this could result in decreasing the total route cost or improving the fitness value of the route.
    ii. Form a new population of routes and assign the offspring as a new generation.

5. Iteration:
    i. Repeat the process (2) to (4).
    ii. Stop the Process when the set number of iteration has been completed or when the best fitness value is completed.
    iii. The output value of the chromosome is the optimal route for the given source to destination link.

A typical mesh network topography with 12 nodes is shown in figure 3. The numbered points shows the nodes which for simplicity could be designated as routers or access points in the network.
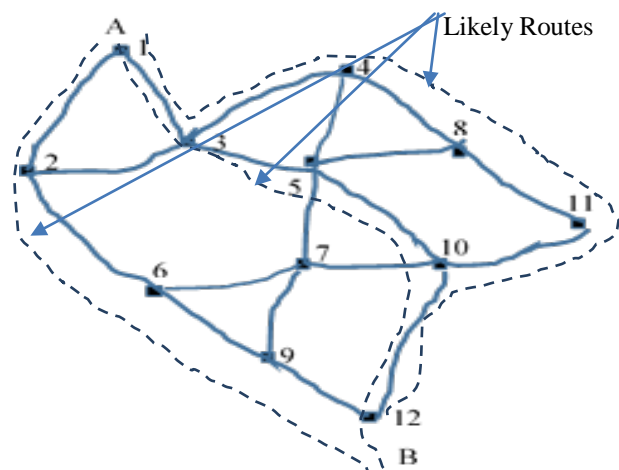
Fig.3: A sample Mesh Topology

The initial population of likely routes from source A to destination B are shown in Table 1.

Table 1: Initial Population of Routes

Route No.	Route	No. of Nodes	FitnessFxn (F(x))	Fitness	Total Route Cost ($\sum C_i$)
1	1-3-4-8-11-10-12	7	F(1)	F1	C1
2	1-3-5-10-12	5	F(2)	F2	C2
3	1-3-5-4-8-11-10-12	8	F(3)	F3	C3
4	1-3-5-8-11-10-12	7	F(4)	F4	C4
5	1-3-5-10-12	5	F(5)	F5	C5
6	1-3-5-7-10-12	6	F(6)	F6	C6
7	1-3-5-7-9-12	6	F(7)	F7	C7
8	1-2-6-9-12	5	F(8)	F8	C8
9	1-3-2-6-9-12	6	F(9)	F9	C9
10	1-2-3-5-7-9-12	7	F(10)	F10	C10
11	1-2-6-7-10-12	7	F(11)	F11	C11
12	1-2-3-5-10-12	6	F(12)	F12	C12

The fitness for each chromosome is calculated using the following expression:

$$Fitness = \frac{F(X)}{Max.F(X)} \qquad (11)$$

Where *Max.F(X)* is the maximum of the fitness function *F(X)* value in the candidate routes.

From table 1, parent routes are randomly selected based on their fitness score *(F(x)*)to undergo the genetic processes of crossover (reproduction) and mutation (flipping). The process is iterated several times to ensure genetic diversity and reaching an equilibrium point where the best route is selected.

3. EXPECTED OUTCOME

Voice communication demands more stringent QoS considerations than data communications. Therefore, it is imperative that when end-to-end VOIP communication is initiated over mesh networks, the routing process should be such that priority considerations for delay, loss and throughput is given.

In the proposed GA technique, the genetic operators are used to ensure that optimal routes are selected for voice communication exchange. In this paper the GA technique is chosen for its simplicity and ability to achieve optimal results. The novelty of the technique proposed in this study is that the objective function used to test the fitness of the candidate routes is derived from the ILA metric, a routing metric that accounts for interference, load, capacity and throughput. Therefore the results obtained would take care of most of the important parameters of voice communication in wireless mesh networks and improve system performance.

4. CONCLUSION

In this paper, we have described a GA based technique used in selecting optimal routes for voice communication in a WLAN based campus communication system. In this technique, it is important that the choice of the objective function be made carefully to reflect some of the important parameters necessary to guarantee quality voice communication on an IP system.

The GA system was chosen for its simplicity and ability to select the optimal route, based on the objective function, from a set of candidate routes in an end-to-end communication link. The optimal route is the route that offers the required bandwidth for the service, low congestion and less interference.

The optimal route guarantees low end-to-end delay, low packet loss, and higher throughput for any instance of connectivity between two nodes.

REFERENCES

Asraf, N. M., Ainon, R. N., &Keong, P. K. (2010).QoS Parameter Optimization using Multi-Objective Genetic Algorithm in MANETs. 2010 Fourth Asia International Conference on Mathematical/Analytical Modelling and Computer Simulation (pp. 138-143). Kota Kinabalu, Malaysia: IEEE.

D. M. Shila and T. Anjali, "Load Aware Traffic Engineering for Mesh Networks," Computer Science, vol. 31, pp. 1460-   1469, 2008.

Ikeda, M., Oda, T., Kulla, E., Honda, T., Barolli, L., &Xhafa, F. (2013). Analysis of WMN-GA Simulation Results: WMN Performance Considering Hotspot Scenario. 2013 IEEE 27th International Conference on Advanced Information Networking and Applications (pp. 318-324). IEEE Computer Society.

Jiang, H., Zheng, L., Liu, Y., & Zhang, M. (2010).Multi-Constratined QOS Routing Optimization of Wireless Mesh Network Based on Hybrid Genetic Algorithm. 2010 International Conference on Intelligent Computing and Integrated Systems ICISS (pp. 862-865). Guillin: IEEE.

Liwlompaisan, W., &Phonphoem, A. (2010). Call Capacity Improvement Techniques for VoIP Over Wireless Mesh Networks. ECTI-CON 6th International Conference (pp. 902-905). Pataya, Chonbury: IEEE.

M. T. Koprivica, M. M. Ilic, A. M. Neskovic and N. J. Neskovic, "An   Empirical Study of the EDCA Qos Mechanism for Voice over WLAN," Telfor Journal, vol. 3, pp. 33-38, 2011.

M. Camelo and C. Omana, "QoS Routing Algorithm Based on Multi-   Objective Optimization for Wireless Mesh Networks,"   in IEEE Latin-American Conference on Communications, 2010.

Pries, R., Staehle, D., &Stoykova, M. (2008).On Optimization of Wireless Mesh Networks using Genetic Algorithm.University of Wurzburg, Computer Science. Wurzburg: University of Wurzburg. Retrieved 2015.

Siddique, A. R., &Kamruzzaman, J. (2008).VoIP Call Capacity over Wireless Mesh Networks. Global Telecommunication Conference, 2008 (pp. 1-6). New Orleans: IEEE.

Siraj, M. (2014).A Survey on Routing Algorithms and Routing Metrics for Wireless Mesh Networks. World Applied Sciences Journal, 30(7), 870-886.

U. Mehjboob, J. Qadir, S. Ali and A. Vasilakos, "Genetic Algorithms in Wireless Networking: Techniques, Applications and   Issues," arXiv preprint arXiv, vol. 1, pp. 1-27, 19 11 2014.

Wang, P., Jiang, H., &Zhuang, W. (2007). Capacity Improvement and Analysis For Voice/Data Traffic over WLANs. IEEE Transactions on Wireless Communications, 6(4), 1530-1541.

REVEGETATION: A POTENTIAL FOR RECLAIMING LANDFILLS AND WASTE CONTAINMENT VICINITY

Agbenyeku Emem-Obong Emmanuel[1*], Muzenda Edison[2], Msibi Mandla Innocent[3]

[1,2]Department of Chemical Engineering, University of Johannesburg, South Africa

[2]Department of Chemical, Materials and Metallurgical Engineering, Botswana International University of Science and Technology, Palapye, Botswana

[3]Research and Innovation Division, University of Johannesburg, South Africa

[*]emmaa@uj.ac.za; kobitha2003@yahoo.com, +27 11 559 6396

ABSTRACT

Landfills have become widespread and unpleasantly a component of the landscape in most communities. Although it is considered a menace to the public, it remains the most common means of disposing waste in general. The growth in human population and industrial activities from the demands of globalization and civilization has triggered increased generated waste destined for landfills. Notably, landfills constitute various environmental and social threats; as byproducts from waste degradation contaminate surrounding soil and water supplies. Therefore the need for proper containment and monitoring systems to curtail such impacts on human and environmental health is dire. However, most countries particularly developing ones are faced with the costly construction, operation and closure of landfills. Research on landfills has revolved around the effects of migrating leachate and gases. However, on the event of landfill closure such massive landfill space becomes idle since constructions on these sites are unstable and costly. Also, the issues of landfill cover, leachate and methane production are of concern. Nevertheless, current challenges of cost and scarcity of virgin lands have drawn attention towards reclamation of landfills. In the developed world there are increasing efforts of converting landfills to assets rather than leaving them as liabilities. Hence, this paper found the need to highlight the potential of revegetation as means of reclaiming wasted land. The paper suggested key factors for successfully reclaiming waste sites by using cheap and available domicile resources such as plants towards a more pleasant and environmental friendly outcome.

Keywords: *Revegetation, Landfill, Plants, Reclamation.*

1. INTRODUCTION

In recent time, series of ecological revegetation and reclamation of waste lands are been done. Idle and abandoned landfills, mine dumps and surrounding vicinity thought to be worthless are drastically being reclaimed for productive functions. As reported by EPA (2005) the revegetation of land where plants and animals can inhabit is part of its functional use. Recently, in knowledge of the need for landfill closure and reclamation it is ensured that the design stage addresses the aesthetic and durable cover system alongside environmental friendly land use considerations in the long term. For instance, as recorded by Robinson and Handel (1995) clay cover liner was found to withstand damage by penetrating roots thereby supporting vegetation growth while allowing its use for recreation and mild sports. Although revegetation and restoration of wasted land has come a long way, the niche still requires a host of substantial records as not much

outcome of this landfill operation has been sufficiently documented. Hence, the study offers highlights based on available documented resources as not much recent works were readily accessible on the potential of revegetation in reclaiming landfills using available indigenous plant resource. In much severe cases like engineered mine dumps and hazardous landfills, where contaminated materials are disposed to protect humans and the environment from exposure as well as curtail contaminant permeation to levels of consequential impacts, require reliable information before revegetation or reclamation processes commence. Issues on the appropriateness to revegetate such sites are often of concern. The anaerobic degradation of waste in landfills expels offensive odors during its service time and when closed. Concerns of escaping contaminants and trash often arise despite the efforts of containment. The migrating contaminants, displaced trash and odoriferous discharge lead to aesthetic

problems and environmental contamination. In some cases, properties situated around such vicinity are devalued. Importantly, landfills should be located out of public view but in certain cases the appropriate geological and hydrological properties necessary for sitting landfills are scarce. As such, landfills happen to be situated around populated human settlements as recorded by Mara et al., (1996). Typically, grasses are planted to help stabilize landfill surfaces and avert erosion by runoffs as reported by Waugh (1994) however trees and shrubs are carefully selected for fear of damaging the cover liners by deep penetrating roots. It should therefore be noted that in revegetating and reclaiming waste sites, information on the nature of the contained waste, location of the containment area and topography are vital to site-specific approaches. Consequently, attempting to convert landfills into assets rather than allow them constitute public nuisance and environmental liability is pertinent. For this reason, this paper posited and outlined general approaches to the use of local plant resource in the recapturing of landfills towards greener and more sustainable ecological benefit. Therefore, for the purpose of this paper, all closed mine dumps, domestic and hazardous fills, abandoned sites and other waste vicinity will be termed landfills.

2. LANDFILL REVEGETATION

2.1. Possibility of Planting on Landfills

Trees, shrubs and other vegetation types can be planted on landfills without compromising standards i.e., its integrity and functionality. For instance, as recorded by EPA (2005) a number of landfills have been revegetated using various plants. Carefully selected flowering plants and grains have been planted on landfills creating a pasture for perching birds and pollinating vectors. However, one main fear of planting on landfills is the ability of plant roots to damage landfill cover liners (LCL) which can affect the integrity of the containment system thereby allowing passage of water

and rodents or causing further damage by desiccative effects. Conversely, findings and experience from Mara et al., (1996) have indicated that, if properly designed and implemented, the integrity of the landfills while revegetated can be maintained as in Figure 1 (a) and (b).

(a)   (b)

Fig. 1: (a) Landfill cover before revegetation (b) Revegetated landfill using indigenous plant species

It should be noted however, that root penetration relies on soil properties as such; compacted clay liner (CCL) or geomembrane (GM) will affect root growth. Hence, a landfill revegetation study by Robinson and Handel (1995) revealed that roots grew sideways once they encountered LCL with no noticeable damage to the LCL was recorded. The soil characteristic depth and quality, supporting climate and topography as well as the intended plant habit are chief to the possibility of revegetating landfills.

2.2. Domicile Plants as Resource for Revegetation

A number of plant species can flourish on landfills however, domicile plants are much considered than foreign ones for adaptative reasons. Since, landfill revegetation is site-specific; plants should be mostly selected by virtue of landfill designs in terms of: irrigation and drainage requirements, geographic conditions, functionality of the vegetative cover, root penetration depth, maintenance requirements and all intended costs. In recent past, domicile species of grass have typically been used as monoculture and rehabilitated habitat in controlling erosion in landfills as shown in Figure 2 (a) and (b). However, Harper (1987) suggested that species may or may not be indigenous to the surrounding habitat and

should be species that are not susceptible to disturbance by inhabitants.

Fig. 2: (a) Indigenous grass specie used as monoculture in landfill erosion control (b) Rehabilitated landfill vegetation of stunted tress and indigenous grass reclamation process

As reported by Waugh (1994) indigenous plants growing around such vicinity for many years may withstand climatic changes and physical disturbances. Revegetation with various plants helps reduce spread of disease and supports broader biological diversity in the recaptured landfill. This will create a more natural ecosystem as stated by Handel et al., (1994) thereby, reducing long-term maintenance requirements and permit self-sustenance. Existing monocultures in landfills can be rehabilitated to diverse indigenous vegetation through careful planning and monitoring. Prescribed burning, tilling and removal of thin topsoil with the monoculture as well as herbicides can aid revegetation preparations. For instance, Handel et al., (1994) reported the conversion of a state landfill from a bare monoculture with eroding areas to flourishing indigenous grassland. The selection of plants for landfills should entail the use of domicile species for revegetation. An indigenous plant as defined by EPA (2005) is a plant that has evolved over many decades in certain expanse and has adapted to the climatic, hydrological and geological changes. Indigenous plants around the landfill vicinity will have a better chance of thriving; as they will require minimal maintenance and be most cost-effective in the long run. Expectedly, landfill revegetation will foster natural conditions that support re-grouping by domicile animal species reliant on the surrounding vicinity. Importantly, incorporating foreign species close to

indigenous plant habitats could possibly overshadow the domicile plants. Hence, it is recommended that the insidious characteristics of the intended specie are investigated. Inclusively, plant succession is bound to happen as noted by Robinson and Handel (1993) such that, initially planted species may die off due to impacts of the elements i.e., regional, whether and climatic factors as well as predatory reasons. Ideally, it is expected that local wildlife, e.g., insects and birds may help in spreading the plant species in and around the revegetated landfills. Furthermore, revegetating landfills in arid zones can be more challenging because the soil will have to be modified using thin vegetation. However, chances of successfully reclaiming such landfills and vicinity depend on certain measures; using soil manure blankets or organic additives, soil modification to boost fertility and moisture retention, ground improvement for water entrapment and planting locally available seeds and seedlings of indigenous plants.

2.3. Vegetative Plants for Landfill Restoration

As earlier stated the selection of vegetative plants is site-specific as such, the types of plant highlighted herein are not applicable to every site but given on general grounds;

- Shrubs: - are known to be woody perennials standing few inches to several feet tall as shown in Figure 3. Selection of shrubs relies on sizes at maturity, root penetration, invasiveness, irrigation requirements and possibility of blocking gas vents, flow channels, wells and maintenance spots among other long-term considerations.

Fig. 3: Vegetative plant shrubs for landfill restoration

- Trees: - are the longest-lived plant groups and have sizable effects on overall vegetative design. Selection

of trees depends on size at maturity as seen in Figure 4, irrigation needs, invasiveness and competition with other plants.

Fig. 4: Vegetative tree plants for landfill reclamation

- Grasses and Wildflowers: - are usually herbaceous and restricted to grassland while wildflowers provide various pleasant aesthetics, root penetration depths and plant heights as shown in Figure 5 (a) and (b). Selection of these plant types depends on their life span, resistance to invasion, root penetration and seeding cycle (Mara et al., 1996).

(a)   (b)

Fig. 5: (a) and (b) Vegetative grasses and wildflowers in and around landfill vicinity

2.4. Factors Affecting Landfill Revegetation

Generally, revegetative processes are site-specific and rely on various factors based on landfill location and design requirements. Steps towards revegetating landfills should tie into a particular eco-region. Conversely, there should be sufficient soil depth to support the intended plant habitat in the revegetated landfill towards sustainability. Furthermore, soil conditions and topography in landfills can be duplicated from surrounding features. A revegetated landfill should duplicate the local indigenous plant profile such that selected plant species are evenly dispersed. Therefore, the general factors that can affect landfill revegetation include:

- Terrain and Slope: - Revegetated landfill could typically be contoured to fit the topography of the vicinity. Many a times, it is mound-shaped with steep slopes which impede plant survival. Biosolids with site-specific modification can prevent desiccation and support seeds till germination and revegetation in steep surfaces. Compost socks, blankets and layers can slow the rate of storm water as well as reduce erosion along steep slopes. The compost retains water which helps revegetation and acts as water filters thereby, improving quality of landfill runoffs.

- Soil and Root Depth: - Soil and root depth are prime factors for landfill revegetation. Generally, high density (not by heavy equipments but loosely compacted), low permeability and poor aeration of the landfill soil prevent deep root penetration. According to Robinson and Handel (1995) there is room for small distance penetration in landfills however, penetration through the entire landfill surface is hindered by slow upward diffusion of landfill gases which reduces the oxygen potential of the soil and can kill plants. Nonetheless, sufficient soil depth (18 to 24 inches optimum) is recommended to support revegetation. A number of steps can be taken in selecting sufficiently rooted trees and shrubs e.g., providing a thicker erosion layer even in small landfill vicinity will improve vegetation spread, compost blankets can also help vicinity with large vegetation. Treated soils e.g., with biosolids can be used to improve poor soils. Trimming taproots is another step for planting seedling in shallow layer of soil to prevent lateral root growth. The lateral roots, up to three times the tree's canopy width, will provide ample anchorage and nutrient absorption for the tree. Indigenous tree species that lack taproot can be used.

- Windthrow and surface reliability: - Blowing down of trees by strong winds on landfills is a challenge as it can compromise the reliability of the LCL while roots can open up soil layers from the collapsed effect. However, with adequate soil depth (14 to 18 inches) trees should remain

firmly rooted although monitoring against windthrow effects is vital. Also, this risk can be averted if trees are removed before they reach heights vulnerable to wind effects or else, planting species that remain relatively short are recommended. Additionally, planting shorter trees around taller ones as recorded by Dobson and Moffat (1995) can break wind effects by slowing the wind and directing wind path over or around the taller trees.

- Soil Quality and Modification: - Failures in landfill revegetation using trees as reported by Watson and Hack (2000) have often arisen from poor soil quality. Other militating factors mostly come from drought, constrained rooting, water logging and poor soil compaction. Soil remains very crucial in revegetation as it promotes plant growth, offers access to water while providing physical support for plant seeds and seedlings. Plants also get nourishment from the soil for proper growth. As such, soils for successful landfill revegetation should; (a) be like topsoil with a healthy layer near the surface (b) be carefully tested for pH, nitrogen, phosphorus, permeability, bulk density, organic matter etc., and (c) be modified with lime in cases of soils with acidic pH before applied over landfills. As noted by Wong and Bradshaw (2002) lime and organic matter can be used to improve revegetation soils 6 inches deep from one to several weeks prior seeding. The topsoil should be loosely distributed with no need for heavy compaction.

- Pests and Invasive Species: - The management of invasive plant species during revegetation is very crucial in the reclamation of landfills. Incorporating indigenous species and habitat of ecosystems in landfill recapture from surrounding vicinity is of importance in terms of conservation and self-sustenance of the vegetation. Planting foreign and invasive species can quickly consume and overshadow domicile ones around such vicinity thus, monitoring is recommended during revegetation processes. Nevertheless, methods such as controlled and prescribed burning, herbicidal or biological approach, and uprooting can be used to get rid of invasive and unwanted species. Proper plant selection can curtail disease spread by migratory insects and birds, micro-organisms, as well rodents and other burrowing animals around landfill vicinity. Care must be taken in cleanup of containment facility since removal of too much material can distort nutritive regeneration qualities and eliminate soil protection and moisture retention (Wong and Bradshaw, 2002).

- Moisture and Irrigation: - Water logging and drought stress limit plant growth and revegetation on landfills and may happen at different times of the year in vicinity with low and erratic rainfall (Wong and Bradshaw, 2002). However, as recorded by Robinson and Handel (1995) trees and shrubs absorb enormous amount of water from soil quickly and efficiently, mitigating water logging. Furthermore, CCL and GM in landfills require soil moisture to avoid desiccative effects. The need for moisture is seasonal and relies on annual rainfall and climate. Moisture is good for vegetative growth but its level must be monitored to avoid compromising the landfill cover.

- Landfill Gas: - Landfill gases can be toxic to vegetative growth caused by oxygen shortage in the root zone. Gas collection systems can both reduce or intensify this problem. Vegetation exposed to high gas concentrations can be defoliated, stunted or even die as such removal and re-population may be the best survival chance. Methanotrophic bacteria in soil are known consume landfill gas (methane formed from decomposition of waste); these bacteria thrive symbiotically with plant roots, existing in concentrations 10 to 100 times higher than in unplanted soils. A well-established root zone can consume vast quantities of landfill gas, even when the plants are dormant (Flower et al., 1981).

2.5. Landfill Revegetation/Planting Requirements

As earlier mentioned site-specific considerations gives a higher chance of revegetation survival. Proper site-specific planting scheme is required for successfully revegetating a landfill or surrounding vicinity. As recorded by Mara et al., (1996) it cost efficient to plant a mixture of indigenous seeds and seedlings in landfill restoration. However, seeding indigenous plants have higher chances of survival than its seedling from nursery beds. Once a landfill is considered properly prepared for revegetation, suitable species can be introduced by planting in clusters. This can propagate seed spread by birds and insects as well as help in the dispersal of domicile species. Generally, the following may be required in landfill planting/reclamation:

i.   The planting of all plant types i.e., wildflowers, grasses, shrubs and trees from the unset of reclamation is a major requirement. Such that, the best result can be achieved from the design towards aiding the survival of the plant habitat. The final plant habitat would be established and gradually mature into the desired vegetation. However, invasive outside plants may flourish if radical control is not ensured.

ii.   Preparing proper soil and environmental conditions to promote indigenous plant growth. This requires close control on plant types to be planted since they will rely much on the changing conditions associated with natural plant succession and survival. Initial soil modifiers with fast growing perennial grass or ground cover will be required to check erosion at the landfills. Notably, plant succession occurs as the selected area matures and the struggle for survival/establishment begins. Typically, grasses with deep taproots and excelling adaptative characteristics will establish early enough. In time, as soil nutrient increases larger perennial plants begin to establish and improve, and ultimately, shrubs and the larger trees dominate the habitat.

iii.   Mixture of planned indigenous plants with featured indigenous species to form the final landfill vegetation. This could allow for high risk of erosion and attracts higher cost of controlling invasive species. Invasive plants normally flourish in early succession habitat and once established are difficult and costly to eradicate. Additionally, they may require more effort and measures in controlling the unwanted species. An effective and cost-efficient approach to revegetation and expansion of habitat is the biological dispersal of seeds and pollination by insects and birds (Robinson and Handel, 1993).

3.   MAINTENANCE FOR/AND AWARENESS ABOUT REVEGETATED LANDFILLS

3.1. Landfill Revegetation Maintenance

Revegetated landfills and surrounding vicinity requires some form of maintenance and maintenance culture. However, one important reason for using indigenous plants is to offer a self-sustaining habitat that greatly reduces cost and lessens other requirements. As such, general maintenance and restoration exercises to foster sustained revegetated landfill may include:

a.   Monitoring and Management of Revegetation after Planting: - This entails the close observation and management of established plants on landfills which may involve re-seeding and irrigating the habitat to aid healthy growth and check invasive outside species. Monitoring against the elements i.e., drought, flood/erosion, windthrow, burrowers, insects, birds, wildlife and other biological pests should be ensured. Diverse control measures can be taken to control and or eradicate invasive species on landfills e.g., prescribed burning, hand uprooting, herbicidal and biological methods. The most appropriate choice of control relies on the function of the revegetated landfill. The frequency of maintenance may reduce with time, and as the habitat matures may be totally stopped. Furthermore, during early stages of revegetation,

mowing must be carefully done to avoid destroying forbs and young trees with weak roots.

b. Long-Term Monitoring and Management of Revegetation: - Methods such as prescribed burning, controlled grazing, mowing, application of herbicides, or combined methods may be initiated at early stages to sustain vegetation succession. After domicile plants are established, the frequency of maintenance will reduce. However, occasional elimination of plants affected by the elements i.e., windblown, drought, diseases etc., may be undertaken (Robinson and Handel, 1993). After plant roots are stable, the habitat can become self-sustaining. Although, stubborn invasive species may continue to thrive but can be periodically controlled. Also, the monitoring of generated landfill leachate quantity and composition can point out the integrity of the LCL. Consequently, leachate generation is expected to be reduced if the landfill is properly covered. Nevertheless, leachate control should be designed for and constantly monitored to avoid soil and groundwater contamination over time (EPA, 2005).

c. Maintaining Landfill Access: - Ensuring that access to revegetated landfill and surrounding vicinity is constantly maintained is of the utmost importance. Such that, access roads, paths and trails leading to vents, outlets and other functional features of the landfill are free of plant barricades and blockages. Post and signage as seen in Figure 6 (a) and (b) may be used to restrict trespassers and mowers, and demarcate freshly planted vicinity.

(a)   (b)

Fig. 6: (a) and (b) Vegetation restriction post and signage

3.2. Awareness for Landfill Revegetation

i. Freshly planted grass in landfills rarely appears green particularly over early ages. During the early stage indigenous plants may take up time growing roots and establishing below the surface. As such, could be mistaken for a futile seeding as only small plant portion may appear above ground. However, as explained by ecologist, most of the growth occurs below surface. Trained restoration experts conversant with indigenous plants will know if planting was successful as such, their services are much required for a successful landfill reclamation process. Nevertheless, some planting sessions may prove abortive at later stages without room for replacement.

ii. Indigenous plant, either seed or seedling is best collected with enough lead time possible. Sufficient lead time carters to likely shortages of desired plant type when needed as well right planting time when the opportunity surfaces. As such, for a successful landfill revegetation project, rush hour purchase and planting is highly discouraged.

iii. For increased revegetation success and reduced failure special hands and equipments i.e., expert plant restorers and drill seeders may be required as seeds and seedlings may pose planting difficulties. For higher successful revegetation outcomes, considerations must be given to proper timing in a planting year as well as appropriate geographical location that supports the intended species to be planted. It should however, be noted that the measure considerable revegetation success can only be done over time and not immediately.

iv. Pests, insects and mammals can constitute a huge problem to fresh vegetation as it attracts re-population. They can attack young grasses, shrubs and trees inflicting significant damage or at worse killing seedlings. Roaming creatures may be hard to control; however, the use of nontoxic repellants is an option to reducing attacks on freshly revegetated landfills. Also studies by EPA (2005)

found providing alternative food sources far from newly revegetated sites keep predators at bay. Furthermore, erecting physical barricades i.e., tall fences, wire nets, cage meshes etc., are optional nonlethal approaches to conserving nature and protecting the freshly revegetated vicinity.

v. It is common sense that if the soil to be used as the landfill cover from the sampling source bulges, it will also bulge wherever it is deposited (except it is treated and modified to meet requirements). Furthermore, it should be noted that if the soil sampling source supported invasive weeds, weed seed will certainly be present on the landfill cover and weed growth will definitely occur which would require cost and energy to control invasion.

vi. Importantly, post and signage as shown in Figure 7 (a) and (b) to caution mowers and sprayers should be put up to avoid accidental damages to the newly revegetated sites.

(a)   (b)

Fig. 7: (a) and (b) Vegetation caution post and signage

4. CONCLUSION

Ongoing challenges of cost and scarcity of land for natural conservation and property development have in recent times, drawn attention towards the reclamation of landfills. There are increased efforts of transforming dump sites into assets rather than allow them constitute liabilities. Thus, the paper highlighted on the potential of revegetation as a landfill recapturing approach. Herein, important factors towards the successful reclamation of waste sites were suggested on, by the use of cheap and available indigenous

plant resources for eco-friendly results. As such, the following conclusions were reached:

o That on the event of landfill closure vast spaces of land become idle and constitutes a nuisance to the general public.

o That the anaerobic decomposition of waste in landfills expels offensive odors during its service time and when closed hence, requires revegetation as a natural conservative measure.

o That contaminants and trash could escape containment. While migrating contaminants, displaced trash and offensive discharges lead to aesthetic problems, human and environmental contamination.

o That abandoned landfills, mine dumps and surrounding vicinity thought to be worthless are now a source of wealth and are drastically reclaimed for productive uses.

o That with appropriate selection and consideration, indigenous plant resource can be successfully utilized in the reclamation and restoration of landfills.

In a nutshell, the reclamation of waste sites gears towards greener and more sustainable ecological benefits. Consequently, since efforts to transform waste sites into worth full end products are in the frontlines of waste management and environmental conservation of natural resources, it was crucial for this paper to address general approaches towards the use of local plant resource in facilitating the ongoing demand for sustainable landfill reclamation.

REFERENCES

Dobson M.C. & Moffat A.J. (1993) "Woodland Establishment on Landfill Sites: Site Monitoring."; http://www.odpm.gov.uk/index.asp?id=1145641.

Environmental Protection Agency (2005) Green Landscaping http://www.epa.gov/greenacres.

Environmental Protection Agency (2005) Land Revitalization Offices&Programshttp://www.epa.gov/swerrims/landrevitalization/index.htm.

Environmental Protection Agency (2005) Municipal Solid Waste LandfillRegulationshttp://www.epa.gov/epaoswer/nonhw/muncpl/landfill/msw_regs.htm

Flower F.B. Gilman E.F. & Leone I.A. (1981) "Landfill Gas, What It Does to Trees and How It's Injurious Effects May Be Prevented." Journal of Agriculture. Vol. 7. Pg 43-52.

Handel S.N. Robinson G.R. & Beattie A.J. (1994) "Biodiversity Resources for Restoration Ecology." Restoration Ecology. Vol. 2, No. 4. Pg 230-241.

Harper J.L. (1987) "The Heuristic Value of Ecological Restoration." Restoration Ecology: A Synthetic Approach to Ecological Research. Cambridge University Press. New York, NY. Pg 35-45.

Mara S. Karen D.H. & John C.J. (1996) Wildflowers as an Alternative for Landfill Revegetation in Spotsylvania County, VA. Virginia Journal of Science. Vol. 47, No. 7. Winter 1996. Pg 281-292.

Robinson G.R. & Handel S.N. (1993) "Forest Restoration on a Closed Landfill: Rapid Addition of New Species by Bird Dispersal." Conservation Biology. Vol. 7, No. 2. Pg 271-278.

Robinson G.R. & Handel S.N. (1995) "Woody Plant Roots Fail to Penetrate a Clay-Lined Landfill: Management Implications." Environmental Management. Vol. 19, No. 1. Pg 57-64.

Watson D. & Hack V. (2000) Wildlife Management and Habitat Creation on Landfill Sites- A Manual of Best Practice. Ecoscope Applied Ecologists. UK.

Waugh W.J. (1994) "Paleoclimatic Data Application: Long-Term Performance of Uranium Mill Tailings Repositories."Workshop Proceedings: Climate Change in the Four Corners and Adjacent Regions. Grand Junction, CO. Sept. 12-14.

Wong M.H. & Bradshaw A.D. (2002) The Restoration and Management of Derelict Land-Modern Approaches. World Scientific Publishing Co. NJ.

EMPIRICAL MODELLING OF ACETIC ACID DEMINERALIZATION OF SHRIMP SHELL USING RESPONSE SURFACE METHODOLOGY

M. S. Galadima[*], A. O. Ameh, and M. O. Agbane
Department of Chemical Engineering Ahmadu Bello University Zaria
[*]galadimams@yahoo.com, +2348052867578.

ABSTRACT

This study focused on the factors affecting the demineralization of shrimp shells using acetic acid through the application of response surface methodology (RSM). The factors considered were concentration and time, while the response was percentage of demineralization achieved. Central Composite Design (CCD) in the Design Expert 6.0.6 package was employed which gave a total of 13 experiments that lead to a linear model relating the response (demineralization) and the variables. Analysis of variance (ANOVA) indicated that the model was significant as indicated in the model F-value of 10.80 or $P>F = 0.0032$. Significant model terms were concentration and time. Optimization of the model indicated acid concentration of 4.5 mol/dm^3 and 30 minutes demineralization time as the optimum conditions for the process. This produced demineralization efficiency of approximately 88% as compared to the experimental value of 80%. Predicted and actual values of the response agreed closely. This indicated that the model can be used to predict acetic acid demineralization of shrimp shell.

Keywords: *RSM, demineralization, shrimp, model, acetic acid.*

1. INTRODUCTION

In seafood industries, shellfish waste management is a huge problem especially the crustacean sector which lacks cost-effective outlets for their waste (Raja *et al*., 2012). Shrimp is one of the important fisheries products worldwide (Hossain and Iqbal, 2014). Conventionally, isolation of chitin from marine waste involves acid treatment to dissolve calcium (demineralization) followed by alkaline extraction to solubilize proteins (deproteinization) (Rinaudo, 2006). These chemical processes are ecologically harmful because of the use of strong acid and alkali solutions for the treatment of chitin properties such as weight and viscosity (Bautista, *et al.* 2001 and Oh, *et al*., 2007). Percot *et al.* (2003) elaborated on the importance of the optimization of the extraction process parameters (pH, time, temperature and solids to acid ratio) in order to minimize chitin degradation and bring the impurity levels down to the satisfactory level for specific applications.

(Mahmoud *et al*,. 2007*)* reported that the effectiveness of using lactic or acetic acids for demineralization of shrimp shells was good comparable to that of using hydrochloric acid and other benefits may include organic acids that are less harmful to the environment, can preserve the characteristics of the purified chitin. This study was therefore aimed at developing a model for the demineralization of shrimp exoskeleton through application of response surface methodology (RSM).

2. METHODOLOGY

Shrimps were obtained from a local market in Port Harcourt, Nigeria. The shells of the shrimp were separated free of loose tissue, dried and ground (250 micro meter sieve).The pretreatment method was similar to that employed by Khorrami *et al*., (2012) and Ameh *et al.*, (2014). A Central Composite Design was employed using Design expert, 6.0.6 (Khajeh, 2011) with concentration and time as the input variables. These factors were varied each at two levels, low and high, resulting in a total of 13 experimental runs. These samples were washed (demineralized) in solutions of acetic acid (with varied

molarity) with their corresponding time (Hossain and Iqbal, 2014; Galadima *et al.*, 2014).

Absorption Atomic Spectra (AAS) analysis was carried out on the resulting samples to evaluate the extent of demineralization.

3. RESULTS AND DISCUSSIONS

Table 1 presents the design matrix and the demineralization obtained from the experimental run. It

can be seen from the Table 1 that 79.85 % and 2.00 % were the highest and the lowest dimeneralization achieved respectively.

Table 1: Central Composite Design matrix with the extent of demineralization.

Runs	A:Conc(mol/dm^3)	B: Time(min)	Demineralization, %
1	3.00	17.50	24.81
2	4.50	30.00	79.85
3	3.00	17.50	22.26
4	3.00	17.50	71.26
5	4.50	5.00	18.32
6	5.12	17.50	74.75
7	3.00	35.18	60.17
8	0.88	17.50	8.57
9	1.50	30.00	21.71
10	3.00	0.18	2.00
11	3.00	17.50	74.53
12	1.50	5.00	8.18
13	3.00	17.50	35.4

Table 2 presents the analysis of variance table, this showed that the model was significant as indicated in the model F-value of 10.80 or P>F = 0.0032. Values of P>F less than 0.0500 indicate model terms are significant. In this case significant model terms were concentration (A) and time (B) due to P>F values of 0.0113 and 0.0061 respectively. The Lack of Fit P>F value of 0.7833 implied the Lack of Fit was not significant relative to the pure error. The model

would then fit experimental data. The results in terms of extent of demineralization compare favourably with literature (Farramae *et al.*, 2015; Mahmoud *et al.*, 2007).

Final equation in terms of real variables is given by equation (1).

$$\text{Sqrt(Demineralization)} = -0.43731 + 1.14863 * \textbf{A} + 0.15425 * \textbf{B} \qquad (1)$$

Where: A = Acid concentration and B = time

Table 2: Analysis of variance (ANOVA) for response surface linear model to identify significant factors affecting demineralization

Source	Sum of Square	DF	Mean square	F Value	Prob > F
Model	53.49	2	26.74	10.80	0.0032*
A	23.75	1	23.75	9.59	0.0113
B	29.74	1	29.74	12.01	0.0061
Residual	24.77	10	2.48		
Lack of Fit	10.68	6	1.78	0.50	0.7833**
Pure Error	14.10	4	3.52		

*significant variable, **not significant
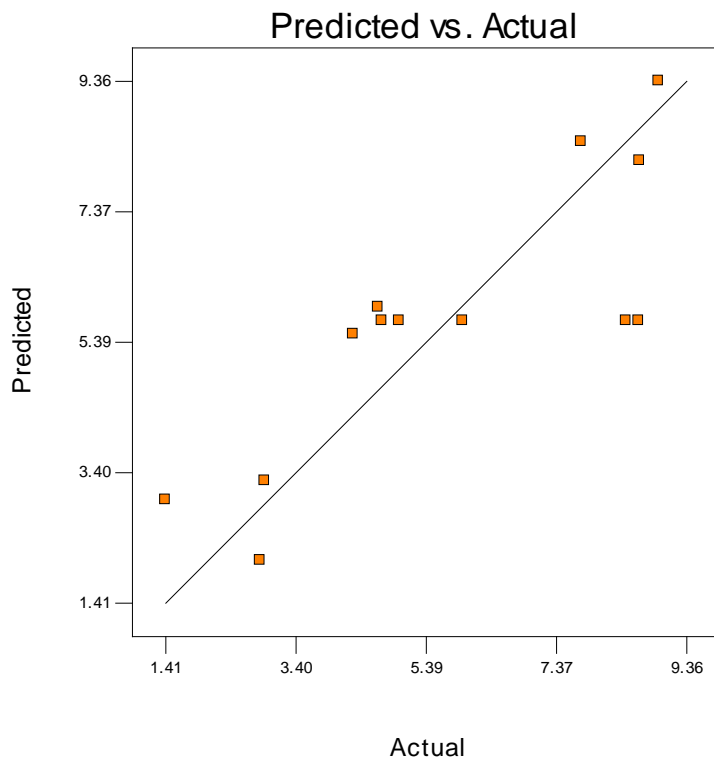
Figure 1: Parity plot of Predicted values (model) versus actual values of the demineralization.

The parity plot shown in Figure 1 compared the values of demineralization from the experimental results and the ones predicted by the model. It can be seen from the plot that the values agree closely.
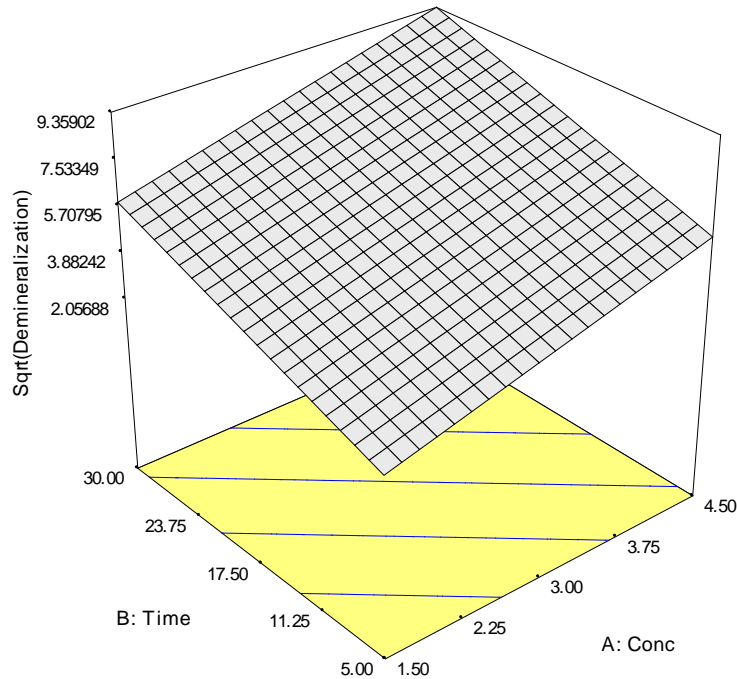
Figure 2: Response surface plot of demineralization versus time and acid concentration.

Figure 2 shows the effect of variation of time and acid concentration with percentage demineralization in the 3 dimensional response surface plot. It shows that that demineralization increases with increase in time and acid concentration.

Tables 3 and 4 present the results of optimization of the demineralization process. The range of concentration and time were presented while the objective function was to maximize demineralization. Numerical optimization was conducted using the Design Expert and it indicated acid concentration of 4.5mol/dm^3 and 30 minutes demineralization time as the optimum conditions for the process.

Table 3: Design of the optimization parameters of the demineralization

Name	Goal	Lower limit	Upper limit
Concentration	In range	1.5 M	4.5 M
Time	In range	5 min	30 min
(Demineralization)	Maximize		

Table 4: Results of the optimization of the demineralization of shrimp shell

No	Conc.	Time	% Demin.	Desirability
1	4.50	30.00	87.59	0.929
2	4.50	29.68	86.66	0.923
3	4.42	30.00	85.99	0.919
4	4.50	29.22	85.36	0.915
5	4.50	28.39	83.01	0.901

Solution: Concentration = 4.5M,   Time = 30 min

Demineralization = 87.59 %

Here, the multiple responses produced showed a variety of concentration with time, as well as their corresponding desirability. The optimum conditions were chosen for which the desirability is highest 0.929.

4. CONCLUSIONS

i. Model for the prediction of demineralization of shrimp shell using acetic acid was developed by application of response surface methodology.

ii. Analysis of variance (ANOVA) indicated that the model was significant as indicated in the model F-value of 10.80 or P>F = 0.0032. Significant model terms were concentration and time.

iii. Optimization of the model indicated acid concentration of 4.5 mol/dm^3 and 30 minutes demineralization time as the optimum conditions for the process. This produced demineralization of 87.59 %.

iv. The Predicted values (by the model) and experimental values of the demineralization agreed closely.

REFERENCES

Ameh A.O., Isa M.T., Abutu D., Rabiu U., (2014). Kinetics of Demineralization of Shrimp. *Leonardo Electronic Journal of Practices and Technologies.,* 24: 13 - 22.

Bautista, J.M., J. Jover, R. Gutierrez, O. Corpas, E. Cremades, F. Fontiveros, Iglesias, *et al.* 2001. Preparation of crayfish chitin by in situ lactic acid production. *Process Biochem.*, 3(37): 229-234.

Francisco F. C., Simora R. M. C., Nuñal S. N., 2015 Deproteination and demineralization of shrimp waste using lactic acid bacteria for the production of crude chitin and chitosan. AACL Bioflux 8(1):107-115.

Galadima M. S., Ameh A. O. and Obomanu J. T., (2014). Application of response surface methodology in demineralization of shrimp shell using lactic acid. Proceedings of Bimonthly Workshops of the Materials Society of Nigeria (MSN), Zaria Chapter, 10: 25 – 27.

Hossain M. S. and Iqbal A., (2014). Production and characterization of chitosan from shrimp waste. *J. Bangladesh Agril. Univ.* 12(1): 153–160.

Khajeh, M. (2011): Optimization of process variables for essential oil components from *Saturejahortensis* by supercritical fluid extraction using Box-Behnken experimental design. *Journal of Supercritical Fluids* 55: 944 – 948.

Khorrami M., Najafpour G.D., Younesi H. and Hosseinpou M. N., (2012). Production of Chitin andChitosan from Shrimp Shell in Batch Culture of *Lactobacillus plantarum. Chem. Biochem. Eng.* 26 (3) 217–223

Mahmoud N.S., Ghaly A.E., Arab F. (2007). Unconventional Approach for Demineralization of Deproteinized Crustacean Shells for Chitin Production, *American Journal of Biochemistry and Biotechnology,* 3(1): 1-9.

Oh, K.T., Y.J. Kim, V.N. Nguyen, W.J. Jung and R.D. Park, 2007. Demineralization of crab shell waste R.D. Park, 2007. by Pseudomonas aeruginosa F722. *Process Biochem.*, 7(42): 1069-1074.)

Percot, A., C. Viton and A. Domard, 2003. Optimization of chitin extraction from shrimp shells. *Biomacromolecules*, 4:12 – 18.

Raja R., Chellaram C., John A. A., 2012 Antibacterial properties of chitin from shell wastes. *Indian Journal of Innovations and Developments* 1:7-10.

Rinaudo, M., 2006. Chitin and chitosan: Properties and applications. *Prog. Polym. Sci.*, 7(31): 603-632.

Structural and Acidity Studies of Sulphated Zirconia Catalyst Prepared from Solid Sulphates by Environmental Friendly Method

Elizabeth J. Eterigho[a]*, T. S. Farrow[b] and Adam P. Harvey[c]

[a,] *Chemical Engineering Department, Federal University of Technology,*
Minna, Niger State, Nigeria

[b]*Chemical and Petroleum Engineering, Niger Delta University*
Wilberforce Island, Bayelsa State, Nigeria

[c]*School of Chemical Engineering and Advanced Materials, Newcastle University,*
NE1 7RU, UK

*Corresponding author. email: jummyeterigho@futminna.edu.ng, 08028648808

ABSTRACT

Non-crystalline sulphated zirconia catalysts were synthesised by a non-aqueous and non-conventional method. The effect of varying the ratio of sulphating agent to zirconium source was also investigated. The samples were characterized by X-ray diffraction, Energy Dispersive X-ray (EDX), Infra-red Spectroscopy (IR), X-ray Photoelectron Spectroscopy (XPS). The surface acidity was measured by the Pyridine-DRIFTS (Diffuse Reflectance Infrared Fourier Transform Spectroscopy) technique. The structural and textural properties of the sulphated zirconias were studied. The EDX and XPS profiles suggested that both sulphated zirconia catalysts have similar zirconia and sulphate structures; however, both catalysts were amorphous. The deconvoluted spectra of oxygen 1s confirmed the presence of oxide oxygen of zirconium and sulphate oxygen on the catalysts. Sample I had a higher amount of sulphate oxygen than sample II. Adsorption of pyridine into both samples indicated higher amounts of Brönsted acid sites in sample I, although, lower amount of sulphate was used during preparation. This opens up the possibility of controlling the degree and type of active sites on a catalyst by the amount of sulphate used for preparation.

Keywords: *Non-conventional method; Sulphated zirconia; characterization; acidity*

1. INTRODUCTION

The use of heterogeneous catalysts have gained attention and recently in the industry because of its advantages over its homogeneous counterpart. Some of the advantages include; easy recovery after reaction, good thermal stability and environmentally friendly. The main challenge is to develop a catalyst that exhibits high activity and selectivity towards the production of the desire product(s). Several routes to synthesizing solid acid catalysts have been developed (Ezekoye *et al*., 2014). Ezekoye *et al*. (2014) reported the synthesis of various super-acid materials over the last 20 years, as well as developing procedures to produce solid super-acids of extreme acidity on several catalyst supports including metal oxides. Among the many heterogeneous solid acid catalysts, zirconium oxide doped with sulphate has attracted considerable attention for selective hydrocarbon isomerisation, esterification and various other acid-promoted reactions (Berrones *et al*., 2014). However, Yadav and Murkute (2006) earlier noted it has a small surface area. Grecea *et al*. (2012) investigated the use of sulphated zirconia as a robust superacid catalyst for multiproduct fatty acid esterification. They observed that the preparation method of the catalyst led to considerable variation in the surface area of the catalyst and in turn the yield of their product. Jiang *et al*. (2010) amongst others specifically reported the preparation method as being pivotal to controlling the catalytic properties of catalysts. Hence, numerous methods of preparation of sulphated zirconia have been developed (Sharma and Singh, 2013) with the aim of optimising its catalytic performance in terms of acid strength and type of acidity to enhance selectivity. Taufiqurrahmi and Bhatia (2011) compared colloidal sol-gel and impregnation technique for preparation of sulphated zirconia catalyst. The catalyst from the colloidal sol-gel was found to retain more

sulphates; with both Lewis and Brönsted acid sites being present (Lewis acid site was predominant). Early reports emphasized the importance of the crystalline phase of zirconia, sulphur species, textural properties and calcination temperature (Thomas and Thomas, 2005)on the generation of acidity of sulphated zirconia. Studies by Berrones*et al*. (2014) indicated that the crucial factor for super acidity in sulphated metal oxides is sulphur concentration instead of coordination and surface density of the sulphate. They reported that lower concentrations of sulphur (< two 'S' atoms/nm^2) resulted in Lewis acidity, and higher concentration (> two 'S' atoms/nm^2) in Brönsted acidity. An interesting controversy is the exact type of acid site responsible for the catalytic activity in a reaction. Muthu *et al*. (2010) claim it is only the Lewis acid sites, whereas Sharma and Singh (2013) claimed that it is only Brönsted and Eterigho *et al*. (2014) agreed both coexist. In this work, non-crystalline sulphated zirconia catalysts were synthesized by non-conventional method. For the purpose of analysis of activity of the catalyst, it was compared with conventional ratio of sulphating agent to the metal oxide. The ultimate aim of this research is to develop sulphated zirconia with active sites for reactions such as isomerisation of n-butane, hydrocracking, alkylation, esterification, transesterification and thermocatalytic cracking of triglycerides.

2. METHODOLOGY

2.1. Sample Preparation

Non aqueous method was used to synthesize sulphated zirconia catalysts. This involved thorough mixing of zirconium oxychlorideoctahydrate(99.5%, Sigma-Aldrich) and ammonium sulphate (97.5%, Sigma-Aldrich) in ratio 1:6 and 1:15 of the reactants respectively. This was done with the aid of mortar and pestle. The mixture was left to age at room temperature for 18h to allow for homogenization before calcination at 600°Cfor 5h. The catalysts were designated as 'sample I and sample II' respectively.

2.2. Catalyst Characterization

The size and morphology of the samples were determined by Energy Dispersive X-ray (EDX).The surface acidity was measured by the Pyridine-DRIFTS (Diffuse Reflectance Infrared Fourier Transform Spectroscopy) technique using a Thermo Avatar FTIR spectrometer. Samples were diluted to 5 wt% in KBr after which they were exposed to pyridine vapour in a vacuum desiccator at room temperature for 20 h.XPS spectra were recorded on Kratos Axis HSi analytical system, equipped with a monochromatedAlKα$_{1, 2}$ X-ray sources and charge neutraliser. Spectra were processed using CasaXPS 2.3.15 software, with energy referencing performed by setting the CH$_x$ peak in the high resolution C 1s spectra. XRD measurements of the samples were made using a PanalyticalX'Pert Pro Multipurpose Diffractometer (MPD) fitted with an X'Celerator and a secondary monochromator to determine the nature of the sample before calcination as well as phases after calcinations. The diffractograms were recorded using Cu Kα radiation with a wavelength of λ = 1.54Å. The BET surface areas were measured using the isothermal adsorption/desorptionN$_2$ at 77K using the Coulter^{TM} SA 3100^{TM} series. The samples were outgassed for 2h at 200°C prior to the analysis. The numbers of Brönsted and Lewis acid sites were calculated using Equation 1(Rattanaphra*et al*., 2010):

$$N_T = \frac{A_L \times C_d}{\in_L m} + \frac{A_B \times C_d}{\in_B m} \qquad (1)$$

where:

N_T is the total number of pyridine/g of sample adsorbed (μmol)

$A_L/A_B$is the integrated absorbance (cm^{-1}) at Lewis (L) or Brönsted (B) sites

C_d is the cross sectional area (cm^2) of the pressed disk

m is the mass (g) of the pressed disk, and

$\varepsilon_L/\varepsilon_B$ is the molar absorption coefficient for pyridine at Lewis (L) or Brönsted (B) sites (cmµmol^{-1}).

3. RESULTS AND DISCUSSIONS

3.1. Catalyst Characterization

The BET surface area and elemental analysis (EDX) of the synthesized catalysts are given in Table 1. Samples were generally found to have better structural properties compared to those reported by other authors (Sun *et al.*, 2008; Sharma and Singh, 2013;Ezekoye *et al.*, 2014). A notable achievement is the BET surface area and the ratio of sulphate oxygen to that of oxide oxygen as shown in Table 1.

Table 1: Textural properties and elemental analysis of the synthesized catalysts

Catalyst	BET (m^2/g)	O$_2$ of SO$_4^{2-}$/ O$_2$ of Zr (from O1s in XPS)	Crystallite size (nm)	Elemental analysis (wt%)		
				Zr	O	S
Sample I	168	10.5	A	35.5	51.6	12.9
Sample II	102	3.2	A	42.1	49.2	8.7

A= amorphous

3.1.1XRD Analysis

The diffractogram patterns of the two prepared sulphated zirconia catalysts by non-aqueous method, designated as sample I and sample II respectively are presented in Figure 1. Both samples were amorphous irrespective of the amount of sulphate used during preparation of the catalyst. The amorphous state of the catalysts is in agreement with Sun *et al.* (2008).
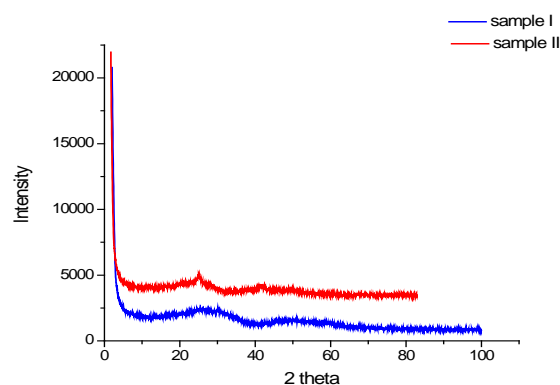
Fig. 1:Diffractogram Patterns of the Samples

3.1.2 FT-IR in the Presence of a Probe Molecule

The sulphate on the catalysts was initially determined by FTIR without pyridine. The spectra are similar as shown in Figure 2; showing strong, broad bands in the region 3550–3000cm^{-1} due to physisorbed and coordinated water followed by weaker absorption at1560-1640cm^{-1} assigned to the bending mode (δHOH) of coordinated water (Sun *et al.*, 2008). The bands at 1300 to 950cm^{-1} for the catalysts are typical of sulphate ions coordinated to the zirconium cation (Ezekoye *et al.*, 2014). However, the intensities of these bands differ with respect to the amount of sulphate used for catalyst preparation. The spectra indicated more sulphate on sample I.
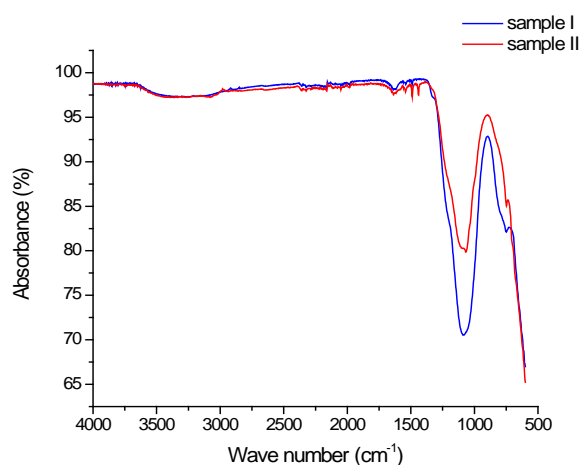
Fig. 2: IR Spectra of the Catalysts

However, this technique could not distinguish between types of acid site. This was instead achieved by DRIFT-pyridine measurements, which indicated different sites according to the sulphur content (Figure 3). The spectra in Figure 3 are a typical pyridine-IR absorption bands for sulphated metal oxides (ASTM D-4824-88). Samples show IR absorption bands between1475 - 1500cm^{-1}, which are assigned to adsorbed pyridine forming Lewis-type adducts. Also a well-defined adsorption bands around 1510-1563cm^{-1}due to Brönsted acid sites.
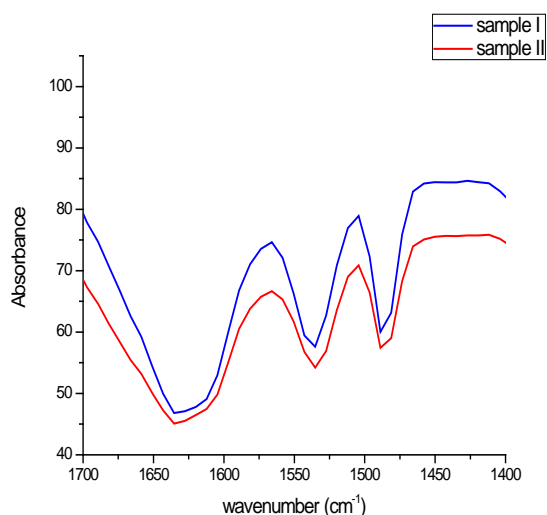
Fig. 3: FT-IR Spectra of AdsorbedPyridine showing bothLewis and Brönsted sites

The absorbance of these bands varies. The intensity of the band between 1510- 1563cm^{-1}assigned to adsorbed pyridine on Brönsted acid site on sample I is 21%, while the intensity on sample II is 12%. Generally, sample II exhibited reduced band intensities of both acid types. This implies sample I was able to retain more sulphate on the surface that interacted with the probe molecules. The percentages of acid sites that were Brönsted and Lewis were estimated using the relative integrated area of the pyridine species adsorbed on the sites (Grecea *et al*., 2012). It was observed that, despite the higher amount of

sulphate being used for samples II, it experienced a substantial reduction in the percentage area of sites that were Brönsted acidic. Using Equation 1 the different amount of Brönsted and Lewis acid sites on the catalysts was evaluated.

3.1.3 X-ray Photoelectron Spectroscopy (XPS)

The XPS data were compared with the standard from Moulder *et al*. (1995). The binding energies as shown in Figure 4, correspond to zirconium in oxidation state of IV and the same binding energy was recorded for both Zr 3d^5 and 3d^3 in both samples.
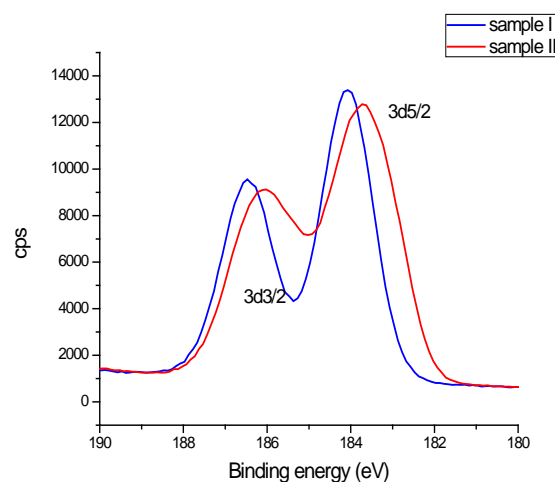
Figure 4: XPS Zr 3d Spectra of the Catalysts

The binding energies of Zr 3d^5 and 3d^3 were at 183.1eV and 185.5eV, respectively. However, the binding energy between the doublets was found to be the same (2.4eV) irrespective of the amount of sulphate during preparation. All samples showed same acidic zirconium species. From this data, the amount of sulphate during preparation seems to have no effect on the XPS Zr state. The binding energies of sulphur were recorded in the region of 2p energies, as presented in Figure 5, which exhibits a pronounced asymmetry.
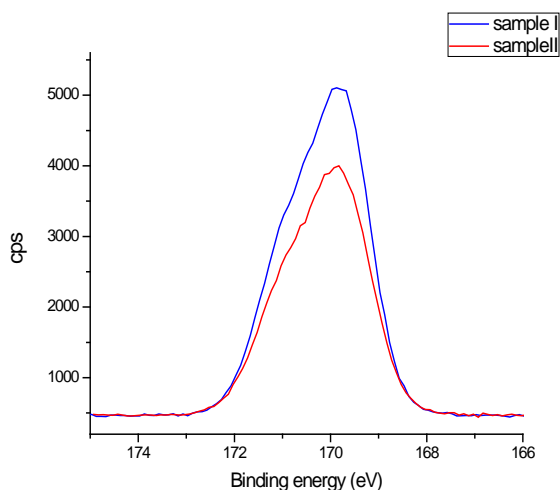
Fig. 5: XPS S 2p Spectra of the Catalysts

Deconvolution of these peaks led to two components, one located around 169.5eV and another between 170/171eV which are attributed to the S $2p_{1/2}$ and $2p_{3/2}$,respectively. These binding energies correspond to sulphur in sulphate; in agreement with other authors (Ezekoye et al., 2014; Grecea et al., 2012). Clearly, the O1s spectra for both samples were consistent as shown in Figure 6, indicating the presence of S^{6+}in SO_4^{2-}. Oxide oxygen of the zirconia at binding energies of 530.5eV/531.0eV and 532.5eV assigned to sulphate oxygen on the surface of the catalyst (Moulder et al., 1995) were observed.
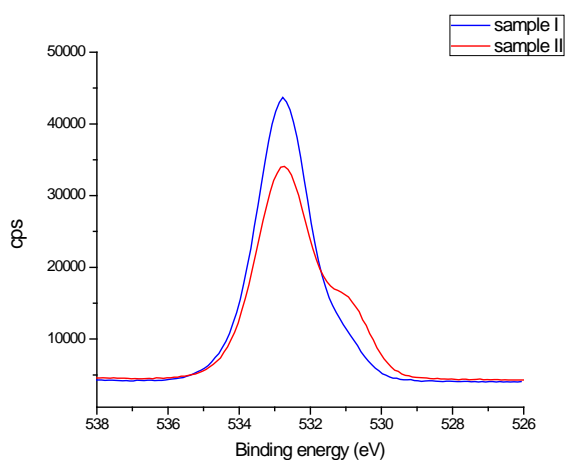
Fig. 6: XPS O 1s Spectra of the Catalysts

The peak at 530.5eV/531.0eV is higher for sample II indicating higher oxide oxygen. However, sample I exhibited higher peaks at binding energy 532.5eV as shown in Figure 7, corresponding to sulphate oxygen which resulted into its higher Brönsted acid site.
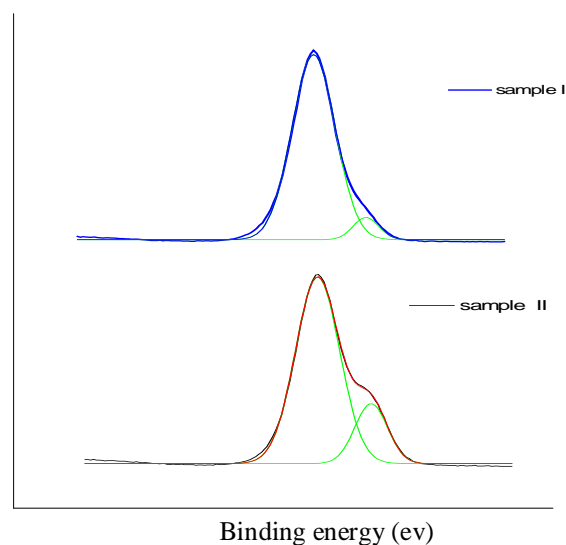
Fig. 7: Deconvoluted O 1s Spectra of the Catalysts

Surprisingly sample I, though prepared with a smaller amount of sulphating agent has its ratio of oxide oxygen and sulphate oxygen to be 10.5, whereas sample II has 3.2 in favour of oxide oxygen. This unique observation is assumed to be due to the controlled ratio of zirconium oxychlorideoctahydrate to ammonium sulphate used in the preparation, which results in a remarkable level of Brönsted acidity from the IR-pyridine analysis on sample I. Although excess sulphate was used in sample II, yet it retained less. One could conclude that the amount of sulphate used for sample II was greater than the threshold value as reported by Berronesial et al. (2014), hence the lower retention of sulphate on the catalyst. The authors reported that at higher sulphate loading the sulphate moves into the bulk phase of the catalyst rather than on the surface. These distinct differences are indications that excess sulphate

may not be necessary for the preparation of an active catalyst.

4. CONCLUSION

Comparing the structural and textural properties of the sulphated zirconias by non-aqueous method in this study with the conventional method as reported by other researchers (Grecea *et al.*, 2012; Berrones*et al.*, 2014) suggest that the non-aqueous method and sulphate source facilitate a better interaction between sulphate groups and zirconia cations. In both samples it is evident that there is a direct relationship between the number of Brönsted acid sites and the amount of sulphate retained on the catalysts: this is in good agreement with Rattanaphra*et al.* (2010). The non-aqueous preparation method resulted into amorphous, Brönsted-dominated catalysts. Increasing the amount of sulphate to improve the structural and textural properties was counterproductive, as it actually decreased the physicochemical properties responsible for activity. In this study it is also shown that the tetragonal phase of sulphated zirconia is not necessarily required for Brönsted acid site formation. Also, that sulphated zirconia catalyst with higher activity properties can be achieved via a non-aqueous and environmentally friendly method.

REFERENCE

ASTM D-4824, STM for determination of catalyst activity by ammonia chemisorptions

Berrones, R., Camas,K., Pérez, Y., Ramírez, E., Pérez, A., Eapen, D and Sebastian, P.J. (2014) 'Synthesis and Performance of Sulphated Zirconia Catalyst in Esterification of Oleic Acid', *Journal of New Materials for Electrochemical Systems*, Vol.17, No 2, pp*99-104*

Eterigho, E. J., Farrow T. Salome and Ogbuka P. Chidi (2014), ''Effect of Modification on Conventional Preparation Method for Sulphated Zirconia on the Production of Fatty Acid Methyl Ester'', *Asian Journal of Engineering and Technology*, Vol. 2 – Issue 03, pp 209-215. http://www.ajouronline.com

Ezekoye, B.A., Ezema,F.I., Ezekoye,V.A., Offor,P.O. and U Uduh, U. (2014) 'Synthesis, structural and surface morphological characterizations of sulphated zirconia Nanoparticles via chemical route', *Nigerian Journal of Technology (NIJOTECH)*, Vol. 33. No.1, pp. 54–59

Grecea, M. L.,Dimian, A. C., Tanase,S., Subbiah, V and Rothenberg, , G. (2012) ' Sulphated zirconia as a robust superacid catalyst for multiproduct fatty acid esterification' *Journal of Catalysis Science and Technology*, Vol. 2, Issue 7, pp 1500-1506

Jiang, S. T., Zhang, F. J. and Pan, L. J. (2010) 'Sodium phosphate as a solid catalyst for biodiesel preparation' *Brazilian Journal of Chemical Engineering*, Vol. 27, No 1, pp 137-144

Moulder, J. F., Chastain, J., Stickle, W. F., Sobol, P. E. and Bomben, K. D. (1995) *Handbook of x-ray photoelectron spectroscopy: a reference book of standard spectra for identification and interpretation of XPS data.* Physical Electronics

Muthu , H., SathyaSelvabala, V., Varathachary, T.K., KiruphaSelvaraj, D., Nandagopal, J. and Subramanian, S. (2010) 'Synthesis of Biodiesel from Neem Oil Using Sulphated Zirconia Via Tranesterification', *Brazilian Journal of Chemical Engineering*, Vol. 27, No. 4, pp. 601 – 608

Rattanaphra, D., Harvey, A. and Srinophakun, P. (2010) 'Simultaneous Conversion of Triglyceride/Free Fatty Acid Mixtures into Biodiesel Using Sulphated Zirconia', *Topics in Catalysis,* 53, (11), pp. 773-782

Sharma, S.D. and Singh, S. (2013) 'Synthesis and Characterization of Highly Effective Nano Sulphated Zirconia over Silica: Core-Shell Catalyst by Ultrasonic Irradiation', *American Journal of Chemistry*, Vol.3 No. 4 pp 96-104

Sun, Y., Yuan, L., Ma, S., Han, Y., Zhao, L., Wang, W., Chen, C. L. and Xiao, F. S. (2008) 'Improved catalytic activity and stability of mesostructured sulphated zirconia by Al promoter', *Applied Catalysis A: General,* 268, (1-2), pp. 17-24.

Taufiqurrahmi, N. and Bhatia, S. (2011) 'Catalytic cracking of edible and non-edible oils for the production of biofuels', *Energy & Environmental Science,* 4, (4), pp. 1087-1112.

Thomas, J. M. and Thomas, W. J. (2005) *Principles and Practice of Heterogeneous Catalysis.*Third Reprint edWeinheim (Germany): VCH Publishers Inc., New York, NY (USA).

Yadav, G. D. and Murkute, A. D. (2006) 'Preparation of a novel catalyst UDCaT-5: Enhancement in activity of acid-treated zirconia - Effect of treatment with chlorosulfonic acid vis-Ã -vissulfuric acid', *Journal of Catalysis,* 224, (1), pp. 218-223

A PACKET SAMPLING THRESHOLD TECHNIQUE FOR MITIGATING DISTRIBUTED DENIAL OF SERVICE (DDoS) ATTACKS IN A UNIVERSITY CAMPUS NETWORK

B. Dominic[1*], H.C. Inyiama[2], A. Ahmed[3], M. B. Abdullahi[4] and O. M. Olaniyi[5]

[1,2,4]Computer Science, Federal University of Technology, Minna

[3,5]Computer Engineering, Federal University of Technology, Minna

aliyu.ahmed@futminna.edu.ng, 07068234414.

ABSTRACT

Over the years, the Distributed Denial of Service (DDoS) attacks have evolved from simple flooding attacks to more complex attacks. With the advent of e-examination and online registration, higher institutions of learning may be exposed to online attacks such as DDoS attacks especially at the application layer.In this paper, a mitigation technique known as Packet Sampling Threshold (PST) technique is developed on a modeled logical Campus network to prevent DDoS attacks on the servers at the application layer. The results obtained from the simulation in OPNET modeler 14.5 showed that the technique was effective and efficient in securing the Campus network against the DDoS attacks.

Keywords:*Packet sampling threshold, distributed denial of service attacks, campus network*

1. INTRODUCTION

Over time, Distributed Denial of Service (DDoS) attacks have grown from simple flooding attacks to more complex attacks. As such, any organization that uses the Internet is vulnerable to attacks online. Nonetheless, the educational sector is also subjected to DDoS attacks following the emergence of school e-examination and online registration. DDoS attackers have modified their attack methods in a pattern that is now more difficult to detect, thereby dimming the line between attacking source and legitimate users (Juniper, 2008).

According to Wesam and Mehdi (2014), DDoS attacks usually overshadow network resources with useless or harmful packets that can prevent legitimate users from gaining access to these resources thereby, infringing on the confidentiality, privacy and integrity of information on the network.

A Campus is a main enterprise location which is made up of one or more buildings that are in close proximity. Usually, a Campus is not necessarily the corporate head-quartersor a major site but rather, it is a multi-floor office building that houses an enterprise, a university or a corporation made up of several buildings in an office complex and the set of interconnected local area networks (LANs) serving the enterprise or the university is referred to a Campus Network (Juniper, 2010). In a Campus Network, all the buildings and floors on the Campus are being connected together in order to share resources and services in a data center either through a campus Local Area Network (LAN) or Wide Area Network (WAN) connections. The Campus could also be connected to remote locations such as branch or regional offices through a WAN (Juniper, 2010).

In today's modern and global world that is Information Technology driven, the necessity and increase values provided by network infrastructures have shown its importance in government organizations, business enterprises and educational institutions most essentially Universities. This has contributed greatly to the achievement of some important goals such as increased productivity, partnership, efficiency and acquiring of knowledge in frequent researches for educational purposes. Therefore, to increase the use of Information Technology in higher institutions of learning requires a robust technical

infrastructure to provide for a secured and reliable network. A University Campus Network is a great necessity for knowledge sharing, easycommunication and aids in collaborative research which are the essential ingredient to building a strong knowledge culture and efficiently support academic mission.

The reminder of this paper is structured as follows: Section 2 presents the review of related works, Section 3 discusses the methodology used in the research and Section 4 presents the Results and discussion while the Conclusion is given in Section 5.

2. REVIEW OF RELATED WORKS

Anjali and Padmavathi (2014) proposed a novel method of detection of DDoS attacks based on Chaos theory and Artificial Neural Networks. The proposed detection technique based on Chaos theory effectively detects DDoS attacks but there is possibility of large prediction error due to busty network traffic.Shalaka, Madhulika, Prajyoti, Sneha and Nilesh (2014) proposed an architecture known as Secure Overlay Services (SOS) to proactively prevent denial of service attacks. Probability of successful attack was reduced by performing intensive filtering near protected network edges, pushing the attack point into the core of the network where high speed routers can handle volume of attack traffic and by introducing randomness and anonymity into the forwarding architecture making it difficult for an attacker to target nodes along the path to a specific SOS protected destination.

Shalaka *et.al*.(2014) used a simple analytical model to evaluate the likelihood that an attacker can successfully launch a DoS attack against an SOS protected network. The result of the proposed SOS architecture showed the resistance of a SOS network against DoS attack as the number of nodes that participate in the overlay increases

but the method is limited to classes of communication where the attackers are known.

The Study of Deepak, Puneet and Vineet (2014) focused on the behaviour of a server or victim machine with regards to various parameters (traffic drop, CPU Utilization, TCP retransmission count, memory free size and processing delay) under DDoS attack using a LAN network simulated in OPNET modeler. A study on prevention strategies and network intrusion prevention techniques for DoS attacks was carried out by Arshey and Balakrishnan (2013). The detection and prevention techniques discussed show that it is effective for small network topologies and can also be adapted for large domains. Arshey and Balakrishnan (2013) reported on some DoS attack mechanisms, how they operate and suggested some basic mitigation strategies that can be adopted to prevent these attacks.

Kharat and Radhakrishna (2013) in their study proposed a threshold based approach technique to detect and prevent DDoS attack before it reaches the victim end with high detection rate and low false positive rate to achieve high performance. Hak (2013) in his study, present DoS attacks and explore several methods of combating these attacks, he describe and analyze the techniques used to detect, prevent and mitigate these DoS attacks.Aamir and Arif (2013) further provided a simulation based analysis of an FTP server performance in a typical enterprise network under DDoS attack. The simulation done in OPNET showed noticeable variations in connection capacity, task processing and delay parameters of the attacked server as compared to the performance without the attack.Lonea, Popescu and Tianfield (2013) proposed a solution using Dempster Shafter Theory (DST) operations in three-valued logic and the Fault-Tree Analysis (FTA) for each virtual machine-based Intrusion Detection System (IDS) in

order to reduce false alarm rates by the representation of the ignorance.

3. METHODOLOGY

Figure3.1 shows the steps that are followed to develop and simulate the Campus Network. It is assumed that the management information system (MIS) unit is responsible for the management of the campus network and thus, houses the core of the network facilities. The design and simulation of the network was carried out in OPNET modeler.
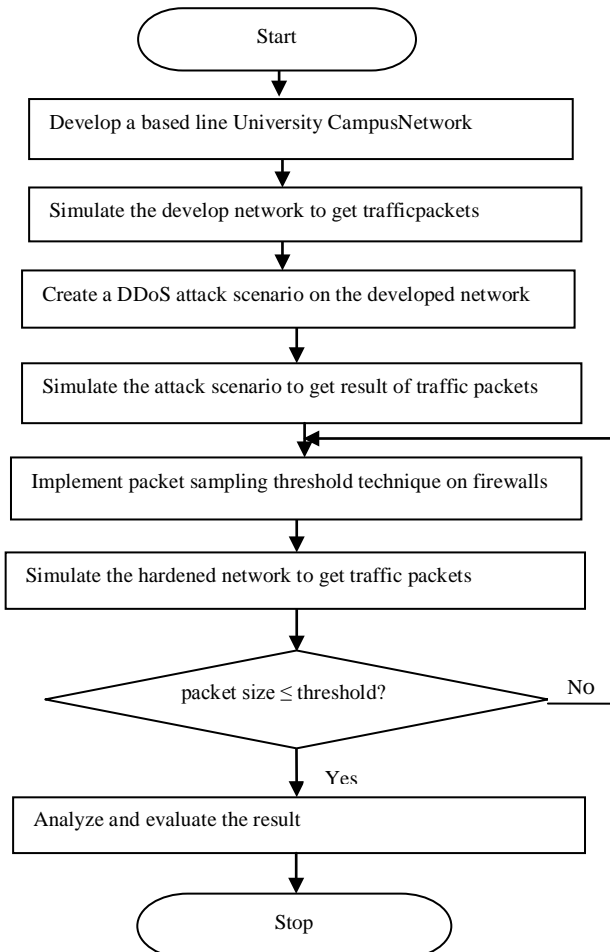
Fig. 3.1: Flow Chart for the Development and Simulation of the Campus Core Network

3.1. Modelling of the Campus Core Network

The Campus Core Network was modelled in OPNET modeler 14.5. The model of the real system was done in three scenarios, namely: the baseline busy scenario, the attack scenario and hardened scenario.

3.1.1. Baseline Busy Model

The baseline scenario was configured adopting the Campus Core Network which served as the baseline scenario busy network in which normal traffic packets were injected into the network and was configured to run under normal circumstances assumed for the normal traffic packets.

The parameters considered for the design of the baseline busy scenario is computed using equations 1 and 2.

$$Tr = \sum_{i=1}^{n} y_i \ (1)$$

$$Ta = \sum \frac{y_i}{N_i} \ (2)$$

Where T_r and T_a are Traffic and average traffic respectively, and y = values of packet traffic on the network and i= 1, 2, 3 ... n. Also the Normal traffic, Nt is calculated using equation 3 assuming a baseline busy traffic of 99% generated.

Thus;

$$Nt = 0.99Tr \ (3)$$

The baseline busy scenario model is shown Figure 3.2, representing the MIS (Management Information System) subnet that houses the FTP server, Web server sand VoIP server. It also shows the core switch

that connects the MIS subnet to other subnets in the network.
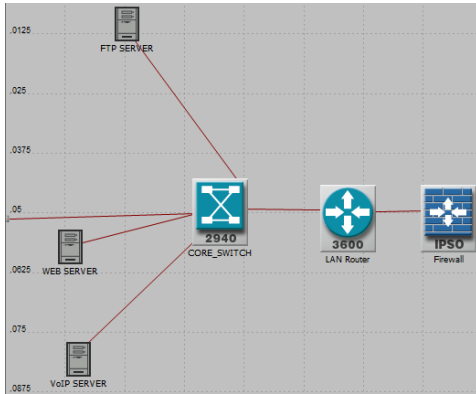
Fig. 3.2: MIS Core subnets for the Baseline Scenario showing the servers

3.1.2. The Attack Model

It is assumed that the attackers got control of the botnets consisting of the zombies and handlers and succeeded to pass through the firewall of the network. A DDoS attack scenario is configured and attack traffic packets are injected into the developed network.10 LAN workstations configured in promiscuous modes served as the botnets consisting of the zombies and the handlers. Botnet 1 is the attacker 1 attacking the FTP server, botnet 2 is the attacker 2 attacking the web (HTTP) server, while botnet 3 is the attacker 3 attacking the VoIP server. Attackers 1 and 2 are operating from remote sites (see Figure 3.3) while attacker 2 is attacking from within (see Figure 3.4). The attacker 1 floods the FTP server with large traffic packets above the assumed normal packets that can be handled by the FTP server; attacker 2 also floods the web server with large request above the normal request packets the web server can handle and attacker 3 also floods the VoIP server with large request above normal thereby affecting the normal performance level of the servers.

For Attack Traffic, A_t, with assumption value of 300% traffic scaling for 10 workstations that make up the zombies and handlers, the derived attack traffic is given in equation 4.

$$A_t = 30Tr \ (4)$$

The Attack Scenario model is shown in Figure. 3.3 and 3.4.
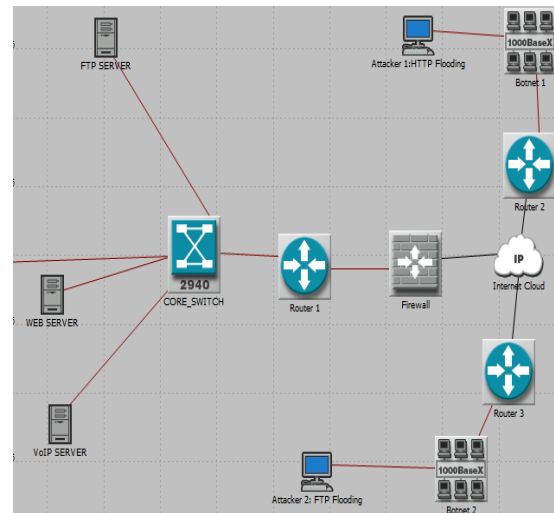
Fig. 3.3: Attack scenario showing attackers from remote sites on the FTP and Web Servers
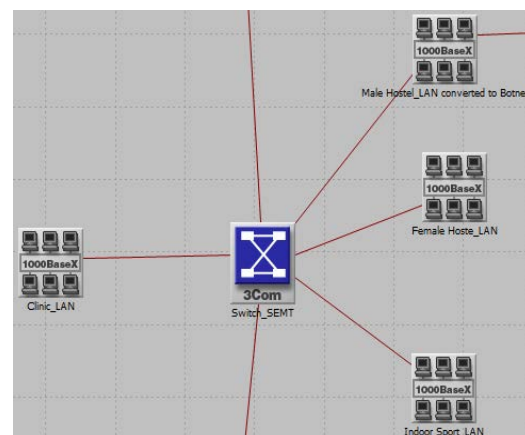
Fig. 3.4: The attack scenario of the VoIP server from within the MIS network.

402

3.1.3. Hardened Network Model

In the modelling of the hardened scenario security is implemented against the DDoS attacks, Packet Sampling Technique (PST) is applied on two separate firewalls on the simulated network, one for inbound traffic and the other for outbound traffic. In the technique, a threshold is set such that once any incoming traffic packet is greater than the set threshold; such a packet is labelled as an attack packet and hence discarded. Therefore, the first firewall is located in the MIS core network at the subnet before the MIS core Switch to secure against attacks from within the network.The second firewall securing against attack from remote sites that is, outbound traffic attack is located between the Internet Service Provider (ISP) and the Router connecting to MIS core servers as shown in Figure3.5.
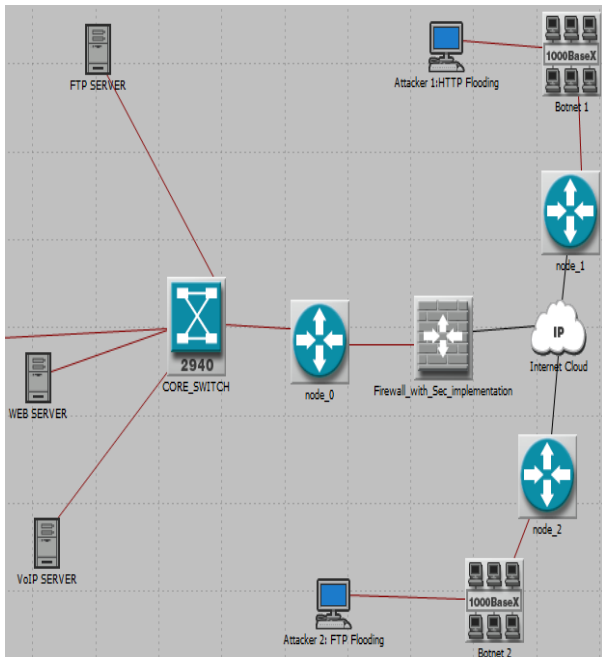
Fig. 3.5: Firewall configured between the ISP and Router before the MIS Core Switch

The implemented PST algorithm is shown Figure3.6.

1: Classify traffic flow using packet sampling

2: Measure traffic flow (T_x) in packet/second

3: Calculate the average traffic (T_a)

4: Compare each traffic flow with average traffic

5: If $T_x > T_a$

6: Mark packet as an attack packet and discard

7: Else,

8: Allow legitimate traffic packet to be delivered.

Fig.3.6: PST algorithm

3.1.4. PST Mechanism

Packet Sampling Scheme detects DDoS attack flows on huge networks by considering measures of flow entropy, average entropy, the entropy of the source port and the number of packets/seconds. It looks at the incoming traffic and extract at an average random, one data packet for sampling during a time window specified by the algorithm. The packet is forwarded or discarded based on the entropy value as compared to the threshold value set. The process is depicted in Figure 3.7.

extracted packet for sampling

Packet Sampling

packet forwarded if entropy value is less than the threshold value or else discarded
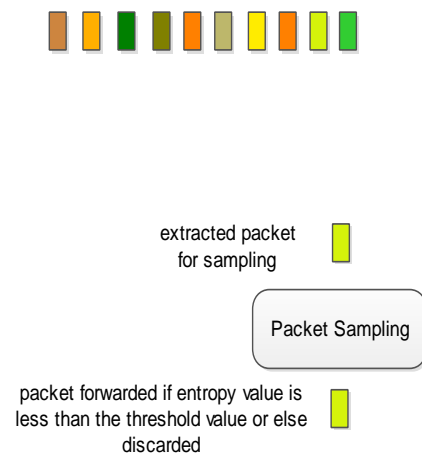
Fig. 3.7: Packet Sampling implemented on router

4. RESULTS AND DISCUSSIONS

Server side parameters such as CPU Utilization, Load response time and Delay are considered to analyse the

effect of the DDoS attack on the performance of the servers in the simulated network.

4.1. Comparison of the Results from the Attack and Hardened Scenarios

It can be seen from the graph in Figure 4.1 that the Web (HTTP) server utilization during the attack scenario is very high, getting to the peak value of 0.28 percent CPU utilization because more traffic packets is being sent by the attacker to the server in order to exhaust the server by requiring more of its processing time. However, the result shows that the web server utilization under the Hardened Network is reduced with initial rise to the peak value of about 0.08 percent and then drastically reduced to almost 0.02 percent CPU Utilization. This indicates that the server was less utilized in the Hardened network scenario as a result of PST that was implemented to help in filtering off the abnormal or flooded traffic thereby maintaining normal CPU utilization and preventing the DDoS attack on the Web server.
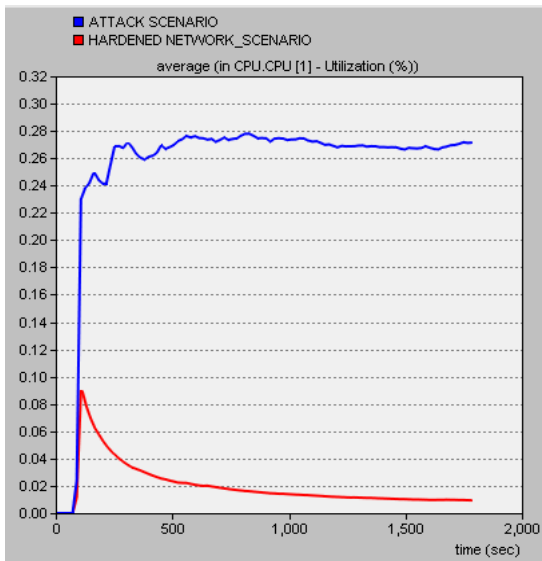
Fig.4.1: Web Server – CPU Utilization (%)

Figure 4.2 shows that under the attack scenario there is a peak rise of email load in sessions per seconds as compared to the result of a low email load under the hardened scenario. In the first instance, because of the over flooding of the web server, more session are requested leading to the rise in load session per seconds while in the hardened scenario, the attack traffic have been filtered thereby reducing the email load on the web server. This shows that the PST was able to block and prevent further attack on the web server.
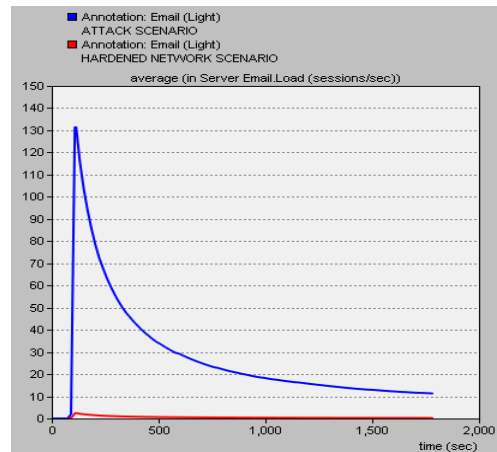
Fig. 4.2: Web Server – Load (Sessions/Sec)

From the graph in Figure 4.3, the result of the VoIP server for the voice called party jitter measured in seconds shows that there is a rise to 600 microseconds for the attack scenario. The attacker floods the server with more traffic packets to exhaust the server. This makes server to be busy processing these packets preventing it to attend to the legitimate requests. However, in the hardened scenario the packets jitter dropped to about 1.6 microseconds. This result has shown that the implemented PST is able to secure the VoIP server from over flooding with the attacker's illegitimate and unnecessary traffic packets.
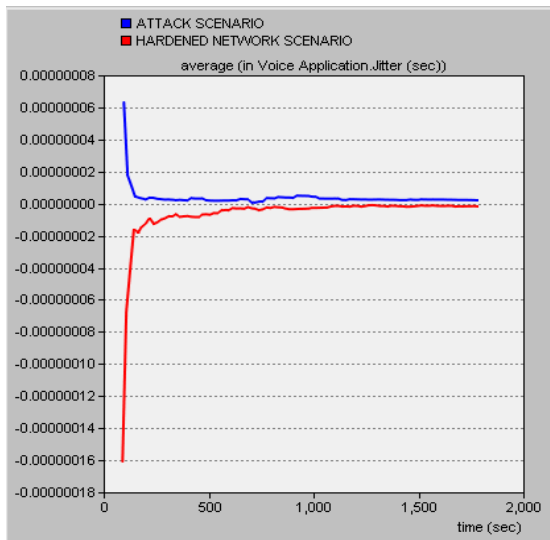
Fig.4.3: VoIP server – Jitter (seconds)

Also, it can be observed from Figure 4.4 that, in the Attack Scenario the load on the FTP server is high to about 0.64 load(requests per seconds) because of the flooding of the server with more requests by the attacker and consequently increasing the connection requests time. However, in the Hardened scenario, the load on the FTP server dropped drastically, which shows that the PST mitigation technique implemented effectively secured the server from the attacker's unnecessary flooding requests.
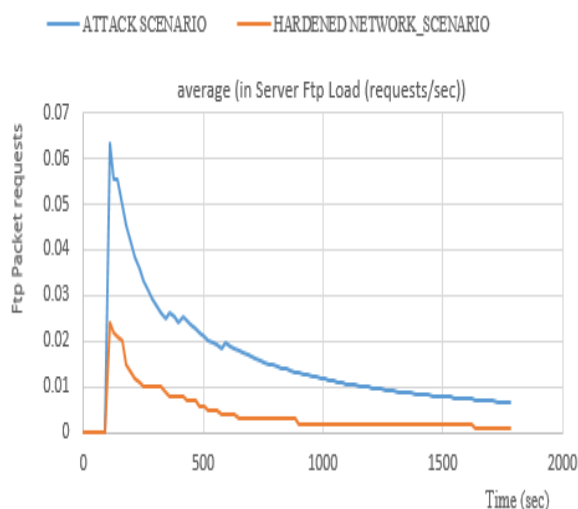
Fig. 4.4: FTP server – Load (request/sec)

5. CONCLUSION

In this paper, Packet Sampling Threshold (PST) technique was implemented on two separate firewalls in a modelled Campus Core Network to mitigate Distributed Denial of Service (DDoS) attack. In the technique, a threshold was set such that once any incoming traffic packet is greater than the set threshold; such a packet is labelled as an attack packet and hence discarded.The results from the simulation carried out on OPNET Modeler 14.5 showed that the PST technique implemented was able to block the DDoS attacks on the servers. In this way, the system load is greatly reduced and DDoS attacks were prevented in real time.

Furthermore, hybrid techniques can be adopted such as the combination of the Packet Sampling Technique (PST) with neural network to improve the effectiveness of the security of a Campus Network against DDoS attacks.

REFERENCES

Anjali, M. & Padmavathi, B. (2014). DDoS Attack Detection Based on Chaos Theory and Artificial Neural Network. *Journal of Computer Science and Information Technologies,* 5(6), 7276-7279.

Arshey, M. & Balakrishnan, C. (2013). Prevention Strategies and Network Intrusion Prevention Techniques for DoS Attacks. *International Journal of Advanced Research in Computer Engineering,* 2 (2),1174-1178.

Deepak, A., Puneet, S. & Vineet, S. (2014). Impact Analysis of Denial of Service (DoS) Due to Packet Flooding. *International Journal of Engineering Research and Applications,* 4 (6),144-149.

Hak, J. K. (2013). An Introspective view of Denial of Service (DoS): Detection, Prevention and Mitigation.

International Journal of Scientific Knowledge, 3 (40),10-15.

Juniper, (2008). Protecting the Network from Denial of Service Floods. Available athttp://www.juniper.net. Retrieved on 01-06-2008. 1-10.
Juniper, (2010). Design Considerations for the High-Performance Campus LAN. Available at http://www.juniper.net. Retrieved on 10-06-2010.

Kharat, J.S. & Radhakrishna, N. (2013). A Vivacious Approach to Detect and Prevent DDoS Attack. *InternationalJournal of Research in Engineering and Technology,* 2 (10), 434-440.

Lonea, A. M., Popescu, D. E. & Tianfield, H. (2013). Detecting DDoS Attacks in Cloud Computing Environment. *International Journal of Communication,* 8 (1), 70-78.

Shalaka, S. C., Madhulika, S. M., Prajyoti, P. S., Sneha, S. P. & Nilesh, S. (2014). Mitigating Denial of Service Attacks using Secure Service OverlayModel. *International Journal of Engineering Trends and Technology,* 8 (9), 479-483.

Wesam, B. & Mehdi, E. M. (2014). Review Clustering Mechanisms of Distributed Denial of Service Attack. *International Journal of Computer Science,* 10 (10), 2037- 2046.

ADAPTIVE BANDWIDTH RESERVATION SCHEME FOR EFFICIENT TRANSMISSION OF TELEMEDICINE TRAFFIC IN CELLULAR NETWORKS

E. J. Obamila[1*], A. J. Onumanyi[2], A. M. Aibinu[3]
[1]Federal University of Technology, P.M.B. 65, Minna, Nigeria
[2,3] Federal University of Technology, P.M.B. 65, Minna, Nigeria
*johnsond12001@yahoo.com, 08064931566.

ABSTRACT

Efficient transmission of Telemedicine traffic is an important aspect of telecommunication engineering because it conveys critical data about a patient's state and vital measurements. Consequently, it is required that such transmissions be accelerated and errorless. This requirement is beyond the norm of only scheduling users at a Base Station, but calls for the provisioning of guaranteed bandwidth reserved for these users within a cell and as they move across different cells. However, this can lead to fairness issues (poor Quality of Service) for regular traffic users within the same cell and also possible wastage of such reserved bandwidth, especially when it is unused. In this paper, we propose an algorithm to address this problem, and term it an adaptive bandwidth reservation scheme based on regular updates of a subscriber's Received Signal Strength. Only details of the algorithm and its working operation are provided here, however, as part of an ongoing work, the algorithm will be subjected in future works to evaluation and validation. Possible expected results are highlighted herein.

Keywords: *Bandwidth reservation, priority order, signal strength update, telemedicine traffic*

1. INTRODUCTION

One of the foremost causes of death in Nigeria is motor vehicle accidents. According to the Federal Road Safety Corps (FRSC), about 3,000 people died in road accidents between January and December 2011 in Nigeria and mortalities were recorded in 2,235 separate road accidents (2015). According to (Ugbeye, 2010), the occurrence of deadly Road Traffic Accidents (RTA) is peak in developing countries and especially in sub-Saharan Africa. The yearly occurrence of trauma deaths in Nigeria alone was put at 1,320 per 100,000 people and remarkably, most of these deaths happened in the first hour of injury, mostly before the patient arrives at the hospital. Basically, though voice communications in most cases, the emergency response teams providing the on-scene pre-hospital assessment takes the patients' vital signs measurements and transmit same to the main health care centres. Because it is mainly voice communication between the response teams and the physician at the main health care centre, assessments will be made based only on the description but

cannot monitor the patient through video communication, receive ECG images, X-ray images etc. Compounding that challenge is the issue of limited health care facilities, which are only located in the cities. Thus inadvertently increasing the time lapse between incident and care, thereby worsening the outcome for the patients (Ugbeye, 2010). Unfortunately, mainly due to vehicular traffic congestion, the arrival of the patients to the main healthcare centre is always delayed. Across Nigeria, the arrival time to the hospital after road traffic accidents is put at 93.6 minutes on the average according to a survey presented in (Ugbeye, 2010). It is therefore clear, that telemedicine systems are necessary where the physician at the main health care centre can remotely monitor and observe the patient and also obtain real time measurements of the patients' vital signs.

The increasing awareness and interest in telemedicine coupled with the advancements in telecommunications technologies has given rise to the many telemedicine applications successfully deployed (Fontelo et al, 2005), (Holopainen et al, 2007), (Maia et al, 2006), (Olariu et

al,2004). The broad range of telemedicine applications include: (i) Teleradiology (ii) Teleconsultation (real-time, store-and-forward) (iii) Telesurgery (iv) Remote Patient Monitoring and (v) Health Care Records Management. In many of these studies, the efficient use of cellular network resources was vital to ensure errorless and accelerated transmission of all telemedicine traffic i.e. video, audio, data etc., chiefly because of the criticality of the transmitted traffic and the limitations of bandwidth availability. The task of transmitting telemedicine data as soon as they get to the Base Stations goes beyond a scheduling task of a scheduler at the base station since the telemedicine user must have bandwidth resources available to transmit before scheduling occur. Therefore, the prioritized or guaranteed transmission of telemedicine traffic by reserving bandwidth for telemedicine traffic is a quick fix to these challenges. The direct consequence of this approach, firstly, is the violation of the Quality of Service (QoS) requirements of regular traffic users and secondly, when reserved bandwidth is left unused, it can result in bandwidth wastage. While a lot of research work is ongoing in this field, a noteworthy observation is that most of these studies concentrate singularly on the transmission of telemedicine traffic over cellular networks, failing to note that regular traffic, which largely constitutes the bulk of traffic in a network also has strict Quality of Service (QoS) requirements as well.

The transmission of the sparse but crucial telemedicine traffic with regular traffic is more complex than just a scheduling challenge. To put that in perspective, in Pavlopoulos et al (1998), 27% of ECG data transmission interruptions occurred in GSM mainly due to traffic congestion in the network. To curb this form of interruptions, telemedicine traffic can be given utmost importance, but doing this will imply creating dissatisfaction to regular users that are already existing and active in the serving cell. Given the crucial and critical

nature of telemedicine traffic, diverse nature of the QoS requirements, appropriate bandwidth reservation is necessary between cells for the purpose of handoff traffic especially telemedicine traffic handoff. The focus of the paper therefore, is that of transmitting the *urgent, critical and crucial* telemedicine traffic by reserving just the appropriate bandwidth throughout the trajectory of the Mobile Station by using the Received Signal Strength Updates measured by the user's MS to predict the direction of movement of the user. Accurate prediction of the movement of the user transmitting telemedicine data is essential so as to ensure that the bandwidth will not be reserved indiscriminately, thus leading to wastage.

Specifically, we are considering the mutual transmission of telemedicine traffics in the form of voice, real-time medical video, ECG signals, and medical images like X-ray scans in a multi-user cellular environment. We also considered the fact that only little tolerance to loss and delay is acceptable in the delivery of medical videos in real-time and other urgent telemedicine traffic. An essential Quality of Service requirement in cellular networks is keeping the probability of handoff packet dropping below a specified limit so that mobile users are able to continue current sessions as they hand-off from one cell to the next.

There are numerous of techniques available to realize mobile stations' movement predictions. These include: (i) an approach that is based on location where the current location and movement direction of an ongoing call from an MS is measured and the location update of the MS is used in predicting the next cell to be entered and (ii) an approach that is history based where the pattern of movement of each MS is predicted based on the mobility history of the MS or by analysing the movements of previous subscribers and then assuming that the ongoing subscribers will travel in that similar pattern (Zander & Karlsson, 2004). The method we are proposing will be

based on the Received Signal Strength updates of the Mobile Station (MS).

In Lee & Hsueh (2004), a predictive channel reservation approach, known as the road-map-based channel reservation scheme (RMCR) was proposed. The intention of the author is to develop a scheme that will improve bandwidth utilization and guarantee that the probability of handoff dropping is reduced. But some assumptions were made in this RMCR approach, that the base stations (BSs) are equipped with road-map information and that mobile stations (MSs) are equipped with global positioning systems (GPS) devices. The MSs intermittently report their GPS location information to their BSs and the BSs evaluate the probability that the MSs will get to the neighbouring cells based the road-map information that is available to the BSs. Thereafter, the BSs compute the amount of bandwidth to be reserved, based on such estimation.

A predictive approach in Choi & Shin (2002) was proposed for bandwidth reservation, in which case the authors develop a method to estimate user mobility based on cumulative history of hand-offs observed in each cell. The history of handoffs observed is then used to probabilistically predict MS directions and hand-off times in a cell. The bandwidth to be reserved for each handoffs is calculated by estimating the total sum of fractional bandwidths of the expected hand-offs within a mobility-estimation time window. The approach (Choi & Shin, 2002) also utilized the location information that is available from the GPS and the mobile's recorded moving history for the prediction. The challenge with this proposed method is that if the MS frequently report their position, the computational load of processing this information will be very high. But since the MS on its own constantly monitors the Signal Strength for the purpose of handoff, this is what our proposed method is exploring so as not adding unnecessary computational load.

The research work by Soh & Kim (2006) proposed a predictive bandwidth reservation approach using road topology information and the positioning of the mobile. For the purpose of prediction of movement of mobile, it is required that the MS reports its position to the serving Base Station periodically i.e. 1s interval. The BS performs the prediction periodically, and the BSs are presumed to have adequate computational and storage capabilities for the purpose of maintaining a database holding some of the required information including the road topology information within the coverage area for prediction purposes. The constraint of this approach is that there is a certain amount of bandwidth utilized by the MSs in periodically updating its position and the computational load increased on the BSs.

In Yu et al (2008), a scheme based on reward reinforcement learning coupled with stochastic approximation was proposed for bandwidth reservation and to implement the algorithm, neural networks was used. But the major constraint in the approach is signalling overhead needed for some feature extraction and local estimation functions. This signalling overheads will need to be eliminated or reduced to the barest, thus reducing the system's complexity and computational load.

Koutsakis (2011) put forward an adaptive bandwidth reservation scheme for telemedicine transmission, in which case the road map approach was used but the approach was based on the assumption that the network provider have check points configured into the MS GPS map. These check points are configured such that it is very close to the cell boundaries, hence once the MSs get to the check point, the next cell to be entered is predicted and bandwidth is thus reserved in that next cell for telemedicine traffic.

The challenges with all the approaches discussed thus far is that of (i) computational load on both the BSs and the MSs (ii) the complexity of the proposed scheme and (iii) memory usage. To design a bandwidth reservation scheme

that will be efficient, these constraints will have to be factored in. But since the MSs periodically updates its Received Signal Strength of both the serving BS and the neighbouring BSs, that approach can be used for predicting the MS movement and thus bandwidth reservation.

The displeasure of experiencing forced call termination by a wireless cellular subscriber while moving between cells is much higher than that of a subscriber who experiences call blocking while attempting to access the network for the first time (Yu et al, 2008). Therefore, it is imperative that the system accommodates newly arriving handoff calls in any cell of the network. For highly critical, crucial and urgent traffic such as telemedicine traffic, it is important that the handoff be seamless. On the other hand, the strategy of reservation of a substantial amount of bandwidth for possible seamless handoff calls may lead to a portion of the bandwidth being left unused because the handoff traffic is of small volumes, meanwhile, the remaining resources available for newly generated traffic from within the cell may not be sufficient. This explains the need for a bandwidth reservation scheme that is adaptable and not fixed.

Bandwidth reservation scheme should be based on priority order of the telemedicine data to be transmitted. The choice of priorities is based on the importance that each of these traffic types currently has for medical care (Bhargava et al, 2003). We will adopt this same priority order for the bandwidth reservation scheme. As for regular traffic, prioritization is based on the strictness of the QoS requirements for each traffic type. Table 1 shows the traffic types we will consider, arranged in descending priority order.

Table 1 – Traffic types to be used arranged in descending order of priority

Traffic Types
Handoff ECG
Handoff X-ray
Handoff Telemedicine Image
Handoff Telemedicine Video
ECG
X-Ray
Telemedicine Image
Telemedicine Video
Handoff Video
Handoff Voice
Handoff Email
Handoff Web
Video
Voice
Email
Web

The remaining part of the paper is arranged thus: Section 2 discusses our proposed methodology, while Section 3 explains the expected results and discussions, the Conclusion is presented in Section 4.

2. METHODOLOGY

2.1. Network Model

Our assumption is that the cell is a hexagonal cell architecture based on the comparative analysis and evaluation of hexagonal cell and circular cell architecture (Baltzis, 2011). Each cell has six neighbour cells as shown in Figure 1. Each Base Stations (BSs) are located at the centre of the cells and the Mobile Stations (MSs) are uniformly distributed within the cell. We also assumed free space loss propagation.
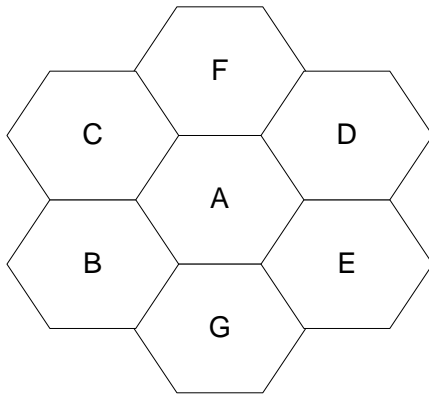
Fig. 1: Cellular network model

2.2. Our Proposed Bandwidth Reservation Scheme

For mobile station (MS) movement prediction for the purpose of bandwidth reservation for telemedicine traffic, we will explore the fact that Mobile Stations continuously takes measurement of the Received Signal Strength from the serving Base Station and other neighboring base stations. Because Signal Strength is a highly unstable parameter due to factors like fading, shadowing, we set two level of checks to make sure that the MS movement from a cell to next cell is accurate. This is to ensure that the prediction of mobile's trajectory is trustworthy and not lead to an unnecessary and indiscriminate reservation bandwidth in the neighboring cell. A minimum acceptable threshold value for Relative Signal Strength (RSS) is set and a hysteresis value is also set. Bandwidth reservation is initiated in the next cell when the serving BS's RSS falls below the Threshold value and one of the neighboring BSs have RSS stronger than the serving BS by the set hysteresis value. To avoid delay in initiation, reservation of bandwidth and actual movement of the mobile into the next cell, we introduced a next check, such that bandwidth reservation is done just before the hysteresis value is attained. Putting in these checks will mitigate against wrong prediction of mobile's movement.

Moreover, rather just reserve a fixed bandwidth for the transmission of the sparse, yet critical telemedicine traffic,

we propose an adaptable reservation, in which case bandwidth reserved will be just the amount of bandwidth needed for the transmission of the remaining data. The algorithm for the realization of the proposed scheme is shown section 2.3 below, with the flowchart is presented in Figure 2.

2.3. Algorithm for Our Bandwidth Reservation Scheme

(i) Set the value of the Minimum acceptable RSS threshold value and hysteresis value.

(ii) For a new user in the system, Bandwidth request is declared in each user's initial request to the BS.

(iii) The value of the RSS is checked at regular intervals to obtain the RSS of the serving BS and those of neighbouring BSs.

(iv) Check if the serving BS's RSS value is below the minimum threshold value.

(v) Check the neighbouring BSs RSS value to see any BS with an RSS value higher than the serving BS's value by an amount equal to or greater than the hysteresis value.

(vi) Reserve bandwidth for the various incoming traffic types into the cell in the Priority order at Table 1.

(vii) Reserve bandwidth that is equal to the remaining bandwidth that the MS will need to complete its transmission for real-time video transmission.

(viii) For all other types of users, reserve bandwidth that is equal to their current bandwidth so that seamless transmission is guaranteed.
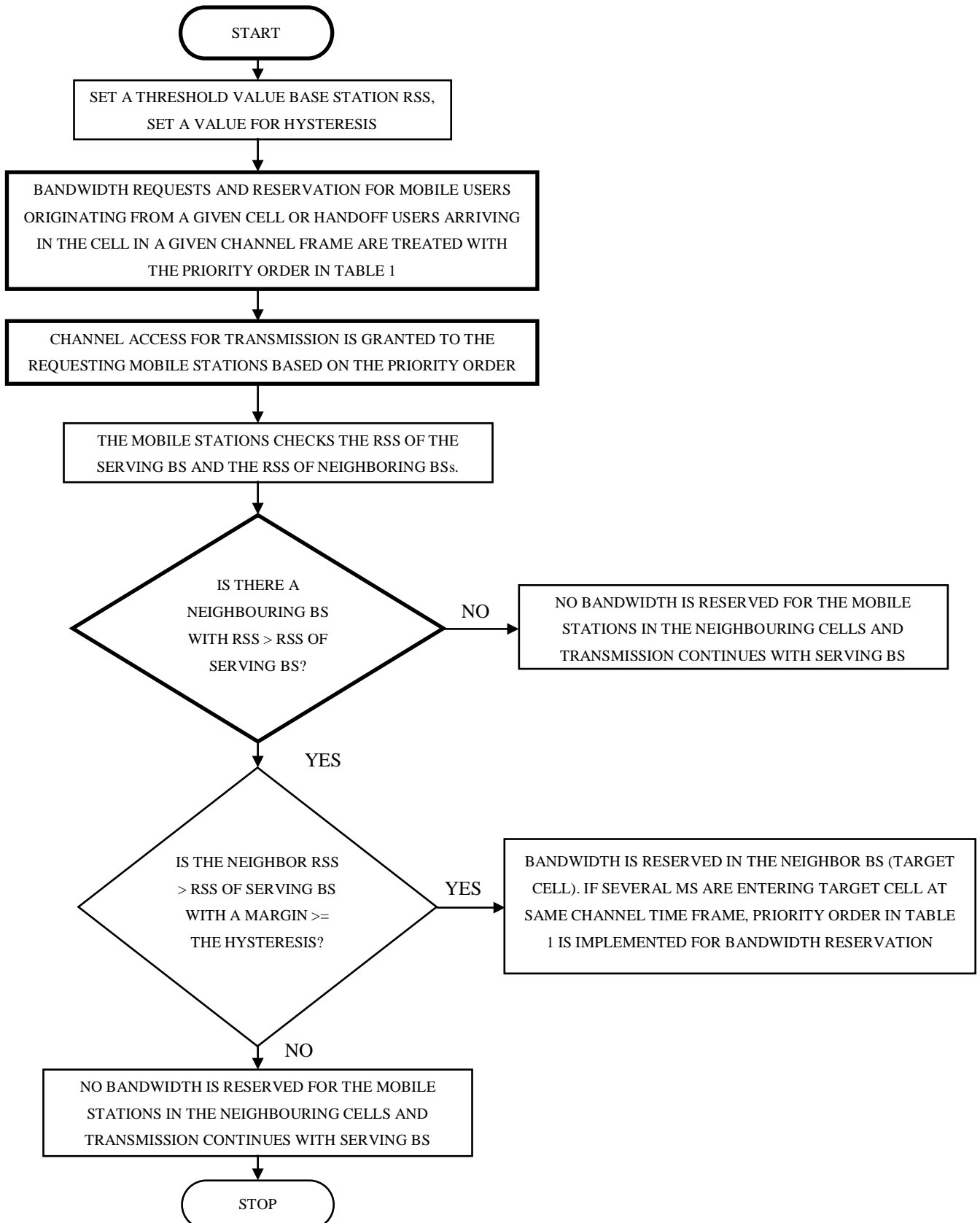
Fig. 2: Flowchart of Our Proposed Bandwidth Reservation Scheme

3. RESULTS AND DISCUSSIONS

The algorithm for the proposed bandwidth reservation method and performance evaluation is to be implemented using MATLAB. The expected outcomes are as follows:-

(i) The proposed scheme assures efficient bandwidth reservation scheme that will not only guarantee prioritized and efficient transmission of telemedicine traffic but ensure efficient bandwidth utilization.

(ii) The scheme also guarantees that the prediction of the mobile's trajectory is accurate thus, bandwidth is not reserved indiscriminately.

3.1. Performance Evaluation

Bandwidth Efficiency is one important parameter used to evaluate the performance of bandwidth reservation scheme, which is obtained using the Equation 1 below.

$$f = NR/NQ \qquad (1)$$

Where: NR is the bandwidth reserved in the next cell

NQ is the actual bandwidth utilized by the handoff users

f is the bandwidth efficiency

Bandwidth Efficiency is achieved when f is as close as possible to 1, which is the goal of our proposed bandwidth reservation scheme.

4. CONCLUSION

The need for accelerated and errorless transmission of telemedicine traffic over cellular networks cannot be over-emphasized. While most studies have focused on the use of GPS, road map information of the radio coverage area, history based approach for the prediction of the trajectory of the MS transmitting telemedicine traffic, we have proposed the use of Signal updates on the MSs for the purpose of prediction and for seamless handoff from one cell to the next. The bandwidth reservation scheme proposed is less complex with little or no computation load and memory usage as compared to others and will guarantee efficient prioritization and transmission of telemedicine traffic.Theongoing work of the researcher is to incorporate bandwidth reservation scheme with a fair scheduling scheme for efficient transmission of telemedicine traffic in next generation wireless access system.

REFERENCE

http://naijagists.com/nigerian-road-accident-statistics-for-2011-3000-deaths-recorded/ Retrieved on July 13, 2015

Baltzis, K. B. (2011). Hexagonal vs Circular Cell Shape: A Comparative Analysis and Evaluation of the Two Popular Modeling Approximations, Cellular Networks - Positioning, Performance Analysis, Reliability. Retrieved from http://www.intechopen.com/books/cellular-networks-positioning-performance-analysis-reliability/hexagonal-vscircular-cell-shape-a-comparative-analysis-and-evaluation-of-the-two-popular-modeling-a

Bhargava, A., Khan, M. F., & Ghafoor, A. (2003). QoS management in multimedia networking for telemedicine applications. In the Proceeding of IEEE Workshop Software Technology, Future Embedded System, (pp. 39 - 42). Hakodate, Japan.

Choi, S.,& Shin, K. G. (2002). Adaptive bandwidth reservation and admission control in QoS sensitive cellular networks. IEEE Trans. Parallel Distributed Systems, 13(9), 882 - 897.

Fontelo, P., DiNino, E., Johansen, K., Khan, A., & Ackerman, M. (2005). Virtual Microscopy: Potential Applications in Medical Education and Telemedicine in Countries with

Developiong Economies. Proceedings of the 38th Hawaii International Conference on System Sciences, (p. 153c).

Health, S. N. (2007). Healthy Ageing, A Challenge for Europe.

Holopainen, A., Galbiati, F., & Voutilainen, K. (2007). Use of smart phone technologies to offer easy-to-use and cost effective telemedicine systems. Proceedings of the First International Conference on the Digital Society (ICDS), (p. 4).

Koutsakis, L. Q. (2011). Adaptive Bandwidth Reservation and Scheduling for Efficient Wireless Telemedicine Traffic Transmission. IEEE Transactions on vehicular Technology, 60, pp. 632 - 643.

Lee, D., & Hsueh, Y. (2004). Bandwidth reservation scheme based on road information for next generation cellular networks. 53(1), 243 - 252.

Maia, S., Wangenheim, A., & Nobre, F. (2006). A Statewide Telemedicine Network for Public Health in Brazil. Proceedings of the 19th IEEE Symposium on Computer-Based Medical Systems (CBMS'06), (pp. 495-500).

Olariu, S., Maly, K., Foudriat, E. C., & Yamany, S. (2004). Wireless Support for Telemedicine in Disaster Management. Proceedings of Tenth International Conference on Parallel and Distributed Systems (ICPADS'04), (pp. 649 - 656).

Pavlopoulos, S., Kyriacou, E., Berler, A., Dembeyiotis, S., & Koutsouris, D. (1998). A novel emergency telemedicine system based on wireless communication technology - AMBULANCE. IEEE Trans. Inf. Technol. Biomed, 2(4), 261 - 267.

Soh, W. S., & Kim, H. S. (2006). A Predictive bandwidth reservation scheme using mobile positioning and road topology information. IEEE/ACM Trans. Network, 14(5), 1078 - 1091.

Ugbeye, M. E. (2010). An Appraisal of Emergency Response System to Victims of Trauma in Nigeria. A conference proceedings on Emergency Response to Victims of Gun Violence and Road Accidents (p. 9). Ikeja, Lagos: CLEEN Foundation, Lagos.

WHO. (2002). Active Ageing: A Policy Framework. A contribution of WHO to the 2nd United Nations World Assembly on Ageing. Madrid, Spain.

Yu, F. R., Wong, V., & Leung, V. (2008). A New QoS provisioning method for adaptive multimedia in wireless networks. IEEE Trans. Vehicular Technology, 57(3), 1899 - 1909.

Zander, R., & Karlsson, J. M. (2004). A rate-based bandwidth borrowing and reservation scheme for cellular networks. In Proceedings of IEEE Vehicular Technology Conference, (pp. 1123 - 1128). Los Angeles, CA.

Application of Inverse method to Reconstruct the form of Pulse During Impulsive damage to Pipelines

Olugboji Oluwafemi Ayodeji[1], Jack Hale[2], Jiya Jonathan Yisa[3] Ajani Clement Kehinde [4*]

[1, 3, 4]Mechanical Engineering Department, Federal University of Technology, Minna Niger State. Nigeria

[2] School of Mechanical and System Engineering, Newcastle University, United Kingdom

[*]clemajan@gmail.com, +2347067674141.

ABSTRACT

Petroleum pipelines damages if untimely detected, poses a tremendous challenge to the oil sector of an economy as it causes oil spillage, theft or explosion of the petroleum products while on transit. It is against this backlash an inverse pulse propagation method for reconstructing the form of pulse generated during pipeline defects was devised and presented in this paper. Inverse problem occurs in several branches of science and engineering. It involves the determination of the parameters of a model that describes or explains a set of observed data .This work deals with an inversion technique that was developed to reconstruct the form of a pulse after it has been propagated along a pipe. To test the suitability of the developed technique, a mathematical model was developed. The theoretical model was validated by experiment using a developed pipeline system. The experimental test rig comprises of a flexible hose pipe 23m long and 19mm diameter with four pressure sensors distributed along the pipeline and connected to the data acquisition system. Static and flowing air in the pipeline were use in the experimental test to validate the developed inverse technique model. The inverse method showed a close relationship to the original pulse.

Keywords:_Pulse,Event,InverseMethod,Sensor._

1. INTRODUCTION

Pipelines serves as one of the means of transporting petroleum products. Unfortunately, they are sometimes subjected to either natural or man-made damages. These damages once untimely detected leads to oil explosion and theft thereby, endangering human lives and properties. During such damages, pressure pulses are generated at the source where these damages has occurred. It is therefore possible to work backwards to the locations where the damages has occurred based on information obtained from the sensors that are located at various intervals along the pipeline. These sensors contains vital information that can be used to work

backwards. A possible method of reconstructing the form of these damage is the use of inverse method. An inverse problem is one that occurs in many branches of science and mathematics where the values of some model parameter(s) must be obtained from the observed data. Inverse methods can be basically considered as an approach for interpolating or smoothing a data set in space and time where a model acts as a dynamical constraint (Evensen, 1994). In geophysics, inverse problems require an understanding of the "forward process" that relates the model to its geophysical response. They also require knowledge of the statistical reliability of the observed data. Aspects that must be considered in inverse problems include the formulation

and parameterization of the problem, the existence, uniqueness and resolution of solutions, strategies for dealing with over-determined and under-determined model parameters, and strategies for introducing independent constraints into the solutions (Ferguson, 2005).

Forward Theory: The (mathematical) process of predicting data based on some physical or mathematical model with a given set of model parameters (and perhaps some other appropriate information, such as geometry, etc.). As an example, consider a two-way vertical travel time t of a seismic wave through M, *layers* of thickness h_i

and velocity v_i. Then t is given by: $t = 2\sum_{i=1}^{M} \frac{h_i}{v_i}$.

The forward problem consists of predicting data (travel time) based on a (mathematical) model of how seismic waves travel. Suppose that for some reason thickness was known for each layer (perhaps from drilling). Then only the M velocities would be considered model parameters. One would obtain a particular travel time t for each set of model parameters one chooses.

Schematically, one might represent this as follows:

| Data | → | Model | → | Predicted model parameters |
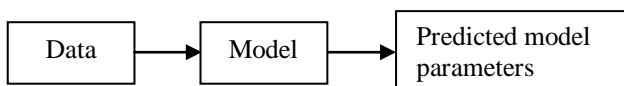
As an example, one might invert the travel time t above to determine the layer velocities. Note that one needs to know the (mathematical) model relating travel time to layer thickness and velocity information. Inverse theory should not be expected to provide the model itself.

The work as carried out by this research is made more difficult as there are no possibilities of making repeat trials, but fortunately this is made possible because a one-dimensional wave guide was considered rather than the three dimensional interior of the Earth.

2. METHODOLOGY

2.1. The Inverse Theory

Inverse problems may be described as problems where

the solutions are known, but not the causes. Alternatively, where the results, or consequences of the problem are known but not what must have caused it. Inverse theory therefore requires knowledge of a forward model capable of predicting data if the model parameters are already known. In an inverse problem measurements are taken of these effects and calculations made to establish what caused them. This requires a description of the data; in most inverse problems the data are simply a table of numerical values, of which a vector provides a convenient means of representing them.

Inverse theory is inherently mathematical and as such does have its limitations. It is best suited to estimating the numerical values of model parameters for some known or assumed mathematical model. It is good for extracting the model parameters that best fit the data.

The basic theory of inverse methods is fully explained by Menke (Menke, 1984).

Briefly, it can be summarized as follows. Suppose in the course of an experiment N measurements are obtained, these numbers may be considered as the elements of the vector **d** of length N. Also, the model parameters can be represented as the elements of the vector **m**, of length M.

Thus, we can write, data: $\mathbf{d} = [d_1, d_2, d_3...,d_N]^T$ (1)

model parameters:

$$\mathbf{m} = [m_1, m_2, m_3,...,m_M]^T \quad (2)$$

In the statement of an inverse problem there is a relationship between the model parameters and the data. This relationship is referred to as the model. The model usually takes the form of one or more formulas that the model parameters and data are anticipated to follow. For example, in trying to determine the resistance of a wire by measuring its voltage and current, there will be two data sets, voltage $\mathbf{d}_1$ and current $\mathbf{d}_2$ respectively, and one

unknown model parameter, resistance (m_1). The model statement would be the resistance times the current equals voltage, which can be represented compactly by vector equation (3),

$$\text{d}_1 = \text{d}_2\, m_1 \qquad\qquad (3)$$

In more realistic situations the relationship between the data and model parameter is more complicated. In the most general case, the data and model parameters are related by one or more implicit equation such as in equation (4),

$$l_1\,(\text{d, m}) = 0$$

$$l_2\,(\text{d, m}) = 0 \qquad\qquad (4)$$

$$l_N\,(\text{d, m}) = 0$$

where, N is the number of equations.

In the above problem concerning the measurements of the resistance, $N = 1$ and $d_2 m_1 = d_1$ would constitute one equation of the form

$$l_1\,(\text{d, m}) = 0$$

(5)These implicit equations, which can be compactly written as the vector equation l (d, m) = 0, summarize what is known about how the measured data and the unknown model parameter are related. The goal of inverse theory, therefore, is to solve, or invert, these equations for the model parameters.

2.2. The Linear Inverse Problem

The simplest form of a linear inverse problem as described by Menke [3], is given by,

$$\mathbf{d = Gm} \qquad\qquad (6)$$

where,

$\mathbf{d}$ = measured data, $\qquad$ $\mathbf{G}$ = data kernel

$\mathbf{m}$ = model parameters

The data and model parameters are functions $d(x)$ and $m(x)$, in which x is some independent variable. Again using the problem of determining the resistance of a wire it is possible to formulate an inverse problem.

Supposing that N voltage measurements V_j are made at current i_j in a circuit, then, the data form a vector $\mathbf{d}$ of N measurements of voltage, where,

$$\mathbf{d} = \left[V_1, V_2, V_3, \ldots, V_N\right]^T \qquad\qquad (7)$$

The current i_j provides auxiliary information that describes the geometry of the experiment. If we assume a model in which the voltage is a linear function of the current;

$$V = a + bi \qquad\qquad (8)$$

The intercept a and the slope b form the two model parameters of the problem, $\text{m} = \left[a, b\right]^T$. According to this model, each voltage observation must satisfy $V = a + bi$:

$$V_1 = a + bi_1$$
$$V_2 = a + bi_2$$
$$\qquad .$$
$$\qquad . \qquad\qquad (9)$$
$$\qquad .$$
$$V_N = a + bi_N$$

These equations can be arranged as the matrix equation d = Gm:

$$\underbrace{\begin{bmatrix} V_1 \\ V_2 \\ . \\ . \\ . \\ V_N \end{bmatrix}}_{d} = \underbrace{\begin{bmatrix} 1 & i_1 \\ 1 & i_2 \\ . & . \\ . & . \\ . & . \\ 1 & i_N \end{bmatrix}}_{G} \underbrace{\begin{bmatrix} a \\ b \end{bmatrix}}_{m} \qquad\qquad (10)$$

For any real set of measurements with experimental errors equation (8) will not be satisfied exactly, but equation 10 can still be used for a least square solution to determine the model parameters a and b.

2.3. Inverse Method Based on Least Squares

The two most common vectors that are concerned with inverse problems are the data-error or misfit vector and the model parameter vector (Menke, 1984). The methods based on data-error or misfit give rise to classic least squares solutions, while methods based on the model

parameter give rise to what is called minimum length solutions.

The improvements over simple least squares and the minimum length solutions include the use of information about noise in the data and a fore-knowledge about the model parameters.

Minimizing the Misfit-Least Squares

The error e_j for each observation is the difference between the observed and predicted datum:

$$e_j = d_j{}^{obs} - d_j{}^{pre} \qquad (11)$$

The jth predicted datum $d_j{}^{pre}$ for the straight line problem is given by

$$d_j{}^{pre} = m_1 + m_2 i_j \qquad (12)$$

where the two unknowns, m_1 and m_2, are the intercept and the slope of the line and i_j is the value along the i axis where the jth observation is made.

For N points we have a system of N such equations that can be written in matrix form as:

$$\begin{bmatrix} d_1 \\ . \\ . \\ . \\ d_N \end{bmatrix} = \begin{bmatrix} 1 & i_1 \\ . & . \\ . & . \\ . & . \\ 1 & i_N \end{bmatrix} \begin{bmatrix} m_1 \\ m_2 \end{bmatrix} \qquad (13)$$

or

$$\text{d} \quad = \quad \text{G} \quad \text{m} \qquad (14)$$
$$(N \times 1) \ (N \times 2) \ (2 \times 1)$$

The total misfit E is given by

$$E = \mathbf{e}^{\mathrm{T}} \mathbf{e} = \sum_{j=1}^{N} \left[d_j{}^{obs} - d_j{}^{pre} \right]^2 \qquad (15)$$

$$= \sum_{j=1}^{N} \left[d_j{}^{obs} - (m_1 + m_2 i_j) \right]^2 \qquad (16)$$

Dropping the "obs" in the notation for the observed data, we have

$$E = \sum_{j}^{N} \left[d_j{}^2 - 2d_j m_1 - 2d_j m_2 i_j + 2m_1 m_2 i_j + m_1{}^2 + m_2{}^2 i_j{}^2 \right] \qquad (17)$$

Taking the partial derivatives of E with respect to m_1 and m_2, and equating them to zero yields:

$$\frac{\partial E}{\partial m_1} = 2Nm_1 - 2\sum_{j=1}^{N} d_j + 2m_2 \sum_{j=1}^{N} i_j = 0 \qquad (18)$$

and $$\frac{\partial E}{\partial m_2} = -2\sum_{j=1}^{N} d_j i_j + 2m_1 \sum_{j=1}^{N} i_j + 2m_2 \sum_{j=1}^{N} i_j{}^2 = 0 \qquad (19)$$

Rewriting equations (5.18) and (5.19) above

$$Nm_1 + m_2 \sum_{j} i_j = \sum_{j} d_j \qquad (20)$$

and

$$m_1 \sum_{j} i_j + m_2 \sum_{j} i_j{}^2 = \sum_{j} d_i i_j \qquad (21)$$

Combining the two equations in matrix notation in the form $\mathbf{Am} = \mathbf{b}$ gives

$$\begin{bmatrix} N & \sum i_j \\ \sum i_j & \sum i_j{}^2 \end{bmatrix} \begin{bmatrix} m_1 \\ m_2 \end{bmatrix} = \begin{bmatrix} \sum d_j \\ \sum d_j i_j \end{bmatrix} \qquad (22)$$

or, simply

$$\mathbf{A} \quad \mathbf{m} \quad = \quad \mathbf{b}$$
(23)
$$(2 \times 2) \ (2 \times 1) \ (2 \times 1)$$

Equation (23) above shows that the problem has been reduced from one with N equations to two unknowns (m_1 and m_2) in $\mathbf{Gm} = \mathbf{d}$ to one with two equations in the same unknowns as in $\mathbf{Am} = \mathbf{b}$.

The matrix equation $\mathbf{Am} = \mathbf{b}$ can also be rewritten in terms of the original $\mathbf{G}$ and $\mathbf{d}$ when it is observed that the matrix $\mathbf{A}$ can be factored as:

$$\begin{bmatrix} N & \sum i_j \\ \sum i_j & \sum i_j^2 \end{bmatrix} = \begin{bmatrix} 1 & 1 & \cdots & 1 \\ i_1 & i_2 & \cdots & i_N \end{bmatrix} \begin{bmatrix} 1 & i_1 \\ 1 & i_2 \\ . & . \\ . & . \\ . & . \\ 1 & i_N \end{bmatrix} = \mathbf{G^T G} \qquad (24)$$

Also, **b** above can be written similarly as

$$\begin{bmatrix} \sum d_j \\ \sum d_j i_j \end{bmatrix} = \begin{bmatrix} 1 & 1 & \cdots & 1 \\ i_1 & i_2 & \cdots & i_N \end{bmatrix} \begin{bmatrix} d_1 \\ d_2 \\ . \\ . \\ . \\ d_N \end{bmatrix} = \mathbf{G^T d} \qquad (25)$$

Substituting equations (24) and (25) into equation (22), gives the equations for the least squares problem:

$$\mathbf{G^T G m} = \mathbf{G^T d} \qquad (26)$$

The least squares solution $\mathbf{m_{LS}}$ is then obtained as

$$\mathbf{m_{LS}} = [\mathbf{G^T G}]^{-1} \mathbf{G^T d} \qquad (27)$$

Assuming that $[\mathbf{G^T G}]^{-1}$ exists, this solution implies that the forward problem as in equation (13) can be used to obtain an explicit relationship between the model parameters (m_1 and m_2) and a measurement of the misfit to the observed data E. The value E is then minimized by taking the partial derivatives of the misfit function with respect to the unknown model parameters, equating the partial derivatives to zero, and solving for the model parameters (U.S. Dept. of transport, 2005).

To formulate the problem into a least-squares inverse problem, we can use the rule governing the attenuation between sensors 2 and 3: that the attenuation coefficient defining propagation is not only frequency dependent, but is proportional to frequency squared (Cao, 2007), and then work backwards from sensor 2 to the event site. Though pulse propagation in a pipeline is in reality non-linear, it is only weakly so if the dispersion effect is not too strong. In this work, the assumption of local linearity is made by neglecting dispersion and so that the problem can be approached by the least–squares inverse method.

The technique developed works in the frequency domain. The pulse signals at the sensor locations 2 and 3 are first transformed into the frequency domain using the fast fourier transform (FFT). Assuming exponential attenuation proportional to the square of each frequency component a best-fit coefficient for the attenuation between locations 2 and 3 is found. Applying this to the pulse signal from sensor 2 the original pulse at the event site is reconstructed in the frequency domain and finally transformed back into the time domain using the inverse FFT.

Pulses propagating in fluid filled pipelines can be expressed in the form:

$$p(x,t) = p_o(t) \exp(-\beta x) \qquad (28)$$

where p is the description of the pulse which is a function of time and distance along the pipe, p_o is the function defining the pulse at $x = 0$, β is frequency dependent attenuation factor, proportional to frequency squared. This formulation is general and is not restricted to any particular pulse shape.

Relating this to the Fourier spectrum in the frequency domain,

$$P_j^1 = P_j^0 e^{-\beta x_{0,1}} \qquad (29)$$

or

$$P_j^1 = P_j^0 e^{-af_j^2 x_{0,1}} \qquad (30)$$

Where P_j^0 and P_j^1 are the pulse functions transformed into the frequency domain, the subscripts denoting the index of the Fourier spectrum components and the superscripts the location of the pulse, 0 being the event location and 1, 2, 3, 4 being locations of the sensors.

$$P_j^3 = P_j^2 e^{-af_j^2 x_{2,3}} \qquad (31)$$

Taking the natural logarithm of both sides of the expression in equation 31 makes this into a linear inverse problem of the form,

f_j= the frequency of the jth Fourier component, $x_{0,1}$= distance between the event 0 and sensor 1.

a = a proportionality constant to be determined.

$$LnP_j^2 = LnP_j^3 + af_j^2 x_{2,3} \qquad (32)$$

In matrix form, this becomes:

$$\begin{bmatrix} LnP_1^2 \\ LnP_2^2 \\ . \\ . \\ . \\ LnP_N^2 \end{bmatrix}_d = \begin{bmatrix} LnP_1^3 & x_{2,3}f_1^2 \\ LnP_2^3 & x_{2,3}f_2^2 \\ . & . \\ . & . \\ . & . \\ LnP_N^3 & x_{2,3}f_N^2 \end{bmatrix}_G \begin{bmatrix} 1 \\ a \end{bmatrix}_m \qquad (33)$$

Which is of the same basic form as equation 13.

Forming the matrix products

$\mathbf{G^TG} =$

$$\begin{bmatrix} LnP_1^3 & LnP_2^3 & \ldots & LnP_N^3 \\ x_{2,3}f_1^2 & x_{2,3}f_2^2 & \ldots & x_{2,3}f_N^2 \end{bmatrix} \begin{bmatrix} LnP_1^3 & x_{2,3}f_1^2 \\ LnP_2^3 & x_{2,3}f_2^2 \\ . & . \\ . & . \\ . & . \\ LnP_N^3 & x_{2,3}f_N^2 \end{bmatrix}$$

$$= \begin{bmatrix} \sum (LnP_j^3)^2 & \sum (LnP_j^3 \times x_{2,3}f_j^2) \\ \sum (x_{2,3}f_j^2 \times LnP_j^3) & \sum x_{2,3}^2 f_j^4 \end{bmatrix} \qquad (34)$$

$$\mathbf{G^Td} = \begin{bmatrix} LnP_1^3 & LnP_2^3 & \ldots & LnP_N^3 \\ x_{2,3}f_1^2 & x_{2,3}f_2^2 & \ldots & x_{2,3}f_N^2 \end{bmatrix} \begin{bmatrix} LnP_1^2 \\ LnP_2^2 \\ . \\ . \\ . \\ LnP_N^2 \end{bmatrix} = \begin{bmatrix} \sum (LnP_j^3 \times LnP_j^2) \times x_{2,3}f_j^2 \\ \sum x_{2,3}f_j^2 LnP_j^2 \end{bmatrix} \qquad (35)$$

$\mathbf{m_{LS}} = [\mathbf{G^TG}]^{-1}\mathbf{G^Td}$

$$= \begin{bmatrix} \sum (LnP_j^3)^2 & \sum (LnP_j^3 \times x_{2,3}f_j^2) \\ \sum (x_{2,3}f_j^2 \times LnP_j^3) & \sum x_{2,3}^2 f_j^4 \end{bmatrix}^{-1} \times$$

$$\begin{bmatrix} \sum (LnP_j^2 \times LnP_j^3) \times x_{2,3}f_j^2 \\ \sum x_{2,3}f_j^2 LnP_j^2 \end{bmatrix} \qquad (36)$$

Equation (36) gives a linear solution to the least square inverse problem obtained based on the general form of the solution set out, from which the estimate of the model parameter a, which defines the frequency dependent attenuation in $\mathbf{m_{LS}}$=[1 a]$^\text{T}$ is determined. This value of the estimated model parameter a in $\mathbf{m_{LS}}$ can then be applied to the Fourier spectrum of the pulse signal at sensor 2 to compute the estimated Fourier spectrum of the form of the pulse to be reconstructed at the start of the event using equation (33)

Since, the Fourier spectrum of the pulse signal at sensor 2 is known, this allows for the computation of the log Fourier spectrum of the pulse at the event that is to be reconstructed, and from which it is a simple matter to convert to the time domain using the inverse FFT.

$$\begin{bmatrix} LnP_1^o \\ LnP_2^o \\ . \\ . \\ . \\ LnP_N^o \end{bmatrix}_d = \begin{bmatrix} LnP_1^2 & x_{o,2}f_1^2 \\ LnP_2^2 & x_{o,2}f_2^2 \\ . & . \\ . & . \\ . & . \\ LnP_N^2 & x_{o,2}f_N^2 \end{bmatrix}_G m_{LS} \qquad (37)$$

2.4. Description of Experimental test rig

Figure 1 shows the test rig that was developed to validate the theories of event location and reconstruction described above. It consists of an air filled pipe along which pressure pulses propagate, a pressure pulse generator and an instrumentation system to capture and record the propagation of the pressure pulses.

This involved the use of the simple pulse data described containing a single frequency component of 53 Hz.

The air filled pipe is a smooth bore flexible hose pipe of 19mm diameter coiled on a circular framework at a

diameter approximately 1.5m, having established that at this curvature the pressure pulses would propagate through it unimpeded, as a waveguide (Evensen, 1994). An advantage in this arrangement is that even though the pressure measurement sensors attached to the pipe of the test rig are located at long distances along the hose pipe they are still physically close together for convenience of monitoring using a single data logger without the need for long cables. Three pressure sensors were located at different positions along the hose pipe and connected to a single data logging device via three charge amplifiers.

The total length of the hose pipe is approximately 23m and the distances of the sensors from one end of the pipe are9.77m for sensor 1, 13.59m for sensor 2 and 15.45m for sensor 3.

2.5. Event Location and Reconstruction in static Air

The experiments in this section were done using thetest rig illustrated in Figure 1 and shown schematically in Figure 2. The simulation here is more realistic since the the pulse is reconstructed from the sensor 2 and 3.

Considering now, the Fourier spectrums of the pulse signals at sensors 2 and 3 along the pipeline in Figure 2, inverse methods pulse reconstruction techniques. The pulse signals at the four sensors were measured and recorded at a sampling rate of 60 kHz.

1.1. Event Reconstruction with Flowing Air

The previous experiments carried out using the test rig were conducted on static air, but this is not representative of real pipeline applications as the gas in the pipeline is expected to be flowing. The test here addresses this by investigating the effects of air flow velocity on event reconstruction. A compressed air supply with pressure control valve was attached to one end of the pipe as shown in Figure 1. This was used to control the pressure of the air at the inlet, and hence the flow rate through the

pipe. The two cases of measurements of air flow velocity through the pipe considered are:
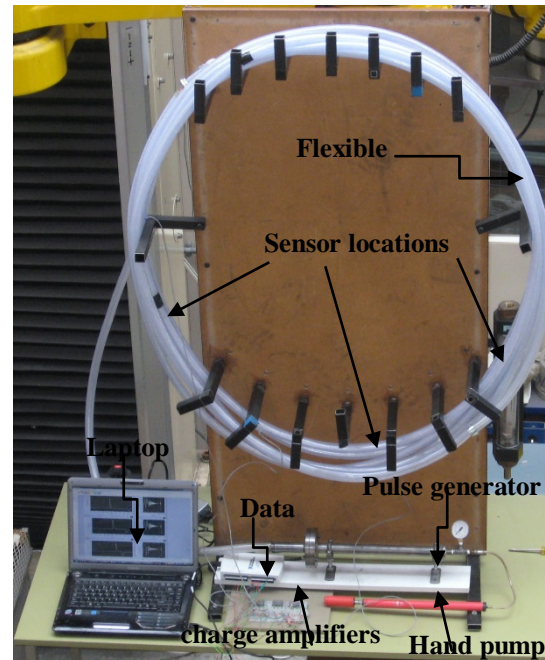
Fig.1 Experimental test rig showing the various

A pressure drop of 0.1 bar along the pipe, giving a computed mean flow velocity between sensors 3 and 4 of 25 m/s.A pressure drop of 0.2 bar along the pipe, giving a mean flow velocity between sensors 3 and 4 of 34 m/s.

2. RESULTS AND DISCUSSIONS
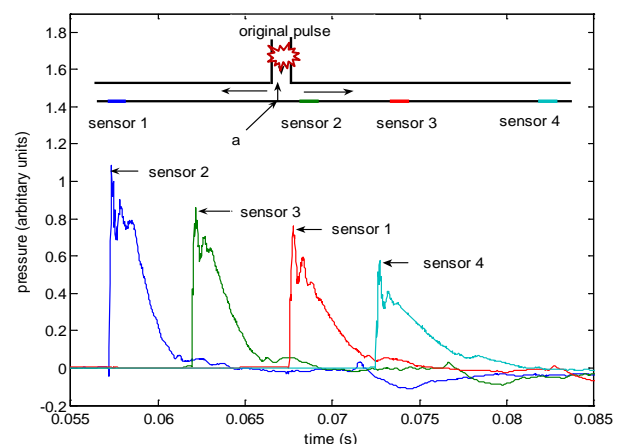
Fig. 2 Typical pressure pulse measured at all four sensors of modified rig (without air flow)

Figure 2 shows a typical pressure pulse from one of the test results obtained at the four sensors located along the pipe of the rig. Sensor 2 was located as close as possible to the tee connector, and hence to the point of arrival of the pulse in the main pipe which defines the event location because this is the place where the pulse enters the main pipe and sets off in both directions, arriving first at sensor 2, followed by sensor 3, then sensor 1 and finally sensor 4. These times of arrival are associated with the distances of the sensors from the position where the generated pressure pulse enters the pipe.

Sensor 2 is the best possible independent measurement of the event (the pulse as it enters the main pipe) because it is close to it and there will be little distortion/attenuation before the pulse propagating from the tee reaches it. The other three sensors are spread out along the pipe to reconstruct the event.

The position "a" shown is the region in the pipe wall where the originally generated pressure pulse reflects back to the source (the pulse generator) and on reaching the end wall of the source, is again reflected back into the pipe. This can be seen as the negative pressure unloading pulse appearing at sensor 2 at approximately the same time as the original pulse arrives at sensor 4.

Figure 3 shows the reconstructed pulse and the true measured pressure pulse at sensor 2, obtained using the inverse method.
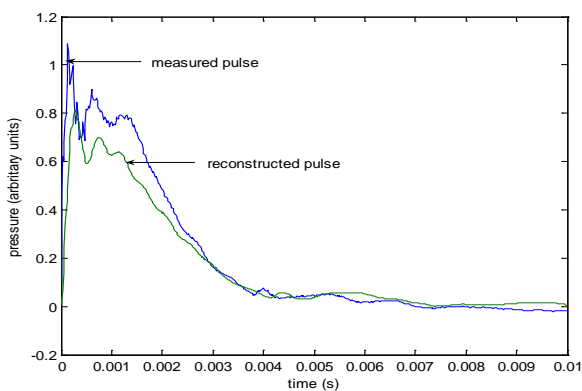
Fig. 3 Reconstructed pulse at sensor 2 by inverse methods with pulse originating between two sensors without airflow.

Figure 4 shows a typical result for the pressure pulse measurements obtained with the pressure pulse entering the main pipe between sensors 1 and 2 and the directions of air flow and pulse propagation.
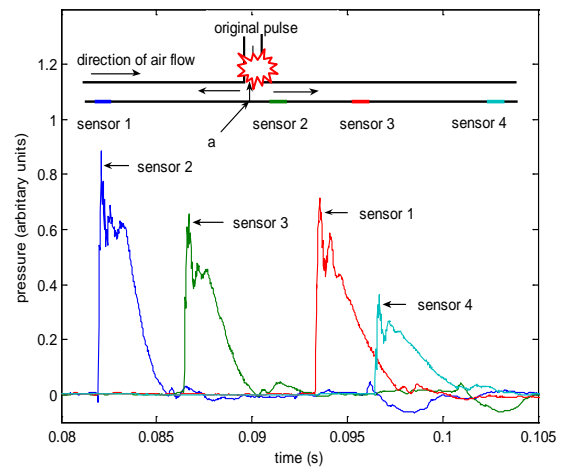
Fig. 4 Typical pressure pulse measurements at all four sensors with pressure pulse enteringbetween sensors 1 and 2 along the pipe with flowing air.

By inspection of Figure 4, it can be seen that the times of arrival of the pressure pulse at the sensors are slightly affected by the air flowing through the pipe. For the case of the flowing air, the velocity with respect to the pipe is increased in the direction of the flow and reduced in the other direction, by an amount equal to the velocity of the air flow. So the arrival times to sensors 2, 3 and 4 is reduced and that to sensor 1 increased accordingly. This reduction in the arrival times is caused by the shorter distance propagated through the air, and so the attenuation of the pulse is expected to be less between sensors 2, 3 and 4.
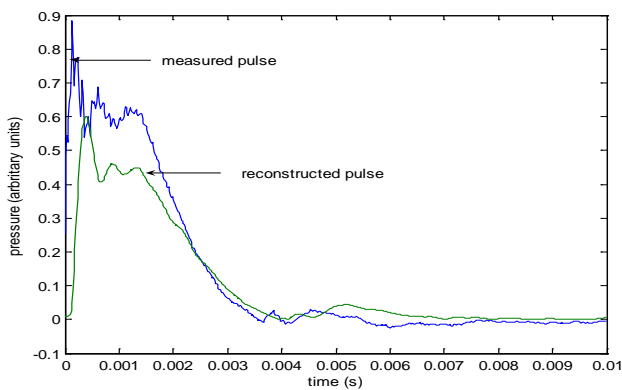
Fig. 5 Reconstructed pulse using inverse (with air flow).

Figure 5 show the form of the reconstructed pulses obtained using the inverse methods of event reconstruction. These reconstructions are typical of a quantity of measurements under the conditions of cases 1 and 2.

From Figure 5 it may be seen that the pulse reconstruction using the inverse method is closely related with the original pulse. The high quality is due to the high frequency components present in the inverse method. As such, the inverse method reconstruction is of value because it gives an underestimate of the pulse size in the range 30-35%.

From Figure 3 the shapes of the reconstructed and measured original pulse at sensor 1 agree quite well.

The magnitude of the reconstructed pulse in each case can be seen to have underestimated the measured pulse by 20%. This result is typical of the fifteen repeat tests, in which the underestimate ranged between 20 % and 22 %.

3. CONCLUSION

From the results obtained for both the static and flowing air it can be inferred that the inverse method shows a good approximation to the original pulse. These experimental results are consistent with the model results which gave a similar level of underestimation. Hence, the technique can be used to predict the cause of a damage to a pipeline.

REFERENCE

Evensen, G., (1994). "Inverse methods and data Assimilation in Nonlinear Ocean models" Nansen*Environmental and remote Sensing Center*, Bergen, Norway Physical.

Ferguson, I. J., (2005). Theory and Application of Geophysical Inversion Methods, Department of Geological Sciences University of Manitoba, *Model parameter* page 1.

Menke, W., (1984)"Geophysical Data Analysis: Discrete Inverse Theory" Academic Press. Orlando,

U.S. Department of Transportation, (2003)"Pipeline Integrity Management in High ConsequenceAreas Gas Transmission Pipelines"*Research and Special Program Administration.*

Cao, C.F, Baik, S., Choi, J.B and Kim, Y.J., (2007)"Protection of Underground Gas Protection of Underground Gas Pipelines from Third Party Damage by On-Line Monitoring Using Piezoelectric Accelerometers". Proceedings of the Institution of Mechanical Engineers, Part E: *Journal of Process Mechanical Engineering.* Volume 221, pp 61 – 67.

AUTOMATIC DETERMINATION OF CALL SETUP TIME AND RING TONE QUALITY IN GSM NETWORK

O. A. Ayo-Bello [1*], A. M. Aibinu [2], A. J. Onumanyi [3]
[1]Department of Telecommunication Engineering
Federal University of Technology, Minna
Niger State, Nigeria
*olatunjioluwabukola@yahoo.com[1], maibinu@gmail.com[2],
adeiza1@yahoo.com[3]

ABSTRACT

One essential Key Performance Indicator (KPI) for mobile network performance assessment is Call setup time (CST). However, there is no standard measurement possible for this parameter, therefore the different operators can measure it differently. In this paper, the possibility of implementing an algorithm for CST measurement using citizen sensing techniques where individual GSM users' can quantify CST from their cell telephone without the utilization of Drive Test is been proposed. Consequently, examination of GSM ringing tone, call time and the sound nature of the ringing tone is analyzed using a Labview and Matlab. The proposed procedure enables the discovery of the territories with unacceptable estimations of Call setup time and relates these to an overview of the Quality of Service of the network.

Keywords: Call Set-up Time, Independent Measurement, Key Performance Indicator, Mobile Network.

1. INTRODUCTION

System execution and Quality of Service (QoS) appraisal of a Global System for Mobile Communication (GSM) is a critical operational prerequisite for Mobile Network Providers (MNP), as it specifically influences the income era and client happiness (Sireesha, Varadarajan, Vivek and Naresh). An MNP has a higher business sector advantage when its QoS is better, this makes the MNPs to put immense effort in monitoring their respective networks and maintain broad and accurate prominence of its quality.

There has been a decrease in the QoS experienced by most end users due to the high demand for GSM services. (Amaldi, Capone, and Malucelli 2008) which has resulted in monitoring the level of QoS maintained by most MNPs (Carvalho de Gouveia, Magedanz 2008). It has been the custom of depending solely on statistics provided by the MNPs in measuring the network QoS. Dependability and reliability of such statistics remain uncertain as the public unfortunately has no access to these data except through legal permission or some cooperation from the vendors.

These made external measurement of QoS status to remain a challenge.

In view of this, new methods to independently measure QoS of the MNP data are being developed. These have formed a recent area of research interest as it has been used in different reports. The Key Performance Indicators (KPIs) used for QoS estimation include Call Setup Time (CST), Call Completion Rate (CCR), Call Drop Rate (CDR), Call Handover Success Rate (CHSR) and Standalone Dedicated Control Channel (SDCCH), but focus here will be on the use of the Call Setup Time (CST) parameter for QoS characterization. Therefore, it is the goal of this paper to provide an overview of high-tech methods used in this regards. As part of an on-going research work, this assessment will provide the different methods in use, the tools being employed, including soft and hardware; their strengths and limitations, and the future direction in this area. In addition, an overview into the development of a comprehensive system for CST measurement is introduced.

Subsequently, the rest of the paper is organized as follows: the details on the process involved in setting up a call in a GSM network and drive test tools used for conducting drive test experiments are given in Section 2, Section 3 describes the working principle of the proposed system for CST measurement and conclusion is drawn in Section 4.

2. METHODOLOGY

The Call Setup Time (CST) is the mean time of the establishment of a call from a subscriber. It is the average setup time of several successful calls. A long call setup time affects the user experience and perception about QoS for the MNPs. Thus, call setup time is one of the KPIs that is of greater concern for Mobile Network Providers (MNP) as it provides a measure to control and assure the Quality of Service (QoS) requirements. Hence, CST is an important key Performance Indicator (KPI) to evaluate the performance of a network (Carvalho de Gouveia 2000).

CST can be calculated from L3 messages and estimated by drive test. For GSM network, CST is the period from Requesting a Channel until Alerting, it is usually 7-8 s for Mobile to Mobile Calls. CST is the duration from Requesting RRC Connection until Alerting for WCDMA, usually 6-7 s for MMC.

Call setup time increases as a result of problem in hardware, transmission, coverage, or interference. A faulty TRX or combiner or an incorrectly connected RF cable makes seizing of the SDCCH or TCH difficult, and thus resulted in call setup time been increased (Yang, C. 2008).

Poor transmission quality, instability of transport links, insufficiency of resources, or bit errors on the Abis and A interfaces may lead to an increase in the error rate on the links, which results in more message retransmissions between switches. Thus, the message transfer delay increases and congestion may occur on the links which in severe cases causes routes to change frequently, which leads to instability and congestion on the links. If the preceding problem occurs during call setup, the call setup time increases (Yang, C. 2008).

The CST can be obtained through traffic measurement and Drive Test (DT). However, based on the need for independent measurement, we discuss the DT approach, which guarantees independence in the next section.

2.1 Drive Test

Coverage, capacity and Quality of Service (QoS) of a mobile radio network can be evaluated with Drive Testing method. It is carried out to check the coverage criteria of the cell site with the RF drive test tool. The procedure involves using a car containing mobile radio network air interface measurement equipment that can detect and keep a wide variety of the physical and virtual parameters of mobile cellular service in a given geographical area. Drive test equipment typically gathers information and services running on the network such as voice or data, radio frequency scanner and GPS information to provide location logging (Amaldi et. al 2008).

There are different types of tools to carry out a DT among which are: JDSU E6474A v15.2, TEMS Investigation, Nemo Outdoor. However, in this research work an algorithm was developed using Matlab and LabView to analyze the ring tone from mobile network providers for their call time characteristics. The result gotten will then be used in the CST Analyzer to predict QoS as explain in the next section.

2.2 Proposed CST Analyzer to Predict QoS of a GSM Network using a Citizen Sensing Approach

Ringtone and CST analyzer to predict QoS of a GSM network is being proposed as part of on going research using a citizen sensing approach. This section only focuses on the discussion of the proposed CST estimation algorithm

which consists of a four distinct stages as shown in Figure 2.

Call tone recording software will be installed on a test phone for acquisition of the required ringing tone. The software will be activated during a call dialing process and when answering a call. The software works in the background or transparently without affecting any call in progress. The recorded data will then be stored in the phone memory for the Format converter to converts the saved file into the right format and checks if it is well converted and save it into the appropriate location. The output of the format converter will be fed into the Call Timer Analyzer to measure the Call Time characteristics such as Silent mode time also known as call setup time, Intra-Burst Time Inter-Burst Time, Number of Burst and Ringing Duration as shown in Figure 2.

Figure 2 shows the flow chart for the ringing tone acquisition and Figure 4 and Figure 5 shows the flow chart for the Call timer Analyzer and Labview design of Sound Quality Analyzer respectively.

From Figure 3, the Silent Mode Time (SMT) can be calculated mathematically, by subtracting the time the counter start from the time the counter stopped

$$SMT = t_{stop} - t_0 \text{---(1)}$$

Where t_{stop} is the silence mode end time and t_0 is the beginning of the silence mode period. Also, Intra Burst Time (IntraBT) can be calculated by subtracting the time the first peak is detected from the time the end of a burst is detected

$$IntraBT = t_2 - t_1 \text{--------------------------------------(2)}$$

Where t_1 and t_2 is the start and end of burst respectively

Inter Burst Time (InterBT) can be calculated by subtracting the time the end of the first burst is detected from the time the next burst started

$$InterBT = t_2 - t_0 \text{---------------------------------------(3)}$$

The sound quality analysis involve three processes namely Signal Quality to Noise Ratio (SQNR) measurement, Amplitude measurement and Frequency measurement.

The analysis of the input signal consist of four distinct stages

1. Compression/Collapsing

2. Flattening of near zero components

3. Differentiating the signal

4. Extraction of relevant parameters

It was discovered that most of the signals have sudden and sporadic zero values occurring. The presence of these zero values is due to high sampling frequency which in this case is 8000Hz per samples. These values however, affect the computational procedure. Hence averaging technique was used to nullify sporadic zero values occurring in the signal i.e. 8000 samples in a second was effectively compressed to 8 samples in the same second. Using thresholding, we reduced the values less than 0.01 that are discovered to be noise to zero. The signal is then differentiated so as to enable the effective tracking of gradients. A positive gradient would indicate the start of a burst and the return of the gradient to zero signifies the end of burst and the start of an inter burst time.

In the Matlab command window, enter these command:
$y = \text{gsm\_voice}(\#, 'all')$;
GetParameters(y);

Where $\# = 0, 1, 2, 3$. These values represent each Mobile network operator. The two command gives the call characteristics of the mobile nework operator in question as shown in Figure1

Figure 1: command Window of Matlab

Figure 2: Typical GSM ring pattern

Figure 3: Flow chart for the ringing tone acquisition

Figure 4: Flow chart for the Call timer Analyzer

3. PRELIMINARY RESULTS AND DISCUSSIONS

The result gotten from the analysis is shown in Table 1. A problem in hardware, transmission, coverage, or interference may result in an increase in the call setup time and also the longer the SMT the less likely a successful call setup.

Table 1: Call Time characteristics for various Mobile Network Providers.

Mobile Operator	Call Setup Time (SMT) (s)	No of Burst	Average Intraburst Time (s)	Average Interbrust Time (s)
Glo - MTN	5	9	1.388	1.458
Glo - Etisalat	6.625	6	1.375	3.604
Glo - A switched OFF phone	3.625	1	5.375	NaN
Glo - Glo 121	6.25	1	25	1.25
Glo - Airtel	10	11	1.261	1.6
Glo - Glo	5.25	11	1.318	3.137
Glo - Busy Destination	0.5	1	11.375	NaN
Etisalat - MTN	5.125	9	1.375	1.5
Etisalat - Glo	9.5	7	1.5	3.25
Etisalat - Airtel	6.375	11	1.397	1.625
Etisalat - Etisalat	4.875	6	1.354	3.645

Figure 5: Labview design of Sound Quality Analyzer
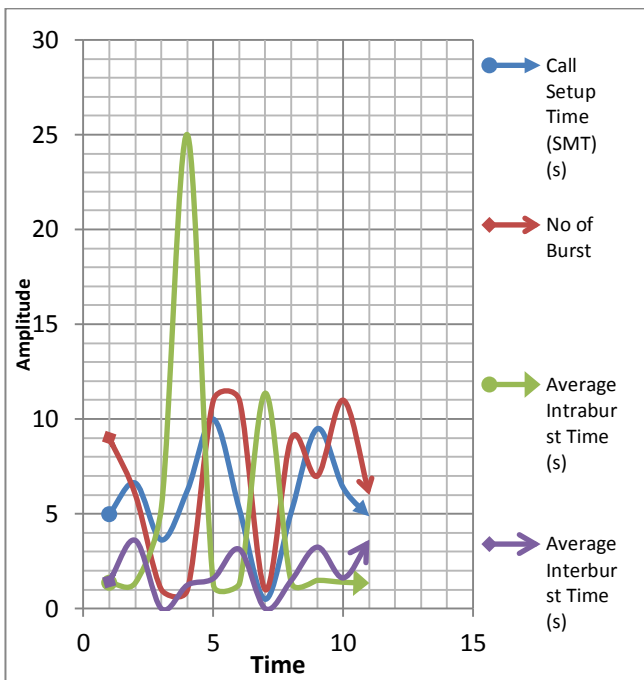
Figure 6: Characteristics of GSM Ring tone

4.   CONCLUSION

This paper provides a tutorial on the process involved in measuring the Call Setup Time (CST) in a GSM network. A practical approach to the CST analyzer to predict QoS and citizen sensing approach have also been presented. It should be noted that this paper forms part of an on-going research effort geared towards developing an analyser to predict QoS through CST measurement using citizen sensing approach.

REFERENCE

Amaldi, A., Capone, A & Malucelli, F. (2008). Journal of Wireless Networks: Radio planning and coverage optimization of 3G cellular networks vol. 14, no. 4, pp. 435–447.

Boulos, N., Bernd, R., David, N., John, G., Gunho, S., Russ, B. William, A., Eduardo J. & Kuo-Yu, S. (2011)

Crowdsourcing, citizen sensing and sensor web technologies for public and environmental health surveillance and crisis management Kamel Boulos et al. International Journal of Health Geographics, 10:67.

Brigham, E. & Oran (1988). The fast Fourier transform and its applications. Englewood Cliffs, N.J.: Prentice Hall. ISBN 0-13-307505-2.

Budhiraja, R. & Jadon J. S. (2013). Study and Implementation of Drive Test For Development of GSM Network. International Journal of Engineering Trends and Technology (IJETT) – Volume 4 Issue 10, pp 4352-4357.

Carvalho de Gouveia, F. & Magedanz, T. (2000). Quality of service in telecommunication networks vol. II, pp. 532– 548.

Cormen, Thomas, H., Charles, E., Leiserson, L., Ronald Rivest, & Clifford Stein. (2001). Chapter 30: Polynomials and the FFT. Introduction to Algorithms (Second ed.). MIT Press and McGraw-Hill.   pp. 822–848. ISBN 0-262-03293-7. esp. section 30.2: The DFT and FFT, pp. 830–838.

Duhamel, P., Piron, B. & Etcheto, J. (1988). On computing the inverse DFT. IEEE Trans. Acoust., Speech and Sig. Processing 36 (2): 285–286. doi:10.1109/29.1519.

Haider, B. & Zafrullah, M., (2009). Radio Frequency Optimization & QoS Evaluation in Operational GSM Network Proceedings of the World Congress on Engineering and Computer Science Vol I.

KOLLÁR, M. (2008). Evaluation Of Real Call Set Up Success Rate In Gsm. Paper presented at the Acta Electrotechnica et Informatica Vol. 8, No. 3, pp 53–56,

Kyriazakos, S., Papaoulakis, N., Nikitopoulos & Gkroustiotis D. (2002). Performance Evaluation of Operational GSM and GPRS Systems under Varying Traffic Conditions. A paper presented at the IST Mobile and Wireless telecommunications Summit, Thessaloniki – Greece.

Kyriazakos, S., Papaoulakis, N., Nikitopoulos & Gkroustiotis D. (2002). A Comprehensive Study on Performance Evaluation of Operational GSM and GPRS Systems under Varying Traffic Conditions. A paper presented at the IST Mobile and Wireless telecommunications Summit, Thessaloniki – Greece.

Oppenheim, Alan, V., Schafer, R. & Buck, J. (1999). Discrete-time signal processing. Upper Saddle River, N.J. Prentice Hall. ISBN 0-13-754920-2.

Sireesha, B., Varadarajan, S., Vivek & Naresh. Increasing Of Call Success Rate In GSM Service Area Using RF Optimization. International Journal of Engineering Research and Applications (IJERA), Vol. 1, Issue 4, pp. 1479-1485

Smith, & Steven, W. (1999). Chapter 8: The Discrete Fourier Transform. The Scientist and Engineer's Guide to Digital Signal Processing (Second ed.). San Diego, Calif.: California Technical Publishing. ISBN 0-9660176-3-3.

Sireesha, B., Varadarajan, S. Vivek and Naresh. "Increasing Of Call Success Rate In GSM Service Area Using RF Optimization. International Journal of Engineering Research and Applications (IJERA), Vol. 1, Issue 4, pp. 1479-1485.

Verma, R., Mandal, S., & Kumar, A. (2012). Improved Voice Quality of GSM Network through Voice Enhancement Device. International Journal of Advanced Research in Computer Science and Software Engineering, Volume 2, Issue 7, PP.77-80

Yang, C. (2008). HUAWEI GSM BSS Network KPI (Call Setup Success Rate) Optimization Manual

3GPP specification: 23.108

COMPARATIVE ANALYSIS OF FUNCTIONAL FEATURES OF TWO DIFFERENT AGRICULTURAL TRACTORS (MF 178 AND X750)

Balami, A. A., [1]Soje, T. M., Dauda, S. M., Aliyu, M.and [2]Mohammed, L.
Department of Agricultural and Bioresources Engineering,
Federal University of Technology, Minna.
1. Research Fellow.
2. Research Assistants.

ABSTRACT

The tractor remains a very important machine in agriculture due to its ability to provide mechanical power to farm implements both on and off the farm. The choice of a tractor based on field performance can be very challenging due to limited information with regards to performance on the field. With a desire to provide some information on the field performance of Massey Fergusson's MF 178 and YTO's X750, Field tests were conducted on a soil that is predominantly sandy loam with an average moisture content of 3.18 % and bulk density of 1.01 g/cm^3 at Sambawa farms, Kaduna. The field parameters evaluated were the fuel consumption, operating speed, wheel slip, draft of implement, effective field capacity, theoretical field capacity, field efficiency, volume of soil disturbed and drawbar power during ploughing and harrowing operations. The data collected was subjected to Duncan's Multiple Range Test at 0.05 % significance levels. From the results, there was significant difference in the field performance of the two tractors. The MF 178 was however found to have a field efficiency of 86.75 % against 74.07 % of the X750. The X750 equally consumed more fuel during both ploughing and harrowing operations by 1.67 L/ha or 2.21 L/h. The MF 178 was then adjudged to give a better performance based on the data analyzed and on the standpoint of operational efficiency and economy.

Keywords:Tractor, Field Performance, Ploughing.

1. INTRODUCTION

The tractor has become a major source of farm power in man's quest to satisfy world hunger thus gradually replacing human power in the field of agriculture thereby saving labour and time in land preparation, food production as well as processing and thus saving cost (Al-Suhaibani *et al.,* 2010; Bellis, 2013; Danfoss, 2013).

Land preparation is one of the most energy demanding operations in agriculture, it involves soil cutting, turning and pulverizing and thus demands high energy, hence the need to optimize tractor performance in order to utilize the available energy. This energy utilization depends on many factors such as soil type and condition, operating depth and speed, and hitch geometry (Sirelkatim *et al.*, 2001).

Due to the cost of energy, efficient energy utilization is of great importance to agricultural engineers and tractor owners thus, optimization of tractor performance is a necessity because it will help in minimizing the fuel consumption and energy loss. Ahaneku *et al.*(2011) stated that ownership of a tractor and associated equipment can involve a substantial investment and hence, improper choice of tractor size can be costly because a very small tractor (lower horse power) can result in long hours of field work, excessive delays and premature replacements, while a too large tractor (higher horse power) can result in excessive operating and overhead costs (Summer and Williams, 2007).

Several factors affect the selection of a tractor and its associated implements. These include soil type, crop type, climatic condition, cost of production, size of field and cultural practices such as tillage system. According to Ahaneku *et al.* (2011), the selection and matching of tractors with implements depends on the availability of

information about the capacity of the tractor and implements as well as the likely load to be imposed on the tractor. Thus, draft requirements will vary with implement size, soil type, speed of operation and depth of operation. Therefore, for effective tractor-implement matching, there is the need to ascertain actual field efficiencies and draft requirements along with other indices of tractive performance (Bukhari *et al.,* 1988).

Sirelkatim *et al.* (2001) stated that agricultural tractor efficiency relies on better tractive effort which can result from increasing the area of contact between the tractor wheels and the soil surface, and reducing the wheel slippage. This will reduce tractor power losses and the amounts of fuel used and consequently allow covering more lands in a given time. Thus, the decision to provide the farm with a new or second hand agricultural tractor is regarded as a responsible task, with little or no room for errors (Pawlak, 2001).

This research work was therefore carried out to compare the field performances of MF 178 and X750 on a sandy loam soil.

2. METHODOLOGY

This research work was carried out on a sandy loam soil at the Sambawa Farms, along Kaduna - Zaria expressway in the north western state of Kaduna, Nigeria. The two tractors whose field performances were evaluated and compared are the MF 178 and YTO X750. The specifications of the tractors are given in Table 1. The implements used for the trials were tractor mounted disc plough and disc harrow. The specifications of the matching implements are given in Table 2. Each tractor was tested on an area of 0.030 hectares (10 x 30 m) laid side by side in a randomized complete block design (RCBD) with three replications (ASABE, 2011; Ashaye, 1983; Ingle, 2011).

Table 1: Specifications of tested tractors

TRACTOR MODEL Specification	MF 178	YTO X750
Engine Power (hp)	73	73
Type of Engine	4-cylinder	4-cylinder
Type of Fuel	Diesel	Diesel
Type of Steering System	Power-assisted	Power-assisted
Type of Injector Pump	In-line injector	In-line injector
Firing Order	1-3-4-2	1-3-4-2
Fuel Tank Capacity (L)	107.9	102
Lifting Capacity (kg)	1927	1800
Rated Engine Speed (rpm)	2200	2400
Type of Cooling System	Water-Cooled	Water-Cooled
Country of Manufacture	Pakistan	China
Front Tyres (size)	7.50 – 16	7.50 – 16
Inflation Pressure (psi)	24	24
Rear Tyres (size)	16.9 – 30	14.9 – 30
Inflation Pressure (psi)	17	17
Weight (kg)	2739	2320

Source: (ASABE, 2011; Ingle, 2011).

Table 2: Specifications of matching implements

Specifications	Disc Plough	Disc Harrow
Implement type	Mounted	Mounted
Overall length (mm)	1800	2200
Overall width (mm)	1500	1700
Number of bottom/blades	3	24
Width of cut (mm)	1310	1080
Diameter of disc (mm)	605	-
Diameter of blade (plane), mm	-	510
Diameter of blade (notched), mm	-	505

Source: (ASABE, 2011; Ingle, 2011).

2.1. Measurements

2.2. Operating Speed

To measure the operating speed, time was recorded when each tractor travelled a distance of 20 m during each operation. The operating speed was then evaluated as a ratio of the distance covered (20 m) to the time recorded.

2.3. Travel Reduction (Wheel Slip)

The travel reduction was determined as follows: a mark was made on the tractor drive wheel with coloured tapes

and allowed to move forward. The distance covered after 10 revolutions under no load and load conditions on same surface were measured and expressed mathematically as expressed in equation 1:

$$TR = \frac{A-B}{A} \times 100\ \% \qquad (1)$$

Where: TR = Travel Reduction (%); A = Distance covered at every 10 revolutions of tractor drive wheel at no load (m); B = Distance covered at every 10 revolutions of tractor drive wheel with load (m)

2.4. Fuel Consumption

The fuel required for each tillage operation was determined by filling the tank of each tractor to full capacity before and after each test. The amount of fuel required to refill after working on each test plot is the fuel consumed during the test.

2.5. Effective Field Capacity

The effective field capacity was evaluated using the relation given in equation 2:

$$S = \frac{A}{T} \qquad (2)$$

Where: S = Effective Field Capacity (ha/h); A = Area covered (ha); T = Time (h)

2.6. Theoretical Field Capacity

The theoretical field capacity was evaluated using the relation given in equation 3:

$$TFC = \frac{S \times W}{10} \qquad (3)$$

Where: TFC = Theoretical field capacity (ha/h); S = Speed (km/h); W = Width (m)

2.7. Field Efficiency

The field efficiency gives an indication of the time lost in the field and the failure to utilize the full working width of

the machine. It was calculated from the test data as given in equation 4:

$$E_f = \frac{\text{Effective field capacity}}{\text{Theoretical field capacity}} \times 100 \qquad (4)$$

Where: Ef = Field efficiency (%)

2.8. Volume of Soil Disturbed

The volume of soil disturbed (m^3/h) was calculated by multiplying the field capacity with the depth of cut. This is given by the relation in equation 5(Al- Suhaibani *et al.*, 2010):

$$V = 10000SD \qquad (5)$$

Where: V = Soil of Volume Disturbed (m3/h); S = Effective Capacity (ha/h); D = Depth ofcut (m).

2.9. Drawbar Power

Drawbar power was evaluated using the relationship between draft and speed as expressed in equation 6.

$$\text{Drawbar Power} = \frac{\text{Draft (kN)} \times \text{Operating Speed (km/h)}}{3.6\ \text{(constant)}} \qquad (6)$$

2.10. Draft of Implement

Draft was measured with the aid of equation 7 developed by Al- Suhaibani *et al.* (2010).

$$UD = \beta_0 + \beta_1 D + \beta_2 D_2 + \beta_{23}\ S + \beta_4 S_2 + \beta_5 DS \qquad (7)$$

Where: UD = Unit draft (N mm-1 or N/tool); D = Tillage depth (cm); S = Travel speed (Km h-1); β0, 1, 2,3,4,5 = Regression coefficients

2.11. Data and Analysis

All data collected were subjected to Duncan's Multiple Range Test using the statistical package SPSS Statistics 20 for windows.

3. RESULTS AND DISCUSSIONS

The results from the field test performed by the two tractors are given in Tables 3 and 4. While the result of the soil analysis tests carried out on the soil is presented in Table 5.

Table 3: Average resultsof parameters from field test performed on MF 178 and X750 during ploughing operation

Parameter	Tractor Model	
	MF 178	X750
Travel reduction (%)	05.86	08.47
Width of cut (cm)	110.0	120.0
Depth of cut (cm)	10.00	08.00
Speed of operation (km/h)	05.50	07.20
Effective field capacity (ha/h)	0.720	0.800
Theoretical field capacity (ha/h)	0.830	01.08
Operation time (h/ha)	1.390	01.25
Field efficiency (%)	86.75	74.07
Draft force (kN)	6.730	08.16
Fuel consumption (L/ha)	10.00	11.67
Fuel consumption (L/h)	07.12	09.33
Soil of volume disturbed (m^3/h)	720.0	640.0
Drawbar power (kW)	10.28	16.32

Table 4: Average results from field test performed on MF 178 and YTO X750 during harrowing operation

Parameter	Tractor Model	
	MF 178	X750
Travel reduction (%)	05.40	06.70
Width of cut (cm)	205.0	212.0
Depth of cut (cm)	04.00	03.50
Speed of operation (km/h)	08.00	08.00
Effective field capacity (ha/h)	01.20	01.20
Theoretical field capacity (ha/h)	01.64	01.64
Operation time (h/ha)	0.830	0.830
Field efficiency (%)	73.17	73.17
Draft force (kN)	05.19	05.34
Fuel consumption (L/ha)	03.33	05.00
Fuel consumption (L/h)	04.00	06.00
Soil volume disturbed (m^3/h)	480.0	420.0
Drawbar power (kW)	11.53	11.87

Table 5: Soil physical properties

Variables	Soil Characteristics
% Sand	79.08
% Clay	13.0
% Silt	7.92
Texture class	Sandy Loam
Bulk density (g/cm^3)	1.01
Soil moisture content (%)	3.18

The soil was found to be predominantly sandy – loam with average moisture content of 3.18 % and bulk density of 1.01 g/cm^3. Tables 6 and 7 show that there is significant difference at 0.05 levels according to Duncan's Multiple Range Test with regards to these parameters and hence there is significant difference in the performance of both tractors. However, each test parameter is discussed as thus:

Fuel Consumption

The fuel consumption rates of the test tractors are depicted in Figures 1 and 2.
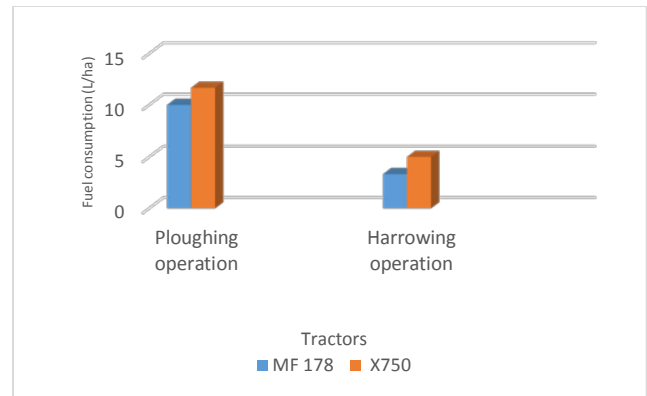
Fig. 1: Fuel consumption of test tractors in litres per hectare
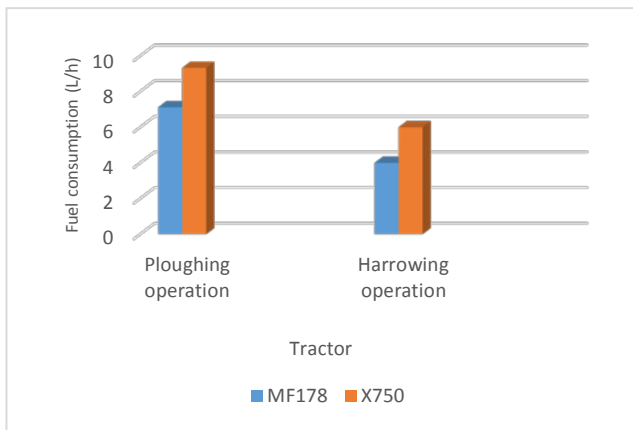
Fig. 2: Fuel consumption of test tractors in litres per hour
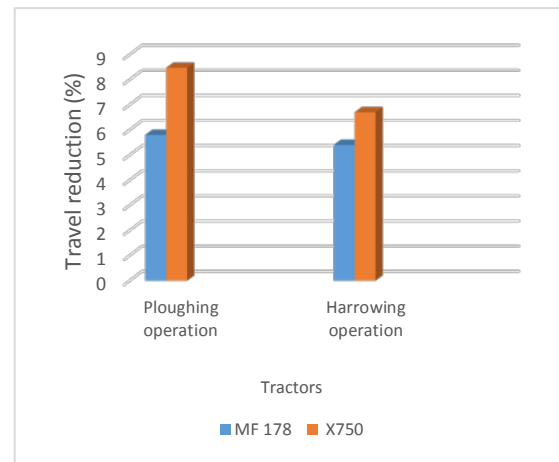
Fig. 3: Travel reduction of test tractors

Figure 1 shows the consumption rate in litres per hectare while Figure 2 shows the consumption rate in litres per hour. Ploughing operations consumed more fuel than harrowing operations for both tractors. The average consumption rate of both tractors is not significantly different as earlier shown in Tables 6 and 7. This is in agreement with the findings of Ahaneku *et al.* (2011) on the comparative evaluation of three models of Mahindra tractors. They reported that the fuel consumption parameter did not show any significant difference when operated at the same condition. However, tractor model X750 consumed more fuel i.e 1.67 L/ha or 2.21 L/h more during ploughing operation and 1.67 L/ha or 2 L/h more during harrowing operation. This could be attributed to its higher speed of travel with higher travel reduction.

Travel reduction (Wheel slip)

Travel reduction tends to affect the traction efficiency of tractive devices. Figure 3 depicts the results of the travel reduction obtained from the field test of MF 178 and X750.

Tractor model X750 consistently gave the higher values of travel reduction or wheel slip during both ploughing and harrowing operations. High values of travel reduction tends to lead to an increase in fuel consumption as useful energy is lost doing little or no work. Hence tractor model X750 is more likely to consume more fuel than MF 178.

Operation time

Time taken to accomplish a task is very vital in production. Results of time taken by test tractors to cover the same area were earlier shown in Tables 3 and 4. Both tractors covered the harrowing operations at the same time while the X750 had a slightly better time than the MF 178.
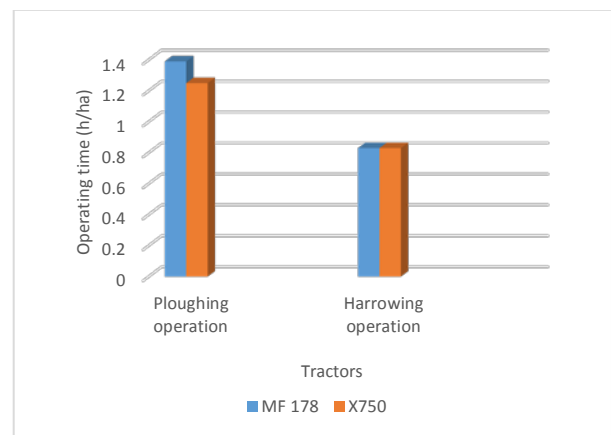
Fig. 4: Operation time of test tractors

Soil volume disturbed

Soil disturbance has been reported as one of the two major factors that determine the performance of tillage implements (Bukhari *et al*., 1988). Soil volume disturbed is a function of the effective field capacity and depth of cut. Comparing the performance of both tractors in terms of soil disturbance as illustrated in Figure 5, tractor model MF 178 achieved a slightly higher soil disturbance than the X750 in both field operations.
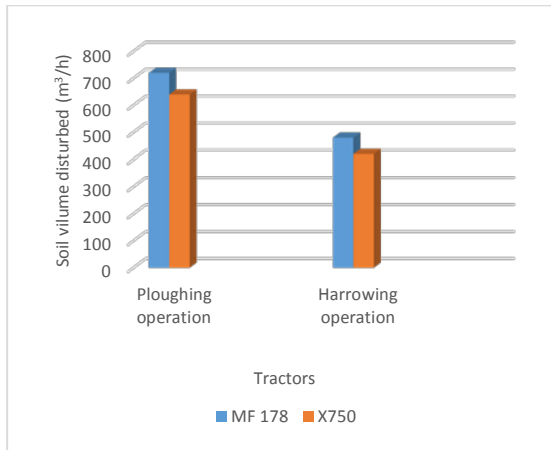
Fig. 5: Soil volume disturbed by test tractors

Field capacity

Field capacity is the other major factor as reported by Bukhari *et al*. (1988) that helps in determining the performance of tillage implements. The field capacity of a machine depends on its width, speed and efficiency of operation. Tractor model X750 achieved a slightly higher field capacity as shown in Figure 6 during the ploughing operation but MF 178 achieved a better field efficiency.
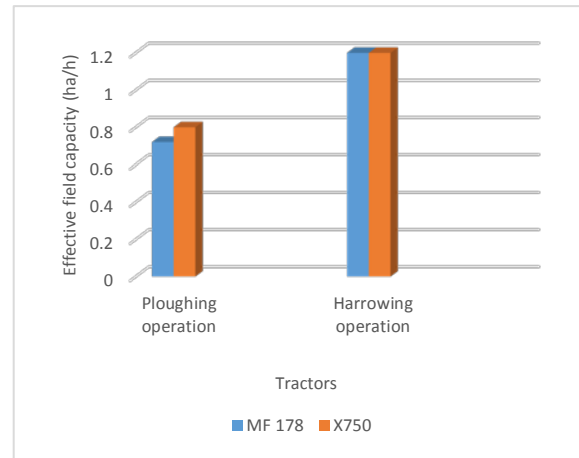
Fig. 6: Effective field capacity of test tractors

Draft of implements

Draft of implements is a function of speed of operation and depth of cut. Figure 7 illustrates the draft (drawbar pull) of both test tractors during ploughing and harrowing operations.
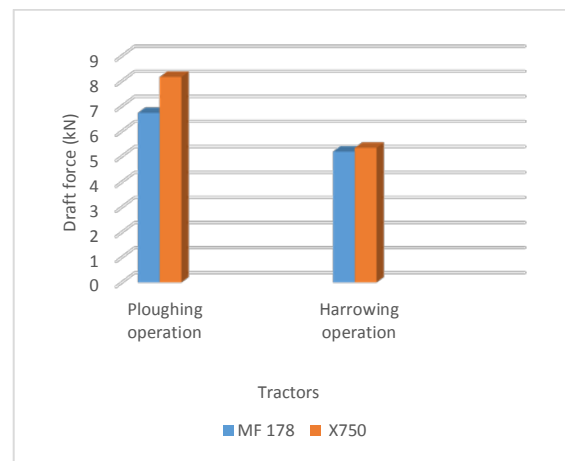
Fig. 7: Draft force of test tractors

Draft recorded during ploughing operations were consistently higher than those of harrowing irrespective of tractor model. The X750 experienced a higher draft. It should be noted that draft recorded were measured with the aid of the equation developed by Al-Suhaibani *et al*. (2010).

Drawbar power

Drawbar power is a function of draft and operating speed. Figure 8 shows the drawbar power of the test tractors recorded during the field operations.
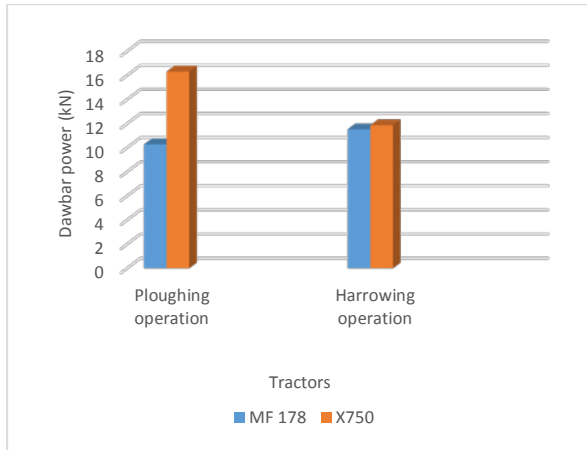
Fig. 8: Drawbar power of test tractors

The drawbar power of X750 was higher than that of MF 178 for both ploughing and harrowing since a large drawbar pull and high speed will result in a large drawbar power as seen with the X750. Drawbar power recorded were higher than those of draft of implements which is essential for doing work.

Field efficiency

Field efficiency is the ratio of the effective field capacity to the theoretical field capacity. It is an indication of time lost in the field and the failure to utilize the full working width of the machine (Ahaneku *et al*., 2011). Hence it represents the amount of work actually done by the machine. Figure 9 illustrates the field efficiency of the test tractors during ploughing and harrowing operations. The MF 178 exhibited a higher field efficiency than the X750 during the ploughing operations.
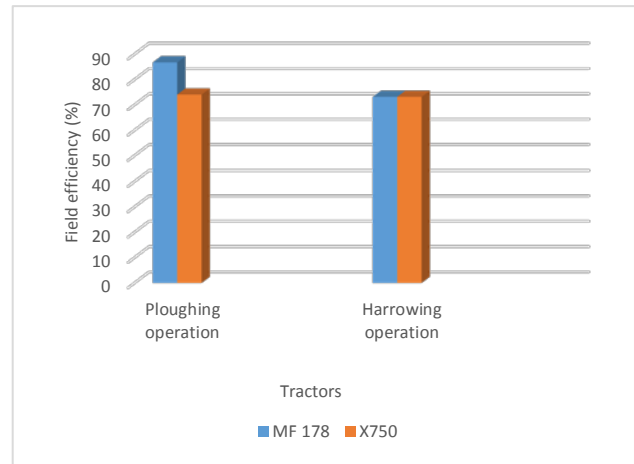
Fig. 9: Field efficiency of test tractors

4. CONCLUSION

It was discovered that there was significant difference in the field performance of the tested tractors. This result can be attributed to the fact that both tractors were tested under identical conditions. However, the MF 178 exhibited a better fuel economy and field efficiency. With the high cost of diesel to run tractors, this will indeed reduce the cost of operation especially during ploughing operations where more energy is required being a primary operation. Also, a more efficient tractor must be able to exhibit a small wheel slip in order to do more work and reduce fuel wastages. This was also exhibited by the MF 178.

REFERENCE

Ahaneku, I. E., O. A. Oyelade and T. Faleye (2011). "Comparative Field Evaluation of Three Models of a Tractor." Retrieved from http:iworx5.webxtra.net/~istroorg/download/Nigeria_conf_downloads/FPM/Ahaneku *et al*.pdf. February, 2015.

Al-Suhaibani, S. A., A. A. Al-Junobi and Y. N. Al-Majhadi (2010). "Development and Evaluation of Tractors and Tillage Implements Instrumentation System." American Journal of Engineering and Applied Sciences 3(2): 363-371.

Ashaye, O. (1983). "Suitability of Nigerian Soils to Mechanical Cultivation." Proceedings of the First National Tillage Symposium of the NSAE: 57-69.

Bellis, M. (2013). "History of Tractors." Retrieved from http://inventors.about.com, February 15th 2015.

Bukhari, S., M. A. Bhutto, J. M. Baloch, A. B. Bhutto and A. N. Mirani (1988). "Performance of Selected Tillage Implements." Agricultural Mechanization in Asia, Africa and Latin America 19(4): 9-14.

Danfoss, U. (2013). "History of the tractor." Retrieved from http://uk.danfossuniverse.com/page2110.aspx, March, 18th 2015.

Grisso, R. D., D. H. Vaughan and G. T. Roberson (2008). "Fuel Prediction for Specific Tractor Models." Applied Eng. Agric 24: 423-428.

Ingle, C. (2011). "Agricultural Tractor Test Standards in America." Retrieved from http://www.strategicstandards.com/files/SES/USTractorTesting.pdf October 23rd, 2014.

Pawlak, J. (2001). "Ocena stanu mechanizacji." Technika Rolnicza, 5: 2-4.

Sirelkatim, K. A., H. A. Alhashem and M. O. Saeed (2001). "The Effect of Some Operating Parameters on Field Performance of A 2WD Tractor." Scientific Journal of King Faisal University (Basic and Applied Sciences), 2(1): 93.

Summer, P. E. and E. J. Williams (2007). "What Size of Farm Tractor Do I Need?" Cooperative Extension Service. University of Georgia college of Agriculture, Athens, G.A. Miscellaneous Publication No. ENG07-003.

DEVELOPING THE FOUNDRY INDUSTRY FOR SUSTAINABLE ECONOMY IN NIGERIA

SUNDAY EDOSA OKUNDAYE
Dept. of Project Management Technology,
School of Entrepreneurship & Management Technology,
Federal University of Technology, Minna, Niger State, Nigeria.
metokunse@gmail.com
08033631288

ABSTRACT

Recently, Nigeria rebases its economy after 25 years to emerge as Africa's largest economy and the 26th in the world amidst expectations that if the Federal Government harnesses the potentials of the economy, especially the metallic extractive industry, it may hit the trillion dollar mark. It is in the light of the above that this paper x-rays the developing of the foundry industry for sustainable development in Nigeria. Further discussion centres on the various linkage industries and their required castings; Basic steps in making sand castings; Foundry machinery, equipment and tools; Small-scale foundry; the Prospects for Small-scale foundry in the Nigerian economy; Objectives of promoting the development of Small-scale foundries; the Role of United Nations Industrial Development Organizations (UNIDO) in establishing foundries in Developing nations; Finance sourcing for establishing small-scale foundries; Future demand projection and finally some recommendations are advanced towards the sustainability of the technological development of Nigeria.

Keywords: Developing, Foundry Industry, Sustainable Economy, Nigeria.

1. INTRODUCTION

Foundry practice has become one of the highly specialized branches of engineering field that embraces many skills including those of the pattern-maker, the moulder, the core-maker, the smelters or furnace-men and the metallurgists. It is one of the intermediary basic industries complementing forging and machining processes through which metallic raw-materials such as ores of iron, copper, aluminium, zinc, tin etc.; coal, coke, deoxidizers, fluxes etc. could be processed, refined and shaped into new products in the form of machine components and spares.

Achieving specific mechanical properties of these components or spares on an industrial scale, requires an in-depth understanding and application of service conditions envisaged for the components which in-turn underlines the need for appropriate casting design, flawless pattern-making, stringent selection of mould and charge materials, appropriate melting, refining and casting techniques and rigorous working and supervisory regimes.

Successive governments in Nigeria since the 70's had tried to put in the country's developmental plans guidelines to diversify the economic base of the country from the dependence on oil which accounted for over 90% of Nigeria's foreign exchange earnings in the last three decades (National Committee on Foundry Development, 1993). The objective was to evolve a new industrial policy which would lead to the much desired technological development and sustainable economy in Nigeria and self-reliant with the metal manufacturing sector being a vehicular medium for bringing this lofty policy into reality. The foundry industry was therefore envisaged to play a pivotal role as a major metal manufacturing activity in line with the independent study reliably conducted by the following bodies: the Federal Office of Statistics, National Committee on Industrial Development (NCID) and the National Committee on foundry Development under the auspices of United Nations Industrial Development (UNIDO) from 1965 to 1985. From these studies, it shows how the National Demand of cast metal products in Nigeria steadily increased form 72, 000 tonnes to 292, 000 tonnes (1985) to 425,000 in (1990s) and 794, 000 tonnes by the turn of the century, for which the National Committee on Foundry Development estimated 40% of these requirements as automotive components (Okundaye, 1995).

From the above collation of various studies, the requirements of foundry products in Nigeria for the infrastructural and industrial development of the country based on the United Nation's index for measuring any Nation's state of industrial development and of course

technological self-reliance, there is the need to have a proliferation of small-scale foundries to enhance the production of cast metal products which could be categorized according to the production process in which they have found utility (Iribhogbe, 1995). These various categories of castings find application in the various linkage industries as presented below.

1.1 Linkage Industry:

The following industries and many others such as the steel, food, plumbing, medical, power generation and distribution, water supply and sanitation etc. that depend on the foundry products (castings) for their day-to-day operation and maintenance for effective throughput and high production are called linkage industries. From the foregoing, it becomes clear that every other manufacturing industry depends on foundry for their machine component parts and spare parts. The following industries as outlined below and many others constitute the linkage industries and they include:

(i) Architectural Designs: Ornamental hardware, architectural fittings etc.

(ii) Agricultural & Agro-Allied Equipment: Parts for mowers, ploughs and cultivating equipment, corn mills parts and plates, oil expellers parts, water pumps, hand pumps etc.

(iii) Automotive Industry: Crank shafts, gears, pinions, rollers, steering knuckles, disc brake callipers, rock arms, brake drums, carburettor bodies connecting rods, pistons, fuel pumps, intake manifold, master cylinder body, master cylinder pistons, transmission housing, crank cases, engine block, cylinder heads etc.

(iv) Building & Road Construction Industry: Man-hole covers, grates, pipe fittings, valves, street lamp housing, door hanger etc.

(v) Ceramic & Refractory Industry: Extrusion press dies, impellers, ceramic press arm, shoe polishing spirals, dies for tiles and bricks, mixing cups etc.

(vi) Electrical Equipment: Motor frames, heads, refrigerator compressor parts for power lines, cast resistor, electric base, change-over switch bodies, and gears switch bodies etc.

(vii) Furniture Industry: Door locks, base for chairs etc.

(viii) Mining and Quarrying: The castings require alloying resulting in high chromium and nickel-chrome iron castings and they include ball mill liners, crushers, sleeves, dredger pump liners, conveyor casting, grinding balls etc.

(ix) Railway Equipment: Brake shoes components, stroke parts etc.

(x) Ship-Building: Pump housing gears, valve bodies, propellers, cylinders, engine blocks, blower housing, water jackets, pistons, pulleys, sleeves, generator housing etc.

(xi) Textile Industry: Pulleys, gears, frames, spanning mules, spindle rails, spinning drive cylinders, sewing machine parts, Tricot beams etc.

(xii) Tool Industry: Housing for power drills, butting machines, power shears, hydro press form blocks, jigs and fixtures, machine and table vices etc.

(xiii) Defence Industry: Warships, submarines, armoured fighting vehicles, bridges, ammunitions, helmets, etc.

(xiv) Cement Industry: Hammers, liners, flanges rollers, grate cooler plates, bolts and nuts, fan impellers, gears etc.

(xv) Petroleum Industry: Steel pipes, storage tanks, tankers bodies, refineries spare-parts etc.

2. FOUNDRY TECHNOLOGY

Foundry Technology can be defined as a metal-forming activity, whereby metallic objects are produced by pouring molten metal into already prepared mould. This mould may be metallic or mineral and may also be permanent or expendable. Through this process, spare-parts or machine components needed in our various manufacturing industries as well as in maintenance or repair activities; which could not have been possible through the other metal-forming and metal-working processes, such as rolling, forging, welding etc. It is on this basis that foundry has been described over the ages as *"the Mother of all industries"* (Ezekwe, 1995).

2.1 Types of Foundry

Based on products, foundry can be classified as follows:
(i)   Captive foundry
(ii)   Jobbing foundry
(iii) Iron casting foundry
(iv)   Steel casting foundry
(v)   Non-ferrous casting foundry
(vi)   Malleable cast iron foundry

2.2 Basic Steps in making sand Castings
(Chukukere, 1988)

The basic steps used in making sand castings are as follows:
(i)   Design
(ii)   Pattern-making

(iii)   Core-making

(iv)   Moulding

(v)   Melting and Pouring

(vi)   Fettling and Cleaning

2.3   Foundry Machinery, Equipment and Tools

(i) Pattern-making: Pattern-making machines and tools include: files, saws, hammers, measuring instruments, planners, band-saw machine, turning lathe, cutting tools etc.

(ii) Core-making: Core-making machines, Core blow-out machines, core boxes, reinforcement wires etc.

(iv) Moulding: Moulding boxes, sieves, shovels, water sprinkler, buckets, strike-rod, sleeker, lifters, spoons, trowels and other basic moulding tools and safety gadgets (e.g. helmets, protective clothes, safety boots etc.).

(v) Melting and Pouring: One melting furnace, preferably open-hearth furnace with two blowers. Others are crucible furnace, electric induction, reverberatory furnace etc.; spoons, tongs, weighing balances, protective clothing, helmet, etc.

(vi) Fettling and Cleaning: Saws, pliers, anvils, files, sand papers, vises, hammers, body fillers, paints, grinding machines, cutting tools, welding and cutting equipment, shot blasting machine, hand drilling machine, stitch saw, hand saw etc.

In a situation where there are no pattern-shop and laboratory and machining facilities, patterns can be purchased and the finished castings could be sent to any machine shop, for machining.

2.4   Foundry Materials and Additives

It is a well-known fact that 65% of the operating materials is obtainable from local resources and over 80% can be locally sourced (i.e. including foreign items that are obtained from Nigerian markets).

2.5   Small-Scale Sector (Foundry) (Definitional Issue)

Considering the conspicuousness of 'small' and 'medium' scale, we may need to spend some time defining what we mean by 'small' in order to put our discussion into a proper perspective. There is no acceptable uniform set International criterion designed for the definition of small and medium-scale industries. They are usually defined in relation to amounts of one or a combination of factors such as investment cost, employment and annual turn-over.

However, set parameters vary from country to country and in the same country over time in response to level of development. For instance, while the United Kingdom defines a small-scale enterprise as one with investment cost not exceeding £2.0 million (i.e. ₦360 million) and paid employment of not more than 200 persons, the United States of America uses only a limit of 500 paid employment in its definition.

The official definition in Nigeria appears broad and quite flexible. The small-scale Industries Division of the Federal Ministry of Industries defined the small-scale industry in 1972 as "all manufacturing units with a total capital investment (excluding cost of land) up to N 50, 000.00 but such an establishment must be wholly Nigerian-owned. The authorities went on to emphasise the need for flexibility in the application of this definition". "Manufacturing units exceeding the limit of investment and employment as stated above may still be considered as small-scale industries if the scale of output is relatively small compared to prepared to prevalent sizes of plants and the technology is fairly labour-intensive."

The Central Bank of Nigeria (CBN), in its credit Policy Guidelines for 1988 fiscal year to financial institutions has defined small-scale, for commercial banks lending purposes, as one with "small turn-over not exceeding N500,000.00". "The CBN also defined, for merchant banks lending, small-scale enterprise as one with a capital investment of not more than N2.0 million (excluding cost of land) or maximum turnover of N5.0 million". (Abdulkadir, 1988).

2.6   The Prospects for Small-Scale Foundries in the Nigerian Economy

While setting up of bigger foundries is desirable in view of various technological and cost factors, the small-scale foundry units also have several economic advantages and social benefits, notably are the following:

(i) Comparatively less capital investment (as infrastructures are not required).
(ii) Quicker turnover.
(iii) Utilization of local raw-materials.
(iv) Meeting local demands
(v) More effective Management control
(vi) Easier modification for alternative products in case of change in demand
(vii) Facilitates the development of indigenous technology

The small jobbing foundry can be found, scattered all over the country. The purpose of a small-scale foundry is to provide elastic services to industry and agriculture, or any sector of the economy that requires small quantities of high quality castings and very rapidly. It must therefore be versatile, flexible and technologically competent, since it will be expected to meet and cast practically all the alloys produced by normal foundry practice and to replace sophisticated parts by spares that must give service at least until an imported spare parts arrive. In addition, the foundry will be expected to select the correct material not always directly related to foundry products or operations.

The small-scale foundry can also substitute locally produced goods for imported ones, thereby saving some foreign exchange. The existence of a small-scale foundry will permit not only the direct substitution of imported castings but in some cases also the local manufacture of equipment in which castings are used even when these castings are of minor importance.

Small-scale foundries promote the establishment of other metal-forming or metal working activities. Within small-scale jobbing foundry in the least developed country, machine shops and sheet-metal working operations are also frequently required with these two essential additional operations. A versatile foundry can offer the most adequate service and can rapidly construct or reconstruct those items of equipment necessary for the progress of the smallest production unit. Collectively, the small-scale industry greatly helps in the creation of an industrial atmosphere.

2.7 Objectives of Promoting the Development of Small-Scale Foundries
The following are the objectives:
(i) Technological self-reliance

(ii) Stimulation of indigenous entrepreneurship
(iii) Transformation of traditional industry
(iv) Creation of employment
(v) Dispersal of industry
(vi) Diversification
(vii) Utilization of resources

2.8 The Role of UNIDO in Establishing Foundries in Developing Nations
It is worth mentioning here that due to the unique role played by the foundry industry, UNIDO endeavours to ensure that the industry shall be provided with the basic general services that will guarantee its operation in developing nations so as to fulfil its mandate "to promote and accelerate industrialization of developing countries with emphasis on the manufacturing sector" (United Nations Development Programmes Publication, 1990). UNIDO regards the foundry industry as one of the essential industries, as it is complementary to any metal working or metal processing activity. UNIDO encourages the establishment of small-scale foundries in developing nations such as ours and provides technical and financial assistance as this will immensely contribute to the sustainability of the economy of such nations.

2.9 Finance Sourcing for Establishing Small-Scale Foundry Industries
Finance sourcing for the establishment and running of small-scale foundries could be met through one or a combination of the following sources:
(i) Short-term funds from development banks.
(ii) Long-term funds from development banks.
(iii) Venture capital
(iv) Borrowing from individuals
(v) Share capital
(vi) Profit retention
(vii) Hiring and factorizing
(viii) Overdraft
(ix) Trade credit
(x) Sales of stocks and shares
(xi) Borrowing funds from various banking institutions, UNIDO, World Bank and

other organizations such as the North/South Co-operation, Africa Development Bank etc.

(xii) Borrowing of funds from National Directorate of Employment (NDE)

(xiii) Partnership venture.

2.10 Future Demand Projection

There will be a strong demand for all major foundry products by the year 2020. Assorted products which are primarily tied to the manufacturing and agricultural

sectors will experience an upward demand, as farming gets a boast from the Government.

A committee set up that carried out a study on the future demand of castings in Nigeria submitted a report prepared for the Federal Government in which, based on the past imports, industrial growth and direct studies on demands, the projection made for short and long range future demand are as shown in Table 1. It is observed that from the average requirement of 191, 800 tonnes in 1977-78, the total potential demand is expected to rise to 292, 200 tonnes in 1981, to 425, 600 tonnes by 1990 and 794, 600 tonnes by the turn of the century. According to Oyinola (1991), the net actual demand of castings in Nigeria is as presented in Table 1.

Table 1: The net actual demand of castings, between a period of 1981 and 2000.

	1981	1985/86	1990	2000
Total Potential Demand (Cast Parts) X 000 Tonnes	191.0	292.1	425.6	794.0
Effective Demand (Cast Parts)	186.5	288.6	694.6	800.00
HNet Actual Demand (Castings) Depending on expected availability of machining.	19.0	80.5	147.3	280.0

Source: Onyinola, 1991

3. DISCUSSION

From table one it can be deduced that the total potential demand of cast parts had increased from 191000 tonnes in 1981 to 794000 tonnes in 2000. The effective demand of cast parts had also increased form 186500 tonnes in 1981 to 800000 tonnes in 2000. Likewise, the net actual demand of castings depending on expected availability of machines is equally observed to have increased from 19000 tonnes in 1981 to 280000 tonnes in 2000. From the above data, it is very clear that the Total Potential Demand, Effective Demand and the Net Actual Demand of castings needed for effective and sooth running of our various linkage industries would have increased tremendously in 2015 and this will continue to increase. Hence, there is the need to develop a foundry industry with a view to sustaining the economic activities in Nigeria.

4. CONCLUSION

Nigeria is presently afflicted and characterised with frightening human suffering and misery index in

comparison other developing nations in the same age bracket e.g. Indian, South Korea, Brazil, Indonesia and Turkey, due to lack of meaningful manufacturing activity, which can only be sustain by the establishment of viable small-scale foundries.

The root cause of our socio-economic, political and technological backwardness is anchored on the promise that our nation failed or rather refused to lay the bedrock for industrialization during the petro-dollar era and instead the nation adopted the import dependent posture.

The establishment of viable small-scale foundries can act as the elixir to all industrial (Manufacturing) development problems. The problems of small-scale foundry development problems of small-scale foundry development in particular and other small-scale industries can be solved unhindered by the political wish of the government of the day.

It is very glaring that the social, political, economic engineering and technological benefits of small-scale foundry are enormous and need not be over-emphasised. All hands need to be on deck.

In view of the above facts, All efforts of industrialization by the government of Nigeria should be directed towards the development of small-scale foundries. In doing this, the following recommendations are advanced:

(i)   Industrial Banks should provide loans to genuine entrepreneurs

(ii) Tariff on imported foundry machinery and equipment should be removed.

(iii) Research and Development (R & D) in foundry materials to aid total input substitution should be encouraged.

(iv) Nigeria should toe the developmental steps taken by India, Malaysia, Brazil, Mexico and other newly industrialized nations (NIN).

REFERENCE

Abdulkabir A. (1988). "Financing Small and Medium Scale Spin-Off Industries in the Steel Sector". Proceedings of the National Seminar marking the 10th Year Anniversary of the Nigerian Metallurgical Society pp. 118-119

Chukwukere, E, U. (1880). "Survival of the Foundry Industry in Nigeria" Unpublished paper presented at a Seminar of the NMS (Ajaokuta Chapter), held at Ajaokuta. pp. 3-7.

Ezekwe, G. (1995). "Foundry is Mother of All Industries". Foundry Chronicle Vol. I No.1. p. 5

Iribhogbe, M. M. (1995): "An Update on Castings for the Nigerian Quarrying and Cement Industries". Proceedings of the Nigerian Metallurgical Society (NMS) p. 72.

National Committee on Foundry Development Report, 1993.

Okundaye, S. E. (1990): "Small-scale Foundry - Vital Downstream Industry for Technological Self-Reliance". Unpublished paper presented at the School of Engineering Maiden Seminar, held at the Federal Polytechnic, Auchi. pp. 1-9, 11-15.

Okundaye, S. E. (1995): "The Role of Small-Scale Foundry Industry in Revitalizing the Depressed Nigerian Economy" Proceedings of the Nigerian Metallurgical Society. pp. 91-98.

Okundaye, S. E. (1989): "Production of Bronze Sleeve (Bushing) and Ornamental Casting at the Foundry Shop, Ajaokuta. A paper presented at the 7th Annual Conference of the Nigerian Metallurgical Society (NMS). pp.1-2.

Oyinola, A. K. (1991): "Non-Destructive Testing Techniques in Foundry Industries". Proceedings of the Nigerian Metallurgical Society. pp. 66-67.

United Nations Development Programme (1990) : Publications on Small-Scale Industry Development in Developing Countries. Pp. 5-8, 10-11.

DEVELOPMENT AND PERFORMANCE EVALUATION OF CHICKEN FEATHER - PLASTIC COMPOSITE PARTICLE BOARD

[1]Umar A. [2]Abdullahi I. and [3]Aliyu A. B.

[1, 2, 3]Department of Mechanical Engineering, Faculty of Engineering, Bayero University, Kano, Nigeria.

E-mail: ibrahimay2k7@gmail.com, Phone: 2348028438580.

ABSTRACT

This work involved the development of chicken feather - plastic composite - using chicken feather particulate as reinforcement and unsaturated polyester as matrix - for particle board production. The physical and mechanical properties of the composite developed were determined. The composite was successfully developed using unsaturated polyester resin as the matrix and chicken feather as reinforcements. The result of the work revealed the following as the average properties of the developed chicken feather – plastic composite: density increased from 0.47- 0.55 g/cm^3; water absorption ranged from 22.0 - 26.0 %; thickness swelling increased from 6.4 – 10 %; the MOR values ranged from 61.2 - 187.8 Mpa; the stiffness strength (MOE) ranged from 3198.8 - 4336.9 Mpa; the ultimate tensile strength ranged from 6.9 - 9.1 Mpa and Young's modulus ranged from 56.86 - 135.4 MPa. From the physical and mechanical properties of the developed composite it was discovered that the chicken feather - plastic composite have satisfied the minimum quality requirements of particle board.

Keywords: *Composite, Matrix, Fibre, Modulus, Feather, Plastic.*

1. INTRODUCTION

Chicken feather is commonly described as a waste by-product and they contribute to environmental pollution due to disposal problems. There are two main types of chicken feather disposal methods that exist, burning and burying (Menandro, 2010). Both of them have negative impact on the environment. Recent studies on the chicken feather waste established that the waste can be a prospective composite reinforcement (Menandro, 2010). The composite reinforcement application of the chicken feather offers a better effective way to handle environmental concerns compared to the traditional disposal methods (Menandro, 2010). Some of the advantages of the chicken feather as a composite reinforcement include lightweight, high thermal insulation, excellent acoustic properties, non-abrasive behavior and excellent hydrophobic properties (Kock, 2006).

Significantly, constituents of composites retain their individual physical and chemical properties: yet together they produce a combination of qualities which individual constituents would be incapable of producing alone (Hull and clyne, 1996). Wood composite boards which have lightweight and high strength are still the best option for construction due to their reasonable costs. However, the growing shortage of wood has led to the development of another suitable means of materials that will meet up with the demand.

Composite

Composites materials are achieved by combining two different materials to produce an overall structure that is better and different from individual components and the new product may be preferred for so many reasons, such as good thermal insulation, lighter in weight, and reduced decaying effect, improved strength among others.

Chicken feather

Chicken feather is an agricultural waste product obtained from the chicken in the food processing industry. Considering the problem caused by this waste and the effect on the National economy therefore, several researchers have investigated and then come up with many ways in which the chicken feather could be used in order to solve this problem and at same time to add value to the National economy.

Winandy et al (2003) reported that, the presence of Keratin in chicken feather poses both hydrophilic and hydrophobic properties which make it to be good in composite production.

Schmidt and Jayasundera (2012) investigated the use of chicken feather as an addition to wood using formaldehyde resin as matrix binder to produce composite and then compared to wood control panels. The amount of the chicken feather used ranged from 20% to 95% and 5% resin. The results of the study showed that, initially, the mechanical properties of chicken feather as an added mixture to wood show some loss in strength and stiffness to all wood control panels and that, physical properties of composite when soaked in water improved, the resistance to water absorption and thickness swelling over all wood control panels which indeed indicated the presence of hydrophobic keratin of feather fiber.

Decay test was also investigated by the addition of chicken feather to wood materials which showed that, the chicken feather inhibited the subsequent decay in the wood fiber (Schmidt and Jayasundera, 2012).

Chicken feathers possess unique properties i.e. low relative

density and good thermal and acoustic insulating properties which would be used as an advantage in a number of applications that will serve as alternatives to feather disposal and meal (Kock, 2006).

Menandro (2010) Studied the chicken feather as an add mixture to cement for reinforcement in a composite production and then the specimens were tested and found out that when the chicken feather was increased - more than 10%, modulus of rupture and modulus of elasticity reduced and also dimensional stability decreased but increase in water absorption and thickness swelling were observed.

Hong and wool (2005) measured the tensile strength of chicken feather fiber directly and reported that the chicken feather has a tensile strength of 41-130MPa which can be compared to that of wood, 95-155MPa.

The hygroscopic nature of chicken feather makes it not compatible with water or mix easily with water which shows that chicken feather product can be used in an area where the product is expected to be in contact with water or in a moist environment (Kock, 2006).

Varieties of Chicken

Chicken originated in Southeast Asia and thereby spreads to the rest of the world by sailors and traders (Acharya and Kumar, 1984) There are many varieties of chicken depending on how is been fed; these includes Corn chicken, Organic chicken, Back yard chicken etc. There are two major categories of chickens in Nigeria base on the Ecotype; these are Fulani chicken and Yoruba chicken (Ajayi, 2010). Fulani chickens are heavy in weight and soft in feather while the Yoruba chickens are Light in weight and with soft Feather (Ajayi, 2010). Back yard chicken was the best option for the production of the particle board due to its strength and all other properties which it has over the Fulani and Yoruba chicken feathers however, may not be available in abundance and as such Fulani chicken feather is chosen for this work.

It is well known that, the role of reinforcement in composite materials is primarily to add mechanical properties to the materials. For example continuous fiber, it provides virtually all of the strength, stiffness, and the ability to carry load. In most applications, the fibers are arranged to form sheets and variety of fiber orientations are possible to achieve different characteristics. (Flym and Belzowski, 1995)

Particleboard is a composite product which is initially made mainly from wood materials (as opposed to sheets or fibers (Kartini et al, 2010). Particleboard is mainly used in structural applications such as construction industry, for bracing walls and flooring (EST, 2006). Although resin-bonded panels are lighter than cement-bonded ones, the latter are lighter than concrete and thus, can replace concrete constructions like prefabricated construction, in elements that are not subjected to loads, like walls. Therefore, these attributes appeal to engineers, contractors, and architects to use it in public and multifamily

residential buildings so as to avoid breaking down of the structures (Papa-dopoulos, 2006)

Hand Lay-Up Technique

Hand lay-up is the most common process used to fabricate composites parts accounting for 40% of composites processed worldwide and it is a relatively simple process with low cost but with much degree of manual handling and it is suitable for making a wide variety of composites products including: boats, tanks, bath ware, truck auto components, ranging from very small to very large Production volume. However, it is feasible to produce substantial production quantities using multiple moulds (Biswal, 2010).

Considering the ecological effects of some materials usage, replacing synthetic fibres such as glass fibre by natural ones is very important in particle board production. The disposal of waste chicken feathers generates greenhouse gases that poses danger to the environment (Menandro, 2010). The traditional ways of handling chicken feather is expensive and at same time dangerous to the environment (Menandro, 2010). They are often burnt in incineration plants, buried in landfills, or recycled into low animal feeds (Menandro, 2010). However, these disposal methods of handling this waste have a restriction or generate greenhouse effect causing gases, such as CO_2 into the atmosphere. If these wastes are converted into a useful material, it may aid towards the achievement of a cleaner, safer and eco-friendly environment.

The main aim of this work is to develop composite using polyester and chicken Feather particulate for the production of particle board. The study involved determining the chemical composition of chicken feather and developing chicken feather - plastic composite of various compositions. The physical and mechanical properties of the developed composite were then determined with a view to comparing the properties with the standard requirements of particle board.

2. MATERIALS AND METHODS

2.1. Materials and Equipment
The materials and equipment used in the various experiments conducted are presented in this section.

2.1.1. Materials and equipment used for the preparation of chicken Feather Particulate
The materials and equipment used in the preparation of chicken feather particulate are: Mill machine, water, sodium chloride, Zinc sheet and sieve.

2.1.2. Materials and equipment used in determination of chemical composition of chicken feather particulate
The materials and equipment used in the determination of the chemical composition of chicken feather are; minipal 4 XRF epsilon panaltical machine and chicken feather particulate.

2.2. Methods

The methods used to carry out the various experiments conducted are presented in this section.

2.2.1. Preparation of Waste Chicken Feather Particulate

Waste chicken feathers were sourced from Sabon gari market Kano, Kano State. The waste feather was washed severally with water mixed with laundry detergent and sodium chloride to remove blood, manure and extraneous materials. The clean feathers were spread on galvanize iron sheets and dried in oven for 4days at 80^0C (Menandro, 2010). The dried feathers were then ground into powder at Abubakar Rimi market Kano, Kano state using mill machine.

2.2.2. Sieve Analysis of the Reinforcement

This was done in order to separate the unwanted elements that may have mixed with the particulate and also for characterizing the particle size using mesh. The particle was sieved using 150μm sieve in accordance with ASTM D 1921-01.

2.2.3. Preparation of Composite

The composites were prepared by hand lay-up technique using chicken feather as filler and polyester as the matrix, methyl ethyl ketone peroxide as the catalyst and cobalt napthalate as an accelerator (table 1).

Table 1: composite Formulation (Nagaraja and Rekha, 2013; Dupont, 2005 and Menandro, 2010)

S/N	CF-%wt	PO-%wt	MEKP-%wt	CoNa%wt
1	5	95	3	1
2	10	90	3	1
3	15	85	3	1
4	20	80	3	1

Where: PO is polyester; MEKP is methyl ethyl ketone peroxide; CF is chicken feather and CoNa is Cobalt nephthalate (accelerator).

2.2.4. Additives Mixing Ratio

Table 2 gives the ratios of catalyst to resin used in producing various compositions of the composite.

Table 2: Catalyst and accelerator mixing Ratios based on resin content

Materials	Mass (g)			
Resin	80.0	85.0	90.0	95.0
MEKP	2.4	2.55	2.7	2.85
CoNap	0.8	0.85	0.9	0.95

2.2.5. Determination of chemical compositions Chicken Feather Particulate

The test was carried out on minipal 4 XRF Epsilon panalytical model machine designed for elemental analysis of wide range of samples in National Geoscience research laboratory Kaduna, Kaduna State. It is an energy dispersive XRF bench top spectrometer which performs non-destructive analysis of elements from sodium right through Uranium, from concentrations down to ppm levels. It offers great levels of sensitivity and versatility with 12 position sample changer. The samples (in powdered form) were weighed and cellulose-powder (binder) and dispersive agent were added and then shaken in small plastic container for 12mins. The mixture was then compressed by applying pressure of 1500kgm^{-2}. The pellets were placed in the computer programmed XRF and the conditions for trace elemental analysis set to generate the results.

2.2.6. Physical Properties of the Composite

Density

Procedure: Samples of chicken feather – plastic composites of various compositions were weighed and their individual weight recorded. The density of the composite was evaluated using (1) as ASTM D 792 and Clyne, 2000.

$$\text{Density} = \frac{mass}{vol} \tag{1}$$

Water absorption Properties

The specimens of the composites of various compositions developed were produced to a dimension of 50mm $\times 50mm$. the specimens were then weighed in order to determine the dry weight of the composite. The specimens were then submerged horizontally in water at room temperature for 24hrs, then removed and patted dry with lint free cloth and then weighed to obtain the wet weight of the composite. (ASTM D570) The water absorption was determined using (2) and thickness swelling using (3).

$$\text{Water Absorption (W/a)} = \frac{W_w - W_d}{W_d} \times 100\% \tag{2}$$

Where: W_w is the wet weight of the composite and W_d is the dry weight of the composite.

$$\text{Thickness swelling (TS)} = \frac{t_w - t_d}{t_d} \times 100\% \tag{3}$$

Where: t_w is the thickness of the wet composite and t_d is the thickness of the dry composite.

2.2.7. Mechanical Properties of the Composite

Modulus of Rupture (MOR)

Composite specimens of dimensions of $125mm \times 12.7mm \times 3.2mm$ were subjected to a load on the universal tensile testing machine with the support span length of 40mm and a head speed of 10mm/min. The specimens were supported at each ends and then loaded at

447

the center. The forward movement of the machine leads to gradual increase of load at the middle span until failure of the test specimens occurred. At the point of failure, the force exerted on the specimen that caused the failure was recorded (ASTM D790). The modulus of rupture (MOR) of the test specimens was evaluated using (4)

$$MOR = \frac{3PL}{2bd^2} \qquad (4)$$

Where: P is the breaking load; L is span Length; b is the sample breath and d is the sample depth.

Modulus of Elasticity (MOE)

The modulus of elasticity (MOE) of the composite was evaluated using (5).

$$MOE = \frac{L^3 m}{4bd^3} \qquad (5)$$

Where;

L is the span length (mm); 'm' is the gradient (i.e slope) of the initial straight-line portion of the load – deflection graph; b is the width of the specimen (mm) and d is the thickness of the specimen or depth (mm).

Ultimate Tensile strength (UTS) and Youngs modulus (E)

The composite specimens were molded in a dumbbell shape of dimension $120mm \times 15mm \times 4mm$ and the samples were then individually subjected to a load on a Universal tensile testing machine. The specimens were hooked up at both ends of gauge length 40mm and then stretched with a head speed of 5mm/min. The movement led to gradual increase of the load at the middle span until failure of the test specimen occurred (ASTM D638). The ultimate tensile strength of the specimen was evaluated using (6).

$$\sigma = \frac{L_b}{w-t} \qquad (6)$$

Where: σ is the ultimate tensile strength, L_b is the load at break, w is the original width of the sample and t is the original thickness of the sample.

The Young's Modulus (E)

The Young's modulus of the samples was determined from the tensile test performed on each specimens and the young's modulus (E) was calculated using (7).

$$E = \frac{\sigma}{\varepsilon} \qquad (7)$$

Where: E is the young's modulus of the sample, σ is the stress and ε is the strain.

Percentage Elongation (El)

Percentage elongation of the samples was evaluated using (8).

$$El = \frac{L_f}{L_o} \times 100\% \qquad (8).$$

Where: El is the percentage elongation of the sample, L_f is the final length and L_o is the original length of the sample.

3. RESULTS AND DISCUSSIONS

3.1. Background
The results obtained in the various experiments conducted are presented in this section. Also presented in this section are the discussions of the results obtained.

3.2 Results
3.2.1 Chemical composition of chicken feather
The chemical composition chicken feather are presented in
3.2 Results
3.2.1 Chemical composition of chicken feather
The chemical composition chicken feather presented in Fig 1.
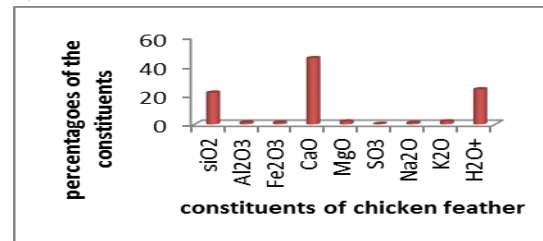
Fig 1: Chemical Composition of chicken feather

3.2.2 Physical Properties and mechanical Properties of composite of various compositions
The properties of the composite developed such as density, water absorption, thickness swelling, modulus of rupture, modulus of elasticity, young modulus, percentage elongation and Ultimate tensile strength are presented below:

Density

The density of the composites of various compositions developed is presented in Fig 2:
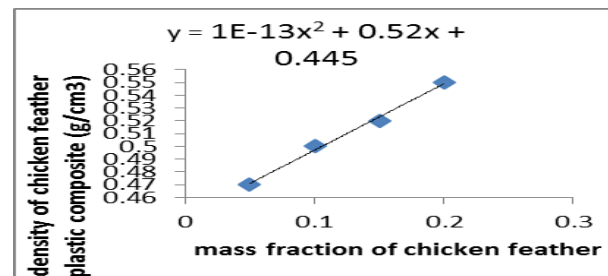
Fig 2: Density of chicken feather - plastic composite versus mass fraction of chicken feather in the composite.

Water Absorption and Thickness Swelling of the plastic composite

The results of the water absorption and thickness swelling of the composite of various compositions are presented in Fig 3.
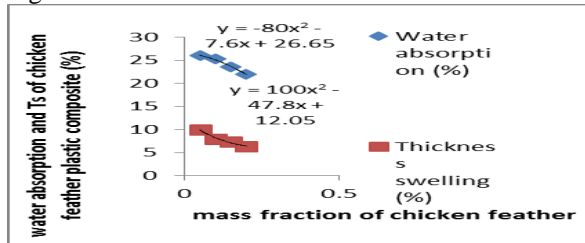
Fig 3: Water absorption and thickness swelling (%) of chicken feather - plastic composite versus mass fraction of chicken feather in the composite.

The load (N) and extension (mm) were obtained for each test conducted, while Modulus of Rupture and Modulus of Elasticity were calculated. The modulus of rupture and modulus of elasticity of the composite is shown in Fig 4.
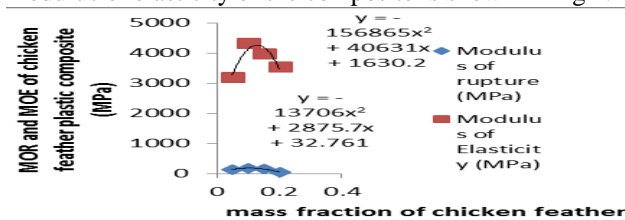
Fig 4: MOR (MPa) and MOE (MPa) of chicken feather - plastic composite versus mass of the chicken feather in the composite.

Ultimate Tensile Strength (UTS), Percentage elongation and Young's Modulus (E) of the chicken feather – plastic composite of various compositions.

The ultimate tensile strength (UTS), Young's modulus, and percentage elongation (El) of the developed composite are presented in Fig 5 and Fig 6.
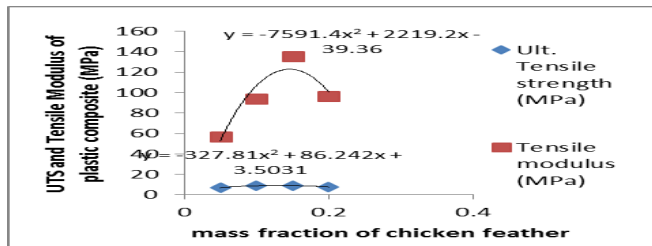
Fig 5: UTS and E vs mass fraction of chicken feather - plastic composite versus chicken feather in the composite.
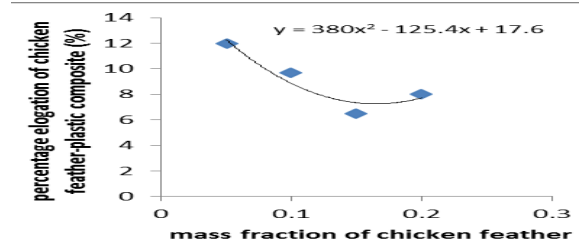
Fig 6: Percentage elongation of chicken feather - plastic composite vs mass fraction of chicken feather in the composite.

3.3. Discussion of Results

3.3.1. The chemical composition of chicken feather

The results shown in fig.1 showed that calcium oxide (CaO) has the highest percentage composition in chicken feather followed by silica (SiO_2). The high present of CaO in chicken feather is an important ingredient that provides strength to chicken feather which makes it sound like cement.

3.3.2. Density of composites developed of various compositions

From the result, the density of chicken feather - plastic composites increased from 0.47- 0.55g/cm^3.These results go in line with (clyne, 2000) and the results of some compositions of the composite have satisfied ASTM (TAS) NO. 1100-2000 for D570 for a good quality particle board ranged 0.5 - 0.9g/cm^3.

3.3.3. Water Absorption of composites developed of various compositions

The average values of the water absorption of the chicken feather - plastic composite ranged from 22.0 - 26.0%. The result obtained showed that the water absorption of the developed composite is low. This is because of the compatibility of chicken feather with the binder was very high. The abundance of amino acid in feather keratin is serine and that each surface of serine has a corresponding free OH and as such CF can absorb water. However, its fine fibers make it to have inherent problem with wettability. This result has satisfied the water absorption recommendation of a good quality particle board of 20 - 75% by ASTM (TAS) No. 1100-2000 for D570.

3.3.4. Thickness swelling of the Composites developed of various compositions

The average values of the thickness swelling of the chicken feather -plastic composite of various compositions increased from 6.4 - 10%. The results obtained showed that the composite produced has a low thickness swelling. The results also have satisfied AST (TAS) No.110-2000 for D570 ranged 5 - 15% thickness swelling for a good quality particle board.

3.3.5. Modulus of Rupture (MOR) of the composites developed of various compositions

The results obtained from the test conducted showed that the mean MOR values of the chicken feather – plastic composite produced ranged from 61.2 - 187.8 MPa. The results showed that the values of MOR increased up to 10wt% and then experienced depreciation with further addition of the mass of reinforcement beyond 10wt% due to the fact that polyester resin has exceeded the saturation point. Therefore, the weight can no longer be coated and bonded properly by the polyester resin. The results obtained satisfied the requirement by the American National Standard Institute (ANSI) for MOR of 14MPa minimum for particle boards developed for interior applications.

3.3.6. Modulus of Elasticity (MOE) of the Composites Developed of Various Compositions
The results obtained showed that, the average values of stiffness strength (MOE) of the chicken feather - plastic composite produced ranged from 3198.8 - 4336.9 MPa. The results obtained met the requirement set by the American National Standard Institute (ANSI) for minimum MOE of 1400MPa for particle board developed for interior use.

3.3.7. Ultimate Tensile Strength (UTS) of Composites Developed of Various Compositions
The results obtained from the test conducted showed that, the average values of ultimate tensile strength of the chicken feather - plastic composite produced ranged from 6.9 - 9.1 MPa. The results also showed that the values of the ultimate tensile strength increased up to 10wt% and then experienced depreciation with further addition of chicken feather beyond 10wt%. The results showed that the tensile strength of the developed composite met requirements set by Emergency number (EN312-2, 1996) of 0.24MPa minimum.

3.3.8. Young's Modulus of the Composites Developed of Various Compositions
The results obtained revealed that, the average values of Young's modulus of the chicken feather - plastic composite developed ranged from 56.86 - 135.4MPa. The results showed that the mean values of Young's modulus of the developed composite increased up to 10wt% and then decreased inconsistently with increase in the weight of chicken feather due to polyester resin that has exceeded the saturation point.

3.3.9. Percentage Elongation (El) of the Composites Developed of Various Compositions
The results obtained from the test conducted revealed that, the average values of the percentage elongation of the chicken feather - plastic composite developed ranged from 6.5 – 12.0%. The results also showed that the percentage elongation of the developed composite decreased as the mass of chicken feather increased. The results obtained met the requirement of 0.3% minimum percentage elongation for (ASTM D638) required for particle board use.

4. CONCLUSION
This research is centred on the development of particle board composite using chicken feather as reinforcement and polyester as the binder for use as an alternative to wood particleboard. The results obtained showed that composites were successfully developed using unsaturated polyester resin as the matrix and chicken feather as reinforcements and also that the chicken feather – plastic composite developed have satisfied the minimum quality requirements for particle board.

RECOMMENDATIONS
Based on the conclusion reached, this study therefore recommends the following:

i. Large scale production and commercialization of particleboard made from chicken feather as reinforcement and polyester resin as matrix should be encouraged to enhance economic growth of the Nation.
ii. The mas of the chicken feather to be added to the polyester resin should not exceeded ten percent by weight (10wt %) for proper coating and bonding in order to obtain high quality particleboard.

REFFERENCE
Acharya, R.M and Kuma, A. (1984). Performance of Local Birds in South Asia. Indian poultry industry yearbook. 7th Edition.

Ajayi, F. O. (2010). Nigerian Indigenous Chicken: A Valuable Genetic Resource for Meat and Egg Production. Asian Journal of Poultry Science, 4, pp 164 – 172.

American National Standard. Particleboard ANSI,A208.1-1999 Table A7p, Gaithersburg.

ASTM D638-02 (2003). American Society of testing materials. Standard test method for tensile properties of plastic. Book of Standard, Vol .14.02 wood. West Conshohocken, PA 19428-2959, United State.

ASTM D792, standard Test Methods for density and specific gravity (relative density) of plastics by displacement, ASTM international, west Conshohocken, PA 2000,www.astm.org

ASTM D790, American Society of Testing materials. Standard test method for flexural properties of plastics, west Conshohocken, ASTM international.

ASTM D570, American Society of Testing materials. Standard test method for water absorption of plastics. Absorption, immersion, plastics, water, immersion-plastics, water analysis-plastics.

Biswal, R. (2010). Study of Wear Behavior of Rice Husk Ceramic Composite. An Unpublished Degree Thesis Presented to the Academic National Institute of Technology, Deem University, Rourkela, pp. 1-50.

Clyne, T. W. (2000). Comprehensive composite materials. Journal of metal matrix composite, Vol 3: pp.1-8

Dupont de Nemour E. I. (2005). Composite polymer fabricating tips. Ashland Canada, www.derakane.com , Accessed march, 2014.

EN 312-2(1996). Particle boards-specification. Part 2. Requirements for general purpose boards for use in dry conditions, European committee for standardization, Brussels, Belgium.

EST (2006).Wood Product: Processes and Use. Environmental Statistic Team. Published by the Product Development and Publishing Business Unite of Statistic New Zealand. p13.www.stats.govt.nz

Flynn, M. S. and Belzowski, B. M. (1995). Barristers to Automotive Structural Composites: Concerns, Completion, and Competence, Proceedings of 11th Annual ASM/ESD Advanced Composites Conference and Exposition, pp. 517-534.

Hong, C.K and Wool, R.P., (2005). Development of Bio-Based Composite Materials from Soybeans Oil and Keratin Fiber. Journal of Applied Polymer Science, Vol. 95, pp.1524-1538.

Hull, D and Clyne, T.W. (1996). An Introduction to Composite Materials. Cambridge University Press, Cambridge.

Kock. J.W. (2006). Physical and Mechanical Properties of Chicken Feather Materials. An unpublished master's degree thesis presented to the School of civil and environmental engineering, Georgia Institute of Technology.

Kartini, K., Mahmud, H. B. and Hamidah, M. S., (2010). Absorption and Permeability Performance of Selangor Rice Husk Ash Blended Grade 30. Concrete Journal of Engineering Science and Technology, Vol. 5, No.1, pp.1-16.

Menandro, N.A. (2010). Waste Chicken Feather as Reinforcement in Cement-Bonded Composites, Philippine Journal of Science, Vol. 139, NO.2, pp. 161-166.

Nagaraja, B.G, and Rekha, B. (2013). A comparative study on tensile behavior of plant and Animal fibre reinforcecomposite. International Journal of Innovation and applied studies, Vol.2, No. 2, pp. 645-648.

Papadopoulos, A. N. (2006). Chemical Modification of Solid Wood and Raw Material for Composites Production with linear Chain Carboxylic Acid Anhydrides: A Brief Review, 5(1)499-506

Schmidt, W.F. and Jayasundera, S. (2012). The Effect of Water Absorption on Mechanical Properties of Wood Flour/Wheat Husk Polypropylene Hybrid. Central Institute of Plastic Engineering and Technology,

Lucknow, India, Material Sciences and Application, 3, pp317-325.

TAS NO.110-2000, testing application standard. Testing requirements for physical properties of roof membranes, insulation, coatings, and other roofing components. ASTM standard.

Winandy, J.E., Muehl, J.H., Micales, J.A., Raina, A. and Schmidt, W. (2003). Potential of Chicken Feather Fibre in Wood, MDF Composite," Proceedings Ecocomp 2003, p20, pp1-6

EFFECT OF AIR FLOW RATE ON QUALITY OF SYNGAS PRODUCED VIA GASIFICATION OF SAWDUST

M. B. Muhammad[1*], J. Salisu[2], B. Mukhtar[3], N. Yusuf[4],A. Y. Atta[5], I.M. Bugaje[6]

[1,2]Department of Chemical Engineering, Ahmadu Bello University, Zaria
[3,4,5]National Research Institute for Chemical Technology, Basawa, Zaria
[*]belloibnmaj@gmail.com, +2347065162100.

ABSTRACT

Current state of affairs in Africa indicates heightening energy demand coupled with degrading environmental issues related to waste generation and disposal. These daunting circumstances prompted a number of extensive researches in the area of renewable and sustainable energy development. This article investigates exclusively the effect of air flow rate on quality of syngas produced via gasification of sawdust. Experimental study was conducted using a pilot scale downdraft gasifier with additional scrubbing units consisting of cyclone, filter and tar collector. The gas products from the gasifier were analysed using an onlinegas analyser capable of detecting and quantifying CO, H_2, CO_2,$CH_4$and O_2. Air flow rates at 0.64, 0.19 and 0.07 litre/min were used for the study. The results obtained shows that the higher air flow levelfavours better quality of syngas. Air flow rate at 0.64 litre/min, generated the best quality of syngas containing 13.55% and 2.59% of CO and H_2, respectively. Gas caloric value of nearly 700kcal/m^3 and a maximum temperature of 550^0C were also recorded.

Keywords: Renewable Energy, Sawdust, Syngas, Gasification, Downdraftgasifier.

1. INTRODUCTION

The global trend today shows significant attention is focused towards renewable energy technologies for sustainable development (Bergerson and Keith, 2006).

Over the past decades biomass gasification has been regarded as a very promising technology, because of its vast potentials suited for applications ranging from traditional domestic usage to modern industrial application (Kirkels and Verbong, 2011).However more extensive applications lie ahead through effective technology for conversion of the biomass into valuable gaseous and liquid products which can be further processed into fuels and commodity chemicals (Reed and Das, 1988).

Another benefit of gasification is the possibility of the utilization of various organic wastes from the local industry and agriculture with a considerable CO_2 emission reduction (Lapuerta et al, 2008).

Gasification refers to the thermo-chemical conversion of any solid or liquid carbon-based material (feedstock) into gaseous fuel through partial oxidation with air, oxygen, water vapour or their mixture. Unlike the full combustion, it uses air/fuel ratios also known as equilibrium ratio (ER) noticeably below the stoichiometric value. Such deficit in supply of the oxidation agent prevents complete conversion of the carbon and the hydrogen present in feedstock into CO_2 and H_2O respectively, and results in formation of combustible components such as CO, H_2 and CH_4. In addition to those components, the producer gas also contains typical products of combustion, namely CO_2, N_2, O_2 and H_2O.

Although the process takes place with a sub-stoichiometric amount of air, it is usual to find a low concentration of oxygen in the gasification products (Martínez et al, 2012).

Gasification is an established technology. However, there is very little research in the country in terms of the process development and optimization of the operating conditions.

The main objective of the present research work is to investigate the effect of varying air flow levels on quality of producer gas derived from gasification of sawdust particles as feedstock. A pilot scale downdraft gasifierwas used for its excellent low tar formation performance.

2. METHODOLOGY

2.1. Material

Sawdust (feedstock) obtained from Sawmills at *KasuwanKatako* of *SabonGari* Local Government Area in Kaduna State, Nigeria, was used as feedstock for the research work. Collected samples were spread dried in an open air and under shade to reduce the moisture content. Ultimate and proximate analyses method published by American Society for Testing and Material (ASTM) E 870 – 82 designated for fuel wood analysis was conducted to characterize feedstock sample.

2.2. Equipment

The gasification experiment was conducted using a downdraft gasifierdeveloped at the National Research Institute for Chemical Technology (NARICT), Zaria, Nigeria. Figure1 depicts a schematic representation of the system used consisting of five separate units namely; gasifier (reactor), cyclone, filter, tar collector and syngas burner. The reactor geometry constitutesof double coaxial cylindrical shells with inner diameter of 30cm and height of 72cm. Carbon steel of 1mm thickness was used as construction material for both internal and external shells of the reactor while galvanized pipe of 1.5 inch (3.81cm) internal diameter connects all the system units together for continuous flow of producer gas. Fresh feedstock is fed manually through the upper section of the gasifierfor every batch operation. An agitator shaft mounted on a suspended grate below the inner shell extended to pass through a small opening on a mild steel circular lid which aids to reduce bridging during feeding process. In a similar manner it serves as a means by which reduced fuel in form of ash and char can be dislodged from the grate.

Air blower mounted at the inlet end of the air nozzle with speed rating of 3600rpm supplies air into the reactor in two stages. At first air reaches a manifold like chamber that goes round the inner reactor shell. At second stage air flows directly across the biomass through perforations around the circumference of the manifold with nearly uniform distribution.

In principle, gasification process occurs sequentially in four distinct reaction zones notably; drying, pyrolysis, oxidation and reduction. However in practice, these zones are not completely distinct from one another rather forms overlap. Drying takes place at the uppermost part of the reactor where moisture and volatile component of the biomass are driven off. Pyrolysis zone lies immediately below where tarry gases and charcoal are produced. The tarry gases then pass downward through the combustion zone where oxidation reactions occur with enormous release of energy in form of heat sufficient to sustain pyrolysis and drying processes. Cracking of tar occurs during the passage of gases through the high temperature oxidation zone. The gas stream flows to the reduction zone at the bottom of the grate where the unconverted carbon reduces to produce more combustible gases by a number of endothermic reactions. Product gas finally leaves the reactor from the bottom of the inner shell via the outer shell.
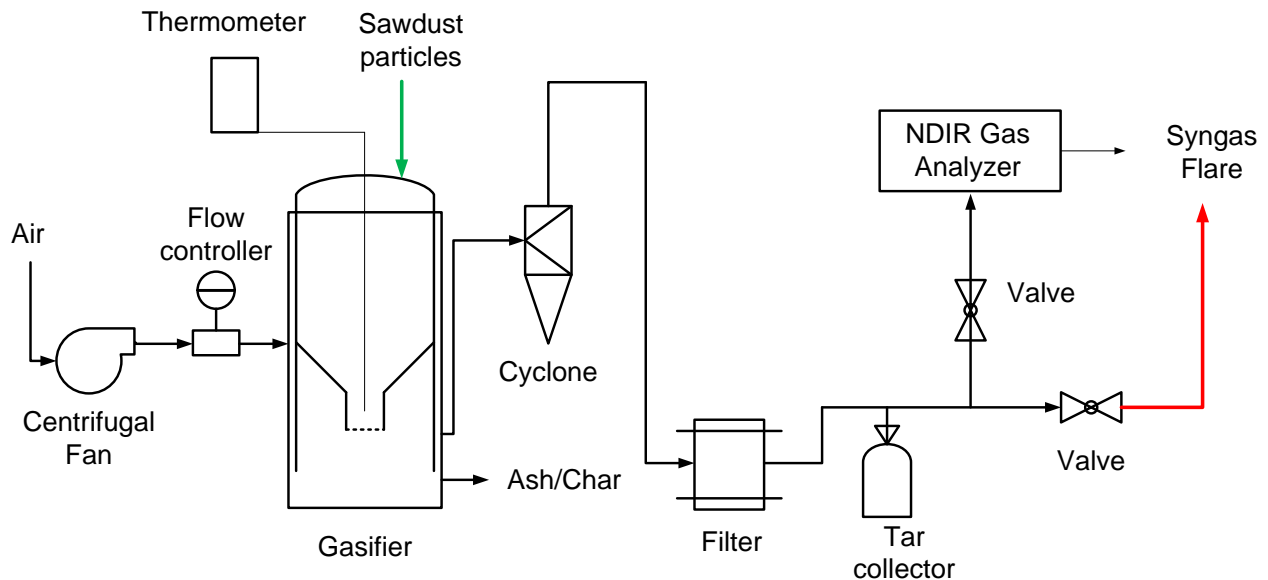
Fig.1: Schematic Diagram of the Gasification Experimental Set-up

2.3. Experimental Start up

Prior to start up procedure a quantity of sawdust feedstock approximately 10kg was charged to fill the internal shell to its brim. The agitator shaft was then mounted to pass through an aperture on a circular mild steel lid to properly close the reactor shell. With the aid of a silicon gasket sealer all possible leakages around the reactor were properly sealed up to avoid loss of product gases. An induce fan blower mounted at inlet end of air nozzle through the suction end allows air draft to flow into the reactor in a reverse mode. While all other valves were shut up tightly as air supply comes exclusively through the ignition aperture. In this way the biomass feedstock is ignited and allowed to attend auto-ignition temperature so as to sustain the started combustion before changing the blower fitting configuration such that discharge end connects to the inlet end of the air nozzle. Ignition aperture was then closed tightly allowing product gas to exit via the bypass duct. With aid of the agitator shaft, the feedstock is then stirred up at intermittent time interval as

reaction proceeds gradually while reducing fresh feedstock to char and ashes.

2.4. Experimental Measurement

After successful start-up procedure, the reactor is allowed to run for about 5 minutes to attend nearly auto-ignition temperature such that operation can be sustained. A flow meter positioned ahead of the blower monitors the rates at which air flows. To keep this flow constant, a 3–12V variable adaptor powering the blower allows selection of constant speed. Reactor temperatures are measured by K–Type thermocouple with readings displayed on digital screen. A thermocouple sensor inserted through an aperture on the reactor lid extends to reach the oxidation zone. Typically axial and radial temperature distributions are trends observed in gasifier reactors. However, within the context of the current study only the maximum temperature zone was prioritized as parameter of interest. Gas composition in percentage volume bases were determined using Non-Dispersal Infrared (NDIR) gas analyser by a way of online sampling of the product gas.

An additional gas washing module with three integrated treatment stages was used to purify gas sample. In this way the analyser sensor is carefully protected to effectively avoid potential damage by trace of contaminant in the product gas.

Percentage gas compositions of CO, H_2, CO_2 and CH_4 were monitored and recorded in addition to combined calorific value product gases.

Varying flow rates of oxidation agents were used separately to investigate the effect of equivalent ratio (ER) on composition of product gas and gasification temperature while keeping moisture content, particle size distribution and feeding rate as constant operation parameters.

3. RESULTS AND DISCUSSIONS

3.1. Ultimate and Proximate Analysis

Both ultimate and proximate analyses were conducted using the standard of American Society of Testing Material (ASTM).

Ultimate analysis determines the composition of dry fuel on weight percentage basis. Typically Hydrogen, Oxygen, Carbon, Nitrogen, Sulphur and Ash content are determined. Figure2 showing ultimate analysis result of sawdust sample indicates that the sawdust sample material contains significant carbon up to 50%, implying the suitability of the feedstock for gasification. Low sulphur and nitrogen contents approximately 0.18 and 0.09 respectively, indicates added advantage in terms of low level contribution to NO_x and SO_x gas emission compared to conventional fossil feedstock.

Proximate analysis determines the moisture content (M), volatile matter (VM), ash content (A) and fixed carbon content (C) of feedstock. Moisture content of biomass sample is analysed by weight loss observed at about 103°C for 16 hours. Subjecting dried biomass further to a temperature of about 950°C drives off volatile content leaving behind the fixed carbon. Figure3 presents

proximate analysis data of sawdust sample material on weight percentage basis.
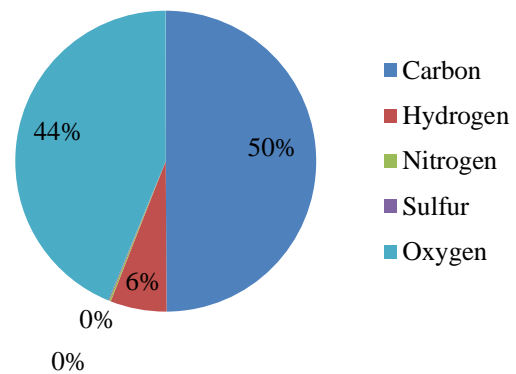
Fig.2: Ultimate Analysis of the Sawdust Sample
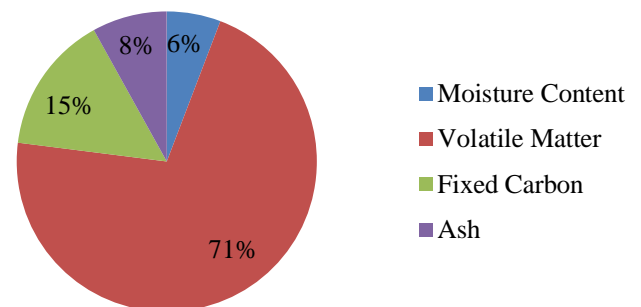
Fig.3: Proximate Analysis of the Sawdust Sample

3.2. Effect of Air Flow Rate on Temperature

The amount of air supplied in thermal conversion of carbon feedstock determines the corresponding term used to describe the process; either pyrolysis or gasification or combustion. Figure4 presents gasification temperature profile with three different flow levels selected to run the experiment. Observed trend indicates that increase in air flow rate corresponds to increase in temperature of the oxidation zone. For about 10 minutes of operation, flow levels; 0.64, 0.19 and 0.07litre per min (LPM) recorded highest temperatures points of 548.7,478.8 and 403.3°C respectively.
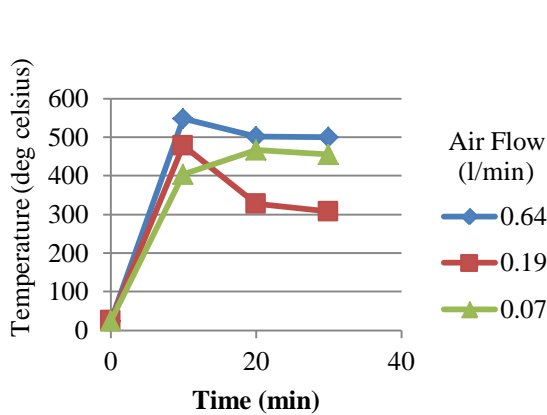
Fig4: Gasification Temperature Profile

3.3. Effects of Air Flow on Syngas Composition

Effects of gasification air flow on syngas composition are presented in Figure5-7. It was observed that level of residual oxygen in syngas decreases with increase in air flow most likely as a result of oxidation reactions taking place to form CO and CO_2. Compositions of CO and H_2 in syngas recorded highest levels of 13.55% and 2.59% respectively with 0.64 LPM air flow as shown in Figure5. However drastic fall in syngas composition was observed apparently as a result of total endothermic oxidation reaction favoured at high temperature as given by (1). Methane formation equally favoured at temperature above 200°C given by (2), also contributes to the fall of syngas quality. Similar trend of gas quality was observed with lower air flow levels of 0.19 and 0.07 LPM.

Typical gas composition from biomass gasification in a downdraft gasifier with air used as oxidizing agentindicates up to 15% CO (McKendry, 2002).

$$CO + {}^1/_2\, O_2 \rightarrow CO_2 \qquad (1)$$

$$CO + 3H_2 \rightarrow CH_4 + H_2O \quad (2)$$
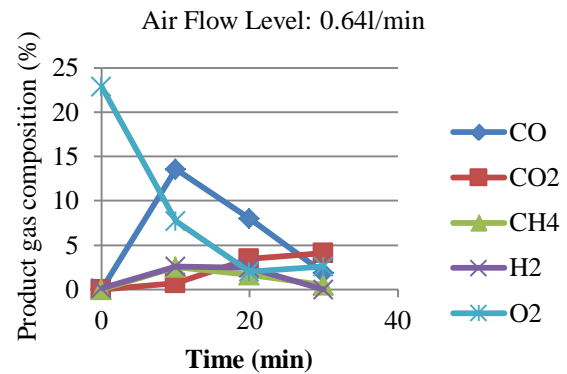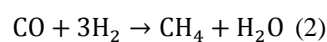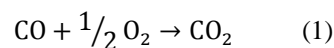
Fig5: Syngas Composition Profile at 0.64 LPM
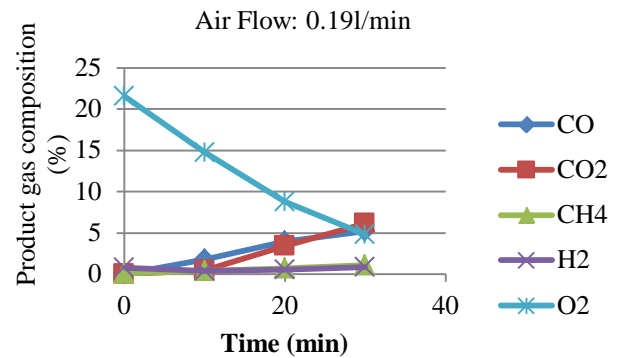
Fig6: Syngas Composition Profile at 0.19 LPM
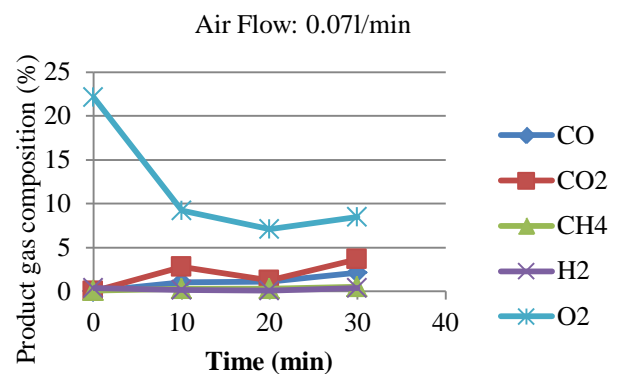
Fig7: Syngas Composition Profile at 0.07 LPM

3.4. Effects of Air Flow on Calorific Value of Syngas

Calorific value also called the heating value is the amount of energy produce by complete combustion of a combustiblematerial sample. Combustible component of

syngas contributes majorly to the combined calorific value. Therefore higher calorific value is expected with higher percentage composition of CO, H_2 and CH_4 in syngas. Figure8 illustrates the proportionality effect of air flow level on caloric value with 0.64 LPM flow level recording the highest calorific value nearly 700kcal/m^3(2.93MJ/m^3).
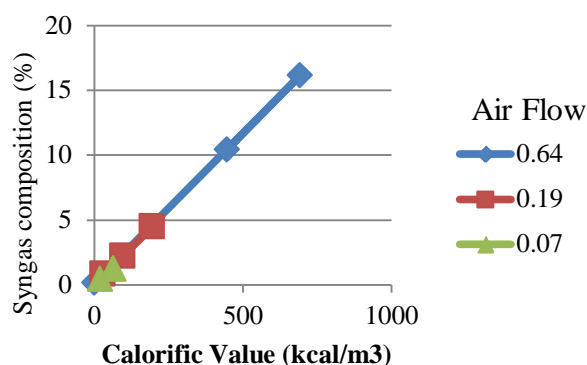
Fig8: Effect of Air flow level on Calorific Value

4. CONCLUSION

The quest for alternative renewable resources for sustainable development and capacity building in local technology is the key motivation for this research work.

Syngas majorly consisting of CO and H_2 in addition to CO_2 and CH_4 was produced via gasification of sawdust feedstock in a downdraft gasifier, using air as gasification agent.

The experimental gasification process carried out indicates considerable trend between air flow rate levels and syngas quality. Increase in air flow rate corresponds to increase in temperature of the oxidation zone. The highest air flow rate of 0.64 LPM gave the best syngas composition of CO and H_2 of 13.55 and 2.59% respectively and the highest calorific value of about 700kcal/m^3.

REFERENCE

Bergerson, J. D., & Keith. (2006). Life Cycle Assessment of Oil Sands Technologies. Alberta Energy Futures Project, Institute for Sustainable Energy, Environment, and Economy (ISEE). University Calgary.

Kirkels, F. A., & Verbong, G. P. (2011). Biomass gasification: Still promising? A 30-year global overview. Renewable and Sustainable Energy Reviews(15), 471–481.

Lapuerta, M., Hernández, J., Pazo, A., & López, J. (2008). Gasification and co-gasification of biomass wastes: effect of the biomass origin and the gasifier operating conditions. Fuel Processing Technology(89), 828-837.

Martínez, J. D., Mahkamov, K., Andrade, R. V., & Lora, E. E. (2011, August 19). Syngas Production In Downdraft Biomass Gasifiers and its Application Using Internal Combustion Engines. Renewable Energy Journal.

McKendry, P. (2002). Energy Production from Biomass (Part 3): Gasification Technologies. Bioresource Technology, 83, 55-63.

Reed, T. B., & Das, A. (1988). Hand Book of Downdraft Gasifier Engine System. Solar technical information program, solar energy research institute, (SERI). Colorado.

Effect of Delignified Coir Fibre Particulate Filler on physical properties of Natural Rubbe vulcanizate.

J.0. Oboh[*], D.O. Agbajelola[2], J.O. Okafor[3]

[2,3]Department of Chemical Engineering, Federal University of Technology, Minna Niger State, Nigeria.
[*]Department of Polymer Technology, Nigerian Institute of Leather and Science Technology. Zaria, Nigeria.

labconsult@yahoo.com. 08035060872

ABSTRACT

Coconut fibre was separated from the fruit shell, washed and a portion of it was washed in boiling water and treated with 5% solution of sodium hydroxide and sodium carbonate (delignification). This was followed by grinding and clarification into particles size of 125µm for both treated (DCFF) and untreated fibre (RCFF). The DCFF and RCCF were characterized to determine their moisture content, pH, density, lignin content and porosity. RCFF had higher values of lignin content, density and lower values of pH, moisture content and porosity compared with DCFF .Different rubber formulations containing 0, 15, 30 45 and 60 parts per hundred rubber of both filler type were compounded and vulcanized. Scanning election micrographs (SEM) of an unfilled vulcanisate, RCFF based vulcanisate and DCFF based vulcanisate were obtained. The RCFF vulcanisate reveals better dispersion of filler in the polymer matrix. The tensile strength, elongation at break, hardness, compression set and abrasion resistance of the vulcanised samples were investigated. The results of test obtained were compared with those obtained from the convectional reinforcing filler carbon black (CB). It was observed that for hardness, both RCFF and DCFF based vulcanizates compared favourably well with the CB reinforced vulcanizate. 75.5, 71 and 75 international rubber hardness density (IRHD) were the highest values for vulcanisate filled RCFF, DCFF and CB respectively. Tensile strength increases with increasing filler loading highest values of 6.6, 7.5 and 18.5 MPa were obtained for vulcanisate with RCFF, DCFF and CB respectively. Thermo gravimetric analysis also shows that all vulcanisates were thermally stable up to 250 ^{o}C. Abrasion resistance and compression set showed an irregular increase with increasing filler loading for all filled vulcanizate while elongation at break showed a falling trend for all the filled vulcanizate as filler loading were increased. The particulate coir fibre compete favorably with the conventional carbon black filler in almost all the properties evaluated except in the case of tensile strength where it fell below 50% of the measured value for carbon black.

Keywords: *Delignified, coir fibre, vulcanizate, rubber*.

1. INTRODUCTION

The search for possible alternative to carbon black filler in the manufacture and application of rubber article has witnessed a steady growth over the years. Carbon black filler is produced through heavy industrial combustion of hydrocarbon process. This process requires tremendous energy utilization and constitutes a potential source of pollution and global warming; this has led to the search for more cost effective and eco – friendly materials for replacement. Raw rubber is usually transformed into a range of materials suitable for application in various uses and in different service environment through compounding and vulcanization. Natural rubber alone does not possess the necessary physico-mechanical properties that are required by rubber manufacturers. Fillers are widely used additives and the largest in quantity among others in the manufacture of rubber product. Particulate fillers such as carbon black, calcium carbonate and china clay are widely used as reinforcing filler in the industries. Calcium carbonate ($CaCo_3$) has attracted considerable interest in recent years due its low cost and availability and the dependence of the traditional carbon on crude oil. The concept of conversion of waste to wealth is of significance since it yields the dual benefits of waste management and sustainable cost efficient production system [19]. Coir fibre is an agro-industrial by-

product generated during the coir defibering process. Coir fibre is a lignocellulosic agro-industrial residue that contains about 38 % lignin (polyphenol) and therefore delignification has to be achieved to loosen the lignocellulose binding and to expose the cellulosic component [20].

The reinforcing strength required of a fibre is possessed by cellulosic component. Direct combination of coir fibre phase with a polymer phase might result to a situation where the lignin (which is weakly bound to the cellulose and hemi cellulose) actually interacts with the polymer phase instead of the desired cellulose phase especially if the surface area of the cellulosic component is not large enough to ensure adequate binding with the polymer phase. This possibly is the reason while other workers [1] and [12] similar works carbonize the coir fibre before using it. The aim of this work is to study the effect of blending delignified coir particulate filler on the reinforcement of natural rubber vulcanizate.

Agricultural residues are low cost materials and readily available in large quantity for use everywhere [15]. In previous report, the use of sugarcane baggasse, cocoa pod husk, rubber seed shell etc. as filler in natural rubber has been investigated [11] &[15]. As for coir fibre the few works reported so far on it showed that they were carbonized [1] & [12]. These study present results of assessment and utilization of particulate coir fibre as filler for the compounding of rubber

2. METHODOLOGY

The main material used during this work was crumb natural rubber of grade NSR-10 and was purchased from Alhson Lab Equipment consult, Zaria Kaduna State, Nigeria. The coir fibre was obtained from Ekpoma, Edo state Nigeria. Other compounding additives and chemical which are of industrial grade used were sulphur, stearic acid, carbon black (N330 HAF), trimethyl quinoline

(TMQ) and mercaptobenzothiazole (MBT) and were all purchased from Alhson Lab Equipment consult, Zaria Kaduna State, Nigeria.

2.1. PREPARATION AND CHARACTERIZATION OF PARTICULATE COIR FIBRE (PCF) FILLERS

The waste outer part of coconut fruit shell were soaked in water for five (5) hours in order to loosen the fibres so as to facilitate easy extraction of the coir fibre. A portion of the extracted fibre was delignified in accordance to a process described by Geethama , 1998. In this process 5 % solution of sodium hydroxide and sodium carbonate was used to soak the coir fibre for a period of 48 hrs and were then thoroughly washed in excess water in order to remove the extraneous materials. The fibres were sun dried for a period of 72hrs and then converted to particulate coir fibre filler by grinding and sieving to $\leq 125\mu m$ particle size with the aid of laboratory grinder (Thomas Wiley lab mill model 4). The particulate coir fibre filler were known as raw coir fibre filler (RCFF) and (DCFF). Both fillers were characterized based on pH value, density and moisture content. .

2.2. Formulation of rubber vulcanizatee

Fifteen different formulations based on 5 by 3 model was adopted, that is five different filler contents of 0, 15, 30, 45 and 60 phr each for rubber compounds filled with delignified coir fibre filer (DCFF), rubber compounds filled with raw coir fibre filler (RCFF) and rubber compounds filled with carbon black (CB).

These are shown on table 1

Table 1: formulation table

Ingredients	Contents(phr)				
Natural rubber	100	100	100	100	100
Zinc oxide	5	5	5	5	5
Stearic acid	2	2	2	2	2
TMQ	1	1	1	1	1
MBT	2	2	2	2	2
Sulphur	3	3	3	3	3
RCFF filler	0	15	30	45	60
CB filler	0	15	30	45	60
DCFF filler	0	15	30	45	60

COMPOUNDING

The rubber was masticated and mixed with chemicals/additives using open roll mill manufactured by Reliable Rubber and Plastic New York, Model 5189 in accordance with standard methods in the American Society for Testing Materials (ASTM D3184-80) for all the composites.

VULCANIZATION

Appropriate test pieces were vulcanized using 11 metric tons Carver inc. model 3851-0 lab curing press at temperature of 150 ^{o}C for 30 minutes.

PROPERTIES DETERMINATION OF RUBBER VULCANIZATES

Tests piece were prepared from the vulcanizates into appropriate shapes and dimensions for various tests and analysis.

Hardness, abrasion resistance, compression set, elongation at break , tensile strength, scanning electron microscopy (SEM) and thermogravimetry analysis (TGA) were carried out. All tests were carried out as specified by American Society for Testing and Materials (ASTM).

3. RESULTS AND DISCUSSIONS

The results for the characterization of fillers are shown on table 2.

Table 2: Characteristics of fillers

paramters	RCFF	DCFF	CB
Lignin content (%)	35	24.5	-
pH value	7.18	8.23	6.5
Density (g/cm^3)	0.36	0.26	0.92
Moisture content (%)	7.14	9.32	2.4
Diameter (µm)	125	125	-

The moisture content, pH value, particle diameter and lignin contents were determined, these properties were evaluated to determine the effect of delignification on the properties of coir fibre. Results obtained showed that there was a reduction in lignin content from 35 to 24.5 %. The effect of delignification on the moisture content, pH value and density of fibre are shown on table 4. The reduction in lignin content means increased surface interaction between the cellulose fibre and the polymer phase. The pH value for RCFF was found to be 7.18 while that of DCFF and CB were 8.23 and 6.5 respectively. Some workers [4],

[11], [12] and [18] showed that the vulcanization rate of rubber composite increases with increasing alkalinity that is higher crosslink density would be achieved for RCFF and DCFF than that of CB within the same vulcanization time. This work did not however study the vulcanization rate of the various composite. The particle diameter used was 125µm while that of carbon black is 40 – 60nm. This is an indication that CB possesses larger surface area necessary for the reinforcement of rubber. Note that the process of particle size reduction of coir fibre is somewhat cumbersome due to its high strength and fibrous nature.
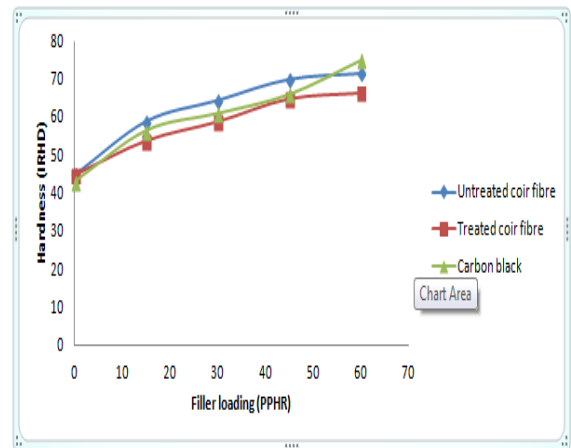
Fig. 1: effect of filler loading on hardness

Hardness was found to increase as filler loading were increased for all fillers loading as shown in fig 1. the untreated filler (RCFF) were found to have higher value of hardness in all filler loading values. CB composite fell in between the untreated fibre composite (RCFF) and the treated fibre composite (DCFF) from 0 – 45 phr and rise above them between 45 – 60 phr of filler content. The possible reason for this is that as more filler are incorporated into the rubber matrix, the vulcanizate become more rigid owing to progressive reduction of polymer chain elasticity. The difference in densities and lignin contents might have affected their level of dispersion and packing thus resulting in different hardness values.
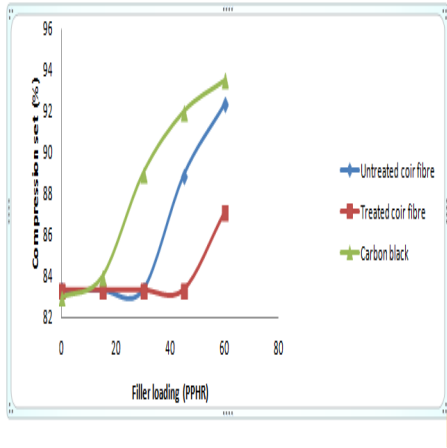
Fig. 2: Effect of filler loading on compression set

The results for compression set as shown in fig.2 reveal similar trend for all fillers based composites. No noticeable change was observed from filler loading of 0 – 15 phr for CB, 0 – 30 phr for RCFF and 0 – 45 for DCFF. They however increased with increasing filler loading as these various points were exceeded. CB was found to posses' superior compression property while DCFF has the least compression set. Note that compression set is the percentage thickness retained after the removal of compressive force. From literature source the compressibility of rubber vulcanizate is connected with the amount of filler incorporated into the rubber matrix, the particle diameter, density and their extent of dispersion. Increase in the filler content of rubber vulcanizate makes it more rigid and less susceptible to compression loading.

The abrasion resistance as presented in fig.3 measures the resistance of a polymer material to mechanical action such as rubbing, scraping or erosion that tends progressively to remove material from the surface. The abrasion resistance took a single step rise as filler content was increased from 0 – 15 phr, after which an irregular trend was observed. DCFF gave highest values when compared with CB and RCFF with the same filler loading of 0 – 15 phr. This is an indication that abrasion resistance might not continue to rise with increase in filler loading. The effect of filler on abrasion property has generally been attributed to the adhesion of particulate filler to the polymer phase, therefore at higher filler loading the adhesion between the polymer phase and the filler weakens as result of high ratio of filler to polymer
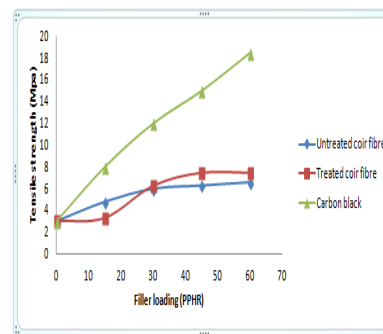
Fig 4: Effect of filler loading on tensile strength of composites

The tensile strength results are shown in fig. 4. Tensile strength is one of the most important properties

Fig. 4: effect of filler loading on tensile strength

The tensile strength results are shown in fig. 4. Tensile strength is one of the most important properties of vulcanized rubber since it application is mostly in the automobile industry. It is a measure of the breaking strength of a material under tensional stress. The tensile strength of CB was found to be higher than those of RCFF and DCFF. However, DCFF was found to give a slightly higher value of tensile strength from filler loading of 30 – 60 phr when compared to its counterpart RCFF. The reasons can be attributed to the reduction of lignin

Fig. 3: Effect of filler loading on abrasion resistance

content(increase interaction between the polymer and cellulose component of the coir fibre) The effect of filler on tensile strength according to [11] and [12] depends on bonding quality between filler and polymer phase, level of dispersion of filler, surface reactivity between filler and rubber matrix and particle size.
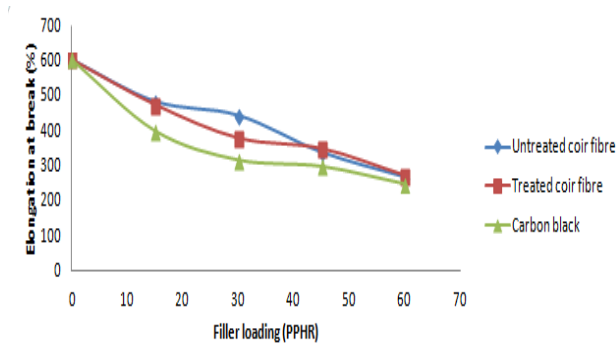
Fig. 5: effect of filler loading elongation at break

The result of elongation at break as displayed in fig. 5 shows that CB vulcanizates gave the lowest value at all filler loadings while DCFF and RCFF revealed the same values of elongation at break between 0 – 15 phr and 45 – 60 phr filler loading, RCFF was however found to give higher value between 15 – 45 phr. Note that the filler with high value of elongation at break gives low reinforcement potential.
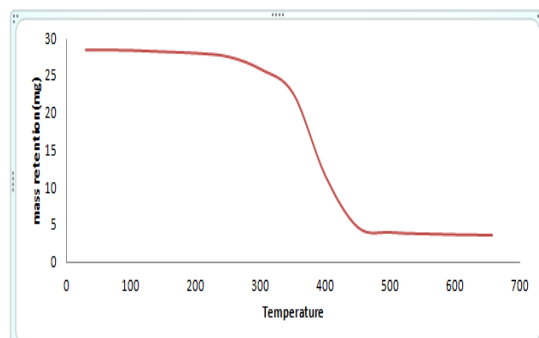
Fig.6a : TGA of RCFF
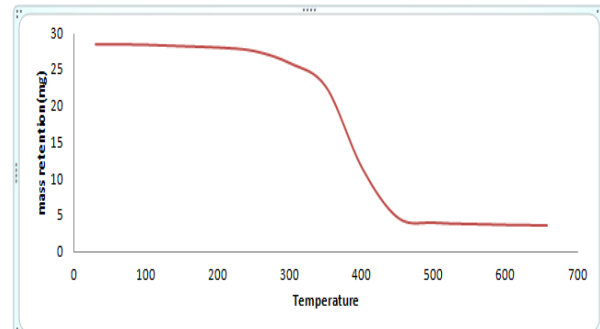
Fig. 6b: TGA of DCFF

The result of thermogravimetric analysis is shown in figs. 6a and 6b. The curves for vulcanizate filled with DCFF and RCFF gave the same values. This is an indication that the presence of lignin does not affect thermal property of the vulcanized rubber.
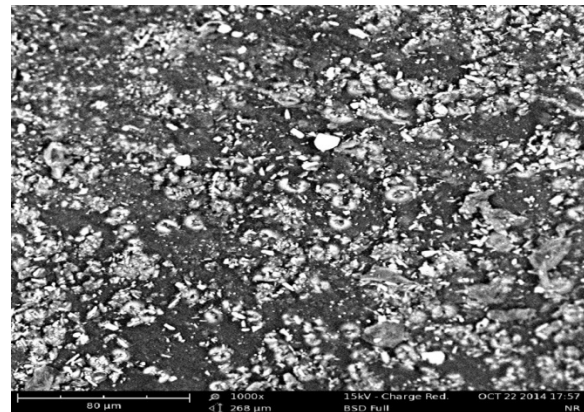
Fig. 7: SEM of unfilled rubber vulcanizate
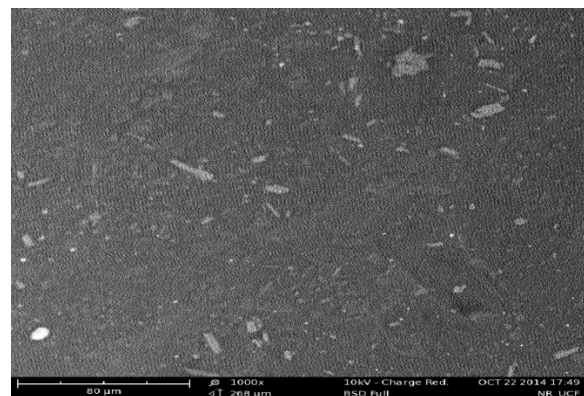
Fig. 8: SEM of RCFF vulcanizate
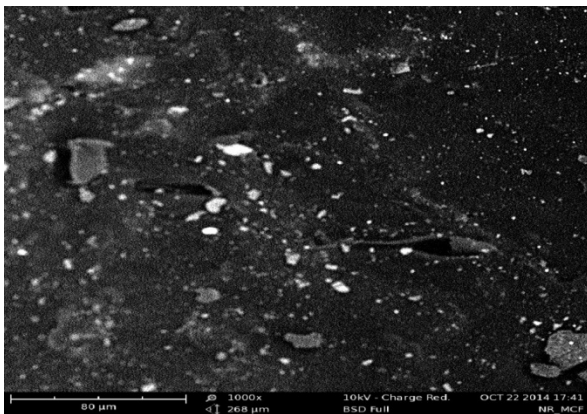
Fig. 8: SEM of DCFF vulcanizate

The scanning electron micrograph of unfilled vulcanizate (rubber vulcanizates without filler), DCFF vulcanizate and RCFF filled vulcanizates were compared. Micrograph of unfilled vulcanizate was found to have large numbers of pores with varying sizes and contours. The RCFF shows little or pores. This is an indication that the pores were all filled with fillers. DCFF shows dark wall and relatively more numbers of pores compared to the RCFF. This might be attributed to better adhesion of the filler phase to the polymer matrix.

4. CONCLUSION.

This work has investigated the effect of delignified coir fibre particulate filler on the reinforced properties of natural rubber vulcanisate. The following conclusions have been made in line with the aim and objectives of this work.

I. Rubber vulcanisates containing alkaline treated coir fibre and untreated coir fibre at various particle sizes were compared with the carbon black filled vulcanisates.

II. It was found that increasing all filler loading within the rubber vulcanisate results in higher values of tensile strength, hardness, compression set and abrasion resistance while elongation at break decreases correspondingly.

III. Thermogravimetric analysis also shows that vulcanisates are thermally stable below 250 ^{o}C

IV. The particulate coir fibre competes favorably with carbon black in almost all the properties evaluated except in the case of tensile strength where it fell below 50% of the measured value for carbon black.

REFERENCE

[1] Aguele, F.G., Madufor, C.I. (2012). Effect of carbonized coir fibre on physical properties of natural rubber composites. *American journal of polymer science 2(3), 28 34.*

[2] Ainsworth, E., & Gillespie, K. (2007). Estimation of Total Phenolics Content and other Oxidation Substrate in Plant Tissue using Ciocalteu Reagent. *Nat.protoc* , 875-877.

[3] Ash, B., Satapathy, D., & Mukherjes P.S. (2001).Characterization and application of activated coir pith. *Journal of Scientific and industrial Research* 165, 1008-102

[4] Asore, E. J. (2000). *Introduction to Rubber Technology*. Benin City: Josen Books.

[5] ASTM D 395 – 03(2008): Standard test method for rubber compression set.

[6] ASTM D 412- 06 Standard test method for tensile strength of rubbers.

[7] ASTM D 1509 –Standard test method for moisture content determination

[8] ASTM D 1512 – Standard test method for pH determination

[9] ASTM D1415 – 06 Standard test method for rubber hardness

[10] ASTM D1415 – 06 Standard test method for rubber hardness

[11] Egwakhide , P.H., Akporhonor, E.E., & Okiemien, F.E. (2007). Effect of coconut fibre filler on the cure characteristics, physical- mechanical and

swelling properties of natural rubber vulcanizate. *Internationa. Journal 0f phyical. Science* 2(2): 39.

[12] Egwakhide , P.H., Akporhonor, E.E., & Okiemien, F.E. (2008). The characterization of carbonized coconut fibre as fillers in natural rubber formulations. *Trend applied Sci. Res.* (3), 53-60

[13] Kline L.M., Douglas, G.H., Alum, R.W., & Nicole, L. (2010) .Simplifies determination of lignin content in hard and soft woods via UV-spectrophotometric analysis of biomass dissolved in ionic liquids. *Bioresources.com*

[14] Mohammad, K.H. (2012). Scanning Electron Microscopy Study of fibre Reinforced Polymeric Nanocomposite. *INTECH* , 732-740.

[15] Okiemien, F.E., & Imannah, J.E. (2005). Physico-mechanical and swelling properties of natural rubber filled with rubber seed shell carbon. *Journal of polymer materials*, 22 (4), 409.

[17]. Rajkumar, K. (2013). Modified Coconut pith – a novel Rubber Additive. *Indian Rubber Manufacturers Research Association* , 1-14.

[18]. South, J.T. (2001). Mechanical properties and durabilityof natural rubber. *Ph.D Thesis* , 34-60.

[19] Kumar, A., Anil and Gupta, k.r.(1998). Fundamentals of polymers. International edition. Mc Graw Hill, Singapore

[20]. Prabu, sathest C. and Murugensan A.G (2010). Effective utilization and management of coir industrial waste for the production of poly-ß-hydroxybutatyral using the bacterium Azobacter beijerincikii. International journal of environmental research, 4(3), 519-524.

[21] Sreenivasan, P., Bharma Iyer, K.R. and Krishna Iyer. (1998). Influence of delignification and alkali treatment on the fine structure of coir fibre. Journal of material science

EFFECT OF PARTIAL REPLACEMENT OF SAND WITH QUARRY DUST ON THE
COMPRESSIVE STRENGTH OF SANDCRETE BLOCKS

Bala A., Sadiku S. and Aguwa J. I.

Department of Civil Engineering, Federal University of Technology, Minna
E-mail:balhaji80@yahoo.com / 08065260435

ABSTRACT

This paper provides the results of an experimental investigation into the effect of partial replacement of sand with quarry dust in production of sandcrete blocks using mix ratio of 1:6. Physical properties of sand and quarry dust were determined in the laboratory in accordance with BS 1377-9 (1990). Blocks were produced using 0, 5, 10, 15, 20, 25, 30, 35, 40, 45, and 50% partial replacement of sand with quarry dust. Compressive strength tests were carried out on the blocks after curing for 7, 14, 21 and 28 days respectively. It was found that optimal compressive strength was achieved at 45% replacement of sand with quarry dust corresponding to a compressive strength of 2.6N/mm^2.

Keywords: *Optimum Compressive strength, Partial replacement, Quarry dust, and Sandcrete blocks.*

1.   INTRODUCTION

Sandcrete blocks are man-made composite materials consisting of measured proportions of cement (as hydraulic binder), sand and water, moulded into different sizes for walling and foundations Barry (1969). They are some times referred to as concrete blocks. Although usually larger in size than fired bricks, they are however stabilized by removing the centre cores to reduce the weight, thereby gaining sufficient strength setting and hardening to be used as walling units. The quality of blocks differs from one manufacturer to the other. This is due to high cost of cement, quantities and properties of aggregate used as well as method of proportion adopted.

They are of sizes and weights that can be handled easily by masons and placed in succession vertically and horizontally in the

wall. Blocks as load bearing walls perform the task of transferring part of the actual load from overlaying structural element to the foundation and must therefore conform to standard recommendation for compressive strength of blocks. The most popular building block sizes recommended in accordance with Nigeria Industrial Standard (NIS 87:2004) include the following; 450mm×225mm×113mm, and 450mm×225mm×150mm. Thus 450mm×225mm×150mm was used for this research work.

However, the popularity of sandcrete blocks and their extensive application as wall materials cannot be over emphasized. Sandcrete blocks when properly produced meet the recommendation of BS 2028, 1364 (1968) for density and compressive strength of structural masonry. Sandcrete block walls are not usually designed to support load other than their own weight. One of the earliest

warning sign of failure is often manifested by the formation of serious critical crack long before the actual failure (Dio and Morries, 2009).

A research work carried out by Abdullahi (2005) on the compressive strength of sandcrete blocks in some selected block industries in Minna revealed that the compressive strengths of their blocks fall bellow the standard. The study therefore suggested improvement on the selection of the materials and curing. In recent past good attention has been placed on the successful utilisation of various industrial by-products such as fly ash, silica fume, rice husk ash, foundry waste to save environmental pollution.

Quarry dust which is a by-product from crushing process during quarrying activities is one of those materials that have recently gained attention to be used as fine aggregates in the production of concrete (Sivakumar and Prakash, 2011). It is against this background that this study is aimed at finding the extent of partial replacement of sand with quarry dust to achieve maximum compressive strength in sandcrete blocks production. Some of the objectives are; to determine the index properties of sand and quarry dust, to produce sandcrete blocks with 0,5,10,15,20,25,30,35,40,45,and 50 % of quarry dust, to cure the blocks for 7, 14,21 and 28 days and to carry out compressive strength tests on the blocks.

2. METHODOLOGY

2.1 Materials

Cement;

The cement referred to in this work is the Ordinary Portland cement produced from Dangote group of company in accordance to NIS 87:2004 part 1. The cement was bought from Usmaniyya Nigeria Ltd cement depot located at Gbakungu Minna, Niger state Nigeria. The cement were kept on a raised platform and adequately protected from external damage by weather.

Sharp sand;

The sharp sand was obtained from a river bed at Gidan-mangoro, Minna, Nigeria. The sand was clean and sharp, free from clay, loam, dirt or organic matters and conforms to the grading requirement in zone 4 (BS EN 12620 : 2008).

Quarry dust;

The quarry dust was collected from Abubakar Umar Investment Ltd (quarry site) located along Anguwandaji by-pass Minna, Nigeria. The aggregate was clean and sharp, free from clay, loam, clay, loam, dirt or organic matters and conforms to the grading requirements in zone 2 (BS EN 12620 : 2008).

Water;

The water used was obtained from the borehole at convocation square Federal University of Technology Minna (Gidan kwano Campus) Nigeria. The physical examination of the water revealed that it was clean, free from deleterious materials and fit for drinking as recommended by BS EN 1008:2002

2.2 Production of block samples

Laboratory tests were carried out on both aggregate (sand and quarry dust) in accordance with BS 1377-9 (1990) Standard, to determine their respective physical properties, such as specific gravity, sieve analysis, bulk density and moisture content. Mix proportions were carried out and were strictly adhered to during the block production.

Two hundred and forty (240) 150mm ×225mm×450mm (6") sandcrete blocks were produced manually using the mix ratio of 1:6 (cement: sand/quarry dust) and cured for 7, 14, 21 and 28 days respectively. Twenty (20) numbers of blocks were produced at each replacement level.

2.3 Curing

The curing of the blocks was carried out using the spraying method. Spraying was done morning and evening for the period of five days. However, the weight of each block was taking with the aid of weighing balance to determine the dry density of each block before compressive strength test.

2.4 Compressive strength test

Compressive strength test on the block samples was determined using the standard procedure for pre-cast sandcrete blocks. Sixty (60) numbers of blocks were subjected to compressive strength test at each curing day. The weight of the block samples was always taken before the compressive strength was conducted. Five (5) blocks were tested at each replacement level for the period of 7, 14, 21 and 28 days after casting, using manual 150KN compressive strength testing machine in the Laboratory of Civil Engineering, Federal University of Technology, Minna, Nigeria.

2.5 Physical properties

The physical properties of both aggregate (sand and quarry dust) were determined in accordance with BS 1377-9 (1990). These include; Specific gravity, Compacted Bulk density, Uncompacted bulk density, moisture content and sieve analysis.

3. RESULTS AND DISCUSSIONS

3.1 Preliminary test for sand and quarry dust

The properties of sand and quarry dust used for the study are summarized in Table 1. While Figure 1 shows their particle size distribution curves.

Table 1: Physical Properties of Constituent Materials

Parameters	Sand	Quarry dust
Specific gravity	2.62	2.67
Compacted Bulk density	1618.30kg/m^3	1991.88 kg/m^3
Uncompacted bulk density	1467.30kg/m^3	1811.41kg/m^3
Moisture content	7.68%	0.4%
Coefficient of uniformity (C_u)	1.67	8.67
Finess modulus	4.28	6.01
Coefficient of concavity (C_c)	1.45	0.46
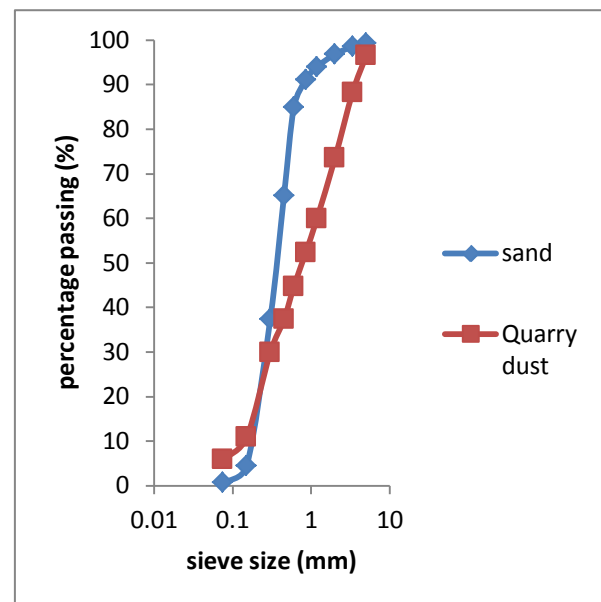
Figure 1: Result of sieve analysis of fine aggregates (sand and Quarry dust).

From the curve, it is clearly shown that the sand is uniformly graded and classified in zone 4 in accordance with BS EN 12620 (2008) classification for aggregate, while quarry dust is well graded, and was classified in zone 2 in accordance with BS EN 12620 (2008) classification for aggregate. The fineness moduli of sand and quarry dust are presented in Table 1. The higher the value of fineness modulus of aggregate, the coarser it is (Lambe and Robert, 2000). The fineness modulus of quarry dust is greater than that of sand which indicates that the quarry dust is coarser than the sand. Also their specific gravities are shown in that table respectively, these values obtained fall within the limit for natural aggregate with the value of specific gravity between 2.6 and 2.7 Neville (1995). The compacted and uncompacted bulk densities of sand and quarry dust are shown in Table 1. The density depends on how densely the aggregate are packed and it is influenced by the nature of compaction adopted in the mix. However, any aggregate with a particle density less than $200kg/m^3$ is defined as light weight aggregate. Thus the aggregates used for this research work are normal weight aggregate Clarke (1993).
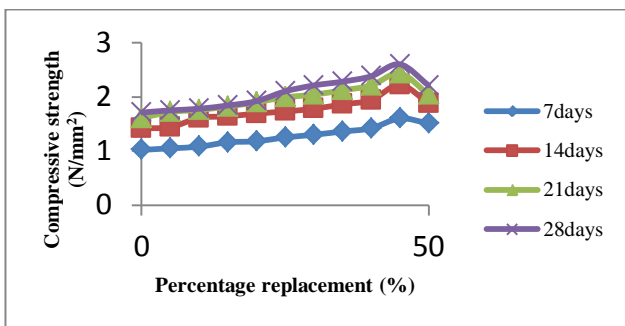
Figure 2: Relationship between compressive strength and percentage of quarry dust replacement for various days.

Figure 2 indicates that the compressive strength increased steadily as the quantity of quarry dust increased up to 45 % replacement where the highest compressive strength of 2.60 N/mm^2 was achieved, and later decreased beyond the 45 % replacement to the strength of 2.21 N/mm^2 at 50

% replacement. The Standards Organization of Nigeria recommends the minimum compressive strength of 1.8 N/mm^2 and 2.5 N/mm^2 for non-load bearing and load bearing hand compacted hollow blocks respectively. The strength of 2.60N/mm^2 obtained at 45 % is very consistent to the standard.

It was also noted that, the strength and density of the block increase along with the increase in quarry dust replacement and curing age. According to Hamza and Yusuf (2009) Curing is the process of preventing the lost of moisture from the blocks, while maintaining a satisfactory temperature required. Preferably, sandcrete blocks should be moist air cured for the first seven days. This is obvious because curing and protection produce very good blocks.

Thus the quarry dust improves the strengths of the blocks made with the sand in zone 4. The increase in strength in all cases can be attributed to better bonding achieved with the surrounding cement matrix which in turn is caused by the reaction of lime in the cement with the roughness and phase angle of the crushed granite surface. Crushed granite consists of either angular, rounded or irregular shaped individual pieces therefore a change in shape of quarry dust from one shape to another will improve the workability and strength considerably unless the mix proportion are changed.

Dio and Morris (2009) recommended the density of light weight blocks to be less than 1500 kg/m^3 and must be greater than 625 kg/m^3, while that of dense weight blocks to be greater 1500 kg/cm^3. Hence, the value obtained for this work as shown in Table 1. is within the required limit of dense weight blocks. It is obvious from Figure 3 that the dry density of the blocks increased along with

increase in curing age and the percentage quarry dust replacement.
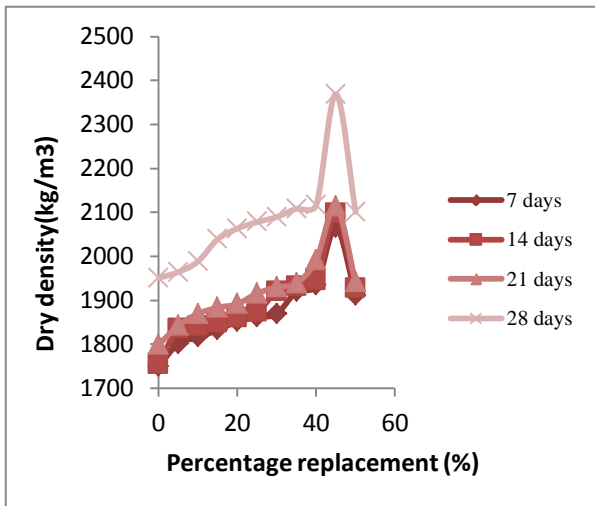
Figure 3: Relationship between Dry density and percentage of quarry dust replacement for various days.

4.   CONCLUSION

The compressive strength increased with the increase in quantity of quarry dust up to 45% and there after decreased. That means that replacement of sand with quarry dust beyond 45% of quarry dust is counter productive as the compressive strength started to decrease. Sand in zone 4 which is generally not good for production of sandcrete blocks can be improved by partial replacement with quarry dust.

REFERENCES

Abdullahi, M. (2005). Compressive Strength of Sandcrete Blocks in Bosso and Shiroro Area of Minna, Nigeria, AU J.T. 9(2): 126-132

BS 2028,1364 (1968) Recommendations for Density and Compressive Strength of Structural Masonry.

BS 12: (1996) Portland cement (Ordinary and Rapid – Hardening) British Standard Institute 2 Park Street, London.

BS EN 12620 (2008) Specification for aggregates from natural sources for concrete.

BS EN 1008 (2002) Mixing water for concrete specification for sampling, testing and assessing the suitability of water.

BS EN 12390 (2002) Testing concrete, Method for determination of compressive strength of concrete cube.

BS EN 12350-1 (2000) Testing fresh concrete

Barry, R. (1969). The Construction of Building 4th Edition, Volume 1, Construction and Materials.

Clarke, J.L. (1993). Structural Light weight Aggregate Concrete, Blackie Academic and Professional. Pp 25–26.

Dio A.W. and Morris E. E. (2009) physio-mechanical behaviour of sandcrete block masonry units. Journal of Building Appraisal vol.4,4,301-309 www.palgravel.journal.com/jba/.

Hamza, A.A. and Yusuf S. (2009). Determination of Compressive Strength of Six Inches hollow Sandcrete Block. A paper presented at 12th annual National Engineering Conference, College of Engineering, Kaduna Polytechnic, Kaduna. 1st to 3rd December, 2009.

Lambe & Robert V. W. (2000). Soil mechanics. Massachuetts Institute of Technology University of Sydeny. Page 29- 38.

Neville, M. (1995). Properties of Concrete. 4th and final Edition. Addison Wesley Longman Limited, England: 451pp.

Nigeria Industrial Standard, NIS 87:2004. Standard for Sandcrete Blocks. Standard Organization of Nigeria Lagos, Nigeria.

Sivakumar A. and Prakash M. (2011) Characteristic studies on the mechanical properties of quarry dust addition in conventional concrete. Journal of Civil Engineering and Construction Technology Vol. 2(10), pp. 218-235

Effects of Degradation on Turbine Entry Temperature (TET) and Combustion Chamber Pressure (CCP) in an Industrial Gas Turbine Performance.

Salihu A.Usman[1*,] A. Nasir[2], [4]H. T. Abdulkarim, S.N. Muhammed[3]

[1]Works and Maintenance Services, Federal University of Technology Minna
[2,3]Mechanical Engineering Department, Federal University of Technology Minna
[4]Department of Electrical/Electronic Technology, College of Education, Minna
[*]s.usman@futminna.edu.ng or imakaydee@gmail.com, 0803 791 5946.

ABSTRACT

Component degradation is a very common problem associated with operating industrial gas turbines. The major components so affected by this phenomenon are compressor, combustor and turbine blades. In some locations, compressor fouling is due to large amount of mixture of sand and oil in engine operating environment. Particularly, in the desert, the weather is highly sandy and dusty most times, therefore, this problem becomes even more obvious when gas turbines operate in the desert. The purpose of this research is to study the effect of degradation on gas turbine performance. The study involves the analysis of operating parameters for Siemens gas turbine engines model SGT 5 – 2000E coded GT11 and GT21 in the power stations. The parameters considered were ambient temperature, exhaust temperature, combustion chamber pressure and turbine entry temperature, GT 11 is degraded whileGT 21 is newly installed engine both in the same location at Geregu I and II power stations in Ajaokuta, Kogi State in the North central part of Nigeria. Simulations were carried out using Gas turb 11 simulation software, results of engine performance parameters were compared. A case study shows that due to component degradation, the TET increased to 1049.67^{o}C, the fuel flow increased by 8.49% and power falls by 7.14% consequently, the cost of power loss in the sum of one hundred and eighty seven million, one hundred and eleven thousand, seven hundred and fifty three naira ninety two kobo ₦187,111,753.92k only for the degraded gas turbine for a period of one year. The analytical approach has shown to be very useful and could be applied to similar gas turbine engines used in power generation station as well as other industrial application. However, the method used in this research work can be adopted by the maintenance Engineers to monitor the trend of components degradation in gas turbine engines for maintenance reliability.

---

1. INTRODUCTION

The history of the gas turbine can be traced as far back to 1791 when John Barbar conceived the ideas for gas and steam turbines. In 1903, a Norwegian, Aegidius Elling, built the first successful gas turbine using a rotary/dynamic compressor and turbines, and is credited with building the first gas turbine that produced excess power of about 8kW. Frank Whittle in England also patented a jet turbine similar to Elling's gas turbine in 1930. The engine consisted of a centrifugal compressor and an axial turbine and was subsequently tested in April 1937 according to (Tony, 2005;Razak, 2007).

Today, gas turbines are used widely in various industries to produce mechanical

470

power and are employed to drive various loads such as generators, pumps, process compressors, or a propeller. The performance and satisfactory operation of gas turbines are of paramount importance to the profitability of industries, varying from civil and military aviation to power generation, and also oil and gas exploration and production. However ,as a result of long operation period, all turbo machinery experiences losses in performance..

Degradation is a decline to a lower condition in performance, quality or level as a result of aging, operating and environmental conditions. The two classes of gas turbine degradation are:

(i)   Recoverable loss and

(ii)   Non-recoverable loss.

Compressor fouling is usually classified as recoverable losses and can be corrected by water washing or by mechanically washing the compressor blades and vanes after operation.

Non-recoverable losses are mainly due to increase in clearance of turbine, compressor and changes in surface finishing and airfoil contour, since this loss is as a result of reduction in components efficiencies. It is hardly recovered by means of external

maintenance or compressor cleaning and operation procedures, except by means of replacement of the effected parts at recommended inspection periods

1.2   Problem Statement

The economic effect of degradation in a gas turbine power can be severe. All gas turbines deteriorate in performance during operation, leading to reduced performance, capacity and thermal efficiency. Loss of capacity results in lost production, affecting revenue. Loss in thermal efficiency increases fuel consumption and therefore leads to higher fuel costs. Both these factors reduce profits. However, degradation in a gas turbine can only be minimized and cannot be eliminated completely.

1.3   Significance of the Study

 The causes, preventions and effects of degradation have been revealed in this research. It has also provided base line information on how to effectively monitor gas turbine components for degradation. However, following the available means of managing degradation provided by this study will improve the performance of gas turbine

2.0   Materials and Methods

The major materials used in this research work are the operating parameters generated from newly installed and old Siemen gas turbines (SGT 5 – 2000E) located at Geregu Ajaokuta

Local Govt.Area of Kogi State. The gas turbines were installed in 2005 and 2013 respectively. Degradation impact on the performance can only be notice after a long period of operation.

Simulation software called GasTurb 11 was also used to generate engine parameters using ISO and design conditions. This was done to provide bases for comparison.

This Siemens gas turbine is used mainly for power generation and designed to the capacities of 145mw and 160mw at base and peak loads respectively.

2.1 Field Stations

Geregu power stations I (GT 11) was in operation since 2005 and Geregu power stations II (GT 21) started operating in 2013 and are both located at Ajaokuta, Kogi state, North Central of Nigeria

2.2 Gas Turbine Performance Data

Performance data of the gas turbine units under investigation are ambient temperature, turbine entry temperature (TET), exhaust temperature (EXT), combustor chamber pressure in bars (CCP) and power output in mega watts (MW). Degraded physical components were also taken cognizance of.

2.3 Analysis

Data collected from Siemens gas turbine SGT5 – 2000E coded GT11 and GT21in the power stations (Degraded and Newly Installed) engines were analyzed by comparison

2.4 Gas Turbine Simulation

Gas Turb 11 was used to produce Design point simulation for the engine

3.0 RESULTS AND DISCUSSIONS

The data which have been collected cover the period from May to October, 2014.The variation of ambient temperature and load from day to day are shown in figs 3.1 and fig 3.2
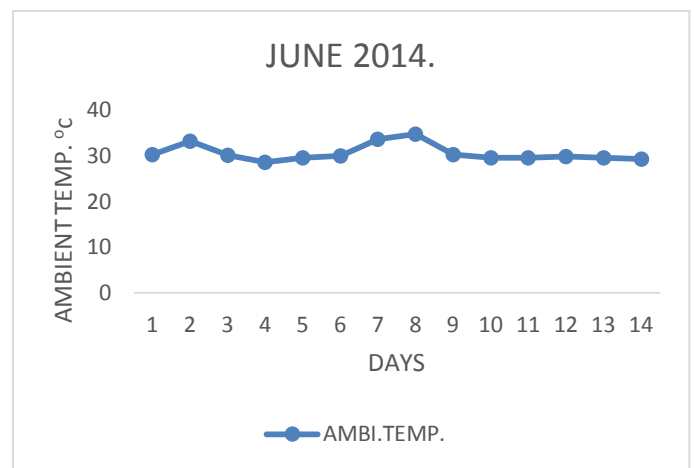
Figure 3.1: Variation of Ambient Temperatures
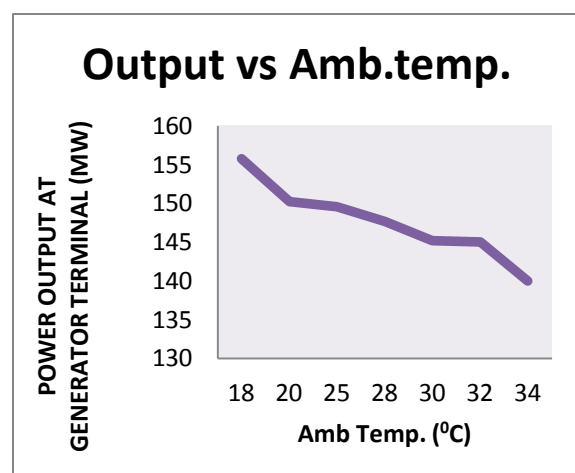
Figure 3.2: Effect of Ambient Temperature on Engine Power Output

Influence of Ambient Temperature on the Output

As can be seen in figure 3.2.The range of ambient temperature in Geregu power station varies typically between 29°C to 34°C in June. In gas turbines generally, temperature variation leads to change in the maximum engine power output as in figure 3.2, but as a result of component degradation on GT 11 and however, due to the changes in the ambient temperature it was difficult to achieve the base load requirement of 145MW, unless the parameters were varied that is, part/peak load. However, all the engine parameters such as CDP, CDT, Mass flow and TET change all the time as a result of changing ambient temperature.

Output power VS Days
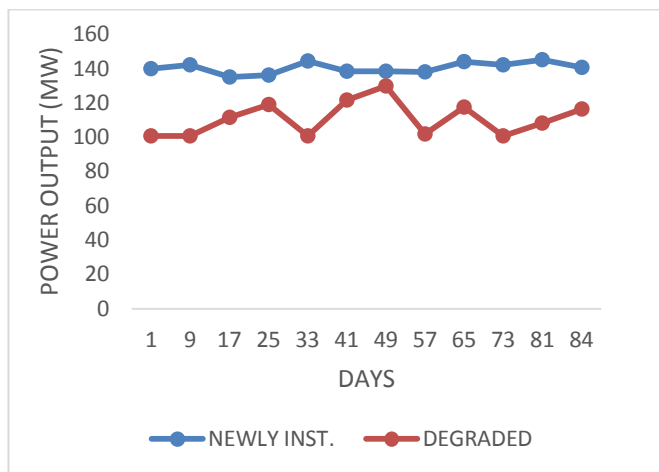
Figure 3.3: Power Variation over 80 days

The two engines were meant to operate on base load at an output of 145MW. From figure 3.3 above, it could be observed that as a result of component degradation, the degraded engine

(GT11) could not achieve the expected output at base load, while the newly installed engine (GT21) could even achieve above the expected Megawatts if the operating conditions are favourable.

3.1 Turbine Entry Temperature (TET) deviation Analysis

Applying the same method, the TET in K was plotted and compared
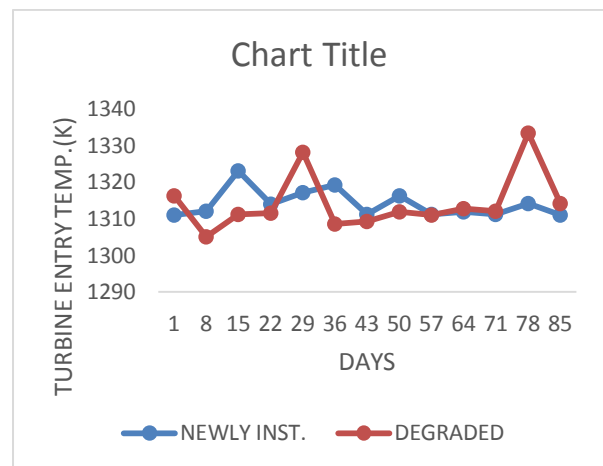
Figure 3.4: Turbine Entry Temperature Deviation Vs Days

From the figure 3.4 above, on 29th day of the study, the degraded engine shows a lower TET, with the progress of time especially at day 78; however, this deviation increases as a result of increase in TET of the degraded engine due to component degradation. Eventually, the degraded engine TET becomes higher than the newly installed engine TET.

The results, however, shows that the degraded engine TET at day 29 was 1328.2 K. The newly

473

installed engine TET was 1317.52 K and deviation between them was 10.68 K, also in the later days as per day 78, the degraded engine TET reached 1333.35 K and the newly installed engine TET reached 1311 K.

3.2 Economic Analysis and Outcome of Degradation

The power loss cost penalty will be calculated, in order to determine the effect of degradation on engine operating cost from the result above as follows:

i.   Simple cycle SGT 5 – 2000E (GT11 and GT21)
ii. Power output at 139.99MW.
iii. Assuming the engine on same load operation for 78 days or 1872 hours.
iv. Cost of electricity is N5/KW.h.
v.   Power loss 7.14% for same period.

3.3 In the first 1872 hours

Power loss = 0.0714 X 139.99 X 1872 = 18711.18MW.h. = 18711175.39KW.h.Cost of power loss = 18711175.39 X 5 = ₦93, 555,876.96k

4.0 Conclusion

In this research, effects of degradation on gas turbine performance have been studied.

The major components affected by degradation are compressors, combustor and turbine blades but the most common form of performance degradation is compressor fouling and this is as a result of ingestion of dirt and dust from the operation environment. Component degradation results in reduced compressor capacity, efficiency, turbine creep life and combustion chamber pressure drop due to high thermal stress.

From the findings of this study, the operating parameters especially, exhaust temperature and turbine entry temperature TET of GT11 increased to 555°C and 1049.67 ^{o}C as against 540 ^{o}C and 1038 ^{o}C of GT21 for a given output of 130.0MW and 139.99MW respectively. If GT11 engine is not overhauled, in a year the company stands to loose the sum of one hundred and eighty seven million, one hundred and eleven thousand, seven hundred and fifty three naira ninety two kobo(₦187, and 111,753.92k) only, to component degradation.

This research did not cover the studies of effects of degradation in aero – derivative engines and aero engine flying air craft.

REFERENCE

Tony,G.W. (2005). Gas Turbine Handbook: Principles and Practices, 3rdEdition,Fairmont Press, Inc, India pp 73-92.

Razak, A.M.Y. (2007). Industrial Gas Turbines: Performance and Operatability, 1st Edition, Woodhead Publishing Ltd, Cambidge Englandpp 25- 40.

Bacos M.P., Dorvaux J.M., Lavigne O., Mevrel R., Poulain M., Rio C. and Vidal-setif M.H(2011).Performance and degradation mechanisms of thermal barrier coatings for turbine blades.*Journal aerospace Lab AL03-03.*

Ezenwa A.O. (2011).Gas turbine performance optimization using compressor online water washing technique.*Scientific Research Journal Engineering,* 2011, 3,500-507.

Jonathan D. B. (2002). Analysis of the Sensitivity of Multistage axial compressor to Fouling at various stages, MSc. thesis in Mechanical Engineering submitted to the Naval Postgraduate School Monterey, California.

Environmental Impact Assessment of Gas Flaring Emission

(A Case Study of Eleme, River State)

Eyitayo A. Afolabi, U.G, Akpan, and A.H, Ameh
Department of Chemical Engineering, Federal University of Technology, Minna, Nigeria.
elizamos2001@yahoo.com; +2348072201514

ABSTRACT
The effect of gas flaring in Niger-Delta part of Nigeria, with Eleme as case study was investigated. The flared gas, resulted in contamination of nearby river water, atmosphere and the soil around the gas flared area. The results revealed that the nearby water might becomes unsafe for drinking as the pH of the water is as low as 5.96, which is considered to be lower than the WHO minimum allowable standard for drinking water (7- 8.5). The soil analysis also revealed that flared gas possibly increased the acidity of the soil from the pH of 6.1 to 5.5. These have led to the decision that flare gas influenced the river water, the soil, as well as the health conditions of the people, which may be responsible for poor yields of some fruit crops and poor health conditions of the people.

Keywords: *Emission, Gas flaring, Environment, Impact assessment*

1. INTRODUCTION

Nigeria has an approximated volume of one hundred and eighty billion cubic feet of natural gas, and this makes it the ninth greatest natural gas concentration in the world (Commery, 2002). Due to the unsustainable exploration routine and lack of gas utilization facilities, Nigeria flares seventy five percent of the natural gas associated with the crude oil and re-ejects just 12% to further improve oil recovery. Therefore, about two billion standard cubic feet of gas happens to be flared in Nigeria per annum and this amount to about 19% of the exact amount of gas flared around the world (Ashton et al; 1999). By the World Bank approximation, about 10% of the world carbon dioxide emission originates from flaring (Watts, 2001).

Gas flaring is a method used to dispose off the natural gases associated with the crude oil. The flared gas consist of numerous other gases such as hydrogen, sulphide, sulphur dioxide, nitrogen dioxide, carbon dioxide, water vapour and hydrogen gases (Argo, 2001; David, 1996). The release of the flared gas residue into the atmosphere has caused a lot of hazards characteristic of the petroleum industry. Hazards associated with gas flaring include

heavy noise, increase in temperature, emission of organic compounds and poisonous particulates that are dangerous to the ecosystem. The need to ascertain the effects of gas flaring are quite overwhelming due to the free-radicals and atoms that control the atmospheric chemistry, though present in low concentration. These pollutants react with gaseous substances in the atmosphere and disturb the ecosystem (Leahey and Preston, 2001; Kindzierski, 2000).

In recent times, gas flaring has become a major issues of concern to communities in Eleme local government area in particular and the Niger Delta in general (O'Rourke and Connolly, 2003; Okonta and Douglas,2001). The consequences of oil production need considerable attention in a bid to reconcile the environmental hazards caused by gas flaring and the developmental processes of these communities. Therefore, it is obvious to ascertain the effects of the flaring in terms of its operational cost and environmental impact assessment. This is important because the gas flared readily reacts with atmospheric substance and thereby have harmful effect on the environment (Ngofa, 2002; Ezzati and Kammen, 2002). Though much research has been carried out on the impact of gas flaring, there is the need for periodical evaluation to

ascertain the present level of gas flaring and effects on man and his environ. Therefore, the aim of this study is to evaluate the effects of gas flaring on the environment and people living in Eleme, River State. This aim is realizable through the collection and analysis of the soil, surface water and atmosphere samples, thereby determining the impact of gas flaring on the people and environment of Eleme. Gas flaring causes noise, elevation of temperature, odour, smoke and release of nitrogenous oxides, sulphur oxides, volatile organic compounds and suspended particulate matter not to mention CO_2, CH_4 and H_2O to the immediate surroundings (Strosher, 1996). Emission connected with carbon dioxide and unburned gases by flares give rise to greenhouse effect and a worldwide increased in temperature and acid deposition. The associated problems with gas flaring into the atmosphere are predominantly found in the Niger-Delta Communities. Amidst conflicting statements, field proof appears to assist the prevalent postulation that gas flaring has a strong connection with acidification and other harmful effects.

Acid deposition could be due to discharge of nitrogen, sulphur and carbon oxides into the atmosphere to form acids which can be deposited on roofing sheets, water, soil and other materials directly or through precipitation. Acid deposition may pollute lakes and stream which is unhealthy for the environment (Gerth and Labaton, 2004). Gas flaring is directly and indirectly linked to various diseases affecting the respiratory system. These diseases include cough, chest pain, dyspnea, noisy breathing/wheezing, asthma and these occur as a result of inhalation of the emitted gases. Moreover, nausea, vomiting, jaundice, diarrhea, flatulence are caused due to the ingestion of contaminated water or affected food crops grown in the affected area (Akanbami, 1999). He noted that although gas flaring alone is not the only emitter of

these gases, the truth is that they play a large contributory role.

2. METHODOLOGY

The experimental procedure for this study was carried out in Eleme Local Government Area in order to investigate the effect of gas flaring by Eleme Petrochemical Company and the Port-Harcourt Refinery, both situated in this area. Soil and water samples were taken at different sampling points for analysis. Questionnaires were designed and administered randomly among 50 different people and statistically analysed to determine the adverse effects of gas flaring on the health of people residing water, atmosphere and the soil in Eleme local government area of River state.

2.1. Sampling Points

Samples of water were collected from five different points for analysis. An area directly behind the Eleme flares at Abgonchia in Egi, area around the beginning of the river at Aleto, which is about 1½ km away from the petrochemical plant were used as the control areas. A point at Alode (the receiving river) 2 km downstream of Eleme was selected. At this point, the impact may or may not be adverse depending on the season. Another sampling point was Alesa, a point where the Port Harcourt Refinery is sited. It is expected that flaring around this area is intense. The last sampling point was about 3 km away from the Port-Harcourt Refinery along the river that flows from Alesa through Okpulu

The soil samples were collected from three stations before the point of flaring, at the point of flaring and after the point of flaring. Soil auger was used to collect soil samples from the top soil surface and bottom soil measured at 30 cm depth from the surface. The soil samples collected were air dried, then 1 g of the dried soil

put in a 100 ml beaker and 20 ml of 3:1 Nitric acid/Perchloric acid mixture added. The sample was heated with heating mantle until a clear digest was obtained. The mixture was allowed to cool, down to room temperature (30 ^oC) and distilled water was added and filtered. The filtrate was made up to 100 ml with distilled water in a 100 ml volumetric flask. The mixture is then analyzed for the presence of heavy metals in the soil around Eleme Local Government Area as a result of flaring activities in the area.

2.2. Water Samples Analysis

The water samples were analyzed in order to determine certain parameters such as temperature, conductivity, pH, total hardness, alkalinity and biochemical oxygen demand in accordance with the standard given by EIA (2003) and Strosher (1996),

2.3. Soil Samples Analysis

The soil samples were also analysed to determine pH, alkalinity, chloride and sulphate contents of the soil polluted. In addition, the presence of heavy metals such as Ni, Mn, Cu, Zn, Fe, Pb in the polluted water and soil

samples were also analyzed in accordance with the standard given by EIA (2003) and Strosher (1996),

3. RESULTS AND DISCUSSIONS

The analyses of water and soil samples in and around Eleme are presented in Tables 1 to 4. The effect of temperature is mostly reflected in increasing the rate of chemical reactions, reducing the solubility of gases, amplifications of taste and odour. Table 1 showed that temperatures of 30 ^oC, 30 ^oC, 31 ^oC, 30 ^oC and 31 ^oC for points 1, 2, 3, 4 and 5 respectively are higher than the standard range of 22-25 ^oC given by WHO (2011). Therefore, these water bodies can be concluded as polluted and need to be treated in order to reduce the temperature of these water bodies. The water samples at all the sample points as shown in Table 1 are acidic as the pH values obtained found to be below the WHO acceptable limit of pH range of 7 – 8.5. The acidic nature is possibly due to the dissolution of CO_2, SO_2, SO_3 and NO_2 effluent into the water bodies.

Table 1: Water Quality Analysis

Sample description	Temp (^oC)	pH	Conductivity ($\mu s/cm$)	DO (mg/l)	BOD (mg/l)	COD (mg/l)	Total hardness (mg/l)	Alkalinity (mg/l)	CO_2 (mg/l)	Ni (mg/l)	Cu (mg/l)	Zn (mg/l)	Fe (mg/l)	Pb (mg/l)
	22-25	7-8.5	≤ 1500		3.00		≤ 60			0.10	1.00	5.00	0.30	0.050
Point 1	30	5.96	1290	16.00	6.00	28.50	8.00	20.00	6.81	0.00	1.00	0.30	5.60	0.00
Point 2	30	5.03	350	12.00	9.00	33.00	10.00	5.50	5.90	0.10	0.80	0.21	6.30	0.00
Point 3	31	4.68	293	6.50	4.00	26.00	23.00	17.00	8.00	0.00	0.66	0.60	4.40	0.01
Point 4	30	6.40	867	6.00	4.00	42.30	18.00	12.00	10.95	0.00	0.79	0.52	5.36	0.01
Point 5	31	6.20	924	8.00	6.00	35.60	14.00	11.80	7.36	0.00	0.83	0.38	3.91	0.01

Table 2: Soil Analysis of Heavy Metals

Sample Description	Mn (mg/l)	Cu (mg/l)	Pb (mg/l)	Ni (mg/l)	Cr (mg/l)	Zn (mg/l)
Alesa Bottom Soil	5.60	2.80	2.00	1.60	3.10	2.40
Alesa Top Soil	4.10	1.70	1.26	2.20	1.90	1.70
Aleto Bottom Soil	1.20	1.30	1.70	0.90	2.60	3.00
Aleto Top Soil	1.00	1.30	1.85	3.70	2.90	3.30
Okpulu Bottom Soil	1.20	1.20	0.00	0.60	0.10	1.80
Okpulu Top Soil	1.10	1.40	0.00	0.10	0.10	1.30

Table 3: The Soil Analysis

	Before Flaring	After Flaring
pH of the Soil	6.1	5.5
Percentage of Organic Matter	82	60

Table 4: Effect on Human Health

	Percentage of People saying Yes	Percentage of People saying No
Cough	30	70
Chest Pain	20	80
Noisy Breathing	20	80
Poor visibility	30	70
Abnormal skin change	32	68
Eyes pain	24	76
Ear ache	20	80
Excessive sweating	38	62
Premature death	32	68
Smoking	22	78

The total hardness of water for the 5 sampling points is 8.00, 10.00, 23.00, 18.00 and 14.00 mg/L respectively. These values are found to be within the acceptable limit and can be classified as soft water due to small amounts of calcium and magnesium present in the water body.

Table 1 showed that the bicarbonate alkalinity is 20.00 mg/L and 17.00 mg/L at sample points 1 and 3 respectively. These values are observed to be rather higher on comparison with 5.50 mg/L, 12.00 mg/L and 11.80

mg/L for sampling points 2, 4 and 5 respectively. Therefore, the water at sampling points 1 and 3 will need treatment such as aeration and neutralization before being used for drinking purposes. The water analysis as showed in Table 1 gives the highest BOD value of 9.00 mg/L at sampling point 2; follow by 6.00 mg/L and 6.00 mg/L at points 1 and 5 respectively. Then after, a least value of 4.00 mg/L and 4.00 mg/L at sampling points 3 and 4 were obtained. However, a BOD value exceeding 3 mg/l affects coagulation and rapid sand-filtration processes thereby requiring expensive advance water treatment.

The soil analysis as shown in Table 3 showed that the pH of the soil before and after flaring was 6.1 and 5.5 respectively. Similarly, the percentage of organic matter before and after flaring was 82% and 60% respectively. This result showed that for high productivity, there is need for the soil to be re-aeration before it could be used for crop planting.

The flaring of natural gas yields substantial toxic gases due to chemical action of CO, CO_2, SO_4, NO and hydrocarbon gases such methane and fluoride compounds. Gas flaring directly and indirectly caused respiratory system diseases like cough, chest pain, noisy breathing and wheezing are as result of direct or indirect inhalation of the emitted gases. For example, the analysis of the results from questionnaire as shown in Table 4 revealed that 78% of the people interviewed do not smoke. but have respiratory related problems. This indicates that inhalation of pollutants from gas flaring operation is a major cause of sickness associated with the respiratory system

4. CONCLUSION

The environmental impact assessment of gas flaring emission on people living in Eleme and its environment

was investigated and the results are summarized as follows:

(1) That the average rise in the temperature of the area is due to emission and radiation into the atmosphere of both the combustible and non-combustible materials like soot.

(2) The physiochemical parameters such as the metallic components of the effluents degrade the soil and soil fertility due to the formation of soil crumb and scorched soil texture.

(3) The biochemical parameter analyzed from the effluent indicates a higher amount of deposit; this has resulted in higher pH and correspondingly higher dissolved oxygen (DO). Thus, the river water needs to be reactivated as the level of dissolve oxygen of 16.00 mg/l, 12.00 mg/l, 6.50 mg/l, 6.00 mg/l, and 8.00 mg/l is far above the acceptable level of 5 mg/l.

REFERENCE

Akinbami, J.F.K (1999); Implications of environmental degradation in Nigeria center for energy research and development, O.A.U Ile- Ife, Nigeria.

Akpan, U.G. (2000), Impact of gas flaring on the Niger Delta Area: A case study of Port Harcourt Metropolis, Journal of Applied Science and Education, 4:67-72

Argo, J.2001. Unhealthy effects of upstream oil and gas flaring, http://www.sierraclub.ca/national/oil-and-gas-exploration/soss-oil-and-gasflaring.pdf, accessed May 7, 2013

Ashton, N.J, Arnott, S and Douglas, O (1999); The human ecosystem of the Niger Delta –an ERA hand book. Environmental Right Action, Lagos. Pp: 224

Commery, P. 2002. Special report oil and gas: major projects in Africa. New African. September 2002.

David, S. (1996); Making the flare safe, Journal of lost prevention in process industries, Vol 9, Pp 363-381.

Energy Information Administration (2003), Country analysis briefs Nigeria retrieved July 5, 2012 from http://www.eia.doe.gov/emeu/cabs/nigeria.html.

Ezzati, M. and D.M. Kammen. 2002. Household energy, indoor air pollution, and health in developing countries: knowledge base for effective interventions. Annual Reviews Energy and Environment 27: 233-270..

Gerth, J. and L. Labaton. 2004. Shell withheld reserves data aid Nigeria. New York Times. March 19, 2004

Kindzierski, W.D. 2000. Importance of human environmental exporsure to hazardous air pollutants from gas flares. Environmental Reviews 8: 41-62

Leahey, D.M. and K. Preston. 2001. Theoretical and observational assessments of flare efficiencies. Journal of the Air & Waste Management Association. 51: 1610-1616.

Ngofa, A. N. (2002); The Effect of gas flaring in Niger Delta Area. (Chemical Engineering department, FUT, Minna (Unpublished B.Eng Project)

Okonta, I. and O. Douglas 2001. Where vultures feast : Shell, human rights, and oil in the Niger Delta. Sierra Club Books, San Francisco. 267 pp.

O'Rourke, D and S. Connolly 2003. Just oil? the distribution of environmental and social impacts of oil production and consumption. Reviews in Advance 28: 05.1- 05.31.

Strosher , M. (1996); Investigation of flare gas emissions in Alberta. Alberta research council, Alberta Canada.

Watts, M. 2001. Petro-violence: community, extraction, and political ecology of a mythic commodity. Pp. 189-212 In Violent environments. Watts, M. and Peluso,N. eds. Cornell University Press.

World Health Organization (2011), Guidelines for Drinking water-quality, fourth ed. http://www.who.int/water_sanitation_health/publications/201/dwq_guidelines/en/

ESTIMATION OF PARTICLE SIZE DISTRIBUTION IN CARBONIZED MUNICIPAL SOLID WASTE USING DYNAMIC LIGHT SCATTERING METHOD

Alhaji A. Yakatun[1], Olalekan D. Adeniyi[2*], Mary I. Adeniyi[2], Manase Auta[2], Aisha A. Faruk[2] and Mohammed Alhassan[2]

[1]*Chemical Engineering Department, Federal Polytechnic, PMB 55, Bida, Nigeria*
[2]*Chemical Engineering Department, Federal University of Technology, PMB 65, Minna, Nigeria*
Lekanadeniyi625@futminna.edu.ng [2*]

Abstract

The study on the estimation of particle size distribution in carbonized municipal solid waste (MSW) using dynamic light scattering (DLS) method was investigated for different solid wastes. The selected MSW are dried grass, waste paper, melon shell, saw dust and sugarcane bagasse. The analysis was conducted at room temperature of 25°C and 0.2μ/m filter unit was used in transferring the dispersed mixture into a plastic cuvette. The Z – average and poly disparity index (PDI) reveals homogeneity, which are 135.2 nm and 0.453 respectively. Carbonized MSW has potential application in carbon nanotubes industry as conductors of electricity, heat generation and fuel cells.

Key words: Estimation, Potential, Carbonized, MSW, PDI, PSD and DLS.

1. INTRODUCTION

Nanotechnology is finding applicability in the field of environmental protection and has great potential in improving air, water, and energy generation (USEPA, 2007). MSW provide a mean of generating nanoparticle carbon fuel which could be used in fuel cells and other technologies. These particle sizes are significant in the applications of these technologies. Engineered nanoparticles can efficiently reduce toxic metal emissions from combustion systems thereby improving air quality by suppressing metal vapor nucleation, promoting metal nanoparticle condensation and coagulation (Babayemi and Dauda, 2009). These applications are often determined by the properties of the nanomaterial, such as size,

surface properties, crystal structures and morphologies (Ujam and Eboh, 2012).

The efficacy and subsequent success of a processing product is strongly dependent on its shelf life and its stability under targeted desired conditions. A typical manifestation of formulation instability is an increase in particle size, due to aggregation of the analyzed or carrier. As the particle size increases, efficacy is diminished, primarily due to the decrease in the active surface area. The correlation between efficacy and size, particle sizing is quickly becoming a routine step in the development of more stable and effective formulations (Yakatun, 2015). On the other hand, the particle sizes could greatly enhance electrochemical

conversion in direct carbon fuel cell (Adeniyi *et al.*, 2014; Adeniyi and Ewan, 2012).

Accurate determination of nanomaterial size is crucial for developing nanoscale technologies, because size governs many of the physical and chemical properties of these materials. For instance, a good photo catalyst needs a large catalytic surface area and the primary size of catalyst nanoparticles defines the surface area available for adsorption and decomposition of organic pollutants (Sørum *et al.*, 2001). In the adsorption and reaction of sulfur dioxide on photocatalytic titanium dioxide nanoparticles, the inherent adsorption capacity of the smaller nanoparticles has been found to be larger because of the greater saturated surface coverage of sulfite adsorbed on the particles .The adverse effects of these materials on human health has prompted research globally to assess the toxicity of the nanomaterial in areas such as metals, metal oxides, fullerenes, and carbon nanotubes (CNT) (Abdulkareem *et al.*, 2007; Sørum *et al.*, 2001).

The excellent electrochemical properties, such as rapid electron kinetics, semi- and superconducting electron transport, high tensile strength composites, and hollow core suitable for storing guest molecules, have attracted attention as an electrode material for electrochemical sensors. The synergetic effects of CNTs and conducting polymer improves the electrical and mechanical properties of polymers in order to develop high performance sensor (Adeniyi et al., 2014; Afolabi et al., 2012).

Nanoscale changes the physical properties of particles, notably by increasing the ratio of surface area to volume, and the emergence of quantum effects. High surface area is a critical factor in the performance of catalysis and structures such as

electrodes, allowing Improvement in performance of such technologies as fuel cell and batteries. The large surface area also results in useful interactions between the materials in nanocomposites, leading to special properties such as increased strength and/or increased chemical/heat resistance. The fact that nanoparticles have dimensions below the critical wavelength of light renders them transparent, an effect exploited in packaging, cosmetics and coatings (Abdulkareem *et al.*, 2007).

2. METHODOLOGY

MSW was pyrolysed at 350°C to produce solid carbon. The size analyses of selected MSW carbon were carrying out at the Federal University of Technology, Minna. Dynamic light scattering (DLS) was used. The analysis was conducted at room temperature of 25°C. 1 mg of the sample was dispersed in 10 ml of distilled water to form a dispersion liquid. 0.2 µm filter unit was used in transferring the mixture into a plastic cuvette using a string. The cuvette was then placed in dynamic light scattering equipment for analysis.

3. RESULTS AND DISCUSSIONS

The result obtained are presented in Figures 1 to 5. Figure 1 shows particle size distribution (PSD) by percentage volume graph of carbonized dried grass

with the peaks. The z-average and poly disparity index (PDI) are 135.2 nm and 0.453 respectively. The PSD with size number of peak 1 (44.65 nm) and peak 2 (5386 nm) corresponds to percentage volume of 98.5 and 1.5, The duration used was 60 s. Carbon nanotube springs have the potential to indefinitely

Fig.1: PSD of carbonized dried grass.

store elastic potential energy at ten times the density of lithium-ion batteries with flexible charge and discharge rates and extremely high cycling durability (Adeniyi and Ewan, 2012; Abdulkareem *et al.*, 2007; Sørum *et al.*, 2001).

Figure 2 shows PSD by percentage volume graph of carbonized melon shell with one peak. The z-average and PDI are 400.6 and 0.411. The PSD with size number of peak 1 (300.3 nm) corresponds to percentage volume (100.0 %). The exceptional electrical and mechanical properties of carbon nanotubes have made them alternatives to the traditional electrical actuators for both microscopic and macroscopic applications. Carbon nanotubes are very good conductors of both electricity and heat, and they are also very strong and elastic molecules in certain directions (Adeniyi and Ewan, 2012; Abdulkareem *et al.*, 2007; Sørum *et al.*, 2001).

Fig.2: PSD of carbonized melon shell
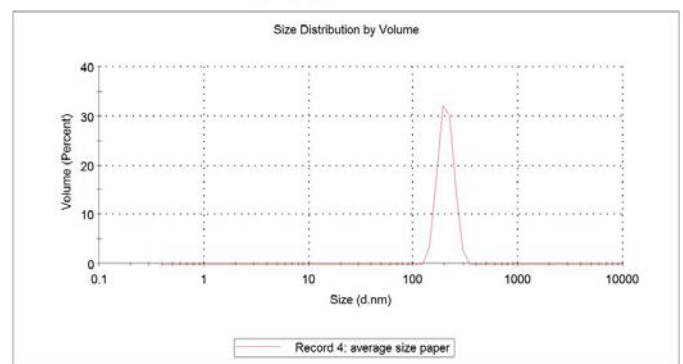
Fig.3: PSD of carbonized paper.
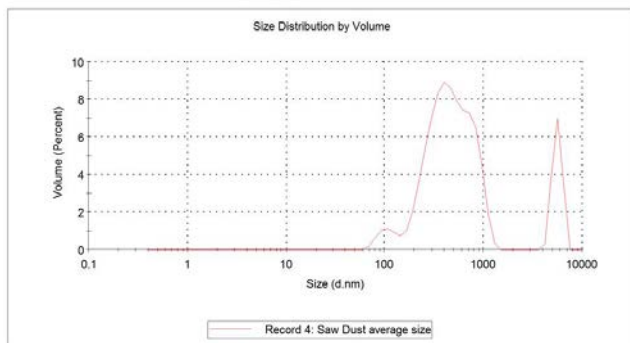
Fig.4: PSD of carbonized saw dust.
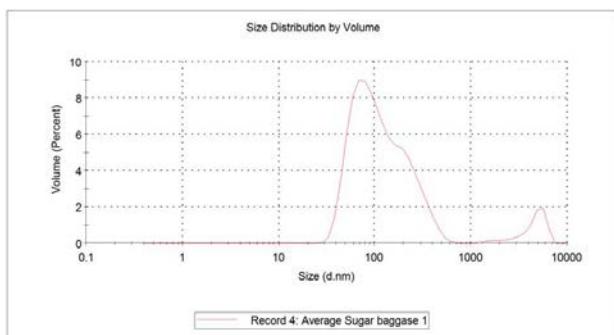
Fig.5: PSD of carbonized sugarcane bagasse.

Figure 3 shows the PSD of carbonized paper with one peak. The z-average and PDI are 1040 nm and 0.875. The PSD with size number of peak 1 (205.1 nm) corresponds to percentage volume (100.0 %). The duration used was 140 s. The carbon particle has potential applications in battery, direct carbon fuel cell, carbon assisted water electrolysis among others (Ewan and Adeniyi, 2013; Adeniyi and Ewan, 2012; Hackett *et al.*, 2007; Cherepy *et al.*, 2005; Hoogers, 2003).

Figure 4 shows the PSD of carbonized saw dust with three peaks. The z-average and PdI are 646.2 nm and 0.572. The PSD with size number of peak 1 (506.7 nm), peak 2 (106.3 nm) and peak 3 (5526 nm) which

corresponds to percentage volume of 80.9, 4.6 and 14.5. Large structures of carbon nanotubes can be used for thermal management of electronic circuits. An approximately 1 mm–thick carbon nanotube layer was used as a special material to fabricate coolers, this material has very low density, ~20 times lower weight than a similar copper structure, while the cooling properties are similar for the two materials (Abdulkareem *et al.*, 2007; Hoogers, 2003).

Figure 5 shows the PSD of carbonized sugarcane bagasse with three peaks. The z-average and PDI are 153.0 nm and 0.276. The PSD with size number of peak 1 (132.9 nm), peak 2 (1687 nm) and peak 3 (4691 nm) which corresponds to percentage volume of 92.4, 0.5 and 7.1. In addition to being able to store electrical energy, there has been some research in using carbon nanotubes to store hydrogen to be used as a fuel source. By taking advantage of the capillary effects of the small carbon nanotubes, it is possible to condense gases in high density inside single-walled nanotubes. This allows for gases, most notably hydrogen (H_2), to be stored at high densities without being condensed into a liquid. Potentially, this storage method could be used on vehicles in place of gas fuel tanks for a hydrogen-powered car (Cherepy *et al.*, 2005; Hackett *et al.*, 2007; Hoogers, 2003).

4. CONCLUSION

The carbon particle morphology show that the high surface area and porosity enhanced storage capability of fuel cell. The particle size results also indicates potential application in nanocarbon tube for energy conversion and storage. The carbon particle has

potential applications in battery, direct carbon fuel cell, carbon assisted water electrolysis. This would contribute in the abatement of environemtal degradation, renewable and susstainable energy generation for the future.

REFERENCES

Abdulkareem A. S., Afolabi .A.S., Iyuke S.E and Piennar C. H vZ (2007): Synthesis of carbon nanotubes by swirled floating catalyst chemical vapour deposition reactor. *Journal of Nanoscience and Nanotechnology*. American scientific publisher, 7 (9), 3233-3238.

Adeniyi O.D. and Ewan B.C.R. (2012), Electrochemical conversion of switchgrass and poplar in molten carbonate direct carbon fuel cell, *International Journal of Ambient Energy*, Taylor & Francis Group LLC, London, U.K, 33:4, 204-208.

Adeniyi O.D., Ewan, B.C.R., Adeniyi M.I. and Abdulkadir M. (2014) The behaviour of biomass char in two direct carbon fuel cell designs, *Journal of Energy Challenges & Mechanics (JECM), Aberdeen, Scotland, United Kingdom*, Vol.1, Iss. 4, article 6, pp.1-6.

Afolabi A.S, Abdulkareem A.S, Iyuke S.E and Pienaar H.C.vZ (2012): Performance and Kinetics of Pt-CNT catalyst electrodes in a PEM fuel cell. *Journal of material research*. 27 (11), 1497-1505.

Babayemi, J.O., & Dauda, K.T. (2009). Evaluation of Solid Waste Generation, Categories and Disposal Options in Developing Countries: A Case Study of Nigeria. J. Applied. Sciences Environment Management: 13 : 83 -88.

Cherepy, N.J., R. Krueger, K.J. Fiet, A.F. Jankowski and J.F. Cooper (2005), "Direct conversion of carbon fuels in a molten carbonate fuel cell*", J. Electrochemical Society,* 152(1) : A80-A87.

Ewan B.C.R. and Adeniyi O.D. (2013), A demonstration of carbon assisted water electrolysis, *Energies*, Basel, Switzerland, 6 (3): 1657-1668.

Hackett, G.A., J.W. Zondlo and R. Svensson (2007), "Evaluation of carbon materials for use in a direct carbon fuel cell", *J Power Sources,* 168:111-118.

Hoogers, G. 2003. Fuel Cell Technology Handbook. Florida,CRC Press LLC.

Sørum, L, Glarborg, P., Jensen, A., Skreiberg, Ø. and Dam-Johansen, K. (2001) "Formation of NO from Combustion of Volatiles from Municipal Solid Waste Components and Their Mixtures", Comb. & Flame : 123:195-212.

Ujam, A. J. and Eboh, F. (2012), Thermal analysis of a small-scale municipal solid waste-fired steam generator: Case study of Enugu state, Nigeria. *Journal of Energy Technologies and policy*. 2 (5) : 38-54.

Yakatun A.A. (2015), Evaluation of municipal solid waste for potential energy production, a case study of Bida metropolis, M.Eng. Thesis, Federal University of Technology, Minna, Nigeria

Load Pull Assessment of WIN PP10 PHEMT Transistor

M. T. Kabir[1], A. S. Yaro[2], A. S. Abubakar[3], B. O. Sadik[3]

[123]Department of Electrical and Computer Engineering, Ahmadu Bello University, Zaria, Nigeria.

mtkabir@abu.edu.ng08136449743

ABSTRACT

Load pull is a measurement technique employed in the design of power amplifiers to determine the optimum load impedance that would ensure the highest efficiency of the amplifier. In this paper, load pull measurement technique was used to determine the optimum impedance of the PHEMT devices from the WIN PP10 foundry process at 25GHz of frequency. This involved running simulations to assess the performance of the transistor devices. The load pull measurement will allow for the impedances to be realized for efficient amplification in class A and AB modes of operation. Furthermore, this paper provides discussion and analysis of the simulated load pull data in terms of the gain, output power and power added efficiency. The simulation was done for a 4x25um device.

Keywords: *Load pull, transistor, PHEMTs, impedance.*

1. INTRODUCTION

The need for high performance power amplifiers in terms of efficiency, output power and gain in the communication industry has increased due high demand and growth. Load pull measurement is one of the techniques and processes used in the design of PAs to meet this high demand. Load pull helps to provide the required load impedance that will yield the optimum performance out of a transistor device. This measurement technique provides very fast, accurate and efficient way to determine the device's performance and characteristics. Also, load pull data enables the development of nonlinear transistor models for various applications (Ebrahimi et al, 2011) (Qi et al, 2006) (Ghannouchi and Hashmi, 2011). Therefore, load pull plays a very important role in the design of high performance power amplifiers.

The term Load-pull is used to describe the process of varying the load impedance of a device under test so as to assess and measure the performance of the device. Load-pull systems help to measure the optimal performance of a device given the biasing conditions and frequency, which helps to set-up the conditions to achieve the best impedances that would bring out the best performance from the device under test. There are different reasons why Load-pull based measurement is used to assess the optimal performance of a device under test. For example for passive elements (linear) s-parameter measurement is enough to analyze the performance of the device. But for active elements like transistors, because they are considered non-linear so they exhibit non-linear characteristic (produce unwanted spectral components and Harmonics), S-parameters cannot be used. Therefore, Load-pull is used in this case to determine and measure the appropriate terminations to the input and output impedances of the device under test to avoid exhibition of these non-linear characteristics. Hence, help in optimizing the performance of the device in terms of the output power, gain and efficiency (Ghannouchi and Hashmi, 2013). Load-pull measurement does not only provide the appropriate terminations of the DUT but also plays an important role in the design of power amplifiers. It enables quick and accurate determination of the optimum parameters for the performance of the PA and also helps in testing the linearity of the PA under different loading conditions (Noori et al, 2006). Therefore, load pull is a technique that helps to analyze a DUT to get the appropriate impedance for optimum performance, which then leads to the design of matching networks (Ghannouchi and Hashmi, 2011). There are different types

of load-pull systems but the two commonly used ones are the passive and active load-pull systems.

The passive Load-pull systems make use of passive tuners, which are used to tune and vary the impedances of the DUT. The tuners are used together with other equipment like the power meters, signal generators, vector network analyzer, bias tees that make up the complete load pull measurement set-up.

a)   Basic passive load   b)   Active   load
      pull system set-up   pull set-up
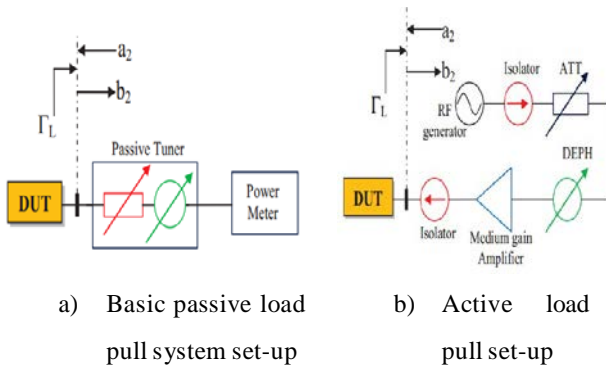
Fig.1 (Ghannouchi and Hashmi, 2011): Types of load pull systems

The Active Load-pull systems do not make use of passive tuners, they produce the desired impedance by injecting a signal directly at the DUT ports (Ghannouchi and Hashmi, 2011). This help to solve the problem of losses introduced by the passive tuners in the passive systems. In this project, passive load-pull systems are going to be used to measure and assess the WIN PP10 devices up to 25GHz of frequency. The passive load pull was used here because of a number of advantages it has over the active system: it can handle high power with no non-linear effects, it is easier to set up than the active system and also cost less to set up and maintain.

2.   SCATTERING PARAMETERS AND STABILITY

Stability is a very important characteristic that must be considered carefully when using or designing circuits with transistor devices for example in amplifier design. When the transistor is not stable oscillation will occur that leads

to large voltages and power levels to be generated in the circuit. The scattering parameters are parameters that are used to help analyze and check the stability of a transistor. The S-parameters of a device are complex numbers that are used determine its stability. They depend on the frequency of operation and the input and output impedance of the device. It will be easier to demonstrate the s-parameter using a simple diagram (Robertson and Lucyszyn, 2001).
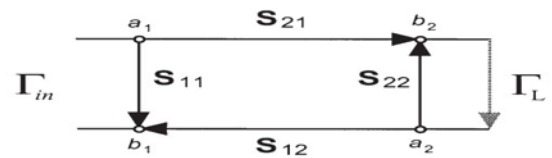
Fig.2 (Robertson and Lucyszyn, 2001): A simple flow graph showing a device with output load

Where, S11 is the input reflection coefficient.

S12 is the reverse transmission gain

S21 is the forward transmission gain

S22 is the output reflection coefficient

From the diagram we can spot that the direction of the reverse transmission gain, S12 shows that the input impedance is dependent on the load reflection coefficient. And also the same applies to the output reflection coefficient and S21. This shows how the s-parameters can be used to find out and analyse the transistors characteristics.

To find the stability of a device that is if the device is stable or not, first the Rollett Stability factor k and the stability measure b need to be examined. These process is a called the k-b stability test. The test is done by using the s-parameters to calculate the values of k and b. if the k-value calculated is greater than one then the device is unconditionally stable and if the b-value is greater than zero then also the device is unconditionally stable. But for the contrary the device is conditionally unstable for the set of s-parameters (Zhirun, 2013).

$$K=(1-|S11|-|S22|+|\Delta|)/2|S12\ S21| >1 \qquad (1.1)$$
$$B= [\![1+|S11|]\!]\ ^2-|S22|^2-|\Delta|^2>0 \qquad (1.2)$$

Where $\Delta=S11*S22-S12*S21$

When a device is conditionally unstable it means that at some frequencies the device is stable but not at some frequencies. To find these frequencies regions where the device is potentially unstable stable, the input and output reflection coefficients are used to draw stability circles. These circles represent the boundary between the stable and unstable regions on the smith chart (Robertson and Lucyszyn, 2001). The input and out reflection coefficients are calculated from the formulas below derived from Fig.2.

$$\Gamma\_in=S11+(S12*S21*\Gamma\_L)/(1-S22*\Gamma\_L) \qquad (1.3)$$
$$\Gamma\_out=S22+(S12*S21*\Gamma\_s)/(1-S11*\Gamma\_s) \qquad (1.4)$$

For the output stability regions, if $|S11|>1$ the region intersecting the smith chart and the stability circle is the stable region and if the $|S11|<1$, the region that has the origin of the smith chart is the stable region. And for the input stability regions, if $|S22|>1$ the region between the smith chart and the stability circle is the stable region and if the $|S22|<1$, the region that has the origin of the smith chart is the stable region (Zhirun, 2013).

3. FIELD EFFECT TRANSISTORS (FET)

A Field effect transistor is a type of transistor device that operates by the effect of an electric field to control the current on the flow of electrons through a semiconductor material. The FET is made up of three channels and current flows through these channels. The channels are: the source channel, gate channel and the drain channel. The source channel is where the current enters the channel and the drain channel is where the leave the channel. The gate channel generates the electric field that in turn controls the drain current. There are different types of FETs based on the way the electric field is generated. The way the field is generated affects the electron flow and hence changes the size and width of the conducting channel.

In this paper, the transistor device used from the WIN PP10 foundry process is a type of HEMT (high-electron mobility transistor) device called the pHEMT (pseudomorphic HEMT). A HEMT device is made up of two materials usually Gallium Arsenide GaAs and Aluminum Gallium Arsenide AlGaAs. The structure is made up of a layer of a large band gap of a doped semiconductor material AlGaAs on a layer of an undoped semiconductor material GaAs. This enables the transfer of electrons from the material with higher conduction band energy to the material with lower conduction band energy. An interface occurs between the two semiconductor materials this is known as a Heterojunction. Near this junction a two-dimensional electron gas (2DEG) is formed. This means that the undoped channel provides a two-dimensional channel for the carriers transferred from the doped channel. This makes it possible for the channel to separate the electrons from their donors so as to reduce scattering and hence provide high mobility of the conducting electrons (Jianjun, 2010) (Brech, 2013).

The pHEMT is a type of HEMT device with an additional layer of Indium Gallium Arsenide InGaAs. This layer is used as the electron gas channel material to help increase the performance of the device. The more InGaAs introduced the more the electron drift velocity in the channel and enhances the electron mobility in the 2DEG layer (Jianjun, 2010).
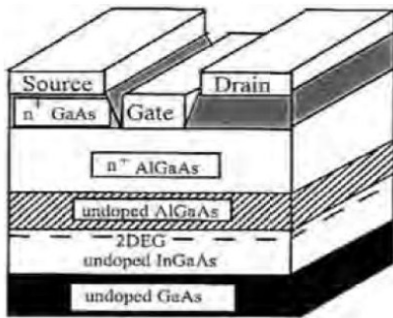
Fig.3 (Brech, 2013): PHEMT device structure

4. LOAD PULL SIMULATION AND ANALYSIS

The simulation was done for operation in class A mode of operation. The bias point for this mode of operation was determined. Using this bias point the s-parameters were generated to determine the stability circles of the transistor.

Table 1: The S-parameters

freq	S(1,1)	S(1,2)	S(2,1)	S(2,2)
0.0000 Hz	1.000 / 0.000	5.867E-5 / 0....	6.282 / -180.0...	0.766 / 0.000
5.000 GHz	0.980 / -24.024	0.038 / 72.687	5.771 / 159.1...	0.765 / -22.117
10.00 GHz	0.933 / -45.940	0.069 / 57.246	5.269 / 139.9...	0.736 / -42.061
15.00 GHz	0.879 / -64.717	0.091 / 44.289	4.655 / 123.3...	0.705 / -58.775
20.00 GHz	0.832 / -80.350	0.106 / 33.723	4.063 / 109.1...	0.680 / -72.282
25.00 GHz	0.795 / -93.303	0.115 / 25.096	3.546 / 96.918	0.664 / -83.093
30.00 GHz	0.770 / -104.1...	0.121 / 17.948	3.111 / 86.196	0.655 / -91.798

From the s-parameters, the complex impedance (smZ1) value that must be presented to the transistor input port (gate) required for conjugate matching and the corresponding maximum gain that the transistor can have at this impedance were calculated for 25GHz of frequency.

Table 2: Smz1 and maximum gain

freq	SmZ1	SmZ2	MaxGain1
0.0000 Hz	2.525E5 + j0.000	80.084 + j0.000	48.427
5.000 GHz	40.897 + j202.784	16.825 + j65.161	20.549
10.00 GHz	124.290 + j100.420	48.254 + j43.944	12.907
15.00 GHz	134.158 + j65.866	47.623 + j40.096	9.241
20.00 GHz	137.442 + j48.263	43.609 + j39.234	6.709
25.00 GHz	138.933 + j37.437	38.849 + j38.698	4.772
30.00 GHz	139.733 + j30.000	34.194 + j37.881	3.204

Note: The reason why smZ1 is calculated only for the input and not for the output is because at the input conjugate match is needed to produce maximum gain from

the transistor. And at the output power match is needed to deliver the maximum power.

Fig.4(a) shows on the right the swept reflection coefficient contours with the radius of 1 and the centre at the middle of the smith chart. The marker points at the load impedance that gives the maximum power added efficiency (PAE) with the corresponding power delivered 13.715 dBm and the gain 3.715 at that point. The PAE at this load impedance 37.715+j26.503 is 18.287%, which is very reasonable for a class A amplifier that ideally has an efficiency of 50%.

The corresponding source impedance for this load is shown in figure 4(b). The marker shows the source impedance point that gives the maximum PAE of 19.559%. Obviously, the PAE for the source pull should be slightly greater than the PAE at the output due to some losses in the circuit. The same for the gain and power delivered to the load.
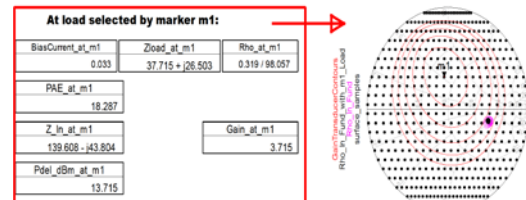
Fig.4(a): The load pull simulation results
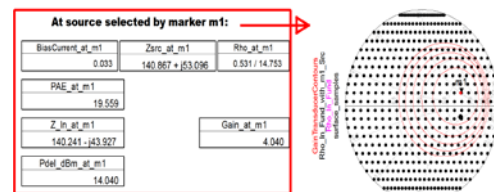
Fig.4(b): The source pull simulation results

Figure 5(a) shows the load pull simulation set up comprising of the matching circuit with the optimum load and source impedance.
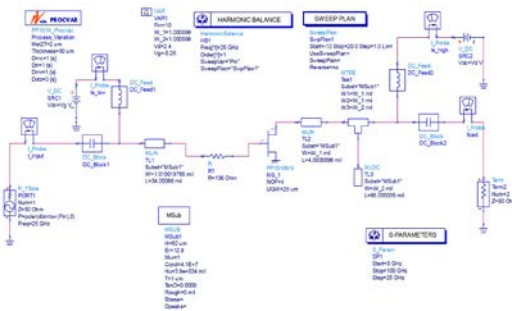
Fig.5(a): the complete circuit for Class A operation
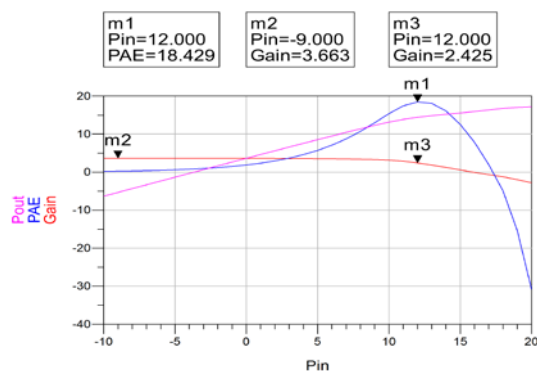
Fig.5(b): the plot of the PAE, gain and output power against the input power

Figure 5(b) shows at marker1 the maximum PAE that was achieved for class A mode of operation which is 18.429% at an input power of 12dBm. This result agrees with that found in the source and load pull simulation. At marker2, the maximum gain of 3.663 was achieved. And marker3 shows the 1dB compression point to be at 12dBm of input power and the output power at this point is 15dBm. This is the point where the gain of the device fall by 1dB and the output power is no longer proportional to the input power (nonlinear). Beyond this point the transistor is in its saturation region. As we can see the maximum PAE was achieved at this point and then starts falling after the point. The results show that the performance of the PP1010 transistor is very good and efficient for class A mode operation.

The same simulation was conducted for the transistor but for class AB mode of operation. Figure 6 shows the plot of the PAE, power output and gain against the swept power input. From the figure, marker 1 shows the point of

maximum PAE, which is about 41%. In ideal case the efficiency of a class AB amplifier is around 65%, therefore this result is practically reasonable for simulation. Marker 2 shows the point where the maximum gain of 7.341 is achieved which is at 7dBm of input power. And marker 3 shows the 1dB compression point of the transistor at the Class AB operating point. The output power at this point is about 16.7dBm. These results compared with the results for the Class A operating point show why the class AB is better than the class A amplifier. The classes AB amplifier also has better efficiency and gain than the class A amplifier.
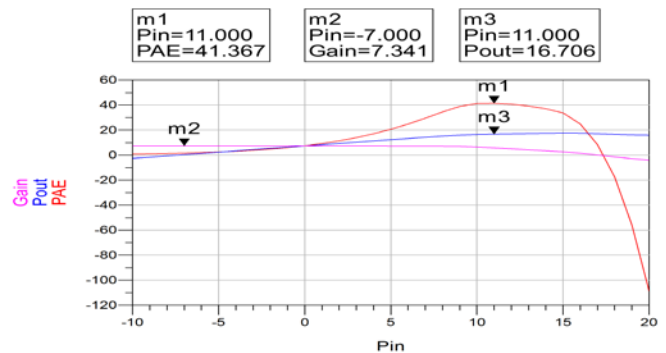
Fig.6: plot of the PAE, gain and output power against the input power

5. CONCLUSION

In this paper, the load pull assessment of the WIN PP10 transistor was performed to find its optimum source and load impedances for operation in both class A and AB mode of operation at 25GHz of frequency. It was clearly shown that in the class AB mode of operation the transistor performed better than in class A mode. The analysis was done in terms of the PAE, the gain and the output power.

6. REFERENCES

Brech H. "The principle of HEMT" available from www.iue.tuwien.ac.at/phd/brech/ch_2.htm, 1998. [accessed on 29th April 2013]

Ebrahimi M. M., M. Helaoui, and F. M. Ghannouchi, "Analytical Approach to Optimize the Efficiency of Switching Mode Pas Loaded with Semi-Distributed Matching Networks," IET Microwaves, Antenna and Propagation, Vol. 5, Issue 1, p. 57, Jan. 2011.

Ghannouchi F., S. M. Hashmi, ''Load-Pull Techniques and their Applications in Power Amplifiers Design'' 2011.

Ghannochi F., S. M. Hashmi, "Load pull techniques with application to power amplifiers" p29 – 38, Springer, 2013.

Jianjun G., "RF and microwave modeling and measurement techniques for compound field effect transistors" p132-133, Scitech publishing Inc, 2010.

Noori B., P. Hart, J. Wood, P.H. Aaen, M. Guyonnet, M. Lefevre, J.A. Pla, J. Jones, Load-pull measurements using modulated signals, in 36th European Microwave Conference, Manchester, UK (Sept. 2006), pp. 1594–1597

Qi H., J. Benedikt, and P. J. Tasker, "A novel approach for effective import of nonlinear device characteristics into CAD for large signal power amplifier design," in Proc. IEEE MTT-S IMS Dig., San Francisco, CA, June 2006, pp. 477–480.

Robertson I. D (Ian D.) and S Lucyszyn (Stepan) "RFIC and MMIC design and technology" Institution of Electrical Engineers. London: Institution of Electrical Engineers 2nd edition, 2001.

Zhirun H., "RF/Microwave circuit design" School of Electrical and Electronic Engineering, University of Manchester, 2013.

Modification of Clay Using A-3 Soil

Alhaji Mohammed Mustapha
Department of Civil Engineering, Federal University of Technology, Minna
[2,]**a.mustapha@futminna.edu.ng**   **(08036133082)**

ABSTRACT

Clay soil classified as A-7-6 according to AASHTO soil classification system and CH according to unified soil classification system was collected from Niger State Polytechnic Zungeru in Niger State. The clay was modified with A-3 soil sieved out from river sand. The clay was replaced with A-3 soil at 0, 10, 20, 30 to 100% by weight of the clay soil. Grain size analysis tests and Atterberg limit tests were carried out on each of the clay-A-3 soil mixtures to evaluate the effect of A-3 soil on the clay soil. Results showed that the liquid limit of the clay reduced from 59.3% at 0% A-3 soil replacement to 23.4% at 80% A-3 soil replacement. The plasticity index reduced from 32.5% at 0% A-3 soil replacement to 6.6% at 60% A-3 soil replacement. These represent 60% reduction in liquid limit and 80% reduction in plasticity index. A-3 soil is therefore an appropriate material for modification of clayey soils and 60% A-3 soil replacement is the maximum required for effective modification of clay soils.

Keywords:modification, A-3 soil, flocculation, Aggregation.

1. INTRODUCTION

It is common in geotechnical practice to encounter lateritic soils which satisfies all requirements for use as sub-base course, or even base course for low trafficked roads according to Nigerian General Specification for Roads and Bridge Works (1992) but is deficient in Atterberg limits of its fines. This is attributed to the nature of the clay present in such type of laterite. Soils that fall under this group may be highly plastic. Placement of these materials during road construction is usually difficult as the plastic clay keep sticking to the rolling drum of the compactor. Sections that are successfully compacted, loose strength drastically with ingress of water due to softening of the clay soil which can result in to instant failure of the road structure. Also, the criteria placed by the Highway Research Board of America (1943) for highly plastic clay soils to be economically stabilized, include that, less than 50% passing sieve 0.075mm, less than 40% liquid limit and less than 18% plasticity index. Soils with index properties above these limits would be modify to reduce these values. Modification of clay will reduce its Atterberg limits and hence put the lateritic soil in an AASHTO classification group that will make it suitable for use as sub-base course or even base course material.

A-3 soils subgroup in AASHTO soil classification system is placed in a lone column without subdivisions like A-1 and A-2. A-3 soils are uniformly fine and non plastic sand which make its use in any component of road structure to be very minimal and almost completely neglected in AASHTO soil classification scheme. It is therefore pertinent to put this class of soil in to any possible engineering use.

Soil modification is the improvement of the physical properties of the soil in order to increase its workability. Materials commonly used for modification are cement, lime and some other pozzolanic admixtures like fly ashes, rice husk ashes, sugarcane Bagasse ashes, e.t.c. According to Ola (1983), modification by these chemicals is caused by flocculation and aggregation of the clay particles which reduces its double layer. This is based on the physico-chemical reaction which reduces the repulsive forces and increases the effective grain size due to agglomeration of the clay particles. The agglomeration will eventually turn clay particles to silt sized particles which cause reduction in the liquid limit. The author studied a lateritic clay soil and observed increase in liquid limit from 36% at 0% lime to 42% at 10% lime while the plastic limit was observed to increase from 18% at 0% lime to 41% at 10% lime. The cumulative effect of these two is the reduction in plasticity index from 18% at 0% lime to 1% at 10% lime. These trend was observed by Osinubi and Gadzama (2008), Osinubi and Katte (1999). Ola (1983b) studied lime stabilization of some Nigerian black cotton soils where lime content of 0, 2, 4 to 10% was used. Findings revealed continue reduction in liquid limit, continues increase in plastic limit and continues decrease in plasticity index. Osinubi and Alhassan (2008) worked on the lime modification of clay using Bagasse ash as pozollana. The researcher used 0, 1, 2 – 4% lime each admixed with 0, 1, 2 – 8% Bagasse ash by dry weight of the soil. The result shows particle size distribution curve shifting from region of fine grained soil to the region of course grained soil as percentage lime and Bagasse ash increases. There was continuous decrease in liquid limit and increase in plastic limit with increase in lime and Bagasse ash. These trends combined to cause reduction in plasticity index with increase in lime and Bagasse ash. Bagasse ash was used to modify shika lateritic clay soil Osinubi and Gadzama (2008). The Bagasse ash was used at 0, 2% - 10% by weight of the clay soil. Results showed increase in liquid limit and plastic limit and subsequently decreases in

plasticity index as Bagasse ash content is increased. However, all these materials used for modification are either expensive or very difficult to source in large quantity hence the requirement to look for cheaper and easy-to-source material for modification of clay soils.

Goodarzi and Salimi (2015) treated dispersive clayey soil with granulated blast furnace slag (GBFS) and basic oxygen furnace slag (BOFS). The slags were added from 2.5 to 30% by weight of the dispersive clay. The index properties result showed continuous reduction in plasticity index from 350.5% to 200% for treatment with GBFS and to 100% for treatment with BOFS. Muazu (2006) studied the effect of sand on the Atterberg limits of four different lateritic soils. The author used 0%, 2%, 4% - 8% sand by weight of lateritic soil. The results revealed continuous reduction in liquid limit, plastic limit and plasticity index as the sand increases up to 8% sand. The researcher did not reduce the sand to predominantly silty sand and cannot evaluate the Atterberg limits beyond 8% sand. Joel and Agbede (2008) studied the possibility of using Igumale sand and lime to stabilize Igumale shale. The author used 0%, 10%, 20% to 50% sand each admixed with 0%, 2%, 4% to 14% lime by weight of dry Igumale shale. Results at 0% lime showed reduction in plasticity index from 45% at 0% sand to 30% at 50% sand. This research does not consider the soil properties beyond 50% sand.

This work is therefore intended towards replacing clay with A-3 soil from 0% to 100% to modify the clay soil.

2. METARIALS AND METHODOLOGY

2.1. *Materials*

The materials used for this study are clay soil collected from Niger State Polytechnic, Zungeru, Niger State. The A-3 soil used for the study was obtained from River Chanchaga in Minna, Niger State. The A-3 soil was collected by sieving the river sand through sieve 0.425mm.

2.2. *Methodology*

The clay soil was properly dried and pulverised before it is being put in to use. The A-3 soil was used to replace the clay soil at 0%, 10%, 20% to 100% by weight of the dried clay soil. Index properties test was conducted on the natural clay soil and silt soils according to the methods highlighted in BS 1377 (1990) while same was done on each of the mixed samples according to the methods highlighted in BS 1924 (1990). Variation in Atterberg limits with percentage A-3 soil replacement were calculated and plotted. The variation in percentage liquid limit and percentage plasticity index with percentage silt replacement was also calculated and plotted.

3. RESULTS AND DISCUSSIONS

3.1. *Grain size analysis*

The result of the grain size analysis is shown in figure 1. The result showed curves moving from well graded nature at 0% A-3 soil replacement to highly uniformly graded nature at 100% A-3 soil replacement. This is because of the uniformly graded A-3 soil used for replacement of well graded clay soil as shown in figure 1.
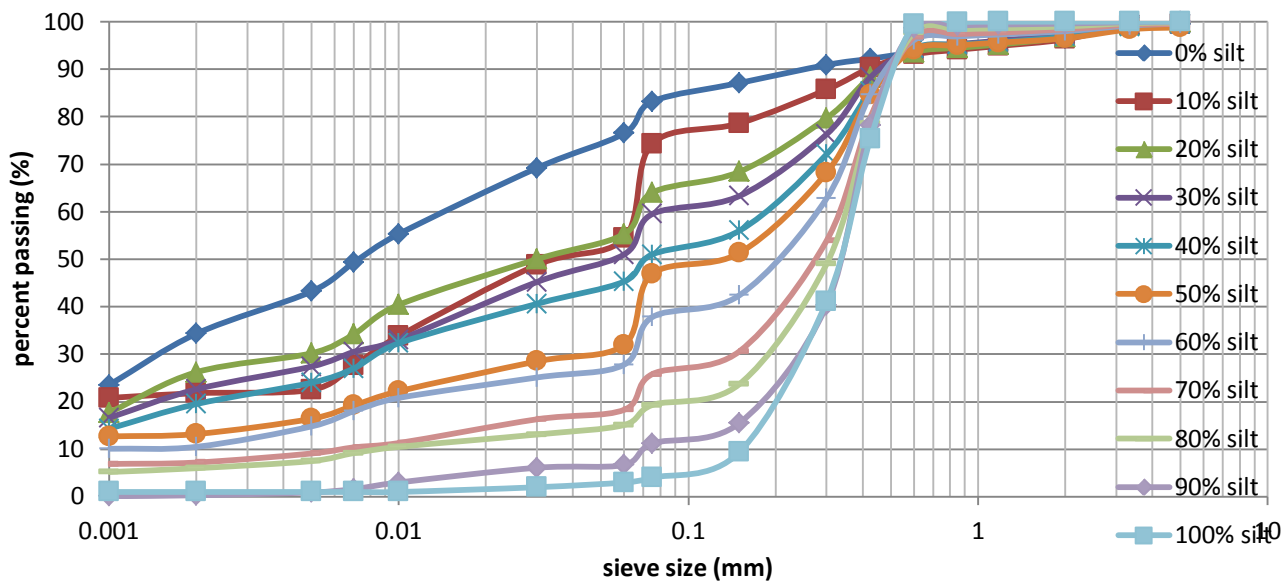
Figure 1: Grain size analysis of the clay soil at various silt replacement

This can probably cause reduction in strength of remoulded clay soils replaced with high composition of A-3 soil.

The result also showed grained size curves moving from the region of fine grained soil towards the region of course grained soils. This agrees with the findings by Osinubi and Alhassan (2008).

3.2 Atterberg limits

The result of the variation in liquid limit, Plastic limit and plasticity index with A-3 soil replacement is shown in figure 2. The liquid limit decreases from 59.3% at 0% A-3 soil replacement to 23.4% at 80% A-3 soil replacement after which the value increased to 28.8% at 100% A-3 soil replacement. The plastic limit behaved similarly with reduction from 26.8% at 0% A-3 soil replacement to 18% at 50% A-3 soil replacement after which the value increased to 20.3% at 60% A-3 soil replacement. This trend is in agreement with Muazu (2006) and Joel and Agbede (2008). The mixture became non plastic beyond this replacement.

The resultant plasticity index reduces from 32.5% at 0% A-3 soil replacement to 6.6% at 60% A-3 soil replacement after which the mixture becomes non plastic. These results are in disagreementwith studies carried out using lime and cement for modifications (Osinubi, 1999). This is because the results of lime and cement modification of clays are commonly characterised by average increase in both the liquid limit and plastic limit with resultant decrease in plasticity index. Unlike lime, cement and some other pozzolanic admixtures that pass through chemical reactions in the process of modifying clay soils, A-3 soil is inactive and do not undergo these reactions.Therefore, the trend observed in this study emanates from the physical process of which A-3 soil particles covers the surfaces of the active clay particles and reduces interaction between

clay to clay particles thus reducing the plastic action of the clay particles.
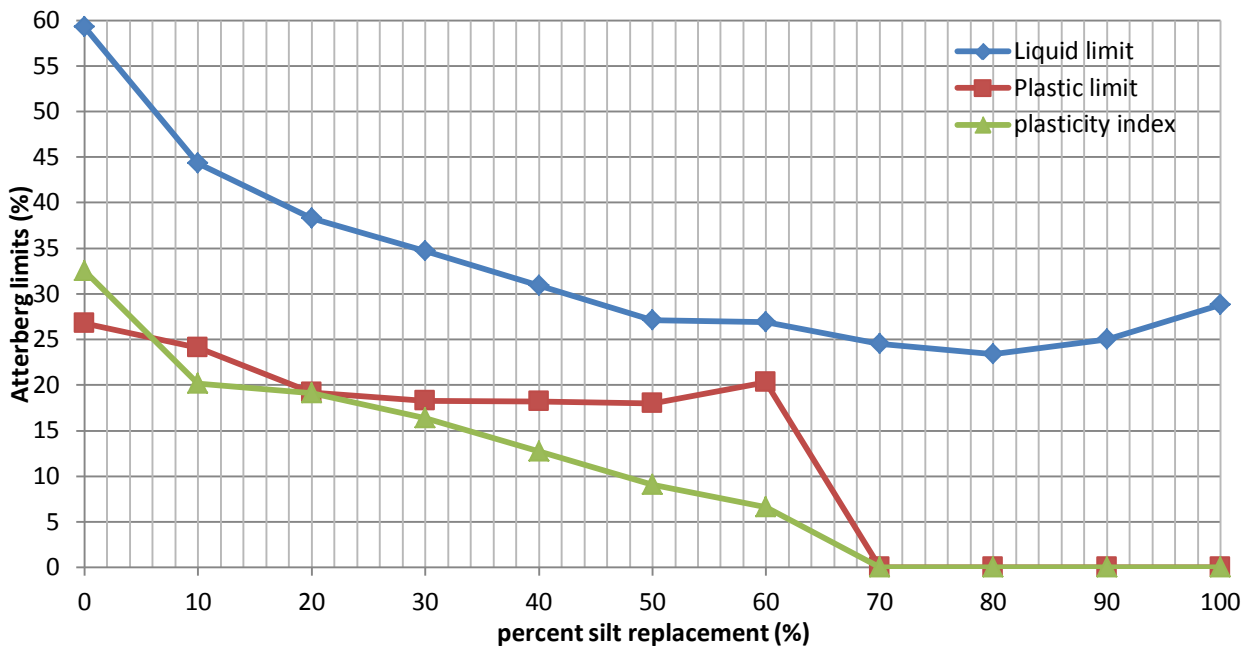
Figure 2: Variation of Atterberg Limits with increase in non-plastic silt replacement

At lower composition of A-3 soil particles, few active clay particles are covered with the A-3 soil which leaves more active clay particles to exhibit plastic action. However, increase in A-3 soil tends to cover more active clay particles and further reduction in both the liquid limit and the plastic limit with resultant decrease in plasticity index.

A point is reached when the whole active clay particles contained in the soil sample are covered with A-3 soil. Increase in A-3 soil beyond this point results in to slight increase in liquid limit with completely non plasticity of the fines contained in the soil. The reduction in Atterberg Limits with
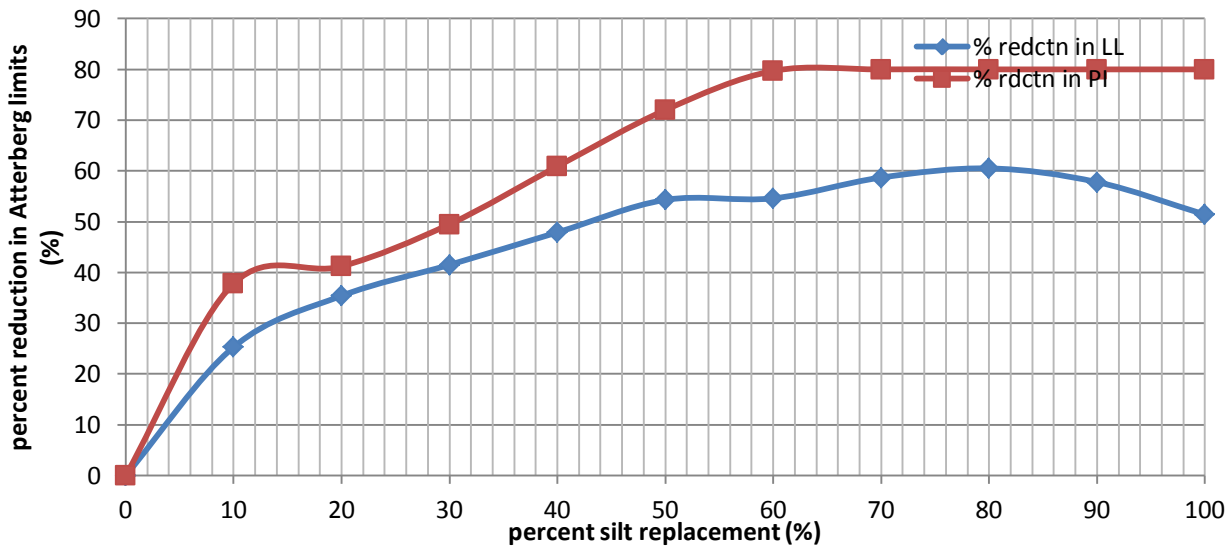
Figure 3: Percentage reduction in Atterberg Limit with percentage silt replacement

increase in A-3 soil replacement represented by percentage reduction on the bases of the maximum Atterberg limit values of the clay is shown in figure 3. This percentage Atterberg limit reduction will help to determine the amount of A-3 soil required to modifying a gravely lateritic soil which is deficient in only the Atterberg limits. The result of the index properties of the clay soil replaced with varied A-3 soil as well as its classifications using the Unified Soil Classification System (USCS) and the American Association of State Highways and Transportation Officers system (AASHTO) classifications is shown below:

Table 1: Summary of index properties and subsequent soil classification with silt replacement

percentage silt	Percent passing sieves (%)				Liquid	Plasticity	Soil Classification	
Replacement (%)	5.0mm	2.0mm	0.425mm	0.075mm	Limit (%)	Index (%)	AASHTO	USCS
0	99.5	96.5	92.2	83.2	59.3	32.5	A-7-6	CH
10	99.4	96.3	90.3	74.3	44.3	20.2	A-7-6	CL
20	99.8	96.7	88.3	64.0	38.3	19.1	A-6	CL
30	99.5	97.4	88.3	59.5	34.7	16.4	A-6	CL
40	99.4	96.9	85.3	51.0	30.9	12.7	A-6	CL
50	98.8	96.5	84.7	46.9	27.1	9.1	A-4	SC
60	99.6	98.0	84.7	37.8	26.9	6.6	A-4	SM-SC
70	99.5	98.4	79.9	25.8	24.5	NP	A-2-4	SM
80	99.8	99.0	78.6	19.3	23.4	NP	A-2-4	SM
90	100	99.6	78.2	11.2	25.0	NP	A-2-4	SM
100	100	100	75.3	4.0	28.8	NP	A-3	SP

The soil classification presented on the table above showed clay of high plasticity at 0% A-3 soil through clay of low plasticity from 10% to 40% A-3 soil. The classification becomes clay sand at 50% A-3 soil and silty sand to clay sand at 60% A-3 soil. Beyond this percentage A-3 soil, the clay soil becomes non plastic. Therefore, 60% A-3 soil is the maximum value required for effective modification of clay soils.

4. CONCLUSION

From the result of the investigation carried out in this study, the following conclusions can be drawn:

1   The clay used in this study classified as A-7-6 under AASHTO classification system and as CH under unified soil classification system.

2   The particle sizes moved from the region of fine grained soil to that of course grained soil with increase in percentage A-3 soil replacement.

3   The index properties decreased continuously from 0% A-3 soil to 60% A-3 soil replacement after which the clay becomes completely non plastic. Therefore, 60% A-3 soil replacement is the maximum required for effective modification of clay soils.

4   Maximum of 60% reduction in liquid limit was achieved at 80% A-3 soil replacement while maximum of 80% reduction in plasticity index was achieved at 60% A-3 soil replacement.

5. RECOMMENDATIONS

1. A maximum of 60% A-3 soil replacement is recommended for effective modification of plastic clays. Beyond this level of replacement, the whole mixture becomes non plastic.

6. REFERENCES

Nigerian General Specification (1992), "Road and Bridge Works", Federal Ministry of Works, Lagos,

Highway Research Board of America (1943), "Use of Soil-Cement Mixture for Base Courses", Water time

Osinubi K. J. and Alhassan M., (2008) "Use of Lime and Bagasse Ashe in the Modification of Laterite", Nigerian Journal of Engineering, Vol. 14, No. 1.

Joel M. and Agbede I. O., (2008) "Lime-Sand Stabilization of Igumale Shale Mixtures for Road Work", Nigerian Journal of Engineering, Vol. 14, No. 1.

AASHTO (1986) "Standard Specifications for Transportation Materials and Methods of Sampling and Testing" 14th Edition, Am. Assoc. of State Hwy. and Transp. Officials. Washington D. C.

B. S. 1377 (1990) "Methods of Testing Soils for Civil Engineering Purposes" British Standard Institute, London.

B. S. 1924 (1990) "Methods of Test for Stabilized Soils", British Standard Institute, London.

.

Road Problems No. 7, Nat. Res. Council, Div. Eng. Indust. Res., Washington D. C.

Ola S. A. (1983) "The geotechnical properties of the black cotton soils of north-eastern Nigeria", In: Tropical Soils of Nigeria for Engineering Practice, Rotterdam, pp. 85-101.

Osinubi K. J. and Gadzama E. W., (2008) "Bagasse Ashe Modification of Shika Laterite", Nigerian Journal of Engineering, Vol. 14, No. 1.

Osinubi, K. J. and Katte V. Y. (1999) "Effect of Elapse Time after Mixing on Grain Size and Plasticity Characteristics II: Soil – Cement Mixes,

Osinubi K. J. (1995), "Lime Modification of Black Cotton Soil", Spectrum Journal, Vol. 2, No. 1 & 2.

Muazu M. A. (2006) "Effect of Sand on Plasticity of Laterite", Biannual Engineering Conference, School of Engineering and Engineering Technology, Federal University of Technology, Minna.

Goodarzi, A. R. and Salimi, M. (2015), "Stabilization Treatment of a Dispersive Clayey soil using Granulated Blast Furnace Slag and Basic Oxygen Furnace Slag", Journal of Applied Clay Science, Vol. 108, PP61-69.

Non-Isothermal Devolatization of Industrial and Chewing Sugarcane Bagasses

[1]Charles Nwatuzor, M. U. Garba[1*], Abdulfatai Jimoh[1], Kariim Ishaq[2], Musa Umaru[1] and Mohammed Alhassan
[1]Chemical Engineering Department Federal Univeristy of Technology Minna, Niger State, P. M. B. 65, Nigeria
[2] Center for Genetic Engineering and Biotechnology, Federal Univeristy of Technology Minna, P. M. B. 65, Niger State, Nigeria
[*]umar.garba@futminna.edu.ng, 08052450032.

ABSTRACT

The devolatilization is the first step of thermochemical processes and requires an in-depth understanding. In this paper, the devolatilization of industrial and chewing sugarcane bagasses has been investigated using thermogravimentric analyser (TGA). The devolatilization of industrial sugarcane bagasse (ISB) and chewing sugarcane bagasse (CSB) were related to it lignocellulose content (cellulose, hemicelluloses and lignin). The component compounds of bagasse exhibit three major mass loss peaks which decompose independently. The first and second mass-loses were associated with hemicellulose and cellulose degradation and are responsible for the appearance of the first peak and second peak with the temperature range of 180–254 ^{o}C and 250–317◦C respectively. Lignin degradation was observed to occur at a much higher temperatures of 317-900 ^{o}C as denoted by the third peak. A comparative evaluation of the bagasse obtained from the two varieties of sugarcane shows that there was an overlaped of TG-CSB over TG-ISB during hemicellulose decomposition which later separated with the emergence of cellulose decomposition. The thermal stability of bagasse decomposition was observed to increase in the following order: hemicellulose < cellulose < lignin. The result of TGA indicated that CSB has higher thermal stability than the ISB. The difference in the lignocellulose fraction provides an explanation for these differences. The percentage of cellulose and lignin content in CSB is greater than that of ISB with lignin content constituting larger percentage of the difference. These experimental results help explain and predict the behaviour of bagasses in practical applications.

Keywords: *Chewing Sugarcane; Industrial Sugarane, Bagasse, TGA/DTG; lignocellulose*

---

1. INTRODUCTION

Hoslistic ultilization of agricultural produce and its resulting by-products in industrial transformation process has been widely acknowledged as a vital aspect of sustaining the environment and conserving the much needed economic resources (Dormo *et al.*, 2004). Sugarcane bagasse is an abundant agricultural waste produced as a by-product of sugarcane processing from sugar industries. In Nigeria, there are two main types of sugarcanes; the industrial and chewing sugarcane. The chewing sugarcane is mainly consumed in it natural form for it sweetness in all community in Nigeria (Ojehomon *et al.*, 1996). It is characterized with a purple colour and is known to be robust with less sucrose and much water. It is often softer than the industrial type with high ability to withstand drought (Ojehomon *et al.*, 1996). In Nigeria, the chewing sugarcane account for 60% of cane production because of it domestic economic viability when compared to industrial cane (Gana, 2011). Chewing cane is in high demand due to high rate of public consumption which has led to the generation of enormous quantity of sugar cane fibre wastes that littered the major streets of most Nigerian cities. In addition to domestic consumption of this sugarcane in its natural form, it is processed into local brown sugar cakes referred to in Hausa language "Alewa and Mazarkwaila" (Gana *et al.*, 2009).

The industrial sugarcane is a major feedstock in sugar mill (Naidu, 1987). It is mainly used for the production of sugar and alcohol (Sun *et al.*, 2004). The stems of the crop are cut and transported from the field to sugarcane mills where they are crushed to produce sugar juice and sugarcane bagasse. The juice is subjected to evaporation until it is concentrated into sugar. The increased in the

importation of raw sugar from Brazil with poor field practice and the need to conserve the nation foreign exchange have stimulated the Nigeria Government interest towards making concerted efforts to foster sugar production (Nzeka *et al*., 2013). Privatization of sugar estates, improved field practices, out growers programme, and efficiencies of the factory and it boilers have generated large amount of bagasse. The continuous accumulation of these bagasse and it non-utilization by the industry presents an agricultural waste problem (Ouensanga, 1988). Sugarcane bagasse is a lignocellulosic plant's cell wall. It is mainly constituted of hemicellulose, cellulose and lignin, which act as a structural support (Idi *et al.*, 2011). The fraction of lignocellulose bagasse is dependent on the sugarcane variety, maturation, soil type or condition, amount of fertilizer applied and the condition harvesting (Lamb *et al*., 1977). Generally, about 280 g of bagasse is generated from 1 tonne of sugarcane (Sun *et al*., 2004). Sugarcane corresponds to approximately 40 wt% of the total stem mass (Sun *et al*., 2004).

A number of possible biotechnological processing route are available for the production of bio-products from agricultural waste (biomass). Among all products biofuel have been of great interest (Demo et al., 2004). These technological schemes used to convert biomass to an alternative energy source include physical, biochemical, thermal and chemical technique (Abdullah, 2010). Thermochemical processes constitute alternative route for biomass utilization (Garba *et al*., 2006; Abdullah, 2010 and Garba *et al*., 2012). Because of its large potentials, it has the ability to become the main energy source in the closest future. Co-firing coal with biomass is a short time opportunity reaps from biomass advantages (Garba *et al*., 2013). Gasification is a benign and efficient alternative for producing upgraded fuel from biomass (Prins *et al*., 2003). Pyrolysis is all-round process for recovering fuel and chemical (Biagini *et al*., 2006). Torrefaction is a fuel upgrading process where raw biomass is heated in the temperatures of 200–300 °C under an inert atmosphere (Garba *et al*., 2014).

Thermogravimetry Analysis (TGA) is an important means of obtaining key information about the vital characteristics such as reaction mechanism, thermal stability, phase transformation and essential data on specific temperature of the heterogeneous reactions taking place during pyrolysis (Abdullah, 2010). TGA comprise of main two components - Thermogravimetry (TG) and differential thermogravimetric (DTG) analyses. In TG, a continuous graph of mass change against temperature or time can be monitor while DTG is an approach performed by detecting the rate of mass loss.

Many researchers have studied thermal characteristics of different biomass materials (Munir *et al*. 2009). For instance Abdullah *et al*. (2010) carried out TGA study of rice husk and oil palm shell while Ouensanga (1988) investigated the thermal degradation of sugar cane bagasse and its components (cellulose and lignin) between room temperature and 700 ^{o}C under atmospheric condition (nitrogen, dry air, oxygen) using thermogravimetric analysis. Recently, Vanita *et al*. (2011) reported their findings on thermal decomposition of bagasse from different locations using thermogravimetry analysis.

The quantum of sugarcane bagasse generated in Nigeria call for a concerted research effort towards it's proper evacuation by converting these waste to energy. As far as the author's knowledge could go there are no documented literatures on the thermal behaviour of sugarcane bagasse originating from Nigeria so as to establish it potential for energy generation. This paper focuss on the study of thermal behaviour of sugarcane bagasse originating from Nigeria. In this work, thermal characteristics of industrial and chewing sugarcane bagasses was studied in an inert atmospheres, leading to a comparative evaluation of the

thermal behaviour in order to explore their energy potential.

2. METHODOLOGY

2.1. Materials

Two sugarcane bagasse from two different varieties of sugarcane namely; Chewing Sugarcane and Industrial Sugarcane were employed in this work. Chewing sugarcane bagasse (CSB) was collected from Wuya Kpansanako Community of Bida, Niger State. Industrial sugarcane bagasse (ISB) was collected from sugar mills located in Bacita, Kwara State, Nigeria. Figure 1 shows the pictorial view of the samples. The samples were not washed to remove the residual sugars because in an industrial setting the sample will be used as received. These samples was then crushed to obtain a particle size less than 250 μm and were kept in air tight bins prior to analysis.

Figure 1. Bagasse Sample (a) CSB (b) ISB

2.2. Determination of Lignocellulose Fraction

Following Van Soest's Fibre method (van Soet *et al*., 1963), neutral detergent fibre (NDF), acid detergent fibre (ADF) and acid detergent lignin (ADL) were measured. The NDF was determined by refluxing bagasse ash for 1h in a neutral buffered detergent solution. The residue corrected ash which is also the total cell (NDF = hemicelluloses + cellulose + lignin) is the NDF. ADF (ADF% =lignin +cellulose) was determined by refluxing the NDF sample in a solution of cetyl ammonium bromide (CTAB) in 2M sulphuric acid. Hemicelluloses dissolves and was removed by filtration. ADL was measure by further treating ADF

sample with strong acid (72% sulphuric acid) to dissolve the cellulose in order to determined the lignin. The hemicellulose content was derived by subtracting NDF values from ADF values while cellulose content was derived by the difference between ADF and ADL.

2.3. Thermogravimetry Analyisis

A TG / DTG non-isothermal test was carried out using Perkin Elmer thermogravimentric analyser (TGA-4000) for the two samples of bagasse: ISB and CSB. The TGA equipment was purged with oxygen gas to simulate conventional combustion with flow rate of 20 ml/min and heating rate of 10 ^{o}C /min, the analysis was performed using a temperature scan range 30 to 900 ^{o}C.The weight of empty crucible was zero and latter load with sample to be analysed.

2.4 Fourier Transform Infrared Spectroscopy Analysis

The FTIR spectra of bagasse samples were obtained using SHIMADZU Series FTIR Spectrophotometer, 400 mg samples of potassium bromide containing about 5 mg of bagasse powder were prepared and subjected to analysis.

3. RESULTS AND DISCUSSIONS

The decomposition profiles as shown by thermograms from TGA reflects characteristic parameters essential for the understanding of the thermal behaviours of a fuel (Munir *et al*., 2009). Different region can be distinguished from the thermograms. These regions represent the beginning and the ending of the derivative of thermogravimetric curve (DTG) which shows the breakdown of organic matter in the samples under inert atmosphere and therefore it is a reflection of the combustion of the release volatiles during partially decomposition organic materials (Idi *et al*., 2011).

Figure 2 and 2 shows the weight loss curve (TG) and derivative thermogravimetric (DTG) evolution profiles of ISC and CSB samples as a function of temperature using heating rate of 10 ^{o}C/min. Table 1 shows the proximate and thermal properties of the ISC and CSB samples. The thermal degradation can be divided into three stages; moisture drying, main devolatilisation and continuous slight devolatilisation (Munir *et al*., 2009). The Stage I is often attributed to dehydration of water (Idris, 2010). The TG and DTG curves in Figure 2 show that ISB dehydration begins at room temperature up to approximately 180 °C which corresponds to the first peak in the DTG evolution with a mass loss of about 10%. Figure 3 shows CSB dehydration begins at slight higher temperature approximately 186 °C with corresponding lower mass loss of approximately 8 %. These values were also indicated in Table 1. The mass loss observed in ISB sample shows quantitative agreement with 10 % for central Pakistan but greater than 6.5 % of South African bagasse sample as reported by Munir *et al*. (2009) and Akinwale *et al*. (2011) respectively. In Stage II, between temperature ranges of 180-250 ^{o}C (for ISB in Figure 2) and 186-255 ^{o}C (for CSB in Figure 3), a negligible weight loss were observed. This stage is followed by the start of devolitilization which is characterized by the sudden weight loss. The negligible weight loss before the start of devolatilization can be attributed to the removal of bound moisture and the start of polysaccharide hydrolysis (Roque-Diaz, 1985, Mansaray 1999). In the third stage, there is no obvious weight loss observed beyond temperature of 500 ^{o}C. Nevertheless, the ISB and CSB samples continue to decompose until beyond temperature of 900 ^{o}C with maximum decomposition at temperature of approximately 906 ^{o}C.

Table 1: Characteristics of the thermogravimetric experiment under N_2 conditions.

Sample	MC (%)	VM (%)	AC (%)	T_p	T_o	Degradation Temperature range (°C)
CSB	7.6	12.12	4.92	228	210	186 - 254
		14.6		297	254	254 - 317
		25.8		351	341	317 - 472
ISB	10.2	7.30	3.42	235	213	180 - 250
		10.5		283	283	251 - 318
		14.7		353	344	318 - 460

The elemental analysis of raw biomass is the starting point in establishing the suitability of a given solid fuel to be burned in a furnace from the thermal behaviour point of view (Garba *et al*., 2012). The high mineral content in bagasse would have a measurable effect on the thermal degradation rate. Both samples of ISB and CSB were subjected to XRF analysis and the results are shown in Table 2. The CaO and Fe_2O_3 content may be particularly important. CaO(s) is refractory in character and it will raise the thermal stability (Mansaray *et al*., 1999). Consequently CSB with higher Ca content (80% CaO compared with 76% CaO for ISB) show higher stability than the ISC.

Table 2: Chemical analysis of bagasse samples.

Oxide (%)	ISB	CSB
SiO_2	14.22	12.21
Al_2O_3	2.51	1.72
TiO_2	0.48	0.40
MgO	0.34	0.3
MnO	0.20	0.19
CaO	76.11	80.01
Na_2O	1.02	0.98
K_2O	2.2	2.31
Fe_2O_3	3.0	1.71

P_2O_5	0.012	0.11
BaO	0.01	-
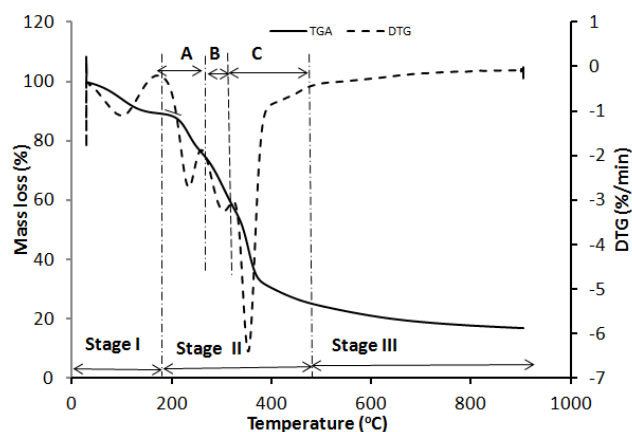
Figure 2. Thermal property of industrial sugarcane bagasse (ISB)
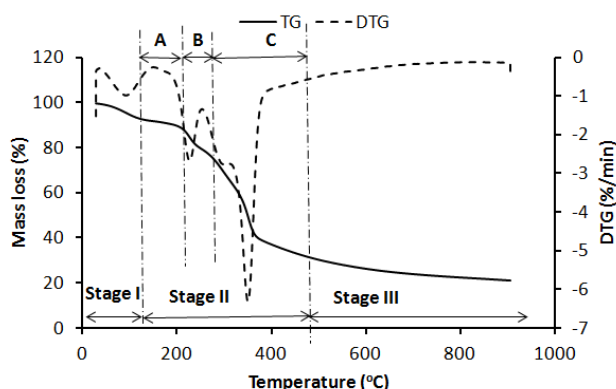
Figure 3. Thermal property of chewing sugarcane bagasse.

Lignocelluloses biomass are majorly composed of hemicelluloses, cellulose and lignin (Shafizadeh, 1982). The Stage II of weight loss exhibits three distinctive regions A, B, and C as depicted Figures 2 and 3. Region A, ranging from a temperature of 180-254 °C and region B from a temperature of 250-317◦C were found to be similar to the curves of decomposition of hemicelluloses (Wang et al., 2011; Nola et al., 2010) and cellulose (Wang et al., 2011; Nola et al., 2010), whereas region C which is the decomposition at higher temperature is thought to be

due to decomposition of the complex and/or aromatic structures such as lignin (Idris et al., 2010).

The small peak in A shown in Figures 2 and 3 are indication of lower stability of this hemicellulose when compared with the B (cellulose). The component C (lignin) shows the main peak at temperature range of 317-900 °C. Lignin degradation occurs gradually over a wide temperature range due to it cross link and aromatic nature resulting in broader peak (Fahmi et al., 2007).

Onset (T_o) and peak temperatures (T_p) are important tool in knowing thermal stability of the fuel (Daniela et al., 2011 and Bao-Guo et al., 2006). The former refers to the temperature when weight loss just begins, while the latter to the temperature of the maximum rate of decomposition.

Figure 2 shows the onset and peak temperatures for degradation of the sample. The onset temperatures for hemicelluloses (To_1), cellulose (To_2) and lignin (To_3) are 213, 283 and 345 °C respectively. Low onset temperature means the component is easier to degradate. Hemicellulose is easily susceptive to heat and less resistance to degradation (Bridgeman et al., 2008). Whereas lignin degradation is more resistance and therefore large amount of heat is required. Figure 4. TG and DTG curves of industrial sugarcane bagasse (ISB) and chewing sugarcane bagasse (CSB).
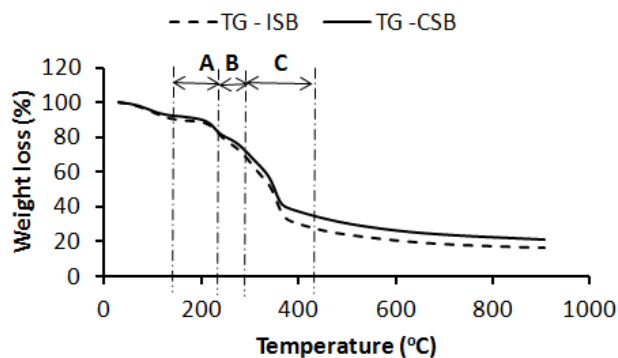
Table 2. Lignocellulose fraction of bagasse

Bagasse	Cellulose	Hemicellulose	Lignin
ISB	38.8	29.4	21.7
CCB	39.2	26.1	24.1

Figure 4 gives a comparison of the TG-DTG profiles for ISB and CSB. It is seen that the TG-CSB lapped over TG-ISB during hemicelluloses decomposition but separated at the emergence of cellulose (B) decomposition and the difference become more apparent during lignin decomposition. This indicated that the thermal stability increase in the order: hemicellulose < cellulose < lignin. The reason for this relatively higher thermal stability of the lignin is probably due to the substantial percentage of lignin in CSB. The difference in the lignocelluloses fraction (Table 2) provides an explanation for these differences. The percentage of cellulose and lignin content of CSB is greater than that of ISB with lignin content constituting larger percentage of the difference.

FTIR spectroscopic investigations provide information on the natural polymer functional group. FTIR spectrum of ISB and CSB were displayed in Figure 3 (a) and (b) respectively. There is a broad band at 3385 cm^{-1}, which is characteristic for the OH- stretching of cellulose and this band gives good information about the hydrogen bonds formation. There is also side - band at 2923 cm^{-1} which represents the C–H stretching of cellulose. The peak at 1634 cm^{-1}, 1040 cm-1 and 407 cm^{-1} assign to C=C stretching of aromatic ring in lignin, C-H deformation of lignin and –COO vibration of acetyl groups in hemicelluloses, respectively. In FTIR spectra, lignin appears in between cellulose and hemicelluloses. This revelation is corroborated by the ample evidence in literature of numerous investigators (Idi *et al.* 2011; Uma *et al.*, 2012) that lignin is embedded in the

hemicellulose and cellulose structure to strengthen the cell wall of plant. ISB exhibit similar wavelength pattern to CCB except at wavelength between 500 - 400 cm^{-1} it shows narrower band. CSB exhibited higher % transmittance.
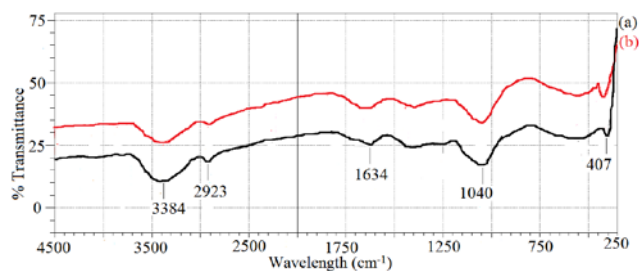
Figure 4. FT-IR Spectra of (a) ISB and (b) CSB.

4. CONCLUSION

Devolatilization of industrial and chewing sugarcane bagasses using TGA have been presented. The devolatilization of bagasse were related to it cellulose, hemicelluloses and lignin which pyrolyse independently. The first, second and third mass-loses were associated with hemicelluloses, cellulose and lignin degradation and thermal stability of bagasse decomposition was observed to increase in the following order: hemicellulose < cellulose < lignin. A comparative evaluation of the bagasse obtained from the two varieties of sugarcane shows that chewing sugarcane bagasse is more thermally stable than industrial sugarcane bagasse.

REFERENCE

Abdullahi, S. S., Yusuf, S. N., Ahmad,M. M., Ramli, A. and Ismail H. (2010) "Thermogravimetry study on pyrolysis of various lignocellulosic Biomass for potential Hydrogen production, *International Journal of chemical and Biological Engineering* Vol. 3 No. 3, pp. 137 – 141.

Biagini , E., Fantei, A., Tognotti, L., (2006) "Effect of the heating rate on the devolatilization of biomass residues" *d. Eng. Chem. Res.* Vol.45, No.13, pp.4486 - 449.

Bridgeman, T. G., Jones , Shield , J. M., I., Williams, P.T. (2008) "Torrefaction of reed canary grass, wheat straw and willow to

enhance solid fuel qualities and combustion properties", *Fuel* 87 pp. 844 – 856.

Dormo, N., Belati-Bako, K., Bartha, L., Elorestein, U, and Gubiczaan, h., (2004) "Manufacturals of an environment – safe biolubricant from fuel iol by enzymatic esterification in solvent free system", *Biochemical Engineering Journal*, Vol. 21, pp. 229 – 234.

Gana, K. A., Shebayan, J. A. Y., Ogunlela, V. B., Odion, E. C., Imolehin, E. D., (2009) "Path coefficient analysis on growth parameters of chewing sugarcane as affected by fertility rates and weed control treatments at Badeggi, Nigeria", *Agricultural tropica et subtropica*, Vol.42, pp.1.

Gana, A. K., (2011a) "Appropriate method for organic manure application for higher sugarcane yield in Nigeria", *Journal of Agricultural Technology*, Vol.7, No.6, pp. 1549-1559

Garba, M., U., Alhassan, M., Kovo, A. S., (2006) "A Review of Advances and Quality Assessment of Biofuels" *Leonardo Journal of Sciences*, pp.167 - 178.

Garba, M., U., Ingham, D., B., Ma, L., Porter, R., T., J., Pourkashnian, M., Tan, M., H., Z. and Alan Williams, (2012) " Prediction of Potassium Chloride Sulphation and Its Effect on Deposition of Biomass-Fired Boilers" *Energy & Fuels*, Vol.26 No.11, pp.6501 - 8.

Garba, M., U., Oloruntoba, J. M., Isah, A. G., Alhassan, M., (2015) "Production of Solid Fuel From Rice Straw Through Torrefaction Process", *International Journal of Science and Engineering Investigations* Vol.4 No.37, pp.1 – 6.

Idris , S. S., Abd Rahman, N., Ismail, K., Alias, A. B., Abd Rashid, Z., (2010) "Investigation on thermochemical behaviour of low rank Malaysian coal,oil palm biomass and their blends during pyrolysis via thermogravimetric", *Bioresource Technology*, Vol.101, pp. 4584 – 4592.

Lamb, B., W., Bilger, R., W.,(1977) "Combustion of bagasse: literature review" *Sugar Technol.* Vol.*4*, pp.89 – 130.

Mansaray, K .G., Ghaly, A. E., (1999) "Determination of kinetic parameters of rice husksin oxygen using thermogravimetric analysis", Biomass and Bioenergy Vol.17 pp.19 – 31.

Ma., B., Li., X., Xu, L., Wang, K., Wang, X. G., (2006) "Investigation on catalyzed combustion of high ash coal by thermogravimetric analysis", Thermochimica Acta Vol.445, pp.19 – 22.

Munir, S., Daood , S. S., Nimmo, Cunliffe , W., A. M., Gibbs, B.M. (2009) "Thermal analysis and devolatilization kinetics of cotton stalk, sugar cane bagasse and shea meal under nitrogen and air atmospheres", *Bioresource Technology* 100, pp. 1413 – 1418.

Naidu, K. M. (1987) "Potential yield in sugar cane and its realization through variety improvement" sugarcane varietal improvement. Sugarcane Breeding Instituet, Coimbatore, India, pp. 1 – 17.

Nola, G. D., Jong, W. D., Spliethoff, H., (2010) "TG–FTIR characterization of coal and biomass single fuels and blends under slow heating rate conditions: partitioning of the fuel-bound nitrogen", *Fuel Process Technol.* Vol.91, pp.103 – 15.

Nzeka, U.,Olaito, P., (2013) Annual Sugar Report for Nigeria 2013, Sugar Annual, pp. 2 – 4.

Ojehomon, V. E. T., Busari, L. D., Ndarubu, A. A., Gana, A. K and Amosun, A., (1996) "Production practices and costs/returns analysis of traditional chewing cane production in Nigeria", *WAFSRN Journal* Vol.6, No.2, pp.14 - 22.

Prins, M., J., Ptasinski, K., J., Janssen F., J., J. G., (2003). "From coal to biomass gasification: comparison of thermodynamic efficiency" In: Houbak, N., Elmegaard, B., Qvale, B., Moran, M., J., editors. Proceedings of 16th Int. Conf. on Efficiency, Costs,

Uma M. C., Obi, K., Muzenda, E., Guduri, B. R., & Varada R. A. (2012) "Extraction and characterization of cellulose microfibrils from agricultural residue – Cocos nucifera L". *Biomass and Bioenergy,* Vol.46, pp. 555 - 563.

Roque-Diaz, P., University, C., Villas, L.C.V., Shemet, V.A., Lavrenko, V.A., (1985) "Studies on thermal decomposition and combustion mechanism ofbagasse under non-isothermal conditions", *Thermochimica Acta* Vol.93 pp. 349 – 352.

Shafizadeh, F. (1982) "Introduction to pyrolysis of biomass", *Journal of Analytical and Applied Pyrolysis*, No. 3, pp. 283 – 305.

Sun, J. F., Sun, R. C. and Su Y. Q., (2004) "Fractiional extraction and structural characterization of sugarcane bagasse hemicelluloses", *Carbonhydrate polymers* Vol.56: pp. 195 – 204.

Van Soest, P. J., (1963) "The use of detergent in the analysis of fibrous feed II: A rapid method for the determination of fibre and lignin", J . Assoc off Agri Chem, Vol.46, pp. 829 - 835.

Vanita, R. M., William, O. S., Doherty, Ray L. F., and Pyam M., (2011) "Thermal Decomposition of Bagasse: Effect of Different Sugar Cane Cultivars" *Ind. Eng. Chem. Res.* Vol.50, pp.791 – 798.

Wang, C., Wu, Y., Liu, Q., Yang, H., Yin, F., (2011) "Analysis of the behavior of pollutant gas emissions during wheat straw/coal cofiring by TG–FTIR", *Fuel Process Technol.* Vol.92, pp.1037 – 41.

PARTIAL REPLACEMENT OF CEMENT WITH CORN COB ASH IN CONCRETE PRODUCTION

Bala A[1*]., H. O. Aminulai[1]., M. Abubakar[1], H. S. Abdulrahman[1] and U. Musa[2]

[1]Department of Civil Engineering, Federal University of Technology, Minna, Nigeria
[2]Department of Chemical Engineering, Federal University of Technology, Minna, Nigeria
*balhaji80@yahoo.com/08065260435

ABSTRACT

The research investigated the effects of partial replacement of cement with corncob ash (CCA). Physical properties of the aggregates and mechanical properties of CCA cement concrete at 0.5 water–cement ratio and mix ratio of 1:2:4 were examined. Sixty concrete (60) cubes of size 150x150x150mm with different percentages by mass of corncob ash to Portland cement in order of 0%, 3%, 6%, 9% and 12% corncob ash were cast and crushed. The specific gravity of corncob ash was 1.16, while a twenty eight (28) day compressive strength of 29.4N/mm^2 was obtained at 3% replacement level, which shows that the 3% CCA replacement for cement is the optimum. While 12% CCA replacement for cement offers the lowest strength (18.6N/mm^2). Hence, the use of supper plasticizers and accelerators may be required to enhance the strength and workability at this replacement level.

Keywords: *Compressive Cube Strength, Corncob Ash, Partial replacement, Cement*

1. INTRODUCTION

Concrete is one of the engineering materials commonly used in building component such as slabs, columns, beams, staircase, foundation, retaining wall, dams etc. However, concrete is the most versatile heterogeneous or composite construction materials and impetus of infrastructural development of any nation. Civil engineering practice and construction work around the world depend to a very large extent on concrete. Concrete is a synthetic construction material made by mixing cement, fine aggregate, coarse aggregate and water in a specified proportion. Each of the components contributes to the strength development of the concrete. Hence, the overall cost of concrete production depends largely on the availability and cost of its constituent material. In Nigeria, cement is averagely the most expensive ingredient in the production of any concrete (Adesanya & Raheem,

2009). Because of the negative impact due to the environmental pollution, degradation of natural resources such as limestone and high cost of Portland cement, there is, therefore, need for cheaper and available substitute for cement in concrete production. One of the practical and economical solution is through the utilization of agricultural and industrial waste such as rice husk ash, coal fly ash (pulverized fuel ash), granulated blast furnace slag, silica fume, met-kaolin (calcium clay), rice husk ash, palm kernel shell ash, and Shea nut shell ash.

In addition, corncob is the hard thick cylindrical central core of maize, however, corn cob is describe as the agricultural waste product obtained from maize or corn, which is the most important cereal crop in sub-Sahara Africa. According to food and agricultural organization data, 589 million tons of maize was produce worldwide in the year 2008 (FAO, 2009). The United States was the largest maize producer having 52% of world production. Africa produce 9% of the world maize (IITA, 2008),

Nigeria was the second largest producer of maize in Africa in the year 2001 with 4.62 million tons (FAO, 2009). Subsequently, facility study reveals that, in Niger state most peasant or subsistence farmer cultivate cereal crop (Grass family crop) such as genuine corn, rice, corn (maize) and so on. However, these further imply that availability of corn cob as a by-product of maize is be assured. However, the significance of this research is to help reduce the cost of concrete production arising from increasing cost of cement, and reduce the volume of solid waste generated from corncob using this waste-to-wealth initiative.

2. METHODOLOGY

Materials used for this study are:

Cement;

The cement used for this research work is Ordinary Portland cement (OPC). The cement was purchased from Kowa cement store located at Gbakungu in Minna, Niger state.

Corncob ash (CCA);

The corncob was collected from Kudu in Mokwa local government, a major corn producing rural community in Niger state, the cob was dried thoroughly and burnt using open air burning. Finally the product was sieve using sieve number 200.

Coarse Aggregate (Gravel);

Crushed granite used was obtained from Triacta crushing plant located at Maikunkele in Minna, Niger state. The aggregate was clean, strong and sharp, free from clay, loam, dirt or organic matters conforming to the requirement of BS EN 12620 (2008).

Fine Aggregate (Sharp Sand)

The sharp sand used was obtained from river located at Gidan-mongoro along Federal University of Technology, Minna. It was air dried for 72 hours in other to reduce the moisture present in it. The sand was also clean and sharp, free from clay, loam, dirt or organic matters and conform to the requirement of BS EN 12620 (2008).

Water;

Tap water was used for mixing and curing of the concrete at the civil engineering laboratory, Federal University of Technology Minna. The physical examination of the water shows that it was clean, free from impurities and fit for drinking as recommended by the standard. BS EN 1008 (2002)

Production of Concrete;

Moulds of (150×150×150) mm were used. They were lubricated with engine oil in order to reduce friction and to enhance removal of cubes from the moulds. They were then filled with concrete in three layers and each layer was tamped 25 times. The moulds containing the cubes were left for 24 hours under a room temperature for the cubes to set before removing the mould. The cubes were removed after 24 hours and were taken to curing tank (BS EN 12390, 2002).

Curing of Cubes;

The method use for curing in this work is the total immersion of the cubes in water for specific age of 7, 14, 21 and 28 days from the day of casting (BS EN 12390-2:2000)

Compressive Strength Test

The concrete cubes were crushed at 7, 14, 21, and 28 days in order to determine the compressive strength of the

cubes. The compressive strength is determined by dividing the maximum of failure load of the specimen during the test by the cross sectional area of the specimen, BS EN 12390 (2002).

Compressive strength is evaluated using the relation;

$$compressive\ strength\ (N/mm2) = \frac{crushing\ load}{cross\ sectional\ area\ of\ concrte\ cube} \quad (1)$$

3. RESULTS AND DISCUSSIONS

Specific gravity;

The result of specific gravity test for both fine and coarse aggregates as presented in Table 1.0 fall within the specification 2.6 -3.0 for natural aggregate.

Bulk density;

The result of bulk density of both fine and coarse aggregates are given in Table 1.0 (loose and compacted bulk density) as 1460.10kg/m^3, 1600.05kg/m^3 and 1477.0kg/m^3, 1644.0kg/m^3 respectively. These values are within the specified range of 1650kg/m^3 to 1850kg/m^3 as reported by Abdullahi and Oyetola (2006).

Table 1.0 Physical Properties of the Aggregates

Parameter	Sand	Gravel	CCA	Cement
Specific gravity	2.68	2.75	1.16	3.16
Compacted Bulk density (kg/m^3)	1600.05	1644	-	-
Uncompacted bulk density (kg/m^3)	1460.10	1477	-	-
Aggregate impact value (AIV)	-	465	-	-

Sieve analysis

The result obtained for sieve analysis of both gravel and sharp sand was plotted as shown in   Tables 2.0 and 3.0. However, from Figure 1.0 the curve shows as S-curve showing that the sharp sand is well graded, which was adequate for producing a workable concrete. Also, Figure 2.0 shows a smooth grading curve which is an indication that the aggregate is adequate for production of workable concrete.

Table 2.0 Sieve analysis of the gravel

Sieve size (mm)	Weight Retained (g)	% Retained	% Cum Passing
37.5	0.000	0.00	100
19.00	12.000	1.20	98.80
13.2	84.000	8.42	90.38
9.5	268.200	26.87	63.52
4.75	625.300	62.64	0.88
Pan	8.790	0.88	0.00
TOTAL		100.00	353.58

Table 3.0 Sieve analysis of the sharp sand

Sieve size (mm)	Weight Retained (g)	% Retained	Cum % Retained	Cum % Passing
5.00	4.94	0.49	0.49	99.51
3.35	6.50	0.65	1.14	98.86
2.00	24.90	2.49	3.63	96.37
1.18	97.90	9.79	13.42	86.58
850	113.65	13.17	26.59	73.41
600	158.50	15.85	42.44	57.56
425	155.91	15.59	58.03	41.97
300	119.95	11.99	70.02	29.98
150	218.43	21.84	91.86	8.14
75	33.15	3.32	95.18	
Pan	48.17	4.82	100	
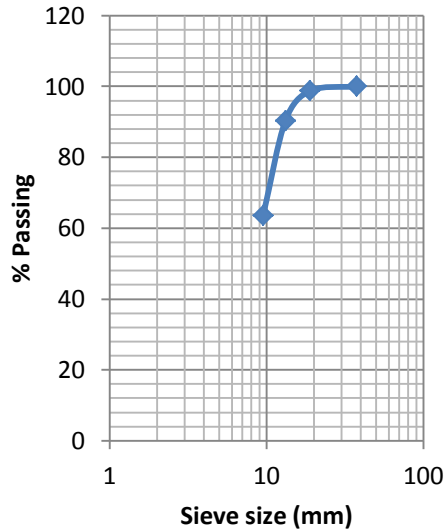
Fig 1: Sieve Analysis of the Gravel
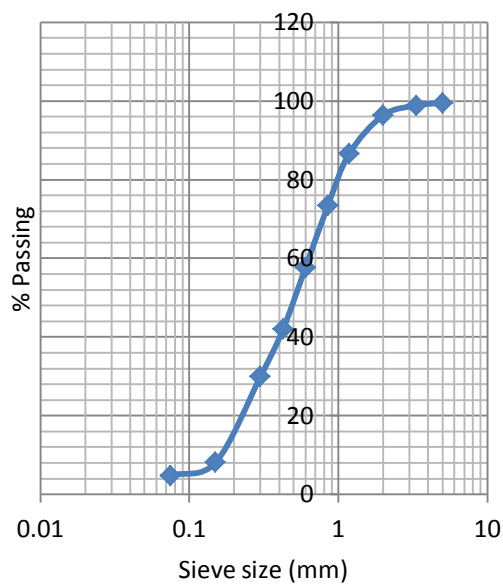
Fig 2: Sieve Analysis of Sharp Sand

Chemical analysis of CCA;

Table 4.0 shows the chemical composition of corn cob ash. The total percentage composition of iron oxide (Fe_2O_3=2.95), Silicon dioxide (SiO_2=68.60) and Aluminum oxide (Al_2O_3=5.15) was found to be 76.7%. The value is within the required value of 70% minimum for Pozzolanas as specified by ASTM C618 (2005). This values a little more than the value obtained by Abdullahi and Oyetola (2006) for rice husk ash (73.15%) which implies that CCA is more pozzolanic.

Table 4.0: Chemical Analysis of Corn Cob Ash

	% Composition	ASTM C618-12 Requirement
SiO_2	68.60	$SiO_2+Al_2O_3+Fe_2O_3\geq70\%$
Al_2O_3	5.15	
Fe_2O_3	2.95	
CaO	4.50	
MgO	2.80	
SO_3	1.44	
K_2O	8.42	
Na_2O	0.45	
Mn_2O_3	0.06	
P_2O_5	2.42	
LOI	8.55	10% max. for Classes N and F, 6% max. for Class C
Specific Gravity	2.50	

Compacting Factor;

The results obtained for the compacting factors of fresh CCA concrete for 0%, 3%, 6%, 9% and 12% were within the range of 0.94 and 0.95. These values fall within the required limit of 0.85-0.98 (Wilby, 1983), which indicates that the workability is satisfactory.

Slump Test;

The variations of the slump with increase in CCA is presented in Table 5.0. The result of the slump test obtained for 0%, 3%, 6%, 9% and 12% CCA are 32mm, 30mm, 28.5mm, 27mm and 27.5mm respectively. According to Wilby, 1983 a very low slump ranges from 0 - 25mm. Hence, from the above range of values it shows that the workability is also satisfactory.

Table 5.0 Slump and Compacting Factor Result CCA Concrete

% CCA	0% CCA	3% CCA	6% CCA	9% CCA	12% CCA
Slump (mm)	32	30	28.5	27	27.5
M_1 (kg)	7038	6882	7661	7933	7614
M_2 (kg)	7650	7580	8150	8350	8100
Compacting factor	0.92	0.90	0.94	0.95	0.94

Compressive Strength of Hardened Corncob Ash (CCA) Concrete;

The values obtained for the compressive strength test for hardened CCA concrete are given in Table 6.0 for 0%, 3%, 6%, 9% and 12%. The strength increases with the increase in age of curing. The mixes containing CCA exhibited downward result as the CCA content increases. It is

observed that the value of compressive strength obtained at 28days crushing for the respective percentage replacement of CCA are 32.1N/mm^2, 29.4 N/mm^2, 23.8 N/mm^2, 21.5 N/mm^2 and 18.6 N/mm^2. This indicates that the optimum replacement level for corncob ash is 3%.

Table 6.0 Summary of Copmressive Strength

% CCA replacement	Compressive Strength (N/mm^2)			
	7days	14days	21days	28days
0%	28.0	30.2	30.5	32.1
3%	25.7	28.3	28.8	29.4
6%	20.5	22.6	23.6	23.8
9%	17.9	18.2	18.6	21.2
12%	15.2	17.4	18.0	18.6
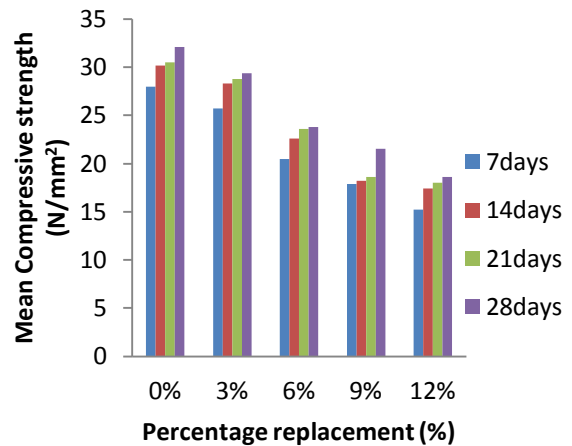
Figure 1: Compressive Strength against % Replacement

4. CONCLUSION

From the tests conducted on OPC/CCA concrete as presented in various sections, the following conclusions are made;

1. Corncob ash is pozzolanic and is therefore suitable for concrete production.
2. The water requirement increases with increase in percentage CCA replacement.
3. The compressive strength of concrete made with OPC/CCA increases with age of curing and decreases as the percentage of CCA increases.
4. The utilization of the corncob for production of concrete will go along way in not only the reduction of overall cost of the concrete, but also reduce the quantity of the waste in the environment.
5. The optimum replacement level of OPC with CCA is 3%

Recommendation

1. 3 percent replacement level of cement with CCA is satisfactory and thus, recommended
2. Concretes with the presence of ash content should be allowed to cure for 90days, by which pozzolanic activity of ash would have been concluded.
3. The use of locally available materials in infrastructural development will be met with the use of corn cob ash as a construction material and ultimately help meet our millennium development goals (MDG), thereby also enhancing the economic power of the rural dwellers if they are encouraged to plant maize from which these corn cobs could be gotten. The global green environment initiative will be greatly influenced by the reduction in solid waste disposal.
4. The volume replacement attempted to get high strength concrete should be enhanced with super-plasticizers and a further reduction in the water-cement ratio so that concrete of very high strength can be achieved.

REFERENCE

Abdullahi, M. and Oyetola, E. B. (2006) The Use of Rice Husk in Low-Cost Sandcrete Block Production", Leonardo Electronic Journal of Practices and Technologies, 8: 58-70.

Adesanya, D. A. and Raheem, A. A. (2007) 'Development of Corn Cob Ash Blended Cement, Construction Building Mater,
doi: 10.1016/j.conbuidmat.2007.11.013
(Article in Press)

ASTM C618 (2005) 'Standard Specification for Coal Fly Ash and Raw or Calcined Pozzalan for use in Concrete' Annual Book of ASTM Standards. Annual Book of ASTM Standards. American Society for Testing and Materials

British Standard Institute (2002) Mixing water for concrete specification for sampling, testing and assessing the suitability of water. BS EN 1008

British Standard Institute (2002) Testing concrete, Method for determination of Compressive Strength of Concrete Cube, BS EN 12390

British Standard Institute (2008) 'Aggregates for Concrete' BS EN 12620

Food and Agricultural Organization, Retrieved December 27, 2009, Available at:
http://apps.fao.org/default.htm.

Wilby C. B. (1983) 'Structural concrete' London, Butterworth & Co. Ltd

The International Institute of Tropical Agriculture (2008). Retrieved from
http://intranet/iita4/crop/maize.htm

Production of Solar Photovoltaic Module Using Dye Extract from Fluted Pumpkin Leaf as Sensitizer

Musa, Nicholas Akhaze[1*] , Nzekwe, Joel Chinedu[2]

Department of Mechanical Engineering

Federal University of Technology, Minna

*Corresponding Author Email Address ; Madonick1@yahoo.com. GSM NO; 08058717209

ABSTRACT

Dye sensitized solar cells (DSSCs) are auspicious class of low cost and moderate performance solar cells. This paper reports the development of DSSCs using dye extract from fluted pumpkin leaf as doping substance and other materials such as titanium dioxide, aluminium foil, copper wires, araldite, glasses, sealants and carbon deposits. From the solar module produced, the maximum voltage obtained was 340Mv at atmospheric temperature of 30^0C and minimum voltage obtained was 9mV at atmospheric temperature of 23^0C. The module performance varies with time due to the sun intensity. The fabrication of dye-sensitized solar cell does not need elaborate material and it is feasible and affordable and it will go a long way alleviating the cost incurred in power generation, supply, and consumption.

Keywords: **Dye-sensitized solar cell, fluted pumpkin leaf, mirror, module, voltage**

1 INTRODUCTION

In our present world, fast industrial development, economic development and rising energy utilization of the growing population, requires more energy in various forms. Since the amount of available energy from fossil fuel resources dwindles on daily basis, as well as environmental hazard associated with the usage, development of renewable energy technologies become imperative to meet the energy demand of the entire populationnow and in time to come. Renewable energy such as wind and ocean current are limited to some areas. However, solar energy is available to everyone during the day. It is a potential resource among the various renewable energy options (Ganguli and Singh, 2010). An opportunity should be grasped to build the most suitable environmental friendly photovoltaic power plant and welcome a better tomorrow. (Bhoye and Sharma, 2014)

Solar energy is the energy that is produced by the sun. This energy is in the form of solar radiation which travels to the earth through space in discrete packets of energy called photon (Microsoft Encarta Premium, 2009). This makes the production of solar electricity possible.

Solar energy can be converted directly to electrical energy by the use of photovoltaic cells and according to Omubo-Pepple (2013), the conversion is based on photovoltaic effect. When sunlight hits the photovoltaic cells, the photons of light excite the electrons in the cells and cause them to flow, thus generating electricity.

There are different types of solar cell based on its constituent. But so far, the single silicon crystal cell is the most commonly used, because of its high energy conversion efficiency as high as 25%, as stated by Lewis and Larry(2010). Theproblem with this solar cell is their high cost of production and installation(Boyo et al., 2012). A type of solar cell known as dye-sensitised solar cell (DSSC) is cheap to produce and does not need elaborate materials. Although its conversion efficiency is less than the best thin-film cells, in theory its price/performance ratio should be good enough to allow them to compete with fossil fuel electrical generation by achieving grid parity (Wikimedia, 2015). In fact, it has been shown that dye-sensitized solar cells are auspicious class of low cost and moderate efficiency solar cells.

Dye-sensitized solar cell (DSSC) was invented by Michael Gratzel and Brian O' Regan in 1991

(Wikimedia, 2015). The original Grätzel cell design comprises four major parts, which include: titanium dioxide (TiO_2) nanoparticle film, dye molecules, electrolyte and transparent conducting electrodes. The TiO_2 nanoparticle film makes available a large surface area for supporting dye molecules, typically ruthenium-based molecules, which are used as chromo pore to absorb sunlight in the visible region.

DSSC uses dye as sensitizers to convert solar energy into electrical energy. Electricity is generated when the dye is illuminated by solar radiation; then it flows to the semi-conductor surface. In this paper, dye-sensitized solar cells were made using natural dye extracted from fluted pumpkin leaf *(Telfairia occidentalis)*. Fluted Pumpkin is a tropical vine cultivated in West Africa as a leaf vegetable and for its edible seeds. It is commonly called "ugu" and indigenous to southern Nigeria. Fluted pumpkin can be found all year round, because it can be cultivated by irrigation in dry season. It is typically grown vertically on trestle-like structures; nevertheless, it can be allowed to spread flat on a field. Fluted pumpkin leaf has been evaluated chemically and found to contain (g/100 dry wt.) 30.5+2.5 crude protein,

3.0+0.15 crude lipid, 8.3+0.5 crude fibre and 8.4+0.5 total ash (Ladeji et al; 1994). The photo-responses of fluted pumpkin leaf have been studied alongside the effect of change in atmospheric temperature, when used to make a dye-sensitized solar module.

2 MATERIALS AND METHODS

2.1 Preparation of natural dye from fluted pumpkin leaf

The leaves were plucked and put in oven made in England by Gallenkamp, for 5 hours at 70^{0}C to dry up. A mortar and a pestle were used to grind the dried leaves and then sieved to obtain smaller particles. 200g of the sieved grounded leaves were wrapped with 14 pieces of filter paper and then placed in a soxhlet extractor made by Electromantle ME, shown in plate I, in batches of two. 500mL of 99.7% concentrated ethanol was poured into a round bottom of flask of the soxhlet extractor and the heater turned on at temperature of 75^{0}C for about 3 hours per batch. The extract which comprises ethanol and the dye was heated at 75^{0}C to obtain a mixture rich in dye in ratio 10: 1. The dye was collected in a sample bottle.

Plate 1: Electromantle ME Soxhlet extractor in WAFT Department Federal University of Technology Minna.

2.2 Preparation and assembling of the solar module

A cell is made of a mirror and a transparent glass of size 100 by 100mm. Thinner was used to remove the paint on the painted side of the mirrors in order to access the conductive silver coating .The pieces of mirrors and the transparent glass were washed with detergent and water; and rinsed with ethanol to enhance adhesion. A piece of aluminium foil cut out in form of a hollow rectangle was glued to each of the transparent glasses to make them conductive.

For the TiO_2 paste, 9mL of weak acid solution prepared by adding 0.1mL of acetic acid to 50mL of distilled water in a beaker; was poured on 6g of TiO_2 inside a ceramic mortal in 1ml increment with the use of pipette while grinding the titanium dioxide with a pestle to obtain smooth colloidal paste. (Khalil, 2011) The TiO_2 paste was uniformly

applied on the conductive side of the mirrors and allowed to dry for about 10 minutes; and then, inserted in an oven for 5 hours, at 130^0C. The TiO_2 coated glasses were brought out and allowed to cool gradually to room temperature. The dye solution was used to stain the TiO_2 coated glasses as shown in plate II and allowed to dry which form the anodes.

Plate II: The anodes formed by staining the TiO_2 coated glasses with natural dye

The other pairs of glasses were burnt on a candle such that the part of the glass with aluminium foil touches the yellow flame. The fume from candle contains carbon which form the cathodes shown in plate III.

Plate III: Cathodes formed by burning the aluminium foil coated transparent glasses on a candle flame.

Three drops of iodine were poured on the anodes and immediately, the cathodes were placed on them. Araldite and masking tape were used to seal the cells. The cells produced were connected in series and arranged on a plastic board to form a solar photovoltaic module

shown in plate IV

Plate; IV Solar photovoltaic   module consisting of nine
series connected solar cells

2.3 Measurement

An ALDA DT-830D digital multimeter and a mercury-in-glass thermometer were used to measure the voltage generated by the solar panel with a constant load connected to it and atmospheric temperature respectively, at different time of the day.

3. RESULTS AND DISCUSSION

The developed solar module (DSSC) was tested in the day, from 7am to 7pm for three days in an interval of 30minutes during raining season. Table 1 depicts the result of the measured voltage of the solar module at constant load and the atmospheric temperatures.

Table1: Measured voltage of the produced solar module and atmospheric temperatures for three days'

Time (Hour)	Day one		Day two		Day three	
	Voltage (mV)	Atmospheric Temperature(^{0}C)	Voltage (mV)	Atmospheric Temperature(^{0}C)	Voltage (mV)	Atmospheric Temperature(^{0}C)
7.00	270.00	27.00	85.00	26.00	11.00	23.00
7.30	290.00	28.00	87.00	27.00	12.00	25.00
8.00	320.00	28.00	85.00	27.00	13.00	26.00
8.30	320.00	29.00	86.00	27.00	13.00	26.00
9.00	300.00	28.00	82.00	27.00	13.00	26.00
9.30	310.00	30.00	81.00	28.00	13.00	24.00
10.00	330.00	29.00	81.00	26.00	12.00	24.00
10.30	340.00	30.00	77.00	27.00	11.00	25.00
11.00	332.00	29.00	80.00	27.00	12.00	25.00
11.30	304.00	29.00	58.00	26.00	11.00	25.00
12.00	250.00	28.00	52.00	27.00	11.00	25.00
12.30	210.00	29.00	50.00	27.00	11.00	25.00

From Table 1, the maximum output voltage obtained within the three days is 340mV at atmospheric temperature of 30^0C. This is higher than the voltage of 306mV realised by Khalil (2011) who used 84g of Yameni Henna dye in his work. More so, higher than 243mV gotten by Zijian

(2012) who used unquantified dye extract from raspberry in his work. However, the maximum voltage of 750mV that was realised in the work of Lee et al (2007) that worked on dye sensitized solar module using platinum as the counter electrode, is found to be higher than the one gotten in this work. The cell performance was affected by rainfall and cloudy weather in day two and three. The maximum voltage for day two and day three are 87mV and 13mV respectively. All these maximum values were obtained at the time of the day when the intensity of the sun was high. That is, high solar module performance is affiliated to high solar irradiance.

The maximum output voltage from the series-connected-cells in the solar panel was low compared to the expected voltage. Considering the fact that, each of the cells produced has a maximum open circuit voltage of 445mV. Consequently, the maximum open circuit voltage of the solar module consisting of nine cells is 4V. Actually, DSSCs produce their maximum voltage immediately after

production when illuminated by sufficient sunlight and afterwards the cell performance will be affected by weather change and wind if not perfectly sealed. Almost all the cells produced, stayed for about 17 hours (throughout the night) before they were connected in series to form the solar module. The sealants used were not sufficient to achieve a perfect seal and the aqueous iodine electrolyte in the cells got dried up a little bit by wind during that period. This in turn affected the electron cycle (Zijian, 2012), hence the voltage. There wer voltage drops across the internal resistance of the solar module, wire contacts, conducting wires and connectors such as the aluminium foil used as terminals of the cells and the silver coating on the conductive side of the mirror.

The variation of voltage from module with time and also with atmospheric temperature for the first, second and third day are shown in Figures 1, 2, 3, 4, 5and 6 respectively.
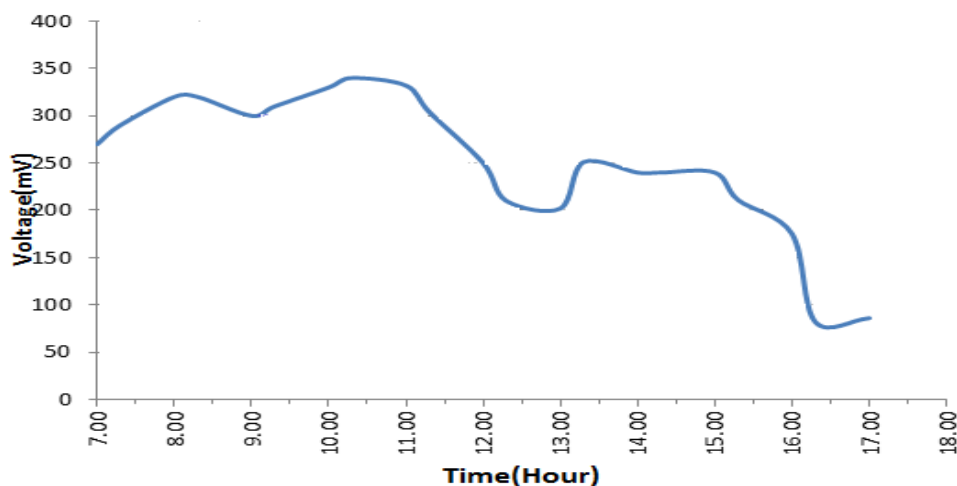
Figure 1: Variation of voltage with time for day one.
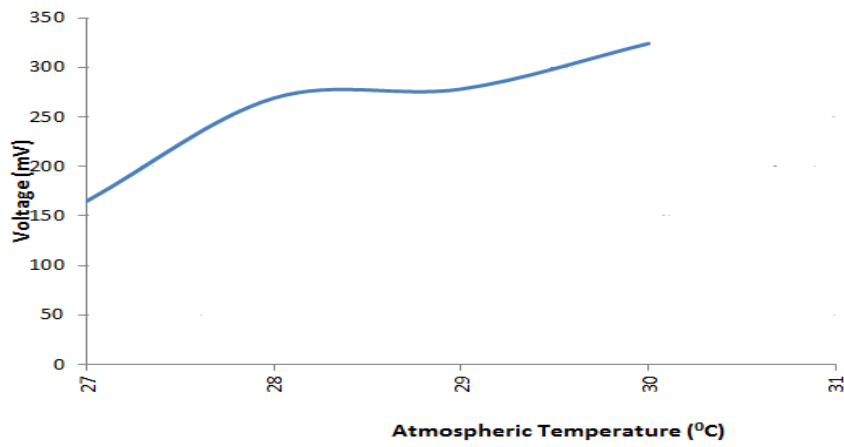
Figure 2: Variation of voltage with respect to atmospheric temperature for day one
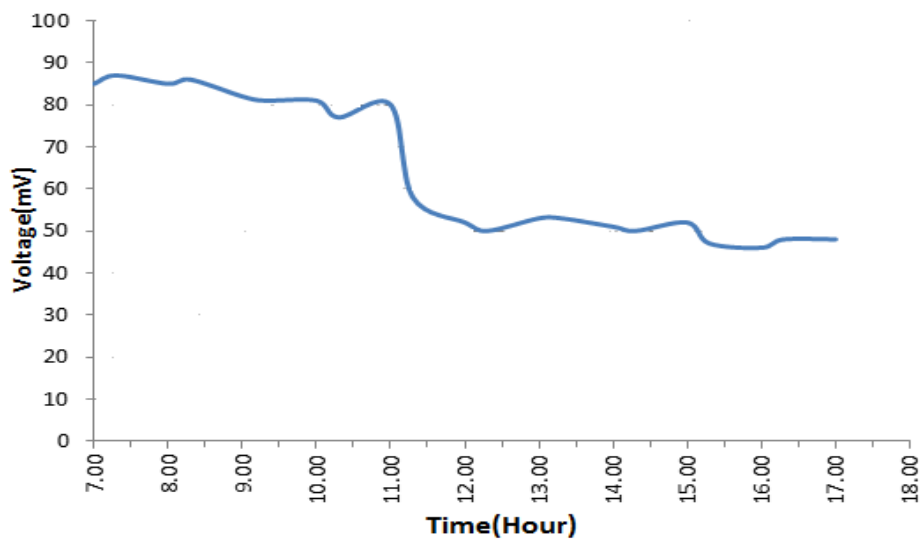
Figure 3: Variation of voltage with time for day two.
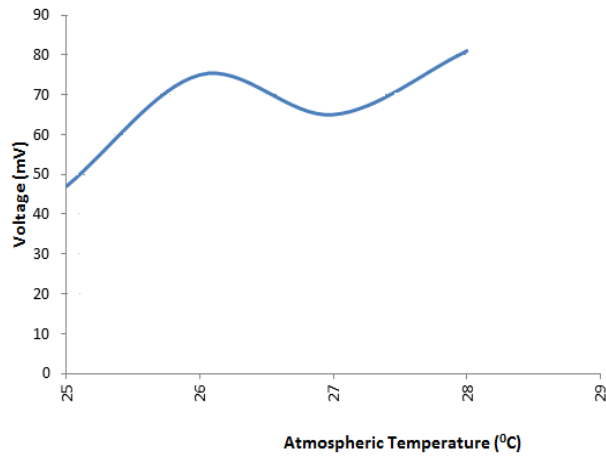
Figure 4: Variation of voltage with respect to atmospheric temperature for day two.
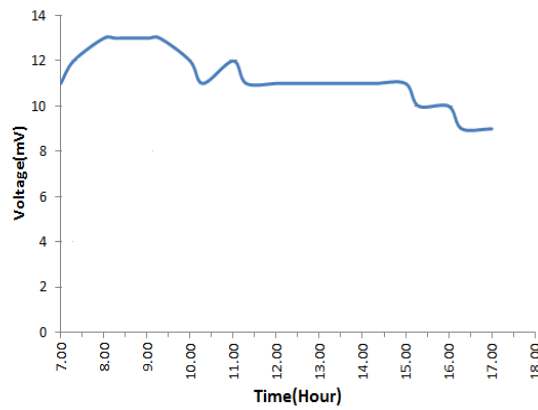
Figure 5: Variation of voltage with time for day three
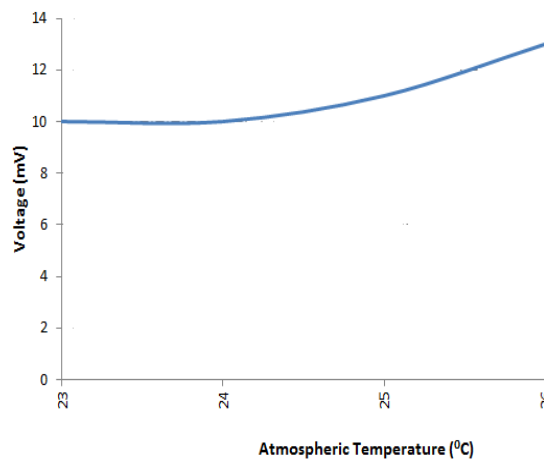
Figure 6: Variation of voltage with respect to atmospheric temperature for day three

.

From Figures 1, 3 and 5, it can be seen that voltage fluctuates with time. This is as a result of variation in solar irradiance during the day.

From Figures 2, 4, and 6, the voltage increased with increased atmospheric temperature. This is a clear indication that ambient temperature increases as solar irradiance increases.

4 CONCLUSIONS

The development of solar photovoltaic module, using dye extract from fluted pumpkin leaf as doping substance was successfully accomplished, showing the ways by which solar energy can be maximize, even as it is easy to get the materials around us. The fabrication of dye-sensitized solar cell does not need elaborate material and it is feasible and affordable.

The cost incurred in the production of the solar module was considerably low. This shows a possible way of replacing semiconductor materials for making solar cell. Although it has low conversion efficiency, yet it stands the chance of competing with fossil fuels because it is renewable and durable with no pollution. If more attention is given to the production of dye-sensitized solar cell, the research will go a long way alleviating the cost incurred from power generation, supply, and consumption.

REFERENCES

Bhoye, H., & Sharma, G. (2014). An analysis of one MW Photovoltaic Solar Power Plant Design. *International Journal of Advance Research in Electrical, Electronics and Instrumentation Engineering,*Volume 3 Issue1, pp6969-697

Boyo, A., Shitta, M., Oluwa, T., & Adeola, S. (2012). Bitter Leaf (Vernonia amygdalin) for Dye Sensitized Solar Cell. *Trends in Applied Sciences Research*,7(7) pp 558-564.

Ganguli, S., & Singh, J. (2010). Estimating the solar photovoltaic generation potential and possible plant capacity in Patiala. *International Journal of Applied Engineering Research, Dindigul*, Volume 1, No. 2 pp253-260.

Holladay, A & Redmond, WA. (2009). *Solar Energy.* Microsoft Encarta.

Khalil, E. J. (2011). *Dye Sensitized Solar Cells - Working Principles, Challenges and Opportunities.* (P. L. Kosyachenko, Ed.) Retrieved March 2, 2015, from InTech: http://www.intechopen.com/books/solar-cells-dye-sensitized-devices/dye-sensitized-solar-cells-working-principles-challenges-and-opportunities

Ladeji, O., Okoye, S., & Ojobe, T. (1995). *Chemical evaluation of the nutritive value of leaf of fluted pumpkin (Telferia occidentalis).*Food Chemistry*,53; 353-355.*

Lee, W .J, Lewis, F., & Larry, P. (2010). *Solar Cells and Thier Application* (2nd ed.). (F. Lewis, & P. Larry, Eds.) A John Wiley & Sons, INC.

Omubo-Pepple, V. (2013). Influence of meteorological parameter on the efficiency of photovoltaic module in some cities in the Niger Delta of Nigeria. *Journal of Asian Scientific Research, 3*(1), 107-133.

Wikimedia (2015). *Dye-sensitized solar cell*. Retrieved March 4, 2015, from Wikipedia Atom feed: http://en.wikipedia.org/wiki/Dye-sensitized_solar_cell

Wikipedia (2015). *Telfairia occidentalis*. Retrieved March 29, 2015, from Wikipedia Atom Feed: http://en.m.wikipedia.org/wiki/Telfairia_occidentalis

Zijain, C. X. (2012). *Characterization of the DyeSensitized Solar Cell*. B.Sc, Project Report submitted to Faculty of Worcester Polytechnic Institute.

QUALITY ASSURANCE OF HOLLOW SANDCRETE BLOCKS: A CASE STUDY OF HOLLOW SANDCRETE BLOCK INDUSTRIES IN MINNA, NIGER STATE, NIGERIA

[1]Tsado T.Y., [2]Auta S.M., [3]James O. and [4]Ahmed S. B.

[1,2,3]Department of civil engineering, School of Engineering and Engineering Technology

Federal University of Technology, Minna, [4]Work and Services Department, Federal University of Technology, Minna

Correspondence: Ty.tsdao@futminna.edu.ng +2348055215092.

ABSTRACT

This paper presents study into construction hollow sandcrete block quality assurance of the block industries in Minna, Niger State, Nigeria. Construction hollow sandcrete blocks are more widely used among other walling materials in Minna and Nigeria in general. However, there have been instances of construction failure due to the fact that the hollow sandcrete blocks used for the construction do not meet construction qualities in terms of material strength. Hence, the mean compressive and characteristic strengths, production and usage of these blocks need to be investigated. Laboratory, work study and field survey methods were used in this research. The Laboratory analyses of the construction sandcrete blocks were carried out on a total of sixteen (16) block producing industries randomly selected. One hundred and sixty (160) in number of six inches (6-inches) and nine inches (9-inches) blocks of dimensions 450 x 225 x 150m and 450 x 225 x 225mm respectively, obtained from the block industries were deployed to the laboratory and considered for water absorption and strength requirements. The water absorption value for 6-inches block were between 15.17 – 18.04% and that of 9-inches, 14.32 – 19.94% which are above 12% as recommended by Nigerian Industrial Standard (NIS) 87:2007. This was due to large volume of fines content. The mean compressive and characteristic strengths of these blocks in the range of 3-14days age, were between 0.45 – 62 N/mm^2 and 0.28 – 0.45N/mm^2 for 6-inches blocks and 0.99-0.62N/mm^2 and 0.29 – 0.42N/mm^2 for 9-inches block respectively. When these values are compared with the recommended standard minimum values for 6-inches of 2.5N/mm^2 and for 9-inches of 3.45N/mm^2 respectively, do not meet the required minimum strength. Therefore, these blocks are not fit to be used for construction purposes. Work study and field survey carried-out through questionnairing administered to the personnel in the sandcrete block production and usages, results reveal that 87% of block industries studied are owned and managed by non-professional and workers are inadequately educated, and so do not test these blocks to ensure standard practice in production. The mixed proportion was found to be between 1: 16-1: 18 as against 1:8 recommended by NIS 87:2007. 95% of the block-end users do not care to demand for strength requirements at the point of purchase. Professionals are recommended to own or manage the block industries and the relevant authorities to ensure quality control so that blocks produced can effectively be use as load bearing walling material and to avoid construction failures.

Keywords: *Construction, Hollow sandcrete block, Block industry, Walling material, Water absorption, strength, Quality*

1. INTRODUCTION

Hollow sandcrete blocks are block made of a mixture of cement and sand (fine aggregate) of mix ratio 1:8 with a varying percentage of water added to the mixture to be able to produce the specified standard (Jackson and Dhir, 1998; Hamza and Yusuf, 2011; NIS 87:2007; Vallenger, 1971). Hollow sandcrete blocks are rectangular in shape of sizes measuring 450mm x 225mm x 225mm with web thickness of 50mm regarded as 9-inches and 450mmx 225mm x 150mm with web thickness of 37.5mm regarded as 6-inches blocks respectively (Barry, 1969; NIS 87:2007). The 9-inches blocks are used as load bearing block wall while the 6-inches blocks are used as non-load bearing block walling material (NIS 87:2004).

Load bearing units must conform to building by-law as it participates mainly in transforming the actual load of the structure to the foundation. In this case the load bearing wall are those walls acting as a supports for the whole structure to transmit the weight to the ground surface underneath it for stability (Alutu and Oghenejobo, 2006; NIS 87:2000). For a long time in Nigeria, hollow sandcrete blocks are manufacture in many parts of the country without any reference to suit local building requirements or good quality work (Oyekan and Kamiyo, 2008).

Hollow sandcrete blocks are widely used in Nigeria, Ghana and virtually all African country as walling unit, and the quality of these blocks produced differs due to the different methods employed in the production and properties of the constituent materials. Over 90% of physical infrastructures in Nigeria are being constructed using sandcrete blocks making it a very important material in building construction worldwide (Aguwa, 2011; Anosike and Oyebade, 2012; Baidan and Tunlo,2004; Gooding and Thomas, 1995; Oyekan and Kamiyo, 2008)).

The hollow sandcrete blocks produced by the block industries in Nigeria, and Niger State, Minna in particular are below the standard resulting into construction failure (Tsado and Yewa, 2013). This may be due to various reasons of mix proportion and production process not carried out in accordance to the specification by the NIS 87:2007.

In the year 2000, and in an attempt to enhance the best materials and manufacturing practice, the Standard Organization of Nigeria (SON) prescribed compressive strength and water absorption properties standard required for different kind of sandcrete blocks (Alufsayo, 2013). Among the objectives of this Nigerian

Industrial Standard (NIS) document are to ensure that all block manufacturers meets a minimum specified standard, as well as to control the quality of blocks produced by these manufacturers. The Nigerian Industrial Standard (NIS) for sandcrete block is a standard reference document developed by the Standard Organization of Nigeria (SON) which prescribes the minimum requirement and uses of sandcrete blocks. These requirements include the quality of materials, the methods and procedure to employ for production and testing of the final products to ensure compliance to prescribed standard. The first standard for sandcrete block in Nigeria was developed in 2000 and known as NIS 87:2000..

In 2004, the document was reviewed and NIS 87:2004; Standard for Sandcrete blocks became the country's standard reference document for sandcrete block. The last review was done in 2007 and known as NIS 87:2007 which emerged as the latest standard reference document for sandcrete block production in Nigeria.

Abdullahi, (2005) investigated the strength characteristic of hollow sandcrete block in Bosso and Shiroro areas Minna, Nigeria. The result revealed that not all type of the fine aggregates used are suitable for block making. The compressive strength of the sandcrete blocks

were below standard as recommended NIS 87: 2000. The study suggested improvement on the selection of materials and curing.

Oyininuola and Olalusi, (2004) reported that a great number of buildings collapse weekly in the country, but did not receive public or official notice and some of those Collapsed building showed that their load bearing walls were not of adequate strength to withstand the applied load on them (Tsado and Yewa, 2013). Over 200 lives were lost in Nigeria due to building collapsed between 1974 and 2006 (Ewa and Ukpata, 2013)

The collapse of several buildings in Minna, the Talba Estate along Minna – Bida road in particular is partly attributed to the use of poor quality blocks in the construction (Tsado and Yewa, 2013). Figure I show hollow block wall failure (Tsado and Yewa, 2013). The authors did not carry-out quality assurance of the hollow blocks used for the construction to ascertain the quality standard of the blocks used for the construction. Frequent collapse of buildings globally calls for proper quality control measures into production of sandcrete blocks especially hollow blocks as walling materials.

Fig. I. Hollow Block Wall Failure

This research investigate among block manufactures in Minna and metropolis area of Niger State the level of conformity to the quality assurance and standard specification, evaluate the production process employed in the production of hollow sandcrete blocks.. The water absorption properties and the compressive strength of various hollow sandcrete blocks with respect to their mode of manufacture were tested using compressive strength machine to crush the block samples in accordance to BS 2028. Secondly, the compressive strength of various sandcrete blocks was compared to NIS 87: 2004 and 2007, so as to assess the quality of sandcrete blocks produced in Minna and metropolis are of, Niger State, Nigeria.

2. METHODOLOGY

Laboratory experiments, work study and field survey were adopted to carry out this study. The field survey involves collection of hollow sandcrete blocks specimen from randomly selected block manufacturing industries in Minna and its environs area of Niger State for laboratory test. Minna and its environs were considered due to large volume of block manufacturing industries and being the capital of Niger State large volume of dwellings are required which involve the use of hollow sandcrete block. The study case area was zone into four (Maikunkele, Chanchaga, Kpankungu and Maitunbi). The water absorption capacity and compressive strength tests were the properties tested on the blocks sample collected. The singular reason being that water absorption percentage and compressive strength are the two major characteristic requirements specified for testing and verifying the quality of sandcrete block apart from appearance and dimension (NIS 87:2007) .

Six inches (6-inches) of 450 x 225 x 150mm and nine inches (9-inches) of 450 x 225x 225mm block sizes were obtained and utilized in evaluating the block sample in accordance to NIS: 87:2004 and 2007. Ten pieces of hollow sandcrete blocks were sampled randomly per block industry among a total of sixteen (16) block producing industries randomly selected. One hundred and sixty (160) in number of six inches (6-inches) and nine inches (9-inches) blocks of dimensions 450 x 225 x 225mm and 450 x 225 x 150m obtained from

the block industries were taken to the laboratory and considered for quality assurance test in terms of water absorption and strength requirement parameters

The date of cast and age of the block samples obtained were within 3 -14days. The main objective of sampling the blocks was to evaluate its quality and compare the results obtained with the recommended minimum standard specification for high quality and performance of sandcrete block by the NIS 87:2007.

Work study and field survey were carried out by direct observation of the techniques employed among block manufactures at the selected sampled industry sites in the production process. Site operation observation includes the batching method and mix ration, placing, compaction, and off course curing and personnel. A well structure questionnaire was prepared and administered to these selected block manufacturing industries, individuals and organizations that use such blocks for construction works to elicit further information on their operation in order to give credibility to some of the observation made during site visits. The well structured questionnaire administered covers areas such as: Experience; Personnel Qualification; Number of Operating team; Management team; Mix proportion; Test of Materials and Age of Blocks.

The block-molding machine generally in use by the sample industries is the Roascometta type, which vibrates the block during filling and compaction, and one block is produced at a time.

Water Absorption Capacity

Each specimen of the deployed block sample was first weigh in a dry state to obtain its dry mass (M_1) and then fully immersed in water for 24hours when the samples were completely wetted, they were removed and the trace of water were wipe off with a damp cloth and then weigh again to obtain wet weight (M_2). This procedure was repeated on other samples and the water absorption capacity was computed from equations 1:

$$\text{Water Absorption}\,(\%) = \frac{M_2 - M_1}{M_1}\ \text{x}\ 100 \qquad (1)$$

Where:

M_1 = Weight of dry block before immersion and

M_2 = Weight of wet block after immersion

The average of the results obtained was regarded as the water absorption of the block and shall not exceed 12% (NIS 583:2007).

Compressive Strength

This test was conducted in accordance to specification given in the NIS 87:2000 code for the production of hollow sandcrete blocks, The

compressive strength of the sandcrete blocks was determined through the crushing of the hollow sandcrete block, this was carried out on all the forty (40) samples of label blocks produced from different industries. The blocks were weighed and a wooden plank was placed underneath the block and carefully placed between the center of the plates of the crushing machine, another wooden plank was placed on top of the block. .This is to enable uniform transfer of the load around the surface of the block. The machine was then switched on and operated to crush the block. During crushing, the machine pointer rose gradually until it drops indicating failure. The reading at this point was noted and recorded. The compressive strength in N/mm^2 of each block was then calculated from the equation 2:

$$\text{Compressive Strength} = \frac{\text{Maximum load at failure(N)}}{\text{Cross sectional Area (mm}^2)} \quad (2)$$

The average results obtained was taken as the crushing strength of the blocks and shall not be less than 3.45N/mm^2 for load bearing hollow sandcrete blocks and 2.5N/mm^2 for non-load bearing hollow sandcrete blocks produced mechanically (NIS 87:2007).

3. RESULTS AND DISCUSSIONS

Water Absorption Capacity

Tables 1 presents water absorption capacity of all the specimens collected from various commercial hollow block manufacturing industries as determine using the relationship, and Figure 1 shows the relationship between the water absorption rate of the hollow sandcrete blocks rate and the sample hollow sandcrete block industries.

Table 1: Mean Values for Water Absorption of all Specimens

Industry	6" Average Absorption capacity (%)	9"Average Absorption capacity (%)	Overall mean Absorption capacity (%)
Maikunkele	18.04	19.94	
Chanchaga	15.78	16.87	
Kpankungu	16.77	16.16	16.63
Maitunbi	15.17	14.32	
Average Absorption capacity	16.44	16.82	
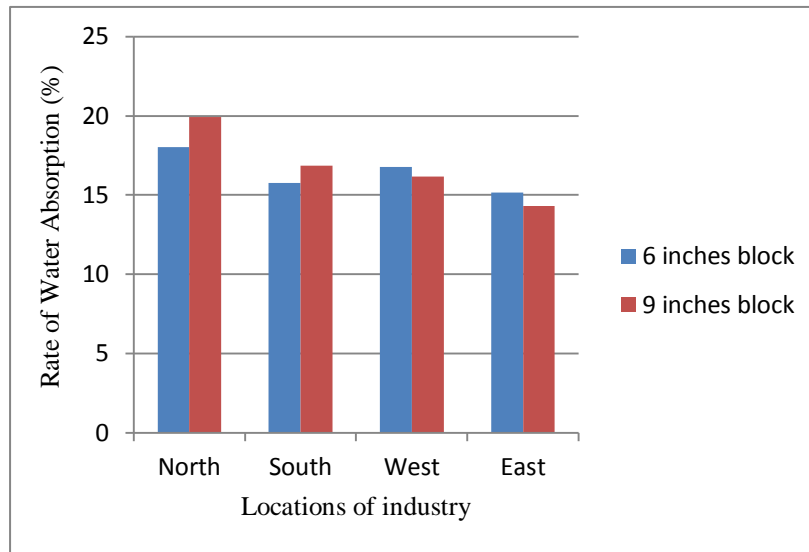
Fig 1: Mean Values for Water Absorption of all Specimens Chart.

From Table 1 and Figure 1 the water absorption capacity values of 6-inches hollow sandcrete block obtained from the four sample zones area of the case study are in the following order with Maikunkele having the highest vale follow by Kpankungu, Chanchaga and Maitunbi (18.04, 16.77, 15.78 and 15.17%) respective . For 9-inches block the order are Maikunkele, Chanchaga, Kpankungu and Maitunbi (19.94, 16.87, 16.16 and 14.32%) respectively. The water absorption capacities value obtained from all the blocks (6- and 9-inches) are above the maximum specified vale of 12% by NIS: 87:2007. The reason for this high absorption is due to high percentages of fines.

Compressive Strength of 6- and 9-inches Hollow Sandcrete Block

Tables 2 and 3 shows the compressive strength of the 6- and 9-inches blocks respectively.

Table 2: Compressive Strength of 6-inches Hollow Sandcrete Block

Sample No	Area of Study	Mean Strength (N/mm^2)	Characteristic Mean Strength (N/mm^2)
A-6	Maikukele	0.62	0.45
B-6	Chanchaga	0.45	0.28
C-6	Kpankungu	0.50	0.40
D-6	Maitumbi	0.49	0.41

Table 3: Compressive Strength of 9-inches Hollow Sandcrete Block

Sample No	Area of Study	Mean Strength (N/mm^2)	Characteristic Mean Strength (N/mm^2)
A-9	Maikukele	0.37	0.29
B-9	Chanchaga	0.39	0.33
C-9	Kpankungu	0.65	0.42
D-9	Maitumbi	0.43	0.35

The Compressive Strength of both 6"and 9" blocks are presented in Tables 1 and 2. From Table 1 it can be observed that the 6-inches block has a mean strength of between 0.45 – 0.62N/mm^2 with characteristic mean strength of between of 0.28 - 0.45N/mm^2. The Sample from Maikunkele area or zone has the highest mean strength value of 0.65N/mm^2, while that of Chinchaga has the lowest value of .45N/mm^2, and also Maikunkele has the highest characteristic mean strength value of 0.45N/mm$^2.$while Chinchaga has the lowest value of 28N/mm^2

Similarly, from Table 2, the 9-inches block has a mean strength value of between 0.39 – 0.65N/mm^2

and characteristic mean strength of between 0.29 - 0.42N/mm^2.The highest mean strength and the characteristic mean strength values of 0.65N/mm^{2}and 0.42N/mm^{2}were from Kpankungu The lowest mean strength and characteristic mean strength were from Maikunkele with the values of 0.37N/mm^2 and 0.29N/mm^{2}respectively.. These when compared with the recommended standard minimum values by the NIS 87:2007 of 2.5N/mm^2 for non–load bearing blocks (6-inches) and 3.45N/mm^2 minimum for load bearing (9-inches) blocks reveals that the hollow sandcrete block from the sample industries did not meet the required minimum strength. Therefore, are not fit to be used for the construction purposes.

2.1 Work study and Field Survey

Tables 4 and 5 presents observations and the responses from the hollow block manufacturing industries and construction companies and /individuals that use these blocks for constructions purpose

Table 4: Response from Block Industries

S/No	Qualified Personnel	Operating Team	Test of materials	Mix Ratio	9-inches Block per bag	6-inches Block per bag	Damage block
1	No	5	No	1:16	40	62	R
2	No	10	No	1:16	42	64	R
3	No	9	No	1:14	45	60	R
4	No	10	No	1:16	43	66	S
5	No	5	No	1:18	44	64	R
6	No	10	No	1:14	45	60	S
7	No	13	No	1:18	40	66	S
8	No	5	No	1:18	43	66	R
9	No	9	No	1:16	42	66	R
10	No	10	No	1:16	40	62	R
11	No	13	No	1:16	44	64	R
12	No	10	No	1:18	45	64	R
13	No	5	No	1:16	45	64	S
14	No	17	No	1:14	42	60	R
15	Yes	15	No	1:16	45	62	R
16	No	5	No	1:18	46	64	R
17	No	8	No	1:18	44	66	R
18	No	10	No	1:18	45	66	R
19	Yes	14	No	1:18	44	66	R
20	No	10	No	1:18	43	64	R
21	No	5	No	1:16	40	62	R
22	No	13	No	1:16	40	64	S
23	Yes	9	No	1:18	41	66	R

| 24 | No | 5 | No | 1:18 | 44 | 66 | R |

Table 5: Response from Construction Companies and Individuals

S/No	Location	Area of purchase	Testing of block	Damage block (Average 200)	Demand for Age	Age
1	G/Kwanu	Kpankungu	No	5	No	-
2	G/kwanu	Kpankungu	No	4	No	-
3	G/kwanu	Kpankungu	No	3	No	-
4	G/Kwanu	W/by pass	No	6	Yes	7
5	G/Mangoro	Chanchaga	No	5	No	-
6	G/Mangoro	W/by pass	Yes	2	No	-
7	G/Mangoro	W/by pass	No	4	No	-
8	Gurara	W/by pass	No	7	No	-
9	Gurara	E/by pass	No	4	No	-
10	Gurara	Maikukele	No	3	No	-
11	Gurara	Maitumbi	No	2	No	-
12	Fadukpe	W/by pass	No	5	Yes	7
13	Fadukpe	W/by pass	No	6	No	-
14	Fadukpe	E/by pass	No	3	No	-
15	Fadukpe	Maikunkele	No	4	No	-
16	Sauka	W/by pass	No	8	No	-
17	Sauka	E/by pass	No	3	No	-
18	Sauka	W/by pass	No	4	No	-
19	Sauka	Kpnakungu	No	6	Yes	14
20	Chachaga	Chanchaga	Yes	4	No	-
21	Chachaga	Chanchaga	No	4	No	-
22	Chachaga	W/by pass	No	5	No	-
23	Chachaga	E/by pass	No	7	No	-

24	Tuga	W/by pass	No	8	No	-
25	Tuga	E/by pass	Yes	4	Yes	7
26	Kwaso	W/by pass	No	4	Yes	3
27	Kwaso	E/by pass	No	6	No	-
28	Kwaso	W/by pass	No	3	No	-
29	Kwaso	Chanchaga	No	3	Yes	14
30	Bosso	E/by pass	No	3	No	-
31	Bosso	W/by pass	No	7	No	-
32	Bosso	W/by pass	No	6	No	-
33	Maikunkele	W/by pass	No	5	No	-
34	Maikunkele	E/by pass	No	5	Yes	7
35	Maikunkele	W/by pass	No	3	No	-
36	Maikunkele	Kpankungu	Yes	4	No	-
37	Tayi	E/by pass	No	8	No	-
38	Tayi	W/by pass	No	10	No	-
39	Tayi	Maitumbi	No	4	No	-
40	Tayi	W/by pass	No	5	No	-
41	Maitumbi	Maitumbi	No	7	No	-
42	Maitumbi	Maitumbi	No	4	No	-
43	Maitumbi	W/by pass	No	3	No	-
44	Maitumbi	Kpankungu	No	4	Yes	3
45	D/Kura	Chanchaga	No	10	No	-
46	D/Kura	Maitumbi	No	10	No	-
47	D/Kura	W/by pass	No	7	No	-
48	Shango	Chanchaga	No	9	No	-
49	Shango	W/by pass	No	8	No	-
50	Shango	W/by pass	No	4	No	-

Moulding method

It was observed that all the four manufacturing industry visited uses vibrating machine of Roascometta type to compact and produce their blocks

Batching method

Batching by volume with the use of the wheel barrow was used in almost of the industries visited to measure the sand (fine aggregate) to an extent referred to as full.

Mix ratio

During the field survey it was observed that specified standards mix ratio of 1:8 cement sand proportion and water cement ratio of 0.6 to achieve the minimum compressive strength value of 2.5N/mm² for non-load bearing or 3.5N/mm²for load bearing walls (NIS 87: 2007) are being undermined by the manufacturers. Majority of the block industries investigated used a ratio of between 1:16 to 1:18 to produced 42-45 number of 450mm x 225mm x 225mm Blocks and 64-70 number of (450mm x225mm x150mm) blocks respectively. A bag of cement and a wheel barrow full of sand is equivalent to three head (3) pan and eight (8) head pan respectively. These result to an average mix proportion of 1:18 by Volume used by most block industries.

Mixing method

It was observed that manual mixing with the help of shovel is used to mix the fine aggregate and cement in all the industries visited. .

Addition of water

In all the industries visited there was no specific volume of water for mixing, but was done at the discretion of the operator depending on the moisture condition of the sand. Water is added arbitrarily to make a paste for the production of the block. The type of water use across the study area ranges from Pipe bone and Borehole water free from impurities' and some well stream water which may contain some impurities (Ewa and Ukpata, 2013).

Curing method and duration

The blocks were observed to be cured by spraying method twice daily for just two to three days which is against the specified 7-day curing (NIS 87: 2007). The blocks are usually left in the open air.

Quality Assurance

There is no quality assurance as it was observed that the manufacturers do not carry out any test on finished blocks before stacking. And poor quality of blocks causes cracks in the walls of buildings which will eventually result to building structural failure or worse still building collapse as is being experienced in Nigeria over the years (Anosike and Oyebade 2011).

Personnel

Personnel used in most of the block industries are known professional. Majority of the Managers, operators and labourers are either secondary leavers or those that do not attend School at all.

Cement

The cement used is whatever brand is available in the market, while the sand used are sharp and plaster sand.

At the backdrop of the forgoing, about 5-10 blocks out of an average of 200blocks are usually lost either during delivery or in the processes of production. The damage blocks are in most Industries re-used. The industries are not organized as a body and individually do not organized any training for their staff. Prices of the blocks are fixed at individual discretion. The Organizations and Individuals that used the blocks do not necessary purchase the blocks from the nearby block industries. The damage blocks of a maximum of 8 blocks from an average of 200blocks on site are used as filling materials and those damage during delivery are returned and replaced. The construction companies and individual who used the blocks do not care to test the blocks before usage. Only a few do care to ask of the age of the blocks before even buying. From Tables 4 and 5, 87% of block industries studied are owned and managed by non-professional and workers are inadequately educated,

and so do not test these blocks to ensure standard practice in production. The mixed proportion was found to be between 1:16-1:18 as against 1:8 recommended by NIS`:587:2007. 95% of the block-end users do not care in demand for strength requirements at the point of purchase.

4. CONCLUSION AND RECOMMENDATION

4.1 Conclusions

The water absorption capacities value obtained from all the blocks (6- and 9-inches) were above the maximum specified vale of 12% by NIS: 87:2007. The reason for this high absorption is due to high percentages of fines, and this results into low compressive strength of the blocks.. The maximum Characteristic strength of the sandcrete block tested was $0.45N/mm^2$ for the load bearing blocks and $0.53N/mm^2$ for the non-load bearing blocks. This is far below the minimum required strength of $3.45N/mm^2$ and $2.5N/mm^2$ for the bearing and no bearing blocks respectively as specified by NIS 78:2007. The mix proportion used is as high as 1:18 in the production of the blocks. The number of 9-inches and 6-inches blocks produced from a bag of cement is as high as 45blocks and 70blocks respectively. There is lack of constant monitory of the block industries by the appropriate organisation. The block industries produces blocks without carrying out any test and the users also buy without testing before usage or demand for a test result. The

management of the production of the blocks seems to be left in the hand of quacks that are less educated in the blocks production. The blocks produced are not properly cured before selling to buyers and end-users. The damaged blocks are usually re-cycled or sold by the block industries and in most cases used as filling material by the users.

4.2 Recommendations

Based on the assessment carried out on the sandcrete produced, there is an urgent need for the authorities (Standard Organization of Nigeria (SON), Nigeria Society of Engineers (NSE) and Council for the Regulation of Engineering in Nigeria (COREN) concerned to monitor the block industries. Block industries should employ the services of professionals. The industries should organize training for their staff from time to time. Construction Companies and individuals who use the blocks should also ensure that they buy matured blocks or use the services of professionals. They should also test or demand the test result of the blocks before buying.

ACKNOWLEDGEMENTS

REFERENCE

Abdullahi, M. (2005). Compressive Strength of Sandcrete Blocks in Bosso and Shiroro Area of Minna, Niger State, Nigeria. *AU Journal of Technology*, 9(2), 126-132.

Aguwa J.I. (2010). Performance of Laterite-Cement Blocks as Walling Units in Relation to Sandcrete Blocks, *Leonardo Electronic Journal of Practices and Technologies* 16, 190-197.

Aguwa J.I. and Tsado T.Y. (2011). Effect of Mixing Water Content on the Compressive Strength of Laterite Cement Blocks as Walling Units in Buildings. *Environmental Technology and Science Journal (ETSJ),* 4(1), 60-67.

Alutu O.E. and Oghenejobo A.E. (2006). Strength, durability and cost effectiveness of Cement-Stabilized laterite hollow blocks, *Journal of Engineering Geology and Hydrogeolog.* 39(1), 65-72

Anosike M.N. and Oyebade A.A. (2012). Sandcrete Blocks and Quality Management in Nigeria Building Industries, *Journal of Engineering, Project and Production Management*, 2(1), 37-46.

Baidan B.K, and Tuuli M. M. (2004). Impact of Quality Control Practice in Sandcrete Blocks Production, *Journal of Architectural Engineering*, 10(20), 35-46.

British Standard Institution, BS 2028 (1970): Precast concrete blocks. Her majesty Stationary office. London, England.

Ewa D. E. and Ukpata J. O. (2013). Investigation of the compressive strengths of commercial sandcrete blocks in Calabar Nigeria. *International Journal of Engineering and Technology,* 3 (4), 477-482.

Gooding D. E. and Thomas T. H. (1995). The potential of cement stabilized building Blocks as an urban building material in developing countries. Working Paper No. 44. Development Technology Unit. University of Warwick.

Hamza A. A and Yusuf S. (2011): Comparing the compressive strength of six and nine inches hand moulded sandcrete block. *Journal of Engineering and Applied Sciences.* 3(4), 64-66

Jackson N. and Dhir R. K, (1998), Civil Engineering Material, Macmillan Education Ltd, Hong Kong.

Nigerian Industrial Standard (NIS 87: 2000). Standards for Sandcrete Blocks Approved by Standard Organization of Nigeria (SON), Lagos, Nigeria

Nigerian Industrial Standard (NIS 87: 2004). Standards for Sandcrete Blocks Approved by Standard Organization of Nigeria (SON), Lagos, Nigeria

Nigerian Industrial Standard (NIS 87: 2007). Standards for Sandcrete Blocks Approved by Standard Organization of Nigeria (SON). Lagos, Nigeria

Okpalla D. C. and Ihaza J. O. (1987). Quality of Sandcrete blocks produced in Benin City, Proceedings of the first UniBen Conference on Engineering and Technological Developments. University of Benin, Nigeria.

Olufsayo A. A. (2013). The strength properties of Sandcrete blocks in Ado-Ekiti, Akure and Ile-Ife, Nigeria. *International Journal of Engineering Science Invention.* 2, 25-34

Oyekan G. L. and Kamiyo O. M. (2008). Effect of Nigeria Rice Husk-Ash on some Engineering properties of Sandcrete Blocks, *Research Journal of Applied Sciences*, 3 (5), 345-351.

Oyetola E. B. and Abdullahi M. (2006). The use of Rice Husk Ash in low-cost Sandcrete block production. *Leonardo Electronic Journal of practices and Technologies.*

Oyininuola G. M. and Olalusi O. O. (2004). Assessment of building failure in Nigeria. Lagos and Ibadan Case Study. *African Journal of Science and Technology . Science and Engineering Series,* P: 75-78.

Tsado T.Y. and Yewa M. (2013). An Investigation into Building Structure Failure – Management Perspective: A Case Study of Talba Housing Estate, Mina .Niger State, Nigeria, Proceedings of .3rd Binomial Engineering Conference, School of Engineering and Engi8neering Technology, Federal University of Technology, Minna, Niger State. 508- 514

Vallenger (1971). Construction Industry Hand Book. Medical and Technical Publishing Co. Limited, Aylesbury, PP.45

AN IMPROVED GSM TECHNOLOGY-BASED MICROCONTROLLER MULTI-SENSOR HOME SECURITY AND MONITORING SYSTEM

S. S. Oyewobi, M. Okwori*, E. U. Mpkuma, W. M. Audu

Department of Telecommunication Engineering, Federal University of Technology, Minna, Niger

*michaelowkori@futminna.edu.ng, 08032903629

ABSTRACT

With increasing rate of crime all over the world, and with no pointer to this rate of crime abating anytime soon, home security has now become a major concern. Therefore most people; rich or poor are taking measures from highly sophisticated to very crude methods to prevent intrusion. This work presents a GSM technology-based home security and monitoring system. However, unlike the traditional magnetic switch alarms equipped on doors and windows, this system has incorporated a fire detector, a motion sensor and a moisture (rainfall) sensor. On any attempt of a break in, rainfall or possible smoke or fire a short message service (SMS) is sent to the house owner. The system is built using a programmed microcontroller interfaced with mobile phone (NOKIA 1209) such that the three major buttons of the mobile phone are switched at intervals to send a message to the owner of the house anytime there is an intruder, rainfall or fire accident. The system was tested and it worked on attempt of intrusion, rainfall (water) and smoke.

Keywords: *GSM, SMS, Sensor, Microcontroller, Mobile phone, Intrusion.*

1. INTRODUCTION

Security has always been an unavoidable part of the human lives right from the olden days down to our contemporary world. However security measures taken by Man has evolved over the Ages, from the use of animals like dogs, parrots, and human beings; padlocks, and also alarm systems to highly sophisticated unmanned security systems as we have them today. In the same vein, the methods as well as the amount of intelligence required to achieve the desired result has also changed from the olden days to the present day. Modern day security ranges from motion detection sensor which can be used for door control and to check intrusion, moisture detecting sensor which can be used to detect high degree of moisture or rain from getting into the home to fire sensor which can be used to detect fire accidents when it senses abnormal rise in temperature in the house or even smoke (Mike, 2012).

Communication is a very important aspect of human life. With advances in technology, smart homes now employ the use of communication systems to provide enhanced and efficient security measures to homes. These smart homes have the capability of allowing the home owner control devices with a single system that could either be local or remote (Raghavendran, 2011; Rosslin and Tai-hoon, 2010).

In this work, modern day security techniques and advancements in communication technology have been explored to build an automated security system capable of detecting intrusion, detecting fire outbreaks and also detecting rainfall in the protected building and reporting same through a short message to a mobile phone that will alert the appropriate authorities to take preventive and corrective measures. The rest of work is presented as follows, section two presents the design and implementation, and section three highlights the testing and results while section four concludes the work.

2. DESIGN AND IMPLEMENTATION

The design is made up of three major blocks, the power supply, the sensing section and the Microcontroller/Communication section. Each of these sections is tasked with functions that contribute to the performance of the entire unit. The block diagram of the

home security and monitoring system showing the different aspect of the design is presented in Figure 1.
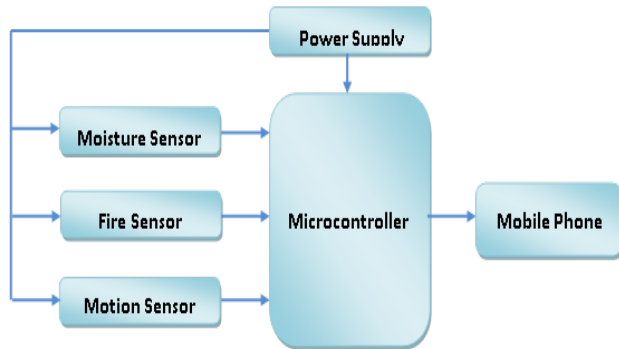
Fig.1: Block Diagram of the Home Security System

2.1. Power Supply Unit

Most electronic devices and circuits require a direct current (DC) source for their proper operation, and a voltage regulator to fix the voltage and make it constant for the load. In line with this principle, the power supply unit in this work was designed to include the following listed subcomponents to achieve a smooth DC for the operation of the system: A step down transformer, a bridge rectifier, filtering capacitors, and voltage regulators as shown in Figure 2.
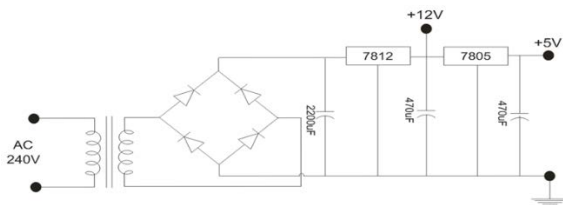
Fig. 2: Power supply unit

Design of Sensing Units

Three separate sensing units were designed in this work, one for preventing intrusion and the other two for monitoring the home. A temperature sensor was used in detecting the accidental occurrence of fire and it works on the principle that any fire accident will immediately increase the temperature of the surrounding environment. A laser-light dependent resistor sensor was used for motion sensing to detect movement in restricted areas. A

printed circuit board together with ferric acid was used to make the rainfall sensor for sensing moisture in the home; the preceding sessions explain the design of the different sensing units in this work in details.

Design of Sensing Units

The sensing unit forfire outbreak detection was effectively designed by the use of a thermistor. A thermistor works on the principle of variance of resistance of some materials with temperature. In this work, a Negative-Temperature-Coefficient (NTC) thermistor was used. Its resistance reduces with decrease in temperature, however to set the analog output of the thermistor to a logic output needed for proper operation of the system, a LM555 operational amplifier was used. The circuit diagram of the fire sensing unit is shown in Figure 3.
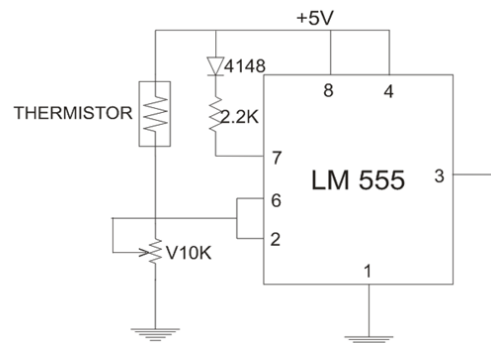
Fig.3:Circuit Diagram Of fire Sensor

Design of Laser Based Motion Sensor

The motion sensing unit was designed by the use of a laser light dependent resistor (LDR). The LDR was connected to a 555 timer that was neither a monostable nor astable connection, because no timing or frequency is required but intrusion detection. The LM 555 is designed to deliver a logic output any time the PIN 2 and 6 is HIGH or LOW, the IN4148 diode is to prevent back flow of current to PIN 7, the variable resistor was connected to set the sensitivity of the LDR, and PIN 6 was loop with

PIN 2 to make its output remain HIGH as long as the PIN 2 is HIGH and LOW immediately PIN 2 goes LOW, PIN 2 needs about 2V to be HIGH while the voltage produced at the output is 5V which was interfaced with the microcontroller for monitoring (Fire Sensor, 2010). The circuit of the motion sensor is shown in Figure 4.
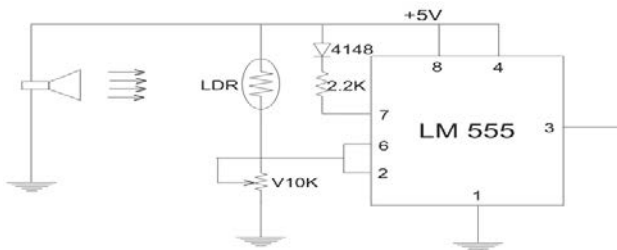
Fig.4:Circuit Diagram Of The Motion Sensor

Design of Moisture Sensor

The moisture sensor was designed by the use of a printed circuit board which was achieved by the use of a software called the printed circuit board wizard (PCB wizard) and ferric acid. The PCB was connected to an LM555 timer that is neither in monostable nor astable connection because no timing or frequencies is required, The LM555 is configured to deliver a logic output any time the PIN 2 and 6 is HIGH or LOW, the IN4148 diode is to prevent back flow of current to PIN 7, The variable resistor was connected to set the sensitivity of the printed circuit board (PCB). The PCB has two terminals one connected to the VCC while the other terminal is connected to the LM555 timer, whenever water touches the board it bridges and that will send an output signal to the LM555 timer which is connected to the microcontroller (Motion Sensor, 2010). Figure 5 is the circuit diagram of the moisture sensing unit.
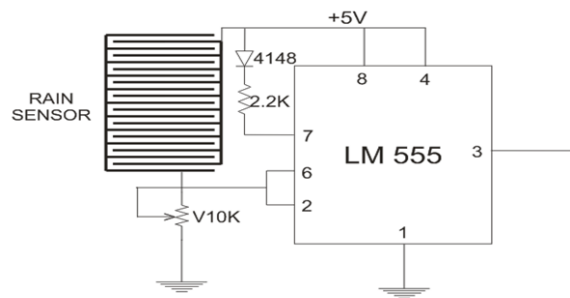
Fig.5:Circuit Diagram of the Moisture (rainfall) Sensor

Design of Output Drivers

Three 12 volts DC relays were used to control the three basic buttons of the mobile phone (NOKIA1209) used; these are the power button, the select button and the scroll down button. The relay is an electromechanical device that deals with electronic and mechanical devices, it has 5 terminals, and terminals 1 and 2 are the coil of the relay while terminals 3, 4, and 5 are Normally Closed (NC), Common (C) and Normally Opened (NC) respectively. If current flows through the coil, the Common will disconnect from the Normally closed (NC) to the Normally opened (NC) and if the current should stops flowing the Common (C) will go back to the Normally closed (NC).

Figure 6 is the circuit diagram of the relay switching circuit used in this design, for this work also, two terminals of the mobile phone were used, one terminal was connected to the Common while the second terminal was connected to the Normally Open (NO) of the relay, when current flows through the coil from the microcontroller, the Common (C) will disconnect from the Normally closed (NC) to the Normally Opened (NO) thereby pressing the required button of the mobile phone (Mehta and Mehta, 2006).
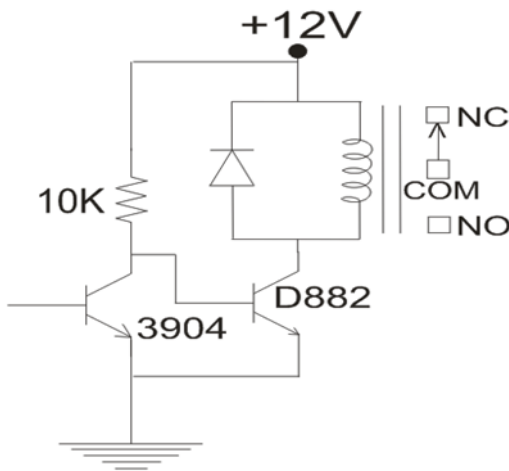
Fig.6: Relay Switching Circuit For The mobile phone

Microcontroller Unit

A microcontroller is a single chip that contains the processor (the CPU), non-volatile memory for the program (ROM or flash), volatile memory for input and output (RAM), a clock and an I/O control unit. This unit acts as the control or brain of the entire system and is responsible for interpreting the messages sent from the sensing unit and sending the appropriate message to the mobile phone. The microprocessor used for this work is **AT89S52** and it belongs to the **8051** family.

89S52 Microcontroller

The **AT89S52** is a low-power, high-performance **CMOS 8-bit** microcontroller with **8K** bytes of in-system programmable flash memory. The device is manufactured using Atmel's high-density nonvolatile memory technology and is compatible with the industry-standard **8051** instruction set and pinout. The on-chip Flash allows the program memory to be reprogrammed in-system or by a conventional nonvolatile memory programmer. By combining a versatile **8-bit** CPU with in-system programmable Flash on a monolithic chip, the Atmel **AT89S52** is a powerful microcontroller, which provides a highly flexible and cost-effective solution to many, embedded control applications.

The **AT89S52** shown in figure 7 provides the following standard features: **8K bytes** of Flash, **256** bytes of RAM, **32 I/O** lines, Watchdog timer, two data pointers, three **16-bit** timer/counters, a six-vector two-level interrupt architecture, a full duplex serial port, on-chip oscillator, and clock circuitry. In addition, the **AT89S52** is designed with static logic for operation down to zero frequency and supports two software selectable power saving modes. The Idle Mode stops the CPU while allowing the RAM, timer/counters, serial port, and interrupt system to continue functioning. The Power-down mode saves the RAM contents but freezes the oscillator, disabling all other chip functions until the next interrupt (Muhammad *et al*, 2005).

For this work, the **AT89S52** microcontroller was interfaced with Nokia (1209) GSM mobile phone to decode the received message and do the required action. The protocol used for the communication between the two is Assembly Language. The microcontroller pulls the SMS received by phone, decodes it, recognizes the Mobile number and then sends a message to the Mobile number.
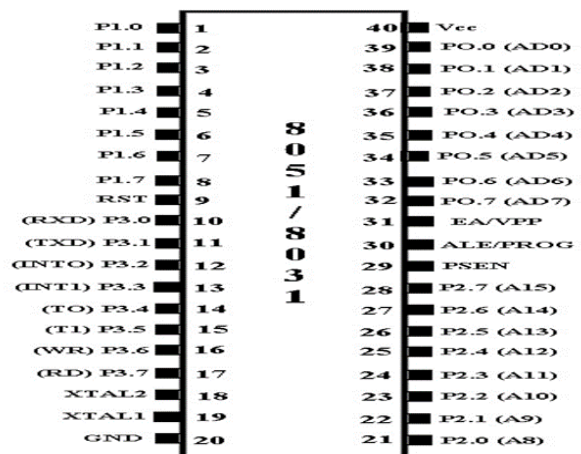
Fig. 7:Pin diagram of the 8051 Microcontroller

The Microcontroller was programmed with the use of assembly language and simulated by the use of edsim51

software before finally burning it on the chip. Figures 8 and figure 9 are the diagrams of the flow chart of the program and the complete circuit diagram of the design respectively.
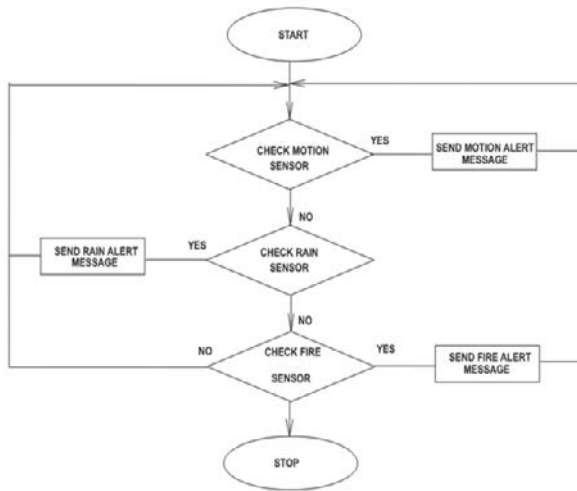
Fig. 8: Program Flowchart
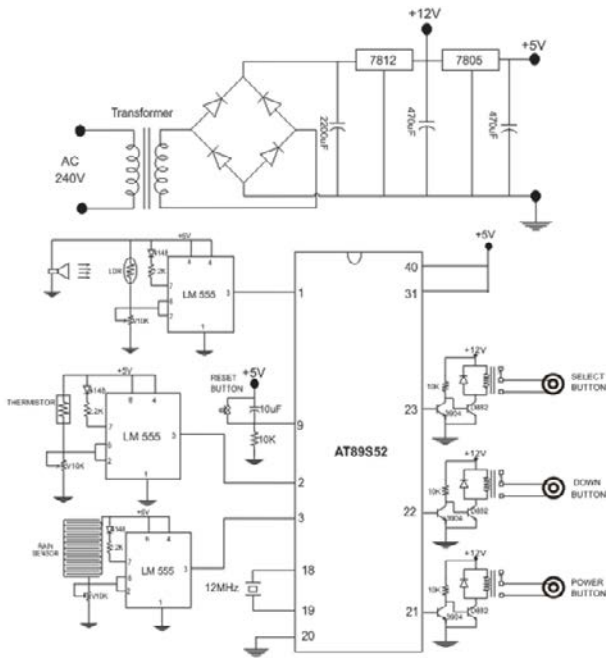
Fig.9:Circuit Diagram

3. RESULTS AND DISCUSSIONS

Performance test was conducted between the system interfaced with the NOKIA (1209) phone and the phone of the owner of the house after connecting the circuit appropriately to check if the circuit will be able to send a message to its appropriate destination if there was to be intrusion, fire accident and rainfall to the owner's home.

3.1. Fire Sensor Test

Heat was put very close to the thermistor and temperatures monitored by a thermometer are recorded and the responses of the system were recorded. Table 3.1 present the results of the test carried out on the fire sensor.

Table 1: Fire sensor results

Test	Temperature (degree Celsius)	Message sent
1	0	No
2	10	No
3	20	No
4	30	No
5	40	No
6	50	Yes
7	60	Yes
8	70	Yes
9	80	Yes
10	90	yes

3.2. Rainfall Sensor Test

The printed circuit board of the rainfall sensor was left without moisture (0) and no message was sent. Then water was dropped on it (1) and it triggered the LM555 time which sent a message to the microcontroller, then the microcontroller with the help of the relays pressed the mobile phone that now sent a rainfall alert message to the owner of the house. Result is presented in Table 2.

Table 2: Rainfall sensor test

Test	Rainfall senor	Message sent
1	0	No
2	1	Yes

3.3. Motion Sensor Test

The laser-light dependent resistor was faced in the direction of light without obstruction **(0)** and no message was sent. Then an obstruction was put over it **(1)** and it triggered the LM555 timer which sent a message to the microcontroller. The microcontroller with the help of the relays pressed the mobile phone and an intruder message was sent to the owner of the house. Table 3 shows results obtained.

Table 3: Motion sensor result.

Test	Motion senor	Message sent
1	0	No
2	1	Yes

4. CONCLUSION

An improved GSM technology-based microcontroller multi-sensor home security and monitoring system has been developed. Test were performed and the system showed a capability of informing a remote owner through an SMS message of an intruder break in, a fire outbreak and rainfall (water) entering an apartment. The SMS sent highlight which of the eventualities have occurred. Extensive test confirms that the system performs accurately and can prevent colossal damage to live and properties.

REFERENCES

Fire Sensor, online at: http://en.wikipedia.org/wiki/fire_sensor, accessed on 12/10/2010.

Mehta, V K., Mehta, R. (2006). Principles of Electronics, S. Chand & Company LTD, 2006.

Mike, J W. (2010). "Home Security History", available online at: http://ezinearticles.com/?Home-Security-History&id=2129354, accessed on 01/10/2012.

Motion Detector, online at http://en.wikipedia.org/wiki/motion_detector, accessed on 12/10/2010.

Muhammad, A M., Janice, G M., Rolin, D M. (2005). The 8051 Microcontroller and Embedded Systems, 2005.

Raghavendran, G. (2011).SMS Based Wirelss Home Appliance Control System, International Conference on Life Science and Technology, vol.3, 2011.

Rosslin, J R., Tai-hoon, K. (2010) A Review on Security in Smart Home Development, International Journal of Advanced Science and Technology, Vol. 15, pp 13-22, 2010.

SECURITY MANAGEMENT: THE ENGINEERING PERSPECTIVE

Ogboo Henry Uchenna, A. Nasir, J. Y. Jiya, H. T. Abdulkarim

Mechanical Eng. Dept. Federal University of Technology Minna Federal University of Technology, Minna, Niger state, Nigeria
Department of Electrical/Electronic Technology, College of Education, Minna

*Corresponding Author: kodosnow@yahoo.com, 08053157614

ABSTRACT

Security management is a difficult task as everyone agrees that security is a problem. As such, this work aims at addressing the ever increasing security challenge confronting us as individuals from the engineering perspective. Throughout human history, engineering has driven the advance of civilization. This can be seen from the metallurgists who ended the Stone Age to the shipbuilders who united the world's people through travels and trades; the past witnessed many marvels of engineering prowess. As civilization grew, it became pertinent that the world became confronted with the challenge of survival and relevance and hence, the desire not to be cut out from the basic necessities of life and existence gave rise to devices by humanity to remain relevance and hence, the field of engineering owes it a responsibility to the world to see that this issue is sorted out as usual as it has always provided respite to the world.

Keywords:. *Countermeasure,Steering,Incentive,Tantalizing*

1. INTRODUCTION

The issue of security has become a global responsibility of all as such, security is no longer a situation free of dangers, but rather an "insurance" as a "technology of risks" and a disposition of the social steering of modern societies. Security has become "a general 'societal idea of value' (wertidee) and a universally employed 'normative concept', that is used with different meanings in an affirmative manner "with a shift of focus from protection against concrete dangers towards insurance in the context of abstract risks (makropoulos, 1995).

"Security measures the absence of threats to acquired values, in an objective sense and in a subjective sense, it is the absence of fear that such values will be attacked ". From an engineering perspective, to design, build, and deploy a secure application, we must integrate security into our application development life cycle by including specific security-related activities in our current engineering processes. Such security-related activities includes identifying security objectives, applying security design guidelines, patterns, and principles, conducting security architecture and design reviews, creating threats models, performing security code reviews, security testing, and conducting security deployment reviews.

In the century just ended, engineering recorded its grandest accomplishments. Some of the highlights from a century in which engineering revolutionized and improved virtually every aspect of human life are the widespread development and distribution of electricity and clean water, airplanes and automobiles, radio and television, spacecraft and lasers, computer and the internet, and antibiotics and medical imaging.

However, as we witnessed a massive population growth and an expansion in its needs and desires, the problem of sustaining civilization's continuing advancement, while still improving the quality of life loomed even more. Threats to personal and public health demand both old and new, required more effective and more readily available treatments hence, vulnerabilities to pandemic diseases, terrorist violence, and natural disasters require serious searches for new methods of protection and prevention. Top on the priority of engineering innovations became products and processes that enhance the joy of living as they have been since the taming of fire and the invention of the wheel.

In each of these broad realms of human concern, the specific grand challenges awaiting engineering solutions are; health, vulnerability, sustainability and joy of living. And, the world's cadre of engineers will seek ways to put knowledge into practice to meet these grand challenges. Engineers will continue the tradition of forging a better future applying the rules of reason, the findings of science, the aesthetics of art, and the spark of creative imagination. Foremost among the challenges confronting engineers are those that must be met to ensure the future itself. The earth we live in is a planet of finite resources and its growing population currently consumes them at a rate that cannot be sustained. Widely reported warnings have emphasised the need to develop a new source of energy and at the same time as preventing or reversing the degradation of the environment. Sunshine has long offered a tantalizing source of environmentally friendly power, bathing the Earth with more energy each hour than the planet's population consumes in a year. But capturing the power, converting it into useful forms, and especially storing it for a rainy day, poses provocative engineering challenges.

And publicized environmental concern involves the atmosphere's dominant component, the element nitrogen. The biogeochemical cycle that extracts nitrogen from the air for its incorporation into plants- and hence food- has become altered by human activity. With widespread use of fertilizers and high- temperature industrial combustion, humans have doubled the rate at which nitrogen is removed from the air relative to pre-industrial times, contributing to smog and acid rain, polluting drinking water, and even worsening global warming. Engineers must design countermeasures for nitrogen cycle problems, while maintaining the ability of agriculture to produce adequate food supplies.

Even as terrorist attacks, medicine epidemics, and natural disasters represents acute threats to the quality of life, more general concerns pose challenges for the continued enhancement of living. Engineers, face the grand challenge of renewing and sustaining the aging infrastructures of cities and services, while preserving ecological balances and enhancing the aesthetic appeal of living spaces.

2. METHODOLOGY

Providing data to feed an informatics system in preparation for bio, chemical or any kind of terror involves engineering challenges in three main categories. The first is surveillance and detection – monitoring the water, air, soil and food for early signs of an attack. Next to it is rapid diagnosis, requiring a system that can analyze and identify the agent of harm as well as track its location and spread within the population. Finally come countermeasures, powered by nimble operations that can quickly develop and small-produce antidotes, vaccines, or other treatments to keep the effects of an attack as small as possible and track how effective the countermeasures are.

2.1 Preventing Nuclear Terror

The material suitable for making a weapon has been accumulating around the world from the beginning of the nuclear age. In certain countries, some bombs may not be adequately secured against theft or sale in certain countries. Scattered about the globe are nuclear reactors for research or power capable of producing the raw material for nuclear devices. Hence, instructions for building explosive devices from such materials have been spreading widely and it should not be assumed that terrorists or other groups wishing to make nuclear weapons cannot read.

Consequently, the main obstacle to a terrorist planning a nuclear nightmare would be acquiring fissile material – plutonium or highly enriched uranium capable of rapid nuclear fission. Nearly 2 million kilograms of each have

already been produced and exist in the world today. It takes less than ten kilograms of plutonium, or a few tens of kilograms of highly enriched uranium, to build a bomb. Nuclear security therefore represents one of the most urgent policy issues of the 21st century. However, in addition to its political and institutional aspects, it poses acute technical issues as well. In short, engineering shares the formidable challenges of finding all the dangerous nuclear materials in the world, keeping track of it, securing it, and detecting its diversion or transport for terrorist use.
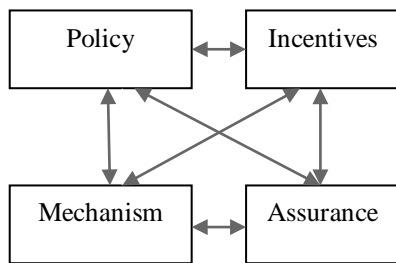
Figure 1.1 Security Analysis Framework

3. RESULTS AND DISCUSSIONS

It has been discovered that the challenges facing the management of security includes how to: secure sensitive materials, detect one especially at a distance, render a potential device harmless, carry out emergency response, cleanup, and public communication after a nuclear explosion or any other major disaster, and determine who did it.

All of these have engineering components; some are purely technical while others are systems challenges. Some of the technical issues are informational – it is essential to have a sound system for keeping tracks of very sensitive weapons and materials known to exist, in order to protect against their theft or purchase on the black market by terrorists. Another possible danger is that very sophisticated terrorist could buy the innards of a dismantled component or fuel from a nuclear power plant,

and build a homemade explosive device. It is conceivable that such a device would produce considerable damage. Hence, a thorough approach needs to be carried out by competent individuals to checkmate this evil trend and come up with a countermeasure against these backlogs. The competent personnel's with competent counter approach (the engineering approach) are the engineers.

Security management from an engineering perspective basically requires four things to come together. There's policy: what we are supposed to achieve. There's mechanism: the ciphers, access controls, hardware tamper-resistance and other machinery that you assemble in order to implement the policy. There's assurance: the amount of reliance you can place on each particular mechanism. Then finally, there's incentive: the motive that the people guarding and maintaining the system have to do their job properly, and also the motives that the attackers have to try to defeat your policy. Security failure can result into devastating consequences that may be very difficult to manage.

In cases of terrorist attacks for instance in places like airports, the reasons why most of the attackers get their weapons such as knives through the airport security is not because of mechanism failure but policy one. In the time past, knives and blades up to three inches were permitted through airports and screeners did their task of keeping guns and explosives off as far as possible. Policy has changed now: first to prohibit all knives, then most weapons. It is also found out that in airports, mechanisms are weak because of things like composite knives and explosives that don't contain nitrogen. Assurances are always poor many tons of harmless passengers possessions are consigned to the trash each month, while well below half of all the weapons taken through screening (whether accidental or for test purposes) are picked up. The question is now why are such policy choices made? And the answer

is quite simply, the incentives on the decision makers favour visible controls over effective ones.

4. CONCLUSION

Although, some individuals may have "Security" in their title or may deal directly with security issues on a daily basis, security still remains everyone's responsibility. There is a popular saying that a chain is only as strong as its weakest link. In as much as security management practices involve balancing security processes and proper management and oversight. Security management confronts the risk of violent and rapidly changing scenarios and addresses the vulnerability of humans in the midst of such a risk: It therefore must be a dynamic and "ever green" system, a framework to guide and provide consistency for future decisions made incrementally. With the widespread of engineering innovations, the issue of security management can successfully become a success story as new measures to counter security challenges will be birthed.

ACKNOWLEDGEMENTS

REFERENCE

Anderson, R (2008). Security Engineering: a guide to building dependable distribution systems pp 3-16.

Bernstein, A., et al. 2002. Nuclear Reactor Safeguards and Monitoring with Antineutrino Detectors. Journal of Applied Physics 91: 4672-4676. DOI: 10.1063/1.1452775.

Bowden, N.S., et al. 2007. Experimental Results from an Antineutrino Detector for Cooperative Monitoring of Nuclear Reactors. Nuclear Instruments and Methods in Physics Research A 572: 985-998.

Garwin, R., and G. Charpak. 2001. Megawatts and Megatons. New York: Knopf.

Hecker, S.S. 2006. Toward a Comprehensive Safeguards System: Keeping Fissile Materials Out of Terrorists' Hands. The Annals of the American Academy of Political and Social Science 607: 121-132.

National Research Council. 2002. Making the Nation Safer: The Role of Science and Technology in Countering Terrorism. Washington, D.C.: National Academies Press. Pp. 39-64.

Nuclear Threat Initiative. 2006. Seeing the Danger Is the First Step: 2006 Annual Report.

Slaughter, D.R., et al. 2007. The Nuclear Car Wash: A System to Detect Nuclear Weapons in Commercial Cargo Shipments.

Nuclear Instruments and Methods in Physics Research A 579: 349-352. DOI: 10.1016/j.nima.2007.04.058.

Luis, E. F. (2000). Beyond Security Planning: Towards a Model of Security Management, Coping with the Security Challenges of the Humanitarian Work, pp 1-6

DETERMINATION OF SPECIFIC PHYSICAL AND COMPACTION PROPERTIES OF SUBGRADE MATERIALS FROM NIGERIAN SOURCES

Abdulfatai Adinoyi MURANA[1*], Adekunle Taiwo OLOWOSULU[2], Manasseh JOEL[3]

[1,2] *Department of Civil Engineering, Ahmadu Bello University, Zaria, Kaduna State, Nigeria*
[3]*Department of Civil Engineering, University of Agriculture, Makurdi, Benue State, Nigeria*
*[*fatinoyi2007@gmail.com](mailto:fatinoyi2007@gmail.com), +234(0)8036376697*

ABSTRACT

As with any other structure, a pavement structure is supported by the underlying soil. The design of the entire pavement structure depends on the condition of the soil. Therefore, characterizing the soil layer (subgrade), is a critical component for pavement design and, thus, the performance and life of the pavement structure. Characterization of subgrade materials involves obtaining material properties (index properties, physical and compaction properties) that identify the material response to external stimuli of traffic loading and environmental conditions. This work aimed at determining specific physical and compaction properties of Nigerian subgrade soils. Samples collected were classified according to AASHTO and the USCS systems. Laboratory testing was conducted on the samples to characterize specific physical and compaction properties. Testing include the standard soils properties tests to determine gradation, Liquid Limit, and Plastic Limit; Hydrometer analysis to determine the percentage of clay and silt content; specific gravity to determine the degree of saturation; the standard Proctor test to determine the Optimum Moisture Content and Maximum Dry Density; Unconfined Compression Test and the CBR test. The AASHTO soil classification shows that the samples were "Fair to Poor" except one "Excellent to Good". The USCS soil classification indicated that the samples were mostly clayed soil. The CBR values indicated that the strength of the subgrades were poor, therefore, capping is required.

Keywords: *Resilient Modulus, subgrade, CBR, UCS*

1. INTRODUCTION

A conventional flexible pavement consists of a prepared subgrade or foundation and layers of sub-base, base and surface courses [1]. The layers are selected to spread traffic loads to a level that can be withstood by the subgrade without failure [2].

The objective of pavement design is to provide a structural and economical combination of materials such that it serves the intended traffic volume in a given climate over the existing soil conditions for a specified time interval. Traffic volume, environmental loads, and soil strength determine the structural requirements of a pavement, and failure to characterize any of them adversely affects the pavement performance. The subgrade may be characterized in the laboratory or by field tests or both [3].

The resilient modulus of fine-grain soils is not a constant stiffness property but depends upon various factors like load state or stress state, which includes the deviator and confining stress, soil type and its structure, which primarily depends on compaction method and compaction effort of a new subgrade. Resilient modulus is found to increase with a decrease in moisture content and an increase in density, and decrease with an increase in deviator stress. Resilient modulus that range between 14 and 140 MPa can be obtained for the same fine-grained subgrade soil by changing parameters such as stress state or moisture content[4]. Resilient modulus of subgrade soils are influenced by the physical condition of the soil (moisture content and unit weight), stress level and soil type. Other factors affecting resilient modulus of subgrade soils include soil type and properties such as amount of fines and plasticity characteristics. In addition, the sample preparation method and the sample size have influence on the test results. Material stiffness is affected by particle size and particle size distribution [5].

It was found that low clay content and high silt content results in lower resilient modulus values and that low plasticity index and liquid limit, low specific gravity, and high organic content result in lower resilient modulus [6]. Other research results indicated that the resilient modulus generally decreases when the amount of fines increases [7]. Also, it was noticed that an increase in maximum particle size leads to an increase in the resilient modulus[8].

The compaction method used to prepare soil samples affected the resilient modulus response. In general, samples that were compacted statically showed higher resilient modulus compared to those prepared by kneading compaction[5].

2.1 Flexible Pavement

Flexible Pavement is usually composed of several asphalt concrete layers, a granular base course and a soil subgrade. For mechanistic design of pavement systems based on elastic theory, a modulus of elasticity must be designated for each design layer including the soil subgrade[9]. A pavement design requires characterization of the component materials in addition to the support soil. The pavement structure may consist of layers of aggregate or other modified soil known as subbase and base layer. The subgrade is the underlying soil, and its characterization allows for the design of a proper foundational support for the pavement. Therefore, subgrade material characterization is needed to design an adequate pavement structure for expected traffic[10].

2.3 Mechanistic-Empirical Pavement Design Guide (MEPDG)

The proposed MEPDG procedure, introduced in NCHRP Project 1-37A [11], is an improved methodology for pavement design and evaluation of paving materials. This is because the MEPDG procedure provides better capability for predicting pavement performance using mechanistic analyses to determine stresses and strains and empirical models to predict performance. To accomplish this improved prediction capability, the MEPDG procedure requires fundamental material properties [12]. Unlike currently used empirical pavement design methods, this new procedure depends heavily on the characterization of the fundamental engineering properties of paving materials [13].

In M-E framework for pavement design, four major inputs are utilized to predict pavement responses and ultimately pavement performance enabling the selection of a cross-section meeting the specified requirements. M-E design enables the mechanical properties of the selected materials to be used in conjunction with empirical performance information and site conditions (traffic and climate). Inputs include an initial pavement structure, climatic data, traffic volume and weight distributions, and material properties of the Hot Mix Asphalt (HMA), base and subgrade materials. In M-E pavement design, accurate representation of material characteristics is imperative to a successful and reliable design. In an M-E framework, accurate material characterization is vital in successfully predicting pavement responses and ultimately pavement performance[14].

MEPDG considers traffic, structural features, materials, construction, and climate far more than ever before. It uses a hierarchical approach to determine design inputs. Depending on the desired level of accuracy of input parameter, three levels of input are provided from Level 1 (highest level of accuracy) to level 3 (lowest level of accuracy). Depending on the criticality of the project and the available resources, the designer has the flexibility to choose any one of the input levels for the design as well as use a mix of levels[15]. The three identifies levels of design input parameters provides the pavement designer with flexibility in achieving pavement design with available resources based on the significance of the project. The three levels of input parameters apply to traffic characterization, material properties, and

environmental conditions[5]. Level 1 input parameters are measured directly and are considered site or project specific. This level requires the greatest amount of testing and data collection. Level 2 input parameters generally are less detailed data sets that are used with correlations or regressions to estimate the corresponding Level 1 parameters. This level of input data requires less testing and data collection efforts. Level 3 input parameters are either "best estimate" or default values and require the least testing and data collection[16].

2. METHODOLOGY

A detailed research plan was develop to collect subgrade materials within the Master Test Section (MTS) for Zone 1 in Kaduna State of Nigeria. The collected soil samples were subjected to different tests to determine their physical properties and compaction characteristics.

3.2 Laboratory Tests

Eighteen subgrade soils from six different MTS collected at 500mm depth were tested.The MTS were selected in connection with a study to develop procedure for overlay design method[17]. A summary of the MTS locations were as presented in Table 1.

Table 1: Master Test Section Locations

MTS	Route Number	Distance from First Node (km)	Node Number and Name
1 – 1	A236	35	241 Zaria (A126) to 394 A236/State Road
1 – 2	A11	4	239 Katabu to 353 Pambegua
1 – 3	A2	40	237 Kaduna (A235) to 711 Kaduna-Niger Border
1 – 4	A235	11	237 Kaduna (A235) to 584 Kachia
1 – 5	A125	11	238 Kaduna to 346 S.B. Gwari
1 – 6	A2	2	239 Katabu to 460 Zaria (A236)

3.2.1 Physical Properties and Compaction Characteristics

Evaluation of soil properties and identification and classification of the investigated soils are important steps to accomplish the research objective. Collected samples were subjected to standard laboratory tests using standard test procedures [18] to determine their physical properties and compaction characteristics. The soil index properties including gradation and hydrometer analysis[19] and[20], Liquid Limit [21], Plastic Limit [22] and specific gravity [23]. The samples were also subjected to Standard Proctor test to determine the Optimum Moisture Content (OMC) and Maximum Dry Density (MDD) adopting the AASHTO standard[24]. Hydrometer analysis were carried out to estimate the percentage of both clay and silt content in each of the samples. Also obtained was the Natural Moisture Content of each of the sample in accordance to [25].

3.2.2 California Bearing Ratio

The test was carried out in accordance to AASHTO standard [26] as a penetration test where a plunger with a cross sectional area was pushed with a constant displacement rate into the compacted sample at OMC and MDD contained in a mold. The CBR value was calculated as the ratio of load needed to have a 0.1-in penetration of the circular spindle. A soaked CBR was also determined after the sample was soaked for 96 hours under water.

3.2.3 Unconfined Compression Test

The soils samples were tested in accordance with AASHTO standard [27] for the unconfined compression test. A continuous stress-strain response was recorded to produce a complete stress-strain diagram. Samples were prepared using

the Proctor hammer (Proctor). The Proctor samples were approximately 38 mm by 85 mm cylindrical. The rate of loading was 1 percent strain per minute.

3. RESULTS AND DISCUSSIONS

4.2 Properties of the Investigated Soils

The results of laboratory tests conducted to evaluate soil properties are presented in Table 2. The data on soil propertiesconsists of particle size analysis (sieve and hydrometer); consistency limits (LL, PL, and PI); specific gravity; MDD and OMC; soil classification using the USCS[28]; and soil classification using the AASHTO method including group index (GI)[29]. The following is a brief description of selected soils.

4.2.1 MTS 1 – 1 (241 Zaria (A126) to 394 A236/State Road)

Test results indicated that the soil samples consists of 72.42%, 77.76% and 48.66% of fine materials with PI of 17, 15 and 13 respectively. From the hydrometer analysis, clay content were 49.76%, 46.88% and 29.60%; and silt content were 22.72%, 30.88% and 19.04% for the three samples respectively.Two of the samples (TP1 and TP2) was classified as lean clay with gravel (CL) while clayed gravel (GC) for TP3 sample according to the USCS and clayey soil (A-6) for all the three samples according to the AASHTO soil classification with a group index, GI of 11, 11 and 3 respectively. Figure 2 shows the particle size distribution curve of MTS 1-1 soil samples. The results of the Standard Proctor test on the samples were depicted in Figure 3a-c. Results showed that the MDD were 1627 kg/m^3, 1598 kg/m^3 and 1848 kg/m^3 and the corresponding OMC were 17.6%, 18.7% and 13.3% for the samples respectively.

Figure 2: Percentage Passing against Sieve Size for MTS 1-1 Soil Samples
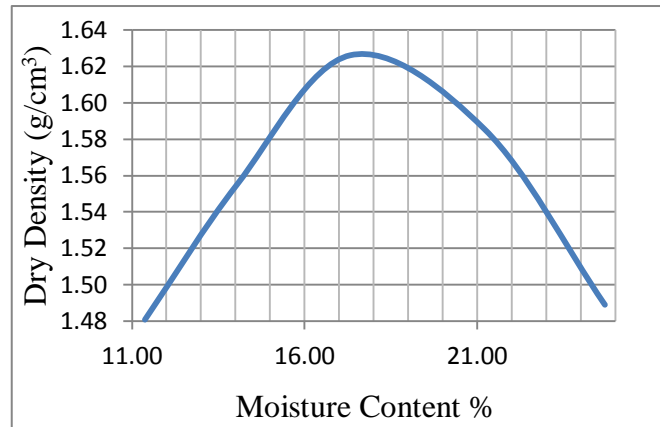
Figure 3a: Graph of Dry Density against Moisture Content for MTS 1-1 TP1

Figure 3b: Graph of Dry Density against Moisture Content for MTS 1-1 TP2
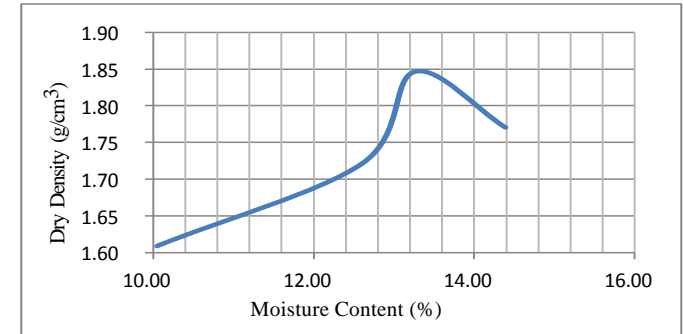
Figure 3c: Graph of Dry Density against Moisture Content for MTS 1-1 TP3

Table 2: Soil Index Properties of samples from Various Master Test Sections

MTS	Passing #200 (%)	Clay (%)	Silt (%)	LL (%	PL %	PI %	Gs	OMC (%)	MDD kg/m^3	USCS	GI	AASHTO
MTS 1-1	72.42	49.76	22.72	37	20	17	2.51	17.6	1627	CL (Lean clay with gravel)	11	A-6 (clayed soils)
	77.76	46.88	30.88	39	24	15	2.44	18.7	1598	CL (Lean clay with gravel)	11	A-6 (clayed soils)
	48.66	29.60	19.04	33	20	13	2.49	13.3	1848	GC (Clayed Gravel)	3	A-6 (clayed soils)
MTS 1-2	22.24	8.48	13.76	36	24	12	2.57	16.2	1664	GC (Clayed Gravel)	0	A-2-4 (Silty or clayed gravel sand)
	73.38	37.28	36.16	29	21	8	2.46	20.0	1618	CL (Lean clay with gravel)	5	A-4 (Silty soils)
	75.84	42.88	32.96	37	18	19	2.51	21.0	1597	CL (Lean clay with gravel)	13	A-4 (Silty soils)
MTS 1-3	66.34	39.84	26.56	39	25	14	2.46	15.6	1768	CL (Gravelly lean clay)	8	A-4 (Silty soils)
	43.76	27.36	16.48	36	26	10	3.31	16.2	1770	SC (Clayed Sand)	2	A-4 (Silty soils)
	55.94	33.44	22.40	31	18	13	2.51	17.8	1612	CL (Gravelly lean clay)	4	A-6 (clayed soils)
MTS 1-4	88.22	69.28	18.88	45	29	16	2.54	22.3	1518	CL (Lean clay)	16	A-7-6 (clayed soils)
	92.70	48.80	48.16	42	25	17	2.55	21.6	1516	CL (Lean clay)	18	A-7-6 (clayed soils)
	85.76	61.60	24.16	32	22	10	2.55	18.5	1575	CL (Lean clay)	8	A-4 (Silty soils)
MTS 1-5	57.82	18.08	39.68	42	28	14	2.58	18.8	1672	CL (Gravelly lean clay)	6	A-7-6 (clayed soils)
	69.08	42.72	26.40	41	31	10	2.50	18.9	1582	CL (Gravelly lean clay)	7	A-5 (Silty soils)
	71.36	50.08	21.28	41	27	14	2.53	21.1	1618	CL (Lean clay with gravel)	9	A-7-6 (clayed soils)
MTS 1-6	57.60	17.28	40.32	30	20	10	2.58	13.9	1768	CL (Gravelly lean clay)	3	A-4 (Silty soils)
	50.48	18.08	32.32	35	21	14	2.46	21.0	1585	CL (Gravelly lean clay)	4	A-6 (clayed soils)
	49.76	30.88	18.88	39	23	16	2.47	16.6	1730	GC (Clayed Gravel)	5	A-4 (Silty soils)

4.2.2 MTS 1 – 2 (239 Katabu to 353 Pambegua)

Figure 4 depicts the particle size distribution curve of MTS 1-2 soils. The soils consists of 22.24%, 73.38% and 75.84% passing sieve #200 with PI of 12, 8 and 19. The clay content were 8.48%, 37.28% and 42.88%; and silt content were 13.76%, 36.16% and 32.96% for the three samples respectively. The samples was classified as lean clay with gravel (CL) for both TP2 and TP3; and GC (Clayed Gravel) for TP1 according to USCS and silty soils (A-4) for both TP2 and TP3 while TP1 was classified as silty or clayed gravel sand (A-2-4) according to the AASHTO soil classification with GI of 0, 5 and 13 for the samples respectively. Standard Proctor test results showed that the MDD were 1664 kg/m^3, 1618 kg/m^3 and 1597 kg/m^3;and the corresponding OMC were 16.2%, 20.0% and 21.0% for the samples respectively, as shown in Figure 5a-c.
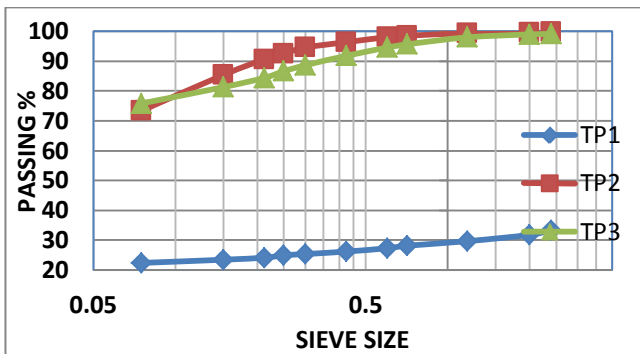
Figure 4: Percentage Passing against Sieve Size for MTS 1-2 Soil Samples
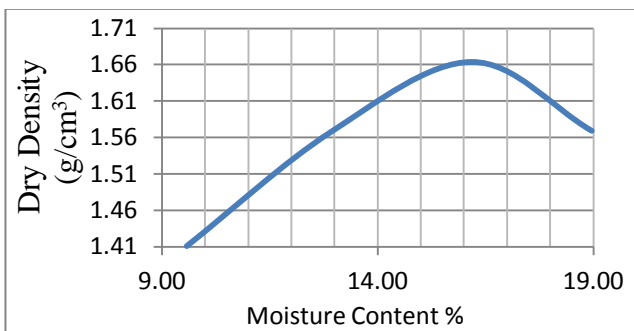
Figure 5a: Graph of Dry Density against Moisture Content for MTS 1-2 TP1
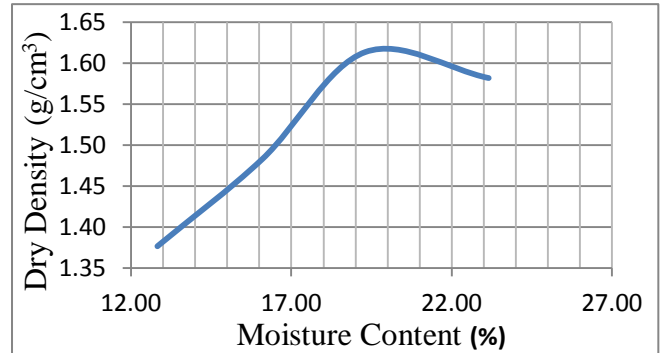
Figure 5b: Graph of Dry Density against Moisture Content for MTS 1-2 TP2
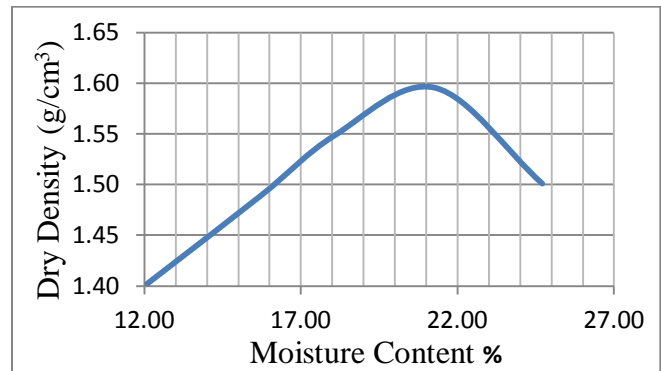
Figure 5c: Graph of Dry Density against Moisture Content for MTS 1-2 TP3

4.2.3 MTS 1 – 3 (237 Kaduna (A235) to 711 Kaduna-Niger Border)

The soils consist of 66.34%, 43.76% and 55.94% passing sieve #200 with plasticity index PI = 14, 10 and 13 for the samples respectively. The clay content were 39.84%, 27.36% and 33.44%; and silt content were 26.56%, 16.48% and 22.40% for the three samples respectively. The TP1 and TP3 samples were classified as gravelly lean clay (CL) and clayed sand (SC) for TP2 sample according to USCS and silty soil (A-4) for TP1 and TP2 samples; and clayed soil (A-6) for TP3 sample according to the AASHTO soil classification with GI of 8, 2 and 4 for the samples respectively. Figure 6 shows the particle size distribution curve of MTS 1-3 soil.Standard Proctor test

results (Figure 7a-c) showed that the MDD were 1768 kg/m³, 1770 kg/m³ and 1612 kg/m³ and the corresponding OMC were 15.6%, 16.2% and 17.8% for TP1, TP2 and TP3 respectively.
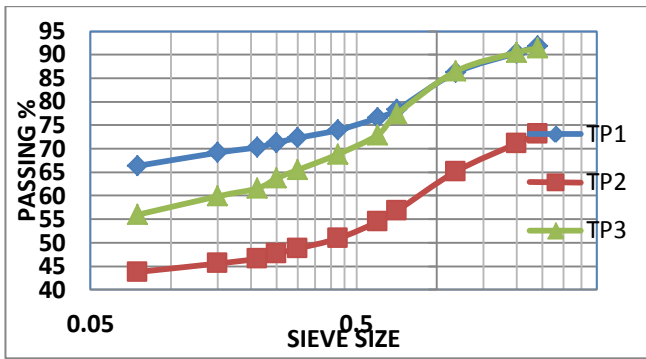
Figure 6: Percentage Passing against Sieve Size for MTS 1-3 Soil Samples
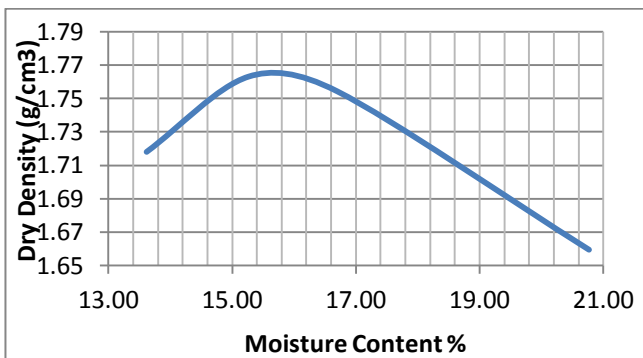
Figure 7a: Graph of Dry Density against Moisture Content for MTS 1-3 TP1
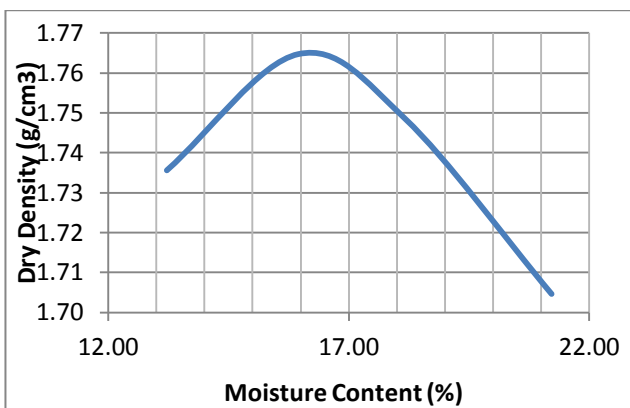
Figure 7b: Graph of Dry Density against Moisture Content for MTS 1-3 TP2
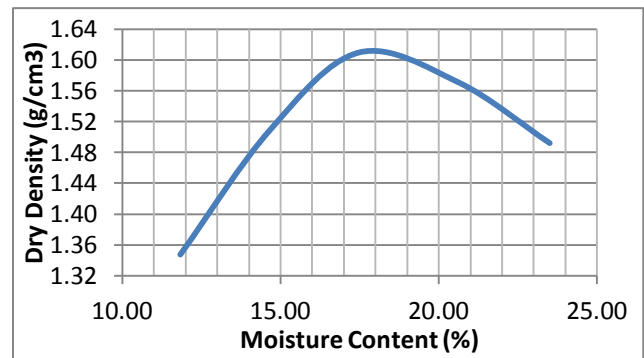
Figure 7c: Graph of Dry Density against Moiture Content for MTS 1-3 TP3

4.2.4 MTS 1 – 4 (237 Kaduna (A235) to 584 Kachia)

Test results showed that the soils consisted of 88.22%, 92.70% and 85.76% passing sieve #200 with PI of 16, 17 and 10 for samples respectively. The hydrometer analysis indicated that clay content were 69.28%, 48.80% and 61.60% and silt content to be 18.88%, 48.16% and 24.16% for the three samples respectively. The samples were classified as lean clay (CL) according to USCS; clayey soil (A-7-6) for TP1 and TP2 samples and silty soil (A-4) for TP3 sample according to the AASHTO soil classification with GI of 16, 18 and 8 respectively.Figure 8 shows the particle size distribution curve of MTS 1-4 soil. Figure 9a-c depicts the results of the Standard Proctor test in which the MDD were 1518 kg/m³, 1516 kg/m³ and 1575 kg/m³ and the corresponding OMC were 22.3%, 21.6% and 18.5% respectively.
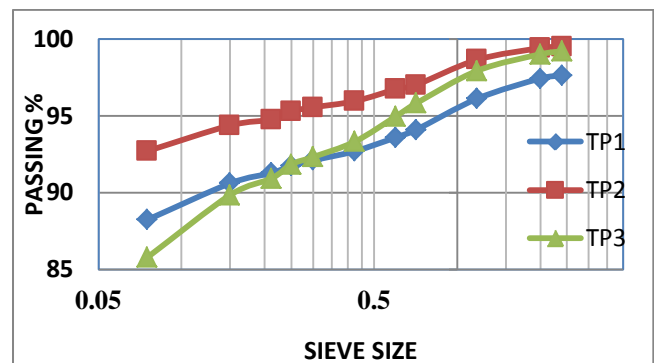
Figure 8: Percentage Passing against Sieve Size for MTS 1-4 Soil Samples
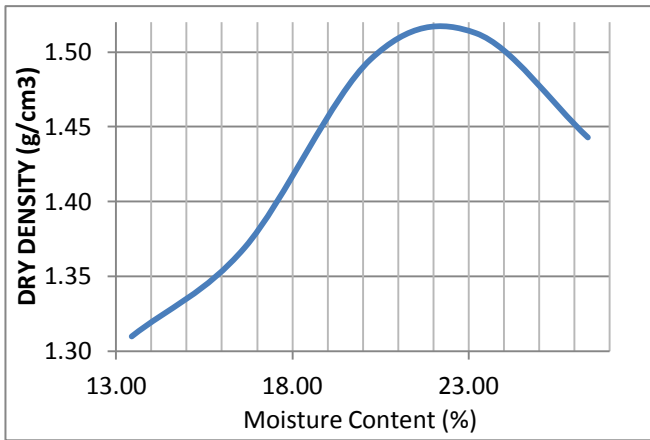
Figure 9a: Graph of Dry Density against Moisture Content for MTS 1-4 TP1
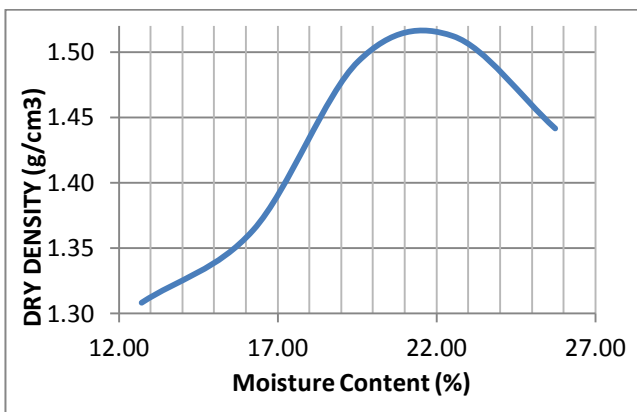
Figure 9b: Graph of Dry Density against Moisture Content for MTS 1-4 TP2
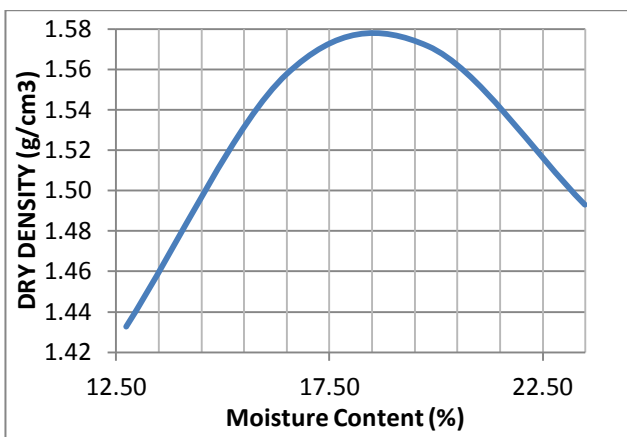
Figure 9c: Graph of Dry Density against Moisture Content for MTS 1-4 TP3

4.2.5   MTS 1 – 5 (238 Kaduna to 346 S.B. Gwari)

Test results showed that the soils consisted of 57.82%, 69.08% and 71.36% passing sieve #200 with PI of 14, 10 and 14 respectively. From the hydrometer analysis, clay content were found to be 18.08%, 42.72% and 50.08% while silt content were 39.68%, 26.40% and 21.28% for the three samples respectively. The samples were classified as clayey soil (A-7-6) for TP1 and TP3 samples and silty soil (A-5) for TP2 sample with GI of 6, 7 and 9 respectively according to AASHTO soil classification and gravelly lean clay (CL) for TP1 and TP2 samples and lean clay with gravel (CL) for TP3 sample according USCS soil classification. Figure 10 shows the particle size distribution curve of MTS 1-5 soil. Figure 11a-c depicts the results of the Standard Proctor test in which the MDD were 1672 kg/m^3, 1582 kg/m^3 and 1618 kg/m^3 and the corresponding OMC were 18.8%, 18.9% and 21.1% respectively.
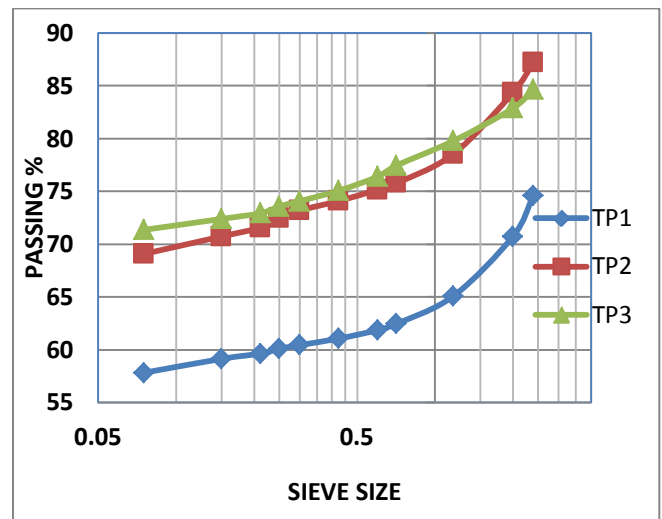
Figure 10: Percentage Passing against Sieve Size for MTS 1-5 Soil Samples
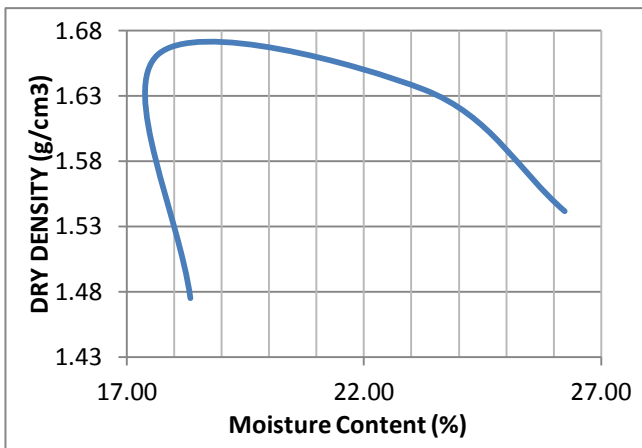
Figure 11a: Graph of Dry Density against Moisture Content for MTS 1-5 TP1
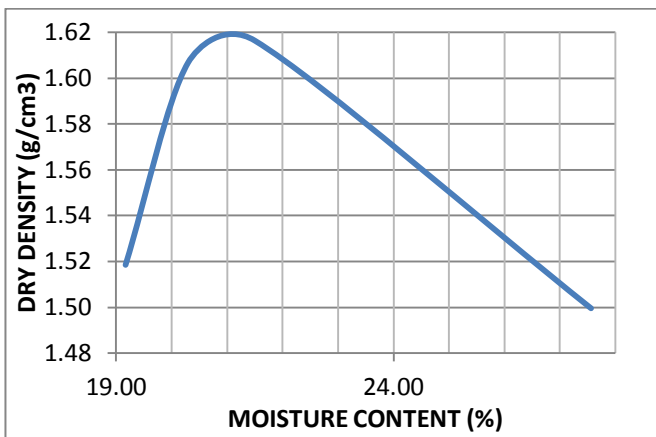
Figure 11b: Graph of Dry Density against Moisture Content for MTS 1-5 TP2
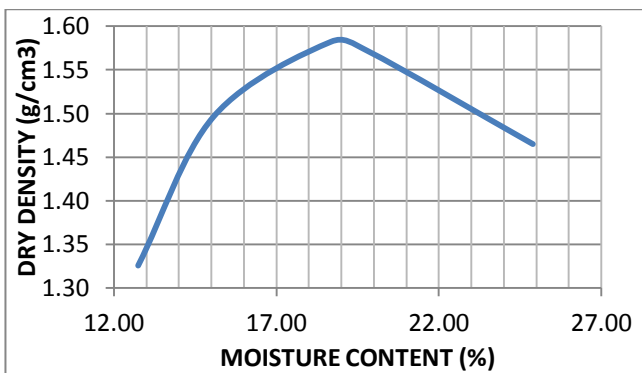
Figure 11c: Graph of Dry Density against Moisture Content for MTS 1-5 TP3

4.2.6   MTS 1 – 6 (239 Katabu to 460 Zaria (A236))

Test results showed that the soils consisted of 57.60%, 50.40% and 49.76% passing sieve #200 with PI of 10, 14 and 16 respectively. the hydrometer analysis showed that clay content were 17.28%, 18.08% and 30.88% while silt content were 40.32%, 32.32% and 18.88% for the three samples respectively. TP1 and TP2 samples were classified as gravelly lean clay (CL) and TP3 as clayed gravel (GC) according to USCS and silty soil (A-4) for TP1 and TP3 samples and clayed soil (A-6) according to the AASHTO soil classification with GI of 3, 4 and 5 respectively. Figure 12 shows the particle size distribution curve of MTS 1-6 soil. Figure 13a-c depicts the results of the Standard Proctor test in which the MDD were 1768 kg/m^3, 1585 kg/m^3 and 1730 kg/m^3 and the corresponding OMC were 13.9%, 21.0% and 16.6% for TP1, TP2 and TP3 respectively.
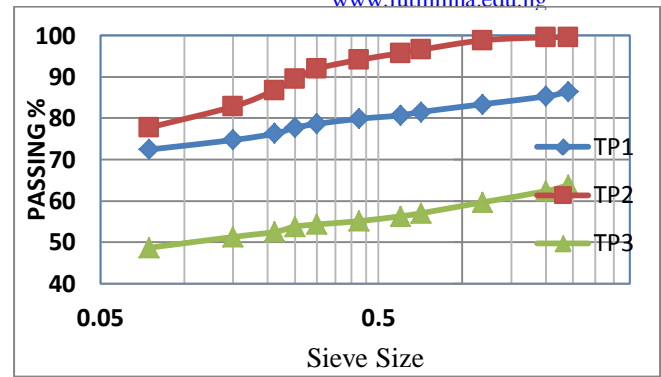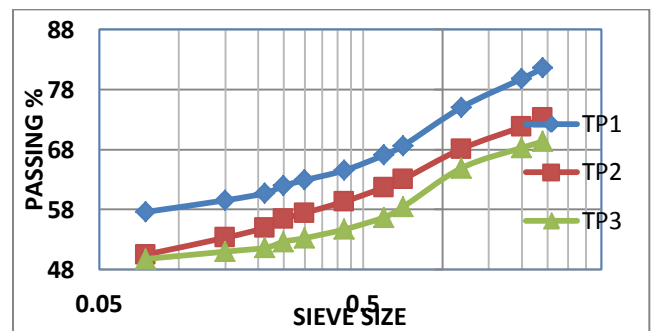

Figure 12: Percentage Passing against Sieve Size for MTS 1-6 Soil Samples

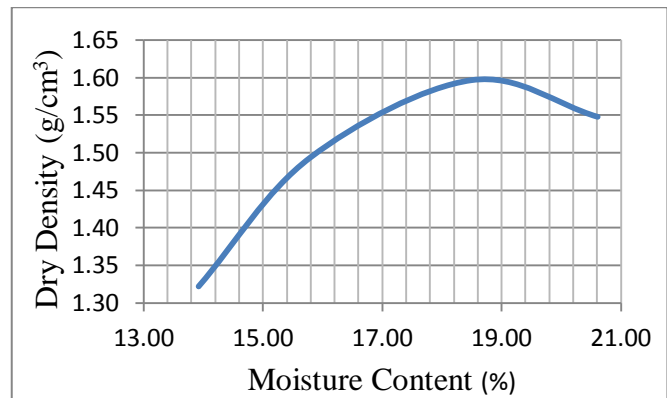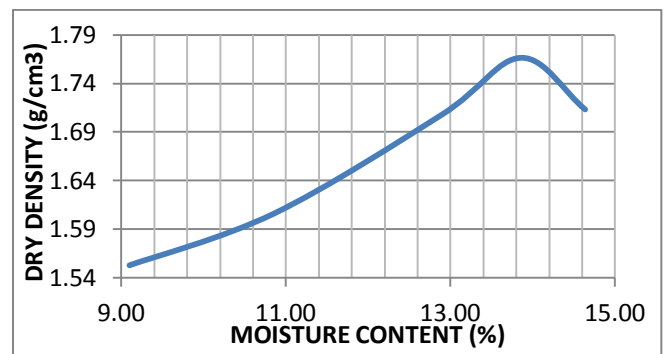Figure 13a: Graph of Dry Density against Moisture Content for MTS 1-6 TP1
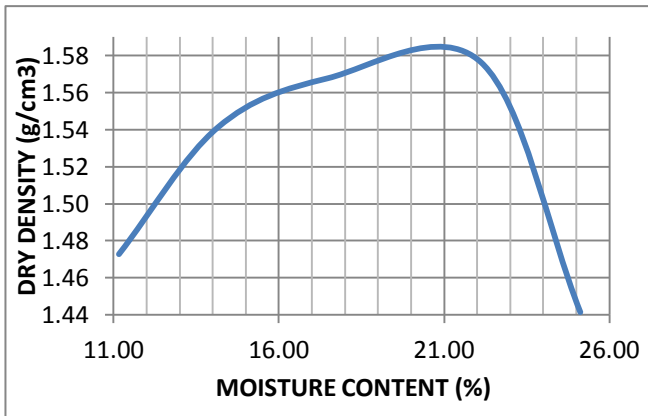
Figure 13b: Graph of Dry Density against Moisture Content for MTS 1-6 TP2
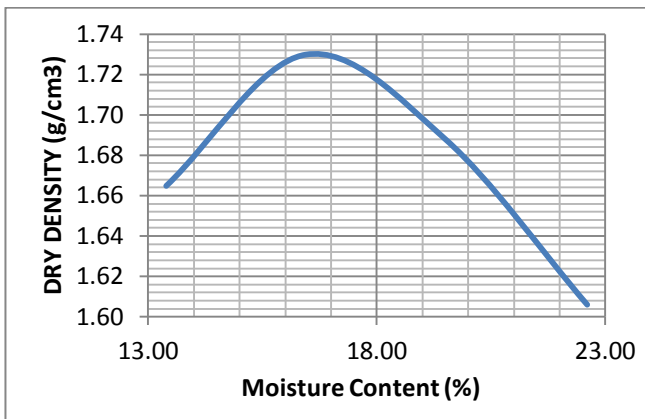
Figure 13c: Graph of Dry Density against Moisture Content for MTS 1-6 TP3

4.3 California Bearing Ratio

The CBR value is determined on the basis of the force F_a at 2.54 mm (0.1 inch) penetration, CBR_{Top}, and the force F_b at 5.08 mm (0.2 inch) penetration, CBR_{Bottom}.

The CBR values obtained on the samples from the test sections are as shown in Table 3.

Table 3: CBR of samples from Various Sections

Master Test Section	CBR (%)	
	UNSOAKED	SOAKED
MTS 1-1	2.30	2.86
	1.02	1.36
	4.52	1.58
MTS 1-2	2.11	1.80
	1.51	2.28
	1.51	1.42

MTS 1-3	0.64	1.80
	4.32	2.77
	1.36	2.44
MTS 1-4	1.44	1.06
	2.27	1.96
	0.79	1.35
MTS 1-5	3.77	5.88
	0.98	7.83
	12.82	0.90
MTS 1-6	1.81	1.89
	1.71	2.56
	0.81	2.16

4.4 Unconfined Compression Test

The unconfined compression test was conducted on the subgrade soil samples. A stress-strain diagram was produced as part of the results. The initial tangent modulus was calculated as the slope of the tangent to the initial straight portion of the curve drawn through the origin. The results obtained are as presented in Table 4.

Table 4: Laboratory results of Samples for Unconfined Compression Test

Master Test Section	Samples	Initial Tangent Modulus (psi)	UCS (psi)
MTS 1 – 1	TP1	1287.240	50.7964
	TP2	1288.870	10.2573
	TP3	1286.330	79.6536
MTS 1 – 2	TP1	1288.430	30.6944
	TP2	1288.760	16.5759
	TP3	1288.040	33.9743
MTS 1 – 3	TP1	1289.010	5.7842
	TP2	1287.600	43.3523
	TP3	1287.210	56.9719
MTS 1 – 4	TP1	1289.150	2.5746
	TP2	1287.410	53.1196
	TP3	1288.380	26.5598
MTS 1 – 5	TP1	1288.380	57.7261
	TP2	1287.110	61.5745
	TP3	1288.180	26.8576
MTS 1 – 6	TP1	1288.990	6.4301
	TP2	1287.930	34.6008
	TP3	1286.340	77.5431

4. CONCLUSION

The following conclusions could be made from the research:

1. The AASHTO soil classification shows that the subgrade soil samples obtained from the MTS were classified to be Clayed soil (A-6 and A-7-6) or silty soils (A-4, A-5 and A-2-4). This implies that the general rating of all the subgrade samples collected within the MTS were "Fair to Poor" except MTS 1-2 (TP1) with rating "Excellent to Good".

2. The USCS soil classification indicated that most of the samples were lean clay soil with gravel (CL) except few that were either clayed gravel (GC) or clayed sand (SC).

3. The CBR values were less than 3% except for samples from MTS 1-5 (TP1 and TP2). This implies that the strength of the subgrades were poor, therefore, capping is required.

5.2   Recommendation

Based on the obtained specific characteristics of the subgrade found around the MTS in Zone 1, it is recommended that the soils should be improved for engineering purposes.

REFERENCE STYLE

[1] AASHTO, Guide for Design of Pavement Structures, 13th ed., Washington, D.C.: American Association of State Highway and Transportation Officials, 1993.

[2] A. Adu-Osei, "Characterization Of Unbound Granular Layers In Flexible Pavements: Research Report ICAR - 502-3," Texas Transportation Institute the Texas A&M University System College Station, Texas, 2001.

[3] K. P. George, "Prediction of Resilient Modulus from Soil Index Properties, FHWA/MS-DOT-RD-04-172," Department of Civil Engineering The University of Mississippi, Mississippi, 2004.

[4] D. Li and E. T. Selig, "Resilient Modulus for Fine-Grained Subgrade Soils," *Journal of Geotechnical Engineering,* vol. 120, no. 6, pp. 939-957, 1994.

[5] H. H. Titi, M. B. Elias and S. Helwany, "Determination of Typical Resilient Modulus Values for Selected Soils in Wisconsin," National Technical Information Service 5285 Port Royal Road Springfield, Milwaukee, 2006.

[6] M. R. Thompson and Q. L. Robnett, "Resilient Properties of Subgrade Soils," *Transportation Engineering Journal, ASCE, 105(TE1),* pp. 71-89, 1979.

[7] F. Lekarp, U. Isacsson and A. Dawson, "State of the Art. I: Resilient Response of Unbound Aggregates," *Journal of Transportation Engineering, ASCE,* vol. 126, no. 1, Jan/Feb 2000.

[8] V. C. Janoo and J. J. Bayer II, "The effect of Aggregate Angularity on Base Course Performance, ERDC/CRREL TR-01-14.," U.S. Army Corps of Engineers, 2001.

[9] J. M. Smolen, "An Improved Alternative Test Method for Resilient Modulus of Fine Grained Soils, Master's Thesis," Graduate School at Trace: Tennessee Research and Creative Exchange, Tennessee, 2003.

[10] S. M. Hossain, "Characterization of Unbound Pavement Materials From Virginia Sources for Use in the New Mechanistic-Empirical Pavement Design Procedure," Virginia Transportation Research Council, Commonwealth of Virginia, Virginia, 2010.

[11] NCHRP, "Mechanistic-Empirical Design of New and Rehabilitated Pavement Structures: NCHRP Project 1-37A," National Research Council, Washington, D.C., 2004.

[12] A. K. Apeagyei and S. D. Diefenderfer, "Asphalt Material Design Inputs for Use with the Mechanistic-Empirical Pavement Design Guide in Virginia: Report No.: FHWA/VCTIR 12-R6," Virginia Center for Transportation Innovation and Research, Virginia, 2011.

[13] G. W. Flintsch, A. Loulizi, S. D. Diefenderfer, K. A. Galal and B. K. Diefenderfer, "Asphalt Materials Characterization in Support of Implementation of the Proposed Mechanistic-Empirical Pavement Design

Guide: Report No. VTRC 07-CR10," Virginia Tech Transportation Institute, Blacksgurg, 2007.

[14] M. M. Robbins, "An Investigation into Dynamic Modulus of Hot-Mix Asphalt and its Contributing Factors: A Thesis Submitted to the Graduate Faculty of Auburn University in Partial Fulfillment of the Requirements for the Degree of Masters of Science," Mary Marjorie Robbins, Auburn, Alabama, 2009.

[15] C. Halil, G. Kasthurirangan and K. Sunghwan, "MEPDG Work Plan Task No. 5: Characterization of Unbound Materials (Soils/Aggregates) for Mechanistic-Empirical Pavement Design Guide," Center for Transportation Research and Education, Iowa, 2009.

[16] S. D. Diefenderfer, "Analysis of the Mechanistic-Empirical Pavement Design Guide Performance Predictions: Influence of Asphalt Material Input Properties, FHWA/VTRC 11-R3," Virginia Transportation Research, Charlottesville, VA 22903, 2010.

[17] G. Claros, R. F. Carmicheal and J. Harvey, "Development of Pavement Evaluation Unit and Rehabilitation Procedure for Overlay Design Method," Texas Research and Development Foundation for the Nigeria Federal Ministry of Works and Housing, Lagos, 1986.

[18] AASHTO, Standard Specifications for Transportation Materials and Methods of Sampling and Testing, 23rd ed., Washington, D.C.: American Association of State Highway and Transportation Officials, 2003.

[19] AASHTO T87, Dry Preparation of Disturbed Soil and Soil Aggregate Samples for Test, 23rd ed., Washington, D.C.: American Association of State Highway and Transportation Officials, 2003.

[20] AASHTO T88, Particle Size Analysis of Soils, 23rd ed., Washington, D.C: American Association of State Highway and Transportation Officials, 2003.

[21] AASHTO T89, Determining the Liquid Limit of Soils, 23rd ed., Washington, D.C.: American Association of State Highway and Transportation Officials, 2003.

[22] AASHTO T90, Determining the Plastic Limit and Plasticity Index of Soils, 23rd ed., Washington, D.C.: American Association of State Highway and Transportation Officials, 2003.

[23] AASHTO T100, Specific Gravity of Soils, 23rd ed., Washington, D.C.: American Association of State Highway and Transportation Officials, 2003.

[24] AASHTO T99, The Moisture-Density Relations of Soils Using a 5.5 lb [2.5 kg] Rammer and a 12-in. [305mm] Drop, 23rd ed., Washington, D.C: American Association of State Highway and Transportation Officials, 2003.

[25] AASHTO T265, Laboratory Determination of Moisture Content of Soils,", 23rd ed., Washington, D.C.: American Association of State Highway and Transportation Officials, 2003.

[26] AASHTO T193, Standard Method of Test for The California Bearing Ratio, 23rd ed., Washington, D.C.: American Association of State Highway and Transportation Officials, 2003.

[27] AASHTO T208, Unconfined Compressive Strength of Cohesive Soil, 23rd ed., Washington, D.C.: American Association of State Highway and Transportation Officials, 2003.

[28] ASTM D2487, Practice for Classification of Soils for Engineering Purposes (Unified Soil Classification System), Philadelphia, PA.: American Society and Testing of Materials, 2000.

[29] AASHTO M145, Classification of soils and Soil-Aggregate Mixtures for Highway Construction Purposes, 23rd ed., Washington, D.C.: American Association of State Highway and Transportation Officials, 2003.

Hybridized Continuous-Repeated Power Flow (HCR-PF) for Electric Power Transfer Capability determination

Ahmad Abubakar Sadiq [1*], M. N. Nwohu [2], M. Saidu [3], A. U. Abraham[4] and U. Abdullahi[5]

[1,2,4]Electrical and Electronics Engineering, Federal University of Technology, Minna
[3,5]Telecomunication Engineering, Federal University of Technology, Minna
[*]Corresponding ahmad.abubakar@futminna.edu.ng, +2348057879333.

ABSTRACT

The ability to accurately and rapidly assess the capabilities of the transmission grid is a key concept in the restructuring of the electric power industry. This paper presents hybridized Continuation-Repeated Power Flow (HCR-PF) for ATC computation. Results of IEEE 9 bus and IEEE 30 bus test systems were presented and comparisons were made with other methods. HCR-PF is seen to provide a good alternative to determine ATC. Single line outage (N–1) criterion is used to simulate the effect of line outages on ATC values thereby identifying overloaded transmission facility. Network response method for results interpretation of ATC is considered appropriate since it takes into consideration the response of the entire network to a given transfer direction. Although any limitation may be considered independently for simulation purposes, in practice any of the limiting constraints can be the most severe, depending on system base case and steady state variables.

Keywords: *Available Power Transfer, Continuation Power Flow, Repeated Power Flow and contingency.*

1. INTRODUCTION

In power systems planning and operations, the ability to accurately and rapidly assess the capabilities of the transmission grid is a key concept in a deregulated electricity market (Sauer, 1997). Information about transfer capability between various interfaces of a power grid is vital for the bulk power market. Power system Engineers and Planners need to know the system bottlenecks (Generation-Transmission interface constraints, Transmission Substation capacity constraints, Transmission wheeling constraints, Transmission-Distribution interface constraints) and system operators must implement transfers within the calculated transfer capability. These bottlenecks if not properly managed result to Load Shedding, Voltage/Frequency instability, and Stranded power (Akinniranye, 2012). Repeated estimation of transfer capabilities are needed to ensure that the combined effects of power transfers resulting from multilateral transactions do not cause undue risk of system overloads, equipment damage, blackouts or system collapse.

Transfer capability of transmission interface can be specified as either Available Transfer Capability (ATC) or Total Transfer Capability (TTC). Transfer capability computations from one point to another (buses) are generally based on a snap shot of the system: system loading, generation dispatch, thermal overload, topology, voltage and/or stability limits as well as contingencies considered (Sadiq A, Nwohu M, et al 2013) (Mark and Chika, 1999; Dobson, et al., 2001).

Hence, there existed different approaches to transfer capability assessment, these are classified as deterministic or probabilistic depending on system parameters considered either fixed or varied during operating conditions. Transfer capability is also catalogued based on different time horizons, planning and operating (real time) capabilities. For real time (on-line) calculations, system generation and load demands are often regarded as fixed values and the entire power network is a snapshot of the highly dynamic system. This assumes a static feasible operating condition upon which an incremental transfer can be imposed on the base case power flow. Operating transfer capability analysis is for real time or immediate future and the aim is focused on contingency analysis. Single line outage (N-1 criterion) contingency is often considered. Transfer capability for planning analysis is in the long-term horizons, due to large number of

uncertainties in system parameter variation. Here, the focus is on considering all likely base cases and contingencies. Hence long term ATC parameters take on probability distribution (Yuan-Kang, 2007).

Four major approaches are suggested in the literature for the calculation of ATC:

I. Sensitivity analysis

Sensitivity analysis employs Factors which include: line outage distribution factors (LODF), Power Transfer distribution factor (PTDF) and Generation sift factors (GSF). These can be based on DC or AC power flow. It does not take into account the non-linear effects of reactive power and voltages (Mark and Chika, 1999, Greene, S., 2002).

II. Optimal power flow (OPF)

Optimal power flow (OPF) method maximizes Transfer Capability between sources and sinks thereby respecting contractual terms and economic dispatch of generation. However, open access allows transaction in practice from/to any point/area (Shaaban, M., Ni, Y., & Wu, F. F. 2000).

III. Continuation power flow (CPFLOW)

Initially introduced to find maximum loadability, CPFLOW is applicable to ATC computation without change in principle. Involve complex parameterization or perpendicular intersection and able to define ATC for thermal, voltage and stability constraints. CPFLOW Implemented by a new Power system software package Power System Analysis Toolbox (PSAT) (Chih-wen, L., et al 2005).

IV. Repeated power flow (RPF)

Easy to implement but involves solving full AC power flow at each transfer step. Similar to CPFLOW it increases complex power demand at sink buses and power supply at sources at a given step until a binding security limit is just encountered. It however does not trace the full nose of the system under simulation (Ejebe, G., et al 1998).

Each of these methods can lend themselves to deterministic or probabilistic method. Equally important in transfer capability assessment is the interpretation of results; often two methods are used; Rated system path (RSP) method and Network response (NR) method. In network response method, transfer capability from bus (A) to another bus (B) is the maximum real power transferable from (A) to (B) by all physical paths connecting buses (A) to (B). While in the rated system path method, transfer capability from bus A to bus B is the real power (maximum) flow over the physical paths directly connecting buses (A) and (B) under a limiting condition which is system-wide (Sauer, 1997). Table 1 shows the performance comparison of various deterministic ATC methods based on the limitations to power transfer (Dobson, I., et al 2001).

1.1 Limitations to Electric Power Transfer

The ability of interconnected transmission network to transfer quality electrical power reliably and economically may be limited by physical, environmental and electrical characteristics of the systems (NERC, 1996). Transfer capability computations are mainly a function of three limits: Thermal limit overload, Voltage limits and Stability limits. (Marannino, *et al.*, 2002). Figure depict Transfer Capability quantities, msrgins and limitations.

Figure1: Transfer Capability Margins and limitations.
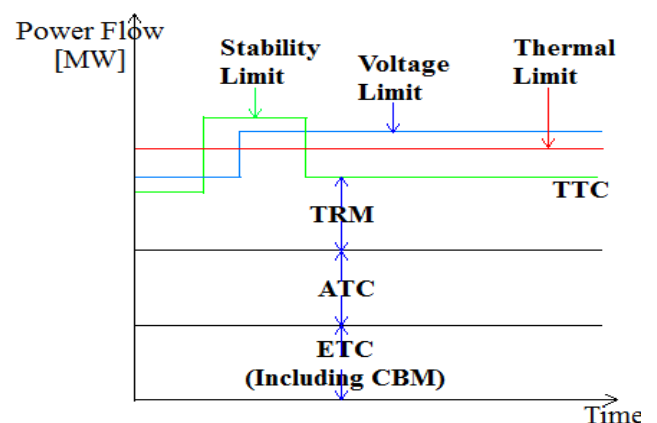
Table 1: Comparison of various Transfer Capability methods.

Method	Constraints Considered		
	Thermal	Voltage	Stability
DCPF	Yes	No	No
PTDF	Yes	No	No
LODF	Yes	No	No
GSF	Yes	No	No
RPF	Yes	Yes	Yes
CPFLOW	Yes	Yes	Yes
OPF	Yes	Yes	Yes

Source: (Hojabri and Hizam, 2011)

1.2 Generic Transfer Capability

Approaches to Transfer Capability computations differs, however, each method adopted should some basic framework as acknowledged by the regulatory agency this makes Transfer Capability peculiar a given Power utility. It is beneficial to consider a simple case of Transfer Capability computation with limited set of network parameter variations. A single Transfer Capability computation between the source-sink buses should yield:

1. A base case (feasible operating condition).
2. Transfer direction including the source, sink and losses (or a lossless Transfer).
3. A solved transfer-limited case which includes the Transfer capability at base case and the incremental transfer imposed that result to binding security limit.
4. The transfer margin is the difference between the power transfer at the base case and the power transfer resulting to the limiting case.

The base case and the transfer direction are inputs to the system while the transfer capability and the limiting constraints are the output.

2. METHODOLOGY

2.1 Reformulation of Power Flow Equation

To apply continuation method to power flow problem, a loading parameter must be inserted into the power flow equations to parameterize the load-flow equation (Venkataramana and Colin, 1992). A constant power load model is documented as follows:

Let the loading parameter (λ) be represented by equation (1)

$$0 \leq \lambda \leq \lambda_{limited} \tag{1}$$

where $\lambda = 0$ corresponds to the base case loading and $\lambda = \lambda_{limited}$ corresponds to the maximum loading parameter above which a binding security limit is encountered. For an n bus system, the normal power flow equation of each bus i can be expressed in equations (2), (3), (4) and (5).

$$P_G^i - P_L^i - P_{injected}^i \tag{2}$$

$$P_{injected}^i = \sum_{j=1}^{n} V_i V_j Y_{ij} \cos(\delta_i - \delta_j + \theta_{ij}) \tag{3}$$

$$Q_G^i - Q_L^i - Q_{injected}^i = 0 \tag{4}$$

$$Q_{injected}^i = \sum_{j=1}^{n} V_i V_j Y_{ij} \cos(\delta_i - \delta_j + \theta_{ij}) \tag{5}$$

where G and L denotes generation and load; bus voltages at buses i and j are given by $V_i \angle \delta_i$ and $V_j \angle \delta_j$ while $Y_{ij} \angle \theta_{ij}$ is the (i, j)th element of the bus admittance matrix.

For Available Transfer Capability calculation, the injected power (Real and Reactive) both at source and sink buses are functions of lambda (λ). In order to simulate a load change, P^i, Q^i and P_G^i terms must be modified such that

each term be made of two components: the base case component and the component due to change in loading parameter (Liang and Ali, 2006; Venkataramana and Colin, 1992). Thus,

$$P_L^i = P_L^{i0}(1 + \lambda K_{pi}) \tag{6}$$

$$Q_L^i = Q_L^{i0}(1 + \lambda K_{Qi}) \tag{7}$$

$$P_G^i = P_G^{i0}(1 + \lambda K_{Gi}) \tag{8}$$

where $P^i{}_G, P^i{}_L, Q^i{}_L$ are the real power generation, load and reactive load at i^{th} bus while $P^{i0}{}_G, P^{i0}{}_L, Q^{i0}{}_L$ are their corresponding base case schedules. K_{Pi}, K_{Qi} and K_{Gi} are participation factor to designate the variation of real and reactive power at PQ buses and real power variation at PV buses (sensitivity of load and generation changes at the ith bus) as lambda (λ) changes.

When these new equations (6), (7) and (8) are inserted into (2) and (4) the resulting power flow equations become parameterized and given in (9), (10).

$$P_G^{i0}(1 + \lambda K_{Gi}) - P_L^{i0}(1 + \lambda K_{pi}) - P_{injected}^i = 0 \tag{9}$$

$$Q_G^{i0} - Q_L^{i0}(1 + \lambda K_{Qi}) - Q_{injected}^i = 0 \tag{10}$$

At generator (PV) buses, the term K_{Qi} is zero while at load (PQ) buses a constant power factor is maintained by making the ratio $\frac{K_{pi}}{K_{Qi}}$ constant.

For an inter-area transfer schedule, the nonlinear power flow equation parameterized with lambda (λ) can be expressed in compact form as in equations (11) and (12).

$$f(x, \lambda) = 0 \tag{11}$$

$$f(x, \lambda) \equiv f(x) - \lambda b \tag{12}$$

where the state variable $x = (\delta, V)$ is a vector of bus voltage magnitude and angles.

The formulation by Mark and Chika, (1999), and Wu and Fischl, (1993), show that there is a close connection between optimization, CPFLOW and repeated power flow (RPF) or successive iterative load flow computation for Transfer Capability computations. CPFLOW can therefore

solve the power flow equation as an optimization problem stated thus (Prabha, *et al.*, 2010):

$$\max(\lambda)$$

Subject to

$$f(x, \lambda) = 0 \tag{13}$$

$$\left|P_G^i\right|_{min} \leq \left|P_G^i\right| \leq \left|P_G^i\right|_{max} \tag{14}$$

$$\left|Q_G^i\right|_{min} \leq \left|P_G^i\right| \leq \left|Q_G^i\right|_{max} \tag{15}$$

$$|V_i|_{min} \leq |V_i| \leq |V_i|_{max} \tag{16}$$

$$\left|P_{ij}\right|_{min} \leq \left|P_{ij}\right| \leq \left|P_{ij}\right|_{max} \tag{17}$$

Equations (13) is the compact power flow equation, (14) and (15) are the PV real and reactive power limitations, (16) is the bus voltage limits while (17) is the thermal limits of lines connecting buses. At the maximum loading parameter (λ_{max}), the ATC is calculated using equation (18) (Chanrasekar and Ramana, 2011; Yan and Chanan, 2002).

$$ATC = \sum_{i \in sink} P_L^i(\lambda_{max}) - \sum_{i \in sink} P_L^{i0} \tag{18}$$

2.2 Hybridized Continuous-Repeated Power Flow (HCR-PF)

The proposed approach to determine ATC is the hybridized Continuous-Repeated (HCR) structure. The continuation power flow (CPFLOW) and repeated power flow (RPF) are both ac power flow methods which give accurate solution in determining the ATC because it considers the effect of reactive power flow and voltage magnitude limit (Othman, 2006). The CPFLOW algorithm effectively increases the controlling parameter in discrete steps and solves the resulting power flow problem at each step. The procedure is continued until a given condition or physical limit preventing further increase is reached. Newton power flow algorithm is used. CPFLOW yields solutions even at voltage collapse points. The ac load flow power system models such as continuation power flow (CPFLOW) can handle the three power flow limits,

namely, thermal, voltage magnitude, and stability constraints (Ejebe, *et al* 1998).

Both CPFLOW and RPF implement transfers by increasing complex load with uniform power factor at every load bus in sink area with corresponding increase in the real power injection at generator buses up to a binding security limit. The proposed algorithm is implemented in Power System Analysis Toolbox (PSAT) and summarized below:

I. Establish a feasible base case, by specifying generation and loading level, bus voltage magnitude and limits as well as line/transformer thermal limits.

II. Run the resulting feasible base case power flow using Newton Raphson (NR) power flow.

III. Specify transfer direction by connecting power supply bid block at all generator buses in source area and connecting power demand bid block at all load buses in sink area

IV. Set up and run CPFLOW in PSAT with specified number of points and step size control.

V. Check for limit violation in IV

VI. If yes, reduced step size else increase step size until the binding security limit is just removed or about to be encountered.

VII. Calculate ATC using equation (3.15) and report ATC value and the binding limitation.

Figure 2 shows the flow chart of the proposed Hybridized Continuous-Repeated Power Flow structure.
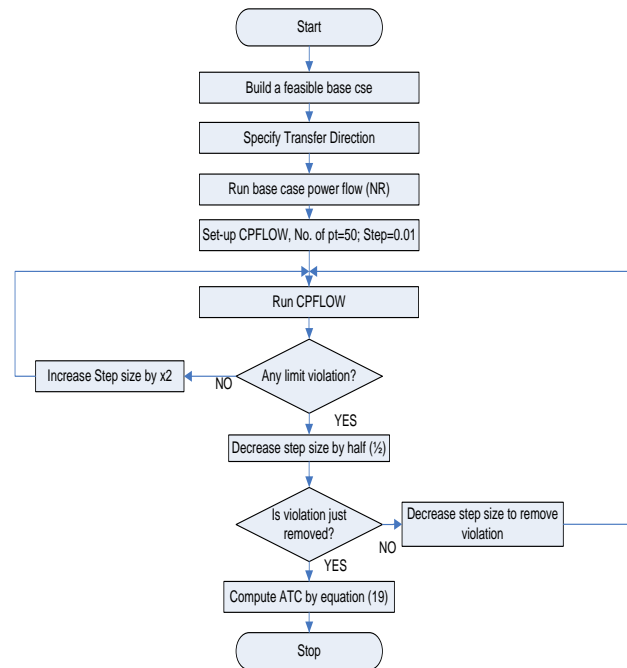
Figure 2: Flowchart of the proposed Hybridized Continuous- Repeated Power Flow Structure.

2.3 Step-size Control of HCR-PF

As shown in Figure 3.6, the step size implementation proposed in the hybridized CPFLOW – RPF structure start with a step – size of 0.01 corresponding to a loading point A. If there is no violation (Line thermal limits, voltage magnitude and generator reactive power), CPFLOW – RPF structure increase the step size to a loading point B (0.02) and then to loading point C (0.04) where a limit violation is encountered. CPFLOW – RPF structure then reduces the step size by half of the increment between point B (0.02) and C (0.04) to a new loading point D (0.03); should there be violation at this new point, the structure move to point E (0.025) and continues in that process.
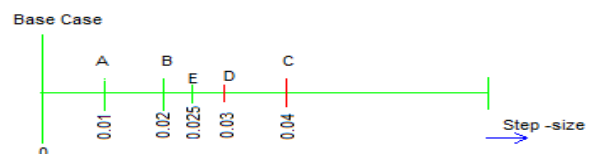
Figure 3: Step-size control implementation of the Hybridized Continuous-Repeated Power Flow Structure.

3. RESULTS AND DISCUSSIONS

3.1 IEEE 9 Bus Test System

The proposed method was implemented on IEEE 9 bus test system. Table 2 gives the results and a comparison is made with Adaptive Neuro-Fuzzy Inference System (ANFIS) method. Figure 4 gives the PSAT model of the IEEE 9 bus test system.

WSCC 3-machine, 9-bus system (Copyright 1977)
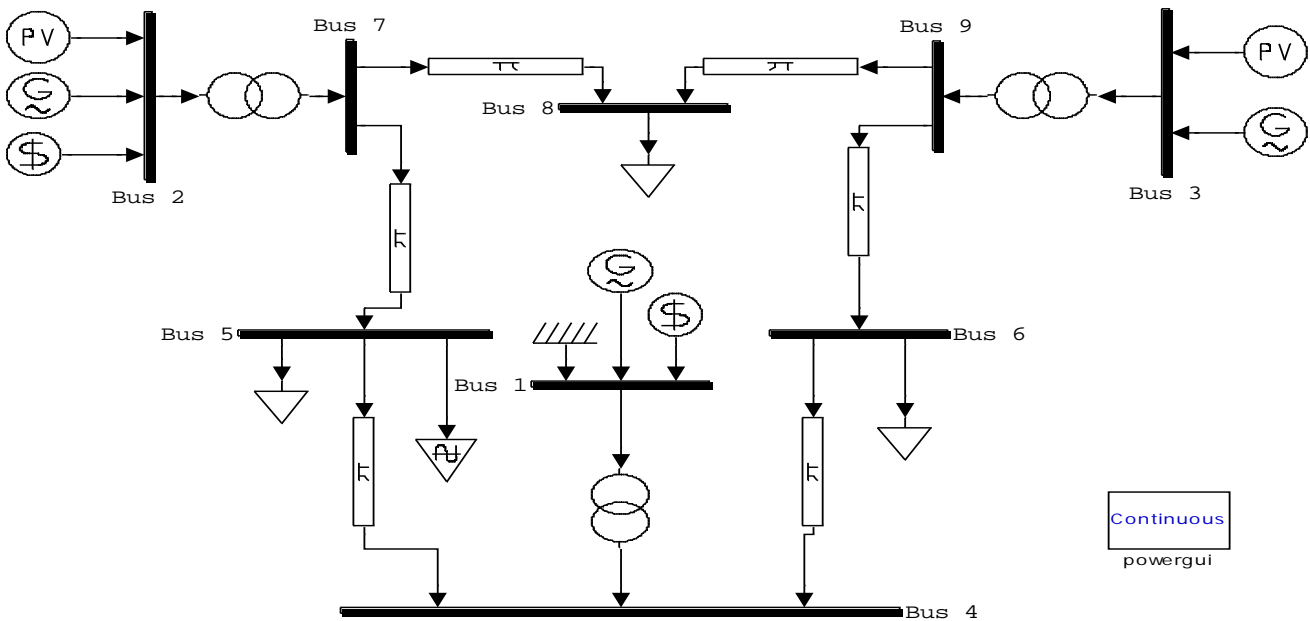
Figure 4: PSAT model of IEEE 9 bus test System.

Table 2: Comparison between HCR-PF and ANFIS method for thermal and voltage limitation various Transactions of IEEE 9 bus test system

TRANSACTION/METHOD	ATC_{TL}(MW) HCR-PF	ATC_{TL} (MW) HCR-PF (Pij)	ATC_{TL}(MW) ANFIS	ATC_{VL} (MW) HCR-PF	ATC_{VL} (MW) HCR-PF (Pij)	ATC_{VL} (MW) ANFIS
T1	66.39	68.11	65.36	146.50	152.37	156.77
T2	67.44	72.99	84.07	106.27	81.56	89.99
T3	88.24	92.70	NO VIOLATION	117.18	123.85	84.22
T4	66.79	71.82	117.05	107.65	117.28	133.78
T5	66.49	73.35	NO VIOLATION	91.16	102.08	79.34
T6	88.45	92.92	73.24	116.53	123.15	154.89
T7	66.83	73.75	144.6	92.95	103.88	127.13

From Table 2, observe that the interpretation of ATC results by either Rated system path (RSP) method or Network response (NR) method using HCR-PF gives different ATC values while ANFIS method gives a too optimistic ATC values. Transactions T3 and T5 shows no violation due to thermal limitation by the ANFIS method, this is rare if not impossible; each transmission line has a rated current carrying capacity which translate to it thermal constraints.

Figure 5 depict comparison between ATC_{TL}(MW) constrained by thermal limitation using HCR-PF and ANFIS. The ATC_{TL}(MW) HCR-PF (Pij) gives the interpretation of ATC results by Rated system path (RSP) while ANFIS method implemented only Rated system path (RSP). From Figure 5, Transactions T3 and T5 by implication mean an infinite ATC.
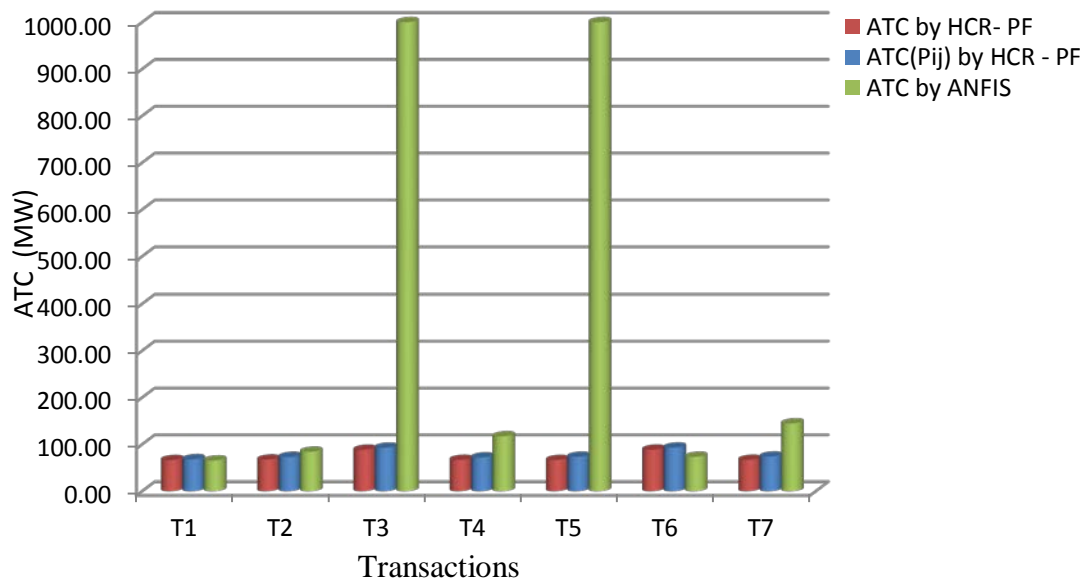
Figure 5: Comparison between ATC_{TL}(MW) constrained by thermal limitation using HCR-PF and ANFIS.

Figure 6 depicts Comparison between ATC_{VL} (MW) constrained by Voltage limitation using HCR-PF and ANFIS. Again ANFIS provides too optimistic results for ATC computation.

In addition, the last corrector step solution result of HCR-PF in PSAT environment which is obtainable in Excels identifies the limitation type and element rather than the searching techniques.

IEEE 30 Bus Test Systems

Table 3 gives the contingency ATC values of IEEE-30 bus system, which shows the comparison between the HCR-PF and that presented in reference (Yuan-Kang, 2007). Various transactions were implemented for both

contingency and normal study cases for IEEE-30 bus system and the results obtained were compared.

Figure 6 depicts the comparison of Table 3. HCR-PF is seen to provide a good alternative to ATC computation. Observe that from Table 3, the limiting lines to the contingency ATC values are same for both method compared.

To further validate the proposed method, ATC expected values among different network buses of the IEEE-30 bus system were also computed as shown in Table 4.
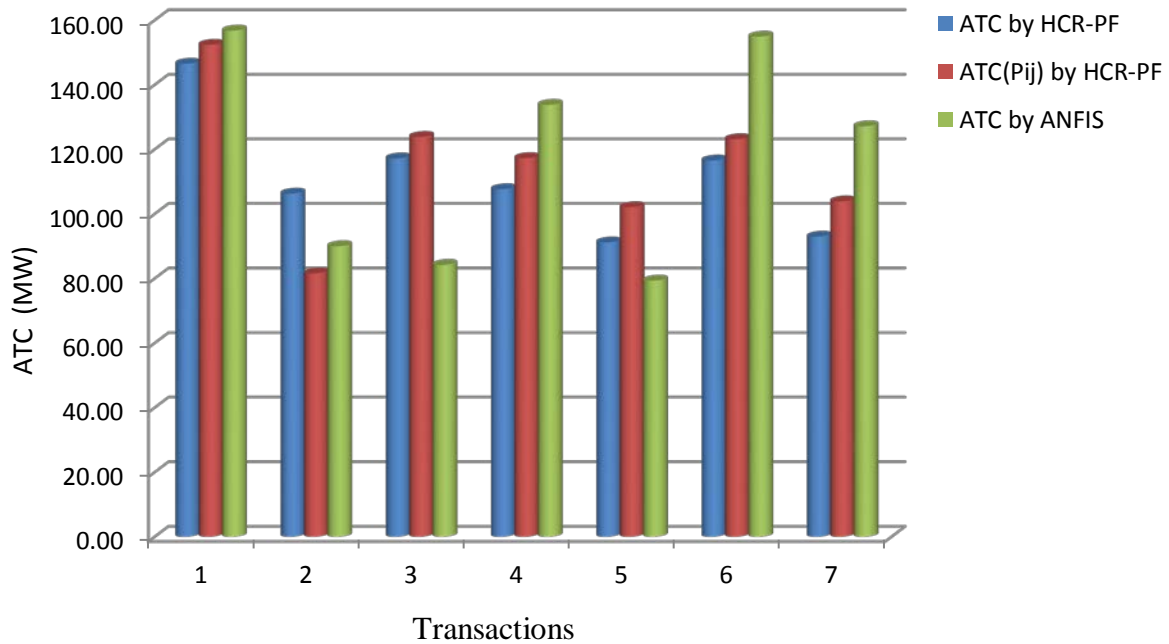
Figure 6: Comparison between ATC_{VL} (MW) constrained by Voltage limitation using HCR-PF and ANFIS.

Table 3: Contingency ATC Values from Bus 14 to Bus 21 of IEEE-30 bus

Bilateral Transaction	Outage Line		Limiting Line		ATC By Hybridized C-RPF	ATC By WU's Method
	From	To	From	To	ATC (MW)	ATC(MW)
From Bus 14 To Bus 21	12	14	14	15	22.2	22.2
	12	15	14	15	13.4131	13.5376
	12	16	14	15	28.77	28.0768
	14	15	10	21	28.49	28.4403
	15	18	10	21	33.7824	33.7682
	15	23	10	21	21.227	21.7515
	16	17	14	15	28.3627	28.8257
	10	17	10	21	29.3251	29.4786
	18	19	10	21	33.4643	32.5241
	19	20	10	21	28.7402	28.7572
	10	20	10	21	27.5504	27.9273
	10	21	21	22	11.669	14.289
	10	22	10	21	12.0471	13.1917
	22	24	10	21	27.8676	27.8809
	23	24	10	21	24.0214	24.1305
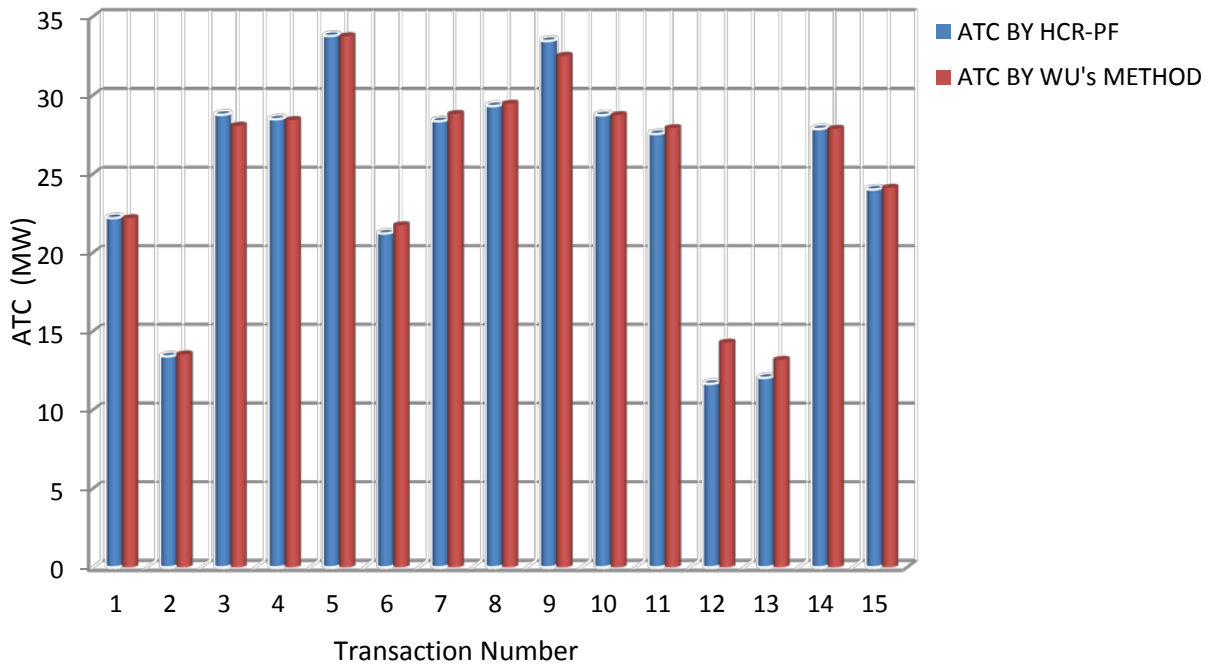
Figure 6: Comparison between ATC using HCR-PF and WU's Method.

4. CONCLUSION

This paper shows that Hybridized Continuous-Repeated power flow (HCR-PF) provides a good approximate alternative for Available transfer capability evaluation. Normal and contingency ATC(s) were computed. Single line (N – 1) outage criterion was used as contingency. It implemented both Rated system path (RSP) method and Network response (NR) method using HCR-PF for ATC results interpretation. Various transactions of IEEE 9 bus and IEEE 30 bus test systems using HCR-PF were implemented.

Table 4: A Comparison between ATC Methods in IEEE-30 bus systems

Comparison on ATC expected values among different network buses in the IEEE-30 bus system												
	ATC Expected values from bus 14 to other buses (MW)											
	From Bus	14	14	14	14	14	14	14	14	14	14	14
1	To Bus	15	16	17	18	19	20	21	23	24	26	29
	ATC (MW) Wu method	25.6	33.9	31.9	15.6	19.9	23.4	28.2	16.7	22.8	12.3	13.6
	ATC (MW) HCR-PF	25.4	32.9	30.8	15.0	16.8	23.0	28.0	13.0	11.0	10.3	13.0
	ATC Expected values from bus 15 to other buses (MW)											
	From Bus	15	15	15	15	15	15	15	15	15	15	15
2	To Bus	14	16	17	18	19	20	21	23	24	26	29
	ATC (MW) Wu method	29.7	41.1	38.2	14.7	18.5	21.5	31.3	15.8	24.3	12.3	13.6
	ATC (MW) HCR-PF	30.6	37.6	32.1	14.3	17.4	20.9	29.3	11.4	12.3	10.4	13.2
	ATC Expected values from bus 16 to other buses (MW)											
	From Bus	16	16	16	16	16	16	16	16	16	16	16
3	To Bus	14	15	17	18	19	20	21	23	24	26	29
	ATC (MW) Wu method	38.9	28.9	19.4	18.8	25.4	26.7	23.0	19.5	18.7	12.3	13.6
	ATC (MW) HCR-PF	37.8	24.2	17.4	18.0	14.6	25.3	22.1	14.1	9.5	11.0	12.6
	ATC Expected values from bus 17 to other buses (MW)											
	From Bus	17	17	17	17	17	17	17	17	17	17	17
4	To Bus	14	15	16	18	19	20	21	23	24	26	29
	ATC (MW) Wu method	36.8	35.7	24.6	21.5	30.7	30.3	25.6	21.6	16.6	12.3	13.6
	ATC (MW) HCR-PF	37.4	28.1	25.2	20.4	27.5	28.5	24.7	14.8	8.9	10.7	12.6
	ATC Expected values from bus 18 to other buses (MW)											
	From Bus	18	18	18	18	18	18	18	18	18	18	18
5	To Bus	14	15	16	17	19	20	21	23	24	26	29
	ATC (MW) Wu method	29.6	28.0	33.4	28.8	16.7	18.7	26.1	17.7	20.3	12.3	13.6
	ATC (MW) HCR-PF	30.3	28.3	33.1	28.3	16.1	18.1	26.3	13.0	11.2	10.7	12.5
	ATC Expected values from bus 19 to other buses (MW)											
	From Bus	19	19	19	19	19	19	19	19	19	19	19
6	To Bus	14	15	16	17	18	20	21	23	24	26	29
	ATC (MW) Wu method	32.4	30.1	35.7	32.3	21.0	42.9	27.3	19.0	18.7	12.3	13.6
	ATC (MW) HCR-PF	32.5	30.0	35.6	32.9	21.2	42.1	26.3	13.4	10.0	10.6	12.6
	ATC Expected values from bus 20 to other buses (MW)											
	From Bus	20	20	20	20	20	20	20	20	20	20	20
7	To Bus	14	15	16	17	18	19	21	23	24	26	29
	ATC (MW) Wu method	33.6	34.9	33.8	31.2	23.2	26.8	26.7	19.8	17.9	12.3	13.6
	ATC (MW) HCR-PF	33.7	34.4	34.5	32.0	23.1	25.0	25.8	14.0	10.0	10.5	12.2
	ATC Expected values from bus 21 to other buses (MW)											
	From Bus	21	21	21	21	21	21	21	21	21	21	21
8	To Bus	14	15	16	17	18	19	20	23	24	26	29
	ATC (MW) Wu method	34.8	35.3	30.1	28.9	22.2	32.1	29.7	21.9	14.5	12.3	13.6
	ATC (MW) HCR-PF	31.5	27.2	30.7	29.3	21.6	29.3	28.4	13.2	6.9	10.5	12.4
	ATC Expected values from bus 23 to other buses (MW)											
	From Bus	23	23	23	23	23	23	23	23	23	23	23
9	To Bus	14	15	16	17	18	19	20	21	24	26	29
	ATC (MW) Wu method	27.1	25.7	31.6	33.8	16.4	21.2	25.2	29.9	22.5	12.3	13.6
	ATC (MW) HCR-PF	26.4	26.1	30.4	31.9	15.8	19.6	24.0	27.6	15.3	10.7	12.3
	ATC Expected values from bus 24 to other buses (MW)											
	From Bus	24	24	24	24	24	24	24	24	24	24	24
10	To Bus	14	15	16	17	18	19	20	21	23	26	29
	ATC (MW) Wu method	33.9	36.3	34.6	31.3	19.3	26.3	32.3	30.2	24.5	12.3	13.6
	ATC (MW) HCR-PF	34.8	36.9	34.8	31.9	18.5	23.6	30.3	30.2	24.2	10.4	12.5

REFERENCE

Akinniranye, O. (2012). *Critical Appraisal Of The Progress On Evacuation Bottlenecks.* Enugu Power Summit: Transmission Company of Nigeria, Retrieved From. http://www.nigeriapowerreform.org/index.php?option=com_rokdownloads&view=folder&Itemid=82

Sadiq, A. M. N. Nwohu J. G. Ambafi and L. J Olatomiwa (2013). *Effect of Contingency on Available Transfer Capability (ATC) of Nigerian 330KV Network:* AU Journal of Technology. Volume 16 Number 4.pp.241 – 246.

Babulal, C., and Kannan, P. (2006). A Novel Approach for ATC Computation in Deregulated Environment. *J. Electrical Systems 2-3* , 146-161.

Chanrasekar, K., and Ramana, N. V. (2011). Fast And Efficient Method to Assess And Enhance Total Transfer Capability in The Presence od FACTS. *International Journal of Advances in Engineering & Technology* , 170-180.

Chih-wen, L., Chen-Sung, C., Joe-Air, J., and Guey-Haw, Y. (2005). Towards a CPFLOW-Based Algorithm to Compute all the Type-1 Load-Flow Solutions in Electric Power Systems. *IEEE Transactions on Circuits and Systems Vol.52, No.3,* , 625-630.

Dobson, I., Scott, G., Rajesh, R., Chritopher, D. L., Fernando, A. L., Mevludin, G., Jianfeng, Z., Ray, Z. (2001). *Electric Power Transfer Capability: Concept, Application, Sensitivity and Uncertainty.* Newyork: Power System Engineering Reaserch Center (PSERC) 01-03.

Ejebe, G., Tong, J., Waight, J., Frame, J., Wang, X., and Tinney, W. (1998). Available Transfer Capability Calculations. *IEEE Transaction on Power Systems, Vol.13, No.4* , 1521-1527.

Greene, S., Dobson, I., and Alvarado, F. L. (2002). Sensitivity of Transfer capability margins with a fast formula. *IEEE Transaction on Power Systems, Vol. 17, NO. 1* , 34-40.

Hojabri, M., and Hizam, H. (2011). Available Transfer capability Calculation. *Application of MATLAB in Science and Engineering* , 143-164.

Liang, M., and Ali, A. (2006). Total Transfer Capability Computation for Multi - Area Power Systems. *IEEE Transactions on Power Systems, Vol. 21, No. 3* , 1141-1147.

Liu, C.-C., and Li, G. (2004). *Available Transfer Capability Determination.* Abuja: Third NSF Workshop on US-Africa Research and Education Collaboration. Retrieved From http://www.docstoc.com/docs/126840418/US-Africa-Abuja-Liu-ATC

Marannino, P., Bresesti, P., Garavaglia, A., Zanellini, F., and Vailati, R. (2002). Assessing The Transmission Transfer Capability Sensitivity to Power System Parameters. *14th PSCC*, pp. 1-7. Sevilla.

Mark, H. G., and Chika, N. (1999). Available Transfer Capability and First order Sensitivity *IEEE Transaction on Power System* , 512-518.

NERC. (1996). *Available Transfer Capability Definitions and Determination.* Newyork:North American Electric Reliability Council. Retrieved From, http://www.nerc.com/docs/docs/pubs/atcfinal.pdf

Othman, M. M., Mohamed, A., and Hussain, A. (2006). Available Transfer Capability assessment using evolutionary programming based capacity benefit margin. *Electrical Power and Energy Systems* , 166-176.

Prabha, U., Venkataseshaiah, C., and Arumungam, S. M. (2010). Assessment of Available Transfer

Capability incorporating Probabilistic Distribution of Load Using Interval Arithmetic Method. *International Journal of Computer and Electrical Engineering. Vol.2, No. 4* , 692-697.

Sauer, P. W. (1997). Technical Challenges of Computing Available Transfer Capability (ATC) in Electric Power Systems. *30th Annual Hawaii International Conference on System Sciences.* Hawaii: PSerc: 97-04.

Shaaban, M., Ni, Y., & Wu, F. F. (2000). Transfer Capability Computations in Deregulated Power Systems. *The 33rd Annual Hawaii International Conference on System Sciences Proceedings, 4-7 January*, (pp. 1-5). Hawaii.

Venkataramana, A., and Colin, C. (1992). The Continuation Power Flow: A Tool for Steady State Voltgae Stability Analysis. *IEEE Transactions Power System* , 416-423.

Wu, T., and Fischl, R. (1993). An Algorithm for detecting the Contingencies which limit the inter-area megawatt Transfer. *North American Power Symposium*, Washington D.C. pp. 222-227.

Yan, O., and Chanan, S. (2002). Assessment of Available Transfer Capability and Margins. *IEEE Transaction on Power Systems, Vol. 17, NO. 2* , 463-468.

Yuan-Kang, W. (2007). A novel algorithm for ATC calculations and applications in deregulated electricity markets. *Electrical Power and Energy Systems* , 810-821.

FORCASTING SOLAR RADIATION INTENSITY USING ANN AND ANFIS (A COMPARATIVE STUDY AND PERFORMANCE ANALYSIS)

Salisu S, Abubakar A. S, Sadiq. B. O, Abdu A.I, Umar A.O

Department of Electrical and Computer Engineering, Ahmadu Bello University, Zaria
Nigeria

s.salisu@live.com, abubakaras@abu.edu.ng

ABSTRACT

This paper focused on developing a short term forecasting model to predict solar radiation intensity. The work adopted the use of both Adaptive neuro-fuzzy inference system and artificial neural network to determine the model that performs best in predicting solar radiation intensity. An experimental set up using TE4 photovoltaic cell apparatus to capture the solar radiation and other relevant data that were used. The model was developed and implemented using MatlabV 7.0. The results revealed that artificial neural network (ANN) based model generated an RMSE and Correlation of 4.1316 and 0.998396217 respectively, which outperform the adaptive neuro-fuzzy inference (ANFIS) with a RMSE and Correlation of 19.7357 and 0.960099 respectively in predicting short term solar radiation intensity.

Keywords: *Solar Radiation Intensity, Artificial neural network, Adaptive neuro-fuzzy inference system and TE4 Photovoltaic cell*

1.0 INTRODUCTION

There have been many different scientific efforts in order to realize better results in the domain of forecasting meteorologicalparameters. Solar radiation forecasting constitutes a very crucial issue for different scientific areas as well as for many different aspects of everyday life. Solar radiation forecasting plays an important role in power

system. To improve the security of the power system and reduce the generation costs, it is necessary to heighten accuracy of the load forecasting in power system. Therefore, establishing high accuracy models of the load forecasting is very important. During the past several decades, load forecasting has been extensively researched and a large number of models have been proposed. Traditional short-term load forecasting methods, which includes classical multiply linear regression (Rewagad and Soanawane, 1998).

Solar power forecasting is playing a key role in solar PV park installation, operation and accurate solar power dispatch ability as well as scheduling. Solar Power varies with time and geographical locations

and meteorological conditions such as ambient temperature, wind velocity, solar radiation and module temperature. The location of Solar PV system is the main reason of solar power variability. Solar variability totally depends on system losses (deterministic losses) and weather parameter (stochastic losses). In the case of solar power, deterministic losses can be found out accurately but stochastic losses are very uncertain and unpredicted in nature. In thispaper, Adaptive Neuro-fuzzy interface system and Artificial neural network are used as powerful tools for solar power Forecasting. The matlab tools are accurately and fast forecasting compared to conventional methods of forecasting. Depending on the forecasting range, broadly we can classify forecasting into four types (Long term forecasting, medium term forecasting and short term forecasting). Various traditional methods like time series method, regression based methods have been used for the prediction of load. The main drawback of this method is the explicit relationship between different variables, requirement of heavy computational time and large amount of memory space. (J.B. Theocharis, 1998)

2.0 DEVELOPED APPROACH

Adaptive Neuro-fuzzy Inference System The methodology adopted for the ANFIS model is as follows:

i. Partitioning of data. 70% of the data was used for training, while 30% was used for checking data.
ii. Load the input data (training data)
iii. Determination of the membership function. The model developed is based on using the fuzzy toolbox MATLAB ® 7.14.0.739(R2012a).
iv. Validation and checking of the model.
v. Determination of root mean square error (RMSE) and Pearson Correlation Coefficient.
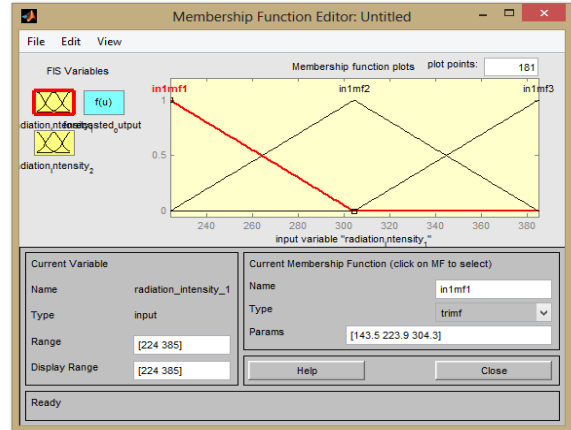
Figure 2. Membership function
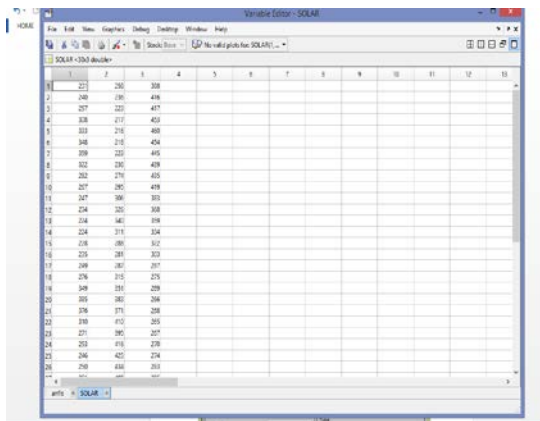
Figure 1. Partitioning of data editor.
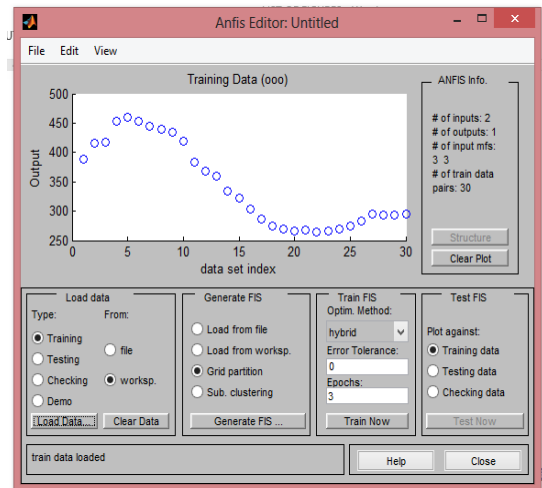
Figure 3. Loading of data

568

Artificial Neural Network (ANN)

The sequential steps adopted for the ANN model is as follows:

i. Partitioning of data. The data was partitioned into three, input variables, target and sample.
ii. Loading of data sample. The data was imported from matlab workspace to network/data manager.
iii. Network creation using feed-forward back-propagation, selection of the number of layers and number of neurons.
iv. Training and Validation of data was carried.

3.0 Performance Index

There various types of performance index, which are error calculation, computation time, comparison of the forecasting models but in this work the root mean square error and pearson correlation coefficient were used.

3.1 The Root Mean Square Error (RMSE)

It measures the performance during training. It is the square of the average squares error between actual output and the corresponding predicted output.

RMSE = √MSE

While the MSE (mean square error) is given by equation (4.1)

$$MSE = \frac{\sum_{i=0}^{n}(Actual\ output - predicted\ output)^2}{number\ of\ outputs}$$

Anfis- Based Model

MSE = 389.5
RMSE = 19.7357

Ann-Based Model

MSE = 17.070186
RMSE = 4.1316

3.2 Correlation Coefficient Analysis

It is a measure of linear relationship between two variables. Its value ranges from +1 to -1, where -1 indicates a perfect correlation, 0 implies absence of correlation and +1 means a perfect positive correlation exists.

The Pearson correlation coefficient is given by $r = \frac{\sum(x - \bar{x})(y - \bar{y})}{\sqrt{\sum(x - \bar{x})\ \sum(y - \bar{y})}}$

Where:

r is the correlation coefficient

x is the actual output

$\bar{x}$ is the mean of the actual output

y is the predicted output

y is the mean of the predicted output

Anfis- Based Model

CORRELATION COEFFICIENT = 0.960099

Ann-Based Model

CORRELATION COEFFICIENT=0.998396217
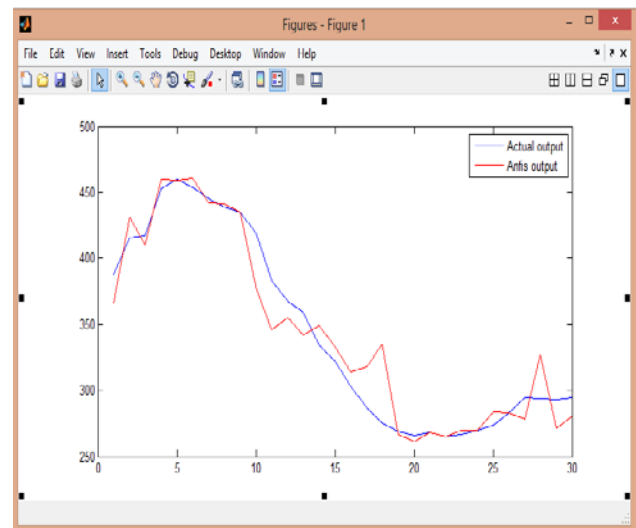
Figure 3.0 ANFIS-BASED Model

Comment on the plot indicates the actual solar radiation obtained for a period of three (3) days while the second plot indicates the predicted solar radiation using the developed ANFIS-BASED model.
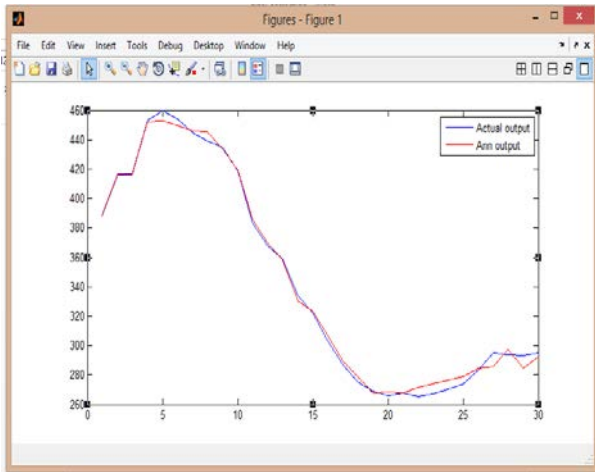
Figure 3.1ANN-BASED Model

Fig 4.0 ANN AND ANFIS BASED Model

Comment on the plot indicates the actual solar radiation obtained for a period of three (3) days while the second plot indicate the predicted solar radiation using the developed ANN-BASED model.

4.0 Comparison of ANFIS and ANN Model
Three meteorological parameters were used for the analysis of solar irradiation. The prediction performance of various artificial neural networks and adaptive neuro-fuzzy inference system were assessed by comparing their forecasted output to actual data obtained, using mean square error (MSE), root mean square error (RMSE) and Pearson correlation coefficient to determine the results which were compared. The comparison between the best structure of best ANN-model (with R=0.998396217) and some ANFIS-model (with R=0.960099) has shown the superiority of the ANN model. These models could be used to evaluate the solar potential of a location. The use of these models in the remote locations that solar measurement devices are not available can be beneficial as an effective tool to select the most efficient locations for using solar energy.

5.0 CONCLUSION
The ANFIS based-model developed generated an RMSE and correlation of 7 and 0.960099 respectively. The ANN-based model developed also generated an RMSE and correlation of 4.1316 and 0.998396217 respectively. These show that both models can be used for Solar Intensity Radiation validation. The ANN provides a better positive correlation coefficient (CoA) 0.998396217 as compared to ANFIS-based model of 0.960099 .The ANN-based model also has an RSME of 4.1316 as compared to the 19.7357 of the ANFIS-based model.
From the statistical analysis carried out on the developed ANFIS based and ANN-based models, both the models can be used to forecast the solar intensity radiation but the ANN-based model outperform the ANFIS-based model using the variables due to the values obtained from the root mean square error and correlation coefficient closeness to absolute one.

REFERENCE:

Jayabharata M. R, and Dusmanta K. M, (2006).
A comparative study of Artificial Neural Network and Fuzzy Inference System Approach for digital relay of transmission line faults,Department of Electrical and Electronic Engineering,Birla Institution of Technology,Mesra,India.

Abdul Azeez, M.A., "Artificial Neural Network Estimation of Global Solar Radiation using Meteorological Parameters in Gusau, Nigeria", Archives of Applied Science Research, 3 (2): 586-595, 2011.

Constatin V. A,(1995). Fuzzy logic and Neuro-Fuzzy Application Explained,173.

Carlos G,. Artificial Neural Network for Beginners.

Jagadish H. Pujar, Fuzzy Ideology based Long Term Load Forecasting, *World Academy of Science, Engineering andTechnology* 64 2010

Takagi, T., and Surgeon, M., "Fuzzy identification of systems and its applications to modeling and control", IEEE Transactions on Systems Man and Cybernetics, 15(1): 116–132, 1985.

Adepoju G. A ,.Ogaunjuyigbe S. O, and Alawode K. O, "Application of neural network to load forecasting in Nigerian electrical power system", *The pacific journal of science and technology*, vol.8, no.1,May 2007, pp.68-72.

Garba (2011), Quality of service,phd. Thesis,electrical engineering department,Ahmadu bello university.

APPENDIX

Table 4.1 Forecasted Solar Intensity Radiation

Actual output	Anfis output	Error	Square Error	Ann output	Error	Square Error
388	366	22	484	388.9516	-0.952	0.9055
416	431	-15	225	416.823	-0.823	0.6773
417	410	7	49	416.1949	0.8051	0.6481
453	460	-7	49	452.2378	0.7622	0.5809
460	459	1	1	452.5724	7.4276	55.1692
454	461	-7	49	449.9686	4.0314	16.2521
445	442	3	9	445.7856	-0.786	0.6171
439	441	-2	4	445.3857	-6.386	40.7771
435	435	0	0	433.4134	1.5866	2.5172
419	377	42	1764	419.512	-0.512	0.2621
383	346	37	1369	385.5817	-2.582	6.6651
368	355	13	169	369.5735	-1.574	2.4759
359	342	17	289	358.6645	0.3355	0.1125
334	349	-15	225	330.7996	3.2004	10.2425
322	333	-11	121	323.132	-1.132	1.2814
303	314	-11	121	306.9135	-3.914	15.3154
287	318	-31	961	289.3584	-2.358	5.562
275	335	-60	3600	279.1868	-4.187	17.5292
269	267	2	4	267.5885	1.4115	1.9923
266	261	5	25	268.0794	-2.079	4.3239
268	268	0	0	267.5259	0.4741	0.22477
265	265	0	0	271.2222	-6.222	38.7157
267	270	-3	9	273.9125	-6.913	47.7826
270	270	0	0	276.7279	-6.728	45.2646
274	284	-10	100	278.8992	-4.899	24.0021
283	283	0	0	284.7967	-1.797	3.2281
295	278	17	289	285.9359	9.0641	82.1579
294	327	-33	1089	297.3466	-3.347	11.1997
293	271	22	484	284.6922	8.3078	69.0195
295	281	14	196	292.4302	2.5698	6.6038
			∑ 11685			∑ 512.10557

DEVELOPMENT OF A COST-FRIENDLY HOME-RANGE TV TRANSMITTER TO PROVIDE SAFE TV CONTENT TO UNDERAGE UNSUPERVISED KIDS

M. Okwori[*], S. S Oyewobi, M. Saidu, U. Abdullahi
Department of Telecommunication Engineering,
Federal University of Technology Minna, Nigeria
[*]michaelowkori@futminna.edu.ng, 08032903629.

ABSTRACT

The security of a nation is directly linked to the moral conduct of her citizens, and this is affected by the kind of upbringing such citizens received as kids. Direct access of kids to video players and satellite TV receivers can lead to unwholesome programs being watched by the Kids especially when they are unsupervised, which can lead to character degradation and deformation. As a solution to this problem, this work is aimed at restricting unsupervised access of underage persons to programs on these electronics devices. Therefore, a low cost home range TV transmitter with pre-select channel-transmit capability, and auto timed turn-on and turn-off was designed. The designed Transmitter powers a Video player or Satellite TV Decoder at a preset time and transmits pre-selected programs on a Video player or Satellite TV Decoder in a restricted region in the house to a Television Set in an unrestricted region in the House that kids have access to for a preset duration. The Transmitter was tested, and it powered the Decoder and transmitted pre-selected programme at the preset time and for the preset duration.

Keywords: *Kids, TV Transmitter, Preset Duration, Restricted Region, Unrestricted Region words.*

1. INTRODUCTION

In this present day, Technology has grown to the level that information dissemination has been made easy and relatively cheap to such an extent that most homes now have access to cable TV and/or a video player. As a result, the level of information at our disposal has increased dramatically with time. Television can be a powerful learning and teaching tool. By means of it, we learn about lands and peoples we may never visit, we watch news as it happens across the globe and insights are gained into politics, history, current events and culture. In fact, Television entertains, instructs and inspires.

However, most of the programmes are neither wholesome nor educational with most portraying scenes of violence, sex, drugs and the use of strong language which might be detrimental to character development in kids in particular and under-aged in general. These scenes of violence are believed to induce aggressive behavior in people and make them less sympathetic towards victims of real life violence. Scenes of sex are also believed to promote promiscuity and

undermine moral standards (Munni and Kana, 2010) (Awake, 2006). The duration spent watching TV can also be detrimental. According to the American Academy of Paediatrics, the average child watches three hours of TV a day, while two hours of quality programming is the maximum recommended by the Academy. Active play time is needed to develop mental, physical and social skills (Amin and Neda, 2011), (American Academy of Pediatrics, 2001), (Seline, 2011).

As a result of the variance in the content of programmes, a classification/rating system was designed to give parents more information about the content and age-appropriateness of TV programmes. But this rating system need to be simplified and made universal to enable parents choose appropriate programmes for kids (Munni and Kana, 2010). Also this rating system has not being effective in this environment (Nigeria) where most at times parents are out seeking for means of catering for the upkeep of the family, and kids are left at home with direct access to video machines and satellite decoders with almost no control as to what they watch. Most satellite decoders now

come with password settings that can be used to lock channels, but this still does not solve the issue of time spent to watch unlocked channels and access to other video players.

TV transmitter is an electronic device that can be used to rebroadcast video signals or Satellite TV throughout your house. TV transmitter is divided into two main components namely: the exciter and RF power amplifier. The exciter provides the signal processing functions required to convert baseband TV signal into a modulated RF signal on the assigned channel while the PA is used to amplify the modulated RF signal to the desired level for transmission (Gerald, Robert, 2011). The PA technology is available commercially in both the solid-state and tube devices. Solid state devices is mostly used for VHF channels but for UHF channels both solid-state and tube devices are used (Gerald, Robert, 2011). In (Marc, Spiwak, 1997) proposed a TV transmitter that combines line level audio and video signals with a transmission power of up to 300 feet. A power efficient Broadcast Facility

Transmission was designed and developed by (Cavell, Martz, 2011). The analog transmitter operates with low power and the life of solid-state device used was improved. However, in our work, a low cost home range TV transmitter with pre-select channel-transmit capability, and auto timed turn-on and turn-off was designed. This work provides a means for only authorized wholesome TV programmes selected by parents to be made available to under aged unsupervised kids. This work is presented in the following order, section two presents the design and implementation, section three highlights the testing and results, section four presents the cost effectiveness and section five concludes the work.

1. DESIGN AND IMPLEMENTATION

This design is made up of basically three main blocks; the power supply, the timer and the transmitter. Each of these units carries out a pertinent task towards achieving the aim of this work. The complete circuit diagrams and the block diagrams are presented in Figures 1 and 2 respectively.
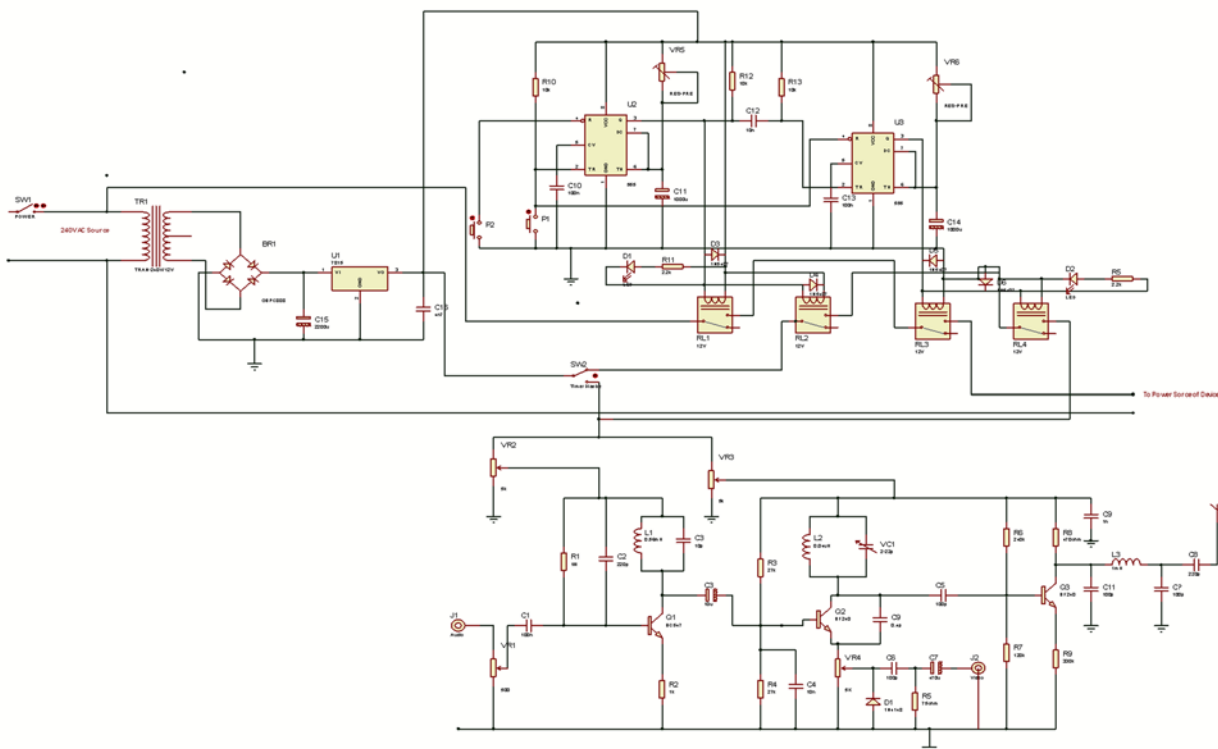
Figure 1: Circuit diagram of Designed Home-range Transmitter
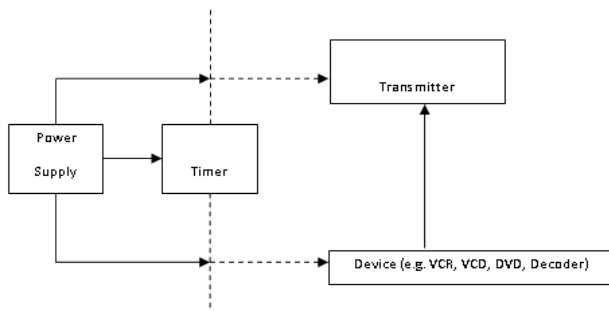
Figure 2: Block diagram of Home-range Transmitter

1.1. Design

The system is powered by a regulated 15V source. It was observed that the quality of the transmitted image is sensitive to the power source voltage, as such a variable resistor was fixed after the regulator to give a variable power supply that can be adjusted to give the optimum transmitted image.

The timer is situated between the designed transmitter and the video source, and determines when and for what duration power gets to both of them. This Timer unit is made up of the wait duration timer, the transmit duration timer, the switching relays and the LED displays. The wait duration timer which is responsible for automatically turning on the transmitter and the video source after a set wait duration. This was achieved using cost friendly 555 timer IC in the monostable mode. The duration of the output pulse on Pin3 of the 555 timer IC depends on the values of the Resistor R1 (between Pin6 and Pin8) and Capacitor C2 (between Pin6 and Pin1) (Schuler, 1999).

The value of the Capacitance was kept fixed at 1000μF, and the Resistance to achieve time durations of 1minute, 30minutes, 1hour and 1hour 30minutes was determined using

$$R = \frac{t}{1.1C} \qquad (1)$$

For t = 1 minute, R1 = 54 545 $\Omega \approx$ 6.9K + 47K.

For t = 30 minutes, R2 = 1 636 364$\Omega \approx$ R1 + 1.5M.

For t = 1 hour, R3 = 3 272 727$\Omega \approx$ R2 + 1.5M.

For t = 1 hour 30 minutes, R 4= 4 909 091$\Omega \approx$ R2 + 1.5M.

Each of the calculated resistance was approximated to easily sourced resistance values and values that have already been used in the circuit to reduce cost and avoid duplication of components. The output of the wait duration timer was coupled through a resistor-capacitor network to pin 2 of the transmit duration timer to achieve edge triggering.

The Transmit duration timer determines the duration that power is supplied to the transmitter and the video source and is similar to the wait timer except that it is edge triggered by the output of the wait duration timer (comes on the instant the input to its pin2 goes low). The time duration of transmission is similar to that of the wait timer analyzed above with variable resistor RV2 (transmit duration variable resistance) having the values as RV1 (wait duration variable resistance).

The time duration is activated with the aid of two Push buttons P1 and P2. Push button P1 starts the wait duration timer and resets the transmit duration timer, while P2 resets or stops the wait duration timer.

Between the timers and the transmitter and video source are situated four relays: RL1, RL2, RL3 and RL4. The first two relays (wait duration relays) are normally open and become closed only when there coils are excited by a voltage greater than their excitation voltage of 12V. The coils are connected to the Vcc and Pin 3 (output) of the delay timer. As such these relays become activated only when delay timer output goes low. At this instant power is fed to the other two relays. The two other relays (transmit duration relays) are also normally closed, but these are activated as the transmit timer comes on because the coils are connected between pin 3 (output) of second 555 timer and the ground. When activated, RL3 and RL4 supplies power to the video source and the transmitter respectively (Thomas, 2007).

The transmitter was designed to be a low cost, low range of 15 meters and a variable frequency transmitter and comprises of the following sections: pre-modulation module, modulation module and the post modulation module. The pre-modulation module was designed to handle signal processing functions to be carried out on the signal in order to achieve efficient radiation of the electromagnetic signal generated at the end. This module takes care of filtering of the input signals (for both the audio and video signals), load matching and DC restoration of the video signal and finally the variable control for the input video and audio input to act as a variable control of the amount of the output of the source that is been fed into the transmitter (Adediran, 2005). The modulation module is responsible for combining both the audio and video signals with high frequency carrier signals to enable efficient radiation.

The audio signal is frequency modulated. The carrier frequency is generated with the use of an oscillator with an LC tank circuit. Setting a carrier frequency of 4.5MHz and using a ceramic capacitor, C3 of capacitance 1nF, the value of the inductance of L1 can be calculated thus (Theraja, 2002):

$$L = \frac{1}{4\pi^2 f_c^2 C} = \frac{1}{4\pi^2 \times (4.5 \times 10^6) \times (1 \times 10^{-9})}$$
$$= 1.25\mu \qquad (2)$$

This inductance was obtained by coiling an SWG 24 coil which has a diameter of 0.56mm. Therefore the number of turns required to achieve that inductance was calculated thus

$$N = \sqrt{\frac{LI}{\mu_o \mu_r A}} = \sqrt{\frac{1.25 \times 10^{-6} \times 0.01}{4\pi \times 10^{-7} \times 1 \times 7.854 \times 10^{-7}}}$$
$$= 112 \ turns \qquad (3)$$

For the video modulation, amplitude modulation was employed. The radio frequency of the video channel has a bandwidth of 7.625MHz, with an attenuation of 20dB at 1.25 and 6.375MHz (Green, 1992). Due to the large bandwidth of the visual signal, it would be unwise to use frequency modulation. The carrier frequency was generated by a tank circuit comprising of inductor, L2 and variable capacitor, VC1. A variable capacitor was used so as to make the frequency of transmission variable. A variable capacitance of 2-22pF was used and an already wound inductor of inductance of 0.04uH was purchased and used. This gives a carrier frequency varying from f_1 to f_2 which are calculated thus:

$$f_1 = \frac{1}{2\pi\sqrt{LC_{max}}} = \frac{1}{2\pi\sqrt{0.04 \times 10^{-6} \times 22 \times 10^{-12}}}$$
$$= 169\ 659\ 739.4 Hz \ \approx 170 MHz \qquad (4)$$
$$f_2 = \frac{1}{2\pi\sqrt{LC_{min}}} = \frac{1}{2\pi\sqrt{0.04 \times 10^{-6} \times 2 \times 10^{-12}}}$$
$$= 562\ 697\ 697.6 Hz \ \approx 563 MHz \qquad (5)$$

The output of the transmitter section comprises of the carrier wave; which is amplitude modulated by the video signal and the already frequency modulated audio at a frequency of *fc+ 4.5MHz*. This output is then amplified using a common emitter amplifier using BF240 transistor. After which it is then passed through a low pass filter to remove the low frequency noise from the output before it is radiated using a 75Ω antenna.

1.2. Mode of Operation

The designed system is aimed at preventing unsupervised kids and unauthorized persons from having direct access to video machines, thereby curtailing the duration spent in front of the TV and also providing a means for restricting the programmes watched to those pre-screened by parents. The device has an audio and video input jack where the video machine's output can be connected to and also has a 240V power socket which powers the video machine. It also has two knobs for setting the timer durations. The first knob determines the duration that the device waits before it powers on both its transmitter and the video machine. Likewise the second knob determines the duration that the

device transmits and powers the video machine. Both knobs have setting for 1minnute (for testing purpose), 30 minutes, and 1 hour and 1 hour 30 minutes durations. The device set-up is depicted in Figure 3.
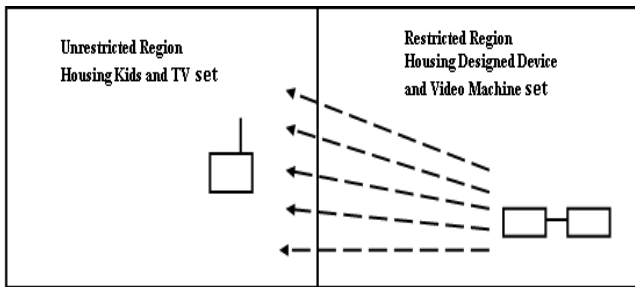
Figure 3: Setting up of designed device

The device and the video machine are situated in a restricted region of the house and TV set is situated in an unrestricted region of the house where kids can have access to. The already screened video or channel is loaded on the video machine, and the duration of both the waiting and transmission is set on the device. At the set time, the device comes on and also powers the video machine, which plays the cued video. The video being played is then transmitted wirelessly to unrestricted regions where kids can watch on a TV set tuned to the frequency of transmission of the device. After the set duration has elapsed, the device turns itself off and cuts power supply to the video machine.

2.   RESULTS AND DISCUSSIONS

The designed and constructed circuit was subjected to a series of tests and the results obtained were analyzed and relevant deductions made. The following tests were carried out: Frequency selection test, Range of coverage test, Time duration test. Due to the limitation of unavailability of spectrum analyzer, a physical eye test was carried out for both the frequency and range of coverage test.

The frequency selection test was performed to determine the frequency at which the transmitted signal was strongest. A video player was connected to the designed circuit and then powered and television set at some distance away was tuned until the best picture and sound was obtained. The frequency at which the best picture and sound was obtained was saved on the set and taken as the frequency of transmission. Figure 4 are pictures of the received image at different reception frequencies. The frequency of the Figure 3(c) was set as the transmission frequency.

The range of coverage test was carried out to determine the range of transmission of the transmitter. A video machine was connected to the designed circuit and then powered. A television set tuned to the frequency of transmission of the transmitter is then moved gradually away from the point of transmission until the maximum distance at which an acceptable image/audio is received at the television. The following images were obtained at the stipulated ranges from the transmission point. From the images as shown in Figure 5, it is best the TV set is placed at a distance of not more than 25 meters from the device, optimal images are received at range less than 15meters

(a) Poor image received   (b) Better image received   (c) Best image received

Figure 4 Images received at various transmission frequencies.
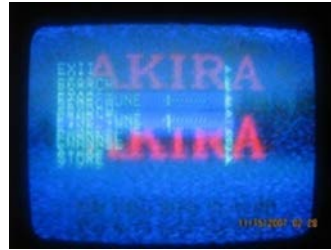
| (a) Range<15m | (b) 15m<Range<25m | (c) Range>25m |
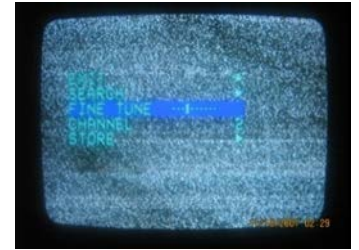
Figure 5 Images received at various transmission ranges

The last test performed was the timer duration test and was performed to determine the actual time at which the device automatically comes on or off as the case may be. The video player was connected to the designed circuit and then powered. A television set was tuned to the frequency of transmission and placed within the range of transmission. The timer knob for both the wait duration and the transmit duration was gradually increased from the 1 minute to the 1 hour 30 minutes duration and the actual time of trip on and off measured with a stopwatch. In Table 1 are the various results on the measured wait and the transmission times as against the calculated or theoretical time.

Table 1: Time Duration Test Results.

THEORETICAL TIME(HR:MM:SS)	WAIT DURATION (HR:MM:SS)	TRANSMIT DURATION(HR:MM:SS)
0:01:00	0:01:02	0:01:00
0:30:00	0:35:01	0:38:38
1:00:00	1:08:40	1:12:20
1:30:00	1:45:10	1:49:05

It can be observed that the actual duration time of the timer differs from the calculated values. This is due to deviances in the values of resistors R and capacitance C, which determine the time, from their stipulated values. Figure 6 shows the resulting errors in the wait time durations and transmit time durations.
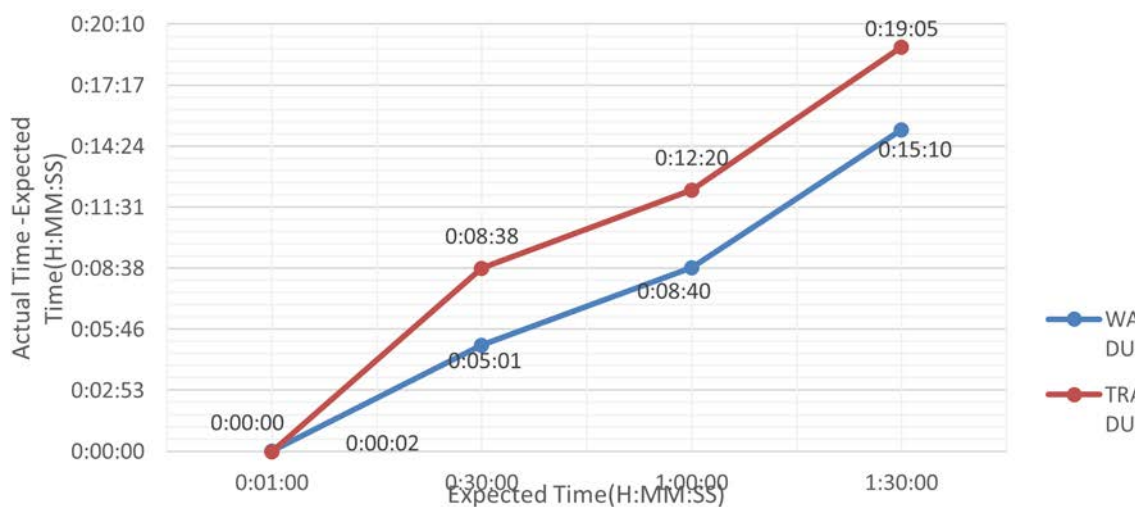
Figure 6 Plot of the Error in Time Durations

This increases as the time duration increases and a maximum value of 19:05 achieved in the 1:30:00 transmit duration. To achieve a higher accuracy level in the timing, a crystal oscillator should be used, but this will increase the cost of the device.

4. COST EFFECTIVENESS

One of the aims of this work is to provide a cost friendly device that would provide parents with a means of providing wholesome TV programs only to unsupervised under aged kids for a set duration of time. The design and implementation of the device made use of easily available and cost effective components. Table 2 shows the components used and the final cost of the device which confirms its cost effectiveness.

Table 2: Cost of Components Used.

S/n	Item	Qty	Unit Cost (Naira)	Total cost (Naira)
1	12V Relay	4	70	280
2	12V, 500mA step down Transformer (centre tap)	1	100	100
3	Variable Resistors	6	30	180
4	555 timer	2	70	140
5	Resistors	13	10	130
6	Diodes	4	10	40
7	LED	2	10	20
8	Casing	1	100	100
9	Veroboard	1	50	50
10	Capacitors	16	20	320
11	Inductors	2	20	40
12	7815 Regulator	1	60	60
13	Variable Capacitors	1	80	80
14	Switches	2	20	40
15	Input Jacks	1	30	30
16	Push buttons	2	10	20
17	Transistors	3	100	300
	TOTAL			**1,930**

The total cost of 1,920 Naira ($9.7) was achieved. Similar home range devices available on online stores were more expensive with price ranging from $20 to $30 (Ebay Online Stores).

5. CONCLUSION

A cost friendly device was designed and developed to provide safe TV content to under aged unsupervised kids. The circuit was realized with easily available components and a simple but effective circuit design. The device designed met the set objectives, but there is still room for improvements. Further work would concentrate on achieving the timing using a microcontroller so that the durations are not restricted to set times and improving the quality of the transmission image.

REFERENCES

Adediran Y A, (2005) Telecommunications Principles and Systems, Finom Associates, Minna, Nigeria.

American Academy of Pediatrics: AAP policy statement: Children Adolescents, and Television (RE0043), February 2001;107:2 (423-426)

Amin A, Neda T, "The Role of Television Advertising and Its Effects on Children", Interdisciplinary Journal of Research in Business, Vol. 1, Issue. 9, (pp.01- 06) September, October, 2011. (Amin and Neda, 2011)

Awake!, (2006) "Television How Does It Influence Your life?", Watchtower Bible and Tract Society of New York, Inc., October 2006 Edition.

Cavell Martz & Associates (2011) "Power Efficient Broadcast Facility Transmission Design for Flexible Advanced Services for Television and Radio on All Devices".

Ebay Online Stores, http://m.ebay.com/itm/wireless-home-broadcasting-system-universal-transmitter-receiver-TV-security-/351159814954?nav=SEARCH, accessed: August, 2015

Gerald W Collins, Robert J Planka, Harris Corporation (2011)

Green D C, (1992) "Transmission systems", Pitman book LTD, 2nd Edition.

Marc Spiwak (1997) "TV Transmitter Use it to rebroadcast video signals throughout your house", Poptronix electronix Handbook.

Munni R, and Kana R J, (2010) "Effect of Electronic Media on Children", Indian Pediatrics, volume 47, pp 561 -568, July 17.

Schuler C A (1999) Electronics Principles and Applications, McGraw-Hill, 5th Edition.

Seline K (2011) "A Study on the Impact of Electronic Media, particularly Television and Computer Consoles, upon Traditional Childhood Play and Certain Aspects of Psychosocial Development amongst Children" International Journal for Cross-Disciplinary Subjects in Education (IJCDSE), Vol 2, Issue 1.

Theraja A K (2002) A Textbook of Electrical Technology, S. Chand & Company LTD, 23rd Edition.

Thomas L F (2007) Electronics Fundamentals: circuits, Devices and Applications, Pearson Education, Upper Saddle River, New Jersey, 7th Edition.

THE EFFECT OF IMMERSION TIME ON THE CORROSION PROTECTION PERFORMANCE OF MILD STEEL BY 3-MERCAPTOPROPYLTRIMETHOXYSILANE SOL-GEL COATING

Abubakar Mohammed[a,*], Nayef M. Alanazi[b] , Heming Wang[a]

[a]Materials and Engineering Research Institute, Sheffield Hallam University, Howard Street, Sheffield S1 1WB, UK
[b] Research and Development Centre, Saudi Aramco, Box 62, Dhahran 31311, Saudi Arabia
*Abubakar.Mohammed@student.shu.ac.uk

ABSTRACT

Corrosion protection can be achieved by depositing a barrier layer such as coating, to prevent the material from coming in contact with the corrosive environment. Sol-gel coatings offer a number of advantages over other methods of protection for metallic materials. 3-mercaptopropyltrimethoxysilane (MPTMS) was used as the precursor for sol-gel coating on mild steel substrate. The effect of immersion time on the coating performance was assessed by Tafel analysis, visual inspection and electrochemical impedance spectroscopy (EIS) in aerated 3.5 wt.%NaCl solution at ambient temperature for 72 h. The electrochemical test of MPTMS coating on mild steel showed that though mild steel was protected by the coating due to coating acting as a barrier to the electrolyte by impeding its contact with the metal surface, the degradation ofthe coating is due to the presence of pores in the coating. Tafel plots revealed that MPTMS sol-gel coating has a porosity of 0.0861 %. Micrograph showed that the pits initiated did not propagate.

KEY WORDS: 3-Mercaptopropyltrimethoxysilane (MPTMS); Sol-gel coating; EIS;immersion time; Mild steel.

1. INTRODUCTION

Metals such as aluminum, copper, iron, and magnesium and their alloys are materials frequently used in marine, oil, construction, automobile and aircraft industries. These materials are the pillars of most engineering operations such as construction, aerospace, containers, packaging, transportation, etc. The use of these materials is mainly due to the properties they possess, such as high strength, workability, low-cost and re-usability (Carvalho *et al.* 2014; Balgude & Sabnis 2012). Metals are extracted in the form of ores in their stable form. The process of converting these ores to metals makes it thermodynamically unstable. Despite the physical characteristics of the resulting materials such as aluminum, copper, iron, and magnesium, they are susceptible to corrosion when they are expose to an aggressive environment as they tend to be in a constant process of reverting to a more stable form in which it was found, such as oxides, sulphates, sulphides, or carbonates. The destruction of metal (Corrosion) takes place in the form chemical or electrochemical reaction with its environment. Corrosion causes loss of valuables and reduces the ability of these metals to function at their optimal abilities.

Chromates conversion coating has been used as the most effective pre-treatment coating on metals for corrosion protection systems (Yasakau *et al.* 2014; Osborne 2001; Kendig & Buchheit 2003).

The new permissible exposure limit (PEL) from the Occupational Safety and HealthAdministration (OSHA) for Cr^{6+} (U.S. Department of Labor *et al.* 2009) has led to a growing restrictions being imposed on the use of hexavalent chromium. Sol–gel derived thin films coating present one of the most viable pre-treatments alternative to the chromate (Akid *et al.* 2011; Zheludkevich *et al.* 2005; Wang *et al.* 2010). A major advantage of the sol–gel process is the possibility of not only forming an inorganic structures, but also forming a hybrid organic-inorganic network structures at low temperatures (Akid *et al.* 2011; Wang *et al.* 2010). Sol–gel coatings have good adhesion to both metallic substrates and organic top coats. In addition, sol-gel films does not require any special processing equipment since the process of applying the sol-gel film is very similar to the conventional coating techniques such as

dip, spin or spray coating and therefore, very cost-effective and can be used for the production of homogeneous films on a large scale (Bechinger *et al.* 2000).

MPTMS has been used as a sole precursor in the preparation of sol-gel coating for Au, Ag, Al, Zinc and copper (Thompson *et al.* 1997; Cai *et al.* 2000; Sinapi *etal.* 2002; Sinapi *et al.* 2003). Recently, Vignesh*et al.*(2014) studied the effect MPTMS concentration as a sole precursor in a Sol-Gel coating Al substrate and revealed that corrosion protection increases with increase in concentration of MPTMS.To the knowledge of the authors, there is no existing literature on the corrosion protection with MPTMS as a sole precursor for the protection of mild steel. In this second paper, the effect of immersion time on the corrosion protection performance of mild steel by 3-mercaptopropyltrimethoxysilane sol-gel coating was examined.

2. EXPERIMENTAL METHODS

2.1. Materials

3-mercaptopropyltrimethoxysilane (MPTMS)-95% was purchased from Sigma-Aldrich and used without any further purification. Nitric acid (70%) and 2-propanol (99.5) were also purchased from Sigma-Aldrich. Deionized water was used for all the experiments and sol preparation.

2.2. Sol-gel preparation

MPTMS sol-gel was prepared by dissolving MPTMS in 2-propanol. Acidified water of 0.1M nitric acid was added drop wise into the mixture. The volume ratio of MPTMS:2-propanol:HNO_3 was 2:1:1 and the mixture was magnetically stirred for 1 hr at the rate of 500 rpm, resulting in a clear and homogenous solution, during which hydrolysis and condensation occurred.

2.3. Substrate preparation

Mild steel panels measuring 102 mm × 25 mm × 1.6 mm were used as the substrate. The chemical composition of the substrate is given in Table 1. The as received panels were soap washed and rinsed with deionized water, then immersed into 2-propanol alcohol to remove inorganic impurities such as oil, grease and fatty residues from the surface. It was then placed into ultrasonic bath for 5 mins for additional cleaning, washed with deionized water and dried with warm nitrogen air. The panels were then placed in a desiccator pending film deposition.

Table 1: Composition of mild steel with Fe as balance

Element	C	Si	Mn	P	S	Ni	Al	Mo	Cu
Wt. (%)	0.02	0.01	0.21	0.007	0.006	0.02	0.054	0.01	0.004

2.4. Coating deposition

Coating was applied on the cleaned mild steel substrate by spray coating using high velocity low pressure (HVLP) of Gen3 system spray coating machine model SB-2900. Thesubstrate was placed at 75 degree to the horizontal and the coating was applied manually using SprayCraft (SP10) spray gun connected the machine. After the deposition, the coatings were left in open air for 10 mins before thermally treated at 100 ^{0}C for 12 hrs in a Genlab oven. The coated mild steels substrate specimens were subsequently cooled to room temperature. An area of 1.0 cm^2 was unmasked on the bare steel and coated substrate by seal the edges and back sides of the steel panels using a beeswax-colophony mixture.

2.5. Electrochemical corrosion test

Electrochemical measurements were conducted on a PARSTAT 2273 electrochemical system in a standard three-electrode cell, where the substrate was the working electrode, with a saturated calomel electrode (SCE) as a reference electrode and the platinum as the counter electrode. The corrosion behaviour of the bare and coated mild steel samples were evaluated by means of open

circuit potential (OCP), Tafel plot and electrochemical impedance spectroscopy (EIS). Electrochemical measurements were carried out at room temperature in aerated 3.5 wt.%NaCl. Prior to starting the polarization, the change in electrode potential with respect to the time was monitored for approximately 1 h in the NaCl solution, until it reached a steady state. Immediately following the stabilisation period, The sample was then polarised to obtaine a Tafel plot, at a scan rate of 1.667 mVs^{-1} from an initial potential of -250 mV (vs. OCP) to the final potential of +250 mV (vs. OCP). Tafel plot for the uncoated mild steel substrate was used for comparison. A sinusoidal A.C. perturbation of 10 mV amplitude was applied for the EIS measurements of the sample at open circuit potential in a frequency range of from 100 kHz to 10 mHz.

3. RESULTS AND DISCUSSIONS

To study the degradation of the MPTMS sol-gel coated on mild steel visual inspection and electrochemical methods were employed. In the electrochemical test, Tafel analysis was used to know estimate the porosity of the coating while EIS was used to monitor the degradation of the coating.

3.1 Tafel Plots

Tafel analysis was carried out to estimate the protection of the steel by MPTMS coating and to estimate the porosity of the coating. Figure 1 shows Tafel plots of bare and MPTMS coated mild steel in 3.5 wt.%NaCl. It was observed that the coated mild steel have a higher corrosion potential compared to the bare steel corrosion potential. Both the cathodic and anodic corrosion current density of the MPTMS coated steel show two and half orders of magnitude lower than those of the bare mild steel. A lower corrosion current density suggest that the corrosion protection offered by the MPTMS coating is due to both blocking of parts of mild steel surface with reduction of

oxygen and metal dissolution occurring in the pores of the coating layers(Phanasgaonkar & Raja 2009). The values of the corrosion potential (E_{corr}) and corrosion current density (i_{corr}) were obtained from the intersection of the anodic and cathodic lines. The Tafel constants (βa and βc) were obtained from the slope of the anodic and cathodic lines. Polarization resistance (R_p) is calculated fromstern-Geary equation①(Stern & Geaby 1957)

$$R_P = \frac{B}{i_{corr}} \qquad ①$$

Where, $i_{corr}$is thecorrosion current density and B is proportionality constant which is calculated from the anodic (β_a) and cathodic (β_c) slopes of Tafel plots as shown by equation②

$$B = \frac{\beta_a * \beta_c}{2.303 * (\beta_a + \beta_c)} \qquad ②$$

The i_{corr} values obtained from equation also confirmed that mild steel is protected when coated with MPTMS sol-gel as evident from the corrosion current density of 5.32 x 10^{-8} Acm^{-2} compared to 1.388 x 10^{-5} Acm^{-2} for bare steel. These values are tabulated inTable 2.

The degradation of this coating was due to porosity and the percentage porosity can be calculated from the relationship(Creus *et al.* 2000; Pepe *et al.* 2006; Raotole *et al.* 2015; Kiruthika *et al.* 2010)

$$P = \frac{R_{ps}}{R_p} * 10^{-\left(\frac{|\Delta E_{corr}|}{\beta a}\right)} * 100 \qquad ③$$

Where, P is the porosity of the coating, R_p is the polarization resistance of the coating, R_{ps} is the polarization resistance of the bare steel, β_a is the anodic Tafel slope of the bare steel and ΔE_{corr} is the difference in corrosion potential between the coated and bare substrate.
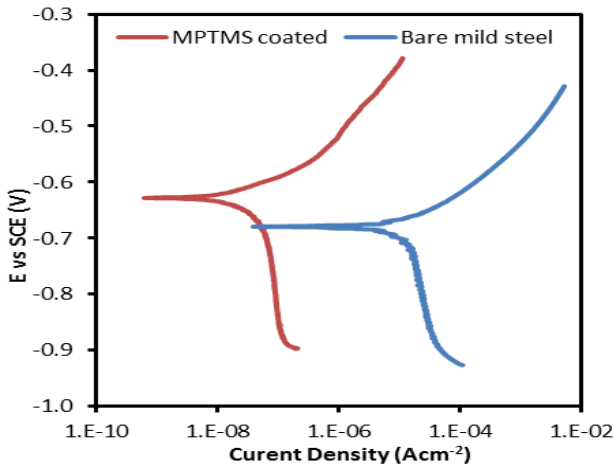
Figure 1:Tafel plots for bare and MPTMS coated mild steel

3.2. EIS

EIS was used to investigate the degradation of theMPTMS coating on mild steel immersed in 3.5 wt.% NaCl for 48hrs as it is considered to be the most viable method for such test (Lamaka *et al.* 2007). The results of the EIS are presented in **Figure 2** (Nyquist plot),Figure 3 (Bode magnitude) andFigure 4 (Bode phase). The plots for the coated steel are characterized by two time constants. The first time constant occur at the high frequency region andis attributed to the barrier properties of the coating, while the second time constant is due to the charge transfer resistance at the intermediate layer between the coating and the substrate. The bare mild steel has a single time constant (**Figure 2**(c)). The values of |**Z**| at 100 kHz and 10 mHz frequencies are correlated to the solution resistance and the MPTMS sol–gel coating performance respectively. The impedance magnitude after 1 h of immersion is about 6 orders of magnitude. However, after 24 h of immersion the magnitude decreases by one order of magnitude. The decrease in impedance magnitude is as a result of coating degradation as immersion time progresses. Increase in immersion time allows more water uptake into the coating through the micropores thereby causing degradation in performance of the coating.
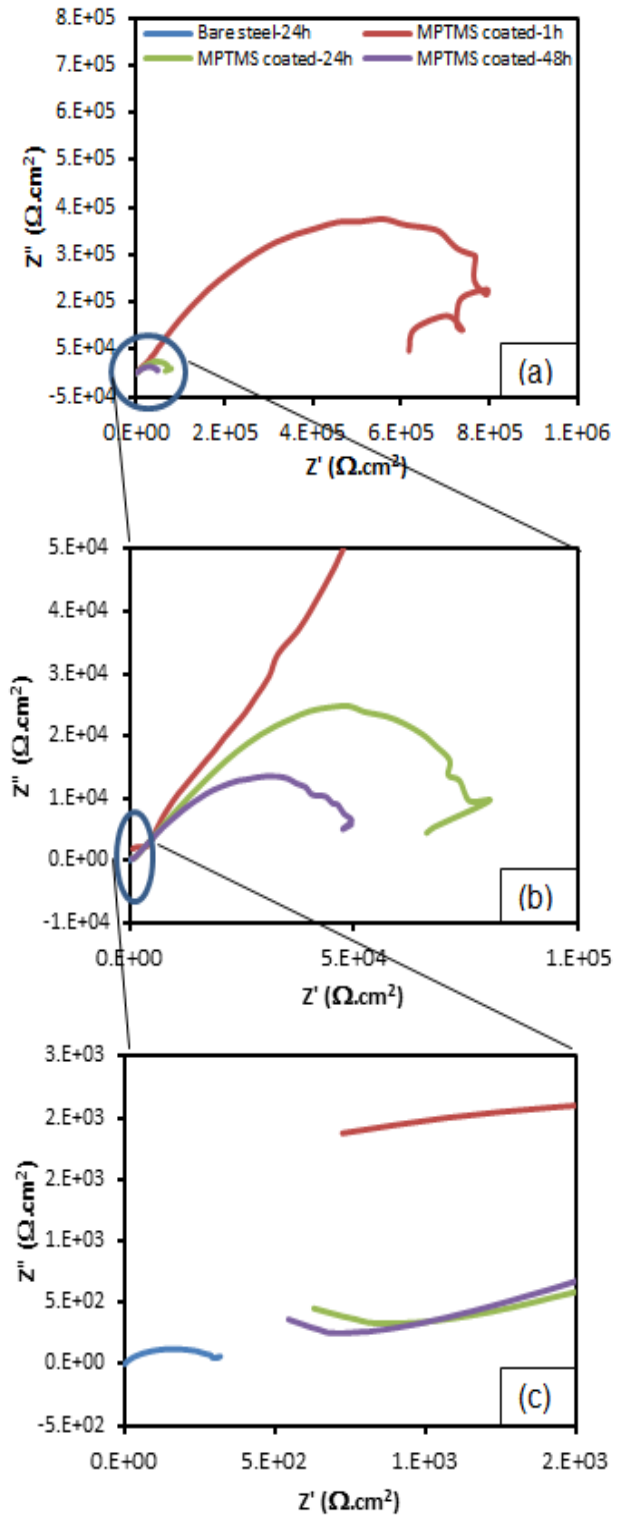
Figure 2: Nyquist plots for coated mild steel in 3.5 wt.%NaCl solution (a), effect of exposure time (b) & showing bare mild steel (c).
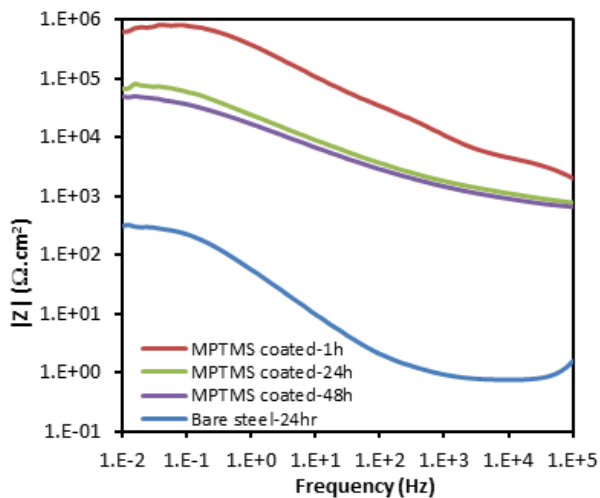
Figure 3: Impedance magnitude vs frequency plots for bare and coated mild steel in 3.5 wt.%NaCl solution.
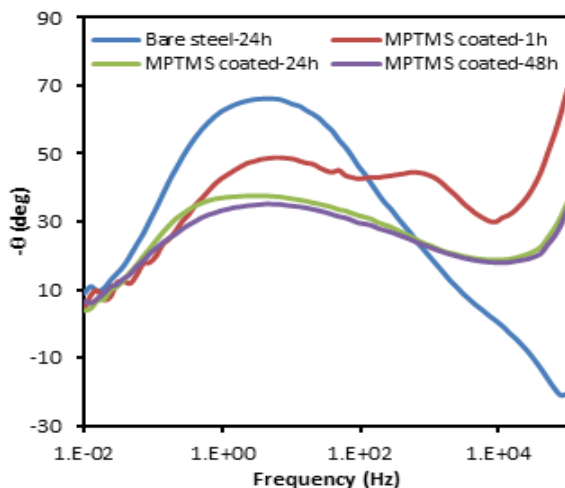
Figure 4: Bode phase angle vs frequency plots for bare and coated mild steel in 3.5 wt.%NaCl solution.

After 48 h immersion, the change in impedance magnitude was negligible. At 100 mHz, it was observed that there is a decrease (Figure 3) in the impedance magnitude for the plots of 1h, 24h and 48h immersion, indicating an inductive effect.

3.3. Mechanism of degradation

A combination of visual observation and electrochemical test were used to study the effect of immersion time on the coating performance. Figure 5(A) shows a micrograph of bare mild steel substrate after cleaning. However, upon application of the transparent MPTMS sol-gel, several patches of green zones were observed (Figure 5(B)). It is suggested that these zones can be attributed to a volatile organic matter in the MPTMS sol. After heat treatment at 100 ºC, the green zones evaporated leaving a transparent film on the surface of the mild steel (Figure 5(C)). However, due to the evaporation of these organic substances, the coating cannot offer an adequate long-term corrosion protection due to the presence of micropores, cracks and areas with low cross-link density due to low temperature elimination of CH_3 group probably located in the surface of open pores after densification (Phanasgaonkar & Raja 2009; Gallardo et al. 2000; Almeida & Pantano 1990). These areas serves as a preferential sites for corrosion initiation as they facilitate the diffusion of aggressive electrolyte to the coating/substrate interface (Phanasgaonkar & Raja 2009). At the early stages of the immersion, the rapid degrease in OCP may be due to initiation of the water uptake through the pores in the coating (Raotole et al. 2015). Figure 5(D) shows the image of MPTMS coated steel with no localized corrosion on the surface after 8 h of immersion in a 3.5 wt.%NaCl. However, after 24 h of immersion, the protective ability of the coating reduces as evident in the decrease in impedance magnitude of the Bode and Nyquist plots. At 24 h of immersion, pits were noticed on the surface of the steel in the areas suspected to region of porosity. However, the presence of a change in the slope in the higher and lower frequency range still reflects the existence of two time constants. The shape of the spectra suggests that the dielectric properties of the coating may be affected due to the immersion process and the phase angle shift indicates a less capacitive response probably due to solution permeation through the coating causing localised corrosion (Liu et al. 2003). These pits show no sign of propagation after 48 h of immersion as evident in the

negligible decrease in the impedance magnitude (**Figure 3**). After 72 h of immersion, brownish areas were noticed on the surface beneath the coating, suggesting that general corrosion is gradually taken place as shown in **Figure 5** (F).

Porosity values calculated according to equation③ using Tafel analysis is presented inTable 2. The Porosity value of 0.0861% suggests that the MPTMS film is acting as a good barrier to the electrolyte. It is important to note that the value of very low porosity obtained was during the first stages of immersion and is in good agreement with the images observed of the coating shown in Figure 5 (C & D) and the high protection percentages recorded(Pepe *et al.* 2006). By contrast the bare mild steel shows severe corrosion in all the areas after just 24 h immersion in 3.5 wt.%NaCl (Figure 5 (E)).
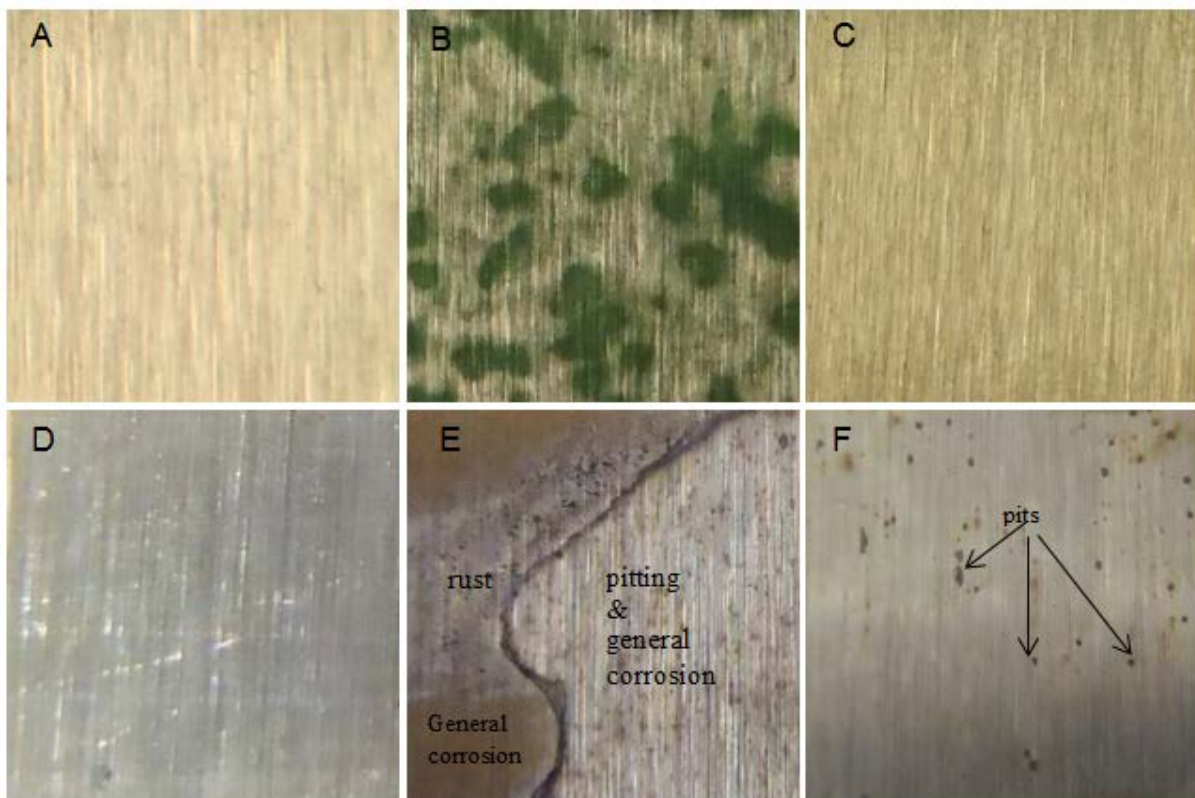
Figure 5: Images of bare mild steel substrate (A), coated surface before curing at 100 ℃ (B), coated surface after curing (C), Coated mild steel after 8 h immersion (D), Bare mild steel after 24 h immersion (E) and MPTMS coated mild steel substrate after 72 h immersion in 3.5 wt.% NaCl

Table 2:Results of Tafel plots measurements for bare and MPTMS coated steel.

Sample	Ecorr (mV)	Icorr (μAcm^{-2})	βa (mVdec^{-1})	βc (mVdec^{-1})	R_p (Ωcm^2)	PE (%)	P (%)
Bare steel	-680	13.88	80	600	2208.2	-	-
MPTMS coated	-628	0.0532	80	580	573872.2	99.62	0.0861

4. CONCLUSION

The results show that MPTMS can be used as a precursor in the development of sol-gel coating on mild steel. The electrochemical test of MPTMS coating on mild steel showed that though mild steel was protected by the coating due to the coating acting as a barrier to the electrolyte by impeding its contact with the metal surface, the degradation of the coating is due to the presence of pores in the coating. Tafel plots revealed that MPTMS sol-gel coating has a porosity of 0.0861 %. Micrograph showed that the pits initiated did not propagate after 72 h of immersion. The results suggest that MPTMS could be used as a corrosion protection coating for mild steel.

ACKNOWLEDGEMENT

REFERENCES

Akid, R., Gobara, M. & Wang, H., 2011. Corrosion protection performance of novel hybrid polyaniline/sol–gel coatings on an aluminium 2024 alloy in neutral, alkaline and acidic solutions. *Electrochimica Acta*, 56(5), pp.2483–2492. Available at: http://www.sciencedirect.com/science/article/pii/S0013468 610016658 [Accessed November 3, 2014].

Almeida, R.M. & Pantano, C.G., 1990. Structural investigation of silica gel films by infrared spectroscopy. *Journal of Applied Physics*, 68(8), p.4225. Available at: http://scitation.aip.org/content/aip/journal/jap/68/8/10.106 3/1.346213 [Accessed June 2, 2015].

Balgude, D. & Sabnis, A., 2012. Sol–gel derived hybrid coatings as an environment friendly surface treatment for corrosion protection of metals and their alloys. *Journal of Sol-Gel Science and Technology*, 64(1), pp.124–134. Available at: http://link.springer.com/10.1007/s10971-012-2838-z [Accessed November 1, 2014].

Bechinger, C. et al., 2000. Submicron metal oxide structures by a sol-gel process on patterned substrates. *Thin Solid Films*, 366(1-2), pp.135–138. Available at: http://www.sciencedirect.com/science/article/pii/S0040609 000008658 [Accessed November 14, 2014].

Cai, M., Ho, M. & Pemberton, J.E., 2000. Surface Vibrational Spectroscopy of Alkylsilane Layers Covalently Bonded to Monolayers of (3-Mercaptopropyl)trimethoxysilane on Ag Substrates. *Langmuir*, 16(7), pp.3446–3453. Available at: http://dx.doi.org/10.1021/la991075n [Accessed August 10, 2015].

Carvalho, J.B.R. et al., 2014. Influence of the annealing temperature and metal salt precursor on the structural characteristics and anti-corrosion barrier effect of CeO2 sol–gel protective coatings of carbon steel. *Ceramics International*, 40(8), pp.13437–13446. Available at: http://www.sciencedirect.com/science/article/pii/S0272884 214007871 [Accessed August 24, 2014].

Creus, J., Mazille, H. & Idrissi, H., 2000. Porosity evaluation of protective coatings onto steel, through electrochemical techniques. *Surface and Coatings Technology*, 130(2-3), pp.224–232. Available at: http://www.sciencedirect.com/science/article/pii/S0257897 299006593 [Accessed July 2, 2015].

Gallardo, J., Galliano, P. & Durán, A., 2000. Thermal Evolution of Hybrid Sol-Gel Silica Coatings: A Structural Analysis. *Journal of Sol-Gel Science and Technology*, 19(1-3), pp.393–397. Available at: http://link.springer.com/article/10.1023/A%3A100877890 9389 [Accessed August 9, 2015].

Kendig, M.W. & Buchheit, R.G., 2003. Corrosion Inhibition of Aluminum and Aluminum Alloys by Soluble Chromates, Chromate Coatings, and Chromate-Free Coatings. *Corrosion*, 59(5), pp.379–400. Available at: http://corrosionjournal.org/doi/abs/10.5006/1.3277570 [Accessed November 8, 2014].

Kiruthika, P. et al., 2010. Effect of plasma surface treatment on mechanical and corrosion protection properties of UV-curable sol-gel based GPTS-ZrO2 coatings on mild steel. *Surface and Coatings Technology*, 204(8), pp.1270–1276. Available at: http://www.sciencedirect.com/science/article/pii/S0257897 209008251 [Accessed June 9, 2015].

Lamaka, S.V. et al., 2007. Nanoporous titania interlayer as reservoir of corrosion inhibitors for coatings with self-healing ability. *Progress in Organic Coatings*, 58(2-3), pp.127–135. Available at: http://www.sciencedirect.com/science/article/pii/S0300944 00600261X [Accessed August 10, 2015].

Liu, C. et al., 2003. An electrochemical impedance spectroscopy study of the corrosion behaviour of PVD coated steels in 0.5 N NaCl aqueous solution: Part I. Establishment of equivalent circuits for EIS data modelling. *Corrosion Science*, 45(6), pp.1243–1256. Available at: http://www.sciencedirect.com/science/article/pii/S0010938 X02002135 [Accessed July 2, 2015].

Osborne, J.H., 2001. Observations on chromate conversion coatings from a sol–gel perspective. *Progress in Organic Coatings*, 41(4), pp.280–286. Available at: http://www.sciencedirect.com/science/article/pii/S0300944 001001436 [Accessed October 27, 2014].

Pepe, A. et al., 2006. Sol-gel coatings on carbon steel: Electrochemical evaluation. *Surface and Coatings Technology*, 200(11), pp.3486–3491. Available at:

http://www.sciencedirect.com/science/article/pii/S0257897205008091 [Accessed August 19, 2014].

Phanasgaonkar, A. & Raja, V.S., 2009. Influence of curing temperature, silica nanoparticles- and cerium on surface morphology and corrosion behaviour of hybrid silane coatings on mild steel. *Surface and Coatings Technology*, 203(16), pp.2260–2271. Available at: http://www.sciencedirect.com/science/article/pii/S025789720900111X [Accessed December 3, 2014].

Raotole, P.M. et al., 2015. Corrosion protective poly(aniline-co-o-anisidine) coatings on mild steel. *Journal of Coatings Technology and Research*. Available at: http://link.springer.com/10.1007/s11998-015-9669-0 [Accessed May 7, 2015].

Sinapi, F. et al., 2003. Self-assembly of (3-mercaptopropyl)trimethoxysilane on polycrystalline zinc substrates towards corrosion protection. *Applied Surface Science*, 212-213, pp.464–471. Available at: http://www.sciencedirect.com/science/article/pii/S0169433203001429 [Accessed July 3, 2015].

Sinapi, F., Delhalle, J. & Mekhalif, Z., 2002. XPS and electrochemical evaluation of two-dimensional organic films obtained by chemical modification of self-assembled monolayers of (3-mercaptopropyl)trimethoxysilane on copper surfaces. *Materials Science and Engineering: C*, 22(2), pp.345–353. Available at: http://www.sciencedirect.com/science/article/pii/S0928493102002102 [Accessed July 3, 2015].

Stern, M. & Geaby, A.L., 1957. Electrochemical Polarization I. A Theoretical Analysis of the Shape of Polarization Curves. *Journal of The Electrochemical Society*, 104(1), p.56. Available at: http://jes.ecsdl.org/content/104/1/56.abstract [Accessed August 10, 2015].

Thompson, W.R. et al., 1997. Hydrolysis and Condensation of Self-Assembled Monolayers of (3-Mercaptopropyl)trimethoxysilane on Ag and Au Surfaces. *Langmuir*, 13(8), pp.2291–2302. Available at: http://dx.doi.org/10.1021/la960795g [Accessed June 7, 2015].

U.S. Department of Labor, Occupational Safety and Health Administration & 3373-10, 2009. *Hexavalent chromium*, Washington.

Vignesh, R.B., Edison, T.N.J.I. & Sethuraman, M.G., 2014. Sol–Gel Coating with 3-Mercaptopropyltrimethoxysilane as Precursor for Corrosion Protection of Aluminium Metal. *Journal of Materials Science & Technology*, 30(8), pp.814–820. Available at: http://www.sciencedirect.com/science/article/pii/S1005030213002600 [Accessed August 12, 2014].

Wang, H., Akid, R. & Gobara, M., 2010. Scratch-resistant anticorrosion sol–gel coating for the protection of AZ31 magnesium alloy via a low temperature sol–gel route. *Corrosion Science*, 52(8), pp.2565–2570. Available at: http://www.sciencedirect.com/science/article/pii/S0010938X10001873 [Accessed November 12, 2014].

Yasakau, K.A. et al., 2014. Influence of sol-gel process parameters on the protection properties of sol–gel coatings applied on AA2024. *Surface and Coatings Technology*, 246, pp.6–16. Available at: http://www.sciencedirect.com/science/article/pii/S0257897214001571 [Accessed November 8, 2014].

Zheludkevich, M.L., Salvado, I.M. & Ferreira, M.G.S., 2005. Sol–gel coatings for corrosion protection of metals. *Journal of Materials Chemistry*, 15(48), p.5099. Available at: http://pubs.rsc.org/en/content/articlehtml/2005/jm/b419153f [Accessed November 8, 2014].

PASSIVE CORROSION PROTECTION OF PIPELINE STEEL BY 3-MERCAPTOPROPYLTRIMETHOXYSILANE SOL-GEL COATING

Abubakar Mohammed[a,*], Nayef M. Alanazi[b] , Heming Wang[a]

[a]Materials and Engineering Research Institute, Sheffield Hallam University, Howard Street, Sheffield S1 1WB, UK
[b] Research and Development Centre, Saudi Aramco, Box 62, Dhahran 31311, Saudi Arabia
*Abubakar.Mohammed@student.shu.ac.uk

ABSTRACT

Sol–gel derived thin films coating can provide both active and passive corrosion protection and present one of the most viable pre-treatments alternatives to the toxic chromate. Passive corrosion protection is achieved by depositing a barrier layer such as coating, to prevent the material from coming in contact with the corrosive environment. Sol-gel coatings offer a number of advantages over other methods of protection for metallic materials. 3-mercaptopropyltrimethoxysilane (MPTMS) was used as the precursor for sol-gel coating on mild steel substrate. The MPTMS sol-gel was characterized by Attenuated total reflectance/Fourier transform infrared spectroscopy (ATR/FTIR) and X-ray diffraction. The corrosion performance of the coating was assessed by linear polarisation resistance (LPR), PDS and electrochemical impedance spectroscopy (EIS) in aerated 3.5 wt.%NaCl solution at ambient temperature for 24 hrs. The protection efficiency of the coating was found to be 99.62% with a corrosion resistance of 500 times more than the bare steel.

KEY WORDS: 3-Mercaptopropyltrimethoxysilane (MPTMS); Sol-gel coating; ATR/FTIR; XRD; LPR; PDS; EIS;

1. INTRODUCTION

Materials such as carbon steel has since cemented its place in various industries such as oil and gas industry for the transportation of petroleum products pipelines, due to their high strength, hardness, toughness (Fouladi & Amadeh 2013) and most importantly low cost. The problem of low corrosion resistance that is associated with carbon steel can be curtailed by a combination of active corrosion protection (modification of corrosive environment) and passive corrosion protection (material surface modification)(Brooman 2002a; Brooman 2002b; Brooman 2002c). Passive corrosion protection is achieved by depositing a barrier layer such as coating, to prevent the material from coming in contact with the corrosive environment (Brooman 2002b; Zheludkevich et al. 2007). Commercially, metals are pre-treated with either oxide, phosphate or chromate based chemical conversion coatings (Balgude & Sabnis 2012). Chromates conversion coating has been used as the most effective pre-treatment coating on metals for corrosion protection systems (Osborne 2001; Kendig & Buchheit 2003; Yasakau et al. 2014). The effectiveness of chromate conversion coatings for the corrosion protection of metals is due to the auto-healing

nature (corrosion inhibiting effect) of the hexavalent chromium (Cr^{6+}) contained in the film as well as the physical barrier presented by the film itself (Carvalho et al. 2014; Balgude & Sabnis 2012). Despite the corrosion protection performance, Cr^{6+} based pre-treatments have not been specifically adopted for use with metals showinglimited passivation, such as carbon steel (Wang & Akid 2008). Again, hexavalent chromium is considered highly toxic and environmentally dangerous due to its carcinogenic effect (Decroly & Petitjean 2005; De Graeve et al. 2007; Zheludkevich et al. 2005; U.S. Department of Health and Human Services et al. 2012; U.S. Environmental Protection Agency 1998). The new permissible exposure limit (PEL) from the Occupational Safety and HealthAdministration (OSHA) for Cr^{6+} (U.S. Department of Labor et al. 2009) has led to a growing restrictions being imposed on the use of hexavalent chromium. Consequently, focus has been shifted from its use as a protective coatings against metal corrosion such as carbon steel (Jiang et al. 2014; Liu et al. 2013; Sá Brito et al. 2012; Wang & Akid 2007). As a result of these drawbacks, there is an increasing demand for the development of an anti-corrosion pre-treatments or thin

films coating for steel that will be non-chromate and environmentally-friendly (Wang & Akid 2008).

Sol–gel derived thin films coating present one of the most viable pre-treatments alternative to the chromate (Akid *et al.* 2011; Zheludkevich *et al.* 2005; Wang *et al.* 2010). MPTMS has been used as a sole precursor in the preparation of sol-gel coating. Thompson*et al.*(1997) investigated the formation of MPTMSself-assemble monolayer on Au and Ag substrates and showed that sol-gel adheres to the substrate. Cai*et al.*(2000)used surface vibrational spectroscopy to study the Alkylsilanelayers covalently bonded to Monolayers of MPTMS on Ag substrates. Sinapi*et al.*(2002)formed a protective film using MPTMS and used XPS and electrochemical evaluation to study the two-dimensional organic films obtained by chemical modification of self-assembled monolayers of MPTMS on copper surfaces. They also studied the corrosion protection of MPTMS by self-assembly on polycrystalline zinc substrates(Sinapi *et al.* 2003). Recently, Vignesh*et al.*(2014)studied the effect MPTMS concentration as a sole precursor in a Sol-Gel coating and revealed the corrosion protection increases with increase in concentration of MPTMS.

To the knowledge of the authors, there is no existing literature on the corrosion protection with MPTMS as a sole precursor for the protection of mild steel. This study presents the corrosion protection of mild steel using MPTMS as a sole precursor in the sol-gel process.

2. EXPERIMENTAL METHODS

2.1. Materials

3-mercaptopropyltrimethoxysilane (MPTMS)-95% was purchased from Sigma-Aldrich and used without any further purification. Nitric acid (70%) and 2-propanol (99.5) were also purchased from Sigma-Aldrich. Deionized water was used for all the experiments and sol preparation.

2.2. Sol-gel preparation

MPTMS sol-gel was prepared by dissolving MPTMS in 2-propanol. Acidified water of 0.1M nitric acid was added drop wise into the mixture. The volume ratio of MPTMS:2-propanol:HNO$_3$ was 2:1:1 and the mixture was magnetically stirred for 1 hr at the rate of 500 rpm, resulting in a clear and homogenous solution, during which hydrolysis and condensation occurred.

2.3. Substrate preparation

Mild steel panels measuring 102 mm × 25 mm × 1.6 mm were used as the substrate. The chemical composition of the substrate is given in Table 1. The as received panels were soap washed and rinsed with deionized water, then immersed into 2-propanol alcohol to remove inorganic impurities such as oil, grease and fatty residues from the surface. It was then placed into ultrasonic bath for 5 mins for additional cleaning, washed with deionized water and dried with warm nitrogen air. The panels were then placed in a desiccator pending film deposition.

Table 1: Composition of mild steel with Fe as balance

Element	C	Si	Mn	P	S	Ni	Al	Mo	Cu
Wt. (%)	0.02	0.01	0.21	0.007	0.006	0.02	0.054	0.01	0.004

2.4. Coating deposition

Coating was applied on the cleaned mild steel substrate by spray coating using high velocity low pressure (HVLP) of Gen3 system spray coating machine model SB-2900. The substrate was placed at 75 degree to the horizontal and the coating was applied manually using SprayCraft (SP10) spray gun connected the machine. After the deposition, the coatings were left in open air for 10 mins before thermally treated at 100 ^{0}C for 12 hrs in a Genlab oven. The coated mild steels substrate specimens were subsequently cooled to room temperature. An area of 1.0 cm^2 was unmasked on the bare steel and coated substrate by seal the edges and

back sides of the steel panels using a beeswax-colophony mixture.

2.5. Characterization of sol-gel coating

Visual observation was used to examine the appearance of the coating for colour, uniformity, transparency, defects and degradation of coated surface.

Attenuated total reflectance/Fourier transform infrared spectroscopy (ATR/FT-IR Nexus 670 ThermoNicolet) was used to obtain spectra from pure MPTMS liquid, deionised water and MPTMS sol before coating. The spectra for MPTMS coated on mild steel substrate were obtained by scratching the coating. Spectra were collected with a 4 cm^{-1} resolution and 160 scans have been accumulated for each spectrum. The IR transmission was measured in a wavenumber range of 4000 to 400 cm^{-1}.

X-ray diffraction (XRD) analysis (Philips X'pert pro X-ray diffractometer) was used to examined the surfaces of the bare steel and coated mild steel with the working condition as Cu$K\alpha$ Ni-filtered radiation, 40 kV, 40 mA and a divergence slit 0.47°. The analyses were carried out on the metal specimen directly inserted into the sample-rack of the instrument, with the X-ray beam pointing directly on the specimen surface.

2.6. Electrochemical corrosion test

Electrochemical measurements were conducted on a PARSTAT 2273 electrochemical system in a standard three-electrode cell, where the substrate was the working electrode, with a saturated calomel electrode (SCE) as a reference electrode and the platinum as the counter electrode. The corrosion behaviour of the bare and coated mild steel samples were evaluated by means of linear polarization resistance (LPR), open circuit potential (OCP), Potentiodynamic polarization scan (PDS) and electrochemical impedance spectroscopy (EIS). Electrochemical measurements were carried out at room temperature in aerated 3.5 wt.%NaCl. Prior to starting the polarization, the change in electrode potential with respect to the time was monitored for approximately 1 hr in the NaCl solution, until it reached a steady state. Immediately following the stabilisation period, LPR was collected from a potential range of -20mV (vs. OCP) to +20 mV (vs. OCP). The sample was then polarised to obtaine a PDS at a scan rate of 1.667 mVs^{-1} from an initial potential of -250 mV (vs. OCP) to the final potential of +1.0 V (vs. OCP). LPR and PDS curves for the uncoated mild steel substrate were used for comparison. A sinusoidal A.C. perturbation of 10 mV amplitude was applied for the EIS measurements of the sample at open circuit potential in a frequency range of from 100 kHz to 10 mHz.

3. RESULTS AND DISCUSSIONS

3.1. ATR-FTIR analysis

ATR-FTIR spectrum of MPTMS sol recorded after hydrolysis/condensation was compared with MPTMS coating over mild steel surface. FTIR of pure MPTMS and deionised water was also recorded to check the effect of densification (**Figure 1**). The ATR-FTIR spectrum of the MPTMS sol and MPTMS coating show broad peak absorption between 3650 cm^{-1} and 3200 cm^{-1} is a characteristics of OH bond stretching. The broad peak reduces after condensation and show further reduction after densification. The pure MPTMS peaks at 2933 cm^{-1} and 2840 cm^{-1} were identified and are associated with symmetrical and asymmetrical CH stretching (CH$_2$ and CH$_3$). These peaks, though reduced, were also present on the MPTMS sol after condensation and densification. The presence of these peaks on the prepared coating suggests that the sol-gel processes have no effect on the linkage between the bonding in the material. The peak at 1625 cm^{-1} on the deionised and MPTMS sol is characteristics of water molecules. The peak diminishes on the

MPTMScoating due to evaporation of water molecules during densification. The strong bands between 1090 and 975 cm^{-1} are attributed to Si-O-Si, the structural backbone of the material. The formation of the Si-O-Si layer protects the metal substrate. The spectrum of the MPTMS coated over mild steel shows absorption bands at 1090, 975, 850 and 673 cm^{-1} could be due to Fe-O-Si. This shows the excellent adhesion of MPTMS sol-gel coating on Mild steel substrate. The process of adhesion is depicted inFigure 3.

3.2. XRD analysis

The bare mild steel and the MPTMS coated surface was examined by XRD (Figure 2). The peaks attributed to Fe of the metal substrate are located at $2\theta = 45°$ and $65°$. These peaks also appeared in the MPTMS coated surface but with reduced intensity. The difference in intensity between the bare steel and the coated substrate was 365 a.u., confirms that the MPTMS coating is serving as a protection to the steel. The peaks located at $2\theta = 21°$ and $26°$ are attributed to silicon and sulphur respectively. The presence of silicon on the coated substrate is a confirmation that MPTMS, which is predominately silicon, was responsible for the reduction in intensity of Fe.

3.3. Electrochemical corrosion test

The corrosion protection performance of MPTMS sol-gel coated on mild steel was tested by using electrochemical methods, such as linear polarisation resistance (LPR), Potentiodynamic polarization scan (PDS) and electrochemical impedance spectroscopy (EIS).

3.3.1 Linear polarisation resistance

Linear polarisation resistance was used as a quick method to measure the resistance of the coated mild steel and compared with that of the bare steel. **Figure 5** and **Figure**

6 show the LPR result for bare and coated steel respectively. From the graphs, the intercept on the y-axis is the OCP, while the slope of the curve is the corrosion resistance of the material and is given as:
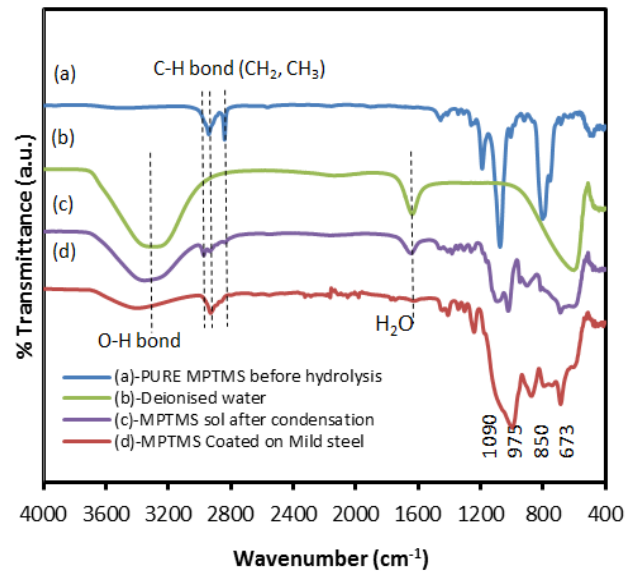
Figure 1: FTIR spectra, (a) pure MPTMS liquid, (b) deionised water, (c) MPTMS sol before coating, (d) MPTMS coated on mild steel substrate.
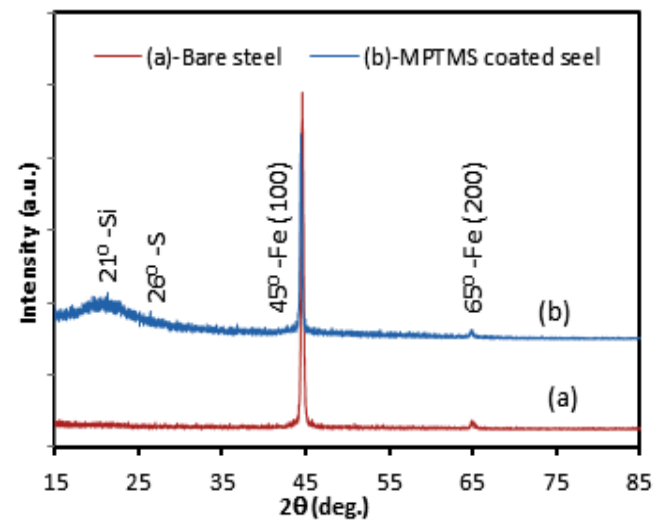
Figure 2: XRD spectra of bare mild steel and MPTMS coated substrate.
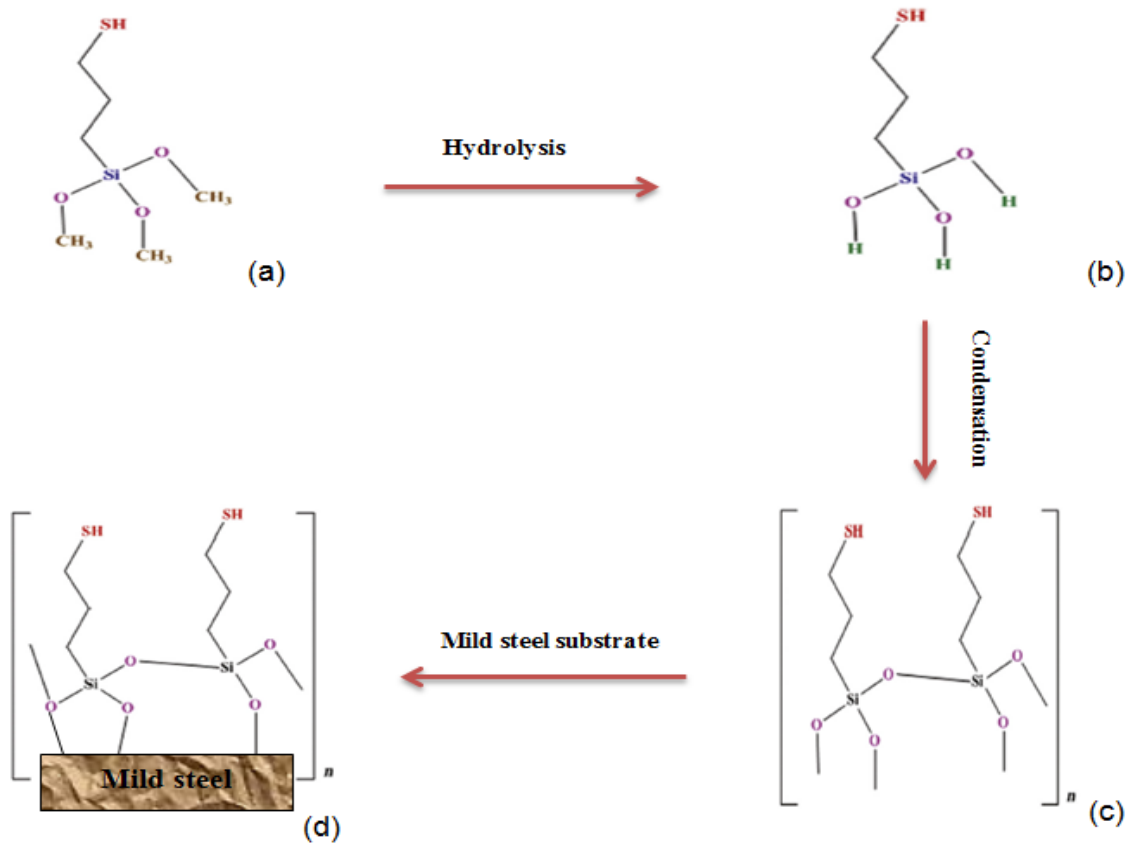
Figure 3: Mechanism of condensation and adhesion on mild steel substrate

$$Slope = R_p = \frac{\Delta E}{\Delta i} \qquad ①$$

$$B = \frac{\beta_a * \beta_c}{2.303 * (\beta_a + \beta_c)} \qquad ③$$

Where, R_p is the polarization resistance, ΔE is the change in voltage and Δi change in current. The corrosion current density can be obtained from the stern-Geary equation (Stern & Geaby 1957).

$$i_{corr} = \frac{B}{R_p} \qquad ②$$

Where, i_{corr} is the corrosion current density and B is proportionality constant which is calculated from the anodic (β_a) and cathodic (β_c) slopes of Tafel plots as shown by equation ③

From **Figure 4** and **Figure 5**, the benefit of coated surface can be observed. The coated mild steel have a higher corrosion potential ($E_{cor} = -628.8$ mV) compared to the bare steel corrosion potential ($E_{cor} = -681.3$ mV). Also, the polarization resistance of the coated substrate is about 500 times more than the bare substrate. The i_{corr} values obtained from equation ② also confirmed that mild steel is protected when coated with MPTMS sol-gel as evident from the corrosion current density of 4.46 x 10⁻⁸ Acm⁻² compared to 2.21 x 10⁻⁵ Acm⁻² for bare steel. These values are tabulated inTable2.

3.3.2 PDS

Dueto the deficiencies associated with LPR, Tafel analysis was carried out to estimate the protection of the steel by MPTMS coating. Figure 6 shows PDSof bare and MPTMS coated mild steel in 3.5 wt.%NaCl. It was observed that the coated mild steel have a higher corrosion potential ($E_{cor} = -628$ mV) compared to the bare steel corrosion potential ($E_{cor} = -680$ mV). Both the cathodic and anodic corrosion current density of the MPTMS coated steel show two and half orders of magnitude lower than those of the bare mild steel. A lower corrosion current density suggest that the corrosion protection offered by the MPTMS coating is due to both blocking of parts of mild steel surface with reduction of oxygen and metal dissolution occurring in the pores of the coating layers(Phanasgaonkar & Raja 2009). The plot also shows sign of passivation at -100 mV. The values of the corrosion potential (E_{corr}) and corrosion current density (i_{corr}) were obtained from the intersection of the anodic and cathodic lines. The Tafel constants (βa and βc) were obtained from the slope of the anodic and cathodic lines. Polarization resistance (R_p) is calculated from equation ② These values are in agreement with the LPR results and are tabulated inTable**2**.
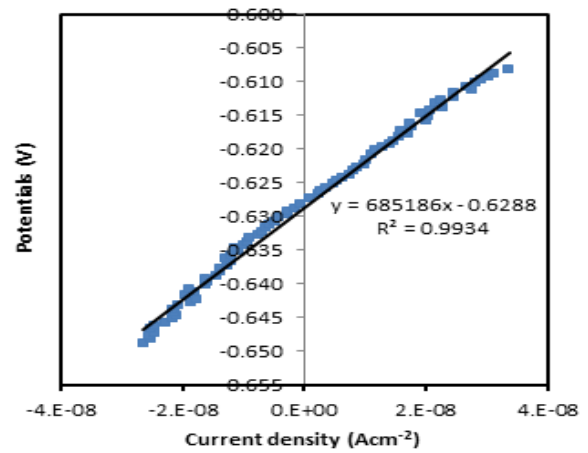
Figure 5:LPR for MPTMS coated mild steel.
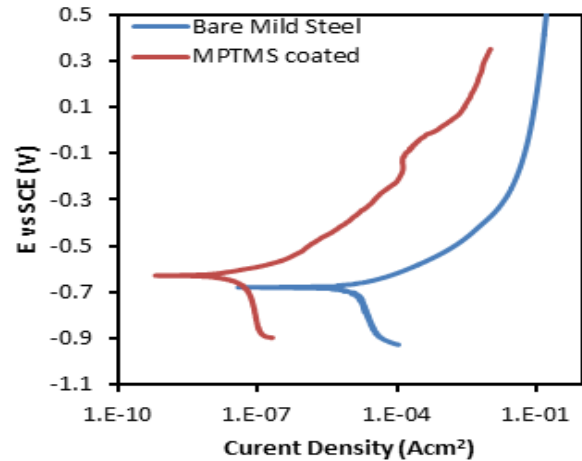
Figure 6:Tafel plots for bare and MPTMS coated mild steel
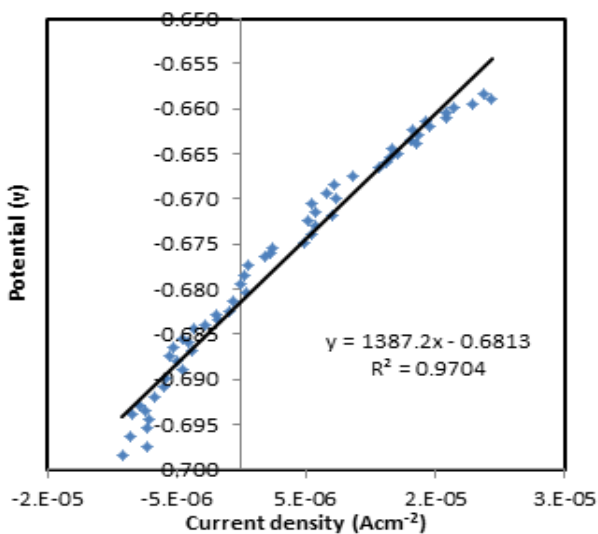
Figure 4:LPR for bare mild steel.
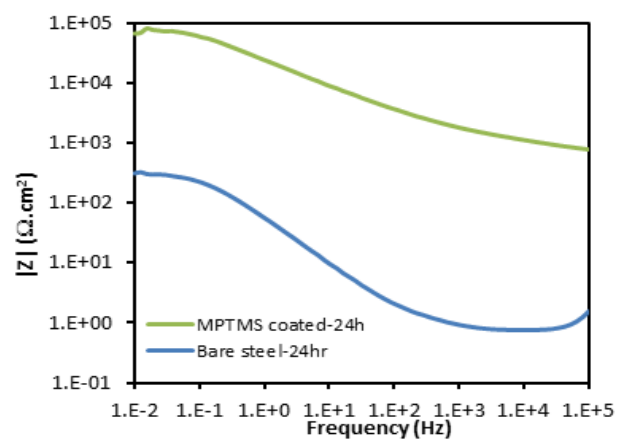
Figure 7: Impedance magnitude vs frequency plots for bare and coated mild steel in 3.5 wt.%NaCl solution.

3.4. EIS

The EIS is generally considered as the most suitable techniques for the investigation and prediction of the anti-corrosion activities (Lamaka *et al.* 2007). EIS was used to investigate the protective abilities of the MPTMS coating on mild steel immersed in 3.5 wt.%NaCl for 24hrs. The results of the EIS are presented in Figure 7. The plot shows that after 24 h of immersion (Figure 7) the coated steel has more than two orders of magnitude higher than the bare steel. The higher impedance is probably due to an area effect where the coating is blocking access of the aggressive electrolyte to the reactive metal surface (Phanasgaonkar & Raja 2009). At 100 mHz, it was observed that there is a decrease (Figure 7) in the impedance magnitude for the plots after 24h immersion, indicating an inductive effect. These analyses are in agreement with the results obtained for LPR and PDS.

3.5. Mechanism of protection

The mechanism of protection is based on the process of hydrolysis to densification and adhesion on the metal substrate. The protection and adhesion is due to the fact that Silane pre-treatment has the ability to form a very dense self-assembled silicon and oxygen rich network. MPTMS $(SH(CH_2)_3Si(OCH_3)_3$ precursor (Figure 3(a)) contains hydrolysable alkoxy groups. These groups are converted to hydrophilic silanol groups (SiOH) after

hydrolysis (Figure 3b). On curing, the condensation reaction takes place thereby forming metallo-syloxane bonds (Fe-O-Si)(Figure 3d) and increasing the adherence of the silanes to the metallic substrates. The excess of the SiOH group present in the adsorbed structure forms a siloxane bond (Si–O–Si) network (Figure 3c). This bond is the structural backbone of the material, as it hinders the penetration of the aggressive species to the metal surface by forming a physical barrier between the substrate and the aggressive environment. The protection efficiency of the coating, PE is calculated using the expression in equation ④(Raotole *et al.*2015; Kiruthika *et al.* 2010).

$$PE = \frac{R_p - R_{ps}}{R_p} * 100 \qquad ④$$

Where, *PE* is the protection efficiency of the coating, $\mathbf{R}_p$ is the polarization resistance of the coating and $\mathbf{R}_{ps}$ is the polarization resistance of the bare steel. A protection efficiency of 99.62% was recorded when Tafel analysis was used. This value increases to 99.80% for the LPR data. The high efficiency is due to the protective ability of the coating. A distinctive characteristic of the sol-gel is seen in the PDS plot showing sign of passivation at -100 mV. This contributes to the protectiveness of the MPTMS sol-gel.

Table 2: Results of LPR and Tafel plots measurements for bare and MPTMS coated steel.

Sample	Ecorr(mV)		Icorr (μAcm^{-2})		βa (mVdec^{-1})	βc (mVdec^{-1})	R_p(Ωcm^2)		PE (%)
	LPR	Tafel plots	LPR	Tafel plots			LPR	Tafel plots	
Bare steel	-681.3	-680	22.10	13.88	80	600	1387.2	2208.2	-
MPTMS coated	-628.8	-628	0.0446	0.0532	80	580	685186	573872.2	99.62

4. CONCLUSION

The results show that MPTMS can be used as a precursor in the development of sol-gel coating on mild steel. The

mechanism of protection of the coating is attributed to the formation of Fe-O-Si linkage on the metallic substrate. The XRD data also confirmed the formation of sol-gel coating

on the mild steel surface. The impedance analysis of MPTMS coating on mild steel showed that the protection is due to coating acting as a barrier to the electrolyte by impeding its contact with the metal surface. PDS plots revealed that MPTMS sol-gel coating on mild steel blocked the anodic sites of the metal and thereby reduced the metal dissolution into the electrolyte solution.

ACKNOWLEDGEMENT

REFERENCES

Akid, R., Gobara, M. & Wang, H., 2011. Corrosion protection performance of novel hybrid polyaniline/sol–gel coatings on an aluminium 2024 alloy in neutral, alkaline and acidic solutions. *Electrochimica Acta*, 56(5), pp.2483–2492. Available at: http://www.sciencedirect.com/science/article/pii/S0013468 610016658 [Accessed November 3, 2014].

Balgude, D. & Sabnis, A., 2012. Sol–gel derived hybrid coatings as an environment friendly surface treatment for corrosion protection of metals and their alloys. *Journal of Sol-Gel Science and Technology*, 64(1), pp.124–134. Available at: http://link.springer.com/10.1007/s10971-012-2838-z [Accessed November 1, 2014].

Brooman, E.W., 2002a. Modifying organic coatings to provide corrosion resistance-Part I: Background and general principles. *Metal Finishing*, 100(1), pp.48–53. Available at: http://www.sciencedirect.com/science/article/pii/S0026057 602800198 [Accessed November 7, 2014].

Brooman, E.W., 2002b. Modifying organic coatings to provide corrosion resistance-Part II: Inorganic additives and inhibitors. *Metal Finishing*, 100(5), pp.42–53. Available at: http://www.sciencedirect.com/science/article/pii/S0026057 602803828 [Accessed October 22, 2014].

Brooman, E.W., 2002c. Modifying organic coatings to provide corrosion resistance-Part III: Organic additives and conducting polymers. *Metal Finishing*, 100(6), pp.104–110. Available at: http://www.sciencedirect.com/science/article/pii/S0026057 602804469 [Accessed November 7, 2014].

Cai, M., Ho, M. & Pemberton, J.E., 2000. Surface Vibrational Spectroscopy of Alkylsilane Layers Covalently Bonded to Monolayers of (3-Mercaptopropyl)trimethoxysilane on Ag Substrates. *Langmuir*, 16(7), pp.3446–3453. Available at: http://dx.doi.org/10.1021/la991075n [Accessed August 10, 2015].

Carvalho, J.B.R. et al., 2014. Influence of the annealing temperature and metal salt precursor on the structural characteristics and anti-corrosion barrier effect of CeO2 sol–gel protective coatings of carbon steel. *Ceramics International*, 40(8), pp.13437–13446. Available at: http://www.sciencedirect.com/science/article/pii/S0272884 214007871 [Accessed August 24, 2014].

Decroly, A. & Petitjean, J.-P., 2005. Study of the deposition of cerium oxide by conversion on to aluminium alloys. *Surface and Coatings Technology*, 194(1), pp.1–9. Available at: http://www.sciencedirect.com/science/article/pii/S0257897 204003913 [Accessed November 8, 2014].

Fouladi, M. & Amadeh, A., 2013. Effect of phosphating time and temperature on microstructure and corrosion behavior of magnesium phosphate coating. *Electrochimica Acta*, 106, pp.1–12. Available at: http://www.sciencedirect.com/science/article/pii/S0013468 613009468 [Accessed November 6, 2014].

De Graeve, I. et al., 2007. Silane coating of metal substrates: Complementary use of electrochemical, optical and thermal analysis for the evaluation of film properties. *Progress in Organic Coatings*, 59(3), pp.224–229. Available at: http://www.sciencedirect.com/science/article/pii/S0300944 006001950 [Accessed October 23, 2014].

Jiang, Q. et al., 2014. Corrosion behavior of arc sprayed Al–Zn–Si–RE coatings on mild steel in 3.5wt% NaCl solution. *Electrochimica Acta*, 115, pp.644–656. Available at: http://www.sciencedirect.com/science/article/pii/S0013468 613019531 [Accessed November 8, 2014].

Kendig, M.W. & Buchheit, R.G., 2003. Corrosion Inhibition of Aluminum and Aluminum Alloys by Soluble Chromates, Chromate Coatings, and Chromate-Free Coatings. *Corrosion*, 59(5), pp.379–400. Available at: http://corrosionjournal.org/doi/abs/10.5006/1.3277570 [Accessed November 8, 2014].

Kiruthika, P. et al., 2010. Effect of plasma surface treatment on mechanical and corrosion protection properties of UV-curable sol-gel based GPTS-ZrO2 coatings on mild steel. *Surface and Coatings Technology*, 204(8), pp.1270–1276. Available at: http://www.sciencedirect.com/science/article/pii/S0257897 209008251 [Accessed June 9, 2015].

Lamaka, S.V. et al., 2007. Nanoporous titania interlayer as reservoir of corrosion inhibitors for coatings with self-healing ability. *Progress in Organic Coatings*, 58(2-3), pp.127–135. Available at: http://www.sciencedirect.com/science/article/pii/S0300944 00600261X [Accessed August 10, 2015].

Liu, Z. et al., 2013. Corrosion behavior of plasma sprayed ceramic and metallic coatings on carbon steel in simulated seawater. *Materials & Design*, 52, pp.630–637. Available at: http://www.sciencedirect.com/science/article/pii/S0261306 913005359 [Accessed November 8, 2014].

Osborne, J.H., 2001. Observations on chromate conversion coatings from a sol–gel perspective. *Progress in Organic Coatings*, 41(4), pp.280–286. Available at:

http://www.sciencedirect.com/science/article/pii/S0300944001001436 [Accessed October 27, 2014].

Phanasgaonkar, A. & Raja, V.S., 2009. Influence of curing temperature, silica nanoparticles- and cerium on surface morphology and corrosion behaviour of hybrid silane coatings on mild steel. *Surface and Coatings Technology*, 203(16), pp.2260–2271. Available at: http://www.sciencedirect.com/science/article/pii/S025789720900111X [Accessed December 3, 2014].

Raotole, P.M. et al., 2015. Corrosion protective poly(aniline-co-o-anisidine) coatings on mild steel. *Journal of Coatings Technology and Research*. Available at: http://link.springer.com/10.1007/s11998-015-9669-0 [Accessed May 7, 2015].

Sá Brito, V.R.S., Bastos, I.N. & Costa, H.R.M., 2012. Corrosion resistance and characterization of metallic coatings deposited by thermal spray on carbon steel. *Materials & Design*, 41, pp.282–288. Available at: http://www.sciencedirect.com/science/article/pii/S0261306912003093 [Accessed November 8, 2014].

Sinapi, F. et al., 2003. Self-assembly of (3-mercaptopropyl)trimethoxysilane on polycrystalline zinc substrates towards corrosion protection. *Applied Surface Science*, 212-213, pp.464–471. Available at: http://www.sciencedirect.com/science/article/pii/S0169433203001429 [Accessed July 3, 2015].

Sinapi, F., Delhalle, J. & Mekhalif, Z., 2002. XPS and electrochemical evaluation of two-dimensional organic films obtained by chemical modification of self-assembled monolayers of (3-mercaptopropyl)trimethoxysilane on copper surfaces. *Materials Science and Engineering: C*, 22(2), pp.345–353. Available at: http://www.sciencedirect.com/science/article/pii/S0928493102002102 [Accessed July 3, 2015].

Stern, M. & Geaby, A.L., 1957. Electrochemical Polarization I. A Theoretical Analysis of the Shape of Polarization Curves. *Journal of The Electrochemical Society*, 104(1), p.56. Available at: http://jes.ecsdl.org/content/104/1/56.abstract [Accessed August 10, 2015].

Thompson, W.R. et al., 1997. Hydrolysis and Condensation of Self-Assembled Monolayers of (3-Mercaptopropyl)trimethoxysilane on Ag and Au Surfaces. *Langmuir*, 13(8), pp.2291–2302. Available at: http://dx.doi.org/10.1021/la960795g [Accessed June 7, 2015].

U.S. Department of Health and Human Services, Public Health Service & Agency for Toxic Substances and Disease Registry, 2012. *Toxicological profile for Chromium*, Atlanta. Available at: http://www.epa.gov/iris/toxreviews/0144tr.pdf.

U.S. Department of Labor, Occupational Safety and Health Administration & 3373-10, 2009. *Hexavalent chromium*, Washington.

U.S. Environmental Protection Agency, 1998. *Toxicological review of hexavalent chromium*, Washington, DC.

Vignesh, R.B., Edison, T.N.J.I. & Sethuraman, M.G., 2014. Sol–Gel Coating with 3-Mercaptopropyltrimethoxysilane as Precursor for Corrosion Protection of Aluminium Metal. *Journal of Materials Science & Technology*, 30(8), pp.814–820. Available at: http://www.sciencedirect.com/science/article/pii/S1005030213002600 [Accessed August 12, 2014].

Wang, H. & Akid, R., 2007. A room temperature cured sol–gel anticorrosion pre-treatment for Al 2024-T3 alloys. *Corrosion Science*, 49(12), pp.4491–4503. Available at: http://www.sciencedirect.com/science/article/pii/S0010938X07001527 [Accessed July 18, 2014].

Wang, H. & Akid, R., 2008. Encapsulated cerium nitrate inhibitors to provide high-performance anti-corrosion sol–gel coatings on mild steel. *Corrosion Science*, 50(4), pp.1142–1148. Available at: http://www.sciencedirect.com/science/article/pii/S0010938X07003307 [Accessed July 1, 2014].

Wang, H., Akid, R. & Gobara, M., 2010. Scratch-resistant anticorrosion sol–gel coating for the protection of AZ31 magnesium alloy via a low temperature sol–gel route. *Corrosion Science*, 52(8), pp.2565–2570. Available at: http://www.sciencedirect.com/science/article/pii/S0010938X10001873 [Accessed November 12, 2014].

Yasakau, K.A. et al., 2014. Influence of sol-gel process parameters on the protection properties of sol–gel coatings applied on AA2024. *Surface and Coatings Technology*, 246, pp.6–16. Available at: http://www.sciencedirect.com/science/article/pii/S0257897214001571 [Accessed November 8, 2014].

Zheludkevich, M.L. et al., 2007. Anticorrosion Coatings with Self-Healing Effect Based on Nanocontainers Impregnated with Corrosion Inhibitor. *Chemistry of Materials*, 19(3), pp.402–411. Available at: http://dx.doi.org/10.1021/cm062066k [Accessed August 20, 2014].

Zheludkevich, M.L., Salvado, I.M. & Ferreira, M.G.S., 2005. Sol–gel coatings for corrosion protection of metals. *Journal of Materials Chemistry*, 15(48), p.5099. Available at: http://pubs.rsc.org/en/content/articlehtml/2005/jm/b419153f [Accessed November 8, 2014].

EFFECTS OF GENERATING PLANT NOISE ON HUMANSAND ENVIRONMENT

A. Babawuya[1], M. D. Bako[2], S. A. Yusuf[3], A. Jibrin[4] and A.J. Elkanah[4]

[1]Department of Mechatronics Engineering, Federal University of Technology, Minna, Nigeria.

[2]Vehicle Inspection Department, Ministry of Transport, Minna, Nigeria.

[3]Mechanical Engineering Department, Waziri Umaru Federal Polytechnic, BirninKebbi, Kebbi State.

[4]Mechanical Engineering Department, Niger state Polytechnic, Zungeru, Nigeria.

*Corresponding Author: babawuyal@futminna.edu.ng,Babawuya@yahoo.com, 07038096888

ABSTRACT

Noise measurements were taken in the morning, afternoon, evening, and night to determine the extent of noise pollution all over the city.A calibrated sound level meter used to measure the generating plant noise. The equivalent sound levels - Leq- were measured at 20 different locations, between 8a.m and 10 p.m. High noise levels were observed throughout the town. The data obtained was analysed and the results hen compared with world health organization standard. The noise equivalent level varied between 99.4 and 83.2 dBA. The results of the study established the fact that generator noise levels are more than the acceptable limit of 60 dBA, that is the daytime government prescribed noise limit for residential and commercial areas. the reaction of the residents to generating plant noise was monitored with a total of 300 questionnaires. The results of the interview questionnaire revealed 97% of the people classified the noise in his/her street as "very high" while 3% says "low"; (III) 89%. And also the respondents answered that noise bother them more in day and night while 11% of the respondent say it is only in the night only. The main outcomes of exposure to generating plant noise were: loss of sleep (100%), hearing loss (100%), annoyance (100%) and disturbance(100%).

1.0 INTRODUCTION

The United States Environmental Protection Agency (EPA) describes noise as "unwanted sound", (Akpan, 2003). Sound being the human sensation of pressure fluctuation in the air.Noise can seriously harm human health and interfere with people's daily activities at school, at work, at home and during leisure time. Akpan,, (2003) Atmaca, (2005) and Oyedepo, (2010) defined noise as unpleasant sounds which disturb the human being physically, physiologically and cause environmental pollution by destroying environmental properties. The most important measurement of noise is its loudness. This loudness depends on the physical sound pressure that is measured on the sensitivity of the human ear to it. According to Levitt, (2001), the sensitivity of the human ear depends on the frequency of the sound. Hearing losses are the most common effects of noise pollution.

According to Mohammed,(2008), increasing noise pollution in the world as affected human being, animals, plants and even inert objects like buildings and bridges. Noise has become a very significant stress factor in the environment, to the level that the term noise pollution has been used to signify the hazard of sound which consequences in the modern day development is immeasurable.

According to Yılmaz et al., (2005), Noise pollution is one of the major problem people facing in urban areas all over the world. As a result of increase in the number of cars and industrialization, noise pollution has also increased. Most of noises in urban areas are increasing every day as a result of more people moving to urban from rural settlements. Noise in

cities, especially along main arteries, has reached up to disturbing levels. Residences far from noise sources and near silent secondary roads are currently very popular. People prefer to live in places far from noisy urban areas. According to Olokochaet al., (2010)Noise disrupts the tranquillity of the environment and can affect climate and human health negatively. Electricity generating plant, vehicle traffic noise and pressure, industrial noise, machinery noise, and construction noise are common sources of noise pollution that contributed directly to climate change.

It was observed at Ilorin metropolis, that generating plants of various designs and sizes are being used, and this resulting in high noise levels. As it bothers people residing in the town. A comfortable environment is one in which there is little or no annoyance and distraction so that working or leisure tasks can be carried out unhindered either physically or mentally. Onuu, (2000), further explain that, environmental noise has become a serious problem in many countries, and it is difficult to regulate by physical means alone.

The U.S. Department of Housing and Urban Development (HUD) recommends the following noise levels for residential areas, measured outdoors:

LAeq ≤ 49 dBA

- Clearly Acceptable.

49 <LAeq ≤ 62 dBA (or LDN ≤65 dBA)

- Normally Acceptable.

62 <LAeq ≤ 76 dBA (or 65 < LDN ≤ 75 dBA) - Normally Unacceptable

LAeq> 76 dBA (or 75 dBA< LDN)

- Clearly Unacceptable.
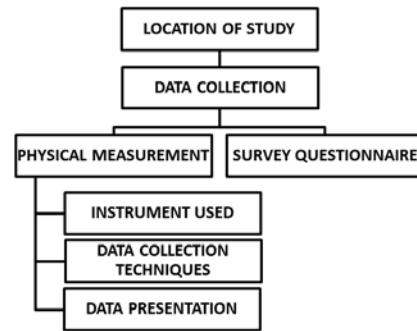
2.0 MATERIALS AND METHODS

2.1 Introduction

The procedure used in gathering and analysing the data is presented in figure 1.

Figure 1: Methodology chart.

3.2 Material used

- **Sound Level Meter –** the sound level meter used is shown in figure 3.

Figure 2: The external features of the digital noise meter.

2.2 Location of study

The study was conducted at 20 different locations in Ilorin metropolis, the capital of Kwara State, Nigeria on May, 2013. The study area is located between latitudes 8° 30' 16'' N and longitudes 4° 34' 13'' E. This is an urban area that is mostly comprise of residential development, shopping complexes, offices

and industries. Actual noise levels in the selected area have been measured and their maximum and minimum values have been record in table 1 and 2. Table 1shows selected location for the noise level measurements in Ilorin metropolis. Figures 2 and 3 shows an overview of Ilorin metropolis showing the noise sample location for this study and the population growth of the city, respectively.

Table 1: Shows selected location for the noise level measurements in Ilorin metropolis

s/No	Locations
1	Geri-Alimi
2	Unity
3	Challenge
4	Post-office
5	Maraba
6	Sabo-Oke
7	Sango
8	Tanke
9	Gaa-akanbi
10	Offa Garage
11	Taiwo
12	Asa-Dam
13	Surulere
14	Agbo-oba
15	Oja-Oba
16	Oloje
17	Ipata
18	Mubo
19	Basin
20	Fate

2.3 Data collection

The two methods used in the data collection were by physical measurement and through survey questionnaire. Physical measurement was used to measure generating plant noise levels while the survey questionnaire involved data collection by using a structured questions blended with some open-ended questions.

The noise meter was fixed at a low range of between 35 – 100 dB. The low range was chosen because it was found to correlate well with human response. The meter was adjusted to "A" weighting so as to determine the noise level. The "A" weighting network was used because it is most commonly employed for industrial and environmental studies, (Avwiri et al.,2003). The rate of hearing loss tends to follow the "A"– scale in that one could tolerate higher levels of low frequency noise for a longer period without hearing impairment. The readings were taken by holding the instrument in such a way that the microphone was at a distance of 1.2m away from any reflecting surface and at 1.0m vertical distance above the ground level in both the living and working environments of the people in order to determine the noise levels to which the people are exposed to.

Four readings were taken of 20 locations, with the aid of the sound level meter, at an interval of 30 seconds for a period of 1hourand the average for each location was recorded. The readings were taken between the hour of (8:00-9:00 am) in the morning, (1:00-2:00 pm) in the afternoon, (4:00-5:00 pm) in the evening, and (9:00-10:00 pm) in the night respectively.

Where L_{Ai} is the ith A-weighted sound pressure level reading dB,N is the total number of readings, L_{Aeq} is the A-weighted equivalent sound pressure level, $L_{AeqM}$is the equivalent sound pressure for the morning measurement, L_{AeqA} is the equivalent sound pressure level for the afternoon measurement, L_{AeqE} is the equivalent sound pressure level for the evening measurement, L_{AeqN} is the equivalent sound pressure level for the night measurement, L_N is night time noise level, L_D is day time noise level, L_{10} is the

noise level exceeded 10% of the time, L_{90} is the noise level exceeded 90% of the time, L_{NP} is noise pollution level, L_{DN} is day-night noise level.

2.4 Survey questionnaire

In order to know the opinion of the citizens from the area about how the generator noise levels have affected their daily life,and their attitude towards it, a questionnaire was developed. The survey questionnaire contained four different parts. The first part had three questions, where the interviewer was identified as to name, sex, age and date of survey. The second part had nine questions, where information about noise levels, major sources of noise and its effects on people's habit was obtained.

In the last part, with three questions, this is all about impacts of generating plant noise, and its effects on people on daily bases. A questionnaire has been applied on a one-to-one basis at selected location. A total of 300 questionnaires were processed. The questionnaire data were aggregated and analysed for the communities from which deductions were made.

3.0 METHOD OF DATA ANALYSIS

In this study, commonly used community noise assessment quantities like the exceedance percentiles L_{10}, and L_{90}, the A-weighted equivalent sound pressure level, L_{Aeq}, the daytime average sound level, L_D, the night time average sound level, L_N, the day-night average sound level, L_{DN}, the noise pollution level, L_{NP}, were manually measured at each site separately(equation 1-5). These noise measures are defined as follows (Saadu et al. 1998):

$$L_{Aeq} = 10\log_{10}\left[\frac{1}{N}\sum_{i=1}^{n}\left(\text{anti}\log\frac{L_{Ai}}{10}\right)n_i\right]$$

$$1 L_D = 10\log_{10}\left[\frac{1}{2}\left(\text{antilog}\frac{L_{AeqM}}{10} + \text{antilog}\frac{L_{AeqA}}{10}\right)\right]$$

$$2$$

$$L_{DN} = 10\log_{10}\left[\frac{1}{24}\left(15 \times \text{antilog}\frac{L_D}{10} + 9 \times \text{antilog}\frac{L_{N+10}}{10}\right)\right] \qquad 3$$

$$L_N = 10\log_{10}\left[\frac{1}{2}\left(\text{antilog}\frac{L_{AeqE}}{10} + \text{antilog}\frac{L_{AeqN}}{10}\right)\right]$$

$$4$$

$$L_{NP} = L_{Aeq} + (L_{10} - L_{90}) \qquad 5$$

4.0 RESULT AND DISCUSSION

4.1 Noise Measurement Results

All the data were obtained on weekdays and under suitable meteorological conditions, i.e., no rain.Four readings each for each location are taken. The measurements that were taken at the 20 located points are given in Table 2 and 3. Table 2 shows the maximum and minimum values obtained during the day, while Table 3 shows the maximum and minimum values obtained during the night.

Table 2: Shows day-time noise levels for measuring point

S/N	Location	Lmax	Lmin
1	Geri-Alimi	92.4	89.1
2	Unity	91.7	89.3
3	Challenge	92.7	86.1
4	Post-Office	98.9	97.3
5	Maraba	91.7	88.1
6	Sabo-Oke	87.7	84.0
7	Sango	91.7	88.0
8	Tanke	97.7	84.3
9	Gaa-Akanbi	88.5	86.2
10	Offa-Garage	90.9	88.1
11	Taiwo	96.9	93.2
12	Asa-Dam	87.9	83.6
13	Surulere	86.9	83.2
14	Agbo-Oba	90.6	88.1
15	Oja-Oba	94.7	92.3
16	Oloje	89.9	87.0
17	Ipata	91.9	89.3

S/N	Location	Lmax	Lmin
18	Mubo	89.9	88.1
19	Basin	85.7	83.3
20	Fate	87.5	84.6

Table 3: Night-time noise levels for measuring point

S/N	Location	Lmax	Lmin
1	Geri-Alimi	92.9	90.2
2	Unity	91.8	88.1
3	Challenge	89.9	75.2
4	Post-Office	99.4	97.2
5	Maraba	91.9	87.0
6	Sabo-Oke	89.8	86.7
7	Sango	90.8	87.9
8	Tanke	89.8	87.7
9	Gaa-Akanbi	89.5	86.1
10	Offa-Garage	90.7	86.0
11	Taiwo	96.9	94.1
12	Asa-Dam	86.7	86.4
13	Surulere	87.9	85.2
14	Agbo-Oba	91.5	88.3
15	Oja-Oba	95.2	93.1
16	Oloje	91.6	88.2
17	Ipata	91.3	88.0
18	Mubo	90.9	88.4
19	Basin	87.9	85.1
20	Fate	88.5	83.2

From Table 2, the day Lmax values range from 85.7dB (A) at point 19 to 98.9dB (A) at point 4, while the Lmin values range from 83.2dB (A) at point 13 to 97.3dB (A) at point 4. From Table 2, the night Lmax values range from 86.7dB (A) at point 12 to 98.9dB (A) at point 4, while the Lmin values range from 83.2dB (A) at point 20 to 97.2dB (A) at point 4. An overview of the two tables revealed that the maximum values and the minimum values obtained have exceeded the governmental legislations for residential area.

The data were also used to evaluate noise descriptors in the form of L_{Aeq}, L_{10}, L_{90}, L_D, L_N, L_{DN} and L_{NP}. The locations are designated with numbers 1 to 42 in Table 4.The average noise descriptors were determined per location. Table 4below shows the daily average values of noise descriptors for all the location surveyed. From Table 4.3, location 4 and 11 has the highest values of L_{Aeq} (56 dBA), L_N (56 dBA), and L_{NP} (57 dBA), while location 4 has the highest L_{10} (99dBA), L_D (58dBA), L_{DN} (63dBA), L_{90} (98dBA). Location 11 has the second highest values of L_{10} (96dBA), L_{DN} (62 dBA), L_{90} (94 dBA),and L_D (56 dBA).

Table 4: Noise levels descriptors computed for day and night in the study area

Location	L_{Aeq}	L_{10}	L_{90}	L_{NP}	L_D	L_N	L_{DN}
1	52	92	91	53	52	52	59
2	51	90	89	52	51	51	57
3	51	89	88	52	52	50	57
4	56	99	98	57	58	56	63
5	51	90	89	52	51	51	57
6	49	87	87	49	47	49	55
7	51	90	90	52	51	51	61
8	48	87	86	49	47	48	55
9	48	88	87	49	48	48	55
10	50	89	88	51	51	50	56
11	56	96	94	57	56	56	62
12	47	84	84	47	47	46	53
13	47	86	86	46	46	48	54
14	50	90	90	50	50	51	57
15	54	94	94	54	54	55	61
16	50	89	87	50	50	51	57
17	51	91	90	52	52	50	57

18	50	90	90	50	50	51	57
19	48	85	85	46	46	47	53
20	47	86	86	46	47	47	54

In order of high noise descriptors, next to these two locations were sites 1 and 15. The average values of noise descriptors of these locations were: L_{Aeq} (52dBA), L_{10}(92dBA), L_{90} (91dBA), L_{NP} (53dBA), L_D(52dBA), L_N (52dBA),L_{DN}(59dBA) and L_{Aeq} (54dBA), L_{10} (94dBA), L_{90} (94 dBA), L_{NP} (54dBA), L_D(54dBA), L_N (55dBA), and L_{DN}(61 dBA) respectively. Locations 1, 4, 11 and 15 were commercial centre and passengers loading park respectively. The background noise levels (L_{90}) at these locations are higher than others locations. This was due to intrusive noise sources from human conversation due to commercial activities, traffic noise, radio player etc. The noise descriptors: L_N, and L_{Aeq} rise from morning and reach peak values in the afternoon and evening but descend in the night. The lowest noise descriptor values were recorded at location 6, 8, 9, 12, 13, 19, and 20 of L_{Aeq}, L_{10}, L_{90}, L_{NP}, L_D, L_N,L_{DN} respectively. These locations are residential areas with some little of commercial activities going on there. Among the factors responsible for differences in noise levels in the centres surveyed include location site, presence of intrusive noise, traffic volume, commercial activities etc.

4.2   Questionnaire Results

The results obtained from the questionnaire survey are presented in figure below.

Table 5: Respondents' Profile

S/N	Variables	Options	Frequency of Occurrence	
			N	%
1	Age (Year)	20-30	150	50
		30-40	82	27
		40-50	42	14
		Above	26	9
		50	300	100
		Total		
2	Sex	Male	163	54
		Female	137	46
		Total	300	100

Table 5 shows that 54% were male and 46% were female, and their ages was 20years and above, 50% were in the age group of 20-30 years old,27% between 30-40years old, 14% between 40-50years old and 9% were 50years above.

The analysis (in table 6) indicates that a very large proportion of respondents in each age group are being affected by noise emanating from the generating plant noise. The range is 100% with overall %age of 100%. Majority of respondents with overall %age of 97% across different age groups feel that traffic noise affects their activities. More than average % of respondents (54%) across different age-groups claims that noise originating from religious functions affects them. A relatively small proportion of respondents (3% across various age groups) acknowledge adverse effect of noise generated by construction and also equal proportion of respondents (3%) across different age-groups claim that noise originating from industries affects them. In another question, the subjects have classified the noise in

their environment as "high" and "low". Fig. 4.1 shows that 97% of the respondents experienced high level of generator noise in their resident and 3% experienced low noise level.

Table 6: Shows sources of noise in terms of age groups

Source of Noise	Age Group									
	20-30		30-40		40-50		Above 50		Total	
	N	%	N	%	N	%	N	%	N	%
Traffic Noise	146	97	82	100	42	100	26	100	296	97
Industrial Noise	4	3	3	4	3	7	-	-	10	3
Generating plant Noise	150	100	82	100	42	100	26	100	300	100
Construction Noise	4	3	3	4	3	7	-	-	10	3
Religious place Noise	84	56	38	46	26	62	13	50	161	54

Fig 4.2 shows that, almost 79% of the respondents have affirmed that they had been living at their resident for years, while 21% had been living at their resident for months. The respondents have been asked "what time does noise bother them more". For this question, Fig. 4.3 below shows that, 89% out of them answered that noise bothers them in the day and night and 11% answered that noise bother them more in the night. The majority of the respondents have answered that they sometimes felt annoyed by generating plant noise in his/her environment.
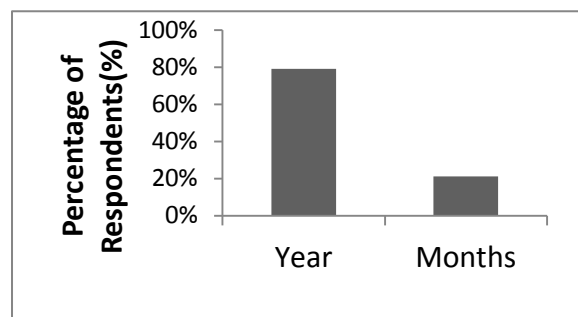
Fig. 4.2: Frequency distributions of respondent's period of living in their resident
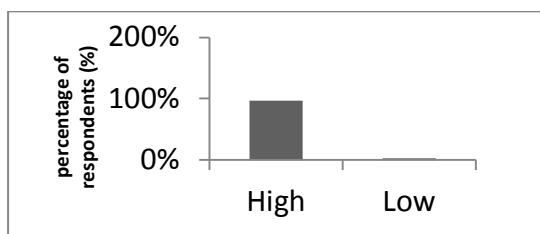
Fig. 4.1: Frequency distributions of generating plant noise levels.
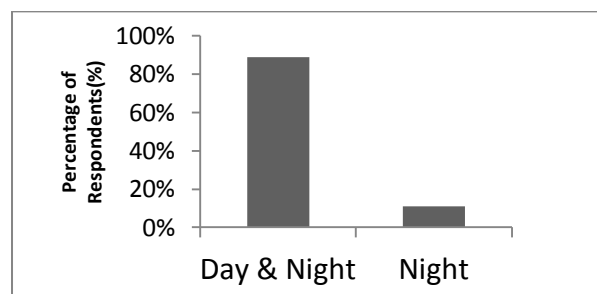
Fig. 6: Frequency distributions of time noise bother respondents

We can visualize (Table 4.6) that generating plant noise causes disturbance, hearing loss, blood

pressure/hypertension, stress, stomach ailments, and annoyance to individuals under its umbrella. Majority of sample respondents exposed to generator noise pollution report occurrence of annoyance, disturbance, loss of sleep and hearing problem. As many as 100% reported the hearing loss, disturbance, loss of sleep and also equal number reported annoyance. The survey data shows that the effect of noise is not similar among various age groups.

Table 7: effect of generating plant noise on different age groups.

Effect of Generating plant noise	Age Groups									
	20-30		30-40		40-50		Above 50		Total	
	N	%	N	%	N	%	N	%	N	%
Hearing loss	150	100	82	100	42	100	26	100	300	100
Annoyance	150	100	82	100	42	100	26	100	300	100
Blood pressure	-	-	-	-	2	5	10	38	12	4
Loss of sleep	150	100	82	100	42	100	26	100	300	100
Stomach ailments	10	7	7	9	3	7	5	19	25	8
Disturbance	150	100	82	100	42	100	26	100	300	100
Stress	118	79	55	67	26	62	22	85	221	74
Total	150	100	82	100	42	100	26	100	300	100

Generally, growing age bears more effect of generator noise pollution. For example, the rising proportion of sample respondents in higher age groups (40years above) acknowledges annoyance, sleeplessness, blood pressure/hypertension, stress, stomach ailment and hearing loss effect. A very large proportion of respondents feel that noise interferes with inter-personal communication and causes annoyance. Extreme effects (i.e. mental stomach ailments and blood pressure) are acknowledged by one third of survey population.

4.3   Discussion

Noise pollution in big cities is a growing problem due to the fact that the urban environment is becoming increasingly crowded and busy. In this study, the measured noise levels were generally high; LAeq, ranged between a maximum of 99.4 dBA and a minimum of 83.2dBA.

The environmental sound levels measured at a given location depend on a number of specific variables. Ugwuanyi, (2004), Paqrvathi, (2003) and Oseji, (2011) have found that the observed sound levels are mainly related to home appliance (i.e. television and music system), road traffic noise, public address system, generating sets, railway and air traffic noise etc. (Ugwuanyi et al., 2004). Several studies have demonstrated that the urban conditions of a given area are also a very important factor influencing the environmental noise levels. There is variation in the noise levels with the period of the day and the nature of the location. From the study carried out, it is observed that there is high noise pollution levels (LNP) in the daytime (7:00 am–3:00 pm) compared with the night-time (8:00 pm–10:00 pm), these always happen mostly in commercial areas. In residential areas where the majority of the residents are always at home after working day hours, the

noise level at night is always high compared to day period as a result of the residents gone for their daily work or business in the day.

Considering the criteria from HUD, only 7 locations representing 35% out of the 20 locations surveyed, can be classified as clearly acceptable, while the remaining locations representing 65% can be classified as normally acceptable. A widely accepted scientific fact is that living in black acoustic zones, where the equivalent sound level is higher than 65 dBA put an urban population in a high risk status for numerous subjective effects of noise, including psychological, sleep and behavioural disorder.

Table 7 shows that 100% of the respondents in each age group believed that the noise emanating from generators affect their hearing. Similar, results are obtained by (Valentine et al., 2010). Nearly 89% of subjects believed that noise bothered them more in the day and night and 11% in the night, as is also reported by other researches (Uris at el., 2001).

The study also revealed that the most unpleasant noise was generating plant and motor traffic followed by religious centred, then by industrial layout, and construction noises.

Interesting results have also been obtained regarding generator noise levels (high and low) are used to determine the level of noise. If the sources are analysed separately, it is noticeable that among the subjects who felt annoyed by the noise in his/her home, 97% pointed out the traffic noise was the main source of annoyance, 100% the generating plant noise.

The study showed that generating plant noise has negative impacts on human health, as is reported by Oseji, (2011), Parvathi et al.,(2003).

4.4 Conclusion

This study explores the sources of noise in Ilorin metropolis, effects, reactions and suggestions for controlling the excessive noise caused by generating plant.It hasalso been revealed that Ilorin is a fast growing metropolis and the generating plant noise pollution has reached a non-acceptable level, as pointed out from the results obtained. Table 6 revealed that the generator noise has become one of the major source of environmental pollution and will require urgently solutions. This were confirmed from the results of the questionnaire interview conducted on the effect of noise pollution on human being. This investigation reveals that noise level at measuring point is higher than the recommended level of 60 dB(A) for commercial and residential areas by World Health Organization(WHO). Hence, the present status of noise pollution in Ilorin metropolis poses a severe health risk to the residents.

REFERENCES

Akpan, A. O., Onuu, M. U., Menkiti, A. I., & Asoquo, U. E. (2003). Measurements and Analysis of Industrial Noise and its Impact Workers in AkwaIbom State, South-Eastern Nigeria. Nig. *Journal of Phys, 15* (2), 41-45.

Atmaca, E. I.,Peker, A.,&Altin, O. (2005). Industrial Noise and Its Effects on Humans. *Polish Journal of Environmental Studies, 14* (6), 721-726.

Cuesta, M., & Pedro, C. (2000). Active control of the exhaust noise radiated by an enclosed generator, *Applied Acoustics, 61,*83-94.

Cuesta, M. & Pedro, C. (2001). Optimization of an active control system to reduce the exhaust noise radiated by a small generator, *Applied Acoustics, 62,* 513 – 526.

Levitt, H. (2001). "Noise Reduction in Hearing Aid" Journal of Rehabilitation Research and Development, 75th street, Jackson Heights, Ny 11370, 38 (1).

Mbamali, I., Stanley, M. A.,&Zubairu I. K. (2012).Environmental, Health and Social Hazards of Fossil Fuel Electricity Generators: A Users' Assessment in

Kaduna, Nigeria. American International Journal of Contemporary Research, 2 (9).

Miltz, S. A., Wilkins III, J.R., Ames A. L., & Witherspoon, M. K.(2008). Occupational Noise Exposure among Three Farm families in Northwest Ohio., *Journal of Agromedicine, 13*(3), 165-174.

Mohammed, J. A. (2008). Effect of Noise Pollution on Hearing of Public Transport Drivers in Lahore City. *Pakistan Journal Of Medical Sciences, 24,1.*

Olokooba, S. M., Ibrahim, I., &Abdulraheem-Mustapha,M. A. (2005). Noise Pollution: A Major Catalyst Climate Change and Human health .*Journal of social sciences Unilorin.*

Oseji, J. O. (2011). Investigating of environmental noise within campus 2, Delta State University, Abraka, Nigeria, 6(2), 11-23.

Oyedepo, S. O, &Saadu, A. A. (2010). Evaluation and analysis of noise levels in Ilorin metropolis, Nigeria. Environ Monit Asses 160, 563-577.

Parvathi, K., &Navaneetha, G. (2003), "Studies On Control Of Noise From Portable Power Generator" Proceedings of the Third International Conference on Environment and Health, Chennai India, Pages 328 – 338.

Saadu, A. A., Onyeonwu, R. O., Ayorinde, E. O., &Ogisi, F. O. (1998). Road Traffic Noise Survey and Analysis in Some Major Urban Centers in Nigeria. Noise Control Eng J, 46, 146–158.

Ugwuanyi, J. U., Ahemen, I., &Agbendeh, A. A. (2004) Assessment of Environmental Noise Pollution in Markurdi Metropolis, Nigeria. *J Pure ApplSci, 6,*134-138.

Yilmaz, H., &Ozer, S. (2005) Evaluation and Analysis of Environmental Noise Pollution in the City of Erzurum, Turkey. Int J Environ Pollut, 23, 438-448.

Quality Control in a Typical Local Casting Workshop

A. Babawuya[1], Saka, A J[2], M. D. Bako[3], Okosi A. P[4].and M. Ibrahim[5]

[1]Department of Mechatronics Engineering,

Federal University of Technology, Minna, Nigeria

[2]Department of Mathematics,

Obafemi Awolowo University, Ile-Ife, Nigeria.

ajsaka@oauife.edu.ng, sakajamiu@gmail.com

[3]Vehicle Inspection Department, Ministry of Transport, Minna, Nigeria

[5]Mechanical Engineering Department,Federal Polytechnic, Bida.

*Corresponding author: babawuyal@futminna.edu.ng,07038096888

ABSTRACT

Being the part of reformation agenda by the current government of Nigeria to give adequate attention to the improvements of the local products, as such, quality improvement on our local products is of paramount. In achieving this aim, Mahmoud Metal Foundry (MMF) in Niger state of Nigeria which uses aluminium alloy for casting non-ferrous metals such as aluminium and brass for customers and other manufacturing ventures was used as a case study. Two consecutive months data set were collected and percentage defective chart (P-chart) analysis was carried out. On the first month, it was observed that the control chartrevealed that the sample number 10 and 11 were outside the control limit and this isevidence that an assignable cause of variation was present. This simply means that the process is not conforming (out of control). It was also observed that the analysis carried out on the data set for the second month revealed that the process is in control, since all the sample points fall within the control limits, the control chart for the second month also testified to this. The establishment of quality control unit should be encouraged in every local firm so as to improve quality of their output.

Keywords: *casting, defective, fractional-defective, p-chart, super QC-pack, quality control*

1.0   INTRODUCTION

Casting is basically melting a solid material, heating to a specific temperature, and pouring the molten material into a cavity or mold, which is in proper shape. Casting has been known by human being since the 4th century B.C. Today it is nearly impossible to design anything which does not involve casting processes. (Brown, 2008). However, one of the problems associated with casting process is defect in the cast which could be as a result of process parameters. Aluminum alloy castings were first produced using processes that had been in historical use for other metals, as mentioned above. The relatively attractive engineering properties of Aluminum - low melting point and castability-quickly led to the adoption of existing casting processes and to developments that broadened the means by which engineered shapes could be produced from molten metal.(www.asminternational.org). The use of Aluminum alloy for casting of domestic and industrial application becames so popular due to its light weight, corrosion resistance and low melting temperature. Achievable casting performance is limited due to defects that emerge during the casting process such as gas, shrink porosity, laminations, inclusion and pattern material. (Brown, *et al*, 1995).

Local foundry workshops have over the years being involved in the use of Al-alloy (recycled Al-alloys) for casting of products such as Al-ports, machine components (such as propeller shafts, cover platesetc. and other esthetic designs for home use).

Mahamoud metal foundry(MMF)located in Tudun wada panteka Kaduna State of Nigeria, is a private local foundry workshop which engages in castings of non-ferrous metals like Aluminum and brass for customers and other manufacturing ventures. They carried out mostly batch production of castings of Al of different shapes and design.(see figure 1). On a daily basis, they carried out a batch production casting of various shapes and design that run into hundreds, this casting are of different quality (standard). These products are sold to customers even if defective.This necessitated the motivation to carry out a statistical quality control on their daily production for one month. So that out of control products can be established.

2.0   LITERATURE REVIEW

2.1   Quality Control in casting

Quality Control begins in early 1900s when factory productions were inspected, that is the final products were inspected for the purpose of accepting or rejecting the product before getting to the consumers. During this time,

F.W.Taylor in his list of basic areas of manufacturing management emphasized on quality including product inspection in it, While Radford was of the view of involving quality consideration early in the product design stage and also to connect together quality, productivity and cost. In 1924, Walter shewhart introduced statistical process control (S.P.C.) by means of charts in order to keep a control over production. After five years Dodge and Romig introduced acceptance sampling inspection tables. This concept of S.P.C. was used in industries till 1940s. However, Second World War remarkably increased the importance of quality control. W. Edward Deming introduced statistical quality control (S.Q.C) in Japan industry.

This resulted in the creation of a quality manufacturing facilities in Japan.

The devastated country in this Second World War posed a tough competition to other leading nations in the area of manufacturing, especially the American manufacturing firms. After this war, in the mid-twentieth century,
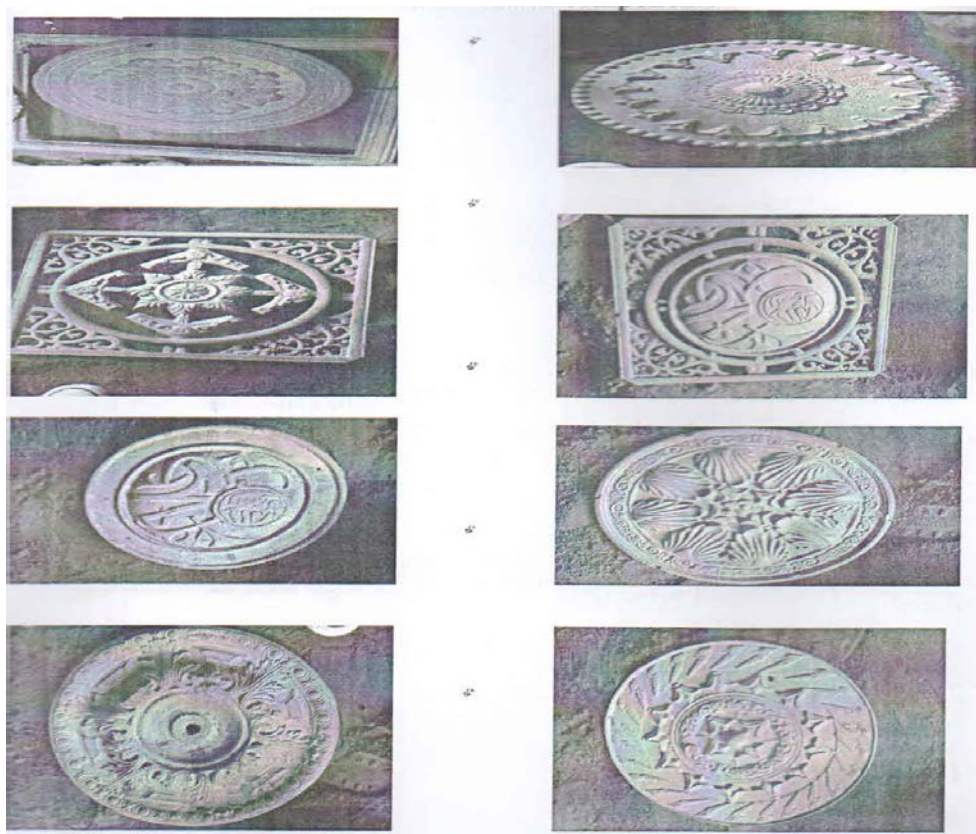
Figure 1: some casted components.

professionals and engineers in the industry hugely benefited by the American universities in terms of training in quality control. This has seen the emergence of "Quality Assurance" evolved out of this development taken place around quality control concept. At about the same time, Joseph Juran began his cost of quality approach, emphasizing accurate and complete identification and measurement of cost of quality. In the mid 1950s Armand Fiegen Baum proposed Total quality control which enlarged the focus of quality control from manufacturing to include product design. During the 1960s, the concept of zero-defects gained favour. Philip Crosby, who was the champion of "zero-defects" concept focused on employee motivation and awareness. In this decade from 1960 to 1970, quality control and management became synonymous with the growth of industrial Revolution in Japan. In late 1980s, Total Quality Management (TQM) gained a lot of popularity even outside Japan and became the main theme revolving around the concept of Quality Control. In the twenty first century the concept of quality has been gathering a total or gross approach in terms of "Business Excellence".

Quality control is very important in our local pot casting shop in that, it is the properties which determine demand of the product, if quality is low certainly demands will be low and if quality is high, demands will certainly be high vise visa. The aim of any business is to make profit, therefore if quality is good, demand will be high and profit will be maximized. Pots like any other products or components need quality control, more so, almost all homes are in need of this product (pot) for one purpose or the other in their daily activities.

2.2   Statistical Process Control

Definition: Statistical Process Control is the use of valid analytical statistical methods to identify the existence of special causes of variation in a process. Statistical process control (SPC) involves using statistical techniques to measure and analyze the variation in processes. Most often

used for manufacturing processes, the intent of SPC is to monitor product quality and maintain processes to fixed targets. Statistical quality control refers to using statistical techniques for measuring and improving the quality of processes and includes SPC in addition to other techniques, such as sampling plans, experimental design, variation reduction, process capability analysis, and process improvement plans (Montgomery, 2005).

2.3   Fractional Defective Chart (P-Chart)

The P-chart is used to monitor or control the proportion or fractional defective produced by a process, (Creswell,1998). P-chart can be used when the subgroup size varies (not constant). It can be applied to any variable where the appropriate performance include scrap reports, inspection data and any other data where you know how many units were inspected and how many either meet some criteria or failed to meet the criteria.

3.0   MATERIAL AND METHODS

3.1   Materials used.

1.   Instrument of data collection (Primary- Questionnaire, Secondary- Interview).

2.   Super QC- pack used for the statistical analysis (P-chart).

3.   Ms Excel pack used for the statistical analysis (correlation and regression).

3.2   Data collection.

Daily production data were collected as shown in Table 1. This includes total numbers of production per day, total defective per day, working hours and numbers of workers for a period of two months.

3.3   Statistical Methodology

In this section we give details of the procedures regarding statistical quality control chart used, specifically fractional

defective chart called P-chart, correlation and regression analysis carried out.

3.4 Control limit for P-chart

According to the control limit for p- chart can be calculated as given in equation 1-4.

Calculate P from each subgroup

$$P = \frac{d}{n} = \frac{Number\ of\ defectives}{Number\ inspected} \qquad (1)$$

Calculate the central line (limit)

$$CL = \bar{P} = \sum_{i=1}^{m} \frac{d_i}{nm}$$

$$\text{or} \qquad \bar{P} = \sum_{i=1}^{m} \frac{p_i}{m} \qquad (2)$$

Compute $3\sigma_p$, where

$$3\sigma_p = \frac{\sqrt{\bar{p}(1-\bar{p})}}{\sqrt{n_i}} \qquad (3)$$

Compute the control limits

- Upper Control Limit (UCL) $= \bar{P} + 3\sigma_p$

- Central Control Limit (CCL or CL) $= \bar{P}$ (4)
- Lower Control Limit (LCL) $= \bar{P} - 3\sigma_p$
- Plot the value of p on the graph and connect them together.
- Plot the central limit and control limits for each of the subgroups

4.0 RESULTS AND DISCUSSION OF THE RESULTS.

4.1 Results

The data collected were presented in table 1 and 2. The data were analysed using super QC- Pack for p-chart and ms excel for correlation and regression. The fractional defective and percentage defective chart were obtained for the two month data collected (see Table 1 and 2). The data were used to obtained the p-chart, correlation and regression. The p-chart for months 1 and 2 are shown in figures 1 and 2. The result of the correlation is presented in table 3, and table 4 and figure 3 are the results of the regression analysis.

Table 1: The number of defectives casted for the first month

Sample Number	Number of Observations Sampled	No. of Defectives Cast	Fractional Defectives
1	39	1	0.03
2	38	2	0.05
3	40	0	0.00
4	35	5	0.14
5	45	5	0.11
6	50	0	0.00
7	30	0	0.00
8	37	3	0.08
9	45	5	0.11
10	40	10	0.25
11	31	9	0.29
12	29	1	0.03
13	36	4	0.11
14	20	0	0.00

15	60	0	0.00
16	60	0	0.00
17	55	5	0.09
18	45	4	0.09
19	39	2	0.05
20	20	2	0.10
21	20	4	0.20
22	20	5	0.25
23	30	3	0.10
24	40	5	0.13
25	20	0	0.00
26	50	5	0.10
27	48	4	0.08
28	25	1	0.04
29	25	2	0.08
30	35	6	0.17
31	30	2	0.07
Total	**1137**	**95**	**2.76**
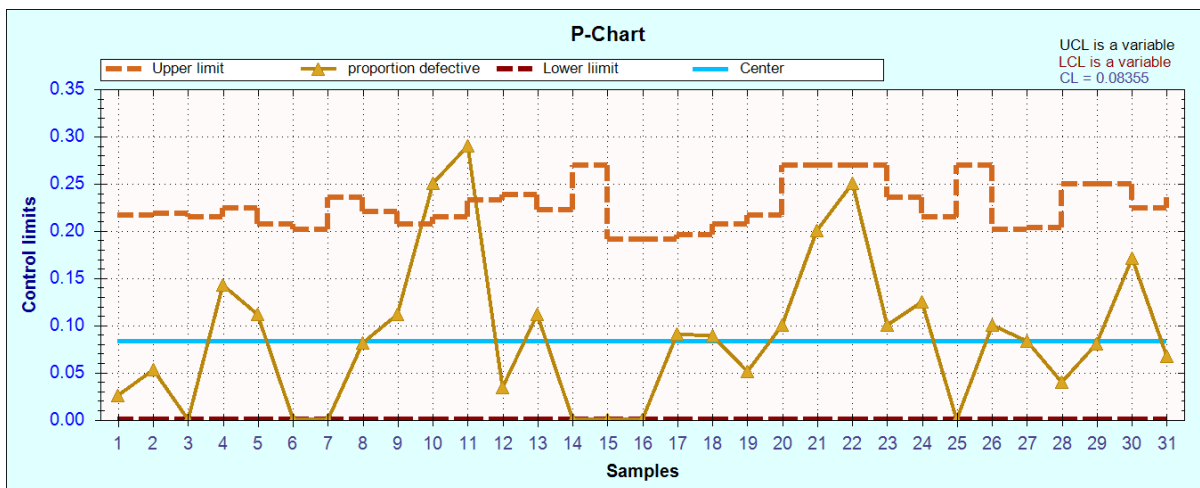
Figure 1: percentage defective chart for the first month.

Table 2: The number of defectives casted for the second month.

Sample Number	Number of Observations Sampled	No of Defectives Cast	Fractional Defectives
1	40	2	0.05
2	35	4	0.11
3	33	1	0.03

4	39	4	0.10
5	36	3	0.08
6	50	5	0.10
7	30	0	0.00
8	37	3	0.08
9	48	0	0.00
10	48	4	0.08
11	31	5	0.16
12	29	1	0.03
13	38	3	0.08
14	40	6	0.15
15	60	7	0.12
16	60	4	0.07
17	55	5	0.09
18	45	4	0.09
19	39	2	0.05
20	40	2	0.05
21	20	4	0.20
22	50	5	0.10
23	38	3	0.08
24	40	5	0.13
25	20	0	0.00
26	50	5	0.10
27	58	4	0.07
28	35	1	0.03
29	45	2	0.04
30	35	6	0.17
31	30	2	0.07
Total	**1254**	**102**	**2.51**
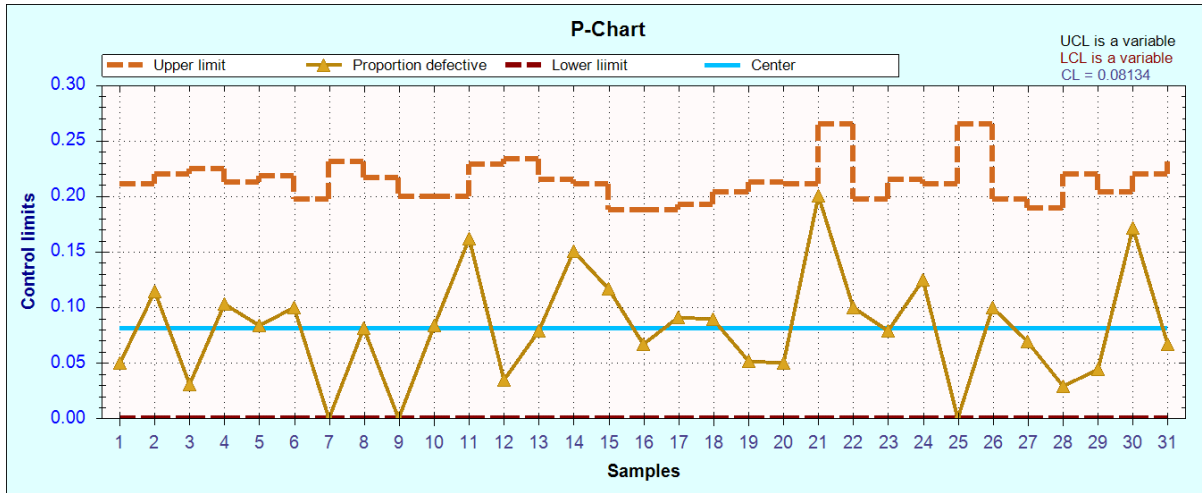
Figure 2: percentage defective chart for the second month.

Table 3: coefficient of correlation between the sampled observations and defective cast.

	Number of Observations Sampled	No of Defectives Cast
Number of Observations Sampled	1	
No of Defectives Cast	0.474280207	1
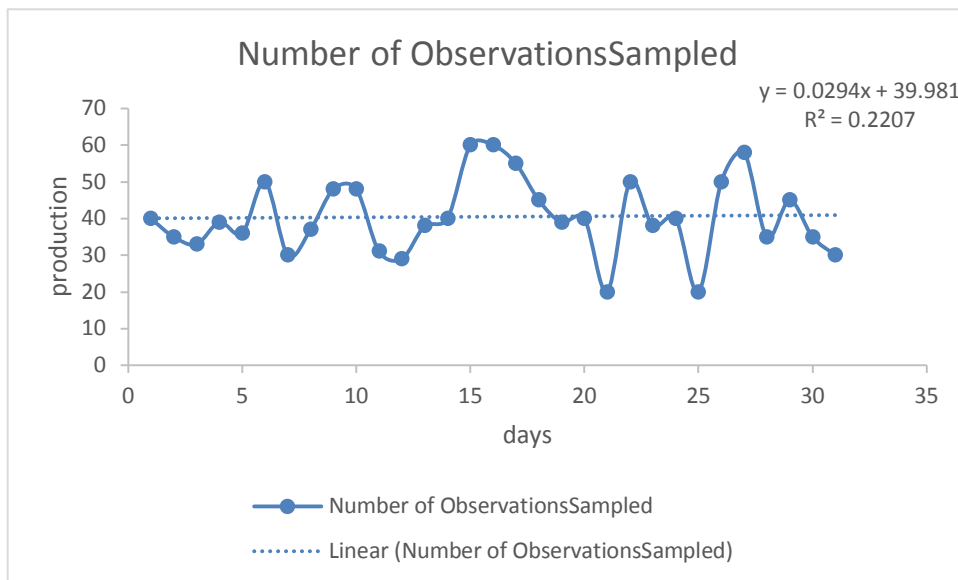
Figure 3: Number of Production per day at MMC during the period of the study
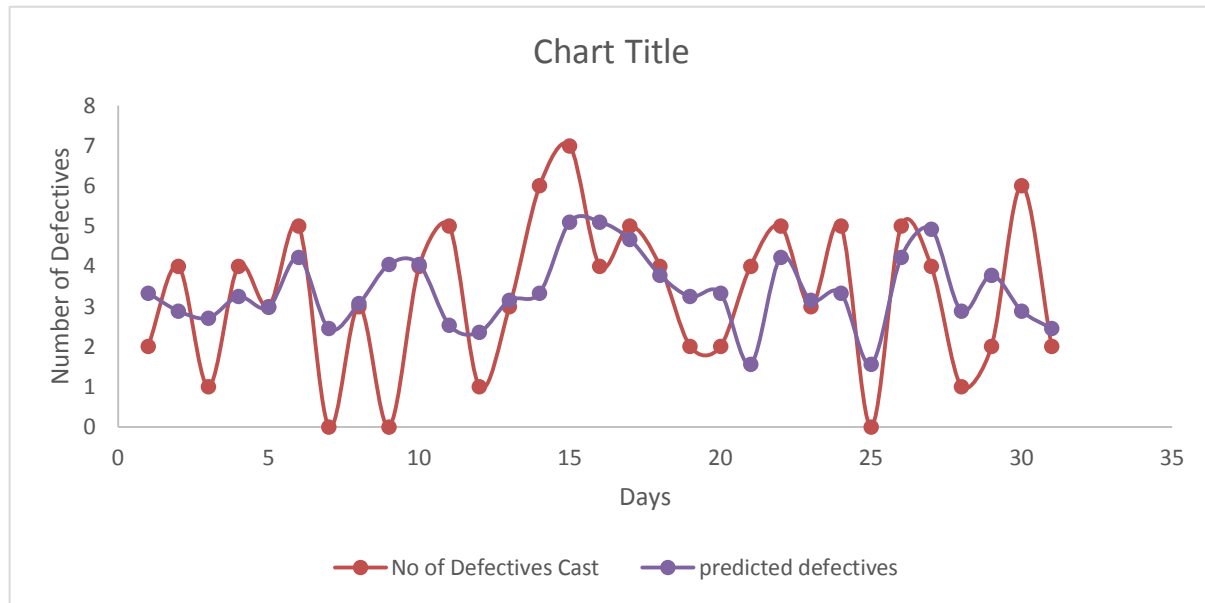
Figure 4: A comparison between daily defects cast and predicted defective

4.2 Discussion of the Results.

For the first month, (see table 1), the total number of product is 1137 total number of defective is 95 and total fractional defective 2.76 for the second, the total numbers of observation sampled 1254, the total number of defective cast, 102 and the total fractional detective 2.51. For the first month, the average observation sampled is 36.7, the average defective cast 3.1, while average fractional detective 0.089. and for the second month, the average observation sampled is 40.5, the average defective cast 3.3, while average fractional detective 0.081. The % defective casted for the 1st month sampled on day 10-11, were out of control limits, while for the second month, there was in control sampled.

The correlation coefficient between the number of production and the number of defectives is 0.472. This means that, as the number of production is increasing, the numbers of the defective are also increasing, but the correlation is not strong. Also, a linear regression between the number of production and the number of defective cast was obtained with a multiple R of 0.475 and R-square of 0.225.

5.0 Conclusion

Based on the analysis carried out in section 4 in respect of data set for the first month and with reference to the control chart in figure 1, it was observed that the sample number 10 and 11 were outside the control limit. And this is evidence that an assignable cause of variation is present. This simply means that the process is not conforming (out of control).It was also observed that the analysis carried on the data set for the second month, revealed that the process is in control, since all the sample points fall within the control limits, the control chart in figure 2 also testified to this. And also there is an intermediate correlation between daily production and daily number of defectives.

On a final note, we hereby, advising our local firm to be embarking continuous processing control in other to have better quality output always.

References

Brown Z, Barnes C, Begelow J and Dodd P., Squeeze cast automotive application of design considerations. In international conference , " High tech Die-casting", Mantichiari, 9-10, April, 2008.

Brown, L. A., Lowe, V. W., &Benham, D. R. (1995). Statistical Process Control (SPC). Chrysler Corporation: For Motor Company; Generation Motors Corporation.

Creswell, J. (1994). Research Design: Qualitative and Quantitative Approaches. SAGE.

Juran, J. M. (1998). Quality Control Process. Blacklisk: McGraw- Hill Professional.

Montgomery, D.C. (2005). Introduction to Statistical Quality Control. Wiley. Robertson, G. H. (1990). Quality through statistical thinking (improving process control and capability).

Nutritional and Organoleptic assessments of sun dried and solar dried *kilishi*

*B.A Orhevba and A.O Moru

Department of Agricultural and Bioresources Engineering, Federal University of Technology, P.M.B 65, Main Campus, Gidan Kwano-Minna, Niger State, Nigeria

* borhevba@yahoo.com, 08061688880

ABSTRACT

This study is aimed at investigating the effect of sun drying and solar drying on the nutritional and organoleptic properties of dried meat (*kilishi*). Nutritional content determined are moisture content, ash content, fat content, crude protein and carbohydrate content by absorption methods. Four hundred grams of meat from beef was divided into two parts (Sample A and Sample B) of two hundred grams each. Sample A was solar dried using a fabricated solar dryer while sample B was sun dried, both were dried for eight hours with respective weight loss recorded hourly. The amount of moisture on wet basis at interval of one hour for solar drying was 12.25%, 21.88%, 27.63%, 33.85%, 37.06, 40.75%, 43.55% and 48.63% , while that of direct sunlight drying had a moisture content of 12.83%, 20.77%, 26.75%, 33.58%, 35.75%, 38.97%, 40.18% 42.65% respectively. Nutritional, Organoleptic and Microbial load count test were carried out with the following results respectively [Nutritional (M.C 9.63%, Fat 1.69%, Crude Protein 50.26%, Ash 24.09%, Carbohydrate and others 12.01%) Organoleptic (Appearance sample A 3.2 and sample B 4.0,Taste sample A 3.1 and sample B 3.2 ,Aroma sample A 4.2 and sample B 4.3 ,feel sample A 3.9 and sample B 3.5) Microbial load count (Sample A >2.5×10^6 and Sample B >4.7×10^8)].. The results shows that *kilishi* is best produced using the solar drying method, as sun drying method contained large number of micro organisms which poses a threat to the health of the consumer.

Keywords: Meat; Kilishi; Organoleptic; Slurry; Nutritional; Drying

1. INTRODUCTION

Meat is one of the essential sources of protein and a wide variety of other nutritional value. It has been widely accepted and consumed by humans as a major food since the primitive era. However, as the consumption rate and the production of meat grew perpetually with time, the nature of the product requires that it be preserved for future use. The high water content of meat makes it extremely perishable. Food preservation is employed to prevent unwanted changes in the nutritive value and sensory quality of food by putting the growth of micro-organisms under control and reducing the physical, chemical and microbiological changes, which in turn increase the economic value of the product (Igene, *et al.,*

1990). *Kilishi* is a dried seasoned meat delicacy majorly from the northern part of the country. This delicacy is popularly enjoyed and consumed across the nation. *Kilishi* is produced in almost all the states of the North-west of Nigeria; it is most popular in Kastina, Sokoto, Kaduna and Kano States (Raw Materials Research and Development Council, 2010). It is a traditionally processed intermediate moisture or semi dry, ready-to-eat, meat product made from beef in Northern Nigeria. It is prepared from the pure flesh of de-boned beef which has been trimmed of all visible fats and connective tissues; the cleaned meat is then weighed and sliced into thin sheets of 0.17- 0.20 cm thick and 60-80 cm long. The sliced meat is sun dried and infused with locally available spices, condiments, and other materials such salt, *magi* seasoning, peanut paste and

water. The local spices and condiments used include; onion, alligator pepper, cloves, chilies, ginger, African nutmeg, black pepper, locust beans, groundnut powder and dry pepper (Igene, *et al.,* 1990).

Nigeria is the highest producer of *kilishi* in West Africa among other countries such as Senegal, Mali, Chad and Niger. It appears to have developed amongst the early Fulani and Hausa headsman as a means of preserving meat in order to enhance its shelf life. *Kilishi* has from time immemorial been part of the trans-saharan trade and even beyond, the product has created an informal export to the Holy land during Hajj period over the years (Raw Materials Research and Development Council, 2010).

The product came about as a means of preserving meat in the absence of facilities for refrigerated storage, by the early Fulani and Hausa herdsmen. In Northern Nigeria, the producing states of *kilishi* include: Borno, Kano, Sokoto, Kaduna and Bauchi. This is made possible because the weather is favourable, consumer demand is high and more than 70 % of the Nigerian cattle population of 10 million can be found in these states (Alaku and Igene 1983).

```
┌─────────────┐
│ Fresh Meat  │
└─────────────┘
       ⇓
┌─────────────┐
│  Trimming   │
└─────────────┘
       ⇓
┌─────────────┐
│   Cutting   │
└─────────────┘
       ⇓
┌─────────────┐
│   Washing   │
└─────────────┘
       ⇓
┌─────────────┐
│  Sun drying │
└─────────────┘
       ⇓
┌─────────────┐
│   Mixing    │
└─────────────┘
       ⇓
```
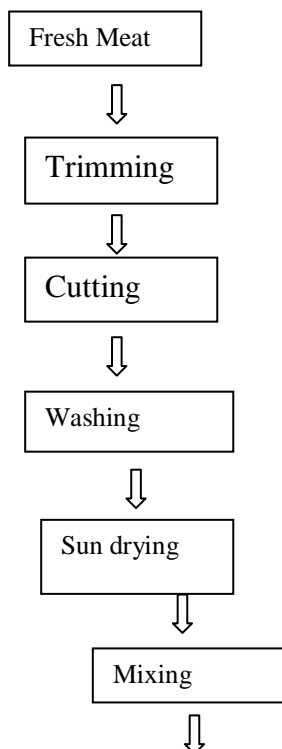
```
┌─────────────┐
│ Sun drying  │
└─────────────┘
       ⇓
┌─────────────┐
│  Roasting   │
└─────────────┘
       ⇓
┌─────────────┐
│  Kilishi    │
└─────────────┘
       ⇓
┌─────────────┐
│ Packaging   │
└─────────────┘
```
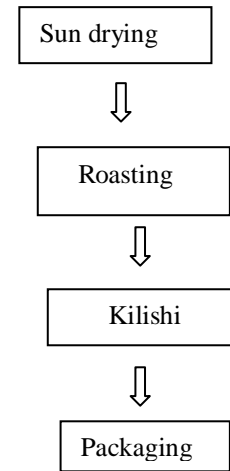
Fig.1.1; Steps involved in the production of dried meat (Kilishi) (Ogunsola and Omojola, 2008)

2. Materials and Methods

2.1 Materials and their Source

Six hundred grams of cow meat (Beef) was bought from Minna abattoir located at Tahi village in Bosso local Government Area of Niger State. The meat was purchased early in the morning to ensure that the meat was fresh and relatively hygienic for processing of *kilishi*. The raw meat was then kept inside a polyethylene bag. The ingredients for the slurry and the packaging material (aluminum foil) were purchased from A. A. Kure ultra modern market, Minna, Niger State.

2.2 Methods

2.2.1 Cleaning process.

The meat obtained was thoroughly washed with water in order to remove dirt and blood stains. Fat and connecting tissues which are not required for the production of *kilishi* were also removed.

2.2.2. Slicing Process.

After cleaning and trimming of the unwanted materials, the meat is cut thinly into slices measuring 3-5 mm thick and

up to 20- 40 mm long, the sliced meat was equally divided into two portions (A and B).

2.2.3 Drying Process.

The first portion (specimen A) of the thin slices were spread out doors on a platform (called 'gadon kara' in Hausa) made from millet stalk, for sun drying, and the second portion (specimen B) placed inside the solar dryer, both were dried for 8 hours and readings were taken every 20 minutes which gave rise to three readings for every hour on each method. This stage of moisture removal is done so as to enable the meat absorb the moisture contained in the ingredient slurry.

2.2.2 Slurry Preparation and Application

The ginger was washed and dried (usually it comes with traces of sand); dried (hot) pepper was grounded together with the other spices including the washed dried ginger, water was then poured into the powder to make a slurry like mixture. The mixture was stirred thoroughly until a red colored paste was obtained. The dried meat was dipped into the slurry for 10 minutes until it completely absorbed the mixed ingredients; it was then spread again on the sorghum stalk mat for a while to drain. This process increased the moisture content of the immersed meat and the surface of the meat is coated with the ingredients. The excess moisture had to be removed using a glowing fire.

2.2.3 Roasting of Immersed Meat and Packaging.

In the final drying process, the infused meat was transferred to where it will be gently roasted with a glowing fire. The height at which the meat is placed on the wire mesh allowed the heat of contact on the meat to be around 100-120 ^{0}C. This enormously reduced the moisture content. It is during this process that kilishi acquires its special flavor from the smoke that was produced from the

fire wood. The hot, sizzling, brown colored kilishi was then removed, cooled to room temperature and ready for consumption. The cooled kilishi was then wrapped in an aluminium foil.

3. Results

The results obtained from the experiment are listed in Tables 1 to 10

Table 1: Mean value of the drying rate and Standard deviation of solar dried Kilishi

Time (hr)	Mean Value (g)	Standard Deviation
0	00.00	0.141421
1	75.50	0.749533
2	56.25	0.480833
3	44.74	0.282843
4	32.30	0.608112
5	25.88	0.282843
6	18.50	0.636396
7	12.90	1.965757
8	02.74	0.141421

Table 2: Mean value of the drying rate and Standard deviation of sun dried *Kilishi*

Time (hr)	Mean Value (g)	Standard Deviation
0	00.00	0
1	74.35	0.070711
2	58.47	0
3	46.50	0.141421
4	32.85	0.59397
5	28.55	3.535534
6	22.06	2.870854
7	19.65	0.46669
8	14.70	0.424264

Table 3: Proximate Composition of solar dried kikishi

Sample	Moisture content	Fat	Crude Protein	Ash	Carbohydrate & Others
A1	9.29	6.26	50.37	24.09	9.99
A2	9.41	6.11	50.41	24.20	9.78
A3	10.20	6.17	50.00	23.98	9.65
Mean	9.63	6.18	50.26	24.09	9.81

Table 4: Proximate Composition of sun dried kikishi

Sample	Moisture content	Fat	Crude Protein	Ash	Carbohydrate & Others
B1	11.56	5.19	49.13	24.39	5.63
B2	11.01	6.17	52.2	23.87	6.75
B3	11.05	6.17	51.53	24.59	6.66
Mean	11.21	5.84	50.95	24.28	6.35

3.2 Organoleptic Assessment of sun dried and solar dried *kilishi*

Table 5: **Scores obtained for Appearance**

	PANELISTS										
Samples	1	2	3	4	5	6	7	8	9	10	Mean
A	5	3	4	3	3	5	4	4	4	5	4
B	3	3	3	2	3	4	4	4	3	3	3.2

Table 6: **Scores obtained for Taste**

	PANELISTS										
Samples	1	2	3	4	5	6	7	8	9	10	Mean
A	3	4	4	3	3	4	3	3	3	2	3.2
B	3	4	3	3	4	4	3	4	3	4	3.1

Table 7: **Scores obtained for Aroma**

	PANELISTS										
Samples	1	2	3	4	5	6	7	8	9	10	Mean
A	4	5	4	5	4	4	4	5	4	3	4.2
B	5	4	5	4	5	3	5	4	4	4	4.3

Table 8: **Scores obtained for Texture**

	PANELISTS										
Samples	1	2	3	4	5	6	7	8	9	10	Mean
A	3	5	4	4	3	4	4	5	4	3	3.9
B	2	3	1	3	2	3	3	4	2	2	3.5

NOTE:

A: *kilishi* prepared by solar drying method

B: *kilishi* prepared by sun drying method

3.3 Microbial analysis of sun dried and solar died *kilishi*

Table 9: Bacteria count in solar dried *kilishi*

Total Aerobic Plate Count (Cfu/m)	Count
Sample	Treatment
A1	$>2.2 \times 10^6$
A2	$>2.5 \times 10^6$
A3	$>2.8 \times 10^6$
Mean	$>2.5 \times 10^6$

Table 10: Bacteria count in sun dried *kilishi*

Total Aerobic Plate Count (Cfu/m)	Count
Sample	Treatment
B1	$>5.1 \times 10^8$
B2	$>4.8 \times 10^8$
B3	$>4.2 \times 10^8$
Mean	$>4.7 \times 10^8$

3.4 Proximate Analysis of sun dried and solar dried *kilishi*

3.4.1 Moisture content

From Tables 3 and 4, moisture content of solar dried sample of 9.63% was slightly lower than that of the sun dried sample of 11.21 %, this could be as a result of the difference in the drying rate of the solar drying method and the sun drying method, as the solar drying method dried faster.

3.4.2 Fat Content

The values of 5.4 % (sun dried) and 6.8 % (solar dried) for fat content are quite close. The difference is slight.

3.4.3 Crude Protein

Regardless of the distinct processing method employed there was no significant difference in the crude protein content values of 50.95 (sun dried) and 50. 26 (solar dried).

3.4.4 Ash Content

There was also no significant difference in the ash content of the dried samples; 24. 28 (sun dried) and 24.08 (solar dried).

3.5 Scores obtained from organoleptic assessment of sun dried and solar dried *kilishi*

3.5.1 Appearance

From Table 5, it can be observed that in appearance, sample A proves to be the highest in terms of acceptability (4.0). The attractive appearance of sample A was as a result of the drying principle of indirect solar dryer which kept the meat out of direct contact with solar radiation (sunlight) and this ensured the retainment of the true color of the meat.

3.5.2 Taste

Table 5 indicates that there were no significant differences in the acceptability of the taste of both samples. The scores for both were 3.1 for sun dried sample and 3. 2 for solar dried sample.

3.5.3 Aroma

The aroma of both samples were highly acceptable with close values of 4.2 for solar dried and 4.3 for sun dried *kilishi*, this shows that the variation in drying method has no effect on the aroma, as the aroma depends on the spicing of the *kilishi*.

3.5.4 Texture

The feel of sample A (solar dried *kilishi,* 3.9) was slightly higher than that of sample A (sun dried *kilishi, 3.5*), this could be due to the variation in the drying rate, as the solar drying method removed moisture faster than the sun drying method which resulted in the solar dried sample having significantly lower moisture content and being more crispy as compared to the sun dried sample.

3.6 Microbial analysis of sun dried and solar dried *kilishi*

The result of the microbial count (Tables 9 and 10) show that the sun dried sample contain significantly higher amount of bacteria as compared to the result of the solar dried sample which also contain bacteria contaminant but in a lower amount, reason being the exposure of the meat to environmental contaminants such as rain, wind/dust, birds ants and rodents during the sun drying process, whereby in the solar drying, the dryer houses the meat and there is no direct impact of sunshine on the sample.

4.0 CONCLUSION

From the results obtained from the study, it can be seen that the method of drying employed, had little or no effect on the proximate content and organoleptic properties of the *kilishi* produced. The results of the microbial analysis however indicates that the sun dried samples contained significantly higher amounts of microbes compared with the solar dried samples; this poses a threat to the health of the consumer.

REFERENCES

Alaku O. and Igene J. O (1983). Seasonal variation in volume of trade cattle moved from Sahelian to the equatorial zone of West Africa with particular reference toNigeria. World Rev. Anim Prod., 19: 69-74.

FAO (2007). Meat processing technology for small to medium-scale producers. *Food and Agricultural Organization, repository document corporate*

Igene, J.O, Farouk, M.M and Akanbi, C. T. (1990). Preliminary study on the traditional processing of Kilishi. Journal of the Science of Food and Agriculture 50, 89-98

Ogunsola O. O. and Omojoba, O. O., (2008),. Qualitative evaluation of kilishi prepared from beef and pork. *Africa journal of biotechnology vol.7 (11), pp. 1753-1758, 3 June, 2008 ISSN1684-5315.c 2008 Academic journal*

Raw Material Research and Development Council (RMRDC) (2010). Upgrade of Indigenous Technology in Kaduna State

AUTOMATIC TRAFFIC SUMMON SYSTEM

A.M. Aibinu[1*], A.A. Saleh[2], A. Mohamud[3], O.J Okubadejo[4], M.J Eyiomika[5]
[1]Federal University of Technology, Minna
[2,3]International Islamic University, Malaysia
*maibinu@gmail.com, abiodun.aibinu@futminna.edu.ng, +234-8029494164.

ABSTRACT

In this paper, we present a novel approach for the detection and transmission of characters in a Vehicle License plate. Our design is made to achieve portability which is not readily available in many traffic control systems. In the detection of car plate numbers, we implement a customized optical character recognition system, useful for traffic systems. Our algorithm uses image and signal processing techniques to correctly transcribe car plate numbers obtained from segmented images into machine readable text. For transmission, we adapt the GPS system to locate the point of incidence and download the road map. We use an SMS platform and email platform to send summon ticket to the offender's mobile phone. Our implementation solves the popular traffic problem called the *summons problem*.

Keywords: *Traffic summon, Automatic traffic summon system, OCR, Optical character recognition*

1. INTRODUCTION

The evolving of transportation over the years, from the days of camels and horses to the development and deployments of motor vehicles, motorcycles, airplanes and all other renaissance travel technology, has enabled people to get to their destination faster and with ease. The inherent ease attributable to these systems and the gradual reduction in cost of these systems has effectively allowed the populace to embrace and crave these systems. However, this desire for mobility and productivity comes at an increased cost to ensure safety.

Due to the effectiveness of road transportation schemes, there has been a steady increase in the use of our roads and the volume of road transportation mechanisms (Vehicles and Motorcycles). This directly infers a need for effective and efficient control, so as to ensure safety on our roads. To fulfil this need, various types of technology such as road traffic surveillance, security, stolen cars detection and tracking system have been invented. However, these innovative technologies are generally not for personal use. As such, the fallout devices manufactured are mainly immobile.

In recent years, License Plate Recognition (LPR) has had huge impact in the bid to ensure safety whilst allowing for maximum use of mobility features and also ensuring productivity. It falls into the bid to use advanced technology to curb or mitigate some of mankind's problems (Anagnostopulous et al., 2006). However, the already outlined problem of immobility of the road surveillance system also affects this system.

We however research a new device design that solves the immobility problem. This device would be used by road traffic management agencies to handle and manage road abuse and misuse by road users.

Using the old system of the traffic summon, traffic policeman will have to record down the traffic offense/summons into traffic violation booklet one for record and another for the summoned person. Then the data of all summon have to be manually keyed in the database. This is inefficient and time consuming.

ANPR is a method that is largely used in the new technology of ITS (1ntelligent Transport Systems) and AVI (automatic vehicle identification). ANPR is a way to retrieve the information on the license plate. In the approach, a camera captures the image of a car and a computer processes the image and recognizes the

information on the plate by applying various image processing and optical pattern recognition techniques (Ying et. al., 2011)

This project focuses more on the image processing algorithm for use in Optical Character Recognition (OCR) using MATLAB and the use of GPS for data transfer. OCR algorithm is used for recognition of license number of a vehicle from the image of the license plate captured by the camera. This research was carried in Malaysia therefore, Malaysian plate number system was used for the testing

With the design and development of better road transportation system and the adoption of these by the people, the design of more efficient and intelligent ways to ensure safety has been researched into, in parallel. The combination of these is proposed to not only allow for mobility and productivity but also ensure security and safety. One of the developed methods is License Plate Recognition (LPR). This plays an important role in application such as unattended parking lot security, access control and traffic safety (Ying et. al., 2011). The design and development of LPR systems is hinged on Optical Character Recognition (OCR), to allow for the accurate detection and interpretation of licence plate numbers and letters.

The goal of Optical Character Recognition (OCR) is to classify optical patterns in a given image (often in a digital image) corresponding to alphanumeric or other characters. The process of OCR involves several steps; the main steps are: segmentation, feature extraction, and classification. However, a typical system for LPR consists of four parts, i.e., obtaining an image of the vehicle, license plate localization and segmentation, character segmentation and standardization, and character recognition (Ying et. al., 2011)

The origins of OCR cannot be traced but it is proposed that it started to aid in telegraphy and the development of braille devices for use by the blind (Shantz and Herbert,

1982) Pioneers of the field include Emanuel Goldberg who created a machine that could decipher characters and convert them to telegraph code. He went on later to design a machine referred to as 'statistical machine', which also performed optical character recognition. Edmund Fournier d'albe developed a device referred to as the Optophone. This mobile handheld device could produce tones to characterize different characters as it reads them (Aibe, 1914). One the modern fathers of optical character recognition Ray Kurzweil, created an optical character recognition system for use by blind people. This device could read and translate any character in any font (Shantz and Herbert, 1982). Today, Optical character recognition is used in Data entry devices, Language translation systems e.t.c
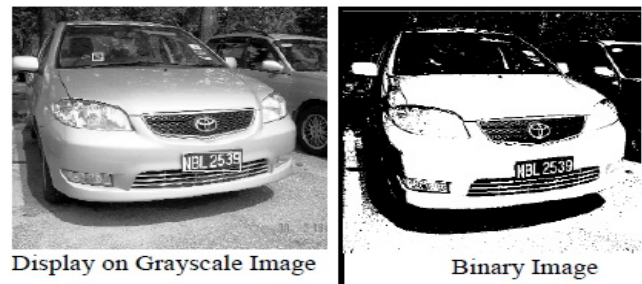
Figure 2.1: Gray to binary conversion

The automatic traffic summons system that this project aims to design uses the LPR technology discussed above and GPS. The integration of these two technologies constitutes the features of the system.

2. METHODOLOGY

2.1 Overview

The automatic traffic summon device can be broken down broadly into two main subcomponents: the image processing subcomponent and the GPS subcomponent. The image processing part is responsible of the license plate number acquisition and the GPS part is concerned with

data transfer from and to the database. The block diagram fig 3.1, shows an overview of the system with its main components.
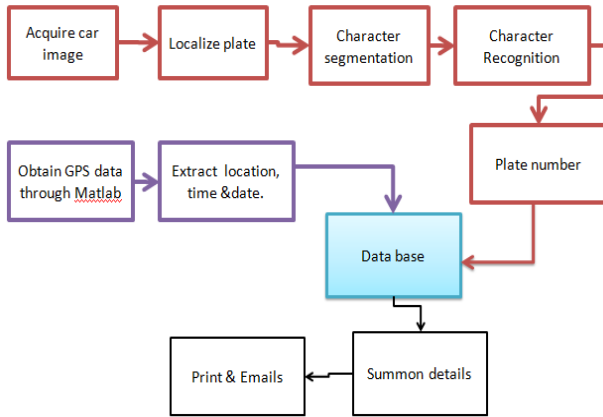
Figure 3.1: Diagram of the overview of the system

The steps used in performing LPR are shown in the flowchart in figure 3.2

Figure 3.3: License Plate Recognition flowchart
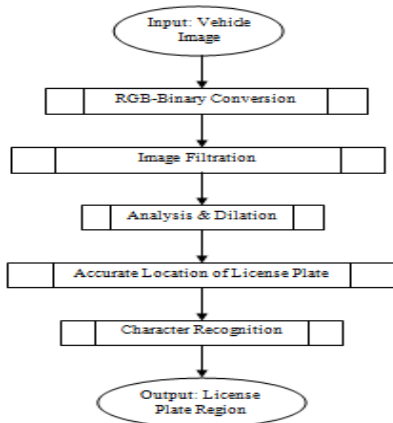
Figure 3.2: License Plate Recognition flowchart

2.2 Car Plate Number Extraction

The first stage in recognizing car plate characters is the vehicle plate number extraction from the car plate images. Before extracting the number plate, the captured vehicle image must be binarized (Otsu, 1978). Binary image {only black and white} consisting of only 1's and 0's by thresholding the pixel values of 0 (black) for all pixels in the input image with luminance less than threshold value and 1 (white) for all other pixels.

After the extraction and binarization of the image, character segmentation is applied to the license plate number in order to outline the individual characters. This step affects greatly the accuracy of the next step which is recognition stage. if the contours of the characters are inaccurate, it might lead to errors in the recognition stage or even to failed recognition stage (Chu et. al., 2004)

The final stage of license plate recognition is character recognition (Chu at. Al, 2004). At this stage the characters segmented in form of images have to be recognized and translated into text. Optical Character Recognition (OCR) algorithm is used to recognize the character with condition, the background of the image has no or very little noise (Quadri and Asif, 2009)

2.3 Evaluation Metrics

During the character recognition process, the extracted character does not always match the character in the database. Since 100% matching is nearly impossible, measuring the similarities between characters is required. Many approaches are available, the most commonly used includes

1. Autocorrelation
2. Mean Square Error (MSE)
3. Structural Similarity Index (SSI)
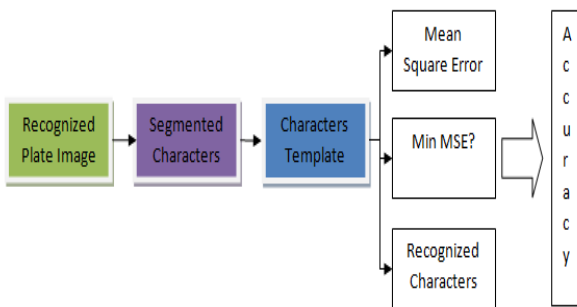
Figure 3.3: Performance measurement

MSE approach is chosen for our application as it gave the best results among the three.

2.4 The SK 53 GPS tracker data extraction

The location data is extracted from the GPS using serial data transfer in Matlab. The chip signal is low when it is used indoor. Therefore it is best used outdoor.

The GPS receiver gives the location in terms of a string of longitude and latitude values. The additional data we are interested in is the time and date. The GPS can provide position accuracy of 2 meters. The receiver is interfaced with the computer through UART.

2.5 Physical Setup

To develop the system, each hardware and software must be set up to make a connection and interaction between both. The system hardware consists of:

i. A computer
ii. A digital camera
iii. GPS tracker sky GPS 53
iv. UART cable interface
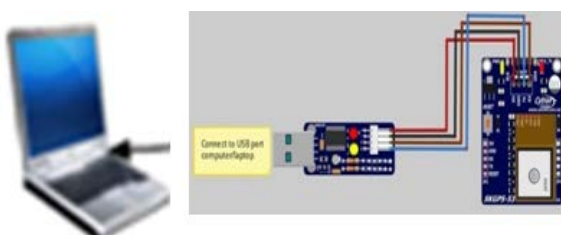
Figure 3.4: system hardware interface

3. RESULTS AND DISCUSSIONS

This section presents the results obtained together with the discussion of the results. The limitations of the system is analyzed based on the system performance. The results of the system is shown in the GUI below

Table 3.1: system performance

Approach	Total Characters	Recognized Characters	Not recognized Characters	Accuracy	False Positive Rate
Mean Square Error	339	324	15	95.6%	4.4%
Auto correlation	339	317	22	93.5%	6.5%
Structural Similarity Index	339	308	31	90.9%	9.1%

4. CONCLUSION

LPR systems are nowadays used in many applications. They are all mainly based on image processing regardless of the software development. A LPR system has to be robust in both hardware and software requirements.

The development of Automatic Traffic Summon Device needs both image processing and communication components to be integrated together for it to function

efficiently. The image processing allows information acquisition and analysis, while communication components permit data reception and transmission from and to database. The system also uses GPS as a tracking system for it to determine the location where is taking place

The algorithm used in this work so far is limited as it can only be applied to some specific types of license plates. It needs further development so that it can be applied efficiently at any type of license plate.

For future development, the image processing part of the Automatic Traffic Summon Device needs further improvement to narrow the limitations discussed. The system also necessitates to be studied further for robustness when it is used in the real time where some types of changes imposed by the environment conditions are to be considered.

REFERENCE

Ahmed Alrabani (2002).Introduction to GPS the global positioning system. Norwood. ARTECH HOUSE, INC.

Anagnostopoulos, C.N.E., Anagnostopoulos, I.E., Loumos, V.& Kayafas, E.(2006).license plate-recognition algorithm for intelligent transportation system applications. *IEEE Intelligent Transportation Systems,* 7(3), pp.377-392.

d'Albe, E. E. F. (1 July 1914). "On a Type-Reading Optophone". Proceedings of the Royal Society A: Mathematical, Physical and Engineering Sciences 90 (619): 373–375. doi:10.1098/rspa.1914.0061.

Ganapathy, v. & Wen, L. D. L.(2008) .A Malaysian Vehicle License Plate Localization and Recognition System. *Journal of Systemics, Cybernetics and Informatics*, 6(1), pp. 1565-1582.

Huin Pan (1998). Publishing. Retrieved from: http://www.usb.org/home .
National Instruments Serial Quick Reference Guide, February 2007
Joakim Ögren. Publishing. Retrieved from: http://cnx.org/content/m12293/latest/

Hsien-Chu W., Chwei-Shyo, T. & Ching-Hao, L. (2004). A license plate recognition system in e-government. *INFORMATION & SECURITY. An International Journal*, 15(2), pp. 199-210.

Otsu, N. (1978). A threshold selection method from gray-level histogram. *IEEE Transactions on Systems and Cyber net, SMC-8*, pp.62-66.

Percival, M.E., Sedgwick, A. & Ellis, T. (204).Road Transport Information and Control.*12th IEE International Conference on Digital Object Identifier*, pp. 211- 213.

Qadri, M. T. and Asif, M. (2009). Automatic Number Plate Recognition System For Vehicle Identification Using Optical Character Recognition. *2009 International Conference on Education Technology and Computer. IEEE Xplore*, pp.335-338.

Negi, C. B. & Krishna B. (2001). *An OCR system for Telugu. In the Proceedings of the Sixth International Conference on Document Processing*, pp.1110-1114.

Rafeal C.G., Richard E.W. (2009). Digital Image Processing. Third edition 2009.

Saleh, Marwan D., Mellah, H., Ahmed Mueen, Salih, N. D. (2008). An Efficient Method for Vehicle License Plate Extraction. *IEEE Xplore*.

Schantz, Herbert F. (1982). The history of OCR, optical character recognition. [Manchester Center, Vt.]: Recognition Technologies Users Association. ISBN 9780943072012.

Shigueo, N., Keiji, Y., Osamu, K., Hiroshi, K., Takayuki, S.(2005). A novel adaptive morphological approach for degraded character image segmentation. *Pattern Recognition*, 38(11), pp.1961-1975.

Shyang-Lih C., Li-Shien C., Yun-Chung C., & Sei-Wan C.(2004). Automatic License Plate Recognition. *IEEE Trans. on Intelligent Transportation Systems*, 5(1), pp. 42-53.

Sunghoon, K., Daechul, K., Younbok, R. & Gyeonghwan, K.(2000).*Pattern Recognition, 2002. IEE Proceedings. 16th International Conference*, 3, PP. 216-219.

William S. Seegar, Protagoras N. Cutchis, Mark R. Fuller, Joseph J. Suter, Vipul Bhatnagar,and Joseph G (1996.)Wall Fifteen Years of Satellite Tracking Development and Application to Wildlife Research and Conservation .JOHNS HOPKINS APL TECHNICAL DIGEST, V. 17(4)

Ying Wen, Yue Lu, Jingqi Yan, Zhenyu Zhou, von Deneen, K.M. and Pengfei Shi.(2011)An Algorithm for License Plate Recognition Applied to IntelligentTransportation System.*IEE Intelligent Transportation Systems*, 12(3), pp.335-338.

Yuntao, C. & Qian, H. (1998). Extracting characters of license plates from video sequences. *Machine Vision and Applications,* pp. 308-320.

BIOMETHANE AND HYDROGEN AS ALTERNATIVE VEHICLE FUELS: AN OVERVIEW

T.O. Kukoyi[1*], E.Muzenda[2,3], A.Mashamba[4], E. Akinlabi[5]

[1]Department of Mechanical Engineering Science, Faculty of Engineering and the Built Environment, University of Johannesburg, Auckland Park Kingsway Campus, Johannesburg, South Africa.

[2]Department of Chemical Engineering, Faculty of Engineering and the Built Environment, University of Johannesburg, Doornfontein Campus, John Orr Building, 3160 Beit Street, Johannesburg, South Africa.

[3]Department of Chemical and Petroleum Engineering, College of Engineering and Technology, Botswana International University of Science and Technology, Private Mail Bag 16, Palapye, Botswana.

[4]Department of Mechanical Engineering Technology, Faculty of Engineering and the Built Environment, University of Johannesburg, Doornfontein Campus, John Orr Building, 3160 Beit Street, Johannesburg, South Africa.

[5]Department of Mechanical Engineering Science, Faculty of Engineering and the Built Environment, University of Johannesburg, Auckland Park Kingsway Campus, Johannesburg, South Africa.

*Corresponding author E-mail: kukoyitemitope@yahoo.com Mobile: +278038855092

ABSTRACT

Human activities over the years have caused massive depletion of the world's fossil fuel reserves which contributes a major percentage of the world's energy source. This coupled with the adverse effects they have on the ecosystem during extraction and subsequent utilization has spurred research for alternative fuels especially in the transport sector. Of all alternative fuels discovered, developed and used, hydrogen and biomethane seem to be viable candidates. This paper reviews the technological and economic viability of both hydrogen and biomethane as eco-friendly alternative fuels for motor vehicles.

Keyword: Fossil fuel, Alternative fuels, vehicles, hydrogen, biomethane

1   INTRODUCTION

The dynamics of the world's economy to a large extent is stimulated and overly dependent on energy. Every aspect of human life today is directly facilitated by the considerable supply of energy, in other words, man's continuous socio-economic relevance is guided by uninterrupted supply of energy. Since the modern history of petroleum began in the 19th century, fossil fuels have been the primary source of energy to mankind, accounting for more than 80% of the world's primary energy consumption (Mohr et al, 2014). Fossil fuels (oil, coal and natural gas) are energy carriers formed from the decay of plants and animal matter over a long period of time (fossilization) (Dincer and Zamfirescu, 2014). The industrial, utility, residential and transport sector are the major consumers of these energy sources which are the major driving forces in any nation's economy (Mohr et al, 2014). These hydrocarbons have been extensively tapped to generate, heat, light, power and propulsion to not only make the earth more habitable but also to convey man and his produce from one point to another. Figure 1 and 2 shows the world's energy demand by fuel and sector(EIA, 2012; EIA, 2013).The dependence on fossil fuels as the sole or major provider of the world's energy demand since the technological revolution has helped promote obvious considerable development but much of these have come at a cost with irrevocable damage to the eco-system. Major concerns on global warming, atmospheric pollution and sustainability of these resources have been raised in the past few decades (De Almedia and Silva, 2009). According to Hubert's Theory, fossil fuels have finite reserves and these

resources are increasingly being depleted. He also cited that the world is certainly at or close to the peak of production of these resources after which a state of terminal decline is expected and they would eventually "dry-up". Another challenge associated with the use of fossil fuels to generate energy is pollution which has overtime caused adverse change to the environment and life on earth. When fossil fuels are extracted or burnt to produce energy, they generate carbon dioxide (CO_2), carbon monoxide (CO), sulphur oxides (SO_X), nitrous oxides (NO_X), hydrocarbons (HC), volatile organic compounds (VOC) and particulate matter (PM) some of which may contributes to green house effect, acid rain or ozone layer depletion (Bardi, 2009) .

Energy sustainability, stringent environmental regulations on exhaust emissions after adoption of the Kyoto Protocol by nations, increase in population which has led to increased demand on petroleum resources and unstable prices has created the need for alternative sources of fuel (Dincer and Zamfirescu, 2009; Crank and Jacoby, 2014). The transport sector consumes a third of the world's energy which is the second highest consumer of fossil fuel after the industrial sector (Yang et al, 2014). 60% of the total crude oil consumed per day is employed to power different modes of transportation. 98% of energy used in this sector comes from fossil fuels; it is also expected to be the fastest growing oil-consuming sector by 2030 with the number of cars expected to hit 1.25 billion from the 700 million currently plying our roads (Yang et al, 2014; Luft, 2014).

The transport sector is constantly hit with increased fuel prices and also accounts for an enormous percentage of green house gas emissions in the atmosphere (EIA, 2013). Recently the transport sector had turned to natural gas (which was mostly used in the industrial sector) as an option

to reduce dependence on the conventional fossil fuels, petrol and diesel produced from fractional distillation of crude oil (Engerer and Horn, 2014). Natural gas which is also a fossil fuel is formed as a result of intense heat and pressure on the decaying matter. It is made up of various hydrocarbons obtained from reservoirs found beneath the earth surface close to oil, rock formations and coal beds; its major constituent is methane with other hydrocarbons like ethane, butane and propane (Curran et al, 2014). Natural gas can be adopted extensively in the transport sector particularly in vehicle engine technology whose acceptance has seen natural gas vehicles increase from 3million in 2003 to about 14.8million in 2014(EIA, 2013). Natural gas consumption is expected to rise from 113 trillion cubic feet in 2010 to 185 trillion cubic feet by 2040 and like other fuel of fossil origin, it is also expected to terminally decline (Engerer and Horn, 2014; Curran et al, 2014). Hence the need for a viable alternative source of energy to keep powering the transport sector as it remains a very important driver of the economy. Some of the energy carriers or fuels that have been utilized in vehicle applications other than the conventional fuels include natural gas, solar energy, electricity, p series, propane, hydrogen, ammonia, steam and different biofuels like biodiesel, ethanol, bio-dimethyl ether and biogas (Gajendra and Subramanian, 2013). Of all these fuels, natural gas, electricity, hydrogen and biofuels especially biodiesel, bioethanol and biogas receive enormous attention all over the world (Larsson, 2008; Gajendra and Subramanian, 2013). However, this paper would dwell on hydrogen and biomethane (with biomethane being scrubbed and upgraded biogas), looking at various published works to accentuate their potentials as viable replacement fuels in vehicle engines. Biomethane is said to the cheapest transport

fuel on the energy market and hydrogen having an enormous prospect as it abounds in nature and performs efficiently in vehicles (Gajendra and Subramanian, 2013); hence the need to highlight the properties of these fuels and compares their performances.
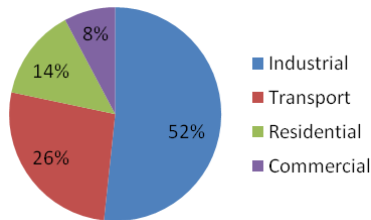
Figure 1: World energy consumption by sector, 2012 (EIA Data)
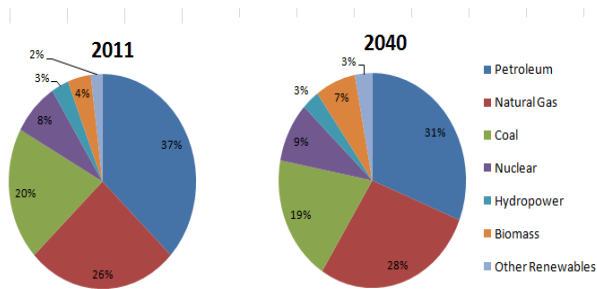
Figure 2: World energy consumption, 2013 (EIA, Data)

2   ALTERNATIVE FUELS

Alternative fuels are energy housing substances or materials other than petroleum. The quest to find alternative fuels has seen various advancements in vehicle technologies and has successfully birthed different fuels but for the fuel to be a viable replacement it must fulfill few criteria such as;

- Sustainability – readily available, long lasting.
- Performance – octane and cetane ratings, energy content per unit volume.

- Economical – lower or competitive price when compared with conventional fuels, life time cost, maintenance cost.
- Safety – safe storage, toxicity.
- Environmental issues – carbon content, volatility, overall GHG emissions, contributions to pollutants.

In summary, for an alternative fuel to be a practical substitute for petrol and diesel in the transport sector it must be able to merge cost competitiveness and infrastructure availability. In other words, infrastructure must be readily available to transport and refuel consumer's vehicles and the cost of the fuel must be lower or competitive when compared to that of petrol and diesel; these would make the fuel attractive and marketable. Taking a look at current trends, alternative fuels are also expected to have similar or better combustion characteristics when compared with diesel or petrol and can be easily integrated into already existing fossil fuel infrastructure as that would cut down on overall cost of the fuel (Gajendra and Subramanian, 2013).

3   HYDROGEN

Henry Cavendish, an English experimental and theoretical chemist discovered hydrogen and called it "inflammable air" in 1776 (West, 2015). The most abundant element on earth, hydrogen is a colourless, odourless, tasteless and non-toxic gas with a molar mass of 2.02kg/kmol, density of 0.0838kg/m^3 at room temperature and net heating value of 119.93MJ/kg. This makes hydrogen the lightest of all molecules and also has the highest energy content per unit mass of all fuels (Ciniviz and Kose, 2011). Despite the profusion of this chemical substance, it can't be found freely in nature. It can be retrieved from water (H_2O), hydrocarbons like methane (CH_4) , biomass, hydrogen

sulphide, boron hydride etc and the herculean task associated with its usage being the extraction of this energy carrier from the compounds that house this useful element (Dell et al, 2010, Gajendra and Subramanian, 2013). Some of the processes to recover hydrogen includes; coal gasification, biomass gasification, natural gas reforming, solar-thermal reforming, electrolysis of water and electrochemical photolysis (Dell et al, 2010). Current trends promote the splitting of water by electrolysis and steam reforming of natural gas as the most cost effective and highly efficient methods in generating large quantities of hydrogen and these methods are currently being employed to produce hydrogen for commercial use. Hydrogen has been extensively employed in aerospace engineering as power source for rockets, metal sintering and annealing, crude oil refining, welding and metal fabrication, glass production, industrial and automotive applications. For the automotive industry and other applications that make use of hydrogen which is gaseous at room temperature, the need to compress hydrogen like any other gaseous fuel remains paramount for storage and transportation (Dell et al, 2010; Dincer and Acar, 2014).

3.1 Hydrogen Storage

There are numerous researches being conducted on storing hydrogen as a vehicle fuel due to its low energy density as it contains lesser energy per unit volume when compared with a gaseous fuel like methane and about 5% of the energy content of gasoline of the same volume. This means the hydrogen tanks would have to be bigger to compensate for the lesser energy density which would affect the overall weight of the vehicle. As the storage pressure of gases increase, the density also increases, hence, hydrogen is compressed into pressure tanks which may be made of aluminum, steel, titanium alloy and recently light weight carbon composite tanks at 350 to 700 bar (IEA, 2006; Karhaman 2005). These composite tanks, though procured at a higher cost than the others are employed as they are able to withstand higher pressures and require no internal heat exchanger when used to store liquid hydrogen. A newer method of storing hydrogen in vehicle is the use of glass microsphere. In this method, the gas enters and is deposited in tiny hollow glass spheres at elevated pressure and temperature (350 -700 bar) and (300^0c) respectively. The energized gas permeates the glass spheres inserted into high pressure vessels; the temperature of the microsphere is then dropped till it reaches room temperature after which it is transferred to a low pressure vehicle tank. This process increases the volume of hydrogen in the tank and when needed for propulsion, the temperature of the tank is increased to (200 -300^0C) to disperse the gas to run the vehicle. It currently provides the greatest advantage for high density storage of hydrogen. In aerospace technology other storing techniques are used or being tested and with time this might be explored in vehicle technology to improve efficiency (IEA, 2006; Sharma and Ghoshal, 2015). Another storage method is the use of metal hydrides which are metallic alloys that absorb hydrogen. As is the case with glass microsphere the rate of absorption and release of the gas is defined by temperature of the hydride. Metallic hydrides are said to absorb hydrogen 1-2% of their weight and this can increase at elevated temperatures with the hydrides holding 5-7% of their weight when heat is applied. Though this method also gives room for more volume of hydrogen to be stored the pores meant for absorption of hydrogen eventually get filled with impurities thereby reducing its holding capacity. Magnesium, lithium, titanium, aluminum, zirconium, lanthanum, could be used for the

hydrides. Carbon nanotubes are tubular cylinders of carbon atoms that are mechanically capable of storing hydrogen within the tube structure. Theoretically they are said to be capable of storing between 4 -65% of their weight in hydrogen. Presently being investigated, it is expected to be the lightest and most efficient way to store hydrogen. Apart from compressing the gas another method of improving the energy density of hydrogen is to cryogenically cool the gas. The temperature is dropped to -260^0C which reduces mass as a result of lower operating pressure. The density of liquid hydrogen is $71kg/m^3$. Liquid hydrogen though more efficient is more expensive and has its drawbacks which include: it requiring a complex storage system, air-tight insulation to reduce evaporation and tank needs to be maintained at constant pressure (Colozza, 2002; IEA, 2006).

3.2 Hydrogen Vehicles

The use of hydrogen in vehicle technology is been considered as the best option at reducing emissions in the transport sector (Dell, 2010). Hydrogen is a highly clean and efficient fuel. It not only can be produced from water which abounds and other available sources but when burnt to produce energy generates only water, though nitrous oxides are produced as oxidation is achieved through atmospheric air (Ramsden et al, 2013). The development of vehicles to accommodate this relatively abundant fuel gas has birthed hydrogen fuel cell vehicles HFCV and hydrogen internal combustion engine vehicles HICEV (Dell, 2010).

3.2.1 Fuel Cell Vehicles

The fuel cell vehicle system is typically made up of the fuel storage tank, the fuel cell stack, electric motor/ power controller unit and the battery. The workings of the HFCV is similar to that of an electric vehicle (EV) as they both use electrical energy to power the motor that propels the vehicle with the only difference being that in electric vehicles, the charge required to power the car is produce from an external source and stored in the battery but for the HFCV the electrical energy is produced on-board via fuel cells which is then discharged and converted to mechanical energy to drive the vehicle. Hydrogen which is the primary fuel is released from the tank and diffuses into the fuel stack. The fuel stack houses the fuel cells (electrochemical devices) which are combined in series to generate adequate electricity to power the vehicle. In each fuel cell there is a reaction between the hydrogen on the anode side and oxygen from the cathode side in the presence of an electrolyte to generate electricity, this reaction is continuous with uninterrupted supply of hydrogen. A battery is included in the system to store electricity from regenerative braking which helps improve the overall efficiency and driving range of the system. HFCV are known to have zero-emissions with the system producing only water and heat. HFCV maximises the energy available in hydrogen using up about 40 – 60% as compared to spark ignition engines that use up about 20% of the energy available in gasoline. They are also known to attain higher thermal efficiencies when compared to spark and compression engines; theoretically it is expected to be above 70% (Dell, 2010; Gajendra and Subramanian, 2013).

3.2.2 Hydrogen internal combustion engine vehicles

Hydrogen has various physical and chemical properties that make it an interesting substitute for gasoline and diesel in internal combustion engines. It burns cleanly and doesn't emit hydrocarbons, carbon monoxide, carbon dioxide, sulphur oxides, volatile organic compounds and particulate matter as it has no carbon content associated with most fossil fuels (Dell, 2010). Its gaseous state permits cold starting

operation. Its lower minimum ignition energy, higher diffusivity, higher burning rate, higher octane number, higher heating value and ability to tolerate diluents delivers higher overall engine efficiencies when drawn with diesel and gasoline engines, this encourages its use particularly in high speed engines. Its wider flammability range 4 – 75% pitched against 1.4 -7.6% of gasoline in ambient air implies that hydrogen can operate at leaner air-fuel mixtures than the theoretical stoichiometric amount which not only aids emission control but also improves the fuel economy of the system (Ciniviz and Kose, 2011). With early researches on hydrogen performed on spark ignition engines, internal combustion engines can accommodate hydrogen as it could be used directly as a vehicle fuel. Hydrogen powered engines are less susceptible to knocks when compared to spark ignition engines because of the higher research octane number of the gas >120 to (91-99) for gasoline.(Gupta, 2008). For SI engines running on pure hydrogen, the use of a gas mixer and gas injector may be employed to introduce the fuel into the combustion chamber and ignited by spark plugs just like petrol as it has relatively high auto-ignition temperature $585^{\circ}C$ (Ciniviz and Kose, 2011). Adjusting spark timing has been proven to improve engine performance (Maharastra, 2014). Hydrogen-fuelled engines can run on leaner combustion ratios which have numerous advantages though decreased power output is experiences because of the low energy density of hydrogen. Pre-ignition and backfire are also issues associated with hydrogen use in internal combustion engines (ICE's) caused by the low ignition energy and fast flame propagation of the fuel; these could be curbed by introducing the pressurized fuel into the combustion chamber just when the piston reaches the top dead centre after closure of the intake valve. Pre-ignition and

further reduction of the NO_X emission could be solved by water injection and exhaust gas recirculation (Dell, 2010; Ciniviz and Kose, 2011). In compression ignition engines hydrogen would require a pilot fuel (diesel 10 -30%) because of its high auto-ignition temperature and trace amounts hydrocarbons and carbon oxides may be formed due to combustion of lubricating oils. Conventional combustion ignition and spark ignition engines can be accommodated to run on mono-fuel engines (hydrogen spark ignition engines), bi-fuel (hydrogen or petrol) and dual-fuel (hydrogen with petrol)(Ciniviz and Kose, 2011). It's important to note that though most researches are conducted retrofitting conventional engines to work on hydrogen, a complete redesign to accommodate the special qualities of this fuel would result in better efficiencies (Gillinham, 2007).

4   BIOMETHANE

Biomethane is another highly researched alternative fuel, also called "green gas", it is the derivative of scrubbed and upgraded biogas. As the name implies, it is made up of primarily methane (90 – 99% CH_4) after removal of the undesired constituents from the biogas the compressed for use in vehicle applications (Ahmad et al, 2012). Biogas, a first generation biofuel, is generated from the anaerobic decomposition of diverse organic material which may include energy crops, farm related wastes (manure, feed and harvest waste), sewage sludge, industrial waste, household waste and from other sources like landfills. It may also be created naturally from sewage streams, swamps and landfills or in controlled environments in an anaerobic digester (AD). The decomposition process is similar to what happens in the digestive tract of a ruminant animal. Microbes acts on organic matter to produce a gas rich in methane (CH_4) with quantities of carbon dioxide, water and other trace gases. The

quantity of methane produced is between (40-75%) depending on if the biogas was produced from natural decomposition or from a controlled process (Persson et al, 2006, Da Costa, 2013).

Anaerobic digestion is a process which has been in existence for centuries with records of it dating back to early Persia and by Marco Polo in China over 2000 years ago. The process has been developed in recent years not only to produce biogas but also aid effective waste management. The first AD plant commenced operation in 1859 at Bombay, India (Monnet, 2003). The digestion of organic matter to produce biogas, a clean, renewable and sustainable energy source involves bacteria which thrive in mesophilic (25 – 40°C) and thermophilic (50 – 65°C) conditions. The phases involved in process include hydrolysis, acidogenesis, acetogenesis and methanisation; these processes involve breakdown of complex matter into methane and other gases that make up biogas. If the system is well balanced the processes are synchronized. The methane production efficiency of AD systems may be improved by mixing the substrates and optimizing other process conditions like the PH, carbon to nitrogen ratio, loading rate and retention time etc. (Muzenda, 2014). Biogas has been extensively used to generate light, heat and power through boilers, combined heat and power, vehicle propulsion and recently fuel cells.

In vehicle application, there is the need to rid the biogas of all impurities except flammable methane which currently can be purified through;

- Physical and chemical absorption (using organic solvents)
- Pressure swing adsorption (using materials like activated carbon)

- High pressure membrane separation
- Cryogenic upgrading (at elevated pressures)

CO_2, O_2, N_2, H_2O, siloxanes, halogenated hydrocarbons are removed as they affect the vehicle engine's performance or damage it (Masebinu, 2014; Persson et al, 2006). Biomethane is also injected into gas grids as evident in many European nations because of its similarities with fossil fuel natural gas and employed in all natural gas applications. In vehicle use biomethane is bottled in cylinders for use. Compressed biogas and compressed natural gas (CNG) have similar methane content and are often referred to as (CNG) in literature. Comparisons have been drawn in their performances at constant speed internal combustion engines. These experiments reported similar engine performances in terms of brake power output, specific gas consumption, thermal efficiency, fuel economy and emissions (Da Costa, 2013; Persson et al, 2006).

4.1 Biomethane storage

As is the case with other gaseous fuels, biomethane is stored by compressing into pressure tanks to aid handling, transportation and increasepressure levels which is required to overcome resistance gas flow (Lemke et al, 2011). The pressure tanks may be made from steel, aluminum and recently composite materials for their strength to weight ratio. They are fitted with safety devices like rupture disks and pressure relief valves. Compression which is done at 200 – 250 bars also helps to improve the energy density of the gas. However, the amount of energy available in the compressed gas is still lesser than what is available in equal volume of liquid fuels like petrol and diesel (Lemke et al, 2011; Persson and Wellinger, 2006). This energy disadvantage could be reduced by cryogenic cooling which

liquefies the gas at a temperature of (-162°C) before being forced into high pressure storage cylinders (Ahman, 2010). The shorter driving ranges experienced with gas vehicles could be improved by fuelling the same vehicles with their liquid form. CNG range limitation is pegged to be at 4:1 volume disadvantage and liquefied natural gas (LNG) is at 1.3:1 volume disadvantage when compared to petrol. In the same vein LNG has a similar energy density to ethanol better than that of liquid methanol but still lower than that of diesel 1.7:1 (Semin, 2008; Kapdi et al, 2005; Ahman, 2010).

Development in CNG storage technology has birthed the use of adsorption to increase the volume of the gas that could be compressed into the pressure tank; it is called adsorped natural gas (ANG). The system makes use of sponge-like materials (eg activated carbon) whose pores soak up or allow gas entry; which to a large extent increases the storage capacity of the tank by lowering the storage pressure and increasing the volume of gaseous fuel that would have been stored in the same container. This system tends to improve driving ranges and if well developed would reduce the bulkiness associated with multiple cylinders on-board vehicles (Zakaria and George, 2011).

4.2 Biomethane vehicles

Biomethane can be used as a renewable fuel in all natural gas applications. The transport sector has utilized natural gas for a while as an alternative fuel with unstable price and inadequate supply plaguing the oil sector. Recent trends have seen biomethane's development and production boost the supply of natural gas with some countries adopting its direct use as a vehicle fuel or injection into their natural gas grids in many sectors, transport inclusive (Persson et al, 2006; Gajendra and Subramanian, 2013; Yang et al, 2014).

Natural gas and biomethane most times referred to as (CNG) are chemically interchangeable with their difference being their source (fossil fuel or renewable organic sources) (Chandra et al, 2011). CNG vehicles have seen a surge in production and acceptance in recent years with a record of about 14.8 million vehicles in 2014 from 3 million vehicles in 2003 (EIA, 2013). Sweden is very much ahead of most countries in biomethane's use in the transport sector with a large percentage of their public vehicle fleets being CNG powered and much of this success is attributed to the governments push for energy sustainability, motivating the production of biomethane to be injected into their natural gas grid. 50% of Sweden's annual biogas production is converted to biomethane to power their vehicles (Persson and Baxter, 2014).

Biomethane is burnt as fuel in internal combustion engines (ICE) with little or no modification required on conventional spark and compression ignition engines. Alterations may be done to their fuel systems to accommodate the gaseous fuel as compared to the regular liquid fuel systems; the basic ICE would burn CNG to produce the desired energy to propel a vehicle (Debabrata and Murugan, 2012).The vehicle system is such that the storage tank often mounted in the trunk of the vehicle discharges the fuel at high pressures (200 bar) through fuel lines (steel tubes) to a pressure reducer allowing a pressure drop to about 3-7 bars before entry into the engine through the air intake or gas injectors. Air is drawn into the combustion chamber which mixes with the fuel injected then allowed to self-ignite (Dual-fuel systems) or burnt with the aid of spark plugs (Bi-fuel or dedicated systems). The combusted air-fuel mixture expands to produce the desired rotational force to propel the vehicle (Semin, 2008).

Some desirable characteristics of biomethane that encourages its use as a vehicle fuel includes its Wobbe index, atomization and motor octane number. When the Wobbe number is kept constant for CNG, there is no noticeable change in air-fuel ratio, laminar velocity (which affects ignition timing) and the knock resistance when compared with conventional fossil fuels(Da Costa, 2013; Chehroudi, 1993). The Wobbe number is the main indicator of interchangeability of fuel gases and similar Wobbe number signify that gaseous fuels could be substituted for a given pressure and valve setting (Persson et al, 2006). Biomethane being a gaseous fuel is completely homogenous with air and doesn't need to be atomized before combustion like liquid fuels (Chandra et al, 2011). This results in improved burning in the combustion chambers which would improve efficiency in dedicated engines and yields lesser hydrocarbon and carbon monoxide pollutions. Cold-start-fuel-enrichment is also not required as fuel is already in its vapour state which is a major source of CO pollutions in cars (Gupta, 2008).

Finally the high motor octane number means engines can attain high compression ratios and efficiencies with little susceptibility to knock. However due to the low volumetric density of the fuel, CNG vehicles have shorter driving ranges than liquid fossil fuels systems with liquefying the CNG (LNG) being an alternative to improve the driving ranges or increasing the number of storage tanks that houses the gas which would cause a weight penalty on the overall system (Gajendra and Subramanian, 2013). CNG also requires a longer duration to combust due to its low burning density which causes a reduction in engine performance and working efficiency in modified spark and combustion ignition engines, this could however be remedied though spark

advance, increasing compression ratios, increasing intake temperature or creating a high-turbulence combustion chamber. Performance might also be improved in dedicated engine designed to optimize the positive burning characteristics of the fuel gas or blending CNG with additives like hydrogen to better its combustive properties (Semin, 2008; Gajendra and Subramanian, 2013).

CNG vehicles may be a dedicated, bi-fuel or dual fuel system. A dedicated system makes use of only CNG as fuel to provide motive force. The system is designed to accommodate the chemical properties of CNG to deliver better outputs as they have single tanks dedicated to just CNG, giving room for more cargo capacity and cleaner emission. The bi-fuel system uses petrol and gasoline alternatively and offers the flexibility of a gasoline engine with the low cost of CNG. In dual fuel systems diesel introduced as the pilot fuel due to its lower auto-ignition temperature then diesel and CNG are simultaneously burnt. These systems have been proven to record reasonable fuel economy (Semin, 2008).

5 DISCUSSION

This section would compare the use of hydrogen and biomethane as alternative fuels in the transport sector using important criteria such as performance in combustion engines, safety, emissions, cost and sustainability. Some of the properties of both fuels are highlighted in the table below. It is important to note that biomethane which would be described in this section is of natural gas quality and might be referred as CNG during discussions.

Table1:Properties of some transport fuels

Property	Gasoline	CNG	Hydrogen
Chemical formula	$C_4 - C_{12}$	CH_4	H_2
Molar Mass	100 - 105	16	2

Carbon	85 - 88	75	0
Specific gravity (15.5°C/15.5°C)	0.72 – 0.78	0.424	0.07
Boiling Temp (°C)	27 - 225	-161	-252
Freezing Temp (°C)	-40	-183	-260
Density at 1atm and 300k (kg/m3)	5.11	0.717	0.082
Stoichiometric composition in air (%vol)	1.65	2.56	3.37
LHV (MJ/kg)	44.76	46.72	119.7
Combustion energy per kg stoichiometric mixture (mJ)	2.79	2.56	3.37
Flammable limits	1.2-6.0	5.3-15.0	4-75
Minimum ignition energy	0.25	0.28	0.02
Laminar flame speed (m/s)	0.37-0.43	0.38	3.46
Auto-ignition temperature (°C)	260-460	540-630	858
Flame temperature (°C)	2307	1914	2207
Diffusivity in air (cm/s)	0.08	N/A	0.63
Octane number	97-98	130	>120

5.1 Performance in internal combustion engines.

The exothermic reactions for the combustion of CNG and Hydrogen at ideal conditions are as follows

$$2H_2 + O_2 \rightarrow 2H_2O \qquad (1)$$
$$CH_4 + O_2 \rightarrow CO_2 + H_2O \qquad (2)$$
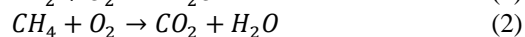
Though both fuels are colourless, odourless and non-toxic gases, combustion of biomethane would yield more unfavourable products than that of hydrogen. Theoretically, as evident in equation "(1)", the combustion of hydrogen gas in internal combustion engines should yield only water vapour but nitrogen (N_2) which is about 79% in air by volume is involved in the reaction, this leads to the production of a considerable amount of nitrous oxides during combustion (Ciniviz and Kose, 2011). However with biomethane, though no particulate matter or soot is emitted as is the case with petrol and diesel, nitrous oxides, carbon dioxide, carbon monoxide is produced. When combustion is incomplete, methane a more potent green house gas than CO_2 is emitted into the atmosphere (Beil and Beyrich, 2013).

In hydrogen's use as fuel, carbon is absent which is not the case with hydrocarbon fuels (CNG inclusive), this distinctive attribute mitigates the production of carbon oxides or hydrocarbons during combustion which have harmful effects on the environment and even when combustion is incomplete, harmless hydrogen is emitted. (Gajendra and Subramanian, 2013).

Table 1 highlights some of the physical properties of gasoline, hydrogen and biomethane (Ciniviz and Kose, 2011; Gupta, 2008;). Hydrogen has the highest energy content per unit mass of any fuel. Its higher and lower heating values are (141.6MJ/kg&119.9MJ/kg) compared to (55.5MJ/kg&50.0MJ/kg) of CNG and (47.3MJ/kg&44.5MJ/kg) of gasoline, these values are used to determine efficiency in gas engines and hydrogen would give the highest gas efficiency when employed. However the low energy density of hydrogen implies that more fuel would have to be stored in terms of volume to get an equivalent amount of CNG on energy basis. As such, storage becomes a major challenge in hydrogen applications as a larger pressure vessel would be needed to get reasonable amount of energy to propel the vehicle (Gupta, 2008; Cinivinz and Kose, 2011).

Hydrogen gas does not possess the reactive attribute of its atom as it requires a reasonable amount of energy to be activated. It has a very high auto ignition temperature, higher than most gaseous fuels (H_2=2584.85°C and CNG=539.85°) when compared to petrol's 256.85°C. This makes ignition difficult for both methane and hydrogen when compressed with air by heat alone without aid from a sparkplug. However when combustion has been initiated hydrogen has a low ignition energy (0.02mJ) which is about a tenth of that of CNG and petrol, this with its high motor octane number

(MON>120) ensures a very continuous rapid burning of the fuel allowing higher thermal efficiencies at high compression ratios without knock and improved engine performance. Though the lower ignition temperature of hydrogen over CNG has its advantage; it also brings in safety concerns as well as increasing the engine's susceptibility to pre-ignition and flashbacks which can be remedied by utilizing an advanced fuel delivery system and water injection (Ciniviz and Kose, 2011; Gupta, 2008; Gajendra and Subramanian, 2013) .

Hydrogen has a wider flammability range; it can burn in wider volume ratios, 4-75% of hydrogen in air when compared with CNG as Gasoline and CNG would optimally burn at 1.2- 6% and 5.3 -15% respectively. Hydrogen's smaller molecules and higher diffusivity makes it slightly more homogenous in air than CNG, this with its flammability limits allows engines to run efficiently at lean mixtures. It can run on air-fuel mixtures from 34:1 (stoichiometric) to 180:1. Operating at such ranges might record power loss but this is compensated for by better fuel economy, lower combustion temperature and lower NOx emissions. Hydrogen has a higher flame speed (3.46m/s) at stoichiometric ratio when compared to CNG (0.38m/s) which allows engines running on hydrogen approach more closely the ideal thermodynamic cycle. However, flame speed is noted to decrease significantly when the engine runs on lean mixtures to improve fuel economy. Thermal efficiency, engine stability and emissions are influenced by flame speed. (Ciniviz and Kose, 2011; Gupta, 2008; Gajendra and Subramanian, 2013).

Hydrogen engines are more susceptible to backfire when compared to engines running on CNG and petrol because of hydrogen's smaller quenching distance at 0.6mm. This is because heat exchange is more difficult as hydrogen flames gets closer to the cylinder walls compared to hydrocarbon fuels (CNG and petrol) leading to backfire (Gupta, 2008; Cinivinz and Kose, 2011).

5.2 Safety.

Hydrogen is more buoyant and diffusive than CNG or gasoline. Hydrogen has very small molecules which find it easier to penetrate through openings compared to other gaseous and liquid fuels. When leaks occur, gaseous fuels don't pool on the ground like liquid fuels, when hydrogen and methane escape into the atmosphere they are both displaced by air which causes them to rise, that with their high ignition temperature reduces tendency for explosion (Gupta, 2008).

Hydrogen has the highest dispersion rate with a diffusion coefficient in air of ($0.63cm^2/s$). When leak occurs hydrogen would disperse and rise faster than CNG or gasoline vapour at ($1.32kg/m^3$ and $5.82kg/m^3$) respectively. Also, CNG with over 3 times the energy density of hydrogen would have more energy loss during leaks (Gupta, 2008; Ciniviniz and Kose, 2011).

When exposed, hydrogen with a wider flammability range tends to be more dangerous than CNG especially when its low ignition energy is considered. However it needs to be in concentrations within the flammability range for detonation to occur which is difficult to achieve in open environments (Gupta, 2008; Sharma and Ghoshal, 2015).

Hydrogen has a higher flame temperature and faster flame velocity (3.46m/s and 2207°C) when compared to CNG's (0.38 m/s and 1917°C) this with hydrogen's lower flame visibility makes it more hazardous during explosion (Gupta, 2008; Cinivinz and Kose, 2011; Karhama, 2005).

5.3 Emissions

Emissions from alternative fuels are ascertained looking at their well to wheel (WTW) values, also referred to as "cradle to grave analysis of fuels" which assess emissions of fuels from production to utilization in vehicles for motive force. The process is broken into two evaluations, well to tank (WTT) which accounts for the GHG emissions associated with sourcing for the fuel, refining, transportation and distribution to storage stations and dispensing into vehicles. The second evaluation takes into account emissions from the combustion of these fuels to produce the desired energy to propel the vehicle, both assessments make up the WTW life cycle analysis. For the tank to wheels assessment TTW, hydrogen combusts to produce water vapour and heat in ICE's with traces of nitrous oxides which is absent when hydrogen is employed fuel cells vehicles (Gajendra and Subramanian, 2013). Meanwhile the combustion of biomethane generates not only nitrous oxide but carbon oxides and hydrocarbons which are all green house gases. Although the GHG emissions are 20-25% lesser when paired with petrol and diesel due to its smaller hydrogen to carbon ratio (Gajendra and Subramanian, 2013). Hydrogen does not produce any carbon emission when utilized in vehicles but its production, depending on the process, yields enormous quantities of green house gases which negates its previous emission advantage in vehicles. The well to wheel GHG life cycle analysis for petrol is about 164g CO_2-eq/km compared to biomethane's 5 -100g CO_2-eq/km depending on the source and upgrading process. Hydrogen well to wheel GHG life cycle analysis is at 8-176g CO_2eq/km depending on its source and production pathway. When manure is used to produce the biomethane to power the vehicle, a 97% reduction in total well to wheel GHG emission is achieved

which is the lowest of any commercially available vehicle fuel. When biomethane is injected into natural gas grids at concentrations of 20% the GHG emission is reduced to 39% when compared with petroleum. Hydrogen's lowest well to wheel GHG emissions is attained at 95% when the production process is 100% wind powered which is not commercially viable, when produced through natural gas reforming or electrolysis via the electric grid the GHG emissions are more than that of a petrol system (DENA, 2010).

5.4 Cost

Economically, a fuel which should be a practical substitute must be cost competitive with available infrastructure in relation with conventional transport fuels. It would also be an advantageous if it could be integrated into existing fossil fuel infrastructure (Gajendra and Subramanian, 2013).

Hydrogen fuelling infrastructure is currently not as developed as that of biomethane. Its commercial production processes, natural gas reforming and electrolysis which both entails splitting hydrogen from water and methane respectively come at very high costs leading to hydrogen gas being sold at more than twice the price of petrol while biomethane at half the price of gasoline on the energy market (Ramsden et al, 2013; Persson et al, 2006; IEA, 2014). It is important to note that 1kg of hydrogen fuel has the energy equivalent of 1 gallon of petrol with price at $4.90/kg - $5.70/kg compared to petrol's $2.32 per gallon (NREL, 2008; Ramsden et al, 2013; Parks et al, 2014).

Biomethane can be integrated into existing natural gas grids as is the case with many European States which has boosted it acceptance, spurred its development and cut down on infrastructural cost. Currently there are millions of CNG

vehicle and thousands filling stations to cater for them compared with hundreds of hydrogen vehicles and filling stations around the world (IEA, 2014;Persson et al, 2006; Gajendra and Subramanian, 2013).

Conversion kits for biomethane to integrate the fuel into available SI and CI vehicles are readily available with conversion costs ranging from $2700 to $10600 depending on the size of the vehicles. For original equipment manufacturers (OEM), the price difference is $1900 to $9000 more for the CNG equivalent of gasoline models and 25-30% more in price than their diesel models (Clarke and DeBruyn, 2012; Sanne and Seisler, 2008). Hydrogen OEM vehicles are very costly and when employed in fuel cells vehicle technology is currently not marketable because of their astronomic prices. Although projections expect the cost to reduce drastically, it would still be more $5300 more than its gasoline counterpart by 2035. It is believed that FCV's could be commercially available by 2020 when cost and technological issues associated with it are resolved (CLIMATE TECH, 2011; Sharma and Ghosal, 2015).

5.5 *Sustainability*

Hydrogen and biomethane are both sustainable and renewable fuels, they can be gotten from diverse sources that have infinite reserves and are ideal substitutes for traditional fossil fuels employed in the transport sector (Gajendra and Subramanian, 2013).

6 CONCLUSION

Hydrogen and biomethane are viable substitute fuels in transport. Though hydrogen performs better in internal combustion engines, its cost of production and expensive infrastructure might be a deterrent in its immediate use.

Biomethane offers significant overall GHG emissions, performs well in dedicated internal combustion engines, is cheaper than gasoline and diesel and can be used with existing natural gas infrastructure and applications. Its reduced performance when compared to hydrogen in internal combustion engines could be improved by blending hydrogen with biomethane and this could be an immediate solution for its use in the transport sector.

REFERENCES

Ahman, M., (2010) "Biomethane in the Transport Sector-An Appraisal of A Forgotten Option", Journal of Energy Policy, Vol 38, pp. 208-217.

Bardi, U., (2009) " Peak oil: The Four Stages of A New Idea", Journal of Energy, Vol 34, pp.323-326.

Beil, M and Beyrich, W; (2013) Biogas Upgrading to Methane; The biogas handbook: Science, production and application, Woodhead publishing; Cambridge UK, pg 342-374, ISBN 978-0-85709-741-5

Chardra, R., Vijay, V., Subarrac, P., (2012) "Vehicular Quality Biomethane Production From Biogas By Using An Automated Water Scrubbing System", ISRN Renewable Energy, pp.1-6.

Chehroudi, B., (1993) "Use of Natural Gas in Internal Combustion Engines", International Non-Renewable Energy Sources Congress, pp. 1-9.

Ciniviz, M and Huseyin, K., (2011) "Hydrogen Use In Internal Combustion Engine: A Review", International Journal of Automotive Engineering and Technologies, Vol 1, pp.1-15.

Clarke, S and DeBruyn, J., (2012). Vehicle Conversion to Natural Gas or Biogas, Ministry of Agriculture, Food and Rural Affairs, Ontario, Canada.

Colozza, A., (2002) "Hydrogen Storage for Aircraft Applications Overview". Analex Corporation, Brook Park, Ohio, National

Aeronautics and Space Administration, Glenn Research Centre. Available at http://gllrs.grc.nasa.gov pg 1-25

Crank, P and Jacoby, L., (2014). Crime Violence and Global Warming, Taylor and Francis, ISBN: 9780323265096.

Curran, S., Wagner, R., Graves, R., Keller, M., Green, J., (2014) "Well-to-Wheel Analysis of Direct and Indirect Use of Natural Gas in Passenger Vehicle", Journal of Energy, Vol 75, pp.194-203.

De Alemeida, P and Silva, P., (2009) "The Peak of Oil Production-Timing and Market Recognition", Journal of Energy Policy, Vol 37, pp.1267-1276.

Debabrata, B and Murugan, S., (2012) "Production and Application of Biogas as a Gaseous Fuel for Internal Combustion Engines" International Journal of Engineering Research and Technology, Vol 1, pp.1-5.

Dell, R., Moseley, P., Rand, D., (2014). Hydrogen Fuel cells and Fuel Cell Vehicles; Towards Sustainable Road Transport, Academic press, Oxford, UK, ISBN 978-0-12-404616-0

Dincer, I and Acar, C., (2014) "Review and Evaluation of Hydrogen Production Methods for Better Sustainability", International Journal of Hydrogen energy, pp.1-18.

Dincer, I., Zamfirescu, C., (2014). Advanced power generation system: Fossil fuel and alternatives, Elsevier, ISBN: 9780123838612, pp.95-141.

Engerer, H and Horn, M., (2010) "Natural Gas Vehicles: An Option for Europe" Journal of Energy Policy, Vol 38, pp.1017-1029.

Gajendra, B. and Subramanian, K., (2013) Alternative Transportation Fuels; Utilization in Combustion Engines, CRC press, Taylor and Francis group, LCC, Boca Raton, ISBN: 13:978-1-4-398-7282-6.

German Energy Agency (DENA)., (2010). The Role of Natural Gas and Biomethane in the Fuel Mix of the Future of Germany: Required Action and Potential Solution to Accelerate Adoption in Transport Applications. Berlin. Germany.

Gillingham, K., (2007). Hydrogen internal combustion engine vehicles: A prudent intermediate step in the wrong direction? Department of Management Science and Engineering Global climate and Energy Project, Precourt Institute for Energy Efficiency, Stanford University, pp.1-28.

Gupta, R., (2008). Hydrogen Fuel: Production Transport and Storage, CRC Press, Taylor and Francis group.

International Energy Agency (IEA)., (2006). Hydrogen Production and Storage: R&D Priorities and Gap; Organisation for Economic Co-operation and Development; Head of Publication Service, Paris, France.

International Energy Agency, (EIA), (2014). Keyworld Energy Statistics; Energy Data Centre, Paris, France.

Kahraman, E., (2005). Analysis of a Hydrogen Fuelled Internal Combustion Engine; MSc Thesis, Graduate School of Engineering and Science of Izmir Institute of Technology, Turkey.

Kapdi, S., Vijay, V., Rajesh, S., Prasad, R., (2005) "Biogas Scrubbing, Compression and Storage Perspective and Prospection in Indian Context", Journal of Renewable Energy, Vol 30, pp.1195-1201.

Larsson E., (2008). Biofuel Production Technologies: Status, Prospect and Implication for Trade Development; Prince Environmental Institute, Princeton University, United Nation Conference on Trade and Development.

Lemke, B., McCann, N., Pourmovahed, A., (2011). "Performance and Efficiency of a Bi-fuel Biomethane/Gasoline Vehicle", International Conference on Renewable Energies and Power Quality, Spain.

Masebinu, S., (2014) "Process Simulation and Parametric Study of a Biogas Upgrading Plant Using Gas Permeation Technique for Methane Enrichment", South African Journal of Chemical Engineering, Vol 19, pp.18-31.

Mohr, S., Wang, J., Ellen, G., Ward, J., Girco, D., (2014) "Projection of world fossil-fuels by country" Journal of Science and Technology of Fuel and Energy, Vol 141, pp.120-135.

Monnet, F., (2003). An Introduction to Anaerobic Digestion of Organic Waste, Remmade, Scotland.

Muzenda, E., (2014) "Biomethane Generation from Organic Waste: A Review", World Congress on Engineering and Computer Science, Vol 2, pp.1-6.

National Renewable Energy Laboratory (NREL)., (2008). Hydrogen Data, DOE/GOI 2008-2597

Parks, G., Boyd, R., Cornish, J., Remick, R., (2014). Hydrogen Station Compression, Storage, and Dispensing Technical Status and Costs, NREL/BK-6A10-58564.

Persson, M and Wellinger, A., (2006). Biogas Upgrading to Vehicle Fuel Standards and Grid Introduction, IEA BIOENERGY, pp.1-32.

Persson, M., Johnsson, O., Wellinger, A., (2006). Biogas Upgrading to Vehicle Standards and Grid Injection; Task 37-Energy from Biogas and Landfill Gas. IEA BIOENERGY, pp.1-16.

Persson, T and Baxter, D., (2014), Task 37 Country Overview-Energy from Biogas, IEA BIOENERGY.

Pew Centre on Global Climatic Change (2011). Hydrogen Fuel Cell Vehicles, CLIMATE – TECH BOOK, Arlington, VA, USA.

Ramsden, T., Ruth M., Diakov, V., (2013). Hydrogen Pathways: Updated Cost, Well-to-Wheels Energy Use and Emission for

Current Technology Status of Ten Hydrogen Production, Delivery and Distribution Scenarios, NREL/TP-6A10-60528.

Ruth, M., (2009) Hydrogen Pathways: Cost. Well-to-Wheel Energy Use and Emissions for the Current Technology Status of Seven Hydrogen Production, Deliveryand Distribution Scenarios, NREL/TP-6A1-46612.

Sanne, M and Seisler, J., (2008). How to Implement Biomethane Project: Decision Maker's Guide, European Natural Gas Association, Sweden.

Semin, R., (2008) "A Technical Review of Compressed Natural as an Alternative for Internal Combustion Engines", American Journal of Engineering and Applied Science Vol 1, pp.302-311.

Sharma, S and Ghosal, K., (2015). "Hydrogen and the Future of Transportation Fuel: From Production to Application", Renewable and Sustainable Energy Reviews, Vol 43, pp.1151-1158.

United States Energy Information Administration, International Energy Outlook, (2013). DOE/EIA-0484

West, J. (2015). Essays on the History of Respiratory Physiology: Perspectives in physiology, Springer, ISBN: 978-1-4939-2362-5

Yang, L., Ge, X., Wan, C., Yu, F., Li, Y., (2014). "Progress and Perspectives in Converting Biogas to Transport Fuels", Journal of Renewable and Sustainable Energy Reviews, Vol 40, pp.1133-1152.

Zakaria, Z and George, T., (2011) "The Performance of Commercial Activated Carbon Absorbent for Adsorbed Natural Gas Storage", International Journal of Research and Reviews in Applied Science, Vol 9, pp.225-230.

Improving the Hardness and Corrosion Resistance of Mild Steel by Aluminization

John Aforo Banyigyi[1], Mahdi Makoyo[2]

[1]National Metallurgical Development Centre, Jos
[2]Mechanical Engineering Department, Bayero University Kano
Corresponding Author's Email: makwayo@gmail.com, Tel: 08039539407

ABSTRACT

The surface of machine elements is the part of the component which is always in contact with external environment while performing its functions. Some failures in machine elements originate from the surfaces making the components to degrade in services thereby leading to failures such as fatigue, wear resistance and oxidation. This work deals with the surface modifications of machine elements' surfaces through the diffusion of aluminium by hot dip aluminizing in order to improve hardness, wear and corrosion resistance. Machine elements made from mild steels were selected for this work. Effect of varying dipping time at different heat treatments and corrosion behaviour of the base steel and aluminized steel were investigated. The aluminized steel when compared with the base steel showed an increased in hardness value by 9.1HRC from 23.1HRC to 33.2HRC within 2.5 hours soaking time. This indicates that aluminization has the ability to improve the hardness value as well as wear resistance of a material. When the steel specimens were immersed in solution of hydrochloric acid, it was observed that the corrosion rate was high in the base steel (controlled specimen) than in the aluminized steel which indicates that a strong bond was obtained between steel and aluminium. While the passive film that makes aluminium to be resistant to corrosion form rapidly but not steadily on the surface of the substrate
It was concluded that aluminized steel possesses a better corrosion resistance properties than steel that was not aluminized when both are exposed to acidic environment for a long period of time.

Keywords: *Aluminization, hardness, corrosion, steel, heat treatment*

1. INTRODUCTION

Surface modification by coating and treatments has become an essential step to improve the surface properties such as resistance to wear, corrosion and oxidation. Various conventional techniques are utilized for depositing the desired material into the substrate to achieve surface modification. These treatment and coating fall into three main categories: hardening achieved by surface heat treatments, hardening achieved by a change in chemical composition near the surface and application of different material on the surface by mechanical or other means (Jacek, 2000). In this study a method termed Aluminization of steel has been adopted to improve the surface hardness of mild steel by surface alloying with aluminium through diffusion and by hot-dipping process

for wear and corrosion resistance application. Aluminium coating provides steel with excellent oxidation and corrosion resistance at elevated temperatures up to $800^{o}C$ and also with reasonable scaling resistance. Aluminizing is one of the most widely used processes for coating steel to increase corrosion and oxidation resistance as well as hardness. Some commonly used aluminization methods are hot dipping, cladding, galvanic coating, calorizing (Avner, 1974). Steel is the widely used metals for engineering purposes and its failures originates from the surface and component degrade in service leading to failures such as fatigue, wear, corrosion and oxidation. Corrosion of steel can reduce load carrying capacity of a component either by generally reducing its size (cross section) or by pitting which not only reduces the effective cross section in the pitted region but also introduces stress raisers that may initiate cracks. Aluminized steel is steel that has been hot dip-coated with aluminium. Hot dip method is economical and widely used. It results in formation of intermetallic alloy layer at the interface and limits the amount of deformation which could be given to the coated steel (Agrawal, 1981). This method is used in the construction, automotive, electronics, ship building and aerospace industries. Aluminized steel is a unique material, as neither steel nor aluminium alone has both of these characteristics. Because it is highly corrosion resistant and conductive, aluminized steel is an ideal metal for electrical chassis application. Also a bond between the steel and the aluminium coating is formed, resulting in a product that has the strength and low cost of steel with the smooth surface of aluminium. The importance of aluminization as a surface finishing operation cannot be overemphasized, it promotes long service life in products such as bolts, washers, joints (Tokai, 2008). Aluminized steel shows a better behaviour against corrosion (Ihom, 2009). It protects the coated steel and improve its physical appearance (Richards, 1994).

2. METHODOLOGY

Aluminization of steel to improve hardness, wear and corrosion resistance processes for producing aluminium coated steel consist of six main steps: sample collection, sample preparation, aluminization, heat treatment, testing of the heat treated aluminized steel and corrosion test for aluminized steel.

2.1 *Sample collection*

Plain iron steel bar of sizes 12mm diameter by 100mm length was sourced from the market. 4 litres of distilled water was obtained. Also300ml of flux, 250ml of sulphuric acid, hydrochloric acid and nitric acid containing 0.5ml each were also obtained. Aluminium wire worth 1.5kg and zinc of 100g was obtained too.

The composition of the steel sample was obtained using an optical emission spectrometer and the result obtained is presented in table 1 below.

Table 1: Composition of steel sample

C	Si	Mn	P	S	Cr	Ni	Mo	Al	Cu	Co	Ti	Nb
0.191	0.179	0.51	0.015	0.025	0.110	0.076	0.019	0.036	0.215	0.0096	<0.0010	<0.0030

V	W	Pb	B	Sn	Zn	As	Bi	Ca	Ce	Zr	La	Fe
0.0012	<0.010	<0.0030	<0.0005	0.0093	0.0054	0.019	<0.002	0.0059	<0.0030	<0.0015	0.0034	98.6

The composition of the aluminium and zinc wires used for preparing the aluminization mixture were obtained by Energy Dispersion (E) X-Ray Fluorescence Spectrometry (ED-XRFS) Test. The results are given in Table 2 and 3.

Table 2: Composition of zinc wire sample

Sample	Al	Si	P	S	K	Ca	Ti	Cr	Mn	Fe
Zinc	3.02	4.60	0.65	0.88	ND	0.56	0.04	0.06	0.02	1.17
	Ni	Cu	Zn	As	Sn	Ba	Co	Pb	Br	Sn
	0.07	1.13	82.01	0.007	0.88	0.02	0.04	0.23	ND	0.01

Table 3: Composition of aluminium wire sample

Sample	Al	Si	P	S	K	Ca	Ti	Cr	Mn	Fe
Aluminium	98.20	0.98	0.31	ND	0.12	0.35	0.03	0.02	0.01	0.22
	Ni	Cu	Zn	As	Sn	Ba	Co	Pb	Br	Sn
	0.02	0.04	0.01	0.002	ND	ND	ND	0.005	ND	ND

2.2 Sample preparation

Plain iron steel bar of 12mm diameter was machined on a lathe machine and 35 pieces were cut to sizes of 10mm diameter by 20mm length. The substrates were thoroughly degreased in 0.5ml sulphuric acid solution for about 10 seconds, scrubbed, wash in distilled water and dried. The average weights of the substrate were measured on a digital weighing scale. The average weight was found to be 12.17g.

2.3 Aluminization process

Mild steel is low carbon steel containing 0.04% to 0.25% carbon with some amount of silicon and sulphur, it does not undergo further martensitic transformation when heated or coated, this makes it suitable for dipping technique (Singh, 2008). Hot dipping consists of immersing the steel in a bath of molten aluminium (Chester, 1989). For the aluminization of the steel pieces (substrates) a crucible of $549.25mm^3$ was used. A mixture of 95% aluminium weighing about 995g and 5% zinc weighing about 45.5g were placed in the crucible and then put into a furnace. The content was heated for 4 hours until the mixture of the aluminium and zinc was melted. The furnace temperature was maintained at $800^{\circ}C$ to enhance higher fluidity of the mixture. The substrates (steel pieces) were grouped into 6 batches of 2 substrates and marked as 1 to 6 (see Plate 1). The first batch of type 1 was dipped in the molten aluminium bath with a tong for time period of 2, 4, 6, 8 minutes respectively without any pretreatment or fluxing. After dipping for the specified duration time, the substrates were withdrawn and cooled in air. One batch was kept as a control sample (not aluminized). The substrates in batches were dipped in 0.1m nitric acid solution between 30 – 40 minutes, wash thoroughly in distilled water, fluxed and then dried. Their weights were then measured using a digital weighing scale.

Plate 1: Aluminized steel samples

2.4 Heat treatment

After the aluminization process, the aluminized steel each from the substrate samples (1 - 5) were taken for diffusion heat treatment in a furnace for about 4 hours to a solution temperature of steel ($800^{\circ}C$ - $900^{\circ}C$) to allow for diffusion of aluminium into the steel substrates. The aluminized steel is heated to form a diffused layer. This treatment improves the adherence between the steel substrate and the aluminium coating. After the diffusion at the various soaking time (hours), the substrate with the aid of a tong were quenched in water and cleaned to remove all traces of fireclay. The test area surfaces were the polished for testing.

2.5 Hardness test

The methods used for testing hardness of materials are Brinell, Vickers and Rockwell (Davies, 1983 and David, 1989). The Rockwell hardness `C' scale (HRC) with a minor load of 98N (9.8 kgf) and a major load of 1471N (150kgf) with diamond cone/pyramid indenter was used. The test pieces, the controlled sample and the aluminized steel samples were marked A, B, C, D, E, and F (see footnote under Table 1). The samples were then heated to austenite temperature of ($800^{\circ}C$-$900^{\circ}C$) for periods of 30 minutes, 1hour, 1½hours, 2 hours and 2½hours respectively. After which the samples were placed on the table of the machine and the indenter was brought into

contact with the prepared surface under a minor load of 98N = 9.8kgf. This takes up the `slack' in the system and the dial indicator is set to zero. The major additional load is then applied (1471N = 150kgf) and when the reading of the dial indicator is steady, the major load is taken off. The piece remains under the minor load, while the hardness value is read directly from the dial indicator of the scale of hardness `C'. Different positional readings are taken on the substrates with the average as shown in Table 4.

2.6 Corrosion Test

Corrosion rate of the controlled and aluminized steel samples when exposed to hydrochloric acid solution was conducted. The corrosion testing method of weight loss measurement was used (Fontana, 1987). The controlled steel sample was marked as A and prepared into A1, A2, A3 and A4 for testing at 72, 144, 216 and 288 hours exposure to the corrosion media (see Table 5). While the aluminized steel samples were marked as B, C, D, E and F and the prepared similarly for the test as in the case of the non-aluminized steel sample (see Table 6). Hydrochloric acid prepared in 0.5m, glass beakers (250ml), digital weighing balance, laboratory oven, distilled water, brush and desiccator are other materials and equipment were the materials used in the corrosion test. Substrates of the controlled and aluminized steel were set into coupons of 10mm diameter by 20mm length sizes. The coupons were mechanically cleaned and scrubbed with emery cloth to expose clean surfaces. The coupons were then washed with distilled waters to remove any contaminant and finally dried in desiccators overnight before weighing using a set digital balance model BL-41OS. The acid solution was prepared using 0.5ml hydrochloric acid (HCl). The weighed coupons were suspended in 250ml beaker containing 0.5mlHCl with the aid of thread at room temperature (Plate 2). Readings were taken at 3 days intervals

for a duration of 12 days. Each specimen or coupon retrieved from the solution was scrubbed with brush in distilled water, degreased in ethanol and dried in a laboratory oven. The dried sample was allowed to cool in a desiccator after which it was weighed using a digital weighing balance. The difference between the initial weight of coupon before and after exposure was recorded as the weight loss.

Plate 2: Corrosion test set-up

3. RESULTS AND DISCUSSIONS

3.1 Results

3.1.1 Hardness test

Table 4 shows the result obtained from the Rockwell hardness `C' scale test (HRC).

Table 4: Result of hardness test for the steel samples

S/N	Sample	Hardness at locations on the sample (HRC)			Average hardness value (HRC)
		Point I	Point II	Point III	
1	A	23.0	24.2	22.0	23.1
2	B	22.1	26.0	21.9	23.5
3	C	24.5	24.7	25.5	24.9

4	D	26.0	28.5	29.0	29.8
5	E	30.5	32.0	34.5	32.3
6	F	30.0	33.8	35.7	33.2

A = Controlled steel sample (i.e. non-aluminized sample), B = Aluminized sample heat treated for 30 minutes, C = Aluminized sample heat treated for one hour, D = Aluminized sample heat treated for one and half hours, E = Aluminized sample heat treated for two hours and F = Aluminized sample heat treated for two and half hours

3.1.2 Corrosion test

Table 5: Corrosion test result for (non-aluminized) controlled steel sample (A))

Exposure Time (Hrs)	Sample identity	Weight of sample (W_1) (g)	Weight of sample (W_2) (g)	Weight loss (W) $(W_1 - W_2)= W$ (g)
72	A_1	12.672	12.407	0.265
144	A_2	12.004	11.649	0.355
216	A_3	12.083	11.663	0.420
288	A_4	12.071	11.591	0.480

A_1 = Control sample for non-aluminized with exposure time of 72 hrs, A_2 = Control sample for non-aluminized with exposure time of 144 hrs, A_3 = Control sample for non-aluminized with exposure time of 216 hrs and A_4 = Control sample for non-aluminized with exposure time of 288 hrs.

Table 6: Corrosion test results for aluminized steel samples (B, C, D, E and F)

Exposure Time (Hours)	Sample Number	Weight of sample (W_1)	Weight of sample (W_2) (g)	Weight loss (W) $(W_1 - W_2)= W$ (g)
Sample B				
72	B_1	12.489	12.289	0.200
144	B_2	11.924	11.693	0.231
216	B_3	12.212	11.930	0.282
288	B_4	12.202	11.852	0.350
Sample C				
72	C_1	12.336	12.165	0.171
144	C_2	12.092	11.886	0.206
216	C_3	13.025	12.785	0.240
288	C_4	12.245	11.953	0.292
Sample D				
72	D_1	12.248	12.110	0.138
144	D_2	12.562	12.392	0.170
216	D_3	12.431	12.231	0.200
288	D_4	12.029	11.789	0.240
Sample E				
72	E_1	12.796	12.676	0.120
144	E_2	12.549	12.395	0.154
216	E_3	12.111	11.921	0.190
288	E_4	12.726	12.501	0.225
Sample F				
72	F_1	13.498	13.418	0.080
144	F_2	12.245	12.134	0.111
216	F_3	13.039	12.909	0.130
288	F_4	12.759	12.604	0.155

Where, B_1 = Aluminized sample of 2 minutes with exposure time of 72 hrs, B_2 = Aluminized sample of 2 minutes with exposure time of 144 hrs, B_3 = Aluminized sample of 2 minutes with exposure time of 216 hrs and B_4 = Aluminized sample of

2 minutes with exposure time of 288 hrs. This similarly applies to samples of C, D, E and F respectively with their exposure hours ranging from 72 to 288.

3.2 Analysis of results
3.2.1 Hardness Test

From Table 4, sample A at different points on the surfaces, three different readings were taken with the highest difference of 2.2 HRC value between 22.0 to 24.2, the average being 23.1HRC.Sample B aluminized heat treated for 30 minutes. Three different readings were taken with the highest of 26.0 and 21.9 being the lowest and the average of 23.5 HRC. Sample C heat treated aluminized for one hour with difference of 1.0 and the average of 24.9 HRC. Sample D aluminized and heat treated for one and half hours with a remarkable difference of 3 and the average HRC value of 29.8. Sample E aluminized and heat treated for two hours with a difference of 4.0 and the average HRC value of 32.3 HRC. Sample F aluminized and heat treated for two and half hours with a difference of 5.7 and the average HRC value of 32. From Figure 1, sample A is the control sample non-aluminized with average HRC value of 23.1. Sample B is the aluminized heat treated sample for 30 minutes with average HRC value of 23.5. Sample C is the aluminized heat treated sample for one hour with average HRC value of 24.9. Similarly, samples D, E and F aluminized heat treated for one and half hours, two hours and two and half hours with average HRC values of 27.8, 32.3 and 33.2, respectively.

3.2.2 Corrosion test

From Table 8, the control specimen (non-aluminized), the weight loss after 72 hours A_1 is 0.265g and after 144 hours A_2 is 0.55g. It increased to 0.42g after 216 hours and 0.488g after 288 hours.

From Table 7, the aluminized steel specimen B, of two minutes and with exposure time of 72 hours, the weight loss recorded was 0.2g of B_1 and increased to 0.231g after 144 hours. There is a further increase of 0.282g and 0.350g after 216 and 288 hours respectively. The aluminized steel specimen of 4 minutes and the exposure time of 72 hours, the weight losses were 0.171g, 0.206g, 0.240g and 0.292g respectively for 144, 216 and 288 hours. The aluminized steel specimen D of 6 minutes and the exposure time of 72, 144, 216 and 288 recorded a gradual increase of weight losses as 0.138g, 0.170g, 0.200g and 0.240g respectively. The aluminized steel specimen E of 8 minutes and exposure time of 72, 144, 216 and 288 hours recorded weight losses of 0.120g, 0.154g, 0.190g and 0.225g respectively. Finally, the aluminized steel specimen F of ten minute and exposure time of 72, 144, 216 and 288 hours recorded weight losses of 0.080g, 0.111g, 0.130g and 0.155g respectively. The corrosion rates of the samples immersed in the acidic environment were determined using the relation. (Singh, 2008).

$$Corrosion\ rate\ (mpy)\ = \frac{534W}{DAT}$$

Where, W is weigh loss (g), D is Density of material g/mm^3, A is total surface area mm^2= 2πr (r+h) and T is Exposure time (hours)

Example of computation of corrosion rate for controlled sample, after 3 days is:

Given W = 0.265g, D = 78.6g/mm^3, A=785.4mm^2 and T =72 hours

$$\frac{534\ x\ 0.265}{78.6\ x\ 785.4\ x\ 72} = 0.000031837 = 31.837\ x\ 10^{-6}\ mm/hrs$$

For 2 minutes of Aluminized steel sample for 3 days, when W= 0.200g and T=72 hours is

$$\frac{534 \times 0.200}{78.6 \times 785.4 \times 72} = 0.0000240284 = 24.0284 \times 10^{-6}$$

mm/hrs

Table 7: Result of rate of corrosion for controlled sample (A) within the specified period of time

Table 8: Result of corrosion rate of the aluminized samples

	Corrosion Rate (mm/hrs) x 10^{-6}			
	72 s	6 Days	9 Days	12 Days
Control	31.837 x 10^{-6}	21.325 x 10^{-6}	16.819 x 10^{-6}	14.417 x 10^{-6}
2 minutes	24.028 x 10^{-6}	13.826 x 10^{-6}	11.241 x 10^{-6}	10.512 x 10^{-6}
4 minutes	20.544 x 10^{-6}	12.874 x 10^{-6}	9.611 x 10^{-6}	8.778 x 10^{-6}
6 minutes	16.579 x 10^{-6}	10.212 x 10^{-6}	8.004 x 10^{-6}	7.228 x 10^{-6}
8 minutes	14.417 x 10^{-6}	9.250 x 10^{-6}	7.609 x 10^{-6}	6.757 x 10^{-6}
10 minutes	9.611 x 10^{-6}	6.667 x 10^{-6}	5.246 x 10^{-6}	4.655 x 10^{-6}

Exp.sure Time (Hrs)	Corrosion Rate (in mm/hrs) x 10^{-6}					
	Sample A	Sample B	Sample C	Sample D	Sample E	Sample F
72	31.837	24.028	20.544	16.579	14.417	9.611
144	21.325	13.826	12.874	10.212	9.250	6.667
216	16.819	11.241	9.611	8.004	7.609	5.246
288	14.417	10.512	8.778	7.228	6.757	4.655

(abrasion) or indentation by another hard body. It is an indication of wear resistance of a material. Processes which increase the hardness of material also increase their tensile strength. At the same, the toughness of the material is reduced as it becomes more brittle.

Figure 1: Soaking Time (Hrs) Against HRC Result (800-900)°C

3.3 Discussion

3.3.1 Hardness Test

It can be seen from Figure 1 below that the controlled sample within 2½ hours of soaking at the temperature range of 1073K – 1173K has a hardness value of 23.1HRC while the aluminized steel sample at the same condition has an increase of 9.1HRC. This has shown that aluminization of materials improves their surface hardness. Thus aluminized steel will possess the ability of a material to withstand scratching

3.3.2 Corrosion Test

Tables 5 and 6 show that control specimen and aluminized steel in different conditions corroded in HCL solution, since decrease in original weight of the materials was recorded.

Comparing the corrosion rate of control specimen and aluminized steel respectively shows that the corrosion increases

in control specimen more than the aluminized specimen especially at the later stage comparing Tables 7 and 8 respectively. The corrosion rate in the tables for the two conditions reveal that the dissolution of control specimen is faster than the aluminized steel within the subsequent days. This may be attributed to the fact that the films formed on the surface of aluminized steel are more passive with time than that of a control specimen. Hence the lower corrosion rate as time of exposure increases.
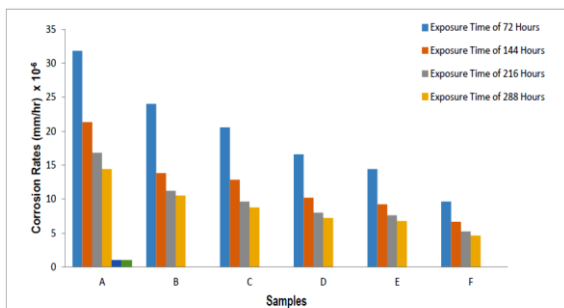
Figure 2: Corrosion Rates for the six samples at Different Exposure Time(hours)

4. CONCLUSION

The hardness test result indicates that the hardness value of aluminized steel increases as the soaking time increases as rightly observed from the test. The hardness increased from $23.1N/mm^2$ to $33.2N/mm^2$ within 2½ hours soaking at the average temperature of 850^oC. The weight loss experiment in HCl solution within the period of 12 days result shows sharp loss of weight in the control sample than observed with the immersion period decreases less with the dipping time increases. The corrosion rate of the control sample is extremely high as compared with the aluminized steel, when computed in the acidic environment from the result of the weight loss experiment. Passive formation was observed to be responsible for the decrease in the corrosion rates of aluminized steel with increase in exposure time in the acidic medium. Therefore, aluminized steel have more corrosion resistance properties than

the control specimen as the time of exposure increases, and the hardness value increase too with more soaking time resulting in a product that has more strength and low cost of steel with the soft and smooth surface of aluminium.

REFERENCE

1. Agrawal, B.K. (1981): Aluminizing of Steel by Gas Atomization Process, Transactions of the Japan Institute of Metals, Vol. 22 No.1 pages 57 to 64.
2. Avner S. H. (1974): Introduction to Physical Metallurgy 2nd edition. McGraw Hill Koga Kusha, Tokyo.
3. Chester F. J. (1989): Hardenability of carbon and alloy steels, Metal handbook, McGraw Hill Book of Company, New York. Volume 1 pg 471, 474-480.
4. David A. R. (1989): Wear resistance, metals handbook, MacMillan Publishing Company, New York. Volume 1, pg 603, 625-626
5. Davies D J and Oelman L A (1983), The structure, properties and heat treatment of metals. 1st Edition, Pitman Publishers, New Zealand
6. Fontana, M.G. (1987): Corrosion Engineering, 3rd Edition, McGraw Hill International, New York. Pages 171, 172 & 237.
7. Ihom A.P. (2009): Seminar Paper published, February 2009, Hot-dip aluminizing of Iron and Steel for improved metal properties (NMDC), Jos.
8. Jacek J et al, (2000): Effect of Chromium Nitride Coating on the Corrosion and Wear Resistance of Stainless Steel, Applied Surface Science, Vol. 156, Issues 1-4, 47-64.
9. Richards, R.W. et al, (1994): Metallurgy of continuous Hot Dip Aluminizing, International Materials Review, Vol. 39 (5), 191 – 212.
10. Singh V. (2008): Physical Metallurgy. Standard Publishers Distributors, Naisarak, Delhi. pg 698, 719, 751-752.
11. Tokai (2008),Aluma Industry Co. Ltd 54 Ichiban – Warishita, Tokai-ciliaichi 476-002 Japan

PRODUCTION AND CHARACTERIZATION OF ORGANIC FERTILIZER FROM ANIMAL WASTE BLEND

Nuhu M[1*]. , Hamisu A.A., Abbas J.A., Mansur S.

Department of Chemical Engineering ABU, Zaria
*Corresponding author phone/email; 08065639034; nmohammed@abu.edu.ng.

ABSTRACT

This research work focused on the production and characterization of organic fertilizer from animal wastes blend (poultry litter and cow dung), where 5.0 kg each of freshly poultry litter and cow dung were collected, dried. Their moisture content was 28.0 and 69% wt. for poultry litter and cow dung respectively. The step employed for the production of the organic fertilizer involved crushing, ball milling and blending of the animal wastes. The characterization of the poultry litter and cow dung was carried out through the method of FTIR analysis to determine the percentage content of nitrogen in the poultry litter, cow dung, poultry litter-cow dung blend ratio and chemical urea fertilizer. The results of the percentage of nitrogen analysis indicate that, poultry litter has 46.02, cow dung 31.47% wt. while the poultry litter-cow dung blend ratios of 1:1,1:2 and 2:1 has 34.29, 32.87 and 42.30% wt. respectively, however the urea chemical fertilizer has 45.17% of the nitrogen. The poultry litter-cow dung blend of 2:1 ratio was found to be more appropriate for the production of the organic fertilizer.

Keywords: *Fertilizer, Animal waste, Environmental pollution, Soil nutrients*

1. INTRODUCTION

The generation and subsequent accumulation of waste generated by continuous increase in human populations is one of the major problems confronting future generations. This was aggravated due to improper waste disposal that often causes greater problems in terms of environmental pollution and disease occurrence not only to human beings but also to animals. Results of a survey on waste generation in the world has indicated that an individual generates an average of 500-600g of waste in one day, with an approximate volume of about 200m3 of the waste collected in one month (Aganon *et al*., 2004). The composition of wastes, collected particularly in the domestic homes ranges from about 40 to 60% (Aganon *et al*., 2004) of biodegradable to the rest as non-biodegradable mostly plastic, foils, wrappers, Styrofoam, bottles and cans (Aganon *et al*.,2004). Considering this huge volume, something has to be done to convert these wastes into useful resources. Based on one of the guiding principles of solid waste management, recycling it would alleviate the problem. On the other hand, the agriculture sector is deemed unsustainable with the negative environmental consequences on the soil condition, since the current agriculture practices are basically chemical-based farming, which make considerable contributions to the degradation of the natural resources, particularly soils. Heavy application of fertilizers has polluted surface and groundwater resources. Intensive cropping to feed the ever expanding population coupled with high erosion rates in the uplands has resulted severe soil nutrient depletion. Based on these scenarios, there is an urgent need to find ways and means of alleviating such problems by creating new and innovative processes would allow this resource to be better utilized and simultaneously reduce environmental impacts. Nowadays, organic-based agricultural production is the rapidly emerging technology in the sector which partly solves waste disposal problems through conversion

of biodegradable wastes into organic compost ensuring the availability of organic fertilizer (Moore *et al*., 1991).

Many organic fertilizers are by products of livestock, fish, food, and other processing industries, but the recent demand for low-cholesterol meat products has led to the tremendous expansion and production of broiler chickens in the poultry industry, leading to naturally abundant supply of chicken litter and this rapid growth of the industry has caused increasing concern about the disposal of poultry wastes with respect to nonpoint source pollution. In view of that poultry litter-based fertilizers have been analysed to be effective plant fertilizers, despite having lower nutrient concentrations than many synthetic fertilizers (Crohn, 2006).

Poultry litter, is a combination of accumulated chicken manure, feathers, and bedding materials (obtained from broiler houses), is a potential biomass feedstock. It can also be described as a mixture of poultry excreta, spilled feed, feathers and material used as bedding in poultry operations. This term is also used to refer to unused bedding materials. Poultry litter is used in confinement buildings used for raising broilers, turkeys and other birds (Godwin et al., 2003). Common bedding materials include wood shavings, sawdust, peanut hulls, shredded sugarcane, straw, and other dry, absorbent, low-cost organic materials. The bedding materials help absorb moisture, thereby limiting the production of ammonia and harmful pathogens (Godwin et al., 2003).

Livestock manure mostly cow dung has been an asset to crop production since the beginning of organized agriculture. The excretions from the cattle contain several essential plant nutrients, they contribute to increased crop yields when properly applied to soils and can be used as valuable sources of fertilizer nutrients for crops. The application of cow dung manure to farmland is an economic sustainable mechanism for increasing crop production, as it is an excellent soil amendment capable of

increasing soil quality due to the provision of large inputs of nutrients and organic material (Pennington *et al.*, 1984). The generation and improper disposal of solid wastes pose a major threat to the environment and high risks to human health, and also the use of synthesized fertilizers for the development of plants cause many problems to the plants, animals, human and environmental health through acidification of the soil, water pollution and contribution to climate change motivated the production and characterization of organic fertilizer from such wastes, which will hopefully reduce environmental pollution, improve soil health and crops productivity.

2. MATERIAL AND METHOD

2.1 Material

The cow dung and poultry litter for the production of the organic fertilizer, were collected from Zango shanu cattle and a broiler chicken homes respectively.

2.2 Method

2.2.1 *Moisture content determination*

The wet samples were weighed using a weighing balance and results recorded as "wt of wet sample". It was then subjected to sun drying for about 2 hours and then to an oven at temperature of 130^0C for three hours, to absorb the moisture completely, the samples were allowed to cool. The cooled samples were weighed and results recorded as "wt of dry sample". The moisture content was calculated using the following equation:

$$Moisture\ Content\ (\%) = \frac{wt\ of\ wet\ sample - wt\ of\ dry\ sample}{wt\ of\ wet\ sample}\ x\ 100 \quad (1)$$

2.2.2 *Sample preparation*

The dried poultry litter and cow dung samples were grinded into smaller particles by the means of a small crusher, in order to reduce their sizes (20-30 microns) for proper milling.

The samples were then grinded into fine particles using a ball milling machine.

The milled samples were then sieved to acquire the desired particles size (5 microns).

2.2.3 Mixing

Mixing is the combination of different substances by blending them together to form a single substance. The poultry litter and cow dung samples were blended together on ratio basis of 1:1, 1:2 and 2:1, for characterization in order to determine the appropriate blending ratio. These ratios where achieved by mixing 50, 50, and 100gpoultry litre with 50, 100, and 50g cow dung.

2.2.4 Characterization

The samples were characterised by determining the nutrient elements present in each of the blended samples through Fourier Transform Infrared (FTIR) method.

The prepared samples were analysed through the Fourier transform infrared in order to know the percentage content of nitrogen present in each of them. The content of the nitrogen present in urea fertilizer sample was also determined. The FITR results obtained were interpreted as follows: The peaks of the Infrared absorptions for the Nitrogen functional group were selected. The areas that correspond to the peaks were also selected from the results Table. The selected areas were added up, divided by the total area and multiply by hundred. The result obtained indicates the percentage content of Nitrogen present in the sample.

3. RESULTS AND DISCUSSIONS

The results obtained from characterization of both the poultry litter and cow dung samples are explained and present under moisture content determination and elemental Nutrients analysis of the samples.

3.1 Moisture Content

Table 1 indicates the result of the moisture content of poultry litter and cow dung samples determined before processing.

Table 1: The moisture content result of poultry litter and cow dung samples

Sample	Wet Sample (kg)	Dry Sample (kg)	Moisture Content (%)
Poultry litter	5.0	3.60	28.0
Cow dung	5.0	1.55	69.0

The results obtained on the moisture content of the poultry litter and cow dung samples calculated indicates that, the poultry litter and the cow dung samples have moisture content of 28.0% and 68.0% respectively. This was comparable with literature value which normally averages between 25 to 75% (Gary et al., 2012).

These values could retain appreciable amount of moisture, allowing the litter to be broken up easily for suitable application to the plant.

3.2 Elemental Nutrients Analysis

The analysis of the elemental nutrients present in the experimental samples was done using the Fourier Transform Infrared (FTIR)to determine the amount of Nitrogen content as major element of interest in the samples as shown in the Figures 1,2,3,4, and 5.
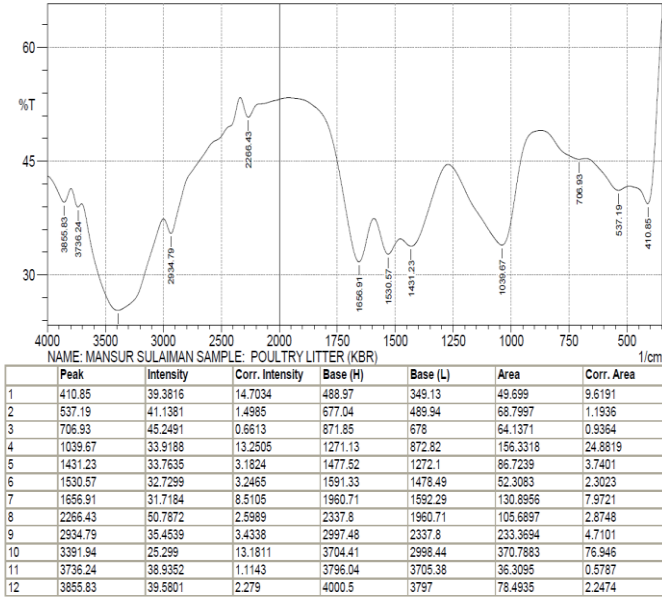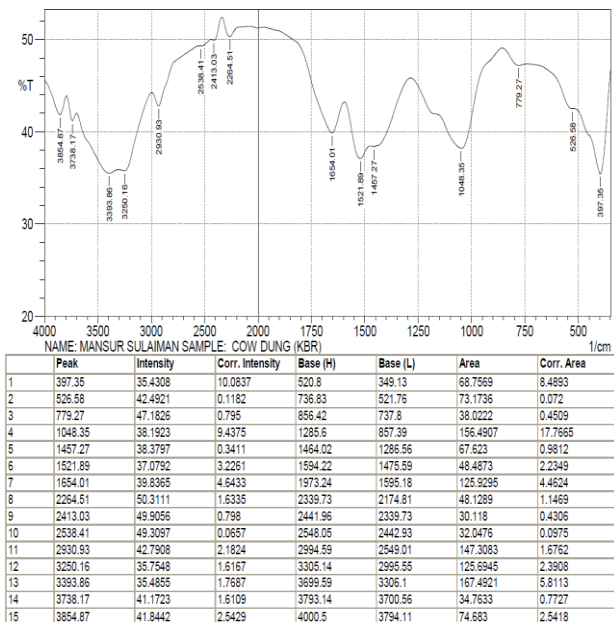
⊕ SHIMADZU

Fig. 1: FTIR analysis result for poultry litter (P) sample

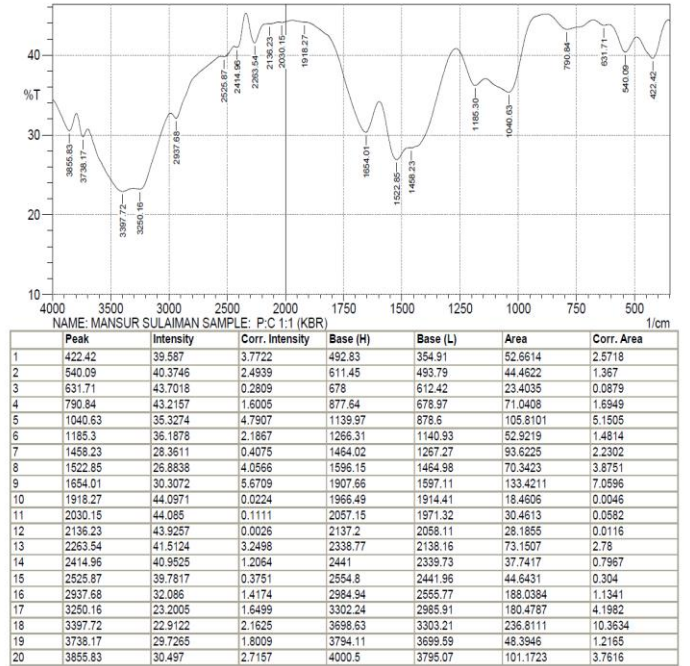FTIR ANALYSIS RESULT NARICT,ZARIA — FTIR- 8400S FOURIER TRANSFORM INFRARED SPECTROPHOTOMETER

NAME: MANSUR SULAIMAN SAMPLE: POULTRY LITTER (KBR)

	Peak	Intensity	Corr. Intensity	Base (H)	Base (L)	Area	Corr. Area
1	410.85	39.3816	14.7034	488.97	349.13	49.699	9.6191
2	537.19	41.1381	1.4985	677.04	489.94	68.7997	1.1936
3	706.93	45.2491	0.6613	871.85	678	64.1371	0.9364
4	1039.67	33.9188	13.2505	1271.13	872.82	156.3318	24.8819
5	1431.23	33.7635	3.1824	1477.52	1272.1	86.7239	3.7401
6	1530.57	32.7299	3.2465	1591.33	1478.49	52.3083	2.3023
7	1656.91	31.7184	8.5105	1960.71	1592.29	130.8956	7.9721
8	2266.43	50.7872	2.5989	2337.8	1960.71	105.6897	2.8748
9	2934.79	35.4539	3.4338	2997.48	2337.8	233.3694	4.7101
10	3391.94	25.299	13.1811	3704.41	2998.44	370.7883	76.946
11	3736.24	38.9352	1.1143	3796.04	3705.38	36.3095	0.5787
12	3855.83	39.5801	2.279	4000.5	3797	78.4935	2.2474

⊕ SHIMADZU

Fig. 2: FTIR analysis result for cow dung (C) sample

FTIR ANALYSIS RESULT NARICT,ZARIA — FTIR- 8400S FOURIER TRANSFORM INFRARED SPECTROPHOTOMETER

NAME: MANSUR SULAIMAN SAMPLE: COW DUNG (KBR)

	Peak	Intensity	Corr. Intensity	Base (H)	Base (L)	Area	Corr. Area
1	397.35	35.4308	10.0837	520.8	349.13	68.7569	8.4893
2	526.58	42.4921	0.1182	736.83	521.76	73.1736	0.072
3	779.27	47.1826	0.795	856.42	737.8	38.0222	0.4509
4	1048.35	38.1923	9.4375	1285.6	857.39	156.4907	17.7665
5	1457.27	38.3797	0.3411	1464.02	1286.56	67.623	0.9812
6	1521.89	37.0792	3.2261	1594.22	1475.59	48.4873	2.2349
7	1654.01	39.8365	4.6433	1973.24	1595.18	125.9295	4.4624
8	2264.51	50.3111	1.6335	2339.73	2174.81	48.1289	1.1469
9	2413.03	49.9056	0.798	2441.96	2339.73	30.118	0.4306
10	2538.41	49.3097	0.0657	2548.05	2442.93	32.0476	0.0975
11	2930.93	42.7908	2.1824	2994.59	2549.01	147.3083	1.6762
12	3250.16	35.7548	1.6167	3305.14	2995.55	125.6945	2.3908
13	3393.86	35.4855	1.7687	3699.59	3306.1	167.4921	5.8113
14	3738.17	41.1723	1.6109	3793.14	3700.56	34.7633	0.7727
15	3854.87	41.8442	2.5429	4000.5	3794.11	74.683	2.5418

Fig.3: FITR Analysis for P:C/1:1 sample

FTIR ANALYSIS RESULT NARICT,ZARIA — FTIR- 8400S FOURIER TRANSFORM INFRARED SPECTROPHOTOMETER

NAME: MANSUR SULAIMAN SAMPLE: P:C 1:1 (KBR)

	Peak	Intensity	Corr. Intensity	Base (H)	Base (L)	Area	Corr. Area
1	422.42	39.587	3.7722	492.83	354.91	52.6614	2.5718
2	540.09	40.3746	2.4939	611.45	493.79	44.4622	1.367
3	631.71	43.7018	0.2809	678	612.42	23.4035	0.0879
4	790.84	43.2157	1.6005	877.64	678.97	71.0408	1.6949
5	1040.63	35.3274	4.7907	1139.97	878.6	105.8101	5.1505
6	1185.3	36.1878	2.1867	1266.31	1140.93	52.9219	1.4814
7	1458.23	28.3611	0.4075	1464.02	1267.27	93.6225	2.2302
8	1522.85	26.8838	4.0566	1596.15	1464.98	70.3423	3.8751
9	1654.01	30.3072	5.6709	1907.66	1597.11	133.4211	7.0596
10	1918.27	44.0971	0.0224	1966.49	1914.41	18.4606	0.0046
11	2030.15	44.085	0.1111	2057.15	1971.32	30.4613	0.0582
12	2136.23	43.9257	0.0026	2137.2	2058.11	28.1855	0.0116
13	2263.54	41.5124	3.2498	2338.77	2138.16	73.1507	2.78
14	2414.96	40.9525	1.2064	2441	2339.73	37.7417	0.7967
15	2525.87	39.7817	0.3751	2554.8	2441.96	44.6431	0.304
16	2937.68	32.086	1.4174	2984.94	2555.77	188.0384	1.1341
17	3250.16	23.2005	1.6499	3302.24	2985.91	180.4787	4.1982
18	3397.72	22.9122	2.1625	3698.63	3303.21	236.8111	10.3634
19	3738.17	29.7265	1.8009	3794.11	3699.59	48.3946	1.2165
20	3855.83	30.497	2.7157	4000.5	3795.07	101.1723	3.7616

Fig.4: FITR Analysis for P:C/1:2 sample

FTIR ANALYSIS RESULT NARICT,ZARIA — FTIR- 8400S FOURIER TRANSFORM INFRARED SPECTROPHOTOMETER

NAME: MANSUR SULAIMAN SAMPLE: P:C 1:2 (KBR)

	Peak	Intensity	Corr. Intensity	Base (H)	Base (L)	Area	Corr. Area
1	422.42	36.2991	8.1745	484.15	349.13	53.4523	5.9826
2	542.02	36.7924	1.3673	608.56	484.15	52.915	0.8941
3	789.88	37.8008	1.0411	866.07	672.21	80.8576	1.1545
4	1044.49	31.6707	3.8342	1155.4	866.07	132.6796	4.4906
5	1437.98	28.7017	0.3358	1445.7	1267.27	87.8547	0.1121
6	1518.03	28.6705	1.5652	1594.22	1484.27	57.5107	1.4337
7	1654.01	30.2826	3.6248	1906.7	1595.18	143.6168	4.6633
8	1910.56	38.5203	0.0011	1913.45	1907.66	2.3974	0
9	1918.27	38.518	0.0109	1965.53	1914.41	21.1495	0.0027
10	2017.61	38.5182	0.0623	2051.36	1970.35	33.5346	0.032
11	2134.31	38.3954	0.0405	2160.35	2055.22	43.6406	0.0314
12	2264.51	37.2249	1.4245	2336.84	2161.31	73.8204	1.2752
13	2413.99	36.9677	0.5355	2441	2337.8	43.8334	0.3974
14	2533.58	36.2759	0.1569	2555.77	2441.96	49.7608	0.1692
15	2934.79	31.3751	1.1544	2986.87	2556.73	200.3252	1.0721
16	3241.48	24.9885	6.6945	3705.38	2987.84	403.1841	43.6324
17	3737.2	30.7657	0.7912	3791.21	3706.34	42.8037	0.4847
18	3854.87	31.0743	1.5938	4000.5	3792.18	102.8505	2.1247

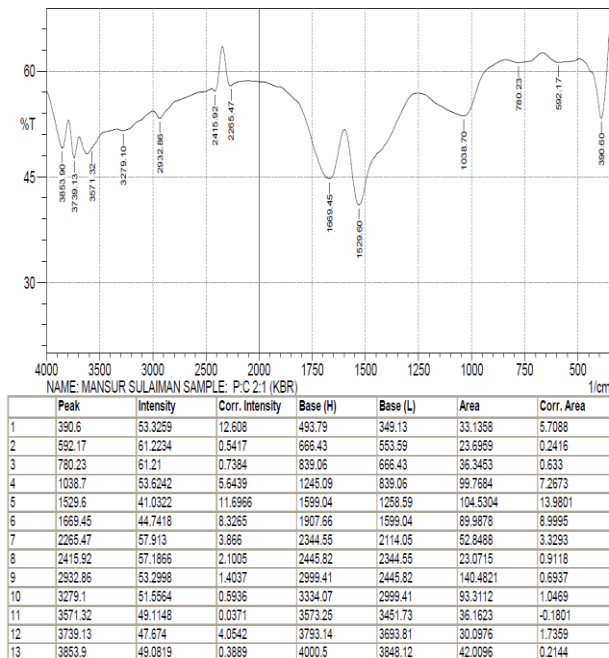**Fig.5:** FITR Analysis for P:C/2:1 sample

The FITR result for analyzing the percentage content of Nitrogen in the samples was interpreted by adding up the selected corresponding areas to the peaks of the infrared absorptions for the Nitrogen functional group derived from the IR absorption Table, divided by the total area and multiply by hundred.

$$Nitrogen\ (wt,\%) = \frac{Nitrogen\ Peaks\ Area}{Total\ Peaks\ Area}\ x\ 100 \quad (2)$$

Table 2, shows the percentage contents of Nitrogen evaluated from the FTIR analysis results. The various Nitrogen group   peaks occur at wave numbers $(1/\lambda)$ of 1530.57, 2266.43, and 3391.94, 1521.89, 2264.51, 3250.16, and 3393.86, 1522.85, 2263.34, 3250.16, and 3397.72, 1518.03, 2264.51, and 3241.48, 1529.6, 2265.47, and 3279.1 cm^{-1} for Poultry litter, Cow dung, poultry litter-cow dung blended ratio of 1:1, 1:2 and 2:1 respectively.

Table 2: The FTIR result of the analyzed samples

Sample	Poultry litter	Cow dung	P:C/1:1	P:C/1:2	P:C/2:1
Nitrogen content (%)	36.89	31.47	34.29	32.87	31.12

Table 2 present the evaluated percentage Nitrogen content in the samples, indicate that poultry litter and cow dung samples have 36.89% and 31.47% respectively, while that of the poultry litter-cow dung blended ratio of 1:1, 1:2 and 2:1 have 34.29%, 32.87% and 31.12% respectively.

The results indicate that poultry litter contains the highest amount of Nitrogen (36.87%), while the blend ratio of P:C/2:1contains the lowest amount of Nitrogen with 31.12%, resulting from the loss of Nitrogen constituents due to the hydrolysis of the NH_2 groups (enzymatic) and then volatilization of N_2O and NH_3 (Gary *et al.*, 2012).

The level of Nitrogen contents in the blended samples was observed to decrease with more of poultry litter due to the large chemical composition of their feed (about 45-50% concentration).

The content of nitrogen analysed for the samples, the nitrogen-cow dung blending ratio of 1:1 with 36.89% is more comparable to standard urea fertilizer with 46% Nitrogen content, thus it is selected as the appropriate mixture of the poultry-cow dung blend to be used in processing the production of the organic fertilizer for effective growth and development of the plants. The blend will provide balance nutrient due to the presence of calcium, potassium and phosphorus among others present in the poultry litter.

4. CONCLUSION

The blend of poultry litter and cow dung of 1:1 blend ratio provide the best formulation for the production of organic fertilizer which can appropriately serve as substitute to the

urea chemical fertilizer, which is cheaper and more environmental friendly than the chemical fertilizer.

REFERENCE

Aganon, C.P., Cruz, N.E., Galindez, J.L., Patricio, M.G., and Roxas, A.C. (2004). *"Production of Organic Fertilizer from Solid Waste"*. The Ecological Solid Waste Management Project". Terminal Report 2004.

Crohn, D. (2006). "Optimizing organic fertilizer applications under steady-state conditions". *Journal of   Environmental Qual. 35:658-669.*

Gary, D.B., and Richard D.M. (2012). *"Causes and prevention of wet litter in broilers houses"*. University   of Florida.

Goodwin, H.L., Jones, F.T., Watkins, S.E., and Hipp, J.S. (2003). *"Use and management of poultry litter and other nutrients".* Arkansas Cooperative Extension Service. University of Arkansas, Little Rock,   Arkansas.

Pennington, J. A., Vandevender, K., and Jennings, A.J. (1984). *"Nutrient and Fertilizer Value of Dairy Manure".*University of Arkansas Division of Agriculture, Cooperative Extension Service in Little   Rock. Arkansas Cooperative Extension Service.

Moore, P.A., Daniel, T.C., Sharpley A.N., and Wood, C.W. (1991).*"Poultry Manure Management".* Arkansas Agricultural Experiment Station, University of Arkansas.

DEVELOPMENT OF A NEW CLASS OF BLOCK IMPLICIT RUNGE-KUTTA TYPE METHOD FOR INITIAL VALUE PROBLEMS

[1] Muhammad R. , [2]Y. A Yahaya , [3]A.S Abdulkareem.

[1&2]Department of Mathematics/Statistics , Federal University of Technology, Minna.

[3]Department of Chemical Engineering, Federal University of Technology, Minna.

[*1]r.muhd@futminna.edu.ng,[2]yusuphyahaya@futminna.edu.ng , [3]kasaka2003@futminna.edu.ng

08036128483, 08034519729, 07068482432

ABSTRACT

In this study, we propose a new class of Runge-Kutta type method with three stages for the solution of initial value problems. The method was developed through the collocation approach and reformulated into a Runge-Kutta type of first order using the Butcher analysis. The first order method was extended to a second order one using the Runge –Kutta Nystrom method. A convergence analysis was carried out in order to determine the order, error constant and stability analysis.Numerical examples carried out on the Initial value problems further substantiate the effectiveness and viability of the methods.

Keywords: *Block,   Implicit, Runge-Kutta type, Initial value problems.*

1. INTRODUCTION

Ordinary Differential Equations arise frequently in the study of the physical problems in aspects of science and engineering.   Unfortunately, many cannot be solved exactly. This is why the ability to solve these equations numerically is important. Traditionally, mathematicians have used one of two classes of methods for solving numerically ordinary differential equations. These are Runge-Kutta methods and Linear Multistep Methods (LMM),(Rattenbury,2005). Runge-Kutta (RK) methods are very popular because of their symmetrical forms, have simple coefficients, very efficient and numerically stable,(Agams, 2012). The methods are fairly simple to program, easy to implement and their truncation error can be controlled in a more straight forward manner than multistep methods, (Kendall, 1989).

The application of Runge-Kutta methodsKutta methods have provided many satisfactory solutions to many problems that have been regarded as insolvable. The popularity and the growth of these methods; coupled with the amount of research effort being undertaken are further evidence that the applications are still the leading source of inspiration for mathematical creativity, (Yahaya & Adegboye, 2011).

The   significance of numerical solution of Ordinary Differential Equations (ODE) in scientific computation cannot be over emphasized as they are used to solve real life problems such as chemical reactions. Most of these problems come in higher order ordinary differential equations. One way of solving these higher order ordinary differential equations is by reduction to a system of first order and then applying any suitable method. This approach has some drawbacks such as waste of computer time and human efforts,(Agams A S, 2012). The idea in

this work is to solve the higher order ODE directly without reduction to first order. This saves computer time and human effort based on the fact that, there is gain in efficiency and accuracy, contains minimal function evaluation and lower computational cost.

In this study, we seek to reformulate the Block Backward Differentiation Formulae (Hybrid and Non-hybrid) for k=1 into Runge Kutta Type Method with three (3) stages for the solution of Initial Value Problems in Ordinary Differential Equations (ODE) of the form

$$y' = f(x, y) \qquad y(x_0) = y \qquad (1)$$

$$y'' = f(x, y) \qquad y(x_0) = y \ \ y'(x_0) = \beta \qquad (2)$$

$$y'' = f(x, y, y') \qquad y(x_0) = y \ \ y'(x_0) = \beta \qquad (3)$$

We consider the numerical solution of the Initial Value Problem that has benefits such as self starting, high order, low error constants, satisfactory stability property such as A-stability and low implementation cost. We emphasize the combination of multistep structure with the use of off grid points and seek a method that is both multistage and multivalue. This will enable us to extend the general linear formulation to the high order Runge-Kutta case by considering a polynomial

$$y(x) = \sum_{j=1}^{t-1} \alpha_j(x) \, y_{n+j} + h \sum_{j=1}^{m-1} \beta_j \, f(\bar{x}_j, y(\bar{x}_j))$$

(4)

Where t denotes the number of interpolation points $x_{n+j}, j = 0,1 \dots t-1$ and m denotes the distinct collocation points $\bar{x}_j \epsilon [x_n, x_{n+k}], j = 0,1 \dots m-1$ chosen from the given step $[x_n, x_{n+k}]$ (Butcher, 2003).

METHODOLOGY

Butcher (2003) defined an S-stage Runge-Kutta method for the first order differential equation in the form

$$y_{n+1} = y_n + h \sum_{i,j=1}^{s} a_{ij} k_i \qquad (5)$$

where for $i = 1,2 \dots \dots s$

$$k_i = f\left(x_i + \alpha_j h, y_n + h \sum_{i,j=1}^{s} a_{ij} k_j\right) \quad (6)$$

The real parameters α_j, k_i, a_{ij} define the method. The method in Butcher array form can be written as

$$\begin{array}{c|c} \alpha & \beta \\ \hline & b^T \end{array}$$

Where $a_{ij} = \beta$

The Runge-Kutta Nystrom (RKN) method is an extension of Runge-Kutta method for second order ODE of the form

$$y'' = f(x, y, y') \qquad y(x_0) = y_0 y'(x_0) = y_0' \quad (7)$$

An S-stage implicit Runge-Kutta Nystrom for direct integration of second order initial value problem is defined in the form

$$y_{n+1} = y_n + \alpha_i h y_n' + h^2 \sum_{i,j=1}^{s} a_{ij} k_j \qquad (8a)$$

$$y_{n+1}' = y_n' + h \sum_{i,j=1}^{s} \bar{a}_{ij} k_j \qquad (8b)$$

where for $i = 1,2 \dots \dots . s$

$$k_i = f(x_i + \alpha_j h, y_n + \alpha_i h y_n' + h^2 \sum_{i,j=1}^{s} a_{ij} k_j, y_n' + h \sum_{i,j=1}^{s} \bar{a}_{ij} k_j) \qquad (8c)$$

The real parameters $\alpha_j, k_j, a_{ij}, \bar{a}_{ij}$ define the method and it is worth mentioning that the method in butcher array form is expressed as

$$\begin{array}{c|c|c} \alpha & \bar{A} & A \\ \hline & \bar{b}^T & b \end{array}$$

$$A = a_{ij} = \beta^2 \bar{A} = \bar{a}_{ij} = \beta \beta = \beta e$$

1.1 Construction of the method

The Consider the approximate solution to equation (1) in the form of power series

$$y(x) = \sum_{j=0}^{t+m-1} \alpha_j x^j \qquad (9)$$

$\alpha \in R, j = 0(1)t + m - 1, y \in C^m(a, b) \subset P(x)$

$$y'(x) = \sum_{j=0}^{t+m-1} j \alpha_j x^{j-1} \qquad (10)$$

Where α_j's are the parameters to be determined, t and m are the points of interpolation and collocation, respectively.

When $K = 1$, we interpolate equation (9) at $j = 0, \frac{1}{2}$ and collocate equation (10) at $j = 1$. Equations (9) & (10) can then be expressed as

$$y(x) = \sum_{j=0}^{t+m-1} \alpha_j x^j = y_{n+j} \quad j = 0, \frac{1}{2} \qquad (11)$$

$$y'(x) = \sum_{j=0}^{t+m-1} j\alpha_j x^{j-1} = f_{n+j} \quad j = 1 \qquad (12)$$

The general form of the proposed method upon addition of one off grid point is expressed as

$$y(x) = \alpha_1(x)y_n + \alpha_2(x)y_{n+\frac{1}{2}} + h\beta_0 f_{n+1} \qquad (13)$$

The matrix D of dimension $(t + m) * (t + m)$ of the proposed method is expressed as:

$$D = \begin{bmatrix} 1 & x_n & x_n^2 \\ 1 & x_n + \frac{1}{2}h & \left(x_n + \frac{1}{2}h\right)^2 \\ 1 & 1 & 2x_n + 2h \end{bmatrix}$$

We invert the matrix D, to obtain columns which form the matrix C. The elements of C are used to generate the continous coefficients of the method as:

$$\left.\begin{array}{l} \alpha_1(x) = C_{11} + C_{21}x + C_{31}x^2 \\ \alpha_2(x) = C_{12} + C_{22}x + C_{32}x^2 \\ \beta_0(x) = C_{13} + C_{23}x + C_{33}x^2 \end{array}\right\} \qquad (14)$$

The values of the continuous coefficients equation (14) are substituted into equation (13) to give the continuous form of the one step block hybrid Backward Differentiation Formula (BDF) with one off step interpolation point.

$$\bar{y}(x) = \left\{ \left(\frac{1}{3}\frac{(2x_n+h)(2x_n+3h)}{h^2} - \frac{8}{3}\frac{x_n+h}{h^2}x + \frac{4}{3h^2}x^2 \right) y_n \right. +$$

$$\left(\frac{-4}{3}\frac{x_n(x_n+2h)}{h^2} + \frac{8}{3}\frac{x_n+h}{h^2}x - \frac{4}{3h^2}x^2 \right) y_{n+\frac{1}{2}} + \left(\frac{1}{3}\frac{x_n(2x_n+h)}{h} - \right.$$

$$\left. \left. \frac{1}{3}\frac{4x_n+h}{h}x + \frac{2}{3h}x^2 \right) f_{n+1} \right\} \qquad (15)$$

Evaluating equation (15) at point $x = x_{n+1}$, and its derivative at $x = x_{n+1/2}$, yields the following two discrete hybrid schemes which are used as a block integrator;

$$y_{n+1} - \frac{4}{3}y_{n+\frac{1}{2}} = -\frac{1}{3}y_n + \frac{1}{3}hf_{n+1}$$

$$(16)$$

$$y_{n+\frac{1}{2}} = y_n + \frac{3}{4}hf_{n+1/2} - \frac{1}{4}hf_{n+1}$$

The equation (16) is of order $[2,2]^T$ with error constant $\left[-\frac{1}{36}, -\frac{5}{24} \right]^T$

By rearranging equation (16) simultaneously, equation (17) was obtained

$$y_{n+\frac{1}{2}} = y_n + \frac{h}{4}\left\{ 3f_{n+\frac{1}{2}} - f_{n+1} \right\}$$

$$(17)$$

$$y_{n+1} = y_n + h\{f_{n+1/2}\}$$

Reformulating equation (17) with the coefficients as characterized by the Butcher array form

$$\begin{array}{c|c} \alpha & \beta \\ \hline & b^T \end{array}$$

Where $a_{ij} = \beta$

gives

0	0	0	0
$\frac{1}{2}$	0	$\frac{3}{4}$	$\frac{-1}{4}$
1	0	1	0
	0	1	0

Using equations (5) and (6), we obtained an implicit 3-stage block Runge-Kutta type method of uniform order two everywhere on the interval of solution

$$y_{n+\frac{1}{2}} = y_n + h(\frac{3}{4}k_2 - \frac{1}{4}k_3)$$

(18)

$$y_{n+1} = y_n + hk_2$$

Where

$$k_1 = f(x_n, y_n)$$

$$k_2 = f(x_n + \frac{1}{2}h, y_n + h\left\{0k_1 + \frac{3}{4}k_2 - \frac{1}{4}k_3\right\})$$

$$k_3 = f(x_n + h, y_n + h\{0k_1 + k_2 + 0k_3\})$$

Extending the method (18) with the coefficients as characterized in the Butcher array form

$$
\begin{array}{c|c|c}
\alpha & \bar{A} & A \\
\hline
 & \bar{b}^T & b
\end{array}
$$

$A = a_{ij} = \beta^2 \bar{A}, \ \bar{a}_{ij} = \beta\beta = \beta e$ gives

$$
\begin{array}{c|ccc|ccc}
0 & 0 & 0 & 0 & 0 & 0 & 0 \\
\frac{1}{2} & 0 & \frac{3}{4} & \frac{-1}{4} & 0 & \frac{5}{16} & \frac{-3}{16} \\
1 & 0 & 1 & 0 & 0 & \frac{3}{4} & \frac{-1}{4} \\
\hline
 & 0 & 1 & 0 & 0 & \frac{3}{4} & \frac{-1}{4}
\end{array}
$$

Using equation (8), we obtained an implicit 3 stage block Runge-Kuttatype method of uniform order 2 everywhere on the interval of solution.

$$y_{n+\frac{1}{2}} = y_n + \frac{1}{2}hy_n' + h^2\left(0k_1 + \frac{5}{16}k_2 - \frac{3}{16}k_3\right),$$

$$y_{n+\frac{1}{2}}' = y_n' + h\left(0k_1 + \frac{3}{4}k_2 - \frac{1}{4}k_3\right)$$

(19)

$$y_{n+1} = y_n + hy_n' + h^2\left(0k_1 + \frac{3}{4}k_2 - \frac{1}{4}k_3\right),$$

$$y_{n+1}' = y_n' + h(0k_1 + k_2 + 0k_3)$$

where

$$k_1 = f(x_n, y_n, y_n')$$

$$k_2 = f(x_n + \frac{1}{2}h, y_n + \frac{1}{2}hy_n' + h^2\left(0k_1 + \frac{5}{16}k_2 - \frac{3}{16}k_3\right),$$

$$y_{n+\frac{1}{2}}' = y_n' + h\left(0k_1 + \frac{3}{4}k_2 - \frac{1}{4}k_3\right))$$

$$k_3 = f(x_n + h, y_n + hy_n' + h^2\left(0k_1 + \frac{3}{4}k_2 - \frac{1}{4}k_3\right),$$

$$y_n' + h(0k_1 + k_2 + 0k_3))$$

The derived method was used to solve existing problems by Sunday etal. (2013) and Odigure et al. (2009).

Problem 1: Sunday J etal.(2013)

This is a first order Initial Value Problem with initial conditions, the eigen value (λ), the steplength (h) and the range of solutions given in equation (20) and the exact solution in equation (21).

$$y' = -\lambda y \qquad y(0) = 1, \quad y'(0) = 1, \quad \lambda = 1, \quad h = 0.01, \qquad 0 \le x \le 0.04 \quad (20)$$

Exact Solution

$$y(x) = e^{-x} \tag{21}$$

Table 1: $K = 1$ first order $RKTM$

x	Exact solution	Computed solution	Error
0.01	0.9901	0.9900	$-4.10E - 08$
0.02	0.9802	0.9802	$-8.11E - 08$
0.03	0.9704	0.9704	$-1.205E - 07$
0.04	0.9608	0.9608	$-1.590E - 07$

Presented in Table1 is the result obtained for exact solution to the problem shown in equation 20. Also presented are the computed results obtained when we applied theRKTM.

It can be observed from the table that the computed solutions are closer to the exact solution with error values in the range $-1.590E-07$ to $-4.10E-08$.

Problem 2 : Odigure etal. (2009)

In their study,Odigure etal. (2009) developed a mathematical model for the process of limestone decarbonization to produce quicklime (CaO) according to chemical reaction shown in equation (22)

$$CaCO_3 \rightarrow CaO + CO_2 \qquad (22)$$

The quality of CaO produced is dependent on the chemical and microstructure composition, density and burning conditions (temperature, CO_2 concentration and particle size). The mathematical model for the decomposition of calcium carbonate is represented by the relationship presented in equation (23)

$$\frac{d^2 T_C}{dr^2} + \frac{2}{r}\frac{dT_C}{dr} - \frac{\rho_p k_1 C_c \Delta H}{k_e} = 0 \qquad (23)$$

$\frac{dT_C}{dr} = 0$ at $r =$

$0 \qquad (24)$

Where

k_e =effective thermal conductivities= $3\ W/m.K$

C_c =concentration of CO_2 in the gas stream

$\rho_p = 2710 kg/m^3$

The concentration of the CO_2 in the gas stream can be estimated from the relationship presented in equation (4)

$$\frac{d^2 C_C}{dr^2} + \frac{2}{r}\frac{dC_C}{dr} - \frac{\rho_p k_1 C_c \Delta H}{(D_k)_e} = 0 (25)$$

$\frac{dC_c}{dr} = 0$ at $r = 0$

The time taken to produce quicklime from calcium carbonate and conversion of calcium carbonate to calcium oxide can be estimated from the relationship shown in equations (26) and (27), respectively;

$$t = \frac{\rho_A}{3 M_A k_m C_c}\frac{(r_s - r)^3}{r^2} (26)$$

$$X_A = 1 - \frac{3 M_A K C_c r^2 t}{\rho_A r_s^3} (27)$$

$$(D_k)_e = 9.70 \times 10^3 \alpha \left(\frac{T_c}{M_A}\right)^{0.5}$$

$$k_1 = A e^{-\frac{E}{R_g T}}$$

$$A = 2.01 E = 4.062 \times 10^4 R_g = 8.314 J/mol.K\ \rho_A$$
$$= 2710 kg/m^3 k_m = 0.03 m/s$$

The performance of the Runge-Kuttatype method (RKTM) on this problem will determine the various temperatures of conversions, the time taken to produce quicklime from calcium carbonate and conversion of calcium carbonate to calcium oxide at various values of the step numbers (k_s).

Table 2: $K = 1$ second order RKTM

r	$T_o = 600^0 C$	$T_o = 650^0 C$	$T_o = 700^0 C$
	T	T	T
0.1	634	684	734
0.2	685	735	785
0.3	736	786	836
0.4	787	837	887
0.5	838	888	938
0.6	889	939	989
0.7	940	990	1040
0.8	991	1041	1091
0.9	1042	1092	1142
1.0	1093	1143	1193

Presented in Table 2 are the solutions to equation 23 using the Runge-Kutta Type Method (RKTM). It can be observed from the table of results that the starting decarbonization temperature and particle size influences the decarbonization temperature.

The time taken and rate of conversion is given in the following Table 3

Table 3: $K = 1$ second order RKTM

r_s	$C_c = 13.204$ C_c	$t(sec)$
0.01	13.2892	0
0.02	13.4169	0.0051
0.03	13.5447	0.0404
0.04	13.6724	0.1351
0.05	13.8002	0.3174
0.06	13.9279	0.6142
0.07	14.0557	1.0517
0.08	14.1834	1.6550
0.09	14.3112	2.4483
0.1	14.4389	3.4552

Based on the obtained simulation results, the rate of conversion $X_A = 0.99$ for the various times and the implication is that there is 99 % conversion of the product.

CONCLUSION

It will be observed that from the table at the initial radius $(r_s = 0.01)$, the time taken and the corresponding conversion rate is 0. This means that at that particular point no reaction has taken place. As the radius increases, we have the various times for the conversion with the same conversion rate at 0.99. This implied that the rate of conversion is 99% which means almost all the limestone is converted to quicklime. The various values obtained will help the engineers to make a very good production management decision.

REFERENCE

Agam, A.S (2013). A sixth order multiply implicit Runge-kutta method for the solution of first and second order ordinary differential equations. Unpublished doctoral dissertation, Nigerian Defence Academy, Kaduna .

Butcher, J.C. (2003). *Numerical methods for ordinary differential equations.* John Wiley &Sons.

Kendall, E. A (1989). *An introduction to numerical analysis*, (2nd ed), John Wiley & Sons.

Odigure, J.O, Mohammad, A., Abdulkareem, A.S (2009). Mathematical Modeling of Limestone Decarbonization Process and Theory of Nanoparticles Reaction Mechanism. *Journal of dispersion science and Technology, 30:305-312.*

Rattenbury, N. (2005). *Almost runge kutta methods for stiff and non-stiff problems.* Unpublished doctoral dissertation, University of Auckland.

Yahaya, Y.A. & Adegboye, Z.A. (2011). Reformulation of quade's type four-step block hybrid multstep method into runge-kutta method for solution of first and second order ordinary differential equations.*Abacus,38(2)*, 114-124.